NEURAL ELECTROCEUTICALS: INTERFACING WITH THE NERVOUS SYSTEM WITH ELECTRICAL STIMULATION

EDITED BY: Giovanni Mirabella, Mikhail Lebedev, Alberto Priori, Julie Duque, Alexei Ossadtchi, Simone Rossi and Olivier David

PUBLISHED IN: Frontiers in Neuroscience

frontiers Research Topics

ISSN 1664-8714
ISBN 978-2-88976-553-9
DOI 10.3389/978-2-88976-553-9

About Frontiers

Frontiers is more than just an open-access publisher of scholarly articles: it is a pioneering approach to the world of academia, radically improving the way scholarly research is managed. The grand vision of Frontiers is a world where all people have an equal opportunity to seek, share and generate knowledge. Frontiers provides immediate and permanent online open access to all its publications, but this alone is not enough to realize our grand goals.

Frontiers Journal Series

The Frontiers Journal Series is a multi-tier and interdisciplinary set of open-access, online journals, promising a paradigm shift from the current review, selection and dissemination processes in academic publishing. All Frontiers journals are driven by researchers for researchers; therefore, they constitute a service to the scholarly community. At the same time, the Frontiers Journal Series operates on a revolutionary invention, the tiered publishing system, initially addressing specific communities of scholars, and gradually climbing up to broader public understanding, thus serving the interests of the lay society, too.

Dedication to Quality

Each Frontiers article is a landmark of the highest quality, thanks to genuinely collaborative interactions between authors and review editors, who include some of the world's best academicians. Research must be certified by peers before entering a stream of knowledge that may eventually reach the public - and shape society; therefore, Frontiers only applies the most rigorous and unbiased reviews.
Frontiers revolutionizes research publishing by freely delivering the most outstanding research, evaluated with no bias from both the academic and social point of view. By applying the most advanced information technologies, Frontiers is catapulting scholarly publishing into a new generation.

What are Frontiers Research Topics?

Frontiers Research Topics are very popular trademarks of the Frontiers Journals Series: they are collections of at least ten articles, all centered on a particular subject. With their unique mix of varied contributions from Original Research to Review Articles, Frontiers Research Topics unify the most influential researchers, the latest key findings and historical advances in a hot research area! Find out more on how to host your own Frontiers Research Topic or contribute to one as an author by contacting the Frontiers Editorial Office: frontiersin.org/about/contact

NEURAL ELECTROCEUTICALS: INTERFACING WITH THE NERVOUS SYSTEM WITH ELECTRICAL STIMULATION

Topic Editors:
Giovanni Mirabella, University of Brescia, Italy
Mikhail Lebedev, Skolkovo Institute of Science and Technology, Russia
Alberto Priori, University of Milan, Italy
Julie Duque, Catholic University of Louvain, Belgium
Alexei Ossadtchi, National Research University Higher School of Economics, Russia
Simone Rossi, University of Siena, Italy
Olivier David, Institut National de la Santé et de la Recherche Médicale (INSERM), France

Citation: Mirabella, G., Lebedev, M., Priori, A., Duque, J., Ossadtchi, A., Rossi, S., David, O., eds. (2022). Neural Electroceuticals: Interfacing With the Nervous System With Electrical Stimulation. Lausanne: Frontiers Media SA.
doi: 10.3389/978-2-88976-553-9

Table of Contents

frontiers in Neuroscience

ORIGINAL RESEARCH
published: 27 November 2017
doi: 10.3389/fnins.2017.00659

A Sub-millimeter, Inductively Powered Neural Stimulator

Daniel K. Freeman[1], Jonathan M. O'Brien[1], Parshant Kumar[1], Brian Daniels[1], Reed A. Irion[1], Louis Shraytah[1], Brett K. Ingersoll[1], Andrew P. Magyar[1], Andrew Czarnecki[1], Jesse Wheeler[1], Jonathan R. Coppeta[1], Michael P. Abban[1], Ronald Gatzke[1], Shelley I. Fried[2], Seung Woo Lee[2], Amy E. Duwel[1], Jonathan J. Bernstein[1], Alik S. Widge[3,4], Ana Hernandez-Reynoso[5], Aswini Kanneganti[5], Mario I. Romero-Ortega[5] and Stuart F. Cogan[5]*

[1] Draper, Cambridge, MA, United States, [2] Department of Neurosurgery, Massachusetts General Hospital, Harvard Medical School, Boston, MA, United States, [3] Department of Psychiatry, Massachusetts General Hospital, Harvard Medical School, Charlestown, MA, United States, [4] Picower Institute of Learning and Memory, Massachusetts Institute of Technology, Cambridge, MA, United States, [5] Department of Bioengineering, University of Texas, Richardson, TX, United States

Wireless neural stimulators are being developed to address problems associated with traditional lead-based implants. However, designing wireless stimulators on the sub-millimeter scale (<1 mm^3) is challenging. As device size shrinks, it becomes difficult to deliver sufficient wireless power to operate the device. Here, we present a sub-millimeter, inductively powered neural stimulator consisting only of a coil to receive power, a capacitor to tune the resonant frequency of the receiver, and a diode to rectify the radio-frequency signal to produce neural excitation. By replacing any complex receiver circuitry with a simple rectifier, we have reduced the required voltage levels that are needed to operate the device from 0.5 to 1 V (e.g., for CMOS) to ~0.25–0.5 V. This reduced voltage allows the use of smaller receive antennas for power, resulting in a device volume of 0.3–0.5 mm^3. The device was encapsulated in epoxy, and successfully passed accelerated lifetime tests in 80°C saline for 2 weeks. We demonstrate a basic proof-of-concept using stimulation with tens of microamps of current delivered to the sciatic nerve in rat to produce a motor response.

Keywords: wireless neural stimulation, implantable neurostimulators, electroceuticals, inductive coupling, microcoil

OPEN ACCESS

Edited by:
Olivier David,
Institut National de la Santé et de la Recherche Médicale, France

Reviewed by:
Paulo M. Mendes,
University of Minho, Portugal
Régis Guillemaud,
CEA Leti, France

****Correspondence:***
Daniel K. Freeman
danielkfreeman@gmail.com

Specialty section:
This article was submitted to Neural Technology, a section of the journal Frontiers in Neuroscience

Received: *14 July 2017*
Accepted: *10 November 2017*
Published: *27 November 2017*

Citation:
Freeman DK, O'Brien JM, Kumar P, Daniels B, Irion RA, Shraytah L, Ingersoll BK, Magyar AP, Czarnecki A, Wheeler J, Coppeta JR, Abban MP, Gatzke R, Fried SI, Lee SW, Duwel AE, Bernstein JJ, Widge AS, Hernandez-Reynoso A, Kanneganti A, Romero-Ortega MI and Cogan SF (2017) A Sub-millimeter, Inductively Powered Neural Stimulator. Front. Neurosci. 11:659. doi: 10.3389/fnins.2017.00659

INTRODUCTION

Wireless neural stimulators are being developed to avoid complications associated with traditional lead-based implants (Sahin and Pikov, 2011). These complications include lead-breakage, scar-tissue growth, MRI restrictions, and undesirable tethering during animal studies (Hamani and Temel, 2012; Desai et al., 2015; Ersen et al., 2015). The smallest wireless stimulators developed to date are passive in nature and are powered electromagnetically from outside the body. This includes radio-frequency powered devices, such as non-radiative inductive coupling (Loeb et al., 2001) or mid-field energy transfer (Ho et al., 2014), as well as optically powered devices, such as near-infrared radiation (Abdo et al., 2011). The radio-frequency powered neural stimulators tend to be considerably larger than the optically-powered devices. However, the challenge with optically-powered devices is that light penetrates very poorly through tissue, allowing only superficial nerve targets. As a result, there is a need for radio-frequency powered stimulators that are on the submillimeter scale (<1 mm^3)

to allow for deeper nerve targets. Stimulators on this size-scale would allow the electronics and antenna to be entirely integrated into a nerve cuff for peripheral nerve stimulation, and could enable wireless deep brain stimulation.

The size of a wireless neural stimulator is often limited by wireless energy transfer, which necessitates antennas that are several millimeters in diameter to operate the device. Passive digital CMOS receivers that have been developed for inductively powered medical implants require at least 1 V to be induced in the implanted coil, which requires coils of at least 1 mm in diameter (Cho et al., 2013; Lee and Ghovanloo, 2013). Low-threshold FETs may allow the required voltage levels to be reduced, but at the expense of reliability (e.g., dropped bits). In order to minimize the amount of voltage that is required to operate an inductively powered neural stimulator, we have developed a simple design that consists only of an antenna to receive inductive power, a diode for rectification, and two electrodes on each of the device for current to flow through in order to excite neurons. Previous studies have explored similar concepts of direct rectification of the received signal, but the devices tend to be large (>1 cm on the longest dimension) (Ha et al., 2012; Towe et al., 2012).

Another factor that influences the size of the implant, aside from the antenna, is the packaging. Implants are commonly made using ceramic or titanium containers that are hermetically-sealed to protect the electronics from the body, and vice-versa. These containers tend to be too large, for example, to integrate onto a nerve cuff. Therefore, we chose to pursue a polymer-based encapsulation in order to maintain a compact form-factor.

Our goal was to design and build an inductively powered wireless neural stimulator that is sub-millimeter scale (<1 mm^3) and can deliver sufficient current for excitation of a peripheral nerve. We present an analytical and computational model to help define the limits on antenna size. We report on a working prototype of the wireless neural stimulator (**Figure 1**). While this device offers stimulation only at a single site, as compared to multi-point stimulation devices, we believe the small size can offer a worthwhile tradeoff for certain applications in neural stimulation therapies.

METHODS

In order to define how much voltage and power is required to operate the device, it is first necessary to define (1) the limits of electromagnetic field exposure, (2) the electrical load of the tissue, and (3) how much current is needed to produce neural excitation.

Defining Limits for Exposure to Electromagnetic Fields

In the United States, the safe level of radio-frequency (RF) exposure is defined by the FCC (see IEEE Std. C95.1; IEEE International Committee on Electromagnetic Safety, 2005). The standard metric used to define safe levels of RF exposure is the specific absorption rate (SAR). SAR measures the amount of RF energy that is absorbed in the body and converted to heat and is expressed in W/kg. The SAR limit for an occupational environment, such as a hospital, is defined as 8 W/kg, while the limits for an uncontrolled environment is 1.6 W/kg (Psathas et al., 2014) averaged over 1 g of tissue.

To estimate SAR as a function of the applied time-varying electromagnetic field, full-wave simulations were conducted in ANSYS Electronics Desktop 2016. We used a model that consists of a four-loop transmit coil of 15.2 cm diameter that is positioned 2.5 cm above biological tissue measuring 25.4 × 25.4 × 6 cm (**Figures 2A,B**). Increasing the size of the tissue volume did not impact the results. Current was driven into the coil at a frequency of 10 MHz using a capacitive T-matching network to transform the inductance of the coil into a 50 Ω input impedance. A frequency of 10 MHz was chosen because the ferrite core in our device becomes lossy at frequencies of >10 MHz. In terms of the electrical properties of the tissue, we used conductivity and relative permittivity values of 0.5 S/m and 100, respectively, representing the approximate value of muscle, fat, and skin as measured at 10 MHz (Gabriel et al., 1996; Foster, 2000). Permittivity was taken to be a real-valued number rather than complex in order to represent the case where there is no dielectric loss due to polarization of the tissue.

The transmit power was varied across a range of power levels, as measured in the percentage of total power available from a benchtop power amplifier (Model AG 1021, T&C Power Conversion). The magnetic field intensity was noted at two specific locations: at the center of the transmit coil, and 7.5 cm axially into the tissue (5 cm beneath the surface of the tissue) (**Figure 2C**). The measurement was also taken when no tissue was present (**Figure 2C**, dashed lines), indicating that the presence of the tissue resulted in a minor attenuation of the applied magnetic field. In the animal experiments discussed later, the animal is placed on a non-conductive plastic table. Our simulations showed that this table had negligible impact on the magnetic field intensities present at the wireless stimulator (not shown).

In addition to measuring the magnetic field intensity, we also measured the SAR level averaged over 1 g of tissue (**Figure 2D**), showing that the limit for uncontrolled environments of 1.6 W/kg is reached for a power level of 27%, while the limit for the controlled environment of 8 W/kg was not encountered for the field levels tested here. It is important to note that the location within the model tissue at which the maximum heating occurred is not necessarily the same location as the implanted device. The goal of these simulations was to determine the magnitude of the magnetic and electric fields at the location of the stimulator while the maximum heating itself can occur in any location in the tissue.

Defining the Electrical Load

In order to determine the level of current that is delivered by the device for a given amount of induced voltage in the implanted coil, it is necessary to define the electrical load of the tissue. When current is delivered to neural tissue with an electrode, there are two general sources of impedance: the electrode-electrolyte interface, and the impedance of the tissue itself. The tissue impedance contains both resistive and capacitive elements, but for bulk tissue, the resistive component is much lower impedance than the capacitive component (Reilly, 1992), and therefore the

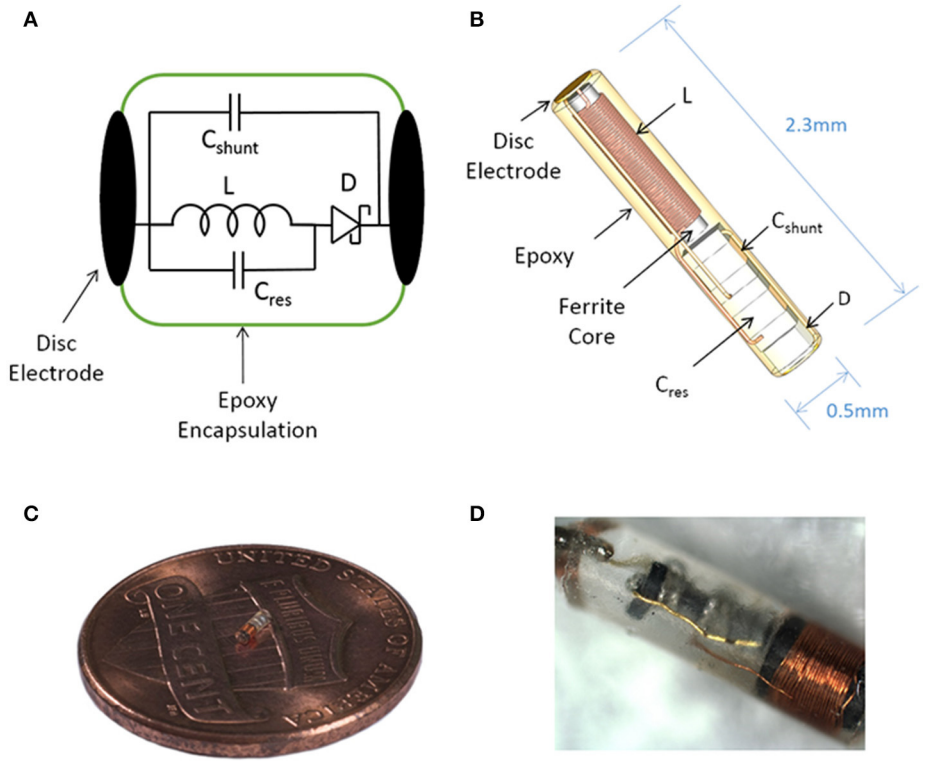

FIGURE 1 | Illustration of the sub-millimeter, wireless stimulator. **(A)** The device consists of a coil (L) to receive inductive power, a capacitor (C_{res}) for resonating the inductor, a Schottky diode (D) for rectification, and a shunt capacitor (C_{shunt}) to facilitate rectification. **(B)** Assembly of the stimulator, with a total volume of 0.45 mm^3. **(C,D)** Images of a built prototype.

tissue is usually considered as a purely resistive medium (Gabriel et al., 1996, 2009; Foster, 2000).

The current is being delivered into the tissue by disc electrodes, and therefore we will approximate tissue resistance with the well-known expression for spreading resistance:

$$R_e = \frac{1}{\sigma d}$$

where d is the diameter of a disc-shaped electrode, σ is the conductivity of the tissue, and R_e is the spreading resistance of a single electrode. Spreading resistance defines the resistance encountered as the current flows from the very conductive metal electrode (e.g., $\sigma_{platinum} \approx 10^7$ S/m) into the moderately conductive tissue. Estimates of tissue conductivity for gray matter vary, but are generally in the range of 0.1–0.3 S/m at low frequencies (<1 kHz) (Gabriel et al., 2009). However, it is not clear that these measurements of bulk tissue conductivity are representative of the micro-environment around a wireless floating stimulator. For example, extracellular fluid has a much higher conductivity (>1 S/m) than bulk tissue. The spreading resistance of a single electrode is plotted over a range of electrode diameters and tissue conductivities (**Figure 3A**). The total tissue resistance (R), is the series combination of the spreading resistance from both electrodes ($R = 2R_e$).

Additionally, the electrode-electrolyte interface will introduce some impedance, which is often described with a parallel combination of double-layer capacitance and a charge-transfer resistance (i.e., Faradaic resistance) (Wei and Grill, 2009). We will assume the voltage levels are too low for electrolysis and therefore we will neglect the Faradaic resistance. The double layer capacitance is ~50 μF/cm^2 for platinum (Geddes, 1997, and unpublished observations). For a disc electrode of diameter 0.4 mm, this corresponds to 65 nF. The impedance of this capacitive interface will depend on the stimulus waveform. If we assume a pulse of 1 ms, then there will be energy out around 1 kHz, and therefore the load of 65 nF will impose 2.4 kΩ. Since we are using roughened platinum with significantly higher capacitance per unit area, the total load will likely be <2.4 kΩ. Taken together, we'll approximate the nominal load resistance to be 10 kΩ, roughly corresponding to two series electrodes of 0.3–0.5 mm with tissue conductivity of 0.5–1 S/m. We will assume the double layer capacitance of the electrodes is negligible when compared to tissue resistance, but it should be noted that this assumption depends heavily on electrode material and on stimulus waveform.

Defining Requirements for Current

The neuronal response to electrical stimulation has been extensively studied (Tehovnkik et al., 2006; Freeman et al., 2011). Typically, electrical stimulation is performed using trains of short-duration pulses on the order of 0.1–1.0 ms, with each pulse consisting of a cathodic phase followed immediately by

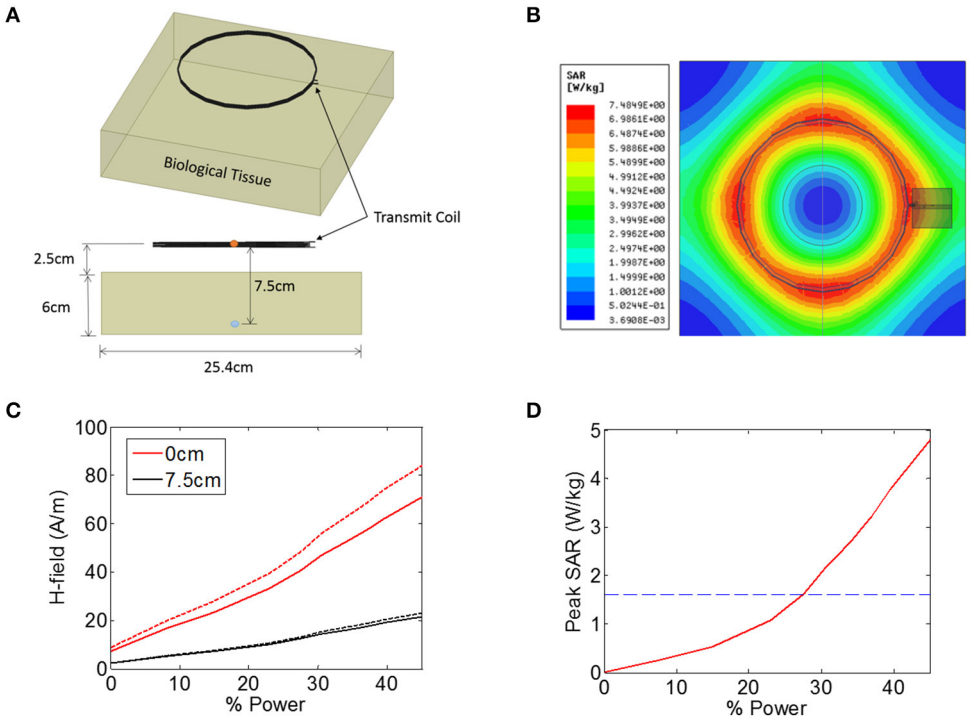

FIGURE 2 | (A,B) Illustration of the finite-element model in ANSYS that was used to estimate the heating of biological tissue in response to an electromagnetic signal from a 15.2 cm diameter coil positioned 2.5 cm from the tissue. The magnetic field intensity was measured in the center the transmit coil (orange circle) and also 7.5 cm from the transmit coil (blue circle). **(C)** Magnetic field (H-field) vs. input power at the center of the transmit coils (0 cm, red solid line), as well as 7.5 cm from the transmitter (black solid line). The measurement was also made when the tissue was not present (dashed lines). **(D)** Peak SAR level simulated across the entire tissue as a function of input power, indicating the maximum allowed SAR level of 1.6 W/kg (blue dashed line).

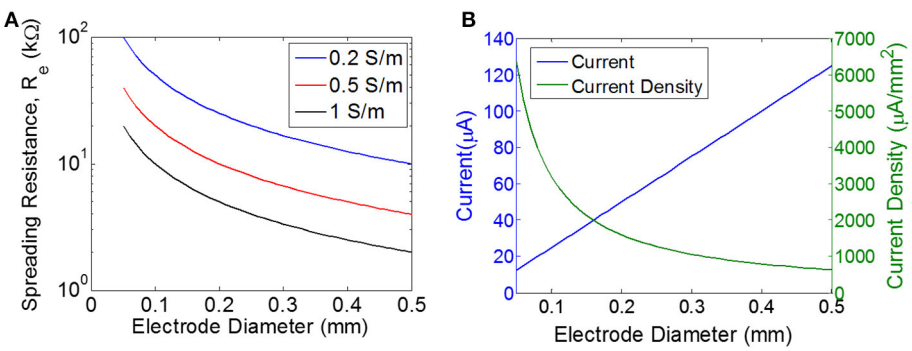

FIGURE 3 | Estimating the load and the required current. **(A)** Spreading resistance of the tissue for a single electrode (R_e) of varying diameter for three different tissue conductivities. **(B)** Current and current density for a single disc electrode of varying diameter, assuming input voltage of 0.5 V for a purely resistive electrode with the load impedance determined purely by the spreading resistance for a tissue conductivity of 0.5 S/m.

an anodic phase (Cogan, 2008). Importantly, our device delivers only monophasic pulses because of the nature of the rectification circuitry. For example, in order to make our device output a pulse of 0.2 ms, the transmitter will emit a short pulse of AC magnetic field for 0.2 ms, and this signal would be received by and rectified by the stimulator, producing a DC output current lasting 0.2 ms. Because of this design, cathodic pulses will always be delivered from one electrode and anodic pulses from the other electrode. Since neurons are more sensitive to cathodic stimulation, we will consider the cathodic electrode to be the primary means of stimulation.

The threshold for excitation of a single neuron is determined by electrode-to-neuron distance and by current density, defined as current per unit area of the electrode surface (Tehovnkik et al., 2006). Unlike neural implants that are driven by a current source, the input to our stimulator is an EMF induced by a time-varying

magnetic field, and therefore the amount of current will depend on the magnitude of the load. The impedance of the load will decrease as the electrodes become larger, which means the total current will increase for larger electrodes. However, the current density will *decrease* as electrodes become larger (**Figure 3B**). Therefore, our choice of electrode size is a trade-off between achieving the highest current density possible, but also aiming for a maximal area of stimulation to excite as many neurons as possible. We chose electrode sizes on the order of 0.3–0.4 mm in diameter as a tradeoff between: (1) smaller electrodes achieve larger current density levels, and (2) larger electrodes will excite a broader area and therefore will recruit more neurons. Because current spreads out as it leaves the electrode, the electrode-to-nerve distance is critical. In our experiments, we do not have precise control over the distance between the electrode and the nerve, but we expect this distance to be on the order of the electrode diameter (<0.3–0.4 mm), and therefore we expect current spreading to have minimal impact on the observed thresholds. Furthermore, this electrode size has been used in similar work to achieve excitation of peripheral nerves in rodent (Romero-Ortega et al., 2015).

Surgical Procedure and Motor Evoked Response Measurements

Four adult Sprague-Dawley rats were used in this study to confirm the ability of the wireless stimulator to elicit action potentials in peripheral nerve axons. The animals were anesthetized with 1.5% isoflurane and the left thigh was shaved and sterilized with 70% ethanol and povidone-iodine. A lateral incision was made in the left hind limb, starting ∼2 cm caudal to the hip bone and in a plane parallel to the femur. The vastus lateralis and biceps femoris muscles were separated exposing the sciatic nerve. The wireless stimulator was placed with the cathode facing the nerve and the anode facing the vastus lateralis muscle. All surgical and experimental procedures were approved by, and conducted in accordance with, the ethical guidelines of the UTA and UTD Institutional Animal Care and Use Committee (IACUC).

The motor response was evaluated by placing the antenna 7.5 cm from the nerve. Video recordings were acquired using Plexon CinePlex Studio V3 and OmniPlex acquisition system at 30 frames/sec. Nerve stimulation was tested using square 250 ms pulses at 2 Hz and at various current levels. The evoked limb movement was tracked using ImageJ to obtain the XY position of the paw in several frames. The Euclidian distance with respect to a baseline was calculated for every frame and plotted with Matlab (Mathworks, Natick, MA).

RESULTS

The wireless neural stimulator (**Figure 1**) consists of a coil (L) to receive inductive power, a tuning capacitor (C_{res}), a diode (D) for rectification, and an optional shunt capacitor (C_{shunt}) to facilitate rectification. This circuit is attached to two disc electrodes to provide stimulation to surrounding tissue. We performed computational analysis of wireless energy transfer through inductive coupling in order to define the number of turns required in the coil.

Computational Model of the Receive Coil

For inductive power transfer, there are analytical expressions that can be used to relate the applied AC magnetic field to the induced voltage in the coil. For coils with a high-permeability core, the induced voltage is typically expressed as a linear function of the relative permeability of the core. For example, a relative permeability of 100 should result in an induced voltage that is increased by a factor of 100. In reality, however, the induced voltage does not scale linearly with permeability, but exhibits complex dependencies on geometry (e.g., length-to-width ratio of the core). To account for these dependencies, we built a computational model of a multi-turn coil with ferrite core using COMSOL (**Figure 4A**). We applied a magnetic field of 40 A/m at 10 MHz to the multi-turn coil and measured the induced voltage (**Figure 4B**). We used a transmit frequency of 10 MHz because the ferrite core becomes lossy above this frequency. We used a field level of 40 A/m because this is the maximum allowed field level that would be seen by a device that is located on the surface of the biological tissue (2.5 cm from the transmitter), at ∼28% input power (**Figure 2C**). This assumes a SAR limit for an uncontrolled environments (1.6 W/kg, see blue dashed line in **Figure 2D**).

The voltage induced in the coil was estimated with and without a 0.2 mm-diameter ferrite core. There was no load present (open circuit) for this simulation and thus no current flowed. This means the coil inductance did not play a role. It is clear that the ferrite will significantly boost the voltage on the coil, although the extent of this increase in voltage depends non-linearly on the number of turns.

Next, we attached a resistive load across the terminals of the coil using the COMSOL-SPICE interface in which the two ends of the coil act as terminals of a load that is input to a SPICE model. In our case, these terminals were attached to a resistive load. Results indicate that the induced voltage is little affected for a load of 10 kΩ (**Figure 4C**). However, for a load resistance of 1 kΩ, the voltage plateaus as the number of turns is increased, as the impedance of the inductor becomes comparable to the load resistance. Despite the fact that the voltage becomes compressed for the 1 kΩ load, the total current is still higher for the 1 kΩ load as compared to the 10 kΩ load (**Figure 4D**). Note that a 1 kΩ load would allow us to reach the required current of 25 μA with very few turns, but unfortunately the tissue load will likely be closer to 10 kΩ than to 1 kΩ (see Methods). A 10 kΩ load would require between 100 and 150 turns to achieve a peak voltage across the load of 250 mV, corresponding to a peak current of 25 μA. This model illustrates how much voltage will be induced for a coil attached to a resistive load. However, we must also account for the impact that the diode and the tuning capacitor will have on the induced voltage.

Incorporating a Diode and Shunt Capacitor

The signals that are used to transmit wireless energy are in the radio frequency regime. These frequencies are too high to excite neurons because the voltage-gated ion channels that underlie

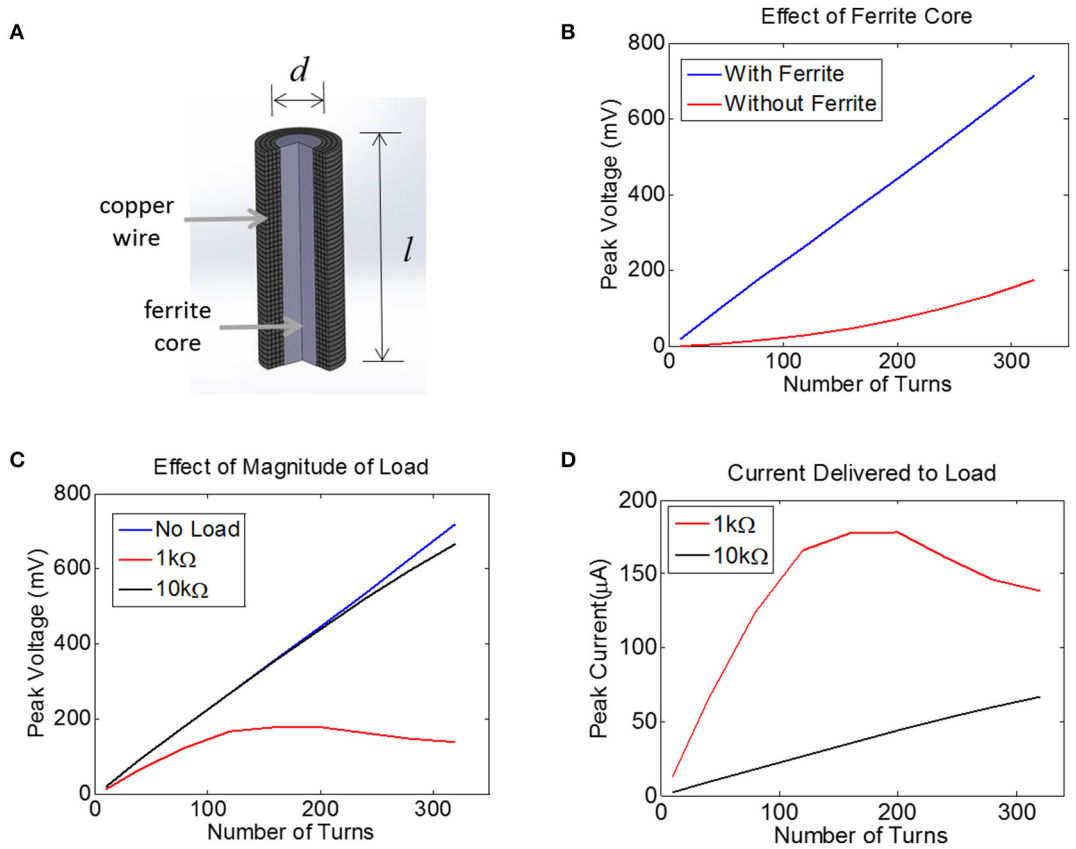

FIGURE 4 | (A) Finite-Element Model of a multi-turn coil with ferrite core used to estimate induced voltage in COMSOL. A cross-section is shown to illustrate winding. **(B)** The peak voltage induced in a coil with $d = 0.2$ mm and $l = 1.0$ mm is plotted as a function of the number of turns, both with a ferrite core (blue) and an air core (red), assuming a 10 MHz transmit frequency with the maximum allowed magnetic field of 40A/m, with 52 AWG copper. **(C)** Assuming a 0.2 mm coil with a ferrite core, the peak voltage is plotted for three different load conditions: no load (open circuit, blue), 1 kΩ (red), and 10 kΩ (black). **(D)** For the data in panel **(C)** the peak current is plotted for two different loads, 1 kΩ and 10 kΩ.

action potentials operate on the 0.1–1.0 ms timescale (1–10 kHz). Therefore, we need some means of converting energy from high-frequency to low-frequency. The simplest technique to do this is to half-wave rectify the signals with a diode, which will produce output current at DC. However, diodes are not perfect rectifiers since there will be some voltage dropped across the diode itself. To maximize the voltage across the load, we require a diode with the lowest possible turn-on voltage.

We tested the ability of a Schottky diode to rectify by first simulating the circuit shown in **Figure 5A** (LTSpice, Linear Technology, Milpitas, CA). A voltage source was used to drive the diode into a 10 kΩ load. An ideal diode was used for the simulations with an additional capacitor (C_{par}) of 0.2pF placed in parallel to the diode to represent parasitic capacitance (see below). The current through the 10 kΩ resistor was measured, containing both AC and DC components. We have plotted the DC component of the current (I_{out}) as a function of sinusoidal input voltage of 1 and 10 MHz (**Figures 5B,C**). Interestingly, we found that more DC current could be achieved when a shunt capacitor (C_{shunt}) was placed in parallel with the resistive load. It is important to note that the role of the capacitor C_{shunt} is not that of a typical smoothing capacitor on a voltage regulator. Rather, this capacitor acts to facilitate rectification by compensating for the parasitic capacitance in the diode; the shunt capacitor was found to have no effect if the diode has zero parasitic capacitance (not shown).

In addition to the simulations, we performed benchtop testing with the test setup shown in **Figure 5A**. We surveyed various types of diodes for this application. Since traditional Schottky diodes do not conduct until around 300 mV, we chose to use a zero-bias Schottky diode that is designed to conduct near zero voltage. The particular diode chosen is designed for RF applications, having a parasitic capacitance of ~0.2 pF (see Methods). These zero-bias diodes have the drawback of having significant reverse leakage current that is not present in standard Schottky diodes. Despite this drawback, we found that the zero-bias diodes were able to rectify the input signal, as shown in the results in **Figures 5D,E**. These data matched well with the simulation results, demonstrating that the inclusion of a shunt capacitor will provide a significant improvement in rectification, at least for 1 MHz.

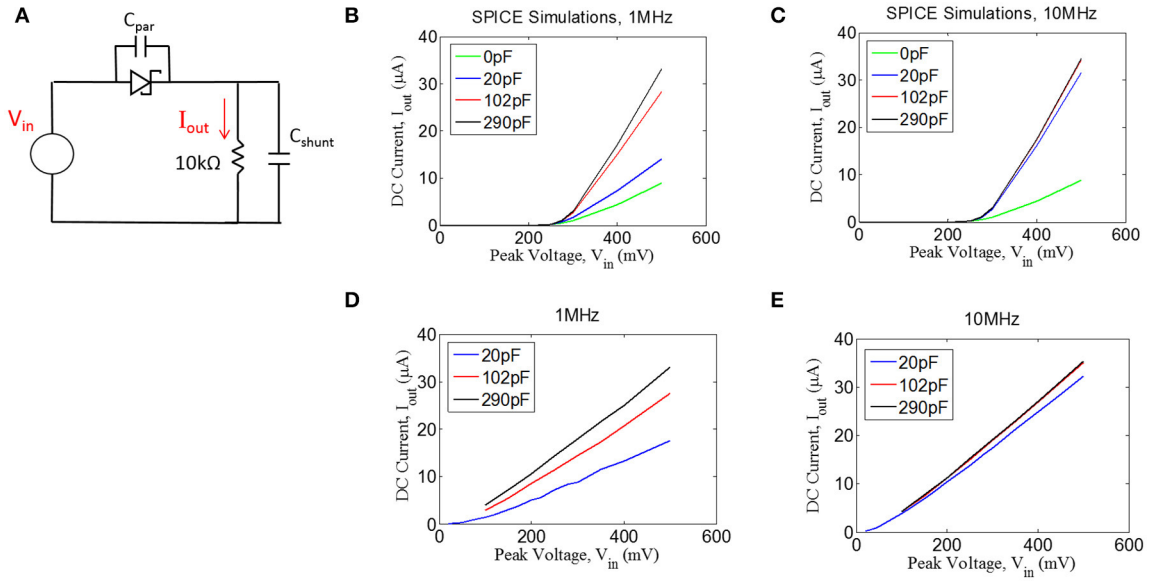

FIGURE 5 | (A) Quantifying rectification by applying an AC signal (V_{in}) and measuring the time-averaged mean of the current, I_{out}, through a resistive load for different values of shunt capacitance (C_{shunt}) for 1 MHz **(B,D)** and 10 MHz **(C,E)**. **(B,C)** Spice simulations showing for the circuit shown in **(A)**, assuming a parasitic capacitance of the diode (C_{par}) of 0.2 pF. **(D,E)** Experimental measurements with an RF Schottky diode.

For the 10 MHz case (**Figure 5E**), it appears as though the impact of the shunt capacitance is minor, but this is primarily because we could not take a measurement for 0 pF of shunt capacitance due to our inability to exclude any parasitic capacitance from the test setup. However, the simulation results at 10 MHz (**Figure 5C**) suggest that some small amount of shunt capacitance (∼10–20 pF) will be necessary to achieve optimal rectification. Future testing will be needed to evaluate whether the tissue itself could produce sufficient capacitance to facilitate rectification, in which case the shunt capacitor could potentially be removed from the design.

Benchtop Testing of Fully Encapsulated Devices

We built a fully encapsulated, functioning device and measured its performance with a series of benchtop tests. The device consisted of a 150-turn coil with 52 AWG wire wrapped around a core of Nickel-Zinc ferrite (#61, Fair-Rite). The coil had an inductance of 31.0 μH, and was tuned to resonate at 10.9 MHz by adding a tuning capacitor of 7.0 pF. The reason for choosing this resonant frequency was that the ferrite becomes significantly lossy for higher frequencies. The device also include an RF Schottky diode and a shunt capacitor of 100 pF. A 10 kΩ resistor was soldered to the platinum disc electrodes during testing to represent the tissue load. The devices were encapsulated in Epoxy (Epo-Tek 301), leaving the disc electrodes exposed. This epoxy was chosen because it has been approved for use by the FDA in medical implants.

A transmitter with diameter of 6″ (15.2 cm) was tuned to 10.9 MHz and the power level was set to 40%. The wireless stimulator was positioned so that the plane of the coil was aligned parallel to the plane of the transmitter. The induced voltage was measured as a function of distance, moving the stimulator along the central axis of the transmitter (**Figure 6A**). As expected, the induced voltage reaches about one-third of its maximum value at a distance equal to half the transmit diameter (compare **Figure 6A** to **Figure 6B**).

The effect of angular rotation of the stimulator with respect to the transmitter showed minor changes in the induced potential up to 60° angle (**Figure 6B**). When the stimulator was positioned 5 cm away from the transmitter and the intensity of the magnetic field was varied, the induced voltage increase monotonically, as expected (**Figure 6C**). The stimulus waveform that is used in the animal studies is also shown (**Figure 6D**), consisting of a train of 1 ms-pulses delivered at 50 Hz. This stimulus was cycled on and off at 2 Hz. These tests show that that the wireless stimulators can produce tens of microamps of current through a 10 kΩ load. Previous studies show that this level of current is sufficient to activate peripheral nerves (Romero-Ortega et al., 2015).

Finally, we performed accelerated lifetime tests to determine whether ingress would occur when the stimulator was exposed to warm saline. Before the tests, the stimulators were confirmed to be functional by performing a diode check between the two disc electrodes with a hand-held multi-meter. Additionally, the device was inspected visually to ensure there were no clear voids within the device. Three stimulators were then placed in 80°C saline for a duration of 2 weeks, and were removed approximately once every 3 days for a diode test. We found that all three devices successfully passed the diode test after 2 weeks, and there was no visible indications of ingress on the devices.

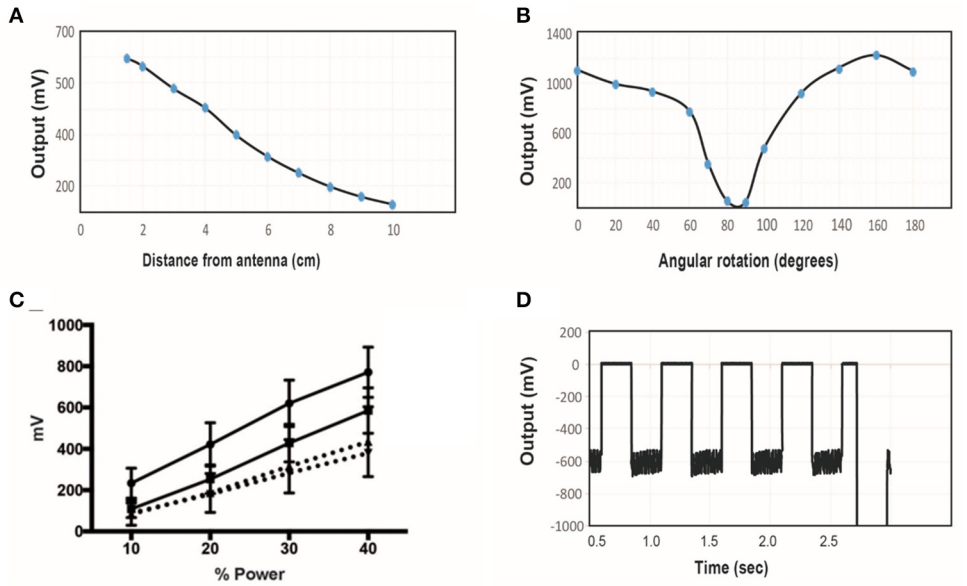

FIGURE 6 | (A) The induced voltage in the electroparticle as a function of distance from the transmitter for an input power of 40%. **(B)** Induced voltage at 0 cm distance measured as a function of rotation angle relative to the plane of the transmitter. **(C)** Electroparticle output as a function of applied magnetic field at a distance of 5 cm for four different devices. **(D)** Induced voltage during square-wave excitation during the waveforms used for motor excitation: a train of 1 ms RF-pulses was delivered at 50 Hz for 250 ms, and this was repeated at 2 Hz. The transmit frequency was 10.9 MHz and the load connected across the two disc electrodes was a 10 kΩ resistor in all cases.

Evoked Nerve Stimulation in the Acute Sciatic Nerve Rat Model

In order to confirm the ability of the wireless stimulator to elicit action potentials in axons, we acutely implanted the stimulator onto the rat sciatic nerve by placing the cathode electrode on the epinerium and the anode to the adjacent muscle (**Figures 7A,B**). The transmitter was positioned 7.5 cm from the stimulator (**Figure 7A**). The power level was set to 45%, corresponding to ∼20–35 A/m of magnetic field at the location of the stimulator (see **Figure 2C**). We do not have control over the precise distance between the electrode and the nerve, but given that the thickness of the epineurium in rat sciatic nerve, we estimate this distance to be on the order of hundreds of microns (Navarro et al., 2005). We evaluated limb movement using a high-speed video camera to observe evoked dorsiflexion of the paw. We found that this power level, stimulation of the sciatic nerve was able to evoke a clearly visible movement of the hindlimb in response to a train of 1 ms-pulses at 50 Hz for 250 ms. **Figure 7C** shows a frame of the paw with a tracing of the evoked movement in one axis. **Figure 7D** illustrates the baseline movement of the limb prior to stimulation (left), as well as the evoked response with the stimulator on (right), which caused >10 mm displacement. If the orientation of the device was flipped so that the anodic electrode was touching the nerve, then no hindlimb movement was observed (not shown).

There was significant variability in the motor responses across trials that was likely due to inconsistent positioning of the stimulator relative to the nerve. This variability was quantified using a single wireless stimulator to stimulate four different nerves, including the left and right nerve of two rodents (**Figure 8**). While two nerves showed very pronounced movements of >10 mm, the other two nerves showed weaker movements around 2–5 mm (**Figure 8**). Despite this variability, it was clear in all cases that increasing the stimulation level caused a greater amount of movement. This variability can be mitigated in future iterations of the design by incorporating the device into a nerve cuff that wraps around the nerve, which will be necessary to hold the device in place for chronic implantation of the device. But for the purposes of this study, these results show clearly that robust neural excitation can be achieved with a sub-millimeter inductively powered stimulator.

Saline Testing of Monophasic Pulsing Strategies

Unlike conventional neural stimulators, the output current of the stimulator presented here is always monophasic and cannot be charge balanced by adding a second phase of opposite polarity. In this circumstance, one electrode in the bipolar pair is polarized only in the negative direction and the other only in the positive direction. After the RF power is turned off at the end of a pulse, each electrode remains polarized and discharges over a time course determined by the tissue resistance and electrode capacitance. If the discharge is not complete before the next pulse, the polarization on the electrodes will build to a steady state value determined by the pulsing parameters. The steady state polarization is determined by the pulse parameters and opposing chemical reactions at the electrodes that act to reestablish the equilibrium potential.

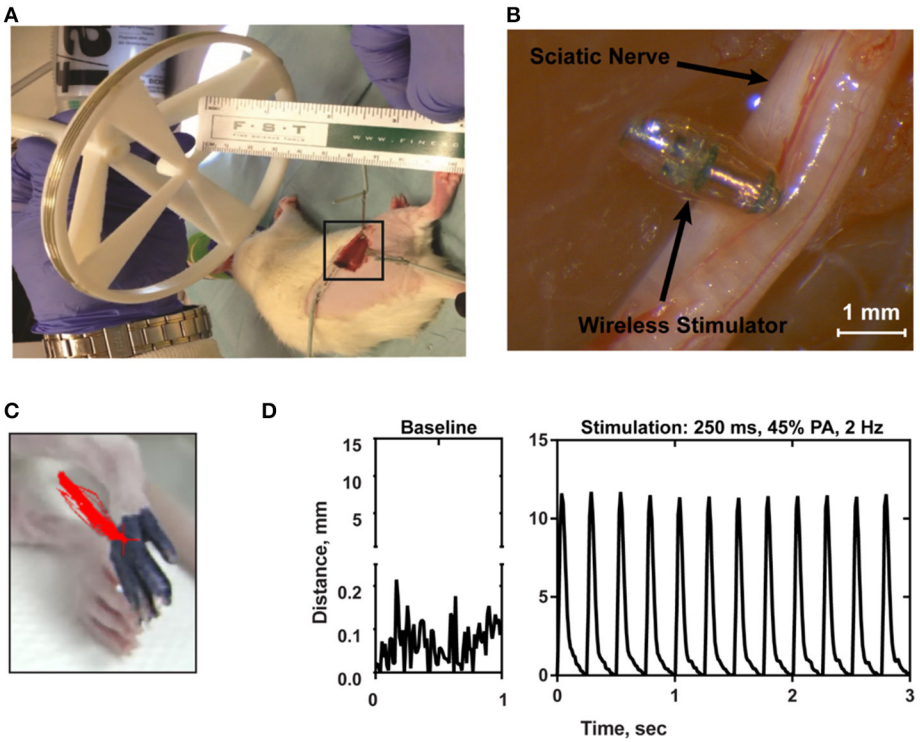

FIGURE 7 | (A) Photograph of the transmitter positioned 7.5 cm from the electroparticle on the hindlimb. **(B)** The electroparticle cathode was placed onto the sciatic nerve, and the power amplifier was set to 45% transmit power. Scale bar = 1.5 mm. **(C)** Videoframe of the rat paw with overlaying traces of the evoked movements (red lines) by stimulation. **(D)** Displacement of the hindlimb by a 2 Hz stimulation shows >10 mm evoked movement.

We conducted preliminary tests in order to quantify the steady state polarization and the ability of the devices to sustain charge injection. The experiment consisted of 400 μm diameter electrodes subjected to isolated monophasic voltage pulses, similar to those that would be generated by RF excitation of the device. Constant voltage rectangular pulses were applied at a pulse rate of 20 Hz and with pulse widths of 200 and 400 μs using a Tektronix AFB2021 arbitrary function generator to switch a custom optical isolator (Sigenics, Chicago IL). The optical isolator switches a DC voltage source on and off according to the waveform provided by the function generator. Current in response to the applied voltage was measured with a low-noise current preamplifier (Stanford Research Systems SR570). During the measurements, the electrodes were in an inorganic model of interstitial fluid (model-ISF) and the polarization of the electrodes measured against a Ag|AgCl reference electrode.

The steady-state current, measured after 300 s of pulsing, sustained at a bipolar pair of platinum electrodes in response to a 400 μs, 0.6 V pulse applied at a pulse frequency of 20 Hz is shown in **Figure 9**. In this data, the voltage is applied between the bipolar pair from 0.3 to 0.7 ms. The slow discharge in the cell voltage can be observed after the applied voltage is turned off. By the next pulse, ∼50 ms, the cell voltage has discharged to about 50 mV. Integration of the current response yielded a steady state charge per phase and charge density of 42 nC/ph and 33 $\mu C/cm^2$, respectively. Similar results were obtained for sputtered iridium oxide (SIROF) and porous TiN electrodes, although the current on these electrodes was more constant over the course of the pulse (not shown). The SIROF had modestly higher charge injection capacity (42 nC/ph, 38 $\mu C/cm^2$) whereas the TiN had a lower capacity (33 nC/ph, 26 $\mu C/cm^2$) than the platinum electrode at steady state.

DISCUSSION

Reducing Antenna Size by Reducing Voltage Requirements

We present here a design for a sub-millimeter, inductively powered, wireless neural stimulator. By removing any transistors, we were able to reduce the voltage levels that must be induced in the implanted coil, and with lower voltage requirements, the size of the coil could be reduced. Another way to describe this rationale is that voltage is, by definition, a form of energy (1 Volt = 1 Joule / Coulomb), and if we operate CMOS off of a supply of 1 V, then this voltage represents a potential energy that is put into the FET and is stored in the p-n junction. Importantly, if we are operating off of wireless power, then this power source must provide a drain-source voltage of 1 V in order to bring the FET out of the triode region and into saturation, and this is true even when zero power is actually being dissipated as heat (e.g.,

for zero gate-source voltage, no power is actually dissipated, even though energy is stored in the p-n junctions). Our device simply removes the requirement to provide this level of drain-source voltage because we don't have any FETs. Because we have relaxed the voltage requirements, we can now make a smaller coil, and this is what enabled the small size of our device.

Clinical and Research Applications for Wireless Neural Stimulators

There are a number of clinical and research applications where this stimulator could be useful. Given the growing interest in the commercialization of peripheral nerve therapies (Famm, 2013), we envision this device being integrated into a nerve cuff. This cuff will wrap around the target nerve and provide electrical stimulation when powered by the external transmitter. For example, treatments for urinary incontinence or chronic migraines could be delivered intermittently by the patient, at home, with a hand-held transmitter. Future testing will be needed to evaluate the extent to which these conditions will respond to intermittent stimulation as opposed to current approach, which often involves continuous stimulation (Noblett and Cadish, 2014). Another factor that must be considered for translation to human peripheral nerves is that when this device is integrated into a nerve cuff, there is the potential that the electrode-to-nerve distance will be larger than in our experiments in which we directly placed the electrode onto the epineurium. This increased distance would increase the threshold necessary for neural excitation. To mitigate this, future designs could involve larger coils in order to provide more current; this will come at the expense of increased device volume.

Therapies involving deep brain stimulation (DBS) could benefit from wireless neural stimulators. For example, totally wireless implants could reduce the level of scar tissue growth that results from tethered leads. However, clinical applications of DBS would be challenging because of the difficulty associated with removing the device in the case of infection. We did not investigate removal strategies in this study. More likely, the device presented here could find applications in animal studies on DBS where tethering the animal is undesirable. This is particularly true for behavioral assays that model aspects of human mental illness using DBS-like stimulation during monitoring of animal behavior (Hamani and Temel, 2012). These experiments often require head-fixation and/or the use of bulky tethers, either of which can limit the full expression of natural behavior, may cue the animal to adopt new behavior patterns, and often limit stimulation to at most a few hours in a special test cage. Human DBS, by contrast, is delivered continuously in a natural environment replete with social interactions and complex decisions. Continuous yet tether-free stimulation could substantially improve the translational relevance of animal models.

Alternative Approaches to Wireless Neural Stimulation

There have been many designs of wireless neural stimulators that are relatively large in size (>1 mm^3) (Okabe et al., 2015; Zargham and Gulak, 2015; Larson and Nurmikko, 2016). The well-known RF BION uses inductive coupling at 2 MHz with a multi-turn coil with ferrite, but is ~10 times larger than our device, measuring 16 mm in length and 2 mm in diameter (Loeb et al., 2001). Another inductively coupled stimulator that was also designed using a simple rectifier included planar coils of 60 mm in diameter, which is considerably larger than the device presented here (Ha et al., 2012). Other stimulators have used higher frequencies for energy transmission, such as a microwave powered stimulator (915 MHz) that measures 10 mm in length and 0.8 mm in diameter (Towe et al., 2012). Another recent design uses so-called mid-field coupling at

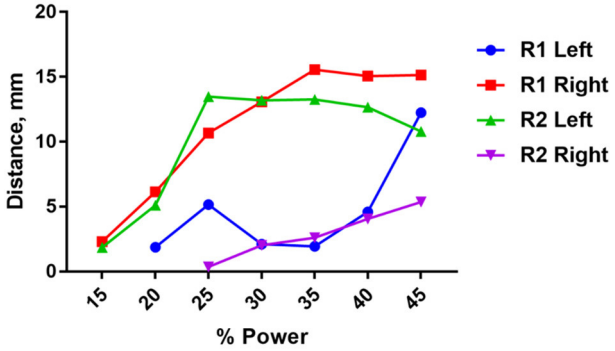

FIGURE 8 | Distance moved by the hindlimb in response to stimulation of the right or left sciatic nerve in two rats (R1 and R2) as a function of input power to the transmit coil. A 10.9 MHz sinusoidal signal was applied to the transmit coil for 1 ms bursts, and these bursts were delivered at 50 Hz for 250 ms. The transmit coil was positioned 7.5 cm from the sciatic nerve.

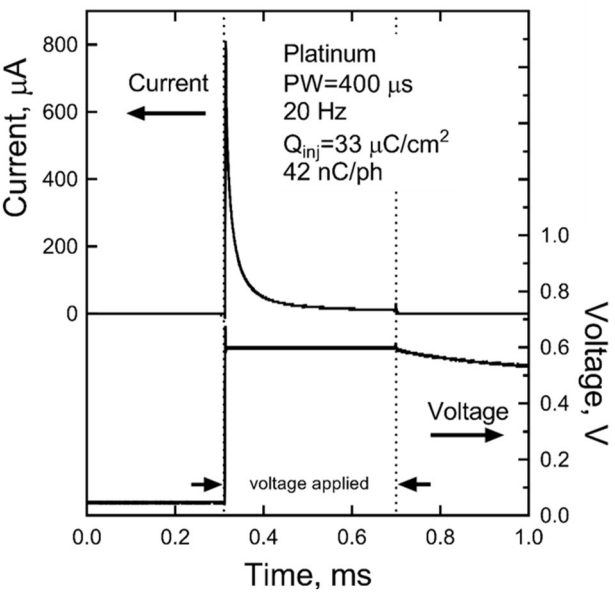

FIGURE 9 | Steady-state current after 300 s of pulsing at 0.6 V and 20 Hz for a platinum bipolar electrode pair. The voltage is applied between 0.3 and 0.7 ms.

1.6 GHz, resulting in a device that is about 5 mm in the longest dimension (Ho et al., 2014). Optically powered stimulators have been developed using photodiodes that are extremely small in scale (<0.01 mm^3), but this approach works only at superficial depths due to the inability of light to penetrate tissue (Abdo et al., 2011; Seymour et al., 2014). This issue with light penetration also presents a challenge for optogenetically modified neurons that can be made sensitive to light (Boyden, 2011).

Nanoparticle-mediated stimulation is an attractive approach if nanoparticles can be delivered through the blood, avoiding the costs and risks of neurosurgery. But even if nanoparticles are designed to be able to cross the blood brain barrier, two challenges remain. First, the inability to control the location of the nanoparticles within the brain will result only in widespread activation (Yue et al., 2012), and therefore may not offer improvements over transcranial magnetic stimulation in terms of the spatial pattern of excitation. Secondly, the amount of nanoparticles needed for excitation can be quite large (Chen et al., 2015), requiring that the nanoparticles are injected directly into the brain rather than through intravenous injection. Another set of studies has attempted to wireless magnetic stimulation with ferritin as a transducer (Stanley et al., 2012; Wheeler et al., 2016), but the interpretation of the results are still under debate (Meister, 2016).

Monophasic Stimulation

Monophasic stimulation without active charge-balance is atypical in neural stimulation. The result is residual polarization of the electrode that slowly discharges during the period between pulses. The limits to monophasic pulsing in terms of deliverable charge and electrode stability are currently being investigated. The preliminary results reported here show that it is possible at steady state (300 s) to sustain modest levels of charge injection (30–40 nC/ph) with 400 μm diameter electrodes. Charge densities increase with decreasing pulse frequency and are higher for shorter periods of pulsing. More detailed characterization of Pt, SIROF, and TiN electrodes under a broad range of monophasic pulsing conditions obtainable with the present wireless stimulation device is ongoing. A significant risk of monopolar stimulation is tissue damage induced by electrode reactions. Measurements of platinum electrode potentials (vs. Ag|AgCl) indicate that the electrodes remain well-within water electrolysis limits during monophasic pulsing with the parameters reported in **Figure 7**. However, histological measures of tissue damage in response to chronic stimulation will be required to assess the safety of wireless monophasic approach.

Risks Associated with the Wireless Stimulator

One of the risks that was not evaluated in this study that tissue encapsulation will increase the tissue impedance enough that the device can no longer deliver therapeutic levels of stimulation. The extent to which tissue encapsulation influence electrode impedance is difficult to predict because there is significant variability in the literature (Ward et al., 2009). Chronic studies with microelectrodes used for recording only, without stimulation, show rapid increases of impedance developing over several weeks after implantation (Prasad and Sanchez, 2012). Other chronic studied have used microelectrodes to stimulate as well as record have found that after an initial period increased electrode impedance, there is a gradual return of impedance to initial values after 12 weeks (Davis et al., 2012).

We can roughly estimate the change in impedance due to scar tissue by taking into account two factors: (1) the expected thickness of the encapsulation layer, which may be on the order of 25 μm (Ersen et al., 2015), and (2) the conductivity of the encapsulation layer, estimated to be ∼0.15–0.3 S/m (Grill and Mortimer, 1994). Taken together, we can estimate the resistance of a 25 μm thick layer of scar tissue on a 300 μm disc electrode with 0.2 S/m conductivity to be 1.8 kΩ. Conversely, with no scar tissue, assuming a conductivity of 0.5 S/m, the same layer of tissue would impose 0.7 kΩ, resulting in an increase of 1.1 kΩ per electrode due to scar tissue. This is a relatively small change in impedance, but these are estimates only that will require animal testing with chronic implants to accurate measure long-term performance.

AUTHOR CONTRIBUTIONS

DF, JO', PK, AD, BD, RI, and JB designed the device. SC, MR-O, AH-R, and AK carried out the experiments. LS and JW carried out computational modeling. MA, AM, JC, and AC fabricated the device. RG, BI, JC, AM, SF, SL, and AW contributed to data analysis.

ACKNOWLEDGMENTS

This work was funded internally at Draper. We would like to acknowledge helpful input from Philip Parks, Chris Yu, Brenan McCarragher, Dale Larson, Carlos Segura, Michael Gary Christiansen, and Ken Gabriel.

REFERENCES

Abdo, A., Sahin, M., Freedman, D. S., Cevik, E., Spuhler, P. S., and Unlu, M. S. (2011). Floating light-activated microelectrical stimulators tested in the rat spinal cord. *J. Neural Eng.* 8:056012. doi: 10.1088/1741-2560/8/5/056012

Boyden, E. S. (2011). A history of optogenetics: the development of tools for controlling brain circuits with light. *F1000 Biol. Rep.* 3:11. doi: 10.3410/B3-11

Chen, R., Romero, G., Christiansen, M. G., Mohr, A., and Anikeeva, P. (2015). Wireless magnetothermal deep brain stimulation. *Science* 347, 1477–1480. doi: 10.1126/science.1261821

Cho, S. H., Xue, N., Cauller, L., Rosellini, W., and Lee, J. B. (2013). A SU-8-Based fully integrated biocompatible inductively powered wireless neurostimulator. *J. Microelectromech. Syst.* 22, 170–176. doi: 10.1109/JMEMS.2012.2221155

Cogan, S. F. (2008). Neural stimulation and recording electrodes. *Annu. Rev. Biomed. Eng.* 10, 275–309. doi: 10.1146/annurev.bioeng.10.061807.160518

Davis, T. S., Parker, R. A., House, P. A., Bagley, E., Wendelken, S., Normann, R. A., et al. (2012). Spatial and temporal characteristics of V1 microstimulation during chronic implantation of a microelectrode array in behaving macaque. *J. Neural Eng.* 9:065003. doi: 10.1088/1741-2560/9/6/065003

Desai, M. J., Hargens, L. M., Breitenfeldt, M. D., Doth, A. H., Ryan, M. R., Gunnarsson, C., et al. (2015). The rate of magnetic resonance imaging in patients with spinal cord stimulation. *Spine* 40, E531–E537. doi: 10.1097/BRS.0000000000000805

Ersen, A., Elkabes, S., Freedman, D. S., and Sahin, M. (2015). Chronic tissue response to untethered microelectrode implants in the rat brain and spinal cord. *J. Neural Eng.* 12:016019. doi: 10.1088/1741-2560/12/1/016019

Famm, K. (2013). A jump-start for electroceuticals. *Nature* 461, 159–161. doi: 10.1038/496159a

Foster, K. R. (2000). "Dielectric properties of tissues," in *The Biomedical Engineering Handbook*, *2nd Edn.,* eds J. D. Bronzino (Boca Raton, FL: CRC Press LLC).

Freeman, D. K., Rizzo, J. F., and Fried, S. I. (2011). Encoding visual information in retinal ganglion cells with prosthetic stimulation. *J. Neural Eng.* 8:035005. doi: 10.1088/1741-2560/8/3/035005

Gabriel, C., Gabriel, S., and Corthout, E. (1996). The dielectric properties of biological tissues: I. Literature survey. *Phys. Med. Biol.* 41, 2231–2249. doi: 10.1088/0031-9155/41/11/001

Gabriel, C., Peyman, A., and Grant, E. H. (2009). Electrical conductivity of tissue at frequencies below 1MHz. *Phys. Med. Biol.* 54, 4863–4878. doi: 10.1088/0031-9155/54/16/002

Geddes, L. A. (1997). Historical evolution of circuit models for the electrode-electrolyte interface. *Ann. Biomed. Eng.* 25, 1–14. doi: 10.1007/BF02738534

Grill, W. M., and Mortimer, J. T. (1994). Electrical properties of implant encapsulation tissue. *Ann. Biomed. Eng.* 22, 23–33. doi: 10.1007/BF02368219

Ha, S., Khraiche, M. L., Silva, G. A., and Cauwenberghs, G. (2012). "Direct inductive stimulation for energy-efficient wireless neural interfaces," *IEEE EMBS Annual International Conference* (San Diego, CA).

Hamani, C., and Temel, Y. (2012). Deep brain stimulation for psychiatric disease: contributions and validity of animal models. *Sci. Transl Med.* 4:142rv8. doi: 10.1126/scitranslmed.3003722

Ho, J. S., Yeh, A. J., Neofytou, E., Kim, S., Tanabe, Y., Patlolla, B., et al. (2014). Wireless power transfer to deep-tissue microimplants. *Proc. Natl. Acad. Sci. U.S.A.* 111, 7974–7979. doi: 10.1073/pnas.1403002111

IEEE International Committee on Electromagnetic Safety (2005). *IEEE Standards for Safety Levels with Respect to Human Exposure to Radio Frequency Electromagnetic Fields, 3kHz to 300GHz, IEEE Std C95.1.*

Larson, L., and Nurmikko, A. (2016). "Microwave communication links for brain interface applications," in *Silicon Monolithic Integrated Circuits in RF Systems (SiRF), 2016 16th Topical Meeting* (Austin, TX), 73–76.

Lee, H. M., and Ghovanloo, M. (2013). A power-efficient wireless capacitor charging system through an inductive link. *IEEE Trans. Circ. Syst.* 60, 707–711. doi: 10.1109/TCSII.2013.2278104

Loeb, G. E., Peck, R. A., Moore, W. H., and Hood, K. (2001). BION system for distributed neural prosthetic interfaces. *Med. Eng. Phys.* 23, 9–18. doi: 10.1016/S1350-4533(01)00011-X

Meister, M. (2016). Physical limits to magnetogenetics. *ELife* 2016:5e17210. doi: 10.7554/eLife.17210

Navarro, X., Krueger, T. B., Lago, N., Micera, S., Stieglitz, T., and Dario, P. (2005). A critical review of interfaces with the peripheral nervous system for the control of neuroprostheses and hybrid bionic systems. *J. Periph. Nerv. Syst.* 10, 229–258. doi: 10.1111/j.1085-9489.2005.10303.x

Noblett, K. L., and Cadish, L. A. (2014). Sacral nerve stimulation for the treatment of refractory voiding and bowel dysfunction. *Am. J. Obstetr. Gynecol.* 2, 99–106. doi: 10.1016/j.ajog.2013.07.025

Okabe, K., Horagodage, P. J., Shota, Y., Takeshi, K., Makoto, I., and Ippei, A. (2015). Co-design method and wafer-level packaging technique of thin-film flexible antenna and silicon CMOS rectifier chips for wireless-powered neural interface systems. *Sensors* 15, 31821–31832. doi: 10.3390/s15229885.

Prasad, A., and Sanchez, J. C. (2012). Quantifying long-term microelectrode array functionality using chronic *in vivo* impedance testing. *J. Neural Eng.* 9:026028. doi: 10.1088/1741-2560/9/2/026028

Psathas, K. A., Kiourti, A., and Nikita, K. S. (2014). "Safety issues in biomedical telemetry," *Handbook of Biomedical Telemetry* (Hoboken, NJ: John Wiley & Sons, Inc.).

Reilly, J. P. (1992). *Applied Bioelectricity: from Electrical Stimulation to Electropathology*. New York, NY: Springer-Verlag.

Romero-Ortega, M., Kanneganti, A., Bendale, G., Seifert, J., Bredeson, S., Troyk, P., et al. (2015)." Chronic and low charge injection wireless intraneural stimulation *in-vivo*," in *2015 37th Annual International Conference of the IEEE Engineering in Medicine and Biology Society (EMBC)* (Milan).

Sahin, M., and Pikov, V. (2011). Wireless microstimulators for neural prosthetics. *Crit. Rev. Biomed. Eng.* 39, 149–164. doi: 10.1615/CritRevBiomedEng.v39.i1.50

Seymour, E. C., Freedman, D. S., Glkkavas, M., Ozbay, E., Sahin, M., and Unlu, M. S. (2014). Improved selectivity from a wavelength addressable device for wireless stimulation of neural tissue. *Front. Neuroeng.* 7:5. doi: 10.3389/fneng.2014.00005

Stanley, S. A., Gagner, J. E., Damanpour, S., Yoshida, M., Dordick, J. S., and Friedman, J. M. (2012). Radio-wave heating of iron oxide nanoparticles can regulate plasma glucose in mice. *Science* 336, 604–608. doi: 10.1126/science.1216753

Tehovnkik, E. J., Tolias, A. S., Sultan, F., Slocum, W. M., and Logothetis, N. K. (2006). Direct and indirect activation of cortical neurons by electrical microstimulation. *J. Neurophysiol.* 96, 512–521. doi: 10.1152/jn.00126.2006

Towe, B. C., Larson, P. J., and Gulick, D. W. (2012). "A microwave powered injectable neural stimulator," *IEEE EMBS Annual International Conference* (San Diego, CA).

Ward, M. P., Rajdev, P., Ellison, C., and Irazoqui, P. P. (2009). Toward a comparison of microelectrodes for acute and chronic recordings. *Brain Res.* 1282, 183–200. doi: 10.1016/j.brainres.2009.05.052

Wei, X. F., and Grill, W. M. (2009). Impedance characteristics of deep brain stimulation electrodes *in vitro* and *in vivo*. *J. Neural Eng.* 6:046008. doi: 10.1088/1741-2560/6/4/046008

Wheeler, M. A., Smith, C. J., Ottolini, M., Barker, B. S., Purohit, A. M., Grippo, R. M., et al. (2016). Genetically targeted magnetic control of the nervous system. *Nat. Neurosci.* 19, 756–761. doi: 10.1038/nn.4265

Yue, K., Guduru, R., Hong, J., Liang, P., Nair, M., and Khizroev, S. (2012). Magneto-electric nanoparticles for non-invasive brain stimulation. *PLoS ONE* 7:44040. doi: 10.1371/journal.pone.0044040

Zargham, M., and Gulak, P. G. (2015). Fully integrated on-chip coil in 0.13 μm CMOS for wireless power transfer through biological media. *IEEE Trans. Biomed. Circuits Syst.* 9, 259–271. doi: 10.1109/TBCAS.2014.2328318

Conflict of Interest Statement: The authors declare that the research was conducted in the absence of any commercial or financial relationships that could be construed as a potential conflict of interest.

frontiers in Neuroscience

ORIGINAL RESEARCH
published: 07 December 2017
doi: 10.3389/fnins.2017.00691

Anodal Transcranial Direct Current Stimulation Increases Bilateral Directed Brain Connectivity during Motor-Imagery Based Brain-Computer Interface Control

*Bryan S. Baxter[1], Bradley J. Edelman[1], Abbas Sohrabpour[1] and Bin He[1,2]**

[1] *Department of Biomedical Engineering, University of Minnesota, Minneapolis, MN, United States,* [2] *Institute for Engineering in Medicine, University of Minnesota, Minneapolis, MN, United States*

Transcranial direct current stimulation (tDCS) has been shown to affect motor and cognitive task performance and learning when applied to brain areas involved in the task. Targeted stimulation has also been found to alter connectivity within the stimulated hemisphere during rest. However, the connectivity effect of the interaction of endogenous task specific activity and targeted stimulation is unclear. This study examined the aftereffects of concurrent anodal high-definition tDCS over the left sensorimotor cortex with motor network connectivity during a one-dimensional EEG based sensorimotor rhythm brain-computer interface (SMR-BCI) task. Directed connectivity following anodal tDCS illustrates altered connections bilaterally between frontal and parietal regions, and these alterations occur in a task specific manner; connections between similar cortical regions are altered differentially during left and right imagination trials. During right-hand imagination following anodal tDCS, there was an increase in outflow from the left premotor cortex (PMC) to multiple regions bilaterally in the motor network and increased inflow to the stimulated sensorimotor cortex from the ipsilateral PMC and contralateral sensorimotor cortex. During left-hand imagination following anodal tDCS, there was increased outflow from the stimulated sensorimotor cortex to regions across the motor network. Significant correlations between connectivity and the behavioral measures of total correct trials and time-to-hit (TTH) correct trials were also found, specifically that the input to the left PMC correlated with decreased right hand imagination performance and that flow from the ipsilateral posterior parietal cortex (PPC) to midline sensorimotor cortex correlated with improved performance for both right and left hand imagination. These results indicate that tDCS interacts with task-specific endogenous activity to alter directed connectivity during SMR-BCI. In order to predict and maximize the targeted effect of tDCS, the interaction of stimulation with the dynamics of endogenous activity needs to be examined comprehensively and understood.

Keywords: brain-computer interface, transcranial direct current stimulation, connectivity, BCI, tDCS

OPEN ACCESS

Edited by:
Alberto Priori,
Università degli Studi di Milano, Italy

Reviewed by:
Makii Muthalib,
Université de Montpellier, France
Danny J. J. Wang,
University of Southern California, United States

***Correspondence:**
Bin He
binhe@umn.edu

Specialty section:
This article was submitted to Neural Technology, a section of the journal Frontiers in Neuroscience

Received: *08 July 2017*
Accepted: *23 November 2017*
Published: *07 December 2017*

Citation:
Baxter BS, Edelman BJ, Sohrabpour A and He B (2017) Anodal Transcranial Direct Current Stimulation Increases Bilateral Directed Brain Connectivity during Motor-Imagery Based Brain-Computer Interface Control. Front. Neurosci. 11:691. doi: 10.3389/fnins.2017.00691

INTRODUCTION

Transcranial Direct Current Stimulation

Transcranial direct current stimulation (tDCS) of the human brain has been increasingly investigated with the resurgence of research into the effects of noninvasive electrical brain stimulation in the early 2000s (Nitsche and Paulus, 2000; Johnson et al., 2013; Paulus and Opitz, 2013; Bestmann et al., 2015). tDCS consists of injecting a low level of current (generally <2 mA) into the head of a subject through multiple electrodes located on the scalp or extracephalically. Modeling studies using both standard two-electrode and multi-electrode configurations have found that current reaches the cortex, and depending on electrode configuration, deeper brain structures, with levels that have been shown *in vitro* to affect the potential of spontaneous neuronal firing (Bikson et al., 2004; Sadleir et al., 2010; Kabakov et al., 2012; Kuo et al., 2013; Opitz et al., 2016). These neuronal effects most likely stem from a variety of sources including membrane depolarization and hyperpolarization of the dendrites and axons of pyramidal cells as well as secondary effects on membrane resistance (Stagg and Nitsche, 2011; Paulus and Rothwell, 2016). Behaviorally, the effects of tDCS on the motor system have been found to affect motor performance and learning when the motor network is stimulated (Reis et al., 2009; Reis and Fritsch, 2011; Buch et al., 2017). A variety of electrophysiological, hemodynamic, and spectroscopic methods have been used to investigate alterations of neural activity from tDCS including increases in the BOLD signal and alterations in excitatory and inhibitory neurotransmitter balance (Jang et al., 2009; Stagg et al., 2009; Antal et al., 2011; Zaehle et al., 2011; Jog et al., 2016; Muthalib et al., 2017). The *in vivo* effects of tDCS on endogenous resting and task specific brain oscillations is less well-understood, and has only recently begun to be investigated with EEG, MEG, and invasive recordings (Soekadar et al., 2013, 2014; Notturno et al., 2014; Roy et al., 2014; Bergmann et al., 2016; Opitz et al., 2016; Krause et al., 2017).

An emerging hypothesis relating the effect of noninvasive neuromodulation to brain activity utilizes a long-term potentiation rationale for targeting brain areas that are specifically active during a task or rest (Bikson and Rahman, 2013). Fox et al. examined the effects of transcranial magnetic stimulation (TMS) targeting and found specifically that if the areas targeted overlapped with correlated or anti-correlated resting state networks, as determined by fMRI, there was an effect on neurological symptoms in patients (Fox et al., 2014). Further work using a similar approach for targeting resting state activity in the motor network with tDCS found an increase in excitability with anodal stimulation of correlated areas as compared to anodal-cathodal stimulation of anti-correlated areas (Fisher et al., 2017). Concurrent stimulation of involved areas during motor performance and learning has specifically led to improvements in performance compared to stimulation prior to, or after, task performance (Buch et al., 2017). Our group recently found a decrease in time to hit and an increase in EEG alpha and beta band power following simultaneous tDCS over the sensorimotor cortex during motor imagery based EEG brain-computer interface (BCI) performance (Baxter et al., 2016).

The Motor System and Noninvasive Brain-Computer Interfaces

The development of noninvasive BCI has allowed individuals with motor dysfunctions to control computers and devices in the lab (Wolpaw et al., 1991; Mak and Wolpaw, 2009; Millán et al., 2010; He et al., 2013, 2015; Scherer and Pfurtscheller, 2013; Yuan and He, 2014) and in the home (Sellers et al., 2009) in real-time using self-modulated brain rhythms or external stimuli. A predominant paradigm for continuous control of an output device is using motor imagination (MI) with sensorimotor rhythm modulation. In order to voluntarily modulate their sensorimotor rhythms, subjects kinesthetically imagine moving a body part without executing the movement. This imagination engages similar networks to motor execution (ME) and generates an event related desynchronization in alpha (8–13 Hz) or beta (15–30 Hz) frequencies, corresponding to a local decrease in power (Pfurtscheller and Lopes da Silva, 1999; Lotze and Halsband, 2006), in the sensorimotor cortical areas responsible for controlling the body part. An event-related synchronization also may occur in contralateral sensorimotor regions. A recent meta-analysis of fMRI studies found premotor (PMC) and somatosensory (S1) regions predominantly active during MI as well as more distributed areas in the frontal and parietal cortices, including the inferior frontal gyrus, supplementary motor area (SMA), primary motor cortex (M1), and superior parietal cortex (PC) (Hétu et al., 2013). While fMRI yields precise localization of an indirect measure of neuronal activity, the temporal resolution is on the order of seconds which does not allow an examination of most oscillatory dynamics.

Regions of the motor network are thought to be responsible for similar tasks during both ME and MI, though there are some known differences in network activity between these two cognitive actions. The PMC is involved in both execution and imagination though different sub-domains are active in each. The PMC is left hemisphere lateralized and is used for motor planning and selection, including selecting the hand to perform a unimanual task (Rushworth et al., 2003). The dorsal PMC also bilaterally increases in activation for contralateral hand execution. For MI, the dorsal and ventral PMC are specifically active (Lotze and Halsband, 2006). The pre- and post-SMA is involved in motor movement preparation, initiation, and execution (Lotze and Halsband, 2006). For MI, the posterior regions of the SMA are specifically active. The sensorimotor cortex (SMC) is involved in both ME and kinesthetic imagination but the degree of activation may depend on the complexity of the imagery movement (Lotze and Halsband, 2006). The contralateral primary motor cortex is active during ME with the contralateral S1 cortex activated with sensory feedback, such as the feeling of pressure on the hand when closing your fingers into a fist. In addition to this activation, there is inhibition from the activated hemisphere to motor cortex ipsilateral to the executed hand movement. The PC, and specifically the PPC is involved in motor preparation and attention as well as visual motor

transformation and performing visuo-motor tasks (Andersen and Buneo, 2002; Rushworth et al., 2003). During motor imagery, orienting visual attention with or without arm movements leads to BOLD increase in differing areas of the PC; these areas may be somewhat lateralized to the left hemisphere (Rushworth et al., 2001). During BCI performance, subjects likely direct visual attention and eye movement to the target and to the cursor during the feedback phase, though this may not be the case when subjects are solely performing MI. In addition to these cortical areas, the cerebellum and subcortical regions are also involved in both ME and MI (Lotze et al., 1999; Lotze and Halsband, 2006).

Source Imaging and BCIs

The temporal resolution of EEG is on the order of milliseconds but standard analysis of EEG data on the sensor level does not allow for high spatial resolution. Source imaging, which involves solving the inverse problem of mapping EEG sensor activity to the brain using Maxwell's equations and the physical properties of head tissues, has been developed over the last few decades (He et al., 1987, 2011b; Hämäläinen and Sarvas, 1989). Based on the specific algorithm for performing this transformation, modeling and event-related potential studies have found localization errors of 7 mm or less (Michel et al., 2004; Im et al., 2007). Source imaging analysis of MI both without and with feedback has been demonstrated to have higher signal-to-noise ratio than sensor data, which can lead to improved MI classification (Qin et al., 2004; Kamousi et al., 2005, 2007; Cincotti et al., 2008; Yuan et al., 2008; Edelman et al., 2016). While source based analysis allows us to examine how brain areas are active over time, more explicit analysis of the interaction of different brain areas are needed to functionally understand how information flows within the network.

Connectivity

There are multiple families of methods that have been used to examine undirected and directed connectivity during cognitive tasks following tDCS using both direct electrophysiological and indirect hemodynamic measurements (Meinzer et al., 2012; Luft et al., 2014). The two activity based classes of connectivity are directed connectivity and functional connectivity; the former is measured via causal directional relationships between two time series, while the latter is measured as a correlation or anti-correlation between two time series (Kaminski and Blinowska, 1991; Baccalá and Sameshima, 2001; Babiloni et al., 2005; Astolfi et al., 2007; He et al., 2011a; Friston et al., 2013).

Connectivity in the Motor System

The connectivity of networks underlying ME and MI has been studied extensively. The unilateral left and right hand ME and motor imagery networks have been compared by applying directed connectivity to fMRI data (Gao et al., 2011). Gao and colleagues reported stronger connectivity amongst the motor network in ME than MI. They found significant intrahemispheric connections within the contralateral hemisphere and between the contralateral and ipsilateral PMC and PPC. Anwar and colleagues used multimodal imaging to examine effective and functional connectivity across the motor network during right-hand finger movement task performance while recording with multiple modalities including fMRI, fNIRS, sensor-based EEG, and source-based EEG and found bidirectional connections between the right dorsolateral prefrontal cortex (DLPFC), right PMC and right SMC (Anwar et al., 2016). Importantly, they found source-based EEG analysis to have the greatest unidirectional flow from SMC to PMC, SMC to DLPFC, and PMC to DLPFC. Other studies have found that PPC is connected to the posterior SMA and PMC (Rizzolatti et al., 1998; Lotze and Halsband, 2006; Davare et al., 2010). Frequency specific connectivity during MI have also been evaluated, though these analyses have generally been confined to the SMC (Kuś et al., 2006; Hamedi et al., 2016). These works examined time and frequency based measures such as Granger causality and coherence metrics and found connections both unilaterally and bilaterally between the SMC and frontal areas during MI. Specific to the BCI context, Billinger and colleagues investigated single trial offline task classification using sensor and source based connectivity measures and found no improvement over power and frequency based features for either sensor or source based analysis (Billinger et al., 2013).

The functionality of these connections has also been investigated through a variety of modalities. The PMC is directly connected to the primary motor cortex; using TMS, the PMC has been found to influence the primary motor cortex during ME depending on parameters of the task, including force delivered and precision of movements, and that this connection is inhibitory during rest (Grafton, 2010; Davare et al., 2011). Connections from the SMA to SMC and PMC inhibit movement execution during MI (Kasess et al., 2008). The function of interhemispheric connections across the corpus callosum between bilateral regions, either inhibitory, excitatory, or both, is an ongoing debate in literature (van der Knaap and van der Ham, 2011).

Connectivity and tDCS

Connectivity analysis using EEG following transcranial current stimulation was initially performed by Polania et al. who found that after the application of anodal tDCS during rest there was an increase in undirected intrahemispheric connectivity in the alpha, beta and high gamma frequencies near the stimulating electrode, and decreased interhemispheric connectivity in the alpha and beta bands, both during motor task performance (Polanía et al., 2011). Further studies examining effects on the motor network also found brain state dependent effects following stimulation. Feurra and colleagues found an increase in TMS MEP amplitude during MI following resting state anodal tDCS of the right PC, whereas this effect was not present during motor action observation (Feurra et al., 2011). Notturno and colleagues examined EEG functional connectivity using coherence and found no difference between anodal and sham stimulation of the motor cortex during motor movement, but altered coherence during rest (Notturno et al., 2014). Polania et al. also examined cortical-subcortical connections with fMRI and found increased functional connectivity between the left primary motor cortex (M1) and the ipsilateral thalamus and caudate nucleus following anodal stimulation (Polanía et al., 2012). Sehm et al. found

functional connectivity effects on the resting state network during and after anodal stimulation of unilateral and bilateral primary S1 (Sehm et al., 2012). Holland et al. examined effective connectivity during a visual object naming task within the left frontal cortex using DCM on concurrent tDCS-fMRI of the inferior frontal cortex. They found a stronger negative backward connection from inferior frontal sulcus to ventral PMC during anodal stimulation compared to sham indicating stronger inhibition from IFS to vPMC, and behaviorally found improved reaction time. Further work examining both task specific (Meinzer et al., 2012) and resting state has shown similar effects due to anodal stimulation (Keeser et al., 2011; Peña-Gómez et al., 2012; Amadi et al., 2014). Combined, these results suggest anodal stimulation increases connectivity near the stimulation electrode as well as to more distant sites intra- and interhemispherically, though the specific effects and regions affected are dependent on the task being performed, the networks involved in the task, and the regions connected to the stimulated area.

Motivation

Sensorimotor rhythm-based BCI is a useful experimental technology to evaluate the interaction of stimulation and endogenous event-related oscillations as unilateral hand imaginations yield different bilateral signals generated by the sensorimotor cortex. Previously we reported changes in performance and localized alpha and beta band power following anodal stimulation (Baxter et al., 2016). The aims of this study were two-fold: (1) to determine connectivity changes during sensorimotor rhythm-based BCI control following simultaneous anodal high-definition (HD)-tDCS of the sensorimotor cortex, and (2) to examine correlations between behavioral metrics and connectivity patterns within the motor imagery network. We utilize HD-tDCS as, based on theory and simulation studies, the current is confined to a smaller region of the brain compared to conventional tDCS, allowing for more precise localization of the effect of stimulation (Dmochowski et al., 2011; Kuo et al., 2013). This improved localization allows us to better understand the effect of local stimulation on both nearby and remote areas, as well as the interconnections of these areas.

We analyzed data recorded during sensorimotor rhythm BCI performance while subjects controlled a moving cursor on the screen prior to and following anodal stimulation of the left sensorimotor cortex. We used a data-driven approach to determine regions-of-interest during BCI control across the cortex, calculated the connectivity between these regions, and determined the changes that resulted from the tDCS. We found alterations in the connectivity of the network based on the laterality of the hand imagination, with a greater number of changes in connectivity during right hand imagination. In addition, we examined the relationship between performance and connectivity measures and found both significant positive and negative correlations between specific connections and performance measures. By combining analyses of connectivity changes after stimulation and the correlations of connectivity values with performance, we aim to inform the functional targeting of networks of interest to maximize stimulation effects and develop multifocal closed loop-noninvasive stimulation on a subject specific level.

MATERIALS AND METHODS

Experimental Setup

Twelve right-handed healthy subjects (8 female) naive to motor imagery (MI) BCI control participated in these experiments (Age: 19–39 years; Mean: 23.58 years; SD: 4.97 years). Subjects were randomly assigned to either Anode or Sham stimulation groups. Included subjects had >62.5% mean accuracy and were considered to have competent control of the BCI (Anode: 72 ± 2% and Sham: 69 ± 2%; mean ± standard error). All procedures and protocols were approved by the University of Minnesota Institutional Review Board.

A 64-channel Biosemi EEG cap with active electrodes and an ActiveTwo amplifier were used to record the EEG signal at 1024 Hz (BioSemi, Amsterdam, Netherlands). A tDCS device with a high-definition (4 × 1) tDCS adapter was used in a Laplacian configuration to deliver 2 mA of current to the center electrode with four return electrodes (Soterix Medical, NY, USA). Conductive gel (Signa Gel, Cortech Solutions) was applied to reduce electrode offsets to below 30 mV for EEG electrodes and impedances under 1 kΩ for tDCS electrodes. The EEG cap was adapted to fit HD-tDCS electrodes adjacent to EEG electrodes arranged according to the international 10/20 system. The center electrode (anode) was placed between C3/CP3 and surround electrodes (cathodes) were placed between CP3/P3, C1/FC1, C5/FC5, and C3/FC3 at a radius of 3.5 cm from the center electrode. For the Anodal group, stimulation consisted of 20 min of 2 mA stimulation with a 30 s ramp up at the start of stimulation and a 30 s ramp down at the end. For the Sham group, for stimulation, the tDCS device ramped up and down over approximately 45 s at the beginning and end of the 20 min.

Subjects were seated in a chair 90 cm from an LCD monitor where experimental stimuli were displayed. Subjects were instructed to remain still during the experimental trials. BCI2000 software was used to present experimental stimuli and record EEG data. Subjects were instructed to kinesthetically imagine opening and closing their respective hand unilaterally based on the target location. The trial structure consisted of a baseline rest period (3 s), planning phase (3 s), and online performance (6 s maximum). Subjects performed 72 trials of the left/right BCI task before stimulation (Prestim); the first 18 trials were removed as at the start of each session the normalizer, embedded in the software, needed to adjust for the subject and session. Following this, the tDCS system was turned on and stimulation was started. During stimulation, subjects performed 90–108 trials depending on individual resting time between runs. The tDCS device was then turned off and the subject immediately performed 72 trials ($Post_0$), followed by a visual oddball task for 13 min to engage the subject in a controlled task, while allowing a rest from the BCI task. Finally, subjects performed 72 trials during the delayed time period from approximately 25 to 37 min post stimulation ($Post_{25}$). Subjects participated in three sessions with the time between sessions at least 48 h.

The control system used the autoregressive filter implemented in BCI2000 (Schalk et al., 2004) to estimate the 11–13 Hz power at the C3/C4 electrodes before and after stimulation to control the cursor during the BCI task. During stimulation, C3 was usually affected by stimulation artifacts and was removed on a session by session basis; in these circumstances a surrounding electrode that was not affected by stimulation artifacts was used instead (see **Figure 2** for example EEG traces of control electrodes). The control signal was calculated based on a linear classifier with inputs composed of the positively weighted power in C4 and the negatively weighted power in C3. A normalizer was used with the classifier to reduce any directional bias in the cursor movement due to a subject's difference in relative power between C3 and C4. After each trial, the normalizer removed the offset by subtracting the mean and scaling the classifier output to unit variance based on the weighted sum of C3 and C4 during the online period of the preceding 30 s. For further details see (Baxter et al., 2016).

Behavioral Measures

The time-to-hit (TTH) behavioral metric is the time from the beginning of the feedback period of a trial to the time the cursor hits the target; subjects had a maximum of 6 s to hit the target. The total correct behavioral metric is the total number of correct trials in each block. Both metrics were divided into right and left hand trials due to previous results suggesting there are directional effects of stimulation (Baxter et al., 2016).

Signal Processing

Raw data was high pass filtered within hardware at 1 Hz and notch filtered at 60 Hz. Offline processing was performed using custom scripts utilizing the EEGLAB toolbox (Delorme and Makeig, 2004) in Matlab (The Mathworks, Inc., MA, USA). Data was low pass filtered at 110 Hz and the mean of each channel was removed. Electrodes were referenced to the common average and downsampled to 250 Hz. Independent Component Analysis (fast-ICA) (Hyvarinen, 1999) was run on concatenated data from all non-stimulation blocks for each session. Components corresponding to eye movement, eye blink, and muscle artifact were removed (Jung et al., 2000). We visually examined the EEG time course data and removed electrodes that displayed a drift from their mean over time and spherically interpolated their activity (Delorme and Makeig, 2004); these were primarily prefrontal or temporal electrodes. Those trials that were contaminated with artifacts during baseline or task performance, respectively, not removed by ICA were discarded. Following removal and interpolation of bad channels, and removal of trials with significant artifactual activity, channels were rereferened to the common average and channel means were removed.

For the mean baseline values used to characterize the noise for source imaging, we included all clean trials remaining after artifact rejection and preprocessing. The 1 s prior to the appearance of the target, during the inter-trial interval, was used as the baseline. For analysis, we removed the first 500 ms of the trial, as there was frequently an ERP artifact due to the cursor appearance, as well as the final 250 ms of the trial, as there was frequently an additional artifact. The data within the 500 ms time window that contained the largest power difference was then used for the analysis of the online data. The time courses were detrended and standardized prior to model fitting and further analysis.

Source Analysis

The BEM forward model was calculated using OPENMEEG (Gramfort et al., 2010) with relative conductivity values of Skin/Skull/Brain: (1/0.0125/1) using a quasistatic approximation mapping 64 electrodes to 15,002 dipoles covering the entire cortical surface. A common head model based on the Colin27 head was used for all source analysis with electrodes located in the Biosemi 64 channel EEG configuration. $M = GD$, with M indicating the EEG sensor measured values, G indicating the gain matrix from the forward problem mapping of noiseless data from the dipole sources to the sensors, and D indicating the dipole current source density. As this is an underdetermined problem, we employed Tikhonov regularization with the weighted minimum norm approach to estimate the dipole current density distribution using Brainstorm (Lawson and Hanson, 1987; Hämäläinen and Ilmoniemi, 1994; Tadel et al., 2011). The weighted minimum norm solution is given by

$$\widehat{D} = \left(W^T W\right)^{-1} G^T \left(G\left(W^T W\right)^{-1} G^T + \lambda I\right)^{-1} M$$

where $\widehat{D}$ is the estimated dipole cortical current density (CCD), W is the weight matrix, λ is the regularization parameter, and I is the identity matrix (Grech et al., 2008). Where $W = \Omega \otimes I$ with $\otimes$ denoting the Kronecker product and Ω being the norm of the columns of G.

The alpha power during the trial and baseline period was computed using 1 Hz resolution Morlet wavelets. The real and imaginary components were separately used to calculate the inverse for each set of values for each trial. To calculate the noise covariance matrix for the inverse calculation, the baseline data from 1 s prior to the start of the trial was mean subtracted on a trial by trail basis. The noise covariance was calculated for each trial and the final matrix was the mean of all artifact free trial matrices for each specific block. To increase the robustness of the solution, we assumed covariance between channels was zero and used the diagonal of the matrix. The orientation of dipoles on the cortical surface were constrained perpendicular to the surface under the assumption that the primary source of the EEG is coherent postsynaptic potentials across populations of pyramidal neurons that are arranged perpendicular to the cortical surface (Buzsáki et al., 2012).

ROI Selection

Our ROI selection method utilized a pipeline similar to our previous work (Yuan et al., 2008). The time course of each electrode was transformed into its time-frequency representation using a 1 Hz band Morlet wavelet and the power in each time window and frequency band (from 1 to 50 Hz) was computed (Qin and He, 2005). Mean amplitude at each sensor in the alpha band (8–13 Hz) was calculated with the real and imaginary parts. Source imaging was then performed with the real and imaginary

parts separately to obtain the corresponding CCD amplitudes which were then combined to compute a total frequency-specific CCD.

Group level ROI selection was performed iteratively based on the mean CCD across all subjects for all sessions. First, all dipoles were assigned an alpha-band score based on the mean CCD across subjects and sessions which was calculated at each dipole over the entire control period for each trial. The dipole with the largest alpha-band score was taken as the center of the first ROI. The extent of the ROI was taken as other dipoles within a 2 cm radius that had an alpha-band score of at least one-quarter of the center dipole. The alpha-band score of all dipoles within a 3 cm radius were then set to zero, and the largest alpha-band score of those remaining was selected and this proceeded iteratively until the top 10 ROIs were determined. ROIs to analyze further for connectivity were selected from the aforementioned set based on knowledge of active areas during MI and BCI task performance (Lotze and Halsband, 2006; Hétu et al., 2013) and were limited to the frontal and parietal cortices. ROI were determined separately for left and right hand imagination (**Figure 1**). For both left and right hand imagination the center of the ROIs were located in 1. Right sensorimotor cortex (SMC), encompassing sections of the premotor, primary motor, and S1 cortices; 2. Left premotor cortex (PMC); 3 SMA, encompassing sections of the SMA bilaterally; 4. Left SMC, encompassing sections of the premotor, motor, and S1 cortex; 5. Bilateral midline SMC. In addition, for left hand imagination, the left PPC was included whereas for right hand imagination the right PPC was included.

Subject specific ROIs on a session by session basis were determined by calculating the highest alpha-band scores across cortical dipoles for each subject within each session, within each of the global ROIs. The ROI activity time course was calculated by taking the mean of the dipoles within a 5 mm radius around the peak dipole. These time courses were used as a source-based virtual channels for analysis. These virtual channels were utilized for fitting the multivariate autoregressive model (MVAR) followed by analysis using the directed transfer function. An overview of the processing pipeline is illustrated in **Figure 2A**.

Connectivity Analysis

The multivariate autoregressive model is defined by

$$X(t) + \sum_{j=1}^{P} A(j) X(t-j) = E(t)$$

Where $X(t) = [X_1(t), X_2(t), \ldots X_k(t)]^T$ are the k time series at time t and $E(t) = [E_1(t), E_2(t), \ldots E_k(t)]^T$ are the k white noise values at time t, and $A(j) = \begin{pmatrix} A_{11}(j) \ldots A_{1k}(j) \\ A_{k1}(j) \ldots A_{kk}(j) \end{pmatrix}$ for $j = 1,\ldots,p$ are model parameters derived from the data.

E(t) is the uncorrelated white noise input driving the system with zero mean. The number of channels, *k*, was determined based on the number of ROIs chosen for connectivity. Model order, *P*, was determined using the AIC with the ARfit toolbox (Schneider and Neumaier, 2001) with each trial in each block being independently fit, then the mean of all trials per block taken as the order for all trials in that block, and each trial refit using the specified model order for that block. For most trials, cross and autocorrelation across 20 time lags exceeded the 2/sqrt(Nt) threshold, where Nt indicates the number of time points in the analysis window, which is a measure of the goodness of fit of the MVAR model, <10% of the time (Ding et al., 2000).

The directed transfer function calculates the connectivity between regions of interest for each frequency of interest. The directed transfer function evaluates the directed influence from one channel to another based on MVAR model fit to the data (Kaminski and Blinowska, 1991; Kaminski et al., 2001).

$$X(f) = H(f) E(f)$$

Where H is the transfer matrix defined in the frequency domain as [where A(0) is the identity matrix].

$$H(f) = \left(\sum_{m=0}^{p} A(m) e^{-2\pi i m f \Delta t} \right)^{-1}$$

This can then be normalized to the total inflow to each channel yielding the normalized directed transfer function.

$$\gamma_{ij}^2(f) = \frac{|H_{ij}(f)|^2}{\sum_{m=1}^{k} |H_{im}(f)|^2}$$

Statistical Analysis

All statistics were performed in R. In order to evaluate changes in connectivity following stimulation, we subtracted the pre-stimulation connectivity values from the $Post_0$ and $Post_{25}$ connectivity values to calculate mean difference values. We applied a general linear model using the nlme package with fixed effects of condition (anode or sham), and random effects of session nested within each subject. The Shapiro test was used to evaluate the Gaussianity of connectivity values and the residuals of the model fit, if Gaussianity was significantly rejected for both of these measures ($p < 0.05$) non-parametric statistical tests (Wilcoxon rank sum test) were used to compare subject mean post-stimulation values across conditions; two sample for between groups and one sample for change from baseline. All values reported in text are mean ± standard error. *p*-values are uncorrected unless otherwise indicated. Cohen's *d* effect sizes were computed between conditions on normally distributed data using the compute.es package.

A generalized linear model with the fixed effects of each connectivity value and random effect of subject with levels by session and block was used to examine the relationship between behavioral measures and connectivity across all subjects regardless of condition. A Poisson link function was used when analyzing the number of correct trials; for time to hit, a Gamma link function was used as this empirically fit the data well. *p*-values are uncorrected unless otherwise indicated.

RESULTS

Composite inflow and outflow characterize the sum influence to and from each ROI (**Figure 3**). For left hand imagination

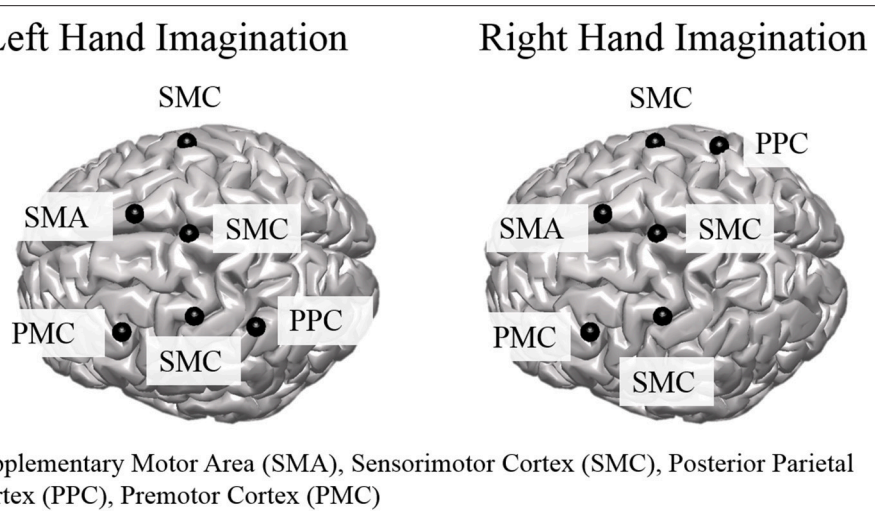

FIGURE 1 | Group level regions of interest for left and right hand imagination. Black sphere indicates the center of the ROI. SMC, Sensorimotor Cortex; SMA, supplementary motor area; PMC, premotor cortex; PPC, posterior parietal cortex.

inflow to the left PMC is largest, while outflow from the left SMC is largest. The difference between inflow and outflow is most positive in the right SMC and left PMC, while the left SMC and midline SMC have the most negative difference. For right hand imagination the greatest inflow is to the left PMC, which also has the largest difference between inflow and outflow. Within each target direction and condition, only a single ROI showed a significant difference in inflow or outflow between post-stimulation time points (Wilcoxon rank sum, $p < 0.05$ uncorrected) therefore the mean of these time points on a subject by subject basis was taken for further analyses. In general, there was a trend toward higher inflow and outflow at the $Post_{25}$ time point compared to the $Post_0$ time point. Total inflow to and outflow from ROIs in the alpha and beta bands changed based on laterality of hand imagination and stimulation condition as measured by the normalized DTF (**Figure 4**). For left-hand imagination there was a difference in total outflow from the left sensorimotor cortex between groups ($p = 00048$; $d = 2.93$), with a significant increase from pre-stimulation in the anodal group (0.19 ± 0.05; $p = 0.016$).

For right-hand imagination there was a significant difference in outflow from left PMC between groups ($p = 0.0084$; $d = 1.89$). There were significant increases in connectivity values in the anodal group across multiple areas of interest including inflow to SMA (0.06 ± 0.015; $p = 0.003$), midline SMC (0.068 ± 0.018; $p = 0.006$), and right PPC (0.062 ± 0.019; $p = 0.020$) and outflow from left SMC (0.063 ± 0.034; $p = 0.031$), left PM (0.082 ± 0.017; $p = 0.011$), and right SMC (0.097 ± 0.030; $p = 0.028$) and in the sham group in SMA inflow (0.054 ± 0.016; $p = 0.02$).

In the beta band there were similar changes from pre-stimulation as there were in the alpha band. There were significant differences in beta frequency band connectivity within and between conditions (**Figure 5**). For left-hand imagination there was a difference between conditions of outflow from the left PPC ($p = 0.048$; $d = 1.30$). There was a significant increase in inflow to the left SMC following anodal stimulation (046 ± 0.015; $p = 0.025$), and a significant increase to the midline SMC in the sham group (0.045 ± 0.015; $p = 0.043$). For right-hand imagination there was a significant difference in inflow to the right PPC between groups ($p = 0.0097$; $d = 1.83$) and outflow from the right SMC ($p = 0.0075$; $d = 1.93$) and left PMC ($p = 0.0023$; $d = 2.34$). There was an increase in SMA (0.032 ± 0.012; $p = 0.044$), midline SMC (0.042 ± 0.009; $p = 0.0023$), and right PPC (0.050 ± 0.016; $p = 0.028$) inflow and right SMC (0.087 ± 0.018; $p = 0.0016$) and left PMC (0.076 ± 0.017; $p = 0.013$) outflow following anodal stimulation.

Directed connections between the ROIs in the alpha band display further differences due to HD-tDCS based on the laterality of hand imagination (**Figure 6**). For left-hand imagination there were significant differences between groups for output from the left SMC to right SMC ($p = 0.011$; $d = 1.81$), left PMC ($p = 0.031$; $d = 1.45$), midline SMC ($p = 0.048$; $d = 1.30$), and left PPC ($p = 0.0037$; $d = 2.17$), with the anodal group having a greater increase than the sham group. The anodal group had increased flow from right SMC to SMA (0.0086 ± 0.0030; $p = 0.010$) and left SMC to right PMC (0.070 ± 0.017; $p = 0.0084$) and SMA (0.029 ± 0.009; $p = 0.028$). The sham group had increased connectivity from SMA to right PPC (0.015 ± 0.0065; $p = 0.043$) and midline SMC to right SMC (-0.029 ± 0.013; $p = 0.036$).

For right-hand imagination there were differences between groups from left PMC to left SMC ($p = 0.037$; $d = 1.64$), midline SMC ($p = 0.033$; $d = 1.42$), and right PPC ($p = 0.002$; $d = 2.37$) with higher changes in connectivity in the anodal group. For the anodal group there was increased connectivity from right SMC to left PMC (0.023 ± 0.007; $p = 0.021$) and left SMC (0.021 ± 0.009; $p = 0.043$), from left PMC to right PMC (0.011 ± 0.005; $p = 0.03$), left SMC (0.038 ± 0.017; $p = 0.037$), and right PPC (0.016 ± 0.005; $p = 0.0039$), and from midline SMC to SMA (0.009 ± 0.004; $p = 0.043$). For the sham group increased connectivity from left SMC to right PPC (0.027 ± 0.007; $p = 0.023$), and midline SMC to SMA (0.026 ± 0.010; $p = 0.021$).

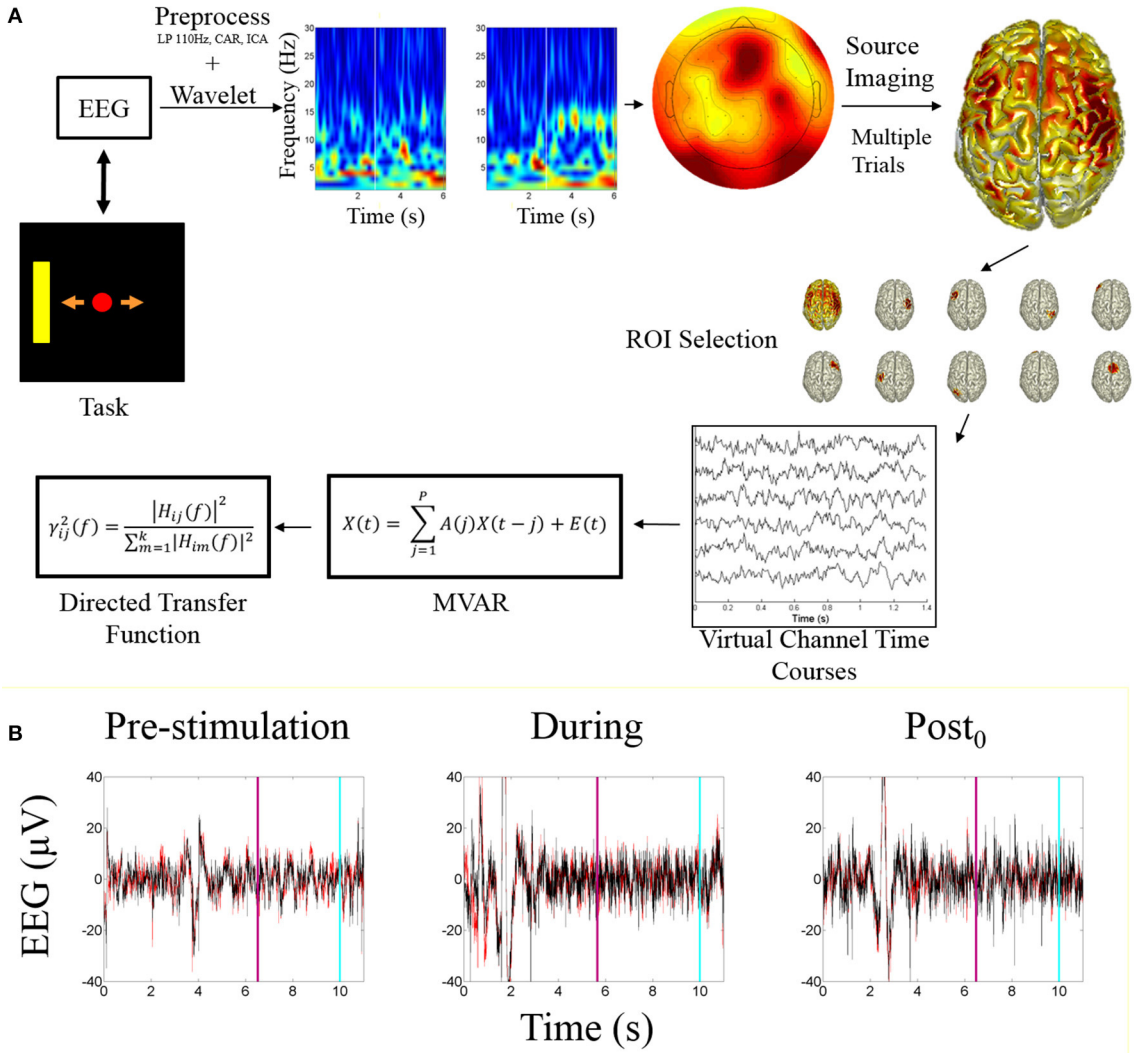

FIGURE 2 | Processing pipeline and EEG data**. (A)** Data analysis processing pipeline. The starting point is the task visualization which is controlled by the EEG data. The included time-frequency transform is an example of a correct trial of right hand imagination, the white bar indicates when online feedback began. The sensor level topograph illustrates alpha band activity during an example trial. The source imaging distribution illustrates the mean alpha power distribution across all subjects for right hand imagination. ROI selection is performed based on the identification of the ROIs described within the text. The peak ROIs are found for each subject each session and the trial specific time courses are extracted and fit with a multivariate autoregressive model to which the directed transfer function is applied. **(B)** Example EEG time course from before, during, and after stimulation. Red trace is C3; Black is C4. Light blue line represents when the trial ended; purple line indicates when the feedback period began.

In order to examine the relationship between alpha band connectivity values and behavioral performance metrics we utilized a generalized linear model with each normalized connectivity value as a fixed effect within the same model. Behavioral metrics across all subjects were: Mean time to hit correct targets for right-hand trials (RH) was 3.511 ± 0.337 s and left-hand trials (LH) was 3.718 ± 198.64 s. Mean correct targets per block were RH: 7.88 ± 1.75 trials and LH: 8.52 ± 2.09 trials. Overall, specific normalized connectivity values were correlated with behavioral outcome measures (**Figure 7**). For right-hand imagination trials, multiple connections correlated with decreased performance, in particular, total inflow to right PMC was significantly correlated with an increased time to hit (β = 7910, $p = 0.039$). Flow from right SMC to left PMC correlated with a decreased total correct (β = −6.24, $p = 0.003$, $p < 0.048$ FDR corrected). Flow from right PPC to left PMC correlated with an increased time to hit (β = 1729, $p < 0.018$). However, other connections correlated with improvements in behavioral measures. Flow from left SMC to right SMC correlated with a decreased time to hit (β = −2478, $p < 0.027$). Flow from left SMC to SMA correlated with an increased total correct (β = 3.22, $p = 0.022$). Flow from right PPC to midline SMC correlated with an increased total correct (β = 2.96, $p = 0.031$). For left-hand imagination trials we found correlations between directed connections and improved behavioral metrics. Flow from left PMC to right SMC correlated with an increased total correct (β =

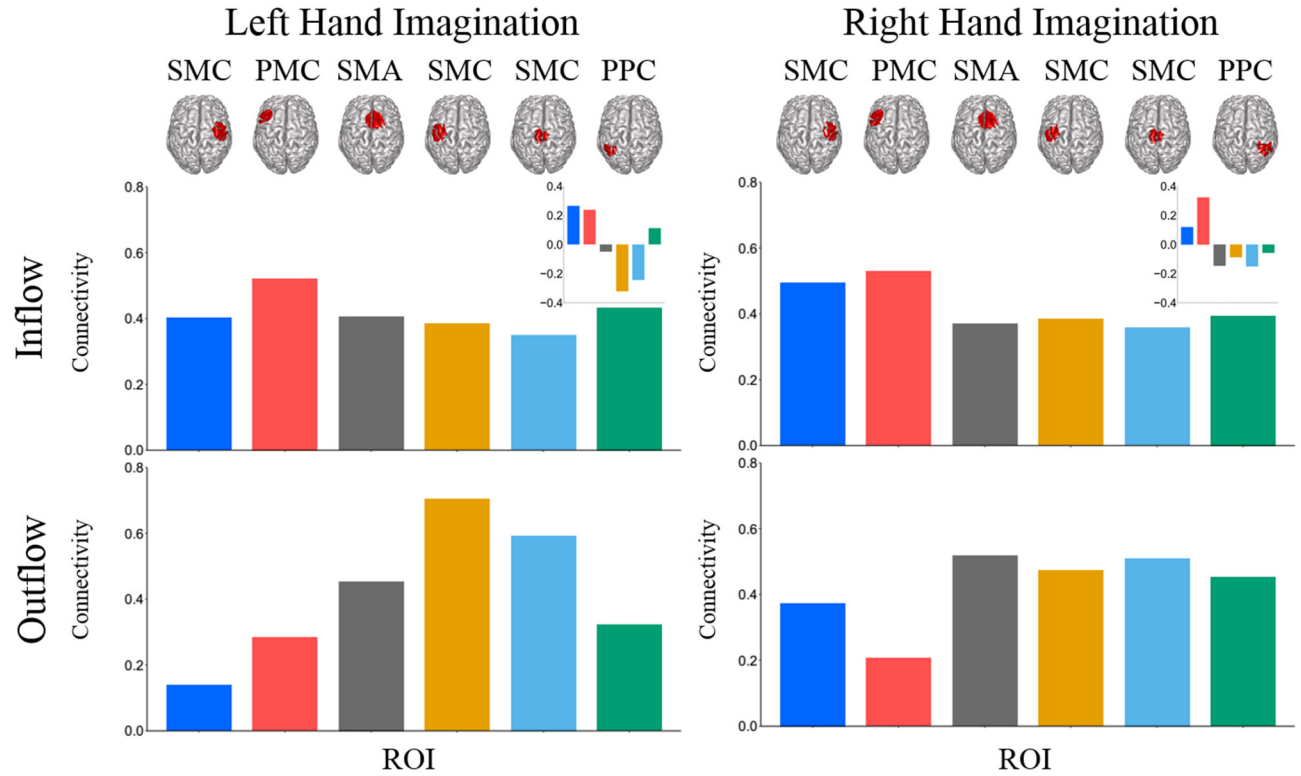

FIGURE 3 | Mean total inflow and outflow across all subjects. Inset represents the difference between inflow and outflow for each ROI. For left hand imagination (Left) inflow to the left PMC is largest, while outflow from the left SMC is largest. The difference between inflow and outflow is most positive in the right SMC and left PMC, while the left SMC and midline SMC have the most negative difference. For right hand imagination (Right) the greatest inflow is to the left PMC, which also has the largest difference between inflow and outflow.

4.78, $p < 0.023$). Flow from left PPC to midline SMC correlated with a decreased time to hit ($\beta = -2{,}955$, $p = 0.007$). Flow from midline SMC to left PPC correlated with an increased total correct ($\beta = 2.33$, $p = 0.019$).

DISCUSSION

Unilateral high-definition anodal tDCS during motor imagery-based brain computer interface performance has bilateral connectivity effects. Stimulation aftereffects differ based on the laterality of hand imagination, with an increased effect on connectivity when performing right-hand imagination, contralateral to the stimulated hemisphere. These results suggest that tDCS interacts with ongoing task-specific endogenous oscillations and affects communication between brain areas involved in task performance. To the best of our knowledge, this is the first study examining connectivity changes following tDCS and correlating connectivity to behavioral performance to examine how planned targeting of the network with stimulation could be used to improve performance.

Motor Network Connectivity

During right-hand imagination, the left sensorimotor cortex desynchronizes (and vice versa for left-hand imagination), which is characterized by a relative decrease in power in the alpha band. This decrease in power is due to networks within the sensorimotor cortex altering their firing patterns when activated by the MI task, this is referred to as event-related desynchronization (ERD) (Pfurtscheller and Lopes da Silva, 1999). The directed connectivity of MI during BCI varies based on the laterality of imagination and there is a large degree of interconnectivity within the sensorimotor cortex bilaterally, including the premotor, motor, and parietal cortices (Gao et al., 2011). These differences and connectivity patterns are likely due to event related synchronization and desynchronization across the motor cortex and the interactions with the rest of the motor imagery network through cortico-cortical connections both intrahemispherically and across the corpus callosum between the two hemispheres connecting the motor and parietal cortices. Gao et al. directly compared directed network activity during ME and MI and found similar connections in both, with ME having multiple significantly stronger connections (Gao et al., 2011). For right-hand imagination, we found greater inflow than outflow in the left PMC and right SMC, with greater outflow than inflow in the SMA and left SMC, and similar inflow and outflow in the right PPC. For left-hand imagination, we found greater inflow than outflow in the right SMC and left PMC, with greater outflow than inflow in the left SMC and midline SMC. Our results differ in relative connectivity when examining the normalized inflow and outflow compared to the work of Gao and

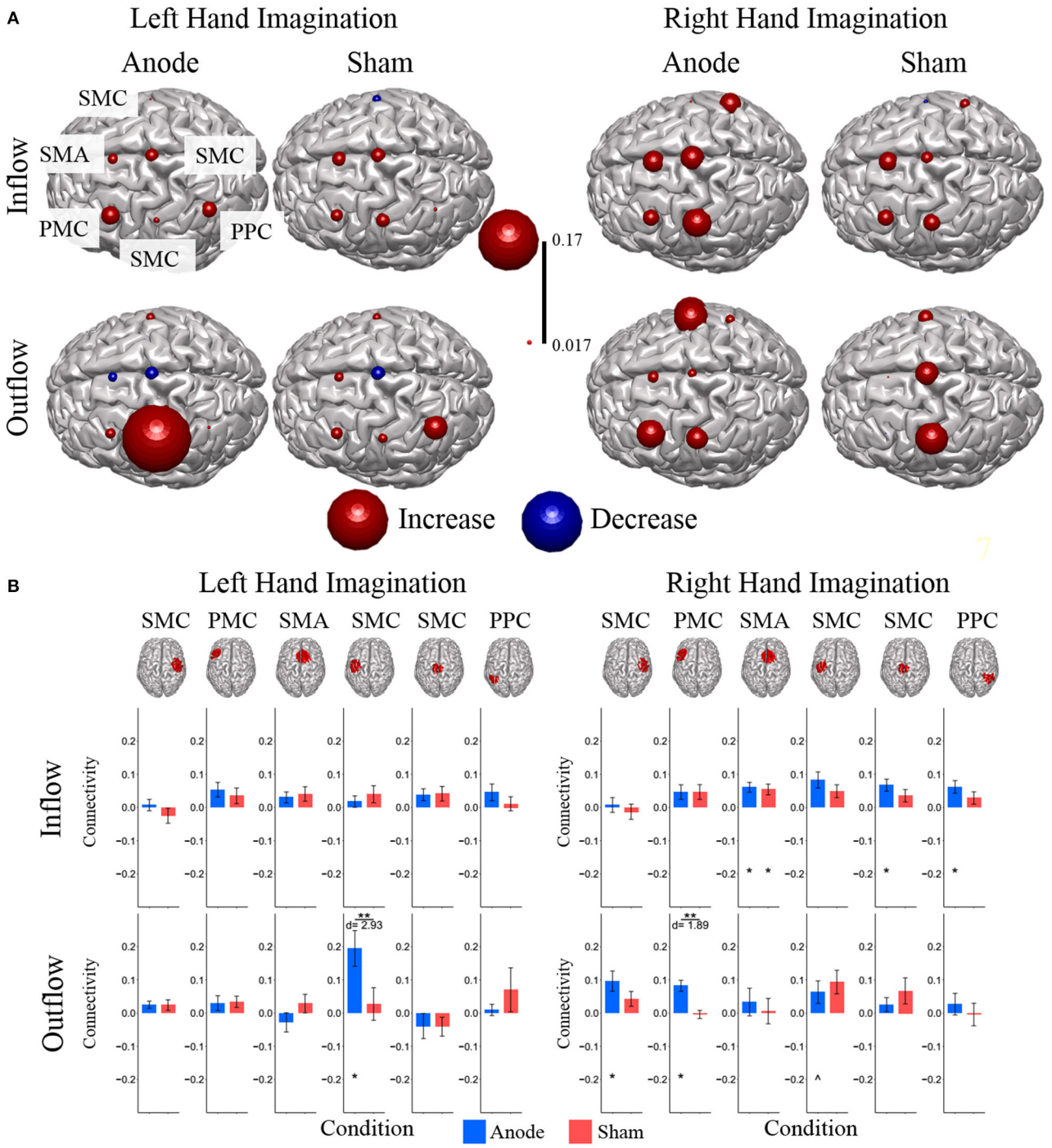

FIGURE 4 | Alpha band normalized DTF total flow for each ROI**. (A)** Change in total connectivity from the pre-stimulation time point mapped onto the peak dipole of each ROI for anode and sham conditions. Color indicates the direction of change and sphere size indicates the absolute change value. **(B)** Mean post-stimulation change in total connectivity between conditions. For left hand imagination (Left) there was a difference in total outflow from the left sensorimotor cortex between groups, with a significant increase from pre-stimulation in the anodal group. For right hand imagination (Right) there was a significant difference in outflow from left PMC between groups. There were significant increases in the inflow to SMA, midline SMC, and right PPC; outflow from left SMC, left PMC, and right SMC in the anodal group and SMA inflow in the sham group. Total inflow to the ROI (top) and total outflow from the ROI (bottom). Bar color indicates the condition: anode (blue) and sham (red). Values are mean across subject; error bars are standard error across subjects. $^{**}p < 0.05$ between conditions. $^{*}p < 0.05$ change from pre-stimulation. ^Wilcoxon rank sum change from pre-stimulation. *d* is Cohen's d effect size.

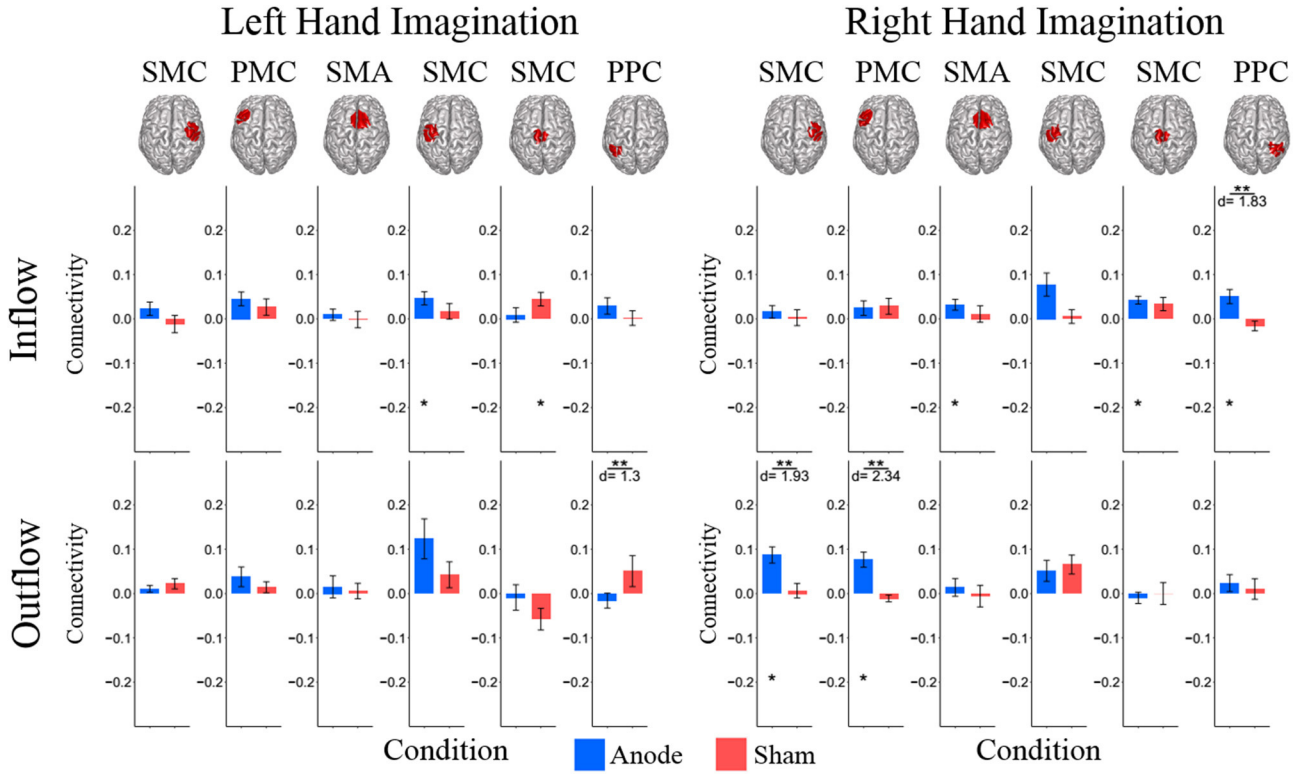

FIGURE 5 | Beta band normalized DTF total flow for each ROI**.** Mean post-stimulation change in total connectivity between conditions. For left hand imagination (Left) there was a difference between conditions of outflow from the left PPC. There was a significant increase in inflow to the left SMC following anodal stimulation, and a significant increase to the midline SMC in the sham group. For right hand imagination (Right) there was a significant difference in inflow to the right PPC between groups and outflow from the right SMC and left PMC. There was an increase in SMA, midline SMC, and left PPC inflow and right SMC and left PM outflow following anodal stimulation. Total inflow to the ROI (top) and total outflow from the ROI (bottom). Bar color indicates the condition: anode (blue) and sham (red). Values are mean across subjects; error bars are standard error across subjects. $^{**}p < 0.05$ between conditions. $^{*}p < 0.05$ change from pre-stimulation. *d* is Cohen's d effect size.

colleagues. A reason for this may be based on the composition of the network, where Gao examine more regions across the cortex, which may offset this balance of inflow and outflow. In addition, we report frequency specific connectivity where previous work examined non-frequency specific BOLD activity.

Specific directed connections have also been investigated during MI and execution. Athanasiou et al. examined connectivity in the alpha band during MI and found information flow from contralateral to ipsilateral M1 and SMA to ipsilateral M1 (Athanasiou et al., 2012). We report connectivity in these directions, though they are not the connections of greatest strength. Anwar et al found a high degree of effective connectivity from SMC to PMC as well as bidirectional SMC–PMC connectivity during ME task performance in the hemisphere contralateral to the hand movement. We find a similarly high connectivity during right hand imagination, from SMC to PMC in the contralateral hemisphere. An important difference in the experimental design of this study was the examination of connectivity as subjects received feedback during imagination through the BCI task. This may account for the differences within the motor network as well as there is constant evaluation of performance and movement which is not present or examined in these previous studies.

Effect of tDCS on Motor Network Activity

Polania et al examined undirected connectivity at the EEG sensor level using graph theory measures and found increased connectivity in the alpha band within the left hemisphere during a right hand motor task following anodal stimulation over the left primary motor cortex (Polanía et al., 2011). During right hand imagination we found increased directed connectivity within the left hemisphere, specifically from the PMC to SMC, which suggests that the undirected connections found by Polania are specific to this direction. In addition, Polania and colleagues found no change or decreased interhemispheric connectivity based on specific electrodes in the alpha band following stimulation, whereas we report an increase in connectivity from the left PMC to the right SMC and right PPC as well as from the right SMC to the left PMC and left PMC. Polania and colleagues used resting state fMRI to examine cortico-thalamic connectivity following anodal tDCS and found increased connectivity between the stimulated left primary motor cortex, and subcortical structures of the ipsilateral thalamus and caudate nucleus (Polanía et al., 2012). As the thalamus has widespread cortico-cortico connections, this is a possible pathway through which the intrahemispheric changes we report occur, though the use of EEG precludes the analysis of connectivity including deep thalamic

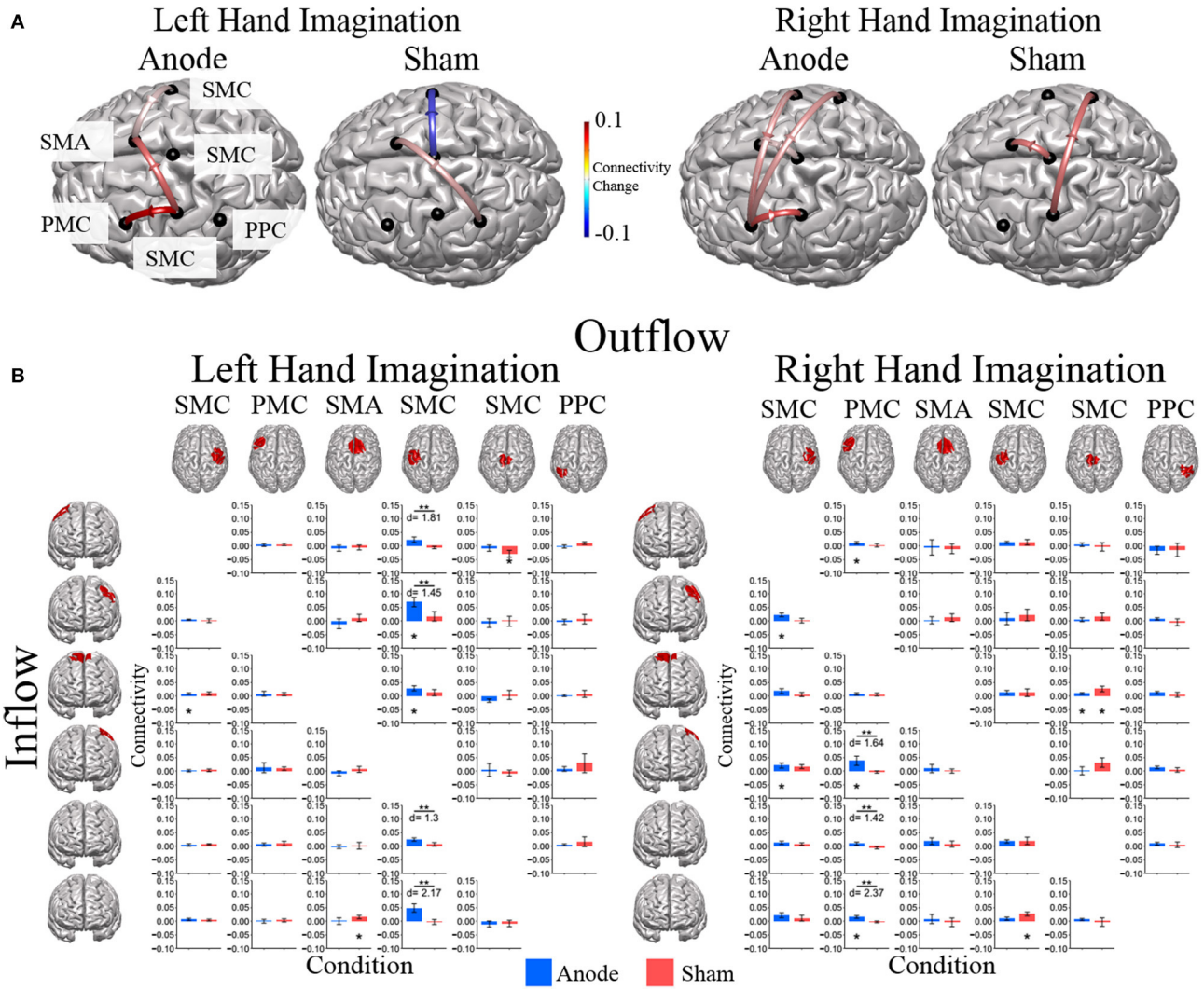

FIGURE 6 | Alpha band normalized DTF flow between each ROI pair**. (A)** Alpha band changes in connectivity after stimulation for right and left hand imagination in the anode and sham stimulation groups. Red indicates and increase in connectivity, blue indicates a decrease in connectivity. Values are mean across subjects across blocks. All included connections had $p < 0.05$ from pre-stimulation baseline. **(B)** Mean post-stimulation change in directed connectivity between conditions. For left hand imagination (Left) there were significant differences between groups for output from the left SMC to right SMC, left PMC, midline SMC, and left PPC, with the anodal group having a greater increase than the sham group. The anodal group had increased flow from right PMC to SMA, left SMC to left PMC and SMA. The sham group had increased connectivity from SMA to right PPC and midline SMC to right SMC. For right hand imagination (Right) there were differences between groups from left PM to left SMC, midline SMC, and right PPC with higher changes in connectivity in the anodal group. For the anodal group there was increased connectivity from right SMC to left PM and left SMC, from left PM to right PMC, left PMC, and right PPC, from midline SMC to SMA. For the sham group increased connectivity from left SMC to right PPC and midline SMC to SMA. Values are mean across subjects; error bars are standard error. $^{**}p < 0.05$ between conditions. $^{*}p < 0.05$ change from pre-stimulation. *d* is Cohen's d effect size.

sources and interhemispheric corpus callosum pathways which in reality may contribute to these changes.

Notturno and colleagues examined functional connectivity using EEG during ME following tDCS with the anodal electrode over the left SMC and found no effect on coherence, an undirected measure, during motor movement between C3 and any other electrode following anodal or cathodal stimulation, though they did not look at pairwise coherence between other electrodes (Notturno et al., 2014). Our results suggest significantly different effects of stimulation in a directed manner. An explanation for the previously found lack of effect by Notturno and colleagues may be the relationship between the timing of stimulation and task performance. These previous studies applied stimulation during rest whereas we had subjects perform the task concurrent with stimulation. During sensorimotor rhythm modulation for controlling a BCI, the control signal is generated from both hemispheres whereby there may be increased interaction between the two

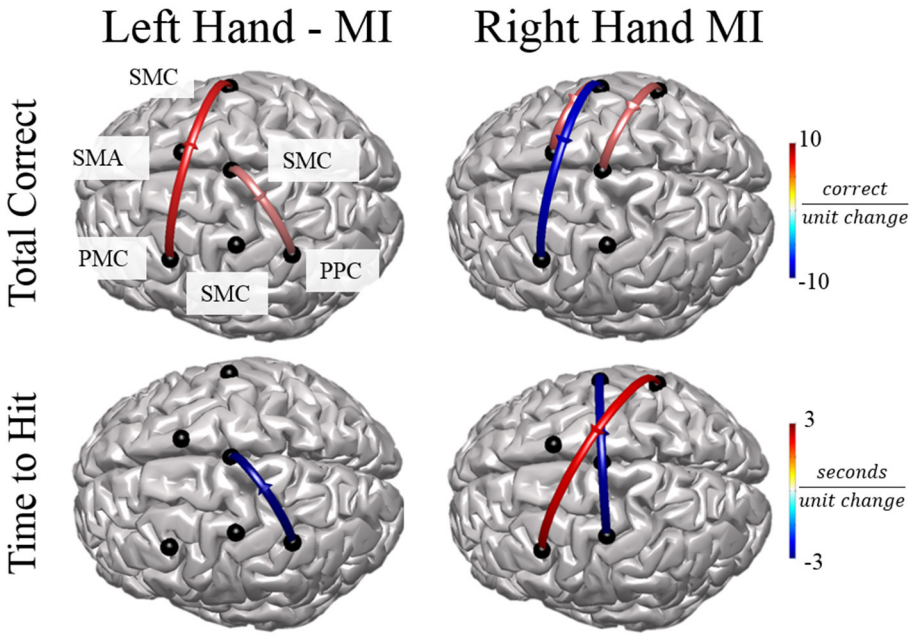

FIGURE 7 | Connectivity Value–Behavioral Correlations**.** For both right and left hand imaginations, flow from the ipsilateral PPC to midline SMC correlated with improved performance. For right hand imagination, inflow to left PMC, in particular from right SMC and PPC correlates with reduced performance through reduced total correct and increased time to hit. Flow from left SMC to right SMC and SMA correlates with improved performance through an increased total correct and decreased time to hit. For left hand imagination, flow from left PMC to right SMC and flow from midline SMC to left PPC correlated with improved performance. Color indicates the beta coefficient value $p < 0.05$ for all displayed connections.

during task performance. Combining task performance with stimulation may then increase both ipsilateral and contralateral connectivity due to task specific activity. These differences highlight the importance of context with stimulation, whereby differing activity during stimulation leads to differing aftereffects of the stimulation on task specific activity, as has been previously suggested (Buch et al., 2017). These differences may also be partially explained by the fact that subjects performed ME in this previous study, even though the motor network connectivity is quite similar between these two activities, as described previously.

A limitation of the current study is that although we instructed subjects to perform kinesthetic imagination of the left and right hand, subjects may have adapted their imagination to improve performance, by using a more complex MI that experimentally allowed them better control of the cursor; for example, throwing a ball or opening a door handle. In order to improve our understanding of the relationship between connectivity and performance, analyses of the connectivity over the time-course of individual trials is needed. Another limitation of this work is the number of subjects used for the analysis. As this was an initial exploratory analysis of the effects of stimulation on connectivity, the number of subjects, and the number of directed connectivity measures, are small and we did not correct our statistics for multiple comparisons. Further studies could utilize more subjects to examine the reproducibility of these analyses and examine specific directional connections based on a priori hypotheses to reduce the number of comparisons.

Connectivity–Behavior Relationship

We found specific connectivity features that correlated with the changes in performance as measured by the number of correct trials and the time to hit correct targets. We do not attempt to predict performance based on these connectivity measures but rather use these correlations to examine how the network interacts during BCI performance. For both right- and left-hand imagination, flow from the ipsilateral PPC to midline SMC correlated with improved performance. The PPC is connected to the SMC and directs attention and visuomotor planning during ME and imagination (Lotze and Halsband, 2006). Generally, there is a slight increase in alpha power in the midline SMC during either right- or left-hand imagination as it is involved in lower limb movement rather than hand movement. This planning input from the ipsilateral PPC may effect this increase in alpha power, which in turn could lead to improved unilateral hand imagination through inhibition of midline SMC.

Right- and left-hand imagination also had differential connections correlated with performance. For right-hand imagination inflow to left PMC, in particular from right SMC and PPC correlated with reduced performance through reduced total correct and increased time to hit. As the left PMC is used in planning of both left and right hand movements, input from the right motor cortex may impair the planning functionality. In addition, the right motor cortex synchronizes during right-hand imagination whereby output may result in an inhibition of relevant information transfer from PMC to downstream regions. There were also connections that correlated with improved

performance for right- and left-hand imagination. Flow from left SMC to right SMC and SMA correlates with improved performance through an increased total correct and decreased time to hit. During right-hand execution and imagination left SMC is desynchronized and is active in directing the movement or imagination. This output to the contralateral SMC may be an inhibitory signal via the corpus callosum, a known direct interhemispheric pathway (van der Knaap and van der Ham, 2011). During left hand imagination, flow from left PMC to right SMC correlated with improved performance. As the left PMC directs bilateral motor planning and as the right PMC is primarily active during left MI, increased information flow in this direction may improve performance. Our findings suggest that increases in the performance of behavioral measures are positively correlated with connections from planning regions, such as PPC and PMC, to sensorimotor cortex whereas a decreases in performance of behavioral measures correlate with connections from the SMC to planning regions.

To the best of our knowledge, there are no comparative works examining the correlation between connectivity and performance of BCI tasks. Though Billinger et al. (2013) examined offline classification performance of EEG source and sensor activity and connectivity features, they did not report specific connectivity features used for classification so we are unable to make comparisons with the current study. In addition, they did not relate connectivity to any online performance metrics but rather examined if connectivity based classifiers can be used to improve classification accuracy.

CONCLUSION

Our results support the hypothesis that tDCS interacts with ongoing endogenous brain oscillations in an activity and task-specific manner. During motor imagery there is a decrease in alpha power in the contralateral sensorimotor cortex due to a desynchronization in the underlying networks, with areas involved in the imagination decoupling from surrounding areas. Based on unilateral sensorimotor stimulation, we see differing interactions of the stimulation aftereffect on network connectivity based on the laterality of hand imagination. We also show both positive and negative correlations between specific directed connection strengths and behavioral metrics, with connections from ipsilateral PPC to midline SMC correlating with behavioral improvements for both right and left hand imagination. However, HD-tDCS over the left SMC did not alter any of these connections that correlate with behavior. The effects of targeting network connections and the most efficacious methodology to alter networks using TCS is still unclear. Future work should examine targeting regions of interest with anodal stimulation to increase excitation and therefore increase the probability of correlating the firing in these areas, however the timing of the firing also needs to be considered as the directional effect of plasticity varies based on these correlations (Müller-Dahlhaus and Ziemann, 2015). Additional work using adaptive or short time directed transfer function, connectivity, and behavioral output to examine how these networks develop across time, will be vital for developing adaptive stimulation.

ETHICS STATEMENT

This study was carried out in accordance with the recommendations of the University of Minnesota Institutional Review Board with written informed consent from all subjects. All subjects gave written informed consent in accordance with the Declaration of Helsinki. The protocol was approved by the University of Minnesota Institutional Review Board.

AUTHOR CONTRIBUTIONS

BB and BH designed the experiments. BB performed experiments. BE assisted in data collection. BB analyzed the data. All authors discussed the results and interpretations. BB and BH wrote the article.

FUNDING

This work was supported in part by NIH AT009263, NIH EB021027, NIH NS096761, NIH MH114233, NIH EY023101, NIH HL117664, NSF CBET-1264782, and NSF DGE-1069104.

ACKNOWLEDGMENTS

We thank Albert You and Nicholas Nesbitt for technical assistance.

REFERENCES

Amadi, U., Ilie, A., Johansen-Berg, H., and Stagg, C. J. (2014). Polarity-specific effects of motor transcranial direct current stimulation on fMRI resting state networks. *Neuroimage* 88, 155–161. doi: 10.1016/j.neuroimage.2013.11.037

Andersen, R. A., and Buneo, C. A. (2002). Intentional maps in posterior parietal cortex. *Annu. Rev. Neurosci.* 25, 189–220. doi: 10.1146/annurev.neuro.25.112701.142922

Antal, A., Polania, R., Schmidt-Samoa, C., Dechent, P., and Paulus, W. (2011). Transcranial direct current stimulation over the primary motor cortex during fMRI. *Neuroimage* 55, 590–596. doi: 10.1016/j.neuroimage.2010.11.085

Anwar, A. R., Muthalib, M., Perrey, S., Galka, A., Granert, O., Wolff, S., et al. (2016). Effective connectivity of cortical sensorimotor networks during finger movement tasks: a simultaneous fNIRS, fMRI, EEG study. *Brain Topogr.* 29, 645–660. doi: 10.1007/s10548-016-0507-1

Astolfi, L., Cincotti, F., Mattia, D., Marciani, M. G., Baccala, L. A., de Vico Fallani, F., et al. (2007). Comparison of different cortical connectivity estimators for high-resolution EEG recordings. *Hum. Brain Mapp.* 28, 143–157. doi: 10.1002/hbm.20263

Athanasiou, A., Lithari, C., Kalogianni, K., Klados, M. A., and Bamidis, P. D. (2012). Source detection and functional connectivity of the sensorimotor cortex during actual and imaginary limb movement: a preliminary study on the implementation of econnectome in motor imagery protocols. *Adv. Hum. Comp. Interact.* 2012:127627. doi: 10.1155/2012/127627

Babiloni, F., Cincotti, F., Babiloni, C., Carducci, F., Mattia, D., Astolfi, L., et al. (2005). Estimation of the cortical functional connectivity with the multimodal

integration of high-resolution EEG and fMRI data by directed transfer function. *Neuroimage* 24, 118–131. doi: 10.1016/j.neuroimage.2004.09.036

Baccalá, L. A. and Sameshima, K. (2001). Partial directed coherence: a new concept in neural structure determination. *Biol. Cybern*. 84, 463–474. doi: 10.1007/PL00007990

Baxter, B. S., Edelman, B. J., Nesbitt, N., and He, B. (2016). Sensorimotor rhythm BCI with simultaneous high definition-transcranial direct current stimulation alters task performance. *Brain Stimul*. 9, 834–841. doi: 10.1016/j.brs.2016.07.003

Bergmann, T. O., Karabanov, A., Hartwigsen, G., Thielscher, A., and Siebner, H. R. (2016). Combining non-invasive transcranial brain stimulation with neuroimaging and electrophysiology: current approaches and future perspectives. *Neuroimage* 140, 4–19. doi: 10.1016/j.neuroimage.2016.02.012

Bestmann, S., de Berker, A. O., and Bonaiuto, J. (2015). Understanding the behavioural consequences of noninvasive brain stimulation. *Trends Cogn. Sci.* 19, 13–20. doi: 10.1016/j.tics.2014.10.003

Bikson, M., and Rahman, A. (2013). Origins of specificity during tDCS: anatomical, activity-selective, and input-bias mechanisms. *Front. Hum. Neurosci*. 7:688. doi: 10.3389/fnhum.2013.00688

Bikson, M., Inoue, M., Akiyama, H., Deans, J. K., Fox, J. E., Miyakawa, H., et al. (2004). Effects of uniform extracellular DC electric fields on excitability in rat hippocampal slices *in vitro*. *J. Physiol*. 557, 175–190. doi: 10.1113/jphysiol.2003.055772

Billinger, M., Brunner, C., and Müller-Putz, G. R. (2013). Single-trial connectivity estimation for classification of motor imagery data. *J. Neural Eng*. 10:46006. doi: 10.1088/1741-2560/10/4/046006

Buch, E. R., Santarnecchi, E., Antal, A., Born, J., Celnik, P. A., Classen, J., et al. (2017). Effects of tDCS on motor learning and memory formation: a consensus and critical position paper. *Clin. Neurophysiol*. 128, 589–603. doi: 10.1016/j.clinph.2017.01.004

Buzsáki, G., Anastassiou, C. A., and Koch, C. (2012). The origin of extracellular fields and currents–EEG, ECoG, LFP and spikes. *Nat. Rev. Neurosci*. 13, 407–420. doi: 10.1038/nrn3241

Cincotti, F., Mattia, D., Aloise, F., Bufalari, S., Astolfi, L., De Vico Fallani, F., et al. (2008). High-resolution EEG techniques for brain-computer interface applications. *J. Neurosci. Methods* 167, 31–42. doi: 10.1016/j.jneumeth.2007.06.031

Davare, M., Kraskov, A., Rothwell, J. C., and Lemon, R. N. (2011). Interactions between areas of the cortical grasping network. *Curr. Opin. Neurobiol*. 21, 565–570. doi: 10.1016/j.conb.2011.05.021

Davare, M., Rothwell, J. C., and Lemon, R. N. (2010). Causal connectivity between the human anterior intraparietal area and premotor cortex during grasp. *Curr. Biol*. 20, 176–181. doi: 10.1016/j.cub.2009.11.063

Delorme, A., and Makeig, S. (2004). EEGLAB: an open source toolbox for analysis of single-trial EEG dynamics including independent component analysis. *J. Neurosci. Methods* 134, 9–21. doi: 10.1016/j.jneumeth.2003.10.009

Ding, M., Bressler, S. L., Yang, W., and Liang, H. (2000). Short-window spectral analysis of cortical event-related potentials by adaptive multivariate autoregressive modeling: data preprocessing, model validation, and variability assessment. *Biol. Cybern*. 83, 35–45. doi: 10.1007/s004229900137

Dmochowski, J. P., Datta, A., Bikson, M., Su, Y., and Parra, L. C. (2011). Optimized multi-electrode stimulation increases focality and intensity at target. *J. Neural Eng*. 8:46011. doi: 10.1088/1741-2560/8/4/046011

Edelman, B. J., Baxter, B., and He, B. (2016). EEG source imaging enhances the decoding of complex right-hand motor imagery tasks. *IEEE Trans. Biomed. Eng*. 63, 4–14. doi: 10.1109/TBME.2015.2467312

Feurra, M., Bianco, G., Polizzotto, N. R., Innocenti, I., Rossi, A., and Rossi, S. (2011). Cortico-cortical connectivity between right parietal and bilateral primary motor cortices during imagined and observed actions: a combined TMS/tDCS Study. *Front. Neural Circuits* 5:10. doi: 10.3389/fncir.2011.00010

Fisher, D. B., Fried, P., Ruffini, G., Ripolles, O., Ketchabaw, T., Santarnecchi, E., et al. (2017). Network-targeted non-invasive brain stimulation with multifocal tdcs. *Brain Stimul*. 10, 411–412. doi: 10.1016/j.brs.2017.01.219

Fox, M. D., Buckner, R. L., Liu, H., Chakravarty, M. M., Lozano, A. M., and Pascual-Leone, A. (2014). Resting-state networks link invasive and noninvasive brain stimulation across diverse psychiatric and neurological diseases. *Proc. Natl. Acad. Sci. U.S.A*. 111, E4367–E4375. doi: 10.1073/pnas.1405003111

Friston, K., Moran, R., and Seth, A. K. (2013). Analysing connectivity with granger causality and dynamic causal modelling. *Curr. Opin. Neurobiol*. 23, 172–178. doi: 10.1016/j.conb.2012.11.010

Gao, Q., Duan, X., and Chen, H. (2011). Evaluation of effective connectivity of motor areas during motor imagery and execution using conditional granger causality. *Neuroimage* 54, 1280–1288. doi: 10.1016/j.neuroimage.2010.08.071

Grafton, S. T. (2010). The cognitive neuroscience of prehension: recent developments. *Exp. Brain Res*. 204, 475–491. doi: 10.1007/s00221-010-2315-2

Gramfort, A., Papadopoulo, T., Olivi, E., and Clerc, M. (2010). OpenMEEG: opensource software for quasistatic bioelectromagnetics. *Biomed. Eng. Online* 9:45. doi: 10.1186/1475-925X-9-45

Grech, R., Cassar, T., Muscat, J., Camilleri, K. P., Fabri, S. G., Zervakis, M., et al. (2008). Review on solving the inverse problem in EEG source analysis. *J. Neuroeng. Rehabil.* 5:25. doi: 10.1186/1743-0003-5-25

Hämäläinen, M. S., and Ilmoniemi, R. J. (1994). Interpreting magnetic fields of the brain: minimum norm estimates. *Med. Biol. Eng. Comput*. 32, 35–42. doi: 10.1007/BF02512476

Hämäläinen, M. S., and Sarvas, J. (1989). Realistic conductivity geometry model of the human head for interpretation of neuromagnetic data. *IEEE Trans. Biomed. Eng*. 36, 165–171. doi: 10.1109/10.16463

Hamedi, M., Salleh, Sh H., and Noor, A. M. (2016). Electroencephalographic motor imagery brain connectivity analysis for BCI: a review. *Neural Comput*. 28, 999–1041. doi: 10.1162/NECO_a_00838

He, B., Baxter, B., Edelman, B. J., Cline, C. C., and Ye, W. W. (2015). Noninvasive brain-computer interfaces based on sensorimotor rhythms. *Proc. IEEE* 103, 1–19. doi: 10.1109/JPROC.2015.2407272

He, B., Dai, Y., Astolfi, L., Babiloni, F., Yuan, H., and Yang, L. (2011a). eConnectome: A MATLAB toolbox for mapping and imaging of brain functional connectivity. *J. Neurosci. Methods* 195, 261–269. doi: 10.1016/j.jneumeth.2010.11.015

He, B., Gao, S., Yuan, H., and Wolpaw, J. (2013). "Brain-computer interface," in *Neural Engineering*, ed B. He (Boston, MA: Springer), 87–151.

He, B., Musha, T., Okamoto, Y., Homma, S., Nakajima, Y., and Sato, T. (1987). Electric dipole tracing in the brain by means of the boundary element method and its accuracy. *IEEE Trans. Biomed. Eng*. 34, 406–414. doi: 10.1109/TBME.1987.326056

He, B., Yang, L., Wilke, C., and Yuan, H. (2011b). Electrophysiological imaging of brain activity and connectivity: challenges and opportunities. *IEEE Trans. Biomed. Eng*. 58, 1918–1931. doi: 10.1109/TBME.2011.2139210

Hétu, S., Grégoire, M., Saimpont, A., Coll, M.P., Eugène, F., Michon, P.E., et al. (2013). The neural network of motor imagery: an ALE meta-analysis. *Neurosci. Biobehav. Rev*. 37, 930–949. doi: 10.1016/j.neubiorev.2013.03.017

Hyvarinen, A. (1999). Fast and robust fixed-point algorithm for independent component analysis. *IEEE Trans. Neur. Net*. 10, 626–634. doi: 10.1109/72.761722

Im, C. H., Gururajan, A., Zhang, N., Chen, W., and He, B. (2007). Spatial resolution of EEG cortical source imaging revealed by localization of retinotopic organization in human primary visual cortex. *J. Neurosci. Methods* 161, 142–154. doi: 10.1016/j.jneumeth.2006.10.008

Jang, S. H., Ahn, S. H., Byun, W. M., Kim, C. S., Lee, M. Y., and Kwon, Y. H. (2009). The effect of transcranial direct current stimulation on the cortical activation by motor task in the human brain: an fMRI study. *Neurosci. Lett*. 460, 117–120. doi: 10.1016/j.neulet.2009.05.037

Jog, M. V., Smith, R. X., Jann, K., Dunn, W., Lafon, B., Truong, D., et al. (2016). *In-vivo* imaging of magnetic fields induced by transcranial direct current stimulation (tDCS) in human brain using MRI. *Sci. Rep*. 6:34385. doi: 10.1038/srep34385

Johnson, M. D., Lim, H. H., Netoff, T. I., Connolly, A. T., Johnson, N., Roy, A., et al. (2013). Neuromodulation for brain disorders: challenges and opportunities. *IEEE Trans. Biomed. Eng*. 60, 610–624. doi: 10.1109/TBME.2013.2244890

Jung, T. P., Makeig, S., Humphries, C., Lee, T. W., McKeown, M. J., Iragui, V., et al. (2000). Removing electroencephalographic artifacts by blind source separation. *Psychophysiology* 37, 163–78. doi: 10.1111/1469-8986.3720163

Kabakov, A. Y., Muller, P. A., Pascual-Leone, A., Jensen, F. E., Rotenberg, A., Antal, A., et al. (2012). Contribution of axonal orientation to pathway-dependent modulation of excitatory transmission by direct current stimulation in isolated rat hippocampus. *J. Neurophysiol*. 107, 1881–1889. doi: 10.1152/jn.00715.2011

Kaminski, M. J., and Blinowska, K. J. (1991). A new method of the description of the information flow in the brain structures. *Biol. Cybern*. 65, 203–210. doi: 10.1007/BF00198091

Kaminski, M., Ding, M., Truccolo, W. A., and Bressler, S. L. (2001). Evaluating causal relations in neural systems: granger causality, directed transfer function and statistical assessment of significance. *Biol. Cybern*. 85, 145–157. doi: 10.1007/s004220000235

Kamousi, B., Amini, A. N., and He, B. (2007). Classification of motor imagery by means of cortical current density estimation and Von Neumann entropy. *J. Neural Eng*. 4, 17–25. doi: 10.1088/1741-2560/4/2/002

Kamousi, B., Liu, Z., and He, B. (2005). Classification of motor imagery tasks for brain-computer interface applications by means of two equivalent dipoles analysis. *IEEE Trans. Neural Syst. Rehabil. Eng*. 13, 166–171. doi: 10.1109/TNSRE.2005.847386

Kasess, C. H., Windischberger, C., Cunnington, R., Lanzenberger, R., Pezawas, L., and Moser, E. (2008). The suppressive influence of SMA on M1 in motor imagery revealed by fMRI and dynamic causal modeling. *Neuroimage* 40, 828–837. doi: 10.1016/j.neuroimage.2007.11.040

Keeser, D., Meindl, T., Bor, J., Palm, U., Pogarell, O., Mulert, C., et al. (2011). Prefrontal transcranial direct current stimulation changes connectivity of resting-state networks during fMRI. *J. Neurosci*. 31, 15284–15293. doi: 10.1523/JNEUROSCI.0542-11.2011

Krause, M. R., Zanos, T. P., Csorba, B. A., Pilly, P. K., Choe, J., Phillips, M. E., et al. (2017). Transcranial direct current stimulation facilitates associative learning and alters functional connectivity in the primate brain. *Curr. Biol*. 27, 3086.e3–3096.e3. doi: 10.1016/j.cub.2017.09.020

Kuo, H. I., Bikson, M., Datta, A., Minhas, P., Paulus, W., Kuo, M. F., et al. (2013). Comparing cortical plasticity induced by conventional and high-definition 4 × 1 ring tDCS: a neurophysiological study. *Brain Stimul*. 6, 644–648. doi: 10.1016/j.brs.2012.09.010

Kuś, R., Ginter, J. S., and Blinowska, K. J. (2006). Propagation of EEG activity during finger movement and its imagination. *Acta Neurobiol. Exp*. 66, 195–206.

Lawson, C. L., and Hanson, R. J. (1987). *Solving Least Squares Problems (Classics in Applied Mathematics*). Philadelphia, PA: Society for Industrial and Applied Mathematics.

Lotze, M., and Halsband, U. (2006). Motor imagery. *J. Physiol. Paris* 99, 386–395. doi: 10.1016/j.jphysparis.2006.03.012

Lotze, M., Montoya, P., Erb, M., Hülsmann, E., Flor, H., Klose, U., et al. (1999). Activation of cortical and cerebellar motor areas during executed and imagined hand movements: an fMRI study. *J. Cogn. Neurosci*. 11, 491–501. doi: 10.1162/089892999563553

Luft, C. D., Pereda, E., Banissy, M. J., and Bhattacharya, J. (2014). Best of both worlds: promise of combining brain stimulation and brain connectome. *Front. Syst. Neurosci*. 8:132. doi: 10.3389/fnsys.2014.00132

Mak, J. N., and Wolpaw, J. R. (2009). Clinical applications of brain-computer Interfaces: current state and future prospects. *IEEE Rev. Biomed. Eng*. 2, 187–199. doi: 10.1109/RBME.2009.2035356

Meinzer, M., Antonenko, D., Lindenberg, R., Hetzer, S., Ulm, L., Avirame, K., et al. (2012). Electrical brain stimulation improves cognitive performance by modulating functional connectivity and task-specific activation. *J. Neurosci*. 32, 1859–1866. doi: 10.1523/JNEUROSCI.4812-11.2012

Michel, C. M., Murray, M. M., Lantz, G., Gonzalez, S., Spinelli, L., and Grave De Peralta, R. (2004). EEG source imaging. *Clin. Neurophysiol*. 115, 2195–2222. doi: 10.1016/j.clinph.2004.06.001

Millán, J. D., Rupp, R., Müller-Putz, G. R., Murray-Smith, R., Giugliemma, C., Tangermann, M., et al. (2010). Combining brain-computer interfaces and assistive technologies: state-of-the-art and challenges. *Front. Neurosci*. 4:161. doi: 10.3389/fnins.2010.00161

Müller-Dahlhaus, F., and Ziemann, U. (2015). Metaplasticity in human cortex. *Neuroscience* 21, 185–202. doi: 10.1177/1073858414526645

Muthalib, M., Besson, P., Rothwell, J., and Perrey, S. (2017). Focal hemodynamic responses in the stimulated hemisphere during high-definition transcranial direct current stimulation. *Neuromodulation*. doi: 10.1111/ner.12632. [Epub ahead of print].

Nitsche, M. A., and Paulus, W. (2000). Excitability changes induced in the human motor cortex by weak transcranial direct current stimulation. *J. Physiol.* 527(Pt 3), 633–639. doi: 10.1111/j.1469-7793.2000.t01-1-00633.x

Notturno, F., Marzetti, L., Pizzella, V., Uncini, A., and Zappasodi, F. (2014). Local and remote effects of transcranial direct current stimulation on the electrical activity of the motor cortical network. *Hum. Brain Mapp*. 35, 2220–2232. doi: 10.1002/hbm.22322

Opitz, A., Falchier, A., Yan, C.G., Yeagle, E. M., Linn, G. S., Megevand, P., et al. (2016). Spatiotemporal structure of intracranial electric fields induced by transcranial electric stimulation in humans and nonhuman primates. *Sci. Rep*. 6:31236. doi: 10.1038/srep31236

Paulus, W., and Opitz, A. (2013). Ohm's law and tDCS over the centuries. *Clin. Neurophysiol*. 124, 429–430. doi: 10.1016/j.clinph.2012.08.019

Paulus, W., and Rothwell, J. C. (2016). Membrane resistance and shunting inhibition: where biophysics meets state-dependent human neurophysiology. *J. Physiol*. 594, 2719–2728. doi: 10.1113/JP271452

Peña-Gómez, C., Sala-Lonch, R., Junqué, C., Clemente, I. C., Vidal, D., Bargalló, N., et al. (2012). Modulation of large-scale brain networks by transcranial direct current stimulation evidenced by resting-state functional MRI. *Brain Stimul*. 5, 252–263. doi: 10.1016/j.brs.2011.08.006

Pfurtscheller, G., and Lopes da Silva, F. (1999). Event-related EEG/MEG synchronization and desynchronization: basic principles. *Clin. Neurophysiol*. 110, 1842–1857. doi: 10.1016/S1388-2457(99)00141-8

Polanía, R., Nitsche, M. A., and Paulus, W. (2011). Modulating functional connectivity patterns and topological functional organization of the human brain with transcranial direct current stimulation. *Hum. Brain Mapp*. 32, 1236–1249. doi: 10.1002/hbm.21104

Polanía, R., Paulus, W., and Nitsche, M. A. (2012). Modulating cortico-striatal and thalamo-cortical functional connectivity with transcranial direct current stimulation. *Hum. Brain Mapp*. 33, 2499–2508. doi: 10.1002/hbm.21380

Qin, L., and He, B. (2005). A wavelet-based time-frequency analysis approach for classification of motor imagery for brain-computer interface applications. *J. Neural Eng*. 2, 65–72. doi: 10.1088/1741-2560/2/4/001

Qin, L., Ding, L., and He, B. (2004). Motor imagery classification by means of source analysis for brain–computer interface applications. *J. Neural Eng*. 1, 135–141. doi: 10.1088/1741-2560/1/3/002

Reis, J., and Fritsch, B. (2011). Modulation of motor performance and motor learning by transcranial direct current stimulation. *Curr. Opin. Neurol*. 24, 590–596. doi: 10.1097/WCO.0b013e32834c3db0

Reis, J., Schambra, H. M., Cohen, L. G., Buch, E. R., Fritsch, B., Zarahn, E., et al. (2009). Noninvasive cortical stimulation enhances motor skill acquisition over multiple days through an effect on consolidation. *Proc. Natl. Acad. Sci. U.S.A*. 106, 1590–1595. doi: 10.1073/pnas.0805413106

Rizzolatti, G., Luppino, G., and Matelli, M. (1998). The organization of the cortical motor system: new concepts. *Electroencephalogr. Clin. Neurophysiol*. 106, 283–296. doi: 10.1016/S0013-4694(98)00022-4

Roy, A., Baxter, B., and He, B. (2014). High-definition transcranial direct current stimulation induces both acute and persistent changes in broadband cortical synchronization: a simultaneous tDCS-EEG study. *IEEE Trans. Biomed. Eng*. 61, 1967–1978. doi: 10.1109/TBME.2014.2311071

Rushworth, M. F., Johansen-Berg, H., Göbel, S. M., and Devlin, J. T. (2003). The left parietal and premotor cortices: motor attention and selection. *Neuroimage* 20, S89–S100. doi: 10.1016/j.neuroimage.2003.09.011

Rushworth, M. F., Krams, M., and Passingham, R. E. (2001). The attentional role of the left parietal cortex: the distinct lateralization and localization of motor attention in the human brain. *J. Cogn. Neurosci*. 13, 698–710. doi: 10.1162/089892901750363244

Sadleir, R. J., Vannorsdall, T. D., Schretlen, D. J., and Gordon, B. (2010). Transcranial direct current stimulation (tDCS) in a realistic head model. *Neuroimage* 51, 1310–1318. doi: 10.1016/j.neuroimage.2010.03.052

Schalk, G., McFarland, D. J., Hinterberger, T., Birbaumer, N., and Wolpaw, J. R. (2004). BCI2000: a general-purpose brain-computer interface (BCI) system. *IEEE Trans. Biomed. Eng*. 51, 1034–1043. doi: 10.1109/TBME.2004.827072

Scherer, R., and Pfurtscheller, G. (2013). Thought-based interaction with the physical world. *Trends Cogn. Sci*. 17, 490–492. doi: 10.1016/j.tics.2013.08.004

Schneider, T., and Neumaier, A. (2001). Algorithm 808: ARfit—a matlab package for the estimation of parameters and eigenmodes of multivariate autoregressive models. *ACM Trans. Math. Softw*. 27, 58–65. doi: 10.1145/382043.382316

Sehm, B., Schäfer, A., Kipping, J., Margulies, D., Conde, V., Taubert, M., et al. (2012). Dynamic modulation of intrinsic functional connectivity by

transcranial direct current stimulation. *J. Neurophysiol.* 108, 3253–3263. doi: 10.1152/jn.00606.2012

Sellers, E. W., McFarland, D. J., Vaughan, T. M., and Wolpaw, J. R. (2009). "BCIs in the laboratory and at home: the wadsworth research program," in *Brain-Computer Interfaces. The Frontiers Collection*, eds B. Graimann, G. Pfurtscheller, and B. Allison (Berlin; Heidelberg: Springer), 97–111. doi: 10.1007/978-3-642-02091-9_6

Soekadar, S. R., Witkowski, M., Cossio, E. G., Birbaumer, N., and Cohen, L. G. (2014). Learned EEG-based brain self-regulation of motor-related oscillations during application of transcranial electric brain stimulation: feasibility and limitations. *Front. Behav. Neurosci.* 8:93. doi: 10.3389/fnbeh.2014.00093

Soekadar, S. R., Witkowski, M., Cossio, E. G., Birbaumer, N., Robinson, S. E., and Cohen, L. G. (2013). *In vivo* assessment of human brain oscillations during application of transcranial electric currents. *Nat. Commun.* 4:2032. doi: 10.1038/ncomms3032

Stagg, C. J., Best, J. G., Stephenson, M. C., O'Shea, J., Wylezinska, M., Kincses, Z. T., et al. (2009). Polarity-sensitive modulation of cortical neurotransmitters by transcranial stimulation. *J. Neurosci.* 29, 5202–5206. doi: 10.1523/JNEUROSCI.4432-08.2009

Stagg, C. G., and Nitsche, M. A. (2011). Physiological basis of transcranial direct current stimulation. *Neuroscience* 17, 37–53. doi: 10.1177/1073858410386614

Tadel, F., Baillet, S., Mosher, J. C., Pantazis, D., and Leahy, R. M. (2011). Brainstorm: a user-friendly application for MEG/EEG analysis. *Comput. Intell. Neurosci.* 2011:879716. doi: 10.1155/2011/879716

van der Knaap, L. J., and van der Ham, I. J. M. (2011). How does the corpus callosum mediate interhemispheric transfer? a review. *Behav. Brain Res.* 223, 211–221. doi: 10.1016/j.bbr.2011.04.018

Wolpaw, J. R., McFarland, D. J., Neat, G. W., and Forneris, C. A. (1991). An EEG-based brain-computer interface for cursor control. *Electroencephalogr. Clin. Neurophysiol.* 78, 252–259. doi: 10.1016/0013-4694(91)90040-B

Yuan, H., and He, B. (2014). Brain-computer interfaces using sensorimotor rhythms: current state and future perspectives. *IEEE Trans. Biomed. Eng.* 61, 1425–1435. doi: 10.1109/TBME.2014.2312397

Yuan, H., Doud, A., Gururajan, A., and He, B. (2008). Cortical imaging of event-related (de)synchronization during online control of brain-computer interface using minimum-norm estimates in frequency domain. *IEEE Trans. Neural Syst. Rehabil. Eng.* 16, 425–431. doi: 10.1109/TNSRE.2008.2003384

Zaehle, T., Sandmann, P., Thorne, J. D., Jäncke, L., and Herrmann, C. S. (2011). Transcranial direct current stimulation of the prefrontal cortex modulates working memory performance: combined behavioural and electrophysiological evidence. *BMC Neurosci.* 12:2. doi: 10.1186/1471-2202-12-2

Conflict of Interest Statement: The authors declare that the research was conducted in the absence of any commercial or financial relationships that could be construed as a potential conflict of interest.

frontiers in Neuroscience

ORIGINAL RESEARCH
published: 11 January 2018
doi: 10.3389/fnins.2017.00748

Conductive Hydrogel Electrodes for Delivery of Long-Term High Frequency Pulses

Naomi A. Staples[1†], Josef A. Goding[1,2†], Aaron D. Gilmour[1], Kirill Y. Aristovich[3], Phillip Byrnes-Preston[1], David S. Holder[3], John W. Morley[4,5], Nigel H. Lovell[1], Daniel J. Chew[6] and Rylie A. Green[1,2]*

[1] Graduate School of Biomedical Engineering, University of New South Wales, Sydney, NSW, Australia, [2] Department of Bioengineering, Imperial College London, London, United Kingdom, [3] Medical Physics and Biomedical Engineering, University College London, London, United Kingdom, [4] School of Medical Science, University of New South Wales, Sydney, NSW, Australia, [5] School of Medicine, Western Sydney University, Sydney, NSW, Australia, [6] Galvani Bioelectronics, Stevenage, United Kingdom

Nerve block waveforms require the passage of large amounts of electrical energy at the neural interface for extended periods of time. It is desirable that such waveforms be applied chronically, consistent with the treatment of protracted immune conditions, however current metal electrode technologies are limited in their capacity to safely deliver ongoing stable blocking waveforms. Conductive hydrogel (CH) electrode coatings have been shown to improve the performance of conventional bionic devices, which use considerably lower amounts of energy than conventional metal electrodes to replace or augment sensory neuron function. In this study the application of CH materials was explored, using both a commercially available platinum iridium (PtIr) cuff electrode array and a novel low-cost stainless steel (SS) electrode array. The CH was able to significantly increase the electrochemical performance of both array types. The SS electrode coated with the CH was shown to be stable under continuous delivery of 2 mA square pulse waveforms at 40,000 Hz for 42 days. CH coatings have been shown as a beneficial electrode material compatible with long-term delivery of high current, high energy waveforms.

Keywords: conductive hydrogel, high frequency stimulation, nerve block, neural interfaces, peripheral nerve cuff array

OPEN ACCESS

Edited by:
Mikhail Lebedev,
Duke University, United States

Reviewed by:
Liang Guo,
The Ohio State University, United States
Kevin J. Otto,
University of Florida, United States

****Correspondence:***
Rylie A. Green
rylie.green@imperial.ac.uk

† Joint first authors.

Specialty section:
This article was submitted to Neural Technology, a section of the journal Frontiers in Neuroscience

Received: *16 October 2017*
Accepted: *22 December 2017*
Published: *11 January 2018*

Citation:
Staples NA, Goding JA, Gilmour AD, Aristovich KY, Byrnes-Preston P, Holder DS, Morley JW, Lovell NH, Chew DJ and Green RA (2018) Conductive Hydrogel Electrodes for Delivery of Long-Term High Frequency Pulses. Front. Neurosci. 11:748. doi: 10.3389/fnins.2017.00748

INTRODUCTION

Recent studies have indicated that electrical therapies, in particular nerve block, may be an effective treatment for chronic conditions such as inflammatory bowel disease, arthritis, asthma, and diabetes (Famm et al., 2013; Birmingham et al., 2014; Langdale et al., 2017). These are disease states where current pharmaceutical approaches have been effective with a large number of patients, but in patients with persistent, non-responsive or resistant cases, treatment options are limited. Recent efforts have therefore focused on engineering a device capable of delivering a flexible range of stimulation, recording and nerve block paradigms for application to the peripheral nervous system (PNS). Such a device is expected to be necessary for tuning system requirements to peripheral nerve fibers within a fascicle and ensuring the health of off-target tissues both adjacent to the device and within, but distal to the neural branch being targeted (for example, organs that are innervated by

the same nerve but not the therapeutic target). While hardware specification, neuromodulation techniques, and biological mapping of visceral nerves are key areas that must be developed, an interfacing device, capable of fitting the many variable and non-uniform fibers of the PNS must also be designed. As specified by Birmingham et al. (2014), new materials and architectures are required to address the largely unmyelinated nerve fibers, irregular neuroanatomy, and movement in the viscera.

Critical to neuromodulator devices is the electrode array, used to interface with and control spatially selective activity within a nerve. To achieve control of a physiological process through nerve modulation within the PNS, it is essential to steer electrical current toward the correct nerve fiber(s) (Lovell et al., 2010). Nerves within the PNS consist of both afferent and efferent fibers that extend to innervate the organs of the body. Afferent fibers carry signals toward the brain, while efferent fibers take signals from the brain to the various peripheral organs and muscles. In an application where organ control is required, such as asthma or diabetes, it is necessary to target the efferent neurons. As most neuro-immune pathways and organ systems are closed-loop, they are reliant on a balance of both afferent inputs and efferent outputs (Pavlov and Tracey, 2017). Inadvertent blocking of the afferent nerves may result in an undesirable/inappropriate response from the brain, ultimately exacerbating the condition being treated. As such, it is critical that an electrode array used for nerve block, can deliver modulating signals to specific areas within the nerve across chronic time frames. One of the most significant challenges to development of such an array, is the need to create a stable electrode-neural interface where the capacity to deliver appropriate and targeted signals does not change over time (Guo, 2016).

A number of electrode array formats have been investigated for application to the PNS, and these are broadly categorized as penetrating and non-penetrating arrays. Penetrating arrays have been shown to be beneficial for spatially selective activation of nerve fibers, being placed within the nerve bundle, beneath the perineurium, and hence closer to the target tissues (Lago et al., 2007; Boretius et al., 2010; Wark et al., 2013). Intrafasicular arrays are specifically designed to sit within the nerve fascicle. However, damage to the perineurium during implantation has been associated with a number of negative consequences, including increased endoneurial pressure, nerve fiber compression, and loss of nerve fibers (Grill et al., 2009). As the neural wound attempts to recover, the chronic presence of a stiff device comprised of foreign material within the nerve, results in growth of fibrous scar tissue that can isolate the electrode arrays and negate the benefit of proximity (Bowman and Erickson, 1985; Zheng et al., 2008). Conversely non-penetrating or cuff arrays, are designed to wrap around the nerve, minimizing damage to the native tissue, but inherently having less spatial selectivity for targeting specific nerve fibers (Tyler and Durand, 2002; Grill et al., 2009). Regardless of the format, these devices are commonly fabricated from conventional electrode array materials, with metallic contacts embedded in polymeric insulators. Some newer approaches based on carbon fibers have been designed to be more flexible, lower profile and biocompatible (Gillis et al., 2017), but the long term *in vivo* performance of these fibers remains unknown.

There are two significant challenges associated with interfacing an electrode array with the visceral nerves of the PNS, one is mechanical and the other is electrical. Regardless of format and placement, there is an inherent mechanical mismatch in the interaction of a relatively stiff electrode array with soft nervous tissues (Green et al., 2008; Grill et al., 2009; Guo, 2016). This mismatch is exacerbated by the substantial displacements of PNS nerve fibers associated with human movement, and can result not only in dislocation of the device but associated damage to the surrounding neural tissue (Grill et al., 2009; Birmingham et al., 2014). Damage and the presence of foreign materials generate inflammatory reactions that lead to fibrous encapsulation of a device. Both the movement of the array and scar tissue encapsulation have resulting impacts on the electrical properties of the neural interface, making spatially selective neuromodulation difficult and unstable over time. The increase in distance between the device and target nerves ultimately leads to the need for application of higher currents to achieve a therapeutic response, at which point, conventional metal electrodes can suffer from electrically-mediated corrosion. This occurs due to high voltages being generated at the electrode-neural interface that cause adverse chemical reactions (including the generation of gases, H^+ ions, and metal redox reactions that result in dissolution). While nerve block waveforms are expected to be in the high frequency range of neuromodulation and the short pulse durations minimizes the time for which a given current is applied and thus a chemical reaction can propagate, the usual techniques for preventing electrical imbalances in the system are not effective. For example, sensory neuroprosthetics often use in line capacitors to block DC currents from being transduced from device to tissue (Cogan et al., 2016b). An alternative approach is to short the electrodes in the array together between stimuli (Wong et al., 2009; Cogan et al., 2016b). Both of these techniques enable the device and tissue to maintain zero net charge and arrest any chemical reactions that may be present. However, at high frequency blocking capacitors are not effective (as they behave as a short rather than open circuit) and there is no interstimulus delay in which to equilibrate the system. As such chronic application of high frequency signals involving nerve block currents can lead to electrode damage and failure where charge balance is not perfectly preserved. This is of particular risk for metallic electrodes where the voltage produced at the interface is high and localized defects in the metal surface can initiate areas of charge imbalance and corrosion.

Conductive hydrogels (CHs) have been shown to be an effective material for mediating the mechanical properties of an electrode and simultaneously improving the electrical properties. CHs are a hybrid material produced from a conductive polymer (CP) and a hydrogel, with a mechanical modulus more than three orders of magnitude below that of platinum (Pt), a conventional bioelectrode material (Green et al., 2012b; Goding et al., 2017). Due to the presence of the hydrogel component, CHs swell in aqueous environments, enabling ingress of ions and forming a three dimensional surface through which charge is transduced. The substantially higher charge transfer area introduced by the

CH enables coated electrodes to inject greater amounts of charge at lower voltage than their uncoated metallic counterparts and hence enable devices with low power consumption (Kim et al., 2004; Sekine et al., 2010; Pan et al., 2012; Hassarati et al., 2014, 2016). In prior studies by Hassarati et al. (2014) it was shown that CH coatings on cochlear implants imparted a reduction in potential transient of over 50% and maintained more stable electrical properties over a simulated 2 years of activity (two billion stimuli delivered continuously over 3 months in artificial perilymph). However, the capacity of these materials to deliver continuous high frequency pulses with relatively large amplitudes (mA as compared to prior studies with μA) is not known. Due to the efficiency in charge transfer of these materials, and their polymeric nature which imparts high electrochemical stability, it was proposed that CH coatings can provide a low voltage interface for delivery of a neural block. It was hypothesized that CH coatings could be used to provide stable, long-term performance of PNS nerve cuffs under high frequency stimulation.

While CH coatings have been routinely applied to Pt or platinum/iridium (PtIr) electrodes used in sensory stimulating neuroprosthetics, it was recognized that by changing the material that interfaces with the neural tissue, it may not be necessary to use a conventional electrode material as the substrate. Stainless steel (SS) has a history in implantable electrodes for recording and also macroelectrodes in cardiac pacing (Bowman and Erickson, 1985; Peixoto et al., 2009; Cogan et al., 2016a), however it is not commonly used in implantable neuroprosthetics. Recent studies by Aristovich et al. (2016) have demonstrated that these arrays are capable of delivering high frequency signals (>1.7 kHz) required for imaging neural activity by electrical impedance tomography (EIT). As an alternate and low-cost platform, SS electrode arrays were compared in this study to commercially available PtIr arrays for delivery of high frequency neural blocking waveforms, both with and without CH coatings. Both arrays types were non-penetrating cuffs, designed to wrap the nerve bundle without penetrating the fascicle. The commercial array was a two electrode pre-curled design, intended to facilitate easy placement around a nerve. The SS array was fabricated in a planar format with increased electrode density and resolution (30 electrode sites), designed for controlled current steering. These arrays were characterized before and after coating for charge transfer properties including maximum cathodic charge injection limit. An *in vitro* high frequency study was undertaken to establish the long term performance and robustness of each of the electrode types.

METHODS

Conductive Hydrogel Fabrication

All conductive hydrogel coatings were fabricated from the same material components, however modification of protocol was required to tailor application to different array formats. All materials and reagents were obtained from SigmaAldrich unless otherwise stated.

The coating procedure was in line with prior literature on macroelectrodes and probe formats (Green et al., 2012b; Hassarati et al., 2014; Goding et al., 2017). This requires a three step protocol consisting of a pre-layer to improve coating adhesion to the underlying electrodes, formation of the non-conductive hydrogel layer and the polymerization of the CP component within the hydrogel to impart conductivity at the electrode sites.

The PEDOT/pTS prelayer was electrodeposited from a solution of 100 mM 3,4-ethylenedioxythiophene (EDOT) and 50 mM sodium p-toluenesulfonate dissolved in 1:1 deionized (DI) water (Baxter Healthcare Pty Ltd.)-acetonitrile solution. The hydrogel macromer solution consisted of 20 wt% poly(vinyl alcohol)-methacrylate-taurine (PVA-taurine) and 0.1 wt% Irgacure® 2959 dissolved in deionized (DI) water. PVA-taurine was synthesized in-house as described previously (Goding et al., 2017). The final step to produce a CH was electrodeposition from a CP solution of 30 mM EDOT and 0.3 mM NaCl dissolved in DI water.

Coating of Pre-curled Commercial Arrays

Commercial cuffs were purchased from Cortec Gmbh. Each cuff consisted of 2 electrode sites, where each electrode was formed by 2 connected pads being 0.7 × 1.15 mm each. The internal diameter of the pre-curled cuff was 1 mm. Cuff electrodes were immersed in PEDOT/pTS prelayer solution in a 2-electrode cell. A thin layer of PEDOT/pTS was galvanostatically deposited onto the PtIr electrodes using 1 mA/cm^2 for 30 s and then rinsed with deionized (DI) water.

The hydrogel coating was applied by injecting 30 μL of hydrogel precursor into an opened cuff prior to closing the cuff around a glass capillary with a 0.7 mm outer diameter. Hydrogel was formed via photopolymerization using 30 mW/cm^2 UV light for 180 s. The coated cuffs were soaked in DI water for 2 min prior to the removal of the glass capillary.

Finally, PEDOT was electrochemically deposited through the PVA-taurine coating immediately after photopolymerization. The coated cuff electrodes were immersed in CH deposition solution in a 2 electrode cell. PEDOT was galvanostatically deposited using 1 mA/cm^2 for 10 min and then rinsed with DI water.

Coating of Planar SS Arrays

Planar electrode arrays were fabricated from 313 L stainless steel with polydimethylsiloxane insulation. The electrode sites were 0.35 × 3 mm. These arrays were cleaned prior to coating, to remove oxides and residual debris from fabrication. The arrays were immersed in 1 M HCl for 2 min, and then sonicated in DI water for 5 min. This process was repeated prior to electrodeposition of the pre-layer. A thin layer of PEDOT/pTS was galvanostatically deposited onto the stainless steel (SS) electrodes using 1.5 mA/cm^2 for 30 s and then rinsed with DI water.

The hydrogel coating was applied by pipetting 30 μL of hydrogel precursor onto the flat cuff. A coverslip was then used to push the solution into the recesses formed by the silicone insulation bordering the electrode sites. Excess macromer solution was removed from the surface of the array. The hydrogel

was crosslinked via photopolymerization using 30 mW/cm^2 UV light for 180 s.

Finally, PEDOT was electrochemically deposited through the PVA-taurine immediately after photopolymerization. The coated cuff electrodes were immersed in an aqueous 0.1 M EDOT solution in a 2 electrode cell. Ten electrode sites were shorted together to enable electrodeposition of multiple sites in parallel. PEDOT was galvanostatically deposited using 1 mA/cm^2 for 10 min and then rinsed with DI water.

Electrochemical Characterization

EIS was conducted using an eDAQ Electrochemical Impedance Analyzer (Z100) in conjunction with an eDAQ Potentiostat (EA163) controlled with the use of Z100 Navigator Software (WonATech Co. Ltd.). Recordings were made using an isolated, leakless Ag/AgCl reference electrode and a platinum wire counter electrode. Measurements were made in 0.9 wt% saline (Baxter Healthcare Pty Ltd.). CH coatings were subjected to a 70 mV sinusoidal voltage amplitude across a frequency range of 10,000 to 1 Hz with a 0 V DC offset voltage.

CV was conducted using an eDAQ e-corder (ED410) in conjunction with an eDAQ Potentiostat (EA163) controlled with the use of EChem software package. Recordings were made in a three electrode cell using an isolated Ag/AgCl reference electrode and a platinum wire counter electrode. Samples were subjected to a cyclical stimulation voltage from −800 to 600 mV at a scan rate of 150 mV/s in 0.9 wt% saline, taking the integral of the 10th cycle to calculate the charge storage capacity (CSC).

Charge Injection Limit

Charge injection comparison was performed in a three electrode cell identical to CV and EIS. Charge injection limit was determined using protocols previously established by Cogan et al. (2005). The limit was defined as the voltage required to reach the reduction potential for water. An in-house biphasic stimulator was used to deliver constant current, charge balanced pulses. Phase length was varied from 0.01 to 0.8 ms, based on standards from the prior literature (Cogan et al., 2005; Green et al., 2014) and also the need to characterize for high frequency stimulation behavior, which is best modeled by short phase length waveforms. The current was increased until the residual interphase voltage (E_{mc}) reached −600 mV vs. Ag/AgCl (see Green et al., 2014 for definition and schematics of E_{mc} relative to the applied biphasic waveform). The charge delivered across a single phase at this point was regarded as the charge injection limit.

Long-Term Delivery of High Frequency Pulses

High frequency stimulation was performed by application of continuous square pulses (charge balanced and net zero DC bias) to electrode pairs in saline. The system used for high frequency stimulation was a custom-built unit comprising an arbitrary waveform charge balance current source (Howland CCS) capable of delivering sine or square waves via four isolated stimulators. The pulse frequency was set to 40 kHz with a peak-to-peak amplitude of 2 mA (1 mA in the positive phase and 1 mA in the negative phase). The total voltage across electrode pairs was monitored daily for the first 2 weeks and then at least twice weekly to ensure there was no drift or DC leakage. Total voltage was defined as the addition of maximum positive and negative voltage (peak to peak voltage). The net voltage (difference between absolute negative and positive voltage) was used as an indicator of imbalance or drift in the waveform. On a weekly basis, electrodes were removed from the high frequency stimulation and characterized using CV and EIS metrics (as detailed in the above protocols). Any changes in performance or appearance of electrodes was recorded and examined where necessary.

RESULTS

CH coatings were applied to both pre-curled and planar electrode arrays, as depicted in **Figure 1**. Due to the different formats, the pre-curled PtIr array was coated such that the entire inner (tissue contacting) surface was coated with a thin layer of PVA hydrogel (∼100 μm). Subsequent electrodeposition of PEDOT resulted in conductive polymer growing in the discrete areas directly above the electrode sites. Parameters were controlled such that PEDOT was not grown beyond the electrode site boundaries, hence preventing bridging between electrodes. This contrasted to the planar array where the recessed electrode sites were filled with PVA hydrogel and subsequently PEDOT growth throughout this hydrogel layer (∼50 μm). In this application the PEDOT is prevented from growing between electrodes as the hydrogel boundaries contain the conductive polymer growth.

Electrochemical Characterization

Electrochemical analysis of each of these arrays was conducted prior to and after coating. The CV curves were integrated to yield CSC, as shown in **Figure 2**. The SS was found to have a CSC more than one order of magnitude lower than PtIr (0.48 mC/cm^2 compared to 5.70 mC/cm^2). The CH coating on the PtIr similarly had a significantly higher CSC (student t-test, $p < 0.05$) than that on the SS, although the difference was substantially lower (not an order of magnitude). The CH coated SS had an average CSC of 85 mC/cm^2 and the CH coated PtIr was recorded as having an average CSC of 212 mC/cm^2. Both CH coatings improved charge transfer by at least two orders of magnitude on their respective substrates.

EIS verified that similar electrochemical performance was observed when using frequency dependant analyses. As depicted in **Figure 3**, SS had a significantly higher impedance at low frequency (around 2 MΩ @ 1 Hz) compared to the PtIr (average of 89 kΩ @ 1 Hz). However, these electrodes do differ in size, and when normalized for geometric charge transfer area have an average impedance of 24.9 and 1.5 kΩ.cm^2 at 1 Hz for SS and PtIr respectively. As frequency is increased the impedance of the SS electrodes decreased to 85.6 Ω.cm^2 at 1 kHz and 14.1 Ω.cm^2 at 10 kHz. Comparatively the PtIr impedance decreases to 11.8 Ω.cm^2 at 1 kHz and further reduced to 9.8 Ω.cm^2 at 10 kHz. It is clearly seen that the SS has a different electrochemical behavior to the PtIr, with capacitive behavior dominating across the entire frequency spectrum. SS has been reported in prior

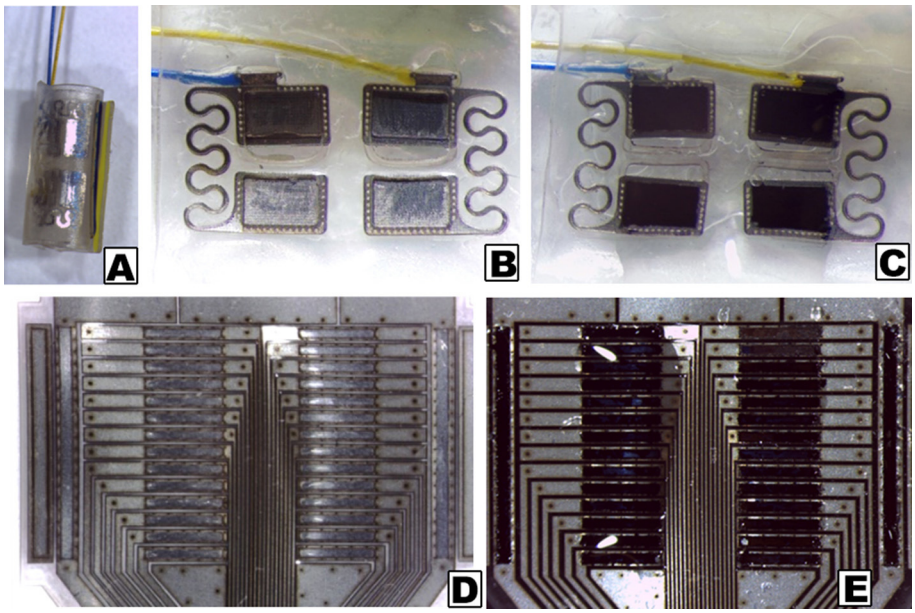

FIGURE 1 | Stereoscopic images of electrode arrays, as received and with CH coatings. **(A)** Pre-curled commercial cuff array; **(B)** Opened cuff showing PtIr electrode sites without coating; **(C)** Opened cuff with CH coating on PtIr electrode sites; **(D)** Uncoated planar SS array; **(E)** CH coated planar SS array.

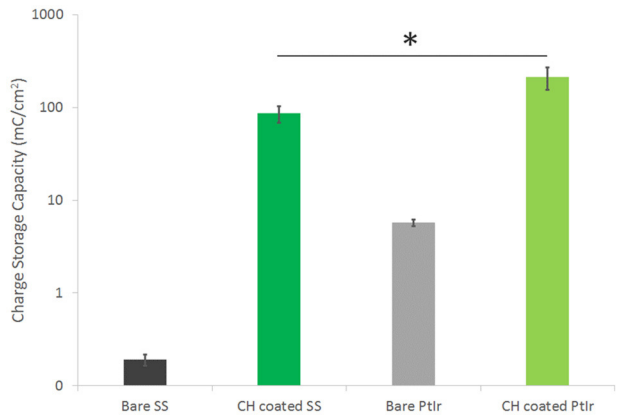

FIGURE 2 | CSC of SS and PtIr electrode arrays before and after CH coating. Error bars are 1 *SD*, $^*p < 0.05$, ($n = 8$). Note log scale on y-axis required to enable SS data to be visualized.

studies as having variable EIS response that is dependent on both degree of passivation and alloy content (Wallinder et al., 1998).

When these arrays were coated with the CH the SS coated arrays experienced an average impedance magnitude of 865 Ω (9.1 Ω.cm^2) at 1 Hz, reducing to 312 Ω (3.3 Ω.cm^2) at 10 kHz. The CH coated PtIr recorded an average impedance magnitude of 497 Ω (8.0 Ω.cm^2) at 1 Hz, reducing to 346 Ω (5.7 Ω.cm^2) at 10 kHz. As such there was no significant difference in frequency dependant impedance performance of the CH on PtIr in comparison to CH on SS. Both arrays experienced significant reductions in impedance compared to their uncoated control arrays across all frequencies, including the high frequency range in which neuromodulation by blocking is expected to be performed (Famm et al., 2013).

Charge Injection Limit

Charge injection limit studies were performed in saline to establish a maximum current that can be passed by each electrode material before electrochemical reactions associated with irreversible Faradaic reactions are enabled. It should be noted that this characterization technique is based on biphasic stimulation and involves the measurement of residual voltage at the electrode interface between cathodic and anodic pulses. As such it is not directly applicable to high frequency nerve block paradigms, however it does provide a metric for comparison related to application of neuromodulation devices, and will also provide guidance on the relative impacts of DC leakage current or drift in the applied nerve blocking waveform. The prior electrochemical analyses are not as well aligned with in-use electrode performance, being related to application of ramped voltage across long time courses (for CV) and application of a wide range of stimulation frequencies (for EIS). As shown in **Figure 4**, CH coatings were able to substantially improve the electrochemical charge injection limit of both electrode types. As with other metrics, it can be seen that the SS arrays are not able to inject levels of charge commensurate with the PtIr at longer phase lengths, until they are coated with the CH. While it is clear that the CH coated SS has the highest charge injection limit at higher phase lengths, the short phase length is most applicable to high frequency stimulations. A 40 kHz square wave has an effective phase length of 0.025 ms. Using this short phase length the CH coated PtIr has an injection limit of 15.8 ± 1.8 μC/cm^2 and the CH coated SS has an injection limit of 13.5 ± 5.1 μC/cm^2. The

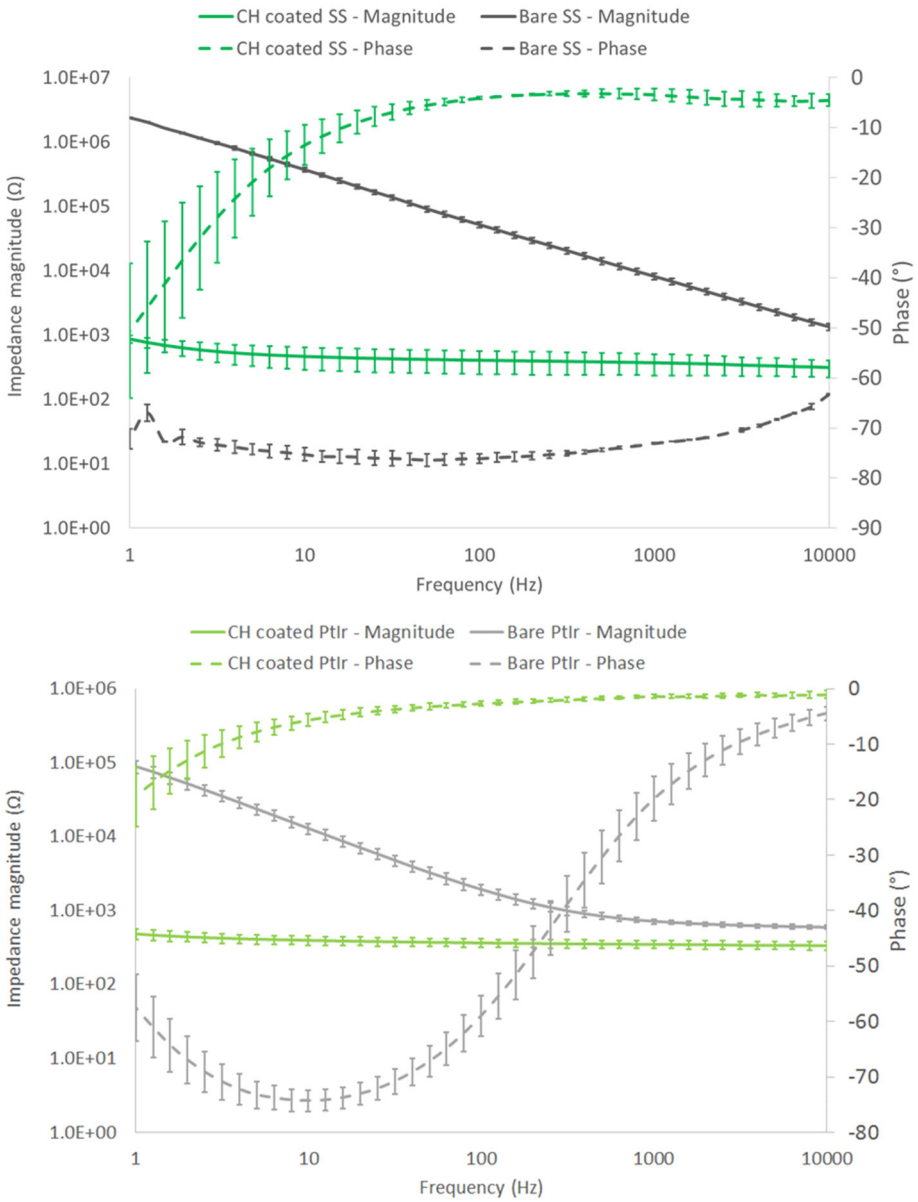

FIGURE 3 | Frequency dependant response of SS **(top)** and PtIr **(bottom)** nerve cuff electrode arrays. Both bare and CH coated arrays are characterized. Error bars are 1 SD, ($n = 8$).

uncoated controls have injection limits of 4.1 ± 0.1 μC/cm^2 for the PtIr and 2.4 ± 0.3 μC/cm^2 for the uncoated SS.

Long-Term Delivery of High Frequency Pulses

CH coating of electrodes was successful and able to improve charge transfer characteristics of arrays irrespective of underlying material type, however the stability and robustness of the system is critical for application in implantable bioelectronics. To understand the operational lifetime and limitations of coated electrodes an *in vitro* test was designed. This assay was based on prior studies that used continuous high frequency stimulation as an accelerated electrical test for coatings on cochlear implants and planar bionic eye electrode arrays (Green et al., 2012a; Hassarati et al., 2014). Due to the restricted channel numbers on the stimulator the commercial arrays and planar arrays were tested in separate studies. The commercial PtIr cuffs were found to have limitations when exposed to continuous high frequency electrical pulses. Initially the bare PtIr electrodes produced an average peak-to-peak voltage of 980 mV and the CH coated PtIr produced an average of 720 mV. However, with continuous stimulation both bare PtIr and CH coated PtIr were found to experience large increases in peak-to-peak voltage, as seen in **Figure 5**. Inspection of these electrodes revealed that failure

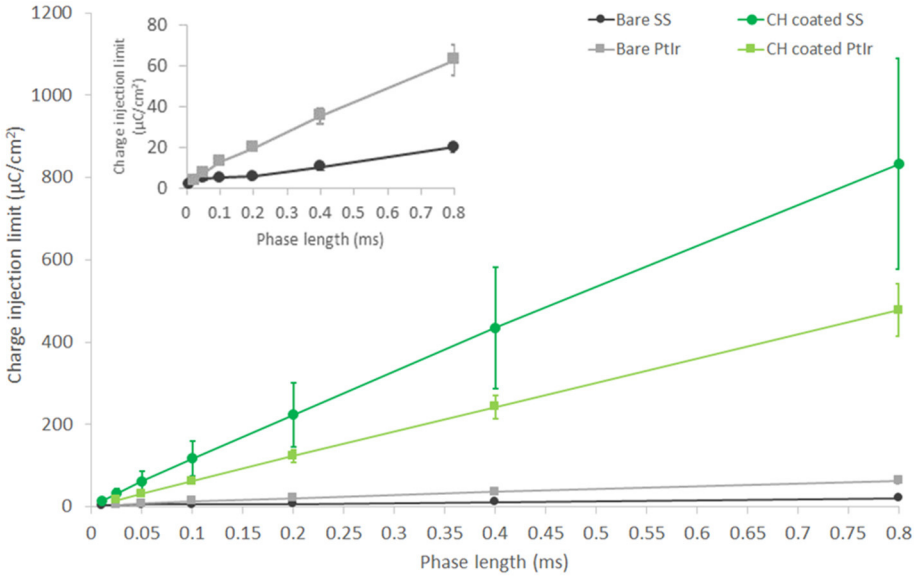

FIGURE 4 | Charge injection limit for both PtIr and SS nerve cuff arrays, bare, and with CH coatings. Inset figure shows charge injection behavior of bare PtIr and SS at short phase lengths. Performed in saline. Error bars are 1SD ($n = 8$).

was occurring at the connection where the wire was bonded to the electrode pad (see **Figure 6**). It should be noted that these commercial cuffs are designed for recording peripheral nerve activity, and as such this application is outside of their typical specification for use. Further investigation revealed that limited cohesion between both the PtIr electrode sites and the laminated silicone insulation led to fluid ingress around the bonding sites, as depicted in **Figure 7**. Due the presence of dissimilar metals and an ionic fluid environment, it is not surprising that some chemical corrosion was able to propagate. Where wire corrosion resulted in high voltage at the bonding point it was found that formation of gas beneath the CH coating resulted in delamination of this material. For both coated and uncoated arrays 2 of the 3 samples failed prior to 14 days and as such this study was not continued on this array format.

In comparison the SS cuffs were found to have greater stability, although the connections for this array were significantly more distant from the electrode sites and were not immersed in the saline electrolyte. The total potential transient on the CH coated arrays was stably maintained over the 42 day study period at a value that was 33% lower than that of the uncoated controls (**Figure 8**).

The electrochemical characteristics of these electrodes were monitored weekly. As shown in **Figure 9**, there was no significant change in CSC across the 42 day testing period for either electrode type following initial conditioning. The SS arrays experienced a significant increase in CSC across the first 7 days of ∼50%. Following this initial change ongoing electroactivity was stable. The CH coated SS electrodes were found to have a slow reduction in CSC across the entire study period, a behavior that has been previously reported for CP based coating materials (Green et al., 2013; Hassarati et al., 2014). The loss of electroactivity by the end of the study was an average of 30% of the initial CSC. This reduction is known to plateau as mobile ions, CP backbone and hydrogel chains within the system reach an equilibrium state (Yamato et al., 1995; Green et al., 2009, 2010). The change in CSC was not expected to be the result of the high frequency stimulation and this was reflected in the electroactivity of the passive controls. At the conclusion of the study passive CH coated controls were found to have an average CSC of 63.23 $\pm$ 8.17 mC/cm^2, compared to the stimulated arrays with a final CSC of 60.04 $\pm$ 10.32 mC/cm^2. Similarly passive SS electrodes were found to have a CSC of 0.23 $\pm$ 0.02 mC/cm^2 at 42 days, compared to the stimulated electrodes with a final CSC of 0.29 $\pm$ 0.09 mC/cm^2.

EIS results depicted in **Figure 10** reflect the same trend seen for the CV, with SS showing a substantial drop in impedance within the first 7 days, followed by continuous stable performance across the remainder of the study. The CH retains a stable EIS response, with a higher resolution image of the impedance magnitude seen in **Figure 11**. There is no significant difference in impedance across the study period and error bars are not shown in **Figure 10**, as they confound visualization of the data. One standard deviation was on average $\pm$ 100 Ω across all frequencies for the CH coated SS. Passive controls for both the SS and CH coated SS demonstrate that unstimulated controls performed similarly to the stimulated electrodes across this period. As such it is unlikely that the high frequency stimulation imparted any significant changes to either material. Finally, the electrode arrays were imaged at the conclusion of the study to establish cohesion of coating and any visible changes in electrode appearance. Neither electrode type was found to have notable changes (images not shown, no discernable difference to **Figure 1**).

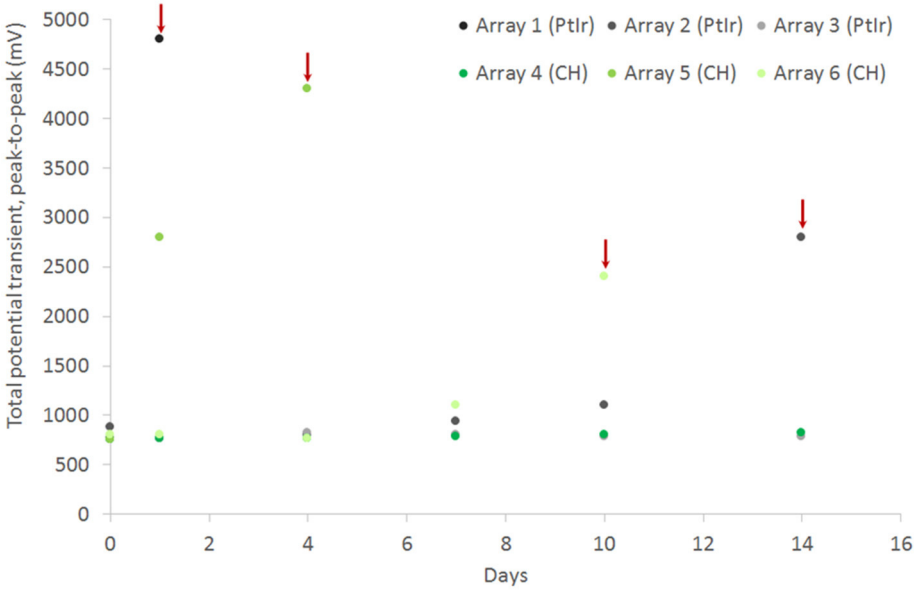

FIGURE 5 | Total voltage drop across commercial PtIr electrode pairs under continuous high frequency stimulation, comparing performance for both bare electrodes and CH coated electrodes. Red arrow indicate an electrode pair that is considered to have failed due to sudden increase in potential transient.

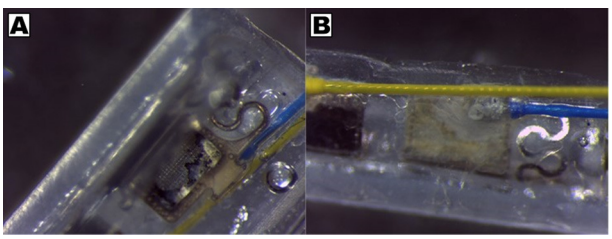

FIGURE 6 | Corrosion of wire and pad connections on PtIr pre-curled cuff arrays, showing **(A)** delamination of CH coating and **(B)** presence of discolored precipitate at bonding point on back of electrode sites.

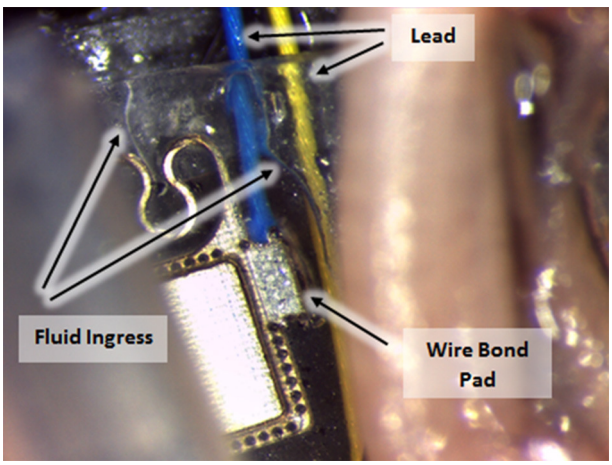

FIGURE 7 | Fluid ingress to commercial cuff connection points, enabling corrosion with continuous electrical stimulation.

DISCUSSION

CH coatings were shown to improve the performance of electrodes irrespective of the underlying metallic substrate. Both PtIr and SS electrodes were coated with a CH comprising the CP PEDOT and the hydrogel PVA-taurine. Despite these electrode arrays having significantly different initial properties, it was shown that the CH coating resulted in comparable electrochemical properties across both array types for a range of properties including CSC, impedance and charge injection limit. The electrode array format was shown to impact on both the electrochemical properties and device stability. The SS arrays were found to be stable under long-term high frequency stimulation and in particular maintained low impedance and high charge storage capacity when coated with the CH.

The majority of past studies into CH coated electrodes have been undertaken using Pt electrodes as the underlying substrate. It is feasible that the interaction between the CH coating and the underlying substrate may influence the electrochemical properties of the resultant electrode. CP coatings and hydrogel coatings have been applied to SS across a range of implants (Meng et al., 2009; Peixoto et al., 2009; Joung et al., 2012), however they are not commonly used in stimulating neuroprosthetics where CH coatings have been focused. In fact, much of the prior literature that encompasses hydrogel application to SS has been focused on imparting bioactivity to orthopedic implants and cardiovascular stents (Meng et al., 2009; Joung et al., 2012). In these applications chemical approaches have been used to covalently link coatings to SS or alternately the hydrogel used has been a degradable component employed for controlled drug

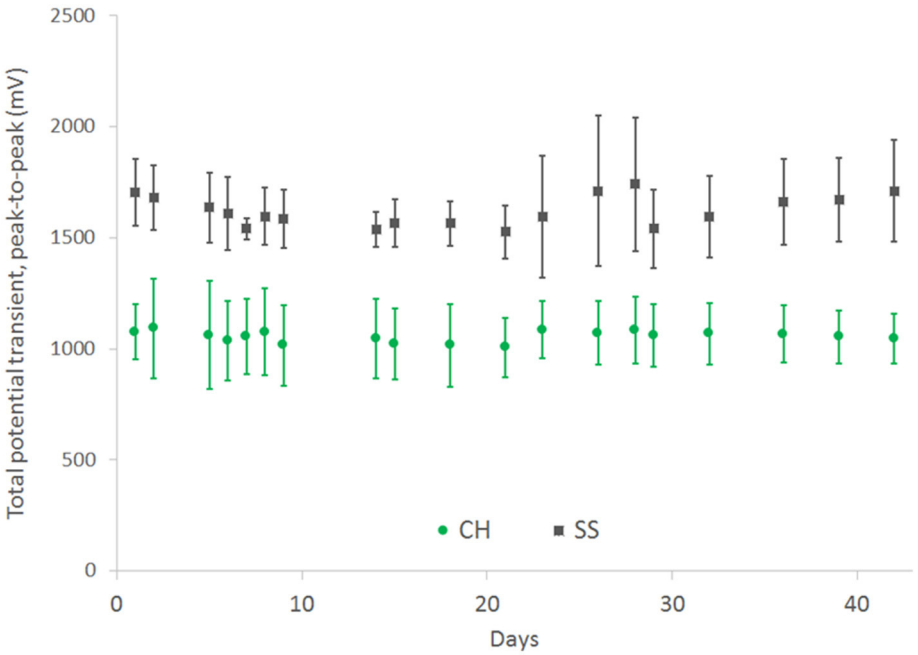

FIGURE 8 | Total voltage drop across SS electrode pairs under continuous high frequency stimulation, comparing performance for both bare electrodes and CH coated electrodes. Error bars are 1 SD ($n = 4$).

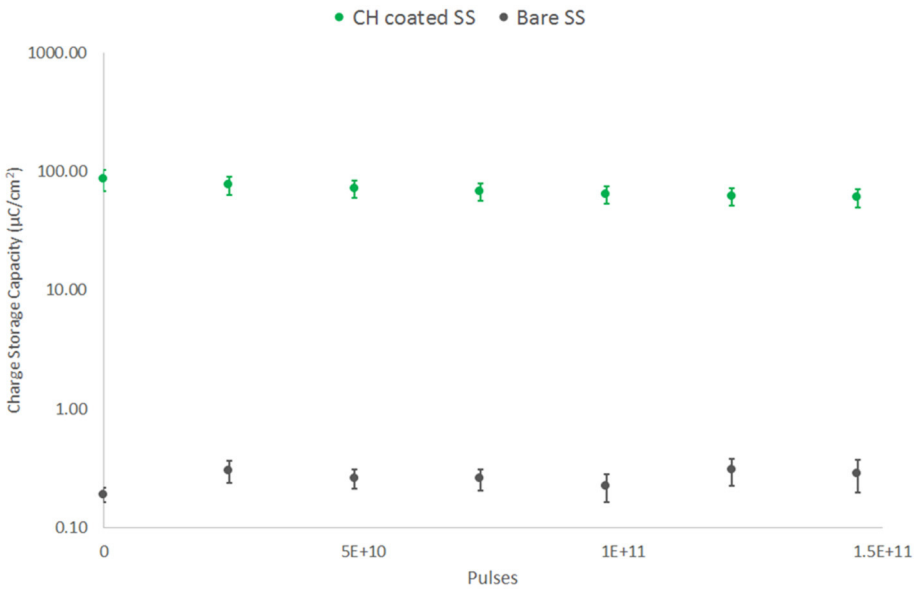

FIGURE 9 | CSC of SS electrodes under high frequency stimulation (40 kHz, 2 mA peak-to-peak). Comparison of CH coated SS and bare SS electrodes over 42 days or 150 billion pulses ($n = 8$).

elution. In this study, the electrochemically grown CP is used to anchor the coating to the implant electrodes. This forms an ionic association and mechanical interaction between the electrode and coating, but there is no covalent chemical bond. Nucleation of the CP at the electrode surface during polymerization will be critical to both electrochemical properties and long-term stability of the CH material (Arteaga et al., 2013; Patton et al., 2015, 2016). For the SS electrode array the cleaning protocol of repeat acid immersions and sonication was critical to reducing passivation and enabling CP deposition on these electrodes. Storage of the arrays within an oxygen accessible environment following cleaning, but prior to coating with the CP prelayer reduced

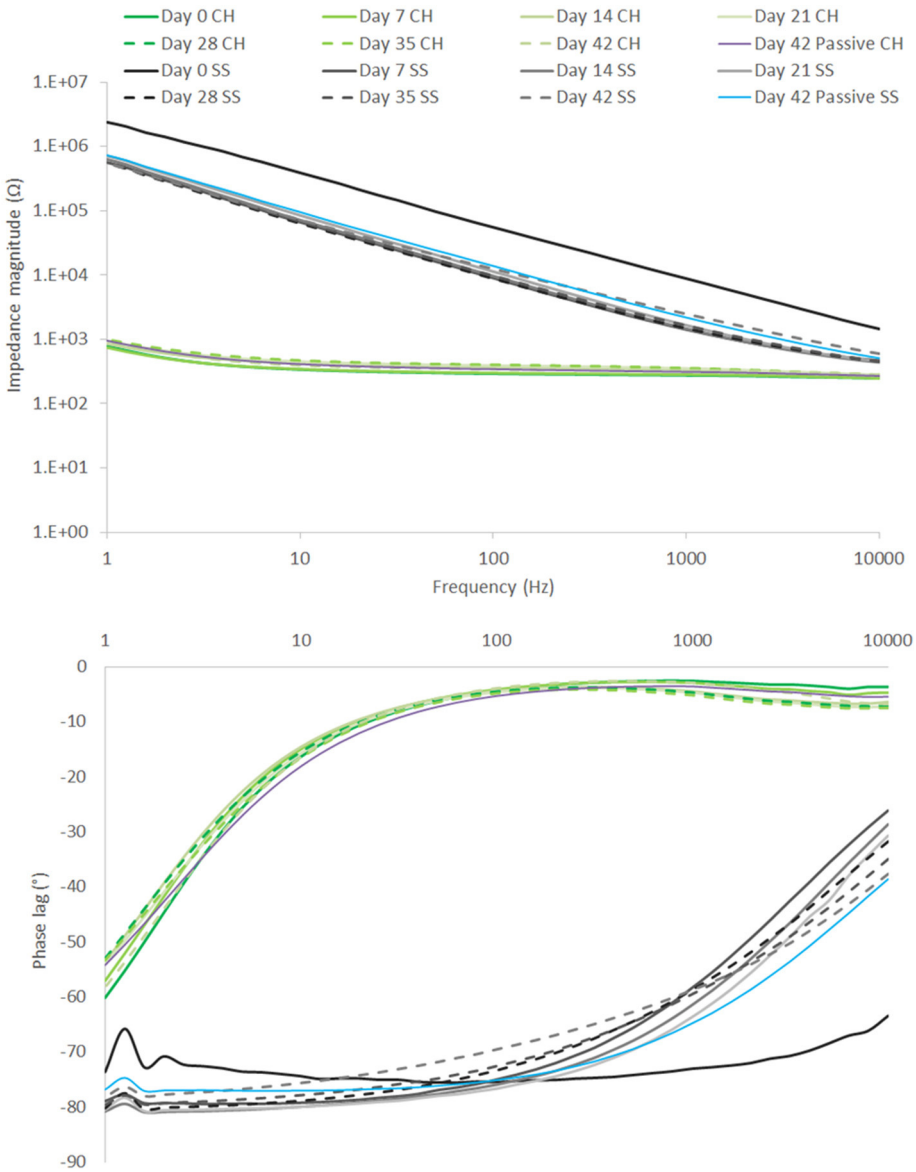

FIGURE 10 | EIS over 42 day period of high frequency stimulation, showing performance of CH coated SS in comparison to uncoated SS. Passive controls are shown at termination of the study ($n = 8$).

the quality of the pre-layer and hence the overall CH coating. Alternately, the PtIr arrays were able to be coated with the same protocols used in prior literature for Pt electrodes. The stability of these arrays was rather impacted by the connections where exposed bonding of wires to the electrode pads led to failure of the device irrespective of the electrode coating.

The electrochemical properties of CH coatings were comparable to prior literature. The increase in CSC achieved by CH coating the SS arrays was 3 orders of magnitude and for the PtIr arrays was 2 orders of magnitude. Prior studies on CH coating of cochlear implants was found to produce electrodes with a CSC of 124 mC/cm^2 (Hassarati et al., 2014), and CH coating of macroelectrodes (1 cm diameter discs) were found to have a CSC of 68.4 mC/cm^2 (Green et al., 2012b) and 114 mC/cm^2 (Goding et al., 2017). In these studies the CSC for the CH coated PtIr electrodes (212 mC/cm^2) was almost double that of prior studies on device electrodes. The CH coated SS electrodes had an average CSC closer to that of the macroelectrodes (85 mC/cm^2). As detailed in the Methods, both of these electrode types are relatively large, having dimensions on the mm scale, and as such could be expected to have properties closer to that of the macroelectrodes. Specifically, the PtIr electrodes have an area of 1.6 mm^2 and the SS electrodes have an area of 0.11 mm^2. It is know that charge transfer on microelectrodes is usually higher than that of macroelectrodes due to edge effects that enable higher charge

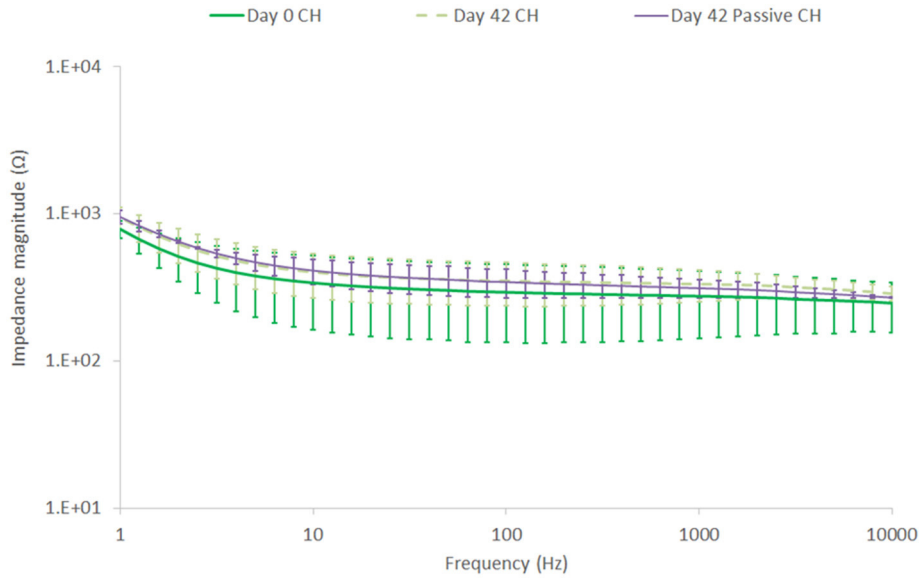

FIGURE 11 | Impedance magnitude changes in the CH coating, comparing Day 0 to Day 42, unstimulated and stimulated at a high frequency of 40 kHz and 2 mA. Error bars are 1 SD, ($n = 8$).

density accumulation at the border regions (Cogan et al., 2016a). However, the PtIr electrodes have substantially higher CSC than both the smaller SS electrodes and macroelectrodes. It is feasible that the pre-curled cuff format influences the electrode behavior when testing by CV. Essentially the curled cuff will form a contained environment which restricts ion diffusion to the much larger volume of electrolyte in which the array is being tested. As a result, ions are likely to be sequestered within this volume and readily available for charge transfer during voltage cycling and associated redox reactions. This is supported by the EIS data which shows very low impedance for CH coated PtIr and also reduced impedance (per area) for uncoated electrodes at low frequency, where capacitive behavior through ionic double layer formation dominates electrical performance. It is important to know that this is a feature of the test system and would not be applicable to an in use cuff that is wrapped around a peripheral nerve.

The charge injection limits recorded in this study appear low when compared to prior literature reports for Pt and CP coated electrodes. This is likely due to the large size of these electrodes and the focus on shorter phase lengths (Rose and Robblee, 1990; Cogan et al., 2005). It is clearly seen in both this study and prior literature that there is a substantial phase dependence related to electrochemical charge injection limit (Green et al., 2012c, 2013, 2014). The majority of studies in the literature have focused only on a single phase length of 0.2 ms, being equivalent to pulse of 5 Hz. For comparison to literature, with a phase length of 0.2 ms the average injection limit of the CH coated SS was 223.3 $\mu C/cm^2$, the CH coated PtIr was 122.8 $\mu C/cm^2$, the bare SS was 6.2 $\mu C/cm^2$, and the bare PtIr was 20.1 $\mu C/cm^2$. At this same length of phase, literature has reported Pt microelectrodes without surface modification to have a charge injection limit within the range of 20–150 $\mu C/cm^2$. Microelectrodes are known to have increased charge injection limit, as edge effects contribute to high charge density at the electrode surface. In a study by Green et al. (2012c) it was shown that Pt electrodes with a diameter of 1 mm produced a charge injection limit that was consistently below 30 $\mu C/cm^2$ (across phase lengths varied from 0.1 to 0.8 ms) when tested in saline under identical conditions to the present study. However, as the focus of this study was high frequency neuromodulation the injection limit at phase lengths below 100 μs is critical. At 40 kHz the injection limit was increased by 5.5 times when SS electrodes were coated with CH and by four times when PtIr electrodes were coated with CH.

Long-term stimulation at 40 kHz and with 2 mA of peak to peak current was conducted using both SS and CH coated SS electrodes. The PtIr electrode arrays were unable to deliver this stimulation due to corrosive failure in the array connections. This was ultimately a factor of the electrode design and future studies will first seek to address areas of electrolyte leakage to the connections. At high frequency all materials act as resistors and the geometric surface area of the electrode is thought to dominate charge transfer behavior. The SS electrode designs have been used in impedance tomography for mapping of neural activity (Aristovich et al., 2016), which supports their use with high frequency pulses, however their stability under continual use for nerve block application was not known. These studies reveal that both SS and CH coated SS support stable delivery of pulses with no significant change in voltage drop across the 42 day period, during which more than 150 billion pulses were delivered. The CSC of the SS was found to increase across the initial period of stimulation and this was matched with a reduction in impedance magnitude and shift in phase lag. This behavior is not uncommon for metals that passivate, and the initial

stimulation period is likely to have conditioned the surface such that charge transfer is more efficient (Williams and Williams, 1974; Miyazaki et al., 2005). Conversely the CH material was found to have a small increase in impedance and reduction in CSC. This is also not uncommon to conductive polymer based materials and known to plateau to yield stable electrochemical characteristics in the long-term (Yamato et al., 1995; Cui and Martin, 2003; Green et al., 2012a, 2013; Goding et al., 2017). The performance of the passive (unstimulated) controls, being not significantly different to that of the stimulated electrodes at 42 days, confirm that these changes in electrochemical performance did not occur as a result of stimulation. In fact, it is most likely that the rearrangement of polymer chains and the loss of mobile, unreacted components are largely responsible for this behavior. This degree of electrochemical stability has been reported for conventional PEDOT coatings before; Wilks et al. (2009) reported a high degree of electrochemical stability of PEDOT coatings on iridium-silicon microelectrodes under continuous biphasic pulsing. After 720,000 stimulation cycles there was no significant change in CSC or impedance, and only minor changes in the charge injection limit of the PEDOT coating. The findings presented in this paper demonstrate that the electrochemical stability of PEDOT is preserved in these CH coatings.

Ultimately, the CH coating reduced the potential transient required to drive the SS electrodes by 33% and maintained a significantly lower impedance and higher CSC across the study period. Since these studies were undertaken in saline without tissue contact, the full benefit of the CH coating has not been fully realized. It is expected that the reduction in stiffness imparted by the hydrogel will result in less scar tissue development over chronic implant periods, and the natural anti-fouling property of the hydrogel (Cheong et al., 2014; Hassarati et al., 2014) will minimize protein blocking at electrode sites. Future work will investigate the application of CH coated SS cuffs *in vivo* over both acute and chronic implant periods.

AUTHOR CONTRIBUTIONS

NS and JG contributed equally as first authors in both experimental work and writing. AG, KA, and PB-P contributed to key aspects of the experimental work and provided input to the manuscript specific to their experimental contributions. DH, JM, and NL were co-investigators and contributed to study design and data analysis. DC was the major industry collaborator and contributed to study design and parameters. RG was the principal investigator contributing to study design, supervision, data analysis, and preparation of the manuscript.

ACKNOWLEDGMENTS

The authors would like to acknowledge funding from Galvani Bioelectronics under Research Collaboration Agreement GSK CRA 160301.

REFERENCES

Aristovich, K. Y., Packham, B. C., Koo, H., Santos, G. S., dos McEvoy, A., and Holder, D. S. (2016). Imaging fast electrical activity in the brain with electrical impedance tomography. *Neuroimage* 124, 204–213. doi: 10.1016/j.neuroimage.2015.08.071

Arteaga, G. C., Del Valle, M. A., Antilén, M., Romero, M., Ramos, A., Hernández, L., et al. (2013). Nucleation and growth mechanism of electro-synthesized poly (pyrrole) on steel. *Int. J. Electrochem. Sci.* 8, 4120–4130. Available online at: http://www.electrochemsci.org/papers/vol8/80304120.pdf

Birmingham, K., Gradinaru, V., Anikeeva, P., Grill, W. M., Pikov, V., McLaughlin, B., et al. (2014). Bioelectronic medicines: a research roadmap. *Nat. Rev. Drug Discov.* 13, 399–400. doi: 10.1038/nrd4351

Boretius, T., Badia, J., Pascual-Font, A., Schuettler, M., Navarro, X., Yoshida, K., et al. (2010). A transverse intrafascicular multichannel electrode (TIME) to interface with the peripheral nerve. *Biosens. Bioelectron.* 26, 62–69. doi: 10.1016/j.bios.2010.05.010

Bowman, B. R., and Erickson, R. C. (1985). Acute and chronic implantation of coiled wire intraneural electrodes during cyclical electrical stimulation. *Ann. Biomed. Eng.* 13, 75–93. doi: 10.1007/BF02371251

Cheong, G. L. M., Lim, K. S., Jakubowicz, A., Martens, P. J., Poole-Warren, L. A., and Green, R. A. (2014). Conductive hydrogels with tailored bioactivity for implantable electrode coatings. *Acta Biomater.* 10, 1216–1226. doi: 10.1016/j.actbio.2013.12.032

Cogan, S. F., Garrett, D. J., and Green, R. A. (2016a). "Electrochemical principles of safe charge injection," in *Neurobionics: The Biomedical Engineering of Neural Prostheses* (Hoboken, NJ: John Wiley & Sons, Inc.), 55–88.

Cogan, S. F., Ludwig, K. A., Welle, C. G., and Takmakov, P. (2016b). Tissue damage thresholds during therapeutic electrical stimulation. *J. Neural Eng.* 13:21001. doi: 10.1088/1741-2560/13/2/021001

Cogan, S. F., Troyk, P. R., Ehrlich, J., and Plante, T. D. (2005). *In vitro* comparison of the charge-injection limits of activated iridium oxide (AIROF) and platinum-iridium microelectrodes. *Biomed. Eng. IEEE Trans.* 52, 1612–1614. doi: 10.1109/TBME.2005.851503

Cui, X., and Martin, D. C. C. (2003). Electrochemical deposition and characterization of poly(3,4-ethylenedioxythiophene) on neural microelectrode arrays. *Sensors Actuat. B Chem.* 89, 92–102. doi: 10.1016/S0925-4005(02)00448-3

Famm, K., Litt, B., Tracey, K. J., Boyden, E. S., and Slaoui, M. (2013). Drug discovery: a jump-start for electroceuticals. *Nature* 496, 159–161. doi: 10.1038/496159a

Gillis, W. F., Lissandrello, C. A., Shen, J., Pearre, B. W., Mertiri, A., Deku, F., et al. (2017). Carbon fiber on polyimide ultra-microelectrodes. *bioRxiv*. doi: 10.1101/123281

Goding, J., Gilmour, A., Martens, P., Poole-Warren, L., and Green, R. (2017). Interpenetrating conducting hydrogel materials for neural interfacing electrodes. *Adv. Healthc. Mater.* 6:1601177. doi: 10.1002/adhm.201601177

Green, R. A., Hassarati, R. T., Bouchinet, L., Lee, C. S., Cheong, G. L. M., Yu, J. F., et al. (2012a). Substrate dependent stability of conducting polymer coatings on medical electrodes. *Biomaterials* 33, 5875–5886. doi: 10.1016/j.biomaterials.2012.05.017

Green, R. A., Hassarati, R. T., Goding, J. A., Baek, S., Lovell, N. H., Martens, P. J., et al. (2012b). Conductive hydrogels: mechanically robust hybrids for use as biomaterials. macromol. *Bioscience* 12, 494–501. doi: 10.1002/mabi.201100490

Green, R. A., Lovell, N. H., and Poole-Warren, L. A. (2009). Cell attachment functionality of bioactive conducting polymers for neural interfaces. *Biomaterials* 30, 3637–3644. doi: 10.1016/j.biomaterials.2009.03.043

Green, R. A., Lovell, N. H., and Poole-Warren, L. A. (2010). Impact of co-incorporating laminin peptide dopants and neurotrophic growth factors on conducting polymer properties. *Acta Biomater.* 6, 63–71. doi: 10.1016/j.actbio.2009.06.030

Green, R. A., Lovell, N. H., Wallace, G. G., and Poole-Warren, L. A. (2008). Conducting polymers for neural interfaces: challenges in developing an effective long-term implant. *Biomaterials* 29, 3393–3399. doi: 10.1016/j.biomaterials.2008.04.047

Green, R. A., Matteucci, P. B. B., Hassarati, R. T. T., Giraud, B., Dodds, C. W., Chen, S., et al. (2013). Performance of conducting polymer electrodes for stimulating neuroprosthetics. *J. Neural Eng.* 10:16009. doi: 10.1088/1741-2560/10/1/016009

Green, R. A., Matteucci, P. B., Dodds, C. W. D., Palmer, J., Dueck, W. F., Hassarati, R. T., et al. (2014). Laser patterning of platinum electrodes for safe neurostimulation. *J. Neural Eng.* 11:56017. doi: 10.1088/1741-2560/11/5/056017

Green, R. A., Toor, H., Dodds, C., and Lovell, N. H. (2012c). Variation in performance of platinum electrodes with size and surface roughness. *Sensors Mater.* 24, 165–180.

Grill, W. M., Norman, S. E., and Bellamkonda, R. V. (2009). Implanted neural interfaces: biochallenges and engineered solutions. *Annu. Rev. Biomed. Eng.* 11, 1–24. doi: 10.1146/annurev-bioeng-061008-124927

Guo, L. (2016). The pursuit of chronically reliable neural interfaces: a materials perspective. *Front. Neurosci.* 10:599. doi: 10.3389/fnins.2016.00599

Hassarati, R. T., Dueck, W. F., Tasche, C., Carter, P. M., Poole-Warren, L. A., and Green, R. A. (2014). Improving cochlear implant properties through conductive hydrogel coatings. *IEEE Trans. Neural Syst. Rehabil. Eng.* 22, 411–418. doi: 10.1109/TNSRE.2014.2304559

Hassarati, R. T., Foster, L. J. R., and Green, R. A. (2016). Influence of biphasic stimulation on olfactory ensheathing cells for neuroprosthetic devices. *Front. Neurosci.* 10:432. doi: 10.3389/fnins.2016.00432

Joung, Y. K., You, S. S., Park, K. M., Go, D. H., and Park, K. D. (2012). *In situ* forming, metal-adhesive heparin hydrogel surfaces for blood-compatible coating. *Colloids Surf. B Biointerfaces* 99, 102–107. doi: 10.1016/j.colsurfb.2011.10.047

Kim, D. H., Abidan, M., and Martin, D. C. (2004). Synthesis and characterization of conducting polymers grown in hydrogels for neural applications. *Mat. Res. Soc. Symp. Proc.* 1, F5.5.1–F5.5.6.

Lago, N., Yoshida, K., Koch, K. P., and Navarro, X. (2007). Assessment of biocompatibility of chronically implanted polyimide and platinum intrafascicular electrodes. *Biomed. Eng. IEEE Trans.* 54, 281–290. doi: 10.1109/TBME.2006.886617

Langdale, C. L., Hokanson, J. A., Sridhar, A., and Grill, W. M. (2017). Stimulation of the pelvic nerve increases bladder capacity in the prostaglandin E2 rat model of overactive bladder running title: pelvic nerve stimulation in the PGE2 OAB rat model. *Am. J. Physiol. Ren. Physiol.* 313, F657–F665. doi: 10.1152/ajprenal.00116.2017

Lovell, N. H., Morley, J. W., Chen, S. C., Hallum, L. E., and Suaning, G. J. (2010). Biological–machine systems integration: engineering the neural interface. *Proc. IEEE* 98, 418–431. doi: 10.1109/JPROC.2009.2039030

Meng, S., Liu, Z., Shen, L., Guo, Z., Chou, L. L., Zhong, W., et al. (2009). The effect of a layer-by-layer chitosan-heparin coating on the endothelialization and coagulation properties of a coronary stent system. *Biomaterials* 30, 2276–2283. doi: 10.1016/j.biomaterials.2008.12.075

Miyazaki, F., Inagawa, Y., Kato, K., Sakaki, M., Ichikawa, H., and Okubo, H. (2005). Electrode conditioning characteristics in vacuum under impulse voltage application in non-uniform electric field. *IEEE Trans. Dielectr. Electr. Insul.* 12, 17–23. doi: 10.1109/TDEI.2005.1394011

Pan, L., Yu, G., Zhai, D., Lee, H. R., Zhao, W., Liu, N., et al. (2012). Hierarchical nanostructured conducting polymer hydrogel with high electrochemical activity. *Proc. Natl. Acad. Sci. U.S.A.* 109, 9287–9292. doi: 10.1073/pnas.1202636109

Patton, A. J., Green, R. A., and Poole-Warren, L. A. (2015). Mediating conducting polymer growth within hydrogels by controlling nucleation. *APL Mater.* 3:14912. doi: 10.1063/1.4904820

Patton, A. J., Poole-Warren, L. A., and Green, R. A. (2016). Mechanisms for imparting conductivity to nonconductive polymeric biomaterials. *Macromol. Biosci.* 16, 1103–1121. doi: 10.1002/mabi.201600057

Pavlov, V. A., and Tracey, K. J. (2017). Neural regulation of immunity: molecular mechanisms and clinical translation. *Nat. Neurosci.* 20, 156–166. doi: 10.1038/nn.4477

Peixoto, N., Jackson, K., Samiyi, R., and Minnikanti, S. (2009). "Charge Storage: Stability measures in implantable electrodes," in *Engineering in Medicine and Biology Society, 2009, EMBC 2009; Annual International Conference of the IEEE* (Minneapolis, MN), 658–661.

Rose, T. L., and Robblee, L. S. (1990). Electrical stimulation with Pt Electrodes; VIII. electrochemically safe charge injection limits with 0.2 ms pulses. *IEEE Trans. Biomed. Eng.* 37, 1118–1120.

Sekine, S., Ido, Y., Miyake, T., Nagamine, K., and Nishizawa, M. (2010). Conducting polymer electrodes printed on hydrogel. *J. Am. Chem. Soc.* 132, 13174–13175. doi: 10.1021/ja1062357

Tyler, D. J., and Durand, D. M. (2002). Functionally selective peripheral nerve stimulation with a flat interface nerve electrode. *IEEE Trans. Neural Syst. Rehabil. Eng.* 10, 294–303. doi: 10.1109/TNSRE.2002.806840

Wallinder, D., Pan, J., Leygraf, C., and Delblanc-Bauer, A. (1998). EIS and XPS study of surface modification of 316LVM stainless steel after passivation. *Corros. Sci.* 41, 275–289. doi: 10.1016/S0010-938X(98)00122-X

Wark, H. A. C., Sharma, R., Mathews, K. S., Fernandez, E., Yoo, J., Christensen, B., et al. (2013). A new high-density (25 electrodes/mm^2) penetrating microelectrode array for recording and stimulating sub-millimeter neuroanatomical structures. *J. Neural Eng.* 10:45003. doi: 10.1088/1741-2560/10/4/045003

Wilks, S. J., Richardson-Burns, S. M., Hendricks, J. L., Martin, D. C., and Otto, K. J. (2009). Poly(3,4-ethylenedioxythiophene) as a micro-neural interface material for electrostimulation. *Front. Neuroeng.* 2:7. doi: 10.3389/neuro.16.007.2009

Williams, D. W., and Williams, W. T. (1974). Prebreakdown and breakdown characteristics of stainless steel electrodes in vacuum. *J. Phys. D Appl. Phys.* 7:315. doi: 10.1088/0022-3727/7/8/315

Wong, Y. T., Chen, S. C., Seo, J. M., Morley, J. W., Lovell, N. H., and Suaning, G. J. (2009). Focal activation of the feline retina via a suprachoroidal electrode array. *Vision Res.* 49, 825–833. doi: 10.1016/j.visres.2009.02.018

Yamato, H., Ohwa, M., and Wernet, W. (1995). Stability of polypyrrole and poly(3,4-ethylenedioxythiophene) for biosensor application. *J. Electroanal. Chem.* 397, 163–170. doi: 10.1016/0022-0728(95)04156-8

Zheng, X., Zhang, J., Chen, T., and Chen, Z. (2008). Recording and stimulating properties of chronically implanted longitudinal intrafascicular electrodes in peripheral fascicles in an animal model. *Microsurgery* 28, 203–209. doi: 10.1002/micr.20465

Conflict of Interest Statement: DC is an employee of Galvani Bioelectronics, the funder of these research activities.

The other authors declare that the research was conducted in the absence of any commercial or financial relationships that could be construed as a potential conflict of interest.

frontiers in Neuroscience

TECHNOLOGY REPORT
published: 24 January 2018
doi: 10.3389/fnins.2017.00734

Evolving Applications, Technological Challenges and Future Opportunities in Neuromodulation: Proceedings of the Fifth Annual Deep Brain Stimulation Think Tank

Adolfo Ramirez-Zamora[1], James J. Giordano[2], Aysegul Gunduz[3], Peter Brown[4], Justin C. Sanchez[5], Kelly D. Foote[6], Leonardo Almeida[1], Philip A. Starr[7], Helen M. Bronte-Stewart[8], Wei Hu[1], Cameron McIntyre[9], Wayne Goodman[10,11], Doe Kumsa[12], Warren M. Grill[13], Harrison C. Walker[14,15], Matthew D. Johnson[16], Jerrold L. Vitek[17], David Greene[18], Daniel S. Rizzuto[19], Dong Song[20], Theodore W. Berger[20], Robert E. Hampson[21], Sam A. Deadwyler[21], Leigh R. Hochberg[22,23,24], Nicholas D. Schiff[25], Paul Stypulkowski[26], Greg Worrell[27], Vineet Tiruvadi[28], Helen S. Mayberg[29], Joohi Jimenez-Shahed[30], Pranav Nanda[31], Sameer A. Sheth[31], Robert E. Gross[32], Scott F. Lempka[33], Luming Li[34,35,36], Wissam Deeb[1] and Michael S. Okun[1]*

[1] Department of Neurology, Center for Movement Disorders and Neurorestoration, University of Florida, Gainesville, FL, United States, [2] Department of Neurology, Pellegrino Center for Clinical Bioethics, Georgetown University Medical Center, Washington, DC, United States, [3] J. Crayton Pruitt Family Department of Biomedical Engineering, Center for Movement Disorders and Neurorestoration, University of Florida, Gainesville, FL, United States, [4] Nuffield Department of Clinical Neurosciences, University of Oxford, Oxford, United Kingdom, [5] Biological Technologies Office, Defense Advanced Research Projects Agency, Arlington, VA, United States, [6] Department of Neurosurgery, Center for Movement Disorders and Neurorestoration, University of Florida, Gainesville, FL, United States, [7] Department of Neurological Surgery, Kavli Institute for Fundamental Neuroscience, University of California, San Francisco, San Francisco, CA, United States, [8] Departments of Neurology and Neurological Sciences and Neurosurgery, Stanford University, Stanford, CA, United States, [9] Department of Biomedical Engineering, Case Western Reserve University, Cleveland, OH, United States, [10] Department of Psychiatry, Icahn School of Medicine at Mount Sinai, New York, NY, United States, [11] Department of Neuroscience, Icahn School of Medicine at Mount Sinai, New York, NY, United States, [12] Division of Biomedical Physics, Office of Science and Engineering Laboratories, Center for Devices and Radiological Health, United States Food and Drug Administration, White Oak Federal Research Center, Silver Spring, MD, United States, [13] Department of Biomedical Engineering, Duke University, Durham, NC, United States, [14] Division of Movement Disorders, Department of Neurology, University of Alabama at Birmingham, Birmingham, AL, United States, [15] Department of Biomedical Engineering, University of Alabama at Birmingham, Birmingham, AL, United States, [16] Department of Biomedical Engineering, University of Minnesota, Minneapolis, MN, United States, [17] Department of Neurology, University of Minnesota, Minneapolis, MN, United States, [18] NeuroPace, Inc., Mountain View, CA, United States, [19] Department of Psychology, University of Pennsylvania, Philadelphia, PA, United States, [20] Department of Biomedical Engineering, University of Southern California, Los Angeles, CA, United States, [21] Physiology and Pharmacology, Wake Forest University School of Medicine, Wake Forest University, Winston-Salem, NC, United States, [22] Department of Neurology, Center for Neurotechnology and Neurorecovery, Massachusetts General Hospital, Harvard Medical School, Harvard University, Boston, MA, United States, [23] Center for Neurorestoration and Neurotechnology, Rehabilitation R and D Service, Veterans Affairs Medical Center, Providence, RI, United States, [24] School of Engineering and Brown Institute for Brain Science, Brown University, Providence, RI, United States, [25] Laboratory of Cognitive Neuromodulation, Feil Family Brain Mind Research Institute, Weill Cornell Medicine, New York, NY, United States, [26] Medtronic Neuromodulation, Minneapolis, MN, United States, [27] Department of Neurology, Mayo Clinic, Rochester, MN, United States, [28] Department of Biomedical Engineering, Georgia Institute of Technology, Emory University School of Medicine, Emory University, Atlanta, GA, United States, [29] Departments of Psychiatry, Neurology, and Radiology, Emory University School of Medicine, Emory University, Atlanta, GA, United States, [30] Parkinson's Disease Center and Movement Disorders Clinic, Department of Neurology, Baylor College of Medicine, Houston, TX, United States, [31] Department of Neurological Surgery, The Neurological Institute, Columbia University Herbert and Florence Irving Medical Center, Colombia University, New York, NY, United States, [32] Department of Neurosurgery, Emory University, Atlanta, GA, United States, [33] Department of Biomedical Engineering, University of Michigan, Ann Arbor, MI, United States, [34] National Engineering Laboratory for Neuromodulation, School of Aerospace Engineering, Tsinghua University, Beijing, China, [35] Precision Medicine and Healthcare Research Center, Tsinghua-Berkeley Shenzhen Institute, Tsinghua University, Beijing, China, [36] Center of Epilepsy, Beijing Institute for Brain Disorders, Beijing, China*

OPEN ACCESS

Edited by:
Ulrich G. Hofmann, Universitätsklinikum Freiburg, Germany

Reviewed by:
Christian K. E. Moll, University Medical Center Hamburg-Eppendorf, Germany
Sabato Santaniello, University of Connecticut, United States

***Correspondence:**
Adolfo Ramirez-Zamora
adolfo.ramirez-zamora@neurology.ufl.edu

Specialty section:
This article was submitted to Neural Technology, a section of the journal Frontiers in Neuroscience

Received: *19 October 2017*
Accepted: *15 December 2017*
Published: *24 January 2018*

Citation:
Ramirez-Zamora A, Giordano JJ, Gunduz A, Brown P, Sanchez JC, Foote KD, Almeida L, Starr PA, Bronte-Stewart HM, Hu W, McIntyre C, Goodman W, Kumsa D, Grill WM, Walker HC, Johnson MD, Vitek JL, Greene D, Rizzuto DS, Song D, Berger TW, Hampson RE, Deadwyler SA, Hochberg LR, Schiff ND, Stypulkowski P, Worrell G, Tiruvadi V, Mayberg HS, Jimenez-Shahed J, Nanda P, Sheth SA, Gross RE, Lempka SF, Li L, Deeb W and Okun MS (2018) Evolving Applications, Technological Challenges and Future Opportunities in Neuromodulation: Proceedings of the Fifth Annual Deep Brain Stimulation Think Tank. Front. Neurosci. 11:734. doi: 10.3389/fnins.2017.00734

The annual Deep Brain Stimulation (DBS) Think Tank provides a focal opportunity for a multidisciplinary ensemble of experts in the field of neuromodulation to discuss advancements and forthcoming opportunities and challenges in the field. The proceedings of the fifth Think Tank summarize progress in neuromodulation neurotechnology and techniques for the treatment of a range of neuropsychiatric conditions including Parkinson's disease, dystonia, essential tremor, Tourette syndrome, obsessive compulsive disorder, epilepsy and cognitive, and motor disorders. Each section of this overview of the meeting provides insight to the critical elements of discussion, current challenges, and identified future directions of scientific and technological development and application. The report addresses key issues in developing, and emphasizes major innovations that have occurred during the past year. Specifically, this year's meeting focused on technical developments in DBS, design considerations for DBS electrodes, improved sensors, neuronal signal processing, advancements in development and uses of responsive DBS (closed-loop systems), updates on National Institutes of Health and DARPA DBS programs of the BRAIN initiative, and neuroethical and policy issues arising in and from DBS research and applications in practice.

Keywords: deep brain stimulation, neuromodulation, epilepsy, Parkinson's disease, tremor, obsessive compulsive disorder, tourette syndrome, memory

INTRODUCTION

Neuromodulation, including cortical and subcortical approaches for management of neurological and neuropsychiatric disorders, continues to rapidly evolve. Technological advancements have enabled an increased understanding of neuronal signals involved in signs and symptoms of a number of neuropsychiatric conditions. The Fifth Annual Deep Brain Stimulation (DBS) Think Tank convened in Atlanta, GA, from May 19th to 21st, 2017 to address evolving applications, technological challenges and future opportunities in neuromodulation. This report highlights the challenges and opportunities addressed in the meeting. There was particular focus on technical developments, design considerations for DBS electrodes, emerging capabilities of responsive DBS (closed-loop systems), updates from the National Institutes of Health (NIH) and Defense Advanced Research Projects Agency (DARPA) DBS-based programs, focus upon advances and knowledge gaps in brain electrophysiology and sensor technology, and address of ongoing and newly arising neuroethical and policy issues generated in and by DBS research and uses in practice.

TECHNICAL DEVELOPMENTS

Technologies Emerging Due to Investigator Demand

Neuromodulation 2.0: Building a bridge from today's tonic pulse generators to tomorrow's adaptive neurological "co-processors."

The burden of neurological disease has significant economic and societal impact. While neuromodulation-based therapeutic devices have forged significant in-roads in treating some neuropsychiatric conditions, overall, the relative success of such approaches has been limited by fundamental questions regarding the pathophysiology and mechanisms underlying both disease processes and DBS-based interventions.

To address the extant knowledge gap, public and private teams are collaborating on building and deploying investigational research tools for studying the human nervous system in both health and disease. The primary goal of this work is to merge (basic and applied) biomedical research with engineering design methods to catalyze the development of next generation neuromodulation therapeutics (see **Figure 1**). The prototyping of therapeutic concepts from a dynamic systems perspective has fostered increased capability of bioelectronic systems that act more as a neurological "co-processor" to address neural system dysfunction, as opposed to the tonic, fixed-pattern stimulators used to date. Emergent technologies include devices that store event triggered recording and improved sensors capable of recording local field potential (LFP) from an increased number of channel combinations. Additional developments include an enhanced capacity to parse signals from the neural noise floor, development of embedded inertial sensors, use of advanced stimulation parameters and patterns, creation of a rechargeable battery (that can increase neurostimulator life to allow more long term applications when utilizing advanced research tools), production of upgradable and smaller devices, improved motion sensing and distance telemetry (e.g., real-time streaming) with higher throughput (not-compressed, multiple channels) and research development kits (greater customization, integration with local and distributed systems). External synchronization has been a challenge in closed loop devices, and implanted device technology with higher bandwidth than current systems has the potential to improve synchronization and to better detect the fast dynamics of neural signals of interest. Toward this end,

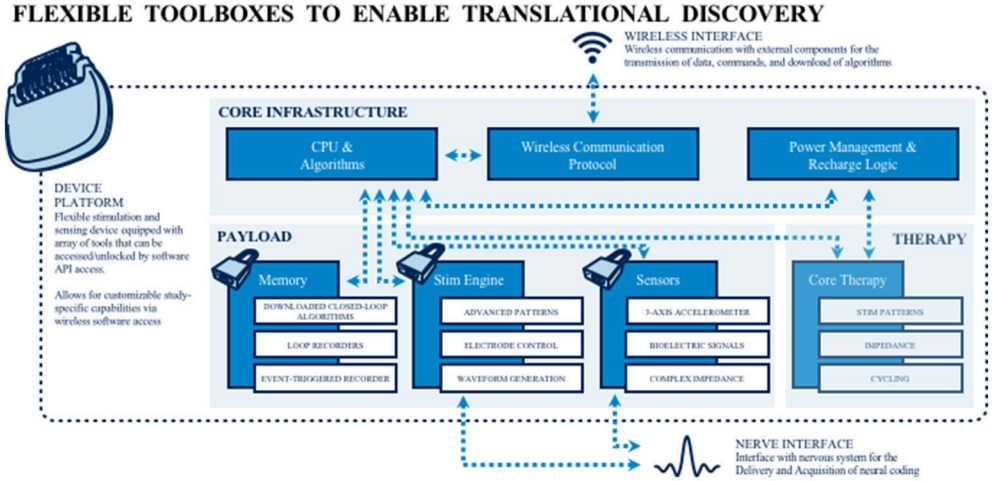

FIGURE 1 | Toolboxes to promote translational neuromodulation research and discovery.

newer networks can select recordings and set specific signals to improve synchronization. The potential release of second-generation devices (e.g., the Medtronic RC+S) for use in certain National Institutes of Health (NIH) projects funded under the United States' Brain Research through Advanced Innovative Neurotechnology (BRAIN) Initiative may address some of these needs. As well, the limited number of lead contacts for closed loop applications has been a constraint. Newer devices will likely facilitate the ability to sample two channels per lead; the use of additional channels could be beneficial to both increase sampling and to pair stimulation in closed-loop devices.

Highlights and Future Directions

- Emerging technological developments include improved sensors, increased device memory, and rechargeable batteries.
- Development of external signals to improve closed loop synchronizations has been identified as being important to next-generation technology capability.
- An increased number of lead electrodes may improve both stimulation and recording capacities of both current and newly developing devices.

Variable Frequency Stimulation as a New Approach to DBS in Defined Applications

There are ongoing efforts to define particular signs and symptoms of neuropsychiatric disorders that may be mitigated by DBS intervention. Freezing of gait (FOG) is defined as a sudden arrest of forward stepping commonly affecting patients with advanced Parkinson's disease (PD) (Nutt et al., 2011). Occurrence and management of FOG is challenging as FOG is often resistant to levodopa treatment in patients with advanced PD. In small case series, low frequency stimulation (LFS) of the subthalamic nucleus (STN) (60–80 Hz) has provided short term benefit in reducing axial symptoms including FOG, although this has raised concerns about the worsening of appendicular symptoms, in particular tremor (Xie et al., 2015; Zibetti et al., 2016). A novel DBS paradigm that combined high and low frequency stimulation in varying patterns (VFS) to address FOG and appendicular PD motor symptoms has been proposed (Jia et al., 2017). Following an open label, doubled blind design, investigators utilized the PINS DBS system to assess the effect of VFS in FOG (NCT02601144). The study included twenty-eight (28) PD subjects presenting with FOG, who were implanted with bilateral STN DBS. At baseline, patients were evaluated under four DBS conditions: DBS off, LFS (60–80 Hz), HFS (130–180 Hz) and VFS for a total of 6 h. All subjects were discharged home on VFS settings and were scheduled for a follow-up second study visit after 6 months, and for a final evaluation at 12 months. Changes in the Unified Parkinson's Disease (UPDRS) motor scale and a 10-meter timed up-and-go (TUG) task were assessed at baseline, and following 1 h of high, low, and VFS. Chronic VFS therapy was assessed at 6 and 12 months with the FOG questionnaire and the gait and falls questionnaire. Initial data suggests that VFS was well tolerated and that it reduces appendicular symptoms and the number of FOG episodes compared to HFS and LFS at 12 months follow up. Finalized publication of the data is pending.

Highlights and Future Directions

- A novel VFS DBS programming paradigm was shown to elicit improved benefit over traditional HFS and LFS programming in an open label design study.
- VFS was well tolerated and was shown to potentially reduce FOG episodes and improve TUG measures.
- The use of external sensing triggered by physiological changes indicative of FOG might be useful a specific biomarker to best utilize VFS.

Biphasic DBS for Essential Tremor and Dystonia

Despite advances in DBS techniques and technology, clinicians continue to face limitations in battery longevity and in

stimulation-induced side effects. The conventional DBS waveform consists of a rectangular biphasic pulse, with an active, high-amplitude and short-duration phase, followed by a passive, low amplitude, charge-balancing phase. Pilot research at the University of Florida in movement disorders reported that square biphasic (sqBIP) pulses (with active rather than passive charge-balancing phase) were well tolerated and provided a greater clinical benefit when compared to commercially available DBS (Akbar et al., 2016).

An open label, pilot trial assessed (over a period of hours) the safety and tolerability of sqBiP DBS in patients with PD, ET, and dystonia (Almeida et al., 2017). Secondary analysis included effects on motor response produced by sqBiP DBS compared to conventional stimulation. Firmware was updated with proprietary software provided by the manufacturer (Medtronic). Patients were tested in at-home settings (conventional DBS), after a 30-min washout, and then at multiple time points after sqBiP DBS was implemented for a total of 3 h for ET and PD, and 2 h for dystonia.

At each evaluation, motor behavior and scales were videotaped, and accelerometer and GAITRite data were collected. There were no adverse events documented in either arm of the study. Significantly positive changes in tremor scores over time, and in accelerometer data were observed. Subsequent *post-hoc* analysis showed significance only between different time points and the washout period. For treatment of dystonia, there was a significant change in cervical dystonia scores, with *post-hoc* analysis revealing differences between other time points and the washout. Interestingly, there was a gradual improvement in GAITRite measures, including cadence, velocity, average step length, and double support time with sqBiP stimulation. sqBiP was well-tolerated in the acute ambulatory setting, with possibly similar benefits produced in motor scores and improved cadence, step stride, and double support gait assessments.

Highlights and Future Directions

- A novel stimulation technique, sqBiP adjusted the pulse frequency and shape of pulses.
- In use against ET, sqBiP DBS improved tremor scales and accelerometer parameters. In treating dystonia sqBiP DBS produced an improvement in gait variables.
- Future studies will explore the mechanisms of sqBiP pulses; long term outcomes; battery consumption, and clinical benefits in treatment of ET, PD, dystonia and other select disorders.

Distributed Network Control with High Density Neuromodulation Technology for the Treatment of Intractable Epilepsy

Anterior thalamic DBS (Salanova et al., 2015) and responsive neuromodulation (Bergey et al., 2015) for treatment epilepsy has been reported to show an approximately 65% reduction in seizures at long term follow-up. Preliminary data using an *in vitro* multi-electrode array in cell culture revealed that asynchronous multi-site stimulation eliminated synchronous epileptogenic activity. Furthermore, in animal models, multi-microelectrodes were more effective than macroelectrodes in terminating seizures through the use of asynchronous theta stimulation (Desai et al., 2016). While such animal studies are promising, it was suggested that the use of a non-human primate model of penicillin induced seizure) would be important (and thus is planned) prior to considering use of this approach in human patients.

A translational study using RC+S (Medtronic) is also currently planned to identify electrophysiological biomarkers and to integrate a closed-loop approach. The initial phase of our studies aims to use an external system to test stimulation in an open loop fashion using asynchronous distributed microelectrode theta stimulation. We will also record biomarkers and use these to design a closed loop neuromodulation algorithm. This will lead in phase 2 to a translational NHP study using RC+S (Medtronic) which will allow both open-loop and closed-loop algorithms based on the previous experiment. The third phase will translate the NHP findings into an early stage feasibility study in epilepsy patients. These studies rely on novel high-channel count electrodes, bidirectional neurostimulation devices and novel computational approaches.

Highlights and Future Directions

- Preliminary data using *in vitro* multielectrode array in cell culture revealed asynchronous multi-site stimulation eliminated synchronous epileptiform activity.
- Multi-microelectrodes were more effective than macroelectrodes in terminating seizures in a rodent model using asynchronous theta stimulation.
- Using an acute non-human primate seizure model of epilepsy, the research will attempt to translate the above findings, and to identify biomarkers to be used in implementation of closed loop seizure control optimization.

ADVANCES IN CLOSED LOOP DBS

Parkinson's Disease

Closed Loop DBS in PD

Specific examples of the application of closed-loop DBS in PD are growing (Rosin et al., 2011; Little et al., 2013, 2016; Malekmohammadi et al., 2016). These cases have demonstrated symptom improvement, with substantial power savings and/or reduction in side-effects attributable to stimulation. The feedback substrates and closed-loop control algorithms involved have varied, but most have relied on the amplitude of beta activity as directly recorded in the basal ganglia-cortical loop. The amplitude of such beta activity correlates with bradykinesia and rigidity and is suppressed by both medications that exert effect on central dopaminergic activity, and high frequency DBS (Meidahl et al., 2017). Thus far, closed-loop control algorithms have either engaged an on-off activity pattern, with short ramping onset and offset (see **Figure 2**), or have employed a more gradual, proportional or hybrid control policy. One important consideration is the optimal reactivity of the closed-loop system, which may impact its efficacy, efficiency and ultimate therapeutic window. In healthy primates, and in patients with PD, beta activity is phasic (Tinkhauser et al., 2017). Longer bursts attain higher amplitudes, indicative of more pervasive

oscillatory synchronization within the neural circuit. Shorter bursts predominate in healthy states; and in patients, the relative proportion of short and long bursts negatively and positively correlate with motor impairment, respectively. Therefore, it might be best to selectively terminate longer, (i.e., pathological) beta bursts through closed-loop DBS to both maximize power savings and to spare the ability of underlying neural circuits to engage in more physiological processing which may involve shorter bursts (Tinkhauser et al., 2017).

The role of more complex feedback signals, including multidimensional central and peripheral inputs, remains to be explored, as do the advantages of more sophisticated control algorithms. In particular, it may prove necessary to tailor control loops to afford improved amelioration of patient-specific patterns of impairment (Meidahl et al., 2017). On the other hand, one of the factors constraining the development of closed-loop DBS is the range of possible feedback signals, control policies, and stimulation patterns. Arguably, the field needs to focus on demonstrating an unequivocal gain over conventional DBS before closed-loop DBS techniques are further nuanced. The key will be to shift from acute trials in post-operative patients—where studies are confounded by stun effects and temporal constraints – to acute and then ultimately to chronic trials in patients who have already undergone conventional DBS. The latter will allow resolution of the stun effect, and will afford time for optimization of conventional DBS so that valid comparisons can be made. However, these types of chronic trials will require further development of enabling technology, together with a more informed understanding of the dynamics of target circuits.

Highlights and Future Directions

- In PD, beta activity is phasic with longer busts attaining higher amplitudes, indicative of more pervasive oscillatory synchronization within the neural circuit. Shorter bursts predominate in the healthy state, and the relative proportion of short and long bursts negatively and positively correlate with motor impairment, respectively.
- Termination of longer, pathological beta bursts through closed-loop DBS might maximize power savings, and spare the ability of underlying neural circuits to engage in more physiological processing.
- The next steps in adaptive DBS involves shifting from acute trials in post-operative patients to longer assessment and evaluation to minimize confounded factors.

Customizing Control Variables and Control Policy Algorithms for Closed Loop DBS to Treat Tremor in Parkinson's Disease

At present DBS is characteristically provided as continuous, open loop, non-responsive input, and uses a "one-size fits all" set of parameters for a wide range of neurological disorders. It cannot respond to the patient's state (asleep/awake, rest/active), dominant symptoms (tremor, bradykinesia, gait impairment) or medication level. In contrast, closed loop (i.e., responsive) DBS (CL– DBS) for PD, using kinematic and/or neural biomarkers, has the potential to deliver more precise and customized neuromodulation, based on state, symptom and level of medication. To be successful CL-DBS requires feedback signals (control variables) that are accurate reflections of the disease state or symptom, and neuromodulation paradigms (control policy algorithms) that are customized for that disease/symptom. Tremor is especially well-suited for responsive or CL-DBS as it varies in amplitude or presence over time and differs between PD subjects. CL-DBS for tremor can be approached using control variables such as a peripheral measure of tremor (Kinematic Cl-DBS) or the STN LFP beta band (13–30 Hz) power (Neural CL-DBS) (Malekmohammadi et al., 2016). Attenuation of STN beta band power by medication or DBS is associated with improvement in both rigidity and bradykinesia and has been the control variable used in CL-DBS studies to date (Kuhn et al., 2008; Whitmer et al., 2012). However, the presence of tremor itself may attenuate beta band power and thus Neural CL-DBS may not be useful for tremor (Shreve et al., 2017).

The effectiveness and efficiency of Kinematic compared to Neural CL-DBS and to open loop DBS were determined in six PD subjects (Malekmohammadi et al., 2016) using a dual threshold control policy algorithm, (**Figure 3**), for either beta band power, (**Figures 3A,B**), or tremor power, measured by a Bluetooth enabled smartwatch (**Figure 3C**). Voltage was increased if either beta or tremor power was above the upper threshold, remained the same if between thresholds, and was decreased if below the lower threshold. Both techniques improved tremor to a similar degree; Kinematic CL-DBS used 10.6% of the total energy that would have been delivered (TEED) during open loop DBS and Neural CL-DBS used 31.5% TEED. Kinematic CL-DBS was significantly more efficient than Neural CL-DBS ($P < 0.05$). Neural CL-DBS was efficacious in treating tremor if the initial voltage was in a therapeutic range; whereas Kinematic CL-DBS required tremor to be present and initial voltage was set at the lower therapeutic limit. This research demonstrates that CL-DBS, using either a neural or kinematic control variable, is more efficient than open loop DBS. Furthermore, it highlights the potential that additional development of patient- and symptom-specific control variables, and control policy algorithms will improve the efficiency, efficacy and specificity of DBS therapy for PD.

Highlights and Future Directions

- Tremor in PD is a symptom especially well-suited for responsive or closed loop DBS as it varies in amplitude or presence over time and differs between patients.
- In a pilot trial, there were no differences between tremor control with adaptive DBS using Kinematic or Neural CL-DBS and Kinematic CL-DBS was significantly more efficient than Neural CL-DBS KCL-DBS.

Closed-Loop DBS for Freezing of Gait in PD

Levodopa-resistant posture, and FOG symptoms are disabling and difficult to address in patients with PD. Recent DBS trials have rarely addressed FOG and specifically "on-medication" freezing and falling. Freezing appears to involve some GABA-ergically-mediated activity of the globus pallidus

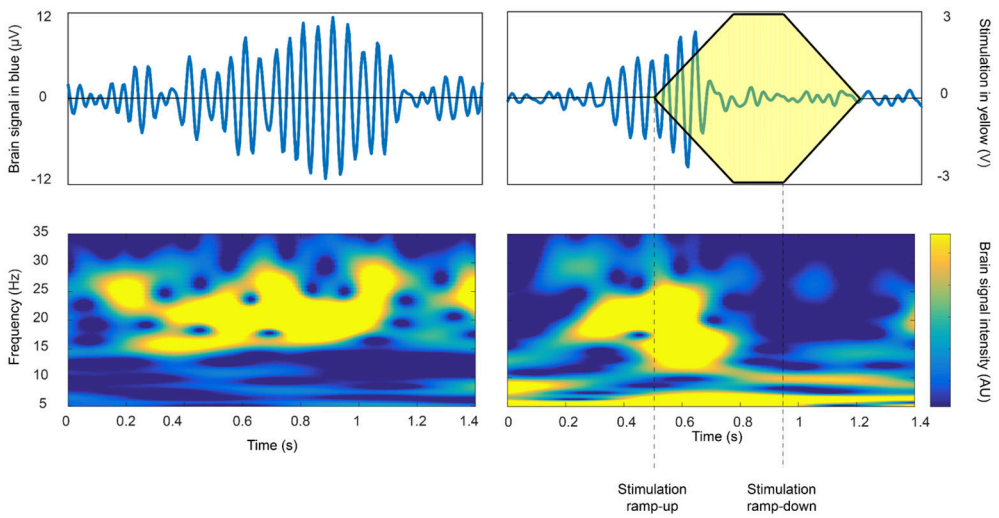

FIGURE 2 | The beta burst duration and amplitude as a potential biomarker for closed loop approaches. On-off feedback control of beta activity recorded in the subthalamic nucleus in a patient with PD so as to terminate long duration, high amplitude beta bursts. Intermittent stimulation may be sufficient to improve motor impairment, whilst sparing more physiological periods of processing and thereby limiting side-effects (Tinkhauser et al., 2017 with permission).

interna (GPi) that leads to dysfunction of the pedunculopontine nucleus (PPN). Human DBS studies have targeted the PPN or the PPN plus STN with mixed—and in many cases, unsatisfactory outcomes (Stefani et al., 2007; Moreau et al., 2009; Moro et al., 2010). However, there is no consensus regarding the best PPN target and both rostral and caudal pedunculopontine nucleus subregions have been targeted (Thevathasan et al., 2017). There is great variability in clinical methodology used among surgical centers and the spread of stimulation and inconsistency in targeting suggests that neighboring brain stem regions may be implicated in any DBS response. Because of the intermittent nature of FOG, a feasibility closed-loop neuromodulation (CL-DBS) approach for bilateral PPN DBS plus conventional bilateral open-loop DBS (OL-DBS) of the GPi to manage on-medication FOG in PD has been initiated at the University of Florida. Five patients with advanced PD and refractory FOG were implanted with Medtronic Activa PC+S implantable neurostimulators leads. The patients were carefully evaluated, so as to define true "on" medication freezers. A closed-loop PPN DBS paradigm has been developed using LFPs occurring in GPi and PPN during normal walking and during maneuvers known to trigger freezing episodes. Assessments are blinded and videotaped including objective gait laboratory analysis. PPN CL-DBS was aimed to deliver stimulation at different frequencies (5, 25, 65, and 130 HZ) at the onset of gait. This PPN CL-DBS paradigm was also used for long-term PPN CL-DBS via the Nexus-E firmware, which allows similar Nexus-D operation, but is a completely embedded, enclosed system with no external triggers or machines. GPi stimulation settings were determined by clinical benefit consistent with current standard of care for optimizing pallidal DBS. The study remains ongoing and will report safety and feasibility of this approach along with clear neurophysiological changes in beta and theta bands that could be potential biomarkers to guide future adaptive DBS approaches.

Highlights and Future Directions

- A novel closed loop DBS system that targets GPi and PPN is currently investigated for treatment of refractory "on" FOG in PD patients. Approach appears safe and applicable.
- Challenges will include establishing the most effective location of PPN contacts, and programming settings, identifying reliable neurophysiological biomarkers of walking and FOG, and refining patient selection in light of wide variability among advanced PD patients.

Closed Loop Deep Brain Stimulation for PD: Update on Use of Cortical Control Signals

Currently used DBS devices generally deliver "open loop" stimulation, continuously stimulating target structures regardless of changes in the brain circuits related to disease expression. Device programming is a labor-intensive process that is based on "trial and error" and requires significant clinical expertise, which are barriers to widespread clinical application. Additionally, continuous open-loop DBS for PD may result in suboptimal control of fluctuating motor signs, stimulation-induced adverse effects, and short battery life (Little et al., 2016).

As previously noted, one approach is to utilize subthalamic beta band activity as the control signal for closed loop stimulation (Little et al., 2013). Advantages of this approach include conceptual simplicity, and that the control signal can be derived from the same electrode array as used for therapeutic stimulation, thereby obviating the need for additional sensor electrodes. Disadvantages include a relatively low amplitude signal with high stimulation artifact, and that the beta band activity is strongly affected by normal movement, not just the severity of Parkinsonian motor signs (Qasim et al., 2016). We have developed an alternative technique for closed loop stimulation in PD using a sensor that is permanently implanted

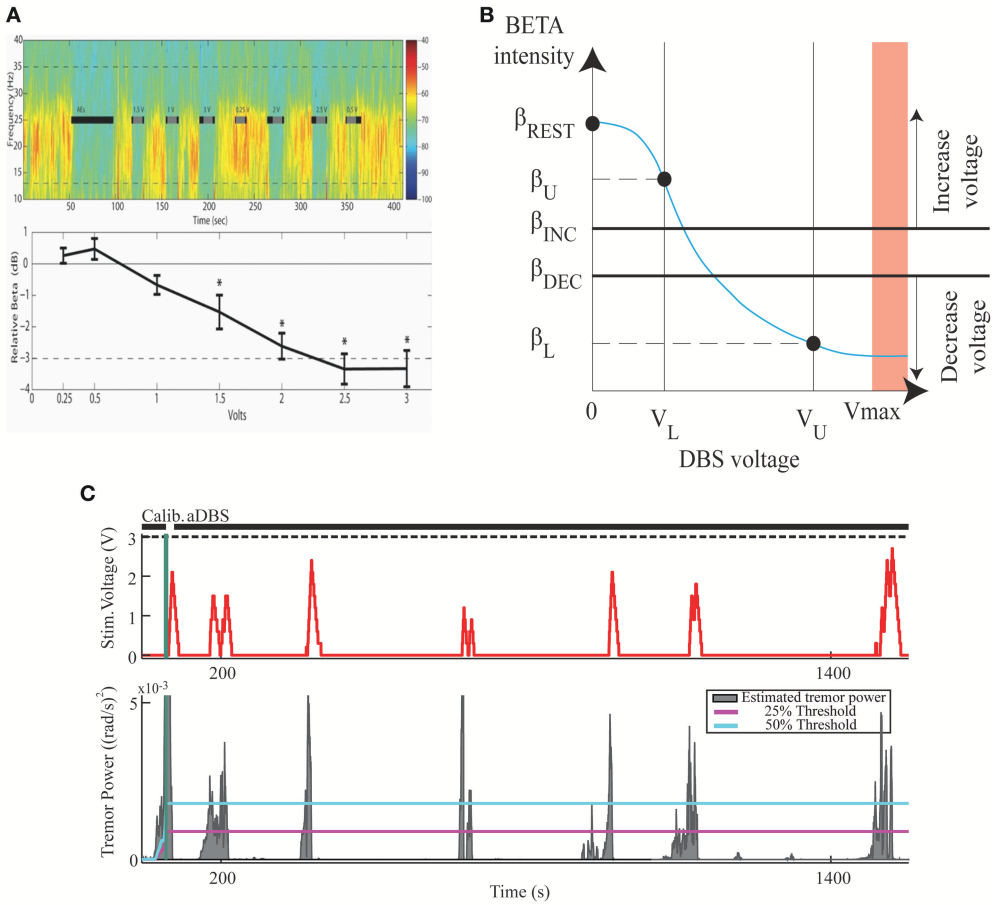

FIGURE 3 | The Development of a Closed Loop System for PD Tremor. **(A)** Voltage dependent attenuation of STN beta band power; top panel- time frequency spectrogram, black bars indicate periods of STN DBS; lower panel group averaged relative beta band power at different DBS voltages. **(B)** Dual threshold control policy diagram; β_{REST}–beta power no DBS at rest; β_U, β_L–beta power at lower and upper limits of DBS voltage; β_{INC}, β_{DEC}–beta power of upper and lower thresholds. **(C).** Example of STN KCL-DBS using dual tremor power thresholds (lower panel blue and magenta lines). DBS voltage (upper panel) follows tremor power and remains off for much of the trial when there is no tremor.

in the subdural space over the primary motor cortex. This is attached, along with the ipsilateral subthalamic stimulating lead, to an investigational pulse generator (Activa PC+S, Medtronic) with sensing as well as stimulation capability that can be used to prototype feedback control algorithms. The control strategy is based on detection of a narrow band gamma oscillation (60–90 Hz) that has previously been shown to be a biomarker of the dyskinetic state (Swann et al., 2016) (**Figure 4**).

We have tested this method in three phases (1) *in vitro* experiments using previously collected cortical signals converted to analog voltages and applied to a saline bath containing a paddle lead attached to an external PC+S; (2) in the clinic, streaming data from an implanted PC+S to an external laptop that controlled the PC+S stimulus via radiotelemetry (Herron and Chizeck, 2014), and (3) in a second clinical application, which evaluated the control algorithm totally embedded in PC+S. In two test subjects, closed loop control (Nexus E) provided 26 and 39% reduction in energy delivered, without adverse effects. Patients in this study did not perceive stimulation-related changes. Cortical contacts were implanted through the same DBS burr hole and appeared to be stable in the long-term (as observed in other recent studies conducted at multiple sites).

Highlights and Future Directions

- A new technique aims to optimize electrophysiological signals used for closed loop DBS using a sensor permanently implanted in the subdural space over primary motor cortex.
- Utilizing an investigational pulse generator (Activa PC+S, Medtronic), the control strategy is based on detection of a narrow band gamma oscillation (60–90 Hz) previously shown to be a biomarker of the dyskinetic state.
- Future challenges include identifying the most effective type of detection; selecting the best type of signal; noise reduction; identifying the ideal frequency band; and discerning between use of single vs. multiple frequencies.

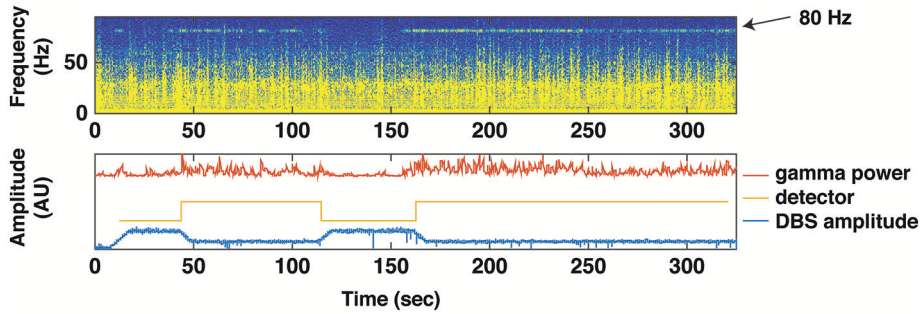

FIGURE 4 | Using Gamma Power as a Biomarker for Closed Loop Deep Brain Stimulation. A brief trial of closed loop stimulation using a cortical detector in a patient with intermittent dyskinesia in spite of therapeutic STN DBS. This trial was implemented with data streaming from PC+S to an external computer (using Nexus D2/3). Top: spectrogram of motor cortex ECoG signal over 300 s, showing several epochs of an 80 Hz oscillation heralding the dyskinetic state. Bottom: transitions in stimulation triggered by the 80 Hz oscillation. Red line depicts the gamma power envelope at 80 Hz center frequency and 5 Hz bandwidth. Gold line depicts the detector that classifies gamma power to high or low values. Blue line depicts spectral power at stimulation frequency (160 Hz). When average gamma power (over 10 s) exceeded or dropped below a threshold (2.5 × standard deviation of gamma power during a calibration recording), stimulation was decreased, or increased, respectively.

Deep Brain Stimulation for Other Neuropsychiatric Conditions

Tourette Syndrome

Tourette syndrome (TS) is a developmental neuropsychiatric disorder characterized by involuntary and vocal tics, which is commonly co-morbid to other conditions, such as attention deficit hyperactivity disorder and obsessive compulsive disorder (Cheung et al., 2007; Kenney et al., 2008). The etiology of TS remains largely unknown; however, a commonly accepted hypothesis implicates dysfunction of corticostriatal and thalamocortical circuits (Albin and Mink, 2006). DBS is an emerging therapy for cases of severe and intractable TS, and next generation DBS devices, such as the Neuropace RNS and Medtronic Activa PC+S, provide tools with which to record electrophysiological signals that can be used to study network effects and pathophysiology in this disorder.

Two studies of TS electrophysiology using DBS have recently been conducted at the University of Florida. The first implanted dual DBS leads in the centromedian- parafascicular complex of the thalamus, and employed a NeuroPace RNS device both to study electrophysiology of tics and to develop a responsive neurostimulation paradigm. Responsive DBS was achieved in one subject, delivering stimulation in response to increases in low-frequency activity (5–15 Hz) in the thalamus that correlated with dystonic tics (Molina et al., 2017). A second study, using the Medtronic Activa PC+S devices targeted the same thalamic nucleus bilaterally, but also included bilateral cortical subdural strips over the motor cortex to study the thalamocortical network of tic generation (Shute et al., 2016).

Long complex tics were shown to be concurrent with a consistently detectable low frequency activity in the thalamus, as shown in other studies. However, stimulation artifacts resulted in the development of a responsive DBS based on the cortical signatures of tic generation, which involved increases in cortical beta activity (Shute et al., 2016). An ongoing NIH study is examining the physiology of tics and closed loop DBS in 10 human subjects. Resetting tic mechanisms to achieve a more normal pattern of oscillatory activity may reduce tics and also lead to less device discharge over longitudinal follow-up.

Highlights and Future Directions

- Pilot studies of responsive neurostimulation in TS patients have been conducted and a larger trial is currently underway.
- Neural activity precedes tic onset, and successful stimulation results in cortical phase amplitude coupling.
- Future challenges—and opportunities—include developing consistent programming algorithms, improving stimulation settings, achieving higher resolution tic detection, and defining additional biomarkers.

Optimizing Neurophysiologic DBS Signal for Treatment of Tourette Syndrome

LFP analysis is a well-established method for investigating disease, and network and stimulation dynamics in PD. Analysis of intraoperative basal ganglia LFPs can potentially predict the optimal stimulation contact (Ince et al., 2010). There is increasing interest in the use of DBS to treat signs and symptoms of TS, and multiple DBS targets have been proposed for the treatment of TS (Viswanathan et al., 2012). LFP analysis using signals captured from a combination of DBS electrodes and cortical recordings has previously shown thalamocortical activity changes during tics in TS (Shute et al., 2016). Limited data exist about the role of LFPs in the posteroventral GPi in TS, although open label stimulation at this site does seem to improve symptoms (Shahed et al., 2007).

LFP recordings from the GPi during an intraoperative testing paradigm capturing the resting state, voluntary movements, and tic activity have been analyzed and reported in 3 subjects with TS (Jimenez-Shahed et al., 2016). The LFP data filtered between 13 and 30 Hz indicated the presence of event related desynchronization with lower amplitude beta band oscillations during tic periods compared to the resting state. During tic periods, there was also amplitude enhancement in the gamma range (40–150 Hz) and higher frequencies (150–500 Hz) in all subjects. Subjects demonstrated individual changes in the

spectral power of LFPs in both the low and high frequency oscillations (HFO) during different states. The resting state was further characterized by coupling between the phase of theta-low alpha oscillations to the amplitude of HFOs in two subjects, while tic activity was associated with beta-HFO phase-amplitude coupling (PAC) in all 3 subjects. These results were in contrast to the novel identification of beta-HFO PAC in the GPi of four un-medicated PD patients at rest. These findings suggest that tic activity can be neurophysiologically distinguished (at the subcortical level) from rest, voluntary movements and akinesia, and that the GPi is a viable target for neuromodulation to decrease tics in TS. Additionally, these data challenge the view that beta-HFO PAC is only a marker of akinesia, since tics represent a hyperkinetic state. These results also highlight the importance of investigating the HFO range of LFP activity.

Given these findings, we posit that continuing investigation of the LFP spectral characteristics and non-linear interactions between different LFP frequency bands across nodes within the basal ganglia-thalamo-cortical network in TS (and other movement disorders) will broaden understanding of the neurophysiologic abnormalities characterizing these conditions. This knowledge will also contribute to the identification of the most appropriate and sensitive signals to trigger closed loop stimulation when different movement patterns are present.

Highlights and Future Directions

- LFP recordings from the GPi demonstrate individual changes in the spectral power in both the low and HFO sub-band during different rest, voluntary movements or tics.
- Tic activity was associated with beta-HFO phase-amplitude coupling in this study.
- Continued investigation of the LFP spectral characteristics of different movement disorders will contribute to the identification of the most appropriate and sensitive signals to trigger and to develop closed loop stimulation.

Studying Oscillatory Activity in Deep Brain Stimulation for Depression

DBS of the subcallosal cingulate white matter (SCCwm) has been shown to elicit durable improvements in depressive symptoms (Riva-Posse et al., 2017). Here, preliminary work is presented that characterizes network-level electrophysiological changes in patients with treatment-resistant depression who were implanted with SCCwm-DBS. Using a prototype bi-directional DBS platform that employed the Activa PC+S (Stanslaski et al., 2012) in conjunction with dense array EEG, preliminary evidence of electrophysiologic changes in the SCC and downstream cortical regions was demonstrated that correlated with both the disease state and stimulation conditions.

In order to assess the validity of any oscillatory biometric captured from patients with chronically implanted prototype devices, preliminary evaluations focused upon limitations of oscillatory analyses in the context of technical device capabilities. In particular, it is known that amplifier limitations are sensitive to disease-independent tissue impedances and impedance changes. Thus, amplifier-related distortions present in bi-directional DBS devices during stimulation were modeled in order to identify potential spurious oscillatory results. Non-linear gain responses from an amplifier that is engaged to its output limits can result in strong high-frequency oscillations and low-to-high phase-amplitude coupling spuriously because of soft-clipping of the input signal. In light of this, we are developing an interactive tool that can be used to assess level of gain compression making analysis and interpretation of oscillatory results more reliable.

Modern analytical approaches were employed to overcome challenges that result from both recording noise and low patient sample sizes. Next, we utilized a machine learning-based algorithm to extract oscillatory biometrics in the chronic PC+S recordings. This approach, when learned on limited, noisy data in a training set, is able to predict the current level of depression severity (as measured by weekly rating scales) with approximately 50% correlation in a testing set of patients. This strategy appears to have technical, analytical, and practical advantages given the limited number of patients, sparseness of sampling, and the known trajectory of clinical depression response(s). This approach, when complemented with standard Fourier-domain approaches, can help to identify useful models for biometrics construction that can be based on correlative analyses.

Despite promising initial results, the exact mechanism of action of SCCwm-DBS still remains unclear, but appears to involve cortical regions beyond the site of stimulation (Mayberg et al., 2005). Using multimodal electrophysiology, we are therefore investigating rapid, transiently induced cortical oscillatory responses to connectomics-optimized SCCwm-DBS. In all patients with simultaneous PC+S LFP and dense EEG, alpha power change patterns can be used to clearly separate stimulation at the optimal SCC contact from stimulation at an adjacent contact on the DBS lead just 1.5 mm away. The complementary accuracy and reliability of this method in confirming current tractographic approaches is the focus of ongoing studies employing a larger cohort.

Highlights and Future Directions

- Various approaches can be used to identify putative biometrics of depression and anatomic sites and networks that be employed in future closed-loop DBS to objectively confirm proper anatomical targeting and potentially optimize therapeutically effective parameters of DBS in treatment of depression.
- Assessment, iterative modification, and expanded testing-set validation will be continued in ongoing investigations with additional subjects.
- Future opportunities will focus upon identifying stimulation settings that will reproduce the putative biomarkers observed on EEG.

Central Thalamic Stimulation for Traumatic Brain Injury (TBI)

Involvement of the central thalamus has been implicated in the pathophysiology of certain types of traumatic brain injury (TBI). As this area links to other relevant brain networks and regions, the involvement of the central thalamus may play an important—and reciprocal—role in other brain responses to TBI, as well. Neural networks mediating arousal project

to the central thalamus, with efferent projections to the anterior forebrain (Schiff, 2016). Pre-clinical animal (non-human primate—NHP) and rodent) models have elucidated these central thalamic to forebrain connections and their functional activation using electrophysiologic methods and optogenetic techniques combined with fMRI (Liu et al., 2015; Baker et al., 2016). Proof of concept that DBS of the central thalamus can produce improvements in cognitive performance and arousal supports the further development of clinical studies (Giacino et al., 2012). Additional studies in human patients with minimally conscious state showed that central thalamic DBS produced improvement(s) in both motor and cognitive function. Notably, a single-subject in minimally conscious state demonstrated motor and cognitive improvement with central thalamic DBS; this patient regained capacity to identify objects and speak after an initial titration phase along with improvements in attention and organized activity of the upper limb. Oral feeding was greatly improved with DBS as well. A clinical trial targeting patients with persistent cognitive difficulties after TBI is planned. Six patients with severe to moderate brain injury (GOSE Outcome level 6–7) at least two years following their initial injury with persistent cognitive impairment limiting regaining vocation and social reentry will be enrolled. The primary outcomes measure will test attention and working memory function. EEG will be used as a secondary physiological marker of cognitive impairment in order to examine physiological mechanisms of DBS effects and to potentially develop adaptive technologies.

Highlights and Future Directions

- Preclinical and clinical data support the role of the central thalamus and its projections in arousal and attention.
- A clinical trial aiming to assess the effect of central thalamic DBS in patients with TBI is underway. Cortical recordings and correlates of cognitive function will be explored using recording DBS technology and EEG.
- Challenges include establishing definitive anatomical substrate(s) for stimulation, selecting ideal candidate patients, obtaining neuroimaging assessments, and developing and implementing the most effective and reliable programming techniques.

Adaptive DBS for Obsessive Compulsive Disorder (OCD)

Ventral Striatum (VS) DBS has FDA humanitarian device exemption approval for treatment of intractable OCD, and has been shown to incur 60% clinical benefit in recent meta-analysis (of open-label studies) (Alonso et al., 2015). However, management and programming strategies are increasingly challenged to provide persistent benefit while limiting the occurrence of DBS-induced behavioral side effects, most notably hypomania (Widge et al., 2016). Programming adjustments have been made largely on the basis of acquiring acute beneficial effects on outcome measures of "anxiety reduction," "improved mood" and "increased energy." Induction of "mirth" has served as a guidepost measure to programming, and has been regarded as predictive of good response to treatment (Haq et al., 2011). However, DBS-induced mirth also represents a potential risk for development of hypomania or mania. Thus, there is a clear need for an adaptive DBS (aDBS) system that can correctly assess hypomania as distinguished from a euthymic mood state, and automatically adjust stimulation accordingly.

A pilot study funded by the NIH BRAIN Initiative aims to develop and to test a prototype aDBS system for intractable OCD that uses LFP signals to automatically adjust DBS parameters to both improve symptom management and reduce stimulation-induced behavioral side effects. One of the challenges of this study was to identify a label for the classifiers that was objective, reliable, and fitting the National Institute of Mental Health (NIMH) Research Domain Criteria (RDoC) Constructs. Positive Valence (e.g., for elevated or euthymic mood) and Negative Valence Constructs (e.g., to encompass depression, anxiety, and disgust associated with worsening OCD) were selected, with facial affect being used to represent the motor output of emotional state; a measure considered to be superior to clinician ratings of affect for tracking changes in real time. The automated facial affect recognition (AFAR) platform (Tian et al., 2001) will be utilized, and time-locked with inputs from LFPs, EEG, motion, physiology, and changes in DBS programming in order to build classifiers for use in this, and future studies.

Highlights and Future Directions

- Ongoing studies are underway toward the development of adaptive technology that can provide accurate classification of acute fluctuations in obsessive ideation and/or compulsive behaviors that can be used to improve DBS programming for use in treatment of OCD.
- The use of an automated facial recognition program will be evaluated as a potential biomarker of emotional state and to determine feasibility for use in adaptive control.
- Challenges include determining how the system can separate physiologic from pathological states, and if and how the system can adequately classify numerous behavioral signals.

Brain State Monitoring for Closed Loop Epilepsy

Epilepsy is an epidemiologically common neurological disease and over 1/3 of patients have drug resistant epilepsy. In select cases, neurosurgical intervention can cure focal epilepsy, but many patients are not surgical candidates because their seizures are poorly localized or originate from brain regions that cannot be safely resected. Seizures are generally treated as random events, and there are currently no proven surrogate biomarkers for seizures. Clinicians must select a treatment and titration plan (drug, dose, stimulation parameters, etc.) based on clinical guidelines, and then wait for a treatment failure to make further treatment adjustments.

Advances in neural engineering have led to implantable devices capable of therapeutic electrical stimulation (Fisher and Velasco, 2014), seizure detection and forecasting (Cook et al., 2013). Electrical stimulation of the anterior nucleus of the thalamus (Fisher et al., 2010; Salanova et al., 2015) and responsive stimulation of detected electrophysiological abnormalities (Morrell and RNS System in Epilepsy Study Group, 2011; Heck et al., 2014; Bergey et al., 2015) were shown to reduce seizure burden in well-designed pivotal trials, but patients rarely

achieved complete seizure freedom. Recently, multiple groups have demonstrated the feasibility of seizure forecasting in both humans (Park et al., 2011; Cook et al., 2013; Brinkmann et al., 2016) and canines (Howbert et al., 2014; Brinkmann et al., 2015) using intracranial EEG. Seizure forecasting has also been demonstrated in ambulatory patients with an implantable device that provides continuous intracranial EEG (iEEG) integrated with a personal assistant device (PAD), running both seizure detection and forecasting algorithms (Cook et al., 2013). Next generation implantable devices are now poised to transform epilepsy management by integrating brain sensing, active brain probing, seizure detection, electronic seizure diaries, seizure forecasting, and intelligent therapeutic stimulation.

The fact that seizure probability fluctuates opens the possibility of directly tracking seizure probability and dynamically adjusting therapy to prevent seizures. Furthermore, it has been shown that the neuronal assemblies activated during seizures may be consolidated in post-seizure slow-wave sleep, i.e., physiological learning mechanisms may strengthen the seizure engram (Bower et al., 2015). This observation suggests targeting neuronal dynamics during post-seizure slow-wave sleep as a brain state dependent therapy. Thus, devices providing continuous brain sensing, probing, and intelligent stimulation based on seizure probability and brain state can open new therapeutic options. In addition, the ability to directly interact with the nervous system could open a new era of brain research.

For example, the RC+S (Bourget et al., 2015) is a rechargeable device, with sensing, stimulation, embedded computational payloads, and continuous iEEG telemetry that affords capability of distributed computing & analytics on a hand-held PAD and cloud environment. It is also rechargeable. Currently pre-clinical development and validation of RC+S in dogs with naturally occurring epilepsy is underway and a human feasibility trial is planned for early 2019 (**Figure 5**).

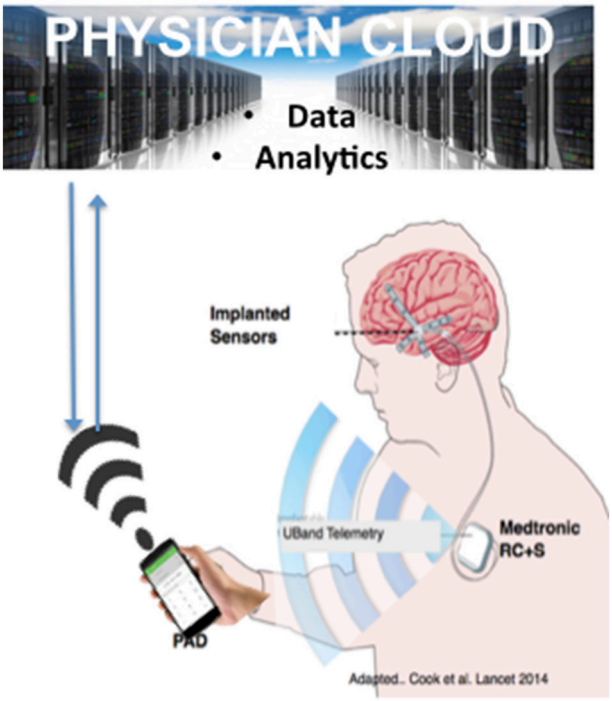

FIGURE 5 | Next Generation Epilepsy Therapy Platform. The implanted, rechargeable Medtronic RC+S provides bi-directional coupling with the brain in patients with epilepsy. The personal assistant device (PAD) provides off-the-body analytics and is bi-directional with a cloud environment. The figure is adapted from Cook et al. with permission (Cook et al., 2013 with permission).

Highlights and Future Directions

- There is a need for developing better tools to precisely identify and analyse seizures. Neuronal ensembles during seizures using scalp EEG have shown that neurons that fire together (at the onset of seizure), wire together (during slow wave sleep).
- Utilizing advanced DBS devices, a currently initiated preclinical study aims to continuously stream EEG data to detect anomalies in epilepsy, and improve seizure forecasting and detection.

DBS ELECTRODES

Electrochemistry of Deep Brain Stimulation Electrodes

The purpose of DBS electrodes is to artificially manipulate neural activity by generating an electric field in the tissue, ultimately resulting in a redistribution of charged particles in the extracellular space. Ideally, the electrode charge is injected capacitively, so that electrons are not transferred between the electrode-tissue interface and charge is rearranged in the tissue in response to the injected charge on the electrode side. The amount of charge injected is transferred via an electron transfer process (i.e., a faradaic reaction), and capacitive reactions occur as well (Merrill et al., 2005). Undesired faradaic reactions include electrode dissolution products that diffuse into tissue (**Figure 6**).

Balancing the amount of charge injected during the stimulation phase by a subsequent phase of the opposite polarity was formerly thought to avoid undesirable faradaic reactions. However, imbalanced charge biphasic waveforms are now known to reduce the amount of platinum (Pt) electrode dissolution when compared to balanced charge biphasic waveforms (Kumsa et al., 2016). In addition to minimization of Pt dissolution, imbalanced charge biphasic waveforms extend the parameter space that could be explored for current steering to selectively activate a target brain region during DBS therapy. More often than not, selection of stimulation parameters is made under consideration for thresholds of tissue damage. While there is no recognized standard addressing safe levels of stimulation, the Shannon plot has been used to set charge and charge density limits. Acute animal data collected used to establish the Shannon plot implies that tissue damage might be dependent on charge injection and surface area of the electrode used. These considerations may guide future selections of electrode materials and/or stimulation parameters.

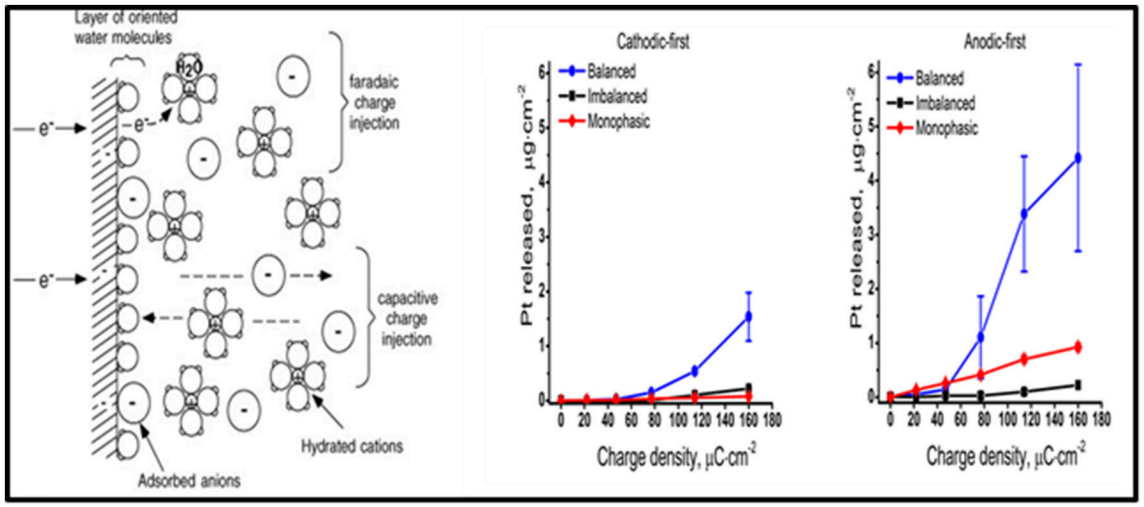

FIGURE 6 | The electrode-electrolyte interface. A schematic representation of the electrode-electrolyte interface [from (Merrill et al., 2005 with permission) far left]. The concentration of Pt measured at different charge densities for cathodic-first (middle) and anodic-first (far right) stimulation waveforms (Kumsa et al., 2016 with permission).

Highlights and Future Directions

- Design considerations for DBS electrodes should incorporate the needs of different spatial and temporal resolutions.
- Charge considerations include safety limits for charge density to avoid tissue damage that can be further characterized by animal studies to demonstrate:
  - Shannon plots of tissue damage thresholds (30 uC/cm^2 warning derived from Shannon plot at 50 Hz); and
  - Charge-balanced biphasic waveforms.
- The threat of stimulation-induced damage has been shown to be dependent on charge injection and the surface area of the electrode.

Biophysics of Recording through Deep Brain Stimulation Electrodes

LFP recordings from DBS electrodes represent an exciting opportunity to study pathological activity in neurological disorders and to provide a potential control signal for closed-loop DBS systems. In PD, these LFP recordings have shown pathological hyper-synchrony within the beta frequency range (e.g., 13–30 Hz) and the oscillations can be reduced with therapeutic DBS (Kuhn et al., 2008; Bronte-Stewart et al., 2009). Closed-loop stimulation using the beta-band LFP as a control signal has demonstrated the potential to improve both the efficiency and possibly the efficacy of DBS (Little et al., 2013; Rosa et al., 2015). New implantable systems can also perform both stimulation and recording through DBS leads (Kuhn and Volkmann, 2017).

Although LFP recordings have the potential to provide disease biomarkers and a control signal for closed-loop stimulation, the origin of the LFP is poorly understood. Because clinical applications of the LFP (e.g., to optimize implant location) exploit the spatial dimensions of the LFP and relative changes in its frequency content (Zaidel et al., 2010), successful application of LFP recordings requires accurate interpretation of the source, recording volume, and various experimental factors (e.g., non-ideal properties of the recording system).

In general, the LFP is believed to be dominated by postsynaptic currents (Kajikawa and Schroeder, 2011). Previous experimental studies with intracortical microelectrodes suggested that the LFP only extends a few 100 µm (Katzner et al., 2009) while contradictory evidence suggest that the LFP can extend several millimeters (Kajikawa and Schroeder, 2011). A computational modeling study showed that the LFP spatial reach is not simple or stationary, but depends on a number of variables, such as neuron morphology, and the distribution and correlations in synaptic activity (Linden et al., 2011). A computational model to specifically characterize LFP recordings from DBS electrodes was previously developed (Lempka and Mcintyre, 2013). Using this model, it was determined that the LFP can extend several millimeters and that its spatial reach was dependent on factors such as the spatial distribution of correlated synaptic activity and the recording configuration, but was independent of the electrode impedance (see **Figure 7**).

To further increase the clinical utility of this modeling approach, a patient-specific LFP model to estimate the region of beta hyper-synchrony within the STN was developed. The model demonstrated that the size and shape of correlated activity within the STN and its relative location to the DBS lead dramatically affect the recorded LFP. It is believed that this patient-specific modeling approach represents an excellent tool to study the neural underpinnings of clinical LFP recordings and to help provide the knowledge necessary to develop effective closed-loop DBS technologies.

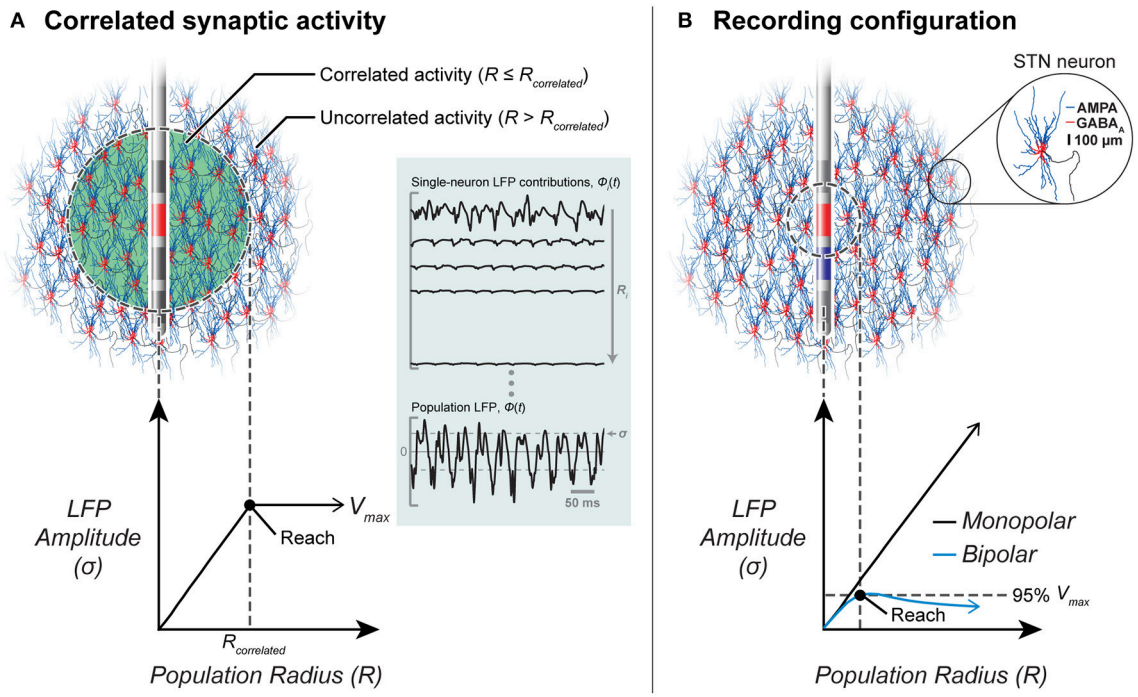

FIGURE 7 | LFP recordings from DBS electrodes. **(A)** Correlated synaptic activity dominates the LFP and determines its spatial reach. A DBS electrode is shown implanted in the center of a volume of STN neurons. Neurons within a population radius ($R \leq R_{correlated}$) receive highly synchronous synaptic inputs while the remaining neurons ($R > R_{correlated}$) receive uncorrelated synaptic inputs. Within correlated regions, an increase in the population radius produces a linear increase in the amplitude of the LFP. Outside of the correlated volume, there is no significant increase in the LFP amplitude. **(B)** Recording configuration effects on the LFP. In this example, all neurons receive correlated synaptic inputs. For a monopolar recording (red electrode only), the LFP amplitude increases linearly with an increase in the population radius and does not converge to a maximum value. However, a bipolar recording (red electrode—blue electrode) limits the amplitude and spatial reach of the LFP recording.

Highlights and Future Directions

- The origin of the LFP is poorly understood with conflicting information regarding LFP's spatial reach.
- A previous computational model determined that the LFP can extend several millimeters and that its spatial reach was dependent on factors, such as the spatial distribution of correlated synaptic activity and the recording configuration, but was independent of the electrode impedance.
- A new computational model demonstrated that the size and shape of correlated activity within the STN and its relative location to the DBS lead dramatically affect the recorded LFP.
- Understanding the neural mechanisms of clinical LFP recordings is necessary to develop effective closed-loop DBS technologies. Future research will focus on determining the LFP construct, LFP interpretation based on electrode position, changes in new directional leads and variation over time.

Coupled Theoretical and Experimental Analysis of DBS Electrodes

Nearly all DBS leads implanted to date consist of a stack of four cylindrical electrode contacts. More recently, directional DBS leads with electrode contacts segmented along and around the lead body have shown utility for more selective targeting of neural pathways of interest while avoiding activation of neural pathways implicated in DBS side-effects (Buhlmann et al., 2011; Martens et al., 2011; Keane et al., 2012; Zitella et al., 2013; Pollo et al., 2014) (See **Figure 8**). Computational models that integrate realistic tissue bioelectrics and cellular biophysics provide a useful framework to assess the design and performance of these directional DBS lead designs.

While many directional DBS lead designs have been proposed, computational models suggest that designs incorporating 3–4 radial electrodes used in concert with multi-channel independent current-controlled stimulation provide a good balance of (1) maintaining safe current density limits when using smaller electrodes at therapeutic stimulation amplitudes; and (2) requirements for higher channel counts to enable better shifting and sculpting of the activation volumes around a DBS lead (Teplitzky et al., 2016; **Figure 8**). Further, computational models have also shown that directional DBS leads can move the center of mass of axonal activation by (at most) 1–1.3 mm tangential to the lead shaft (Teplitzky et al., 2016). This suggests that directional DBS leads, while an enabling technology, may not be able to

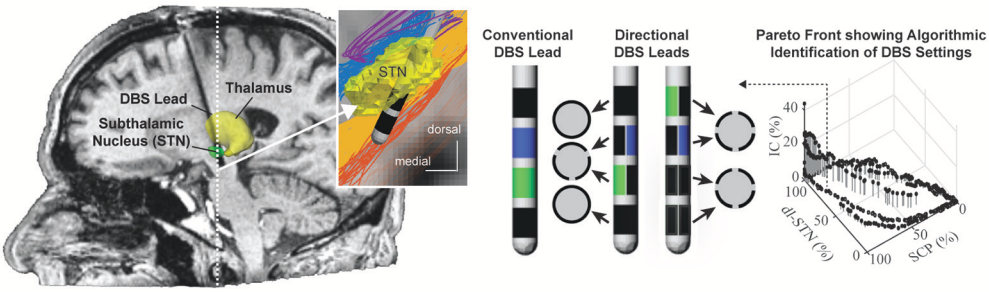

FIGURE 8 | Programming of directional DBS lead designs. Conventional and directional DBS lead designs targeting the subthalamic nucleus for the treatment of Parkinson's disease. Computational programming algorithms can accommodate multiple regions of interest such as the dorsolateral subthalamic nucleus (dl-STN) and the superior cerebellar peduncle (SCP) as well as multiple regions of avoidance, i.e., the corticospinal tract within the internal capsule (IC). Shown is an example of a Pareto Front resulting from the particle swarm optimization algorithm approach to identify stimulation settings that maximize activation in regions of interest and minimize activation of regions of avoidance. Images courtesy of Edgar Peña, Julia Slopsema, and Matthew Johnson (with permission).

rescue therapy for DBS leads that are implanted significantly (>1–1.3 mm) off target. Models also suggest that axonal tracts oriented parallel, in comparison to perpendicular, to the applied electrical field will have lower activation thresholds (Lehto et al., 2017). Such orientation selectivity might help with structural leads design and avoid adverse side effects with DBS.

Once a DBS lead is implanted, stimulation settings are typically tested in a trial-and-error process by stimulating through combinations of electrode contacts to identify stimulation settings that optimize the therapeutic effect based upon clinical outcome measures (Volkmann et al., 2006). Recent developments in subject-specific computational bioelectric models and visualization of the predicted neuronal pathways activated have shown promise in identifying DBS settings that avoid inducing side effects (Frankemolle et al., 2010; Chaturvedi et al., 2013) Leveraging these computational models, several novel semi-automated programming algorithms have been advanced to assist with the selection of stimulation parameters. These algorithms have a basis in machine learning (Chaturvedi et al., 2013; Teplitzky et al., 2016), convex optimization theory (Xiao et al., 2016), and most recently particle swarm optimization (Peña et al., 2017), which allow clinicians to use multiple objectives in their identification of optimal DBS settings.

Highlights and Future Directions

- Computational models support the safety of designs incorporating 3–4 radial electrodes used in concert with multi-channel independent current controlled stimulation.
- Computational bioelectric models and visualization of the predicted neuronal pathways activated have shown promise in identifying DBS settings to deliver therapy and avoid inducing side effects.
- Orientation selective DBS that leverages directional lead technology is poised to improve clinical outcomes (Lehto et al., 2017).
- Future clinical implementation of direction leads will likely leverage novel semi-automated programming algorithms to assist with the selection of stimulation parameters.

DBS TARGETING AND METRICS

Noninvasive Biomarkers to Advanced Emerging DBS Electrode Technologies

Directional DBS electrode technology, as available from multiple vendors, is now entering the commercial market. However, there is a lack of robust tools with which to efficiently implement increasingly adaptable and complex DBS systems. To address this problem, new putative biomarkers to measure patient-specific cortical activation patterns elicited by DBS with combined electroencephalography and electrocorticography (EEG/ECoG) have been investigated.

Clinical applicability of effective contacts with a new directional lead incurs a number of challenges, including the number of contacts to be used, potential combinations of contacts, and complex interactions with anatomical structures. Therefore, a goal is to innovate new approaches to tailor DBS programming adjustments in individuals and to more rapidly arrive at effective, well-tolerated stimulator settings with directional lead technology by using software to remove stimulus artifacts. This should facilitate measurement of fast dynamics of brain responses where there is a short latency to stimulation of the cortex. Such knowledge will be important and useful (1) to better understand the concept of DBS dose, and this may have broad applications for the development of minimally invasive biomarkers; (2) to refine surgical targeting of the DBS electrode in real time; and (3) to inform emerging closed loop stimulation strategies.

Highlights and Future Directions

- Technological advances are aimed at developing adaptable devices and biomarkers to measure patient-specific cortical activation patterns elicited by DBS with combined electroencephalography and electrocorticography (EEG/ECoG).

- There is a need to continuously develop and improve effective and simple stimulation settings, surgical targeting, and manipulation of the field of stimulation.
- Questions remain regarding the effects of different stimulation settings among different structures in the basal ganglia (and elsewhere).

Temporal Pattern of Stimulation Is a New Dimension of Therapeutic Innovation

In the course of experiments intended to test the hypothesis that the reductions of symptoms by DBS required regularization of the firing patterns of neurons (Grill et al., 2004), it was discovered that the effects of DBS were strongly dependent on the temporal pattern of stimulation. Specifically, random patterns of subthalamic nucleus DBS were not as effective as regular frequency DBS at relieving motor symptoms in the 6-OHDA lesioned rat model of PD (Mcconnell et al., 2016) or in humans with PD (Dorval et al., 2010). Similarly, random patterns of thalamic DBS were not as effective as regular frequency DBS at relieving tremor in persons with essential tremor (Birdno et al., 2007, 2008, 2012). In addition to supporting the importance of regularization of neural firing to the efficacy of DBS, this finding inspired the idea of explicitly designing temporal patterns of stimulation to increase the efficacy and energy efficiency of DBS.

However, the design space for temporal patterns is enormous—for example a 200 ms duration train, composed of 1 ms bins each which may or may not contain a pulse, results in 10^{50} different possible patterns of stimulation. Therefore, a model-based design approach employing computational evolution to design optimized temporal patterns of stimulation was developed. Computational evolution works analogously to biological evolution, and the organisms in this approach are temporal patterns of stimulation, and the fitness of any particular pattern is evaluated using a model-based proxy for symptoms (Brocker et al., 2017). Thus, an innovative approach to make a temporary direct connection to the brain lead during surgical replacement of the battery-depleted implantable pulse generator (IPG) (Swan et al., 2014), and to conduct short-term intraoperative testing of the model-optimized patterns. The results demonstrated that the optimized patterns either addressed bradykinesia more effectively than conventional regularly patterned DBS (Brocker et al., 2013), or enabled equivalent treatment of bradykinesia but with a substantial reduction in the required energy (Brocker et al., 2017). This latter finding is important, as it enables increases in the battery life of IPGs, reduction in IPG size, or longer intervals between recharging.

Subsequently a start-up company, Deep Brain Innovations, Inc. conducted a multi-center double-blinded trial comparing temporally optimized patterns of stimulation to conventional high frequency DBS. The results of this study demonstrated that temporally optimized patterns of stimulation produced equivalent or better symptom reduction and substantially reduced energy requirements. In addition to their promise to improve DBS therapy for PD, these data suggest that the temporal pattern of stimulation might be a new dimension of therapy parameter adjustment that can be exploited in other applications of neuromodulation.

Highlights and Future Directions

- The effects of DBS were strongly dependent on the temporal pattern of stimulation and computational models can provide optimized patterns to improve efficacy or improve efficiency.
- Optimized patterns improved bradykinesia more effectively than conventional regularly patterned intraoperative DBS.
- Preliminary results showed that stimulation was well tolerated and produced equivalent or better symptom reduction and substantial reduced energy requirement in some patients.

Using Human Connectome Data to Map Deep Brain Stimulation Targets

Stereotactic targeting of the anterior limb of the internal capsule (ALIC) has been used for decades to treat patients with refractory OCD, depression, and other neuropsychiatric disorders. However, there is uncertainty about optimal targeting within the ALIC, as different locations appear to have variable efficacy/effectiveness. Using diffusion tensor imaging (DTI), the ALIC was anatomically segmented based on prefrontal connectivity in order to evaluate the effect of various stereotactic targets.

ALIC segmentations based on frontal Brodmann area (BA) connectivity were generated and combined for 40 subjects from the Human Connectome Project (HCP) using connectivity-based seed classification (Nanda et al., 2017). A literature review revealed five stereotactic targets within the ALIC. Targets were modeled as 5 mm spheres and were evaluated for overlap with various DTI-defined ALIC segments. Deterministic tractography was performed on an 842-subject HCP DTI template using modeled targets as seeds to identify involved connectomic networks (**Figure 9**).

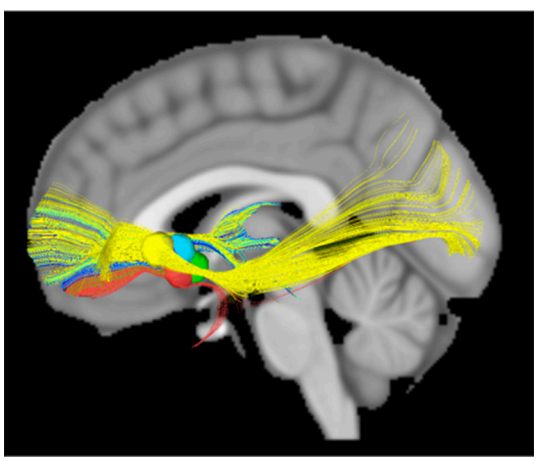

FIGURE 9 | DTI modeled structural connectivity. Tracts running through the five modeled targets (colored spheres in the diagram) according to the HCP 842-subject diffusion data template.

All 40 ALIC segmentations exhibited a dorsal-ventral axis of organization. On average, the combined segmentation was accurate for 66.2% of individuals. The region assigned to BA11 (orbitofrontal cortex, OFC) exhibited the greatest consistency across individuals, with 12.1% being consistently assigned in all 40 subjects. According to the segmentation, a mean of 63.9% of modeled lesion volume within the ALIC intersected with the BA11 region. All five modeled targets exhibited connectivity to OFC in the 842-subject HCP template.

These results clarify the organization and variability of the ALIC. This variability suggests that patients may benefit from pre-operative tractography for individualized targeting, although current stereotactic targets tend to involve the most consistent ALIC sub-regions. These findings also suggest that stereotactic targeting within the ALIC likely involves modulation of prefrontal-subcortical tracts connecting the OFC, which bears relevance to the cortico-striato-thalamo-cortical (CSTC) model of neuropsychiatric pathophysiology.

Highlights and Future Directions

- The Anterior limb of the internal capsule (ALIC) is a frequent DBS target for treatment of psychiatric diseases.
- Using a DTI-based template from the Human Connectome, a study was undertaken to map this region to better understand these tracts for DBS application.
- This research demonstrated that the ALIC has a general axis of orientation but variability is present and can be probabilistically quantified (some loci show differences).

RAD-PD: Registry for the Advancement of DBS in Parkinson's Disease

PD DBS is well known to improve motor function and quality of life in patients experiencing motor complications. However, numerous questions remain about best practices related to DBS, which cannot be answered through traditional clinical trials methods. The Registry for the Advancement of DBS in Parkinson's Disease (RAD-PD) has been proposed as a partnership between the Parkinson Study Group (PSG), Neuropoint Alliance (NPA) and Neurotargeting, LLC, to establish a quality improvement (QI) registry for DBS.

The QI design of RAD-PD will allow for continuous benchmarking of selected data and the opportunity to review those findings via regular dash-boarding and discussion at periodic study group meetings. The registry can support research functions, secondary analysis, linkage to other databases, sub-studies analysis, data collection and use of a de-identified dataset to answer research questions. Multiple clinical questions that cannot otherwise be practically answered will be investigated regarding the best practices surrounding DBS therapy, adverse effects of DBS (and their determinants), the health economics of PD DBS, as well as the correlates of disparities in outcomes among individuals receiving the therapy (**Figure 10**).

The project design has potential to gather longitudinal, prospective data from over 1,000 participants with PD across a 5-year period of DBS therapy, with a data collection and analysis period of up to 10 years. The project is currently under review for funding. Once implemented, the potential exists to extend the RAD-PD infrastructure for the capture and analysis of similar data from patients with other conditions being treated with DBS.

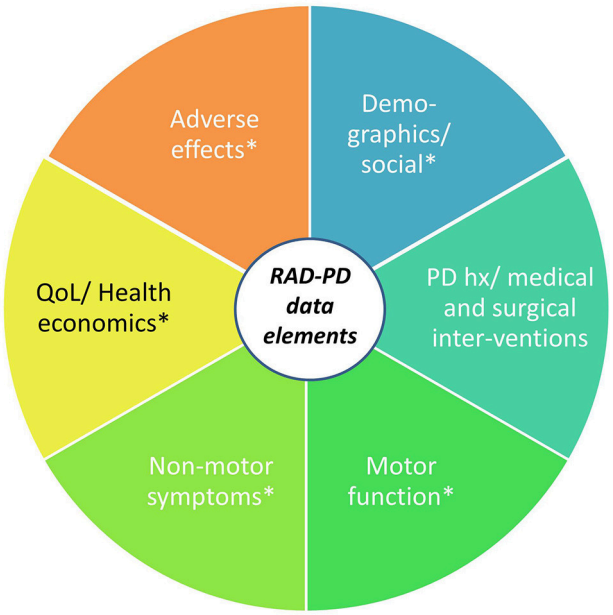

FIGURE 10 | RAD-PD: Registry for the Advancement of DBS in Parkinson's Disease. The RAD-PD data elements include clinician-measured and patient-reported outcomes (indicated by *), which will be collected at baseline (pre-operatively), 6 months, 1 year, and annually through 5 years. The total project period will last 10 years.

Highlights and Future Directions

- The Registry for the Advancement of DBS in Parkinson's Disease (RAD-PD) is a DBS Registry for PD to address numerous clinical questions.
- The registry would integrate different groups for analysis including Neurotargeting, Neuropoint Alliance, and the Parkinson's Study Group (PSG).
- The registry will focus on a Quality Improvement Registry utilizing a data-driven approach.

Diagnostic Data Management in Closed-Loop Cortical Stimulation for Epilepsy

The RNS® System is an FDA approved therapy for treating medically refractory partial onset epilepsy in individuals 18 years of age or older (Bergey et al., 2015). The RNS System consists of an implantable neurostimulator and leads (depths or strips), a physician operated programmer, a patient operated remote monitor and a secure website referred to as the Patient Data Management System (PDMS). The neurostimulator records data of frequency, timing, and location of electrographic activity specific to each patient. The neurostimulator also stores electrocorticograms (ECOGs) as well as counts and timing of various events (detected patterns, long duration events,

high amplitude events and magnet placements). These data are collected via the physician programmer and the patient operated remote monitor to provide a long-term record of patient electrographic activity. These data are then organized and made available for clinician review via the PDMS (**Figure 11**).

In the clinical care environment, physicians must be able to quickly assess data trends and make programming changes within the constraints of a typical clinic visit. The PDMS provides concise summary data and capabilities to quickly sort and view classes of ECOGs and graph trends of various events. It also allows physicians to determine detection settings by clicking on ECOG locations of epileptiform activity they intend to detect. The system then runs a series of algorithms to suggest initial settings. The clinician can rapidly review the suggested settings performance against the library of stored ECOGs and make adjustments to achieve the detection performance desired.

Highlights and Future Directions

- NeuroPace PDMS (Patient Data Management System) allows remote storage on data bank and can simulate detection rate based on the parameter selection and previously data.
- The PDMS provides concise summary data capabilities to quickly sort and view classes of ECOGs and to graph trends of various events to determine detection settings by clicking on ECOG locations of epileptiform activity.

FEDERAL INITIATIVES

Updates on DBS Directions from the NIH P50 Udall Program

NIH Udall Center grants aim to foster multidisciplinary work with nine centers around the United States. Despite years of clinical success and efforts to improve clinical outcomes, the degree of therapy achieved with DBS varies widely among patients for both STN DBS and GPi DBS (Deep-Brain Stimulation for Parkinson's Disease Study Group et al., 2001). Such variability across centers and within any given center likely stems from multiple factors, including patient phenotype(s), assessment protocol, patient health, DBS target, DBS lead location within the target, and the stimulation parameters used to deliver the therapy (Kleiner-Fisman et al., 2006).

To address these challenges, the NIH recently awarded a Morris K. Udall Center of Excellence for Parkinson's Disease Research grant to the University of Minnesota (PI: Jerrold L. Vitek). The University of Minnesota's (UMN) NIH Udall Center is focused on understanding the electrophysiological features that underlie individual motor signs of PD and developing new DBS strategies to treat these motor signs more effectively and more consistently. This is being accomplished in humans through a combination of intra-operative microelectrode, externalized lead recordings, post-operative LFP recordings using the Medtronic RC+S "Brain Radio," and DBS therapy implemented through the lens of novel targets and stimulation paradigms. These

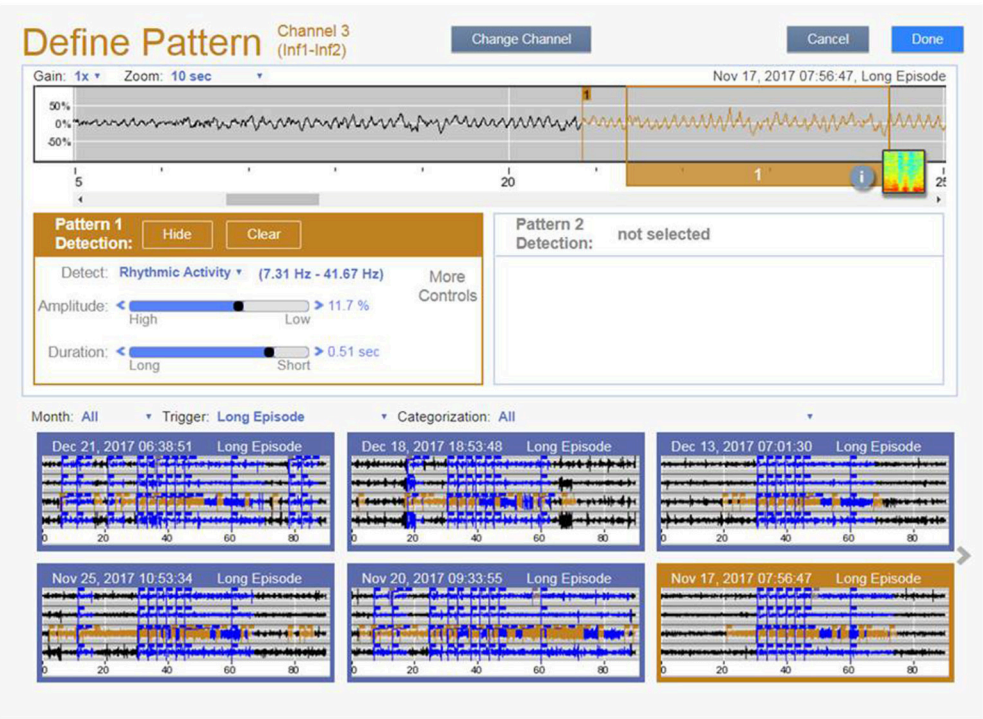

FIGURE 11 | Defining Pattern feature in PDMS. The clinician clicks on the ECOG in the top panel and the PDMS suggests initial detection settings that are immediately simulated in the bottom panel. Sliders in the middle panel allow the physician to make adjustments to achieve the desired performance.

data will be complemented by electrophysiological studies in preclinical animal models of Parkinson's disease with directional DBS implants, and by the development and electrophysiological characterization of optimization tools for improving subject-specific precision of DBS therapy.

Highlights and Future Directions

- The UMN NIH Udall Center is focused on understanding the electrophysiological features that underlie individual motor signs of PD and in developing and advancing new DBS targets and stimulation paradigms through a combination of intra-operative microelectrode and post-operative LFP recordings.
- Specific goals of the UMN Udall Center include:
  - Project 1 (Human): Understand PD pathophysiology as it relates to DBS.
  - Project 2 (Human): Identify mechanisms and pathways mediating the motor effects of pallidal DBS.
  - Project 3 (Pre-clinical Research): Identify electrophysiological mechanisms underlying the clinical variability with DBS therapy for Parkinson's disease.

High Bandwidth Wireless Interfaces in Quadraplegia

The BrainGate consortium is a multi-center effort to restore communication and movement capabilities to people with paralysis and to develop next generation neurotechnologies. The study has recruited 13 participants with over 9,310 total implant days. A completely implantable brain computer interface has also been developed for potential future human use, toward neurally controlled point-and-click (keyboard, communication devices) and for multi-dimensional control of robotic assistive devices or one's own arm and hand. Patients with severe neurological motor disability from ALS, brainstem stroke, or cervical spinal cord injury have demonstrated impressive control of communication and mobility technologies. The core technology, consisting of the decoding of ensembles of single neurons, could provide a neurophysiological signature that could be deployed as part of a closed loop neuromodulation device in both neurologic or psychiatric disorders. Wireless arrays record broad band intracortical physiology and are able to provide external responsive stimulation to contracting implanted muscles. In the future, wirelessly connected cortical arrays capable of recording broadband intracortical signals will also be able to direct the movement of functionally electrical stimulation systems for the restoration of limb movement. The long term aims of the BrainGate trial are to neuroengineer improved BCI capabilities; communicate the validity and viability of BCI-based approaches to both the medical community and representative stake-holders (i.e., patients and the public), and assist and restore function to patients in need.

Highlights and Future Directions

- BrainGate is a multicenter effort dedicated to restoring movement capabilities to motor-impaired individuals. The initiative initially focused on achieving decoding accuracy, and this is being extended by research into improvements in the efficiency of filter calibration and adaptation.
- Future challenges include designing of devices that are portable, fully implanted, compact, wireless, and available around-the-clock to support useful applications and activities of daily living.
- Important questions and challenges remain regarding the number and configuration of electrodes, methods to assess the stability of decoders, personal assessments (to each patient) that balance the risks vs. potential performance as compared the risk/benefit provided by BCIs that record from the scalp.

Updates from DARPA: Restoring Active Memory (RAM)

Neurotechnology: Bridging the Gap between Mind and Machine

DARPA's innovations in neurotechnology are making possible real-time, seamless translation between human brains and machines. These technologies have enabled initial approaches that enable analyses of the ways that diffuse and varied signals from arrays of firing neurons affect brain function. DARPA's current investments in neural interfaces and related technologies build upon this understanding of neural encoding and decoding, developing multi-scale computational models with high spatial and temporal resolution to target a variety of neurologic functions, and these research approaches are synergized by studies that address engineering challenges of designing implantable, closed-loop systems. Key DARPA-funded capability demonstrations include controlling and receiving feedback from a prosthetic arm using sensors in the motor and somatosensory cortices; receiving feedback from a virtual hand using implants in peripheral nerves; and improving declarative memory through stimulation of specific brain regions. DARPA's work is establishing a basis of what is currently possible, revealing how neurotechnology could facilitate symbiotic human-machine interfacing, and engaging assessment and address of the ethical, legal, social, and policy issues fostered by emerging neurotechnologies (see also, below).

Modulating Human Memory Using Direct Brain Stimulation

The Restoring Active Memory (RAM) project aims to develop implantable therapies to treat veterans with TBI by increasing their ability to encode information. In this study, the hypothesis that targeted electrical stimulation can modulate neural encoding states and subsequent memory outcomes was tested. Using recordings from neurosurgical epilepsy patients with intracranially implanted electrodes, multivariate classifiers were trained to discriminate spectral activity during the encoding of words that predicted whether patients would later remember or forget these words; and stimulation was applied to various brain regions to modulate performance.

It was found that stimulation modulates performance, with large variability across the population and across the various brain regions stimulated. Hippocampal stimulation tended to impair recall performance while lateral temporal

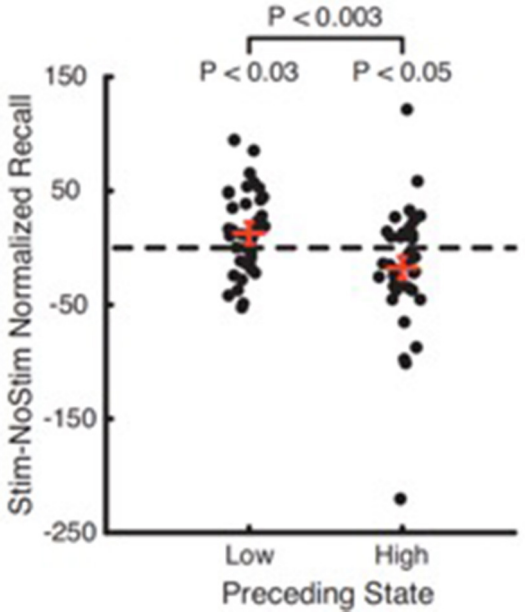

FIGURE 12 | The effect of stimulation is dependent on brain state. Recall performance increased if stimulation was delivered when the brain was in a low encoding state ($p < 0.03$) and decreased if delivered in a high encoding state ($p < 0.05$). The difference between low and high stimulation was also significant ($p < 0.003$). Red bars show mean SE of the difference.

cortex stimulation significantly improved recall performance. In addition, stimulation increased recall performance if delivered when the classifier indicated low encoding efficiency but had the reverse effect if stimulation was delivered when the classifier indicated high encoding efficiency (**Figure 12**). These data suggest strategies for therapeutically treating memory dysfunction using closed-loop brain stimulation.

Highlights and Future Directions

- Electrical stimulation can modulate neural encoding states and subsequent memory outcomes.
- The timing of stimulation and strict anatomical targeting appear critical to enhance memory. Developing patient-specific classifiers and stimulation patterns that adjust over time might provide sustained benefits.
- Current work provides proof of concept for the future of cognitive enhancement in other areas, including attention or focus, using closed-loop neurostimulation technologies.
- Future steps include determining the number of contacts needed for sensing and stimulation, and the translation of these technologies into patients with mild cognitive impairment (MCI) and/or Alzheimer's dementia (AD).

Hippocampal Memory Prostheses: Neural Code-Based DBS

A hippocampal memory prosthesis is defined as a closed-loop system that bypasses damaged hippocampal region(s) to restore or enhance memory functions (Berger et al., 2011). Like closed-loop DBS systems, it consists of a recording unit (e.g., multi-electrode array), a signal processing/control unit, and a stimulator (e.g., stimulating electrodes). Differing from DBS systems, which typically deliver stereotypical stimulation patterns (e.g., HFS or LFS) to target regions to modulate neural activities, hippocampal memory prostheses utilize neural code-based stimulation patterns to reinstate neural signal transmission and thus mimic brain functions. Hippocampal memory prostheses have been developed and tested in rodents (Song et al., 2007, 2009; Berger et al., 2011, 2012; Hampson et al., 2012a,b), nonhuman primates (Hampson et al., 2013), and human epilepsy patients (Song et al., 2016; Hampson et al., in preparation).

This technique is now being applied to human studies in which multi-electrode "macro-micro" depth electrodes are implanted in the hippocampus of epilepsy patients undergoing Phase II invasive monitoring for seizure localization (**Figure 13**). Hippocampal CA3 and CA1 neural ensembles are recorded while patients perform a delayed match-to-sample (DMS) task. Multi-input, multi-output (MIMO) nonlinear dynamical models are built to describe the transformation from CA3 (input) spatio-temporal patterns (codes) of spikes to CA1 (output) spatio-temporal patterns (codes) of spikes using CA3 and CA1 data recorded from success trials of DMS tasks, and further drive stimulations to the CA1 region (Song et al., 2013, 2016). In combination with the modeling from human data, results from preclinical testing in rodents and nonhuman primates (Hampson et al., 2013) demonstrate that (1) MIMO models accurately predict CA1 codes in real-time from ongoing CA3 codes; and (2) closed-loop electrical microstimulation of CA1 using the MIMO-predicted CA1 codes improves DMS performance in those same subjects, indicating improvement of working memory function.

Highlights and Future Challenges

- Hippocampal neurostimulators implanted in epilepsy patients, multi-input, multi-output (MIMO) nonlinear dynamical models have been built to describe the transformation from CA3 (input) spatio-temporal patterns (codes) of spikes to CA1 (output).
- MIMO models accurately predict CA1 codes in real-time from ongoing CA3 codes and improve DMS performance and delayed recognition of DMS visual stimuli.
- An increased level of complexity in memory decoding is expected going forward. Certain limitations apply to current stimulating electrode and improved electrode design might be necessary to facilitate research.
- Future research to determine the most effective location for stimulation, changes in plasticity and stimulating parameters is needed.

ETHICAL AND POLICY ISSUES

As evidenced in the this report, there are ample new developments in DBS technology. These include increasingly sophisticated electrodes and electrode arrays (that enable both stimulation and recording), iterative BCI systems' hard- and

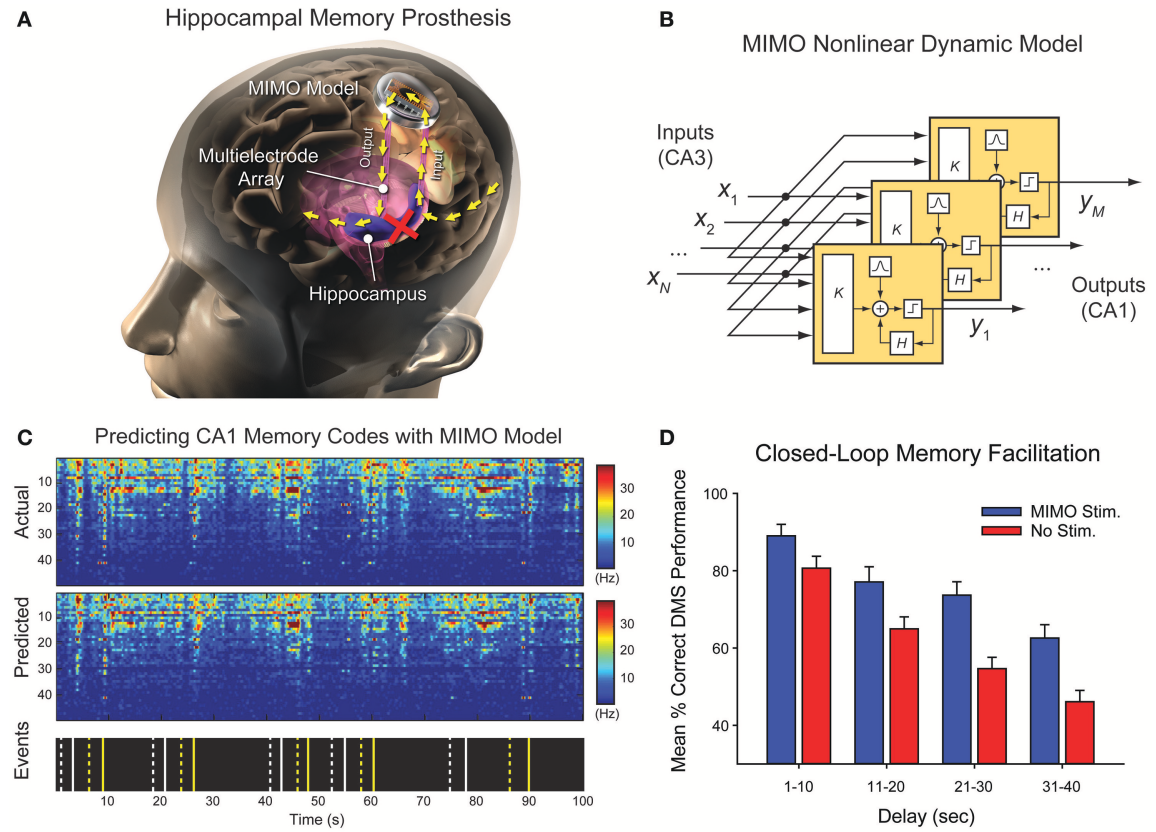

FIGURE 13 | Hippocampal memory prosthesis. **(A)** Hippocampal prosthesis restores memory functions by reinstating neural signals and thus bypassing damaged brain region. **(B)** A MIMO model serves as the computational basis of hippocampal memory prostheses. **(C)** A MIMO model accurately predicts CA1 (output) codes based on CA3 (input) codes in human. **(D)** MIMO-stimulation enhances memory functions in preclinical animal testing.

software, and closed-loop adaptive systems. As well, a building body of research—as presented here - demonstrates the efficacy of various forms of DBS in mitigating signs and symptoms of disorders beyond PD, dystonia and epilepsy (e.g., Tourette syndrome; depression; OCD; memory loss in TBI and AD). This suggests, if not supports, an expanding translational viability and potential value of such approaches. This widening scope of capability and use fosters ethical and policy issues, which can be parsed into (1) those inherent to the characteristics of the technology and/or technique, and (2) those derived from the uses of such technologies in medicine and other applications in the social sphere (for complete address of specific neuroethico-legal and social issues, see: Buniak et al., 2014; Darragh et al., 2015; Giordano, 2017). These are not mutually exclusive: the relative novelty of technologies and techniques spawns questions about the intermediate and ongoing safety and effects in practical use (Giordano, 2015). The prompts questions of if and when these approaches will represent an accepted standard of care for certain disorders; where and under what conditions/contingencies DBS will be situated in the plan/algorithm of care for these pathologies, and if and to what extent medical and/or socio-economic and legal means of support will be provided to enable such care—in both the short and long term. Current problems in the subsidy of DBS treatment of certain movement and psychiatric disorders undergird the importance and need for continuing discourse and deliberation focal to these issues (Rossi et al., 2017).

As well, questions persist as to whether and how implantable neuromodulation might affect aspects of neuropsychological function that are associated with identity, "free will" and autonomy, and what this incurs and infers for the ethically sound use of DBS both to treat defined medical conditions, as well as to potentially optimize/enhance particular aspects of cognition, emotion and/or behavior (Giordano, 2015). We have posited that any new developments in neurotechnology entail effort to define and address the neuroethico-legal and social issues that may, and are likely to be generated by such research and its trsanslation in medical and/or other applications (Shook and Giordano, 2015), and unapologetically reiterate that assertion here. To effect such effort, it will be therefore important—and necessary—to both employ extant ethical and policy constructs and to revisit, and in some cases revise these concepts and processes so as to better meet the exigencies borne of emerging technology and techniques, and of the social contingencies and concerns that affect and are affected by

Indication/use	Weighted average	Last year's scores
DBS for Parkinson's	5.43	5.18
DBS for essential tremor	5.14	5.03
Cochlear implant	4.86	5.17
VNS for epilpsy	4.50	
Spinal cord stimulation for pain management	4.18	4.18
Imaging to guide surgical targeting	3.96	3.51
Imaging post DBS implant	3.70	4.08
MRI safety of neurotechnology implants	3.51	3.18
DBS for depression	3.42	3.26
Sacral nerve stimulation for overactive bladder	3.32	
DBS for epilepsy	3.27	3.38
FES for SCI - bladder control	3.14	2.48
DBS for OCD	3.10	2.74
DBS for Tourette's	3.00	2.43
Transcranial magnetic stimulation	2.87	2.83
PNS stimulation for chronic pain	2.71	
FES for foot drop	2.61	2.40
EEG for decoding limb movement (chronic use)	2.53	1.98
Modeling to guide surgical targeting	2.43	2.80
DBS for chronic pain	2.40	2.40
ECoG for decoding limb movement (chronic use)	2.35	1.69
Retinal implant	2.24	2.15
Closed-loop feedback	2.15	1.59
Microelectrodes in the CNS for decoding limb movement (chronic use)	2.04	2.03
FES for SCI - Limb control	2.00	2.08
Telemetric cortical redcording and stimulation	2.00	
Bi-directional wireless telemetry	1.98	1.47
Neural stimulation for stroke symptoms	1.94	1.90
DBS for Alzheimer's	1.91	1.99
Wireless power for implants	1.78	1.57
Reliable implantable high-channel count connectors (>= 100 channels)	1.68	1.12
ECoG for encoding sensory feedback (chronic use)	1.59	1.48
Low-intensity focused ultrasound	1.58	1.45
VNS for obesity	1.54	
DBS for obesity	1.54	1.54
Microelectrodes in the PNS for decoding limb movement (chronic use)	1.54	1.57
Microelectrodes in the CNS for encoding sensory feedback (chronic use)	1.45	1.60
Microelectrodes in the PNS for encoding sensory feedback (chronic use)	1.41	1.45
Neuromagnetic interfaces	1.30	0.93
DBS for TBI	1.27	1.28
Optogenetics for clinical neutral interfaces	1.16	1.05
DBS for addiction	1.15	1.32
VNS for rheumatoid arthritis	1.13	
VNS for heart failure	1.11	
DBS for PTSD	1.00	1.06

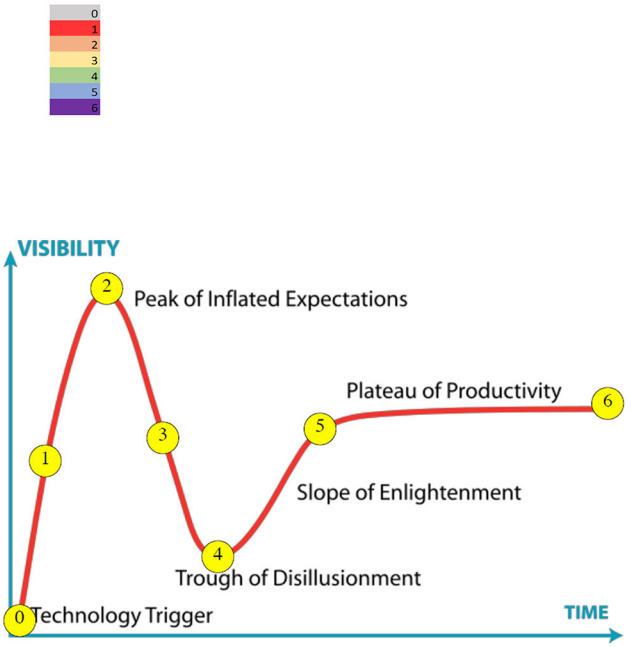

FIGURE 14 | Representation of the anonymous annual survey results, polling the participants of the DBS Think Tank on the hype cycle positions of different DBS related neurotechnological advances and indications. On the right side, the hype cycle graph (adapted Jackie Fenn, "When to leap on the hype cycle," Decision Framework DF-08-6751, Research Note, GartnerGroup RAS Services, June 30, 1999 with permission) that represents the different stages of development. On the left side, a table summarizing the weighted averages of the position of the different neurotechnological indications or uses on the hype cycle graph. Positions 0 to 6 are color coded as noted.

their use in international contexts (Shook and Giordano, 2014; Giordano, 2015). Our ongoing work remains dedicated to these tasks.

SUMMARY AND CONCLUSION

In this paper, we have provided views to the relevant topics and updates discussed at The Fifth Annual DBS Think Tank in Atlanta, GA. Similar to prior years' ThinkTank meetings, an anonymous 40 question poll was sent online to assess participants' perspectives and attitudes toward the current and near-term future developments and applications in the field. Sixty two participants responded. **Figure 14** presents a summary of these responses, compares them to last year's responses, and depicts this year's responses as positioned in various points upon the hype cycle graph. It is notable that some participants' views of DBS applications (e.g., closed loop feedback) moved to the peak of inflated expectations, while, others (e.g., DBS for Tourette's) dropped from this position on the hype cycle graph, and yet others (e.g., Imaging to guide surgical targeting and spinal cord stimulation for pain management) remained in the trough of disillusionment. Consistently, the use of DBS for PD and essential tremor has reached the plateau of productivity and among most participants, cautious optimism remains regarding the use of neuromodulation for several neuropsychiatric conditions, non-neurological indications and the development of newer technologies.

In conclusion, the Fifth Annual DBS Think Tank provided a nexus for discussion and vector for the exchange of ideas about the current and near-term state and direction of DBS research, ongoing technological, scientific and clinical challenges and opportunities, and ethical and policy concerns and possible resolutions important to shaping the future of DBS research and use in practice.

ETHICS STATEMENT

Individual studies were approved by the local Institutional Review Board of participating institutions in this technical report and written informed consent was obtained from all participants.

AUTHOR CONTRIBUTIONS

AR-Z, JG, AG, PB, JS, KF, LA, PhS, HB-S, WH, CM, WG, DK, WMG, HW, MJ, JV, DG, DR, DS, TB, RH, SD, LH, NS, PaS, GW, VT, HM, JJ-S, PN, SS, RG, SFL, LL, WD, and MO fulfilled the authorship criteria by substantial contributions to the conception of the work, providing data for the work, revisiting it critically for important intellectual content, approving the final version, and agreeing to be accountable for all aspects of the work

in ensuring that questions related to the accuracy or integrity of any part of the work are appropriately investigated and resolved.

ACKNOWLEDGMENTS

SFL would like to thank Erika Woodrum (Louis Stokes Cleveland Veterans Affairs Medical Center) and Nicholas Maling, Ph.D. (Case Western Reserve University) for assistance generating **Figure 7**. JG is supported in part by funding from the European Union's Horizon 2020 Research and Innovation Program under grant agreement 720270: HBP SGA1, by the AEHS Foundation, and by federal funds UL1TR001409 from the National Center for Advancing Translational Sciences (NCATS), National Institutes of Health, through the Clinical and Translational Science Awards Program (CTSA), a trademark of the Department of Health and Human Services, part of the Roadmap Initiative, "Re-Engineering the Clinical Research Enterprise." DS, TB, RH, and SD: this work was supported by DARPA RAM program (N66001-14-2-4032, N66001-14-C-4016). The views, opinions and/or findings expressed are those of the author and should not be interpreted as representing the official views or policies of the Department of Defense or the U.S. Government. SS would like to acknowledge the Sackler and Gerstner Foundation for their support. JJ-S would like to thank the Michael J Fox Foundation for Parkinson's Research for providing a project planning grant for the development of RAD-PD design and infrastructure. Furthermore, RAD-PD is an approved study through the Parkinson Study Group and includes participation of Patient Advocates from the Parkinson Disease Foundation. JJ-S also would like to acknowledge the following collaborators and co-investigators: Nuri F. Ince, Ph.D.; Ilknur Telkes, Ph.D.; Ashwin Viswanathan, MD. LL would like to acknowledge grant support NSFC No. 81527901, No. 61601258, and 2016YFC0105502 2016YFC0105900. HW is supported by NIH grant UH3NS100553.

REFERENCES

Akbar, U., Raike, R. S., Hack, N., Hess, C. W., Skinner, J., Martinez-Ramirez, D., et al. (2016). Randomized, blinded pilot testing of nonconventional stimulation patterns and shapes in Parkinson's disease and essential tremor: evidence for further evaluating narrow and biphasic pulses. *Neuromodulation* 19, 343–356. doi: 10.1111/ner.12397

Albin, R. L., and Mink, J. W. (2006). Recent advances in Tourette syndrome research. *Trends Neurosci.* 29, 175–182. doi: 10.1016/j.tins.2006.01.001

Almeida, L., Martinez-Ramirez, D., Ahmed, B., Deeb, W., Jesus, S., Skinner, J., et al. (2017). A pilot trial of square biphasic pulse deep brain stimulation for dystonia: the BIP dystonia study. *Mov. Disord.* 32, 615–618. doi: 10.1002/mds.26906

Alonso, P., Cuadras, D., Gabriels, L., Denys, D., Goodman, W., Greenberg, B. D., et al. (2015). Deep brain stimulation for obsessive-compulsive disorder: a meta-analysis of treatment outcome and predictors of response. *PLoS ONE* 10:e0133591. doi: 10.1371/journal.pone.0133591

Baker, J. L., Ryou, J. W., Wei, X. F., Butson, C. R., Schiff, N. D., and Purpura, K. P. (2016). Robust modulation of arousal regulation, performance, and frontostriatal activity through central thalamic deep brain stimulation in healthy nonhuman primates. *J. Neurophysiol.* 116, 2383–2404. doi: 10.1152/jn.01129.2015

Berger, T. W., Hampson, R. E., Song, D., Goonawardena, A., Marmarelis, V. Z., and Deadwyler, S. A. (2011). A cortical neural prosthesis for restoring and enhancing memory. *J. Neural Eng.* 8:046017. doi: 10.1088/1741-2560/8/4/046017

Berger, T. W., Song, D., Chan, R. H., Marmarelis, V. Z., Lacoss, J., Wills, J., et al. (2012). A hippocampal cognitive prosthesis: multi-input, multi-output nonlinear modeling and VLSI implementation. *IEEE Trans. Neural Syst. Rehabil. Eng.* 20, 198–211. doi: 10.1109/TNSRE.2012.2189133

Bergey, G. K., Morrell, M. J., Mizrahi, E. M., Goldman, A., King-Stephens, D., Nair, D., et al. (2015). Long-term treatment with responsive brain stimulation in adults with refractory partial seizures. *Neurology* 84, 810–817. doi: 10.1212/WNL.0000000000001280

Birdno, M. J., Cooper, S. E., Rezai, A. R., and Grill, W. M. (2007). Pulse-to-pulse changes in the frequency of deep brain stimulation affect tremor and modeled neuronal activity. *J. Neurophysiol.* 98, 1675–1684. doi: 10.1152/jn.00547.2007

Birdno, M. J., Kuncel, A. M., Dorval, A. D., Turner, D. A., and Grill, W. M. (2008). Tremor varies as a function of the temporal regularity of deep brain stimulation. *Neuroreport* 19, 599–602. doi: 10.1097/WNR.0b013e3282f9e45e

Birdno, M. J., Kuncel, A. M., Dorval, A. D., Turner, D. A., Gross, R. E., and Grill, W. M. (2012). Stimulus features underlying reduced tremor suppression with temporally patterned deep brain stimulation. *J. Neurophysiol.* 107, 364–383. doi: 10.1152/jn.00906.2010

Bourget, D., Hank, B., Scott, S., David, L., Chris, A., Tom, A., et al. (2015). "An implantable, rechargeable neuromodulation research tool using a distributed interface and algorithm architecture," in *Neural Engineering (NER) 7th International IEEE/EMBS Conference* (Montpellier).

Bower, M. R., Stead, M., Bower, R. S., Kucewicz, M. T., Sulc, V., Cimbalnik, J., et al. (2015). Evidence for consolidation of neuronal assemblies after seizures in humans. *J. Neurosci.* 35, 999–1010. doi: 10.1523/JNEUROSCI.3019-14.2015

Brinkmann, B. H., Patterson, E. E., Vite, C., Vasoli, V. M., Crepeau, D., Stead, M., et al. (2015). Forecasting seizures using intracranial EEG measures and SVM in naturally occurring Canine Epilepsy. *PLoS ONE* 10:e0133900. doi: 10.1371/journal.pone.0133900

Brinkmann, B. H., Wagenaar, J., Abbot, D., Adkins, P., Bosshard, S. C., Chen, M., et al. (2016). Crowdsourcing reproducible seizure forecasting in human and canine epilepsy. *Brain* 139, 1713–1722. doi: 10.1093/brain/aww045

Brocker, D. T., Swan, B. D., So, R. Q., Turner, D. A., Gross, R. E., and Grill, W. M. (2017). Optimized temporal pattern of brain stimulation designed by computational evolution. *Sci. Transl. Med.* 9:eaah3532. doi: 10.1126/scitranslmed.aah3532

Brocker, D. T., Swan, B. D., Turner, D. A., Gross, R. E., Tatter, S. B., Koop, M. M., et al. (2013). Improved efficacy of temporally non-regular deep brain stimulation in Parkinson's disease. *Exp. Neurol.* 239, 60–67. doi: 10.1016/j.expneurol.2012.09.008

Bronte-Stewart, H., Barberini, C., Koop, M. M., Hill, B. C., Henderson, J. M., and Wingeier, B. (2009). The STN beta-band profile in Parkinson's disease is stationary and shows prolonged attenuation after deep brain stimulation. *Exp. Neurol.* 215, 20–28. doi: 10.1016/j.expneurol.2008.09.008

Buhlmann, J., Hofmann, L., Tass, P. A., and Hauptmann, C. (2011). Modeling of a segmented electrode for desynchronizing deep brain stimulation. *Front. Neuroeng.* 4:15. doi: 10.3389/fneng.2011.00015

Buniak, L., Darragh, M., and Giordano, J. (2014). A four-part working bibliography of neuroethics: part 1: overview and reviews–defining and describing the field and its practices. *Philos. Ethics Humanit. Med.* 9:9. doi: 10.1186/1747-5341-9-9

Chaturvedi, A., Lujan, J. L., and Mcintyre, C. C. (2013). Artificial neural network based characterization of the volume of tissue activated during deep brain stimulation. *J. Neural Eng.* 10:056023. doi: 10.1088/1741-2560/10/5/056023

Cheung, M. Y., Shahed, J., and Jankovic, J. (2007). Malignant tourette syndrome. *Mov. Disord.* 22, 1743–1750. doi: 10.1002/mds.21599

Cook, M. J., O'brien, T. J., Berkovic, S. F., Murphy, M., Morokoff, A., Fabinyi, G., et al. (2013). Prediction of seizure likelihood with a long-term, implanted seizure advisory system in patients with drug-resistant epilepsy: a first-in-man study. *Lancet Neurol.* 12, 563–571. doi: 10.1016/S1474-4422(13)70075-9

Darragh, M., Buniak, L., and Giordano, J. (2015). A four-part working bibliography of neuroethics: part 2–Neuroscientific studies of morality and ethics. *Philos. Ethics Humanit. Med.* 10:2. doi: 10.1186/s13010-015-0022-0

Deep-Brain Stimulation for Parkinson's Disease Study Group, Obeso, J. A., Olanow, C. W., Rodriguez-Oroz, M. C., Krack, P., Kumar, R., et al. (2001). Deep-brain stimulation of the subthalamic nucleus or the pars interna of the globus pallidus in Parkinson's disease. *N. Engl. J. Med.* 345, 956–963. doi: 10.1056/NEJMoa000827

Desai, S. A., Rolston, J. D., Mccracken, C. E., Potter, S. M., and Gross, R. E. (2016). Asynchronous distributed multielectrode microstimulation reduces seizures in the dorsal tetanus toxin model of temporal lobe epilepsy. *Brain Stimul.* 9, 86–100. doi: 10.1016/j.brs.2015.08.008

Dorval, A. D., Kuncel, A. M., Birdno, M. J., Turner, D. A., and Grill, W. M. (2010). Deep brain stimulation alleviates parkinsonian bradykinesia by regularizing pallidal activity. *J. Neurophysiol.* 104, 911–921. doi: 10.1152/jn.00103.2010

Fisher, R., Salanova, V., Witt, T., Worth, R., Henry, T., Gross, R., et al. (2010). Electrical stimulation of the anterior nucleus of thalamus for treatment of refractory epilepsy. *Epilepsia* 51, 899–908. doi: 10.1111/j.1528-1167.2010.02536.x

Fisher, R. S., and Velasco, A. L. (2014). Electrical brain stimulation for epilepsy. *Nat. Rev. Neurol.* 10, 261–270. doi: 10.1038/nrneurol.2014.59

Frankemolle, A. M., Wu, J., Noecker, A. M., Voelcker-Rehage, C., Ho, J. C., Vitek, J. L., et al. (2010). Reversing cognitive-motor impairments in Parkinson's disease patients using a computational modelling approach to deep brain stimulation programming. *Brain* 133, 746–761. doi: 10.1093/brain/awp315

Giacino, J., Fins, J. J., Machado, A., and Schiff, N. D. (2012). Central thalamic deep brain stimulation to promote recovery from chronic posttraumatic minimally conscious state: challenges and opportunities. *Neuromodulation* 15, 339–349. doi: 10.1111/j.1525-1403.2012.00458.x

Giordano, J. (2015). A preparatory neuroethical approach to assessing developments in neurotechnology. *Virtual Mentor.* 17, 56–61. doi: 10.1001/virtualmentor.2015.17.01.msoc1-1501

Giordano, J. (2017). Toward an operational neuroethical risk analysis and mitigation paradigm for emerging neuroscience and technology (neuroS/T). *Exp. Neurol.* 287, 492–495. doi: 10.1016/j.expneurol.2016.07.016

Grill, W. M., Snyder, A. N., and Miocinovic, S. (2004). Deep brain stimulation creates an informational lesion of the stimulated nucleus. *Neuroreport* 15, 1137–1140. doi: 10.1097/00001756-200405190-00011

Hampson, R. E., Song, D., Chan, R. H., Sweatt, A. J., Riley, M. R., Gerhardt, G. A., et al. (2012a). A nonlinear model for hippocampal cognitive prosthesis: memory facilitation by hippocampal ensemble stimulation. *IEEE Trans. Neural Syst. Rehabil. Eng.* 20, 184–197. doi: 10.1109/TNSRE.2012.2189163

Hampson, R. E., Song, D., Chan, R. H., Sweatt, A. J., Riley, M. R., Goonawardena, A. V., et al. (2012b). Closing the loop for memory prosthesis: detecting the role of hippocampal neural ensembles using nonlinear models. *IEEE Trans. Neural Syst. Rehabil. Eng.* 20, 510–525. doi: 10.1109/TNSRE.2012.2190942

Hampson, R. E., Song, D., Opris, I., Santos, L. M., Shin, D. C., Gerhardt, G. A., et al. (2013). Facilitation of memory encoding in primate hippocampus by a neuroprosthesis that promotes task-specific neural firing. *J. Neural Eng.* 10:066013. doi: 10.1088/1741-2560/10/6/066013

Haq, I. U., Foote, K. D., Goodman, W. G., Wu, S. S., Sudhyadhom, A., Ricciuti, N., et al. (2011). Smile and laughter induction and intraoperative predictors of response to deep brain stimulation for obsessive-compulsive disorder. *Neuroimage* 54(Suppl. 1), S247–S255. doi: 10.1016/j.neuroimage.2010.03.009

Heck, C. N., King-Stephens, D., Massey, A. D., Nair, D. R., Jobst, B. C., Barkley, G. L., et al. (2014). Two-year seizure reduction in adults with medically intractable partial onset epilepsy treated with responsive neurostimulation: final results of the RNS System Pivotal trial. *Epilepsia* 55, 432–441. doi: 10.1111/epi.12534

Herron, J., and Chizeck, H. J. (2014). "Prototype closed-loop deep brain stimulation systems inspired by Norbert Wiener," in *IEEE Conference on Norbert Wiener* (Boston, MA).

Howbert, J. J., Patterson, E. E., Stead, S. M., Brinkmann, B., Vasoli, V., Crepeau, D., et al. (2014). Forecasting seizures in dogs with naturally occurring epilepsy. *PLoS ONE* 9:e81920. doi: 10.1371/journal.pone.0081920

Ince, N. F., Gupte, A., Wichmann, T., Ashe, J., Henry, T., Bebler, M., et al. (2010). Selection of optimal programming contacts based on local field potential recordings from subthalamic nucleus in patients with Parkinson's disease. *Neurosurgery* 67, 390–397. doi: 10.1227/01.NEU.0000372091.64824.63

Jia, F., Hu, W., Zhang, J., Wagle Shukla, A., Almeida, L., Meng, F. G., et al. (2017). Variable frequency stimulation of subthalamic nucleus in Parkinson's disease: rationale and hypothesis. *Parkinsonism Relat. Disord.* 39, 27–30. doi: 10.1016/j.parkreldis.2017.03.015

Jimenez-Shahed, J., Telkes, I., Viswanathan, A., and Ince, N. F. (2016). GPi oscillatory activity differentiates tics from the resting state, voluntary movements, and the unmedicated Parkinsonian state. *Front. Neurosci.* 10:436. doi: 10.3389/fnins.2016.00436

Kajikawa, Y., and Schroeder, C. E. (2011). How local is the local field potential? *Neuron* 72, 847–858. doi: 10.1016/j.neuron.2011.09.029

Katzner, S., Nauhaus, I., Benucci, A., Bonin, V., Ringach, D. L., and Carandini, M. (2009). Local origin of field potentials in visual cortex. *Neuron* 61, 35–41. doi: 10.1016/j.neuron.2008.11.016

Keane, M., Deyo, S., Abosch, A., Bajwa, J. A., and Johnson, M. D. (2012). Improved spatial targeting with directionally segmented deep brain stimulation leads for treating essential tremor. *J. Neural Eng.* 9:046005. doi: 10.1088/1741-2560/9/4/046005

Kenney, C., Kuo, S. H., and Jimenez-Shahed, J. (2008). Tourette's syndrome. *Am. Fam. Phys.* 77, 651–658.

Kleiner-Fisman, G., Herzog, J., Fisman, D. N., Tamma, F., Lyons, K. E., Pahwa, R., et al. (2006). Subthalamic nucleus deep brain stimulation: summary and meta-analysis of outcomes. *Mov. Disord.* 21(Suppl. 14), S290–S304. doi: 10.1002/mds.20962

Kuhn, A. A., Kempf, F., Brucke, C., Gaynor Doyle, L., Martinez-Torres, I., Pogosyan, A., et al. (2008). High-frequency stimulation of the subthalamic nucleus suppresses oscillatory beta activity in patients with Parkinson's disease in parallel with improvement in motor performance. *J. Neurosci.* 28, 6165–6173. doi: 10.1523/JNEUROSCI.0282-08.2008

Kuhn, A. A., and Volkmann, J. (2017). Innovations in deep brain stimulation methodology. *Mov. Disord.* 32, 11–19. doi: 10.1002/mds.26703

Kumsa, D., Hudak, E. M., Montague, F. W., Kelley, S. C., Untereker, D. F., Hahn, B. P., et al. (2016). Electrical neurostimulation with imbalanced waveform mitigates dissolution of platinum electrodes. *J. Neural Eng.* 13:054001. doi: 10.1088/1741-2560/13/5/054001

Lehto, L. J., Slopsema, J. P., Johnson, M. D., Shatillo, A., Teplitzky, B. A., Utecht, L., et al. (2017). Orientation selective deep brain stimulation. *J. Neural Eng.* 14:016016. doi: 10.1088/1741-2552/aa5238

Lempka, S. F., and Mcintyre, C. C. (2013). Theoretical analysis of the local field potential in deep brain stimulation applications. *PLoS ONE* 8:e59839. doi: 10.1371/journal.pone.0059839

Linden, H., Tetzlaff, T., Potjans, T. C., Pettersen, K. H., Grun, S., Diesmann, M., et al. (2011). Modeling the spatial reach of the LFP. *Neuron* 72, 859–872. doi: 10.1016/j.neuron.2011.11.006

Little, S., Pogosyan, A., Neal, S., Zavala, B., Zrinzo, L., Hariz, M., et al. (2013). Adaptive deep brain stimulation in advanced Parkinson disease. *Ann. Neurol.* 74, 449–457. doi: 10.1002/ana.23951

Little, S., Tripoliti, E., Beudel, M., Pogosyan, A., Cagnan, H., Herz, D., et al. (2016). Adaptive deep brain stimulation for Parkinson's disease demonstrates reduced speech side effects compared to conventional stimulation in the acute setting. *J. Neurol. Neurosurg. Psychiatr.* 87, 1388–1389. doi: 10.1136/jnnp-2016-313518

Liu, J., Lee, H. J., Weitz, A. J., Fang, Z., Lin, P., Choy, M., et al. (2015). Frequency-selective control of cortical and subcortical networks by central thalamus. *Elife* 4:e09215. doi: 10.7554/eLife.09215

Malekmohammadi, M., Herron, J., Velisar, A., Blumenfeld, Z., Trager, M. H., Chizeck, H. J., et al. (2016). Kinematic adaptive deep brain stimulation for resting tremor in Parkinson's disease. *Mov. Disord.* 31, 426–428. doi: 10.1002/mds.26482

Martens, H. C., Toader, E., Decre, M. M., Anderson, D. J., Vetter, R., Kipke, D. R., et al. (2011). Spatial steering of deep brain stimulation volumes using a novel lead design. *Clin. Neurophysiol.* 122, 558–566. doi: 10.1016/j.clinph.2010.07.026

Mayberg, H. S., Lozano, A. M., Voon, V., Mcneely, H. E., Seminowicz, D., Hamani, C., et al. (2005). Deep brain stimulation for treatment-resistant depression. *Neuron* 45, 651–660. doi: 10.1016/j.neuron.2005.02.014

Mcconnell, G. C., So, R. Q., and Grill, W. M. (2016). Failure to suppress low-frequency neuronal oscillatory activity underlies the reduced effectiveness of random patterns of deep brain stimulation. *J. Neurophysiol.* 115, 2791–2802. doi: 10.1152/jn.00822.2015

Meidahl, A. C., Tinkhauser, G., Herz, D. M., Cagnan, H., Debarros, J., and Brown, P. (2017). Adaptive deep brain stimulation for movement disorders: the long road to clinical therapy. *Mov. Disord.* 32, 810–819. doi: 10.1002/mds.27022

Merrill, D. R., Bikson, M., and Jefferys, J. G. (2005). Electrical stimulation of excitable tissue: design of efficacious and safe protocols. *J. Neurosci. Methods* 141, 171–198. doi: 10.1016/j.jneumeth.2004.10.020

Molina, R., Okun, M. S., Shute, J. B., Opri, E., Rossi, P. J., Martinez-Ramirez, D., et al. (2017). Report of a patient undergoing chronic responsive deep brain stimulation for Tourette syndrome: proof of concept. *J Neurosurg*.29, 1–7. doi: 10.3171/2017.6.JNS17626

Moreau, C., Defebvre, L., Devos, D., Marchetti, F., Destee, A., Stefani, A., et al. (2009). STN versus PPN-DBS for alleviating freezing of gait: toward a frequency modulation approach? *Mov. Disord.* 24, 2164–2166. doi: 10.1002/mds.22743

Moro, E., Hamani, C., Poon, Y. Y., Al-Khairallah, T., Dostrovsky, J. O., Hutchison, W. D., et al. (2010). Unilateral pedunculopontine stimulation improves falls in Parkinson's disease. *Brain* 133, 215–224. doi: 10.1093/brain/awp261

Morrell, M. J., and RNS System in Epilepsy Study Group. (2011). Responsive cortical stimulation for the treatment of medically intractable partial epilepsy. *Neurology* 77, 1295–1304. doi: 10.1212/WNL.0b013e3182302056

Nanda, P., Banks, G. P., Pathak, Y. J., and Sheth, S. A. (2017). Connectivity-based parcellation of the anterior limb of the internal capsule. *Hum. Brain Mapp*. 38, 6107–6117. doi: 10.1002/hbm.23815

Nutt, J. G., Bloem, B. R., Giladi, N., Hallett, M., Horak, F. B., and Nieuwboer, A. (2011). Freezing of gait: moving forward on a mysterious clinical phenomenon. *Lancet Neurol.* 10, 734–744. doi: 10.1016/S1474-4422(11)70143-0

Park, Y., Luo, L., Parhi, K. K., and Netoff, T. (2011). Seizure prediction with spectral power of EEG using cost-sensitive support vector machines. *Epilepsia* 52, 1761–1770. doi: 10.1111/j.1528-1167.2011.03138.x

Peña, E., Zhang, S., Deyo, S., Xiao, Y., and Johnson, M. D. (2017). Particle swarm optimization for programming deep brain stimulation arrays. *J. Neural Eng.* 14:016014. doi: 10.1088/1741-2552/aa52d1

Pollo, C., Kaelin-Lang, A., Oertel, M. F., Stieglitz, L., Taub, E., Fuhr, P., et al. (2014). Directional deep brain stimulation: an intraoperative double-blind pilot study. *Brain* 137, 2015–2026. doi: 10.1093/brain/awu102

Qasim, S. E., De Hemptinne, C., Swann, N. C., Miocinovic, S., Ostrem, J. L., and Starr, P. A. (2016). Electrocorticography reveals beta desynchronization in the basal ganglia-cortical loop during rest tremor in Parkinson's disease. *Neurobiol. Dis.* 86, 177–186. doi: 10.1016/j.nbd.2015.11.023

Riva-Posse, P., Choi, K. S., Holtzheimer, P. E., Crowell, A. L., Garlow, S. J., Rajendra, J. K., et al. (2017). A connectomic approach for subcallosal cingulate deep brain stimulation surgery: prospective targeting in treatment-resistant depression. *Mol. Psychiatry*. doi: 10.1038/mp.2017.59. [Epub ahead of print].

Rosa, M., Arlotti, M., Ardolino, G., Cogiamanian, F., Marceglia, S., Di Fonzo, A., et al. (2015). Adaptive deep brain stimulation in a freely moving Parkinsonian patient. *Mov. Disord.* 30, 1003–1005. doi: 10.1002/mds.26241

Rosin, B., Slovik, M., Mitelman, R., Rivlin-Etzion, M., Haber, S. N., Israel, Z., et al. (2011). Closed-loop deep brain stimulation is superior in ameliorating parkinsonism. *Neuron* 72, 370–384. doi: 10.1016/j.neuron.2011.08.023

Rossi, P. J., Giordano, J., and Okun, M. S. (2017). The problem of funding off-label deep brain stimulation: bait-and-switch tactics and the need for policy reform. *JAMA Neurol.* 74, 9–10. doi: 10.1001/jamaneurol.2016.2530

Salanova, V., Witt, T., Worth, R., Henry, T. R., Gross, R. E., Nazzaro, J. M., et al. (2015). Long-term efficacy and safety of thalamic stimulation for drug-resistant partial epilepsy. *Neurology* 84, 1017–1025. doi: 10.1212/WNL.0000000000001334

Schiff, N. D. (2016). Central thalamic deep brain stimulation to support anterior forebrain mesocircuit function in the severely injured brain. *J. Neural Transm.* 123, 797–806. doi: 10.1007/s00702-016-1547-0

Shahed, J., Poysky, J., Kenney, C., Simpson, R., and Jankovic, J. (2007). GPi deep brain stimulation for Tourette syndrome improves tics and psychiatric comorbidities. *Neurology* 68, 159–160. doi: 10.1212/01.wnl.0000250354.81556.90

Shook, J. R., and Giordano, J. (2014). A principled and cosmopolitan neuroethics: considerations for international relevance. *Philos. Ethics Humanit. Med.* 9:1. doi: 10.1186/1747-5341-9-1

Shook, J. R., and Giordano, J. (2015). Principled research ethics in practice? Reflections for neuroethics and bioethics. *Cortex* 71, 423–426. doi: 10.1016/j.cortex.2015.03.017

Shreve, L. A., Velisar, A., Malekmohammadi, M., Koop, M. M., Trager, M., Quinn, E. J., et al. (2017). Subthalamic oscillations and phase amplitude coupling are greater in the more affected hemisphere in Parkinson's disease. *Clin. Neurophysiol.* 128, 128–137. doi: 10.1016/j.clinph.2016.10.095

Shute, J. B., Okun, M. S., Opri, E., Molina, R., Rossi, P. J., Martinez-Ramirez, D., et al. (2016). Thalamocortical network activity enables chronic tic detection in humans with Tourette syndrome. *Neuroimage Clin.* 12, 165–172. doi: 10.1016/j.nicl.2016.06.015

Song, D., Chan, R. H., Marmarelis, V. Z., Hampson, R. E., Deadwyler, S. A., and Berger, T. W. (2007). Nonlinear dynamic modeling of spike train transformations for hippocampal-cortical prostheses. *IEEE Trans. Biomed. Eng.* 54, 1053–1066. doi: 10.1109/TBME.2007.891948

Song, D., Chan, R. H., Marmarelis, V. Z., Hampson, R. E., Deadwyler, S. A., and Berger, T. W. (2009). Nonlinear modeling of neural population dynamics for hippocampal prostheses. *Neural Netw.* 22, 1340–1351. doi: 10.1016/j.neunet.2009.05.004

Song, D., Robinson, B., Hampson, R., Marmarelis, V., Deadwyler, S., and Berger, T. (2016). Sparse large-scale nonlinear dynamical modeling of human hippocampus for memory prostheses. *IEEE Trans. Neural Syst. Rehabil. Eng.* doi: 10.1109/TNSRE.2016.2604423. [Epub ahead of print].

Song, D., Wang, H., Tu, C. Y., Marmarelis, V. Z., Hampson, R. E., Deadwyler, S. A., et al. (2013). Identification of sparse neural functional connectivity using penalized likelihood estimation and basis functions. *J. Comput. Neurosci.* 35, 335–357. doi: 10.1007/s10827-013-0455-7

Stanslaski, S., Afshar, P., Cong, P., Giftakis, J., Stypulkowski, P., Carlson, D., et al. (2012). Design and validation of a fully implantable, chronic, closed-loop neuromodulation device with concurrent sensing and stimulation. *IEEE Trans. Neural Syst. Rehabil. Eng.* 20, 410–421. doi: 10.1109/TNSRE.2012.2183617

Stefani, A., Lozano, A. M., Peppe, A., Stanzione, P., Galati, S., Tropepi, D., et al. (2007). Bilateral deep brain stimulation of the pedunculopontine and subthalamic nuclei in severe Parkinson's disease. *Brain* 130, 1596–1607. doi: 10.1093/brain/awl346

Swan, B. D., Grill, W. M., and Turner, D. A. (2014). Investigation of deep brain stimulation mechanisms during implantable pulse generator replacement surgery. *Neuromodulation* 17, 419–424; discussion 424. doi: 10.1111/ner.12123

Swann, N. C., De Hemptinne, C., Miocinovic, S., Qasim, S., Wang, S. S., Ziman, N., et al. (2016). Gamma oscillations in the hyperkinetic state detected with chronic human brain recordings in Parkinson's disease. *J. Neurosci.* 36, 6445–6458. doi: 10.1523/JNEUROSCI.1128-16.2016

Teplitzky, B. A., Zitella, L. M., Xiao, Y., and Johnson, M. D. (2016). Model-based comparison of deep brain stimulation array functionality with varying number of radial electrodes and machine learning feature sets. *Front. Comput. Neurosci.* 10:58. doi: 10.3389/fncom.2016.00058

Thevathasan, W., Debu, B., Aziz, T., Bloem, B. R., Blahak, C., Butson, C., et al. (2017). Pedunculopontine nucleus deep brain stimulation in Parkinson's disease: a clinical review. *Mov. Disord.* doi: 10.1002/mds.27098. [Epub ahead of print].

Tian, Y. L., Kanade, T., and Cohn, J. F. (2001). Recognizing action units for facial expression analysis. *IEEE Trans. Pattern Anal. Mach. Intell.* 23, 97–115. doi: 10.1109/34.908962

Tinkhauser, G., Pogosyan, A., Little, S., Beudel, M., Herz, D. M., Tan, H., et al. (2017). The modulatory effect of adaptive deep brain stimulation on beta bursts in Parkinson's disease. *Brain* 140, 1053–1067. doi: 10.1093/brain/awx010

Viswanathan, A., Jimenez-Shahed, J., Baizabal Carvallo, J. F., and Jankovic, J. (2012). Deep brain stimulation for Tourette syndrome: target selection. *Stereotact. Funct. Neurosurg.* 90, 213–224. doi: 10.1159/000337776

Volkmann, J., Moro, E., and Pahwa, R. (2006). Basic algorithms for the programming of deep brain stimulation in Parkinson's disease. *Mov. Disord.* 21(Suppl. 14), S284–S289. doi: 10.1002/mds.20961

Whitmer, D., De Solages, C., Hill, B., Yu, H., Henderson, J. M., and Bronte-Stewart, H. (2012). High frequency deep brain stimulation attenuates subthalamic and cortical rhythms in Parkinson's disease. *Front. Hum. Neurosci.* 6:155. doi: 10.3389/fnhum.2012.00155

Widge, A. S., Licon, E., Zorowitz, S., Corse, A., Arulpragasam, A. R., Camprodon, J. A., et al. (2016). Predictors of hypomania during ventral capsule/ventral striatum deep brain stimulation. *J. Neuropsychiatry Clin. Neurosci.* 28, 38–44. doi: 10.1176/appi.neuropsych.15040089

Xiao, Y., Pena, E., and Johnson, M. D. (2016). Theoretical optimization of stimulation strategies for a directionally segmented deep brain stimulation electrode array. *IEEE Trans. Biomed. Eng.* 63, 359–371. doi: 10.1109/TBME.2015.2457873

Xie, T., Vigil, J., Maccracken, E., Gasparaitis, A., Young, J., Kang, W., et al. (2015). Low-frequency stimulation of STN-DBS reduces aspiration and freezing of gait in patients with PD. *Neurology* 84, 415–420. doi: 10.1212/WNL.0000000000001184

Zaidel, A., Spivak, A., Grieb, B., Bergman, H., and Israel, Z. (2010). Subthalamic span of beta oscillations predicts deep brain stimulation efficacy for patients with Parkinson's disease. *Brain* 133, 2007–2021. doi: 10.1093/brain/awq144

Zibetti, M., Moro, E., Krishna, V., Sammartino, F., Picillo, M., Munhoz, R. P., et al. (2016). Low-frequency subthalamic stimulation in Parkinson's disease: long-term outcome and predictors. *Brain Stimul.* 9, 774–779. doi: 10.1016/j.brs.2016.04.017

Zitella, L. M., Mohsenian, K., Pahwa, M., Gloeckner, C., and Johnson, M. D. (2013). Computational modeling of pedunculopontine nucleus deep brain stimulation. *J. Neural Eng.* 10:045005. doi: 10.1088/1741-2560/10/4/045005

Conflict of Interest Statement: The authors declare that the research was conducted in the absence of any commercial or financial relationships that could be construed as a potential conflict of interest.

frontiers in Neuroscience

OPINION
published: 12 February 2018
doi: 10.3389/fnins.2018.00065

Therapeutic Effects of Electrical Stimulation: Interpretations and Predictions Based on the Visceral Theory of Sleep

Ivan N. Pigarev[1]* *and Marina L. Pigareva*[2]

[1] *Institute for Information Transmission Problems (Kharkevich Institute), Russian Academy of Sciences, Moscow, Russia,*
[2] *Institute of Higher Nervous Activity and Neurophysiology, Russian Academy of Sciences, Moscow, Russia*

Keywords: electrical Stimulation, visceral theory of sleep, Sleep pressure, visceral nerves, sleepiness

Edited by:
Mikhail Lebedev,
Duke University, United States

Reviewed by:
Zurab Silagadze,
Budker Institute of Nuclear Physics (RAS), Russia
Ugo Carraro,
Università degli Studi di Padova, Italy

***Correspondence:**
Ivan N. Pigarev
pigarev@iitp.ru

Specialty section:
This article was submitted to Neural Technology, a section of the journal Frontiers in Neuroscience

Received: *11 October 2017*
Accepted: *26 January 2018*
Published: *12 February 2018*

Citation:
Pigarev IN and Pigareva ML (2018) Therapeutic Effects of Electrical Stimulation: Interpretations and Predictions Based on the Visceral Theory of Sleep. Front. Neurosci. 12:65. doi: 10.3389/fnins.2018.00065

Attempts to use electrical stimulation for treatment of various diseases began even before the nature of both, nervous system and electricity, were discovered (e.g., Devinsky, 1993). Later scientific interpretations of therapeutic effects of electrical stimulations have been based on the functional properties of neural circuits established for wake conditions. Here we discuss a different set of mechanisms for the stimulation therapy, which emerge from our recent investigations into the visceral theory of sleep (Pigarev, 2014).

This theory is based on the observations that, during sleep, neurons in various cortical areas, including the primary visual cortex (area V1), switched from the processing of exteroceptive information (visual, somatosensory and so on) to processing of signals coming from various visceral organs like the stomach, intestine and cardiovascular and respiratory systems (Pigarev, 1994; Pigarev et al., 2006, 2013; Pigarev and Pigareva, 2014). Taking into account these observations, we proposed that, during sleep, the cerebral cortex and other brain regions perform maintenance of body organs, including the brain itself, and generate the host responses to any pathological deviations in their states.

It is well known that sleep deprivation leads to unavoidable death of animals (i.e., Everson et al., 1989), and it is generally recognized that impairments of sleep are connected with various visceral disorders in humans (for reviews see i.e., Knutson and Van Cauter, 2008; Pigarev and Pigareva, 2012; Ali et al., 2013; Surani, 2014). On the other hand, improvement of disturbed sleep or restoration of normal sleep patterns has a therapeutic effect in the case of various diseases (Cizza et al., 2010; Chaput and Tremblay, 2012). But how can this be related to electrical stimulation? Actually, this link is rather direct, and is connected with the probable mechanism of transition from wakefulness to sleep. Details of this approach were presented in our previous study (Pigarev and Pigareva, 2013). Briefly, the transition from wakefulness to sleep and back, we consider, as the balance between two groups of needs—needs of wakefulness and needs of sleep. Needs of wakefulness are determined by the activity of an organism in the surrounding environment, and are based on information coming from extero- and proprio-receptors. Needs of sleep are determined by the states of all visceral organs of the organism, and are based on interoceptive information. But which kind of interoceptive information will increase the need for sleep and provoke sleepiness? If the purpose of sleep is to restore functionality of an organism, it would be logical to propose that needs of sleep should be related to interoceptive error signals. While all interoceptive parameters are within the genetically determined normal range, organisms may stay awake and continue to realize their needs of wakefulness. However, as soon as these parameters decline from safe values, this abnormality will be perceived as tiredness and necessity to sleep. Thus, deviation of the current visceral afferentation from the normal range should provoke sleepiness.

Based on these considerations, it is reasonable to suggest that electrical stimulation could mimic visceral sensory signals and contribute to the transitions between the awake and sleep states. In the first studies where electrical stimulations were applied, it was naturally considered that such stimulation could produce functional responses normally associated with the nervous structure being activated. However, later it became clear that electrical stimulations disrupts normal activity of neuronal circuits instead of activating them in a meaningful way. Even being applied to the peripheral nerves, skin or muscles, electrical stimulation provokes absolutely artificial combinations of fiber activation, which can hardly be imagined in any natural conditions. We should remember that in all parts of a body, thousands of terminals of interoceptive nerves are distributed, and electrical stimulation will excite them also in uncommon ways. This uncommon stimulation of the visceral afferents will be considered as error signals, and will increase the need for sleep. In particular cases sleep might be an immediate reaction, but more likely this stimulation will just increase the need for sleep, which may improve the quality of sleep during the subsequent night or nights. This improved sleep, but not the stimulation itself, may lead to more efficient body restoration, and in the case of any diseases, will facilitate treatment. Thus practically any electrical stimulation potentially may cause nonspecific general therapeutic effects.

The somnolent effect of visceral nerve stimulation was noticed long ago, even before the discovery of electricity. It was known that mechanical stimulation of a neck along the carotid artery evoked sleep—the carotid artery is sometimes even called the "sleep artery." Now we know that this effect is related to stimulation of the vagus nerve, which passes along the carotid artery. In animal experiments it was shown that electrical stimulation of the vagus nerve did indeed provoke sleep (Juhasz et al., 1985). But in order to promote sleep it is not necessary to stimulate all of a nerve. Local stimulation of some peripheral branches might also be sufficient.

In our previous study, we investigated neuronal activity in the cat visual cortex during sleep, and applied visceral electrical stimuli in the area of the small intestine (Pigarev, 1994). We were afraid that intraperitoneal electrical stimulation could decrease the depth of sleep. However, we soon noticed that intestinal stimulation, on the contrary, shifted sleep to an even deeper level. Later we found that this somnolent effect of intestinal stimulation had already been noticed and described by Hungarian scientists (Kukorelli and Juhasz, 1976).

Sleep-promoting effects of visceral stimulation, as with any other responses of the nervous system, are habituating. The strongest effect is observed in response to first presentations. This effect will be less on the next day, and it can disappear after several days of application. An interval of non-stimulation for a couple of weeks restores the initial reaction. We have not studied these habituation effects systematically, and we mention them only because permanent changing of the stimulating parameters might be useful to avoid such habituation.

It is noteworthy that direct brain stimulation in certain cases can promote sleep and even act as anesthesia. While these effects are mostly based on the specific functions of the stimulated brain structures, some contribution is possible from the nonspecific mechanisms similar to the described above.

We found only one study where electrical stimulation of skin surface was efficiently used for improvement of sleep quality (Indursky et al., 2013). However, for this purpose the acupuncture - a mechanical counterpart of electrical stimulation is often used. In many special studies it was shown that acupuncture is effective in improvement of sleep quality and treatment of sleep disorders. See, for example, Cao et al. (2009), Bosch et al. (2014) and Fu et al. (2017). Within the frame of the visceral theory of sleep we also have proposed that acupuncture efficiency for treatment of various health problems, at least partly, could be related with improvement of sleep quality after acupuncture sessions (Pigarev, 2014).

The sleep-inducing effect could be minor compared to the other positive effects of electrical stimulation. But some impact of increased sleepiness can be expected in many cases of such stimulation. It would be very useful if investigators could pay special attention to the quality of sleep of their patients before and after stimulating procedures.

The high probability of growing sleepiness after procedures of electrical stimulation should be taken into account if patients have to use cars after these procedures, because increased risk of car accidents can be expected. On the other hand it might be reasonable to try to use electrical stimulations distributed in various locations over the body, and having variable combinations of stimulating parameters. If our theoretical considerations are correct, one may expect to get a substantial somnolent effect of this procedure, probably capable of replacing, in some cases, the use of pharmacological agents, with the added benefit of being free from the often unpleasant side effects of these drugs.

AUTHOR CONTRIBUTIONS

All authors listed have made a substantial, direct and intellectual contribution to the work, and approved it for publication.

FUNDING

This study was supported by Russian Foundation for Basic Research grants 16-04-00413, and 15-06-19390\OGON.

ACKNOWLEDGMENTS

We are very thankful to Dr. Denys Garden for critical reading of the manuscript and helpful comments.

REFERENCES

Ali, T., Choe, J., Awab, A., Wagener, T. L., and Orr, W. C. (2013). Sleep, immunity and inflammation in gastrointestinal disorders. *World J. Gastroenterol.* 19, 9231–9239. doi: 10.3748/wjg.v19.i48.9231

Bosch, P., Staudte, H., van den Noort, M., and Lim, S. (2014). A case study on acupuncture in the treatment of schizophrenia. *Acupunct Med.* 32, 286–289. doi: 10.1136/acupmed-2014-010547

Cao, H., Pan, X., Li, H., and Liu, J. (2009). Acupuncture for treatment of insomnia: a systematic review of randomized controlled trials. *J. Altern. Complement. Med.* 15, 1171–1186. doi: 10.1089/acm.2009.0041

Cizza, G., Marincola, P., Mattingly, M., Williams, L., Mitler, M., Skarulis, M., et al. (2010). Treatment of obesity with extension of sleep duration: a randomized, prospective, controlled trial. *Clin. Trials* 7, 274–285. doi: 10.1177/1740774510368298

Chaput, J. P., and Tremblay, A. (2012). Adequate sleep to improve the treatment of obesity. *CMAJ* 184, 1975–1976. doi: 10.1503/cmaj.120876

Devinsky, O. (1993). Electrical and magnetic stimulation of the central nervous system. Historical overview. *Adv. Neurol.* 63, 1–16.

Everson, C. A., Bergmann, B. M., and Rechtschaffen, A. (1989). Sleep deprivation in the rat: III. Total sleep deprivation. *Sleep* 12, 13–21.

Fu, C., Zhao, N., Liu, Z., Yuan, L. H., Xie, C., Yang, W. J., et al. (2017). Acupuncture improves peri-menopausal insomnia: a randomized controlled trial. *Sleep.* 40:zsx153. doi: 10.1093/sleep/zsx153

Juhasz, G., Détári, L., and Kukorelli, T. (1985). Effects of hypnogenic vagal stimulation on thalamic neuronal activity in cats. *Brain Res. Bull.* 15, 437–441.

Indursky, P. A., Markelov, V. V., Shakhnarovich, V. M., and Dorokhov, V. B. (2013). Low_frequency rhythmic electrocutaneous hand stimulation during slow_wave night sleep: physiological and therapeutic effects. *Hum. Physiol.* 39, 642–654. doi: 10.1134/S0362119713060054

Knutson, K. L., and Van Cauter, E. (2008). Associations between sleep loss and increased risk of obesity and diabetes. *Ann. N.Y. Acad. Sci.* 1129, 287–304. doi: 10.1196/annals.1417.033

Kukorelli, T., and Juhasz, G. (1976). Sleep induced by intestinal stimulation in cats. *Physiol. Behav.* 19, 355–358.

Pigarev, I. N. (1994). Neurons of visual cortex respond to visceral stimulation during slow wave sleep. *Neuroscience* 62, 1237–1243. doi: 10.1016/0306-4522(94)90355-7

Pigarev, I. N. (2014). "Transmission of the visceral and somatosensory information to the brain via spinal cord in sleep-wake cycle: towards the physiological ground of acupuncture," in *BIT's 5th Annual World Congress of Neurotalk-2014* (Nanjing).

Pigarev, I. N., Almirall, H., Pigareva, M. L., Bautista, V., Sánchez-Bahillo, A., Barcia, C., et al. (2006). Visceral signals reach visual cortex during slow wave sleep. Study in monkeys. *Acta Neurobiol. Exp.* 66, 69–73.

Pigarev, I. N., Bagaev, V. A., Levichkina, E. V., Fedorov, G. O., and Busigina, I. I. (2013). Cortical visual areas process intestinal information during slow-wave sleep. *Neurogastroenterol. Motil.* 25, 268–275.e169. doi: 10.1111/nmo.12052

Pigarev, I. N., and Pigareva, M. L. (2012). Sleep and the control of visceral functions. *Neurosci. Behav. Physiol.* 42, 948–956. doi: 10.1007/s11055-012-9661-4

Pigarev, I. N., and Pigareva, M. L. (2013). Sleep, emotions and visceral control. *Hum. Physiol.* 39, 590–601. doi: 10.1134/s036211971306008x

Pigarev, I. N., and Pigareva, M. L. (2014). Partial sleep in the context of augmentation of brain function. *Front. Syst. Neurosci.* 8:75. doi: 10.3389/fnsys.2014.00075

Surani, S. R. (2014). Diabetes, sleep apnea, obesity and cardiovascular disease: Why not address them together? *World J. Diabetes* 5, 381–384. doi: 10.4239/wjd.v5.i3.381

Conflict of Interest Statement: The authors declare that the research was conducted in the absence of any commercial or financial relationships that could be construed as a potential conflict of interest.

frontiers in Neuroscience

ORIGINAL RESEARCH
published: 08 March 2018
doi: 10.3389/fnins.2018.00139

Using a Double-Coil TMS Protocol to Assess Preparatory Inhibition Bilaterally

Pierre Vassiliadis[*†], *Julien Grandjean*[†], *Gerard Derosiere, Ysaline de Wilde, Louise Quemener and Julie Duque*

Institute of Neuroscience, Université Catholique de Louvain, Brussels, Belgium

Transcranial magnetic stimulation (TMS) applied over the primary motor cortex (M1), elicits motor-evoked potentials (MEPs) in contralateral limb muscles which are valuable indicators of corticospinal excitability (CSE) at the time of stimulation. So far, most studies have used single-coil TMS over one M1, yielding MEPs in muscles of a single limb—usually the hand. However, tracking CSE in the two hands simultaneously would be useful in many contexts. We recently showed that, in the resting state, double-coil stimulation of the two M1 with a 1 ms inter-pulse interval (double-coil$_{1\ ms}$ TMS) elicits MEPs in both hands that are comparable to MEPs obtained using single-coil TMS. To further evaluate this new technique, we considered the MEPs elicited by double-coil$_{1\ ms}$ TMS in an instructed-delay choice reaction time task where a prepared response has to be withheld until an imperative signal is displayed. Single-coil TMS studies have repetitively shown that in this type of task, the motor system is transiently inhibited during the delay period, as evident from the broad suppression of MEP amplitudes. Here, we aimed at investigating whether a comparable inhibitory effect can be observed with MEPs elicited using double-coil$_{1\ ms}$ TMS. To do so, we compared the amplitude as well as the coefficient of variation (CV) of MEPs produced by double-coil$_{1\ ms}$ or single-coil TMS during action preparation. We observed that MEPs were suppressed (smaller amplitude) and often less variable (smaller CV) during the delay period compared to baseline. Importantly, these effects were equivalent whether single-coil or double-coil$_{1\ ms}$ TMS was used. This suggests that double-coil$_{1\ ms}$ TMS is a reliable tool to assess CSE, not only when subjects are at rest, but also when they are involved in a task, opening new research horizons for scientists interested in the corticospinal correlates of human behavior.

Keywords: transcranial magnetic stimulation, motor-evoked potentials, primary motor cortex, corticospinal excitability, coefficient of variation, action preparation, inhibition

OPEN ACCESS

Edited by:
Ioan Opris,
University of Miami, United States

Reviewed by:
Winston D. Byblow,
University of Auckland, New Zealand
Florent Lebon,
INSERM U1093 Université de Bourgogne Franche Comté, France

***Correspondence:**
Pierre Vassiliadis
pierre.vassiliadis@student.uclouvain.be

[†]*These authors have contributed equally to this work.*

Specialty section:
This article was submitted to Neural Technology, a section of the journal Frontiers in Neuroscience

Received: *22 October 2017*
Accepted: *21 February 2018*
Published: *08 March 2018*

Citation:
Vassiliadis P, Grandjean J, Derosiere G, de Wilde Y, Quemener L and Duque J (2018) Using a Double-Coil TMS Protocol to Assess Preparatory Inhibition Bilaterally. Front. Neurosci. 12:139. doi: 10.3389/fnins.2018.00139

INTRODUCTION

Transcranial magnetic stimulation (TMS), a technique used to assess corticospinal excitability (CSE), has gained substantial attention since it was first described about 30 years ago (Ziemann, 2017). The amplitude of motor-evoked potentials (MEPs) elicited in muscles of the contralateral limb (often the hand) by TMS over the primary motor cortex (M1) is a precious indicator of CSE

at the time of stimulation (Bestmann and Krakauer, 2015; Bestmann and Duque, 2016; Duque et al., 2017). Comparing MEP amplitudes in different conditions have helped to characterize the corticospinal correlates of various neural processes including those underlying action preparation and stopping (Duque et al., 2010, 2012, 2013; van den Wildenberg et al., 2010; Greenhouse et al., 2012; Majid et al., 2012; Quoilin and Derosiere, 2015), decision making and reward processing (Klein et al., 2012; Klein-Flügge and Bestmann, 2012; Cos et al., 2014; Zénon et al., 2015; Derosiere et al., 2017a,b), sustained attention (Derosière et al., 2015), speech (Labruna et al., 2011b; Neef et al., 2015), and motor imagery (Ruffino et al., 2017). TMS has also proved useful in characterizing the corticospinal correlates of behavioral deficits in several neurologic disorders (Badawy et al., 2012) including stroke (Auriat et al., 2015; Stinear et al., 2015; Smith and Stinear, 2016; Boddington and Reynolds, 2017), Parkinson's disease (Valls-Solé et al., 1994; Lefaucheur, 2005; Soysal et al., 2008; Benninger and Hallett, 2015), or Alzheimer's disease (Guerra et al., 2011).

To date, almost all TMS-based CSE studies have recorded MEPs from muscles of a single hand following the application of TMS over one M1 only. Hence, in most experiments, the MEP data have only provided researchers with half of the story, increasing the probability of seeing data being misinterpreted. This occurs because applying TMS over both M1 in separate blocks doubles the duration of the experiment, making it impossible to fit all the conditions in a single session. For example, studies investigating inhibitory processes during action preparation have typically recorded MEPs from left hand muscles (following right M1 TMS) in instructed-delay choice RT tasks where subjects have to withhold cued left or right hand responses (e.g., left or right index finger key-presses) until an imperative signal is displayed (Duque and Ivry, 2009; Duque et al., 2010; Greenhouse et al., 2015b; Lebon et al., 2016; Quoilin et al., 2016): left MEPs are deeply suppressed in this context (compared to a baseline), a phenomenon often referred to as preparatory inhibition (Duque et al., 2017). Critically, many studies have reported a stronger left MEP suppression in conditions where the target muscle is selected for the forthcoming movement (i.e., left response) compared to when it is non-selected (i.e., right response) and it has been commonly accepted that this difference results from the distinct function (selected vs. non-selected) of the left hand muscle in these two situations (Duque et al., 2010, 2014; Labruna et al., 2014). That is, preparatory inhibition is thought to be more prominent for selected than non-selected effector representations. Yet, there is a substantial confound here because besides the function (selected vs. non-selected), conditions also differ in regard to the hand being cued for the response (left vs. right). Hence, the stronger left MEP suppression with left than right hand responses may be due to the use of the non-dominant vs. dominant hand rather than to the distinct function of the targeted muscle in these trials.

Recently, we have proposed the use of double-coil TMS over both M1, to obtain MEPs from bilateral muscles at once (Wilhelm et al., 2016; Grandjean et al., 2018). In these previous studies, we tested a double-coil TMS method where the two M1 are stimulated with a 1 ms inter-pulse interval (double-coil$_{1\,ms}$ TMS). An interval between the two TMS pulses is necessary to avoid direct electromagnetic interference between the two stimulating coils. Yet, the latter must be kept short enough to avoid cortical interactions through the corpus callosum occurring with delays as small as 4 ms (Ferbert et al., 1992; Hanajima et al., 2001; reviewed in Reis et al., 2008). In Grandjean et al. (2018), MEPs elicited using this new double-coil$_{1\,ms}$ approach (MEP_{double}) were recorded for five different intensities of stimulation while participants were completely relaxed, at rest, and were compared to those elicited in the same conditions using single-coil TMS (MEP_{single}) applied successively over the two M1. Note that given the 1 ms inter-pulse interval in double-coil$_{1\,ms}$ trials, MEP_{double} were either evoked by a 1st ($MEP_{double-1}$) or a 2nd ($MEP_{double-2}$) TMS pulse. Importantly, the study revealed that $MEP_{double-1}$ and $MEP_{double-2}$ are comparable to MEP_{single} when elicited at rest, regardless of the TMS intensity, suggesting that this method may be used to assess CSE bilaterally. However, it still remains to be determined whether double-coil$_{1\,ms}$ TMS produces comparable MEPs as single-coil TMS in the context of a task.

In the present study, we compared $MEP_{double-1\&2}$ and MEP_{single} during action preparation, applying double-coil$_{1\,ms}$ or single-coil TMS in an instructed-delay choice RT task where subjects have to withhold a cued response until an imperative signal is displayed (Bestmann and Duque, 2016; Quoilin et al., 2016; Duque et al., 2017). We compared the strength of preparatory inhibition when probed using double-coil$_{1\,ms}$ or single-coil TMS. Some of these results have already been reported in abstract form (Grandjean et al., 2017a,b).

MATERIALS AND METHODS

Participants

A total of 15 right-handed healthy subjects participated in the present study ($n = 15$; 10 women; 22.4 ± 1.63 years old). Handedness was determined via a shortened version of the Edinburgh Handedness inventory Oldfield (1971) and all subjects filled out a TMS safety questionnaire. None of the participants suffered from any neurological disorder or had a history of psychiatric illness, drug or alcohol abuse; neither was anybody undergoing a drug treatment that could influence their performance or their neural activity. All subjects were financially compensated for their participation and provided written informed consent. The protocol was approved by the Ethics Committee of the Université Catholique de Louvain.

The "Rolling Ball" Task

Participants sat in front of a 21-inch monitor screen positioned about 60 cm in front of them with their arms semi-flexed and both hands resting palm-down on a response device developed in our laboratory (Quoilin et al., 2016). They performed an instructed-delay choice reaction time (RT) task, which required them to choose between abduction movements of the left or right index finger. The task was implemented with Matlab 7.5 (the Mathworks, Natick, Massachusetts, USAS) using the Psychophysics Toolbox extensions (Brainard, 1997; Pelli, 1997). The refresh rate of the monitor was set at 100 Hz.

The task consisted in a virtual "Rolling Ball" game previously used in another study (Quoilin et al., 2016; **Figure 1A**). In this game, participants were informed that the position of a preparatory cue (i.e., a ball separated from a goal by a gap) indicated the movement side for the forthcoming response: if the ball was on the left side of the screen, subjects had to prepare a left index finger response (to get ready to "shoot the ball into the goal") and if the ball was on the right side, subjects had to prepare a right index finger response. Subjects were explicitly told to withhold their response until the onset of an imperative signal (i.e., a bridge). The latter appeared 1,000–1,200 ms after the ball and remained on the screen until a finger movement was detected or for a maximum duration of 500 ms. When the bridge was on the screen, subjects had to respond as fast as possible to allow the ball to roll on it and to quickly reach the goal. Subjects knew that they would get a score after each trial reflecting how fast and accurate they had been on the previous trial. Note that in each block, some catch trials (trials in which the bridge did not appear; 5% of all trials) were included. Subjects were required not to respond on these trials and were penalized if they did so. Hence, they had to avoid initiating their response prematurely, before the bridge onset. Trials were separated by the presentation of a blank screen lasting for a duration that varied between 2,050 and 2,300 ms (**Figure 1B**).

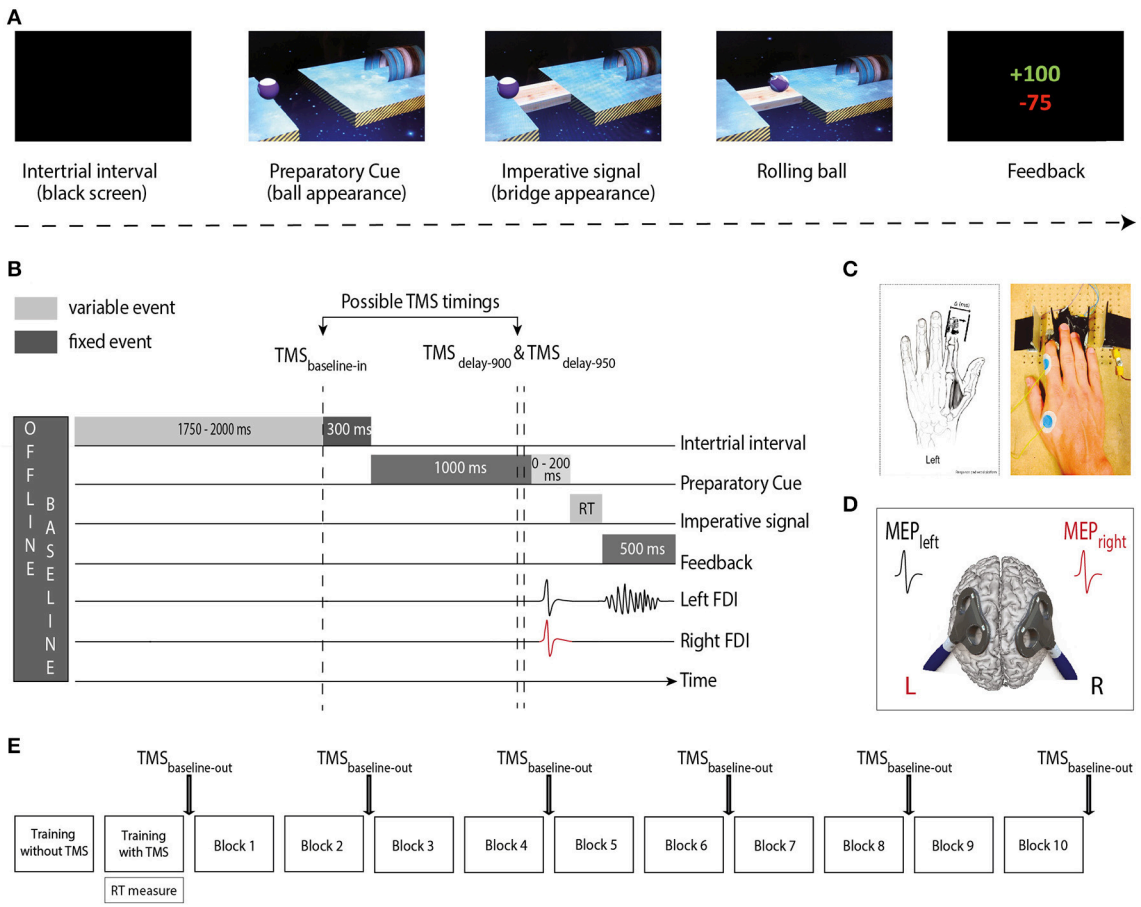

FIGURE 1 | (A) "Rolling Ball" task. Subjects were asked to choose between responding with the left or right index finger according to the position of a ball (Preparatory cue) appearing on the left or right part of the screen (left in the current example). They had to wait until the onset of a bridge (Imperative signal) to release their response. The ball then rolled on the bridge (when the subjects answered correctly) to reach a goal located on the other side of the gap. A feedback reflecting how fast and accurate the subjects had been concluded each trial. **(B)** Time course of a trial. Each trial started with a blank screen (intertrial interval; 2,050–2,300 ms). Then, the preparatory cue appeared for a variable delay period (1,000–1,200 ms), followed by the imperative signal until the reaction time (RT). The feedback was presented at the end of each trial for 500 ms. TMS pulses occurred either during the intertrial interval (1,750–2,000 ms after the blank screen onset; $TMS_{baseline-in}$), or during the delay period (900 or 950 ms after the preparatory cue onset; $TMS_{delay-900}$ and $TMS_{delay-950}$). In Double-$coil_{1\ ms}$ trials, motor-evoked potentials (MEPs) were elicited in the first dorsal interosseous (FDI) of both hands at a near simultaneous time (1 ms delay); in single-coil trials, MEPs were elicited in the left or right hand. The figure displays a left hand trial with double-$coil_{1\ ms}$ at $TMS_{delay-950}$. **(C)** The response device. Index finger responses were recorded using a home-made device positioned under the left (graphic representation) and right (photographic representation) hands **(D)** TMS protocol. Two figure-eight-shaped coils were placed over the subject's primary motor cortex (M1), eliciting MEPs in the left and/or right FDI. **(E)** Time-course of the experiment. After two training blocks (see section Materials and Methods), subjects executed 10 blocks of 40 trials during which MEPs were elicited at $TMS_{baseline-in}$ or TMS_{delay}; MEPs were also elicited outside the blocks ($TMS_{baseline-out}$), before block 1 and after blocks 2, 4, 6, 8, and 10.

The home-made response device (**Figure 1C**) was composed of two pairs of metal edges fixed on a wooden platform (one for each hand) and each trial of the Rolling Ball game required participants to move one index finger from the outer to the inner metal edge (i.e., abduction of the index finger). The contact between the finger and the metal parts of the device was continuously monitored using a Makey Makey printed circuit board with an ATMega32u4 microcontroller running the Arduino Leonardo firmware, based on the principle of high resistance switching between two electrical contacts. This device provided us with a very precise measure of the RTs (precision = 1 ms) and allowed us to control for any anticipated movement. That is, the device permanently checked the initial position of each index finger (which had to be in contact with the outer metal edge) and any contact release before the onset of the imperative signal led to the cancellation of the trial and to a penalty.

Subjects received a feedback of their performance at the end of each trial. On correct trials, the feedback score (displayed in green) was inversely proportional to the reaction time (RT): the faster the subjects, the higher the score. The RT was defined as the time interval between the onset of the bridge and the time when the index finger left the outer metal edge of the response device. The score was determined based on the following equation, with $\propto = 0,8$ *median RT* measured at the end of the training session just before the main experiment:

$$x = \frac{(100.(\propto))}{\left(\propto + \left(\frac{RT-\propto}{10}\right)^{2,4}\right)}$$

Using this equation, scores on correct trials ranged from 1 to 100. Incorrect responses were penalized with negative scores displayed in red. They involved responses occurring too early, referred to as "anticipation errors" (penalized by 75 points), responses occurring too late, referred to as "time-out errors" (penalized by 50 points), responses provided with the incorrect hand (penalized by 20 points), referred to as "choice errors" and responses provided on catch trials (penalized by 12 points), referred as "catch errors." Anticipation errors consisted in responses provided either before the bridge onset or after its onset but with a RT smaller than 100 ms. Time-out errors consisted in responses provided in more than 500 ms (after the bridge offset). Note that when subjects succeeded not to respond on a catch trial, they were rewarded by +12 points. The total score was always displayed at the end of each block.

TMS Protocol

TMS was delivered through one or two small figure-of-eight shaped coils (wing internal diameter 35 mm), each connected either to a Magstim 200[2] magnetic stimulator (Magstim, Whitland, Dyfed, UK) or a Magstim Bistim[2] magnetic stimulator. Both stimulators delivered monophasic pulses and their relationship to a specific hemisphere was counterbalanced between subjects. Each coil was placed tangentially over one primary motor cortex (M1) with the handle pointing backward and laterally at a 45° angle away from the midline, approximately perpendicular to the central sulcus (**Figure 1D**). Small coils were chosen because in most subjects, it is not possible to place two large coils over the two M1s at the same time. For each M1, the optimal scalp position to elicit a contralateral MEP in the first dorsal interosseous muscle (FDI) was identified and marked on a head cap placed on the subject's scalp to provide a reference mark throughout the experiment (Duque et al., 2014, 2016; Klein et al., 2014). Importantly, this was done by always checking for the fact that the two coils could be positioned simultaneously on the head without touching each other; to reduce electromagnetic interference it was sometimes necessary to adjust the orientation of the coils a little but these adaptations remained marginal and did not preclude us from obtaining the best MEP amplitudes.

The resting Motor Threshold (rMT) was determined at the hotspot for each M1 as the minimal TMS intensity required to evoke MEPs of about 50 μV peak-to-peak in the relaxed FDI muscle in at least 5 out of 10 consecutive trials. Across participants, the rMTs corresponded to 41.7 ± 5.05 and 40.8 ± 6.39% of the maximum stimulator output for the left and the right FDI, respectively. The intensity of TMS used throughout the experiment was always set at 115% of the individual rMT for each hemisphere.

Experimental Procedure

The experiment started with two training blocks. The first one (20 trials) was conducted without TMS whereas the second one (40 trials) involved TMS, exactly as in the main experiment. Thereby, the subjects could first practice the task without being disturbed by the TMS pulse and then get used to the stimulations while performing the task in the second training block. The latter block also served to obtain the median RTs, used to individualize the scores on correct trials (see below). Then, during the main phase of the experiment, subjects performed 10 blocks of 40 trials (**Figure 1E**). Using these numbers, we obtained 20 MEPs in each condition.

The goal of the present experiment was to compare the amplitude of MEPs elicited during motor preparation using either single-coil or double-coil$_{1\,ms}$ TMS. In half of the trials, single-coil TMS was used, eliciting MEPs in a single hand (MEP_{single}), either in the left or the right FDI in a balanced proportion. In the other half, MEPs were elicited in both hands at once (MEP_{double}) using a double-coil$_{1\,ms}$ method where the two M1 are stimulated with a 1 ms inter-pulse interval (double-coil$_{1\,ms}$; Grandjean et al., 2018). In all subjects, half of the double-coil$_{1\,ms}$ trials involved a pulse over left M1 first whereas the other half of the trials involved a pulse over the right M1 first. Therefore, for each hand, $MEPs_{double}$ could either result from a first ($MEP_{double-1}$) or a second pulse ($MEP_{double-2}$). Importantly, the single- and double-coil$_{1\,ms}$ trials were always randomized within a block so that the subject could not anticipate the type of pulse (single or double) they would have next, an aspect that could bias MEPs, as suggested in a previous study (Wilhelm et al., 2016).

Single- and double-coil$_{1\,ms}$ TMS pulses were applied at three different timings during the Rolling Ball task (only one pulse per trial; **Figure 1B**). First, some TMS pulses occurred during the intertrial interval, at a random time falling 1,750–2,000 ms

after the blank screen onset; these trials were used to compare MEP_{single} and MEP_{double} at baseline (rest) within the blocks ($TMS_{baseline-in}$, 20% of all trials). In the remaining trials, the TMS was delivered during the delay period either 900 ms ($TMS_{delay-900}$, 40% of all trials) or 950 ms ($TMS_{delay-950}$, 40% of all trials) after the occurrence of the preparatory cue. Based on previous studies (reviewed in Duque et al., 2017), we assumed that at these TMS_{delay} timings, inhibitory changes would be substantial whether MEPs are elicited in a selected condition (e.g., left MEPs elicited in a left hand trial) or a non-selected condition (e.g., left MEPs elicited in a right hand trial). Finally, we also recorded baseline MEPs outside the blocks ($TMS_{baseline-out}$), at six different times (before block 1 and after blocks 2, 4, 6, 8, and 10; 20 MEPs each). These MEPs provided us with a measure of CSE outside the context of the task, at complete rest. Moreover, the comparison of MEP_{single} and MEP_{double} at $TMS_{baseline-out}$ allowed us to check whether we could replicate our previous observations (Grandjean et al., 2018).

Electromyography (EMG) Recording

EMG activity was recorded from surface electrodes (Neuroline, Medicotest, Oelstykke, Denmark) placed over the left and right FDI. MEPs recorded from these homonymous muscles offered a measure of CSE changes occurring in muscles that are involved in the task (whether selected or non-selected). Note that for all participants, stimulating the hotspot for the FDI also elicited reliable MEPs in the abductor digiti minimi (ADM), a pinkie abductor muscle which is irrelevant for the task. These MEPs were also considered in the present study. EMG data were collected for 1,000 ms on each trial, starting 300 ms before the TMS pulse. The EMG signals were amplified (x1,000), bandpass filtered online (10–500 Hz; NeuroloLog; Digitimer), and digitalized at 2,000 Hz for offline analysis.

Trials with background EMG activity (root mean square computed from −250 to −50 ms before the TMS pulse) exceeding 3 standard deviations (*SD*) around the mean were discarded for the following analyses. This was done to prevent contamination of the MEP measurements by significant fluctuations in background EMG (Duque et al., 2014, 2016; Klein et al., 2014). The remaining MEPs were classified according to the experimental condition within which they had been elicited. Trials in which subjects made an error were also removed from the data set; the task was easy so these trials remained rare and errors were not analyzed.

For each condition, we excluded trials with a peak-to peak MEP amplitude exceeding 3 *SD* around the mean. After screening the data for errors, background EMG activity and outliers, a total of 15.9 ± 2.7 trials per condition were left to evaluate CSE changes during action preparation. One subject had to be taken off the MEP analyses because we encountered a technical problem during the experiment (remaining $n = 14$ subjects).

Statistical Analyses

Analyses were carried out with the RStudio software (version 1.0.153., RStudio, Inc., Boston, MA). The assumptions of normality and homogeneity of variance were tested before analyses. All data were systematically tested for the sphericity assumption using Maunchley's tests. The Greenhouse–Geisser correction was used for sphericity when necessary.

Reaction Time

The RT data were classified according to whether subjects performed a movement with the left or right index finger (Mvt_{SIDE}: Mvt_{left} or Mvt_{right}). In addition, trials were divided depending on the time of the TMS pulse (TMS_{TIMING}: $TMS_{baseline-in}$ or TMS_{delay}; trials with $TMS_{delay-900}$ and $TMS_{delay-950}$ pooled together for the RT analysis). Finally, RTs were considered separately for trials in which double-$coil_{1\,ms}$ or single-$coil_{1\,ms}$ TMS was used and for the latter condition we also distinguished trials according to whether the responding hand corresponded to the one in which the MEP was elicited or not ($MEP_{CONDITION}$: MEP_{double}, $MEP_{single-Resp}$, $MEP_{single-NonResp}$). These data were analyzed using a two-way analysis of variance for repeated measures ($ANOVA_{RM}$) with the factors Mvt_{SIDE}, TMS_{TIMING}, and $MEP_{CONDITION}$.

MEP Amplitude

Analyses considered three main types of MEPs (MEP_{TYPE} = MEP_{single}, $MEP_{double-1}$, and $MEP_{double-2}$) elicited in the left or right hand ($MEP_{SIDE} = MEP_{left}$, MEP_{right}), at one of four different timings ($TMS_{TIMING} = TMS_{baseline-out}$, $TMS_{baseline-in}$, $TMS_{delay-900}$, and $TMS_{delay-950}$), during preparation of a left or right side movement ($Mvt_{SIDE} = Mvt_{left}$ or Mvt_{right}).

In a first analysis, we focused on MEPs elicited at rest, when subjects were not preparing a response, considering both MEPs obtained outside the blocks ($TMS_{baseline-out}$) and those acquired within the blocks ($TMS_{baseline-in}$). These MEPs were log-transformed in order to normalize the data distribution. A three-way $ANOVA_{RM}$ was then conducted on the normalized MEP data, with TMS_{TIMING} ($TMS_{baseline-out}$ or $TMS_{baseline-in}$), MEP_{TYPE} (MEP_{single}, $MEP_{double-1}$, or $MEP_{double-2}$), and MEP_{SIDE} (MEP_{left} or MEP_{right}) as within-subject factors.

Second, we aimed at comparing the strength of MEP suppression during the delay period according to whether a single- or double-$coil_{1\,ms}$ procedure was used. To do so, MEPs elicited at $TMS_{delay-900}$ and $TMS_{delay-950}$ were expressed in percentage of MEPs acquired at $TMS_{baseline-in}$ for each condition. These data were log-transformed and multiple one-sided *t*-tests were performed to compare the MEPs elicited at $TMS_{delay-900}$ and $TMS_{delay-950}$ to a constant value of 2 [standing for the $TMS_{baseline-in}$ MEPs because $\log(100) = 2$]. In a second step, we analyzed these data using a four-way $ANOVA_{RM}$ with TMS_{TIMING} ($TMS_{delay-900}$ or $TMS_{delay-950}$), MEP_{TYPE} (MEP_{single}, $MEP_{double-1}$, or $MEP_{double-2}$), MEP_{SIDE} (MEP_{left} or MEP_{right}), and Mvt_{SIDE} (Mvt_{left} or Mvt_{right}) as within-subject factors.

In a further analysis, we assessed the statistical equivalence of MEP amplitudes elicited using a single-coil or double-$coil_{1\,ms}$ procedure. We did so by testing "average bioequivalence hypotheses" [Schuirmann, 1987; U.S. Food and Drug Administration, 2001; Luzar-Stiffler and Stiffler, 2002]; a procedure detailed in our previous study (Grandjean et al., 2018).

Briefly, $MEP_{double-1}$ and $MEP_{double-2}$ elicited at $TMS_{baseline}$ ($TMS_{baseline-in}$ and $TMS_{baseline-out}$) and TMS_{delay} ($TMS_{delay-900}$ and $TMS_{delay-950}$) were expressed as a percentage of MEP_{single} elicited at the same TMS_{TIMING}. We then computed the log of the percentage obtained to further normalize the distribution of the data in each experimental condition. To be considered as equivalent to MEP_{single}, the normalized data needed to be significantly different from the boundaries of a ±0.4 window centered around 2 (corresponding to a MEP_{double} data fitting within a ±20% window centered on 100% of MEP_{single} in log) [U.S. Food and Drug Administration, 2001; Luzar-Stiffler and Stiffler, 2002; Grandjean et al., 2018]. This was tested for each experimental condition, using two one-sided *t*-tests (one for each boundary) given our a priori hypotheses (Grandjean et al., 2018). In a second step, we also determined the smallest significant boundary for each condition. To do so, one-sided *t*-tests starting at ±0.4 around 2 (i.e., ±20% around 100% in log) and decreasing by ±0.02 (i.e., 1% of 2) were performed until we found the narrowest windows between which $MEP_{double-1}$ and $MEP_{double-2}$ significantly fitted ($p < 0.05$).

MEP Coefficient of Variation (CV)

The variability of MEP amplitudes was assessed by computing a coefficient of variation (CV = [*SD*/mean MEP amplitude] × 100) in each experimental condition (Klein-Flügge et al., 2013). Similar to the procedure followed for the analysis of MEP amplitudes, we first focused on CVs at rest (at $TMS_{baseline-out}$ and $TMS_{baseline-in}$; three-way $ANOVA_{RM}$, same factors as for MEP amplitudes). Then, after having expressed the CVs at $TMS_{delay-900}$ and $TMS_{delay950}$ as a percentage of CVs at $TMS_{baseline-in}$, we considered changes during the delay period (four-way $ANOVA_{RM}$, same factors as for MEP amplitudes). The CVs were also log-transformed for these analyses as the data were not normally distributed. Finally, bioequivalence of CVs obtained in the context of double-$coil_{1\,ms}$ and single-coil TMS was also estimated for the $TMS_{baseline}$ and TMS_{delay} timings, using the exact same procedure as for the MEP amplitudes.

Post-hocs comparisons were always conducted using the Fisher's Least Significant Difference (LSD) procedure. All of the data are expressed as mean ± SE and the significance level was set at $p \leq 0.05$.

RESULTS

Reaction Time (RT)

The RTs are shown on **Figure 2** separately for the left and right hand trials. The $ANOVA_{RM}$ revealed a significant influence of TMS_{TIMING} [$F_{(1,14)} = 124.015$ and $p \leq 0.001$]: RTs were generally faster with TMS_{delay} (272.6 ± 36.4 ms) than with $TMS_{baseline-in}$ (309.4 ± 38.8 ms), consistent with many previous reports showing that a TMS pulse applied close to the imperative signal can speed up the release of a motor response (Duque et al., 2012; Labruna et al., 2014; Greenhouse et al., 2015b). Furthermore, the $MEP_{CONDITION}$ also influenced the RTs [$F_{(2,\,28)} = 6.007$, $p = 0.007$]: Fisher LSD *post-hoc* tests revealed that RTs were significantly longer in the $MEP_{single-Resp}$ condition than in the $MEP_{single-NonResp}$ and MEP_{double} conditions (both $p \leq 0.004$); the two latter were not different ($p = 0.597$). These results indicate that the RTs were slower in the presence of a single pulse eliciting a MEP in the responding hand compared to when the MEP was elicited in the non-responding hand or in both hands at once. Finally, the Mvt_{SIDE} × TMS_{TIMING} × $MEP_{CONDITION}$ interaction was significant [$F_{(2,\,28)} = 5.125$, $p = 0.013$]. As such, the slowing effect of $MEP_{single-Resp}$ reported above was systematically observed with TMS_{delay} in both hands (all $p \leq 0.038$). Yet, in trials with $TMS_{baseline-in}$, it was only present for right hand (both $p \leq 0.023$) but not for left hand trials (both $p \geq 0.198$).

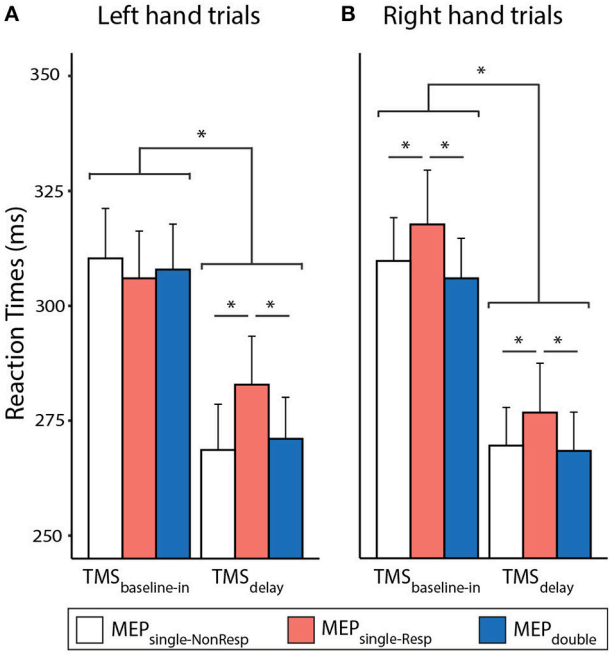

FIGURE 2 | Left **(A)** and Right **(B)** hand reaction times (RTs, in ms) recorded in trials with $TMS_{baseline-in}$ or TMS_{delay} ($TMS_{delay-900}$ and $TMS_{delay-950}$ pooled together), eliciting a MEP_{single} in the responding or non-responding hand ($MEP_{single-Resp}$ or $MEP_{single-NonResp}$, respectively) or MEP_{double} in both hands. *Significantly different ($p \leq 0.05$).

MEP Amplitude

FDI MEPs Recorded at $TMS_{baseline}$

First, we considered FDI MEPs acquired at rest, either during the blocks ($TMS_{baseline-in}$) or outside them ($TMS_{baseline-out}$). As evident on **Figure 3A**, MEPs were generally larger at $TMS_{baseline-in}$ (1.8 ± 0.79 mV) than at $TMS_{baseline-out}$ (1.3 ± 0.70 mV; $p \leq 0.001$). Hence, MEP amplitudes were increased when elicited in the context of the task, as shown in previous reports (Labruna et al., 2011a; Klein et al., 2014; Duque et al., 2016). Importantly this increase was equivalent in all conditions and occurred in the same proportion whether MEPs were elicited using single-coil (MEP_{single}) or double-$coil_{1\,ms}$ TMS ($MEP_{double-1}$ and $MEP_{double-2}$); the different MEP_{TYPE} never differed from one another, whether elicited at $TMS_{baseline-out}$ or $TMS_{baseline-in}$ [$F_{(2,\,26)} = 0.405$, $p = 0.671$].

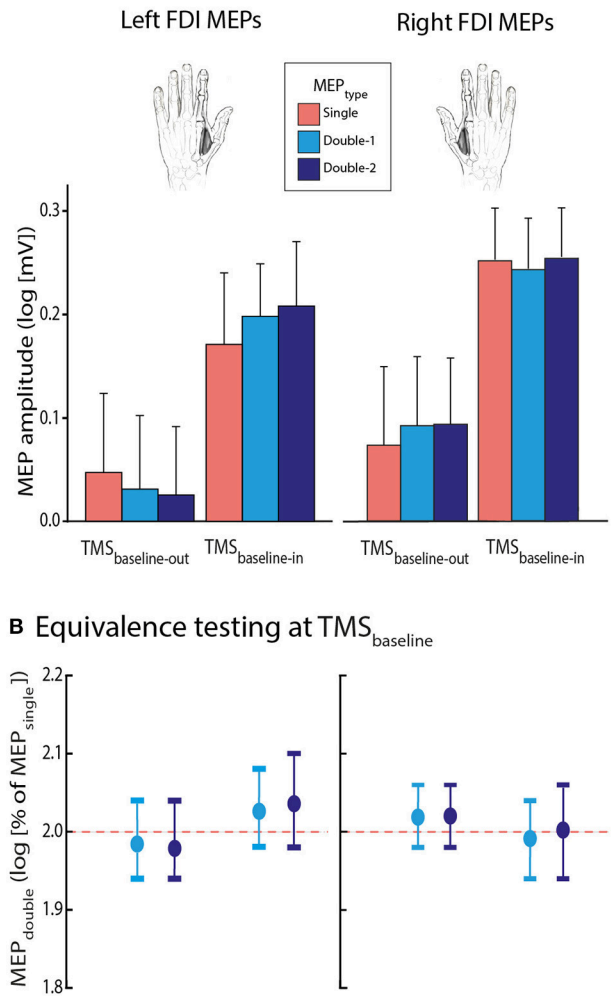

FIGURE 3 | (A) Log-transformed MEP_{single} (red bars), $MEP_{double-1}$ (light blue bars), and $MEP_{double-2}$ (navy blue bars) at $TMS_{baseline-out}$ and $TMS_{baseline-in}$, elicited in the left or right first dorsal interosseous (FDI) muscle. Note that MEP amplitudes at $TMS_{baseline-in}$ were significantly larger than at $TMS_{baseline-out}$; $p \leq 0.001$. **(B)** $MEP_{double-1}$ and $MEP_{double-2}$ amplitudes (expressed as log-transformed percentages of MEP_{single}) significantly fitted in windows ranging between 1.94 and 2.10 l.u. [log(100) = 2], indicating comparable amplitudes for all MEP_{TYPE}. The vertical bars represent the smallest significant boundaries around the mean for each condition. Each plot refers to the above color-coded condition on the x-axis.

Second, we aimed to further assess the bioequivalence of the FDI MEP_{TYPE} at $TMS_{baseline}$. To do so, similar to the procedure used in a previous study (Grandjean et al., 2018), we expressed the $MEP_{double-1}$ and $MEP_{double-2}$ data as a percentage of MEP_{single}. We compared these percentages with boundaries set at ±20% around 100% (corresponding to MEP_{single}), through multiple one-sided *t*-tests (Luzar-Stiffler and Stiffler, 2002). Notably, because the percentages were log-transformed for the analyses, this involved comparing them with boundaries set at ±0.4 around 2 log units (l.u) [because log(100) = 2]. At $TMS_{baseline-out}$ as well as at $TMS_{baseline-in}$, the log-transformed normalized $MEP_{double-1}$ and $MEP_{double-2}$ amplitudes significantly fitted into the ±0.4 window. As we can see on **Figure 3B**, the $MEP_{double-1}$ and $MEP_{double-2}$ even fitted in smaller windows (all $MEP_{double-1}$ between 1.94 and 2.08 l.u.; i.e., between 97 and 104% of MEP_{single} and all $MEP_{double-2}$ between 1.94 and 2.10 l.u. [97–105%], all $p \leq 0.05$).

FDI MEPs Recorded at TMS_{delay}

Then, we evaluated FDI MEP amplitudes during action preparation. To do so, MEPs elicited at $TMS_{delay-900}$ and $TMS_{delay-950}$ were expressed as a percentage of MEPs elicited at $TMS_{baseline-in}$. On average, MEPs equalled 69.7 ± 18.85 and 70.0 ± 21.13% of baseline when elicited at $TMS_{delay-900}$ and $TMS_{delay-950}$, respectively. These data were log-transformed for the analyses (**Figure 4A**); all normalized MEPs were smaller than 2 [i.e., log(100); all $t \leq -3.442$, $p \leq 0.003$], reflecting a consistent suppression of MEPs during the delay period, both at $TMS_{delay-900}$ and $TMS_{delay-950}$. Importantly, the $ANOVA_{RM}$ did not reveal any significant effect of the factor MEP_{TYPE} [$F_{(2, 26)} = 0.513$, $p = 0.685$]: the MEPs acquired with double-$coil_{1\,ms}$ TMS, either by a first ($MEP_{double-1}$) or second pulse ($MEP_{double-2}$), were comparable to MEP_{single}. Besides, MEP amplitudes were the same at both TMS_{TIMING} [$F_{(1, 13)} = 0.115$ and $p \geq 0.45$] and did not depend on whether they were elicited in the left or right FDI [MEP_{SIDE}: $F_{(1, 13)} = 3.241$, $p = 0.095$], or on whether they occurred during a left or right hand trial [Mvt_{SIDE}: $F_{(1, 13)} = 4.182$, $p = 0.062$], although there was a small non-significant trend for the MEP suppression to be more pronounced preceding left hand trials, especially when probed in the left hand. None of the interactions were significant (all $F \leq 1.159$, all $p \geq 0.330$).

Concerning the bioequivalence testing at $TMS_{delay-900}$ and $TMS_{delay-950}$, the log-transformed $MEP_{double-1}$ and $MEP_{double-2}$ data (initially expressed in percentage of MEP_{single}) significantly fitted into the ±0.4 window around 2. These data even fitted in smaller windows as shown on **Figure 4B** (all $MEP_{double-1}$ between 1.96 and 2.08 l.u. [i.e., between 98 and 104% of MEP_{single}] and all $MEP_{double-2}$ between 1.92 and 2.08 l.u. [96–104%]; all $p \leq 0.05$).

Additional Analyses on FDI MEP Amplitudes

We performed a three-way $ANOVA_{RM}$ focusing on the normalized MEP_{single} data, with TMS_{TIMING} ($TMS_{delay-900}$, $TMS_{delay-950}$), MEP_{SIDE} (MEP_{left} or MEP_{right}), and Mvt_{SIDE} (Mvt_{left} or Mvt_{right}) as within-subject factors to ensure that the absence of effect between conditions in which the muscle was selected or not selected for the forthcoming response was not related to the inclusion of additional MEP_{TYPES} ($MEP_{double-1}$ and $MEP_{double-2}$). This $ANOVA_{RM}$ did not reveal any significant MEP_{SIDE} x Mvt_{SIDE} interaction [$F_{(1,13)} = 0.457$, $p = 0.511$], neither did this interaction interact with the factor TMS_{TIMING} [TMS_{TIMING} x MEP_{SIDE} x Mvt_{SIDE}: $F_{(1,13)} = 1.99$, $p = 0.182$]. Hence, the level of inhibition was comparable in selected and non-selected conditions in the present study, regardless of whether a single- or double-coil procedure was used.

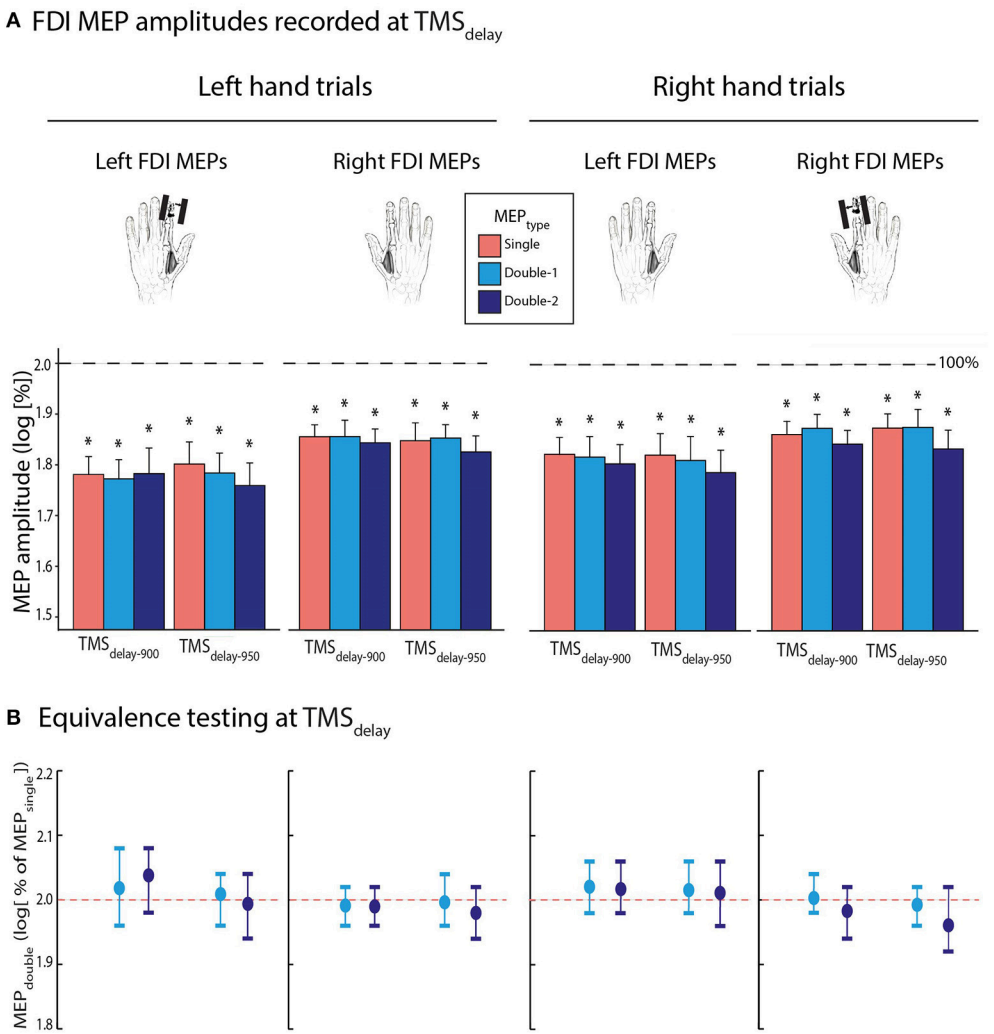

FIGURE 4 | (A) Log-transformed MEP_{single} (red bars), $MEP_{double-1}$ (light blue bars), and $MEP_{double-2}$ (navy blue bars) at $TMS_{delay-900}$ and $TMS_{delay-950}$ (initially expressed as a percentage of $TMS_{baseline-in}$), elicited in the left or right first dorsal interosseous (FDI). Data are shown separately for left (left panel) and right hand (right panel) trials. **(B)** Log-transformed $MEP_{double-1}$ and $MEP_{double-2}$ amplitudes at TMS_{delay} (initially expressed in percentage of MEP_{single}). These data significantly fitted in windows ranging from 1.92 to 2.08 l.u. [i.e., between 96 and 104% of MEP_{single} in log], indicating comparable amplitudes for MEP_{double} and MEP_{single} during action preparation. The vertical bars represent the smallest significant boundaries around the mean for each condition. Each plot refers to the above color-coded condition on the x-axis. *$p \leq 0.005$.

Additional Analyses on ADM MEP Amplitudes

As mentioned above, stimulation of the hotspot for the FDI, also elicited MEPs in the ADM, a pinkie abductor. Although this muscle is irrelevant in the "Rolling Ball" game, its MEPs basically showed the same changes as those observed in the FDI, although in an attenuated manner. At rest, ADM MEPs were globally larger at $TMS_{baseline-in}$ than $TMS_{baseline-out}$ [$F_{(1, 13)} = 24.791$, $p \leq 0.001$]. Most importantly, $ANOVA_{RM}$ revealed that single-coil and double-$coil_{1\,ms}$ TMS elicited comparable ADM MEPs at rest [MEP_{TYPE} $F_{(2, 26)} = 0.148$, $p = 0.863$]. Consistently, the bioequivalence tests showed that all log-transformed $MEP_{double-1}$ and $MEP_{double-2}$ amplitudes (initially expressed in percentage of MEP_{single}) significantly fitted into smaller windows than ±0.4 around 2: all $MEP_{double-1}$ and $MEP_{double-2}$ amplitudes fitted in a 1.92–2.08 window, i.e., 96–104%, all $p \leq 0.05$).

In addition, ADM MEPs were also suppressed during the delay period (all $t \leq -2.042$, all $p \leq 0.031$), regardless of the TMS_{TIMING} [$F_{(1, 13)} = 0.036$, $p = 0.853$] or the MEP_{SIDE} [$F_{(1, 13)} = 0.149$, $p = 0.705$]. Note that the MEP suppression was significantly less pronounced preceding right than left hand movements [$F_{(1, 13)} = 5.165$, $p = 0.041$]. Importantly, the factor MEP_{TYPE} was non-significant [$F_{(2, 26)} = 0.157$, $p = 0.855$]. At both delay timings, all $MEP_{double-1}$ and $MEP_{double-2}$ amplitudes fitted in 1.94–2.08 [97–104%] and 1.92–2.06 [96–103%] windows, respectively. Thus the double-$coil_{1\,ms}$ protocol seemed to induce comparable MEPs as single-coil TMS in an irrelevant muscle as well.

Coefficient of Variation (CV) of MEPs

CV of FDI MEPs Recorded at $TMS_{baseline}$

First, we focused on the CV of FDI MEPs elicited at $TMS_{baseline-out}$ and $TMS_{baseline-in}$ (**Figure 5A**). Overall, they equalled 54.8 ± 18.91% and 47.1 ± 17.88% at these two TMS timings, respectively. The $ANOVA_{RM}$ revealed a significant effect of TMS_{TIMING} on the log-transformed data [$F_{(1, 13)} = 5.14$, $p = 0.041$], with smaller CVs at $TMS_{baseline-in}$ than at $TMS_{baseline-out}$. Hence, MEPs were generally larger and less variable when elicited at rest but in the context of a task, than when elicited outside the blocks. This effect tended to be stronger for MEPs elicited in the right than in the left FDI, but the TMS_{TIMING} x MEP_{SIDE} interaction did not reach significance [$F_{(1, 13)} = 4.092$, $p = 0.064$]. Though, the factor MEP_{SIDE} was significant [$F = 7.67$; $p = 0.02$]: CVs were smaller for MEPs elicited in the right FDI compared to when they were evoked in the left FDI, indicating an overall smaller variability of MEPs in the dominant hand. Importantly, all these effects occurred regardless of whether the MEPs were elicited using a single-coil or a double-$coil_{1\,ms}$ procedure. That is, neither the factor MEP_{TYPE} [$F_{(2, 26)} = 0.049$, $p = 0.952$], nor its interaction with the other factors (all $F \leq 1.431$, all $p \geq 0.257$) were significant. Similar to the MEP amplitudes, in order to assess the statistical bioequivalence of the double-$coil_{1\,ms}$ and single-coil CVs, we expressed the CVs of $MEP_{double-1}$ and $MEP_{double-2}$ as log-transformed percentages of MEP_{single} and tested whether these normalized data were significantly different from boundaries set at ±0.4 around 2. As we can see on **Figure 5B**, the $MEP_{double-1}$ and $MEP_{double-2}$ even fitted in smaller windows (all $MEP_{double-1}$ between 1.88 and 2.14 l.u. [i.e., between 94 and 107% of MEP_{single}] and all $MEP_{double-2}$ between 1.90 and 2.14 l.u. [95–107%]; all $p \leq 0.05$).

CV of FDI MEPs Recorded at TMS_{delay}

Then, we turned to the CV of MEPs elicited during the delay period (**Figure 6A**). On average, they reached 90.2 ± 28.63 and 92.8 ± 36.12% of baseline values at $TMS_{delay-900}$ and $TMS_{delay-950}$, respectively. The *t*-tests performed on the log-transformed data revealed that CVs tended to show a further decrease at both TMS_{delay} timings compared to $TMS_{baseline-in}$, although this effect was only significant for 37.5% of conditions; it was close to significance in 46.7% of the remaining conditions ($0.05 \leq p \leq 0.10$). The four-way $ANOVA_{RM}$ did not reveal any further difference. None of the interactions or factors, including the MEP_{TYPE} [$F_{(2, 26)} = 0.692$, $p = 0.509$], were significant.

Again, at both delay timings, the log-transformed $MEP_{double-1}$ and $MEP_{double-2}$ data (initially expressed in percentage of MEP_{single}) significantly fitted into a ±0.4 window around 2. As evident on **Figure 6B,** the $MEP_{double-1}$ and $MEP_{double-2}$ CVs even fitted in smaller windows (all $MEP_{double-1}$ between 1.90 and 2.12 l.u. [i.e., between 95 and 106% of MEP_{single}] and all $MEP_{double-2}$ between 1.88 and 2.12 l.u. [94–106 %]; all $p \leq 0.05$).

Hence, altogether, these data show that the double-$coil_{1\,ms}$ protocol is associated with comparable MEP amplitudes and CVs as the single-coil TMS procedure, whether these MEP parameters are assessed at rest or during action preparation.

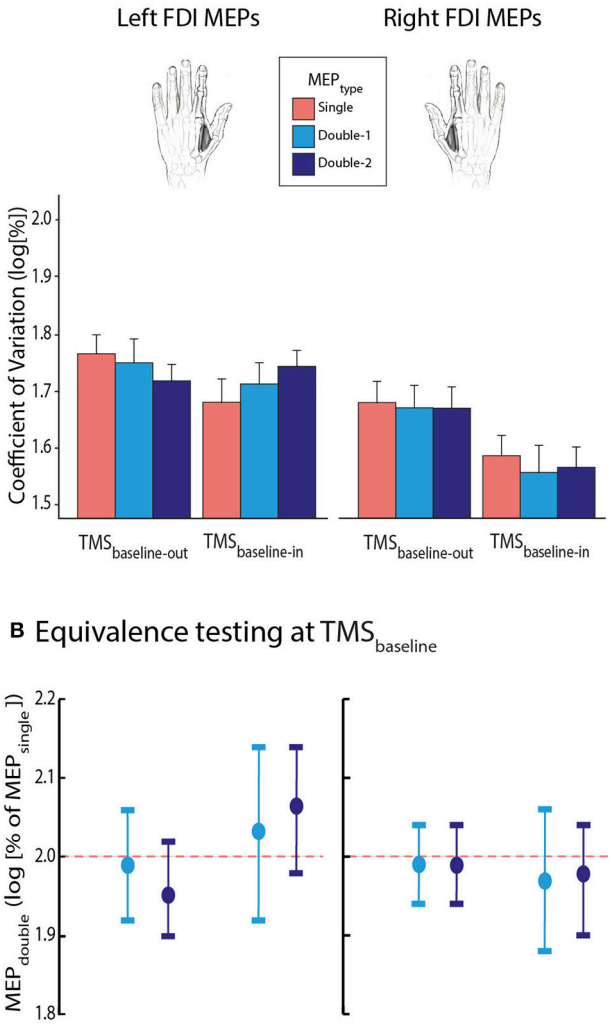

FIGURE 5 | (A) Log-transformed coefficients of variation (CV) of MEP_{single} (red bars), $MEP_{double-1}$ (light blue bars), and $MEP_{double-2}$ (navy blue bars) at $TMS_{baseline-out}$ and $TMS_{baseline-in}$, elicited in the left or right first dorsal interosseous (FDI) muscle. Note that CVs were significantly reduced at $TMS_{baseline-in}$ compared to $TMS_{baseline-out}$. Also, MEPs were generally less variable in the right than in the left FDI; $p \leq 0.05$ for both effects. **(B)** $MEP_{double-1}$ and $MEP_{double-2}$ CVs significantly fitted in windows ranging between 1.88 and 2.14 l.u. [log(100) = 2] indicating comparable CVs for all left and right FDI MEP_{TYPE}. The vertical bars represent the smallest significant boundaries around the mean for each condition. Each plot refers to the above color-coded condition on the x-axis.

Additional Analyses on CV of ADM MEPs

The CVs were also computed for the ADM MEPs. Globally, we observed the same changes as those observed for the FDI. At rest, the CVs of ADM MEPs were globally smaller at $TMS_{baseline-in}$ than $TMS_{baseline-out}$ [$F_{(1, 13)} = 18.314$, $p = 0.001$] but comparable for the different MEP_{TYPE} [$F_{(2, 26)} = 1.011$, $p = 0.378$]. Consistently, the bioequivalence tests showed that all $MEP_{double-1}$ and $MEP_{double-2}$ amplitudes

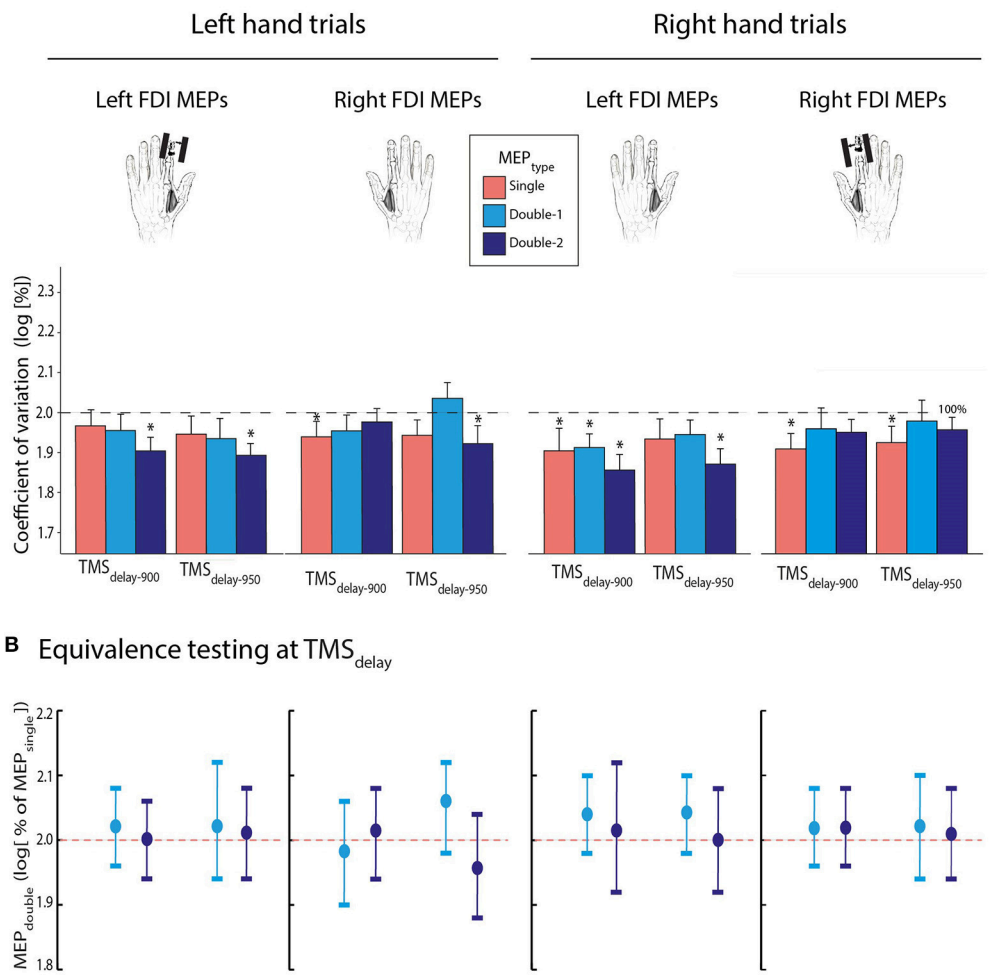

FIGURE 6 | (A) Log-transformed coefficient of variation (CV) of MEP_{single} (red bars), $MEP_{double-1}$ (light blue bars), and $MEP_{double-2}$ (navy blue bars) at $TMS_{delay-900}$ and $TMS_{delay-950}$ (initially expressed as a percentage of $TMS_{baseline-in}$), for the left or right first dorsal interosseous (FDI) muscles. Data are shown separately for MEPs acquired during left (left panel) and right hand (right panel) trials. Note that the factor MEP_{TYPE} was never significant. **(B)** Log-transformed CV of $MEP_{double-1}$ and $MEP_{double-2}$ at TMS_{delay} (initially expressed in percentage of MEP_{single}). These data significantly fitted in windows ranging from 1.88 to 2.12 l.u. [i.e., between 94 and 106% of MEP_{single} in log], indicating comparable CVs for MEP_{double} and MEP_{single} during action preparation. The vertical bars represent the smallest significant boundaries around the mean for each condition. Each plot refers to the above color-coded condition on the x-axis. *$p \leq 0.05$.

significantly fitted into smaller windows than ±0.4 (all $MEP_{double-1}$ between 1.94 and 2.14 l.u. [97–107%] and all $MEP_{double-2}$ between 1.92 and 2.20 l.u. [96–110%]; all $p \leq 0.05$).

There was also a small trend for ADM CVs to decrease during the delay period with respect to $TMS_{baseline-in}$ (but reaching significance in only 20.8% of TMS_{delay} conditions). Similarly to FDI CVs, the $ANOVA_{RM}$ showed that CVs across the MEP_{single}, $MEP_{double-1,}$ and $MEP_{double-2}$ conditions were similar [$F_{(2, 26)} = 1.284$, $p = 0.294$]. No other interaction was found (all $F \leq 3.036$, all $p \geq 0.105$]. At both delay timings, all $MEP_{double-1}$ and $MEP_{double-2}$ CVs fitted in 1.94–2.12 [97–106 %] and 1.90–2.10 [95–105%] windows, respectively. Thus, MEPs elicited in an irrelevant muscle also displayed a CV that was comparable for the single-coil and $double\text{-}coil_{1\,ms}$ protocols.

DISCUSSION

Summary of Study Goals

The goal of the present study was to assess whether the MEPs acquired using $double\text{-}coil_{1\,ms}$ are equivalent to those obtained by means of a classical single-coil TMS method. To do so, we compared MEPs elicited by a first ($MEP_{double-1}$) or second ($MEP_{double-2}$) $double\text{-}coil_{1\,ms}$ TMS pulse to MEPs obtained using single-coil TMS (MEP_{single}). Both the amplitude and coefficient of variation (CV) of MEPs were considered. We compared these MEP variables in the context of a motor task

requiring subjects to prepare and delay left or right index finger responses until the onset of an imperative signal. MEP_{single} are typically suppressed during the delay period (Bestmann and Duque, 2016; Duque et al., 2017). Here, we show that comparable inhibitory changes can be observed with $MEP_{double-1}$ and $MEP_{double-2}$. The MEPs exhibited comparable amplitudes and CVs, regardless of whether they had been elicited using a single- or double-$coil_{1\,ms}$ TMS approach.

Comparing the Amplitude of MEP_{single} and MEP_{double} During Action Preparation

The amplitude of MEPs was much smaller at TMS_{delay} compared to $TMS_{baseline-in}$, consistent with many previous reports (Duque and Ivry, 2009; Greenhouse et al., 2015b; Lebon et al., 2016; Quoilin et al., 2016; Wilhelm et al., 2016). This effect was observed regardless of whether the MEPs were recorded from a muscle that was selected or non-selected for the forthcoming response. This result may seem inconsistent with previous work (Greenhouse et al., 2015a,b; Klein et al., 2016). However, several recent studies have failed to observe a difference of inhibition between selected and non-selected conditions, suggesting that this effect is not consistent and does not systematically show up (Quoilin et al., 2016; Wilhelm et al., 2016, 2017). As suggested in Quoilin et al. (2016), it is likely to depend on the task details, including the use (or not) of response devices, the presence (or not) of catch trials, the time at which TMS is delivered and eventually, the presentation of a feedback (or not). Inhibition at TMS_{delay} was also observed for a muscle that was irrelevant in the task, corroborating the idea that withholding a prepared action is associated with widespread inhibitory influences suppressing CSE until the movement can be initiated (reviewed in Duque et al., 2017). The suppression of MEPs tended to be deeper in the left compared to the right hand, consistent with the view that inhibitory changes are often more pronounced on the non-dominant compared to the dominant side (Leocani et al., 2000; Duque et al., 2007; Quoilin et al., 2016; Wilhelm et al., 2016). Note that this tendency was not observed in a previous work (Klein et al., 2016). Yet, an important difference there is that Klein et al. (2016) registered MEP_{left} and MEP_{right} in separate blocks, reducing the signal to noise ratio when comparing these conditions. Furthermore, we found that MEPs were similarly decreased at $TMS_{delay-900}$ and $TMS_{delay-950}$, probably because preparatory inhibition had reached a plateau by the time TMS was applied, in accordance with recent observations (Lebon et al., 2016).

Most importantly, the strength of the inhibitory effect at TMS_{delay} was comparable across all MEP_{TYPE}. As such, bioequivalent analyses revealed that MEP_{single}, $MEP_{double-1,}$ and $MEP_{double-2}$ displayed the exact same level of suppression during action preparation. This result may stand at odds with another study in which we observed differences between MEP_{single} and MEP_{double} at TMS_{delay} (Wilhelm et al., 2016). However, an important weakness in that work is that the single and double-$coil_{1\,ms}$ protocols were tested in separate blocks. Hence, the difference between MEP_{single} and MEP_{double} was likely due to the fact that subjects were more vigilant or alert when they expected two pulses to occur (increasing MEP amplitudes) compared to when only one pulse was anticipated (Labruna et al., 2011a; Klein et al., 2012, 2014). By intermingling all conditions within each block, the present study allowed to control for this bias: our data show that in its absence, all MEP_{TYPE} display a comparable degree of suppression during action preparation. Note however that, because MEPs are rather global readouts of CSE, these results do not allow to rule out completely the occurrence of some bilateral interactions following double-$coil_{1\,ms}$ TMS. Yet, even if present, these interactions do not alter MEP amplitudes in a systematic way and do not preclude from obtaining measures of preparatory inhibition that are comparable to those acquired with single-coil TMS.

Comparing the CV of MEP_{single} and MEP_{double} During Action Preparation

In order to evaluate changes in the variability of CSE during action preparation, we measured the CV of MEPs elicited using single-coil or double-$coil_{1\,ms}$ TMS. Overall, we observed a decrease in the CV of MEPs at TMS_{delay} compared to $TMS_{baseline-in,}$ even if this effect was not present in all conditions. Therefore, CSE tended to be less variable during action preparation compared to rest, consistent with a previous report (Klein-Flügge et al., 2013). Such a decrease in the variability of CSE during action preparation may reflect an optimization process of neuronal firing rates in the motor cortex (Churchland, 2006). Following this view, firing rates progressively become more consistent during action preparation, reaching a specific state to produce the desired movement (Rickert et al., 2009). Interestingly, this small decrease in the CV of MEPs at TMS_{delay} was not only observed for the FDI but also for the ADM. Hence, the variability of CSE decreased for both task-relevant and irrelevant muscles; the tuning of motor activity during action preparation may thus not be completely specific to the agonist effectors (Churchland et al., 2010; Klein-Flügge et al., 2013). Most importantly, changes in the CV from $TMS_{baseline-in}$ to TMS_{delay} were equivalent for MEP_{single}, $MEP_{double-1}$ and $MEP_{double-2}$, suggesting that double-$coil_{1\,ms}$ TMS is as effective as single-coil TMS to capture changes in the variability of CSE during action preparation.

Comparing the Amplitude and CV of MEP_{single} and MEP_{double} at Rest

In the present study, we acquired two baseline measures of MEPs at rest. That is, MEPs were elicited during the intertrial interval ($TMS_{baseline-in}$) within the blocks, but also outside the blocks ($TMS_{baseline-out}$). At both timings, MEP amplitudes were generally comparable when elicited in the left or right hand, confirming that measures of CSE are highly comparable for both hemispheres at rest (Davidson and Tremblay, 2013). Yet, the CV of FDI MEPs was smaller in the right than in the left hand. Hence, neuronal firing rate may be steadier on the dominant side. Interestingly, MEP amplitudes were larger when acquired within the blocks compared to outside them and this effect was associated with a decrease in the CV of MEPs. Hence, CSE was

larger and less variable when probed within the context of the motor task compared to when the subjects were at complete rest, outside the blocks. Such an effect on MEP amplitudes has been reported in a previous study comparing different baseline conditions (Labruna et al., 2011a). That is, Labruna et al. (2011a) showed that MEPs were larger when elicited in the context of a task requiring subjects to passively view hand or landscape pictures than when elicited outside the task, suggesting that the level of vigilance has a significant influence on CSE.

Importantly, our bioequivalence analyses revealed that MEP_{single}, $MEP_{double-1,}$ and $MEP_{double-2}$ were comparable in all baseline conditions. The bioequivalence of MEPs at complete rest ($TMS_{baseline-out}$) had already been reported in a previous study (Grandjean et al., 2018). Here, we show that this equivalence persists when baseline MEPs are elicited in the context of a motor task ($TMS_{baseline-in}$).

Comparing the Impact of MEP_{single} and MEP_{double} on Reaction Times (RTs)

First of all, RTs were generally faster with TMS_{delay} than with $TMS_{baseline-in}$, consistent with many previous reports showing that a TMS pulse applied close to the imperative signal can prime subjects to respond faster (Duque et al., 2012; Labruna et al., 2014; Greenhouse et al., 2015b; Quoilin et al., 2016) probably because the TMS sound triggers the release of the movement that is being prepared (Carlsen et al., 2007, 2011). Interestingly, we also found that RTs were longer in trials where a MEP_{single} occurred in the responding hand compared to when the MEP_{single} fell in the non-responding hand, or in both hands at once (MEP_{double}). This effect was present in all conditions at TMS_{delay}, indicating that the boosting effect of the TMS sound was slightly attenuated when the MEP fell specifically in the responding hand, compared to when it fell in the other hand or in both hands, consistent with other works (Duque et al., 2013; Wilhelm et al., 2016). Surprisingly this effect of the MEP condition was also observed with $TMS_{baseline-in}$ in right hand trials but not left hand trials. This result was unexpected given that here, MEPs were elicited during the intertrial interval and should thus not affect behavior, an issue for future investigation.

Advantages of Double-$Coil_{1\,ms}$ TMS and Future Directions

The double-$coil_{1\,ms}$ protocol shows many advantages over the regular single-coil technique. First, the number of MEPs that can be collected in a given amount of time is doubled. This is a crucial aspect as it gives the opportunity to test more conditions within the same duration than could be done with a regular single-coil method. Second, CSE is probed bilaterally on the same trial meaning that both hands can be probed simultaneously. Hence, dominant and non-dominant hand MEPs are elicited in the exact same conditions during the task (Duque et al., 2013). This obviously increases the signal to noise ratio in a significant way. Third, the acquisition of MEPs in both hands allows researchers to make direct comparisons between bilateral MEPs on a single-trial basis and to develop new measures such as indexes reflecting the ratio between the CSE of the two hands. In fact, one may be interested in studying the impact of various task parameters (e.g., instruction, presence of reward, sensory evidence, level of urgency, effort required etc.) on the relationship between bilateral MEP amplitudes and CVs. Hence, the present technique opens new horizons in the study of how both hemispheres interact in various task settings (Verleger et al., 2009; Klein et al., 2016).

CONCLUSION

The present study suggests that the double-$coil_{1\,ms}$ TMS can be used to probe CSE within the context of a motor task. As such, we show that MEPs elicited using a double-$coil_{1\,ms}$ technique are equivalent to those obtained by means of single-coil TMS, both at rest and during action preparation. This new method is promising since it allows to record MEPs from both hands simultaneously, doubling the amount of data that can be acquired in a given period of time. The development of double-$coil_{1\,ms}$ TMS might participate in the actual expansion of TMS in a broad range of neurophysiological as well as neurological studies.

AUTHOR CONTRIBUTIONS

PV and JG: contributed equally; PV, JG, GD, and JD: designed research; PV, JG, YdW, and LQ: performed research; PV, JG, GD, YdW, LQ, and JD: analyzed data; PV and JD: wrote the article.

FUNDING

This work was supported by grants from the Fonds Speciaux de Recherche (FSR) of the Universite catholique de Louvain, the Belgian National Funds for Scientific Research (FRS—FNRS: MIS F.4512.14) and the Fondation Medicale Reine Elisabeth (FMRE). JG was a graduate student supported by a Fund for Research Training in Industry and Agriculture (FRIA). GD was a postdoctoral fellow supported by the FNRS and a MSCA-FSR COFUND.

REFERENCES

Auriat, A. M., Neva, J. L., Peters, S., Ferris, J. K., and Boyd, L. A. (2015). A review of transcranial magnetic stimulation and multimodal neuroimaging to characterize post-stroke neuroplasticity. *Front. Neurol.* 6:226. doi: 10.3389/fneur.2015.00226

Badawy, R. A., Loetscher, T., Macdonell, R. A., and Brodtmann, A. (2012). Cortical excitability and neurology: insights into the pathophysiology. *Funct. Neurol.* 27, 131–145.

Benninger, D. H., and Hallett, M. (2015). Non-invasive brain stimulation for Parkinson's disease: current concepts and outlook 2015. *Neurorehabilitation* 37, 11–24. doi: 10.3233/NRE-151237

Bestmann, S., and Duque, J. (2016). Transcranial magnetic stimulation. *Neuroscience* 22, 392–405. doi: 10.1177/1073858415592594

Bestmann, S., and Krakauer, J. W. (2015). The uses and interpretations of the motor-evoked potential for understanding behaviour. *Exp. Brain Res.* 233, 679–689 doi: 10.1007/s00221-014-4183-7

Boddington, L. J., and Reynolds, J. N. (2017). Targeting interhemispheric inhibition with neuromodulation to enhance stroke rehabilitation. *Brain Stimul.* 10, 214–222. doi: 10.1016/j.brs.2017.01.006

Brainard, D. H. (1997). The psychophysics toolbox. *Spat. Vis.* 10, 433–436. doi: 10.1163/156856897X00357

Carlsen, A. N., Dakin, C. J., Chua, R., and Franks, I. M. (2007). Startle produces early response latencies that are distinct from stimulus intensity effects. *Exp. Brain Res.* 176, 199–205. doi: 10.1007/s00221-006-0610-8

Carlsen, A. N., Maslovat, D., Lam, M. Y., Chua, R., and Franks, I. M. (2011). Considerations for the use of a startling acoustic stimulus in studies of motor preparation in humans. *Neurosci. Biobehav. Rev.* 35, 366–376. doi: 10.1016/j.neubiorev.2010.04.009

Churchland, M. M. (2006). Neural variability in premotor cortex provides a signature of motor preparation. *J. Neurosci.* 26, 3697–3712. doi: 10.1523/JNEUROSCI.3762-05.2006

Churchland, M. M., Yu, B. M., Cunningham, J. P., Sugrue, L. P., Cohen, M. R., Corrado, G. S., et al. (2010). Stimulus onset quenches neural variability: a widespread cortical phenomenon. *Nat. Neurosci.* 13, 369–378. doi: 10.1038/nn.2501

Cos, I., Duque, J., and Cisek, P. (2014). Rapid prediction of biomechanical costs during action decisions. *J. Neurophysiol.* 112, 1256–1266. doi: 10.1152/jn.00147.2014

Davidson, T., and Tremblay, F. (2013). Hemispheric differences in corticospinal excitability and in transcallosal inhibition in relation to degree of handedness. *PLoS ONE* 8:e70286. doi: 10.1371/journal.pone.0070286

Derosière, G., Billot, M., Ward, E. T., and Perrey, S. (2015). Adaptations of motor neural structures' activity to lapses in attention. *Cereb. Cortex* 25, 66–74. doi: 10.1093/cercor/bht206

Derosiere, G., Vassiliadis, P., Demaret, S., Zénon, A., and Duque, J. (2017a). Learning stage-dependent effect of M1 disruption on value-based motor decisions. *Neuroimage* 62, 173–185. doi: 10.1016/j.neuroimage.2017.08.075

Derosiere, G., Zénon, A., Alamia, A., and Duque, J. (2017b). Primary motor cortex contributes to the implementation of implicit value-based rules during motor decisions. *Neuroimage* 146, 1115–1127. doi: 10.1016/j.neuroimage.2016.10.010

Duque, J., Greenhouse, I., Labruna, L., and Ivry, R. B. (2017). Physiological markers of motor inhibition during human behavior. *Trends Neurosci.* 40, 219–236 doi: 10.1016/j.tins.2017.02.006

Duque, J., and Ivry, R. B. (2009). Role of corticospinal suppression during motor preparation. *Cereb. Cortex* 19, 2013–2024. doi: 10.1093/cercor/bhn230

Duque, J., Labruna, L., Cazares, C., and Ivry, R. B. (2014). Dissociating the influence of response selection and task anticipation on corticospinal suppression during response preparation. *Neuropsychologia* 65, 287–296. doi: 10.1016/j.neuropsychologia.2014.08.006

Duque, J., Labruna, L., Verset, S., Olivier, E., and Ivry, R. B. (2012). Dissociating the role of prefrontal and premotor cortices in controlling inhibitory mechanisms during motor preparation. *J. Neurosci.* 32, 806–816. doi: 10.1523/JNEUROSCI.4299-12.2012

Duque, J., Lew, D., Mazzocchio, R., Olivier, E., and Ivry, R. B. (2010). Evidence for two concurrent inhibitory mechanisms during response preparation. *J. Neurosci.* 30, 3793–3802. doi: 10.1523/JNEUROSCI.5722-09.2010

Duque, J., Murase, N., Celnik, P., Hummel, F., Harris-Love, M., Mazzocchio, R., et al. (2007). Intermanual differences in movement-related interhemispheric inhibition. *J. Cogn. Neurosci.* 19, 204–213. doi: 10.1162/jocn.2007.19.2.204

Duque, J., Olivier, E., and Rushworth, M. (2013). Top–Down inhibitory control exerted by the medial frontal cortex during action selection under conflict. *J. Cogn. Neurosci.* 25, 1634–1648. doi: 10.1162/jocn_a_00421

Duque, J., Petitjean, C., and Swinnen, S. P. (2016). Effect of aging on motor inhibition during action preparation under sensory conflict. *Front. Aging Neurosci.* 8:322. doi: 10.3389/fnagi.2016.00322

Ferbert, A., Priori, A., Rothwell, J. C., Day, B. L., Colebatch, J. G., and Marsden, C. D. (1992). Interhemispheric inhibition of the human motor cortex. *J. Physiol.* 453, 525–546. doi: 10.1113/jphysiol.1992.sp019243

Grandjean, J., Derosiere, G., Vassiliadis, P., Quemener, L., de Wilde, Y., and Duque, J. (2017a). Validation of a double-coil TMS method to assess corticospinal excitability. *Brain Stimul.* 10:507. doi: 10.1016/j.brs.2017.01.480

Grandjean, J., Derosiere, G., Vassiliadis, P., Quemener, L., Wilde, Y., and Duque, J. (2018). Towards assessing corticospinal excitability bilaterally: validation of a double-coil TMS method. *J. Neurosci. Methods* 293, 162–168. doi: 10.1016/j.jneumeth.2017.09.016

Grandjean, J., Vassiliadis, P., Derosiere, G., de Wilde, Y., Quemener, L., and Duque, J. (2017b). A new double-coil tms method to assess corticospinal excitability bilaterally *Front. Neurosci. Conference Abstract: 12th National Congress of the Belgian Society for Neuroscience.* doi: 10.3389/conf.fnins.2017.94.00118

Greenhouse, I., Oldenkamp, C. L., and Aron, A. R. (2012). Stopping a response has global or nonglobal effects on the motor system depending on preparation. *J. Neurophysiol.* 107, 384–392. doi: 10.1152/jn.00704.2011

Greenhouse, I., Saks, D., Hoang, T., and Ivry, R. B. (2015a). Inhibition during response preparation is sensitive to response complexity. *J. Neurophysiol.* 113, 2792–2800. doi: 10.1152/jn.00999.2014

Greenhouse, I., Sias, A., Labruna, L., and Ivry, R. B. (2015b). Nonspecific inhibition of the motor system during response preparation. *J. Neurosci.* 35, 10675–10684. doi: 10.1523/JNEUROSCI.1436-15.2015

Guerra, A., Assenza, F., Bressi, F., Scrascia, F., Del Duca, M., Ursini, F., et al. (2011). Transcranial magnetic stimulation studies in Alzheimer's Disease. *Int. J. Alzheimers. Dis.* 2011:263817. doi: 10.4061/2011/263817

Hanajima, R., Ugawa, Y., Machii, K., Mochizuki, H., Terao, Y., Enomoto, H., et al. (2001). Interhemispheric facilitation of the hand motor area in humans. *J. Physiol.* 531, 849–859. doi: 10.1111/j.1469-7793.2001.0849h.x

Klein, P.-A., Duque, J., Labruna, L., and Ivry, R. B. (2016). Comparison of the two cerebral hemispheres in inhibitory processes operative during movement preparation. *Neuroimage* 125, 220–232. doi: 10.1016/j.neuroimage.2015.10.007

Klein, P.-A., Olivier, E., and Duque, J. (2012). Influence of reward on corticospinal excitability during movement preparation. *J. Neurosci.* 32, 18124–18136. doi: 10.1523/JNEUROSCI.1701-12.2012

Klein, P.-A., Petitjean, C., Olivier, E., and Duque, J. (2014). Top-down suppression of incompatible motor activations during response selection under conflict. *Neuroimage* 86, 138–149. doi: 10.1016/j.neuroimage.2013.08.005

Klein-Flügge, M. C., and Bestmann, S. (2012). Time-Dependent changes in human corticospinal excitability reveal value-based competition for action during decision processing. *J. Neurosci.* 32, 8373–8382. doi: 10.1523/JNEUROSCI.0270-12.2012

Klein-Flügge, M. C., Nobbs, D., Pitcher, J. B., and Bestmann, S. (2013). Variability of human corticospinal excitability tracks the state of action preparation. *J. Neurosci.* 33, 5564–5572. doi: 10.1523/JNEUROSCI.2448-12.2013

Labruna, L., Fernández-del-Olmo, M., and Ivry, R. B. (2011a). Comparison of different baseline conditions in evaluating factors that influence motor cortex excitability. *Brain Stimul.* 4, 152–155. doi: 10.1016/j.brs.2010.09.010

Labruna, L., Fernández-del-Olmo, M., Landau, A., Duqué, J., and Ivry, R. B. (2011b). Modulation of the motor system during visual and auditory language processing. *Exp. Brain Res.* 211, 243–250. doi: 10.1007/s00221-011-2678-z

Labruna, L., Lebon, F., Duque, J., Klein, P.-A., Cazares, C., and Ivry, R. B. (2014). Generic inhibition of the selected movement and constrained inhibition of nonselected movements during response preparation. *J. Cogn. Neurosci.* 26, 269–278. doi: 10.1162/jocn_a_00492

Lebon, F., Greenhouse, I., Labruna, L., Vanderschelden, B., Papaxanthis, C., and Ivry, R. B. (2016). Influence of delay period duration on inhibitory processes for response preparation. *Cereb. Cortex* 26, 2461–2470. doi: 10.1093/cercor/bhv069

Lefaucheur, J. P. (2005). Motor cortex dysfunction revealed by cortical excitability studies in Parkinson's disease: influence of antiparkinsonian treatment and cortical stimulation. *Clin. Neurophysiol.* 116, 244–253. doi: 10.1016/j.clinph.2004.11.017

Leocani, L., Cohen, L. G., Wassermann, E. M., Ikoma, K., and Hallett, M. (2000). Human corticospinal excitability evaluated with transcranial magnetic stimulation during different reaction time paradigms. *Brain* 123, 1161–1173. doi: 10.1093/brain/123.6.1161

Luzar-Stiffler, V., and Stiffler, C. (2002). Equivalence testing the easy way. *J. Comput. Inf. Technol.* 10, 233–239. doi: 10.2498/cit.2002.03.12

Majid, D. S., Cai, W., George, J. S., Verbruggen, F., and Aron, A. R. (2012). Transcranial magnetic stimulation reveals dissociable mechanisms for global versus selective corticomotor suppression underlying the stopping of action. *Cereb. Cortex* 22, 363–371. doi: 10.1093/cercor/bhr112

Neef, N. E., Hoang, T. N. L., Neef, A., Paulus, W., and Sommer, M. (2015). Speech dynamics are coded in the left motor cortex in fluent speakers but not in adults who stutter. *Brain* 138, 712–725. doi: 10.1093/brain/awu390

Pelli, D. G. (1997). The VideoToolbox software for visual psychophysics: transforming numbers into movies. *Spat. Vis.* 10, 437–442. doi: 10.1163/156856897X00366

Quoilin, C., and Derosiere, G. (2015). Global and specific motor inhibitory mechanisms during action preparation. *J. Neurosci.* 35, 16297–16299. doi: 10.1523/JNEUROSCI.3664-15.2015

Quoilin, C., Lambert, J., Jacob, B., Klein, P.-A., and Duque, J. (2016). Comparison of motor inhibition in variants of the instructed-delay choice reaction time task. *PLoS ONE* 11:e0161964. doi: 10.1371/journal.pone.0161964

Reis, J., Swayne, O. B., Vandermeeren, Y., Camus, M., Dimyan, M. A., Harris-Love, M., et al. (2008). Contribution of transcranial magnetic stimulation to the understanding of cortical mechanisms involved in motor control. *J. Physiol.* 586, 325–351. doi: 10.1113/jphysiol.2007.144824

Rickert, J., Riehle, A., Aertsen, A., Rotter, S., and Nawrot, M. P. (2009). Dynamic encoding of movement direction in motor cortical neurons. *J. Neurosci.* 29, 13870–13882. doi: 10.1523/JNEUROSCI.5441-08.2009

Ruffino, C., Papaxanthis, C., and Lebon, F. (2017). Neural plasticity during motor learning with motor imagery practice: review and perspectives. *Neuroscience* 341, 61–78. doi: 10.1016/j.neuroscience.2016.11.023

Schuirmann, D. J. (1987). A comparison of the two one-sided tests procedure and the power approach for assessing the equivalence of average bioavailability. *J. Pharmacokinet. Biopharm.* 15, 657–680. doi: 10.1007/BF01068419

Smith, M.-C., and Stinear, C. M. (2016). Transcranial Magnetic Stimulation (TMS) in stroke: READY for clinical practice? *J. Clin. Neurosci.* 31, 10–14. doi: 10.1016/j.jocn.2016.01.034

Soysal, A., Sobe, I., Atay, T., Sen, A., and Arpaci, B. (2008). Effect of therapy on motor cortical excitability in Parkinson's disease. *Can. J. Neurol. Sci.* 35, 166–172. doi: 10.1017/S0317167100008581

Stinear, C. M., Petoe, M. A., and Byblow, W. D. (2015). Primary motor cortex excitability during recovery after stroke: implications for neuromodulation. *Brain Stimul.* 8, 1183–1190. doi: 10.1016/j.brs.2015.06.015

U.S. Food and Drug Administration (FDA) (2001) *Guidance for Industry: Statistical Approaches to Establishing Bioequivalence*. Rockville, MD.

Valls-Solé, J., Pascual-Leone, A., Brasil-Neto, J. P., Cammarota, A., McShane, L., and Hallett, M. (1994). Abnormal facilitation of the response to transcranial magnetic stimulation in patients with Parkinson's disease. *Neurology* 44, 735–741.

van den Wildenberg, W. P., Burle, B., Vidal, F., van der Molen, M. W., Ridderinkhof, K. R., and Hasbroucq, T. (2010). Mechanisms and dynamics of cortical motor inhibition in the stop-signal paradigm: a TMS study. *J. Cogn. Neurosci.* 22, 225–239. doi: 10.1162/jocn.2009.21248

Verleger, R., Kuniecki, M., Möller, F., Fritzmannova, M., and Siebner, H. R. (2009). On how the motor cortices resolve an inter-hemispheric response conflict: an event-related EEG potential-guided TMS study of the flankers task. *Eur. J. Neurosci.* 30, 318–326. doi: 10.1111/j.1460-9568.2009.06817.x

Wilhelm, E., Duque, J., and Grandjean, J. (2017). Testing the influence of various parameters on preparatory motor inhibition: a possible explanation for discrepancies between previous studies? *Front Neurosci Conf Abstr 12th Natl Congr Belgian Soc Neurosci*. doi: 10.3389/conf.fnins.2017.94.00080

Wilhelm, E., Quoilin, C., Petitjean, C., and Duque, J. (2016). A double-coil TMS method to assess corticospinal excitability changes at a near-simultaneous time in the two hands during movement preparation. *Front. Hum. Neurosci.* 10:88. doi: 10.3389/fnhum.2016.00088

Zénon, A., Klein, P. A., Alamia, A., Boursoit, F., Wilhelm, E., and Duque, J. (2015). Increased reliance on value-based decision processes following motor cortex disruption. *Brain Stimul.* 8, 957–964. doi: 10.1016/j.brs.2015.05.007

Ziemann, U. (2017). Thirty years of transcranial magnetic stimulation: where do we stand? *Exp. Brain Res.* 235, 973–984. doi: 10.1007/s00221-016-4865-4

Conflict of Interest Statement: The authors declare that the research was conducted in the absence of any commercial or financial relationships that could be construed as a potential conflict of interest.

frontiers in Neuroscience

ORIGINAL RESEARCH
published: 28 March 2018
doi: 10.3389/fnins.2018.00151

Changes in H-Reflex Recruitment After Trans-Spinal Direct Current Stimulation With Multiple Electrode Configurations

Alexander Kuck[1,2], *Dick F. Stegeman*[3], *Herman van der Kooij*[1,4] *and Edwin H. F. van Asseldonk*[1]*

[1] Laboratory of Biomechanical Engineering, Department of Engineering Technology, University of Twente, Enschede, Netherlands, [2] Neuronal Rhythms in Movement Unit, Okinawa Institute of Science and Technology Graduate University, Onna-son, Japan, [3] Department of Neurology/Clinical Neurophysiology, Radboud University Medical Center, Donders Institute for Brain, Cognition and Behavior, Nijmegen, Netherlands, [4] Department of Biomechanical Engineering, Faculty of Mechanical, Maritime and Materials Engineering, Delft University of Technology, Delft, Netherlands

Trans-spinal direct current stimulation (tsDCS) is an electro-modulatory tool with possible application in the rehabilitation of spinal cord injury. TsDCS generates a small electric field, aiming to induce lasting, functional neuromodulation in the targeted neuronal networks. Earlier studies have shown significant modulatory effects after application of lumbar tsDCS. However, for clinical application, a better understanding of application specific factors is required. Our goal was to investigate the effect of different electrode configurations using lumbar spinal tsDCS on spinal excitability. We applied tsDCS (2.5 mA, 15 min) in 10 healthy subjects with three different electrode configurations: (1) Anode and cathode placed over vertebra T11, and the posterior left shoulder respectively (LSC-S) (one polarity), and (2) Both electrodes placed in equal distance (ED) (7 cm) above and below vertebra T11, investigated for two polarities (ED-Anodal/Cathodal). The soleus H-Reflex is measured before, during and after tsDCS in either electrode configuration or a sham condition. To account for genetic predispositions in response to direct current stimulation, subject BDNF genotype was assessed. Stimulation in configuration ED-Cathodal induced an amplitude reduction of the H-reflex, 30 min after tsDCS with respect to baseline, whereas none of the other configurations led to significant post intervention effects. BDNF genotype did not correlate with post intervention effects. Furthermore, we failed to replicate effects shown by a previous study, which highlights the need for a better understanding of methodological and subject specific influences on tsDCS outcome. The H-reflex depression after tsDCS (Config. ED-Cathodal) provides new insights and may foster our understanding of the working mechanism of tsDCS.

Keywords: tsDCS, H-reflex, neuromodulation, spinal cord, neurorehabilitation

OPEN ACCESS

Edited by:
Alberto Priori,
Università degli Studi di Milano, Italy

Reviewed by:
Simon Giszter,
Drexel University, United States
Xiaoli Li,
Beijing Normal University, China

***Correspondence:**
Edwin H. F. van Asseldonk
e.h.f.vanasseldonk@utwente.nl

Specialty section:
This article was submitted to Neural Technology, a section of the journal Frontiers in Neuroscience

Received: *15 July 2017*
Accepted: *26 February 2018*
Published: *28 March 2018*

Citation:
Kuck A, Stegeman DF, van der Kooij H and van Asseldonk EHF (2018) Changes in H-Reflex Recruitment After Trans-Spinal Direct Current Stimulation With Multiple Electrode Configurations. Front. Neurosci. 12:151. doi: 10.3389/fnins.2018.00151

INTRODUCTION

The targeted application of electrotherapy to the rehabilitation of nervous system disorders has been a lasting vision in rehabilitation research. In recent years, trans-spinal direct current stimulation (tsDCS), a variant of transcranial Direct Current Stimulation (tDCS), has received an increasing scientific interest as a proposed novel electrotherapeutic protocol. Aiming to modulate

pathways in the Spinal Cord, tsDCS imposes a small electric field (EF) to the spinal neural circuitry. The ultimate goal is the ability to facilitate spinal plasticity and promote rehabilitation after neural injury of the spinal cord, via a meaningful and targeted application of tsDCS, in combination with established rehabilitation techniques.

Earlier research on the neural effects of DC stimulation, which originates mainly from studies on direct current stimulation of the cortex, has revealed a collection of multiple neural working mechanisms (Bikson et al., 2013; Miranda, 2013; Ruffini et al., 2013) depending on electric field magnitude and direction (Salvador et al., 2010; Dmochowski et al., 2011; Rampersad et al., 2014), the underlying neuroanatomy and its alignment with the imposed EF (Tranchina and Nicholson, 1986; Radman et al., 2009; Arlotti et al., 2012; Kabakov et al., 2012) as well as the ongoing neural activity (Reato et al., 2010; Ranieri et al., 2012; Bikson et al., 2013; Lapenta et al., 2013) and genetic predispositions (Bikson et al., 2013; Lamy and Boakye, 2013; Chhabra et al., 2015).

Consequently, previous studies which have applied tsDC-stimulation on the lumbar spinal cord, also revealed a complex picture of its effects on the spinal motor circuitry (for a thorough overview, see: Cogiamanian et al., 2012). It has been shown, that anodal tsDCS can lead to a significant increase (Hubli et al., 2013), or more specifically, a left shift of the H-reflex recruitment curve (Lamy et al., 2012), whereas cathodal stimulation had no significant effect. Also, cathodal and anodal tsDCS, were able to up- and downregulate cortically evoked motor evoked potentials (MEPs) at lumbar spinal level respectively (Bocci et al., 2015). Furthermore, it was shown that lumbar tsDCS has a significant modulatory effect on spinal reflex presynaptic inhibition (Yamaguchi et al., 2013) and post-activation depression (Winkler et al., 2010). As for tDCS, also in tsDCS genetic factors have been implicated to have an effect on the outcome of DC stimulation protocols (Chhabra et al., 2015). In particular, a polymorphism (*Val66Met*) of Brain-derived Neurotropic Factor (*BDNF*), has been of particular interest. Thereby, Lamy and Boakye showed that the H-reflex recruitment curve modulation after tsDCS significantly differs in carriers and non-carriers of the *BDNF Met allele* (Lamy and Boakye, 2013).

For a successful application of tsDCS in a clinical setting, a better understanding of its application specific effects is needed. This includes knowledge about proper electrode placement, the resulting electric field at the target region and its effects on the targeted neural circuitry. Based on studies simulating the electric field generated by transcutaneous DC stimulation, the EF-vector for a pair of surface electrodes is expected to be largest and tangential to the skin—surface about half-way between electrodes. Below the electrodes the EF vector will be comparably lower and perpendicular to the skin-surface (Kuck et al., 2017). Given that the neural effect of DC stimulation is dependent on EF strength and direction, the modulatory outcomes are expected to vary across tsDCS protocols employing different electrode configurations. However, since all previous studies utilized a similar electrode configuration (passive electrode on the shoulder, active electrode above the lumbar spinal cord), current knowledge does not allow conclusions about electrode placement specific effects of tsDCS.

In this study, our goal was therefore to investigate the effect of tsDCS on the soleus H-reflex with three electrode configurations (**Figure 1**). We compared the commonly used electrode configuration to a new bipolar electrode placement, with both electrodes placed in equal distance, above and below the lumbar spinal cord. We measured the soleus H-Reflex before, during and after tsDCS with both configurations and a sham condition. The commonly used placement was tested in anodal configuration only, which had previously shown to be effective in modulating the soleus H-Reflex (Lamy et al., 2012; Hubli et al., 2013). To probe for polarity specific effects, for the new electrode placement both anodal and cathodal configuration were investigated. We were primarily interested in the changes in H-Reflex amplitude post-tsDCS with respect to baseline. Additionally, we tested for a relationship between the amplitude changes during—compared to those after tsDCS. To take into account the possible differences in tsDCS modulatory response for BDNF met allele carriers (Lamy and Boakye, 2013), we assessed BDNF genotype in all subjects.

MATERIALS AND METHODS

Subjects

We included 10 healthy volunteers with a mean age of 23 (range: 20–29) years. All participants gave their written informed consent before data collection and the study protocol was approved by the local ethics committee of Twente (Enschede, The Netherlands).

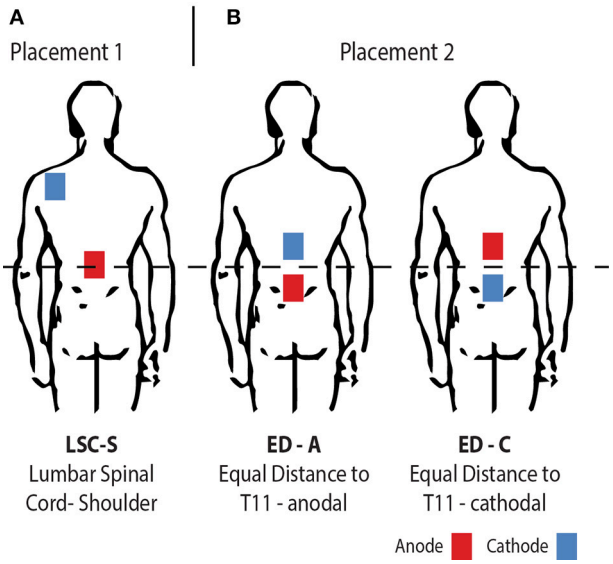

FIGURE 1 | Illustration of the electrode placement configurations investigated. From left to right: **(A)** The traditionally used placement with one anodal electrode centered on the lumbar spinal cord and a return electrode placed on the left posterior shoulder (LSC-S); **(B)** Both electrodes placed in equal distance to the lumbar spinal cord, for opposite polarities (ED-A and ED-C).

tsDCS

As announced, tsDCS was applied in two different electrode placement configurations (**Figure 1**). The amplitude was 2.5 mA and the duration 15 min using a NeuroConn DC-Stimulator PLUS (neuroCare Group GmbH, Munich, Germany). The electrode configurations chosen were: LSC-S: Lumbar Spinal Cord (T11)-left posterior Shoulder (**Figure 1A**) and ED: Equal Distance 7 cm above and below T11 (Lumbar Spinal Cord) (**Figure 1B**). LSC-S was applied in anodal configuration only, whereas for configuration ED the effect of both polarities was investigated. We refer to the polarity of the lower electrode for configuration naming for all configurations (e.g., ED-A and ED-C). Vertebra T11 was determined via manual palpation of the spinal processes, staring at vertebra C7 and counting until vertebra T11 was reached. This process was repeated three times, with the final position estimate determined by taking the mean of the three initial estimates. Sham stimulation, included in the utilized stimulation device, was achieved by applying a 110 μA pulse with a pulse-width of 3 ms and an interval of 550 ms for a duration of 15 min.

H-Reflex Measurement

To determine the changes induced to the H-reflex by tsDCS in one of the three configurations, we chose to characterize the H-reflex recruitment curve at four characteristic points (**Figure 2**): H-Reflex threshold (H_{thresh}), 50% of H-reflex maximum ($H_{max50\%}$), the point at which the ascending part of the recruitment curve begins to settle (H_{settle}) as well as the maximum H-wave (H_{max}). These points were chosen for their ability: (1) to reflect the anticipated changes of the H-reflex recruitment curve (left/right shift, based on Lamy et al., 2012), or overall amplitude modulation, as well as (2) to sufficiently approximate the ascending part of the recruitment curve. The points were determined from a detailed H-reflex recruitment curve, recorded at the start of each experiment. The recruitment curve was sampled at stimulation intervals I (see: Experimental Protocol). Thereby, M_{max}, H_{max}, and H_{thresh} were determined manually, with H_{max} defined as the peak value of the average H-wave recruitment curve and M_{max} the amplitude immediately after peak settling amplitude of the M-wave recruitment curve. H_{thresh} was defined as the first visible H-Wave, in response to a stimulus. H_{settle} and $H_{max50\%}$ were determined via fitting of a sigmoid function $f(s)$ to the recorded recruitment curve: $f(s) = H_{max}/(1 + e^{-m(s-S_{max50\%})})$. Thereby, m is the function slope at $f(S_{max50\%})$, $S_{max50\%}$ the stimulus needed to evoke 50% of H_{max}, H_{max} the maximum value of the recruitment curve and S_{max} the corresponding stimulation amplitude. $H_{max50\%}$ and H_{settle} are then defined as $f(S_{max50\%})$ and $f(S_{settle})$ respectively, given $f''(S_{settle}) = \min(f''(s))$. For each point, the closest multiple of I was chosen as a stimulation amplitude.

EMG

Bipolar, EMG was recorded using a TMSi Porti amplifier (TMSi, Oldenzaal, NL) from the belly of the right lateral soleus muscle with electrode centers placed ~3 cm apart, 4 cm below the initiation of the gastrocnemius tendon. The sampling frequency was set to 2048 samples/s.

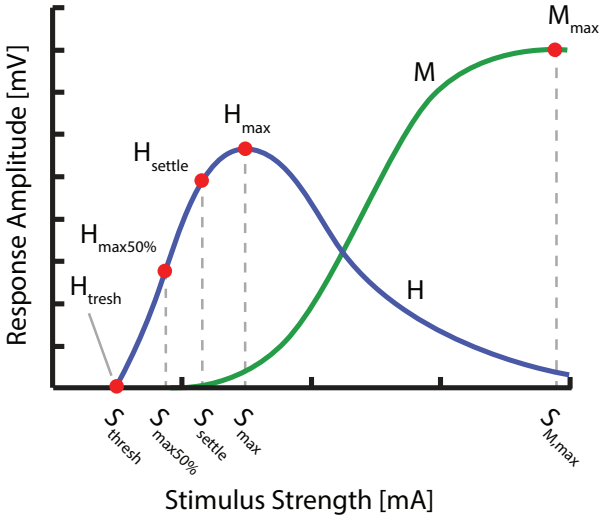

FIGURE 2 | Overview of the distinct points measured within the H- and M-Wave recruitment curves: H-Reflex threshold (H_{thresh}), 50% of H-reflex maximum ($H_{max50\%}$), the point at which the ascending part of the recruitment curve begins to settle (H_{settle}), the maximum H wave (H_{max}) as well as the maximum M-wave (M_{max}).

Nerve Stimulation

H-Reflex responses were evoked using electrical stimulation of the tibial nerve (Micromed Matrix Light, Micromed S.p.A., Mogliano Veneto, Italy). Adhesive active-cathodal (1.5 × 1.5 cm) and return -anodal (5 × 5 cm) electrodes were placed over the tibial nerve in the popliteal fossa and above the patella respectively. The stimulation consisted of a biphasic pulse with a pulse width of 0.5 ms and stimulation amplitudes ranging from 0 to 80 mA.

BDNF Genotyping

Saliva samples were collected (Oragene Dx, DNA Genotek Inc., Ottawa, Canada) from each subject. Subsequently all samples were analyzed to detect the BDNF Val66Met polymorphism using Taqman (rs6265). Additionally, BDNF concentration and sample purity (260/280) were detected.

Experimental Protocol

The experiment was set up in a randomized double-blind placebo controlled design, whereby both experimenter and subject were blinded with respect to the intervention type (real or sham). Interventions consisted of the three stimulation configurations and one sham stimulation. For each intervention, an individual experiment was performed in a randomized order with experiments planned with an interval of at least 7 days. The configuration by which sham was performed was randomized across subjects.

Subjects were instructed to avoid drinking coffee or consume other stimulants on the day of the experiment. Preparatory steps

before attachment of EMG and tibial nerve stimulation electrodes included skin disinfection with alcohol, shaving and exfoliating of the desired skin section. With the subject lying on a medical bench in a prone position, EMG electrodes and nerve stimulation counter electrode in place, a handheld stimulation probe was used to determine the optimal position to stimulate the tibial nerve. Indicators for an appropriate stimulation position were a clear EMG response and visible contraction of the soleus, while excluding the contraction of other muscles such as the tibialis anterior, to avoid stimulation of the peroneal nerve. Additionally, an approximate H-reflex threshold was determined during this procedure, used for the determination of the needed stimulation increment for recruitment curve sampling.

After placement of the active stimulation amplitude, the subject was comfortably seated in an inclined medical chair, head and arms supported (Ankle angle: ∼110°, Knee angle: ∼150°, Hip angle: ∼120°, similar to Lamy et al., 2012). Thereafter, the protocol was executed as shown in **Figure 3**, for which the subject was instructed to remain entirely still and to avoid movement or muscle tension throughout the course of the experiment.

As a first step, an entire recruitment curve was measured at small intervals, later used to determine the stimulation amplitude of four relevant H-wave points (**Figure 2**). Starting at a stimulation amplitude at which no response was visible, the amplitude was increased gradually in predetermined intervals I, while measuring six times at each increment. I was set according to the previously approximated threshold amplitude. For thresholds below 10 mA, increments were set to threshold/10, otherwise an interval of 1 mA was used. The recruitment curve was sampled until reaching its declining portion after H_{max}, after which the amplitude was increased at larger increments, until after the maximum M-wave was reached.

After completion of the initial curve mapping process, the stimulation amplitudes for H_{thresh}, $H_{max50\%}$, H_{settle}, H_{max}, and M_{max} were identified within the recorded recruitment curve (see: H-reflex measurement:). These stimulation amplitudes were then held constant throughout the experiment.

After an additional baseline measurement, the tsDCS intervention was started. Post measurements were performed immediately after (t0) and 30 min following the intervention (t30). To assess the acute stimulation effects, additional measurements, 2 min (S1) and 9 min (S2) in the course of the intervention, were conducted. To reduce interference with effects of tsDCS, only $H_{max50\%}$, H_{settle}, and M_{max} were measured at S1 and S2. The protocol was repeated for each electrode configuration and a sham condition.

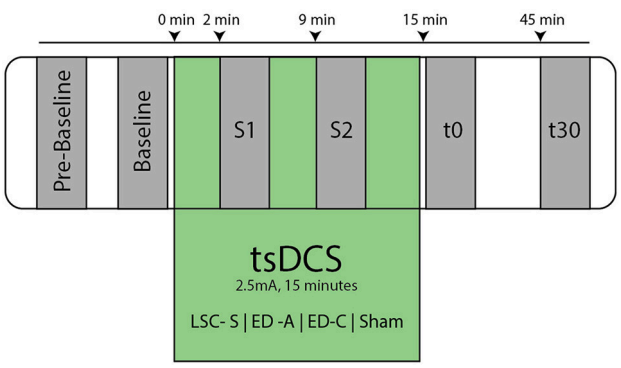

FIGURE 3 | Overview of experimental protocol. At Pre-Baseline an initial recruitment curve mapping took place to determine characteristic points within the H- and M- Wave recruitment curves (see **Figure 2**). After an additional baseline measurement, the tsDCS intervention was started with an amplitude of 2.5 mA and a duration of 15 min. During tsDCS, the H-reflex is probed after 2 min (S1) and 9 min (S2), measuring only H_{settle}, H_{max}, and M_{max}. Post tsDCS measurements follow immediately (t0) and 30 min (t30) after the intervention.

Data Analysis

Data processing was performed with a custom Matlab script (Matlab v.2015a, MathWorks Inc., Natick, USA). EMG signals were high pass filtered at 5 Hz after which H- and M- wave peak-to-peak amplitudes were determined automatically. Thereafter, all amplitudes were normalized with their corresponding M_{max}. Extreme outliers, such as null responses, were removed manually.

We expressed each obtained data point by its difference to baseline. This difference is normalized by the value of H_{max} at baseline and therefore expressed as a fraction of initial, overall H-reflex amplitude allowing comparison between sessions.

As an additional outcome-measure, we calculated the area below the sampled characteristic points, which gives an indication about the curve as a whole. Again, the area was expressed as its difference to the area calculated for its respective baseline. The resulting area difference was normalized by the overall area at baseline.

Because the H-reflex during stimulation was only measured at two sample points ($H_{max50\%}$ and H_{settle}), we also calculated the area difference to baseline restricted to the interval between $H_{max50\%}$ and H_{settle}. This was done in order to compare measurements during, to those before and after tsDCS.

Statistics

Statistical analysis was performed using IBM SPSS Statistics v.23 (IBM Corporation, New York, USA). For each stimulation condition a Friedman's one-way ANOVA was used to test for significant effects in time and for each time interval for significant effects of stimulation configuration. This was performed on changes in curve area and data point amplitudes at H_{max} and $H_{max50\%}$. The significance level was set to $p = 0.05$. *Post-hoc* pairwise comparison was performed using Dunn's–test (Dunn, 1964) with an adjusted p-value of 0.0083. Effect size r was calculated via $r = \frac{Z}{\sqrt{2N}}$ with N being the number (10) of subjects (Pallant, 2013). Furthermore, we calculate the mean (m_{abs}) and interquartile range (IQR_{abs}) of the absolute difference from baseline for conditions found to be significant by *post-hoc* comparison.

To differentiate between a recruitment curve threshold shift and overall amplitude shift, we use Friedman repeated measures ANOVA to compare within measurement values for $H_{max50\%}$ and H_{max} for *post-hoc* measurements significant with respect to baseline. We thereby assume that a change in recruitment curve threshold, which is visible in a left or right shift of the recruitment

curve, will result in a significantly larger amplitude change measured at $S_{max50\%}$ compared to those at S_{max}. Consequently, an overall amplitude decrease will result in no significant difference between the changes at $H_{max50\%}$ and H_{max}.

Furthermore, correlation analysis is used to rule out that changes in H wave could be attributed to a change in M_{max}. In order to investigate differences between genotype groups, a Kruskal-Wallis test is performed for each measurement in which a significant difference was found, with the genotype as between group factor. For conditions across which a significant difference was found, we assess two-tailed Pearson and Spearman correlations by using the area between the corresponding measurement and baseline in a range from $H_{max50\%}$ to H_{settle}.

RESULTS

Subject Safety

Throughout the course of the study, all subjects underwent the experiments without adverse effects, neither during or after the applied tsDCS, nor during the tibial nerve stimulation.

Changes in H-Reflex

A typical measurement for an exemplary subject, including sampled H- and M-wave datapoints and average EMG traces at $s_{max50\%}$, for condition ED-C is illustrated in **Figure 4**. An overview of all H-Reflex datapoints, expressed as a percentage difference of H_{max} at baseline, for all subjects and conditions is shown in **Figure 5**. The total area, as a percentage difference of the area at baseline (see also **Figure 4**), quantifies the overall change (see **Figure 6**), whereas differences in mean datapoint amplitudes for H_{max} and $H_{max50\%}$ (**Figure 5**) can be interpreted as changes in overall amplitude and threshold respectively.

Responses to the different stimulation paradigms show high inter and intra subject variability. The changes observed for all sham measurements and those obtained during curve mapping before baseline give an indication of the natural changes that can be expected without intervention. Thereby the fluctuation in changes in area for all combined pre-baseline and sham measurements normalized by their baseline had an interquartile range of 21%. Similarly, for H_{max}: IQR = 13%, and $H_{max50\%}$: IQR = 45%. Across subjects, most post-intervention changes are within the amplitude range of effects observed without intervention, as visible in **Figures 5**, **6**.

For configurations LSC-S and ED-A, observed changes lie within the same standard deviation range as the sham condition. Furthermore, for both stimulation conditions, responses in either direction are visible, resulting in no statistically significant net-change with respect to baseline (**Table 1**). Similarly, for the sham condition, responses in both directions resulted in no statistically significant changes with respect to baseline.

For configuration ED-C, differences in curve area (**Figure 6**) as well as data points $H_{max50\%}$ and H_{max} (**Figure 5**) reveal clear tsDCS effects post-intervention compared to baseline. This is indicated by overall significant changes in area [$\chi 2_{(3)} = 8.76$, $p = 0.033$], H_{max} [$\chi 2_{(3)} = 16.56$, $p = 0.001$], and $H_{max50\%}$ [$\chi 2_{(3)} = 8.76$, $p = 0.033$]. *Post-hoc* analysis reveals a significant difference of t30 to pre-baseline (H_{max}: Z = 1.8, $p = 0.011$, $r = 0.4$, $m_{abs} = 0.15$, $IQR_{abs} = 0.19$) and baseline (area: Z = 1.7, $p = 0.019$, $r = 0.38$, $m_{abs} = 0.22$, $IQR_{abs} = 0.24$; H_{max}: Z = 2.2, $p < 0.001$, $r = 0.49$, $m_{abs} = 0.15$, $IQR_{abs} = 0.19$; $H_{max50\%}$: Z = 1.7, $p = 0.019$, $r = 0.38$, $m_{abs} = 0.4$, $IQR_{abs} = 0.24$) measurements. To constrain the character of the observed recruitment curve changes, we compared the data points at $H_{max50\%}$ with those at H_{max}, within configuration ED-C at time t30. Thereby no significant differences were found ($p = 0.114$). Thus, the population trend with respect to baseline for condition ED-C appears to be an overall H-reflex decrease instead of a curve shift to the right, revealed by a significant decrease in area, $H_{max50\%}$ and H_{max}.

The observed effects in $H_{max50\%}$, H_{max} and curve area could not be explained by changes in nervous excitation during tibial nerve stimulation as changes in these measures were unrelated to changes in M_{max}. We also explored whether changes during tsDCS (measurements S1 and S2) were predictive for changes post intervention. However, from correlation analysis it appeared that this was not the case.

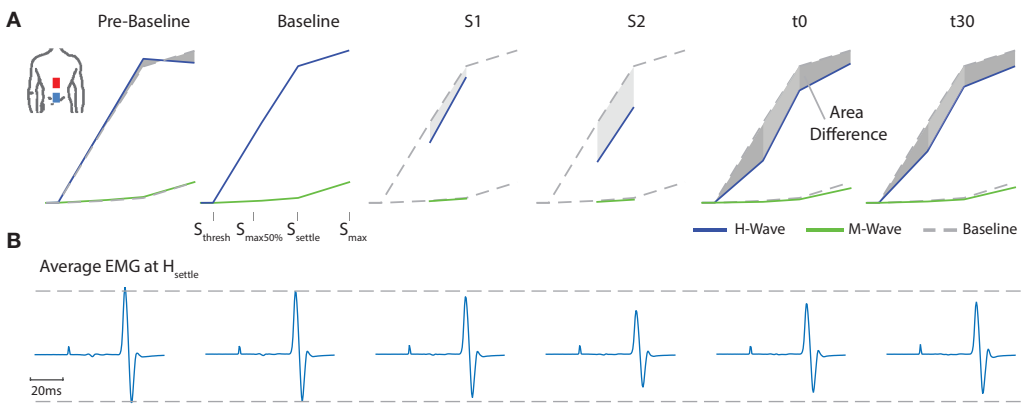

FIGURE 4 | For an exemplary subject **(A)** all average H- and M- Wave datapoints are shown. For clarity, the figure exemplifies the area between a corresponding measurement and baseline. **(B)** Average EMG traces at H_{settle} for configuration ED-C.

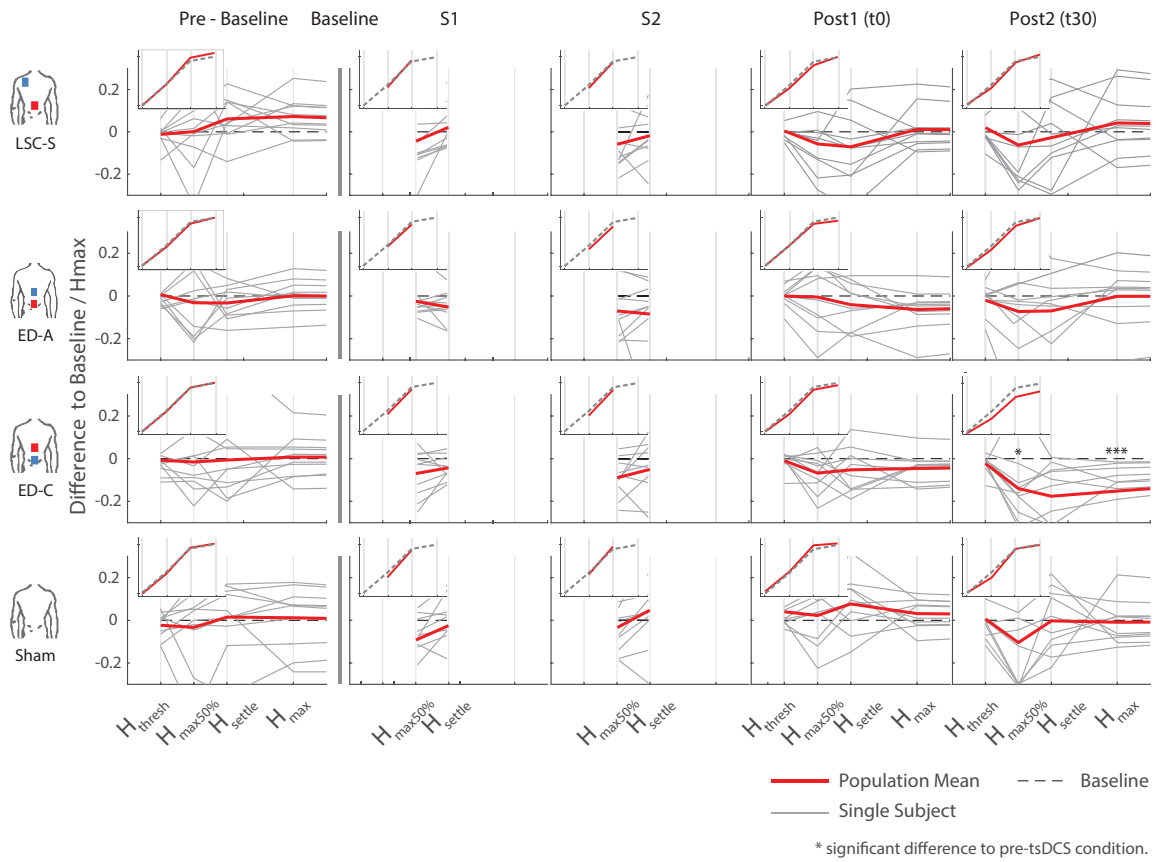

FIGURE 5 | Overview of all differences to baseline, as a percentage of the corresponding H_{max} at baseline, for all configurations and measurements. The inlays show the average trend over all subjects with respect to a generic s-function representing baseline. Significant differences with respect to pre-intervention measurements arose for configuration ED-C, 30 min after intervention (last column).

Testing for time effects across configurations, Friedman's test reveals differences in H_{max} for measurements at t0 [$\chi 2_{(3)} = 7.8$, $p = 0.05$]. However, whereas the highest difference was found between configuration ED-A and sham ($Z = -1.4$, $p = 0.09$), *post-hoc* pairwise comparisons did not lead to significant results. Furthermore, analysis reveals a notable statistical trend [$\chi 2_{(3)} = 7.56$, $p = 0.06$] across conditions at time t30.

To explain the high variability across subjects, BDNF genotype was tested. Thereby, 5 out of 10 subjects were tested positive for the Vall66Met polymorphism. The corresponding subjects' genotype is included by coloring the bars in **Figure 6**. Generally, there is no consistent difference in stimulation response between genotype groups. For conditions exhibiting significant differences compared to baseline, Kruskal-Wallis' test reveals no significant differences between the responses exhibited by the two genotype groups. Thus, the high intersubject variability, which remains within genotype groups, cannot be explained by or, otherwise stated, prohibits explanation of an effect of subject genotype.

DISCUSSION

The goal of this study was to investigate electrode placement specific changes of lumbar trans-spinal direct current stimulation on the soleus H-reflex before, during and after intervention. We introduced a new electrode placement configuration (ED), which generates an electric field vector dominant in longitudinal direction at lumbar spinal motoneuron level, by placing both electrodes equidistant above and below the lumbar spinal cord (Kuck et al., 2017). We show that the newly introduced electrode configuration (ED-C) was able to induce significant changes to the approximated H-reflex recruitment curve 30 min after intervention. This was indicated by a significant and consistent depression of H_{max}, $H_{max50\%}$, and area. The equal distance placement in anodal setting (ED-A) had no significant effect, which confirms the polarity dependency often observed in DC stimulation protocols. Additionally, the effects observed post tsDCS were unrelated to the deviations from baseline measured during DC stimulation. Strikingly, we were not able to observe the effects previously reported for configuration LSC-S (Lumbar

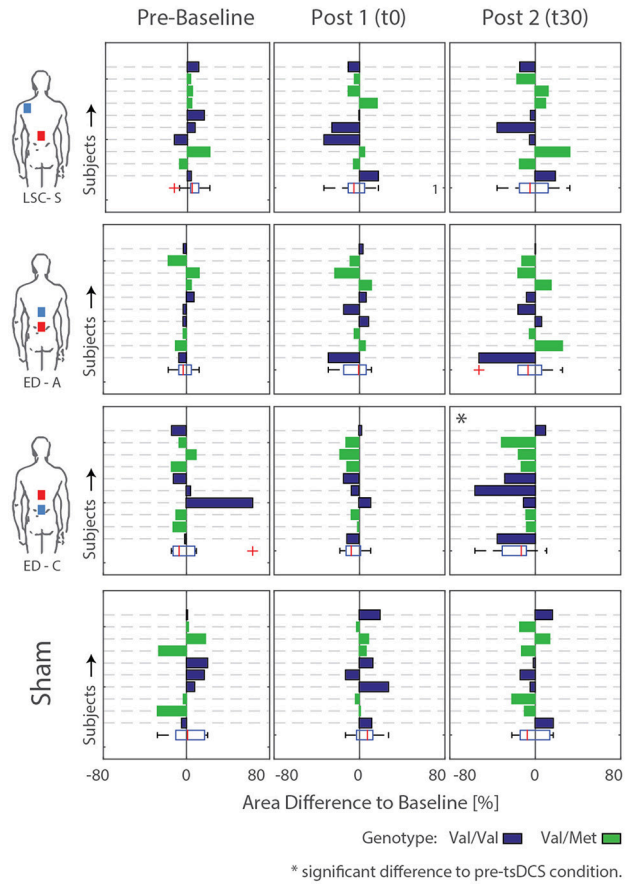

FIGURE 6 | Difference areas between baseline and pre-baseline as well as post tsDCS (t0 and t30) for all subjects. Rows/Bars within each graph correspond to the measured subjects. Additionally, the subject genotype is color coded: Val/Val = Blue, Val/Met = Green. Significant differences to pre-tsDCS measurements are detected for configuration ED-C at time t30.

TABLE 1 | Statistical analysis of general differences within conditions and measurement times, across conditions, after Friedman repeated measures analysis.

	Significance		
	Area difference	H_{max}	$H_{max50\%}$
CONFIGURATION			
LSC-S	0.51	0.16	0.51
ED-A	0.66	0.24	0.073
ED-C	**0.033***	**0.001*****	**0.033***
Sham	0.26	0.54	0.15
MEASUREMENT TIME			
Pre-Baseline	0.16	0.39	0.78
t0	0.06	**0.05***	0.52
t30	0.095	0.06	0.78

*Bold highlights significance. *$p \leq 0.05$, ***$p \leq 0.001$.*

Spinal Cord—Shoulder), which had been shown to induce a significant left shift of the H-reflex recruitment curve (Lamy et al., 2012).

The specific post intervention response to stimulation with configuration ED-C appears to be an overall amplitude reduction of the H-reflex, indicated by a relative decrease in H_{max}, $H_{max50\%}$ and area. This is qualitatively different from the left shift reported after anodal tsDCS (LSC-S) in previous studies and may consequently indicate the involvement of different working mechanisms. Cellular targets of lumbar spinal DCS that have been suggested by previous studies, are the Ia-motoneuron synapse (Lamy et al., 2012; Hubli et al., 2013; Kuck et al., 2017), Ia-presynaptic inhibition (Yamaguchi et al., 2013), or channels mediating persistent inward current excitability (Elbasiouny and Mushahwar, 2007).

We argue, that conductivity changes at the Ia-motoneuron synapse seem less likely, as this would lead to a left shift or right shift of the H-Reflex recruitment curve, not an amplitude modulation (Kuck et al., 2017). Thus, also changes in Ia-presynaptic inhibition appear unlikely. It can however not be excluded, that the observed effect in H-Reflex reduction could in part be caused by a downregulation of Ca^{2+} persistent inward current. Elbasiouny and Mushahwar investigated the effect of motoneuron polarization on spinal motoneuron firing and PIC modulation (Elbasiouny and Mushahwar, 2007). Thereby a constant EF was able to directly surpress motoneuron firing by reducing Ca^{2+} current. In analogy to that, the tsDCS generated electric field in this study, could have led to a similar polarization profile of the lumbar spinal motoneurons (Kuck et al., 2017), which may in turn have resulted in a downregulation of motoneuron activity.

In an effort to understand inter-individual response differences, we investigated the relationship between tsDCS acute and after effects as well as differences in BDNF genotype. To test the relationship between acute and after effects, we correlated the conditions found to be significant, to the changes from baseline measured during tsDCS within the same experiment. However, no relationship was detected.

A possible reason that a relation between acute and long-term effects was not found in this study, could be that the stimulation intensities usually used for human subjects were too low to elicit measurable acute effects. This is different in animal and in *in-vitro* DC experiments, which show measurable acute effects during DC stimulation, which scale with stimulation intensity (Ahmed, 2011; Rahman et al., 2013). The relationship between DCS acute and after effects is complex, as shown by Ahmed (2011), whereby MEP evoked muscle twitches in the hindlimb where inversed during, compared to after tsDCS. Furthermore, this directional relationship was altered by associative stimuli during tsDCS.

Genetic dependencies for the response to tsDCS have been shown for Met allele carriers of brain derived neurotropic factor (BDNF) (Val66Met polymorphism) (Lamy and Boakye, 2013; Wiegand et al., 2016). However, BDNF genotyping in our subject population reveals that the level of variability remains within the two genotype groups and thus no statistical difference between the responses exhibited by the two subject groups was found.

This does however not rule out the influence of other genetic dependencies (Wiegand et al., 2016).

We did not observe a consistent recruitment curve left shift after tsDCS with configuration LSC-S, as reported previously (Lamy et al., 2012). Based on Lamy et al. we had expected a substantial increase of $H_{max50\%}$ with respect to baseline (for configuration LSC-S at time T30). However, with a mean difference from baseline for $H_{max50\%}$ of −6.3% (95% CI [−20.81, 8.26%]), the population response observed here is substantially different from that. However, this is in line with observations by Hubli et al. who showed no significant modulatory effects after anodal tsDCS tested in healthy individuals (Hubli et al., 2013). We therefore assume that the absence of a modulatory effect after tsDCS in configuration LSC-S, must be attributed to experimental and/or subject-specific factors.

The two main methodological differences between the protocol used here and the one of Lamy et al. are the amount of measurements taken during tsDCS as well as sample size. For the former, Lamy et al. sampled two complete H-reflex recruitment curves during tsDCS at a stimulus frequency of 0.33 Hz, and a measurement time of 3–4 min for each curve. In contrast to that, we intentionally reduced the number of measurements during tsDCS, to prevent interactions with the artificially induced neural activity and therefore influence intervention outcome. With each measurement lasting ∼1–2 min (thus overall 2–4 min during tsDCS), the amount of induced neural activity was substantially lower as compared to the protocol performed by Lamy et al. (6–8 min during tsDCS). Along this line, Hubli and colleagues did not measure during tsDCS and stimulation was applied during rest, thus reducing neural activity during DC stimulation to a resting level (Hubli et al., 2013). Since the outcome of DC stimulation is thought to be neural activity dependent (Bikson et al., 2013), the agreement of our results with those reported by Hubli et al. (2013) and the discrepancies with those observed by Lamy et al. may be explained via the differences in induced neural activity during tsDCS.

With regards to sample size, we included a smaller number of subjects (N = 10) compared to Lamy et al. (N = 17), which may suggest limited statistical power to show an otherwise significant effect. However, based on the mentioned population mean for $H_{max50\%}$, 30 min after tsDCS with configuration LSC-S, the responses obtained here are substantially different from those reported by Lamy et al. Furthermore, our results agree with those of Hubli et al. who had included the same number of subjects (N = 17) as Lamy et al. Out of these reasons, it is unlikely that sample size is able to account for the mentioned differences in intervention outcome.

CONCLUSION

The presented results are a further step toward forming a basic understanding of tsDCS and may potentially contribute to a more targeted application in the future. In the light of the knowledge obtained by others, the overall reduction of the H-reflex after stimulation with configuration ED-C indicates that by changing EF direction with respect to the target structure the network response can be changed. This implies that different cellular targets may be dominant depending on EF orientation, which is in line with current state of the art knowledge. Against our expectations, we were not able to observe the same recruitment-curve left shift for configuration LSC-S as previously reported by others, which could be accounted for by methodological or subject specific differences as discussed. In addition to the depression effects discussed earlier, this highlights the complexity of the underlying mechanisms, which have to be understood before tsDCS can find its way into clinical application.

AUTHOR CONTRIBUTIONS

AK, DS, HvdK, and EvA took part in initial planning. AK carried out the experiments and data analysis. AK, DS, HvdK, and EvA contributed to the interpretation of the results. AK took the lead in writing the manuscript. All authors provided critical feedback and helped shape the research, analysis, and manuscript.

FUNDING

This research was supported by ZonMw (Grant Nr. 10-10400-98-008) as part of the NeuroControl—Assessment and Stimulation (NeurAS) consortium.

REFERENCES

Ahmed, Z. (2011). Trans-spinal direct current stimulation modulates motor cortex-induced muscle contraction in mice. *J. Appl. Physiol.* 110, 1414–1424. doi: 10.1152/japplphysiol.01390.2010

Arlotti, M., Rahman, A., Minhas, P., and Bikson, M. (2012). Axon terminal polarization induced by weak uniform DC electric fields: a modeling study. *Conf. Proc. IEEE Eng. Med. Biol. Soc.* 2012, 4575–4578. doi: 10.1109/EMBC.2012.6346985

Bikson, M., and Rahman, A. (2013). Origins of specificity during tDCS: anatomical, activity-selective, and input-bias mechanisms. *Front. Hum. Neurosci.* 7:688. doi: 10.3389/fnhum.2013.00688

Bocci, T., Marceglia, S., Vergari, M., Cognetto, V., Cogiamanian, F., Sartucci, F., et al. (2015). Transcutaneous Spinal Direct Current Stimulation (tsDCS) modulates human corticospinal system excitability. *J. Neurophysiol.* 114, 440-446. doi: 10.1152/jn.00490.2014

Chhabra, H., Shivakumar, V., Agarwal, S. M., Bose, A., Venugopal, D., Rajasekaran, A., et al. (2015). Transcranial direct current stimulation and neuroplasticity genes: implications for psychiatric disorders. *Acta Neuropsychiatr.* 28, 1–10. doi: 10.1017/neu.2015.20

Cogiamanian, F., Ardolino, G., Vergari, M., Ferrucci, R., Ciocca, M., Scelzo, E., et al. (2012). Transcutaneous spinal direct current stimulation. *Front. Psychiatry* 3:63. doi: 10.3389/fpsyt.2012.00063

Dmochowski, J. P., Datta, A., Bikson, M., Su, Y., and Parra, L. C. (2011). Optimized multi-electrode stimulation increases focality and intensity at target. *J. Neural Eng.* 8:46011. doi: 10.1088/1741-2560/8/4/046011

Dunn, O. J. (1964). Multiple comparisons using rank sums. *Technometrics* 6, 241–252. doi: 10.1080/00401706.1964.10490181

Elbasiouny, S. M., and Mushahwar, V. K. (2007). Suppressing the excitability of spinal motoneurons by extracellularly applied electrical fields: insights from computer simulations. *J. Appl. Physiol.* 103, 1824–1836. doi: 10.1152/japplphysiol.00362.2007

Hubli, M., Dietz, V., Schrafl-Altermatt, M., and Bolliger, M. (2013). Modulation of spinal neuronal excitability by spinal direct currents and locomotion after spinal cord injury. *Clin. Neurophysiol.* 124, 1187–1195. doi: 10.1016/j.clinph.2012.11.021

Kabakov, A. Y., Muller, P. A., Pascual-Leone, A., Jensen, F. E., and Rotenberg, A. (2012). Contribution of axonal orientation to pathway-dependent modulation of excitatory transmission by direct current stimulation in isolated rat hippocampus. *J. Neurophysiol.* 107, 1881–1889. doi: 10.1152/jn.00715.2011

Kuck, A., Stegeman, D. F., and van Asseldonk, E. (2017). Modeling trans-spinal direct current stimulation for the modulation of the lumbar spinal motor pathways. *J. Neural Eng.* 14:56014. doi: 10.1088/1741-2552/aa7960

Lamy, J.-C., and Boakye, M. (2013). BDNF Val66Met polymorphism alters spinal DC stimulation-induced plasticity in humans. *J. Neurophysiol.* 110, 109–116. doi: 10.1152/jn.00116.2013

Lamy, J.-C., Ho, C., Badel, A., Arrigo, R. T., and Boakye, M. (2012). Modulation of soleus H reflex by spinal DC stimulation in humans. *J. Neurophysiol.* 108, 906–914. doi: 10.1152/jn.10898.2011

Lapenta, O. M., Minati, L., Fregni, F., and Boggio, P. S. (2013). Je pense donc je fais: transcranial direct current stimulation modulates brain oscillations associated with motor imagery and movement observation. *Front. Hum. Neurosci.* 7:256. doi: 10.3389/fnhum.2013.00256

Miranda, P. C. (2013). "Chapter 29 - Physics of effects of transcranial brain stimulation," in *Brain Stimulation Handbook of Clinical Neurology*, eds A. M. Lozano and M. Hallett (New York, NY: Elsevier), 353–366.

Pallant, J. (2013). *SPSS Survival Manual: a Step by Step Guide to Data Analysis Using SPSS*. Berkshire.

Radman, T., Ramos, R. L., Brumberg, J. C., and Bikson, M. (2009). Role of cortical cell type and morphology in subthreshold and suprathreshold uniform electric field stimulation *in vitro*. *Brain Stimul.* 2, 215.e3–228.e3. doi: 10.1016/j.brs.2009.03.007

Rahman, A., Reato, D., Arlotti, M., Gasca, F., Datta, A., Parra, L. C., et al. (2013). Cellular effects of acute direct current stimulation: somatic and synaptic terminal effects. *J. Physiol.* 591, 2563–2578. doi: 10.1113/jphysiol.2012.247171

Rampersad, S. M., Janssen, A. M., Lucka, F., Aydin, Ü., Lanfer, B., Lew, S., et al. (2014). Simulating transcranial direct current stimulation with a detailed anisotropic human head model. *IEEE Trans. Neural Syst. Rehabil. Eng.* 22, 441–452. doi: 10.1109/TNSRE.2014.2308997

Ranieri, F., Podda, M. V., Riccardi, E., Frisullo, G., Dileone, M., Profice, P., et al. (2012). Modulation of LTP at rat hippocampal CA3-CA1 synapses by direct current stimulation. *J. Neurophysiol.* 107, 1868–1880. doi: 10.1152/jn.00319.2011

Reato, D., Rahman, A., Bikson, M., and Parra, L. C. (2010). Low-Intensity electrical stimulation affects network dynamics by modulating population rate and spike timing. *J. Neurosci.* 30, 15067–15079. doi: 10.1523/JNEUROSCI.2059-10.2010

Ruffini, G., Wendling, F., Merlet, I., Molaee-ardekani, B., Mekonnen, A., Salvador, R., et al. (2013). Transcranial Current Brain Stimulation (tCS): models and technologies. *IEEE Trans. Neural Syst. Rehabil. Eng.* 21, 333–345. doi: 10.1109/TNSRE.2012.2200046

Salvador, R., Mekonnen, A., Ruffini, G., and Miranda, P. C. (2010). Modeling the electric field induced in a high resolution realistic head model during transcranial current stimulation. *Conf. Proc. IEEE Eng. Med. Biol. Soc.* 2010, 2073–2076. doi: 10.1109/IEMBS.2010.5626315

Tranchina, D., and Nicholson, C. (1986). A model for the polarization of neurons by extrinsically applied electric fields. *Biophys. J.* 50, 1139–1156. doi: 10.1016/S0006-3495(86)83558-5

Wiegand, A., Nieratschker, V., and Plewnia, C. (2016). Genetic modulation of transcranial direct current stimulation effects on cognition. *Front. Hum. Neurosci.* 10:651. doi: 10.3389/fnhum.2016.00651

Winkler, T., Hering, P., and Straube, A. (2010). Spinal DC stimulation in humans modulates post-activation depression of the H-reflex depending on current polarity. *Clin. Neurophysiol.* 121, 957–961. doi: 10.1016/j.clinph.2010.01.014

Yamaguchi, T., Fujimoto, S., Otaka, Y., and Tanaka, S. (2013). "Effects of transcutaneous spinal DC stimulation on plasticity of the spinal circuits and corticospinal tracts in humans," in *6th international IEEE/EMBS Conference on Neural Engineering, 2013* (San Diego, CA), 275–278.

Conflict of Interest Statement: The authors declare that the research was conducted in the absence of any commercial or financial relationships that could be construed as a potential conflict of interest.

frontiers in Neuroscience

MINI REVIEW
published: 10 April 2018
doi: 10.3389/fnins.2018.00239

Vagus Nerve Stimulation (VNS) and Other Augmentation Strategies for Therapy-Resistant Depression (TRD): Review of the Evidence and Clinical Advice for Use

Helge H. O. Müller[1], Sebastian Moeller[2], Caroline Lücke[1], Alexandra P. Lam[1], Niclas Braun[1,2] and Alexandra Philipsen[1]*

[1] Department of Psychiatry and Psychotherapy, Universitätsklinikum Bonn, Bonn, Germany, [2] Department of Psychiatry and Psychotherapy, Carl von Ossietzky Universität Oldenburg, Oldenburg, Germany

In addition to electroconvulsive therapy (ECT) and repetitive transcranial magnetic stimulation (rTMS), vagus nerve stimulation (VNS) is one of the approved neurostimulation tools for treatment of major depression. VNS is particularly used in therapy-resistant depression (TRD) and exhibits antidepressive and augmentative effects. In long-term treatment, up to two-thirds of patients respond. This mini-review provides a comprehensive overview of augmentation pharmacotherapy and neurostimulation-based treatment strategies, with a special focus on VNS in TRD, and provides practical clinical advice for how to select TRD patients for add-on neurostimulation treatment strategies.

Keywords: vagus nerve stimulation, therapy-resistant depression, neurostimulation, clinical practice, affective disorders

OPEN ACCESS

Edited by:
Mikhail Lebedev,
Duke University, United States

Reviewed by:
Gianluca Serafini,
Dipartimento di Neuroscienze e Organi di Senso, Ospedale San Martino (IRCCS), Italy
Angela J. Grippo,
Northern Illinois University, United States

****Correspondence:***
Helge H. O. Müller
helge.mueller@ukbonn.de

Specialty section:
This article was submitted to Neural Technology, a section of the journal Frontiers in Neuroscience

Received: *22 November 2017*
Accepted: *27 March 2018*
Published: *10 April 2018*

Citation:
Müller HHO, Moeller S, Lücke C, Lam AP, Braun N and Philipsen A (2018) Vagus Nerve Stimulation (VNS) and Other Augmentation Strategies for Therapy-Resistant Depression (TRD): Review of the Evidence and Clinical Advice for Use. Front. Neurosci. 12:239. doi: 10.3389/fnins.2018.00239

INTRODUCTION

Major depressive disease (MDD) is recognized worldwide as a frequently recurring or chronic and highly prevalent psychiatric disease (Beaucage et al., 2009; Maske et al., 2015). In addition to alterations in the typical domains of affective and mood symptoms, MDD is directly associated with high rates of suicidality and overall mortality as well as a well-established increased risk of death due to comorbid somatic disorders, such as myocardial infarction and stroke (Lasserre et al., 2017; Slepecky et al., 2017; Tesio et al., 2017; Vandeleur et al., 2017). Therefore, it has been projected that MDD will be the second leading cause of disability worldwide by the year 2020 (Michaud et al., 2001; Effinger and Stewart, 2012; Manetti et al., 2014). In addition to psychotherapeutic strategies, pharmacotherapy is usually used as a first-line treatment for MDD, yet many patients do not sufficiently respond to monotherapy with an established medication, such as a selective serotonin reuptake inhibitor (SSRI) (Fava and Davidson, 1996). Some progress has been made in developing safe and efficacious antidepressant treatments and novel pharmacotherapy-based treatment strategies, such as ketamine or selective NMDA receptor subtype 2B (NR2B) antagonists (Serafini et al., 2015; Andrade, 2017) with mechanisms other than monoamine neurotransmitter reuptake inhibition. Ketamine was found to quickly reduce depressive symptoms within hours of a single administration, thus further demonstrating the important role of glutamate in the development of depression (Serafini et al., 2014). However, data on the remission and recurrence rates of

TRD under ketamine are still lacking. In summary, there currently seem to be no fundamental emerging innovations for the long-term treatment of MDD with antidepressant pharmacotherapy. Supportive, noninvasive add-on strategies, such as light-based therapy and exercise as well as alternative strategies, such as acupuncture and yoga, are used alongside pharmacological treatment strategies; however, their status within current treatment regimens is yet to be established, and many strategies are difficult to apply in an outpatient setting. Although evidence-based psychosocial interventions (Hunot et al., 2013; Hayes and Hofmann, 2017) are also under development, unfortunately, up to 50% of all patients with MDD do not achieve remission with currently available treatments (Zhou et al., 2015; Murphy et al., 2017). This subtype of MDD is classified as therapy-resistant depression (TRD) (Rush et al., 2006a,b; Mojtabai, 2017), which is defined by a lack of response or failure to fully respond or achieve remission after trials of at least two proven antidepressants with adequate dosing and duration (Bschor, 2010; Wiles et al., 2014; Holtzmann et al., 2016). At least one-third of all MDD patients are considered "therapy-resistant" (Rush et al., 2006a,b) (ongoing controversy discussed). Therefore, TRD disproportionally accounts for the largest proportion of the disease, underscoring the importance of innovative add-on therapy strategies for this particular type of TRD (McCullough, 2003; "Yoga for anxiety...", 2009; Rizzo et al., 2011; Oldham and Ciraulo, 2014; Lucas et al., 2017; Sakurai et al., 2017).

Add-on or augmentation therapy means the combination of first-line antidepressive pharmacotherapy with a second treatment approach. In addition to pharmacological add-on therapy, neurostimulation techniques are increasingly used. Today, the most promising neurostimulation tools used to treat TRD are (1) Electroconvulsive therapy (ECT), (2) Transcranial direct current stimulation (tDCS), (3) Repetitive transcranial magnetic stimulation (rTMS), (4) Deep brain stimulation (DBS), (5) Magnetic seizure therapy (MST), (6) Cranial electrotherapy stimulation (CES), and (7) Vagus nerve stimulation (VNS). Each has a different application procedure, and there is a large variation in their effects and the clinical expertise required.

This mini-review provides a comprehensive overview of neurostimulation-based treatment strategies with a special focus on VNS in TRD and finally, aims to provide practical clinical advice for their use when selecting TRD patients for add-on neurostimulation treatment strategies.

ADJUNCTIVE BIOLOGICAL OPTIONS FOR TREATING TRD ALONGSIDE ANTIDEPRESSANT PHARMACOTHERAPY

Augmentation Pharmacotherapy

Lithium

Lithium augmentation is (still) the state-of-the-art treatment in add-on and augmentative therapy with antidepressants when facing the challenge of TRD. Solid evidence from both large open-label and placebo-controlled trials highlights its efficacy in the treatment of resistant depression (Stage et al., 2007; Young, 2013; Nelson et al., 2014). Its notable effects include regulation of mood and circadian rhythms, and it also has a positive effect on suicidality and overall mortality. Lithium augmentation has significantly better antidepressant effects than the placebo, with a mean response rate of 41.2% (vs. 14.4%). Nevertheless, the risk of side effects (e.g., metabolic, cardiovascular, nephrologic) is significant, and its toxicity, especially when inadequate doses limit the clinical use of lithium, is notable (Edwards et al., 2013, 2014; Nelson et al., 2014; Hincapie-Castillo and Daniels, 2017).

Atypical Antipsychotics

Atypical antipsychotics comprise the most-studied class of augmenting agents for SSRIs and serotonin-norepinephrine reuptake inhibitors (SNRIs) for depression (Kato and Chang, 2013; Fornaro et al., 2016; Bartoli et al., 2017). The FDA has approved both quetiapine and aripiprazole as well as the combination of olanzapine with fluoxetine for augmentation. Other agents include ziprasidone and risperidone, which have also been shown to be effective in treating MDD/TRD (Gabriel, 2013; Nelson, 2015).

Patients treated with atypical antipsychotics are approximately twice as likely to reach remission as patients treated with the placebo, as highlighted in several studies (De Fruyt et al., 2012; Spielmans et al., 2013; Wright et al., 2013; Fornaro et al., 2016). The use of atypical antipsychotics involves a careful risk-benefit assessment because these agents possess serious short- and long-term treatment-emergent (potentiated through combination therapies) side effects (e.g., sedation, central obesity, metabolic syndrome, and extrapyramidal side effects) (Shirzadi and Ghaemi, 2006; Fraguas et al., 2008; Temmingh, 2012; Sykes et al., 2017).

Thyroid Augmentation

Thyroid hormones are an additional established option for the adjunctive treatment of TRD. Specifically, triiodothyronine (*T3*) is preferred for augmenting antidepressants due to its bioactivity in the CNS. In a meta-analysis of *T3* augmentation (25–50 μg/day) in probands who failed to respond to tricyclics, Aronson and colleagues found that *T3*-treated patients were twice as likely to respond as placebo-treated-patients (Aronson et al., 1996). In STAR*D, *T3* augmentation resulted in a 24.7% remission rate compared with a 15.9% remission rate for lithium augmentation in treatment-resistant patients who failed two previous antidepressant trials (Nierenberg et al., 2008; Warden et al., 2009). A disadvantage of T3 medication is its interference with thyroid metabolism in patients without hypothyroidism. Thus, treatment should be restricted to a few weeks, making this option unsuitable as a maintenance treatment (Cadieux, 1998).

Additional Agents Used for Pharmacologic Augmentation

A number of further drugs of diverse neuropsychopharmacological classes and properties are used as augmentation strategies of first-line antidepressive treatment for TRD. These drugs, which include bupropion, buspirone, methylphenidate, dopamine agonists, anticonvulsants, mirtazapine, modafinil, and pindolol (Dording, 2000), have been shown to possibly add to the antidepressive effect of

first-line antidepressive treatment for TRD when administered in combination therapy. However, the scientific evidence for most of these agents is still comparably limited. In a recent meta-analysis of pharmacological augmentation strategies (Zhou et al., 2015), bupropion, buspirone, lamotrigine, methylphenidate, and pindolol all failed to show a superior effect compared to placebo.

Neurostimulation Options

Some promising neurostimulation tools for TRD in addition to VNS are described below.

ECT and rTMS (which has lower effect sizes) still stand as the gold standards for treatment with level I evidence (Pagnin et al., 2004; Minichino et al., 2012; Berlim et al., 2013b). MST and tDCS seem to be an option, especially when serious side effects occur during treatment with ECT. For DBS, the data are still limited due to small study groups, but the available data and experiences are promising.

Electroconvulsive Therapy (ECT)

ECT is the oldest neurostimulation therapy for treating TRD. It has been widely used in large-scale clinical studies of depression and has been found to be more effective than antidepressant drug use alone. It is also the most common therapeutic option for severe and recurrent depression when medication and psychotherapy have been unsuccessful (Kellner et al., 2012; Berlim et al., 2013b; Kellner, 2014). Based on solid data from six trials, a meta-analysis concluded that real ECT is significantly more effective than simulated (sham) ECT (standardized effect size 0.91, 95% CI −1.27 to −0.54) (The UK ECT Review Group, 2003).

Patients are given general anesthesia and a muscle relaxant before ECT and are continuously monitored throughout the procedure. Then, an electric current used to stimulate cerebral brain regions induces a generalized central seizure. The electrode placement is relevant to both efficacy and the development of side effects. The symmetric bitemporal electrode placement, which covers a large brain volume and induces a high level of seizure generalization, has high efficacy but produces more side effects than other placements. Unilateral ECT, in which the electrodes are placed on the right temple and to the right of the vertex, lowers the seizure generalization, efficacy and side effects (Calev et al., 1995; Prudic, 2008; Sidhom and Youssef, 2014; Muller et al., 2017b).

In clinical practice, the acute ECT treatment phase typically comprising 3 treatments/week can be followed by a taper phase with a reduction to 1–2x/week and then to 1x/week for several weeks. Many patients will then receive further maintenance ECT with a single treatment every 3–6 weeks. Importantly, there is no evidence for a need to limit the lifetime number of treatments in patients who need ongoing treatment (Kellner et al., 2012).

Overall, it can be concluded that ECT is a valid therapy for the treatment of TRD, including its severe and resistant forms. After remission, ECT is often replaced with maintenance ECT (mECT) to prevent relapse. However, good clinical outcomes, are diminished through high relapse rates of up to 50%" (Rifkin, 1988; Kho et al., 2003; Charlson et al., 2012; Pinna et al., 2016). Therefore, there is a 57% relapse rate with optimized pharmacotherapy and a 65% rate after a successful ECT series. The relapse rate remains 37% despite optimized pharmacotherapy and lavish and costly mECT sessions (Kellner et al., 2006; Eschweiler et al., 2007; Post et al., 2015).

Magnetic Seizure Therapy (MST)

MST is a non-invasive convulsive neurostimulation therapy that induces an electric field in the brain and elicits a generalized tonic-clonic seizure. MST is being investigated as an alternative to ECT for use under general anesthesia with assisted ventilation and continuous electroencephalographic (EEG) monitoring. MST has the potential for fewer side effects, such as cognitive dysfunction, than ECT (Lisanby et al., 2003; Allan and Ebmeier, 2011), but optimal stimulation parameters for MST are still being investigated. Most studies have used a coil placed at the vertex with a frequency of stimulation of 100 Hz, a pulse width of 0.2–0.4 ms, and a stimulation duration of 10 s (Kito, 2017). There are no large-scale studies comparing MST to sham stimulation and no large-scale controlled studies of relapse following maintenance MST (mMST) with regard to prevention strategies, so the therapy is still in the experimental stage (Allan and Ebmeier, 2011).

Transcranial Direct Current Stimulation (tDCS)

In tDCS, cortical areas are stimulated non-invasively via a low-intensity direct current. Stimulation via sponge-based rectangular pads lasts for 10–20 min and modulates the neuronal excitability in target cerebral regions (Tschirdewahn et al., 2015; Palm et al., 2016b). The stimulation is focused on the left dorsolateral prefrontal cortex region (DLPFC) to minimize hypo-activity of the left DLPFC, which is a main target region in depression (Berlim et al., 2013a; Dell'Osso and Altamura, 2014; Meron et al., 2015). This therapy has almost no side effects and is well tolerated among all treatment groups. Stimulation of cortical regions may result in changes in membrane resting potentials and modify synaptic transmission in the DLPFC, which ultimately results in a significant, but only moderate, reduction of depression (Liebetanz et al., 2006; Palm et al., 2016a).

Repetitive Transcranial Magnetic Stimulation (rTMS)

Clinically used since the mid-80s, rTMS delivers external magnetic pulses to the cortex. These pulses induce an electrical potential in the brain tissue that depolarizes target neurons (Bulteau et al., 2017; McClintock et al., 2018). Stimulation can be high frequency (1 Hz) or low frequency (<1 Hz), and rTMS can also be used in the form of maintenance rTMS (mrTMS) (Rachid, 2018). Low-frequency rTMS inhibits certain cortical regions, whereas high-frequency rTMS activates the stimulated regions (Baeken et al., 2009; Bakker et al., 2015). It has been used to reduce depression, even in patients with medication-resistant major depression, with very few side effects and up to a 60% response rate, but has only a small antidepressant effect during follow-up after short and acute treatment in the absence of active maintenance treatment (Dell'osso et al., 2011; Kedzior et al., 2015). Similarly, rTMS response rates are poor

in patients for whom ECT has failed (Kedzior et al., 2017). These findings indicate that rTMS should be considered prior to pursuing ECT or as an add-on strategy and that patients who have not responded to ECT are unlikely to respond to rTMS treatment sessions alone (McClintock et al., 2018). The side effects of rTMS are mild and of short duration. Therefore, rTMS is a therapy that can be used for common depression treatment and is beneficial when combined with other standard treatments, such as pharmacotherapy and/or psychotherapy and other neurostimulation options (Perera et al., 2016). In recent years, there has also been growing evidence that, in addition to improvement of mood, rTMS might have a positive effect on cognitive functioning, which is often significantly reduced in patients with major depression. Aspects of cognitive performance reported to improve under rTMS include verbal memory, executive functioning, visuospatial ability, and recognition of facial expressions (Demirtas-Tatlidede et al., 2013). This may be an important advantage of rTMS, since cognitive impairment in MDD is insufficiently targeted by many other treatment options.

Deep Brain Stimulation (DBS)

DBS is an invasive neurosurgical procedure for TRD. The targeted approach involves stereotaxic placement of unilateral and/or bilateral electrodes in predefined brain regions. These electrodes are then connected to an implanted neurostimulator. Although the mode of action remains unclear, it is hypothesized that chronic, high-frequency stimulation (130–185 Hz) reduces cerebral neural transmission by inactivating voltage-dependent ion channels and clinically restores the activity of specific neuronal circuits involved in TRD ("Deep brain stimulation...", 2010; Cusin and Dougherty, 2012; Berlim et al., 2014). The targeted regions include the inferior thalamic peduncle, nucleus accumbens, lateral habenula, ventral striatum and subgenual cingulate cortex. Depending on the regions of interest, DBS is supposed to have antidepressant, strong antianhedonic, and antianxiety effects in TRD patients. It results in improvements related to social functioning, physical health and mood and anhedonic symptoms within TRD (Buhmann et al., 2017). No significant adverse effects of DBS (when implanted) have been recorded, thus highlighting DBS as promising in serious and chronic TRD. However, at this time only few clinical data sets with small sample sizes are available because the procedure is complex and requires direct brain surgery (Schlaepfer and Lieb, 2005; Kennedy et al., 2011; Jiménez et al., 2013; Lozano and Lipsman, 2013).

Cranial Electrotherapy Stimulation (CES)

In pulsed CES, low-amplitude electric currents (<1 mA) are broadly applied to the brain via scalp electrodes. CES has been approved for the treatment of anxiety, depression, and insomnia by the FDA (Gilula and Barach, 2004; Gunther and Phillips, 2010; Kavirajan et al., 2014). CES may affect the reticular activating system, the limbic system, and the hypothalamus (Kirsch and Nichols, 2013). How CES exerts its antidepressant effect is not fully understood. A recent study showed that CES could deactivate cortical brain activity and alter connectivity in the default-mode network (Kavirajan et al., 2014). Clinically, CES also seems to decrease comorbid depression in anxiety disorders (Feusner et al., 2012; Kirsch et al., 2014). However, a Cochrane library review indicates that methodologically rigorous studies of the antidepressant effects of CES in the treatment of acute depression are still lacking (Kavirajan et al., 2014). How CES modulates underlying neuroplasticity or signaling pathways also needs clarification.

Vagus Nerve Stimulation (VNS)

After decades of animal experimentation and application and after significant reductions in the frequency and severity of seizures were observed in response to stimulation of the vagus nerve, VNS was first applied in a human case of refractory epilepsy in 1988 (Rutecki, 1990; Uthman et al., 1990). VNS was then commercially approved for treatment of resistant epilepsy in 1997 (McLachlan, 1997; DeGiorgio et al., 2000; Henry, 2002). After showing its remarkable antidepressive clinical mode of action in a spin-off study and other controlled studies of TRD, it received approval for TRD in Europe and Canada in 2001–2005 (Sackeim et al., 2001; Topfer and Hailey, 2001; Marangell et al., 2002; Kosel and Schlaepfer, 2003). The therapy was then approved by the FDA for chronic depression and TRD in patients aged 18 years or older who do not respond to other antidepressant treatments (Nahas et al., 2006). Over 100,000 patients/year (both neurological and psychiatric indications) are treated worldwide (Cusin and Dougherty, 2012).

Surgical implantation is achieved by means of minor surgery, mainly neurosurgical, or otolaryngologic (Ng et al., 2010; Elliott et al., 2011).VNS requires an implantable pulse generator, which is surgically inserted under the skin of the chest and connected to an electrode placed in one of the vagus fibers in the neck. The repeatedly stimulated vagus nerve sends impulses from the periphery, where the electrode is placed, to the brain. Electrical stimulation of the vagus nerve centrally stimulates the nucleus tractus solitarius, which in turn is able to modulate multiple regions of the brain via its neuronal connections to anatomically distributed cortical and subcortical regions of the brain, the raphe nuclei and locus coeruleus, especially the limbic system. The right vagus nerve is not used because of the risk of potential severe bradycardia or arrhythmias. The left vagus nerve, whose fibers point to the central region, is used in VNS, which mainly stimulates the afferent fibers that communicate with the target regions to achieve improvement in mood. Therefore, this location is responsible for one of the main clinical effects of VNS.

In its mode of action, VNS modulates the concentrations of neurotransmitters (especially serotonin, norepinephrine, GABA and glutamate) and their metabolites while producing changes in the functional activity of CNS regions, which makes the mode of action of VNS similar to that of most antidepressants. Neuroimaging studies have shown evidence that activity in the thalamus and cortex in depressed patients is altered by VNS therapy. Changed activity in the orbital and ventromedial prefrontal cortices has also been recorded (Chae et al., 2003; Muller et al., 2013b). The most frequent acute complications of VNS implantation include temporary salivation, coughing, paralysis of the vocal cords, lower facial weakness, rarely

TABLE 1 | Neurostimulation options for treatment of TRD.

Technique	Main stimulation target region	Mode of action	Evidence	Pro	Con
ECT	Cerebral cortex	Small currents and generalized seizure induction	Strong	First line therapy for patients who failed in pharmacotherapy, rapid antidepressive effects, long-lasting clinical experiences	Relapse rates, effort, cognitive side effects
tDCS	Cerebral cortex	Anode and cathode sending constant low current (0.5–2 mA) directly to the brain	Weak-moderate	Non-invasive, rapid effects	Less clinical experience
rTMS	Cerebral cortex	Magnetic pulses to depolarize cerebral neurons	Strong	Non-invasive, approved	Relapse rates, effort, small effect sizes
DBS	Nucleus accumbens, lateral habenula, ventral striatum, inferior thalamic nucleus, peduncle, subgenual cingulate	High-frequency stimulation (130–185 Hz); reduction of neuronal transmission by inactivating voltage-dependent ion channels; modulation of neuronal circuits	Moderate, experimental	Probably highly effective	Implantation procedure
MST	Cerebral cortex	Based on ECT, probably effects increased glucose metabolism	Weak-moderate	Less side effects than ECT	No broad evidence
CES	Probably affects limbic system, reticular activating system, hypothalamus	Electrical currents (<1 mA)	Weak-moderate	Non-invasive, supposed antidepressive mode of action, FDA-approved	No broad evidence
VNS	Left peripheral vagus nerve	(Long-term) modulation of neurotransmitters	Moderate-strong	Anti-suicidal effects and rates of remittance, combination option with nearly all other treatment options, FDA-approved	Latency in antidepressive efficacy

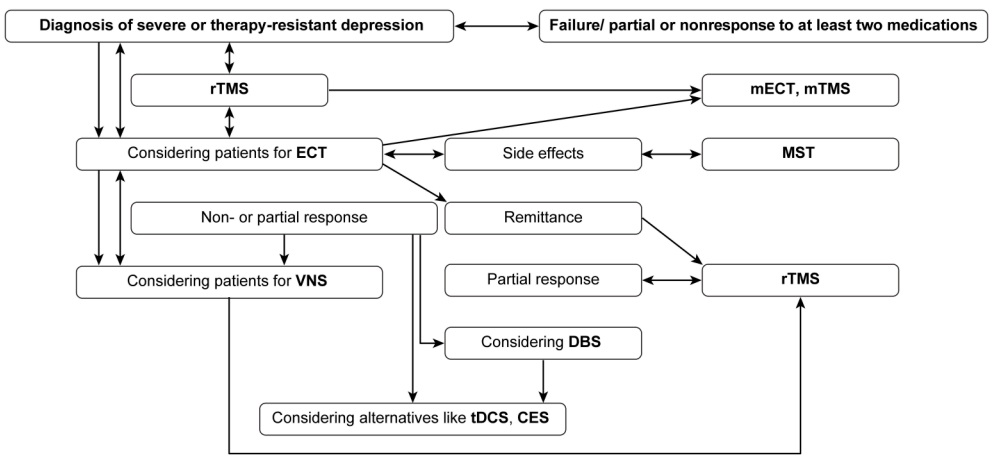

FIGURE 1 | Clinical pathways when choosing neurostimulation techniques.

bradycardia, and, very rarely, asystole; all side effects are generally fully reversible (Elliott et al., 2011; Schneider et al., 2015).

In a nutshell, there is growing and promising evidence for the use of VNS for depression in a 12-month trial. In a recent double-blind trial with 331 TRD patients, adjunct VNS at low (0.25 mA, 130 ls pulse width), medium (0.5–1.0 mA, 250 ls), and high (1.25–1.5 mA, 250 ls) currents was effective over 1 year (Aaronson et al., 2013; Feldman et al., 2013; Muller et al., 2013a).

Smaller studies also showed high levels of remittance of TRD over longer periods (>5 y) (Muller et al., 2013a, 2017a). Recently, Aaronson et al. provided a large set of data showing improved outcomes for adjunctive VNS observed in both ECT responders and non-responders. Within the D-23 VNS registry (489 in the VNS arm and 276 in the treatment-as-usual arm), cumulative remission, based on an MADRS total score, demonstrated that over time, patients in the VNS arm were significantly more likely to experience remission than those in the treatment-as-usual arm (43.3 and 25.7%, respectively), demonstrating significant efficacy. The MADRS is a popular scale because of its high inter-rater reliability and high sensitivity to detect changes in treatment effects. Due to these features, the MADRS has been widely used in mood disorder studies. Higher scores indicate greater symptom severity. As demonstrated in previous studies, the scale has good parallel form reliability. The 5-year cumulative response rate for patients in the VNS arm who had previously responded to ECT was 71.3% compared with 56.9% for the ECT responders in the treatment-as usual arm. For ECT non-responders in the VNS arm, the response rate was 59.6%, compared with 34.1% (95% for ECT non-responders in the treatment-as usual arm). These results show that VNS is promising, particularly, but not only, as a feasible adjunctive tool for ECT responders (Aaronson et al., 2017). In addition to the antidepressive mode of action, a remarkable finding is that VNS seems to have a specific lower all-cause mortality rate and an anti-suicidal effect (Aaronson et al., 2013, 2017; Berry et al., 2013). Therefore, the longer-term results of VNS are encouraging, and VNS can be considered for patients with chronic depression, particularly in situations where treatment resistance may be an issue. A limitation of the available studies on VNS stimulation cited above is the lack of a control group receiving sham stimulation. Sham stimulation is used as a placebo treatment in neurostimulation trials, i.e., specific sham coils, which mimic the feeling of the real stimulation procedure, are used in randomized controlled rTMS trials. Sham stimulation in VNS treatment is much more problematic on an ethical level not only because surgery is required but also because a long period of >6 months of sham stimulation would be required due to the delayed entry of treatment effects under VNS. This seems unethical in light of the seriousness of MDD, including the possible risk of suicide (Aaronson et al., 2013). Thus, the possibility cannot be excluded that a placebo effect influenced the results of the studies cited above. Nonetheless, due to the solid magnitude of effects and the addition of a control group receiving other antidepressive treatment to the large D-23 registry trial (Aaronson et al., 2017), it seems unlikely that the observed effects were due to the placebo effect alone.

CONCLUSION

Selection of Patients for Adjunctive Neurostimulation

The harm of chronic and TRD highlights the need for evidence-based adjunctive treatment options. ECT and others, especially/in addition to rTMS, are primarily delivered for seriously ill depressed probands. Alternative and/or add-on strategies, such as DBS or VNS, should be strongly recommended to patients (**Table 1**, **Figure 1**) as promising adjunctive options to ECT (the gold standard), especially when treatment resistance occurs. Additionally, the combination of rTMS and ECT is promising, and when side effects of ECT occur, MST is a possible alternative. Only ECT and rTMS have level I evidence for regular treatment; VNS is also approved for the indication group for which r-TMS and CES are FDA-approved.

Compared to other neurostimulation techniques, VNS has the advantages of more solid scientific evidence for efficacy compared to MST, tDCS and CES and, after initial implantation, a comparably small burden of time and effort for maintenance treatment compared to ECT and rTMS. Compared to maintenance ECT, VNS is also less invasive in the long term. However, a disadvantage of VNS is the delay of effects after implantation, with substantial treatment effects often only occurring after 3–12 months of treatment.

For MST, tDCS, and CES as adjunctive treatments alone, there is not yet sufficient evidence to recommend them in the first line, but as add-on strategies, they probably should be considered.

In summary, it seems that a special future focus should be placed on therapy based on powerful (especially when combined) augmentative neurostimulation options. Particularly because of the promising results from neurostimulation combination strategies (e.g., ECT followed by VNS and ECT/r-TMS), the expected augmentation effects of combining neurostimulation techniques should be strictly further evaluated in future controlled clinical studies.

AUTHOR CONTRIBUTIONS

HM and AP: Conceived the review's focus; HM, SM, AL, CL, and NB: Conducted the literature review; SM, HM, and NB: Designed the tables and figures; HM and AP: Wrote the first draft, summarized, and finalized the manuscript. All the authors critically commented on drafts, gave expert opinions on neurostimulation and approved the final manuscript.

REFERENCES

(2009). Yoga for anxiety and depression. Studies suggest that this practice modulates the stress response. *Harv. Ment. Health Lett.* 25, 4–5.

(2010). Deep brain stimulation shows promise for Alzheimer's, depression treatment. Doctors also now have more options in how DBS is used to treat Parkinson's disease. *Duke Med. Health News* 16, 1–2.

Aaronson, S. T., Carpenter, L. L., Conway, C. R., Reimherr, F. W., Lisanby, S. H., Schwartz, T. L., et al. (2013). Vagus nerve stimulation therapy randomized to different amounts of electrical charge for treatment-resistant depression: acute and chronic effects. *Brain Stimul.* 6, 631–640. doi: 10.1016/j.brs.2012.09.013

Aaronson, S. T., Sears, P., Ruvuna, F., Bunker, M., Conway, C. R., Dougherty, D. D., et al. (2017). A 5-year observational study of patients with treatment-resistant depression treated with vagus nerve stimulation or treatment as usual:

comparison of response, remission, and suicidality. *Am. J. Psychiatry* 174, 640–648. doi: 10.1176/appi.ajp.2017.16010034

Allan, C. L., and Ebmeier, K. P. (2011). The use of ECT and MST in treating depression. *Int. Rev. Psychiatry* 23, 400–412. doi: 10.3109/09540261.2011.614223

Andrade, C. (2017). Ketamine for depression, 4: in what dose, at what rate, by what route, for how long, and at what frequency? *J. Clin. Psychiatry* 78, e852–e857. doi: 10.4088/JCP.17f11738

Aronson, R., Offman, H. J., Joffe, R. T., and Naylor, C. D. (1996). Triiodothyronine augmentation in the treatment of refractory depression. A meta-analysis. *Arch. Gen. Psychiatry* 53, 842–848. doi: 10.1001/archpsyc.1996.01830090090013

Baeken, C., De Raedt, R., Van Hove, C., Clerinx, P., De Mey, J., and Bossuyt, A. (2009). HF-rTMS treatment in medication-resistant melancholic depression: results from 18FDG-PET brain imaging. *CNS Spectr.* 14, 439–448. doi: 10.1017/S1092852900020411

Bakker, N., Shahab, S., Giacobbe, P., Blumberger, D. M., Daskalakis, Z. J., Kennedy, S. H., et al. (2015). rTMS of the dorsomedial prefrontal cortex for major depression: safety, tolerability, effectiveness, and outcome predictors for 10 Hz vs. intermittent theta-burst stimulation. *Brain Stimul.* 8, 208–215. doi: 10.1016/j.brs.2014.11.002

Bartoli, F., Dell'Osso, B., Crocamo, C., Fiorillo, A., Ketter, T. A., Suppes, T., et al. (2017). Benefits and harms of low and high second-generation antipsychotics doses for bipolar depression: a meta-analysis. *J. Psychiatr. Res.* 88, 38–46. doi: 10.1016/j.jpsychires.2016.12.021

Beaucage, C., Cardinal, L., Kavanagh, M., and Aubé, D. (2009). Major depression in primary care and clinical impacts of treatment strategies: a literature review. *Sante. Ment. Que.* 34, 77–100. doi: 10.7202/029760ar

Berlim, M. T., McGirr, A., Van den Eynde, F., Fleck, M. P., and Giacobbe, P. (2014). Effectiveness and acceptability of deep brain stimulation (DBS) of the subgenual cingulate cortex for treatment-resistant depression: a systematic review and exploratory meta-analysis. *J. Affect. Disord.* 159, 31–38. doi: 10.1016/j.jad.2014.02.016

Berlim, M. T., Van den Eynde, F., and Daskalakis, Z. J. (2013a). Clinical utility of transcranial direct current stimulation (tDCS) for treating major depression: a systematic review and meta-analysis of randomized, double-blind and sham-controlled trials. *J. Psychiatr. Res.* 47, 1–7. doi: 10.1016/j.jpsychires.2012.09.025

Berlim, M. T., Van den Eynde, F., and Daskalakis, Z. J. (2013b). Efficacy and acceptability of high frequency repetitive transcranial magnetic stimulation (rTMS) versus electroconvulsive therapy (ECT) for major depression: a systematic review and meta-analysis of randomized trials. *Depress. Anxiety* 30, 614–623. doi: 10.1002/da.22060

Berry, S. M., Broglio, K., Bunker, M., Jayewardene, A., Olin, B., and Rush, A. J. (2013). A patient-level meta-analysis of studies evaluating vagus nerve stimulation therapy for treatment-resistant depression. *Med. Devices* 6, 17–35. doi: 10.2147/MDER.S41017

Bschor, T. (2010). Therapy-resistant depression. *Expert Rev. Neurother.* 10, 77–86. doi: 10.1586/ern.09.137

Buhmann, C., Huckhagel, T., Engel, K., Gulberti, A., Hidding, U., Poetter-Nerger, M., et al. (2017). Adverse events in deep brain stimulation: a retrospective long-term analysis of neurological, psychiatric and other occurrences. *PLoS ONE* 12:e0178984. doi: 10.1371/journal.pone.0178984

Bulteau, S., Sébille, V., Fayet, G., Thomas-Ollivier, V., Deschamps, T., Bonnin-Rivalland, A., et al. (2017). Efficacy of intermittent Theta Burst Stimulation (iTBS) and 10-Hz high-frequency repetitive transcranial magnetic stimulation (rTMS) in treatment-resistant unipolar depression: study protocol for a randomised controlled trial. *Trials* 18:17. doi: 10.1186/s13063-016-1764-8

Cadieux, R. J. (1998). Practical management of treatment-resistant depression. *Am. Fam. Physician* 58, 2059–2062.

Calev, A., Gaudino, E. A., Squires, N. K., Zervas, I. M., and Fink, M. (1995). ECT and non-memory cognition: a review. *Br. J. Clin. Psychol.* 34 (Pt 4), 505–515. doi: 10.1111/j.2044-8260.1995.tb01485.x

Chae, J. H., Nahas, Z., Lomarev, M., Denslow, S., Lorberbaum, J. P., Bohning, D. E., et al. (2003). A review of functional neuroimaging studies of vagus nerve stimulation (VNS). *J. Psychiatr. Res.* 37, 443–455. doi: 10.1016/S0022-3956(03)00074-8

Charlson, F., Siskind, D., Doi, S. A., McCallum, E., Broome, A., and Lie, D. C. (2012). ECT efficacy and treatment course: a systematic review and meta-analysis of twice vs. thrice weekly schedules. *J. Affect. Disord.* 138, 1–8. doi: 10.1016/j.jad.2011.03.039

Cusin, C., and Dougherty, D. D. (2012). Somatic therapies for treatment-resistant depression: ECT, TMS, VNS, DBS. *Biol. Mood Anxiety Disord.* 2:14. doi: 10.1186/2045-5380-2-14

De Fruyt, J., Deschepper, E., Audenaert, K., Constant, E., Floris, M., Pitchot, W., et al. (2012). Second generation antipsychotics in the treatment of bipolar depression: a systematic review and meta-analysis. *J. Psychopharmacol.* 26, 603–617. doi: 10.1177/0269881111408461

DeGiorgio, C. M., Schachter, S. C., Handforth, A., Salinsky, M., Thompson, J., Uthman, B., et al. (2000). Prospective long-term study of vagus nerve stimulation for the treatment of refractory seizures. *Epilepsia* 41, 1195–1200. doi: 10.1111/j.1528-1157.2000.tb00325.x

Dell'Osso, B., and Altamura, A. C. (2014). Transcranial brain stimulation techniques for major depression: should we extend TMS lessons to tDCS? *Clin. Pract. Epidemiol. Ment. Health* 10, 92–93. doi: 10.2174/1745017901410010092

Dell'osso, B., Camuri, G., Castellano, F., Vecchi, V., Benedetti, M., Bortolussi, S., et al. (2011). Meta-review of metanalytic studies with repetitive transcranial magnetic stimulation (rTMS) for the treatment of major depression. *Clin. Pract. Epidemiol. Ment. Health* 7, 167–177. doi: 10.2174/1745017901107010167

Demirtas-Tatlidede, A., Vahabzadeh-Hagh, A. M., and Pascual-Leone, A. (2013). Can noninvasive brain stimulation enhance cognition in neuropsychiatric disorders? *Neuropharmacology* 64, 566–578. doi: 10.1016/j.neuropharm.2012.06.020

Dording, C. M. (2000). Antidepressant augmentation and combinations. *Psychiatr. Clin. North Am.* 23, 743–755. doi: 10.1016/S0193-953X(05)70195-7

Edwards, S. J., Hamilton, V., Nherera, L., and Trevor, N. (2013). Lithium or an atypical antipsychotic drug in the management of treatment-resistant depression: a systematic review and economic evaluation. *Health Technol. Assess.* 17, 1–190. doi: 10.3310/hta17540

Edwards, S. J., Wakefield, V., Nherera, L., and Trevor, N. (2014). Systematic review and mixed treatment comparison of lithium or an atypical anti-psychotic (AAP) used to augment a selective serotonin reuptake inhibitor (SSRI) in treatment resistant depression (TRD). *Value Health* 17:A455. doi: 10.1016/j.jval.2014.08.1242

Effinger, J. M., and Stewart, D. G. (2012). Classification of co-occurring depression and substance abuse symptoms predicts suicide attempts in adolescents. *Suicide Life Threat. Behav.* 42, 353–358. doi: 10.1111/j.1943-278X.2012.00092.x

Elliott, R. E., Morsi, A., Tanweer, O., Grobelny, B., Geller, E., Carlson, C., et al. (2011). Efficacy of vagus nerve stimulation over time: review of 65 consecutive patients with treatment-resistant epilepsy treated with VNS > 10 years. *Epilepsy Behav.* 20, 478–483.

Eschweiler, G. W., Vonthein, R., Bode, R., Huell, M., Conca, A., Peters, O., et al. (2007). Clinical efficacy and cognitive side effects of bifrontal versus right unilateral electroconvulsive therapy (ECT): a short-term randomised controlled trial in pharmaco-resistant major depression. *J. Affect. Disord.* 101, 149–157. doi: 10.1016/j.jad.2006.11.012

Fava, M., and Davidson, K. G. (1996). Definition and epidemiology of treatment-resistant depression. *Psychiatr. Clin. North Am.* 19, 179–200. doi: 10.1016/S0193-953X(05)70283-5

Feldman, R. L., Dunner, D. L., Muller, J. S., and Stone, D. A. (2013). Medicare patient experience with vagus nerve stimulation for treatment-resistant depression. *J. Med. Econ.* 16, 62–74. doi: 10.3111/13696998.2012.724745

Feusner, J. D., Madsen, S., Moody, T. D., Bohon, C., Hembacher, E., Bookheimer, S. Y., et al. (2012). Effects of cranial electrotherapy stimulation on resting state brain activity. *Brain Behav.* 2, 211–220. doi: 10.1002/brb3.45

Fornaro, M., Stubbs, B., De Berardis, D., Perna, G., Valchera, A., Veronese, N., et al. (2016). Atypical antipsychotics in the treatment of acute bipolar depression with mixed features: a systematic review and exploratory meta-analysis of placebo-controlled clinical trials. *Int. J. Mol. Sci.* 17:241. doi: 10.3390/ijms17020241

Fraguas, D., Merchan-Náranjo, J., Laita, P., Parellada, M., Moreno, D., Ruiz-Sancho, A., et al. (2008). Metabolic and hormonal side effects in children and adolescents treated with second-generation antipsychotics. *J. Clin. Psychiatry* 69, 1166–1175. doi: 10.4088/JCP.v69n0717

Gabriel, A. (2013). Risperidone, quetiapine, and olanzapine adjunctive treatments in major depression with psychotic features: a comparative study. *Neuropsychiatr. Dis. Treat.* 9, 485–492. doi: 10.2147/NDT.S42745

Gilula, M. F., and Barach, P. R. (2004). Cranial electrotherapy stimulation: a safe neuromedical treatment for anxiety, depression, or insomnia. *South Med. J.* 97, 1269–1270. doi: 10.1097/01.SMJ.0000136304.33212.06

Gunther, M., and Phillips, K. D. (2010). Cranial electrotherapy stimulation for the treatment of depression. *J. Psychosoc. Nurs. Ment. Health Serv.* 48, 37–42. doi: 10.3928/02793695-20100701-01

Hayes, S. C., and Hofmann, S. G. (2017). The third wave of cognitive behavioral therapy and the rise of process-based care. *World Psychiatry* 16, 245–246. doi: 10.1002/wps.20442

Henry, T. R. (2002). Therapeutic mechanisms of vagus nerve stimulation. *Neurology* 59, S3–S14. doi: 10.1212/WNL.59.6_suppl_4.S3

Hincapie-Castillo, J. M., and Daniels, P. F. (2017). Use of lithium in patients with unipolar depression. *Lancet Psychiatry* 4, 662–663. doi: 10.1016/S2215-0366(17)30317-6

Holtzmann, J., Richieri, R., Saba, G., Allaïli, N., Bation, R., Moliere, F., et al. (2016). [How to define treatment-resistant depression?]. *Presse Med.* 45, 323–328. doi: 10.1016/j.lpm.2016.02.002

Hunot, V., Moore, T. H., Caldwell, D. M., Furukawa, T. A., Davies, P., Jones, H., et al. (2013). 'Third wave' cognitive and behavioural therapies versus other psychological therapies for depression. *Cochrane Database Syst. Rev.* CD008704. doi: 10.1002/14651858.CD008704.pub2

Jiménez, F., Nicolini, H., Lozano, A. M., Piedimonte, F., Salín, R., and Velasco, F. (2013). Electrical stimulation of the inferior thalamic peduncle in the treatment of major depression and obsessive compulsive disorders. *World Neurosurg.* 80, S30.e17– S30.e25. doi: 10.1016/j.wneu.2012.07.010

Kato, M., and Chang, C. M. (2013). Augmentation treatments with second-generation antipsychotics to antidepressants in treatment-resistant depression. *CNS Drugs* 27(Suppl. 1), S11–S19. doi: 10.1007/s40263-012-0029-7

Kavirajan, H. C., Lueck, K., and Chuang, K. (2014). Alternating current cranial electrotherapy stimulation (CES) for depression. *Cochrane Database Syst. Rev.* CD010521. doi: 10.1002/14651858.CD010521.pub2

Kedzior, K. K., Reitz, S. K., Azorina, V., and Loo, C. (2015). Durability of the antidepressant effect of the high-frequency repetitive transcranial magnetic stimulation (rTMS) In the absence of maintenance treatment in major depression: a systematic review and meta-analysis of 16 double-blind, randomized, sham-controlled trials. *Depress. Anxiety* 32, 193–203. doi: 10.1002/da.22339

Kedzior, K. K., Schuchinsky, M., Gerkensmeier, I., and Loo, C. (2017). Challenges in comparing the acute cognitive outcomes of high-frequency repetitive transcranial magnetic stimulation (HF-rTMS) vs. electroconvulsive therapy (ECT) in major depression: a systematic review. *J. Psychiatr. Res.* 91, 14–17. doi: 10.1016/j.jpsychires.2017.03.002

Kellner, C. (2014). Review: maintenance antidepressants reduce risk of relapse in the 6 months following ECT in people with major depression. *Evid. Based Ment. Health* 17:8. doi: 10.1136/eb-2013-101663

Kellner, C. H., Greenberg, R. M., Murrough, J. W., Bryson, E. O., Briggs, M. C., and Pasculli, R. M. (2012). ECT in treatment-resistant depression. *Am. J. Psychiatry* 169, 1238–1244. doi: 10.1176/appi.ajp.2012.12050648

Kellner, C. H., Knapp, R. G., Petrides, G., Rummans, T. A., Husain, M. M., Rasmussen, K., et al. (2006). Continuation electroconvulsive therapy vs. pharmacotherapy for relapse prevention in major depression: a multisite study from the Consortium for Research in Electroconvulsive Therapy (CORE). *Arch. Gen. Psychiatry* 63, 1337–1344. doi: 10.1001/archpsyc.63.12.1337

Kennedy, S. H., Giacobbe, P., Rizvi, S. J., Placenza, F. M., Nishikawa, Y., Mayberg, H. S., et al. (2011). Deep brain stimulation for treatment-resistant depression: follow-up after 3 to 6 years. *Am. J. Psychiatry* 168, 502–510. doi: 10.1176/appi.ajp.2010.10081187

Kho, K. H., van Vreeswijk, M. F., Simpson, S., and Zwinderman, A. H. (2003). A meta-analysis of electroconvulsive therapy efficacy in depression. *J. ECT* 19, 139–147. doi: 10.1097/00124509-200309000-00005

Kirsch, D. L., and Nichols, F. (2013). Cranial electrotherapy stimulation for treatment of anxiety, depression, and insomnia. *Psychiatr. Clin. North Am.* 36, 169–176. doi: 10.1016/j.psc.2013.01.006

Kirsch, D. L., Price, L. R., Nichols, F., Marksberry, J. A., and Platoni, K. T. (2014). Military service member and veteran self reports of efficacy of cranial electrotherapy stimulation for anxiety, posttraumatic stress disorder, insomnia, and depression. *US Army Med. Dep. J.* 46–54.

Kito, S. (2017). [Magnetic stimulation therapy for mood disorder]. *Brain Nerve* 69, 239–246. doi: 10.11477/mf.1416200733

Kosel, M., and Schlaepfer, T. E. (2003). Beyond the treatment of epilepsy: new applications of vagus nerve stimulation in psychiatry. *CNS Spectr.* 8, 515–521. doi: 10.1017/S1092852900018988

Lasserre, A. M., Strippoli, M. F., Glaus, J., Gholam-Rezaee, M., Vandeleur, C. L., Castelao, E., et al. (2017). Prospective associations of depression subtypes with cardio-metabolic risk factors in the general population. *Mol. Psychiatry* 22, 1026–1034. doi: 10.1038/mp.2016.178

Liebetanz, D., Fregni, F., Monte-Silva, K. K., Oliveira, M. B., Amâncio-dos-Santos, A., Nitsche, M. A., et al. (2006). After-effects of transcranial direct current stimulation (tDCS) on cortical spreading depression. *Neurosci. Lett.* 398, 85–90. doi: 10.1016/j.neulet.2005.12.058

Lisanby, S. H., Luber, B., Schlaepfer, T. E., and Sackeim, H. A. (2003). Safety and feasibility of magnetic seizure therapy (MST) in major depression: randomized within-subject comparison with electroconvulsive therapy. *Neuropsychopharmacology* 28, 1852–1865. doi: 10.1038/sj.npp.1300229

Lozano, A. M., and Lipsman, N. (2013). Probing and regulating dysfunctional circuits using deep brain stimulation. *Neuron* 77, 406–424. doi: 10.1016/j.neuron.2013.01.020

Lucas, N., Hubain, P., Loas, G., and Jurysta, F. (2017). Treatment resistant depression: actuality and perspectives in 2017. *Rev. Med. Brux.* 38, 16–25.

Manetti, A., Hoertel, N., Le Strat, Y., Schuster, J. P., Lemogne, C., and Limosin, F. (2014). Comorbidity of late-life depression in the United States: a population-based study. *Am. J. Geriatr. Psychiatry* 22, 1292–1306. doi: 10.1016/j.jagp.2013.05.001

Marangell, L. B., Rush, A. J., George, M. S., Sackeim, H. A., Johnson, C. R., Husain, M. M., et al. (2002). Vagus nerve stimulation (VNS) for major depressive episodes: one year outcomes. *Biol. Psychiatry* 51, 280–287. doi: 10.1016/S0006-3223(01)01343-9

Maske, U. E., Busch, M. A., Jacobi, F., Beesdo-Baum, K., Seiffert, I., Wittchen, H. U., et al. (2015). Current major depressive syndrome measured with the Patient Health Questionnaire-9 (PHQ-9) and the Composite International Diagnostic Interview (CIDI): results from a cross-sectional population-based study of adults in Germany. *BMC Psychiatry* 15:77. doi: 10.1186/s12888-015-0463-4

McClintock, S. M., Reti, I. M., Carpenter, L. L., McDonald, W. M., Dubin, M., Taylor, S. F., et al. (2018). Consensus recommendations for the clinical application of repetitive transcranial magnetic stimulation (rTMS) in the treatment of depression. *J. Clin. Psychiatry* 79:16cs10905. doi: 10.4088/JCP.16cs10905

McCullough, J. P. Jr. (2003). Treatment for chronic depression using Cognitive Behavioral Analysis System of Psychotherapy (CBASP). *J. Clin. Psychol.* 59, 833–846. doi: 10.1002/jclp.10176

McLachlan, R. S. (1997). Vagus nerve stimulation for intractable epilepsy: a review. *J. Clin. Neurophysiol.* 14, 358–368. doi: 10.1097/00004691-199709000-00002

Meron, D., Hedger, N., Garner, M., and Baldwin, D. S. (2015). Transcranial direct current stimulation (tDCS) in the treatment of depression: systematic review and meta-analysis of efficacy and tolerability. *Neurosci. Biobehav. Rev.* 57, 46–62. doi: 10.1016/j.neubiorev.2015.07.012

Michaud, C. M., Murray, C. J., and Bloom, B. R. (2001). Burden of disease–implications for future research. *JAMA* 285, 535–539. doi: 10.1001/jama.285.5.535

Minichino, A., Bersani, F. S., Capra, E., Pannese, R., Bonanno, C., Salviati, M., et al. (2012). ECT, rTMS, and deepTMS in pharmacoresistant drug-free patients with unipolar depression: a comparative review. *Neuropsychiatr. Dis. Treat.* 8, 55–64. doi: 10.2147/NDT.S27025

Mojtabai, R. (2017). Nonremission and time to remission among remitters in major depressive disorder: revisiting STAR*D. *Depress. Anxiety* 34, 1123–1133. doi: 10.1002/da.22677

Müller, H. H., Kornhuber, J., Maler, J. M., and Sperling, W. (2013a). The effects of stimulation parameters on clinical outcomes in patients with vagus nerve stimulation implants with major depression. *J. ECT* 29, e40–e42. doi: 10.1097/YCT.0b013e318290f7ed

Müller, H. H. O., Lücke, C., Moeller, S., Philipsen, A., and Sperling, W. (2017a). Efficacy and long-term tuning parameters of vagus nerve stimulation in long-term treated depressive patients. *J. Clin. Neurosci.* 44, 340–341. doi: 10.1016/j.jocn.2017.06.020

Müller, H. H. O., Reike, M., Grosse-Holz, S., Röther, M., Lücke, C., Philipsen, A., et al. (2017b). Electroconvulsive therapy hasn't negative effects on short-term memory function, as assessed using a bedside hand-held device. *Ment. Illn.* 9:7093. doi: 10.4081/mi.2017.7093

Müller, H. H., Reulbach, U., Maler, J. M., Kornhuber, J., and Sperling, W. (2013b). Facilitative effects of VNS on the motor threshold: implications for its antidepressive mode of action? *J. Neural. Transm.* 120, 1507–1510. doi: 10.1007/s00702-013-1043-8.

Murphy, J. A., Sarris, J., and Byrne, G. J. (2017). A review of the conceptualisation and risk factors associated with treatment-resistant depression. *Depress. Res. Treat.* 2017:4176825. doi: 10.1155/2017/4176825

Nahas, Z., Burns, C., Foust, M. J., Short, B., Herbsman, T., and George, M. S. (2006). Vagus nerve stimulation (VNS) for depression: what do we know now and what should be done next? *Curr. Psychiatry Rep.* 8, 445–451. doi: 10.1007/s11920-006-0049-4

Nelson, J. C. (2015). Adjunctive ziprasidone in major depression and the current status of adjunctive atypical antipsychotics. *Am. J. Psychiatry* 172, 1176–1178. doi: 10.1176/appi.ajp.2015.15091220

Nelson, J. C., Baumann, P., Delucchi, K., Joffe, R., and Katona, C. (2014). A systematic review and meta-analysis of lithium augmentation of tricyclic and second generation antidepressants in major depression. *J. Affect. Disord.* 168, 269–275. doi: 10.1016/j.jad.2014.05.053

Ng, W. H., Donner, E., Go, C., Abou-Hamden, A., and Rutka, J. T. (2010). Revision of vagal nerve stimulation (VNS) electrodes: review and report on use of ultra-sharp monopolar tip. *Childs Nerv. Syst.* 26, 1081–1084. doi: 10.1007/s00381-010-1121-2

Nierenberg, A. A., Alpert, J. E., Gaynes, B. N., Warden, D., Wisniewski, S. R., Biggs, M. M., et al. (2008). Family history of completed suicide and characteristics of major depressive disorder: a STAR*D (sequenced treatment alternatives to relieve depression) study. *J. Affect. Disord.* 108, 129–134. doi: 10.1016/j.jad.2007.10.011

Oldham, M. A., and Ciraulo, D. A. (2014). Bright light therapy for depression: a review of its effects on chronobiology and the autonomic nervous system. *Chronobiol. Int.* 31, 305–319. doi: 10.3109/07420528.2013.833935

Pagnin, D., de Queiroz, V., Pini, S., and Cassano, G. B. (2004). Efficacy of ECT in depression: a meta-analytic review. *J. ECT* 20, 13–20. doi: 10.1097/00124509-200403000-00004

Palm, U., Ayache, S. S., Padberg, F., and Lefaucheur, J. P. (2016a). [Transcranial direct current stimulation (tDCS) for depression: results of nearly a decade of clinical research]. *Encephale* 42, 39–47. doi: 10.1016/j.encep.2015.06.003

Palm, U., Hasan, A., Strube, W., and Padberg, F. (2016b). tDCS for the treatment of depression: a comprehensive review. *Eur. Arch. Psychiatry Clin. Neurosci.* 266, 681–694. doi: 10.1007/s00406-016-0674-9

Perera, T., George, M. S., Grammer, G., Janicak, P. G., Pascual-Leone, A., and Wirecki, T. S. (2016). The Clinical TMS Society consensus review and treatment recommendations for TMS therapy for major depressive disorder. *Brain Stimul.* 9, 336–346. doi: 10.1016/j.brs.2016.03.010

Pinna, M., Manchia, M., Oppo, R., Scano, F., Pillai, G., Loche, A. P., et al. (2016). Clinical and biological predictors of response to electroconvulsive therapy (ECT): a review. *Neurosci. Lett.* 669, 32–42. doi: 10.1016/j.neulet.2016.10.047

Post, T., Kemmler, G., Krassnig, T., Brugger, A., and Hausmann, A. (2015). [Efficacy of continuation and maintenance electroconvulsive therapy (c/m ECT) in the treatment of patients with therapy-resistant affective disorders: a retrospective analysis]. *Neuropsychiatrie* 29, 133–138. doi: 10.1007/s40211-015-0150-1

Prudic, J. (2008). Strategies to minimize cognitive side effects with ECT: aspects of ECT technique. *J. ECT* 24, 46–51. doi: 10.1097/YCT.0b013e31815ef238

Rachid, F. (2018). Maintenance repetitive transcranial magnetic stimulation (rTMS) for relapse prevention in with depression: a review. *Psychiatry Res.* 262, 363–372. doi: 10.1016/j.psychres.2017.09.009

Rifkin, A. (1988). ECT versus tricyclic antidepressants in depression: a review of the evidence. *J. Clin. Psychiatry* 49, 3–7.

Rizzo, M., Creed, F., Goldberg, D., Meader, N., and Pilling, S. (2011). A systematic review of non-pharmacological treatments for depression in people with chronic physical health problems. *J. Psychosom. Res.* 71, 18–27. doi: 10.1016/j.jpsychores.2011.02.011

Rush, A. J., Kraemer, H. C., Sackeim, H. A., Fava, M., Trivedi, M. H., Frank, E., et al. (2006a). Report by the ACNP Task Force on response and remission in major depressive disorder. *Neuropsychopharmacology* 31, 1841–1853. doi: 10.1038/sj.npp.1301131

Rush, A. J., Trivedi, M. H., Wisniewski, S. R., Nierenberg, A. A., Stewart, J. W., Warden, D., et al. (2006b). Acute and longer-term outcomes in depressed outpatients requiring one or several treatment steps: a STAR*D report. *Am. J. Psychiatry* 163, 1905–1917. doi: 10.1176/ajp.2006.163.11.1905

Rutecki, P. (1990). Anatomical, physiological, and theoretical basis for the antiepileptic effect of vagus nerve stimulation. *Epilepsia* 31(Suppl. 2), S1–S6. doi: 10.1111/j.1528-1157.1990.tb05843.x

Sackeim, H. A., Rush, A. J., George, M. S., Marangell, L. B., Husain, M. M., Nahas, Z., et al. (2001). Vagus nerve stimulation (VNS) for treatment-resistant depression: efficacy, side effects, and predictors of outcome. *Neuropsychopharmacology* 25, 713–728. doi: 10.1016/S0893-133X(01)00271-8

Sakurai, H., Suzuki, T., Yoshimura, K., Mimura, M., and Uchida, H. (2017). Predicting relapse with individual residual symptoms in major depressive disorder: a reanalysis of the STAR*D data. *Psychopharmacology* 234, 2453–2461. doi: 10.1007/s00213-017-4634-5

Schlaepfer, T. E., and Lieb, K. (2005). Deep brain stimulation for treatment of refractory depression. *Lancet* 366, 1420–1422. doi: 10.1016/S0140-6736(05)67582-4

Schneider, U. C., Bohlmann, K., Vajkoczy, P., and Straub, H. B. (2015). Implantation of a new Vagus Nerve Stimulation (VNS) Therapy(R) generator, AspireSR(R): considerations and recommendations during implantation and replacement surgery–comparison to a traditional system. *Acta Neurochir.* 157, 721–728. doi: 10.1007/s00701-015-2362-3

Serafini, G., Gonda, X., Rihmer, Z., Pompili, M., Girardi, P., Nasrallah, H. A., et al. (2015). NMDA receptor antagonists for depression: critical considerations. *Ann. Clin. Psychiatry* 27, 213–220.

Serafini, G., Howland, R. H., Rovedi, F., Girardi, P., and Amore, M. (2014). The role of ketamine in treatment-resistant depression: a systematic review. *Curr. Neuropharmacol.* 12, 444–461. doi: 10.2174/1570159X12666140619204251

Shirzadi, A. A., and Ghaemi, S. N. (2006). Side effects of atypical antipsychotics: extrapyramidal symptoms and the metabolic syndrome. *Harv. Rev. Psychiatry* 14, 152–164. doi: 10.1080/10673220600748486

Sidhom, E., and Youssef, N. A. (2014). Ultra-brief pulse unilateral ECT is associated with less cognitive side effects. *Brain Stimul.* 7, 768–769. doi: 10.1016/j.brs.2014.06.013

Slepecky, M., Kotianova, A., Prasko, J., Majercak, I., Gyorgyova, E., Kotian, M., et al. (2017). Which psychological, psychophysiological, and anthropometric factors are connected with life events, depression, and quality of life in patients with cardiovascular disease. *Neuropsychiatr. Dis. Treat.* 13, 2093–2104. doi: 10.2147/NDT.S141811

Spielmans, G.I., Berman, M.I., Linardatos, E., Rosenlicht, N.Z., Perry, A., and Tsai, A. C. (2013). Adjunctive atypical antipsychotic treatment for major depressive disorder: a meta-analysis of depression, quality of life, and safety outcomes. *PLoS Med.* 10:e1001403. doi: 10.1371/journal.pmed.1001403

Stage, K. B., Kristoffersen, J., and Sørensen, C. H. (2007). Lithium versus antidepressants in prevention of unipolar depression. A survey of a Cochrane review. *Ugeskr Laeger* 169, 3953–3955.

Sykes, D. A., Moore, H., Stott, L., Holliday, N., Javitch, J. A., Lane, J. R., et al. (2017). Extrapyramidal side effects of antipsychotics are linked to their association kinetics at dopamine D2 receptors. *Nat. Commun.* 8:763. doi: 10.1038/s41467-017-00716-z

Temmingh, H. S. (2012). Extrapyramidal side-effects and antipsychotics: are second-generation agents still indicated? *Br. J. Psychiatry* 201:247. doi: 10.1192/bjp.201.3.247

Tesio, V., Marra, S., Molinaro, S., Torta, R., Gaita, F., and Castelli, L. (2017). Screening of depression in cardiology: a study on 617 cardiovascular patients. *Int. J. Cardiol.* 245, 49–51. doi: 10.1016/j.ijcard.2017.07.065

The UK ECT Review Group (2003). Efficacy and safety of electroconvulsive therapy in depressive disorders: a systematic review and meta-analysis. *Lancet* 361, 799–808. doi: 10.1016/S0140-6736(03)12705-5

Topfer, L. A., and Hailey, D. (2001). Vagus nerve stimulation (VNS) for treatment-resistant depression. *Issues Emerg. Health Technol.* 25, 713–728.

Tschirdewahn, J., Vignaud, P., Pfeiffer, A., Nolden, J., Padberg, F., and Palm, U. (2015). Transcranial direct current stimulation (tDCS) for the treatment of depression. *MMW Fortschr. Med.* 157, 46–48. doi: 10.1007/s15006-015-7540-y

Uthman, B. M., Wilder, B. J., Hammond, E. J., and Reid, S. A. (1990). Efficacy and safety of vagus nerve stimulation in patients with complex partial seizures. *Epilepsia* 31(Suppl. 2), S44–S50. doi: 10.1111/j.1528-1157.1990.tb05849.x

Vandeleur, C. L., Fassassi, S., Castelao, E., Glaus, J., Strippoli, M. F., Lasserre, A. M., et al. (2017). Prevalence and correlates of DSM-5 major depressive and related disorders in the community. *Psychiatry Res.* 250, 50–58. doi: 10.1016/j.psychres.2017.01.060

Warden, D., Rush, A. J., Wisniewski, S. R., Lesser, I. M., Kornstein, S. G., Balasubramani, G. K., et al. (2009). What predicts attrition in second step medication treatments for depression?: a STAR*D Report. *Int. J. Neuropsychopharmacol.* 12, 459–473. doi: 10.1017/S1461145708009073

Wiles, N., Thomas, L., Abel, A., Barnes, M., Carroll, F., Ridgway, N., et al. (2014). Clinical effectiveness and cost-effectiveness of cognitive behavioural therapy as an adjunct to pharmacotherapy for treatment-resistant depression in primary care: the CoBalT randomised controlled trial. *Health Technol. Assess.* 18, 1–167, vii–viii. doi: 10.3310/hta18310

Wright, B. M., Eiland, E. H. III., and Lorenz, R. (2013). Augmentation with atypical antipsychotics for depression: a review of evidence-based support from the medical literature. *Pharmacotherapy* 33, 344–359. doi: 10.1002/phar.1204

Young, A. H. (2013). Review: lithium reduces the risk of suicide compared with placebo in people with depression and bipolar disorder. *Evid. Based Ment. Health* 16, 112. doi: 10.1136/eb-2013-101493

Zhou, X., Ravindran, A. V., Qin, B., Del Giovane, C., Li, Q., Bauer, M., et al. (2015). Comparative efficacy, acceptability, and tolerability of augmentation agents in treatment-resistant depression: systematic review and network meta-analysis. *J. Clin. Psychiatry* 76, e487–e498. doi: 10.4088/JCP.14r09204

Conflict of Interest Statement: HM received travel grants and speaker's compensation from LivaNova Germany within the last year.

The other authors declare that the research was conducted in the absence of any commercial or financial relationships that could be construed as a potential conflict of interest.

frontiers in Neuroscience

CLINICAL TRIAL
published: 24 April 2018
doi: 10.3389/fnins.2018.00225

Improvement of Olfactory Function With High Frequency Non-invasive Auricular Electrostimulation in Healthy Humans

Ashim Maharjan[1], *Eunice Wang*[2], *Mei Peng*[2] *and Yusuf O. Cakmak*[1,3,4]*

[1] Department of Anatomy, School of Biomedical Sciences, University of Otago, Dunedin, New Zealand, [2] Department of Food Science, University of Otago, Dunedin, New Zealand, [3] Brain Health Research Centre, Dunedin, New Zealand, [4] Medical Technologies Centre of Research Excellence, Auckland, New Zealand

In past literature on animal models, invasive vagal nerve stimulation using high frequencies has shown to be effective at modulating the activity of the olfactory bulb (OB). Recent advances in invasive vagal nerve stimulation in humans, despite previous findings in animal models, used low frequency stimulation and found no effect on the olfactory functioning. The present article aimed to test potential effects of non-invasive, high and low frequency vagal nerve stimulation in humans, with supplementary exploration of the orbitofrontal cortex using near-infrared spectroscopy (NIRS). Healthy, male adult participants (n = 18) performed two olfactory tests [odor threshold test (OTT) and supra-threshold test (STT)] before and after receiving high-, low frequency vagal nerve stimulation and placebo (no stimulation). Participant's olfactory functioning was monitored using NIRS, and assessed with two behavioral olfactory tests. NIRS data of separate stimulation parameters were statistically analyzed using repeated-measures ANOVA across different stages. Data from olfactory tests were analyzed using paired parametric and non-parametric statistical tests. Only high frequency, non-invasive vagal nerve stimulation was able to positively modulate the performance of the healthy participants in the STT ($p = 0.021$, Wilcoxon sign-ranked test), with significant differences in NIRS (p = 0.014, *post-hoc* with *Bonferroni correction*) recordings of the right hemispheric, orbitofrontal cortex. The results from the current article implore further exploration of the neurocircuitry involved under vagal nerve stimulation and the effects of non-invasive, high frequency, vagal nerve stimulation toward olfactory dysfunction which showcase in Parkinson's and Alzheimer's Diseases. Despite the sufficient effect size (moderate effect, correlation coefficient (r): 0.39 for the STT) of the current study, future research should replicate the current findings with a larger cohort.

Keywords: vagal nerve stimulation, olfaction, near-infrared spectroscopy, orbitofrontal cortex, non-invasive electrostimulation

OPEN ACCESS

Edited by:
Mikhail Lebedev,
Duke University, United States

Reviewed by:
Xiaoli Li,
Beijing Normal University, China
Marco Capogrosso,
University of Fribourg, Switzerland

***Correspondence:**
Yusuf O. Cakmak
yusuf.cakmak@anatomy.otago.ac.nz

Specialty section:
This article was submitted to Neural Technology, a section of the journal Frontiers in Neuroscience

Received: *05 December 2017*
Accepted: *22 March 2018*
Published: *24 April 2018*

Citation:
Maharjan A, Wang E, Peng M and Cakmak YO (2018) Improvement of Olfactory Function With High Frequency Non-invasive Auricular Electrostimulation in Healthy Humans. Front. Neurosci. 12:225. doi: 10.3389/fnins.2018.00225

Abbreviations: VOR, venous oxygen reserve; OTT, odor threshold test; STT, supra-threshold test; DMV, dorsal nucleus of the vagus nerve; OFC, orbitofrontal cortex; Pre-S, Pre-stimulation; S, stimulation; Post-S, post-stimulation; $VWrSO_2$, Venous Weighted percent of regional oxygen saturation.

INTRODUCTION

The olfactory system plays a fundamental role in our interactions with the environment, from detecting hazards to determining food consumption (Doty, 2012; Huart et al., 2013). Interconnected olfactory areas are responsible for various processes of the central nervous system in relation to smell, including memory (Velayudhan et al., 2013), spatial navigation (Alves et al., 2014), pleasure, mood and sensation (Sobel et al., 2003; Katata et al., 2009). Within the olfactory system, the olfactory bulb (OB) is the first communication structure responsible for processing smell. The olfactory nerve fibers, after arriving at the cranial cavity, connect to the mitral and tufted cells of the OB, and through the olfactory tract and olfactory tubercle, project to the olfactory cortex (Powell et al., 1965; Savic et al., 2000). The olfactory tract projects to the primary olfactory (cerebral) centers which includes the entorhinal cortex, piriform cortex and the parahippocampal gyrus, and then to the secondary olfactory (cerebral) centers which includes the hypothalamus, thalamus and the orbitofrontal cortex (OFC) (Savic et al., 2000; Sobel et al., 2003; Katata et al., 2009). An integral component of the olfactory system, the OFC, functions as the main neocortical projection, acting as a relay station for all arriving afferent inputs from numerous olfactory areas and sending feedback accordingly (Gottfried, 2006; Patel and Pinto, 2014).

Approximately half of the elderly population between the age of 65 and 80 years present olfactory impairments (Doty et al., 1984b; Duffy et al., 1995; Murphy et al., 2002). In addition, olfactory dysfunction is found to be a common complaint at the early stages of neurological diseases such as Alzheimer's disease (AD) and Parkinson' disease (PD), with more than 90% prevalence and higher incidence in men (Duff et al., 2002; Doty, 2012; Alves et al., 2014). Particularly with AD, odor discrimination (Fusetti et al., 2010) and identification abilities (Rezek, 1987; Motomura and Tomota, 2006), are impaired from the earliest stage of the disease. The presence of olfactory impairments at the early stage of AD has been linked to several factors occurring initially at the entorhinal cortex, one of the main terminals in the primary olfactory cortex. This includes the pathological compounds of AD (tau and amyloid precursor protein) (Naslund et al., 2000; Desikan et al., 2012), alongside reduction of cerebral blood volume (Khan et al., 2014) and thinning of cortical area (Fennema-Notestine et al., 2009; Karow et al., 2010; Velayudhan et al., 2013). Impairments in the entorhinal cortex is also seen as the link to olfactory dysfunction in the associated interconnected cortical regions (Khan et al., 2014).

In PD, impairments in odor detection (Doty, 2012), odor identification, odor discrimination (Mesholam et al., 1998) and olfactory supra-threshold measures (Doty and Kamath, 2014), are one of the earliest non-motor symptoms, preceding motor symptoms by several years (Ross et al., 2008; Doty, 2012). Impairments in PD are associated with the presence of lewy bodies, which represent distinctive inclusion bodies that underlie neuroanatomical dysfunctions in this condition. Lewy bodies are present from the earliest stage of PD, identified in the olfactory nucleus and the OB, but also in the dorsal nucleus of the vagus nerve (DMV) (Li et al., 2016). The spread of lewy bodies throughout the stages of PD, initially begins at the DMV, then spreads throughout the brainstem nuclei to the substantia nigra-pars compacta and finally the cortex (Braak et al., 2003; Doty, 2012; Li et al., 2016). This evidence points to an important connection between the vagus nerve and the olfactory processing areas of the cortex which is responsible for the early development of olfactory dysfunction in PD.

García-Díaz et al. (1984) conducted the very first study on animal models to demonstrate the capacity of invasive vagus nerve stimulation (VNS) in modulating the neuronal activity of the OB. This study showed that the ipsilateral OB neurons exhibited an increase in firing activity under high frequency (80 Hz) VNS but not under low frequency (20–40 Hz) VNS. In subsequent studies, invasive VNS in human patients with medically intractable epilepsy (Kirchner et al., 2004) and therapy-resistant depression (Sperling et al., 2011), used low frequency stimulation, where no significant effects of VNS on functional olfactory tests were found. Indeed, research has not yet addressed the question of whether high frequency VNS, as demonstrated in previous research on animal models (García-Díaz et al., 1984), is capable of modulating the olfactory performance in humans.

In a recent study, Frangos et al. (2015) has demonstrated that non-invasive VNS of the auricular branch of the vagus nerve via the left cymba conchae of the external ear, produced similar effects to invasive VNS. This finding highlights the potential benefits of using non-invasive VNS, similar to the application of invasive VNS in previous studies (García-Díaz et al., 1984; Kirchner et al., 2004; Sperling et al., 2011). To explore the potential benefits of high frequency VNS, based on a previous study using invasive VNS in animal models (García-Díaz et al., 1984), the present study aimed to examine the potential effects of non-invasive, high and low frequency VNS in humans, with supplementary exploration of OFC activation using near-infrared spectroscopy (NIRS).

METHODS

Participants

A total of 18 Caucasian male, healthy, non-smokers participated in this study (age range = 21–38 years, mean: 24.55 years, standard deviation: 3.8 years). The participants were asked to refrain from food and non-water beverage for 2 h prior to the experiment and abstain from applying any fragrance product/s on the day of the study. This study was carried out in accordance with the recommendations of 'Otago Human Participants Ethics Committee' with written informed consent from all subjects. All subjects gave written informed consent in accordance with the Declaration of Helsinki. The study is approved by Otago Human Participants Ethics Committee (Reference: H16/148) and registered to the Australian New Zealand clinical trials registry (ANZCTR; registration ID: ACTRN12617000034336).

Procedure

To measure and compare the participants in this study with the standard criteria required to meet the normative healthy

responses for odor identification and memory, put forward by Doty et al. (1984a), odor identification test (Sensonics International, Haddon Heights, NJ 08035 USA; **Table 1**) and odor discrimination/memory test (Sensonics International, Haddon Heights, NJ 08035 USA) were completed after the placebo session. Each participant attended three, 60 min sessions with a minimum of 24 h apart. The experimental room consists of an isolated environment where no additional olfactory or visual stimuli representing food or providing any distractions were present. The experimental room kept at steady temperature ($23 \pm 1^{\circ}C$). The participants were informed not to sniff during the olfactory tests to eliminate the potential effects of sniffing. The participant was seated opposite to the experimenter performing the olfactory tests and signed consent and exclusion criteria forms to qualify the participant for the study. A brief rundown of the experimental stages was given to the participant and a second experimenter conducted the stimulation (enforcing the double-blind design). Odor threshold test (OTT) and supra-threshold test (STT) were performed before and after VNS or placebo stimulation. **Figure 1** displays the experimental design of the current article. The current study followed a within participant design. In each session, participants were randomly assigned to one of the three experimental conditions: high frequency VNS, low frequency VNS or placebo session. Orders of experimental conditions were counterbalanced across the participants.

Odor Threshold Test (OTT)

Odor Threshold Test (OTT) was performed using "Snap and Sniff Olfactory Test System" (Sensonics International, Model: 02400, Hadden Heights, NJ)—a pen-like odor dispensing device. This testing battery comprises five blank-odor pens and 15 odorant pens (phenyl ethanol; concentration ranges: 10^{-2}—10^{-9}, 0.5log apart). Inter-stimuli-interval was approximately 3 s; the inter-trial-interval was approximately 20 s. The experimental procedure for the OTT followed that of previous studies (Hummel et al., 1997; Ehrenstein and Ehrenstein, 1999). Individual thresholds were estimated using the standard data analysis method for the staircase test, by averaging the concentrations at which the last four points occurred (Hummel et al., 1997).

Supra-Threshold Test (STT)

A sensory discrimination test was selected to assess olfactory perception in the supra-threshold range (Lawless and Heymann, 2010). This method is referred to as the STT in the current paper. The test used Vanillin as the odorant sample (Sensient; CAS number: 121-22-5; purity: 99%). A series of aqueous solutions with varying concentrations—8, 16, and 32 ppm—were prepared using a serial dilution method while blank samples were distilled water. The STT comprised of three trials. In each trial, five samples were presented to the participants, of which two were the target and others were blank samples. Participants were asked to identify both target samples. A delay of 30 s was implemented between stimuli, and a 1 min delay between trials. One point was awarded if the participants correctly identified both target odors on each trial and a maximum of three points could be awarded.

TABLE 1 | Results from the pre-screening odor identification test ($n = 18$) scoring the participants in the corresponding criteria determined by their scores on the tests.

Test score	Smell identification test
6–18 (Total Anosmia)	0
19–25 (Severe Anosmia)	1
26–29 (Moderate Anosmia)	0
30–33 (Mild Microsmia)	6
34–40 (Normosmia)	11

Vagal Nerve Stimulation

Non-invasive VNS was applied using "TENS ECO-2" (SCHWA-MEDICO, France) by the same experimenter, using transcutaneous electrical nerve stimulation (TENS) of three different parameters: high (80 Hz) frequency VNS, low (10 Hz) frequency VNS and placebo (no stimulation but the device was still attached). Previous studies on cranial nerves suggested that the parasympathetic nerve axons reach the human ear with the aid of two divisions of the auricular branch of the vagus nerve. One of the branches follows the external ear canal dispersing predominantly to the cavum and cymba conchae area of the auricular skin while the second branch travels through the posterior auricular nerve of the facial nerve, following the trajectory of the posterior auricular nerve (Schuknecht, 1974; Lang, 1983; Mulazimoglu et al., 2017). For this reason, the VNS in the current study was applied to the internal (covering the cavum concha and extending to cymba concha) and external portions of the ear (**Figures 2a–c**). This enforced stimulation to both branches of the auricular branch of the vagus nerve. The left vagus nerve is the preferred side of stimulation as it avoids cardiac effects, in comparison to the right vagus nerve which innervates the cardia atria (Henry, 2002). The strength of the VNS stimulation (amplitude) was between 10 and 15 milliamps and the pulse bandwidth was 180 μs in square waveform. The stimulation was only continued if there was no perceived pain by the participant.

Near-Infrared Spectroscopy (NIRS)

NIRS (COVIDIEN INVOS OXIMETER, Model 5100C-PA, Mansfield, MA) was used to measure participants' activity from the OFC (set up as shown in **Figure 2**). Although electroencephalography (EEGs) have been used to detect different patterns of odor effects in past literature, this methodology runs the risk of misinterpretation of data due to spatial smearing, which occurs during recording of the scalp EEGs. In addition, EEGs does not provide the high spatiotemporal resolution that is supported by the NIRS (Harada et al., 2006). Several studies have displayed the effectiveness of the NIRS in monitoring the activation of the OFC under olfactory stimulus (Hongo et al., 1995; Cho et al., 1998; Edmonds et al., 1998; Ishimaru et al., 2004; Harada et al., 2006; Kobayashi et al., 2012). Specifically, Harada et al. (2006), Ishimaru et al. (2004), and Kobayashi et al. (2012), have suggested that functional magnetic resonance

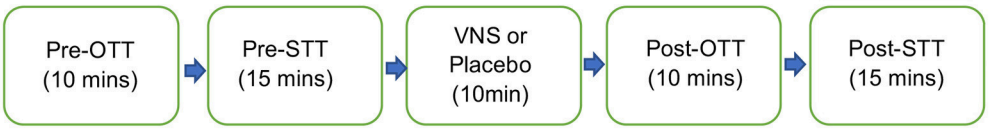

FIGURE 1 | Schematic sequence of each stage of the experiment. OTT, Odor Threshold Test; STT, Supra-Threshold Test. A brief 5-min introduction, prior to the experiment comprised of obtaining participant's consent and device set up.

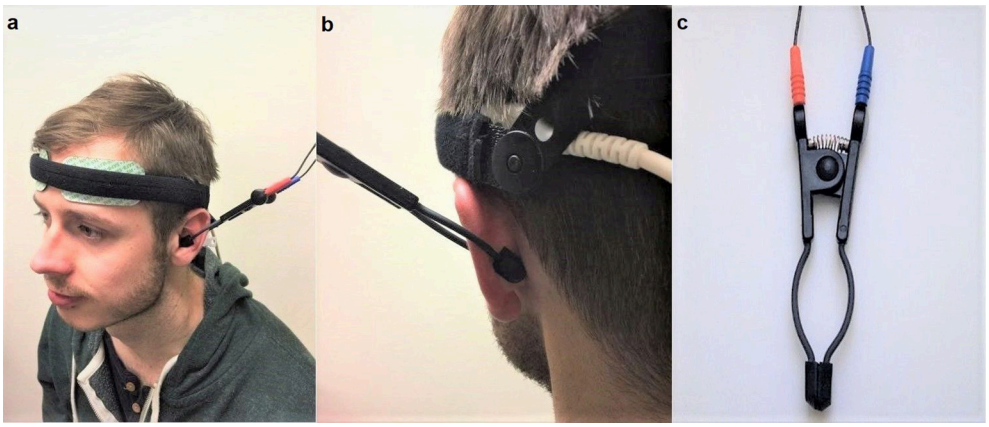

FIGURE 2 | (a) (Left) Set up of the near-infrared spectroscopy (NIRS) electrodes on the forehead. Location and set-up of the non-invasive VNS (Auricular TENS) electrode in the cavum and cymba conchae area of the external ear. **(b)** (Right) shows location of the non-invasive VNS (auricular TENS) electrode in posterior aspect of the external ear in the current experiment. **(c)** shows the auricular TENS electrode (Schwa-Medico, France). Written informed consent was obtained from the participant for the publication of this image.

imaging (fMRI) localization of olfactory expression is under the lateral and anterior orbito-frontal gyri of the frontal lobe. On the basis of this information, Harada et al. (2006) placed the NIRS recording over the orbito-frontal region (secondary olfactory cortex), with the supplementary exploration of other regions (the temporal, parietal and occipital lobes) and found that oxygenated hemoglobin (HbO2) concentration increased only over the orbito-frontal region during olfactory stimulation.

Regional hemoglobin oxygen saturation (rSO_2) monitoring NIRS systems permit the continuous and non-invasive measurement of the cerebral regional oxygen balance in the cortex. NIRS, briefly, is a useful non-invasive method of monitoring regional tissue oxygenation. By using the modified Beer-Lambert law for the light attenuation changes through the illuminated tissue, NIRS sequentially detects concentration changes of oxygenated and deoxygenated hemoglobin in the brain. As oxygenated hemoglobin concentration represents an increase in blood flow, this, in turn reflects neuronal activation measured by the NIRS (Harada et al., 2006). The INVOS monitors the cortical activity while excluding information from the skin and scalp blood flow. The INVOS system sensors uses two near-infrared light sources at 2 different wavelengths (730 and 810 nm) and two photodiode detectors at a distance. Light travels from the sensor's light emitting diode to either a proximal or distal detector in parabolic path, permitting separate data processing of shallow and deep optical signals with an algorithm of subtraction of the short travel distance of the light from the longer distance of travel in order to eliminate the contribution of the skin and scalp. The INVOS system's ability to localize the area of measurement with the process of suppressing the influences of extra-cerebrally reflected photons, called spatial resolution, has been empirically validated in human subjects (Hongo et al., 1995). It uses a clinically validated algorithm that allows absolute, real time data accuracy from the cortex with its multi-sensors on the same sensor (Hongo et al., 1995; Cho et al., 1998; Edmonds et al., 1998, 2004; Roberts et al., 1998; Higami et al., 1999; Singer et al., 1999; Yao et al., 2001; Alexander et al., 2002; Iglesias et al., 2003). INVOS measures both the venous and arterial blood in a 3:1 ratio to monitor cortical activity. In this context, INVOS measures the venous-weighted percent of rSO_2 ($VWrSO_2$) in the cortex, which provides real-time information concerning the balance of oxygen supply and demand and in turn, calculates the venous oxygen reserve (VOR) that reflects the remaining oxygen after extraction by tissues and vital organs (Hongo et al., 1995; Cho et al., 1998; Edmonds et al., 1998, 2004; Roberts et al., 1998; Higami et al., 1999; Singer et al., 1999; Yao et al., 2001; Alexander et al., 2002; Iglesias et al., 2003). This system allows a sensitive and real-time measurement of VOR (measured as $VWrSO_2$). In addition, the quality of INVOS system recording can be assessed by inspection of the signal strength index (SSI) for each channel by 5 unit bar scale system. Any stable SSI signal display of >1

bar is reported to be strong and stable enough to generate an accurate $VWrSO_2$ [Chapter 6.4.16 and 11.7.4 in the INVOS NIRS 5100c manual (Covidien, 2013)]. The SSI bar were monitored throughout the recordings to ensure the highest quality of signal (5/5 SSI). We used disposable INVOS electrodes for each participant to ensure hygiene and data quality. In addition to self-adhesive feature of the disposable INVOS sensors, we also improved the stabilization of the electrodes and cables with a rigid head band (**Figure 2**).

In the context of the extensive literature and clinical validation studies, we used FDA approved INVOS NIRS for the present study. With the NIRS, each section of the experiment was mapped, to ensure that each part of the experiment (*experimental stages shown in* **Figure 1**) could have an average (mean) recording of $VWrSO_2$ (that represents VOR) for the participant from the left and right hemisphere of the OFC.

Data Analysis

Data from the NIRS device was transferred to the INVOS software which accommodated data presentation. We used average (mean) recordings of $VWrSO_2$ data of specific time periods marked for each segment of each session which was in line with the previous research (Cho et al., 1998; Murkin et al., 2007). Repeated-measures analyses of variance (ANOVA) were applied separately to data obtained from three stimulation parameters (High VNS, low VNS and placebo) for assessing $VWrSO_2$ changes in the left and right hemispheric OFC across stages of the experiment (pre-stimulation, stimulation and post-stimulation) within participants ($n = 18$). Specifically, the repeated-measures ANOVA was applied to STT and OTT periods separately in order to provide synchronized analyses of NIRS data with the functional olfactory tests and stimulation (i.e., preSTT-Stimulation-postSTT periods of NIRS and preOTT-Stimulation-postOTT periods of NIRS). In addition to this 3-stage analysis of NIRS, an additional 5-stage analysis of NIRS (preOTT-preSTT-Stimulation-postOTT-postSTT, in the order of experiment, see **Figure 1**) were also performed to reveal any potential influence of OTT over STT (if any). Post hoc test using pairwise comparison with *Bonferroni correction*, was applied to understand any significance at alpha level of 5% in all ANOVA tests. To insure the baseline activity was consistent across three different stimulation parameters for OTT, STT, and NIRS data, repeated measures ANOVA was also applied to data that obtained at pre-stimulation stage (**Table 2**).

For data obtained from the olfactory tests, normality tests using the *Shapiro-Wilk correction* (Ghasemi and Zahediasl, 2012) were performed on the differences between the scores before and after stimulation for all three parameters (High VNS, low VNS, and placebo). This test was separately applied to the STT and OTT data. Data for participants under low frequency VNS and placebo stimulation for OTT and for participants under placebo stimulation for STT, passed the normality test ($p > 0.05$). Thus, a paired sample *t*-test was performed on these data. The rest of the data (high frequency VNS for both OTT and STT tests, and low frequency VNS for STT test) failed the normality test ($p < 0.05$), so a non-parametric (Wilcoxon signed rank test- Gibbons and Chakraborti, 2011) was performed for this set of data. All the analyses were performed using SPSS software (IBM SPSS Statistics, Ver. 20, St Leonards, NSW).

RESULTS

Pre-screening Olfactory Test Results

The results from the odor identification and memory tests used to ensure that the healthy participants in the current study represented the standard criteria required to meet the normative healthy responses for odor identification (**Table 1**) and memory tests (Doty et al., 1984a, 1995). Seven of the eighteen participants displayed values outside of Normosmia, but none of the participants displayed total anosmia which was the exclusion criteria for the current study in line with the past olfactory research (Doty et al., 1984a, 1995). In this context, all the participants were eligible for the current study.

OTT Results With 3-Stage (PreOTT-Stimulation-PostOTT) Analysis of NIRS Data

Figure 3 shows each participant ($n = 18$) results from the OTT, before and after VNS stimulation, for all three stimulation parameters (high- and low frequency VNS and placebo). There was no significant difference in the performance of the OTT after VNS stimulation under any of the three stimulation parameters [high frequency VNS, $p = 0.523$ (Wilcoxon signed-rank test); low frequency VNS, $p = 0.186$ (paired sample *t*-test); placebo stimulation, $p = 0.904$ (paired sample *t*-test)]. Individual results are provided in **Figure 3**. In the NIRS recording of the OFC in the left and right hemispheres during the OTT, there were no significant differences in $VWrSO_2$ (%) under all three stimulation parameters in all three stages of the experiment (Pre-S, S, Post-S) (left hemisphere High frequency VNS, $p = 0.643$; left hemisphere Low frequency VNS, $p = 0.570$; left hemisphere Placebo, $p = 0.061$; right hemisphere High frequency VNS, $p = 0.233$; right hemisphere Low frequency VNS, $p = 0.565$; right hemisphere Placebo, $p = 0.098$). Individual results are presented in **Figure 3**.

STT Results With 3-Stage (PreSTT-Stimulation-PostSTT) Analysis of NIRS Data

Figure 4 shows each participant ($n = 18$) results from the STT, before and after VNS stimulation, for all three stimulation parameters (high- and low frequency VNS and placebo). There were significant differences in the STT scores after high frequency VNS [$p = 0.021$ (Wilcoxon signed-rank test), correlation coefficient (r): 0.39] but not under the low frequency VNS [$p = 0.439$ (Wilcoxon signed-ranked test) or placebo stimulation ($p = 0.083$ (paired sample *t*-test)]. Individual results are presented in **Figure 4**. In the NIRS recording of the OFC in the right hemisphere, there were significant differences in $VWrSO_2$ (%) between the three stages of the experiment after high frequency VNS ($p = 0.031$). *Post-hoc* tests using the *Bonferroni correction* revealed that there were significant differences in NIRS OFC recording on the right hemisphere between Pre-S stage

TABLE 2 | Results of the repeated-measures ANOVA that assessed the potential difference (if any) of olfactory test (OTT, STT) and also the NIRS ($VWrSO_2$) data in all of the three different stimulation parameters (high- and low frequency VNS and placebo) at the pre-stimulation stage of testing.

Olfactory tests and NIRS recordings (h = hemisphere)	Stimulation (H = High, L = Low and P = Placebo)	Mean	S.D.	*F*-value DF (1, 17)	*P*-value
Pre-S OTT scores	H	6.02	1.41	0.099	0.889
	L	5.83	1.71		
	P	5.92	1.53		
Pre-S STT scores	H	1.55	1.20	2.006	0.152
	L	1.78	0.94		
	P	2.11	0.76		
Left-h $VWrSO_2$ at Pre-S OTT	H	76.72	9.73	1.156	0.319
	L	76.23	8.48		
	P	74.72	9.84		
Right-h $VWrSO_2$ at Pre-S OTT	H	76.91	9.05	2.129	0.142
	L	78.04	9.81		
	P	75.55	9.74		
Left-h $VWrSO_2$ at Pre-S STT	H	76.65	9.49	1.663	0.210
	L	75.58	8.85		
	P	74.26	9.91		
Right-h $VWrSO_2$ at Pre-S STT	H	77.35	10.06	2.016	0.156
	L	76.21	9.09		
	P	74.75	10.59		

S.D., standard deviation; DF, Degrees of Freedom. STT scores range = 0–3, OTT scores range = 2–9. H, hemisphere; H, High Frequency Stimulation; L, Low frequency Stimulation; P, Placebo.

and S stage ($p = 0.014$). There were no significant differences in $VWrSO_2$ (%) between the three stages of the experiment after high frequency VNS in the left hemisphere ($p = 0.253$), or after low frequency VNS in both hemispheres (left hemisphere, $p = 0.693$; right hemisphere, $p = 0.732$) or after placebo (left hemisphere, $p = 0.697$; right hemisphere, $p = 0.849$). Individual results are presented in **Figure 4**. Additional scatterplot chart of each individual participant, before and after stimulation parameters (high frequency VNS, low frequency VNS and placebo stimulation), STT scores and the corresponding right hemispheric OFC NIRS recordings (pre-stimulation, stimulation and post-stimulation) are provided as **Supplementary Files 1–3**.

5-Stage (PreOTT-PreSTT-Stimulation-PostOTT-PostSTT) Analysis of NIRS

An additional ANOVA analysis of the 5-stage NIRS periods (preOTT-preSTT-Stimulation-postOTT-postSTT, **Figure 1**.) in the order of experiments for all stimulation parameters (low, high and placebo) for the right and left hemisphere demonstrated a significance only in the high frequency stimulation group for the right hemisphere (p:0.037) and pairwise comparisons demonstrated the significance (p:0.046, *post-hoc* tests using the *Bonferroni correction*) only in between the preSTT and stimulation periods of NIRS in this group, similar to the results derived from the 3-stage (preOTT-Stimulation-PostOTT and preSTT-Stimulation-postSTT) analysis of NIRS.

Pre-stimulation, Intergroup Differences From OTT and STT, and Respective NIRS Recordings From OFC

Table 2 displays results of the repeated-measures ANOVA that assessed the potential difference (if any) of olfactory test (OTT, STT) and also the NIRS ($VWrSO_2$) data in all of the three different stimulation parameters (high, low frequency VNS and placebo) at the pre-stimulation stage of testing. There was no significant difference in the pre-stimulation stage for both olfactory tests and NIRS $VWrSO_2$ (%) data under any stimulation parameter (**Table 2**).

DISCUSSION

The current study tested the effects of non-invasive, high and low frequency VNS on olfactory sensory tests in healthy adult participants, with the addition of functional imaging technique in the OFC. To our knowledge, this was the first data suggesting non-invasive high frequency (80 Hz) VNS can positively modulate olfactory performance in healthy participants. Indeed, olfactory performance was improved after the implementation of high frequency VNS in the STT, although

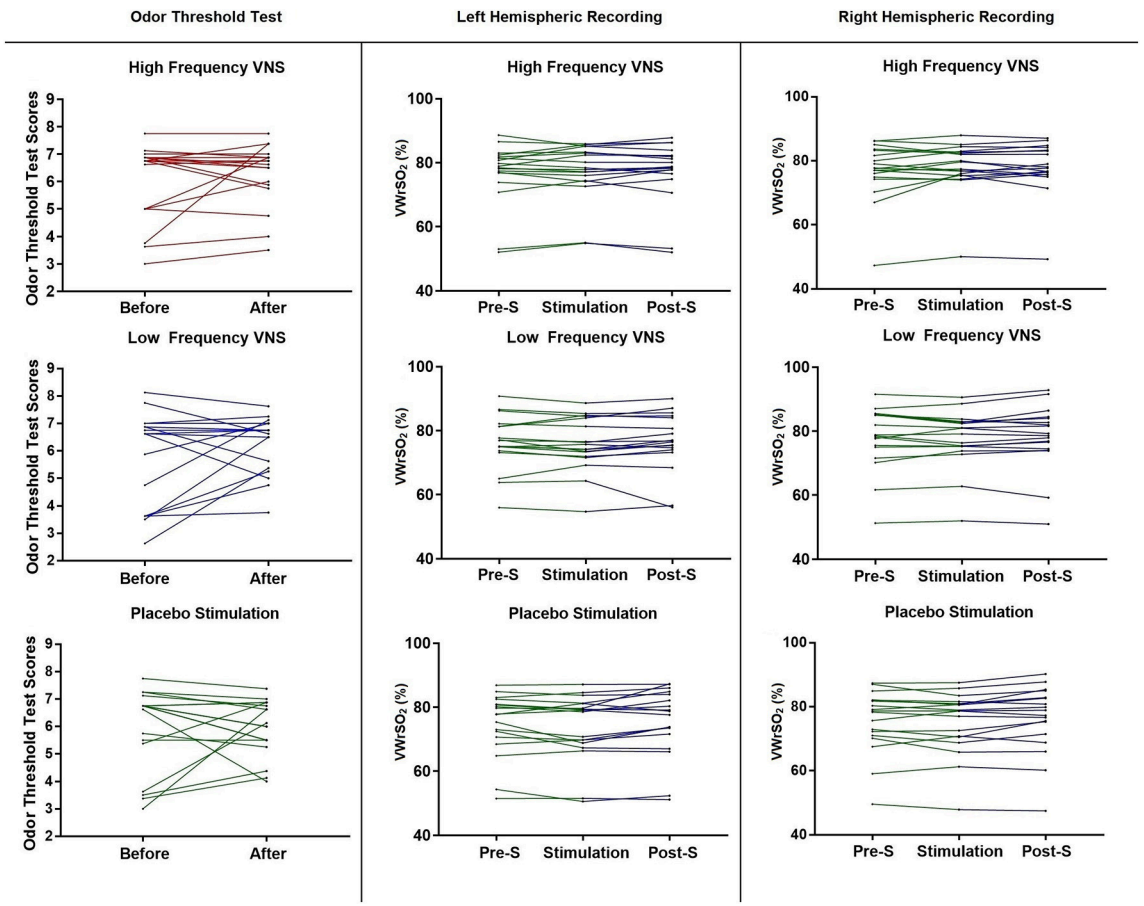

FIGURE 3 | Each participant's scores, before and after each of the stimulation parameters (high frequency VNS, low frequency VNS and placebo) for the OTT, and each participant's recordings for all three stages of the experiment (pre-stimulation OTT; Pre-S, stimulation and post-stimulation OTT; Post-S) for each stimulation parameter (high frequency VNS, low frequency VNS and placebo) from both the left and the right hemispheres of the OFC, measuring venous oxygen reserve-($VWrSO_2$ %) using NIRS. OTT scores range = 2–9.

not in the OTT. In contrast, non-invasive low frequency (10 Hz) VNS and placebo did not show any effect on modulating performance in the olfactory sensory tests. These results were supported by increased $VWrSO_2$ in the NIRS recordings of the OFC in the right hemisphere.

In the current article, non-invasive, low frequency VNS did not change the ability to influence olfactory function in the healthy participants. This result is in line with previous research using invasive, low frequency VNS on humans (Kirchner et al., 2004; Sperling et al., 2011). It should be stated that previous studies in humans were performed on patients with medically intractable epilepsy (Kirchner et al., 2004) or patients with therapy-resistant depression (Sperling et al., 2011), not healthy controls. The use of invasive low frequency VNS in these previous articles fitted the stimulation parameters for patients with medically intractable epilepsy (Kirchner et al., 2004) and therapy-resistant depression (Sperling et al., 2011) instead of stimulation parameters that could potentially impact olfactory function. As the previous articles in VNS used invasive procedures on patients requiring VNS therapy rather than healthy controls, it was infeasible to access different VNS of higher frequencies. This includes the exploration of high frequency VNS of 80 Hz, which in previous animal models showed to be effective in modulating the activity of the OB (García-Díaz et al., 1984).

In contrast to the low frequency VNS, non-invasive, high frequency VNS was demonstrated to result in significant improvements on STT performance. This is in support of previous research where low and high frequency stimulation had opposite autonomic nerve system responses in previous human studies of peripheral nerve stimulation (Cakmak et al., 2008, 2016, 2017; Zhao, 2008). Previous studies have reported that different olfactory measures such as the odor identification test, odor recognition test or the OTT could be processed under the same cortical/subcortical areas associated with olfaction (Mesholam et al., 1998). Furthermore, in healthy participants, olfactory functioning from the OTT was highly correlated with that of the odor identification test (Doty et al., 1989, 1994). However, in both these articles, there were no measures observing the olfactory functioning through the STT.

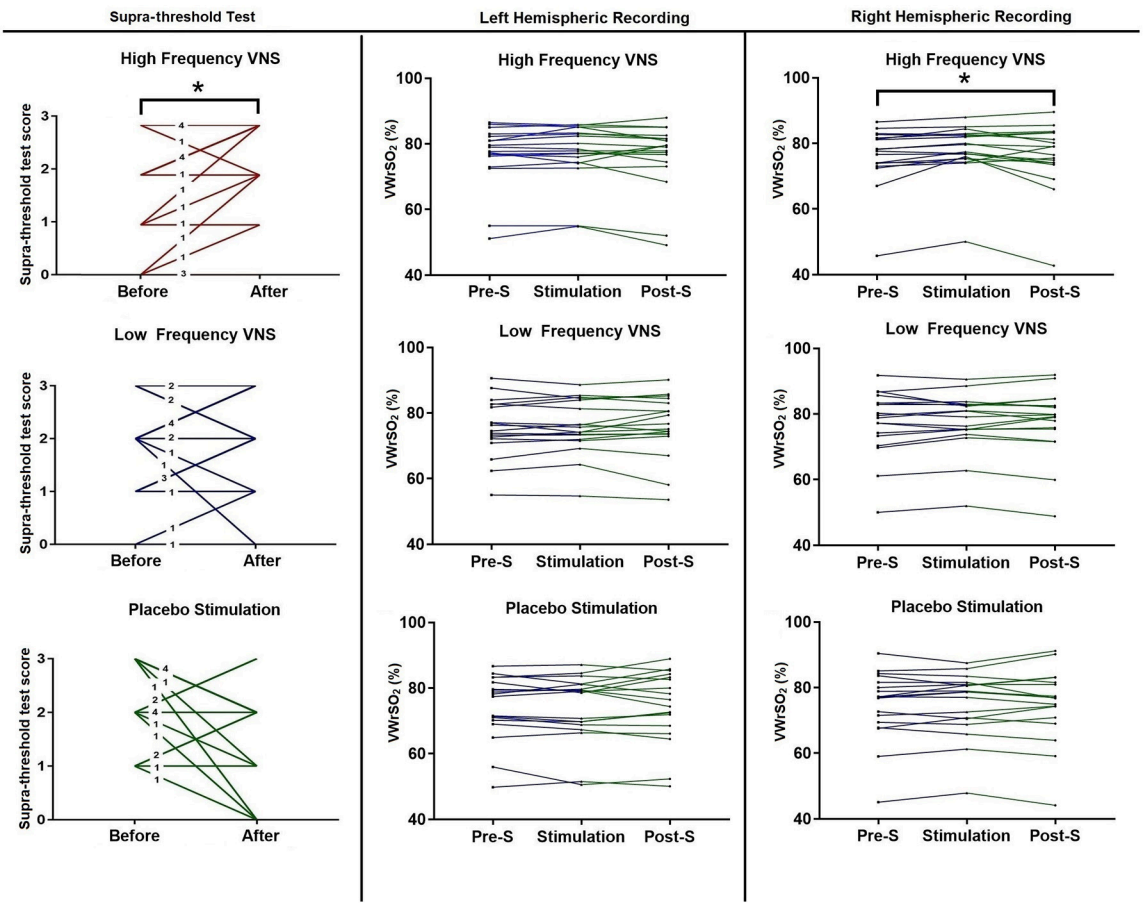

FIGURE 4 | Each participant's scores, before and after each of the stimulation parameters (high frequency VNS, low frequency VNS and placebo) for the STT, and each participant's recordings for all three stages of the experiment (pre-stimulation STT; Pre-S, stimulation and post-stimulation STT; Post-S) for each stimulation parameter (high frequency VNS, low frequency VNS and placebo) from both the left and the right hemispheres of the OFC, measuring venous oxygen reserve ($VWrSO_2$ %) using NIRS. The numbers in each line for the STT scores represents the number of cases that represent the corresponding result. STT scores range = 0–3. *Statistically significant ($p < 0.05$).

In a recent study (Hedner et al., 2010), cognitive variables from different types of olfactory tests such as the OTT, odor discrimination test and the odor identification test were observed. They suggested that OTT is governed by sections of the cortex that is responsible for low-level perceptual function (such as the volume of the OBs related to the peripheral sensory input of olfactory processes) whereas tests of odor discrimination/recognition/identification tests poses more cognitive demands and are represented in cortical areas for higher-level perceptual functions. This could explain the variability seen in the current study where no expression of change was seen in the OTT scores after all stimulation parameters, nor was there any chance in the OFC recording while STT scores improved after high frequency stimulation, alongside the increase of OFC activity on the right hemisphere (represented through the increased $VWrSO_2$). Future research is required to observe olfactory structures that are engaged during the STT that differentiates it from separate olfactory functional tests mentioned previously. This could represent the results from this current article, where only the STT displayed improvements after high frequency VNS. The investigation of STT during VNS or straight after VNS could also be performed in a future study to observe if there would be a more prominent effect on the STT scores than what was observed after the stimulation in the current article. However, the results from the current study showed a statistical significance in the NIRS recordings between pre-stimulation and stimulation stages in the pairwise comparison using *Bonferroni correction* for the STT, but this was not the case for the stimulation and the post-stimulation stages. Therefore, this may exclude the potential washing out effect of auricular vagal nerve stimulation on STT scores. In addition, 5-stage analysis of NIRS data demonstrated a significance only in high frequency stimulation group on the right hemisphere with an indication of the difference between the preSTT and stimulation periods of NIRS. However, there was no significant difference between the OTT and STT periods of NIRS data, suggesting that the OTT test did not exert influence on STT in terms of NIRS recording.

Exploration of the neuroanatomical structures that are affected by high frequency VNS would aid in the understanding of how the olfactory centers are influenced by the vagus nerve. In the past literature, García-Díaz et al. (1984) reported that only high frequency VNS increased the activity of the OBs, with the potential effect of VNS through the periglomerular layer of OBs. It is also understood that the cholinergic elements of the OBs originate in the olfactory tubercle (OT) (Shute and Lewis, 1967) and it has been demonstrated (Gervais, 1979) that the OT modulates the centrifugal control over the OB (**Figure 5**). This therefore also implies the presence of an oligosynaptic pathway by which the vagus nerve influences the OB via the OT. OT is heavily innervated by numerous neuromodulatory centers in the brain and brainstem (Wesson and Wilson, 2011). The OT receives noradrenergic fibers of locus Coeruleus (LC) and serotonergic fibers of Raphe nucleus (Solano-Flores et al., 1980; Guevara-Guzman et al., 1991). The last but not the least, Raphe nucleus also acts on OT through the dopaminergic pathway that passes through the ventral tegmental area (Pierce et al., 1976; Hervé et al., 1987). Both the LC (via paragigantocellular nucleus) (Chandler et al., 2014) and raphe nucleus have afferents from nucleus of the tractus solitarius (NTS) and it has been demonstrated that both structures can be stimulated with auricular vagal nerve stimulation (Sawchenko, 1983; Ruggiero et al., 2000; Mello-Carpes and Izquierdo, 2013; Frangos et al., 2015). NTS has a role as the hub to convey the neuromodulatory effects of the auricular vagal nerve stimulation (Frangos et al., 2015). In the context of underlined numerous interconnections of the OT, it can be considered that OT can easily be modulated with auricular vagal nerve stimulation and it is considered as likely the contributor to state-dependent olfactory processing (Wesson and Wilson, 2011; **Figure 5**).

OFC is the secondary order station of olfactory system that can be modulated by OT or directly by LC or raphe nucleus (Kannan and Yamashita, 1985; Mooney et al., 1987; Ikemoto, 2007; Price, 2010; Wesson and Wilson, 2011; Chandler et al., 2014; Zhou et al., 2015). LC and Raphe nucleus acts directly on the OFC via noradrenergic and serotonergic pathways respectively (Wesson and Wilson, 2011; Chandler et al., 2014; Zhou et al., 2015). In addition to the OT, OFC is also prone to modulation by auricular vagal nerve stimulation. The vagus nerve could also stimulate the NTS-locus Coeruleus (or raphe nucleus)-OFC pathways (Kannan and Yamashita, 1985; Samuels and Szabadi, 2008; Wesson and Wilson, 2011; Mello-Carpes and Izquierdo, 2013; Chandler et al., 2014; Frangos et al., 2015). Furthermore, LC can also act on basolateral nucleus of the amygdala and/or paraventricular nucleus of the hypothalamus (Samuels and Szabadi, 2008; Mello-Carpes and Izquierdo, 2013). Both the basolateral nucleus of the amygdala and paraventricular nucleus of the hypothalamus acts on the OT (Samuels and Szabadi, 2008; Wesson and Wilson, 2011). The NTS can also project directly to the hypothalamic paraventricular nuclei which act on the OT (Kannan and Yamashita, 1985; Wesson and Wilson, 2011; Zhou et al., 2015). In summary, OT, OB and OFC can be modulated via serotonergic, noradrenergic, cholinergic and dopaminergic pathways by auricular vagal nerve stimulation (**Figure 5**).

In past research on rat-animal models (Ziomber et al., 2012), the use of invasive, low frequency VNS had reported inhibitory effects on the dopamine system in the nucleus accumbens, frontal cortex, ventral tegmental area and the striatum. Ziomber et al. (2012) indicated that invasive low frequency VNS displayed similar effects on dopaminergic impairments to vagotomy. Previous studies have also linked the dopaminergic system with olfactory function, indicating that the dopaminergic modulation can alter odor detection thresholds and odor discrimination abilities (Ziomber et al., 2012). However, the use of low frequency, non-invasive VNS in the current article did not have any effects on olfactory performance. It was hypothesized that although low-frequency VNS, through the potential modulation of the dopaminergic system, leads to an impaired VN function, in contrast, high-frequency stimulation could potentially have the opposite effects (Cakmak et al., 2008, 2016, 2017; Zhao, 2008). This hypothesis is supported by the current findings, where only high frequency VNS was capable of improving olfactory performance in the STT. These results in the current article implore future research to encapsulate the exact mechanism of action of how different frequencies of non-invasive VNS affects the dopaminergic system. This could explain the results from both stimulation parameters in the current article, and detail how each stimulation parameter affects the dopaminergic system.

The use of functional imaging techniques, alongside VNS is a crucial step toward understanding the effects of VNS on the olfactory system. In the current article, NIRS was used as the functional imaging technique to observe VNS effects on the OFC. The OFC is considered the communication station of olfaction in the brain (Patel and Pinto, 2014) with a direct pathway to the neocortex. The OFC is involved in multiple complex sensory pathways that provide input from most of the major sensory and limbic structures, highlighting its role in multisensory integration (Shepherd, 2009). Previous reports using functional brain imaging techniques (Handforth et al., 1998; Henry et al., 1999; Bohning et al., 2001; Lomarev et al., 2002) have also reported that invasive VNS stimulation of 20–30 HZ caused significant increases in blood flow in the bilateral OFC, which did not occur in the invasive VNS stimulation of 1 Hz. In contrast to the previous studies using VNS of 20–30 Hz, (Handforth et al., 1998; Henry et al., 1999; Bohning et al., 2001; Lomarev et al., 2002; Kirchner et al., 2004; Sperling et al., 2011; Frangos et al., 2015) but in support of VNS using 1 Hz (Bohning et al., 2001; Lomarev et al., 2002), the current article did not present any significant effects under VNS using 10 Hz in the OFC. In comparison, high frequency VNS of 80 Hz, displayed significant differences in the contralateral-right hemispheric OFC. In summary, the spectrum of different frequencies of VNS results in differentiating effects on the OFC, with 1–10 Hz presenting no effect on either hemisphere of the brain, 20–30 Hz presenting bilateral OFC activation and 80 Hz presenting contralateral OFC activation. This could be the key to understanding why only high frequency VNS of 80Hz was effective in modulating olfactory performance in the current article.

In the meta-analysis and review (Li et al., 2016), it was reported that PD patients presented a significantly larger OB

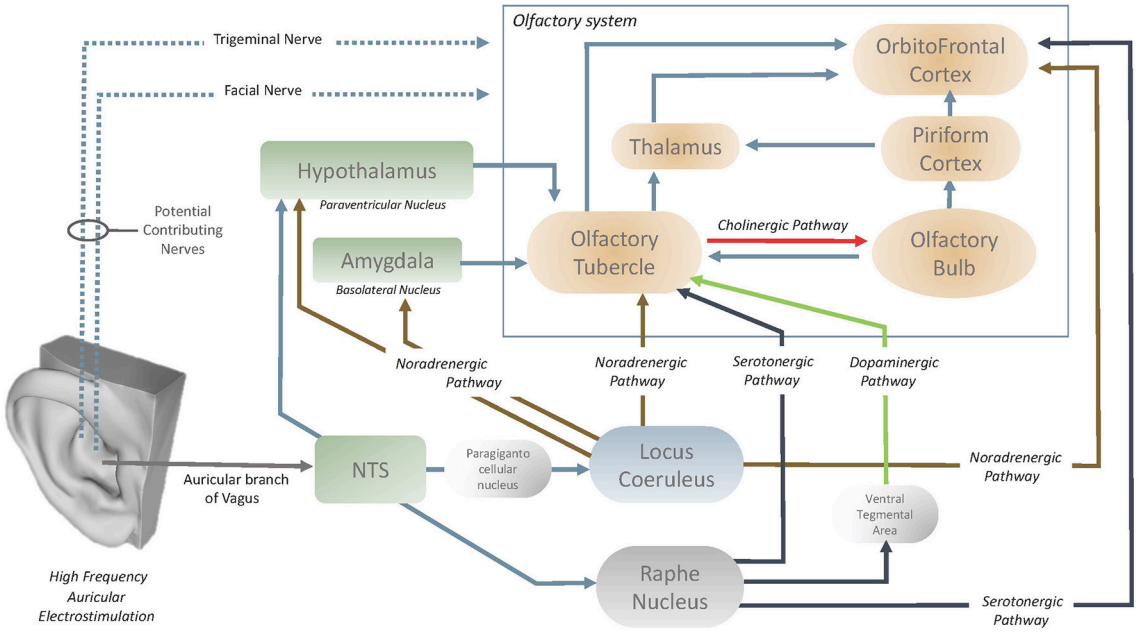

FIGURE 5 | Pathways from the auricular vagus nerve to the olfactory system.

volume on the right hemisphere, indicating the presence of lateralized differences between the two hemispheres. In support, several articles have indicated that the right hemisphere is more important for higher-order processing of smell sensation that the left hemisphere (Zatorre et al., 1992; Jones-Gotman and Zatorre, 1993; Hummel et al., 1995). Functional imaging studies attribute the right-side lateralized differences to odors inducing increased activation within the right piriform cortex and OFC, which are core anatomical structures in olfactory processing (Zatorre et al., 1992). The current article is in support of the aforementioned studies, as the improved olfactory performance was attributed to increased activation of the contralateral, right hemispheric OFC. With the support from the results of the current article, it could be acknowledged that improvements in the STT under high frequency VNS was through the activation of the contralateral OFC activation, in contrast to previous reports of bilateral OFC activation through low frequency VNS (Handforth et al., 1998; Henry et al., 1999; Bohning et al., 2001; Lomarev et al., 2002; Kirchner et al., 2004; Sperling et al., 2011; Frangos et al., 2015).

The loss of olfactory function is very common in neurological diseases including AD, PD, vascular dementia and fronto-temporal dementia (Kovács, 2004; Alves et al., 2014; Godoy et al., 2015). The loss of olfactory functioning is an early symptom in AD and PD and is seen, not only as a pre-mediator of the disease, but a factor that could affect separate symptomology of the disease (Alves et al., 2014). It has been indicated that the higher the olfactory dysfunction is at baseline in patients diagnosed with PD, the higher the risk of developing visual hallucinations and greater cognitive dysfunction (Doty, 2012). Furthermore, loss of olfactory function in PD separates this neurological disorder from other movement disorders (Doty, 2012). A recent article reported that patients with PD had reduced STT scores in comparison with healthy controls (Doty and Kamath, 2014). It is also worth to note that the recovery of the olfactory function induces the neuroplasticity in patients with smell loss (Kollndorfer et al., 2014). In a previous study, our group (Cakmak et al., 2017) demonstrated clinically significant improvements in PD motor symptoms with high frequency (130 Hz) auricular electrostimulation including auricular vagal nerve territory. In this context, as high frequency VNS in the current article improved healthy participant's olfactory abilities in the STT, a potential beneficial effect of high frequency vagal nerve stimulation on olfactory function in early AD and PD needs to be investigated. Further exploration toward the effects of VNS on olfactory processes should use the non-invasive approach as it has not only exhibited similar effectiveness as the invasive approaches (Frangos et al., 2015) but it also, eliminates the risk associated with surgical implementation (Handforth et al., 1998; Fahy, 2010).

There are some limitations to consider in the present study. We acknowledged that there are various olfactory behavioral tasks available. While the STT was employed in the present research, future should replicate these findings with other types of tasks. In addition, NIRS monitoring was only performed to observe the OFC, therefore unable to encapsulate the entire cortex including the piriform cortex. fMRI would be convenient option to visualize entire networks of the olfactory system that could be influenced with auricular vagal nerve stimulation. A previous fMRI study with low frequency, auricular vagal nerve stimulation demonstrated alterations in numerous different

brain regions (Frangos et al., 2015). In this context, a potential effect of high frequency, auricular vagal nerve stimulation on different neuronal networks cannot be excluded. However, low frequency cervical and auricular VNS has been used as a treatment option for intractable epilepsy, chronic treatment-resistant depression (Howland, 2014), pain (Ellrich, 2011; Howland, 2014), primary headaches and medication-overuse headaches (Gaul et al., 2016), and lately high frequency auricular VNS has been used by our group in Parkinson's Disease (Cakmak et al., 2017). To our knowledge, there have been no side effects reported of non-invasive VNS in the context of cortical activity and therefore, a negative effect through the use of non-invasive VNS would be a rare possibility in the context of previous research. In addition, it is also worth to mention that trigeminal and facial nerves have the potential to modulate NTS and as a consequence, the olfactory function (Escanilla et al., 2015). The anatomical connections in between the facial and trigeminal nerves were demonstrated (Cobo et al., 2017) and the auricular stimulation zone in the present study comprises both the external and the posterior aspect of the auricle as shown in **Figures 2a,b**. Both of these zones include potential contributions from the facial and trigeminal nerve branches, therefore potential contributions of the facial and trigeminal nerve on the observed olfactory modulatory effects of auricular stimulation cannot be excluded.

Although the NIRS monitoring have the advantages of real-time, non-invasive and continuous monitoring of changes in regional oxygen saturation, it has some limitations. Within the wavelength region of interest (730–810 nm), melanin and water are also in the light spectrum of photon absorption, fortunately it has been demonstrated that INVOS NIRS recordings were relatively unaffected by normal skin pigmentation in the adults (Misra et al., 1998; Damian and Schlosser, 2007). It is worth to note that the within-subject design of the present study also helped to ameliorate potential biasing effects (if any) due to inter-individual differences in skin color. Hair or hair follicles can produce excessive photon scattering in NIRS and it may result with artifactual low rSO_2 (Orihuela-Espina et al., 2010). Therefore, only the clinically validated placement for the sensors (the frontal head-hair free area) were used in the present study. Skull and skin perfusion data can also alter the NIRS recordings however the NIRS-INVOS (5100c model in the present study) uses two specific wavelengths of near-infrared light to determine oxygen hemoglobin saturation in the tissue beneath the sensor, with two detectors (shallow and deep) that allows the suppression of superficial tissue. This allows accurate measurement of site-specific tissue oxygenation (Thavasothy et al., 2002; Edmonds et al., 2004; Hessel et al., 2014). Cranial bone anomalies, frontal sinus inflammation, dyshemoglobinemias like local or systemic pathologies are also reported to be the potential artifact factors for NIRS recordings (Gopinath et al., 1995; de Letter et al., 1998; Madsen et al., 2000; Sehic and Thomas, 2000; Boulos et al., 2007; McRobb et al., 2011). In addition, NIRS is also susceptible to ambient light and motion artifacts of relative movement between an optical fiber and the scalp. All of these underlined potential artifacts are reported to be resolved by fluctuating/unstable bar signal alert of SSI data quality monitoring system of the INVOS (NIRS 5100c) (Chapter 6.4.16 and 11.7.4 in the INVOS NIRS 5100c manual; Covidien, 2013). In the context of the knowledge of any stable SSI bar display of >1 is an accurate signal of $WVrSO_2$ and our stable signal at 5/5 SSI bar in the present study, we can conclude that our recordings with NIRS are in highest quality of clinically validated INVOS system. It is also worth to note that we only enrolled healthy participants in our study to eliminate such potential pathological artifacts but also to interact with a healthy olfactory system. In addition, we also kept the room temperature and the position of the participants constant during the experiments for a potential effect on NIRS measurements.

Results of the present study were obtained in 18 participants in a within-subject study with three conditions—a placebo and 2 different stimulation conditions (low and high VNS). In addition to presented *p*-values for the statistical significance, the effect size [correlation coefficient (r): 0.39 for the STT test with the significant output after high frequency VNS] indicated a medium/moderate effect in the context of Cohen's thresholds for interpreting the effect size (r:0.1 small effect, r:0.3 moderate effect, r:0.5 large effect, Cohen, 1988). Future studies are needed to replicate our study with a larger cohort. In addition, the present study included only healthy male participants due to difficulties of enrolling female participants in the same period of their menstrual cycle. Future studies are also needed to investigate the potential different responses of neuromodulation on female cohorts in the context of hormonal influences over the olfactory system.

In conclusion, the present article exhibited, for the first time in human research, that non-invasive high frequency auricular vagal nerve stimulation is effective in improving the healthy adult olfactory function in the STT, accompanied by increased activation of the right hemispheric orbitofrontal cortex. The present study underlies the significance of the frequency in auricular vagal nerve stimulation to modulate olfactory function. Further studies are needed to investigate potential effects of different frequencies of vagal nerve stimulation on olfactory function and related neural networks.

AUTHOR CONTRIBUTIONS

YC: The research concept idea; YC and MP: Study design and methodology; YC, EW and AM: Performing the experiments; AM and MP: Statistical Analysis; AM, MP and YC: Analyzing the results; AM, MP and YC: Writing the manuscript.

FUNDING

Otago University, School of Biomedical Sciences, Dean's Bequest Fund.

ACKNOWLEDGMENTS

Authors would like to thank 3dscanstore/Ten24 Media LTD for the 3D scan of the external ear in **Figure 5**.

SUPPLEMENTARY MATERIAL

The Supplementary Material for this article can be found online at: https://www.frontiersin.org/articles/10.3389/fnins.2018.00225/full#supplementary-material

Supplementary Files 1–3 | Scatterplot graph which displays each participant's scores, before and after each stimulation parameter (high frequency VNS, low frequency VNS and placebo) for the STT scores (scores range = 0–3) in combination with participant's recordings for all three stages of the experiment (pre-stimulation STT; Pre-S, stimulation and post-stimulation STT; Post-S) for the right hemisphere of the OFC, measuring venous oxygen reserve ($VWrSO_2$ %) using NIRS. In the STT score figures (Figure on top), "Red" color represents participants who improved, while on the STT right hemisphere NIRS recordings (Figure on bottom), "Red" color represents improvements (increased % in $VWrSO_2$) in the stimulation stage from the pre-stimulation stage and "Orange" color represents improvements (increased % in $VWrSO_2$) in the post-stimulation stage from the pre-stimulation stage. Supplementary file 1 shows the results from high frequency VNS, Supplementary file 2 shows the results from the low frequency VNS and Supplementary file 3 shows the results from the placebo stimulation.

REFERENCES

Alexander, J. C., Knonenfeld, M. A., and Dance, G. R. (2002). Reduced postoperative length of stay may result from using cerebral oximetry monitoring to guide treatment. *Annu. Thoracic Surg.* 73:s373. doi: 10.1016/S0003-4975(01)03537-8

Alves, J., Petrosyan, A., and Magalhaes, R. (2014). Olfactory dysfunction in dementia. *World J. Clin. Cases* 2, 661–669. doi: 10.12998/wjcc.v2.i11.661

Bohning, D. E., Lomarev, M. P., Denslow, S., Nahas, Z., George, M. S., Shastri, A., et al. (2001). Feasibility of vagus nerve stimulation – synchronized blood oxygenation level – Dependent functional MRI. *Invest. Radiol.* 36, 470–479. doi: 10.1097/00004424-200108000-00006

Boulos, P. R., Knoepp, S. M., and Rubin, P. A. (2007). Green bone. *Arch. Ophthalmol.* 125, 380–386. doi: 10.1001/archopht.125.3.380

Braak, H., Del Tredici, K., Rüb, U., De Vos, R. A. I., Jansen Steur, E. N. H., and Braak, E. (2003). Staging of brain pathology related to sporadic Parkinson's disease. *Neurobiol. Aging* 24, 197–211. doi: 10.1016/S0197-4580(02)00065-9

Cakmak, Y. O., Akpinar, I. N., Ekinci, G., and Bekiroglu, N. (2008). Point- and frequency-specific response of the testicular artery to abdominal electroacupuncture in humans. *Fertil. Steril.* 90, 1732–1738. doi: 10.1016/j.fertnstert.2007.08.013

Cakmak, Y. O., Akpinar, I. N., and Yoldemir, T. (2016). Decreasing the uterine blood flow with electroacupuncture: bidermatomal and monodermatomal applications. *Gynecol. Obstet. Invest.* 82, 151–156. doi: 10.1159/000446947

Cakmak, Y. O., Apaydin, H., Kiziltan, G., Gündüz, A., Ozsoy, B., Olcer, S., et al. Ertan, S. (2017). Rapid alleviation of Parkinson's disease symptoms via electrostimulation of intrinsic auricular muscle zones. *Front. Hum. Neurosci.* 11:338. doi: 10.3389/fnhum.2017.00338

Chandler, D. J., Gao, W.-J., and Waterhouse, B. D. (2014). Heterogeneous organization of the locus coeruleus projections to prefrontal and motor cortices. *Proc. Natl. Acad. Sci. U.S.A.* 111, 6816–6821. doi: 10.1073/pnas.1320827111

Cho, H., Nemeto, E. M., Yonas, H., Balzer, J., and Sclabassi, R. J. (1998). Cerebral monitoring by means of oximetry and somatosensory evoked potentials during carotid endarterectomy. *J. Neurosurg.* 89, 533–538. doi: 10.3171/jns.1998.89.4.0533

Cobo, J. L., Solé-Magdalena, A., Menéndez, I., de Vicente, J. C., and Vega, J. A. (2017). Connections between the facial and trigeminal nerves: anatomical basis for facial muscle proprioception. *JPRAS Open* 12, 9–18. doi: 10.1016/j.jpra.2017.01.005

Cohen, J. (1988). *Statistical Power Analysis for the Behavioral Sciences.* 2nd Edn. Hillsdale, MI: Erlbaum Associates.

Covidien. (2013). *Operations Manual INVOS System, Model 5100C.* Mansfield. Available online at: http://www.wemed1.com/downloads/dl/file/id/7947/product/10495/manual_for_mo_s_5100c.pdf

Damian, M. S., and Schlosser, R. (2007). Bilateral near infrared spectroscopy in space-occupying middle cerebral artery stroke. *Neurocrit. Care* 6, 165–173. doi: 10.1007/s12028-007-0010-3

de Letter, J. A., Sie, T. H., Moll, F. L., Algra, A., Eikelboom, B. C., and Ackerstaff, G. A. (1998). Transcranial cerebral oximetry during carotid endarterectomy: agreement between frontal and lateral probe measurements as compared with an electroencephalogram. *Cardiovasc. Surg.* 6, 373–377. doi: 10.1016/S0967-2109(98)00020-9

Desikan, R. S., McEvoy, L. K., Thompson, W. K., Holland, D., Brewer, J. B., Aisen, P. S., et al. (2012). Amyloid-β-Associated clinical decline occurs only in the presence of elevated P-tau. *Arch. Neurol.* 69, 709-713. doi: 10.1001/archneurol.2011.3354

Doty, R. L. (2012). Olfactory dysfunction in Parkinson disease. *Nat. Rev. Neurol.* 8, 329–339. doi: 10.1038/nrneurol.2012.80

Doty, R. L., and Kamath, V. (2014). The influences of age on olfaction: a review. *Front. Psychol.* 5, 1–20. doi: 10.3389/fpsyg.2014.00020

Doty, R. L., McKeown, D. A., Lee, W. W., and Shaman, P. (1995). A study of the test-retest reliability of 10 olfactory tests. *Chem. Senses* 20, 645–656. doi: 10.1093/chemse/20.6.645

Doty, R. L., Riklan, M., Deems, D. A., Reynolds, C., and Stellar, S. (1989). The olfactory and cognitive deficits of Parkinson's disease: evidence for independence. *Ann. Neurol.* 25, 166–171. doi: 10.1002/ana.410250210

Doty, R. L., Shaman, P., and Dann, M. (1984a). Development of the University of Pennsylvania Smell Identification Test: a rapid quantitative olfactory function test for the clinic. *Physiol. Behav.* 32, 489–502. doi: 10.1016/0031-9384(84)90269-5

Doty, R. L., Smith, R., McKeown, D. A., and Raj, J. (1994). Tests of human olfactory function: principal components analysis suggests that most measure a common source of variance. *Percept. Psychophys.* 56, 701–707. doi: 10.3758/BF03208363

Doty, R. L., Shaman, P., Applebaum, S., Giberson, R., Siksorski, L., and Rosenberg, L. (1984b). Smell identification ability: changes with age. *Science* 226, 1441–1443.

Duff, K., McCaffrey, R. J., and Solomon, G. S. (2002). Test : successfully discriminating probable and major depression. *J. Neuropsychiatr.* 14, 197–201. doi: 10.1176/jnp.14.2.197

Duffy, V. B., Rackstrand, J. R., and Ferris, A. M. (1995). Olfactory dysfunction and related nutricional risk in free-living, elderly women. *J. Am. Diet. Assoc.* 95, 879–884. doi: 10.1016/S0002-8223(95)00244-8

Edmonds, H. L., Singer, I., Sehic, A., and Strickland, T. J. (1998). Multimodality neuromonitoring for neurocardiology. *J. Intervent. Cardiol.* 11, 197–204. doi: 10.1111/j.1540-8183.1998.tb00119.x

Edmonds, H. L. Jr., Ganzel, B. L., and Austin, E. H. II. (2004). Cerebral oximetry for cardiac and vascular surgery. *Semin. Cardiothorac. Vasc. Anesth.* 8, 147–166. doi: 10.1177/108925320400800208

Ehrenstein, W. H., and Ehrenstein, A. (1999). Psychophysical Methods. *Modern Tech. Neurosci. Res.* 43, 1211–1241. doi: 10.1007/978-3-642-58552-4_43

Ellrich, J. (2011). Transcutaneous vagus nerve stimulation. *Eur. Neurol. Rev.* 6, 254–256. doi: 10.17925/ENR.2011.06.04.254

Escanilla, O. D., Victor, J. D., and Di Lorenzo, P. M. (2015). Odor-taste convergence in the nucleus of the solitary tract of the awake freely licking rat. *J. Neurosci.* 35, 6284–6297. doi: 10.1523/JNEUROSCI.3526-14.2015

Fahy, B. G. (2010). Intraoperative and perioperative complications with a vagus nerve stimulation device. *J. Clin. Anesth.* 22, 213–222. doi: 10.1016/j.jclinane.2009.10.002

Fennema-Notestine, C., McEvoy, L. K., Hagler, D. J., Jacobson, M. W., and Dale, A. M. (2009). Structural neuroimaging in the detection and prognosis of pre-clinical and early AD. *Behav. Neurol.* 21, 3–12. doi: 10.1155/2009/698156

Frangos, E., Ellrich, J., and Komisaruk, B. R. (2015). Non-invasive access to the vagus nerve central projections via electrical stimulation of the

external ear: FMRI evidence in humans. *Brain Stimul.* 8, 624–636. doi: 10.1016/j.brs.2014.11.018

Fusetti, M., Fioretti, A. B., Silvagni, F., Simaskou, M., Sucapane, P., Necozione, S., et al. (2010). Smell and preclinical Alzheimer disease: study of 29 patients with amnesic mild cognitive impairment. *J. Otolaryngol. Head Neck Surg.* 39, 175–181. doi: 10.2310/7070.2009.090046

García-Díaz, D. E., Aguilar-Baturoni, H. U., Guevara-Aguilar, R., and Wayner, M. J. (1984). Vagus nerve stimulation modifies the electrical activity of the olfactory bulb. *Brain Res. Bull.* 12, 529–537. doi: 10.1016/0361-9230(84)90168-0

Gaul, C., Diener, H.-C., Silver, N., Magis, D., Reuter, U., Andersson, A., et al. (2016). Non-invasive vagus nerve stimulation for PREVention and Acute treatment of chronic cluster headache (PREVA): a randomised controlled study. *Cephalalgia* 36, 534–546. doi: 10.1177/0333102415607070

Gervais, R. (1979). Unilateral lesions of the olfactory tubercle modifying general arousal effects in the rat olfactory bulb. *Electroencephalogr. Clin. Neurophysiol.* 46, 665–674. doi: 10.1016/0013-4694(79)90104-4

Ghasemi, A., and Zahediasl, S. (2012). Normality tests for statistical analysis: a guide for non-statisticians. *Int. J. Endocrinol. Metab.* 10, 486–489. doi: 10.5812/ijem.3505

Gibbons, J. D., and Chakraborti, S. (2011). "Nonparametric statistical inference," in *International Encyclopedia of Statistical Science*, eds W. R. Schucany, A. M. Kshirsagar, M. F. Neuts, and E. G. Schilling (Berlin: Springer), 977–979.

Godoy, M. D. C. L., Voegels, R. L., Pinna, F. D. R., Imamura, R., and Farfel, J. M. (2015). Olfaction in neurologic and neurodegenerative diseases: a literature review. *Int. Arch. Otorhinolaryngol.* 19, 176–179. doi: 10.1055/s-0034-1390136

Gopinath, S. P., Robertson, C. S., Contant, C. F., Narayan, R. K., Grossman, R. G., and Chance, B. (1995). Early detection of delayed traumatic intracranial hematomas using near-infrared spectroscopy. *J. Neurosurg.* 83, 438–444. doi: 10.3171/jns.1995.83.3.0438

Gottfried, J. A. (2006). Smell: central nervous processing. *Adv. Otorhinolaryngol.* 63, 44–69. doi: 10.1159/000093750

Guevara-Guzman, R., García-Díaz, D. E., Solano-Flores, L. P., Wayner, M. J., and Armstrong, D. L. (1991). Role of the paraventricular nucleus in the projection from the nucleus of the solitary tract to the olfactory bulb. *Brain Res. Bull.* 27, 447–450. doi: 10.1016/0361-9230(91)90140-F

Handforth, A., DeGiorgio, C. M., Schachter, S. C., Uthman, B. M., Naritoku, D. K., Tecoma, E. S., et al. (1998). Vagus nerve stimulation therapy for partial-onset seizures: a randomized active-control trial. *Neurology* 51, 48–55. doi: 10.1212/WNL.51.1.48

Harada, H., Tanaka, M., and Kato, T. (2006). Brain olfactory activation measured by near-infrared spectroscopy in humans. *J. Laryngol. Otol.* 120, 638–643. doi: 10.1017/S002221510600123X

Hedner, M., Larsson, M., Arnold, N., Zucco, G. M., and Hummel, T. (2010). Cognitive factors in odor detection, odor discrimination, and odor identification tasks. *J. Clin. Exp. Neuropsychol.* 32, 1062–1067. doi: 10.1080/13803391003683070

Henry, T. R. (2002). Therapeutic mechanisms of vagus nerve stimulation. *Neurology* 59(6 Suppl. 4), S3–S14. doi: 10.1212/WNL.59.6_suppl_4.S3

Henry, T. R., Votaw, J. R., Pennell, P. B., Epstein, C. M., Bakay, R. A. E., Faber, T., et al. Hoffman, J. M. (1999). Acute blood flow changes and efficacy of vagus nerve stimulation in partial epilepsy. *Neurology* 52, 1166–1166. doi: 10.1212/WNL.52.6.1166

Hervé, D., Pickel, V. M., Joh, T. H., and Beaudet, A. (1987). Serotonin axon terminals in the ventral tegmental area of the rat: fine structure and synaptic input to dopaminergic neurons. *Brain Res.* 435, 71–83. doi: 10.1016/0006-8993(87)91588-5

Hessel, T. W., Hyttel-Sorensen, S., and Greisen, G. (2014). Cerebral oxygenation after birth–a comparison of INVOS® and FORE-SIGHT™ near-infrared spectroscopy oximeters. *Acta Paediatr.* 103, 488–493. doi: 10.1111/apa.12567

Higami, T., Kozawa, S., Asada, T., Obo, H., Gan, K., Iwahashi, K., et al. (1999). Retrograde cerebral perfusion versus selective cerebral perfusion as evaluated by cerebral oxygen saturation during aortic arch reconstruction. *Ann. Thoracic Surg.* 67, 1091–1096. doi: 10.1016/S0003-4975(99)00135-6

Hongo, K., Kobayashi, S., Okudera, H., Hokama, M., and Nakagawa, F. (1995). Noninvasive cerebral optical spectroscopy: depth-resolved measurements of cerebral haemodynamics using indocyanine green. *Neurol. Res.* 17, 89–93. doi: 10.1080/01616412.1995.11740293

Howland, R. H. (2014). New developments with vagus nerve stimulation therapy. *J. Psychosoc. Nurs.* 52, 11–14. doi: 10.3928/02793695-20140218-01

Huart, C., Rombaux, P., and Hummel, T. (2013). Plasticity of the human olfactory system: the olfactory bulb. *Molecules* 18, 11586–11600. doi: 10.3390/molecules180911586

Hummel, T., Pauli, E., Schuler, P., Kettenmann, B., Stefan, H., and Kobal, G. (1995). Chemosensory event-related potentials in patients with temporal lobe epilepsy. *Epilepsia* 36, 79–85. doi: 10.1111/j.1528-1157.1995.tb01670.x

Hummel, T., Sekinger, B., Wolf, S. R., Pauli, E., Kobal, G., and Hummel, T. (1997). "Sniffin" sticks': olfactory performance assessed by the combined testing of odor identification, odor discrimination and olfactory threshold. *Chem. Senses* 22, 39–52.

Iglesias, I., Murkin, J. M., Bainbridge, D., and Adams, S. (2003). Monitoring cerebral oxygen saturation significantly decreases postoperative length of stay: a prospective randomized blinded study. *Heart Surg. Forum* 6:204.

Ikemoto, S. (2007). Dopamine reward circuitry: two projection systems from the ventral midbrain to the nucleus accumbens-olfactory tubercle complex. *Brain Res. Rev.* 56, 27–78. doi: 10.1016/j.brainresrev.2007.05.004

Ishimaru, T., Yata, T., Horikawa, K., and Hatanaka, S. (2004). Near-infrared spectroscopy of the adult human olfactory cortex. *Acta Otolaryngol.* 124, 95–98. doi: 10.1080/03655230410017751

Jones-Gotman, M., and Zatorre, R. J. (1993). Odor recognition memory in humans role of right temporal and orbitofrontal regions. *Brain Cogn.* 22, 182–198. doi: 10.1006/brcg.1993.1033

Kannan, H., and Yamashita, H. (1985). Connections of neurons in the region of the nucleus tractus solitarius with the hypothalamic paraventricular nucleus: their possible involvement in neural control of the cardiovascular system in rats. *Brain Res.* 329, 205–212. doi: 10.1016/0006-8993(85)90526-8

Karow, D. S., McEvoy, L. K., and Fennema-Notestine, C. (2010). Relative capability of mr imaging and fdg pet to depict changes associated with purpose : methods : results : *Radiol.* 256, 932-942. doi: 10.1148/radiol.10091402

Katata, K., Sakai, N., Doi, K., Kawamitsu, H., Fujii, M., Sugimura, K., et al. (2009). Functional MRI of regional brain responses to "pleasant" and "unpleasant" odors. *Acta Otolaryngol.* 129, 85–90. doi: 10.1080/00016480902915715

Khan, U. A., Liu, L., Provenzano, F. A., Berman, D. E., Profaci, C. P., Sloan, R., et al. Small, S. A. (2014). Molecular drivers and cortical spread of lateral entorhinal cortex dysfunction in preclinical Alzheimer's disease. *Nat. Neurosci.* 17, 304–311. doi: 10.1038/nn.3606

Kirchner, A., Landis, B. N., Haslbeck, M., Stefan, H., Renner, B., and Hummel, T. (2004). Chemosensory function in patients with vagal nerve stimulators. *J. Clin. Neurophysiol.* 21, 418–425. doi: 10.1097/01.WNP.0000141755.28070.14

Kobayashi, E., Karaki, M., Touge, T., Deguchi, K., Ikeda, K., Mori, N., et al. (2012). "Olfactory assessment using near-infrared spectroscopy," in *2012 ICME International Conference on Complex Medical Engineering (CME)* (Kobe), 517–520.

Kollndorfer, K., Kowalczyk, K., Hoche, E., Mueller, C. A., Pollak, M., Trattnig, S., et al. (2014). Recovery of olfactory function induces neuroplasticity effects in patients with smell loss. *Neural Plast.* 2014:140419. doi: 10.1155/2014/140419

Kovács, T. (2004). Mechanisms of olfactory dysfunction in aging and neurodegenerative disorders. *Ageing Res. Rev.* 3, 215–232. doi: 10.1016/j.arr.2003.10.003

Lang, J. (1983). *Clinical Anatomy of the Head: Neurocranium*. Orbit, Craniocervical Regions. Berlin: Springer-Verlag,

Lawless, H. T., and Heymann, H. (2010). *Sensory Evaluation of Food*. New York, NY: Springer.

Li, J., Gu, C. Z., Su, J. B., Zhu, L. H., Zhou, Y., Huang, H. Y., et al. (2016). Changes in olfactory bulb volume in Parkinson's disease: a systematic review and meta-analysis. *PLoS ONE* 11:e0149286. doi: 10.1371/journal.pone.0149286

Lomarev, M., Denslow, S., Nahas, Z., Chae, J. H., George, M. S., and Bohning, D. E. (2002). Vagus nerve stimulation (VNS) synchronized BOLD fMRI suggests that VNS in depressed adults has frequency/dose dependent effects. *J. Psychiatr. Res.* 36, 219–227. doi: 10.1016/S0022-3956(02)00013-4

Madsen, P. L., Skak, C., Rasmussen, A., and Secher, N. H. (2000). Interference of cerebral near-infrared oximetry in patients with icterus. *Anesth. Analg.* 90, 489–493. doi: 10.1213/00000539-200002000-00046

McRobb, C., Walczak, R., Lawson, S., Lodge, E., Lockhart, N., and Bandarenko, I. I. I., R. (2011). Carboxyhemoglobinemia in a pediatric cardiopulmonary bypass

patient derived from a contaminated unit of allogenic blood. *Perfusion* 26, 302–307. doi: 10.1177/0267659111406993

Mello-Carpes, P. B., and Izquierdo, I. (2013). The nucleus of the solitary tract→ nucleus paragigantocellularis→ locus coeruleus→ CA1 region of dorsal hippocampus pathway is important for consolidation of object recognition memory. *Neurobiol. Learn. Mem.* 100, 56–63. doi: 10.1016/j.nlm.2012.12.002

Mesholam, R. I., Moberg, P. J., Mahr, R. N., and Doty, R. L. (1998). Olfaction in neurodegenerative disease. *Arch. Neurol.* 55:84. doi: 10.1001/archneur.55.1.84

Misra, M., Stark, J., Dujovny, M., Widman, R., and Ausman, J. I. (1998). Transcranial cerebral oximetry in random normal subjects. *Neurol. Res.* 20, 137–141. doi: 10.1080/01616412.1998.11740496

Mooney, K. E., Inokuchi, A., Snow, J. B. Jr., and Kimmelman, C. P. (1987). Projections from the ventral tegmental area to the olfactory tubercle in the rat. *Otolaryngol. Head Neck Surg.* 96, 151–157. doi: 10.1177/019459988709600207

Motomura, N., and Tomota, Y. (2006). Olfactory dysfunction in dementia of Alzheimer's type and vascular dementia. *Psychogeriatrics* 6, 19–20. doi: 10.1111/j.1479-8301.2006.00119.x

Mulazimoglu, S., Flury, R., Kapila, S., and Linder, T. (2017). Effects of a sensory branch to the posterior external ear canal : coughing, pain, Ramsay Hunt' s syndrome and Hitselberger' s sign. *J. Laryngol. Otol.* 131, 329–333. doi: 10.1017/S0022215117000160

Murkin, J. M., Adams, S. J., Novick, R. J., Quantz, M., Bainbridge, D., Iglesias, I., et al. (2007). Monitoring brain oxygen saturation during coronary bypass surgery: a randomized, prospective study. *Anesth. Analg.* 104, 51–58. doi: 10.1213/01.ane.0000246814.29362.f4

Murphy, C., Cruickshanks, K. J., Klein, B. E. K., Klein, R., and Nondahl, D. M. (2002). Prevalence of olfactory impairment. *JAMA* 288, 2307–2312. doi: 10.1001/jama.288.18.2307

Naslund, J., Haroutunian, V., Mohs, R., Davis, K. L., Davies, P., Greengard, P., et al. (2000). Correlation between elevated levels of amyloid ? -peptide in the brain and cognitive decline. *JAMA* 283, 1571–1577. doi: 10.1001/jama.283.12.1571

Orihuela-Espina, F., Leff, D. R., James, D. R. C., Darzi, A. W., and Yang, G. Z. (2010). Quality control and assurance in functional near infrared spectroscopy (fNIRS) experimentation. *Phys. Med. Biol.* 55, 3701–3724. doi: 10.1088/0031-9155/55/13/009

Patel, R. M., and Pinto, J. M. (2014). Olfaction : anatomy, physiology, and disease. *Otolaryngol. Head Neck Surg.* 60, 54–60. doi: 10.1002/ca.22338

Pierce, E. T., Foote, W. E., and Hobson, J. A. (1976). The efferent connection of the nucleus raphe dorsalis. *Brain Res.* 107, 137–144. doi: 10.1016/0006-8993(76)90102-5

Powell, B. Y. T. P. S., Cowan, W. M., and Raisman, G. (1965). The central olfactory connexions. *J. Anat.* 99, 791–813.

Price, J. L. (2010). *Olfactory Higher Centers Anatomy*. St. Louis, MO: Elsevier Ltd.

Rezek, D. L. (1987). Olfactory deficits as a neurologic sign in dementia of the Alzheimer type. *Arch. Neurol.* 44, 1030–1032. doi: 10.1001/archneur.1987.00520220036012

Roberts, K. W., Crnkowic, A. P., and Linneman, L. J. (1998). Near-infrared spectroscopy detects critical cerebral hypoxia during carotid endarterectomy in awake patients. *Anesthesiology* 9:A933. doi: 10.1097/00000542-199809160-00038

Ross, G. W., Petrovitch, H., Abbott, R. D., Tanner, C. M., Popper, J., and Masaki, K. (2008). Association of olfactory dysfunction with risk for future Parkinson's disease. *Ann. Neurol.* 63, 167–173. doi: 10.1002/ana.21291

Ruggiero, D. A., Underwood, M. D., Mann, J. J., Anwar, M., and Arango, V. (2000). The human nucleus of the solitary tract: visceral pathways revealed with an "*in vitro*" postmortem tracing method. *J. Auton. Nerv. Syst.* 79, 181–190. doi: 10.1016/S0165-1838(99)00097-1

Samuels, E. R., and Szabadi, E. (2008). Functional neuroanatomy of the noradrenergic locus coeruleus: its roles in the regulation of arousal and autonomic function part I: principles of functional organisation. *Curr. Neuropharmacol.* 6, 235–253. doi: 10.2174/157015908785777229

Savic, I., Gulyas, B., Larsson, M., and Roland, P. (2000). Olfactory functions are mediated by parallel and hierarchical processing. *Neuron* 26, 735–745. doi: 10.1016/S0896-6273(00)81209-X

Sawchenko, P. E. (1983). Central connections of the sensory and motor nuclei of the vagus nerve. *J. Auton. Nerv. Syst.* 9, 13–26. doi: 10.1016/0165-1838(83)90129-7

Schuknecht, H. F. (1974). *Pathology of the Ear*. Cambridge: Harvard University.

Sehic, A., and Thomas, M. H. (2000). Cerebral oximetry during carotid endarterectomy: signal failure resulting from large frontal sinus defect. *J. Cardiothorac. Vasc. Anesth.* 14, 444–446. doi: 10.1053/jcan.2000.7946

Shepherd, G. M. (2009). "16 New perspectives on olfactory processing and human smell," in *The Neurobiology of Olfaction*, ed A. Menini (Boca Raton, FL: Taylor & Francis Group, LLC), 395–403.

Shute, C. C. D., and Lewis, P. R. (1967). The ascending cholinergic reticular system: neocortical, olfactory and subcortical projections. *Brain* 90, 497–520. doi: 10.1093/brain/90.3.497

Singer, I., Dawn, B., Edmonds, H., and Stickland, T. J. (1999). Syncope is predicted by neuromonitoring in patients with ICDs. *Pac. Clin. Electrophysiol.* 22, 216–222. doi: 10.1111/j.1540-8159.1999.tb00336.x

Sobel, N., Johnson, B. N., and Mainland, J. (2003). "Functional neuroimaging of human olfaction," in *Handbook of Olfaction and Gustation*, ed R. L. Doty (New York, NY: Marcel Dekker).

Solano-Flores, L. P., Aguilar-Baturoni, H. U., and Guevara-Aguilar, R. (1980). Locus coeruleus influences upon the olfactory tubercle. *Brain Res. Bull.* 5, 383–389. doi: 10.1016/S0361-9230(80)80008-6

Sperling, W., Biermann, T., Spannenberger, R., Clepce, M., Padberg, F., Reulbach, U., et al. Thuerauf, N. (2011). Changes in gustatory perceptions of patients with major depression treated with vagus nerve stimulation (VNS). *Pharmacopsychiatry* 44, 67–71. doi: 10.1055/s-0030-1268427

Thavasothy, M., Broadhead, M., Elwell, C., Peters, M., and Smith, M. (2002). A comparison of cerebral oxygenation as measured by the NIRO 300 and the INVOS 5100 Near-Infrared Spectrophotometers. *Anaesthesia* 57, 999–1006. doi: 10.1046/j.1365-2044.2002.02826.x

Velayudhan, L., Pritchard, M., Powell, J. F., Proitsi, P., and Lovestone, S. (2013). Smell identification function as a severity and progression marker in Alzheimer's disease. *Int. Psychogeriatr.* 25, 1157–1166. doi: 10.1017/S1041610213000446

Wesson, D. W., and Wilson, D. A. (2011). Sniffing out the contributions of the olfactory tubercle to the sense of smell: hedonics, sensory integration, and more? *Neurosci. Biobehav. Rev.* 35, 655–668. doi: 10.1016/j.neubiorev.2010.08.004

Yao, F. S. F., Tseng, C. C., Woo, D., Huang, S. W., and Levin, S. K. (2001). Maintaining cerebral oxygen saturation during cardiac surgery decreased neurological complications. *Anesthesiology* 95:A152.

Zatorre, R. J., Jones-Gotman, M., Evans, A. C., and Meyer, E. (1992). Functional localization and lateralization of human olfactory cortex. *Nature* 360, 339–340.

Zhao, Z. Q. (2008). Neural mechanism underlying acupuncture analgesia. *Prog. Neurobiol.* 85, 355–375. doi: 10.1016/j.pneurobio.2008.05.004

Zhou, J., Jia, C., Feng, Q., Bao, J., and Luo, M. (2015). Prospective coding of dorsal raphe reward signals by the orbitofrontal cortex. *J. Neurosci.* 35, 2717–2730. doi: 10.1523/JNEUROSCI.4017-14.2015

Ziomber, A., Thor, P., Krygowska-Wajs, A., Zalecki, T., Moskala, M., Romanska, I., et al. Antkiewicz-Michaluk, L. (2012). Chronic impairment of the vagus nerve function leads to inhibition of dopamine but not serotonin neurons in rat brain structures. *Pharmacol. Rep.* 64, 1359–1367. doi: 10.1016/S1734-1140(12)70933-7

Conflict of Interest Statement: The authors declare that the research was conducted in the absence of any commercial or financial relationships that could be construed as a potential conflict of interest.

frontiers in Neuroscience

ORIGINAL RESEARCH
published: 25 June 2018
doi: 10.3389/fnins.2018.00426

TMS Motor Thresholds Correlate With TDCS Electric Field Strengths in Hand Motor Area

Marko Mikkonen[1], Ilkka Laakso[1], Motofumi Sumiya[2], Soichiro Koyama[3], Akimasa Hirata[4] and Satoshi Tanaka[5]*

[1] Department of Electrical Engineering and Automation, Aalto University, Espoo, Finland, [2] Department of System Neuroscience, National Institute for Physiological Sciences, Okazaki, Japan, [3] School of Health Sciences, Faculty of Rehabilitation, Fujita Health University, Toyoake, Japan, [4] Department of Computer Science and Engineering, Nagoya Institute of Technology, Nagoya, Japan, [5] Laboratory of Psychology, Hamamatsu University School of Medicine, Hamamatsu, Japan

Transcranial direct current stimulation (TDCS) modulates cortical activity and influences motor and cognitive functions in both healthy and clinical populations. However, there is large inter-individual variability in the responses to TDCS. Computational studies have suggested that inter-individual differences in cranial and brain anatomy may contribute to this variability via creating varying electric fields in the brain. This implies that the electric fields or their strength and orientation should be considered and incorporated when selecting the TDCS dose. Unfortunately, electric field modeling is difficult to perform; thus, a more-robust and practical method of estimating the strength of TDCS electric fields for experimental use is required. As recent studies have revealed a relationship between the sensitivity to TMS and motor cortical TDCS after-effects, the aim of the present study was to investigate whether the resting motor threshold (RMT), a simple measure of transcranial magnetic stimulation (TMS) sensitivity, would be useful for estimating TDCS electric field strengths in the hand area of primary motor cortex (M1). To achieve this, we measured the RMT in 28 subjects. We also obtained magnetic resonance images from each subject to build individual three-dimensional anatomic models, which were used in solving the TDCS and TMS electric fields using the finite element method (FEM). Then, we calculated the correlation between the measured RMT and the modeled TDCS electric fields. We found that the RMT correlated with the TDCS electric fields in hand M1 ($R^2 = 0.58$), but no obvious correlations were identified in regions outside M1. The found correlation was mainly due to a correlation between the TDCS and TMS electric fields, both of which were affected by individual's anatomic features. In conclusion, the RMT could provide a useful tool for estimating cortical electric fields for motor cortical TDCS.

Keywords: tDCS, TMS, resting motor threshold, electric field estimation, FEM

OPEN ACCESS

Edited by:
Alberto Priori,
Universitá degli Studi di Milano, Italy

Reviewed by:
Marco Iacoboni,
University of California, Los Angeles, United States
Serena Fiocchi,
Istituto di Elettronica e di Ingegneria dell'Informazione e delle Telecomunicazioni (IEIIT), Italy

Mayank Jog contributed to the review of Marco Iacoboni

****Correspondence:***
Marko Mikkonen
marko.mikkonen@aalto.fi

Specialty section:
This article was submitted to Neural Technology, a section of the journal Frontiers in Neuroscience

Received: *13 October 2017*
Accepted: *06 July 2018*
Published: *25 June 2018*

Citation:
Mikkonen M, Laakso I, Sumiya M, Koyama S, Hirata A and Tanaka S (2018) TMS Motor Thresholds Correlate With TDCS Electric Field Strengths in Hand Motor Area. Front. Neurosci. 12:426. doi: 10.3389/fnins.2018.00426

INTRODUCTION

Transcranial direct current stimulation (TDCS) is a non-invasive method of stimulating the brain and is capable of eliciting changes in cortical activity that outlast the stimulation period (Priori et al., 1998; Nitsche and Paulus, 2000, 2001). Studies suggest that these TDCS-induced changes have the potential to serve as a treatment for various cerebrovascular, psychiatric, and neurological diseases

such as stroke (Marquez et al., 2015), depression (Meron et al., 2015), and schizophrenia (Fröhlich et al., 2016). However, this potential is hindered by inter-individual variations in its efficacy (López-Alonso et al., 2014; Wiethoff et al., 2014; Chew et al., 2015; López-Alonso et al., 2015) which may be related to differences in the induced electric fields (EFs).

Computational studies have suggested that these differences in the induced EFs may arise from anatomical differences between individuals: The distance from the surface of the scalp to the surface of the brain, in terms of subcutaneous fat thickness (Truong et al., 2013), skull thickness (Opitz et al., 2015), and especially the amount of CSF (Laakso et al., 2015; Opitz et al., 2015), has been found to have an effect on the electric fields in the adult brain. Similar results have also been found in children (Kessler et al., 2013; Fiocchi et al., 2016). In fact, induced cortical EFs may be a more useful parameter for determining the appropriate TDCS dose (Bestmann and Ward, 2017), compared to the input current that is commonly employed (Horvath et al., 2015) in TDCS studies.

As it is virtually impossible to non-invasively measure the strength of TDCS-induced EFs *in vivo*, the EFs are often modeled computationally. Unfortunately, estimating the EFs that are induced in a subject's brain with a computer model is a tedious process involving magnetic resonance imaging (MRI), segmentation of the acquired images, and computer simulations, making it an impractical approach in the clinical environment. Developing a simpler and more-robust method of estimating the strength of TDCS EFs would be beneficial because it would permit obtaining more-uniform TDCS stimulation intensities in terms of the induced EFs.

Transcranial magnetic stimulation (TMS) is a commonly used method for studying the excitability of the motor cortex (Ilmoniemi et al., 1999). TMS works by different mechanism from TDCS, magnetically inducing a brief pulsed EF that activates cortical neurons, which, in the case of motor cortical TMS, evokes responses that can be easily measured using electromyography. Theoretically, the EFs induced by TMS depend mainly on the distance below the scalp surface (Tofts, 1990). This has been confirmed in electrophysiological studies, which have shown that the scalp–cortex distance explains 50–70% of inter-subject variability in the motor threshold (MT) (Kozel et al., 2000; Stokes et al., 2007; Herbsman et al., 2009). Modeling studies have shown that, in addition to the scalp–cortex distance, the EFs induced by TMS are affected by the distribution of the CSF and orientation of the gyri with respect to the direction of the induced EF (Opitz et al., 2013, 2014; Laakso et al., 2014; Bungert et al., 2016; Laakso et al., 2018). These anatomical features, namely the thicknesses of the scalp tissues, skull, and CSF, as well as the orientation of gyri and sulci, also affect the EFs produced by TDCS (Datta et al., 2009; Truong et al., 2013; Laakso et al., 2015; Opitz et al., 2015). Therefore, the EFs of TMS and TDCS may be linked, despite the fact that TDCS and TMS act via different mechanisms. Based on this, our hypothesis was that the MTs measured using TMS may be indirectly related to the TDCS EFs.

Recent studies have indicated that individual TMS thresholds may indeed affect the after-effects of TDCS (Labruna et al., 2016; Jamil et al., 2017): Labruna et al. (2016) studied the relationship between TDCS efficacy and individual sensitivity to TMS using 1 mA anodal and cathodal stimulation. This was extended to a range of 0.5–2 mA by Jamil et al. (2017). Both studies found TMS thresholds to have a modest effect on the after-effects of anodal 1 mA TDCS at early epoch (0–30 min after stimulation). However, neither study found significant effects for cathodal stimulation, at later epochs, or for other stimulation currents.

The aim of the present study was to study whether TMS motor thresholds, namely the resting motor threshold (RMT), would also be a useful parameter for estimating the strength of TDCS EFs in the hand area of primary motor cortex (M1). We also investigated the relationship between the EFs of TDCS and TMS.

METHODS

Subjects

Twenty-eight healthy subjects (7 women and 21 men; mean age ± standard deviation [SD] = 27.1 ± 6.4 years) participated in the study. All subjects participated in both the RMT measurements and the MRI. The subjects were neurologically healthy and had no family history of epilepsy. The Human Research Ethics Committee at the National Institute for Physiological Sciences approved all experimental procedures. All subjects provided both informed and written consent before participating in the experiment. Both the left- and right-handed subjects were included in this study, as no significant interhemispheric differences have been found in responses to TMS (Bashir et al., 2013).

RMT Measurement

We determined the RMT for the left abductor pollicis brevis muscle as a measure of cortical excitability using a figure-eight-shaped coil (diameter of the individual loop: 9 cm) connected to a Magstim 200 magnetic stimulator (Magstim Company, UK). The coil and stimulator were applied to elicit motor-evoked potentials (MEPs) in two separate sessions that were performed on different days. The coil handle was held perpendicular to the central sulcus. For each subject, the location of the hand M1 region (hand knob)

TABLE 1 | List of segmented tissues and the electric conductivities used in modeling TDCS and TMS.

Tissue	σ_{TDCS} (S/m)	σ_{TMS} (S/m)
GM	0.20	0.215
WM	0.14	0.142
CSF	1.8, (Baumann et al., 1997)	1.8, (Baumann et al., 1997)
Compact bone	0.008, (Akhtari et al., 2002)	0.009, (Akhtari et al., 2002)
Spongy bone	0.027, (Akhtari et al., 2002)	0.034 (Akhtari et al., 2002)
Fat	0.08, (Gabriel et al., 2009)	0.15, (Wake et al., 2016)
Skin	0.08, (Gabriel et al., 2009)	0.43, (Wake et al., 2016)
Muscle	0.16, (Gabriel et al., 2009)	0.18, (Gabriel et al., 2009)
Dura	0.16	0.18
Blood	0.7, (Gabriel C. et al., 1996)	0.7, (Gabriel S. et al., 1996)
Eye humor	1.5, (Lindenblatt and Silny, 2001)	1.6, (Lindenblatt and Silny, 2001)

was identified using an individual T1-weighted MR image and a frameless stereotaxic navigation system (Brainsight 2; Rogue Research, Montreal, Canada). For the RMT measurements, the coil was placed directly above the center of the hand knob, as identified by the navigation system. The RMT was defined as the lowest stimulation intensity required to elicit MEPs with a peak-to-peak amplitude of 50-μV in five of ten trials (Rossini et al., 1999).

MRI

All MRI scans were acquired using a 3.0 T MRI scanner (Verio; Siemens, Ltd., Erlangen, Germany). Structural T1-weighted MRI of all subjects were acquired using a Magnetization Prepared Rapid Acquisition in Gradient Echo (MPRAGE) sequence (TR/TE/TI/FA/FOV/voxel size/number of slices = 1,800 ms/1.98 ms/800 ms/9° /256 mm/1.0 mm x 1.0 mm x 1.0 mm/176). In addition, T2-weighted MRI were acquired for the same subjects (TR/TE/FOV/voxel size/slice number = 4,500 ms/368 ms/256 mm/1.0 mm x 1.0 mm x 1.0 mm/224 slices).

Volume Conductor Models

The MR-images were segmented with an in-house software (Laakso et al., 2015). Details of the segmentation process have been described previously (Laakso et al., 2015, 2016). In short, the FreeSurfer image analysis software (Dale et al., 1999; Fischl et al., 1999; Fischl and Dale, 2000; Desikan et al., 2006) was used for segmenting the brain. Non-brain tissues were segmented using a semi-automatic procedure that uses both T1 and T2 weighted MR images, which were first divided into three compartments: the scalp, skull and the contents of the skull (without brain). These compartments were then further segmented into individual tissues (see **Table 1**). The segmentation process also ensured that the minimum distance between the brain and the inner skull surface was not shorter than 0.5 mm. Volume conductor models with a resolution of 0.5 mm were built for each subject from the segmented data by assigning conductivity values to each voxel in a cubical grid. The tissue conductivities we used were assumed to be linear and isotropic.

For modeling TDCS, a gray matter conductivity of 0.2 S/m was selected, as existing literature suggests that its value typically varies from 0.1 to 0.3 S/m (Freygang and Landau, 1955; Stoy et al., 1982; Ranck, 1963; Gabriel C. et al., 1996; Latikka et al., 2001; Akhtari et al., 2006). Similarly, white matter conductivity is approximately 30% less than that of gray matter (Freygang and Landau, 1955; Stoy et al., 1982; Gabriel C. et al., 1996); thus, we used a white matter conductivity of 0.14 S/m. For modeling TMS, the gray and white matter conductivity values were extrapolated to the frequency of 3 kHz of the magnetic stimulator (Nieminen et al., 2015) using a Cole–Cole parametric model (Gabriel S. et al., 1996) from human *in vivo* values of 0.26 and 0.17 S/m measured at 50 kHz (Koessler et al., 2017), respectively. Thus, 0.215 S/m was used for gray matter and 0.142 S/m for white matter. The conductivity values for other tissues are presented in **Table 1**. The conductivity values for compact and spongy bone were increased by 30% to compensate for the room temperature measurements, and the dura conductivity was chosen arbitrarily to be the same as that of muscle.

EF Modeling

An in-house finite element method (FEM) solver (Laakso and Hirata, 2012), which employed the volume conductor model voxels as elements, linear basis functions, and the geometric multigrid method, was used to establish the electric scalar potential ϕ that was induced at the vertices of each voxel by TDCS and TMS stimulation.

For TDCS, the solver was used to iteratively calculate ϕ from the potential equation

$$\nabla \cdot \sigma_{\mathrm{TDCS}} \nabla \phi = 0, \tag{1}$$

where σ_{TDCS} is the electric conductivity. The iteration was continued until the relative residual of the numerical solution was less than 10^{-6}, which typically results in less than 0.1% error in the EF (Laakso and Hirata, 2012). The EF was determined from $\vec{E} = -\nabla\phi$. The active electrode was located above the hand knob (**Figure 1A**) and the reference electrode was located at the

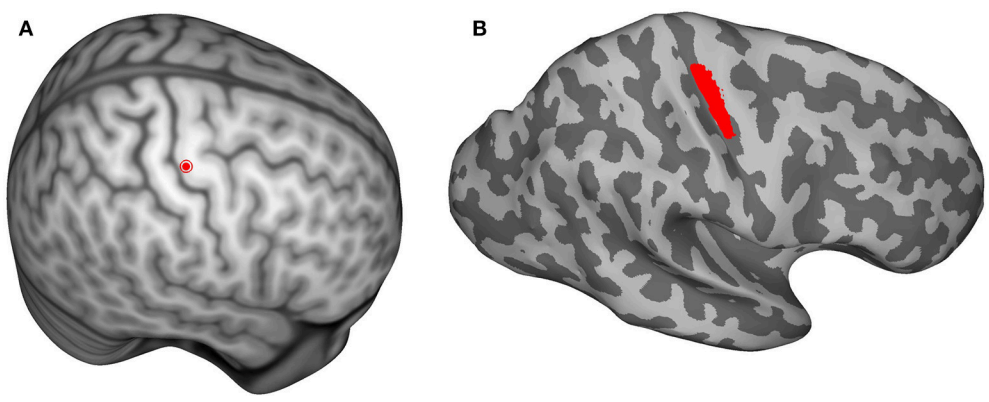

FIGURE 1 | (A) The center of the hand knob is shown as a red dot on the Montreal Neurological Institute (MNI) template brain. The hand-knob location was mapped from the MNI template to each individual subject's brain using an inter-subject registration method in order to keep the anode and coil locations consistent. **(B)** The location of the region of interest (shown in red) that was used during data analysis. The shading represents the gyral structure (dark = sulci, light = gyri).

contralateral forehead (Fp1) for each subject. The electrodes were modeled based on a realistic two-compartment design (Saturnino et al., 2015) consisting of 5 × 5-cm and 6-mm thick saline-soaked sponges ($\sigma = 1.6$ S/m) and a 1-mm thick rubber sheet ($\sigma = 0.1$ S/m). The connector was modeled as a disk with a radius of 5 mm that was located beneath the rubber sheet, with the current source/sink placed uniformly on the disk. The rubber sheet surrounded the connector, with 1 mm of rubber on all sides. A 1-mA input current was used.

To model TMS, the quasistatic approximation was used, i.e., the electric and magnetic fields were assumed to vary very slowly with time. This assumption is valid because the energy of the stimulation waveform is concentrated at frequencies lower than 10 kHz (Wang and Eisenberg, 1994). Furthermore, the magnetic skin effect can be ignored because the conductivities of biological tissues are very small compared to those of metals. Under these assumptions, the EF can be represented as $\vec{E} = -\nabla\phi - \frac{\partial}{\partial t}\vec{A}$, where t denotes time, and $\vec{A}$ is the magnetic vector potential. The scalar potential ϕ was determined with the following equation:

$$\nabla \cdot \sigma_{\mathrm{TMS}} \nabla\phi = \nabla \cdot \sigma_{\mathrm{TMS}} \frac{\partial}{\partial t}\vec{A}. \quad (2)$$

TABLE 2 | Subjects' handedness and measured RMTs from both sessions.

Subject	Handedness	RMT_A (%)	RMT_B (%)
1	R	55	52
2	R	50	48
3	R	36	32
4	R	46	48
5	L	60	63
6	R	50	50
7	R	40	45
8	R	54	52
9	R	46	48
10	R	52	42
11	R	42	48
12	R	45	46
13	R	60	62
14	L	45	48
15	R	43	46
16	R	46	54
17	R	70	72
18	R	60	62
19	R	44	48
20	R	44	46
21	R	42	43
22	R	32	32
23	R	34	28
24	R	36	34
25	R	64	70
26	R	48	50
27	R	38	36
28	R	40	40

Under the quasistatic approximation, the current in the coil windings was constant, and $\vec{A}$ was solved analytically via the Biot–Savart law using a coil current (1.74 A/μs, Laakso et al., 2018) that produced the same peak EF as a monophasic pulse of the Magstim 200 stimulator at 1% of the maximum output. The choice of the stimulator intensity for computer modeling is arbitrary as the induced EFs change linearly with stimulator output (Nieminen et al., 2015), and thus, EFs at any other stimulator output can be obtained by multiplication. The model of the figure-8 coil consisted of two circular wings of thin wire with nine windings each (Laakso et al., 2018). The outer and inner diameters of the wings were 9.7 and 7.2 cm, respectively. The dimensions were based on the Magstim 70-mm figure-8 coil (Thielscher and Kammer, 2004). The coil windings were located on a tangential plane above the hand knob at a height of 5.5 mm from the skin, to account for the thickness of the coil (1.1 cm), and oriented 45° from the anteroposterior direction.

In order to keep the anode and the coil locations consistent for each subject, the center of the hand knob was selected on the Montreal Neurological Institute (MNI) template brain (**Figure 1A**) and mapped to each subject's brain using an inter-subject registration method (Laakso et al., 2016). The closest point on the scalp to the mapped hand-knob center was where the center of the anode and TMS coil were positioned.

All simulations presented in this study were executed with MATLAB (version 2014a, Mathworks Inc., Natick, MA, USA) on a computer with 8-core Intel Xeon processor (3.4 GHz) and 32 GB of memory. On average, the models contained 33 million elements and took 45 s to solve.

Data Analysis

All data analyses were performed using MATLAB (version 2014a, Mathworks Inc., Natick, MA, USA). Linear regression analysis was used to study the correlation between RMTs of the two sessions. The absolute values of the EFs in each subject were determined on a surface located 1 mm below the gray-matter surface. The surface EFs were mapped onto the surface of the MNI template brain (**Figure 1B**) using a previously described inter-subject registration procedure (Laakso et al., 2016). The surfaces used in analyses are triangular meshes constructed using Freesurfer.

The region of interest (ROI; **Figure 1B**) was defined as the area on the MNI template brain surface within a probabilistic cytoarchitectonic map of Brodmann area 4, as defined by FreeSurfer (Fischl et al., 2007), that was within 1.5 cm of the center of the hand knob [MNI coordinates (Maki et al., 2008): x = 37.41, y = −24.00, z = 57.41]. The spatial mean and maximum EFs were calculated in the ROI for each subject. Linear regression analysis was used to examine the correlations between the RMTs and the TDCS EFs in the ROI, as well as the correlations between the TDCS EFs and TMS EFs in the ROI. Studentized residuals were used to find outliers in the analyses with 95% confidence interval, and the found outliers were omitted.

To study the spatial extent of the correlations, linear regression analyses between the RMTs and TDCS EFs as well as between the TDCS EFs and TMS EFs were performed nodewise

on the triangular MNI brain surface mesh (consisting of 149,319 nodes). To exclude the nodes with low average TDCS EFs from the analysis, the analyses were only performed at the 31039 nodes where the subject-wise mean TDCS EF magnitude was higher than 50% of the maximum. The Benjamini-Hochberg procedure was used to control the false discovery rate (FDR) at a level of 5%.

RESULTS

RMTs

Table 2 presents the subject handedness and measured RMTs. The level of RMTs remained consistent intra-individually between the two measurements, differing by only three percentage points on average and strongly correlating ($R^2 = 0.88$, $P < 0.0001$). In contrast, the inter-individual variance was large, with the largest individual mean RMT (71%) being 40 percentage points higher than the lowest mean RMT (31%); for all subjects and both sessions, the mean and SD of the RMTs were 47.6% and 9.9%, respectively.

EF Modeling

The TDCS EFs in the right hemisphere for each subject are presented in **Figure 2**. Although the stimulation parameters were identical, the modeled EFs varied inter-individually. For all subjects, the mean ± SD of the maximum absolute EF in the ROI was 0.61 ± 0.09 V/m, with the highest and lowest maximum

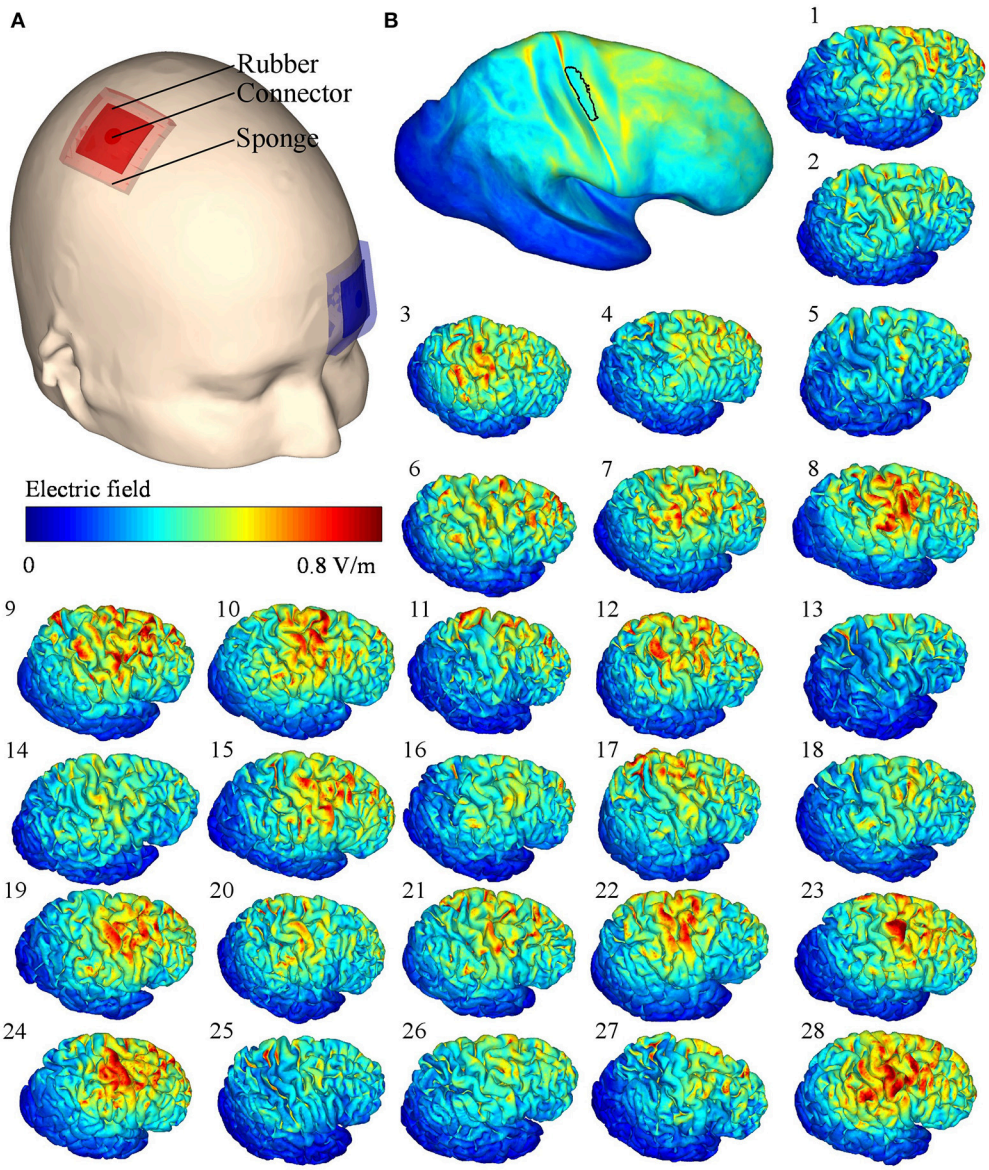

FIGURE 2 | (A) Transcranial direct current stimulation (TDCS) electrode locations on the scalp. **(B)** Mean of the electric fields (EFs) mapped onto the Montreal Neurological Institute template, the black outlined area represents the region of interest; (1–28) simulated TDCS EFs of each subject on the right hemisphere.

values being 0.85 and 0.47 V/m, respectively. The mean EF in the ROI was 0.34 ± 0.07 V/m.

Correlation Between the RMTs and TDCS EFs

As the RMTs correlated significantly between sessions, we calculated the mean of the two RMT measurements for each subject and used the means in the analysis. Linear regression analysis revealed a significant correlation between the mean TDCS EF strengths and RMTs ($R^2 = 0.58$, $P < 0.001$, see **Figure 3A**, regression coefficients are presented in **Table 3**) , one data point was omitted based on the outlier analysis. Specifically, subjects with a higher RMT tended to have a smaller mean TDCS EF. Our nodewise examination (see **Figure 3B**) of the correlation between the TDCS EFs and RMTs revealed an area with a significant (with a 5% FDR) negative correlation beneath the TDCS electrode. This suggests that the EFs within this region could be estimated using the RMT. However, as seen in **Figure 3B**, the correlation between the RMT and the EFs in regions anterior to the precentral gyrus were not significant.

Correlation Between TMS and TDCS EFs

As RMT is measured using TMS, we hypothesized that the EFs induced by TMS would be connected to those produced by TDCS, which could explain the correlation between the TDCS EF strengths and the RMT. To test this, we modeled the TMS-induced EFs in each subject. The modeled TMS EFs and their mean are presented in **Figure 4**. Scaled to the level of individual RMTs (**Table 2**), the mean TMS EF strength within the ROI was 75 ± 15 V/m, and the maximum EF strength was 207 ± 43 V/m.

Linear regression analysis of the mean EF strengths in the ROI showed a significant correlation between the TMS and TDCS EFs ($R^2 = 0.36$, $P < 0.001$, see **Figure 5A**). No outliers were detected. Our nodewise examination (see **Figure 5B**) of the correlation between the TDCS and TMS EFs revealed a significant (with a 5% FDR) positive correlation in a wide region of the cortex, mainly in the precentral gyrus and frontal areas. Spatially, there are significant correlations located also on the gyri anterior to the ROI. This is most likely due to these regions being far away from the sources of the EFs for both TMS and TDCS, and thus, the EFs in these regions might be similarly affected by the individual anatomy in both cases. Note that especially the TMS EFs are rather weak in the anterior regions (**Figure 4B**), where the highest EFs take place on the gyral crowns in similar manner to the TDCS EFs (**Figure 2B**).

We also studied the spatial correlation between the RMT and TMS EF strengths (**Figure 6**). Although the average TMS EF strength in the ROI was found to correlate with the RMT ($R^2 = 0.44$, $P < 0.001$), no significant correlations were found in nodewise analysis using 5% FDR. Regions outside M1 did not seem to exhibit any systematic correlation between the TMS EF strength and RMT (**Figure 6B**), which is similar to the case with TDCS EFs (**Figure 3B**). This result is in line with the hypothesis that far from the sources, the EFs may be mainly affected by individual anatomic differences, not RMT.

DISCUSSION

In the present study, we measured the TMS RMTs and modeled realistic and individual TDCS and TMS EFs for 28 subjects. We found that the RMT was correlated with the modeled TDCS

TABLE 3 | Coefficients for linear regression EF = $E_0 + k \times \text{RMT} + \epsilon$, presented in **Figure 3A**.

	Predicted value	95% Confidence interval
E_0	0.6152	[0.5167, 0.7137]
k	−0.0059	[−0.0080, −0.0039]

EF is the mean TDCS EF in the ROI (V/m), E_0 is the intercept (V/m), k is the slope of the regression line (V/m per % of stimulator output), and ϵ is the residual.

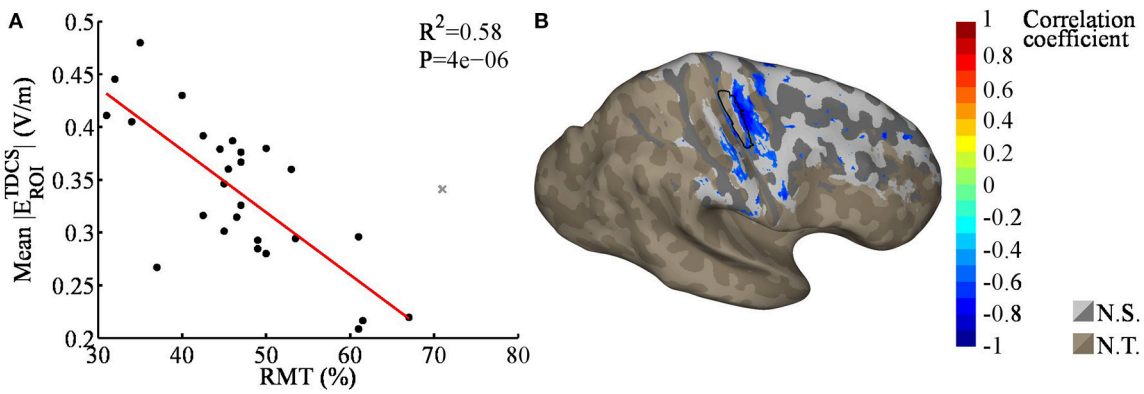

FIGURE 3 | (A) Regression plot of the mean transcranial direct current stimulation electric fields (TDCS EFs) within the region of interest [ROI; black outlined area in **(B)**], as a function of the resting motor threshold (RMT); the gray cross marks the outlier that was omitted from the analysis. The RMT was found to correlate significantly with the TDCS EFs. **(B)** Nodewise correlation between the RMT and individual TDCS EFs; the significant correlation coefficients are shown in color, the non-significant coefficients in gray (N.S.), and the unstudied areas (average TDCS EF lower than 50% of the maximum) in brown (N.T.). The shading in the gray/brown areas represents the gyral structure of the brain (dark = sulci, light = gyri).

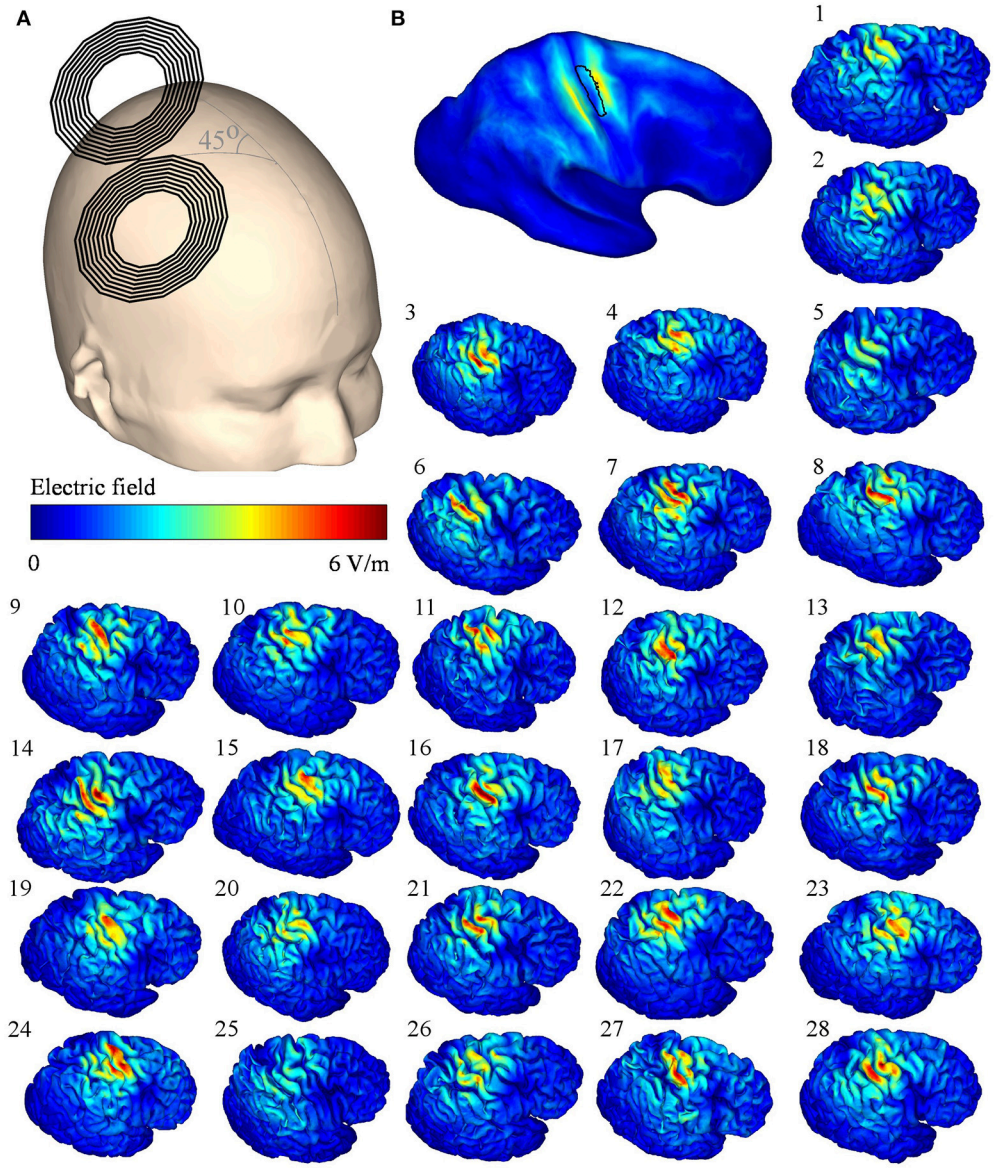

FIGURE 4 | (A) Transcranial magnetic stimulation (TMS) coil orientation on the template head. **(B)** Mean of the electric fields (EFs) mapped onto the Montreal Neurological Institute template, the black outlined area represents the region of interest; (1–28) simulated TMS EFs of each subject on the right hemisphere. The TMS stimulator output was set to 1% of the maximum stimulator output.

EF strength in hand M1 ($R^2 = 0.58$, $P < 0.001$), a finding that has important implications for both the interpretation and design of TDCS experiments. No obvious correlations were identified in regions outside M1. The correlation between the calculated TDCS EF strengths and the measured RMTs that we identified beneath the TDCS anode may provide a simple method by which to estimate the TDCS EF strengths in hand M1 of individual subjects, making it a valuable tool for designing motor cortical TDCS protocols. Here, we found that the individuals with low RMTs tended to have larger TDCS-induced EFs in hand M1 than did subjects with high RMTs. This may be the physical mechanism underlying the recent findings of Jamil et al. (2017) and Labruna et al. (2016) showing that inter-individual sensitivity to TMS might affect the after-effects of anodal TDCS.

In order to understand the correlation between the TDCS EFs and RMT, we studied the relationship between the EFs of TDCS and TMS by modeling the TMS-induced EFs. A linear regression analysis revealed a positive correlation between the EF strengths of TMS and TDCS in hand M1. This positive correlation is interesting, because it suggests that both the stimulus (i.e., TDCS) and the method for measuring the effect of stimulation (i.e., TMS) are related to each other and that this relationship should be considered when designing TDCS experiments. Our

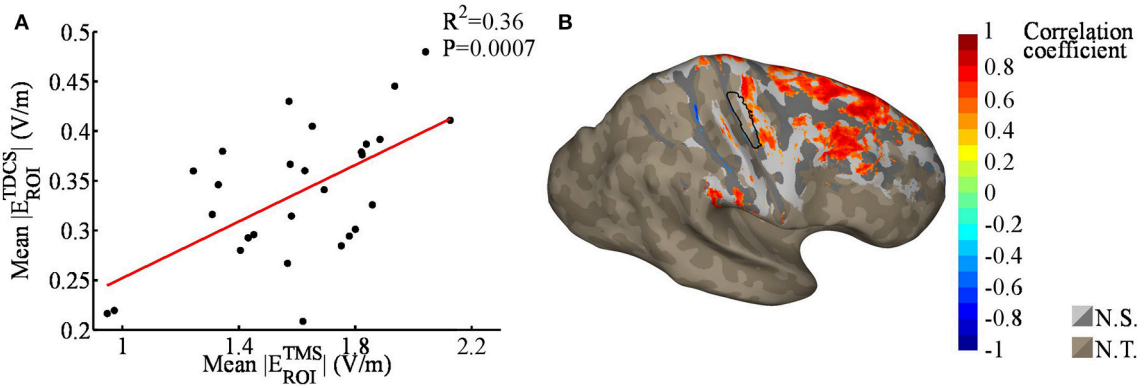

FIGURE 5 | (A) Regression plot of the mean absolute transcranial direct current stimulation (TDCS) electric fields (EFs) within the region of interest [ROI; black outlined area in **(B)**], as a function of the mean absolute transcranial magnetic stimulation (TMS) EFs within the ROI. The TMS EFs were significantly correlated with the TDCS EFs. **(B)** Nodewise correlation between individual TDCS and TMS EFs; significant correlation coefficients are shown in color, the non-significant coefficients in gray (N.S.), and unstudied areas (average TDCS EF lower than 50% of the maximum) in brown (N.T.). The shading in the gray/brown areas represents the gyral structure of the brain (dark = sulci, light = gyri).

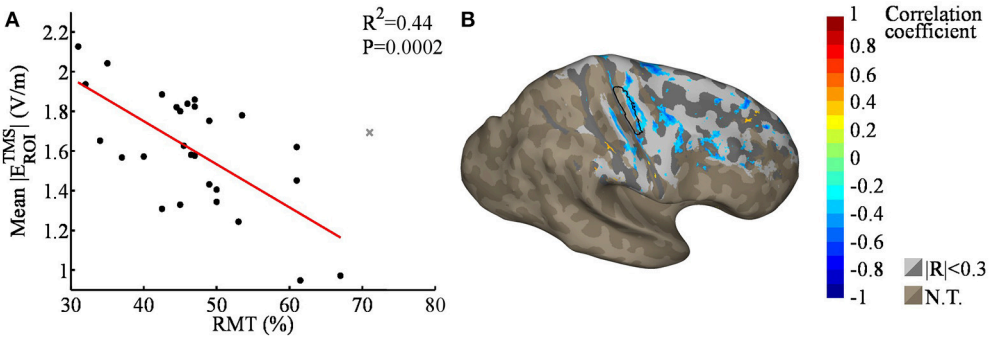

FIGURE 6 | (A) Regression plot of the mean TMS EF strengths within the ROI [black outlined area in **(B)**], as a function of the RMT; the gray cross marks the outlier that was omitted from the analysis. The average TMS EF strength was found to correlate significantly with RMT. **(B)** Nodewise correlation between individual RMT and TMS EFs; correlation coefficients with $|R| > 0.3$ are shown in color, smaller coefficients in gray, and unstudied areas (average TDCS EF lower than 50% of the maximum) in brown (N.T.). The shading in the gray/brown areas represents the gyral structure of the brain (dark = sulci, light = gyri). None of the correlations were significant with 5% FDR.

results suggest that recipients of high TMS EFs may also receive high TDCS EFs, potentially biasing the experimental results of motor cortical TDCS toward subjects who are more sensitive to TMS. However, the TMS stimulator intensity in motor cortical experiments is typically either 110–150% of the RMT or set such that approximately 1 mV MEPs are produced at baseline (Horvath et al., 2015), thus approximately leveling the TMS EFs over subjects and minimizing the potential bias.

It should also be noted that the strength is not the only parameter when talking about the efficacy of TDCS in terms of EFs: also the polarity (anodal/cathodal) and the direction [parallel/perpendicular to the cortical surface (Rawji et al., 2018)] of the EFs should be taken into account when determining the dose. Thus further research is required in order to study whether the RMTs could also be used to predict the efficacy of TDCS. Also, only a single electrode montage for anodal/cathodal stimulation of the motor cortex was considered in this study, so care must be taken in extrapolating these results to other electrode montages and especially to other cortical target sites, as we found that RMT and TDCS EF strengths to correlate significantly only in the M1. Furthermore, instead of the usual approach used in measuring RMT, where the TMS coil is moved on the scalp to pinpoint the stimulation hot spot, we placed the coil guided solely by the MR images without attempting to find the hot spot.

Our computational modeling approach appears to be valid based on the relationship we identified between the measured data (RMTs) and the modeled EFs. However, there are a number of uncertainties inherent in the EF model, including the conductivity values (Akhtari et al., 2006, 2010; Laakso et al., 2016) and the segmentation process (Laakso et al., 2015). The amplitudes of the EFs we observed were within the same ranges as those found in previous simulation studies (Datta et al., 2009, 2012; Laakso et al., 2015, 2016), with the slight differences likely resulting from the different conductivity values and electrode

sizes used in each study. In general, calculated EFs are higher than are those measured *in vivo* (Opitz et al., 2016; Huang et al., 2017), likely due to limitations in the conductivity values and to the experimental difficulties in measuring TDCS EFs *in vivo*.

CONCLUSIONS

The present study revealed that TMS RMTs could be used as a simple measure for estimating the strength of TDCS EFs in hand M1. Subjects having higher RMTs tended to have lower TDCS EFs, implying that the RMT has the potential to serve as a meaningful tool for estimating the EF dose in motor cortical TDCS. Additionally, we demonstrated a correlation between the EFs of TDCS and TMS, suggesting that subjects who are more sensitive to TMS also have higher TDCS EFs in hand M1. Nevertheless, more research on how to convert the observed correlation between TDCS EF strengths and RMTs into a clinically useful method is required.

AUTHOR CONTRIBUTIONS

IL, AH, and ST designed the study. SK and MS performed the measurements and analyzed the measured data. MM and IL performed the computational analysis and analyzed the data. MM, IL, and ST wrote the paper.

FUNDING

The experiment was supported (payment for subject etc.) by grants from the Grants-in-Aid for Scientific Research (KAKENHI: 16H03201 and 17H00869).

REFERENCES

Akhtari, M., Bryant, H., Mamelak, A., Flynn, E., Heller, L., Shih, J., et al. (2002). Conductivities of three-layer live human skull. *Brain Topogr.* 14, 151–167. doi: 10.1023/A:1014590923185

Akhtari, M., Mandelkern, M., Bui, D., Salamon, N., Vinters, H. V., and Mathern, G. W. (2010). Variable anisotropic brain electrical conductivities in epileptogenic foci. *Brain Topogr.* 23, 292–300. doi: 10.1007/s10548-010-0144-z

Akhtari, M., Salamon, N., Duncan, R., Fried, I., and Mathern, G. W. (2006). Electrical conductivities of the freshly excised cerebral cortex in epilepsy surgery patients; correlation with pathology, seizure duration, and diffusion tensor imaging. *Brain Topogr.* 18, 281–290. doi: 10.1007/s10548-006-0006-x

Bashir, S., Perez, J., Horvath, J. C., and Pascual-Leone, A. (2013). Differentiation of motor cortical representation of hand muscles by navigated mapping of optimal tms current directions in healthy subjects. *J. Clin. Neurophysiol.* 30, 390–395. doi: 10.1097/WNP.0b013e31829dda6b

Baumann, S., Wozny, D., Kelly, S., and Meno, F. (1997). The electrical conductivity of human cerebrospinal fluid at body temperature. *IEEE Trans. Biomed. Eng.* 44, 220–223.

Bestmann, S., and Ward, N. (2017). Are current flow models for transcranial electrical stimulation fit for purpose? *Brain Stimul.* 10, 865–866. doi: 10.1016/j.brs.2017.04.002

Bungert, A., Antunes, A., Espenhahn, S., and Thielscher, A. (2016). Where does TMS stimulate the motor cortex? Combining electrophysiological measurements and realistic field estimates to reveal the affected cortex position. *Cereb. Cortex* 27, 5083–5094. doi: 10.1093/cercor/bhw292

Chew, T., Ho, K.-A., and Loo, C. K. (2015). Inter- and intra-individual variability in response to transcranial direct current stimulation (tdcs) at varying current intensities. *Brain Stimul.* 8, 1130-1137. doi: 10.1016/j.brs.2015.07.031

Dale, A. M., Fischl, B., and Sereno, M. I. (1999). Cortical surface-based analysis. I. segmentation and surface reconstruction. *Neuroimage* 9, 179–194. doi: 10.1006/nimg.1998.0395

Datta, A., Bansal, V., Diaz, J., Patel, J., Reato, D., and Bikson, M. (2009). Gyri-precise head model of transcranial direct current stimulation: improved spatial focality using a ring electrode versus conventional rectangular pad. *Brain Stimul.* 2, 201–207. doi: 10.1016/j.brs.2009.03.005

Datta, A., Truong, D., Minhas, P., Parra, L. C., and Bikson, M. (2012). Inter-individual variation during transcranial direct current stimulation and normalization of dose using MRI-derived computational models. *Front. Psychiatry* 3:91. doi: 10.3389/fpsyt.2012.00091

Desikan, R. S., Ségonne, F., Fischl, B., Quinn, B. T., Dickerson, B. C., Blacker, D., et al. (2006). An automated labeling system for subdividing the human cerebral cortex on MRI scans into gyral based regions of interest. *Neuroimage* 31, 968–980. doi: 10.1016/j.neuroimage.2006.01.021

Fiocchi, S., Ravazzani, P., Priori, A., and Parazzini, M. (2016). Cerebellar and spinal direct current stimulation in children: computational modeling of the induced electric field. *Front. Hum. Neurosci.* 10:522. doi: 10.3389/fnhum.2016.00522

Fischl, B., and Dale, A. M. (2000). Measuring the thickness of the human cerebral cortex from magnetic resonance images. *Proc. Natl. Acad. Sci. U.S.A.* 97, 11050–11055. doi: 10.1073/pnas.200033797

Fischl, B., Rajendran, N., Busa, E., Augustinack, J., Hinds, O., Yeo, B. T., et al. (2007). Cortical folding patterns and predicting cytoarchitecture. *Cereb. Cortex* 18, 1973–1980. doi: 10.1093/cercor/bhm225

Fischl, B., Sereno, M. I., and Dale, A. M. (1999). Cortical surface-based analysis. II: Inflation, flattening, and a surface-based coordinate system. *Neuroimage* 9, 195–207. doi: 10.1006/nimg.1998.0396

Freygang W. Jr., and Landau, W. (1955). Some relations between resistivity and electrical activity in the cerebral cortex of the cat. *J. Cell. Compar. Physiol.* 45, 377–392. doi: 10.1002/jcp.1030450305

Fröhlich, F., Burrello, T. N., Mellin, J. M., Cordle, A. L., Lustenberger, C. M., and Gilmore, J. H. (2016). Exploratory study of once-daily transcranial direct current stimulation (tDCS) as a treatment for auditory hallucinations in schizophrenia. *Eur. Psychiatry* 33, 54–60. doi: 10.1016/j.eurpsy.2015.11.005

Gabriel, C., Gabriel, S., and Corthout, E. (1996). The dielectric properties of biological tissues: I. Literature survey. *Phys. Med. Biol.* 41, 2231–2249. doi: 10.1088/0031-9155/41/11/001

Gabriel, C., Peyman, A., and Grant, E. H. (2009). Electrical conductivity of tissue at frequencies below 1 MHz. *Phys. Med. Biol.* 54, 4863–4878. doi: 10.1088/0031-9155/54/16/002

Gabriel, S., Lau, R. W., and Gabriel, C. (1996). The dielectric properties of biological tissues: III. Parametric models for the dielectric spectrum of tissues. *Phys. Med. Biol.* 41, 2271–2293. doi: 10.1088/0031-9155/41/11/003

Herbsman, T., Forster, L., Molnar, C., Dougherty, R., Christie, D., Koola, J., et al. (2009). Motor threshold in transcranial magnetic stimulation: the impact of white matter fiber orientation and skull-to-cortex distance. *Hum. Brain Mapp.* 30, 2044–2055. doi: 10.1002/hbm.20649

Horvath, J. C., Forte, J. D., and Carter, O. (2015). Evidence that transcranial direct current stimulation (tDCS) generates little-to-no reliable neurophysiologic effect beyond mep amplitude modulation in healthy human subjects: a systematic review. *Neuropsychologia* 66, 213–236. doi: 10.1016/j.neuropsychologia.2014.11.021

Huang, Y., Liu, A. A., Lafon, B., Friedman, D., Dayan, M., Wang, X., et al. (2017). Measurements and models of electric fields in the *in vivo* human brain during transcranial electric stimulation. *Elife* 6:e18834. doi: 10.7554/eLife.18834

Ilmoniemi, R. J., Ruohonen, J., and Karhu, J. (1999). Transcranial magnetic stimulation–a new tool for functional imaging of the brain. *Crit. Rev. Biomed. Eng.* 27, 241–284.

Jamil, A., Batsikadze, G., Kuo, H.-I., Labruna, L., Hasan, A., Paulus, W., et al. (2017). Systematic evaluation of the impact of stimulation intensity on neuroplastic after-effects induced by transcranial direct current stimulation. *J. Physiol.* 595, 1723–1288. doi: 10.1113/JP272738

Kessler, S. K., Minhas, P., Woods, A. J., Rosen, A., Gorman, C., and Bikson, M. (2013). Dosage considerations for transcranial direct current stimulation in children: a computational modeling study. *PLoS ONE* 8:e76112. doi: 10.1371/journal.pone.0076112

Koessler, L., Colnat-Coulbois, S., Cecchin, T., Hofmanis, J., Dmochowski, J. P., Norcia, A. M., et al. (2017). *In-vivo* measurements of human brain tissue conductivity using focal electrical current injection through intracerebral multicontact electrodes. *Hum. Brain Mapp.* 38, 974–986. doi: 10.1002/hbm.23431

Kozel, F. A., Nahas, Z., deBrux, C., Molloy, M., Lorberbaum, J. P., Bohning, D., et al. (2000). How coil-cortex distance relates to age, motor threshold, and antidepressant response to repetitive transcranial magnetic stimulation. *J. Neuropsychiatry Clin. Neurosci.* 12, 376–384. doi: 10.1176/jnp.12.3.376

Laakso, I., and Hirata, A. (2012). Fast multigrid-based computation of the induced electric field for transcranial magnetic stimulation. *Phys. Med. Biol.* 57, 7753–7765. doi: 10.1088/0031-9155/57/23/7753

Laakso, I., Hirata, A., and Ugawa, Y. (2014). Effects of coil orientation on the electric field induced by tms over the hand motor area. *Phys. Med. Biol.* 59, 203–218. doi: 10.1088/0031-9155/59/1/203

Laakso, I., Murakami, T., Hirata, A., and Ugawa, Y. (2018). Where and what tms activates: experiments and modeling. *Brain Stimul.* 11, 166–174. doi: 10.1016/j.brs.2017.09.011

Laakso, I., Tanaka, S., Koyama, S., De Santis, V., and Hirata, A. (2015). Inter-subject variability in electric fields of motor cortical tdcs. *Brain Stimul.* 8, 906–913. doi: 10.1016/j.brs.2015.05.002

Laakso, I., Tanaka, S., Mikkonen, M., Koyama, S., and Sadato, N. (2016). Electric fields of motor and frontal tdcs in a standard brain space: a computer simulation study. *Neuroimage* 137, 140–151. doi: 10.1016/j.neuroimage.2016.05.032

Labruna, L., Jamil, A., Fresnoza, S., Batsikadze, G., Kuo, M.-F., Vanderschelden, B., et al. (2016). Efficacy of anodal transcranial direct current stimulation is related to sensitivity to transcranial magnetic stimulation. *Brain Stimul.* 9, 8–15. doi: 10.1016/j.brs.2015.08.014

Latikka, J., Kuurne, T., and Eskola, H. (2001). Conductivity of living intracranial tissues. *Phys. Med. Biol.* 46, 1611–1616. doi: 10.1088/0031-9155/46/6/302

Lindenblatt, G., and Silny, J. (2001). A model of the electrical volume conductor in the region of the eye in the ELF range. *Phys. Med. Biol.* 46, 3051–3059. doi: 10.1088/0031-9155/46/11/319

López-Alonso, V., Cheeran, B., Rio-Rodriguez, D., and Fernández-Del-Olmo, M. (2014). Inter-individual variability in response to non-invasive brain stimulation paradigms. *Brain Stimul.* 7, 372–380. doi: 10.1016/j.brs.2014.02.004

López-Alonso, V., Fernández-Del-Olmo, M., Costantini, A., Gonzalez-Henriquez, J. J., and Cheeran, B. (2015). Intra-individual variability in the response to anodal transcranial direct current stimulation. *Clin. Neurophysiol.* 126, 2342-2347. doi: 10.1016/j.clinph.2015.03.022

Maki, Y., Wong, K. F. K., Sugiura, M., Ozaki, T., and Sadato, N. (2008). Asymmetric control mechanisms of bimanual coordination: an application of directed connectivity analysis to kinematic and functional MRI data. *Neuroimage* 42, 1295–1304. doi: 10.1016/j.neuroimage.2008.06.045

Marquez, J., van Vliet, P., McElduff, P., Lagopoulos, J., and Parsons, M. (2015). Transcranial direct current stimulation (tDCS): does it have merit in stroke rehabilitation? a systematic review. *Int. J. Stroke* 10, 306–316. doi: 10.1111/ijs.12169

Meron, D., Hedger, N., Garner, M., and Baldwin, D. S. (2015). Transcranial direct current stimulation (tDCS) in the treatment of depression: systematic review and meta-analysis of efficacy and tolerability. *Neurosci. Biobehav. Rev.* 57, 46–62. doi: 10.1016/j.neubiorev.2015.07.012

Nieminen, J. O., Koponen, L. M., and Ilmoniemi, R. J. (2015). Experimental characterization of the electric field distribution induced by tms devices. *Brain Stimul.* 8, 582–589. doi: 10.1016/j.brs.2015.01.004

Nitsche, M. A., and Paulus, W. (2000). Excitability changes induced in the human motor cortex by weak transcranial direct current stimulation. *J. Physiol.* 527(Pt 3), 633–639. doi: 10.1111/j.1469-7793.2000.t01-1-00633.x

Nitsche, M. A., and Paulus, W. (2001). Sustained excitability elevations induced by transcranial DC motor cortex stimulation in humans. *Neurology* 57, 1899–1901. doi: 10.1212/WNL.57.10.1899

Opitz, A., Falchier, A., Yan, C.-G., Yeagle, E. M., Linn, G. S., Megevand, P., et al. (2016). Spatiotemporal structure of intracranial electric fields induced by transcranial electric stimulation in humans and nonhuman primates. *Sci. Rep.* 6:31236. doi: 10.1038/srep31236

Opitz, A., Legon, W., Rowlands, A., Bickel, W. K., Paulus, W., and Tyler, W. J. (2013). Physiological observations validate finite element models for estimating subject-specific electric field distributions induced by transcranial magnetic stimulation of the human motor cortex. *Neuroimage* 81, 253–264. doi: 10.1016/j.neuroimage.2013.04.067

Opitz, A., Paulus, W., Will, S., Antunes, A., and Thielscher, A. (2015). Determinants of the electric field during transcranial direct current stimulation. *Neuroimage* 109, 140–150. doi: 10.1016/j.neuroimage.2015.01.033

Opitz, A., Zafar, N., Bockermann, V., Rohde, V., and Paulus, W. (2014). Validating computationally predicted TMS stimulation areas using direct electrical stimulation in patients with brain tumors near precentral regions. *Neuroimage* 4, 500–507. doi: 10.1016/j.nicl.2014.03.004

Priori, A., Berardelli, A., Rona, S., Accornero, N., and Manfredi, M. (1998). Polarization of the human motor cortex through the scalp. *Neuroreport* 9, 2257–2260. doi: 10.1097/00001756-199807130-00020

Ranck, J. B. (1963). Specific impedance of rabbit cerebral cortex. *Exp. Neurol.* 7, 144–152.

Rawji, V., Ciocca, M., Zacharia, A., Soares, D., Truong, D., Bikson, M., et al. (2018). tDCS changes in motor excitability are specific to orientation of current flow. *Brain Stimul.* 11, 289–298. doi: 10.1016/j.brs.2017.11.001

Rossini, P. M., Berardelli, A., Deuschl, G., Hallett, M., Maertens de Noordhout, A. M., Paulus, W., et al. (1999). Applications of magnetic cortical stimulation. The international federation of clinical neurophysiology. *Electroencephalogr. Clin. Neurophysiol. Suppl.* 52, 171–185.

Saturnino, G. B., Antunes, A., and Thielscher, A. (2015). On the importance of electrode parameters for shaping electric field patterns generated by tDCS. *Neuroimage* 120, 25–35. doi: 10.1016/j.neuroimage.2015.06.067

Stokes, M. G., Chambers, C. D., Gould, I. C., English, T., McNaught, E., McDonald, O., et al. (2007). Distance-adjusted motor threshold for transcranial magnetic stimulation. *Clin. Neurophysiol.* 118, 1617–1625. doi: 10.1016/j.clinph.2007.04.004

Stoy, R. D., Foster, K. R., and Schwan, H. P. (1982). Dielectric properties of mammalian tissues from 0.1 to 100 mhz; a summary of recent data. *Phys. Med. Biol.* 27:501. doi: 10.1088/0031-9155/27/4/002

Thielscher, A., and Kammer, T. (2004). Electric field properties of two commercial figure-8 coils in TMS: calculation of focality and efficiency. *Clin. Neurophysiol.* 115, 1697–1708. doi: 10.1016/j.clinph.2004.02.019

Tofts, P. S. (1990). The distribution of induced currents in magnetic stimulation of the nervous system. *Phys. Med. Biol.* 35, 1119–1128. doi: 10.1088/0031-9155/35/8/008

Truong, D. Q., Magerowski, G., Blackburn, G. L., Bikson, M., and Alonso-Alonso, M. (2013). Computational modeling of transcranial direct current stimulation (tDCS) in obesity: impact of head fat and dose guidelines. *Neuroimage Clin.* 2, 759–766. doi: 10.1016/j.nicl.2013.05.011

Wake, K., Sasaki, K., and Watanabe, S. (2016). Conductivities of epidermis, dermis, and subcutaneous tissue at intermediate frequencies. *Phys. Med. Biol.* 61:4376. doi: 10.1088/0031-9155/61/12/4376

Wang, W., and Eisenberg, S. (1994). A three-dimensional finite element method for computing magnetically induced currents in tissues. *IEEE Trans. Magnet.* 30, 5015–5023. doi: 10.1109/20.334289

Wiethoff, S., Hamada, M., and Rothwell, J. C. (2014). Variability in response to transcranial direct current stimulation of the motor cortex. *Brain Stimul.* 7, 468–475. doi: 10.1016/j.brs.2014.02.003

Conflict of Interest Statement: The authors declare that the research was conducted in the absence of any commercial or financial relationships that could be construed as a potential conflict of interest.

frontiers in Neuroscience

METHODS
published: 26 June 2018
doi: 10.3389/fnins.2018.00376

Effect of Stimulation Waveform on the Non-linear Entrainment of Cortical Alpha Oscillations

Axel Hutt[1], *John D. Griffiths*[2,3], *Christoph S. Herrmann*[4] *and Jérémie Lefebvre*[3,5]*

[1] Deutscher Wetterdienst, Department FE12-Data Assimilation, Offenbach am Main, Germany, [2] Rotman Research Institute, Baycrest Health Sciences, Toronto, ON, Canada, [3] Krembil Research Institute, University Health Network, Toronto, ON, Canada, [4] Experimental Psychology Lab, Department of Psychology, Cluster of Excellence "Hearing4all", European Medical, School, Carl von Ossietzky University, Oldenburg, Germany, [5] Department of Mathematics and Institute for Biomaterials and Biomedical Engineering, University of Toronto, Toronto, ON, Canada

In the past decade, there has been a surge of interest in using patterned brain stimulation to manipulate cortical oscillations, in both experimental and clinical settings. But the relationship between stimulation waveform and its impact on ongoing oscillations remains poorly understood and severely restrains the development of new paradigms. To address some aspects of this intricate problem, we combine computational and mathematical approaches, providing new insights into the influence of waveform of both low and high-frequency stimuli on synchronous neural activity. Using a cellular-based cortical microcircuit network model, we performed numerical simulations to test the influence of different waveforms on ongoing alpha oscillations, and derived a mean-field description of stimulation-driven dynamics to better understand the observed responses. Our analysis shows that high-frequency periodic stimulation translates into an effective transformation of the neurons' response function, leading to waveform-dependent changes in oscillatory dynamics and resting state activity. Moreover, we found that randomly fluctuating stimulation linearizes the neuron response function while constant input moves its activation threshold. Taken together, our findings establish a new theoretical framework in which stimulation waveforms impact neural systems at the population-scale through non-linear interactions.

Keywords: stimulation waveform, synchrony, entrainment, neural dynamics, networks, oscillations

OPEN ACCESS

Edited by:
Olivier David,
Institut National de la Santé et de la Recherche Médicale (INSERM), France

Reviewed by:
Thomas R. Knösche,
Max-Planck-Institut für Kognitions- und Neurowissenschaften, Germany
Tamer Demiralp,
Istanbul University, Turkey

***Correspondence:**
Jérémie Lefebvre
jeremie.lefebvre@uhnresearch.ca

Specialty section:
This article was submitted to Neural Technology, a section of the journal Frontiers in Neuroscience

Received: *02 March 2018*
Accepted: *16 May 2018*
Published: *26 June 2018*

Citation:
Hutt A, Griffiths JD, Herrmann CS and Lefebvre J (2018) Effect of Stimulation Waveform on the Non-linear Entrainment of Cortical Alpha Oscillations. Front. Neurosci. 12:376. doi: 10.3389/fnins.2018.00376

INTRODUCTION

Oscillatory brain activity results from the collective and synchronous discharge of large populations of neurons, and is thought to play an important role in homeostasis, neural communication and information processing (Singer and Gray, 1995; Engel and Singer, 2001; Varela et al., 2001; Lakatos et al., 2008). In humans, such oscillations have been shown to be important for cognitive functions, and disturbed brain oscillations can result in cognitive deficits or neurological and psychiatric diseases (Uhlhaas and Singer, 2006). Many years of correlational analysis have shown that parameters of brain oscillations correlate with human perception, attention, memory, and behavior (Engel et al., 2001; Buzsáki and Draguhn, 2004; Hipp et al., 2011). Recent studies using TMS and tACS to modulate brain oscillations revealed a *causal* role of brain oscillations for such cognitive functions (e.g., Helfrich et al., 2014; Cecere et al., 2015; Dreyer and Herrmann, 2015). Importantly, all parameters of brain

oscillations (amplitude, frequency, and phase) have been related to certain aspects of cognitive functions. While it has been repeatedly shown that e.g., tACS can up-regulate the amplitude of brain oscillations (Thut and Miniussi, 2009; Helfrich et al., 2014), less is known about down-regulating their amplitude or frequency, and how this depends on stimulation waveform. Intuitively, repetitive trains of negative and positive current pulses should have opposite effects on the frequency of brain oscillations. Do positive and negative pulse trains simply mirror each other with respect to the entrainment of alpha oscillations? Are pulses equivalent to sinusoids? Can noise-induced-like effects be triggered by deterministic signals? Answering these key questions would significantly improve our understanding of the role played by stimulation pattern on oscillatory brain dynamics, and catalyze the development of new clinical stimulation paradigms meant to engage neural populations and cortical oscillations.

This study sets out to answer some of these questions by harnessing computational and mathematical techniques and study the effect of stimulation waveform on cortical alpha oscillations. Alpha oscillations have been implicated in a wide variety of physiological and cognitive functions (Başar, 2012; Mierau et al., 2017), and have repeatedly been targeted using non-invasive stimulation in investigations aimed at obtaining a better understanding of the functional properties of cortical circuits (Fröhlich and McCormick, 2010; Cecere et al., 2015; Romei et al., 2016). Alpha oscillations have been shown to be maintained by large scale processes (Hindriks et al., 2014) supported by delayed network interactions (Cabral et al., 2014), and to build on slower and more global inhibitory processes (Klimesch et al., 2007; Womelsdorf et al., 2014). As such, to understand the effect of stimulation on these collective oscillations, a population-scale approach—in which networks of neurons are considered as opposed to individual cells—is necessary.

To provide new insight into the effects of brain stimulation on neural populations, we use two computational models in parallel and explore the impact of stimulation waveform and polarity on alpha oscillations. The first model, which we study numerically, is a cortical microcircuit network model which has been used before by the authors to investigate alpha resonance and entrainment in the cortex (Herrmann et al., 2016). The second model is a reduced neural oscillator model (Lefebvre et al., 2015; Hutt et al., 2016), which we derive from the cortical microcircuit model and analyze to understand the relationship between stimulation waveform and peak oscillation frequency. We combine insights provided by these two models to better understand, from a population-scale perspective, how stimulation waveforms can be tuned to either accelerate or slow down cortical alpha activity. We examine both near-resonant stimulation frequencies, where phase locking with the stimulation waveform can be observed, and higher frequencies, where we see the occurrence of non-linear entrainment. Through this approach, we develop a framework in which the effects of high-frequency stimuli with various waveform shapes on neural oscillations can be characterized by analyzing the associated transformation of the neurons' input/output (i.e., response) function. Recent experimental and computational studies have shown that the shape of the neural response function is altered in the presence of direct cortical stimulation, through a combination of somatic and synaptic effects (Lafon et al., 2017). To validate these results, and see how they are impacted by stimulation waveform, we systematically analyze neural population dynamics in the presence of repetitive pulse trains of positive and negative polarities, as well as sinusoidal drive and Gaussian white noise. We compare each case by deriving the associated mean-field dynamics, using a formalism that directly incorporates the effects of stimulation into the model equations. We then explore the influence of stimulation frequency and amplitude on network oscillations. In addition, our analysis suggests that, from a population perspective, the high-dimensionality of stimulation waveform parameter space can be significantly reduced by observing that seemingly distinct waveforms may possess equivalent entrainment properties. Our results further provide new perspectives on the waveform-specific interaction between stimulation and non-linear feedback in neural networks.

MATERIALS AND METHODS

Cortical Microcircuit Model

To study the influence of different stimulation waveforms on oscillatory dynamics in cortical microcircuits, we here consider a model of interacting cortical populations and investigate changes in limit cycle solutions when subjected to stimulation. This model has been thoroughly discussed and analyzed in previous work (Herrmann et al., 2016), and thus we present it here briefly only.

This cortical network consists of spatially extended excitatory (e) and inhibitory (i) populations, whose activities are governed by the dynamics and interactions of neuronal ensembles. These ensembles, or sub-networks, include recurrently coupled neurons subjected to excitatory and inhibitory synaptic input, respectively. The ensemble spiking activity of each patch is modeled by the non-homogeneous Poisson processes

$$X_n^j(t) \to Poisson\left(f\left[u_n^j(t)\right]\right) \tag{1}$$

where $X_n^j(t) = \sum_{t_l} \delta_n^j(t - t_l)$ is the ensemble spike train of the jth patch and $n = e, i$ indicate excitatory and inhibitory populations, respectively. The firing rate function $f[u]$, also called the response function, sets the relationship between input potentials and output firing rates (Hutt and Buhry, 2014; Lefebvre et al., 2015; Herrmann et al., 2016). It exhibits a sigmoidal shape given by $f\left[u_n^j\right] = \left(1 + \exp\left[-\beta(u_n^j - h)\right]\right)^{-1}$ i.e., the firing rate probability approaches $f = 1$ for large membrane potentials, where the gain is $\beta > 0$ and the firing rate threshold is h. This defined, the model combines both the spiking of single cells as well as a dependence on the firing rate of the whole population. Such a hybrid cortical model thus combines both spiking and rate driven dynamics. The excitatory and inhibitory potentials $u_e^j(t)$ and $u_i^j(t)$ represent ensemble-averaged potentials proportional to averaged dendritic currents. They obey the set of non-linear

stochastic equations

$$\alpha_n^{-1}\frac{du_n^j(t)}{dt} = L[u_n^j(t)] + \sum_m G_{nm}^j(t) + \sqrt{2D_n}\,\xi_n^j(t) + S(t) \quad (2)$$

with $n = e, i$ and the temporal rate constants α_n. The linear operator $L[U] = k\,U$ represents membrane leaks. All cells in the network are driven by an external global stimulation $S(t)$ exhibiting various waveforms. The cross-population recurrent inputs $G_{nm}^j(t)$ are defined by

$$G_{nm}^j(t) = \sum_{k=1}^{N_m} W_{nm}^{jk}(c)\cdot PSP_m^k\left(t-\tau^{jk}\right) \quad (3)$$

where $PSP_m^k(t)$ refers to mean post-synaptic potential of patch k in population m at time t. Interactions between subnetworks k and l are subjected to intracortical propagation delays $\tau^{jk} = \left|x(k) - x(i)\right| v^{-1}$, with v being the axonal conduction velocity, set here to v =0.13 m/s (Hutt et al., 2003). They are computed by convolving the time-delayed ensemble spike trains with exponential synapses of the form

$$PSP_m^k(t) = \int_o^t X_m^k(s)\,\frac{1}{a_m}e^{-\frac{t-s}{a_m}}\,ds \quad (4)$$

with synaptic time constant a_m.

Excitatory and inhibitory populations are subjected to endogenous sources of noise $\xi_n^j(t)$, assumed to follow spatially and temporally independent Gaussian white noise profiles with fixed variance D_n. Synaptic weights within $(W_{ee}^{jk}(c), W_{ii}^{jk}(c))$ and between $(W_{ei}^{jk}(c), W_{ie}^{jk}(c))$ excitatory and inhibitory populations exhibit sparse exponential profiles (Hellwig, 2000) with connection probability c, that is

$$W_{nm}^{jk}(c) = w_{nm}^o(c)\exp\left[-\sigma_{n,m}^2\left|x(j) - x(k)\right|\right] \quad (5)$$

Neuron ensembles in the network are distributed randomly within a one-dimensional spatial domain Ω. The constants $\sigma_{n,m}^2 = \sigma_e^2$, σ_i^2 correspond to the range of the excitatory and/or inhibitory interactions, $x(k)$ refers to the spatial location of neurons in patch k and the connection probability is $c = 0.6$ i.e., 40% of the synaptic weights were randomly set to zero. The spatially-averaged neuroelectric network activity is a weighted sum over potentials of the excitatory and inhibitory population

$$A(t) = \frac{1}{N_e}\sum_{k=1}^{N_e}\phi_e^k u_e^k(t) + \frac{1}{N_i}\sum_{k=1}^{N_i}\phi_i^k u_i^k(t) \quad (6)$$

where $\phi_{e,i}^k$ are real positive coefficients. Here we assume that the network fine scale structure is unknown, and thus consider random weights i.e., $\phi_{e,i}^k$ =[0,1] (Herrmann et al., 2016). We did this to take into account various sources of observational variability that we do not model explicitly. However, specific choices of coefficient distributions can be made to increase the similarity of the neuroelectric output to signals such as LFPs and EEG (e.g., see Lindén et al., 2010). Model parameters are given in **Table 1**.

Spectral Analysis

Spectral analysis was performed using a fast Fourier transform routine using freely available C++ scripts (Press et al., 2007). The power spectrum for each simulation condition is an average over five independent trials, each computed as the magnitude of the Fourier transform (with rectangular time window) of a time series of 4,000 ms duration. The long duration of the time series ensures negligible spectral leakage effects.

Reduced Neural Oscillator Model

To better understand the mechanism involved in shaping oscillations in the cortical microcircuit model, we use a scalar and reduced non-linear network as a prototype to rigorously analyze the role of delayed and non-linear interactions in shaping emergent oscillations, and specifically how those are impacted by stimulation waveform. This simplified model sacrifices many physiological details in comparison to the cortical microcircuit model but preserves key components underlying the rhythmic activity seen in the cortical microcircuit model while remaining analytically tractable. Our goal here is to obtain a qualitative assessment of the different phenomena observed in our results.

Oscillations in the cortical microcircuit model arise due to delayed recurrent inhibition conveyed by inhibitory synapses. In this regime, inhibitory interactions dominate the dynamics, and the cortical microcircuit model can be significantly simplified, preserving the key components responsible of the oscillations. Specifically, we focus on parameters that result in an inhibition driven regime in which

$$G_{ee}^j, G_{ei}^j \ll G_{ie}^j, G_{ii}^j. \quad (7)$$

Consequently, the dynamics of the cortical model obeys in good approximation

$$\begin{aligned}\alpha_e^{-1}\frac{du_e^j(t)}{dt} &\approx L[u_e^j(t)] + G_{ie}^j(t) + \sqrt{2D_e}\xi_e^j(t) + S(t)\\ \alpha_i^{-1}\frac{du_i^j(t)}{dt} &\approx L[u_i^j(t)] + G_{ii}^j(t) + \sqrt{2D_i}\,\xi_i^j(t) + S(t)\end{aligned} \quad (8)$$

This approximation renders independent the dynamics of the inhibitory population from the activity of the excitatory cells. The excitatory membrane potential is thus, on average, driven by the activity of the inhibitory population, such that one may fully characterize the activity of the network by considering inhibitory ensemble dynamics. Assuming that the firing rate is high and that σ_i is small enough, i.e., broad spatial connectivity, we can write

$$\begin{aligned}G_{ii}^j(t) &\approx \sum_{k=1}^{N_m} W_{ii}^{jk}(c)\cdot f\left[u_i^k\left(t-\tau^{jk}\right)\right]\\ &\approx w_{ii}^o\sum_{k=1}^{N_m} f[u_i^k(t-\bar{\tau})]\end{aligned} \quad (9)$$

TABLE 1 | Cortical microcircuit network model parameters.

Symbol	Definition	Value
Ω	Network spatial size	10 mm
N_e	Number of excitatory neurons	800
N_i	Number of inhibitory neurons	200
β	Response function gain	300 a.u.
h	Response function threshold	−0.1 a.u.
τ_m	synaptic time constant	10 ms
α_e	Dendritic rate constant – excitatory	1.0
α_i	Dendritic rate constant – inhibitory	1.5
v	Conduction velocity	0.128 m/s
c	Connection probability	0.6
w^o_{ee}	$e \to e$ synaptic connection strength	60
w^o_{ei}	$e \to i$ synaptic connection strength	70
w^o_{ie}.	$i \to e$ synaptic connection strength	−70
w^o_{ii}	$i \to i$ synaptic connection strength	−70
σ^2_e	Excitatory synaptic spatial decay rate	1.0 a.u.
σ^2_i	Inhibitory synaptic spatial decay rate	0.5 a.u.
D	Intrinsic noise level	0.0001
dt	Integration time step	1 ms

where $\bar{\tau} = \int_0^\infty \tau g(\tau)\, d\tau \approx 25$ ms is the mean propagation delay and$g(\tau) = \frac{2c^2}{\Omega^2}\left(\frac{\Omega}{c} - \tau\right) \mid 0 \leq \tau \leq \frac{\Omega}{c}$. is the distribution of delays in our model. Taken together, now we may fully describe the response of the cortical populations to stimulation in the inhibitory-driven regime by the following scalar equation,

$$\alpha^{-1}\frac{d}{dt}U^j(t) = L\left[U^j(t)\right] + gN^{-1}\sum\nolimits_{j=1}^{N} f[U^j(t-\bar{\tau})] + S(t) \tag{10}$$

where $\alpha^{-1} \equiv \alpha_i^{-1}$ and $U^j(t) \equiv u_i^j(t)$ was introduced to distinguish the more detailed cortical microcircuit model and the reduced model in the subsequent calculations. The mean synaptic connectivity $w^o_{ii} = gN^{-1}$ has also been introduced to indicate the average evaluated over all possible pairs of inhibitory neurons. According to the derivations above the mean synaptic action is inhibitory with $g < 0$. The non-linear response function above remains the same with $f[u] = \left(1 + \exp\left[-\beta\left(u - h\right)\right]\right)^{-1}$. This kind of approximation has been used frequently in the literature (e.g., Curtu and Ermentrout, 2004) to express the dynamics of excitatory and inhibitory networks from the perspective of a particular cellular species. For the rest of the analysis, we assume that $L[U] = -U$.

Mean Field Dynamics in Presence of Stimulation

A common approach when trying to understand the essential dynamical characteristics of an otherwise high-dimensional system is to derive mean-field representations. What is different here is that we apply the mean field reduction by including stimulation in the calculations. As such, let us further assume that limit cycle solutions occur in a mean-driven regime in which the local dynamics can be seen as small independent fluctuations around a slowly varying mean $\bar{U}$ i.e.,

$$U^j(t) = \bar{U}(t) + V^j(t) \tag{11}$$

where $\bar{U}$ is given by

$$\bar{U}(t) = N^{-1}\sum_{i=1}^{N} U^j(t) \equiv < U >_N \tag{12}$$

and $< \ >_N$ is an average performed over the N units of the network. As an ansatz, local fluctuations V^j from the mean obey the zero mean processes

$$\frac{d}{dt}V^j = -V^j + S(t) - \mu_S, \tag{13}$$

where we have used the fact that $L[U] = -U$ and where

$$\mu_S = \int_t^{t+T} S(s)\, ds \tag{14}$$

for T sufficiently small. Then taking the mean over N neurons in Equation (10) above yields the mean dynamics of the network in presence of stimulation

$$\frac{d}{dt}\bar{U}(t) = -\bar{U}(t) + gF\left[\bar{U}(t-\bar{\tau})\right] + \mu_S\,. \tag{15}$$

Now the network dynamics are governed by the effective neuron response function (Hutt et al., 2016)

$$F\left[\bar{U}\right] = \int_{\Omega(\nu)} f\left[\bar{U} + V\right]\rho(V)dV \tag{16}$$

where $\rho(V)$ is the probability density function of the solution of Equation (13). According to this framework, the effect of a dynamic stimulus $S(t)$ with stationary statistics can be characterized by looking at the probability density function $\rho\,(V)$ associated to the linear and zero-mean processes whose dynamics obey Equation (13) and its convolution with the response function of the network as per Equation (16). We note that the mean field equation must be interpreted.

RESULTS

Response of Cortical Neurons to Stimulation

To better understand the role of stimulation waveforms on the entrainment of network oscillations, we integrated numerically Equation (2) for different functional forms of the input term $S(t)$: positive pulses, negative pulses, sinusoidal stimulation, and Gaussian white noise. In each case, all model parameters, except those related to the stimuli, were kept constant. Representative network responses to different waveforms are plotted in **Figure 1**. As seen in **Figure 1A**, without any stimulation, and for the set of parameters chosen, the network stabilizes into alpha-like synchronous activity. Spiking of the neurons is locked to these emergent global oscillations, resulting in a clear peak frequency of 10 Hz. When a pulse train stimulus with positive polarity was applied continuously at a rate of 50 Hz, network oscillations were found to accelerate with respect to baseline, stabilizing at a frequency of about 12 Hz. As shown in **Figure 1B**, the power of the associated oscillations and spike coherence were also both increased. We here recover the results of Herrmann et al. (2016), in which high-frequency (positive) pulse trains trigger non-linear acceleration of endogenous oscillations by changing the natural frequency of the solution of Equation (2). In **Figure 1C** however, when the network is stimulated continuously with a pulse train of negative polarity at a rate of 50 Hz, the opposite occurs: endogenous oscillations are slowed-down with respect to baseline. This novel effect, in contrast to the positive pulses, was not predicted by previous theoretical work. When sinusoidal stimulation was applied as shown in **Figure 1D**, endogenous oscillations were found to be entrained in a similar fashion as with positive pulses (cf. **Figure 1A**). Uncorrelated Gaussian white noise was found to have an analogous yet more pronounced effect (**Figure 1E**). Taken together, these results indicate that different stimulation waveforms have variable impact on the entrainment of endogenous network oscillations.

To understand how these results depend on stimulation settings and waveforms, we measured the response of the network while stimulation parameters were changed. For pulse trains and sinusoidal inputs, frequencies were systematically varied between 0 and 100 Hz with fixed amplitude. In the case of Gaussian white noise, the intensity of the noise was gradually increased between 0 and 0.01. Results are shown in **Figure 2**. **Figure 2A** shows that for positive pulses, increasing the stimulation frequency gradually shifted the peak response frequency from 10 to 12 Hz (Herrmann et al., 2016). The results were quite different with negative pulses: In **Figure 2B**, the peak frequency was slowed down and decreased in intensity (power decreases) until endogenous oscillations lost stability. Acceleration of endogenous oscillation was also observed in **Figures 2C,D** when sinusoidal input and Gaussian white noise were used, respectively. The different periodic stimulation cases are also depicted in **Figure 3**, where the range of stimulation frequencies is narrowed to a range about the endogenous frequency.

For stimulation frequencies close to but larger than the endogenous frequency, positive pulses and sinusoidal stimulation entrain the endogenous rhythm. Conversely, negative pulses entrain the endogenous rhythm for a more narrow range of frequencies.

Impact of Stimulus Waveform on Alpha Oscillations: Theoretical Insights

To understand the mechanism behind the numerical observations made with the cortical microcircuit model (**Figures 1**, **2**), we developed a reduced non-linear network model based on a mean-field approximation that preserved the mean features of the initial model, but remained analytically tractable (see section Materials and Methods).

As a first step to understand how the stimulation waveform affects endogenous oscillations, we applied the reduced neural oscillator model to characterize the effect of different stimulation waveforms on the response function of the network in Equation (15). These computations show that different stimulation patterns—leading to different statistics of the fluctuations around the activity mean—shape the effective response function in a plurality of waveform-dependent ways. The cases analyzed below are sequentially illustrated in **Figure 4**.

1. Pulse Train Stimulation

Let us first consider the stimulus waveform

$$S\,(t) = S\sum\nolimits_n \delta\left(t - \frac{2\pi}{r}n\right), \tag{17}$$

where $\delta\,(0) = 1$ and zero otherwise. This pulse train has a rate r and an intensity of$S$. Using the mean-field formalism we have detailed earlier, fluctuations about the mean network activity $\bar{u}$ obey

$$\frac{d}{dt}V^j = -V^j + S\sum\nolimits_n \delta\left(t - \frac{2\pi}{r}n\right) - \mu_S \tag{18}$$

with $\mu_S = Sr$. To obtain the effective neuron response function, one has to convolve the firing rate function f with the normalized probability density $\rho(V)$ for the process (18) according to Equation (16)

$$\rho\,(V) = \begin{cases} \frac{r}{V-\mu_S} \mid V \in [Se^{-\frac{1}{r}}, S] \\ 0 \mid \text{otherwise} \end{cases} \tag{19}$$

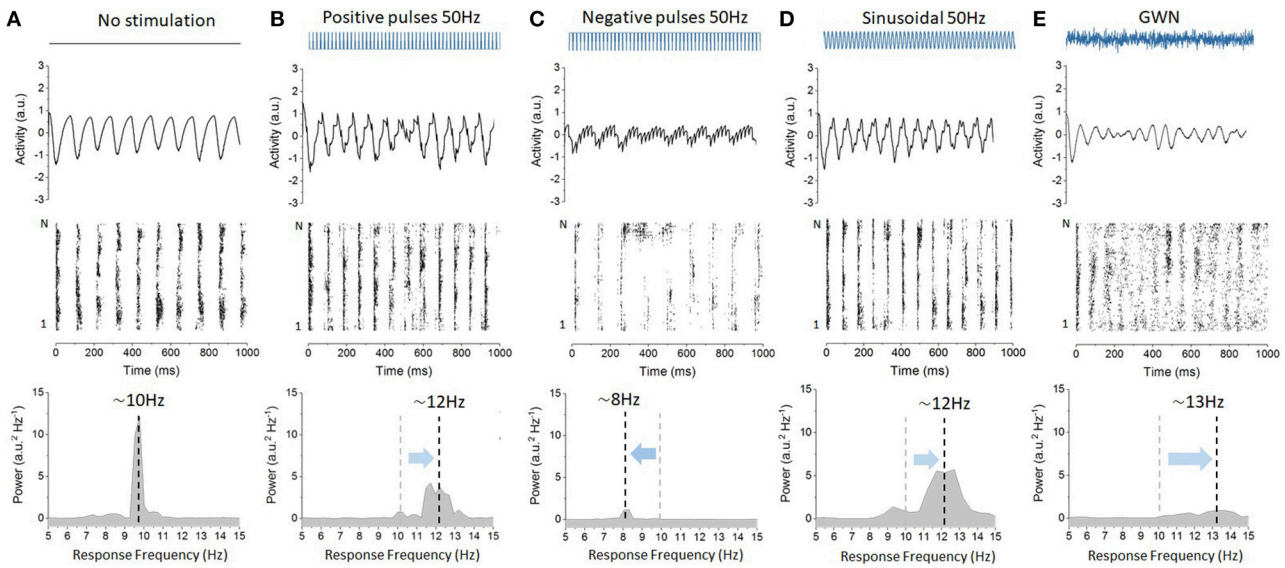

FIGURE 1 | Variability of the cortical microcircuit network responses to stimulation with diverse waveforms. Stimulation has different impact on network resting state oscillations depending on the waveform applied. **(A)** Baseline oscillatory activity in absence of stimulation. The network neuroelectric output is plotted (top), as well as the spiking activity of the excitatory neurons (middle) and the power spectral density of the network output (bottom). The network displays stable oscillations of 10 Hz and ensemble spiking is phase locked to these intrinsic oscillations. **(B)** Positive pulses with a frequency of 50 Hz are found to accelerate endogenous oscillatory activity from 10 Hz **(A)** up to 12 Hz, entraining the neurons into faster cycles. Here, $S = 2.5$. Power expressed at the peak frequency also decreases with respect to baseline. **(C)** Negative pulses at 50 Hz, in contrast, decelerate endogenous oscillations from 10 Hz to about 8 Hz, and significantly suppress the power of endogenous oscillations. Here $S = 2.5$. **(D)** A sinusoidal waveform delivered at 50 Hz is also found to accelerate endogenous oscillations. The intensity of the sinusoidal signal, by virtue of being a continuous (i.e., not a discontinuous) was set to a smaller amplitude. Here $S = 0.5$. **(E)** For reference, Gaussian white noise (GWN) is also applied, and the 10 Hz oscillations are significantly accelerated from 10 Hz **(A)** up to 13 Hz. Here the noise intensity was increased from $D = 0.0001$ **(A–D)** to $D = 0.01$.

In the limit of high gain, $f[U] \approx H[U-h]$, then the effective response function becomes

$$F\left[\bar{U}\right] = r\int_{S}^{S\,e^{-\frac{1}{r}}} \frac{H\left[\bar{U}+V-h\right]}{V}dV$$
$$= -rH\left[\bar{U}+S-h\right]\left(\ln\left[-\bar{U}\right]-\ln\left[S\right]\right)+rH\left[\bar{U}+S\exp\left(-\frac{1}{r}\right)-h\right]$$
$$\left(\ln\left[-\bar{U}\right]-\ln\left[S\exp\left(-\frac{1}{r}\right)\right]\right). \quad (20)$$

Then the network mean activity $\bar{u}$ obeys the mean-field dynamics

$$\frac{d}{dt}\bar{U}(t) = -\bar{U}(t) + gF\left[\bar{U}(t-\bar{\tau})\right] + S\,r. \quad (21)$$

Note that in these calculations, we have made no assumptions on the value of S and as such the result above holds for both positive and negative pulse trains. These two cases ($S > 0$, $S < 0$) are illustrated in **Figures 4B,C**.

2. Sinusoidal Stimulation

Let us now consider the periodic stimulation

$$S(t) = S\,\sin(2\pi\omega_s t) \quad (22)$$

with angle frequency ω_s. Fluctuations around the mean obey

$$\frac{d}{dt}V^j = -V^j + S\,\sin(2\pi\omega_s t) \quad (23)$$

since $\mu_S = 0$. This case was studied in detail in Hutt et al. (2016). One can show that the associated normalized probability density function $\rho(V)$ reads (Baker, 2006)

$$\rho(V) = \frac{1}{\pi\sqrt{(S/2\pi\omega_s)^2 - V^2}} \quad (24)$$

and consequently the effective non-linearity is given by

$$\tilde{F}\left[\bar{U}\right] \approx \int_{-\mu}^{\mu} \frac{H\left[\bar{U}+V-h\right]}{\pi\sqrt{\left(\frac{S}{2\pi\omega_s}\right)^2 - V^2}}dv = \frac{1}{\pi}\sin^{-1}(2\pi\omega_S\bar{U}/S)$$
$$+\frac{1}{2},\ -1 \le 2\pi\omega_S\bar{U}/S \le 1 \quad (25)$$
$$\tilde{F}\left[\bar{U}\right] = 1,\ 2\pi\omega_S\bar{U}/S > 1$$
$$\tilde{F}\left[\bar{U}\right] = 0,\ 2\pi\omega_S\bar{U}/S < -1$$

As illustrated in **Figure 4D**, the effective response function of the system is primarily linearized locally near the inflection point (i.e., $h = 0$).

3. Gaussian White Noise Stimulation

Next, we study Lefebvre and Hutt (2013):

$$S(t) = S_j(t) = \sqrt{2D}\,\xi_j(t), \quad (26)$$

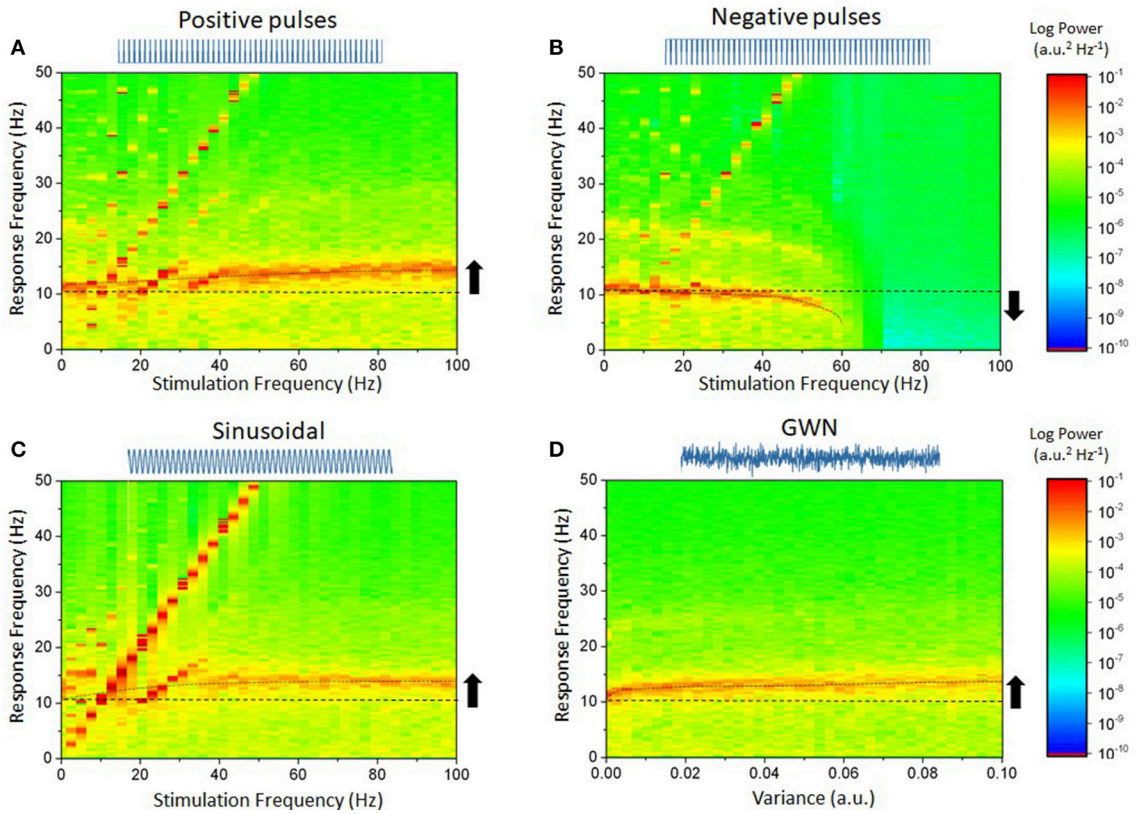

FIGURE 2 | Diverse effects of stimulation waveform and frequency on the power spectrum in the cortical microcircuit network model. In each case, a waveform was chosen and used to stimulate the network. Stimulation frequency was increased while the power spectrum of the network responses was calculated. **(A)** Positive pulses, of frequencies ranging from 1 Hz up to 100 Hz are found to shape endogenous activity. The diagonal lines, representing the linear contribution of the stimulation waveform, delineate regions of entrainment. For slower frequencies, the network peak frequency shifts from its endogenous value to the stimulation's: neurons ensemble spiking is phased locked to the stimulation. For higher stimulation frequencies, endogenous oscillations accelerate, indicating non-linear entrainment. **(B)** Negative pulses do the opposite. Entrainment is weaker, and endogenous oscillations are gradually slowed down until they are suppressed as stimulation frequency is increased. **(C)** Sinusoidal inputs show a similar yet more pronounced effect as positive pulses. **(D)** By increasing the variance of the Gaussian white noise (GWN) input, the network's oscillations also accelerate. No entrainment can be seen as the stimulation possessed no dominant frequency. Parameters are as in **Figure 1**.

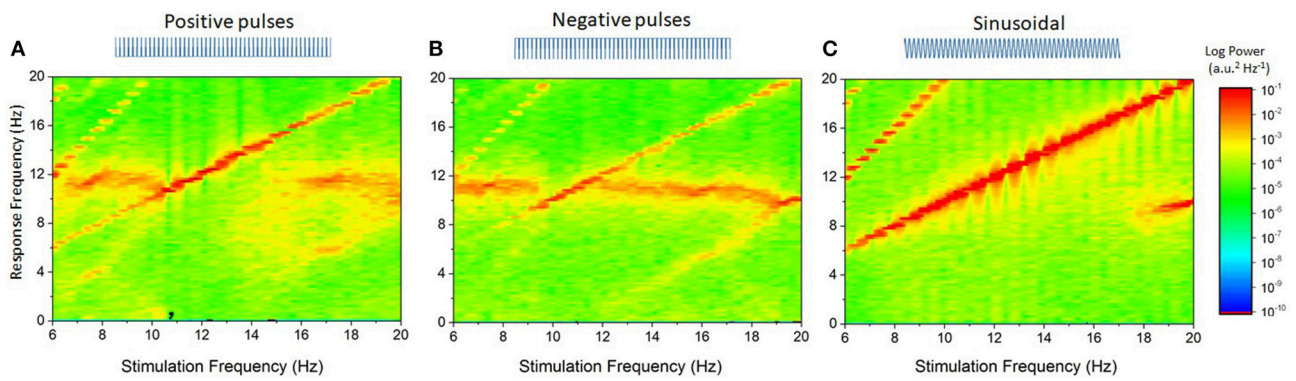

FIGURE 3 | Impact of stimulation waveform on endogenous oscillations for near-resonant stimulation frequencies. This represents a close-up of the data plotted in **Figure 2**, over the interval 8–20 Hz. **(A)** Positive pulses with frequency ranging from 8 to 20 Hz shows that entrainment of network activity occurs for stimulation frequencies near the endogenous frequency of 10 Hz. The entrainment region is also non-symmetrical around that frequency: phase-locking is more pronounced to the right than to the left, indicating that the endogenous frequency accelerates as the stimulation frequency changes. **(B)** Negative pulses have a narrower entrainment region, and the network slowing down can readily be seen dominating the dynamics. **(C)** Sinusoidal stimulation is clearly more effective at entraining endogenous oscillations: the network dynamics is fully phase-locked to the stimulation frequency over this interval. Gaussian white noise (GWN) is here omitted because no entrainment occurs (see **Figure 2**). In all panels, the stimulation amplitude is the same. Parameters are as in **Figure 2**.

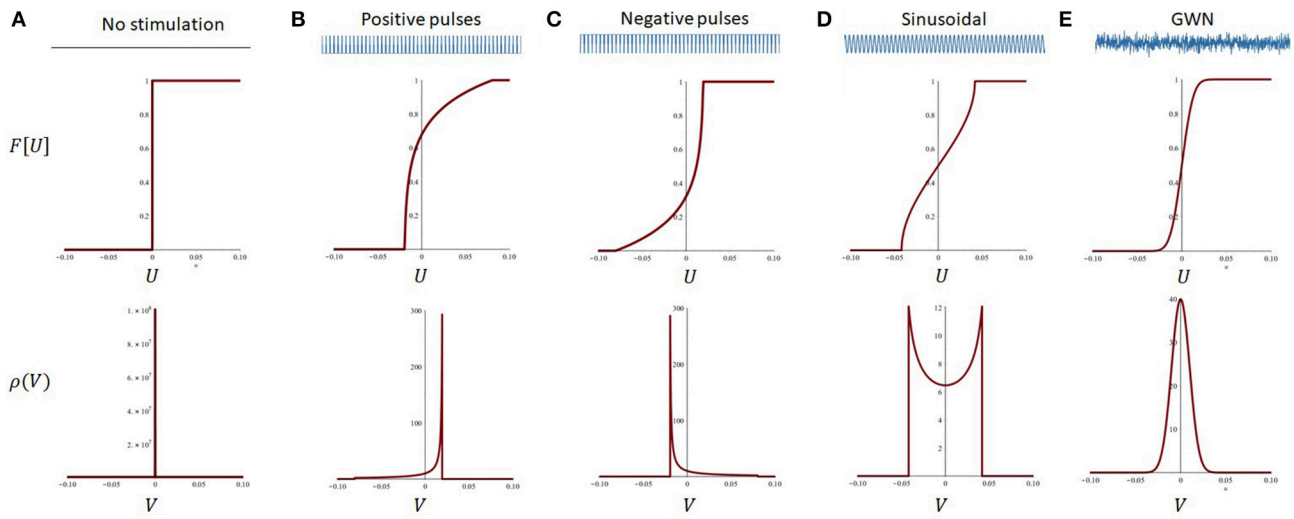

FIGURE 4 | Effect of stimulation polarity and fluctuation distribution on the effective response function of the reduced model. Stimulation-driven fluctuations around the mean change the effective response function of the system in a waveform-dependent way. **(A)** In absence of stimulation, or in the case of a constant DC shift, the system's response function remains unchanged (top): the probability density function of the fluctuations is a delta function centered at 0. **(B)** For positive pulses, the network response function is linearized but primarily over the positive U axis. This is due to the asymmetrical shape of the probability density function. Note the change in effective threshold, due to the non-zero mean of the stimulation. Here $S = 1$, $r = 0.2$. **(C)** Analogous effect in presence of negative pulses, where the effective response function of the system is now linearized toward the negative U axis. Here $S = -1$, $r = 0.2$. **(D)** The sinusoidal input shapes the response function in a hybrid but symmetrical way, as its mean is centered at U =0. Here $S = 0.1$, ω_S =12 Hz. **(E)** Gaussian white noise (GWN) fully smoothes the system's response function, where the probability density function of the fluctuations are normally distributed and also centered around 0. Here $D = 0.0001$. All other parameters are as in **Table 2**.

TABLE 2 | Reduced model parameters.

Symbol	Definition	Value
N	Number of Interacting Units	100
β	Response function gain	300 a.u.
h	Response function threshold	−0.1 a.u.
$\bar{\tau}$	Effective mean delay	25 ms
g	Mean synaptic coupling	−15 a.u.
k	Linear operator gain constant	−1 a.u.
dt	Integration time step	1 ms

where ξ_j are Gaussian white noise processes such that $< \xi_j \xi_k >= \delta_{jk}$ i.e., all neurons in the network experience independent stochastic input of intensity$D$. This case was also studied in detail in Hutt et al. (2016). Fluctuations around the mean obey the stochastic Langevin equations

$$\frac{d}{dt}V^j = -V^j + \sqrt{2D}\,\xi_j(t) \tag{27}$$

where $\mu_S = 0$. The associated probability density function $\rho(V)$ is a symmetric Gaussian

$$\rho\,(V) = \frac{1}{\sqrt{2\pi D}}\exp[-\frac{V^2}{2D}]. \tag{28}$$

Convolving with the threshold non-linearity yields

$$\tilde{F}\left[\bar{U}\right] \approx \frac{1}{\sqrt{2\pi D}}\int_{-\mu}^{\mu} H\left[\bar{U}+V-h\right]\exp\left[-\frac{V^2}{2D}\right]dv = \frac{1}{2}+\frac{1}{2}\mathrm{erf}[\frac{\bar{U}}{\sqrt{2D}}]. \tag{29}$$

This equation states that additive noise linearizes the effective neuron response function as D is increased, cf. **Figure 4E**.

4. Continuous Stimulation

At last, let us consider the simple tonic stimulus

$$S\,(t) = S = constant \tag{30}$$

In this particular case, the input has zero variance and the effective response function is thus unchanged

$$F\,[U] = H\left[U-h\right] \approx f[U] \tag{31}$$

The effect on the dynamics can be understood by introducing the change of variable

$$\bar{U} \to \bar{U} - S \tag{32}$$

which leads to the mean–field dynamics

$$\frac{d}{dt}\bar{U}(t) = -\bar{U}(t) + g\tilde{F}\left[\bar{U}(t-\bar{\tau})\right] \tag{33}$$

with $\tilde{F}[U] = H[U - \tilde{h}]$ and $\tilde{h} = h - S$. As such, the impact of continuous stimulation is analogous to a change in the response function threshold. This is in good agreement with the reported change in input/output response functions measured experimentally using tDCS (Lafon et al., 2017).

Impact on Alpha Peak Frequency

As the derivations above have pointed out, stimulation statistics are reflected by changes in the effective response function, leading to mean-field equations with variable non-linear structures. Moreover, linear stability of the equilibria will also depend on stimulation statistics, which will be reflected on the features of oscillatory solutions. Regardless of stimuli waveform, limit cycle solutions are deployed around the implicitly defined equilibrium

$$\bar{U}_o = gF\left[\bar{U}_o\right] + \mu_S\,. \tag{34}$$

The linearized dynamics around the steady state $\bar{u}_o$ is

$$\frac{d}{dt}\bar{U}(t) = -\bar{U}(t) + R[\bar{U}_o]\,\bar{U}(t-\bar{\tau}) \tag{35}$$

where $R\left[\bar{U}_o\right] = g\,F'[\bar{U}_o]$ and $R\left[\bar{U}_o\right] < 0$ for the cases in **Figure 4**. We highlight here that the linear gain $R[\bar{U}_o]$ depends explicitly on the stimulation waveform through the convolved statistics in the effective function F and implicitly through the stimulus corrected equilibrium state $\bar{U}_o$. To determine the frequency of emergent alpha oscillations, the iterative Galerkin method (He, 2005; Liu, 2005) is helpful to find a frequency ω minimizing the measure

$$J = \int_0^{2\pi/\omega} \left(\frac{d}{dt}\bar{U} - F[\bar{U}(t-\bar{\tau})]\right)\cdot\cos(\omega t)dt \tag{36}$$

Here we may consider small input stimuli i.e., $S \ll 1$and gain in the linear case

$$J_{lin} = \int_0^{2\pi/\omega} \left(\frac{d}{dt}\bar{U} - R[\bar{U}_o]\bar{U}(t-\bar{\tau})\right)\cdot\cos(\omega t)dt \tag{37}$$

Using the ansatz $\bar{U}(t) = A\cos(\omega t) + \bar{U}_o$, one obtains for the first iteration

$$J_{lin} = -\frac{A\pi\left(R[\bar{U}_o]\cos(\omega\tau) - 1\right)}{\omega} \tag{38}$$

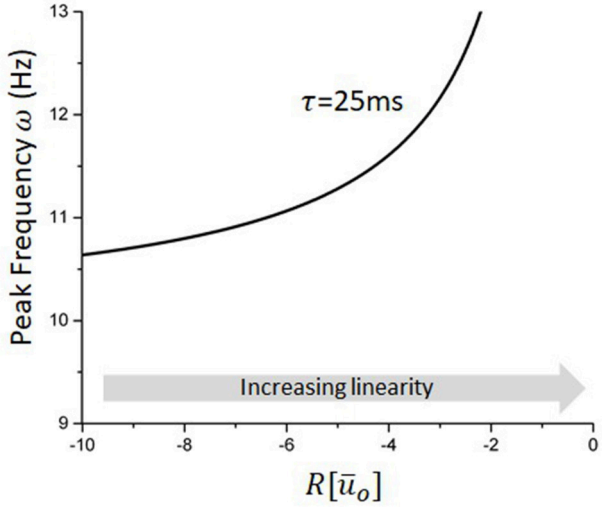

FIGURE 5 | Peak frequency of the reduced model as a function of the linear gain. For a fixed delay, changes in the linear gain due to the stimulation will mediate the non-linear entrainment of the endogenous oscillations. Increases in $|R|$ will cause a slowing down of endogenous oscillations, e.g., negative pulses, while decreases in $|R|$ will do the opposite and increase the network peak frequency.

Setting $J_{lin} = 0$ and solving for ω yields an approximation of the linear frequency as a function of $R[\bar{u}_o]$ and delay τ i.e.

$$\omega \approx \frac{\arccos\left(\frac{1}{R[\bar{U}_o]}\right)}{\bar{\tau}} \tag{39}$$

Equation (36) approximates well the dependence of the network peak frequency on stimulation statistics whenever the stimulation amplitude remains small and its frequency high. **Figure 5** illustrates how the network endogenous frequency depends on the linear gain for the delay considered in our model (i.e., $\bar{\tau} = 25$ms). Although $R[\bar{U}_o]$ cannot always be computed analytically due to the implicit condition for the equilibrium (34), some specific cases such as Gaussian white noise for instance, remain tractable and accurate (Hutt et al., 2016), and can otherwise be computed numerically.

According to the local approximations above, effects of stimulation waveform on equilibrium states and oscillations can be characterized by local, stimulus-induced changes in the linearized gain, evaluated at the fixed point $\bar{U}_o$. Equation (39) above states that ω is inversely proportional to $|R|$: increases (resp. decreases) in the linear gain R in Equation (35), i.e., decreases (resp. increases) of the slope of $F[\bar{U}_o]$, translates into an acceleration (resp. deceleration) of the network peak frequency. For the stimulation types studied and shown in **Figure 4**, this implies that network oscillations slow down whenever the system becomes locally non-linear, i.e., the transfer function becomes steeper, and accelerate when the network is pushed toward the linear regime (Hutt et al., 2016), i.e., the transfer function becomes more flat. **Figure 4** (bottom panels) shows the non-linear response function and we observe that

the slopes $F'[\bar{U}_o]$ of symmetric probability densities ρ are symmetric with respect to the threshold h, set here to 0, whereas the slopes of non-symmetric probability densities are non-symmetric. Since $F'\left[\bar{U}_o\right] \sim R$ for symmetric probability densities, the effect of external stimulation depends on the distance of the equilibrium state to the threshold only in contrast to non-symmetric probability densities. This highlights the importance of the shape of the probability density function and the equilibrium state.

According to this framework, mathematically the sensitivity of network oscillations to the stimulation waveform depends fully on how the probability density $\rho(V)$ interacts with the network response function f. An important implication of this result is that different stimulus waveforms that possess the same statistical properties, i.e., the same probability density function $\rho(V)$, will affect oscillations in the same way since the effective response function will possess an identical non-linear structure. This significantly reduces the dimensionality of the stimulus waveform parameter space, in the context of the optimization of non-linear acceleration/deceleration.

Using the approach outlined above, we computed the peak frequency of oscillations for various stimulation waveforms and compared them to the values computed numerically in the reduced network model. Results are presented in **Figure 6**. For all waveforms considered, the convolution approach (Equation 39) captured well the major effect of high-frequency stimuli on non-linear oscillations for small values of S, linking statistics of the input waveforms to the system's response. The mean field analysis confirms that positive (resp. negative) pulse trains accelerate (resp. slow down) ongoing oscillations, while both sinusoidal and Gaussian white noise inputs increased the endogenous frequency of the network.

The results above hold for high-frequency (or stochastic) stimulation; what happens if this condition is relaxed? We investigated this question numerically and results are plotted in **Figure 7**. For slower frequencies, the network dynamics were found to be dominated by (super- and sub-) harmonic entrainment: endogenous oscillations maintain stable phase relationships with the stimuli, sequentially jumping from one harmonic to the next, as seen from the Arnold tongue patterns portrayed in both **Figures 7A,B**. There, the waveform-dependent non-linear interactions between stimulation and network oscillations can be observed through the presence of tilted Arnold tongues, due to non-linear shifts in the natural frequency of the system (Lefebvre et al., 2015; Herrmann et al., 2016; Hutt et al., 2016). Surprisingly, negative pulses were found to be more efficient at entraining ongoing oscillations. Indeed, **Figures 7A,B** show that Arnold tongues are wider for negative pule trains ($S < 0$) compared to positive ones ($S > 0$). Also, negative pulses were found to suppress network oscillations beyond specific values of stimulation amplitude and frequency. We note that this is fully analogous with the dynamics observed in **Figure 2** where peak power is gradually suppressed by negative pulse trains whose frequency exceeds $\sim$50 Hz for $S = 2.5$. Beyond this point, the network does not exhibit any internal resonances and the peak frequency is the same as the stimulation frequency.

DISCUSSION

Electromagnetic brain stimulation has become increasingly popular to support a wide variety of clinical interventions. It is routinely used in the treatment of various types of neuropsychiatric disorders such as treatment-resistant depression (Ferrucci et al., 2009), Parkinsonism (Hess, 2013), Schizophrenia (Hoy et al., 2016), and the number of potential applications is increasing rapidly. Both invasive (e.g., DBS) and non-invasive (e.g., TMS, TACS) paradigms are emerging as strong alternatives to pharmaceutical treatments and have further raised the fascinating prospect of entraining brain rhythms to engage neural circuits at a functional level (Fröhlich, 2015). However, the relationship between stimulation waveform and entrainment outcomes remains a difficult and open problem. How the different stimulation temporal patterns interact with the intrinsic non-linear structure of cortical circuits to shape synchronous neural dynamics is also poorly understood.

To answer some of these questions, we have combined computational and mathematical methods to reconcile the effect of stimulation at the mesoscopic neural ensemble and macroscopic population scales using mean-field techniques. Using a detailed cortical microcircuit model, we have numerically explored the effect of stimulation pulse trains, sinusoidal inputs and Gaussian white noise stimulation on resting state alpha oscillations. First, our simulations have confirmed that, as expected, distinct waveforms have different entrainment properties. Notably, while positive pulse trains were found to accelerate ongoing oscillations, negative pulses did the opposite. To understand the source of this novel finding, we have developed a framework in which the mesoscopic and waveform-dependent effects of stimulation on oscillatory activity can be characterized by a change in the neuron response function, mathematically speaking through a convolution with the probability density function associated with stimulation-induced fluctuations around the mean. Using this approach, it was possible to relate the statistics of stimuli to the acceleration/slowing down of non-linear oscillations using a reduced neural oscillator model that preserved the non-linear structure of the more detailed cortical microcircuit model. Taken together, these results show that the core differences in entrainment properties between various stimulation waveforms can be explained by population-scale changes in the effective response function of the network—an emerging perspective in line with recent findings in the literature (Kar et al., 2017; Lafon et al., 2017). The approach we have put forward is relevant especially in cases where the relative phase of stimulation with respect to ongoing oscillations is not known and where the stimulus and the ongoing activity coexist on different time scales. Brain stimulation, especially in the non-invasive case, engages populations of neurons with effects that go beyond single cells and extend whole circuits. As such, the use of mean-field techniques is warranted, providing appropriate description of the dynamics at these larger spatial scales. The non-linear structure of neuron response functions reflects the combined effect of multiple neurophysiological mechanisms such as ion channel dynamics (e.g., Hutt and Buhry, 2014), adaptation

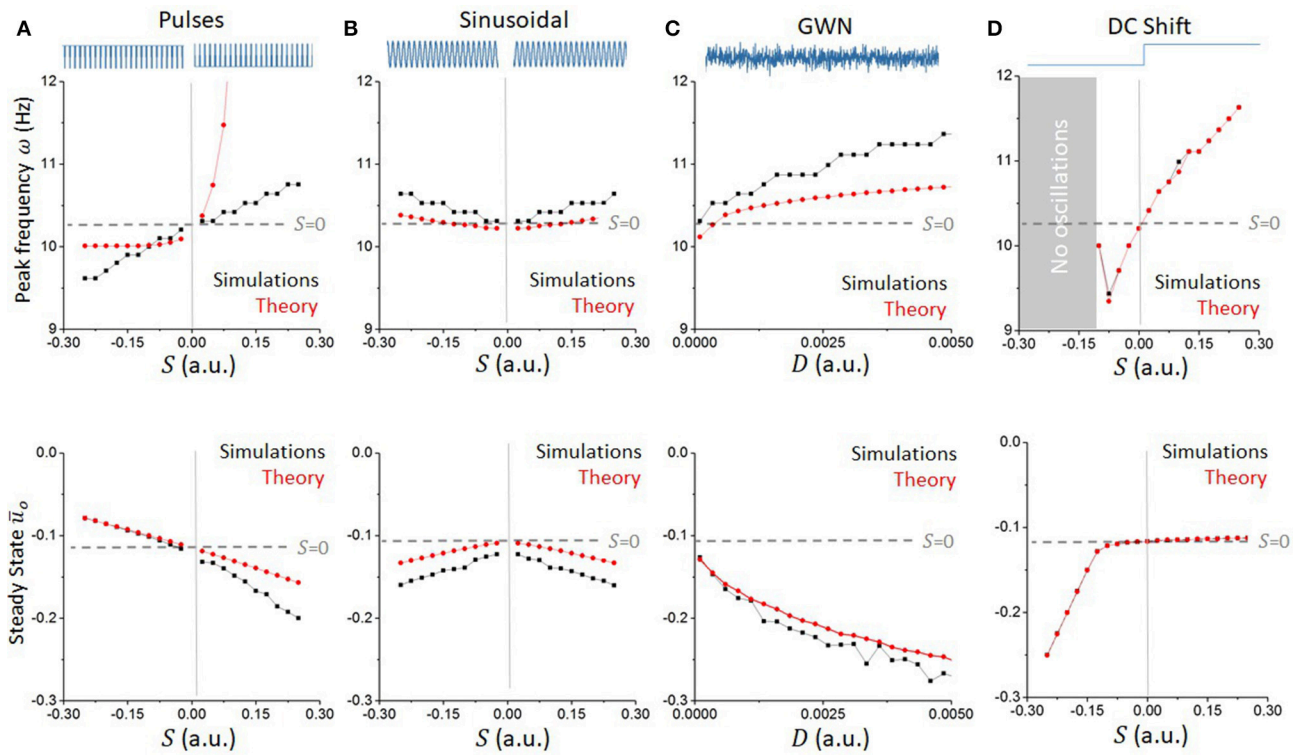

FIGURE 6 | Waveform-dependent non-linear entrainment of endogenous oscillations in the reduced model. The convolution approach allows us to compute the dependence of the system's peak frequency on the stimulation parameters. **(A)** Peak endogenous frequency as a function of the amplitude of pulses, either positive or negative (top). The theoretical calculations (red line), based on local linear analysis, are accurate for small pulse amplitudes, and diverge away from the simulated dynamics (black line) from there. The effect of pulses on the network peak frequency is monotonic and asymmetrical. The effect of the pulses' amplitude on the steady state $\bar{u}_o$ is also plotted (bottom). **(B)** Expectedly, sinusoidal waveforms have a symmetrical effect whether the amplitude is positive or negative, and are found to accelerate the system's peak frequency in both cases. **(C)** Gaussian White noise (GWN) also accelerates endogenous oscillations, in a more pronounced way. **(D)** For comparison, a constant DC-shift input has an analogous effect as positive pulses, but the effect on the system's steady state is different.

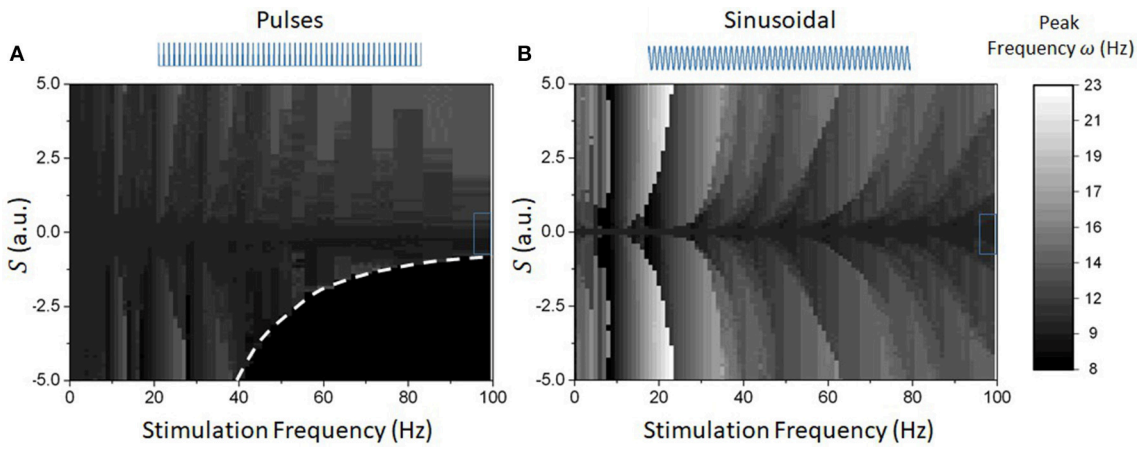

FIGURE 7 | Numerically computed Arnold Tongues of reduced model for different waveforms. Given the different impact of the stimulation on the network response function and oscillatory properties, different waveforms possess different entrainment properties (linear or not). **(A)** Peak endogenous frequency as a function of varying stimulation frequency and amplitude for pulse waveforms. The triangular regions represent Arnold tongues were the system's activity is phase locked to the stimulus drive. The resulting map is asymmetrical, where acceleration can be seen for positive pulses, and slowing down (and loss of stability) can be observed for negative pulses. Notice also that the Arnold tongues are bent to the right, a clear signature of a change in endogenous frequency due to non-linear entrainment. The dashed line denotes the parameter border below which network activity vanishes. **(B)** In contrast, sinusoidal inputs have fully symmetrical entrainment regions. These are analogously bent to the right, as expected.

(e.g., Benda et al., 2007) as well as recurrent feedback (e.g., Sutherland et al., 2009). As such, our results suggest that distinct waveforms engage neural circuits through a plurality of neurophysiological mechanisms, yet generate equivalent outcomes as far as synchronous oscillations are concerned.

The analysis we have conducted has revealed that in regimes of high frequency stimulation, distinct waveforms may have similar impact on non-linear neural oscillations. Indeed, positive pulses, sinusoidal inputs and Gaussian white noise were all found to have similar influence on ongoing oscillations when the stimulation frequency (or intensity D for Gaussian white noise) is high, indicating that, within these regimes, it is possible to reduce the high-dimensionality of the stimulation waveform parameter space: multiple stimulation patterns have equivalent effect on synchronous oscillations.

Our analysis has shown that, in first approximation, the local features of the effective response function F near the fixed point $\bar{U}_o$ determine primarily the impact of stimulation waveforms on limit cycle solutions. This means that the stimulation efficacy is highly dependent on the state: changes to the response function are commensurate with the proximity of the fixed point, implying that the same waveform will have different impact on endogenous oscillations if the equilibrium location in phase space differs. This is in complete agreement with numerous recent findings showing the state dependence of entrainment efficacy (Neuling et al., 2013; Alagapan et al., 2016).

The results presented in this study are aimed at obtaining a better understanding of the properties of mesoscopic neural population activity in regimes where the dynamics are dominated by recurrent inhibition. In our model, this arises due to differential spatial profiles of excitatory vs. inhibitory connections. Specifically, excitatory connections dominate at smaller spatial scales, whereas inhibitory connections dominate at larger spatial scales. This is the 1-D analog of classic "Mexican Hat" profiles of lateral connectivity, as observed for example in visual cortex (Amari, 1977; Kang et al., 2003). Other neural population-scale mechanisms of rhythmogenesis that have been studied in the experimental and theoretical literature include intra-columnar circuit motifs (Wilson and Cowan, 1972; Jansen and Rit, 1995; Womelsdorf et al., 2014) and long-range thalamocortical loops (Lopes da Silva et al., 1974; Robinson et al., 2001). Distinguishing the differential contributions of these and other mechanisms to a given set of empirical observations is a challenging and active research topic. However, despite major differences in their exact neuroanatomical and neurophysiological components, many of these different circuit mechanisms can be understood as having in common the same core rhythmogenic phenomenon—namely delayed recurrent inhibition. As such, the mathematical techniques developed and insights obtained in the present study regarding changes in neural population response functions under different stimulation waveform regimes may, we suggest, also prove useful for characterizing analogous responses in other modeling and experimental contexts.

In order to fully characterize the effects of electromagnetic brain stimulation, it is necessary to consider both local effects at the stimulation site, and distal effects that result from propagation of stimulated response throughout the brain via long-range white matter pathways (Massimini et al., 2005). Our focus in this study has been on the first of these, with the neural population and mean field models presented describing oscillatory responses to various stimulation waveforms in an isolated patch of cortex. An important direction for future work shall be to extend this approach to investigate polysynaptic and large-scale network effects. Such networks, extending on larger spatial scales, are built of interconnected population patches, as considered here. The rapidly growing literature on stimulation and control problems in macro-connectomics has primarily used relatively simple descriptions of neural population dynamics such as planar oscillators (e.g., Spiegler et al., 2016), phase oscillators (e.g., Gollo et al., 2017), or linear integrators (e.g., Betzel et al., 2016), and typically focuses on spatial pattern formation and recovery or modulation of canonical fmri-derived resting state networks. A number of studies have examined power spectrum changes in M/EEG-relevant frequency ranges following focal stimulation (Spiegler et al., 2010; Cona et al., 2011, 2014; Fung and Robinson, 2014). Recent work by Spiegler and colleagues (Kunze et al., 2016) observed a sharpening and acceleration of peak oscillatory frequencies, as well as an increase in long-range synchrony, following simulated transcranial direct current stimulation in a model of coupled neural masses. Importantly, these authors found that heterogeneity in the level of neural population response function saturation—which arose due to the network topology and to the spatially diffuse effect of electrical brain stimulation—played a major role in shaping large-scale network activity. Likewise, developing a spatially mapped characterization of node-wise variation in response function modifications due to diffuse and inhomogeneous stimulation current distributions shall be important for translating the theoretical insights obtained in the present study to improved experimental paradigms and clinical treatments. Taken together and in conjunction with previous studies, our results reinforce the notion that stimulation effects and optimization has to be considered from multiple spatial scales. Indeed, previous work from the authors have demonstrated that delays, which become non-negligible as the spatial scale considered increases, play an important role not only on the immediate response of the stimulated networks (Hutt and Atay, 2007; Lefebvre et al., 2015; Hutt et al., 2016), but also on post-stimulation after effects (Alagapan et al., 2016), and thus play a key role in defining the entrainment properties of non-linear neural systems.

AUTHOR CONTRIBUTIONS

AH and JL conceived the principle idea of the work. JL performed the numerical analysis. AH, JG, and JL have worked out the analytical results. JL and CH structured the manuscript and all authors have written the manuscript.

ACKNOWLEDGMENTS

This work has been supported by the Natural Sciences and Engineering Research Council of Canada (JL).

REFERENCES

Alagapan, S., Schmidt, S. L., Lefebvre, J., Hadar, E., Shin, H. W., and Fröhlich, F. (2016). Modulation of cortical oscillations by low-frequency direct cortical stimulation is state-dependent. *PLoS Biol.* 14:e1002424. doi: 10.1371/journal.pbio.1002424

Amari, S. (1977). Dynamics of pattern formation in lateral-inhibition type neural fields. *Biol. Cybern.* 27, 77–87. doi: 10.1007/BF00337259

Baker, G. L. (2006). Probability, pendulums, and pedagogy. *Am. J. Phys.* 74, 482–489. doi: 10.1119/1.2186689

Başar, E. (2012). A review of alpha activity in integrative brain function: fundamental physiology, sensory coding, cognition and pathology. *Int. J. Psychophysiol.* 86, 1–24. doi: 10.1016/j.ijpsycho.2012.07.002

Benda, J., Bethge, M., Hennig, M., K., Pawelzik, K., and Herz A. V. M. (2007). Spike-frequency adaptation: phenomenological model and experimental tests. *Neurocomputing* 38–40, 105–110. doi: 10.1016/S0925-2312(01)00545-8

Betzel, R., Gu, S., Medaglia, J., Pasqualetti, F., and Bassett, D. (2016). Optimally controlling the human connectome: the role of network topology. *Sci. Rep.* 6:30770. doi: 10.1038/srep30770

Buzsáki, G., and Draguhn, A. (2004). Neuronal oscillations in cortical networks. *Science* 304:1926. doi: 10.1126/science.1099745

Cabral, J., Luckhoo, H., Woolrich, M., Joensson, M., Mohseni, H., Baker, A., et al. (2014). Exploring mechanisms of spontaneous functional connectivity in MEG: how delayed network interactions lead to structured amplitude envelopes of band-pass filtered oscillations. *Neuroimage* 90, 423–435. doi: 10.1016/j.neuroimage.2013.11.047

Cecere, R., Rees, G., and Romei, V. (2015). Individual differences in alpha frequency drive crossmodal illusory perception. *Curr. Biol.* 19, 231–235. doi: 10.1016/j.cub.2014.11.034

Cona, F., Lacanna, M., and Ursino, M. (2014). A thalamo-cortical neural mass model for the simulation of brain rhythms during sleep. *J. Comput. Neurosci.* 37, 125–148. doi: 10.1007/s10827-013-0493-1

Cona, F., Zavaglia, M., Massimini, M., Rosanova, M., and Ursino, M. (2011). A neural mass model of interconnected regions simulates rhythm propagation observed via TMS-EEG. *Neuroimage* 57, 1045–1058. doi: 10.1016/j.neuroimage.2011.05.007

Curtu, R., and Ermentrout, B. (2004). Pattern formation in a network of excitatory and inhibitory cells with adaptation. *SIAM J. Appl. Dyn. Syst.* 3, 191–231. doi: 10.1137/030600503

Dreyer, A. M., and Herrmann, C. S. (2015). Frequency-modulated steady-state visual evoked potentials: a new stimulation method for brain-computer interfaces. *J Neurosci. Methods* 241, 1–9. doi: 10.1016/j.jneumeth.2014.12.004

Engel, A. K., and Singer, W. (2001). Temporal binding and the neural correlates of sensory awareness. *Trends Cogn. Sci.* 5, 16–25. doi: 10.1016/S1364-6613(00)01568-0

Engel, A. K., Fries, P., and Singer, W. (2001). Dynamic predictions: oscillations and synchrony in top-down processing. *Nat. Rev. Neurosci.* 2, 704–716. doi: 10.1038/35094565

Ferrucci, R., Bortolomasi, M., Vergari, M., Tadini, L., Salvoro, B., Giacopuzzi, M., et al. (2009). Transcranial direct current stimulation in severe, drug-resistant major depression. *J. Affect. Disord.* 118, 215–219. doi: 10.1016/j.jad.2009.02.015

Fröhlich, F. (2015). Experiments and models of cortical oscillations as a target for non-invasive brain stimulation. *Prog. Brain Res.* 222, 41–73. doi: 10.1016/bs.pbr.2015.07.025

Fröhlich, F., and McCormick, D. A. (2010). Endogenous electric fields may guide neocortical network activity. *Neuron* 67, 129–143. doi: 10.1016/j.neuron.2010.06.005

Fung, P. K., and Robinson, P. A. (2014). Neural field theory of synaptic metaplasticity with applications to theta burst stimulation. *J. Theor. Biol.* 340, 164–176. doi: 10.1016/j.jtbi.2013.09.021

Gollo, L., Roberts, J., and Cocchi, L. (2017). Mapping how local perturbations influence systems-level brain dynamics. *Neuroimage* 60, 97–112. doi: 10.1016/j.neuroimage.2017.01.057

He, J. H. (2005). Periodic solutions and bifurcations of delay-differential equations. *Phys. Lett.* A 347, 228–230. doi: 10.1016/j.physleta.2005.08.014

Helfrich, R. F., Schneider, T. R., Rach, S., Trautmann-Lengsfeld, S. A., Engel, A. K., and Herrmann, C. S. (2014). Entrainment of brain oscillations by transcranial alternating current stimulation. *Curr. Biol.* 24, 333–339. doi: 10.1016/j.cub.2013.12.041

Hellwig, B. (2000). A quantitative analysis of the local connectivity between pyramidal neurons in layers 2/3 of the rat visual cortex. *Biol. Cybern.* 82, 111–121. doi: 10.1007/PL00007964

Herrmann, C., Ionta, S., Hutt, A., Murray, M. M., and Lefebvre, J. (2016). Shaping intrinsic oscillatory neural activity with periodic stimulation. *J. Neurosci.* 36, 5328–5337. doi: 10.1523/JNEUROSCI.0236-16.2016

Hess, C. W. (2013). Modulation of cortical-subcortical networks in Parkinson's disease by applied field effects. *Front. Hum. Neurosci.* 7:565. doi: 10.3389/fnhum.2013.00565

Hindriks, R., van Putten, M. J. A., and Deco, G. (2014). Intra-cortical propagation of EEG alpha oscillations. *Neuroimage* 103, 444–453. doi: 10.1016/j.neuroimage.2014.08.027

Hipp, J. F., Engel, A. K., and Siegel, M. (2011). Oscillatory synchronization in large-scale cortical networks predicts perception. *Neuron* 69, 387–396. doi: 10.1016/j.neuron.2010.12.027

Hoy, K. E., Whitty, D., Bailey, N., and Fitzgerald, P. B. (2016). Preliminary investigation of the effects of γ-tACS on working memory in schizophrenia. *J Neural Transm.* 123, 1205–1212. doi: 10.1007/s00702-016-1554-1

Hutt, A., and Atay, F. M. (2007). Spontaneous and evoked activity in extended neural populations with gamma-distributed spatial interactions and transmission delay. *Chaos Sol. Fract.* 32, 547–560. doi: 10.1016/j.chaos.2005.10.091

Hutt, A., and Buhry, L. (2014). Study of GABAergic extra-synaptic tonic inhibition in single neurons and neural populations by traversing neural scales: application to propofol-induced anaesthesia. *J Comput Neurosci.* 37, 417–437. doi: 10.1007/s10827-014-0512-x

Hutt, A., Bestehorn, M., and Wennekers, T. (2003). Pattern formation in intracortical neuronal fields. *Netw. Comput. Neural Syst.* 14, 351–368. doi: 10.1088/0954-898X_14_2_310

Hutt, A., Mierau, A., and Lefebvre, J. (2016). Dynamic control of synchronous dynamics in networks of spiking neurons. *PLoS ONE* 11:e0161488. doi: 10.1371/journal.pone.0161488

Jansen, B. H., and Rit, V. G. (1995). Electroencephalogram and visual evoked potential generation in a mathematical model of coupled cortical columns. *Biol. Cybern.* 73, 357–366. doi: 10.1007/BF00199471

Kang, K., Shelley, M., and Sompolinsky, H. (2003). Mexican hats and pinwheels in visual cortex. *Proc. Natl. Acad. Sci. U.S.A.* 100, 2848–2853. doi: 10.1073/pnas.0138051100

Kar, K., Duijnhouwer, J., and Krekelberg, B. (2017). Transcranial alternating current stimulation attenuates neuronal adaptation. *J. Neurosci.* 30, 2266–2216. doi: 10.1523/JNEUROSCI.2266-16.2016

Klimesch, W., Sauseng, P., and Hanslmayr, S. (2007). EEG alpha oscillations: the inhibition-timing hypothesis. *Brain Res. Rev.* 53, 63–88. doi: 10.1016/j.brainresrev.2006.06.003

Kunze, T., Hunold, A., Haueisen, J., Jirsa, V., and Spiegler, A. (2016). Transcranial direct current stimulation changes resting state functional connectivity: a large-scale brain network modeling study. *Neuroimage* 140, 174–187. doi: 10.1016/j.neuroimage.2016.02.015

Lafon, B., Rahman, A., Bikson, M., and Parra, L. C. (2017). Direct Current stimulation alters neuronal input/output function. *Brain Stimul.* 10, 36–45. doi: 10.1016/j.brs.2016.08.014

Lakatos, P., Karmos, G., Mehta, A. D., Ulbert, I., and Schroeder, C. E. (2008). Entrainment of neuronal oscillations as a mechanism of attentional selection. *Science* 320, 110–113. doi: 10.1126/science.1154735

Lefebvre, J., and Hutt, A. (2013). Additive noise quenches delay-induced oscillations. *Europhys. Lett.* 102:60003. doi: 10.1209/0295-5075/102/60003

Lefebvre, J., Hutt, A., Knebel, J. F., Whittingstall, K., and Murray, M. M. (2015). Stimulus statistics shape oscillations in nonlinear recurrent neural networks. *J. Neurosci.* 35, 2895–2903. doi: 10.1523/JNEUROSCI.3609-14.2015

Lindén, H., Pettersen, K. H., and Einevoll, G. T. (2010). Intrinsic dendritic filtering gives low-pass power spectra of local field potentials. *J. Comput. Neurosci.* 29, 423–444. doi: 10.1007/s10827-010-0245-4

Liu, H. M. (2005). Approximate period of nonlinear oscillators with discontinuities by modified Lindstedt-Poincare method. *Chaos Solit. Fract.* 23, 577-579. doi: 10.1016/j.chaos.2004.05.004

Lopes da Silva, F. H., Hoeks, A., Smits, H., and Zetterberg, L. H. (1974). Model of brain rhythmic activity. *Kybernetik* 15, 27–37. doi: 10.1007/BF00270757

Massimini, M., Ferrarelli, F., Huber, R., Esser, S. K., Singh, H., and Tononi, G. (2005). Breakdown of cortical effective connectivity during sleep. *Science* 309, 2228–2232. doi: 10.1126/science.1117256

Mierau, A., Klimesch, W., and Lefebvre, J. (2017). State-dependent alpha peak frequency shifts: experimental evidence, potential mechanisms and functional implications. *Neuroscience* 360, 146–154. doi: 10.1016/j.neuroscience.2017.07.037

Neuling, T., Rach, S., and Herrmann, C. S. (2013). Orchestrating neuronal networks: sustained after-effects of transcranial alternating current stimulation depend upon brain states. *Front. Human Neurosci.* 7:161. doi: 10.3389/fnhum.2013.00161

Press, W. H., Teukolsky, S. A., Vetterling, W. T., and Flannery, B. P. (2007). *Numerical Recipes: The Art of Scientific Computing, 3rd Edn*. Cambridge: Cambridge University Press.

Robinson, P. A., Rennie, C. J., Wright, J. J., Bahramali, H., Gordon, E., and Rowe, D. L. (2001). Prediction of electroencephalographic spectra from neurophysiology. *Phys. Rev. E* 63:021903. doi: 10.1103/PhysRevE.63.021903

Romei, V., Bauer, M., Brooks, J. L., Economides, M., Penny, W., Thut, G., et al. (2016). Causal evidence that intrinsic beta-frequency is relevant for enhanced signal propagation in the motor system as shown through rhythmic TMS. *Neuroimage* 125, 120–130. doi: 10.1016/j.neuroimage.2015.11.020

Singer, W., and Gray, C. M. (1995). Visual feature integration and the temporal correlation hypothesis. *Annu. Rev. Neurosci.* 18, 555–586. doi: 10.1146/annurev.ne.18.030195.003011

Spiegler, A., Hansen, E., Bernard, C., McIntosh, A., and Jirsa, V. (2016). Selective activation of resting-state networks following focal stimulation in a connectome-based network model of the human brain. *eNeuro* 3:ENEURO.0068–16.2016. doi: 10.1523/ENEURO.0068-16.2016

Spiegler, A., Kiebel, S. J., Atay, F. M., and Knösche, T. R. (2010). Bifurcation analysis of neural mass models: impact of extrinsic inputs and dendritic time constants. *Neuroimage* 52, 1041–1058. doi: 10.1016/j.neuroimage.2009.12.081

Sutherland, C., Doiron, B., and Longtin, A. (2009). Feedback-induced gain control in stochastic spiking networks. *Biol. Cybern.* 100, 475–489. doi: 10.1007/s00422-009-0298-5

Thut, G., and Miniussi, C. (2009). New insights into rhythmic brain activity from TMS–EEG studies. *Trends Cogn. Sci.* 13, 182–189. doi: 10.1016/j.tics.2009.01.004

Uhlhaas, P. J., and Singer, W. (2006). Neural synchrony in brain disorders: relevance for cognitive dysfunctions and pathophysiology. *Neuron* 52, 155–168. doi: 10.1016/j.neuron.2006.09.020

Varela, F., Lachaux, J.-P., Rodriguez, E., and Martinerie, J. (2001). The brainweb: phase synchronization and large-scale integration. *Nat. Rev. Neurosci.* 2, 229–239. doi: 10.1038/35067550

Wilson, H. R., and Cowan, J. D. (1972). Excitatory and inhibitory interactions in localized populations of model neurons. *Biophys. J.* 12, 1–24. doi: 10.1016/S0006-3495(72)86068-5

Womelsdorf, T., Valiante, T. A., Sahin, N. T., , Miller, K. J., and Tiesinga, P. (2014). Dynamic circuit motifs underlying rhythmic gain control, gating and integration. *Nat. Neurosci.* 17, 1031–1039. doi: 10.1038/nn.3764

Conflict of Interest Statement: The authors declare that the research was conducted in the absence of any commercial or financial relationships that could be construed as a potential conflict of interest.

frontiers in Neuroscience

METHODS
published: 23 July 2018
doi: 10.3389/fnins.2018.00472

Development of an Activity-Dependent Epidural Stimulation System in Freely Moving Spinal Cord Injured Rats: A Proof of Concept Study

*Avi Rascoe[1,2], Pawan Sharma[1] and Prithvi K. Shah[1,2]**

[1] Division of Rehabilitation Sciences, Department of Physical Therapy, School of Health Technology and Management, Stony Brook University, Stony Brook, NY, United States, [2] Department of Neurobiology and Behavior, Stony Brook University, Stony Brook, NY, United States

Purpose: Extensive pre-clinical and clinical experimentation has yielded data on the robustness and versatility of epidural stimulation (ES) strategies to activate spinal neural circuitry to produce functional benefits. Increasing studies are now reporting that closed-loop electrical stimulation delivery methods significantly enhance the neuromodulation effects of stimulation, to in turn, improve physiological outcomes of the intervention. No studies have yet explored the feasibility and usage of closed-loop systems to neuromodulate the cervical spinal cord using ES.

Methods: We developed an activity-dependent system that utilizes electromyography (EMG) activity to trigger epidural stimulation (tES) of the cervical spinal cord in awake, freely moving rats. Experiments were performed on rats that were implanted with chronic forelimb EMG and cervical epidural implants, with (n = 7) and without (n = 2) a complete C4 spinal hemisection.

Results: Our results show that the EMG triggered activity-dependent system can be reliably applied and reproduced for: (i) stimulating multiple rats simultaneously throughout the night during free home-cage activity and (ii) use as a mobile system for testing and training during various short-term behavioral testing conditions. The system was able to consistently generate stimulation pulse trains in response to attempted EMG activity that crossed a user-defined threshold in all rats for all experiments, including the overnight experiments that lasts for 7 h/session for 6 days/week through the 3-month period.

Conclusion: The developed closed-loop system can be considered to represent a class of bidirectional neural prostheses via a circuit that enables two-way interactions between neural activity (real-time processing of EMG activity) and external devices (such as a stimulator). It can operate autonomously for extended periods of time in unrestrained rats, allowing its use as a long-term therapeutic tool. It can also enable us to study the long-term physiological effects of incorporating electrical stimulation techniques into the nervous system. The system can also be experimented for connecting several neural

OPEN ACCESS

Edited by:
Giovanni Mirabella, Sapienza Università di Roma, Italy

Reviewed by:
Xuefeng F. Wei, The College of New Jersey, United States
Parag Gad, University of California, Los Angeles, United States

***Correspondence:**
Prithvi K. Shah
prithvi.shah@stonybrook.edu

Specialty section:
This article was submitted to Neural Technology, a section of the journal Frontiers in Neuroscience

Received: *09 December 2017*
Accepted: *21 June 2018*
Published: *23 July 2018*

Citation:
Rascoe A, Sharma P and Shah PK (2018) Development of an Activity-Dependent Epidural Stimulation System in Freely Moving Spinal Cord Injured Rats: A Proof of Concept Study. Front. Neurosci. 12:472. doi: 10.3389/fnins.2018.00472

systems into a *Brainet* by combining neural signals from multiple rats dynamically and in real-time so as to enhance motor performance. Studies are ongoing in our laboratory to test the usefulness of this system in the recovery of hand function after cervical spinal cord injuries.

Keywords: activity-dependent electrical stimulation, closed-loop stimulation, epidural stimulation, cervical spinal cord injury, hand function, rats

INTRODUCTION

Electrical epidural stimulation (ES) of the spinal cord has gained increased attention as a successful neuromodulatory strategy for functional recovery after a severe spinal cord injury (SCI) in humans. After prescribed delivery and hence *training* with ES, patients with a complete SCI have demonstrated restoration of critical body functions including voluntary leg (Carhart et al., 2004; Angeli et al., 2014; Grahn et al., 2017) and arm (Lu et al., 2016) movements, independent standing (Harkema et al., 2011; Rejc et al., 2015) posture, bladder, bowel (Harkema et al., 2011; Angeli et al., 2014), and physiological cough performance (DiMarco et al., 2009, 2014). It is now becoming clear that spinal ES not only activates peripheral afferents, dorsal columns and motoneurons (Capogrosso et al., 2013; Minassian et al., 2016), but also has a neuromodulatory effect on a variety of segmental spinal interneurons (Gad et al., 2013; Taccola et al., 2017). Consequently, this results in drastic alterations in the excitability state of spinal neuronal circuits as well as of spared descending supraspinal connections to a level at which spinal circuitries can generate voluntary functional motor output.

Two major advancements in electrical stimulation strategies portend the continued success of ES as a crucial tool for neuromodulation in the field of SCI neurorehabilitation: first, multi-site stimulation of the spinal cord has gained increased attention because of its ability to spatially and functionally activate wide and discrete neuronal populations to synergistically influence and modulate the excitability of sensorimotor pathways for an effective motor output, more so than single site stimulation of localized individual segments (Angeli et al., 2014; Gerasimenko et al., 2015; Sayenko et al., 2015; Shah et al., 2016). As such, differential excitation of local spinal segments seems to be the key to neuromodulate appropriate neuronal networks for functionally beneficial outcomes.

Second, the advent of closed-loop electrical stimulation systems has become an attractive option in neurorehabilitation. Closed-loop is defined as the "delivery of any form of therapy, either to a target or systemically, exclusively in response to a specific cue or command" (Osorio et al., 2001). Closed-loop electrical stimulation techniques involve delivery of stimulation in response to an endogenous neural drive, such as a neural or behavioral event, to permit modulation of active neurological signals without experimenter input. In biological studies, the term closed-loop is also used for a technique in which bio-signals from the subject determine the timing of stimulus delivery and stimulation delivery is continually adapted in response to physiological changes (Sun and Morrell, 2014; Krook-Magnuson et al., 2015; McPherson et al., 2015). This is in contrast to studies that deliver open-loop stimulation protocols in which the stimulus is delivered regardless of ongoing activity and according to a predefined offline script (Gerasimenko et al., 2008; Shah et al., 2016). Indeed, increasing studies are now reporting that such closed-loop electrical stimulation delivery methods that control the timing of stimulation delivery so as to pair it with an ongoing neural activity, significantly enhance the neuromodulation effects of stimulation, to in turn, improve physiological outcomes of the intervention (Fountas et al., 2005; Rolston et al., 2009; Venkatraman et al., 2009; McPherson et al., 2015; Zareen et al., 2017). The purported mechanism is a direct test of Hebb's postulate (Hebb, 1949), showing that natural patterns of neuronal firing can lead to input-specific plasticity when paired with appropriate postsynaptic depolarization during normal behavior (Jackson et al., 2006a; McPherson et al., 2015). As such, it is not surprising that stimulation that is delivered precisely at the initiation of activity leads to potentiation of an already active circuitry to produce functional benefits (McPherson et al., 2015; Mercier et al., 2016). Additionally, there is also evidence for the retention of long term functional reorganization of neuronal circuitry with closed-loop stimulation (Jackson et al., 2006a).

The majority of closed-loop stimulation protocols currently employed are used to stimulate brain structures and are utilized for the treatment of a variety of neurological disorders in humans (Fountas et al., 2005; Little et al., 2013; Krook-Magnuson et al., 2015). Most closed-loop systems also adopt circuitry designs that are complex and expensive, require custom building of neuro-chips, demand tester supervision, not particularly tested for chronic stimulation and/or do not necessarily provide modifiable circuit schematics (Zanos et al., 2011). Although pre-clinical studies utilizing closed-loop stimulation techniques of the spinal cord have just begun to surface (Fuentes et al., 2009; Wenger et al., 2014; Zimmermann and Jackson, 2014; McPherson et al., 2015; Mercier et al., 2016), most of these systems either utilize cortical signals for stimulation (Fuentes et al., 2009), use intraspinal microstimulation techniques (Fitzsimmons et al., 2007; Fuentes et al., 2009; Zimmermann and Jackson, 2014; McPherson et al., 2015; Mercier et al., 2016) or have been tested for ES of the lumbosacral cord (Wenger et al., 2014). Experiments that use kinematics and/or electromyography (EMG) to trigger lumbo-sacral ES in thoracic spinal rats incorporate half an hour of neuromodulatory rehabilitative training sessions under tester supervision (Gad et al., 2012; Wenger et al., 2014). No studies have yet explored the feasibility and usage of closed-loop systems to neuromodulate the cervical spinal cord using ES, nor have demonstrated the effects of chronic ES of the cervical cord during overnight activity.

In the present study, we assemble a closed-loop activity-dependent system capable of delivering low-latency stimuli subsequent to detection of a user-defined bio-signal. Although this system has varied applications, we specifically demonstrate a closed-loop stimulation technique that effectively allows multi-channel ES of the cervical spinal cord triggered by EMG activity (tES) of forelimb muscles in awake, freely moving rats. This application is a preamble to ongoing experiments in our laboratory that aim to recover upper limb sensory-motor function after a cervical SCI in rodents. We present details of the setup with demonstration of its application in rats with and without a cervical hemisection injury. In this proof of concept study, we highlight unique features of the technique and validate the feasibility and reliability of the closed loop system, and delivery of tES (i) during overnight long-term stimulation in the rat's home-cage during overnight activity (7 h/day, 6 days/week for ∼1–3 months) without tester supervision in multiple rats simultaneously and (ii) during short-term stimulation during a variety of motor activities in controlled experimental conditions.

MATERIALS AND METHODS

Animals and Experimental Design

This study was carried out in accordance with the recommendations of National Institutes of Health Guide for the Care and Use of Laboratory Animals. The protocol was approved by the Stony Brook University Chancellor's Animal Research Committee (National-Research-Council, 2011).

An outline of experimental procedures is shown in **Figure 1A**. A total of nine adult female Sprague-Dawley rats (240–260 g body weight) underwent surgical procedures for chronic EMG and epidural stimulating electrode implantation. Two rats served as non-injured controls and 7 rats were subject to a complete cervical hemisection (CHx) at the C4 spinal segment. We first tested feasibility of implementing the closed-loop system that consisted of EMG triggered ES (tES) in non-injured rats ($n = 2$). Specifically, we tested if the developed system could deliver ES triggered from muscle activity during the rat's night activity in its home cage with a 7 h tES training protocol (non-mobile setup, described below). The functionality of the closed-loop system to deliver tES was also tested during different motor behaviors (mobile setup, described below). Reliability and validity of the closed-loop system to deliver tES was then assessed by exposing CHx injured rats to tES for both the mobile and non-mobile setups throughout the experimental period for 3 months ($n = 7$).

Surgeries

All surgeries were performed under aseptic conditions with the rats deeply anesthetized with isoflurane gas (1.0–2.5% via facemask as needed). Surgery was performed with the rats on a heated surgery table (Shor-Line, Kansas City, MO, United States) and maintained at 37°C to maintain body temperature. All incisions were closed in layers using 5.0 Vicryl for the muscle and fascial layers, and staples for the skin. After surgery, the rats were placed in an incubator until fully recovered and administered antibiotics and analgesics as needed for up to 5 days. Thereafter, the rats were housed singly in cages to avoid damaging each others' head plugs through social interaction. The room was maintained at 26 ± 1°C, 40% humidity and a 12:12 h light:dark cycle with access to food and water *ad libitum*. The cage floors were covered with Alpha-Dri Bedding (Shepard Specialty Papers, Watertown, TN, United States). Pieces of fruit were given during each animal care session. For rats that underwent CHx, the bladders of all rats were expressed manually two times daily for the first 1–3 days until they regained complete bladder control.

Electromyography Implants

A small incision was made at the mid-line of the skull. The muscles and fascia were retracted laterally, few superficial cuts were made in the skull with a scalpel (to roughen the skull surface to accommodate dental cement), and the skull was dried thoroughly. One connector with Teflon-coated stainless-steel wires (Omnetics, Part # AS632; Cooner Wire Co., Chatsworth, CA, United States) was attached securely to the skull with screws (**Figure 1B-i**) and dental cement as previously described (Roy et al., 1991; Shah et al., 2012). While the screws hold the head plug in place, the dental cement firmly secures the screw and head plug unit onto the skull, making this 'head mount' on the skull a permanent one for use in chronic stimulation experiments. A skin incision was made in the upper-dorsal region of the back and wires from the connector were routed subcutaneously (**Figure 1B-ii**). Two wires were coiled subcutaneously so that they could be easily retrieved for implantation as ES electrodes on the spinal cord at a later time point (see below). Skin and fascial incisions were made to bilaterally expose belly of the deltoid, pronator, flexor digitorum, and extensor digitorum muscles (**Figure 1B-iii**). Muscle identity was verified using direct muscle electrical stimulation. Wires were routed subcutaneously from the back incision to each muscle site. Bipolar intramuscular EMG electrodes were formed and secured into the mid-belly of each muscle as shown in **Figure 1B-iv** and as described previously (Roy et al., 1991). The proximal ends of EMG wires outside the muscle were coiled near each implant site as well as in the mid-back region and placed beneath adjacent fascia. The coiled wires provided room for stress relief during rat movement. After electrode implantation into the muscle, we verified proper placement of the EMG electrodes into the desired muscle by stimulating the muscle via the head plug connector. Approximately 1cm of Teflon coating was stripped at the distal end of an additional wire that served as a reference electrode: this wire was placed subcutaneously on the right side of the vertebral column at the level of the inferior scapular angle.

Epidural Implantation

Epidural electrodes were implanted as described previously (Shah et al., 2012, 2016; Alam et al., 2015). Briefly, a longitudinal skin incision was made on the upper back using the C2 and T2 spinous processes as landmarks. Underlying fascia and upper back muscles (trapezius, rhomboid, and splenius) were then retracted with blunt dissection to expose the cervical vertebral column. A partial laminectomy was performed at vertebral levels C4, C5, and C7. Laminectomies at C5 and C7 were adequate to expose spinal cord segments C6 and C8, respectively. Partial

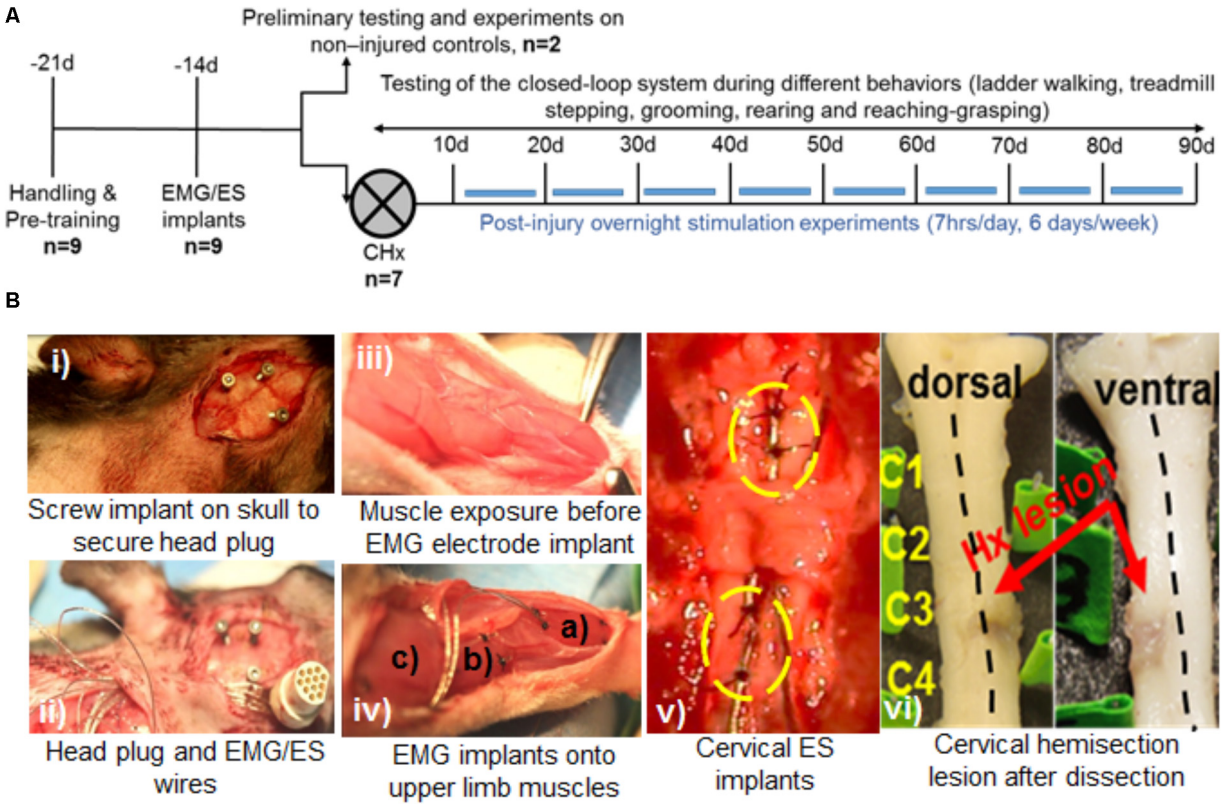

FIGURE 1 | Experimental outline, behavioral and surgical procedures. **(A)** Rats were initially handled prior to all experiments and trained for treadmill stepping and reaching-grasping activities. Later, rats underwent EMG and ES implants and were randomized into two experiments: *Experiment I:* two rats served as non-injured controls and were subjected to several pilot trials for initial testing of the closed-loop ES system in a variety of motor behaviors (open field walking, ladder walking, treadmill stepping, and grooming) and overnight stimulation experiments. *Experiment II:* seven rats received a cervical hemisection injury at the C4 spinal segment (CHx). They were trained with triggered ES (tES) during normal night cage activity for ∼7 h/day, 6 days/week for starting at 10 days after injury. Open field, ladder stepping, rearing, reaching-grasping and grooming tests were performed at multiple time points throughout the study. **(B)** Still photographs of EMG/ES implants and the CHx site. **(i)** Three screw implants on the skull were used to secure the head plug connector. **(ii)** EMG/ES electrode wires are routed subcutaneously underneath the neck region and routed toward the upper back. **(iii)** Exposure of forelimb muscles prior to EMG implantation. **(iv)** Select forelimb muscles [**(a)** flexor digitorum **(b)** pronator **(c)** deltoid] are implanted with EMG electrodes. **(v)** Epidural implants are shown at C6 (upper circle) and C8 (lower circle) spinal segments with two suture knots (black knots within circles) to secure the implants. **(vi)** Gross dorsal and ventral views of the cervical spinal cord shows the CHx lesion site at C4 replaced with scar tissue.

laminectomy of C4 vertebra allowed passage of the Teflon-coated stainless-steel wires. These wires were pulled toward the deeper back musculature and then inserted beneath the partial C4 vertebrae and passed epidurally to each partial laminectomy site. One additional wire that served as a reference electrode was placed subcutaneously on the left side of the vertebral column at the level of the inferior scapular angle. A small region (∼1 mm notch) of the Teflon coating was removed from each wire to form the stimulating electrodes that were then secured to the dura at the mid-line of the spinal cord at each site with 8.0 Ethilon sutures (**Figure 1B-v**). The wires were coiled at the exit site from the vertebral column to provide stress relief.

Cervical Spinal Cord Hemisection

A dorsal mid-line skin incision was made and the paravertebral muscles and fascia from ∼C2 to T2 vertebral body levels were reflected laterally to expose the vertebrae. A partial laminectomy was performed via removal of the spinous processes and a portion of the lateral bodies of the C3 and C4 vertebrae, effectively exposing the spinal cord. A 30-gauge needle was inserted into the midline of the cord to demarcate the right and half halves of the spinal cord. Micro-scissors were used to transect the right half of the spinal cord at ∼C4. Injury was verified by gently passing a fine glass probe through the hemisection site. Post-mortem, all injuries were verified histologically (**Figure 1B-vi** shows gross lesions, histology data not shown).

Development of a Closed-Loop ES System

We developed and tested a closed-loop ES system for the cervical cord by integrating key components of an effective closed-loop system (Krook-Magnuson et al., 2015) for use in freely moving rodents: *(i) Input trigger:* provided by salient EMG signals from forelimb muscles implanted with chronic EMG electrodes. *(ii) Real-time processing of the bio-signal to trigger stimulation*:

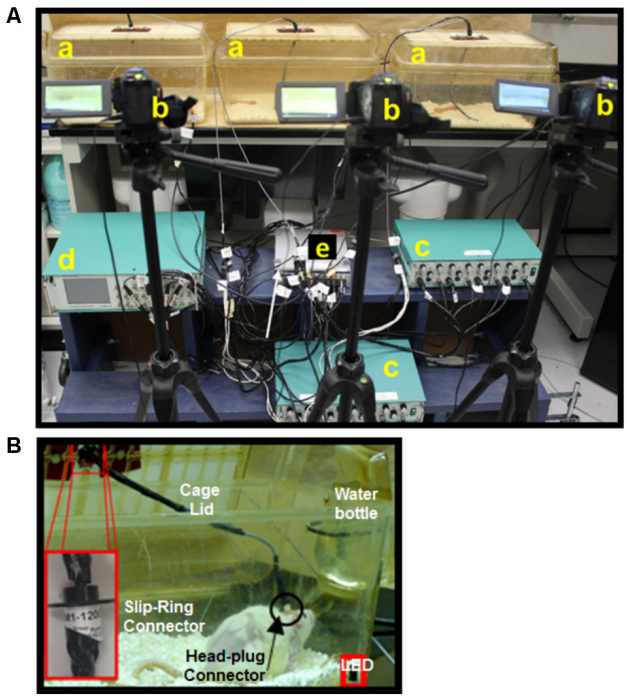

FIGURE 2 | Non-mobile experimental setup for long-term closed-loop spinal epidural stimulation (ES) in multiple rats. **(A)** Picture of the experimental setup showing multiple home cages **(a)**, cameras **(b)**, amplifiers **(c)**, a stimulator **(d)**, and a DAU **(e)**. **(B)** Picture of the rat in its modified home-cage allows full access to water without compromising movement due to the cable. A slip-ring connector (insert) linked to the head plug cable is attached into the cage lid and allows the rat a full 360 degrees of range of motion in the home-cage.

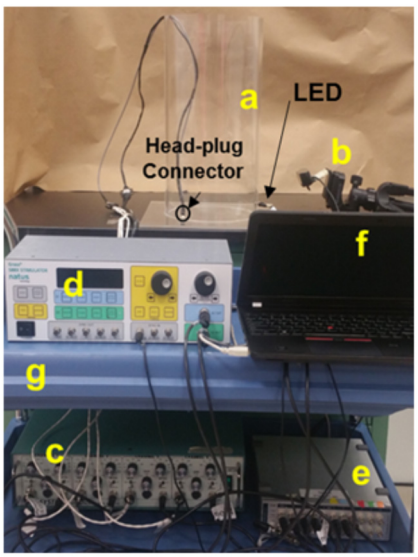

FIGURE 3 | Mobile experimental setup utilizing the closed-loop spinal ES system. Picture of the experimental setup for an individual rat shows an acrylic cylinder used for obtaining EMG data during grooming and rearing behaviors **(a)**, camera **(b)**, amplifier **(c)**, stimulator **(d)**, DAU **(e)**, and laptop **(f)**, all situated on a mobile cart **(g)**. The camera setup is particularly different than the non-mobile experiments and the setup is handy for training and testing in short experiments.

performed by the data acquisition unit (DAU). *(iii) Closed-loop delivery of stimulation*: via chronically implanted cervical epidural electrodes. This loop although does not implement a feedback controlled error correction mechanism by determining the 'correctness' of occurrence of that signal, the system is closed-loop in that it utilizes a recurrent biosignal-machine interface wherein real-time neural activity from the subject determines the timing, stimulation frequency and the length of stimulus delivery to the target. Additionally, the stimulation delivery stops once the rat stops to move. This is in contrast to open-loop stimulation strategies that we and others have used previously to continuously and independently deliver stimulation to the subject (Courtine et al., 2009; Shah and Gerasimenko, 2016). Although the hardware assembly may be used for a variety of applications, we demonstrate feasibility and usage of this setup in two experimental settings relevant to our laboratory: Chronic longitudinal experiments that require overnight training with tES for 7 h/day for 6 days/week for ∼3 months (non-mobile setup, **Figure 2**) and experiments aimed at assessment and training in a variety of rehabilitative motor tasks (mobile setup, **Figure 3**). Details of the setups are described in 'setup for data collection' below. In both setups, the amplified EMG signal is conveyed from the rat to the DAU, which signals the stimulator for delivery of ES.

From the Rat to the Data Acquisition Unit (DAU)

The built closed-loop circuitry for ES triggered by EMG signal is shown schematically in **Figure 4A**. Twelve pin circular plastic connectors (Part # A22004-001; Omnetics Connector Corp., Minneapolis, MN, United States) implanted on the rat's skull conveyed EMG signal from the forelimbs to the DAU through an amplifier. Nine of the pins (for EMG) from the mating connector were connected to one end of a 12-connector cable (Part # NMUF 12/30-4046SJ; Cooner Wire Co., Chatsworth, CA, United States). The remaining three pins (for ES) were soldered to three hook-up wires. Ends of these cables/wires were soldered to the rotary end of a slip-ring commutator (Part # 312M1-1200; Orbex Group, Fremont, CA, United States) implanted in the cage lid (**Figure 2B**). Commutators were used to ensure that free movement of rats in the cage is not limited by cable rotations. Non-rotary end of the slip-ring were connected to two D-SUB 9 connectors, one each for EMG and ES. The mating D-SUB connector for the EMG cable were soldered onto the ends of a 3′ input cable (Part #692000; A-M Systems, Sequim, WA, United States) for use with an amplifier (A-M Systems, Sequim, WA, United States). The mating D-SUB connector for the ES cable received input from the stimulator. Note that for the mobile experimental setup, the wires and cables that are soldered to the mating connector were attached directly to the D-SUBs without slip rings. The amplifier settings were as follows: Gain: x1000, Low Cut-off frequency: 10 Hz, High Cut-off frequency: 5 kHz, Notch settings were adjusted to '*In.*' The amplifier was connected to the analog input channels on the DAU (ADI Inc., Colorado Springs, CO, United States).

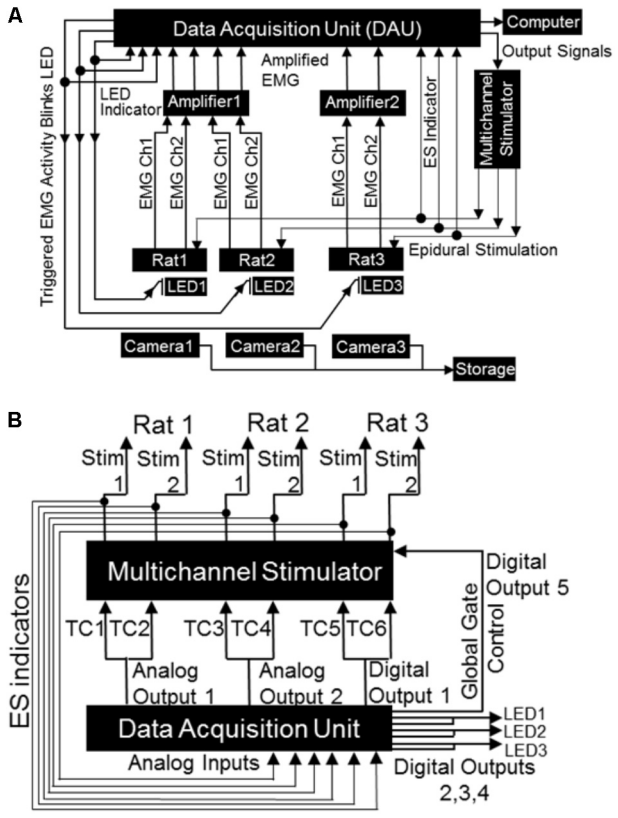

FIGURE 4 | Block diagrams depicting electrical connections of the mobile closed-loop spinal ES system. **(A)** Shown is a setup for a non-mobile closed-loop ES system for three rats. Detected EMG signal (shown are two EMG channels per rat) from implanted electrodes is amplified and sent to the DAU. When the EMG signal crosses a user defined threshold, the DAU triggers the multi-channel stimulator and synchronizing LED. A head plug cable transmits the stimulation pulse to the rat's spinal cord. The synchronizing LED pulse is visible as a bright light on the camera each time the EMG signal crosses the threshold. Concurrent inputs into the DAU monitors the LED pulse as well as sends output signals to the stimulator. A computer records all inputs that is fed into the DAU (EMG signal, LED pulse, stimulation pulse). An infrared camera records rat activity throughout the long-term night experiments. **(B)** Expanded block diagram from **(A)** above shows detailed connections and ES indicator loops from the DAU to the stimulator. Included are the global gate output control for the stimulator, the LED outputs and LED indicator loops (TC: stimulator trigger input channel).

From the DAU to the Stimulator and LEDs

The DAU was connected to the stimulator (for delivery of ES) and to LEDs (for visual syncing of infrared cameras and EMG activity) as follows (**Figure 4B**). Each of the two DAU analog output channels were split so as to send signals to two separate external trigger channels of the stimulator (A-M Systems or Grass S88x Natus Medical Inc., Pleasanton, CA, United States). To create additional output channels (one for a third stimulation trigger for a third rat, one for global gate control and three for LEDs), a single D-SUB 15 cable was custom constructed and outputted from the digital outputs on the DAU. This cable was soldered to a two row DSUB-15F connector and had the following connections: (a) three BNC connectors and LEDs with resistors. The BNC cables connected in-line with the LEDs monitored LED pulses via the DAU. These LED-BNCs were then connected to analog-in channels of the DAU for viewing as separate channels on the software. (b) A stimulator trigger channel (for the third rat), the digital output of which was split similar to the analog output channels. (c) A digital out channel that was used for the stimulator global gate control, which served as a master on/off switch for delivery of stimulation, ultimately controlled by the software. Note that the digital outputs of DAU for the additional rats can be used to expand the setup to include five rats (with two triggering muscles, one DAU, and one stimulator) or to a maximum of eight rats (with two triggering muscle, two DAU and one stimulator) simultaneously, but we demonstrate here a setup for only three rats. For the mobile experimental setup, a single LED was soldered onto one end of a BNC cable and attached to a splitter connected to the analog output of the DAU. The remaining end of the splitter was connected to an analog input channel on the DAU to allow for recording of LED pulses by the DAU. In all cases, the LEDs were placed near the rat's cage within the field of view of the cameras that captured all motor behavior either for overnight or mobile experiments. An infrared (IR) camera was used for the overnight filming (Bell & Howell, Elite Brands Inc., New York, NY, United States), and a webcam for the mobile experiments.

From the Stimulator to the Rat and DAU

Each output channel of the stimulator was split using a BNC splitter. One BNC cable was connected to an analog input channel on the DAU to monitor the outputted voltage from the stimulator and the other connected to a DSUB-9 from where a cable connected with the rat's head plug on the skull.

Software and Stimulation Protocols

All control settings of the closed-loop system were made in either ADI's Labchart or AM-Systems 3800 software. For the mobile system, ES was directly controlled via the stimulator. The software settings for EMG and ES were as follows.

Delivery of a trigger pulse initiated by EMG activity

An EMG threshold for triggering ES was first identified by collecting 3–5 min of baseline EMG data while the rat freely moved around in the cage. In order to prevent the stimulator from delivering multiple trigger outputs during the same EMG event, hysteresis was set to 1–3%, thereby necessitating a decrease in signal to 1–3% of the total dynamic range to generate the subsequent trigger pulse. This value was set depending upon baseline noise levels and amplitude of EMG signals. The triggering pulse width was set to 5 ms for the stimulation and LED triggers. Software settings also allowed for (i) comment placements on a separate digital channel to identify which muscle in each animal triggered the stimulation (ii) automatically start the stimulation after 30 min of baseline data collection, and (iii) obtain additional 30 min of data after the termination of the stimulation period. For the non-injured rats, the deltoid muscle was used to trigger stimulation since it was the first muscle to become activated during most cage activity. Note that for injured rats too, the deltoid muscle EMG threshold continued to trigger ES (since the C4 injury resulted in partial sparing of the muscle).

In addition, stimulation was triggered off the wrist extensor muscle, which showed some activity by 10 days post-injury (dpi) in most rats.

Delivery of ES triggered by onset of EMG activity (tES)

Stimulation on/off was controlled by a digital output channel attached to the global gate of the stimulator (see output signals in **Figure 4B**). With the rat connected to the setup, the stimulation intensity was first identified to elicit the lowest visually detectable upper limb muscle twitching (in both injured and non-injured rats). This was repeated for both channels (C6 and C8) for each rat. In both non-injured and injured rats, we used minimal visible twitching of the upper limb to identify the stimulation threshold. And this measure remained same throughout the study. Note that we were able to detect forelimb muscle twitching in response to ES at 10 dpi. Intensity of stimulation voltage for all experiments was then set at 90% of the obtained motor threshold (ES threshold voltage). Sub-motor threshold stimulation intensities were utilized to avoid interference with voluntary movement, eating, drinking and sleeping activities during the stimulation. In the current experiments, we used voltage stimulation to simulate our previous works (Shah et al., 2012; Alam et al., 2015; Shah and Lavrov, 2017). Note that for experiments when current output is desired, stimulation is possible for up to 10 h, being limited by the battery life of the stimulus isolator units (data not shown). Once the stimulation intensity threshold was set, our software was programmed to deliver this ES threshold voltage only when the EMG amplitude on the desired channel went above a user-defined EMG threshold based off EMG activity during attempted movement (EMG threshold). This EMG threshold was necessary to take into account any baseline electrical noise and avoid unnecessary delivery of ES independent of EMG activity. The software then triggered delivery of ES from onset of EMG activity or EMG spikes within a burst.

As proof of principle, we demonstrate two kinds of stimulation parameters using the closed-loop system. First, a 500 ms pulse train at 40 Hz that consisted of biphasic rectangular pulses (200 μs duration) was triggered by onset of EMG burst during free cage activity (**Figures 5A-i–iii**). Stimulation was delivered to the C6 and/or C8 spinal segments with monopolar configurations of C6-Ref+ and C8-Ref+ as described before (Alam et al., 2015; Alam et al., 2017). The length of the train was set to 500 ms at 40 Hz frequency based off an average bursting period of 0.5 ms for most muscles during motor activity. Thus, once a train of ES pulses was delivered in response to initiation of EMG burst activity, subsequent spiking activity from the EMG burst did not generate any new stimulation pulses until the train was completed. The setup also permitted multi-channel stimulation with varied time intervals between stimulation pulses at the different spinal segments. This method allowed for stimulation of the cord at an optimal frequency of 40 Hz to neuromodulate activity of spinal networks below the lesion, as described previously (Shah et al., 2012, 2016; Alam et al., 2015). 90% stimulation threshold was used to avoid undesired stimulation of the cord.

Second, we tested if our setup allowed individual spiking activity within the EMG burst to trigger single ES pulses to modulate timed activity of individual EPSPs (**Figures 5B-iv–vii**), as described previously for intraspinal microstimulation (McPherson et al., 2015). The main rationale of this stimulation strategy was to modulate activity of individual spikes within a burst, presuming that each spike is an excitatory post-synaptic response generated from supraspinal descending drive or spinal activity. The stimulation pulse delivered in the specific spike window would then modulate activity of active neural circuitry to allow for the delivery of stimulation at a user-defined frequency (McPherson et al., 2015; Zareen et al., 2017). Indeed, this stimulation strategy proved to be highly customized for each trial within and between rats and yielded unique resultant (effective) frequencies of tES delivery (see section "Results"). An inter-stimulation interval of 10 ms was imposed after each stimulus pulse to prevent stimulation artifacts from retriggering stimulation (**Figure 5B-vi**).

Algorithm for stimulation delivery

A feature of 'Fast Response Output' in our software monitored incoming EMG data and let users configure output signals (analog or digital) based on threshold values of raw input voltages. All of the threshold and hysteresis checking was done in the software by the PowerPC embedded processor in the DAU, after the input signal is delivered out of the system's Analog to Digital converter. For our purposes, each digital output was linked to 2 input channels (i.e., digital output 1 was linked to input 1 and input 2; output 2 to input 3 and 4, etc.). When the raw voltage of a monitored input crossed the set level of 0.2 V, a fixed width pulse of 0.005 s was triggered in the digital output. A hysteresis of 3% meant that the input signal needs to go above or below 0.2 V by 0.006 V before another output can be triggered again by each input pair. These Fast Response Output settings were saved in the random-access memory (RAM) in the DAU and are downloaded whenever a particular file is loaded.

Setup for Data Collection

Application of the closed-loop system for cervical spinal cord tES was tested in two experimental conditions: A non-mobile experimental setup, tailored to deliver tES in multiple rats simultaneously during overnight activity for 7 h/day for 6 days/week for ∼3 months (**Figure 2**). The second, a mobile setup, for experiments aimed at assessment and training in a variety of rehabilitative motor tasks (**Figure 3**).

Non-mobile Setup for Multiple Rats

We constructed a non-mobile system that is capable of simultaneously delivering the tES for 7 h/session to multiple rats, limited mainly by the units of equipment used. In our previous experiments that involved training with ES, we have been able to train only one rat at a time because of technical limitations with our experimental setup (Shah et al., 2016). This limitation becomes exaggerated for overnight experiments where rats need to be exposed to the stimulation for long hours, because data can then be collected from only one rat at a time (Gad et al., 2013). Shown in **Figure 2** is a setup for three rats

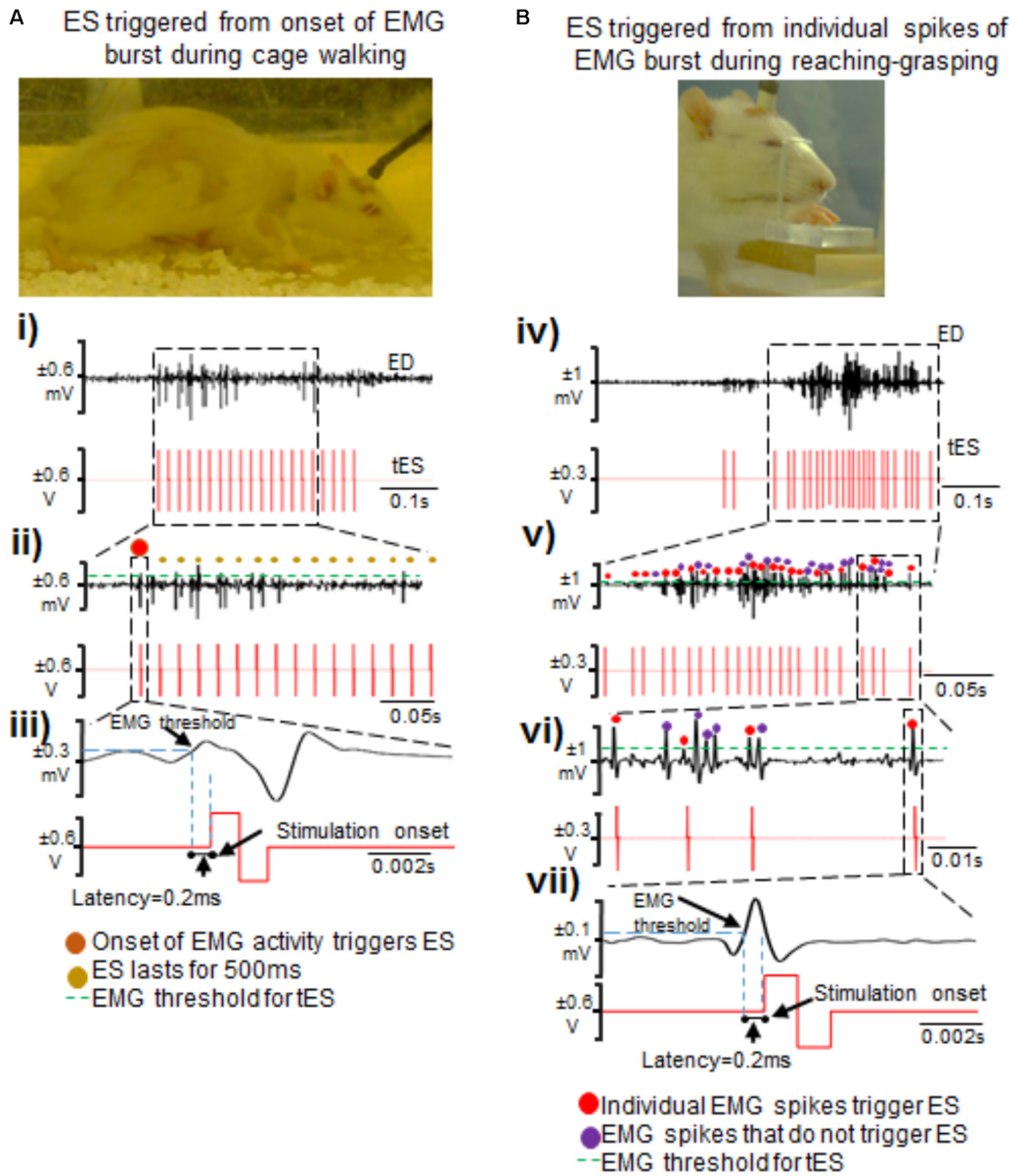

FIGURE 5 | Two methods of triggering ES from EMG signals during attempted activity. **(A)** Shown are standstill images of a rat receiving tES triggered from the onset of the extensor digitorum (ED) muscle bursting activity during walking in the home-cage. **(i)** Single ED burst during walking with corresponding stimulation train. **(ii)** Shown is a zoomed-in view of the EMG burst. The red dot represents the first spike that initiated the train of ES pulses (shown as red biphasic waveform). **(iii)** A single spike along with corresponding ES pulse triggered from that spike is zoomed to demonstrate latency for onset of stimulation pulse after the EMG spike crosses a set threshold. **(B)** Shown are standstill images of a rat receiving tES triggered from individual spikes (EPSPs) in an EMG burst during a reaching-grasping task. **(iv)** Biphasic stimulation pulses are delivered in response to individual spikes in an EMG burst that crosses a user defined threshold. **(v)** Zoomed-in view of the EMG signal shows individual spikes and corresponding stimulation pulses. Red dots are the spikes that triggered tES. Violet dots are the spikes that cross the user-defined threshold, but do not trigger tES because of the preset inter-stimulation interval time. **(vi)** Expanded view of individual spikes that triggered (red dots) or failed to trigger (violet dots) tES. In this example, an inter-stimulation interval is set to 10 ms to prevent stimulation artifacts from retriggering stimulation. **(vii)** Note the latency of ∼0.2 ms from time of spiking activity to delivery of tES, similar to what is seen in **(iii)**.

that utilizes two amplifiers, one 8-channel stimulator, a desktop and one DAU; assuming two channels of multi-site stimulation, triggered by two EMG channels, and one LED pulse per rat. Each rat is housed individually in its own cage throughout the experiment. Importantly, training with tES for all rats can be started at the same time. Data collection from video as well as EMG can be controlled by a common software source. Any errors in delivering the ES or data collection steps can be easily detected and all data are also stored to a common backup simultaneously. A standard rat cage was modified to integrate the flexible swivel connector within the rat's cage lid that connected to the stimulation device. Three holes matched to the slip-ring

manufactured screw placement were drilled into a piece of hard plastic. The slip-ring was secured to the hard plastic using three screws and nuts. The hard plastic with the slip-ring was then secured to the cage lid via bolts. A curved water bottle spout was connected to the rat's water bottle and inserted into the bottom hole and secured. Modifying the home-cage in this way ensured that the rats could move freely in their cage while the stimulation is on. During the overnight session, rats were filmed using an IR camera to visually observe overnight cage activity concomitant with EMG recording.

Mobile Setup for Experiments in an Individual Rat

We scaled down the non-mobile system into a mobile system for tES delivery in an individual rat to include a single amplifier, stimulator, camera and a laptop (**Figure 3**). Although all connections of the mobile setup were similar to the non-mobile setup, a webcam was used that was controlled by a recording software that automatically synced the video feed to the EMG traces. The setup also was less cumbersome requiring minimal maintenance with cable and rat-cage usage, enough for testing or training an individual rat. We tested its functionality in a variety of portable experimental settings for motor behavioral testing in our laboratory.

Data Collection

Data were collected in two experimental phases described below.

Overnight Experiments

We tested the capability of the non-mobile closed-loop stimulation system to deliver tES throughout the night in response to the EMG activity during the rat's free activity in its home-cage. This was done in non-injured rats to test the logistics, feasibility and implementation of the 7 h protocol prior to employing it in injured rats. A full night-time session lasted for 7 h and consisted of 30 min of baseline EMG and video recording in the home cage, followed by 6 h of stimulation and recording, and a subsequent 30 min of post-stimulation recording. The deltoid, pronator or extensor muscle was chosen to trigger tES because our preliminary EMG data revealed that these muscles are the first to activate during any attempted locomotor movement of the forelimb, including isometric contractions. tES was triggered from onset of EMG burst or spiking EMG activity as described above.

We then determined if long-term closed-loop tES could be applied in the rat's home-cage without the need for supervision in multiple rats after the injury. Seven CHx rats underwent long-term overnight exposure to tES for 7 h/day for 6 days/week for 1–3 months, beginning at 10 days post-injury. Our preliminary data show that 10 days post-injury is the time when rats with a complete hemisection at C4 have regained adequate control of their hindlimbs and trunk to move around in the cage. These rats are also most physiologically stable by day 10 after an initial insult to the rostral cervical cord. The stimulation protocols were the same for non-injured and injured rats, as descried above in *stimulation protocol*.

Mobile Experiments

The feasibility of the closed-loop system was then assessed for use in mobile experiments. Specifically, ES was triggered from onset of EMG activity and/or individual spiking activity (EPSPs) in the EMG burst during different motor behaviors: ladder walking, treadmill walking, rearing and grooming behavior and reaching-grasping. Rearing and grooming behaviors were chosen because these are the rat's most naturally occurring behaviors. For ladder walking, a rat was placed on a horizontal ladder consisting of unevenly spaced rungs with cages on either end of the ladder serving as end points (Metz and Whishaw, 2009). For treadmill walking, rats were placed on a custom-built rat treadmill similar to the one used previously (Shah et al., 2013) and the speed was set to 13 cm/s. For the rearing behavior, rats were placed in a custom built acrylic cylinder that readily prompted the rearing behavior. The grooming behavior in the cylinder was obtained via natural grooming activity or grooming induced manually by placing few water drops on the rat's head between the ears (Gensel et al., 2006). For reaching-grasping pellet retrieval task, rats were assessed on their ability to reach and grasp sugar pellets successfully as described previously (Zemmar et al., 2015; Alam et al., 2017). The rats were placed individually in an acrylic reaching and grasping chamber (18 cm × 15 cm × 31 cm) with a small slit in the front wall (3 cm × 1.5 cm). Rats were offered with a 45 mg banana-flavored sugar pellets (Bio-Serv, United States) and encouraged to reach and grasp the sugar pellet placed on the platform 1cm away from the slit with the preferred forepaw.

All sessions were recorded throughout the experiments so as to obtain EMG and video data during these functional activities. The EMG signals were filtered (band passed, 10 Hz–5 KHz) and amplified (1000×) using an analog amplifier (differential AC amplifier, AM-systems Inc., United States). The signal then was digitized at a 10 KHz sampling rate and stored on a computer using a data acquisition card (NI-DAQ; National Instruments Inc., United States) using a custom-written program. Data obtained from these experiments were set to automatically store into our lab servers for use in our current and future works.

Data Analysis

Electromyography and video data were synchronized to match movement with corresponding EMG activity. For this, we first find the first frame where the LED sync is on (LED onset) in the video (example: 50). In the associated EMG file the LED onset corresponds to the first rise in voltage in the *LED sync* channel (example: 5 s). From a range of video frames that contain a motor event (example: reaching/grasping) (example: 500–1500), frame values are converted to values relative to the LED onset frame (example: 450–1450). The relative frame values are then converted to time values by dividing with the video's frame rate (4.5–14.5 s for a 100 fps video). For the EMG file, all time points before the LED onset in the EMG file are cropped to create a new file. As such, the time values generated from the video then match the EMG file (the software automatically takes care of the sampling rate for the EMG file). Note that EMG signals were band-passed filtered (20–1000 Hz) for data analysis. Data were

analyzed to verify if stimulation was triggered secondary to the appropriate EMG trigger. The latency to onset of stimulation was obtained as the time difference between EMG activity triggering ES and onset of stimulation.

For all data, representations of EMG bursts from the most clearly visible cycles during ladder walking, treadmill walking, reaching-grasping, grooming and rearing activities on the video were selected for data analysis. Clear motor activity was first identified on the video and corresponding EMG activity detected to show success of the closed-loop system at delivering ES triggered from onset of bursting activity for overnight experiments as well as from individual spikes for motor behaviors in the mobile setup. We watched videos for gross behavior and then the corresponding EMG activity was retrieved to study which muscle triggered the tES. All EMG analysis for this manuscript was limited to identifying the appropriate muscles for tES and testing the feasibility, reliability and validity of the closed-loop tES.

RESULTS

Feasibility

In this work, we successfully assembled a functional and simple closed-loop system without the need for designing complex electrical circuit boards or electrical neuro chips. We were able to establish use of the setup for overnight experiments requiring overnight tES of the spinal cord in injured rats, possessing capabilities to function without tester supervision (**Table 1**). The system could also be implemented in a variety of experimental settings for use in motor behavioral studies.

Reliability

We were able to reliably implement the closed-loop system to deliver the stimulation protocol for several sessions throughout 1–3 months, a prime requirement for our future chronic training experiments (**Table 2**). Although there was no problem with the system itself, in one rat, experimentation was stopped by ∼1 month because the headplug failed. We also encountered an epidural implant failure in a couple of rats.

The closed-loop system allowed successful tES delivery simultaneously in multiple rats during overnight activity for 7 h/day for 6 days/week for 1–3 months. We were able to start experiments for all rats at the same time, the system automatically stopped the experiments at the end of 7 h, ran the 7 h protocol homogenously for all rats, and EMG-video data were collected and saved automatically without any software system errors. The head plug connectors, cables, swivel connectors and customized home-cages functioned well without major errors throughout the experimental timeline. The cables remained viable and did not interfere with night activity, food or water access in the cage. Note that although we demonstrate feasibility of the system to deliver tES to three rats simultaneously in this work, preliminary data from our lab now show that we can expand this system to deliver tES in eight rats. Application of the closed-loop system in the mobile setup too was successful in a variety of experimental settings that involved motor assessment. In all rats, the deltoid and extensor muscle EMG activity readily triggered ES in response to some proximal arm movement and/or distal wrist movements, respectively, by day 10 post injury during the rat's overnight motor activity in the cage. In comparison to pre-injury levels, the EMG threshold required to trigger ES increased earlier after the injury. For example, EMG threshold to trigger ES from the deltoid changed from ∼0.03 mV (pre-injury) to ∼0.15 mV

TABLE 1 | Features of the closed-loop system.

Feature	Description
Off-the-shelf parts	No requirement of complex circuit boards/chips.
Versatile and customizable	The system can be customized to receive input and provide output from/to a variety of different sensor and stimulation sources, custom tailored to individual experiments.
Expandable	We demonstrate an electronic setup for up to three animals in **Figure 2** (assuming two amplifiers, one DAU, and 1 stimulator using 2 channel EMG, stim, and LED). The system as is further expandable to more animals, if needed.
Low latency	Latency times are 0.2 ms between the EMG signal crossing threshold and the stimulation activation (**Figure 5**).
High number of inputs and outputs	The system, assuming one DAU, allows for 16 channels of input and 10 channels of output. Adding a second DAU allows for an additional 16 channels of input (no extra output channels).
Can trigger off multiple inputs separately or simultaneously	The system can be configured to initiate multi-site stimulation based off individual or simultaneous threshold activation (**Figures 6**, **7**).
A/C controlled	The system is A/C powered allowing for lengthy recording times.
Application for chronic experiments	System is feasible and reliable for use in overnight stimulation studies that does not require supervision.
Portable	The system is mobile, easily transportable in a cart, making it ideal for a variety of behavioral testing and training protocols.

TABLE 2 | Success of conducting night experiments using the closed-loop system over select time points.

Rat identity	Pre-injury testing and experiments (non-injured rats)								
Rat 1					✓				
Rat 2					✓				
	Post-injury testing and experiments (injured rats)								
	10	**20**	**30**	**40**	**50**	**60**	**70**	**80**	**90**
Rat 3	✓	✓	✓	✓	✓	✓	✓	✓	✓
Rat 4	✓	✓	✓	✓	✓	✓	✓	✓	✓
Rat 5	✓	✓	✓	✓	✓	✓	✓	NR*	NR*
Rat 6	✓	✓	✓	✓	✓	✓	✓	✓	✓
Rat 7	✓	✓	✓	Omnetics connector malfunction. Testing and experiments discontinued					
Rat 8	✓	✓	✓	NR*	NR*	NR*	NR*	NR*	NR*
Rat 9	✓	✓	✓	✓	✓	✓	✓	✓	✓

*✓ – Testing and experiments successfully performed. *NR – Non-responsive to tES due to epidural implant failure.*

(post-injury). Likewise, EMG threshold to trigger ES from the extensor changed from ∼0.05 mV (pre-injury) to ∼0.2 mV (post-injury). The increase is most likely due to elevated motoneuronal excitability states that leads to overall increase in baseline bursting EMG activity and baseline noise after the injury, a commonly observed phenomena early after a cervical SCI (Alam et al., 2017). We are, however, considering adopting more robust EMG threshold detection techniques (such as signal noise ratios) for our current experiments. Interestingly too, stimulation intensities that induced muscle twitch after the injury were generally higher for up to 3–6 weeks post injury (0.03–0.06 V pre-injury versus 0.25–1.5 V post-injury), and gradually decreased over time. The elevated stimulation intensities that were required to induce limb movement indicate that the relatively more rigid forelimb observed from elevated spasticity after a SCI necessitated greater strengths of stimulation to allow visualization of a muscle twitch (and perhaps overcome the co-contraction). Details of these observations are currently under investigation in our laboratory and beyond the scope of the current manuscript.

Sensitivity of ES Delivery

Our system was able to detect the set EMG thresholds to deliver stimulation 100% of the times. Additionally, there were no false negatives, that is, the current was delivered only when the set threshold for that muscle was reached.

Validity

Our data confirm that for both the overnight as well as mobile setups, the closed-loop system is capable of reliably generating a pre-defined signal parameter that surpasses a user-defined threshold to reliably trigger the DAU to in turn, activate the stimulator to output the desired stimulation protocol without user input. For overnight closed-loop tES in multiple rats, the 7 h tES protocol remained constant over the 3 months. Stimulation pulse trains were consistently generated and applied over the full 6 h in response to selected EMG bursts that crossed a user-defined threshold for muscle activation. Delivery of stimulation was possible by trigger from single (**Figure 6A**) or multiple muscles (**Figure 6B**). The synchronizing LED pulse verified that the EMG signal surpassed threshold and only then generated the stimulation output. Out of the 6 h for which ES was prescribed for delivery, the total actual stimulation time ranged from 4 to 5 h per rat, depending upon the night activity of that rat. Video recording and the stimulation protocol lasted for the 6 h with half hour of baseline data collection pre-and post the tES delivery session, making it suitable for chronic implementation in injured rats. Video data generated from the IR cameras proved useful in linking patterns of EMG activity with quality of movements during free cage activity.

For behavioral experiments that are done in different physical locations, transporting the mobile tES system proved beneficial since the overnight training setup is cumbersome. For ladder (**Figure 7A**) and treadmill walking (**Figure 7B**), for example, flexor and extensor muscles independently triggered stimulation. **Figures 7C,D** show the versatility of the closed-loop system in detecting spiking EMG activity to initiate stimulation while rats performed rearing and grooming behaviors.

Importantly too, the closed-loop system delivered tES from the onset of muscle burst or muscle spike within the burst as determined by the tester. This was consistent between rats, across trials and between behavioral conditions (representative two rats are shown across two representative time points and two testing conditions in **Figure 8**). There were no noticeable movement artifacts and interference of motor activity from cable or rat movement in any instances.

Latency to stimulation: During tES, the latency to onset of stimulation consistently occurred after crossing the user-defined muscle threshold. This was ∼0.2 ms, irrespective of whether the stimulation was triggered from onset of burst activity or by spikes within the EMG (**Figures 5-iii,v**).

Limitations of the Closed-Loop System and Its Application for Chronic Experiments

(i) Note that the duration for which every rat receives tES is directly dependent on the voluntary activity level of rats. As such, the total treatment time using tES is variable between rats, especially after an injury. Based on our preliminary data for overnight experiments, for example, the number of hours during which tES is actually delivered to each rat ranges between 4 to 5 h per rat per session. In any case, our setup allows us to overcome this variability by customizing the training time for each rat, easily programmable into the software. (ii) Although we did not encounter any obvious problems with use of the technique itself, implementing the closed-loop system for the overnight experiments was more demanding than the mobile setup. Some complications related to this application include: (a) in rare instances, rats tend to chew on the cables. Using a shrink-wrap around the cable resolved the issue without restricting rat movement. (b) All rats were able to sustain the long durations of stimulation for the 3 months. It was however, not uncommon for rats to attempt to remove the connecting cable with their contralateral upper limb in the initial days of training. This limitation was overcome when the connection between the connecting cable and head plug was *tightened* using a thin layer of a solvent (such as nail-polish). (c) Complete failure of the head plug and/or ES wires too are other complications associated with long-term training. (d) The non-mobile setup for tES in multiple rats is cumbersome and requires committed space. Robustness of the setup is, however, ideal for chronic experiments such as those pursued in our laboratory.

DISCUSSION

We present herein an activity-dependent closed-loop electrical stimulation system that features an assembly of off-the-shelf components and allows for ES of the cervical spinal cord triggered from prescribed motor movements in real time. To our knowledge, this is the first study that incorporates the delivery of cervical ES triggered by EMG activity in freely moving rats after a cervical SCI. Our results show that the tES system can be successfully implemented during a variety of motor behaviors

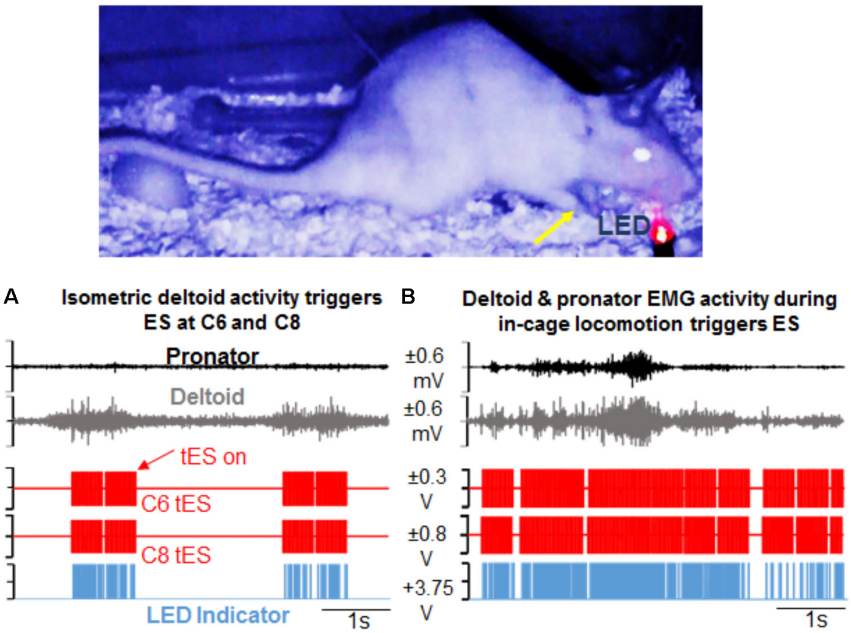

FIGURE 6 | Demonstration of activity-dependent ES of the cervical cord segments triggered by pre-defined EMG signal thresholds (tES) during overnight training in the rat's home cage. **(A)** Standstill image that corresponds to a frame in the video is synced with precise time of an ongoing forelimb EMG activity. The EMG signal corresponds to forelimb weight support (yellow arrow) in the rat's home cage at night. Note that activity in the deltoid muscle alone triggers ES of the C6 and C8 spinal cord segments (red pulses). Stimulation occurs in response to muscle activity measured via EMG signal only at a defined threshold (tES on). With no muscle activity present, tES shuts off automatically. LED on the video blinks red when the EMG signal crosses a threshold to trigger ES and is also recorded as a pulse (blue) in the data collection software. **(B)** Shown is a similar snapshot of a video frame that corresponds to deltoid and pronator muscle EMG activity during a forelimb locomotor task in the cage. The deltoid muscle threshold keeps the ES switched on for a longer duration.

during different experimental settings. We also demonstrate the feasibility of the system for use as a long-term rehabilitative therapeutic tool for multiple rats in a chronic overnight training regimen without the need for tester supervision. Experiments in our laboratory are underway to determine if chronic intervention with tES will restore upper limb motor function from paralysis after a cervical SCI.

Unique Features of the Developed Closed-Loop System and Experimental Setup

The closed-loop system constructed from off-the-shelf commercially available components offers wide versatility for use with both freely moving animals as well as in constrained experimental conditions. In this work, we show that delivery of cervical ES is possible for long durations (7 h/day for 6 days/week for 1–3 months) without any interruptions in a given session and without need of supervision by a person. Multiple rats can be trained at the same time, thereby greatly increasing the efficiency of experiments that utilize long-term rehabilitative protocols. Our experiments that lasted for 3 months did not suffer from any major problems in the hardware or software components of the system. Simple modifications of the home-cage with commutators and infrared capabilities when integrated with the setup, permit training rats and monitoring their night activity for long hours without tester supervision. Stimulation sequences can be pre-programmed or triggered off ongoing EMG. Additionally, depending on rodent behavior in the cage, the stimulation parameters (time of stimulation, frequency of stimulation) are continually *adapted* (in the millisecond range) throughout the treatment session in response to feedback from physiological changes (EMG activity) at any given time in the treatment session. For example, the frequency of stimulation varies continuously throughout the training period, varying between 20 and 40 Hz, depending upon the extent of motor activity by the rat (see **Figures 5B**, **8**). The stimulation also stops as soon as the rat stops moving. A feedback loop from bio-signals that control the stimulation delivery parameters therefore make it a real-time adaptive (closed-loop) system (Krook-Magnuson et al., 2015; McPherson et al., 2015). This is in contrast to open-loop stimulation protocols in which the stimulus is delivered regardless of the ongoing activity and according to a pre-defined offline script. The uniqueness of this system is also the ability to use the raw EMG signal from a single and/or variety of muscles and/or motor activities within the same experimental session so as to deliver a single or multi-site stimulation pulse within a short period of time (latency of 0.2 ms). The setup can allow the use of other bio-signals (such as mechanomyography and force plate sensors) as stimulation triggers. Additionally, a streamlined platform for closed-loop experimentation using simple point electrodes makes it a promising tool for use with multi-array electrodes.

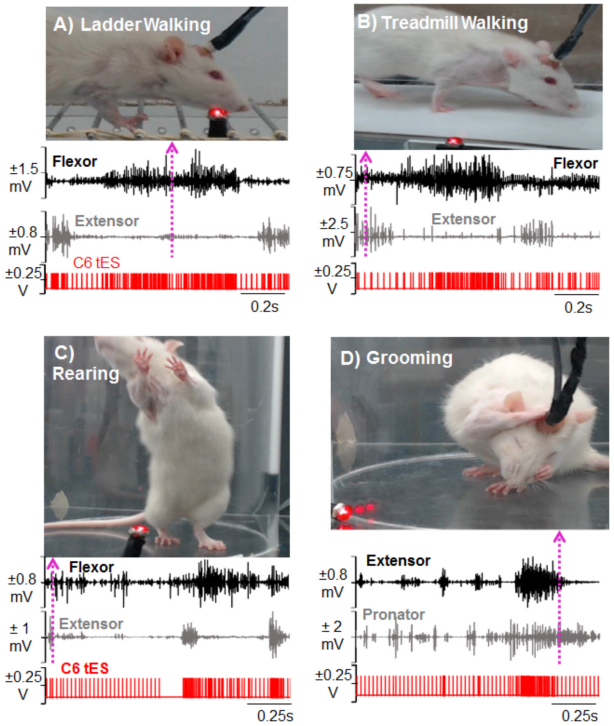

FIGURE 7 | Demonstration of activity-dependent ES of the cervical cord segments triggered by pre-defined EMG signal thresholds (tES) in a mobile experimental setup designed for a multitude of motor tasks. Standstill image that corresponds to a frame in the video is synced with precise timing of an ongoing forelimb EMG activity (dotted arrow matches the frame with the time in the EMG trace). The portable closed-loop setup permitted obtaining data for ladder walking **(A)**, treadmill walking **(B)**, rearing **(C)**, and grooming **(D)** motor behaviors. Note that during each task, tES occurred following every spike in the EMG burst based upon a user-defined threshold for muscle activity.

Closed-Loop ES of the Lumbar Spinal Cord

There is growing interest in spinal ES as a means of facilitating motor output after a SCI. Most of the previous works on ES has been *open-loop* that entails delivery of continuous ES at a constant rate, not timed to EMG activity related to the task (Carhart et al., 2004; Courtine et al., 2009; Harkema et al., 2011; Shah et al., 2012; Angeli et al., 2014; Shah and Gerasimenko, 2016) for review, see (Shah and Lavrov, 2017).

In contrast to an algorithm that is embedded within our designed software, note that previous ES studies for spinal cord stimulation have employed algorithms operated by customized neuro-chips to create a closed-loop system. One of the most elegant closed-loop ES systems implemented in SCI studies integrated feedback from hindlimb kinematic activity and muscle EMG to control lower limb kinematics during continuous bipedal stepping in real time in rats spinalized at T8 (Wenger et al., 2014). This system utilized control algorithms and advanced technological platforms that interfaced feedback signals and feed-forward mechanisms to match ongoing modulated neural activity in real time. In another study involving rats that were spinalized at the thoracic cord, ES in the lumbosacral spinal cord was triggered from EMG activity of the biceps brachii muscles (Gad et al., 2012). In both these reports, ES was delivered in a setup that involved restraining the spinal rat and ES continued for as long as the rehabilitative training lasted under tester supervision. Gad et al. (2012) used an analog multiplexer controlled by a target board debugging interface (MSP-EZ430) to detect the start and stop times of EMG bursting activity in the forelimb to deliver lumbosacral stimulation. The goal of this experiment was to achieve indirect volitional control of ES (by forelimb EMG activity) to facilitate quadrupedal stepping in spinal rats. A moving window step-detection algorithm was implemented in a small microprocessor to detect the on-off EMG patterns of a single forelimb muscle that initiated and terminated lumbosacral ES during walking on a treadmill. No feedback control of the bio-signal to correct stimulation parameters were employed. The latency to stimulation from trigger was longer than 1 s (almost two step cycles) and involved signal processing (ex: FFT of raw signal) prior to stimulation delivery. This is in contrast to detection of raw spiking activity of multiple muscles that are activated during volitional motor activity in the rat's home-cage in our setup. Our algorithm detects threshold of EMG activity with each spiking activity within 0.2 ms of spike activity onset. Our system is also set to deliver chronic periods of stimulation (for ∼7 h) independent from supervision by a tester; with the primary goal of promoting long-term plasticity in spinal neural circuitry, similar to what has been shown with intraspinal microstimulation (McPherson et al., 2015).

Collectively, our implementation of the system and algorithm is the first application of a closed-loop system for cervical spinal cord ES as well as the only one so far for chronically delivering cervical ES without tester supervision in freely moving rats during the rat's home-cage activity.

Novel Closed-Loop Stimulation Strategies of the Cervical Spinal Cord

Our current experiments were inspired by studies that demonstrate that triggered intraspinal microstimulation of the cervical spinal cord controlled by cortical neurons or EMG activity will evoke movements of the arm and hand in primates (Jackson et al., 2006b) and also improve hand function after a SCI in rats (McPherson et al., 2015). In the present work, we built an activity triggered ES system that allowed training rats with tES without tester supervision. The system involved utilizing EMG activity from the affected forelimb muscles to trigger stimulation of the cervical cord so as to facilitate ongoing forelimb movement patterns during routine activity in the rat's home-cage environment.

We were able to implement two unique protocols for triggered stimulation. The first tES strategy was the delivery of a continuous 500 ms train of ES (40 Hz) triggered from the first spike of EMG bursting activity that reached a prescribed threshold value during attempted movement. Although descending supraspinal neuronal control is integral to regulate locomotion, bilateral rhythmic alternating neural activity necessary for treadmill and overground locomotion

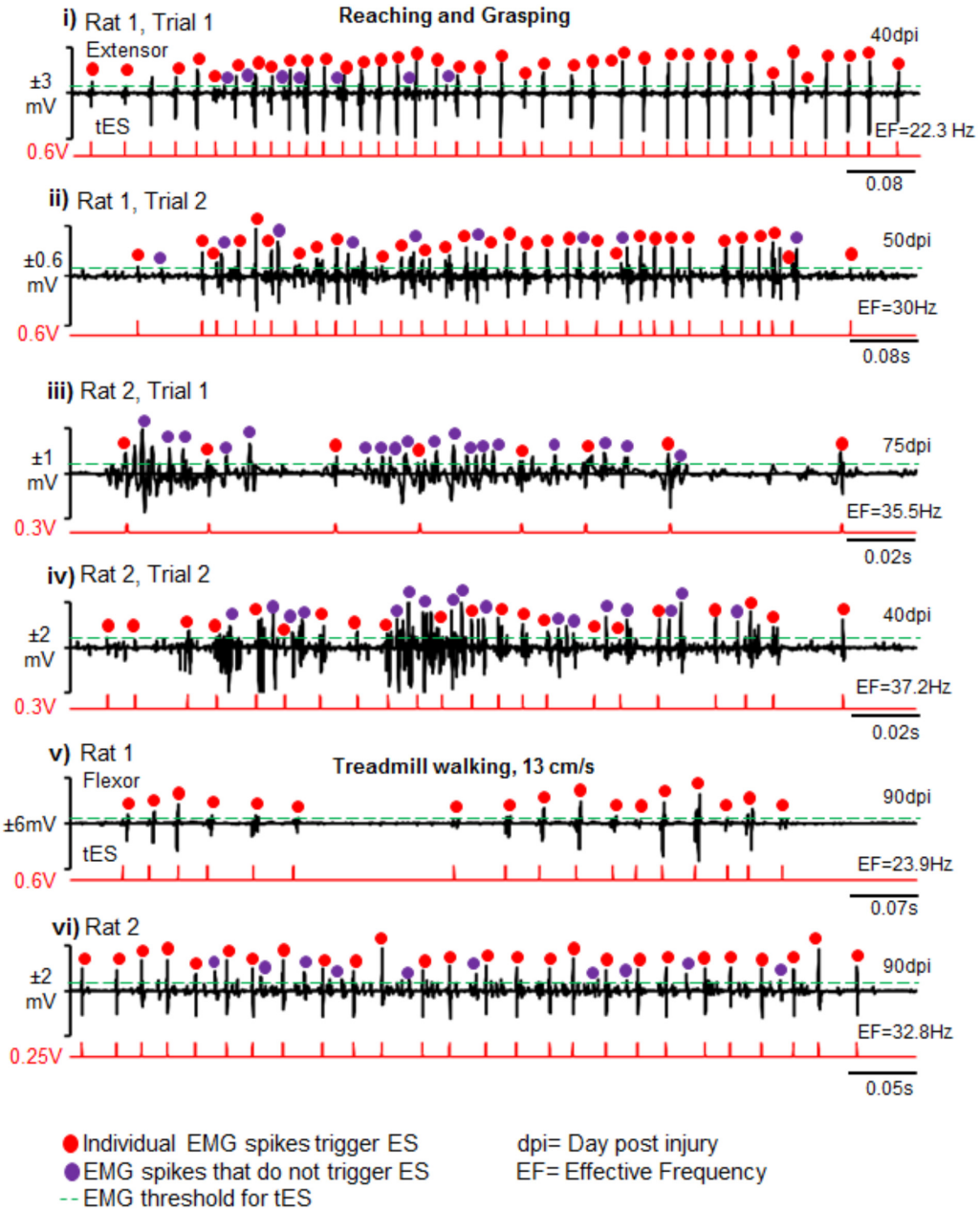

FIGURE 8 | Reliability and validity of closed-loop spinal ES system. Shown are representative EMG bursts along with corresponding tES during two trials of reaching-grasping activity for Rat 1 **(i,ii)** and Rat 2 **(iii,iv)** at different days post injury (dpi). **(v,vi)** Similarly, representative EMG data from a single trial are shown from two rats (Rat 1 and Rat 2) during treadmill walking at 13 cm/s. Red dots are EMG spikes that trigger tES. Violet dots are spikes that cross the user-defined threshold, but do not trigger tES because of the preset inter-stimulation interval time. As expected, the closed-loop system consistently delivered tES in response to the EMG spikes (red dots) that crossed a tester defined threshold (green line) for a multitude of motor tasks between and within rats. Note that the resultant effective frequency (EF) directly depends upon bursting activity of the task.

does not rely heavily on descending drive (Grillner and Zangger, 1979; Edgerton et al., 2008). We therefore tested a stimulation strategy that permitted continuous delivery of ES to target forelimb locomotion in this study. The idea that a prescribed 40 Hz frequency will globally activate locomotor networks in the cervical cord was adopted from previous reported works that demonstrate that 40 Hz can effectively facilitate pattern generated hindlimb locomotor activity after severe hindlimb paralysis [for review, see (Shah and Lavrov, 2017)]. Moreover, previous studies that have employed cervical ES (Alam et al., 2015, 2017) or cervical intraspinal microstimulation (Sunshine et al., 2013; Mondello et al., 2014) have shown success in modulating cervical networks at these frequencies.

The main feature of the tES mode was to trigger ES secondary to initiation of any attempted activity in the cage, instead of continually delivering ES even when the muscles were at rest. Our data indicate that at rest, EMG activity during tES was close to zero as is desired during the muscles' resting phase, to eliminate unnecessary levels of excitation from the muscle. Although continuous delivery of electrical stimulation has shown improvements in a variety of physiological functions after a severe SCI in both animals and humans [for review see (Shah and Lavrov, 2017)], findings from literature demonstrate that delivering ES triggered by EMG activity is a far better stimulation strategy than continually delivering ES even during the rested no-EMG activity phases (Krook-Magnuson et al., 2015; McPherson et al., 2015). This is most likely because the excess delivery of electrical current into a relatively inactive neural circuitry zone does not necessarily result in neuromodulation that is otherwise required when 'demanded' of the nervous system, as during an attempted movement. This concept is supported by clinical studies in humans with a functionally complete SCI. In these works, although ES is continuously delivered during volitional attempts made by the subject, greater gains in voluntary leg movements are seen in those subjects when ES also accompanies volitional effort and intent to move (Angeli et al., 2014; Grahn et al., 2017; Rejc et al., 2017). It is reasonable to hypothesize that delivery of stimulation at a time when the circuits are 'primed' for activity, will produce functional benefits than when delivered without volitional attempts to move. These questions, however, need to be addressed systematically and are some of the objectives of our future experiments.

The second tES strategy presented here involved delivery of single ES pulses triggered from individual spikes of EMG activity. In this protocol, each stimulation pulse was delivered in response to spikes in forelimb EMG burst in a spike-activity dependent manner during free home-cage or reaching and grasping activity. The fundamental premise of this stimulation strategy is to amplify an individual excitatory post-synaptic response by enhancing supraspinal descending drive in a specific window to facilitate long term potentiation and modulate activity of active neural circuitry to allow for the delivery of stimulation at a user-defined frequency (McPherson et al., 2015; Zareen et al., 2017). In an *in vitro* experiment, after a cervical spinal cord hemisection in adult rats, inspiratory bursting in the tongue muscle that is used to trigger intraspinal microstimulation resulted in activation of diaphragm motor units during the inspiratory phase (Mercier et al., 2016). This paradigm evoked short-term potentiation of spontaneous inspiratory activity in the previously paralyzed hemidiaphragm (i.e., bursting that persists beyond the stimulus period). Moreover, chronic treatment with intraspinal microstimulation of the cervical spinal cord that is timed with spiking EMG activity during reaching and grasping function, greatly enhanced motor function (McPherson et al., 2015). None of the rats in the present study were exposed to any training using this protocol, but the presented data are proof of concept for implementing the EPSP triggered ES as a more refined technique to control a more precise supraspinally driven skilled motor output. Experiments in our laboratory are currently under way to determine the effects of this ES protocol on skilled reaching and grasping function in injured rats.

Note that we have not reported the benefits of this system over the use of continuous ES for the cervical cord after a cervical SCI, but this question is currently beyond the scope of the present report. Instead, the methodology for tES described here has laid the foundation for pursuing this and similar crucial research questions with use of the proposed technique.

Overnight Activity-Dependent Chronic Stimulation

One of the major advantages of our setup has also been the ability to stimulate the spinal cord for prolonged hours through the rat's night cycle. After severe cervical spinal cord injuries, the motor deficits are persistent (Filli et al., 2011) and therapies to enable motor function of the paralyzed limb often necessitate chronic intervention periods of motor and/or neuromodulatory strategies (Angeli et al., 2014; Grahn et al., 2017). However, intervention time for a given therapy is limited both in the standard pre-clinical and clinical setting. There is therefore a need for automation in motor therapies delivered, but in a way that integrates the subject's intentional activity and functional capability. Moreover, as expected, the effects of stimulation training are maximum when the subject is actively engaged in training (Angeli et al., 2014; Buick et al., 2016). As such, delivering stimulation in the rat's active (i.e.) night cycle will deliver stimulation for a longer period – each time the rat attempts to move. The delivered stimulation in turn will activate spinal circuits to further permit movements that were otherwise not possible – thereby creating a positive feedback mechanism of increased 'self-training.' Indeed, experiments that utilize such long-term activity-dependent stimulation during overnight activity have gained increased attention (Zimmermann and Jackson, 2014; McPherson et al., 2015) and are highly relevant for pre-clinical studies that necessitate long intervention periods for effective clinical translation.

CONCLUDING REMARKS

In the clinical setting, the use of closed-loop systems is used for a variety of neurological disorders [see review (Krook-Magnuson et al., 2015)] including its proven use for suppressing clinical seizures in humans (Fountas et al., 2005) and treating movement disorders in patients with Parkinson's disease (Little et al., 2013). The idea that residual proximal limb movements trigger pre-programmed stimulation to cause the paralyzed muscles to contract has proved successful for closed-loop functional electrical stimulation systems controlling limb activity in humans [for review see (Ethier and Miller, 2015)].

Given the clinical use of ES in persons with a SCI (Harkema et al., 2011; Angeli et al., 2014; Grahn et al., 2017; Rejc et al., 2017), it is not surprising that much effort is being expended in improvising on ES techniques as a training tool to restore physiological functions after a SCI. Moreover, with the extreme reliance of upper limb motor function on supraspinal pathways (Fouad et al., 2001;

Ballermann and Fouad, 2006; Hurd et al., 2013), it is worthwhile developing a neuro-rehabilitative feedback based intervention that integrates spinal cord stimulation with attempted voluntary movements of the hands or legs. This is especially relevant in instances of functionally incomplete SCIs that have some descending control of movement.

With the surge in evidenced-based motor rehabilitation practice, one of the main hurdles for effective translation of neuro-rehabilitative motor therapies into the community is the limited amount of time spent by patients in rehabilitation clinics (Newitt et al., 2016). To combat this limitation, carefully designed feedback based home-therapy programs have indeed become an integral part of modern evidence-based neuro-rehabilitation practice (Buick et al., 2016; Zbogar et al., 2016). The successful development of the tES technique presented herein can operate autonomously for extended periods of time in unrestrained rats, allowing its use as a long-term therapeutic tool. The system can also be used in concurrence with motor rehabilitative training procedures to facilitate the effects of the training. It can also enable us to study the short-term as well as long-term physiological effects of incorporating electrical stimulation techniques into the nervous system. It might be worthwhile for example, to investigate if an activity-dependent closed loop ES technique in combination with rehabilitative motor training will prove effective in regaining skilled upper limb reaching and grasping function in the more clinically relevant contusion injury model. Spinal ES has received attention in the treatment of neurological damage that is beyond a SCI, such as in ameliorating motor symptoms of a Parkinson's disease (Fuentes et al., 2009). Triggering ES during resting states (as compared to during EMG activity) is another feasible application of the closed-loop system. The system can therefore prove effective both as a supplement to existing rehabilitative motor therapies in the clinic or laboratory setting, or could be used independently as a feedback based training tool.

The developed closed-loop system can also be considered to represent a class of bidirectional neural prostheses (Jackson et al., 2006b) via a circuit that enables two-way interactions between neural activity (real-time processing of EMG activity) and external devices (such as a stimulator). Recently, elaborate computational platforms such as the Brainet (Pais-Vieira et al., 2015; Ramakrishnan et al., 2015), which allows sharing neural information between multiple study subjects to engage in a common motor behavior, have gained increased attention in the field of neuroscience. This closed-loop ES technique can be experimented for connecting several neural systems into a Brainet by combining neural signals from multiple rats dynamically and in real-time so as to enhance motor performance. EMG or spinal neural activity can be recorded from the chronically implanted epidural electrodes and analyzed in real time to be delivered to the spinal cord of all rats connected in the setup. It is our hope that the features and usability of this system will encourage researchers to capitalize on the exciting possibilities inherent in closed-loop devices for ES neuromodulation studies.

AUTHOR CONTRIBUTIONS

AR built the proposed technology, performed the experiments, collected data, generated figures, and wrote the manuscript. PS collected data, performed all animal training experiments, analyzed and interpreted the data, generated figures, and edited the manuscript. PKS built the proposed technology, designed the experiments, performed the surgeries, performed experiments, interpreted the data, and wrote the manuscript. All authors read, edited, and approved the final draft of the manuscript.

FUNDING

This work was supported by the Craig Neilsen Grant 338237 granted to PKS. PKS was also supported by a grant from the New York State Spinal Cord Injury Institutional Grant # DOH01-C30839GG-3450000.

ACKNOWLEDGMENTS

We extend our sincere thanks to ADInstruments for their help with technical expertise and advice.

REFERENCES

Alam, M., Garcia-Alias, G., Jin, B., Keyes, J., Zhong, H., Roy, R. R., et al. (2017). Electrical neuromodulation of the cervical spinal cord facilitates forelimb skilled function recovery in spinal cord injured rats. *Exp. Neurol.* 291, 141–150. doi: 10.1016/j.expneurol.2017.02.006

Alam, M., Garcia-Alias, G., Shah, P. K., Gerasimenko, Y., Zhong, H., Roy, R. R., et al. (2015). Evaluation of optimal electrode configurations for epidural spinal cord stimulation in cervical spinal cord injured rats. *J. Neurosci. Methods* 247, 50–57. doi: 10.1016/j.jneumeth.2015.03.012

Angeli, C. A., Edgerton, V. R., Gerasimenko, Y. P., and Harkema, S. J. (2014). Altering spinal cord excitability enables voluntary movements after chronic complete paralysis in humans. *Brain* 137(Pt 5), 1394–1409. doi: 10.1093/brain/awu038

Ballermann, M., and Fouad, K. (2006). Spontaneous locomotor recovery in spinal cord injured rats is accompanied by anatomical plasticity of reticulospinal fibers. *Eur. J. Neurosci.* 23, 1988–1996. doi: 10.1111/j.1460-9568.2006.04726.x

Buick, A. R., Kowalczewski, J., Carson, R. G., and Prochazka, A. (2016). Tele-supervised fes-assisted exercise for hemiplegic upper limb. *IEEE Trans. Neural. Syst. Rehabil. Eng.* 24, 79–87. doi: 10.1109/TNSRE.2015.2408453

Capogrosso, M., Wenger, N., Raspopovic, S., Musienko, P., Beauparlant, J., Bassi Luciani, L., et al. (2013). A computational model for epidural electrical stimulation of spinal sensorimotor circuits. *J. Neurosci.* 33, 19326–19340. doi: 10.1523/JNEUROSCI.1688-13.2013

Carhart, M. R., He, J., Herman, R., D'Luzansky, S., and Willis, W. T. (2004). Epidural spinal-cord stimulation facilitates recovery of functional walking following incomplete spinal-cord injury. *IEEE Trans. Neural. Syst. Rehabil. Eng.* 12, 32–42. doi: 10.1109/TNSRE.2003.822763

Courtine, G., Gerasimenko, Y., van den Brand, R., Yew, A., Musienko, P., Zhong, H., et al. (2009). Transformation of nonfunctional spinal circuits into functional states after the loss of brain input. *Nat. Neurosci.* 12, 1333–1342. doi: 10.1038/nn.2401

DiMarco, A. F., Kowalski, K. E., Geertman, R. T., Hromyak, D. R., Frost, F. S., Creasey, G. H., et al. (2009). Lower thoracic spinal cord stimulation to restore

cough in patients with spinal cord injury: results of a National Institutes of Health-Sponsored clinical trial. Part II: clinical outcomes. *Arch. Phys. Med. Rehabil.* 90, 726–732. doi: 10.1016/j.apmr.2008.11.014

DiMarco, A. F., Kowalski, K. E., Hromyak, D. R., and Geertman, R. T. (2014). Long-term follow-up of spinal cord stimulation to restore cough in subjects with spinal cord injury. *J. Spinal Cord Med.* 37, 380–388. doi: 10.1179/2045772313Y.0000000152

Edgerton, V. R., Courtine, G., Gerasimenko, Y. P., Lavrov, I., Ichiyama, R. M., Fong, A. J., et al. (2008). Training locomotor networks. *Brain Res. Rev.* 57, 241–254. doi: 10.1016/j.brainresrev.2007.09.002

Ethier, C., and Miller, L. E. (2015). Brain-controlled muscle stimulation for the restoration of motor function. *Neurobiol. Dis.* 83, 180–190. doi: 10.1016/j.nbd.2014.10.014

Filli, L., Zorner, B., Weinmann, O., and Schwab, M. E. (2011). Motor deficits and recovery in rats with unilateral spinal cord hemisection mimic the Brown-Sequard syndrome. *Brain* 134(Pt 8), 2261–2273. doi: 10.1093/brain/awr167

Fitzsimmons, N. A., Drake, W., Hanson, T. L., Lebedev, M. A., and Nicolelis, M. A. (2007). Primate reaching cued by multichannel spatiotemporal cortical microstimulation. *J. Neurosci.* 27, 5593–5602. doi: 10.1523/JNEUROSCI.5297-06.2007

Fouad, K., Pedersen, V., Schwab, M. E., and Brosamle, C. (2001). Cervical sprouting of corticospinal fibers after thoracic spinal cord injury accompanies shifts in evoked motor responses. *Curr. Biol.* 11, 1766–1770. doi: 10.1016/S0960-9822(01)00535-8

Fountas, K. N., Smith, J. R., Murro, A. M., Politsky, J., Park, Y. D., and Jenkins, P. D. (2005). Implantation of a closed-loop stimulation in the management of medically refractory focal epilepsy: a technical note. *Stereotact. Funct. Neurosurg.* 83, 153–158. doi: 10.1159/000088656

Fuentes, R., Petersson, P., Siesser, W. B., Caron, M. G., and Nicolelis, M. A. (2009). Spinal cord stimulation restores locomotion in animal models of Parkinson's disease. *Science* 323, 1578–1582. doi: 10.1126/science.1164901

Gad, P., Choe, J., Shah, P., Garcia-Alias, G., Rath, M., Gerasimenko, Y., et al. (2013). Sub-threshold spinal cord stimulation facilitates spontaneous motor activity in spinal rats. *J. Neuroeng. Rehabil.* 10:108. doi: 10.1186/1743-0003-10-108

Gad, P., Woodbridge, J., Lavrov, I., Zhong, H., Roy, R. R., Sarrafzadeh, M., et al. (2012). Forelimb EMG-based trigger to control an electronic spinal bridge to enable hindlimb stepping after a complete spinal cord lesion in rats. *J. Neuroeng. Rehabil.* 9:38. doi: 10.1186/1743-0003-9-38

Gensel, J. C., Tovar, C. A., Hamers, F. P., Deibert, R. J., Beattie, M. S., and Bresnahan, J. C. (2006). Behavioral and histological characterization of unilateral cervical spinal cord contusion injury in rats. *J. Neurotrauma* 23, 36–54. doi: 10.1089/neu.2006.23.36

Gerasimenko, Y., Gorodnichev, R., Puhov, A., Moshonkina, T., Savochin, A., Selionov, V., et al. (2015). Initiation and modulation of locomotor circuitry output with multisite transcutaneous electrical stimulation of the spinal cord in noninjured humans. *J. Neurophysiol.* 113, 834–842. doi: 10.1152/jn.00609.2014

Gerasimenko, Y., Roy, R. R., and Edgerton, V. R. (2008). Epidural stimulation: comparison of the spinal circuits that generate and control locomotion in rats, cats and humans. *Exp. Neurol.* 209, 417–425. doi: 10.1016/j.expneurol.2007.07.015

Grahn, P. J., Lavrov, I. A., Sayenko, D. G., Van Straaten, M. G., Gill, M. L., Strommen, J. A., et al. (2017). Enabling task-specific volitional motor functions via spinal cord neuromodulation in a human with paraplegia. *Mayo Clin. Proc.* 92, 544–554. doi: 10.1016/j.mayocp.2017.02.014

Grillner, S., and Zangger, P. (1979). On the central generation of locomotion in the low spinal cat. *Exp. Brain Res.* 34, 241–261. doi: 10.1007/BF00235671

Harkema, S., Gerasimenko, Y., Hodes, J., Burdick, J., Angeli, C., Chen, Y., et al. (2011). Effect of epidural stimulation of the lumbosacral spinal cord on voluntary movement, standing, and assisted stepping after motor complete paraplegia: a case study. *Lancet* 377, 1938–1947. doi: 10.1016/S0140-6736(11)60547-3

Hebb, D. (1949). *The Organization of Behavior: The Neuropsychological Theory*. Hoboken, NJ: Wiley, 334.

Hurd, C., Weishaupt, N., and Fouad, K. (2013). Anatomical correlates of recovery in single pellet reaching in spinal cord injured rats. *Exp. Neurol.* 247, 605–614. doi: 10.1016/j.expneurol.2013.02.013

Jackson, A., Mavoori, J., and Fetz, E. E. (2006a). Long-term motor cortex plasticity induced by an electronic neural implant. *Nature* 444, 56–60. doi: 10.1038/nature05226

Jackson, A., Moritz, C. T., Mavoori, J., Lucas, T. H., and Fetz, E. E. (2006b). The neurochip bci: towards a neural prosthesis for upper limb function. *IEEE Trans. Neural. Syst. Rehabil. Eng.* 14, 187–190. doi: 10.1109/TNSRE.2006.875547

Krook-Magnuson, E., Gelinas, J. N., Soltesz, I., and Buzsaki, G. (2015). Neuroelectronics and biooptics: closed-loop technologies in neurological disorders. *JAMA Neurol.* 72, 823–829. doi: 10.1001/jamaneurol.2015.0608

Little, S., Pogosyan, A., Neal, S., Zavala, B., Zrinzo, L., and Hariz, M. (2013). Adaptive deep brain stimulation in advanced Parkinson disease. *Ann. Neurol.* 74, 449–457. doi: 10.1002/ana.23951

Lu, D. C., Edgerton, V. R., Modaber, M., AuYong, N., Morikawa, E., Zdunowski, S., et al. (2016). Engaging cervical spinal cord networks to reenable volitional control of hand function in tetraplegic patients. *Neurorehabil. Neural Repair* 30, 951–962. doi: 10.1177/1545968316644344

McPherson, J. G., Miller, R. R., and Perlmutter, S. I. (2015). Targeted, activity-dependent spinal stimulation produces long-lasting motor recovery in chronic cervical spinal cord injury. *Proc. Natl. Acad. Sci. U.S.A.* 112, 12193–12198. doi: 10.1073/pnas.1505383112

Mercier, L. M., Gonzalez-Rothi, E. J., Streeter, K. A., Posgai, S. S., Poirier, A. S., Fuller, D. D., et al. (2016). Intraspinal microstimulation and diaphragm activation following cervical spinal cord injury. *J. Neurophysiol.* 117, 767–776. doi: 10.1152/jn.00721.2016

Metz, G. A., and Whishaw, I. Q. (2009). The ladder rung walking task: a scoring system and its practical application. *J. Vis. Exp.* 12:1204. doi: 10.3791/1204

Minassian, K., McKay, W. B., Binder, H., and Hofstoetter, U. S. (2016). Targeting lumbar spinal neural circuitry by epidural stimulation to restore motor function after spinal cord injury. *Neurotherapeutics* 13, 284–294. doi: 10.1007/s13311-016-0421-y

Mondello, S. E., Kasten, M. R., Horner, P. J., and Moritz, C. T. (2014). Therapeutic intraspinal stimulation to generate activity and promote long-term recovery. *Front. Neurosci.* 8:21. doi: 10.3389/fnins.2014.00021

National-Research-Council (2011). *Guide for the Care and Use of Laboratory Animals*. Wahington, DC: The National Academies Press, 220.

Newitt, R., Barnett, F., and Crowe, M. (2016). Understanding factors that influence participation in physical activity among people with a neuromusculoskeletal condition: a review of qualitative studies. *Disabil. Rehabil.* 38, 1–10. doi: 10.3109/09638288.2014.996676

Osorio, I., Frei, M. G., Manly, B. F., Sunderam, S., Bhavaraju, N. C., and Wilkinson, S. B. (2001). An introduction to contingent (closed-loop) brain electrical stimulation for seizure blockage, to ultra-short-term clinical trials, and to multidimensional statistical analysis of therapeutic efficacy. *J. Clin. Neurophysiol.* 18, 533–544. doi: 10.1097/00004691-200111000-00003

Pais-Vieira, M., Chiuffa, G., Lebedev, M., Yadav, A., and Nicolelis, M. A. (2015). Building an organic computing device with multiple interconnected brains. *Sci. Rep.* 5:11869. doi: 10.1038/srep11869

Ramakrishnan, A., Ifft, P. J., Pais-Vieira, M., Byun, Y. W., Zhuang, K. Z., Lebedev, M. A., et al. (2015). Computing arm movements with a monkey brainet. *Sci. Rep.* 5:10767. doi: 10.1038/srep10767

Rejc, E., Angeli, C., and Harkema, S. (2015). Effects of lumbosacral spinal cord epidural stimulation for standing after chronic complete paralysis in humans. *PLoS One* 10:e0133998. doi: 10.1371/journal.pone.0133998

Rejc, E., Angeli, C. A., Atkinson, D., and Harkema, S. J. (2017). Motor recovery after activity-based training with spinal cord epidural stimulation in a chronic motor complete paraplegic. *Sci. Rep.* 7:13476. doi: 10.1038/s41598-017-14003-w

Rolston, J. D., Gross, R. E., and Potter, S. M. (2009). A low-cost multielectrode system for data acquisition enabling real-time closed-loop processing with rapid recovery from stimulation artifacts. *Front. Neuroeng.* 2:12. doi: 10.3389/neuro.16.012.2009

Roy, R. R., Hutchison, D. L., Pierotti, D. J., Hodgson, J. A., and Edgerton, V. R. (1991). EMG patterns of rat ankle extensors and flexors during treadmill locomotion and swimming. *J. Appl. Physiol.* 70, 2522–2529. doi: 10.1152/jappl.1991.70.6.2522

Sayenko, D. G., Atkinson, D. A., Floyd, T. C., Gorodnichev, R. M., Moshonkina, T. R., Harkema, S. J., et al. (2015). Effects of paired transcutaneous electrical stimulation delivered at single and dual sites over lumbosacral spinal cord. *Neurosci. Lett.* 609, 229–234. doi: 10.1016/j.neulet.2015.10.005

Shah, P., Sureddi, S., Alam, M., Zhong, H., Roy, R. R., Edgerton, V. R., et al. (2016). Unique spatiotemporal neuromodulation of the lumbosacral circuitry shapes locomotor success after spinal cord injury. *J. Neurotrauma* 33, 1709–1723. doi: 10.1089/neu.2015.4256

Shah, P. K., Garcia-Alias, G., Choe, J., Gad, P., Gerasimenko, Y., Tillakaratne, N., et al. (2013). Use of quadrupedal step training to re-engage spinal interneuronal networks and improve locomotor function after spinal cord injury. *Brain* 136(Pt 11), 3362–3377. doi: 10.1093/brain/awt265

Shah, P. K., and Gerasimenko, Y. (2016). Multi-site spinal stimulation strategies to enhance locomotion after paralysis. *Neural Regen. Res.* 11, 1926–1927. doi: 10.4103/1673-5374.197131

Shah, P. K., Gerasimenko, Y., Shyu, A., Lavrov, I., Zhong, H., Roy, R. R., et al. (2012). Variability in step training enhances locomotor recovery after a spinal cord injury. *Eur. J. Neurosci.* 36, 2054–2062. doi: 10.1111/j.1460-9568.2012.08106.x

Shah, P. K., and Lavrov, I. (2017). Spinal epidural stimulation strategies. *Neuroscientist*. doi: 10.1177/1073858417699554 [Epub ahead of print].

Sun, F. T., and Morrell, M. J. (2014). Closed-loop neurostimulation: the clinical experience. *Neurotherapeutics* 11, 553–563. doi: 10.1007/s13311-014-0280-3

Sunshine, M. D., Cho, F. S., Lockwood, D. R., Fechko, A. S., Kasten, M. R., and Moritz, C. T. (2013). Cervical intraspinal microstimulation evokes robust forelimb movements before and after injury. *J. Neural Eng.* 10:036001. doi: 10.1088/1741-2560/10/3/036001

Taccola, G., Sayenko, D., Gad, P., Gerasimenko, Y., and Edgerton, V. R. (2017). And yet it moves: recovery of volitional control after spinal cord injury. *Prog. Neurobiol.* 160, 64–81. doi: 10.1016/j.pneurobio.2017.10.004

Venkatraman, S., Elkabany, K., Long, J., Yao, Y., and Carmena, J. (2009). A System for neuronal recording and closed loop intracortical microstimulation in awake rodents. *IEEE Trans. Biomed. Eng.* 56, 15–22. doi: 10.1109/TBME.2008.2005944

Wenger, N., Moraud, E. M., Raspopovic, S., Bonizzato, M., DiGiovanna, J., Musienko, P., et al. (2014). Closed-loop neuromodulation of spinal sensorimotor circuits controls refined locomotion after complete spinal cord injury. *Sci. Transl. Med.* 6:255ra133. doi: 10.1126/scitranslmed.3008325

Zanos, S., Richardson, A. G., Shupe, L., Miles, F. P., and Fetz, E. E. (2011). The Neurochip-2: an autonomous head-fixed computer for recording and stimulating in freely behaving monkeys. *IEEE Trans. Neural Syst. Rehabil. Eng.* 19, 427–435. doi: 10.1109/TNSRE.2011.2158007

Zareen, N., Shinozaki, M., Ryan, D., Alexander, H., Amer, A., Truong, D. Q., et al. (2017). Motor cortex and spinal cord neuromodulation promote corticospinal tract axonal outgrowth and motor recovery after cervical contusion spinal cord injury. *Exp. Neurol.* 297, 179–189. doi: 10.1016/j.expneurol.2017.08.004

Zbogar, D., Eng, J. J., Miller, W. C., Krassioukov, A. V., and Verrier, M. C. (2016). Physical activity outside of structured therapy during inpatient spinal cord injury rehabilitation. *J. Neuroeng. Rehabil.* 13:99. doi: 10.1186/s12984-016-0208-8

Zemmar, A., Kast, B., Lussi, K., Luft, A. R., and Schwab, M. E. (2015). Acquisition of a high-precision skilled forelimb reaching task in rats. *J. Vis. Exp.* 22:e53010. doi: 10.3791/53010

Zimmermann, J. B., and Jackson, A. (2014). Closed-loop control of spinal cord stimulation to restore hand function after paralysis. *Front. Neurosci.* 8:87. doi: 10.3389/fnins.2014.00087

Conflict of Interest Statement: The authors declare that the research was conducted in the absence of any commercial or financial relationships that could be construed as a potential conflict of interest.

frontiers in Neuroscience

ORIGINAL RESEARCH
published: 22 November 2018
doi: 10.3389/fnins.2018.00858

Simulation Study of Intermittent Axonal Block and Desynchronization Effect Induced by High-Frequency Stimulation of Electrical Pulses

Zheshan Guo[1], Zhouyan Feng[1], Yang Wang[1] and Xuefeng Wei[2]*

[1] Key Lab of Biomedical Engineering for Ministry of Education, College of Biomedical Engineering and Instrument Science, Zhejiang University, Hangzhou, China, [2] Department of Biomedical Engineering, The College of New Jersey, Ewing, NJ, United States

OPEN ACCESS

Edited by:
Mikhail Lebedev,
Duke University, United States

Reviewed by:
Constance Hammond,
Institut National de la Santé et de la Recherche Médicale (INSERM), France
Tatiana Kameneva,
Swinburne University of Technology, Australia

****Correspondence:***
Zhouyan Feng
fengzhouyan@139.com

Specialty section:
This article was submitted to Neural Technology, a section of the journal Frontiers in Neuroscience

Received: *04 May 2018*
Accepted: *02 November 2018*
Published: *22 November 2018*

Citation:
Guo Z, Feng Z, Wang Y and Wei X (2018) Simulation Study of Intermittent Axonal Block and Desynchronization Effect Induced by High-Frequency Stimulation of Electrical Pulses. Front. Neurosci. 12:858. doi: 10.3389/fnins.2018.00858

Deep brain stimulation (DBS) has been successfully used in treating neural disorders in brain, such as Parkinson's disease and epilepsy. However, the precise mechanisms of DBS remain unclear. Regular DBS therapy utilizes high-frequency stimulation (HFS) of electrical pulses. Among all of neuronal elements, axons are mostly inclined to be activated by electrical pulses. Therefore, the response of axons may play an important role in DBS treatment. To study the axonal responses during HFS, we developed a computational model of myelinated axon to simulate sequences of action potentials generated in single and multiple axons (an axon bundle) by stimulations. The stimulations are applied extracellularly by a point source of current pulses with a frequency of 50–200 Hz. Additionally, our model takes into account the accumulation of potassium ions in the peri-axonal spaces. Results show that the increase of extracellular potassium generates intermittent depolarization block in the axons during HFS. Under the state of alternate block and recovery, axons fire action potentials at a rate far lower than the frequency of stimulation pulses. In addition, the degree of axonal block is highly related to the distance between the axons and the stimulation point. The differences in the degree of block for individual axons in a bundle result in desynchronized firing among the axons. Stimulations with higher frequency and/or greater intensity can induce axonal block faster and increase the desynchronization effect on axonal firing. Presumably, the desynchronized axonal activity induced by HFS could generate asynchronous activity in the population of target neurons downstream thereby suppressing over-synchronized firing of neurons in pathological conditions. The desynchronization effect generated by intermittent activation of axons may be crucial for DBS therapy. The present study provides new insights into the mechanisms of DBS, which is significant for advancing the application of DBS.

Keywords: high-frequency stimulation, potassium accumulation, axonal block, desynchronization, model of myelinated axon

INTRODUCTION

Deep brain stimulation (DBS) is an effective clinical treatment for diseases of motor nervous system, such as Parkinson's disease, essential tremors, and dystonia (Mehanna and Lai, 2013; Cury et al., 2017). It also exhibits potentials in treating epilepsy and other mental illness such as depression and obsession (Bergey, 2013; Blomstedt et al., 2013; Narang et al., 2016). However, the precise mechanisms of DBS action are still under debate.

Normally, DBS therapy is performed with continuous stimulation of electrical pulses. The efficacy of DBS is strongly related to the frequency of pulses, which is adjusted for optimal outcome of individual patient. The frequency range of effective stimulation in clinic is 90–200 Hz (commonly around 130 Hz), hence the stimulation is called high-frequency stimulation (HFS) (Birdno and Grill, 2008; Eusebio et al., 2011; Zhong et al., 2011; McConnell et al., 2012).

Both HFS and lesion therapy are found to produce similar effects on the relief of symptoms, thus HFS is originally assumed to inhibit the neuronal activity of stimulated areas in brain (Boraud et al., 1996; Anderson, 2006). For example, HFS activates axon terminals connecting inhibitory synapses, thus enhances the release of inhibitory neurotransmitters thereby inhibiting the activity of postsynaptic neurons (Johnson and McIntyre, 2008; Deniau et al., 2010; Chiken and Nambu, 2013). However, some research showed a contrary effect that HFS could facilitate the action potential firing of target neurons (Reese et al., 2011; Cleary et al., 2013). A recent hypothesis claims that desynchronization is more noteworthy than excitability change (Medeiros Dde and Moraes, 2014). Since over-synchronized activity of neurons is a pathological feature for many brain disorders such as Parkinson's disease and epilepsy (Hammond et al., 2007; Jiruska et al., 2013), the role of HFS might be to decrease the synchronization among neurons (Deniau et al., 2010; Medeiros Dde and Moraes, 2014; Feng et al., 2017). However, it is not clear how HFS generates desynchronization.

Electrical pulses delivered from stimulating electrode are applied simultaneously on different elements of surrounding neurons, among which axon membrane is most inclined to be activated. Action potential may initiate at axon, even if soma locates closer to the stimulating electrode (Ranck, 1975; Nowak and Bullier, 1998; McIntyre and Grill, 1999). Therefore, the response of axon may play an important role in the action of DBS (Chomiak and Hu, 2007; Udupa and Chen, 2015). Some research showed that continuous HFS could generate depolarization block on axons, making axons fail to fire an action potential following every stimulating pulse (Jensen and Durand, 2009; Zheng et al., 2011; Feng et al., 2013, 2014). This depolarization block of axons may be an important mechanism underlying the desynchronization effect of HFS.

Previous studies suggest that accumulation of K^+ in peri-axonal sub-myelin space during HFS contributes to the depolarization block of axons (Bellinger et al., 2008; Zheng et al., 2011). We hypothesize here that the depolarization block could be intermittent because of the fluctuation of sub-myelin K^+ concentration during HFS thereby causing the axons to fire action potentials at a rate far lower than the frequency of stimulation pulses. Under this situation, the axonal firing generated within an axon bundle would be asynchronous thereby desynchronizing neuronal activity in the downstream projecting area.

To verify this hypothesis, we developed a computational model to simulate thin myelinated axons in brain and to study the effects of HFS on single and multiple axons (an axon bundle). Since current techniques of *in vivo* experiments do not allow intracellular recordings of multiple thin axons simultaneously to trace their reactions, this modeling study is significant for unraveling the desynchronization mechanism of axonal role in DBS.

MATERIALS AND METHODS

To investigate the responses of axons to HFS, we utilized a computational model of thin myelinated axon in the central nervous system using NEURON v7.4. The axonal model was modified from a previous model (Bellinger et al., 2008). Bellinger's model was adapted from motor nerve fibers (McIntyre and Grill, 2002; McIntyre et al., 2004). To simulate more closely the responses of brain neurons to HFS, we replaced the kinetic equations of ionic channels with those from axons of pyramidal neurons of brain (Bianchi et al., 2012) and altered other parameters such as axonal diameters, lengths of internode parts, and number of myelin lamella accordingly. Details of the model are described below, including the structures and parameter settings, the accumulation of extracellular K^+, the administration of stimulation by a point source of current pulses extracellularly, as well as signal recording and analyzing.

Morphological Parameters of the Axon Model

The myelinated axon consists of 21 nodes of Ranvier (abbreviated as Node) and 20 internode parts (**Figure 1**). The outer diameter of the myelin sheath is set to 1 μm to simulate the thin axons of brain neurons (Wang et al., 2008). Thus, the internode length is set to 100 μm according to the ratio of axon diameter to internode length of 1:100 (Frijns et al., 1994). In this case, the total length of the axon is ∼2 mm. Additionally, according to the linear relationship between the thickness of myelin sheath and axon diameter (Schröder, 1972), the number of myelin lamellae is set to 15 layers. The morphological parameters of different parts of the axon model are listed in **Table 1**.

As shown in **Figure 1**, inside the myelin sheath, each internode part is divided into two halves, each with three sections: a paranodal junction (PNJ), a juxtaparanode (JXP), and ½ internode (IND), from either side to the middle (Bellinger et al., 2008; Rasband and Peles, 2016). Therefore, each internode part contains two PNJ, two JXP, and one IND. These sections differ in both length and diameter. Particularly, IND is far longer than PNJ and JXP. "Peri-axonal space" refers to the space between axon membrane and surrounding myelin sheath, and its width changes along the internode parts (see **Table 1**).

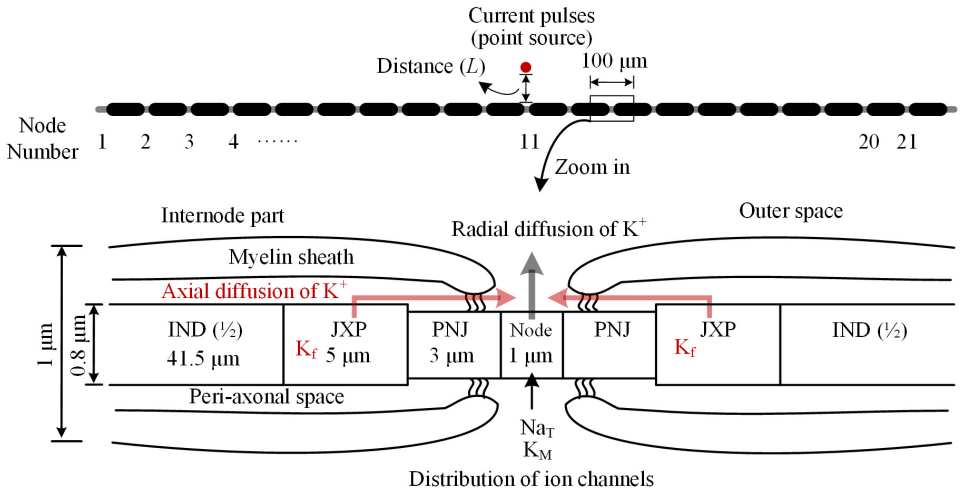

FIGURE 1 | Schematic diagram of the model for thin myelinated axon, including structures, dimensions, and distributions of ionic channels. *Top*: Overview of the entire axon with 21 nodes of Ranvier (Node) and 20 internode parts. *Bottom*: Magnified view of a nodal region with the three sections surrounding each node: paranodal junction (PNJ), juxtaparanodes (JXP), and internode (IND). Axial and radial diffusion of K^+ are shown by pink and gray arrow-lines, respectively.

TABLE 1 | Morphological parameters of the axon model.

Parameter	Value	Unit
Outer diameter of axon	1	µm
Internode length	100	µm
Total axon length	2	mm
Node diameter	0.7	µm
Node length	1	µm
PNJ diameter	0.7	µm
PNJ length	3	µm
JXP diameter	0.8	µm
JXP length	5	µm
IND diameter	0.8	µm
IND length	83	µm
PNJ peri-axonal space width	1.8	nm
JXP peri-axonal space width	8	nm
IND peri-axonal space width	8	nm
Number of myelin lamella	15	

TABLE 2 | Electrical parameters of the axon model.

Parameter	Value	Unit
Axoplasmic resistivity (ρ_a)	70	Ω·cm
Capacitance of the axon membrane (c_m)	1	µF/cm^2
Leakage conductance (g_{Lk})	0.0001	S/cm^2
Leakage reversal potential (E_{Lk})	−66	mV
Capacitance of the myelin (c_{my})	0.1	µF/cm^2
Conductance of the myelin (g_{my})	0.001	S/cm^2
Resting potential	−66	mV
Potassium reversal potential (initial value)	−95	mV
Sodium reversal potential	45	mV
Max. conductance of transient Na^+ (Na_T) on Node	2	S/cm^2
Max. conductance of M-type K^+ (K_m) on Node	0.003	S/cm^2
Max. conductance of fast K^+ (K_f) on JXP	0.03	S/cm^2

TABLE 3 | Parameters for modeling dynamics of K^+ concentration.

Parameter	Value	Unit
Intracellular K^+ concentration	106	mM
Extracellular K^+ concentration (initial value)	3	mM
Intracellular Na^+ concentration	10	mM
Diffusion coefficient (*D*)	1.85	µm^2/ms
Axial area of diffusion zone at IND	0.02	µm^2
Axial area of diffusion zone at JXP	0.02	µm^2
Axial area of diffusion zone at PNJ	0.004	µm^2
Radial area of diffusion zone at Node	2.2	µm^2
Max. current of NaK pump (I_{NaKmax})	2.46	µA/cm^2
K^+ equilibrium binding constant (KmK)	5.3	mM
Na^+ equilibrium binding constant (KmNa)	27.9	mM

Electrical Parameters of the Axon Model

The axon contains both passive and active electrical features (**Table 2**). The parameters of passive features include: resistivity for the axoplasm (ρ_a); capacitance (c_m), leakage conductance (g_{Lk}), and leakage reversal potential (E_{Lk}) for the axon membrane; capacitance (c_{my}) and conductance (g_{my}) for the myelin. Resting potential of the axon membrane is set to −66 mV (Staff et al., 2000). The sodium (Na^+) reversal potential is set to a fixed value 45 mV (Bianchi et al., 2012), whereas the potassium (K^+) reversal potential varies with the changes of extracellular K^+ concentration during HFS. The initial value of K^+ reversal potential is −95 mV calculated by Nernst equation based on the initial K^+ concentrations inside and outside the axon membrane (**Table 3**).

The parameters of active features include the values of maximum conductance for three types of voltage-gated ionic channels: transient Na^+ channel (Na_T) and M-type K^+ channel

(K_M) distributed on Node membrane; fast K^+ channel (K_f) distributed on JXP membrane (**Table 2** and **Figure 1**).

At node membrane, the Na_T channels mainly correspond to an integration of sodium channel isoforms of Nav1.1 and Nav1.6 (Caldwell et al., 2000; Duflocq et al., 2008). The kinetic equation of Na_T channels is adopted from literature (Bianchi et al., 2012), which was modified from the work with experimental results (Migliore et al., 1999). The maximum conductance of Na_T is set to 2 S/cm^2 according to the range of maximum Na^+ conductance 1.3 ∼ 2.6 S/cm^2, i.e., 1000 ∼ 2000 channels/μm^2 and 13 pS/channel (Scholz et al., 1993; Waxman and Ritchie, 1993). The K_M channels represent KCNQ isoforms (Kv7.2/7.3) (Devaux, 2004; Schwarz et al., 2006). The kinetic equation and maximum conductance of K_M are adopted from literature (Bianchi et al., 2012). At JXP membrane, the K_f channel has been commonly used in computation modeling (Schwarz et al., 1995; McIntyre et al., 2004; Bellinger et al., 2008) to represent the ionic current of potassium corresponding to an integration of Kv isoforms such as Kv1.1 and Kv1.2 (Wang et al., 1993; Rasband and Trimmer, 2001; Rasband and Peles, 2016). The kinetic equation of K_f is adopted from previous models (McIntyre et al., 2004), and its maximum conductance is set to 0.03 S/cm^2 (Bellinger et al., 2008). The three types of voltage-gated channels are dominant for generation and conduction of action potentials in myelinated brain axons (Rasband and Peles, 2016; Nelson and Jenkins, 2017).

Change of K^+ Concentrations in the Peri-Axonal Space

Our axon model also takes into account NaK pumps and K^+ diffusion as previous report (Bellinger et al., 2008). The concentration of K^+ inside the axon membrane is set to constant 106 mM, and K^+ concentration outside of the axon membrane ($[K^+]_o$) is initially set to 3 mM (**Table 3**). The K^+ inside the membrane can only outflow through the K^+ channels on the Node and JXP membranes. The outflowing K^+ on the Node diffuses to the outer space radially. The outflowing K^+ on the JXP can first flow into the peri-axon space, then diffuse axially to the outside of the Node and finally diffuse into outer space radially (**Figure 1**).

Both axial and radial diffusions of K^+ follow the Fick's law:

$$J = D \times A \times \left(\frac{\mathrm{d}[K^+]_o}{\mathrm{d}x}\right) \quad (1)$$

where J is the diffusion flux; D is the diffusion coefficient 1.85 μm^2/ms; A is the cross section area of the diffusion zone; $[K^+]_o$ is extracellular K^+ concentration; x is the diffusion distance. Based on the data in **Table 1**, the axial area of the peri-axon space outside IND, JXP, and PNJ are 0.02, 0.02, and 0.004 μm^2, respectively; the radial area of Node surface is 2.2 μm^2, much larger than the axial area of peri-axon space (**Table 3**).

$[K^+]_o$ is also regulated by NaK pump, which pumps out three Na^+ and pumps in two K^+ per ATP hydrolyzed. Assuming the NaK pumps are distributed evenly on the entire axon membrane, the ionic current (I_{NaK}) of NaK pump per unit area is (Bellinger et al., 2008):

$$I_{NaK} = I_{NaKmax}\left(\frac{[K^+]_o}{[K^+]_o + KmK}\right)\left(\frac{[Na^+]_i^{1.5}}{[Na^+]_i^{1.5} + KmNa^{1.5}}\right) \times \left(\frac{V+150}{V+200}\right) \quad (2)$$

where V is the membrane potential; $[Na^+]_i$ is intracellular Na^+ concentration; I_{NaKmax} is the maximum transport current per unit area; KmK and KmNa are the equilibrium binding constants of K^+ and Na^+, respectively (**Table 3**).

The parameter values of formulae (1) and (2) are listed in **Table 3**. The two formulae were used to simulate the dynamic changes of the K^+ concentrations outside axon membrane.

Extracellular Stimulation and Signal Recording

Electrical stimulation is a sequence of monophasic current pulses with pulse width of 0.1 ms, pulse intensity of −0.1 to −0.5 mA, pulse frequency of 50, 130, or 200 Hz, and stimulation duration of 1 min.

Extracellular point source of stimulation is located above the 11th node of Ranvier ($Node_{11}$), which is the center of axon (**Figure 1**). The extracellular potential (φ) at a specific part on the axon membrane generated by the stimulation point is:

$$\varphi = I/4\pi\sigma r \quad (3)$$

where σ is the extracellular conductivity, which is set to 0.286 S/m; I is the pulse intensity of stimulations; r is the distance between the stimulation point, and the specific part of the axon.

An effective action potential induced by stimulation is defined as one that can spread to both axon ends successfully. Because the action potentials induced at the central node ($Node_{11}$) can spread in both orthodromic and antidromic directions equally, the numbers of effective action potentials during stimulation periods are counted only at one end node ($Node_1$) to evaluate the axonal conduction. Also, the membrane potential of the central $Node_{11}$ together with the $[K^+]_o$ in the peri-axonal space of the neighboring JXP are recorded to investigate the relation between accumulated K^+ and HFS-induced action potentials.

Additionally, an index called "induction ratio" of axonal action potentials was used to evaluate the degree of intermittent depolarization block induced by the stimulations. The value of the index, represented as percentage, was defined as the reciprocal of the number of stimulation pulses in between two successive evoked action potentials. For example, if a second action potential is evoked following three successive pulses, that is, two of the pulses fail to induce effective action potential; then the induction ratio is 33%.

Evaluation of Action Potential Synchronization by Responses of an Axon Bundle to Stimulation

To study the integrate responses of multiple axons to HFS, 11 identical axons are spaced in parallel at an interval of

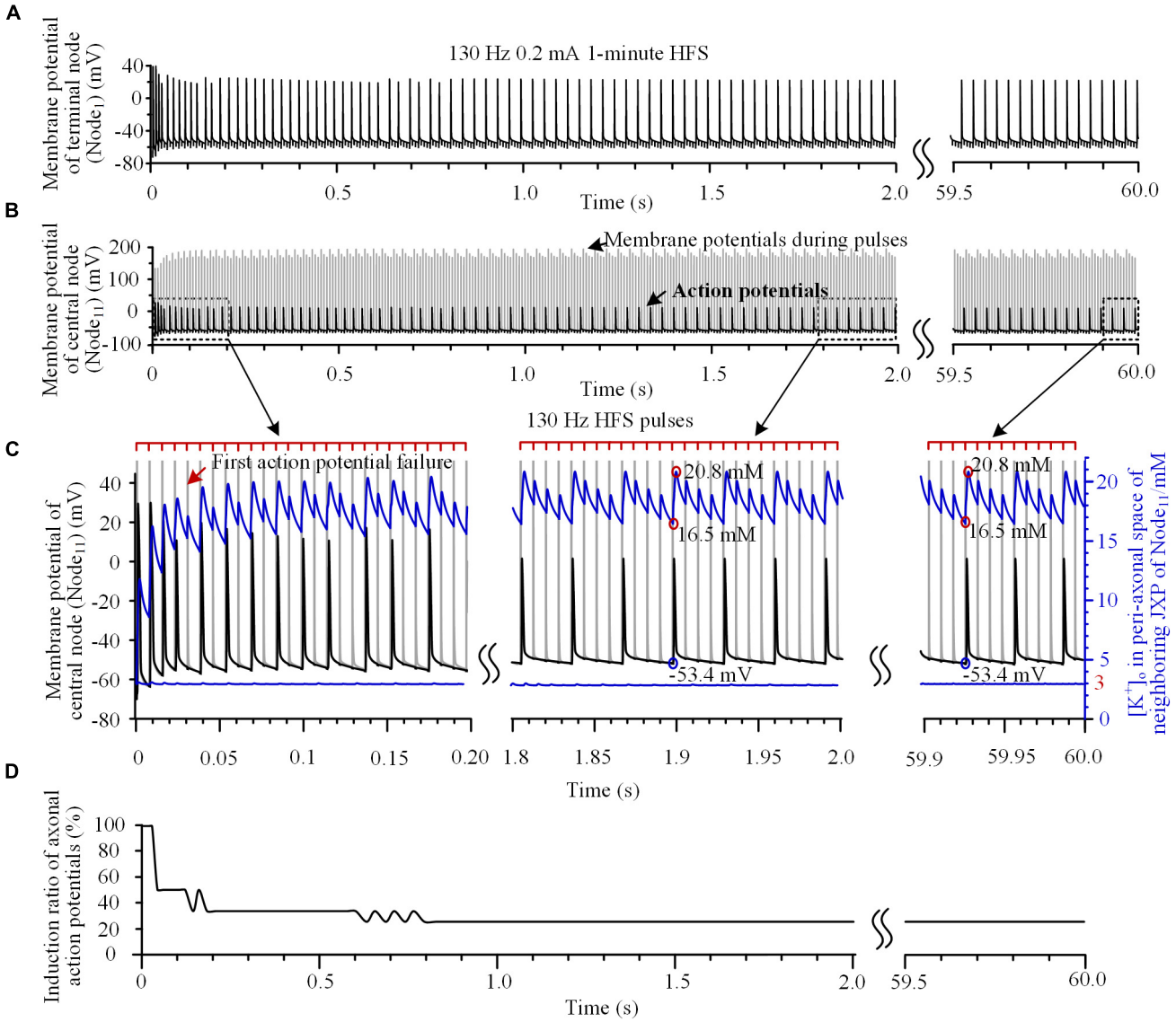

FIGURE 2 | Action potentials and $[K^+]_o$ induced by high-frequency stimulation (HFS). **(A,B)** Membrane potentials recorded simultaneously at the end node ($Node_1$) and the central node ($Node_{11}$) during a 1-min train of 130 Hz pulse stimulation with 0.2 mA intensity. For clarity, recordings in 2.0 ~ 59.5 s are omitted. **(C)** Magnified plots of membrane potentials at $Node_{11}$ (black curves), $[K^+]_o$ at $Node_{11}$ (blue curves below) and $[K^+]_o$ in the peri-axonal space of neighboring JXP (blue curves up) during the first 0.2 s, middle 1.8 ~ 2.0 s and last 0.1 s of the 1-min HFS. Cathodic monophasic pulses of extracellular HFS are represented by the tick marks on the red lines above. The gray curves in **(B,C)** represent changes of membrane potentials induced by pulses at $Node_{11}$. These large potentials are trimmed in the enlarged plots in **(C)**. **(D)** Change of induction ratio of axonal action potentials by pulses of HFS.

10 μm in a simplified model of axon bundle. The stimulation point is located at the same plane as the axons, above the axon center ($Node_{11}$) of the topmost axon with a distance of 20 μm. Thus, the distances (L) from the stimulation point to the central nodes ($Node_{11}$) of the 11 axons are in a range of 20–120 μm. Percentage ratio of effective action potentials in the 11 axons induced by each pulse is calculated, which is defined as "synchronization ratio." If all of the 11 axons are activated by a pulse synchronously, the synchronization ratio is 100%. The curve of synchronization ratio is smoothed by sliding average of every 10 data points.

RESULTS

$[K^+]_o$ Fluctuation Induces Intermittent Axonal Block

Our simulation results showed dynamics of the axonal responses to the pulses of HFS. For example, when a 130 Hz HFS was applied 50 μm above the central node ($Node_{11}$) of axon (**Figures 2A,B**), the initial four pulses could all induce action potentials, which propagated to the end of axon ($Node_1$) (**Figures 2A,C**). However, the fifth pulse only caused a change of

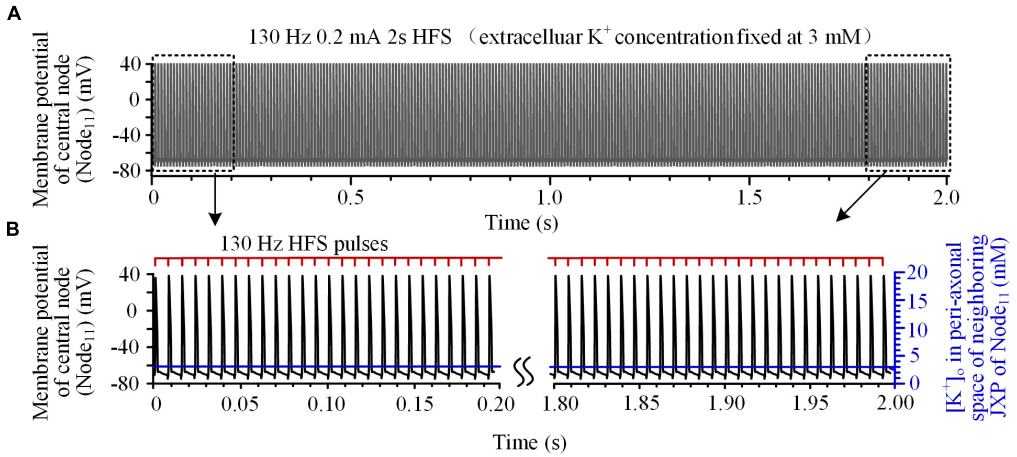

FIGURE 3 | Axonal responses during high-frequency stimulation (HFS) when the extracellular K^+ concentration was fixed at 3 mM: **(A)** Action potentials induced by 130 Hz pulses during 2-s HFS. **(B)** Membrane potential at $Node_{11}$ (black curves) and $[K^+]_o$ in the peri-axonal space of neighboring JXP (blue curves) during the first and last 0.2 s of the 2-s HFS shown in **(A)**. Every stimulation pulse induces an action potential.

potential on the $Node_{11}$ membrane during the pulse and did not induce an action potential following the pulse (see the red arrow in **Figure 2C**). During the HFS, the induction ratio of action potentials gradually decreased from 100% to a steady value of 25% after 1.5 s of stimulation and maintained to the end of 1-min stimulation (**Figure 2D**), indicating that only one of every four pulses induces an action potential, intermittently.

To test the hypothesis that the intermittent block of axon results from the fluctuation of sub-myelin $[K^+]_o$ during HFS, we monitored $[K^+]_o$ within the peri-axon space of JXP next to the central node ($Node_{11}$). During the initial four pulses of HFS, the $[K^+]_o$ increased rapidly from baseline 3 mM to over 14 mM (see the blue curve and right coordinate in **Figure 2C**). After the induction ratio of action potentials became stable (∼1.5 s after the onset of HFS), $[K^+]_o$ fluctuated with lower and upper limits of 16.5 and 20.8 mM, respectively. The outflow of K^+ during each action potential caused a large jump in $[K^+]_o$ between the two concentration limits (circled in red on the blue curve in **Figure 2C**). A pulse that did not induce an action potential also caused a small increase in $[K^+]_o$ due to an elevation of membrane potential. Because of the persistent effects of NaK pump and ion diffusion that remove K^+ from the peri-axon space, $[K^+]_o$ gradually decreased in a saw-toothed fashion in the intervals of action potentials and in the intervals of pulses. The changes of $[K^+]_o$ were also steady after ∼1.5 s of stimulation accompanying the stabilization of induction ratio of action potentials. Since the axonal activity changed from transient to steady state after ∼1.5 s of stimulation, we only provide the data of first 2-s stimulation in the subsequent results.

The increase of $[K^+]_o$ elevated the basic membrane potential of $Node_{11}$ from −66 mV up to above −53.4 mV. When the $[K^+]_o$ intermittently fell below 16.5 mM and the membrane potential fell below −53.4 mV, an action potential could be induced again (circled by blue on the black curve in **Figure 2C**). Nevertheless, the $[K^+]_o$ immediately outside $Node_{11}$ stayed at ∼3 mM during the entire HFS (**Figure 2C**, the blue line below). Therefore, the membrane depolarization caused by the increase of $[K^+]_o$ within the peri-axon space of JXP might be the reason why the axon failed to fire an action potential following each stimulation pulse.

To verify this hypothesis, the mechanism of K^+ accumulation outside the axon membrane was removed, i.e., the $[K^+]_o$ was fixed at 3 mM. Then, during the same 130 Hz stimulation, every pulse could induce an action potential at $Node_{11}$ (**Figures 3A,B**) that spread to the axon ends.

These results indicate that the fluctuation of $[K^+]_o$ induced by HFS causes intermittent block and intermittent recovery in axons, which results in a firing rate of axonal action potentials far lower than the pulse frequency of HFS. For multiple axons, their action potentials might be induced by different pulses thereby resulting in misalignment in time and asynchronous firing of action potentials. We next test the hypothesis by simulating the responses of multiple axons to HFS.

Asynchronous Firing of Multiple Axons Induced by High Frequency Stimulation

To investigate the integrated activity induced on multiple axons located at various distances from a stimulation point, we analyzed the responses of an axon bundle composed of 11 axons to HFS. Due to the different distances of axons to the stimulation point, the degree of axonal block was different for individual axons (**Figure 4A**). Axons closer to the stimulation point had lower induction ratios of effective action potentials. During a HFS train of 130 Hz with 0.2 mA intensity, after ∼1.5 s stimulation, the steady-state values of induction ratio were ∼14% for the axon with the shortest distance of 20 μm and ∼50% for the axon with the longest distance of 120 μm (**Figure 4B**).

The differences of block degrees would cause differences in firing time of the multiple axons responding to stimulation pulses thereby resulting in asynchronous firing of action potentials during HFS. For example, during the last seven pulses of HFS period (**Figure 4A** *right*), the first of the seven pulses (indicated

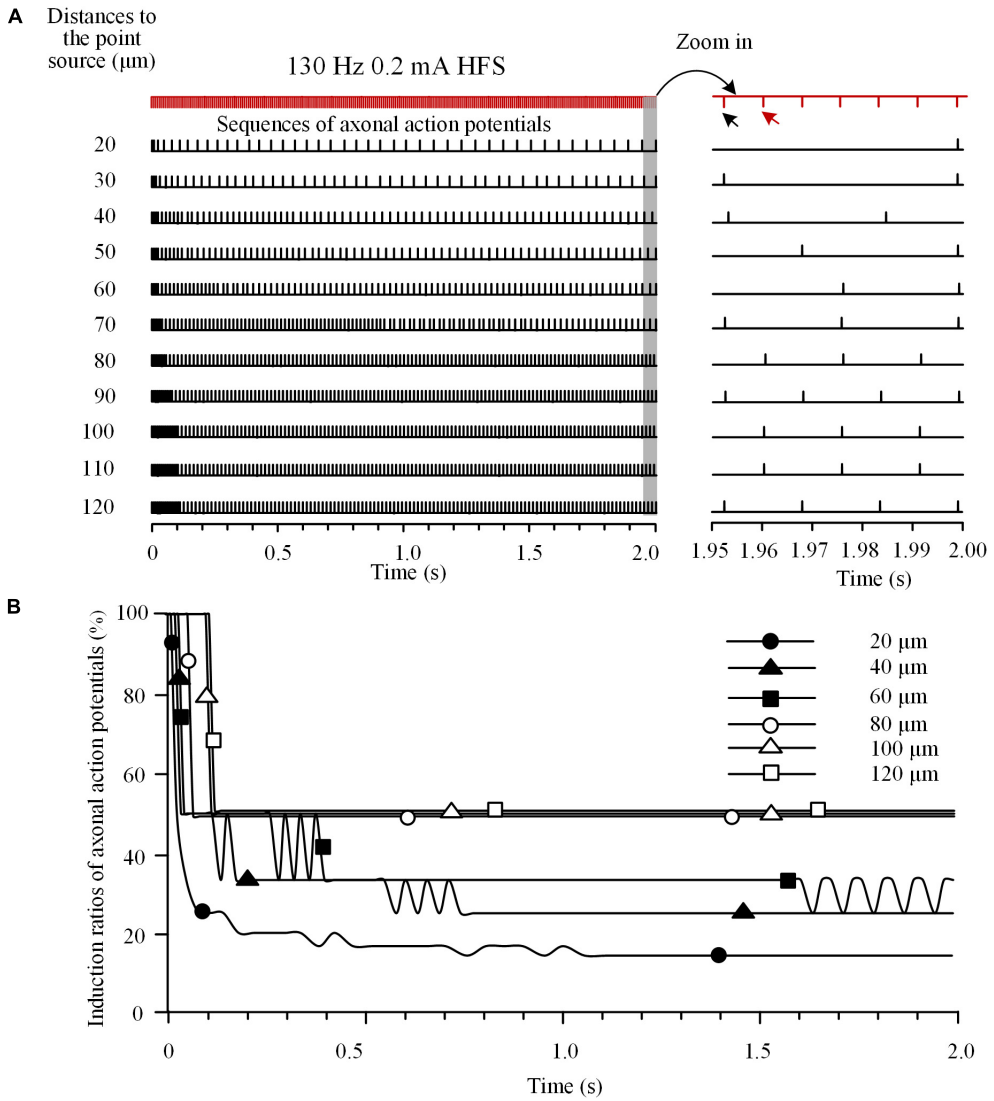

FIGURE 4 | Responses of a bundle of axons to high-frequency stimulation (HFS). **(A)** Sequences of action potentials generated by 130 Hz HFS (0.2 mA) in 11 axons with different distances to the point source of stimulation. Axonal responses to the last seven pulses at the end of 2-s HFS are expanded at *right*. **(B)** Changes of induction ratios of action potentials for the six axons with distances of 20, 40, 60, 80, 100, and 120 μm to the stimulation source during HFS.

by the black arrow) induced action potentials only on axons at 30, 40, 70, 90, and 120 μm distances, while the next pulse (indicated by the red arrow) induced action potentials only on axons at 80, 100, and 110 μm. Therefore, the two pulses induced asynchronous action potentials in different axons.

The number of axons activated by each pulse decreased rapidly at the beginning of HFS (**Figure 5**). The initial pulses could induce action potentials simultaneously in all 11 axons, and thereby the synchronization ratio of action potentials was 100%. After that, the synchronization ratio decreased and was down to a steady value of ∼36% after 1.5 s stimulation.

These results indicate that HFS could cause various degrees of depolarization block to the axons within a bundle, which decreased the synchronization of the overall firing of action potentials. However, the activation of axons was related to not only the distance from the stimulation point, but also the frequency and intensity of the stimulation. Therefore, we next examined the changes of synchronization ratios of multiple axons by stimulations of various frequencies and intensities.

Effect of Stimulation Frequency and Intensity on the Synchronization of Induced Action Potentials in Axon Bundle

With a fixed stimulation intensity of 0.3 mA, HFS at different frequencies of 50, 130, and 200 Hz decreased the synchronization ratio of the 11 axons with different speeds (**Figure 6A**). For a lower frequency of 50 Hz, the synchronization ratio decreased slowly to ∼90% at 0.2 s and stabilized at ∼88% after 1.5 s. For

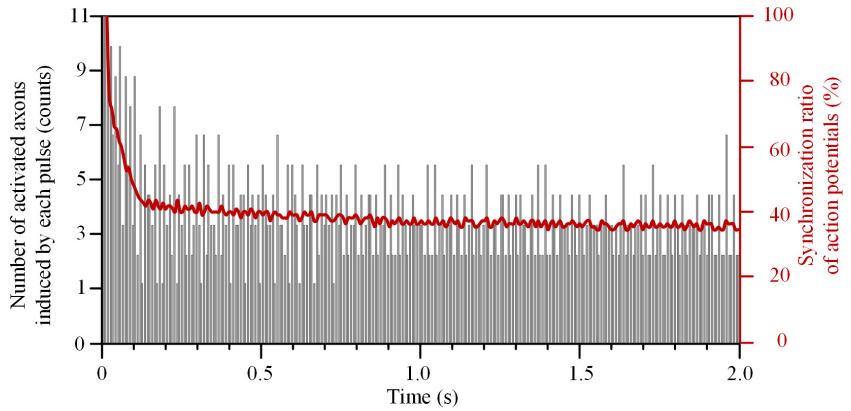

FIGURE 5 | Synchronization ratio of action potentials generated in a bundle of 11 axons during high-frequency stimulation.

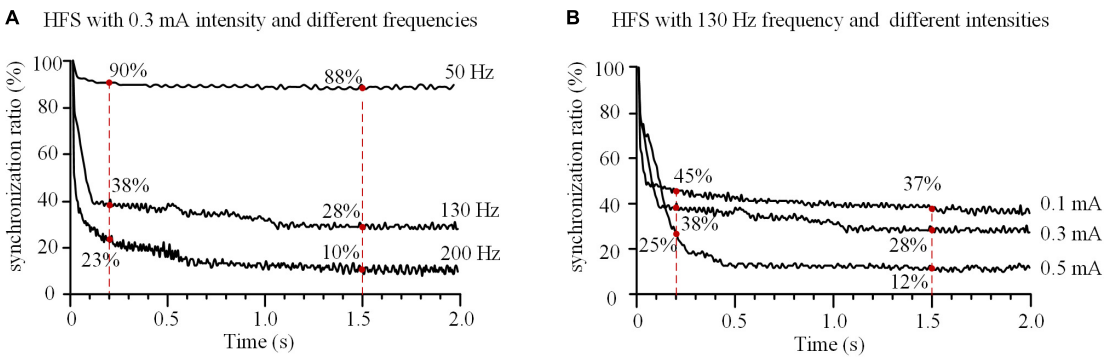

FIGURE 6 | Effects of frequency and intensity of high-frequency stimulation (HFS) on the synchronization of action potential firing of an axonal bundle. **(A)** Changes of the synchronization ratios during HFS with different frequencies at a fixed intensity (0.3 mA). **(B)** Changes of the synchronization ratios during HFS with different intensities at a fixed frequency (130 Hz).

higher frequencies of 130 and 200 Hz, the synchronization ratios decreased more rapidly, to ∼38 and ∼23% at 0.2 s, and stabilized at ∼28 and ∼10% after 1.5 s, respectively. These results indicate that the higher the HFS frequency, the faster the actions of axons desynchronized and the lower synchronization ratios at steady state.

With a fixed stimulation frequency of 130 Hz, HFS at different stimulation intensities of 0.1, 0.3, and 0.5 mA decreased the synchronization ratio of the axons in the assumed bundle to different degrees (**Figure 6B**). At 0.2 s, the synchronization ratios decreased to ∼45, ∼38, and ∼25%, respectively; after 1.5 s, they stabilized at ∼37, ∼28, and ∼12%, respectively, for the three stimulation intensities. These results indicate that the greater the stimulation intensity, the more desynchronized the action potentials of axons and the deeper the degree of axonal block.

DISCUSSION

In the present study, we utilized a computational model to investigate the responses of thin myelinated axons in brain to high-frequency pulse stimulation (HFS). The major findings are (1) the accumulation of K^+ in the peri-axon space during HFS can cause intermittent depolarization block in axons and result in a firing rate of action potentials in axons far lower than the stimulation frequency; (2) the HFS-induced intermittent block can generate asynchronous firing of action potentials in multiple axons within a bundle; (3) differences in frequency and intensity of HFS generate different degrees of the axonal block and of the asynchronous activity thereby resulting in different modulation effects of HFS. Possible mechanisms of these findings and their implications are discussed below.

Intermittent Depolarization Block and Its Implications

In-vitro studies on central nerves have shown that repeated stimulation can elevate $[K^+]_o$ thereby resulting in a decreased speed of axonal conduction until final block of the conduction. Artificially increasing $[K^+]_o$ can also generate axonal block (Förstl et al., 1982; Poolos et al., 1987). The simulation results of our study are consistent with those previous studies. Nevertheless, we further reveal an intermittent feature of the axonal block.

The stimulation-induced depolarization and action potentials are generated mainly in the Ranvier nodes, not in the internode

parts, because of the high impedance of myelinated membrane of internodes and the sole distribution region of Na^+ channel in the nodes (**Figure 1**). In contrast, the K^+ accumulation is generated in the internode parts (**Figure 2C**), not immediately outside the nodes, because of the small peri-axon space around axon membrane of internodes and the dense distribution of K^+ channel in the JXP section (Debanne et al., 2011). Due to a fast diffusion of K^+ outside the Ranvier nodes (imitating the K^+ buffering effect of nearby glial cells), our simulation results show that the $[K^+]_o$ at nodes stays at ∼3 mM (**Figure 2C**), and does not change obviously. Nevertheless, the accumulated $[K^+]_o$ around JXP sections and the excitation of nearby nodes can still interact with each other by the spread of potential changes along axonal membrane.

With the interaction, the HFS-induced depolarization of nodes can increase $[K^+]_o$ of JXP repeatedly following each stimulation pulse; whereas the increased $[K^+]_o$ in turn can cause persistent depolarization of axonal membrane by decreasing the Nernst potential of K^+. A substantial depolarization may lead to depolarization block via the inactivation of sodium channels on the node and prevent the node from continuously generating action potential following each pulse of HFS (Hille, 2001; Qian et al., 2014; Kameneva et al., 2016). K^+ accumulation in JXP sections is counteracted by K^+ clearance via mechanisms of NaK pump and K^+ diffusion. An action potential can be re-induced by a stimulation pulse when $[K^+]_o$ returns to an adequately low level (**Figure 2C**), which generates intermittent block and recovery of axonal activity.

Previous experimental studies have shown that HFS can induce partial block of axonal conduction, but not complete (Jensen and Durand, 2009; Zheng et al., 2011). Based on extracellular recording of population spikes from multiple axons under HFS, two possible mechanisms might underlie the partial block: (1) a part of the axons are completely blocked and the rest are not; (2) each axon produces intermittent block. Previous simulation study has suggested that the mechanism for axonal depolarization block is the former (Bellinger et al., 2008). If it was true that a part of the axons were completely blocked, the downstream projecting neurons would respond in two opposite scenario: either remain silent, or fire at a frequency close to the stimulation. However, the results of *in vivo* animal experiments suggest otherwise; the firing frequency of downstream neurons increase during HFS, but much lower than the stimulation frequency (Feng et al., 2017). Moreover, completely blocking of axon fibers requires stimulation frequencies up to thousands of Hertz (Kilgore and Bhadra, 2014; Couto and Grill, 2016), and the frequencies below 200 Hz used in clinical DBS are unlikely to produce complete axonal block. Therefore, the intermittent axonal block mechanism presented in this paper provides a more reasonable explanation for the experimental observations.

Asynchronous Neuronal Firing and Its Implications

Our simulation results on an axon bundle indicate that intermittent block of individual axons can cause asynchronous firing of the entire axon bundle (**Figures 4**, **5**). Axons at various distances from the stimulation point experience various degrees of depolarization block. Upon intermittent recovery from the block, these axons fire action potentials at different rates and different timings thereby generating asynchronous firing.

HFS-induced desynchronization has important implication to the mechanisms of DBS therapy, because synchronized firing is related to pathological conditions of many brain disorders. In movement disorders such as Parkinson's disease, there is an increase in synchronization of neuronal activity in the basal ganglia and thalamus (Birdno and Grill, 2008; Gale et al., 2008). In epilepsy, populations of neurons fire excessively and synchronously at the onset of seizures (Lopes da Silva et al., 2003; Shiri et al., 2016). HFS could induce asynchronous firing of target neurons to replace the pathological synchronous activity in Parkinson's disease (Cleary et al., 2013; Udupa and Chen, 2015), or suppress hyper-synchronous epileptiform activity (Good et al., 2009; Medeiros Dde and Moraes, 2014). Previous experimental study has proposed an intermittent block of axonal excitation as a possible mechanism for the generation of desynchronization by HFS (Feng et al., 2017). However, the underling mechanism of intermittent block has not been determined.

To our knowledge, this is the first simulation study addressing the intermittent block of axons and the desynchronization effect induced by HFS by incorporating the mechanism of submyelin K^+ accumulation from the scale of axonal ultrastructure. Although the effect of extracellular K^+ accumulation on axonal block was previously simulated in a modeling study (Bellinger et al., 2008), the simulation only presented a complete block of axon, not intermittent block. Therefore, it cannot explain the desynchronization mechanism of HFS.

Moreover, the present study shows that within the DBS frequency range (50–200 Hz), as the stimulation frequency increases, the desynchronization speed of axon bundle accelerates at the initial phase of stimulation and the steady-state level of synchronization ratio decreases (**Figure 6A**). This is consistent with the observations of frequency-dependent axonal block induced by HFS in animal experiments (Jensen and Durand, 2009; Feng et al., 2013, 2014). It is well reported that the efficacy of DBS is dependent on the frequency of stimulation, with effective frequency >90 Hz (Birdno and Grill, 2008; Zhong et al., 2011; McConnell et al., 2012). The results of our simulation study suggest that at a higher stimulation frequency, DBS could replace the pathological synchronization of target neuronal populations with more asynchronous activity thereby treating the diseases. This may underline the mechanism of the frequency-dependent efficacy of DBS.

Limitations of the Simulation Study

One of the limitations of the present study is the use of monophasic (cathodic) stimulation pulses, not biphasic pulses. Clinic DBS commonly uses asymmetrical biphasic pulses, each consisting a cathodic phase, an inter-pulse delay, and a charge-balancing anodic phase (Butson and McIntyre, 2007). The cathodic phase exerts activation

effects; whereas the anodic second phase aims to balance the charge for the safety of DBS. The anodic phase is designed to have longer pulse width yet smaller amplitude in order to minimize its hyperpolarization effect, therefore it would not arrest the activation generated by the cathodic first phase. To simplify the simulation, the anodic phase was not included in the simulated pulses because of its small effects on activation. Further studies with biphasic pulses are needed to mimick the stimulations more consistent with the clinic situation.

Another limitation of the study is that the extracellular potential generated by the point source of stimulation was calculated based on homogeneous conductivity (equation 3), whereas the true extracellular volume conductor is highly heterogeneous. The heterogeneity may alter the location of largest potential change along the axon, thereby moving the position of action potential initiation to other nodes, not exactly the central node (i.e., $Node_{11}$ in our simulation). However, no matter which node is first activated, the subsequent propagation of action potential and the reaction inside the axon would be similar because the high impedance of myelin sheath would prevent the extracellular stimulation from acting on the structures under the myelin sheath (**Figure 1**). It was the reaction of underneath structures (e.g., potassium accumulation) that determined the generation of intermittent block. Therefore, similar conclusions would be obtained with heterogeneous extracellular volume conductor. Nevertheless, a more realistic model accounting for heterogeneity may improve the fidelity of the model predictions.

Summary

The present study shows that the accumulation of potassium ions in the peri-axon space during high HFS can induce intermittent block of axons, which causes asynchronous firing of action potential in an axon bundle. This desynchronized firing of axons could presumably generate asynchronous activity in the projected neurons downstream, thereby suppressing the pathological synchronization of target nuclei. The results provide important insights into the therapeutic mechanisms of DBS, which may lead to the development of novel DBS strategies and the extension of the DBS applications.

AUTHOR CONTRIBUTIONS

ZF and ZG designed the study. ZG, YW, and XW contributed to the model modification. ZG performed the simulation. ZF and ZG interpreted the results. ZG drafted the manuscript. ZF, XW, and YW revised the manuscript critically. All authors gave final approval of the submission.

FUNDING

This work was supported by the National Natural Science Foundation of China (No. 30970753).

REFERENCES

Anderson, T. R. (2006). Selective attenuation of afferent synaptic transmission as a mechanism of thalamic deep brain stimulation-induced tremor arrest. *J. Neurosci.* 26, 841–850. doi: 10.1523/JNEUROSCI.3523-05.2006

Bellinger, S. C., Miyazawa, G., and Steinmetz, P. N. (2008). Submyelin potassium accumulation may functionally block subsets of local axons during deep brain stimulation: a modeling study. *J. Neural Eng.* 5, 263–274. doi: 10.1088/1741-2560/5/3/001

Bergey, G. K. (2013). Neurostimulation in the treatment of epilepsy. *Exp. Neurol.* 244, 87–95. doi: 10.1016/j.expneurol.2013.04.004

Bianchi, D., Marasco, A., Limongiello, A., Marchetti, C., Marie, H., Tirozzi, B., et al. (2012). On the mechanisms underlying the depolarization block in the spiking dynamics of CA1 pyramidal neurons. *J. Comput. Neurosci.* 33, 207–225. doi: 10.1007/s10827-012-0383-y

Birdno, M. J., and Grill, W. M. (2008). Mechanisms of deep brain stimulation in movement disorders as revealed by changes in stimulus frequency. *Neurotherapeutics* 5, 14–25. doi: 10.1016/j.nurt.2007.10.067

Blomstedt, P., Sjöberg, R. L., Hansson, M., Bodlund, O., and Hariz, M. I. (2013). Deep brain stimulation in the treatment of obsessive-compulsive disorder. *World Neurosurg.* 80, e245–e253. doi: 10.1016/j.wneu.2012.10.006

Boraud, T., Bezard, E., Bioulac, B., and Gross, C. (1996). High frequency stimulation of the internal Globus Pallidus (GPi) simultaneously improves parkinsonian symptoms and reduces the firing frequency of GPi neurons in the MPTP-treated monkey. *Neurosci. Lett.* 215, 17–20. doi: 10.1016/S0304-3940(96)12943-8

Butson, C. R., and McIntyre, C. C. (2007). Differences among implanted pulse generator waveforms cause variations in the neural response to deep brain stimulation. *Clin. Neurophysiol.* 118, 1889–1894. doi: 10.1016/j.clinph.2007.05.061

Caldwell, J. H., Schaller, K. L., Lasher, R. S., Peles, E., and Levinson, S. R. (2000). Sodium channel Nav1.6 is localized at nodes of Ranvier, dendrites, and synapses. *Proc. Natl. Acad. Sci. U.S.A.* 97, 5616–5620. doi: 10.1073/pnas.090034797

Chiken, S., and Nambu, A. (2013). High-frequency pallidal stimulation disrupts information flow through the pallidum by GABAergic inhibition. *J. Neurosci.* 33, 2268–2280. doi: 10.1523/JNEUROSCI.4144-11.2013

Chomiak, T., and Hu, B. (2007). Axonal and somatic filtering of antidromically evoked cortical excitation by simulated deep brain stimulation in rat brain. *J. Physiol.* 579, 403–412. doi: 10.1113/jphysiol.2006.124057

Cleary, D. R., Raslan, A. M., Rubin, J. E., Bahgat, D., Viswanathan, A., Heinricher, M. M., et al. (2013). Deep brain stimulation entrains local neuronal firing in human globus pallidus internus. *J. Neurophysiol.* 109, 978–987. doi: 10.1152/jn.00420.2012

Couto, J., and Grill, W. M. (2016). Kilohertz frequency deep brain stimulation is ineffective at regularizing the firing of model thalamic neurons. *Front. Comput. Neurosci.* 10:22. doi: 10.3389/fncom.2016.00022

Cury, R. G., Fraix, V., Castrioto, A., Pérez Fernández, M. A., Krack, P., Chabardes, S., et al. (2017). Thalamic deep brain stimulation for tremor in Parkinson disease, essential tremor, and dystonia. *Neurology* 89, 1416–1423. doi: 10.1212/WNL.0000000000004295

Debanne, D., Campanac, E., Bialowas, A., Carlier, E., and Alcaraz, G. (2011). Axon physiology. *Physiol. Rev.* 91, 555–602. doi: 10.1152/physrev.00048.2009

Deniau, J.-M., Degos, B., Bosch, C., and Maurice, N. (2010). Deep brain stimulation mechanisms: beyond the concept of local functional inhibition. *Eur. J. Neurosci.* 32, 1080–1091. doi: 10.1111/j.1460-9568.2010.07413.x

Devaux, J. J. (2004). KCNQ2 is a nodal K+ channel. *J. Neurosci.* 24, 1236–1244. doi: 10.1523/JNEUROSCI.4512-03.2004

Duflocq, A., Le Bras, B., Bullier, E., Couraud, F., and Davenne, M. (2008). Nav1.1 is predominantly expressed in nodes of Ranvier and axon initial segments. *Mol. Cell. Neurosci.* 39, 180–192. doi: 10.1016/j.mcn.2008.06.008

Eusebio, A., Thevathasan, W., Doyle Gaynor, L., Pogosyan, A., Bye, E., Foltynie, T., et al. (2011). Deep brain stimulation can suppress pathological synchronisation in parkinsonian patients. *J. Neurol. Neurosurg. Psychiatry* 82, 569–573. doi: 10.1136/jnnp.2010.217489

Feng, Z., Wang, Z., Guo, Z., Zhou, W., Cai, Z., and Durand, D. M. (2017). High frequency stimulation of afferent fibers generates asynchronous firing in the downstream neurons in hippocampus through partial block of axonal conduction. *Brain Res.* 1661, 67–78. doi: 10.1016/j.brainres.2017.02.008

Feng, Z., Yu, Y., Guo, Z., Cao, J., and Durand, D. M. (2014). High frequency stimulation extends the refractory period and generates axonal block in the rat hippocampus. *Brain Stimul.* 7, 680–689. doi: 10.1016/j.brs.2014.03.011

Feng, Z., Zheng, X., Yu, Y., and Durand, D. M. (2013). Functional disconnection of axonal fibers generated by high frequency stimulation in the hippocampal CA1 region in-vivo. *Brain Res.* 1509, 32–42. doi: 10.1016/j.brainres.2013.02.048

Förstl, J., Galvan, M., and ten Bruggencate, G. (1982). Extracellular K+ concentration during electrical stimulation of rat isolated sympathetic ganglia, vagus and optic nerves. *Neuroscience* 7, 3221–3229. doi: 10.1016/0306-4522(82)90244-5

Frijns, J. H. M., Mooij, J., and ten Kate, J. H. (1994). A quantitative approach to modeling mammalia myelinated nerve fibers for electrical prostheis design. *IEEE Trans. Biomed. Eng.* 41, 556–566. doi: 10.1109/10.293243

Gale, J. T., Amirnovin, R., Williams, Z. M., Flaherty, A. W., and Eskandar, E. N. (2008). From symphony to cacophony: pathophysiology of the human basal ganglia in Parkinson disease. *Neurosci. Biobehav. Rev.* 32, 378–387. doi: 10.1016/j.neubiorev.2006.11.005

Good, L. B., Sabesan, S., Marsh, S. T., Tsakalis, K., Treiman, D., and Iasemidis, L. (2009). Control of synchronization of brain dynamics leads to control of epileptic seizures in rodents. *Int. J. Neural Syst.* 19, 173–196. doi: 10.1142/S0129065709001951

Hammond, C., Bergman, H., and Brown, P. (2007). Pathological synchronization in Parkinson's disease: networks, models and treatments. *Trends Neurosci.* 30, 357–364. doi: 10.1016/j.tins.2007.05.004

Hille, B. (2001). *Ion Channels of Excitable Membranes*. Sunderland, MA: Sinauer.

Jensen, A. L., and Durand, D. M. (2009). High frequency stimulation can block axonal conduction. *Exp. Neurol.* 220, 57–70. doi: 10.1016/j.expneurol.2009.07.023

Jiruska, P., de Curtis, M., Jefferys, J. G. R., Schevon, C. A., Schiff, S. J., and Schindler, K. (2013). Synchronization and desynchronization in epilepsy: controversies and hypotheses. *J. Physiol.* 591, 787–797. doi: 10.1113/jphysiol.2012.239590

Johnson, M. D., and McIntyre, C. C. (2008). Quantifying the neural elements activated and inhibited by globus pallidus deep brain stimulation. *J. Neurophysiol.* 100, 2549–2563. doi: 10.1152/jn.90372.2008

Kameneva, T., Maturana, M. I., Hadjinicolaou, A. E., Cloherty, S. L., Ibbotson, M. R., Grayden, D. B., et al. (2016). Retinal ganglion cells: mechanisms underlying depolarization block and differential responses to high frequency electrical stimulation of ON and OFF cells. *J. Neural Eng.* 13:16017. doi: 10.1088/1741-2560/13/1/016017

Kilgore, K. L., and Bhadra, N. (2014). Reversible nerve conduction block using kilohertz frequency alternating current. *Neuromodulation Technol. Neural Interface* 17, 242–255. doi: 10.1111/ner.12100

Lopes da Silva, F., Blanes, W., Kalitzin, S. N., Parra, J., Suffczynski, P., and Velis, D. N. (2003). Epilepsies as dynamical diseases of brain systems: basic models of the transition between normal and epileptic activity. *Epilepsia* 44(Suppl. 1), 72–83. doi: 10.1111/j.0013-9580.2003.12005.x

McConnell, G. C., So, R. Q., Hilliard, J. D., Lopomo, P., and Grill, W. M. (2012). Effective deep brain stimulation suppresses low-frequency network oscillations in the basal ganglia by regularizing neural firing patterns. *J. Neurosci.* 32, 15657–15668. doi: 10.1523/JNEUROSCI.2824-12.2012

McIntyre, C. C., and Grill, W. M. (1999). Excitation of central nervous system neurons by nonuniform electric fields. *Biophys. J.* 76, 878–888. doi: 10.1016/S0006-3495(99)77251-6

McIntyre, C. C., and Grill, W. M. (2002). Extracellular stimulation of central neurons: influence of stimulus waveform and frequency on neuronal output. *J. Neurophysiol.* 88, 1592–1604. doi: 10.1152/jn.2002.88.4.1592

McIntyre, C. C., Grill, W. M., Sherman, D. L., and Thakor, N. V. (2004). Cellular effects of deep brain stimulation: model-based analysis of activation and inhibition. *J. Neurophysiol.* 91, 1457–1469. doi: 10.1152/jn.00989.2003

Medeiros Dde, C., and Moraes, M. F. D. (2014). Focus on desynchronization rather than excitability: a new strategy for intraencephalic electrical stimulation. *Epilepsy Behav.* 38, 32–36. doi: 10.1016/j.yebeh.2013.12.034

Mehanna, R., and Lai, E. C. (2013). Deep brain stimulation in Parkinson's disease. *Transl. Neurodegener.* 2, 1–10. doi: 10.1186/2047-9158-2-22

Migliore, M., Hoffman, D. A., Magee, J. C., and Johnston, D. (1999). Role of an A-type K+ conductance in the back-propagation of action potentials in the dendrites of hippocampal pyramidal neurons. *J. Comput. Neurosci.* 7, 5–15. doi: 10.1023/A:1008906225285

Narang, P., Retzlaff, A., Brar, K., and Lippmann, S. (2016). Deep brain stimulation for treatment-refractory depression. *South. Med. J.* 109, 700–703. doi: 10.14423/SMJ.0000000000000554

Nelson, A. D., and Jenkins, P. M. (2017). Axonal membranes and their domains: assembly and function of the axon initial segment and node of Ranvier. *Front. Cell. Neurosci.* 11:136. doi: 10.3389/fncel.2017.00136

Nowak, L. G., and Bullier, J. (1998). Axons, but not cell bodies, are activated by electrical stimulation in cortical gray matter. *Exp. Brain Res.* 118, 489–500. doi: 10.1007/s002210050305

Poolos, N. P., Mauk, M. D., and Kocsis, J. D. (1987). Activity-evoked increases in extracellular potassium modulate presynaptic excitability in the CA1 region of the hippocampus. *J. Neurophysiol.* 58, 404–416. doi: 10.1152/jn.1987.58.2.404

Qian, K., Yu, N., Tucker, K. R., Levitan, E. S., and Canavier, C. C. (2014). Mathematical analysis of depolarization block mediated by slow inactivation of fast sodium channels in midbrain dopamine neurons. *J. Neurophysiol.* 112, 2779–2790. doi: 10.1152/jn.00578.2014

Ranck, J. B. (1975). Which elements are excited in electrical stimulation of mammalian central nervous system: a review. *Brain Res.* 98, 417–440. doi: 10.1016/0006-8993(75)90364-9

Rasband, M. N., and Peles, E. (2016). The nodes of Ranvier: molecular assembly and maintenance. *Cold Spring Harb. Perspect. Biol.* 8, 1–15. doi: 10.1101/cshperspect.a020495

Rasband, M. N., and Trimmer, J. S. (2001). Subunit composition and novel localization of K+ channels in spinal cord. *J. Comp. Neurol.* 429, 166–176. doi: 10.1002/1096-9861(20000101)429:1<166::AID-CNE13>3.0.CO;2-Y

Reese, R., Leblois, A., Steigerwald, F., Pötter-Nerger, M., Herzog, J., Mehdorn, H. M., et al. (2011). Subthalamic deep brain stimulation increases pallidal firing rate and regularity. *Exp. Neurol.* 229, 517–521. doi: 10.1016/j.expneurol.2011.01.020

Scholz, A., Reid, G., Vogel, W., and Bostock, H. (1993). Ion channels in human axons. *J. Neurophysiol.* 70, 1274–1279. doi: 10.1152/jn.1993.70.3.1274

Schröder, J. M. (1972). Altered ratio between axon diameter and myelin sheath thickness in regenerated nerve fibers. *Brain Res.* 45, 49–65. doi: 10.1016/0006-8993(72)90215-6

Schwarz, J. R., Glassmeier, G., Cooper, E. C., Kao, T. C., Nodera, H., Tabuena, D., et al. (2006). KCNQ channels mediate IKs, a slow K+ current regulating excitability in the rat node of Ranvier. *J. Physiol.* 573, 17–34. doi: 10.1113/jphysiol.2006.106815

Schwarz, J. R., Reid, G., and Bostock, H. (1995). Action potentials and membrane currents in the human node of Ranvier. *Pflugers Arch. Eur. J. Physiol.* 430, 283–292. doi: 10.1007/BF00374660

Shiri, Z., Manseau, F., Lévesque, M., Williams, S., and Avoli, M. (2016). Activation of specific neuronal networks leads to different seizure onset types. *Ann. Neurol.* 79, 354–365. doi: 10.1002/ana.24570

Staff, N. P., Jung, H. Y., Thiagarajan, T., Yao, M., and Spruston, N. (2000). Resting and active properties of pyramidal neurons in subiculum and CA1 of rat hippocampus. *J. Neurophysiol.* 84, 2398–2408. doi: 10.1016/0959-4388(93)90214-j

Udupa, K., and Chen, R. (2015). The mechanisms of action of deep brain stimulation and ideas for the future development. *Prog. Neurobiol.* 133, 27–49. doi: 10.1016/j.pneurobio.2015.08.001

Wang, H., Kunkel, D. D., Martin, T. M., Schwartzkroin, P. A., and Tempel, B. L. (1993). Heteromultimeric K+ channels in terminal and juxtaparanodal regions of neurons. *Nature* 365, 75–79. doi: 10.1038/365075a0

Wang, S. S.-H., Shultz, J. R., Burish, M. J., Harrison, K. H., Hof, P. R., Towns, L. C., et al. (2008). Functional trade-offs in white matter axonal scaling. *J. Neurosci.* 28, 4047–4056. doi: 10.1523/JNEUROSCI.5559-05.2008

Waxman, S. G., and Ritchie, J. M. (1993). Molecular dissection of the myelinated axon. *Ann. Neurol.* 33, 121–136. doi: 10.1002/ana.410330202

Zheng, F., Lammert, K., Nixdorf-Bergweiler, B. E., Steigerwald, F., Volkmann, J., and Alzheimer, C. (2011). Axonal failure during high frequency stimulation of rat subthalamic nucleus. *J. Physiol.* 589, 2781–2793. doi: 10.1113/jphysiol.2011.205807

Zhong, X. L., Yu, J. T., Zhang, Q., Wang, N. D., and Tan, L. (2011). Deep brain stimulation for epilepsy in clinical practice and in animal models. *Brain Res. Bull.* 85, 81–88. doi: 10.1016/j.brainresbull.2011.03.020

Conflict of Interest Statement: The authors declare that the research was conducted in the absence of any commercial or financial relationships that could be construed as a potential conflict of interest.

frontiers in Neuroscience

ORIGINAL RESEARCH
published: 03 December 2018
doi: 10.3389/fnins.2018.00877

A Real-Time Phase-Locking System for Non-invasive Brain Stimulation

*Farrokh Mansouri[1], Peter Fettes[2], Laura Schulze[2], Peter Giacobbe[3,4,5], Jose Zariffa[1,6] and Jonathan Downar[2,3,4,7]**

[1] Institute of Biomaterial and Biomedical Engineering, University of Toronto, Toronto, ON, Canada, [2] Institute of Medical Science, University of Toronto, Toronto, ON, Canada, [3] Department of Psychiatry, University of Toronto, Toronto, ON, Canada, [4] Centre for Mental Health, University Health Network, Toronto, ON, Canada, [5] Harquail Centre for Neuromodulation, Sunnybrook Health Sciences Centre, Toronto, ON, Canada, [6] Toronto Rehabilitation Institute, University Health Network, Toronto, ON, Canada, [7] Krembil Research Institute, University Health Network, Toronto, ON, Canada

Non-invasive brain stimulation techniques are entering widespread use for the investigation and treatment of a range of neurological and neuropsychiatric disorders. However, most current techniques are 'open-loop', without feedback from target brain region activity; this limitation could contribute to heterogeneous effects seen for nominally 'inhibitory' and 'excitatory' protocols across individuals. More potent and consistent effects may ensue from closed-loop and, in particular, phase-locked brain stimulation. In this work, a closed-loop brain stimulation system is introduced that can analyze EEG data in real-time, provide a forecast of the phase of an underlying brain rhythm of interest, and control pulsed transcranial electromagnetic stimulation to deliver pulses at a specific phase of the target frequency band. The technique was implemented using readily available equipment such as a basic EEG system, a low-cost Arduino board and MATLAB scripts. The phase-locked brain stimulation method was tested in 5 healthy volunteers and its phase-locking performance evaluated at 0, 90, 180, and 270 degree phases in theta and alpha frequency bands. On average phase locking values of 0.55° ± 0.11° and 0.52° ± 0.14° and error angles of 11° ± 11° and 3.3° ± 18° were achieved for theta and alpha stimulation, respectively. Despite the low-cost hardware implementation, signal processing time generated a phase delay of only 3.8° for theta and 57° for alpha stimulation, both readily accommodated in the pulse trigger algorithm. This work lays the methodological steps for achieving phase-locked brain stimulation for brief-pulse transcranial electrical stimulation (tES) and repetitive transcranial magnetic stimulation (rTMS), facilitating further research on the effect of stimulation phase for these techniques.

Keywords: closed-loop brain stimulation, synchronized brain stimulation, real-time phase tracking, phase-locked brain stimulation, transcranial electric stimulation

OPEN ACCESS

Edited by:
Mikhail Lebedev, Duke University, United States

Reviewed by:
Ali Yadollahpour, Ahvaz Jundishapur University of Medical Sciences, Iran
Xiaoli Li, Beijing Normal University, China
Marianna Semprini, Fondazione Istituto Italiano di Technologia, Italy

***Correspondence:**
Jonathan Downar
jonathan.downar@uhn.ca

Specialty section:
This article was submitted to Neural Technology, a section of the journal Frontiers in Neuroscience

Received: *26 June 2018*
Accepted: *12 November 2018*
Published: *03 December 2018*

Citation:
Mansouri F, Fettes P, Schulze L, Giacobbe P, Zariffa J and Downar J (2018) A Real-Time Phase-Locking System for Non-invasive Brain Stimulation. Front. Neurosci. 12:877. doi: 10.3389/fnins.2018.00877

INTRODUCTION

Non-invasive brain stimulation is entering increasingly widespread use as both a research tool and a clinical intervention for neuropsychiatric disorders. A wide range of non-invasive brain stimulation techniques, such as transcranial magnetic stimulation (TMS) (Hallett, 2000), transcranial electrical stimulation (tES) (Paulus, 2011), and transcranial pulsed ultrasound (TPU) (Tufail et al., 2011),

have been developed as ways to modulate brain activity (Polanía et al., 2018). While these methods have demonstrated applications in treating a number of neuropsychiatric disorders (Schulz et al., 2013; Kuo et al., 2014), they are still hampered by several important limitations. One such limitation is the heterogeneity of effect across individuals. For example, nominally 'excitatory' or 'inhibitory' rTMS protocols can show the opposite-to-expected effect in up to 50% of individuals (Maeda et al., 2000; Hamada et al., 2013). Several hypotheses have been proposed to explain this heterogeneity of effect; prominent among them is a variable degree of synchronization between the applied stimulation and the underlying brain activity when the stimulator is employed in an 'open-loop' fashion (Chung et al., 2018). At present, most non-invasive brain stimulation techniques use 'open-loop,' i.e., applying stimulation at a set protocol without feedback guidance from the actual activity of the target region. A 'closed-loop' system, in contrast, would read the activity of the target region and use this information to guide the parameters of stimulation: for example, the pattern, frequency, phase, or timing of stimulation.

Closed-loop stimulation systems may be considered a worthwhile objective if there is evidence that the effects of stimulation depend on the brain state at the time of stimulation, and indeed there is ample literature support for this proposal. Current models of brain function posit that brain regions operate as integrated networks bound by coherent activity, and task-specific activation of these networks is seen across various brain states (Seager et al., 2002; Park and Friston, 2013; Pessoa, 2014). The state of the brain during the stimulation can change the outcome of the intervention (Silvanto et al., 2008); an elementary example would be the observation that the active motor threshold is substantially lower than the resting motor threshold for stimulation of the primary motor cortex (Hallett, 2007). On a related point, there is mounting evidence that brain stimulation, especially the types that use energies below the threshold for action potential elicitation (e.g., tES), are more consistent in effect when synchronized to the underlying brain activity (Fröhlich and McCormick, 2010; Reato et al., 2013). In one early study, electrical stimulation of hippocampal brain slices showed that when the stimulation was delivered at the peak or the trough of the theta rhythm of tissue, the changes in the evoked potentials were opposite (Hyman et al., 2003). In another example, while TMS effects could vary depending on the phase of the underlying brain network, TMS pulses applied at the peak or trough of the μ-rhythm of the motor cortex have been shown to have opposite plastic effects (Zrenner et al., 2017). Recently, phase-locked stimulation of the sensorimotor cortex in monkeys showed phase specific bidirectional synaptic plasticity (Zanos et al., 2018). Thus, open-loop stimulation, by applying pulses at various phases of the intrinsic brain activity, is proposed to contribute to the observed heterogeneity of effect for stimulation across individuals and across sessions within a given individual. Given these findings, a system enabling phase-locked stimulation could potentially allow more precise control of the direction of effect of the stimulation, as well as a more consistent effect overall, within and across individuals. Such an approach would build upon other efforts to reduce sources of heterogeneity in non-invasive brain stimulation via straightforward, user-friendly, clinically translatable methods (e.g., (Mansouri et al., 2018)).

In tES, the electrical currents applied create a small electric field that can alter the ongoing activity of the brain (Nitsche and Paulus, 2000; Ohn et al., 2008; Utz et al., 2010; Reato et al., 2013). In one example, the frequency of the stimulation matched to the underlying alpha oscillation can modulate the intrinsic alpha rhythms (Vossen et al., 2015). Moreover, frequency- and phase-specific effects of transcranial alternating current stimulation have been shown in a number of specific experiments in motor activity (Guerra et al., 2016; Nakazono et al., 2016), cognition (Polanía et al., 2012) and auditory system (Riecke et al., 2015). However, open-loop implementation of the stimulation techniques in these studies confine them to their experimental settings and inhibit them from being used in a wider scope of applications. Due to the technical challenges of closed-loop brain stimulation, namely real-time implementation of phase tracking algorithms and the presence of stimulation artifacts in the recordings, it has been very difficult to explore the effects of these stimulation techniques in a wide range of models and experimental settings. For example, when applying the sinusoidal alternating current stimuli of transcranial alternating current stimulation (tACS), it becomes difficult to model out the artifact of the stimulation itself in order to recover the original signal from the target brain region, which is needed to recover information about dominant frequency or phase in order to enable closed-loop, phase-locked stimulation. As such, phase-locked tACS or rTMS, although potentially useful in theory for enhancing stimulus potency and consistency, is difficult to accomplish in practice due to challenges in recovering the source signal for closed-loop stimulation.

Here, we describe a novel apparatus for a closed-loop stimulation system that can provide real-time, phase-locked brain stimulation and can be applied with a wide range of neuromodulation techniques. The approach relies on the use of brief pulses of stimulation (as are employed in rTMS, or in this case with brief-pulse tES), such that only a small proportion of the data samples in each cycle are contaminated by stimulus artifact (c.f., Neuropace patent US 6690974B2). The non-contaminated data samples are sufficient for reconstruction of dominant frequency and phase information, and this information can be used in real-time to deliver the stimulation pulses at any desired phase: 0°, 90°, 180°, or 270°. In this work, we have tested our method using pulsed-transcranial electrical stimulation (ptES) (Alon et al., 2012; Berenyi et al., 2012; Morales-Quezada et al., 2015; Vasquez et al., 2016), and lay out the steps essential for implementation of this technique for closed-loop, phase-locked non-invasive brain stimulation. The intended scope of this paper is to describe the technique and provide a preliminary proof-of-concept *in vivo* demonstration. Subsequent work will examine in detail the behavioral effects of phase-locked vs. non-phase-locked stimulation in a larger validation sample.

MATERIALS AND METHODS

We have developed a closed-loop brain stimulation technique that is able to read electroencephalography (EEG) data, analyze it in real-time to extract specific phase and frequency information, and control the stimulator based on the phase and frequency of the underlying signal. The system includes an EEG amplifier, MATLAB signal processing scripts and an Arduino interface to control the brain stimulation (**Figure 1**). In this section we describe all components of this system in detail.

Real-Time Brain Recording and Preprocessing

A Brain Products V-AMP 16 channel EEG amplifier (Brain Products GmbH, Munich, Germany) was used in this setup. The amplifier was connected to a Windows 7 computer (Intel® Core™ i5-3470 3.2 GHz) via USB. OpenVibe (Renard et al., 2010) was used as an interface to stream data from the amplifier in real-time. The EEG system sampled the data at 2 kHz and downsampled the data to 512 Hz in hardware, while applying the appropriate anti-aliasing filters. The data was buffered and sent 4 samples at a time to the OpenVibe software. The V-AMP amplifier used a 32-bit data resolution with a wide dynamic range. This ensured that the amplifier was not saturated during the recording due to the stimulation and resulting artifacts.

For recording/stimulation sessions, the stimulation electrodes were first placed on the scalp (stimulation: F3, F4 for theta stimulation and O3, O4 for alpha stimulation; recording: Fz for theta stimulation and Oz for alpha stimulation); Ten20 conductive gel (Weaver and Company, Aurora, CO, United States) was applied to the electrodes and the scalp until the impedances of the electrodes were below 5 kΩ. Next, a 16-channel passive-electrode EEG cap (EasyCap GmbH, Germany) was worn by the volunteers on top of the stimulation electrodes and HiCL Abrasive EEG Gel (EasyCap GmbH, Germany) was applied to reduce the impedance of each of the recording electrodes to below 5 kΩ.

Signal Processing

A MATLAB script was called within OpenVibe every 10ms (100Hz) to analyze the recorded signal. The script was developed to analyze the EEG signal recorded from the EEG channel of interest (Fz for theta recording and Oz for alpha recording) and control the stimulator based on the method presented in our previous work (Mansouri et al., 2017). In summary, this script first removes the stimulation artifact from the recorded EEG; second, it analyzes the EEG to extract the timing for the next

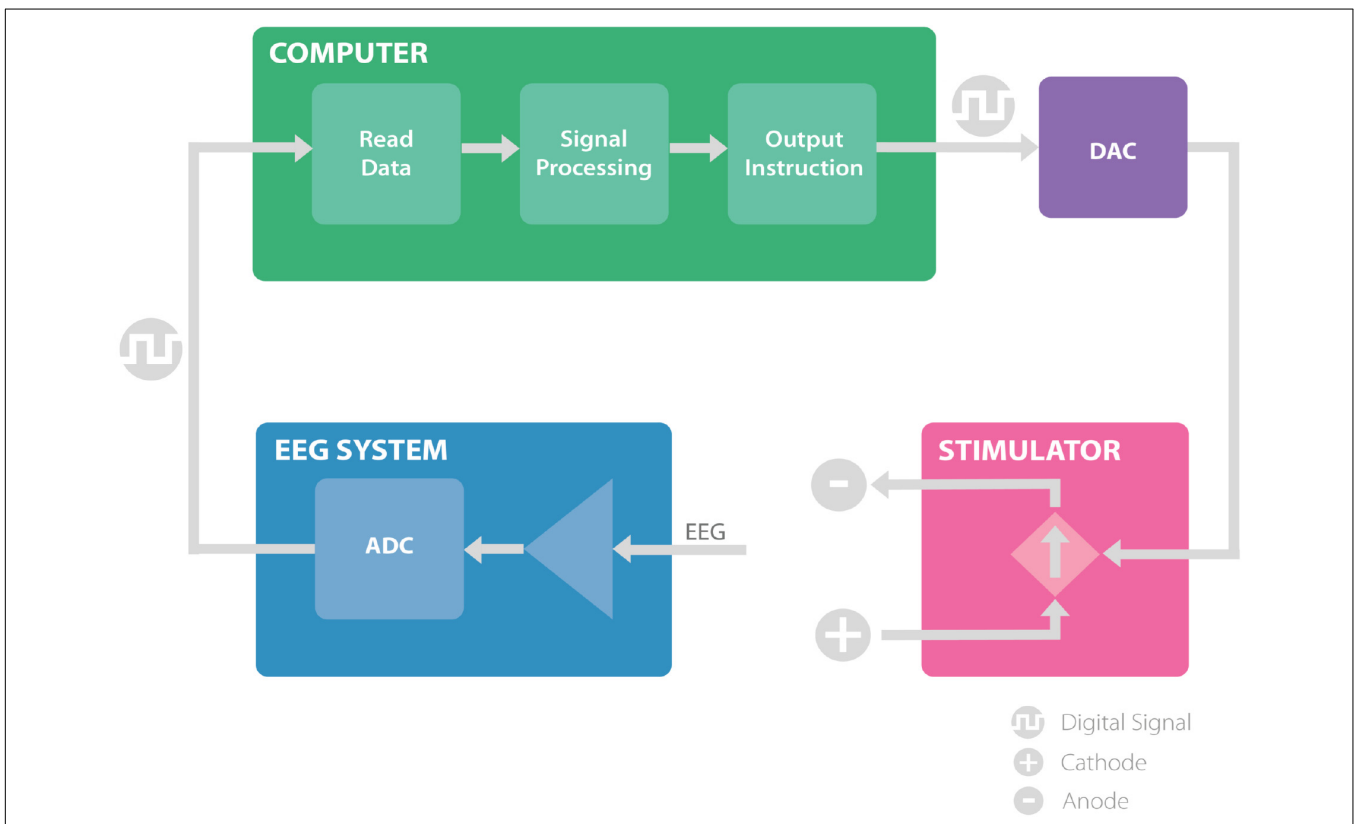

FIGURE 1 | The proposed system, consisting of EEG amplifier (blue) records the EEG signal and transmit the digital data to the computer. The computer (green) receives the EEG recordings and analyze the signal to extract the timing of the stimulation and communicates the instruction through a digital to analog converter to the stimulator. The stimulator (pink), provides the stimulation based on the information received and allows for closed loop brain stimulation. ADC, analog to digital converter; DAC, digital to analog converter.

stimulation pulse and, finally, it communicates with an Arduino Due board to control the stimulator output in real-time.

Artifact Removal

Accurate recovery and analysis of EEG activity occurring simultaneously with a large stimulation artifact is a challenging objective. To date, few methods have been proposed that can remove the electrical stimulation artifacts in short-window recordings (<1 s) in real-time. For stimulation methods such as transcranial alternating current stimulation (tACS), which delivers a continuous sine-wave stimulation pulse, closed-loop stimulation is particularly challenging, as it is difficult to recover the underlying EEG signal accurately, or determine its phase in a given frequency component during active stimulation.

An alternative, workaround approach is to minimize the proportion of EEG samples that are affected by stimulation artifact, by using a tES waveform consisting of short, square-wave pulses rather than continuous sinusoidal stimulation. During brief-pulse stimulation, only a small portion of the EEG samples are contaminated with the stimulation artifact, so that much of the EEG signal (and in particular, its phase in a given frequency component) remains recoverable over a given window of time. For this reason, we used short pulsed stimulation in this work, which enabled us to assess the feasibility of closed-loop, phase-locked tES without the confounding presence of a stimulation artifact (c.f. Neuropace US patent 6690974B2), using readily available and inexpensive components commonly employed in laboratory settings.

The recorded EEG generally has amplitudes smaller than 50 μV, while the stimulation artifacts are orders of magnitude larger (>1 mV). The amplitude of the signal compared with its local median (window size of 20 samples) was used to detect the large artifact (McNames et al., 2004). The empirically selected threshold of 50 μV on the difference between the signal and its median was used to identify the timing of the pulses. Next, the signal contaminated with the artifact was deleted and replaced with an interpolated signal using a spline interpolation method (Waddell et al., 2009).

This method worked well only when the duration of the artifact was much smaller than the period of the underlying brain oscillation. In our case, the 5ms pulses generated 20 ms of artifact, while the underlying brain oscillation of interest in the alpha frequency band has a period of ∼100 ms and in the theta frequency band has a period of ∼160 ms, which is much larger than the duration of the artifact itself (**Figure 2**). For the purposes of this proof-of-concept study, we selected theta (4–8 Hz) and alpha (8–13 Hz) bands for testing this closed-loop phase locking method. To assess the artifact removal method performance, stimulation at arbitrary phase and frequency was applied to study the artifact duration and the artifact detection method. Pulses of 5 ms duration were delivered at random intervals of 100–200 ms. Averaging of 500 epochs of stimulation artifact recordings, time-locked to the onset of the stimulation pulse, was used to assess the lasting effect of the artifact after the onset of the pulse (see Results below).

Signal Processing and Frequency and Phase Extraction

As described in our previous work (Mansouri et al., 2017), we first use a segment of the recorded signal and apply an IIR bandpass filter to isolate a frequency band of interest. Based on our previous simulations offline, we used a 10th order elliptical filter, converted the quantized filter to second-order sections, and applied it to the recording.

Next, the Fast Fourier Transform (FFT) of the filtered signal segment was computed. The filtered signal was first zero-padded to increase the bin resolution in the FFT. The FFT bin with maximum power in the frequency range of interest was selected as the dominant frequency and its phase and frequency were used to calculate the timing of the next stimulation pulse. To correct for the small delays in the system or a small phase shift that was introduced by the filter or other components of the

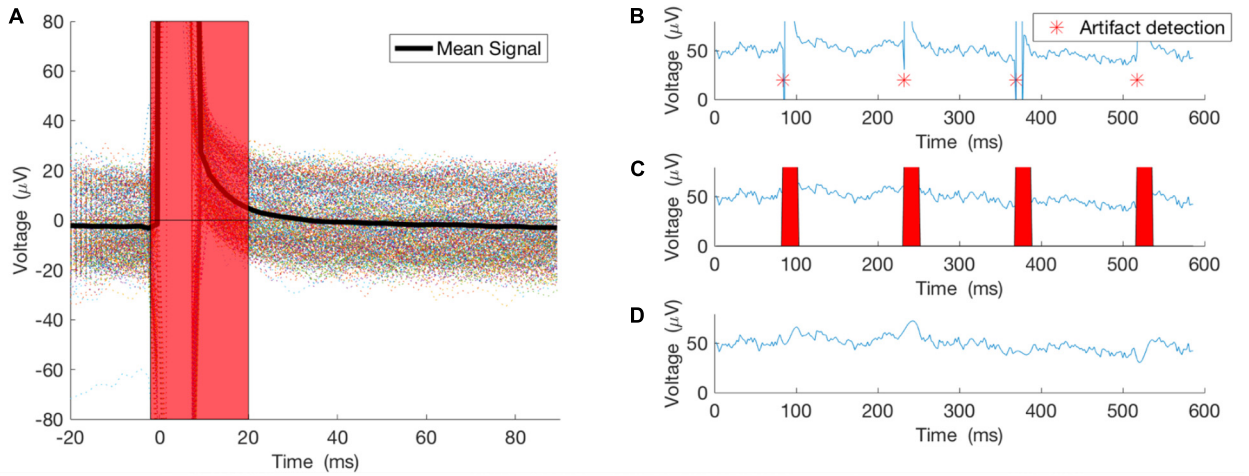

FIGURE 2 | Artifacts from 500 pulses were averaged to study the true effect of the stimulation on the recording. **(A)** The 500 epochs and their average. **(B)** An example of the pulse detector, asterisk showing location of the detected pulses. **(C,D)** Pulses removed and signal interpolated using spline interpolation.

signal processing or hardware delays, an empirically calculated correction time was added to the calculated pulse time.

Real-Time Control of the Stimulator

The timing of the next pulse was communicated to an Arduino Due Microcontroller boar (Arduino) through serial USB communication. First, a serial connection was made through the MATLAB Serial Port Interface (MATLAB version 7.9.0), and at every iteration of the code the timing of the next pulse was communicated to the Arduino Due, which then produced a pulse through its true analog output pin with microsecond resolution. The Arduino analog output is connected to the "remote control" port on the Neuroconn DC-Plus stimulator (Neuroconn Ltd., Ilmenau, Germany). In this system, the stimulator follows the Arduino-generated voltage waveforms and produces a current-controlled output proportional to that voltage.

In vivo Demonstration

In order to demonstrate the potential applicability of the present technique across different brain regions, different states (resting vs. on-task), and different recording types (ongoing activity vs. evoked potential on-task), we studied both alpha and theta rhythms, both occipital and frontal regions, and both resting and on-task (evoked) brain states. Occipital regions are particularly potent and well-studied generators of resting alpha rhythms, particularly during the resting eyes-closed state, and are thus widely used in studies of EEG alpha activity (Lehmann, 1971; Vossen et al., 2015). Likewise, midline frontal regions are particularly potent and well-studied generators of theta rhythms, particularly during cognitive control tasks, which are likewise widely used in EEG studies of cognition in healthy controls and individuals with illness (Frank et al., 2004, 2005; Cavanagh and Frank, 2014). Such studies commonly employ evoked potentials rather than resting-state activity (Frank et al., 2004, 2005; Cavanagh and Frank, 2014).

The system was tested by providing phase-locked stimulation at theta (4–8 Hz) and alpha (8–13 Hz) in mid-frontal and occipital human brain regions, respectively. The testing was performed during eyes closed EEG for alpha-band testing (5 min). For theta-band testing sessions (5 min), the participants played a computer-based reinforcement learning game (Frank et al., 2004, 2005). In this reinforcement learning game, participants were presented with pairs of Japanese characters and asked to choose one by pressing left or right key on a keyboard, followed by a visual feedback (won or lost) (Frank et al., 2004, 2005). 5 millisecond square-wave monophasic pulses of 2 mA current were delivered at 0, 90, 180, or 270 phase angle. Each stimulation (alpha and theta) was applied for 50 pulses for each of 0°, 90°, 180° and 270° phase angles. Phase-locking values for each band and phase-angle were computed as below, along with their distributions for each phase and band.

Participants

Participants were 5 healthy volunteers (3 male, 2 female, ages 27–30, mean age 28.0 ± 1.6 (mean ± SD), 2 left-handed). All recruitment, informed consent, and experimental procedures were approved by the Research Ethics Board of the University Health Network (UHN REB 16-5270) in accordance with the principles of the Declaration of Helsinki.

Analysis

To measure the phase of the underlying brain oscillation during the stimulation, the stimulation artifact was first removed and the signal interpolated using the methods described earlier. Then, the bandpass filter was applied. The phase of the EEG was measured as the angle of the Hilbert transformation during the stimulation pulse. We use polar histogram plots to visualize the phase of the stimulation compared to the phase of the underlying brain oscillations. Further, we calculated Phase Locking Value (PLV) (Equation 1) and the mean angle of the phase (Equation 2). PLV is a value between 0 and 1; higher PLV shows better phase locking. In these equations, φ is the phase angle of the underlying EEG frequency component of interest during the stimulation pulse, and N is the number of pulses used to calculate PLV and mean angle. All values in this manuscript are reported as mean ± standard deviation.

Equation 1:

$$\mathrm{PLV} = \left| \left| \frac{1}{N} \sum_{\mathrm{n}=1}^{\mathrm{N}} e^{\varphi_{\mathrm{n}} i} \right| \right|$$

Equation 2:

$$\mathit{Mean\ Angle} = \angle \left(\frac{1}{N} \sum_{\mathrm{n}=1}^{\mathrm{N}} e^{\varphi_{\mathrm{n}} i} \right)$$

RESULTS

Artifact Removal

As noted above, stimulation at arbitrary phase and frequency was applied to study the artifact duration and the artifact detection method. Pulses of 5ms duration were delivered at random intervals of 100–200 ms. Averaging 500 epochs of stimulation artifact recordings, time-locked to the onset of the stimulation pulse, illustrates the lasting effect of the artifact after the onset of the pulse (**Figure 2A**). Thus, our artifact removal method is set to remove 20 ms of the recording and interpolate the signal for that duration (**Figures 2B–D**).

System Timing Corrections

Alpha and theta stimulation were conducted on a healthy volunteer to test the system delays and calculate the angle corrections for each of the stimulations. The stimulation was applied for 300 pulses and the analysis showed that alpha stimulation is delayed 57 degrees, while theta stimulation is delayed 3.8 degrees (**Figure 3**). A PLV of 0.68 was found for theta stimulation, while alpha stimulation achieved a PLV of 0.75. For the subsequent testing work that followed these measurements, a timing correction was implemented in the system to compensate for the delays.

In vivo Demonstration

Both alpha and theta stimulation sessions were applied successfully in all 5 participants. The volunteers reported no pain

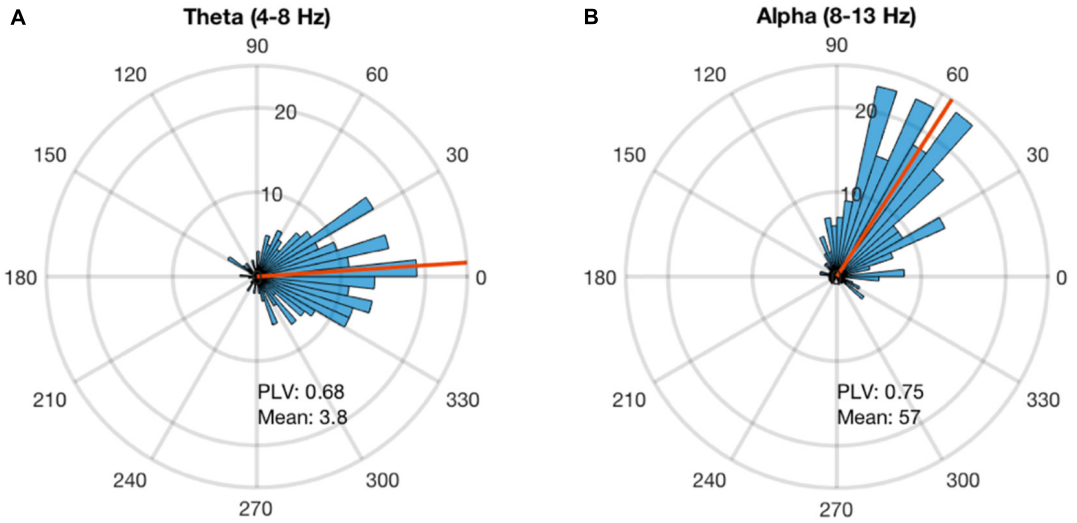

FIGURE 3 | Phase-locking delay for theta and alpha sessions. The phase-locked stimulation without any phase correction shows a constant delay. This delay is calculated for each stimulation frequency. **(A)** The stimulation at theta band for 300 pulses showed that the system has a delay of 3.8 degrees and PLV of 0.68. **(B)** The stimulation at alpha for 300 pulses showed that the system has a delay of 57 degrees and PLV of 0.68.

from the stimulation and there were no phosphene experiences reported. A minor tingling sensation was reported by 3 of the participants. All stimulation electrodes and the recording electrodes had impedances of smaller than 5 kΩ throughout the experiment.

A minimum of 0.34 PLV and maximum of 0.79 PLV and average of 0.55 ± 0.11 was achieved for theta stimulation. A minimum of 0.27 PLV and maximum of 0.75 PLV and average of 0.52 ± 0.14 was achieved for alpha stimulation. The average error in the angles were 11° ± 11° for theta and 3.3° ± 18° for alpha stimulation. Thus, the distribution of phase angles of stimulation for each of the 4 phase angles remained well within in their particular quadrant (i.e., with standard deviations 2.5–4 times smaller than ± 45° in each instance) (**Figure 4**).

DISCUSSION

Endogenous brain activity during stimulation is a key factor determining the effect of the stimulation (Herrmann et al.,

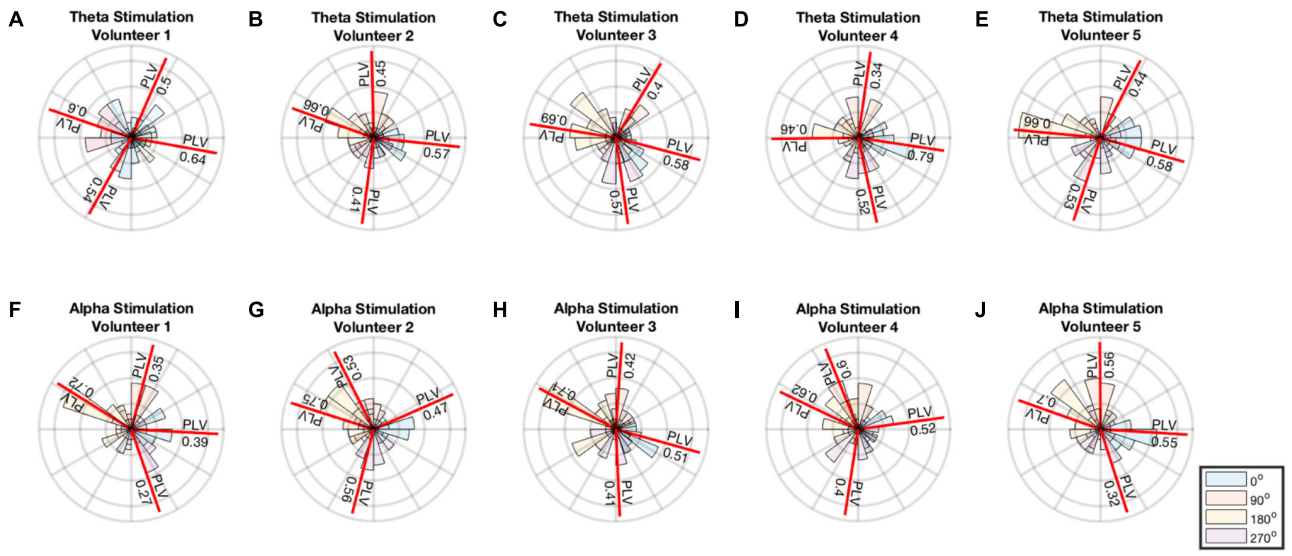

FIGURE 4 | (A–E) Polar histogram showing performance of theta stimulation in theta band for 4 different phase angles. **(F–J)** Polar histogram showing performance of theta stimulation in theta band for 4 different phase angles. The mean angle for each stimulation is shown by the red line and the PLV value is reported on the red line.

2013; Fröhlich, 2014). As a result, conventional 'open-loop' brain stimulation techniques such as rTMS, tDCS, or tACS that do not make efforts to synchronize their activity to the endogenous activity of the target brain region risk the possibility of an unwelcome heterogeneity in the magnitude, or even direction, of their effect. For example, nominally 'inhibitory' rTMS protocols such as 1 Hz or continuous theta-burst stimulation show the opposite effect (i.e., facilitation) in up to 50% of individuals; conversely, inhibitory effects are seen in a substantial proportion of subjects for nominally 'excitatory' rTMS protocols such as 10 Hz or intermittent theta-burst stimulation (Maeda et al., 2000; Hamada et al., 2013). Regarding one possible factor behind this heterogeneity, recent results indicate that phase-locking the stimulation in- or out-of-phase to the endogenous activity of the target can render a given protocol either inhibitory or excitatory (Zrenner et al., 2017), highlighting the importance of phase-locking specifically, and of the need for closed-loop brain stimulation methods in general. Closed-loop brain stimulation thus has the potential to overcome a major current hindrance to the effectiveness of neuromodulation techniques, by improving the potency and consistency of effect (Karabanov et al., 2016).

Here we have implemented a closed-loop brain stimulation that is suitable for operation in real time, targeting specific EEG bands of common interest in research and clinical settings: the theta and alpha EEG frequency bands. The methods introduced in this work demonstrate a functioning apparatus for the development and testing of stimulation phase effects on the underlying brain oscillation. The phase measurement of the stimulation from the recording would be unlikely to arise from a pick-up of the stimulation artifact, because this would mean that the phase measured would always be the same, and thus would not allow phase locking at 4 different phases, as illustrated in **Figure 4**. Using a simple apparatus whose components offer the advantages of low cost and wide availability, we developed a system that can analyze the EEG using our previously published algorithm (Mansouri et al., 2017) and provide real-time control of the stimulation. In this study, the analysis of the phase relies on a single channel recorded at the scalp location of interest. The technique is for this reason compatible with larger, higher-density arrays, but also works successfully in more limited arrays, as the present study illustrates. Using larger EEG systems would not affect performance of the proposed technique given that a single channel is used for input.

One major hurdle for closed-loop brain stimulation is the artifact introduced by the stimulator itself. Yet, despite extensive and inventive work to solve this problem (Kohli and Casson, 2015; Dowsett and Herrmann, 2016; Noury et al., 2016; Noury and Siegel, 2017, 2018; Kasten et al., 2018), to our knowledge there is still no effective solution for this issue that leverages inexpensive, routinely available components suitable for routine clinical/translational use. In the present work, we suggest that a viable workaround is to employ brief stimulation pulses (as is the case with rTMS, or brief-pulse tES) so as to minimize the proportion of samples affected by artifacts, and avoid using the segments of the recording that have been contaminated with the artifact. We used pulsed stimulation and showed that in our recording system, each 5 ms pulse of stimulation contaminates at most ∼20 ms of the recording. Considering that the target frequency bands have periods much larger than 20 ms, it is possible to use the recordings with missing 20 ms sections and still determine the phase and frequency of the underlying brain activity with good accuracy.

In this work, we have tested this system on theta and alpha bands, noting that these bands are often of interest in EEG and tACS studies (Jaušovec and Jaušovec, 2014; Pahor and Jaušovec, 2014; Vossen et al., 2015; Vosskuhl et al., 2015) and that they have long enough wavelengths to enable successful extraction of phase and frequency information even after artifact removal. Another feature of the present system lies in circumventing the effects of the artifact by applying the stimulation in a discontinuous mode. By introducing a delay between the stimulation pulses and providing enough recording time between the pulses, the artifact of the first stimulation pulse will not be present in the recordings used for estimating the timing of the next pulse. Of note, novel non-electromagnetic stimulation modalities, such as focused ultrasound (e.g., TPU), can be applied without contaminating the EEG signal with any artifact at all. Such forms of neuromodulation will perhaps eventually allow us to circumvent the problem of electromagnetic stimulation-induced artifacts altogether.

It is worth noting that signal processing components, such as the hardware filters used in EEG recording instruments, and the software filters applied to the signal during processing, can introduce frequency dependent delays to the recordings. Additionally, computation time delays and hardware delays communicating the stimulation instructions to the stimulator are inevitable. In this work, we addressed this issue by measuring the phase delay introduced by all the components of the combined system, and then applying a phase correction to achieve the desired stimulation phase. The execution time of the MATLAB code in this study was ∼1 ms. This delay is proximately constant and adjusted for through empirically calculated phase correction. Considering that the delay in the MATLAB computation time is two orders of magnitude smaller than the period of the oscillation of interest (∼100–200 ms), small changes in the computation time do not significantly affect the accuracy of the phase locking method. Using faster hardware and more optimized signal processing techniques can potentially reduce these delays, but not remove them entirely; thus, the phase delay lag should ideally be addressed via a phase-adjustment correction factor that can help improve the overall phase-locking performance of the system.

It is also important to note that the applicability of our approach is not limited to pulsed electrical stimulation; rather, it is also suitable for a number of pulsed stimulation techniques including rTMS, tES and TPU. The present method is applicable to any stimulation technique in which the stimulation pulses are brief compared to the overall period of the endogenous waveform of interest. For rTMS pulses, which are <1 ms in duration, the present method is suitable not only for theta- and alpha-band locking, but potentially also for higher-frequency bands of interest such as the beta or gamma bands. For low-field electromagnetic stimulation (Rohan et al., 2014) or transcranial

pulsed electromagnetic field stimulation (Martiny et al., 2010),the stimulation pulses are likewise much briefer than the period of the EEG bands of interest, and the present method may be applicable to enable phase-locked stimulation. Since the effects of phase and timing for these stimulation modalities are still only just beginning to be explored, the approach presented here may enable exploration of previously neglected dimensions of the parameter space for non-invasive brain stimulation protocols.

An important limitation of the present work, and a topic for future study, concerns the actual effects of this short-pulse (5 ms) ptES waveform on brain activity and behavior across a larger sample of individuals sufficient to generate an estimate of the distribution of performances in the general population. A future study will address this larger aim; the more limited purpose of the present study was to describe the technique and apparatus, and to demonstrate its successful use as proof of concept. Although in this study we were able to introduce a closed-loop brain stimulation method in a relatively small group, its effect on the target brain region's electrical oscillations themselves remains uncharacterized. In addition, the effect of the ptES on behavioral measures of brain function (e.g., working memory performance, or reaction times on a cued-response task) remains to be characterized in more detail. The available evidence to date suggests that short pulses of transcranial electrical stimulation, similar to those used in the present study, are indeed capable of modulating brain activity and behavior. For example, transcranial pulsed electrical stimulation can modulate spike and waves of seizures in an epileptic rat model (Berenyi et al., 2012). Furthermore, Alon et al. (2012) have shown acute improvement in gait and balance recovery in a Parkinson's disease population using this type of stimulation. Furthermore, pulsed stimulation has been recently shown to alter cognitive performance and heart rate variability (HRV) across a range of cognitive tasks (Morales-Quezada et al., 2015). In addition, Vasquez et al. (2016) showed pulsed stimulation significantly increases alpha and theta coherence in frontal regions. Nonetheless, the specific effects of in- and out-of-phase stimulation for the brief, 5 ms, 2 mA pulses of the present study on brain activity and behavior remain to be characterized in future studies.

In conclusion, there is mounting evidence that brain stimulation at different phases of the underlying brain oscillation can have quite different effects on brain activity and its behavioral sequelae (Polanía et al., 2012; Brittain et al., 2013; Riecke et al., 2015; Guerra et al., 2016; Nakazono et al., 2016). At the same time, research on the effects of phase-locked stimulation has been hampered by the challenges of recovering accurate EEG signal from a target brain region, while simultaneously stimulating that same region with sinusoidal waveforms, such as those used in tACS. The workaround of the present study is to apply brief, square-wave tES pulses, such that the artifact is limited to only a small proportion of samples and the phase information can still be recovered from the EEG signal with good accuracy. A system composed of readily available, off-the-shelf components can recover the phase information using this method, and can apply it in real time to control pulse timing, while compensating for processing lags to maintain phase-locked stimulation in both the alpha and the theta bands. This work therefore presents a straightforward and inexpensive, yet viable, approach to achieving closed-loop, phase-locked brain stimulation. With further validation, this method may allow a systematic assessment of the effect of phase-locking on the neurobiological and behavioral effects of ptES in both healthy volunteers and patient populations. If phase-locking can indeed reduce the heterogeneity of effect for non-invasive brain stimulation, then there may be potential for marked increases in the efficacy of tES, rTMS, and other brain stimulation techniques in the years to come.

AUTHOR CONTRIBUTIONS

All authors listed have made a substantial, direct and intellectual contribution to the work, and approved it for publication.

FUNDING

This work was supported by a MITACS Accelerate Grant (#IT05799) to author FM.

REFERENCES

Alon, G., Yungher, D. A., Shulman, L. M., and Rogers, M. W. (2012). Safety and immediate effect of noninvasive transcranial pulsed current stimulation on gait and balance in parkinson disease. *Neurorehabil. Neural Repair* 26, 1089–1095. doi: 10.1177/1545968312448233

Berenyi, A., Belluscio, M., Mao, D., and Buzsaki, G. (2012). Closed-loop control of epilepsy by transcranial electrical stimulation. *Science* 337, 735–737. doi: 10.1126/science.1223154

Brittain, J. S., Probert-Smith, P., Aziz, T. Z., and Brown, P. (2013). Tremor suppression by rhythmic transcranial current stimulation. *Curr. Biol.* 23, 436–440. doi: 10.1016/j.cub.2013.01.068

Cavanagh, J. F., and Frank, M. J. (2014). Frontal theta as a mechanism for cognitive control. *Trends Cogn. Sci.* 18, 414–421. doi: 10.1016/j.tics.2014.04.012

Chung, S. W., Sullivan, C. M., Rogasch, N. C., Hoy, K. E., Bailey, N. W., Cash, R. F. H., et al. (2018). The effects of individualised intermittent theta burst stimulation in the prefrontal cortex: a TMS-EEG study. *Hum. Brain Mapp.* doi: 10.1002/hbm.24398 [Epub ahead of print].

Dowsett, J., and Herrmann, C. S. (2016). Transcranial alternating current stimulation with sawtooth waves: simultaneous stimulation and EEG recording. *Front. Hum. Neurosci.* 10:135. doi: 10.3389/fnhum.2016.00135

Frank, M. J., Seeberger, L. C., and O'Reilly, R. C. (2004). By carrot or by stick: cognitive reinforcement learning in Parkinsonism. *Science* 306, 1940–1943. doi: 10.1126/science.1102941

Frank, M. J., Woroch, B. S., and Curran, T. (2005). Error-related negativity predicts reinforcement learning and conflict biases. *Neuron* 47, 495–501. doi: 10.1016/j.neuron.2005.06.020

Fröhlich, F. (2014). Endogenous and exogenous electric fields as modifiers of brain activity: rational design of noninvasive brain stimulation with transcranial alternating current stimulation. *Dialogues Clin. Neurosci.* 16, 93–102.

Fröhlich, F., and McCormick, D. A. (2010). Endogenous electric fields may guide neocortical network activity. *Neuron* 67, 129–143. doi: 10.1016/j.neuron.2010.06.005

Guerra, A., Pogosyan, A., Nowak, M., Tan, H., Ferreri, F., Di Lazzaro, V., et al. (2016). Phase dependency of the human primary motor cortex and cholinergic

inhibition cancelation during beta tACS. *Cereb. Cortex* 26, 3977–3990. doi: 10.1093/cercor/bhw245

Hallett, M. (2000). Transcranial magnetic stimulation and the human brain. *Nature* 406, 147–150. doi: 10.1038/35018000

Hallett, M. (2007). Transcranial magnetic stimulation: a primer. *Neuron* 55, 187–199. doi: 10.1016/j.neuron.2007.06.026

Hamada, M., Murase, N., Hasan, A., Balaratnam, M., and Rothwell, J. C. (2013). The role of interneuron networks in driving human motor cortical plasticity. *Cereb. Cortex* 23, 1593–1605. doi: 10.1093/cercor/bhs147

Herrmann, C. S., Rach, S., Neuling, T., and Strüber, D. (2013). Transcranial alternating current stimulation: a review of the underlying mechanisms and modulation of cognitive processes. *Front. Hum. Neurosci.* 7:279. doi: 10.3389/fnhum.2013.00279

Hyman, J. M., Wyble, B. P., Goyal, V., Rossi, C. A., and Hasselmo, M. E. (2003). Stimulation in hippocampal region CA1 in behaving rats yields long-term potentiation when delivered to the peak of theta and long-term depression when delivered to the trough. *J. Neurosci.* 23, 11725–11731. doi: 10.1523/JNEUROSCI.23-37-11725.2003

Jaušovec, N., and Jaušovec, K. (2014). Increasing working memory capacity with theta transcranial alternating current stimulation (tACS). *Biol. Psychol.* 96, 42–47. doi: 10.1016/j.biopsycho.2013.11.006

Karabanov, A., Thielscher, A., and Siebner, H. R. (2016). Transcranial brain stimulation: closing the loop between brain and stimulation. *Curr. Opin. Neurol.* 29, 397–404. doi: 10.1097/WCO.0000000000000342

Kasten, F. H., Negahbani, E., Fröhlich, F., and Herrmann, C. S. (2018). Non-linear transfer characteristics of stimulation and recording hardware account for spurious low-frequency artifacts during amplitude modulated transcranial alternating current stimulation (AM-tACS). *Neuroimage* 179, 134–143. doi: 10.1016/j.neuroimage.2018.05.068

Kohli, S., and Casson, A. J. (2015). Removal of Transcranial a.c. Current Stimulation artifact from simultaneous EEG recordings by superposition of moving averages. *Proc. Annu. Int. Conf. IEEE Eng. Med. Biol. Soc. EMBS* 2015, 3436–3439. doi: 10.1109/EMBC.2015.7319131

Kuo, M.-F., Paulus, W., and Nitsche, M. A. (2014). Therapeutic effects of non-invasive brain stimulation with direct currents (tDCS) in neuropsychiatric diseases. *Neuroimage* 85, 948–960. doi: 10.1016/j.neuroimage.2013.05.117

Lehmann, D. (1971). Multichannel topography of human alpha EEG fields. *Electroencephalogr. Clin. Neurophysiol.* 31, 439–449. doi: 10.1016/0013-4694(71)90165-9

Maeda, F., Keenan, J. P., Tormos, J. M., Topka, H., and Pascual-Leone, A. (2000). Interindividual variability of the modulatory effects of repetitive transcranial magnetic stimulation on cortical excitability. *Exp. Brain Res.* 133, 425–430. doi: 10.1007/s002210000432

Mansouri, F., Dunlop, K., Giacobbe, P., Downar, J., and Zariffa, J. (2017). A fast EEG forecasting algorithm for phase-locked transcranial electrical stimulation of the human brain. *Front. Neurosci.* 11:401. doi: 10.3389/fnins.2017.00401

Mansouri, F., Mir-Moghtadaei, A., Niranjan, V., Wu, J. S., Akhmedjanov, D., Nuh, M., et al. (2018). Development and validation of a 3d-printed neuronavigation headset for therapeutic brain stimulation. *J. Neural Eng.* 15, 046034. doi: 10.1088/1741-2552/aacb96

Martiny, K., Lunde, M., and Bech, P. (2010). Transcranial low voltage pulsed electromagnetic fields in patients with treatment-resistant depression. *Biol. Psychiatry* 68, 163–169. doi: 10.1016/j.biopsych.2010.02.017

McNames, J., Thong, T., and Aboy, M. (2004). Impulse rejection filter for artifact removal in spectral analysis of biomedical signals. *Conf. Proc. IEEE Eng. Med. Biol. Soc.* 1, 145–148.

Morales-Quezada, L., Cosmo, C., Carvalho, S., Leite, J., Castillo-Saavedra, L., Rozisky, J. R., et al. (2015). Cognitive effects and autonomic responses to transcranial pulsed current stimulation. *Exp. Brain Res.* 233, 701–709. doi: 10.1007/s00221-014-4147-y

Nakazono, H., Ogata, K., Kuroda, T., and Tobimatsu, S. (2016). Phase and frequency-dependent effects of transcranial alternating current stimulation on motor cortical excitability. *PLoS One* 11:e0162521. doi: 10.1371/journal.pone.0162521

Nitsche, M. A., and Paulus, W. (2000). Excitability changes induced in the human motor cortex by weak transcranial direct current stimulation. *J. Physiol.* 527, 633–639. doi: 10.1111/j.1469-7793.2000.t01-1-00633.x

Noury, N., Hipp, J. F., and Siegel, M. (2016). Physiological processes non-linearly affect electrophysiological recordings during transcranial electric stimulation. *Neuroimage* 140, 99–109. doi: 10.1016/j.neuroimage.2016.03.065

Noury, N., and Siegel, M. (2017). Phase properties of transcranial electrical stimulation artifacts in electrophysiological recordings. *Neuroimage* 158, 406–416. doi: 10.1016/j.neuroimage.2017.07.010

Noury, N., and Siegel, M. (2018). Analyzing EEG and MEG signals recorded during tES, a reply. *Neuroimage* 167, 53–61. doi: 10.1016/j.neuroimage.2017.11.023

Ohn, S. H., Park, C.-I., Yoo, W.-K., Ko, M.-H., Choi, K. P., Kim, G.-M., et al. (2008). Time-dependent effect of transcranial direct current stimulation on the enhancement of working memory. *Neuroreport* 19, 43–47. doi: 10.1097/WNR.0b013e3282f2adfd

Pahor, A., and Jaušovec, N. (2014). The effects of theta transcranial alternating current stimulation (tACS) on fluid intelligence. *Int. J. Psychophysiol.* 93, 322–331. doi: 10.1016/j.ijpsycho.2014.06.015

Park, H.-J., and Friston, K. (2013). Structural and functional brain networks: from connections to cognition. *Science* 342:1238411. doi: 10.1126/science.1238411

Paulus, W. (2011). Transcranial electrical stimulation (tES - tDCS; tRNS, tACS) methods. *Neuropsychol. Rehabil.* 21, 602–617. doi: 10.1080/09602011.2011.557292

Pessoa, L. (2014). Understanding brain networks and brain organization. *Phys. Life Rev.* 11, 400–435. doi: 10.1016/j.plrev.2014.03.005

Polanía, R., Nitsche, M. A., Korman, C., Batsikadze, G., and Paulus, W. (2012). The importance of timing in segregated theta phase-coupling for cognitive performance. *Curr. Biol.* 22, 1314–1318. doi: 10.1016/j.cub.2012.05.021

Polanía, R., Nitsche, M. A., and Ruff, C. C. (2018). Studying and modifying brain function with non-invasive brain stimulation. *Nat. Neurosci.* 21, 174–187. doi: 10.1038/s41593-017-0054-4

Reato, D., Rahman, A., Bikson, M., and Parra, L. C. (2013). Effects of weak transcranial alternating current stimulation on brain activity—a review of known mechanisms from animal studies. *Front. Hum. Neurosci.* 7:687. doi: 10.3389/fnhum.2013.00687

Renard, Y., Lotte, F., Gibert, G., Congedo, M., Maby, E., Delannoy, V., et al. (2010). OpenViBE: an open-source software platform to design, test, and use brain-computer interfaces in real and virtual environments. *Presence Teleoperators Virtual Environ.* 19, 35–53. doi: 10.1162/pres.19.1.35

Riecke, L., Formisano, E., Herrmann, C. S., and Sack, A. T. (2015). 4-Hz transcranial alternating current stimulation phase modulates hearing. *Brain Stimul.* 8, 777–783. doi: 10.1016/j.brs.2015.04.004

Rohan, M. L., Yamamoto, R. T., Ravichandran, C. T., Cayetano, K. R., Morales, O. G., Olson, D. P., et al. (2014). Rapid mood-elevating effects of low field magnetic stimulation in depression. *Biol. Psychiatry* 76, 186–193. doi: 10.1016/j.biopsych.2013.10.024

Schulz, R., Gerloff, C., and Hummel, F. C. (2013). Non-invasive brain stimulation in neurological diseases. *Neuropharmacology* 64, 579–587. doi: 10.1016/j.neuropharm.2012.05.016

Seager, M. A., Johnson, L. D., Chabot, E. S., Asaka, Y., and Berry, S. D. (2002). Oscillatory brain states and learning: impact of hippocampal theta-contingent training. *Proc. Natl. Acad. Sci. U.S.A.* 99, 1616–1620. doi: 10.1073/pnas.032662099

Silvanto, J., Muggleton, N., and Walsh, V. (2008). State-dependency in brain stimulation studies of perception and cognition. *Trends Cogn. Sci.* 12, 447–454. doi: 10.1016/j.tics.2008.09.004

Tufail, Y., Yoshihiro, A., Pati, S., Li, M. M., and Tyler, W. J. (2011). Ultrasonic neuromodulation by brain stimulation with transcranial ultrasound. *Nat. Protoc.* 6, 1453–1470. doi: 10.1038/nprot.2011.371

Utz, K. S., Dimova, V., Oppenländer, K., and Kerkhoff, G. (2010). Electrified minds: transcranial direct current stimulation (tDCS) and Galvanic Vestibular Stimulation (GVS) as methods of non-invasive brain stimulation in neuropsychology-A review of current data and future implications. *Neuropsychologia* 48, 2789–2810. doi: 10.1016/j.neuropsychologia.2010.06.002

Vasquez, A., Malavera, A., Doruk, D., Morales-Quezada, L., Carvalho, S., Leite, J., et al. (2016). Duration dependent effects of transcranial pulsed current stimulation (tPCS) indexed by electroencephalography. *Neuromodulation* 19, 679–688. doi: 10.1111/ner.12457

Vossen, A., Gross, J., and Thut, G. (2015). Alpha power increase after transcranial alternating current stimulation at alpha frequency (a-tACS) reflects plastic changes rather than entrainment. *Brain Stimul.* 8, 499–508. doi: 10.1016/j.brs.2014.12.004

Vosskuhl, J., Huster, R. J., and Herrmann, C. S. (2015). Increase in short-term memory capacity induced by down-regulating individual theta frequency via transcranial alternating current stimulation. *Front. Hum. Neurosci.* 9:257. doi: 10.3389/fnhum.2015.00257

Waddell, C., Pratt, J. A., Porr, B., and Ewing, S. (2009). "Deep brain stimulation artifact removal through under-sampling and cubic-spline interpolation," in *Proceedings of the 2nd Int Congr Image Signal Process CISP'09 2009* (Piscataway, NJ: IEEE).

Zanos, S., Rembado, I., Chen, D., and Fetz, E. E. (2018). Phase-locked stimulation during cortical beta oscillations produces bidirectional synaptic plasticity in awake monkeys. *Curr. Biol.* 28, 2515.e4–2526.e4. doi: 10.1016/j.cub.2018.07.009

Zrenner, C., Desideri, D., Belardinelli, P., and Ziemann, U. (2017). Real-time EEG-defined excitability states determine efficacy of TMS-induced plasticity in human motor cortex. *Brain Stimul.* 11, 374–389. doi: 10.1016/j.brs.2017.11.016

Conflict of Interest Statement: The authors declare that the research was conducted in the absence of any commercial or financial relationships that could be construed as a potential conflict of interest.

frontiers in Neuroscience

ORIGINAL RESEARCH
published: 13 December 2018
doi: 10.3389/fnins.2018.00949

Increasing Human Performance by Sharing Cognitive Load Using Brain-to-Brain Interface

Vladimir A. Maksimenko[1], Alexander E. Hramov[1], Nikita S. Frolov[1], Annika Lüttjohann[2], Vladimir O. Nedaivozov[1], Vadim V. Grubov[1], Anastasia E. Runnova[1], Vladimir V. Makarov[1], Jürgen Kurths[3,4,5] and Alexander N. Pisarchik[1,6]**

[1] REC "Artificial Intelligence Systems and Neurotechnology", Yuri Gagarin State Technical University of Saratov, Saratov, Russia, [2] Institute of Physiology I, University of Münster, Münster, Germany, [3] Potsdam Institute for Climate Impact Research, Potsdam, Germany, [4] Department of Physics, Humboldt University, Berlin, Germany, [5] Institute for Complex Systems and Mathematical Biology, University of Aberdeen, Aberdeen, United Kingdom, [6] Center for Biomedical Technology, Technical University of Madrid, Madrid, Spain

OPEN ACCESS

Edited by:
Giovanni Mirabella,
Sapienza University of Rome, Italy

Reviewed by:
Mikhail Lebedev,
Duke University, United States
M. Van Hulle,
KU Leuven, Belgium
Aleksandra Vuckovic,
University of Glasgow,
United Kingdom

***Correspondence:**
Vladimir A. Maksimenko
maximenkovl@gmail.com
Alexander N. Pisarchik
alexander.pisarchik@ctb.upm.es

Specialty section:
This article was submitted to Neural Technology, a section of the journal Frontiers in Neuroscience

Received: 20 July 2018
Accepted: 29 November 2018
Published: 13 December 2018

Citation:
Maksimenko VA, Hramov AE, Frolov NS, Lüttjohann A, Nedaivozov VO, Grubov VV, Runnova AE, Makarov VV, Kurths J and Pisarchik AN (2018) Increasing Human Performance by Sharing Cognitive Load Using Brain-to-Brain Interface. Front. Neurosci. 12:949. doi: 10.3389/fnins.2018.00949

Brain-computer interfaces (BCIs) attract a lot of attention because of their ability to improve the brain's efficiency in performing complex tasks using a computer. Furthermore, BCIs can increase human's performance not only due to human-machine interactions, but also thanks to an optimal distribution of cognitive load among all members of a group working on a common task, i.e., due to human-human interaction. The latter is of particular importance when sustained attention and alertness are required. In every day practice, this is a common occurrence, for example, among office workers, pilots of a military or a civil aircraft, power plant operators, etc. Their routinely work includes continuous monitoring of instrument readings and implies a heavy cognitive load due to processing large amounts of visual information. In this paper, we propose a brain-to-brain interface (BBI) which estimates brain states of every participant and distributes a cognitive load among all members of the group accomplishing together a common task. The BBI allows sharing the whole workload between all participants depending on their current cognitive performance estimated from their electrical brain activity. We show that the team efficiency can be increased due to redistribution of the work between participants so that the most difficult workload falls on the operator who exhibits maximum performance. Finally, we demonstrate that the human-to-human interaction is more efficient in the presence of a certain delay determined by brain rhythms. The obtained results are promising for the development of a new generation of communication systems based on neurophysiological brain activity of interacting people. Such BBIs will distribute a common task between all group members according to their individual physical conditions.

Keywords: brain-computer interface (BCI), brain-to-brain interface (BBI), human-to-human interaction, visual attention, brain states recognition, cognitive performance, cognitive reserve, mental fatigue

1. INTRODUCTION

The brain-computer interface (BCI) development is a novel multidisciplinary research topic in neuroscience, physics and engineering. Many applications, including medicine, industry, robotics, etc. (Chen et al., 2015; Bowsher et al., 2016; Kawase et al., 2017; Spüler, 2017; Maksimenko et al., 2017a) are in dire need of this modern technology. The BCI is based on the characteristic forms of electrical or magnetic brain activity and their real-time transformation into computer commands. Today, the developed neuro-computer interfaces allow controlling a cursor 2D movement (Wolpaw and McFarland, 2004, partially synthesize speech Birbaumer et al., 1999, and simplest human movements Ma et al., 2017). The BCIs can be effectively used in neuroprosthetics Ma et al. (2017), rehabilitation Daly and Wolpaw (2008), exoskeletons Kawase et al. (2017), and robots Peternel et al. (2016). In addition, recent advances in cognitive neuroscience provide the possibility of using BCIs for enhancing cognitive abilities and treating mental disorders (Hillard et al., 2013). Moreover, BCIs are expected to enhance human performance, such as to shorten reaction time, to improve error processing and unsupervised learning (Mirabella and Lebedev, 2016), etc.

Since the main goal of BCI is to repair and/or increase human performance in solving different tasks (Zander and Kothe, 2011; Chaudhary et al., 2016), the machine controlled by the brain activity takes a part of the cognitive or physical human load. Similarly to the human-machine interaction, a human-to-human interaction can be improved by enhancing human collaboration with the help of BCI. In this situation, the machine component of traditional BCI can be replaced by another human linked to the first one by an interface, whose assistance would enhance the subject performance in managing a particular task. Such a brain-to-brain interface (BBI) would be very helpful for a group of people subjected to a common task which requires sustained attention. In everyday practice, this is a common occurrence, for example, among office workers, pilots of military (Estrada et al., 2012) or civil aircrafts (Sallinen et al., 2017), power plant operators, and other teams, whose routine work includes continuous monitoring of instrument readings, and requires sustained alertness and concentration (Baker et al., 1990; Jensen, 1999; Takahashi et al., 2005). The human-to-human interaction through computers could help the members of such groups to effectively interact by estimating and monitoring physical conditions of each person, in particular, degree of alertness, in order to distribute workloads among all participants according to their current physiological status.

In this paper, we propose a special BBI to heighten human-to-human interaction while performing a common collective task. The efficiency of the proposed BBI is estimated in experimental sessions, where the participants perform a prolonged task of classification of bistable visual stimuli of different degree of ambiguity. In bistable perception, the ambiguity is related to the probability of different interpretations of the presented image; highest ambiguity results in about 50% probability. In our experiment, we explore a classical example of visual ambiguous stimuli, the Necker cube (see **Figure 1**). This bistable image is very convenient for research, because unlike other ambiguous images, its ambiguity can be adjusted by varying the control parameter $g \in [0, 1]$ related to the contrast of the inner ribs, which define the volume structure of this 2D image. The values $g = 0$ and $g = 1$ correspond to unambiguous left- and right-oriented cubes, respectively. The parameter g controls the probability of the cube orientation interpretation. For instance, the probability of the left-oriented cube interpretation is 100% when $g = 0$ and 0% when $g = 1$. We assume that the complexity of the cognitive task in the cube classification as left or right oriented one is closely related to the cube ambiguity. Evidently, the stimuli with low ambiguity can be classified easier than the stimuli with high ambiguity (see section 2.). Therefore, the classification of unambiguous or weakly ambiguous images is considered as a low-complexity (LC) task, whereas the classification of highly ambiguous images as a high-complexity (HC) task.

TABLE 1 | Parameters of the experiment.

Parameter	Value
Time interval of visual stimuli presentation	randomly chosen between 1 and 1.5 s
Time interval between visual stimuli presentations	randomly chosen between 3 and 5 s
Number of presented visual stimuli	200
Total duration of experimental session	30 min
Location of EEG scalp electrodes	International 10–20 system
EEG recording sampling rate	250 Hz
EEG recording filtering	1–30 Hz
Considered EEG channels	O_1, O_2, P_3, P_4, P_z
Considered EEG bands	α-waves (8–12 Hz), β-waves (15–30 Hz)

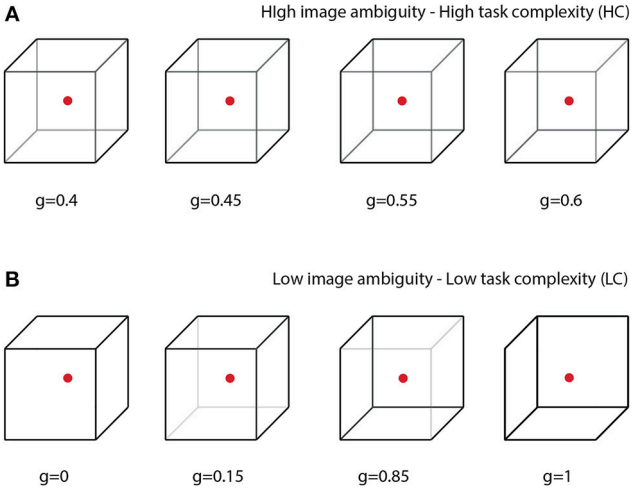

FIGURE 1 | Complete set of visual stimuli split into two sets: **(A)** cubes with high degree of ambiguity representing tasks of high complexity (HC) and **(B)** cubes with low degree of ambiguity representing tasks of low complexity (LC).

2. MATERIALS AND METHODS

2.1. Participants

Twenty healthy unpaid volunteers, 12 males and 8 females, between the ages of 20 and 43 with normal or corrected-to-normal visual acuity participated in the experiment. All of them provided informed written consent before participating. The experimental studies were performed in accordance with the Declaration of Helsinki and approved by the local research Ethics Committee of the Yuri Gagarin State Technical University of Saratov. The participants did not exhibit substantial differences in factors characterizing properties of attention according to the results of psychodiagnostic tests (Maksimenko et al., 2018).

2.2. Visual Task

All participants were subjected to the visual task of classification of consistently presented Necker cubes as left- or right-oriented (**Figure 1**). The Necker cube (Necker Esq, 1832) is a popular object of many psychological experiments (Mathes et al., 2006; Kornmeier et al., 2011; Pisarchik et al., 2014). An observer without any perceptional abnormalities perceives the Necker cube as a bistable 3D-object due to the specific position of the cube's ribs. Bistability in perception consists in interpretation of the cube orientation, depending on the contrasts of the inner ribs. To control the cube ambiguity, we used the normalized value $g = y/255 \in [0, 1]$, where y is the brightness of three inner lines centered in the left middle corner (according to the 8-bit grayscale palette) (Runnova et al., 2016; Hramov et al., 2017). The values $g = 1$ and $g = 0$ correspond, respectively, to 0 (black) and 255 (white) pixels' luminance of these lines. The Necker cube images with different g were created using a standard graphics software. One can see that the parameter g controls the cube orientation. Along with samples of unambiguous left- ($g = 0$) or right- ($g = 1$) oriented cubes, as well as a fully ambiguous cube ($g = 0.5$), we successively presented cubes of various ambiguity with ($0 < g < 0.5$) and ($0.5 < g < 1$), each of which differed from the previous one.

The value of g was considered as a *degree of complexity* in the cube classification, because the cubes with g close to 1 or 0 can easily be interpreted as left- or right-oriented, respectively, whereas the interpretation of the cubes with g close to 0.5 is a more complex task. According to the difficulty of the classification task, the whole set of the presented stimuli with $g = (0, 0.15, 0.4, 0.45, 0.55, 0.6, 0.85, 1)$ was split into two subsets: the task of high complexity (HC) to classify highly ambiguous images with $g = (0.4, 0.45, 0.55, 0.6)$ (**Figure 1A**) and the task of low complexity (LC) to classify weakly ambiguous cubes with $g = (0, 0.15, 0.85, 1)$ (see **Figure 1B**). The subjects were asked to classify the cubes as left/right oriented according to their first impression.

2.3. Experimental Procedure

All participants were instructed to press either left or right key depending on their first impression on the cube orientation at each presentation, the left key when they saw the left-oriented cube and the right key otherwise. The subjects were randomly divided into 10 pairs. Each pair was subjected to two different experiments: EXP1 and EXP2, both containing two sessions: session 1 (S1) and session 2 (S2), each lasted 30 min. In S1, the cubes with randomly selected g were simultaneously presented to both subjects in each pair; every set of stimuli was presented for about 30 times. In S2, the whole set of stimuli was split into two subsets: stimuli with high ambiguity (HC) (see **Figure 1A**) and stimuli with low ambiguity (LC) (see **Figure 1B**), and cubes from different subsets were presented depending on brain responses of the participants.

- EXP1: S1–both subjects simultaneously observed the same cubes, randomly selected from a whole set of stimuli; S2–task complexity was distributed among participants based on their instantaneous alertness; the subject with higher alertness received a HC stimulus, while his/her partner received a LC stimulus. S2 was associated with human-human interaction through a non-delayed coupling, i.e., task complexity was distributed based on instantaneous alertness of the participants.
- EXP2: S1–both subjects simultaneously observed the same cubes, randomly selected from a whole set of stimuli (the same as in EXP1); S2–the subject with higher alertness received HC stimuli, while his/her partner received LC stimuli only in the case when the difference between their degrees of alertness became >10%. S2 was associated with delayed coupling between the participants because the task was not switched immediately.

In addition, we carried out a third experiment, where subjects were not arranged in pairs, but each performed the individual classification task. This additional experiment also consisted of two sessions, each lasted 30 min, during which the participant observed low ambiguous stimuli (in the first session) and high ambiguous stimuli (in the second session). Other parameters of the experiment are shown in **Table 1**.

2.4. EEG Recording

To record EEG data, we used cup adhesive Ag/AgCl electrodes placed on the "Tien–20" paste. Immediately before the experiments started, we performed all necessary procedures to increase the conductivity of the skin and reduce its resistance using abrasive "NuPrep" gel. The impedance values were measured after the electrodes were installed, and monitored during the experiments. Usually, the impedance varied in the interval of 2–5 kΩ. The ground electrode N was located in front of the head at the Fpz electrode location. The EEG signals were filtered by a band-pass filter with cut-off points at 1 Hz (HP), both 100-Hz (LP) and 50-Hz Notch filters. The electroencephalograph "Encephalan-EEGR-19/26" (Medicom MTD company, Taganrog, Russian Federation) with multiple EEG channels and two-button input device (keypad) was used for amplification and analog-to-digital conversion of the EEG signals. This device possessed the registration certificate of the Federal Service for Supervision in Health Care No. FCP 2007/00124 of 07.11.2014 and the European Certificate CE 538571 of the British Standards Institute (BSI).

To diminish artifacts of the muscular origin, we asked the participants to take a pose which excluded excessive tension of neck muscles. Recent studies showed that these

artifacts affect time frequency properties in occipital area in the spectral bandwidth of muscle activity (∼20–300 Hz) (Muthukumaraswamy, 2013). It is slightly overlapped with the frequency band of 1–30 Hz explored in the present work. On the other hand, the amplitude of muscular artifacts in the occipital area was strongly related to the subject's posture during experiment. Since we only estimated relative changes in spectral properties during time intervals when the stimuli were presented with respect to the intervals when the subject did not receive the stimuli, the effect of muscular artifacts uncorrelated with the stimuli presentation was not strong.

2.5. Estimation of the Brain Response

The perception of visual stimuli is known to be associated with an increase in the electrical activity in visual areas in the occipital lobe (Mulckhuyse, 2011; Gleiss and Kayser, 2014) and attentional areas in the parietal lobe (Laufs, 2006). Therefore, the most informative channels are in these lobes. This allowed us to restrict our analysis to the EEG recordings from five electrodes only (O_1, O_2, P_3, P_4, P_z), located in the occipital (O1 and O2) and parietal (P3, P4, Pz) lobes according to the 10–20 electrode layout (Niedermeyer and da Silva, 2014), to be able to perform fast analysis in real time.

The EEG data was analyzed using the continuous wavelet transform (Pavlov et al., 2012). The wavelet energy spectrum $E^n(f,t) = \sqrt{W_n(f,t)^2}$ was calculated for each EEG channel $X_n(t)$ in the $f \in [1,30]$-Hz frequency range. Here, $W_n(f,t)$ is the complex-valued wavelet coefficients calculated as

$$W_n(f,t) = \sqrt{f} \int_{t-4/f}^{t+4/f} X_n(t)\psi^*(f,t)dt, \quad (1)$$

where $n = 1,...,N$ is the EEG channel number ($N = 5$ being the total number of channels used for the analysis) and "$*$" defines the complex conjugation. The mother wavelet function $\psi(f,t)$ is the Morlet wavelet often used for the analysis of neurophysiological data, defined as

$$\psi(f,t) = \sqrt{f}\pi^{1/4} e^{j\omega_0 f(t-t_0)} e^{f(t-t_0)^2/2}, \quad (2)$$

where $\omega_0 = 2\pi$ is the central frequency of the Morlet mother wavelet (Sitnikova et al., 2014).

Every EEG signal associated with the presentation of a single visual stimulus was analyzed separately in the alpha and beta frequency bands during a 1-s interval preceding the presentation (τ_i^1) and a 1-s interval followed by the moment of the stimulus presentation (τ_i^2) (**Figure 2**). A special software controlled digital triggering to initiate the calculation process together with stimulus presentation.

As a result, the values A_i^1, A_i^2, B_i^1, B_i^2 were calculated for each i-th presentation as

$$A_i^{1,2} = \sum_{n=1}^{N} \int_{t\in\tau_i^{1,2}} \xi^n(t')dt', \quad (3)$$

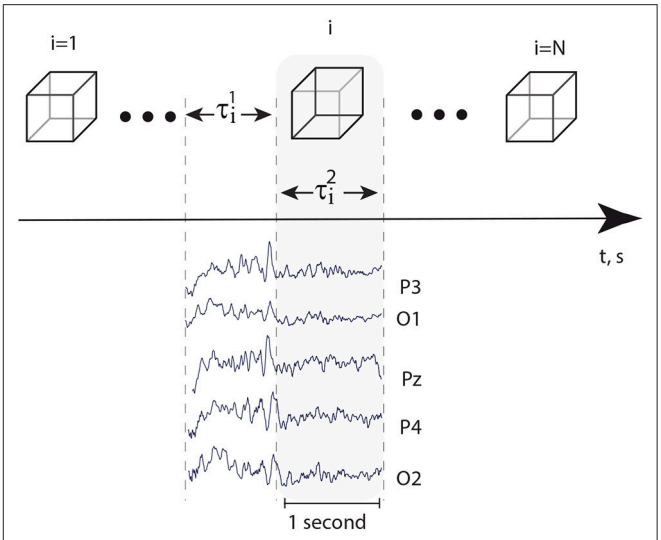

FIGURE 2 | Top: successively presented visual stimuli and time intervals $\tau_i^1 = 1$ s and $\tau_i^2 = 1$ s, preceded stimuli presentation and followed immediately by the moment of stimulus presentation, respectively. **Bottom:** typical EEG traces registered in occipital area during time intervals τ_i^1 and τ_i^2.

$$B_i^{1,2} = \sum_{n=1}^{N} \int_{t\in\tau_i^{1,2}} \xi^n(t')dt', \quad (4)$$

where

$$\xi^n(t) = \begin{cases} 1, \text{ if } f_{max}^n \in \Delta f_{\alpha,\beta}, \\ 0, \text{ if } f_{max}^n \notin \Delta f_{\alpha,\beta}, \end{cases} \quad (5)$$

where $N = 5$ is the number of EEG channels and f_{max}^n is the location of the maximal spectral component. The values given by Equations (3, 4) quantify neural activity in α- and β-frequency bands. According to the recent work (Maksimenko et al., 2018), visual attention is related to the interplay between these bands in occipital and parietal areas. In particular, changes in α-activity are associated with visual (Sauseng et al., 2005) or auditory attention (Foxe and Snyder, 2011), while changes in β-activity are associated with stimuli processing (Sehatpour et al., 2008) and switching the brain to an attention state (Wróbel, 2000; Gola et al., 2013). The role of alpha and beta activity in the perceptual process is also highlighted in Michalareas et al. (2016) in the context of information transfer in visual areas.

The control characteristic $I(i)$ was calculated as follows

$$I(i) = \frac{(a_i^1 - a_i^2) - (b_i^2 - b_i^1)}{2}, \quad (6)$$

where $a_i^{1,2}$ and $b_i^{1,2}$ were obtained as

$$a_i^{1,2} = \frac{1}{6}\sum_{n=i-6}^{i} A_n^{1,2}, \quad (7)$$

$$b_i^{1,2} = \frac{1}{6}\sum_{n=i-6}^{i} B_n^{1,2} \quad (8)$$

by averaging $A_i^{1,2}$ and $B_i^{1,2}$ values over six presentations.

The value of $I(i)$ calculated in real time using Equation (6) reflects the intensity of the brain response on the appearing visual stimuli. Large $I(i)$ is associated with a high response due to more careful image processing by the subject, whereas small $I(i)$ is related to a low response, which takes place when the subject does not pay much attention on the classification task.

The design of our algorithm allowed us to take into account changes in the time-frequency EEG structure associated with the stimulus perception and neglect the influence of unrelated oscillations, e.g., muscular artifacts which occurred in the EEG signals at the moments uncorrelated with the stimuli presentation.

2.6. Brain-to-Brain Interface (BBI)

The scheme of the proposed BBI is illustrated in **Figure 3A**. The BBI performs human-to-human interaction in the following way:

- The stimulus (Necker cube) is simultaneously presented to a pair of operators (subject 1 and subject 2) on the corresponding client personal computers (PC1 for subject 1 and PC2 for subject 2). Each subject is able to see only his/her screen, but not the screen of another subject.
- Subjects' EEGs are simultaneously recorded and transmitted in real time to the corresponding PCs. The operator's performance is estimated using stimulus-related brain response $I(i)$ to every presented i-th stimulus on the base of the EEG spectral properties (see Methods).
- Brain responses $I_1(i)$ and $I_2(i)$ of subject 1 and subject 2, respectively, are transmitted to the computational server for a comparative analysis.
- Depending on the result in this comparison, the corresponding control command is sent to each PC to adjust the ambiguity range of the presented stimuli for each subject. For example, if $I_1(i) > I_2(i)$, then subject 1 receives a stimulus with higher ambiguity, while subject 2 receives a stimulus with weaker ambiguity.

The BBI was built based on the "Encephalan-EEGR-19/26" (Medicom MTD, Russia). The EEG data recorded from each subject were initially processed by local computers, where the values of the brain response were calculated individually for each subject using home-made software based on C++. Then, these values were sent to a calculation server with markers containing the information about presented stimuli through the IP-message. The server software (also developed in C++) analyzed the incoming information and sent control commands back to the local computers through IP-messages. The control commands were used to realize switches between the sets of stimuli. The information about the set number was sent back to the server. As a result, the dataset containing the values of brain responses and the stimuli set numbers were saved to a data file at every time moment.

2.7. Connectivity Analysis

The connectivity analysis for every pair of participants was performed via the Recurrence-based Measure of Dependence (RMD) proposed and described in details in Goswami et al. (2013). Using this approach, we could either identify coupling directions and time lags between interacting systems or prove that they were independent.

Let $I_1(i)$ and $I_2(i)$ be L (leader) and A (assistant) brain response time series, respectively. The RMD is calculated as

$$\mathrm{RMD}(\tau) = \log_2\left(\frac{1}{N'}\sum_{i=1}^{N'}\mathrm{RMD}_i(\tau)\right),$$

$$\mathrm{RMD}_i(\tau) = \frac{P(I_1(i), I_2(i+\tau))}{P(I_1(i))\,P(I_2(i+\tau))},$$

where τ is a time lag, $P(I_k = I_k(i))$ is a probability for I_k to take the value $I_k(i)$, and $P(I_1(i), I_2(i)) = P(I_1 = I_1(i))\,P(I_2 = I_2(i))$ is a joint probability that $I_1 = I_1(i)$ at the same time, where $I_2 = I_2(i)$ and $N' = N - \tau$. The probabilities P determined by a recurrence matrix (Marwan et al., 2007), is calculated as

$$P(I_k(i)) = \frac{1}{N}\sum_{j=1}^{N}\mathbf{R}_k(i,j),$$

$$P(I_1(i), I_2(i)) = \frac{1}{N}\sum_{j=1}^{N}\mathbf{JR}(i,j),$$

$$\mathbf{JR} = \mathbf{R}_1(i,j)\,\mathbf{R}_2(i,j),$$

where $\mathbf{R}_k(i,j)$ is a recurrence matrix of k-th participant and $\mathbf{JR}(i,j)$ is a joint recurrence matrix.

Next, we carried out the statistical test of significance of the obtained RMD(τ) values using surrogate data of the observed time series. For this aim, we generated so-called twin surrogates, which were independent realizations of the entire system via the recurrence-based approach proposed in Thiel et al. (2006) and Ramos et al. (2017). The observed values of RMD(τ) implied a statistically significant dependence of I_2 on I_1 if RMD exceeded 95 percentile (confidence interval) of the test RMD(τ) distribution calculated for I_1 surrogate time series. In the framework of this approach, we found that for $\tau > 0$ a non-zero RMD exceeding the confidence interval determined the dependence of I_2 on I_1, and the converse was true for $\tau < 0$. On the contrary, if RMD lied inside the confidence interval, the participants acted independently.

2.8. Statistical Analysis

The statistical analysis was performed using IBM SPSS Statistics. The values of the brain response $I(t)$ calculated during different sessions (or for different participants) were compared as two independent samples using an independent samples t-test. The mean values of the brain response $I(t)$ within the group of participants were compared for different experimental sessions as paired samples. First, we applied the Shapiro-Wilk normality test to the corresponding samples. If the data set did not pass this test ($p < 0.05$), we applied the Wilcoxon signed rank test, otherwise, t-test was used. The tests used for the statistical analysis are indicated in the caption of **Figure 3**.

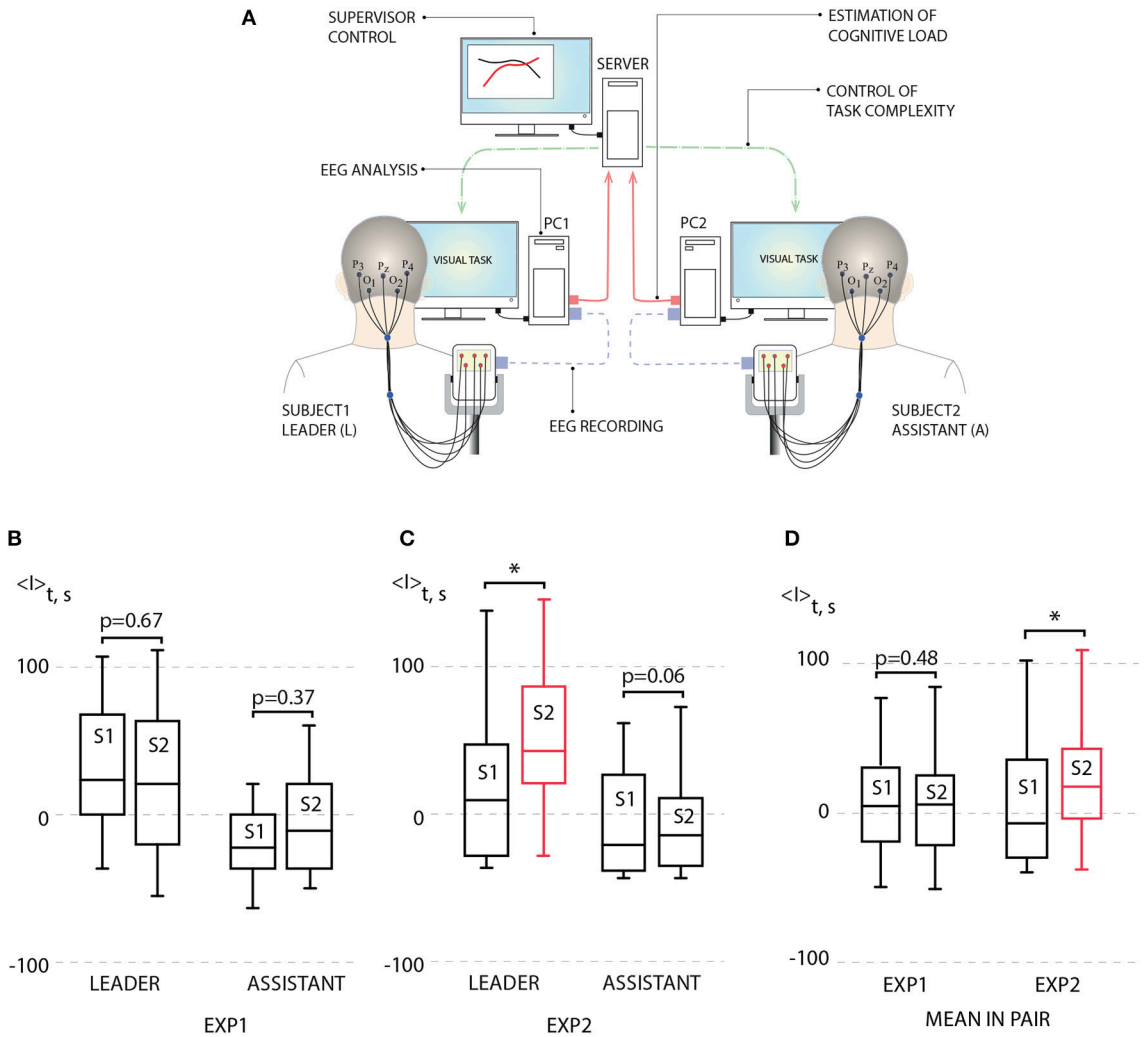

FIGURE 3 | (A) Schematic illustration of human-to-human interaction through BBI. **(B)** Left: average leader's brain response $\langle I \rangle$ during first experiment (EXP1): session 1 (S1) [no link between subjects, $p = 0.938$ by Shapiro-Wilk normality test (SWNT)] and session 2 (S2) (no delay in coupling between subjects, $p = 0.965$ by SWNT) (not significant, $n = 10$, $p = 0.67$ by paired sample t-test); right: average assistant's brain response $\langle I \rangle$ during EXP1: S1 (no link between subjects, $p = 0.402$ by SWNT) and S2 (no delay in coupling between subjects, $p = 0.485$ by SWNT) (not significant, $n = 10$, $p = 0.37$ by paired sample t-test). **(C)** Left: average leader's brain response $\langle I \rangle$ during second experiment (EXP2): S1 (no link between subjects, $p = 0.131$ by SWNT) and S2 (delayed coupling between subjects, $p = 0.889$ by SWNT) (significant change, $n = 10$, $^*p < 0.05$ by paired sample t-test); right: average assistant's brain response $\langle I \rangle$ during EXP2: S1 (no link between subjects, $p = 0.099$ by SWNT) and S2 (delayed coupling between subjects, $p = 0.169$ by SWNT) (not significant, $n = 10$, $p = 0.06$ by paired sample t-test). **(D)** Left: mean brain response $\langle I \rangle$ for pairs during EXP1: S1 (no link between subjects, $p = 0.979$ by SWNT) and S2 (no delay in coupling between subjects, $p = 0.847$ by SWNT) (not significant, $n = 10$, $p = 0.48$ by paired sample t-test); right: mean brain response $\langle I \rangle$ for pairs during EXP1: S1 (no link between subjects, $p = 0.108$ by SWNT) and S2 (no delay in coupling between subjects, $p = 0.622$ by SWNT) (significant change, $n = 10$, $^*p < 0.05$ by paired sample t-test). Medians (bars), 25–75 percentiles (box) and outlines (whiskers) are shown.

3. RESULTS

For each session, average performance $\langle I \rangle$ was calculated for each subject by averaging his/her brain response I over 200 image presentations. According to $\langle I \rangle$ estimated during preliminary non-coupled session (S1), the subjects in each pair were classified as a leader (L) (subject with higher $\langle I \rangle$) and an assistant (A) (subject with lower $\langle I \rangle$). Then, $\langle I \rangle$ of L and A obtained during uncoupled and coupled sessions were calculated and compared.

The results of this comparison for EXP1 are presented in **Figure 3B** in the form of box-and-whiskers diagrams which show average performance $\langle I \rangle$ for leaders and assistants in all pairs. One can see that according to the group analysis, the interaction between subjects in EXP1 did not bring a significant effect on the degree of performance for leaders and assistants. On the contrary, we uncovered a significant increase in the degree of alertness of the leader in EXP2 shown in **Figure 3C**, where the task complexity was changed if a 10% difference appeared between values of $I_1(i)$ and $I_2(i)$. The observed changes in the

assistants' degree of alertness were insignificant. Such an increase in the leader's performance caused an enhancement of the pair's performance. This can be seen from **Figure 3D**, where we plot the value of $\langle I \rangle$ averaged over all participants' performances.

In order to understand the obtained result, let us now consider the evolution of the brain response during one experimental session. The typical dependence $I(i)$ reflects a change in the amplitude of the brain response as the number of presented Necker cubes i is increased. The result shows oscillations whose period varies from 15 to 40 presented stimuli (see **Figure 4A**). Such a behavior of the brain response can be associated with the relaxation of the neural ensemble. The restoration state is needed for cognitive recovery after mental fatigue caused by the HC task (**Figure 4B**). The degree of image ambiguity (or complexity of the visual task) strongly affects the amplitude of the brain response. In **Figure 4C** we plot the average values of the brain response calculated for the preliminary experimental session conducted individually for each participant, where visual stimuli with low degree of ambiguity were presented. The base value was chosen when the observer was subjected to highly ambiguous stimuli. In **Figure 4D** typical dependence I(i) are compared for LC and HC tasks. We found that an increase in the degree of image ambiguity (or an increase in the task complexity) leads to a corresponding increase in the average amplitude of the brain response $\langle I \rangle$. According to our recent study (Maksimenko et al., 2017b), such a change in the brain response is caused by an increase in alertness. In this case, the time-frequency structure of the EEG signals exhibits significant changes for each subsequent i-th stimulus. The origin of these changes is in the contribution of α and β brain rhythms. From the viewpoint of neural dynamics, this means that a large neural population participates in image classification (Maksimenko et al., 2017c). As the image ambiguity grows, the average response $I(i)$ increases.

According to the above result, one can assume that effective classification can be obtained if the image ambiguity is adjusted according to the current value of the brain response. This can be implemented with the help of biological feedback according to the following situations: (i) in the case of high operator performance defined by a high value of the brain response base line, the operator is subjected to stimuli with high degree of ambiguity, i.e., the task complexity is being increased with corresponding cognitive load increment, (ii) as the cognitive load is increased, it leads to an augmentation in neuronal tiredness which immediately causes a decrease in the brain response, (iii) in contrast, having a low brain response the operator is subjected to stimuli with a low degree of ambiguity, i.e., the cognitive load decreases, and (iv) a decrease in cognitive load causes a faster restoration.

In the case of two operators, each of them was subjected to the same stimuli ambiguity cycle in antiphase. This design offers two main advantages: (i) the most complicated (or most important) task is being processed by the operator with highest momentary skill, (ii) the switch to the less complicated task, when the operator is tired, allows decreasing the restoration time. The combination of both features enables to efficiently manage the whole workload distribution. Obviously, the efficiency of the described approach depends on the coincidence quality between complexity and operator's performance skills, namely, high performance has to be correlated with high complexity, and the restoration phase should be correlated with low complexity defined by the frequency of $I(i)$ oscillations.

In order to check how this criterium of coincidence was satisfied in two conducted experiments, EXP1 and EXP2, we carried out the detailed analysis of the results obtained in the corresponding experimental sessions. When comparing the sub-plots in **Figure 5A**, one can clearly see that during EXP1, when the task complexity switches immediately as soon as the amplitude of the brain response of one subject ($I_1(i)$) exceeds the brain response of the other subject ($I_2(i)$), there are many short switches with $\Delta < 5$, smaller than the period of $I(i)$ oscillations. In this case, the dependencies $I_1(i)$ and $I_2(i)$ obtained for both subjects do not demonstrate an antiphase mode. On the contrary, the values of $I(i)$ obtained for the subjects during experiment EXP2 behave mostly in antiphase and switches appear less frequently. In **Figure 5B** the box-and-whiskers diagram compares the mean number of switches $\langle N_{TC} \rangle$ averaged over subjects during EXP1 and EXP2. One can see that in EXP2 the number of switches significantly decreases (significance is judged from $p < 0.05$ estimated via paired t-test).

One can surmise that in EXP1 the multiple unnecessary spontaneous switches, caused by low-frequency fluctuations of $I(i)$, interfered with the establishment of the antiphase mode between oscillations I_1 and I_2 of the leader and assistant in pair. Unlike experiment EXP1, during EXP2 such switches appeared more scarcely and the interval Δ between two successive switches matched the period of $I(i)$ oscillations which was estimated to vary from 15 to 40 stimuli presentations. In both experiments, Δ was distributed within the interval of [0, 40] (see **Figure 5C**). This distribution displays a significantly larger number of rapid switches (< 5 presented cubes) observed during EXP1, whereas medium (5–10 presented cubes) and optimal (11–20 presented cubes) intervals between switches dominated in EXP2. Taking into account that the period of $I(i)$ oscillations occurred in the same range, we can conclude that the switching regime in EXP2 mostly satisfied the criterium described above, and therefore led to an increase in operator's performance.

Figures 5D,E illustrate the results of the connectivity analysis in coupled pairs during EXP1 and EXP2. We estimated directions and time lags in coupling between participants by calculating the Recurrence-based Measure of Dependence (RMD) (Goswami et al., 2013) (see detailed description in section 2.) using time series $I_1(i)$ and $I_2(i)$ recorded during EXP1 and EXP2. The time lag τ was introduced by a relevant shifting of one of the time series relative to the other by τ units. We found that during EXP1 (**Figure 5D**) the participants mostly performed their tasks independently or rarely influencing each other at short lags (about 10 image presentations). Indeed, a large number of fast spontaneous switches between high and low complexity tasks could not determine the effective interaction between participants. On the contrary, during EXP2 (**Figure 5E**) the delayed coupling between participants caused the establishment of unidirectional dependence of the assistant on the leader, that was reproduced for all pairs of participants. Notably, the most significant time lag of this dependence, observed in the most of

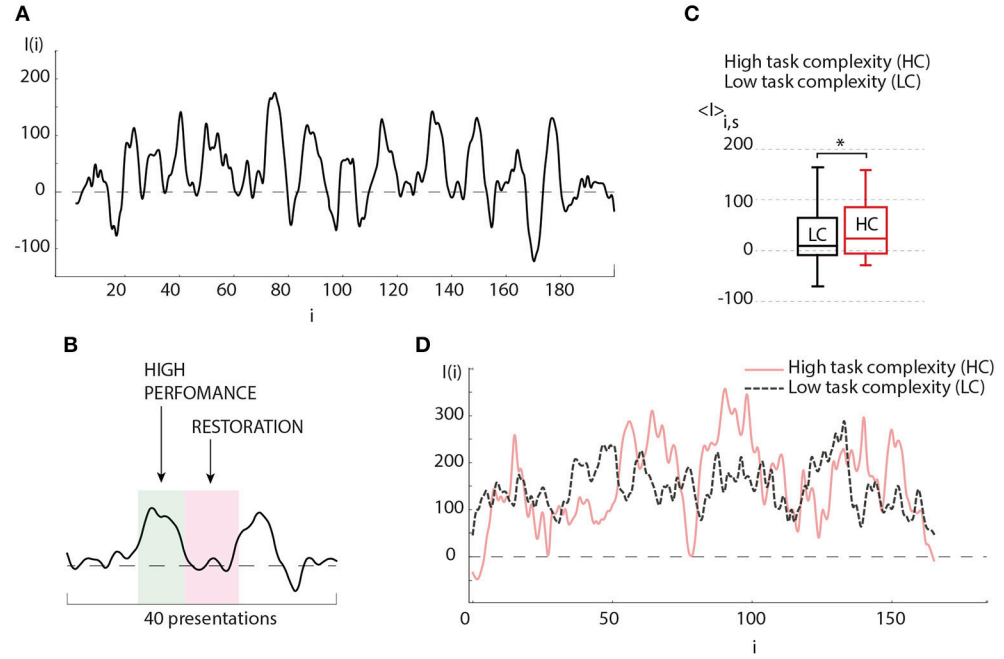

FIGURE 4 | (A) Typical oscillations of the brain response value (I) depending on the number of presented visual stimuli during the experimental session. **(B)** Detailed illustration of a single period of (I) oscillations ($\approx$ 20 presented stimuli), where "hump" and "hollow" demonstrate the states of high brain performance and restoration, respectively. **(C)** Average brain response $\langle I \rangle$ of the subject during experimental session, when images with low degree of ambiguity (LC) ($p = 0.436$ by Shapiro-Wilk normality test) and high degree of ambiguity (HC) ($p = 0.434$ by Shapiro-Wilk normality test) were presented (session contains 200 presentations) (significant change, $n = 10$, $^*p < 0.05$ by paired sample t-test). Medians (bars), 25–75 percentiles (box) and outlines (whiskers) are shown. **(D)** Typical oscillations of the brain response value (I) depending on the number of presented visual stimuli during the perception of images of high degree (solid curve) and low degree (dashed curve) of ambiguity.

pairs and corresponded to approximately 20 image presentations, is associated with natural frequency of individual brain response oscillations.

4. DISCUSSION

The possibility to estimate and control the human psychophysiological condition, and the ability to accomplish mental tasks via BCI is of great fundamental and practical interest (Borghini et al., 2017). In this context, the estimation and control of such human factor as alertness is very important (Lim et al., 2012; Liu et al., 2013; Ko et al., 2017). Alertness manifests itself as an active attentional state marked by high sensory awareness to be watchful and ready for any potential danger or emergency, or fast to respond to it. As it was shown in neurophysiological studies, a person who has to be alerted during his/her work, such as air traffic controllers or pilots, often has a trouble to maintain alertness. In some situations, people use drugs in order to increase attention, but a safer and more effective way is to use BCI to improve the human ability to maintain alertness. Such BCIs can give rise to the development of training systems, in particular, for children with attention deficit hyperactivity disorder (Lim et al., 2012; Hillard et al., 2013), as well as assistant systems which allow to control the attention during long-lasting job tasks. Moreover, they can be used for the development of BCI for completely paralyzed people (Hill and Schölkopf, 2012; Jin et al., 2017).

The BCIs which are aimed at increasing human brain abilities are known as passive BCIs. These BCIs use biomarkers extracted from brain signals to improve human's cognitive performance with no aim of voluntary control of the system (Zander and Kothe, 2011). The main goal of such systems is to enhance cognitive performance of healthy humans and to recover mild cognitive impairment. In this context, traditional definition of BCI is more suitable for active BCIs. They imply that operator voluntarily generates specific patterns of brain activity which can be automatically detected in real time and translated into commands for controlling a technical device by thought. Active BCIs mostly aim to help paralyzed people to communicate and interact with external environment (Wolpaw et al., 2002).

Passive BCIs are able to estimate degree of alertness in real time based on changes in the time-frequency structure of human EEG and provide possibility for alertness control by biological feedback (Maksimenko et al., 2017b). At the same time, the ability of such BCIs to immediately improve human alertness is not reported in literature. The recent review on the methods for the improvement of cognitive performance (Taya et al., 2015) states that brain abilities can be enhanced by prolonged and systematic cognitive training. In this paper, we propose an alternative approach. We demonstrate that human alertness

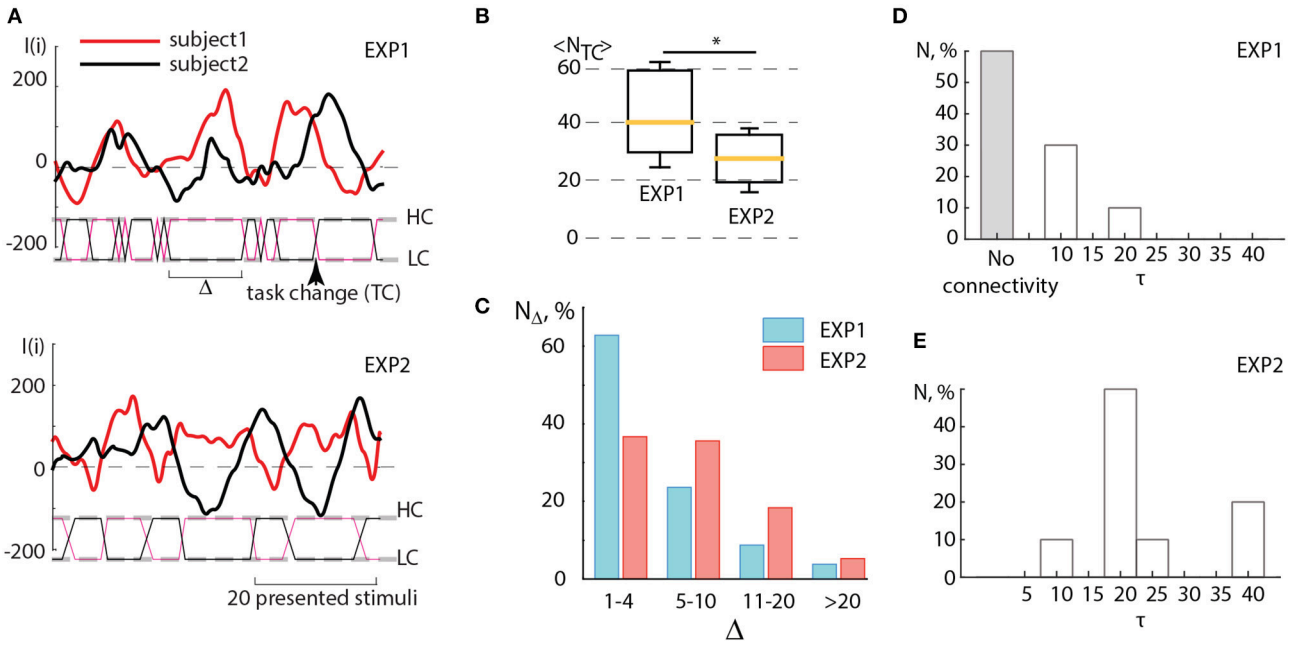

FIGURE 5 | (A) Detailed illustration of the BBI performance during experiments EXP1 and EXP2. Solid curves represent the brain response *I*(*i*) of two partners, dashed lines marked as HC and LC indicate two types of visual tasks associated with high and low complexity, solid lines between these dashed lines indicate switches (TC) between the tasks, the arrow shows the moment of a single switch. The length of the interval (Δ) between two successive switches is measured in the number of presented stimuli. **(B)** Comparison between the number of switches $< N_{TC} >$ averaged over subjects during experiments EXP1 and EXP2. Statistical significance is estimated via paired *t*-test. Medians (yellow bars), 25–75 percentiles (box) and outlines (whiskers) are shown. **(C)** Distribution of time intervals between switches Δ calculated by taking into account four ranges: rapid switches (1–4 units), medium switches (5–10 units), optimal switches (11–20 units) and long switches (> 20 units). **(D,E)** Connectivity analysis. Histograms reflecting distribution of coupling time lags τ over all pairs of participants showing the change in the character of coupling in **(D)** EXP1 and **(E)** EXP2. $^*p < 0.05$ by paired sample *t*-test.

can be immediately improved via human-to-human interaction. In particular, we shown, for the first time to the best of our knowledge, that human performance to perform a cognitive load can be increased using BBI which monitors working ability of every person in the group and distributes the load among all participants according to their individual ability, in order to perform a common task more efficiently. This became possible due to specific EEG hallmarks associated with degree of alertness.

Having analyzed the mean degree of alertness, we have found that in each pair of participants, the subject who initially demonstrated higher degree of alertness in the experiments without any interaction, exhibited increasing alertness in the experiment with human-to-human interaction due to the assistance of his/her partner. It was surprising that the increasing alertness was only observed in the experiment, where the task complexity was changed as soon as the difference in the degree of alertness between the partners exceeded 10%. We have shown that this effect is caused by the oscillatory behavior of the degree of alertness, determined by the average period of cognitive recovery after mental fatigue. In this respect, the effective interval between switches of the task complexity should coincide with this brain rhythm.

The obtained results demonstrate the principal difference between human-machine and human-to-human interactions. While in the former case, the machine performs a part of a cognitive or a physical human load, in the latter case, the machine is replaced by another human, so that a feedback is required to compare the subjects' brain states in order to decide who is more suitable for the action. This is especially important for systems aimed at increasing human cognitive performance. Since brain ability to consciously perceive and process information is limited (Marois and Ivanoff, 2005), the human exhibits a state of mental fatigue manifested as brain inability to complete the mental task which requires a high level of sustained attention in the absence of discernible cognitive failure (Chaudhuri and Behan, 2000).

Human-to-human interaction can also be implemented via special brain-to-brain interfaces which along with active and passive BCIs, have become a hot topic in neuroscience, physics and IT-technologies. Recently, the possibility of human-to-human interaction via BBI was performed in a way, where motor information registered in the cortical region was transmitted to the motor cortex region of another subject with the help of brain stimulation. Such possibility was first demonstrated by Pais-Vieira et al. (2013) in rats. One year later, human-to-human interaction was considered by Rao et al. (2014), who proposed a noninvasive interface which combined EEG with transcranial magnetic stimulation (TMS) for delivering information to brain. Their BBI detected motor imagery in EEG signals recorded from one subject ("sender") and transmitted this information

over Internet to the motor cortex region of another subject ("receiver").

The brain-to-brain interaction was also implemented in the form of human-animal interaction (Yoo et al., 2013), where the human volunteer's intention was translated to stimulate a rat's brain motor area responsible for the tail movement. Another type of BBI was demonstrated by Mashat et al. (2017) in a closed-loop form, where the intention signal from a sender was recognized using EEG and sent out to trigger TMS of a receiver to induce hand motion; meanwhile, TMS resulted in a significant change in the motor evoked potentials recorded by electromyography of the receiver's arm, which triggered functional electrical stimulation applied to the sender's arm and generated hand motion.

Although these studies provided the experimental evidence of the information transmission between brains, they did not demonstrate the possibility to improve the performance of a sender and a receiver. The control command was translated to the receiver's brain in any case, not considering its willingness to perform an action. In other words, previously proposed systems did not take into account brain states of interacting people. Instead, our BBI analyses and compares human brain states, as a core feature of the human-to-human interaction, to improve human performance in tasks which require sustained attention, in particular, in classification of consecutively presented ambiguous images. At the same time, possible applications of proposed BBI are widespread. The distribution of cognitive or physical load unequally over all participants depending on their current psychophysiological conditions is a very efficient way to improve the working performance of the group of people.

5. CONCLUSION

The presented results contributed in the multidisciplinary field of science, especially, in physics and brain-to-brain interface development. From a physical point of view, we have considered interacting human brains as a mutually coupled dynamical system and revealed nonlinear phenomena caused by particular features of electrical brain activity. In particular, we have found that the brain activity, while performing a cognitive load, oscillates in time with a certain mean period which can be related to periodic cognitive recovery after mental fatigue caused by a difficult task. The modulation of the cognitive load complexity with a frequency close to this "natural" frequency of cognitive recovery allows maintaining a high brain performance for a prolonged time. Moreover, such a modulation increases the amplitude of the brain response, similar to a resonant behavior of a dynamical system subjected to an external periodic forcing. This principle underlies the proposed BBI aimed to increase human performance due to brain-to-brain interaction.

The obtained results can be a starting point for the development of systems for neural-based communication between humans which allow to "feel" conditions of the partner and make the human-to-human interaction more efficient. This would be very helpful for a group of people subjected to a common task which requires sustained attention and alertness. The BBI could help such people to have effective interactions by estimating and monitoring physical conditions of each team member, in particular, degree of alertness, in order to distribute workloads among all participants according to their current physiological status. Starting from the case of two interacting persons, this system can be extended to the large network of people working on a common project.

AUTHOR CONTRIBUTIONS

VAM, AEH, ANP, and JK conceived the study. VVG, AL, and AER performed experiments. VAM and VON implemented data processing algorithm. VVM and NSF analyzed the data. VAM, AEH and ANP wrote the manuscript.

FUNDING

This work was supported by the Russian Foundation for Basic Research (Grant 18-32-20129) and the President Program (Project NSH-2737.2018.2). JK was supported within the scope of the IRTG 1740/TRP 2015/50122-0, funded by the DFG/FAPESP. ANP acknowledges support from the Ministry of Economy and Competitiveness (Spain) (Ref. SAF2016-80240-P).

REFERENCES

Baker, T. L., Campbell, S. C., Linder, K. D., and Moore-Ede, M. C. (1990). *Control-Room Operator Alertness and Performance in Nuclear Power Plants.* Report EPRI-NP–6748 United States Vol. 23.

Birbaumer, N., Ghanayim, N., Hinterberger, T., Iversen, I., Kotchoubey, B., Kübler, A., et al. (1999). A spelling device for the paralysed. *Nature* 398, 297–298.

Borghini, G., Aricó, P., Di Flumeri, G., Cartocci, G., Colosimo, A., Bonelli, S., et al. (2017). EEG-based cognitive control behaviour assessment: an ecological study with professional air traffic controllers. *Sci. Rep.* 7:547. doi: 10.1038/s41598-017-00633-7

Bowsher, K., Civillico, E. F., Coburn, J., Collinger, J., Contreras-Vidal, J. L., Denison, T. et al. (2016). Brain-computer interface devices for patients with paralysis and amputation: a meeting report. *J. Neural Eng.* 13:023001. doi: 10.1088/1741-2560/13/2/023001

Chaudhary, U., Birbaumer, N., and Ramos-Murguialday, A. (2016). Brain–computer interfaces for communication and rehabilitation. *Nat. Rev. Neurol.*12, 513–525. doi: 10.1038/nrneurol.2016.113

Chaudhuri, A., and Behan, P. O. (2000). Fatigue and basal ganglia. *J. Neurol. Sci.* 179, 34–42. doi: 10.1016/S0022-510X(00)00411-1

Chen, X., Wang, Y., Nakanishi, M., Gao, X., Jung, T. P., and Gao, S. (2015). High-speed spelling with a noninvasive brain-computer interface. *Proc. Natl. Acad. Sci. U.S.A.* 112, E6058–E6067. doi: 10.1073/pnas.1508080112

Daly, J. J., and Wolpaw, J. R. (2008). Brain-computer interfaces in neurological rehabilitation. *Lancet Neurol.* 7, 1032–1043. doi: 10.1016/S1474-4422(08)70223-0

Estrada, A., Kelley, A. M., Webb, C. M., Athy, J. R., and Crowleym J. S. (2012). Modafinil as a replacement for dextroamphetamine for sustaining alertness in military helicopter pilots. *Aviat. Space Environ. Med.* 83, 556–64. doi: 10.3357/ASEM.3129.2012

Foxe, J. J., and Snyder, A. C. (2011). The role of alpha-band brain oscillations as a sensory suppression mechanism during selective attention. *Front. Psychol.* 2:154. doi: 10.3389/fpsyg.2011.00154

Gleiss, S., and Kayser, C. (2014). Acoustic noise improves visual perception and modulates occipital oscillatory states. *J. Cogn. Neurosci.* 26 699–711. doi: 10.1162/jocn_a_00524

Gola, M., Kaminski, J., Brzezicka, A., and Wrobel, A. (2013). Beta-band activity as a correctness predictor in a sustained attention task. *Int. J. Psychophysiol.* 89, 334–341. doi: 10.1016/j.ijpsycho.2013.05.007

Goswami, B., Marwan, N., Feulner, G., and Kurths, J. (2013). How do global temperature drivers influence each other? *Eur. Phys. J. Special Top.* 222, 861–873. doi: 10.1140/epjst/e2013-01889-8

Hill, N. J., and Schölkopf, B. (2012). An online brain-computer interface based on shifting attention to concurrent streams of auditory stimuli. *J. Neural Eng.* 9:026011. doi: 10.1088/1741-2560/9/2/026011

Hillard, B., El-Baz, A. S., Sears, L., Tasman, A., and Sokhadze, E. M. (2013). Neurofeedback training aimed to improve focused attention and alertness in children with adhd: a study of relative power of EEG rhythms using custom-made software application. *Clin. EEG Neurosci.* 44, 193–202. doi: 10.1177/1550059412458262

Hramov, A. E., Maksimenko, V. A., Pchelintseva, S. V., Runnova, A. E., Grubov, V. V., Musatov, V. Y., et al. (2017). Classifying the perceptual interpretations of a bistable image using EEG and artificial neural networks. *Front. Neurosci.* 11:674. doi: 10.3389/fnins.2017.00674

Jensen, R. C. (1999). Alertness-supporting activities for control room operators in automated industrial plant. *Hum. Factors Ergon. Soc. Ann. Meet. Proc.* 43, 752–756. doi: 10.1177/154193129904301225

Jin, J., Zhang, H., Daly, I., Wang, X., and Cichocki, A. (2017). An improved P300 pattern in BCI to catch user's attention. *J. Neural Eng.* 14:036001. doi: 10.1088/1741-2552/aa6213

Kawase, T., Sakurada, T., Koike, Y., and Kansaku, K. (2017). A hybrid BMI-based exoskeleton for paresis: EMG control for assisting arm movements. *J. Neural Eng.* 14:016015. doi: 10.1088/1741-2552/aa525f

Ko, L. W., Komarov, O., Hairston, W. D., Jung, T. P., and Lin, C. T. (2017). Sustained attention in real classroom settings: An EEG study. *Front. Hum. Neurosci.* 11:388. doi: 10.3389/fnhum.2017.00388

Kornmeier, J., Pfäffle, M., and Bach, M. (2011). Necker cube: Stimulus-related (low-level) and percept-related (high-level) EEG signatures early in occipital cortex. *J. Vis.* 11:12. doi: 10.1167/11.9.12

Laufs, H., Holt, J. L., Elfont, R., Krams, M., Paul, J. S., Krakow, K., et al. (2006). Where the BOLD signal goes when alpha EEG leaves. *Neuroimage* 31, 1408–1418. doi: 10.1016/j.neuroimage.2006.02.002

Lim, C. G., Lee, T. S., Guan, C., Fung, D. S., Zhao, Y., Teng, S. S., et al. (2012). A brain-computer interface based attention training program for treating attention deficit hyperactivity disorder. *PLoS ONE* 7:e46692. doi: 10.1371/journal.pone.0046692

Liu, N. H., Chiang, C. Y., and Chu, H. C. (2013). Recognizing the degree of human attention using EEG signals from mobile sensors. *Sensors (Basel)* 13, 10273–10286. doi: 10.3390/s130810273

Ma, T., Li, H., Deng, L., Yang, H., Lv, X., Li, P., et al. (2017). The hybrid BCI system for movement control by combining motor imagery and moving onset visual evoked potential. *J. Neural Eng.* 14, 026015. doi: 10.1088/1741-2552/aa5d5f

Maksimenko, V. A., Heukelum van, S., Makarov, V. V., Kelderhuis, J., Luttjohann, A., Koronovskii, A. A., et al. (2017a). Absence seizure control by a brain computer interface. *Sci. Rep.* 7:2487. doi: 10.1038/s41598-017-02626-y

Maksimenko, V. A., Lüttjohann, A., Makarov, V. V., Goremyko, M. V., Koronovskii, A. A., Nedaivozov, V., et al. (2017c) Macroscopic and microscopic spectral properties of brain networks during local and global synchronization. *Phys. Rev. E* 96:012316. doi: 10.1103/PhysRevE.96.012316

Maksimenko, V. A., Runnova, A. E., Frolov, N. S., Makarov, V. V., Nedaivozov, V., Koronovskii, A. A., et al. (2018). Multiscale neural connectivity during human sensory processing in the brain. *Phys. Rev. E* 97:052405. doi: 10.1103/PhysRevE.97.052405

Maksimenko, V. A., Runnova, A. E., Zhuravlev, M. O., Makarov, V. V., Nedayvozov, V., Grubov, V. V., et al. (2017b) Visual perception affected by motivation and alertness controlled by a noninvasive brain-computer interface. *PLoS ONE* 12:e188700. doi: 10.1371/journal.pone.0188700

Maksimenko, V. A., Runnova, A. E., Zhuravlev, M. O., Protasov, P., Kulanin, R., Khramova, M. V., et al. (2018). Human personality reflects spatio-temporal and time-frequency EEG structure. *PLoS ONE* 13:e0197642. doi: 10.1371/journal.pone.0197642

Marois, R., and Ivanoff, J. (2005). Capacity limits of information processing in the brain. *Trends Cogn. Sci.* 9, 296–305. doi: 10.1016/j.tics.2005.04.010

Marwan, N., Romano, M. C., Thiel, M., and Kurths, J. (2007). Recurrence plots for the analysis of complex systems. *Phys. Rep.* 438, 237–329. doi: 10.1016/j.physrep.2006.11.001

Mashat, M. E. M., Li, G., and Zhang, D. (2017). Human-to-human closed-loop control based on brain-to-brain interface and muscle-to-muscle interface. *Sci. Rep.* 7, 11001. doi: 10.1038/s41598-017-10957-z

Mathes, B., Strüber, D., Stadler, M. A., and Basar-Eroglu, C. (2006). Voluntary control of necker cube reversals modulates the EEG delta- and gamma-band response. *Neurosci. Lett.* 402, 145–149. doi: 10.1016/j.neulet.2006.03.063

Michalareas, G., Vezoli, J., van Pelt, S., Schoffelen, J. M., Kennedy, H., and Fries, P. (2016). Alpha-beta and gamma rhythms subserve feedback and feedforward influences among human visual cortical areas. *Neuron* 89, 384–397. doi: 10.1016/j.neuron.2015.12.018

Mirabella, G., and Lebedev, M. A. (2016). Interfacing to the brain's motor decisions. *J. Neurophysiol.*117, 1305–1319. doi: 10.1152/jn.00051.2016

Mulckhuyse, M., Kelley, T. A., Theeuwes, J., Walsh, V., and Lavie, N. (2011). Enhanced visual perception with occipital transcranial magnetic stimulation. *Eur. J. Neurosci.* 34, 1320–1325. doi: 10.1111/j.1460-9568.2011.07814.x

Muthukumaraswamy, S. (2013). High-frequency brain activity and muscle artifacts in MEG/EEG: a review and recommendations. *Front. Hum. Neurosci.* 7:138. doi: 10.3389/fnhum.2013.00138

Necker Esq, L. A. (1832). Lxi. observations on some remarkable optical phenomena seen in Switzerland; and on an optical phenomenon which occurs on viewing a figure of a crystal or geometrical solid. *Lond. Edinb. Dublin Philos. Mag. J. Sci.* 1, 329–337. doi: 10.1080/14786443208647909

Niedermeyer, E., and da Silva, F. L. (2014). *Electroencephalography: Basic Principles, Clinical Applications, and Related Fields, Nonlinear Dynamics* (Philadelphia, PA: Lippincot Williams & Wilkins).

Pais-Vieira, M., Lebedev, M., Kunicki, C., Wang, J., and Nicolelis, M. A. (2013). A brain-to-brain interface for real-time sharing of sensorimotor information. *Sci. Rep.* 3:1319. doi: 10.1038/srep01319

Pavlov, A. N., Hramov, A. E., Koronovskii, A. A., Sitnikova, Y. E., Makarov, V. A., and Ovchinnikov, A. A. (2012). Wavelet analysis in neurodynamics. *Phys. Uspekhi* 55, 845–875. doi: 10.3367/UFNe.0182.201209a.0905

Peternel, L., Noda, T., Petrič, T., Ude, A., Morimoto, J., and Babič, J. (2016). Adaptive control of exoskeleton robots for periodic assistive behaviours based on emg feedback minimisation. *PLoS ONE* 11:e148942. doi: 10.1371/journal.pone.0148942

Pisarchik, A. N., Jaimes-Reátegui, R., Magallón-García, C. D., and Castillo-Morales, C. O. (2014). Critical slowing down and noise-induced intermittency in bistable perception: Bifurcation analysis. *Biol. Cybern.*. 108, 397–404. doi: 10.1007/s00422-014-0607-5

Ramos, A. M. T., Builes-Jaramillo, A., Poveda, G., Goswami, B., Macau, E. E. N., Kurths, J., et al. (2017). Recurrence measure of conditional dependence and applications. *Phys. Rev. E* 95:052206. doi: 10.1103/PhysRevE.95.052206

Rao, R. P., Stocco, A., Bryan, M., Sarma, D., Youngquist, T. M., Wu, J., et al. (2014). A direct brain-to-brain interface in humans. *PLoS ONE* 9:e111332. doi: 10.1371/journal.pone.0111332

Runnova, A. E., Hramov, A. E., Grubov, V., Koronovsky, A. A., Kurovskaya, M. K., and Pisarchik, A. N. (2016). Theoretical background and experimental measurements of human brain noise intensity in perception of ambiguous images. *Chaos Solitons Fractals* 93, 201–206. doi: 10.1016/j.chaos.2016.11.001

Sallinen, M., Sihvola, M., Puttonen, S., Ketola, K., Tuori, A., Härmä, M., et al. (2017). Sleep, alertness and alertness management among commercial airline pilots on short-haul and long-haul flights. *Accid. Anal. Prev.* 98, 320–329. doi: 10.1016/j.aap.2016.10.029

Sauseng, P., Klimesch, W., Stadler, W., Schabus, M., Doppelmayr, M., Hanslmayr, S., et al. (2005). A shift of visual spatial attention is selectively associated with human EEG alpha activity. *Eur. J. Neurosci.* 22, 2917–2926. doi: 10.1111/j.1460-9568.2005.04482.x

Sehatpour, P., Molholm, S., Schwartz, T. H., Mahoney, J. R., Mehta, A. D., Javitt, D. C., et al. (2008). A human intracranial study of long-range oscillatory coherence across a frontal-occipital-hippocampal brain network during visual object processing. *Proc. Natl. Acad. Sci. U.S.A.* 105, 4399–4404. doi: 10.1073/pnas.0708418105

Sitnikova, E., Hramov, A. E., Grubov, V., and Koronovsky, A. A. (2014). Time-frequency characteristics and dynamics of sleep spindles in wag/rij rats with absence epilepsy. *Brain Res.* 1543, 290–299. doi: 10.1016/j.brainres.2013.11.001

Spüler, M. (2017). A high-speed brain-computer interface (BCI) using dry EEG electrodes. *PLoS ONE* 12:e172400. doi: 10.1371/journal.pone.0172400

Takahashi, M., Tanigawa, T., Tachibana, N., Mutou, K., Kage, Y., Smith, L., et al. (2005). Modifying effects of perceived adaptation to shift work on health, wellbeing, and alertness on the job among nuclear power plant operators. *Ind. Health* 43, 171–178. doi: 10.2486/indhealth.43.171

Taya, F., Sun, Y., Babiloni, F., Thakor, N., and Bezerianos, A. (2015) Brain enhancement through cognitive training: a new insight from brain connectome. *Front. Syst. Neurosci.* 9:44. doi: 10.3389/fnsys.2015.00044

Thiel, M., Romano, M. C., Kurths, J., Rolfs, M., and Kliegl, R. (2006). Twin surrogates to test for complex synchronisation. *Europhys. Lett.* 75:535. doi: 10.1209/epl/i2006-10147-0

Wolpaw, J. R., Birbaumer, N., McFarland, D. J., Pfurtscheller, G., and Vaughan, T. M. (2002). Brain-computer interfaces for communication and control. *Clin. Neurophysiol.* 133, 767–791. doi: 10.1016/S1388-2457(02)00057-3

Wolpaw, J. R., and McFarland, D. J. (2004). Control of a two-dimensional movement signal by a noninvasive brain-computer interface in humans. *Proc. Natl. Acad. Sci. U.S.A.* 101, 17849–17854. doi: 10.1073/pnas.0403504101

Wróbel, A. (2000). Beta activity: a carrier for visual attention. *Acta Neurobiol. Exp.* 60, 247–260.

Yoo, S. S., Kim, H., Filandrianos, E., Taghados, S. J., and Park, S. (2013). Non-invasive brain-to-brain interface (BBI): establishing functional links between two brains. *PLoS ONE* 8:e60410. doi: 10.1371/journal.pone.0060410

Zander, T. O., and Kothe, C. (2011). Towards passive brain-computer interfaces: applying brain-computer interface technology to human-machine systems in general. *J. Neural Eng.* 8, 025005. doi: 10.1088/1741-2560/8/2/025005

Conflict of Interest Statement: The authors declare that the research was conducted in the absence of any commercial or financial relationships that could be construed as a potential conflict of interest.

frontiers in Neuroscience

ORIGINAL RESEARCH
published: 31 January 2019
doi: 10.3389/fnins.2019.00036

Small Changes in Inter-Pulse-Intervals Can Cause Synchronized Neuronal Firing During High-Frequency Stimulations in Rat Hippocampus

Zhouyan Feng, Weijian Ma, Zhaoxiang Wang, Chen Qiu and Hanhan Hu*

Key Lab of Biomedical Engineering for Ministry of Education, College of Biomedical Engineering and Instrument Science, Zhejiang University, Hangzhou, China

OPEN ACCESS

Edited by:
Olivier David, Institut National de la Santé et de la Recherche Médicale (INSERM), France

Reviewed by:
Veronique Coizet, INSERM U1216 Grenoble Institut des Neurosciences (GIN), France
Andrei Barborica, University of Bucharest, Romania
Pascale Quilichini, INSERM U1106 Institut de Neurosciences des Systèmes, France

***Correspondence:**
Zhouyan Feng
fengzhouyan@139.com

Specialty section:
This article was submitted to Neural Technology, a section of the journal Frontiers in Neuroscience

Received: *01 November 2018*
Accepted: *15 January 2019*
Published: *31 January 2019*

Citation:
Feng Z, Ma W, Wang Z, Qiu C and Hu H (2019) Small Changes in Inter-Pulse-Intervals Can Cause Synchronized Neuronal Firing During High-Frequency Stimulations in Rat Hippocampus. Front. Neurosci. 13:36. doi: 10.3389/fnins.2019.00036

Deep brain stimulation (DBS) traditionally utilizes electrical pulse sequences with a constant frequency, i.e., constant inter-pulse-interval (IPI), to treat certain brain disorders in clinic. Stimulation sequences with varying frequency have been investigated recently to improve the efficacy of existing DBS therapy and to develop new treatments. However, the effects of such sequences are inconclusive. The present study tests the hypothesis that stimulations with varying IPI can generate neuronal activity markedly different from the activity induced by stimulations with constant IPI. And, the crucial factor causing the distinction is the relative differences in IPI lengths rather than the absolute lengths of IPI nor the average lengths of IPI. In rat experiments *in vivo*, responses of neuronal populations to applied stimulation sequences were collected during stimulations with both constant IPI (control) and random IPI. The stimulations were applied in the efferent fibers antidromically (in alveus) or in the afferent fibers orthodromically (in Schaffer collaterals) of pyramidal cells, the principal cells of hippocampal CA1 region. Amplitudes and areas of population spike (PS) waveforms were used to evaluate the neuronal responses induced by different stimulation paradigms. During the periods of both antidromic and orthodromic high-frequency stimulation (HFS), the HFS with random IPI induced synchronous neuronal firing with large PS even if the lengths of random IPI were limited to a small range of 5–10 ms, corresponding to a frequency range 100–200 Hz. The large PS events did not appear during control stimulations with a constant frequency at 100, 200, or 130 Hz (i.e., the mean frequency of HFS with random IPI uniformly distributed within 5–10 ms). Presumably, nonlinear dynamics in neuronal responses to random IPI might cause the generation of synchronous firing under the situation without any long pauses in HFS

sequences. The results indicate that stimulations with random IPI can generate salient impulses to brain tissues and modulate the synchronization of neuronal activity, thereby providing potential stimulation paradigms for extending DBS therapy in treating more brain diseases, such as disorders of consciousness and vegetative states.

Keywords: high-frequency stimulation, temporal patterns, population spike, synchronous firing, axonal stimulation, hippocampal CA1 region

INTRODUCTION

Deep brain stimulation (DBS) has been developed to treat brain disorders for decades, including Parkinson's disease, essential tremor, dystonia, epilepsy, obsessive-compulsive disorder, addiction, depression, and Alzheimer's disease (Fridley et al., 2012; Udupa and Chen, 2015; Wichmann and DeLong, 2016; Cury et al., 2017). Despite the most successful application of the therapy for treating movement disorders such as Parkinson's disease, DBS treatment for other diseases is not mature currently. New stimulation paradigms have been designed and tested for extending DBS therapy in treating more neurological and psychiatric disorders (Rizzone et al., 2001; Kuncel et al., 2006; Brocker et al., 2017).

Commonly, DBS utilizes biphasic pulse sequences of so-called high-frequency stimulation (HFS) with a constant pulse frequency, that is, a constant inter-pulse-interval (IPI). The efficient pulse frequency for treating movement disorders in clinic is in a range of 90–185 Hz (Rizzone et al., 2001; Kuncel et al., 2006). To improve therapy effects, irregular temporal patterns of stimulation with varying IPI or with pauses have been studied in animal experiments, computational models as well as in clinical treatments (Swan et al., 2016; Brocker et al., 2017; Cassar et al., 2017). However, the results are inconclusive. Many studies have shown that varying IPI may decrease DBS effectiveness. Even if the mean frequency of varying stimulation is as high as constant stimulation, the effectiveness of varying stimulations may be still poorer than constant stimulations (Dorval et al., 2010; Birdno et al., 2012; Kuncel et al., 2012; McConnell et al., 2016).

These studies on therapeutic effects of varying stimulation patterns have been mostly evaluated in relieving the symptoms of movement disorders (Dorval et al., 2010; Swan et al., 2016). The mechanism of effective DBS for treating these disorders has been considered to mask pathological oscillations and abnormal synchronous activity by replacing them with HFS-induced patterns of activity (Eusebio et al., 2011; Wilson et al., 2011; Medeiros and Moraes, 2014; Herrington et al., 2016). Therefore, it has been inferred that long pauses in the stimulations may fail to mask the intrinsic activity or fail to suppress the synchronous activity in the pathological brain regions, thereby decreasing the DBS effectiveness (Llinás et al., 1999; Birdno and Grill, 2008; Swan et al., 2016; McConnell et al., 2016).

However, even pauses as short as 15–25 ms inserted in a basic sequence of constant HFS at a low rate (∼2–4 Hz) are sufficient to decrease the efficacy of DBS (Birdno et al., 2007; Swan et al., 2016). It seems unlikely that such narrow and infrequent gaps could allow the target neurons to recover their intrinsic activity, because a period of seconds to minutes is needed for the neurons to return to original activity after withdrawal of constant HFS (Popovych and Tass, 2014; Feng et al., 2017). On the other hand, even a short pause (e.g., 20 ms) during constant HFS (100- or 200-Hz) can result in generation of highly synchronized population firing of neurons that differs from the asynchronous firing induced by constant HFS (Feng et al., 2014). Therefore, we propose here an alternative hypothesis for the effects of varying IPI: even if the lengths of all IPI are short enough, small changes of IPI can generate neuronal responses quite different from that induced by stimulations of constant IPI. These differences in HFS-induced activity, not a recovery of intrinsic activity, might cause different effects in DBS therapy.

To test the hypothesis, we compared the responses of neuronal populations in the hippocampal CA1 region of anesthetized rats to applied stimulation sequences with both constant IPI (control) and varying IPI in the efferent or afferent axonal fibers of pyramidal cells, the principal cells of CA1 region. The dense compact of CA1 pyramidal cells facilitates the evaluation of synchronous firing of neuronal populations by recording population spikes (PS) *in vivo*. A waveform of PS is generated from the superposition of many, simultaneous single-unit spikes surrounding the recording site (Theoret et al., 1984; Andersen et al., 2000, 2007). Furthermore, axonal activations induced by electrical pulses have been shown to play a crucial role in DBS therapy (Gradinaru et al., 2009; Hess et al., 2013; Girgis and Miller, 2016; Herrington et al., 2016). Therefore, we examined neuronal responses by directly stimulating axonal fibers. In addition, given the fact that hippocampus is a focus region of brain diseases such as epilepsy and Alzheimer's disease (Sankar et al., 2015; Udupa and Chen, 2015), the results of the study can provide important clues for developing new stimulation paradigms to treat more brain diseases.

MATERIALS AND METHODS

Animal Surgery and Electrode Implantation

All animal procedures used in this study conformed to the Guide for the Care and Use of Laboratory Animals (China Ministry of Health). The protocol was approved by the Institutional Animal Care and Use Committee, Zhejiang University. Twenty male Sprague-Dawley rats (adult, 310 ± 48 g) were used for *in vivo* experiments under anesthesia by urethane (1.25 g/kg, i.p.). Surgical procedures and electrode placements were similar to previous reports (Feng et al., 2013, 2017).

Briefly, one recording electrode (RE) and two stimulating electrodes (SE) were inserted into the left hippocampal region of brain. The RE was a 16-channel array (Model Poly2, NeuroNexus Technologies Inc., United States) and was perpendicularly positioned in the CA1 region of hippocampus. The two SE were bipolar concentric stainless-steel electrodes (Model CBCSG75, FHC Inc., United States) and were positioned in the alveus and the Schaffer collaterals of hippocampal CA1 region for antidromic and orthodromic activations of CA1 pyramidal cells, respectively. The waveforms of antidromically- and orthodromically evoked population potentials as well as signals of unit spikes appeared serially in the 16 channel recording array were used to guide the correct positioning of the electrodes.

Recording and Stimulating

Raw signals collected in the hippocampal CA1 region were amplified 100 times by a 16-channel extracellular amplifier (Model 3600, A-M System Inc., United States) with a band-pass filtering range 0.3–5000 Hz. The amplified signals were then sampled by a PowerLab data acquisition system (Model PL3516, ADInstruments Inc., Australia) with a sampling rate of 20 kHz.

Stimulations were sequences of biphasic current pulses with each phase width of 0.1 ms and were generated by a programmable stimulator (Model 3800, A-M System Inc., United States). The current intensity of pulses was 0.3 or 0.4 mA that evoked approximately 75% maximal amplitude of PS according to an input-output curve. The curve was made by applying single pulses with a gradually increased intensity and measuring corresponding evoked PS potentials. The setting of current intensity (75% saturation value) could ensure enough activation to target region and avoid over stimulation simultaneously.

Both constant IPI and varying IPI were used. The pulse frequency of constant IPI was 100, 200, or 130 Hz. The varying IPI changed randomly in a range of 20–600 Hz (i.e., 1.67–50 ms, with a mean pulse frequency 100 Hz) or in a range of 100–200 Hz (i.e., 5–10 ms, with a mean pulse frequency ∼130 Hz).

The duration of stimulation sequences was 80, 140, or 180 s. To compare the differences between effects of random IPI and constant IPI directly, most stimulation sequences started with a 50-s period of constant IPI to reach a steady state of neuronal responses, then switched to a 10-s period random IPI and finally switched back to constant IPI for another 20 s to make a total duration 80 s. In some of the stimulations, the 60-s period (50-s constant + 10-s random IPI) was repeated twice to make a total duration of 140 s. To eliminate the possible impacts of the changes of brain state and other uncontrolled facts, in statistical evaluations, the 10-s (40 to 50 s) period of constant IPI immediately preceding the 10-s (50 to 60 s) period of random IPI was used as a control representing the "steady-state" response induced by constant IPI stimulation. Stimulation sequences with sole random IPI through a whole duration of 3 min (180 s) were also applied to show the persistent of effects induced by random IPI.

Two to four stimulation sequences with different paradigms were performed in each rat experiment. The intervals between stimulation sequences were greater than half an hour to ensure recovery from previous stimulation.

Data Analysis

Amplitudes and areas of PS waveforms were used to evaluate the neuronal responses induced by stimulation sequences. The PS amplitude was measured as the potential difference between the negative peak of PS and the baseline before PS. The PS area was measured as the product of amplitude and half-height width of PS (Theoret et al., 1984). Additionally, "maximum amplitude" of PS within a specific period of stimulation was calculated as the average amplitude of ten largest PS waveforms to eliminate the impact of interference.

All statistical data were represented as mean ± standard deviation. "n" represents the number of rats for data collections or the number of stimulation sequences. Student t-test was used to judge the statistical significance of the differences between data groups.

In addition, to clarify the recording signals in figures, stimulation artifacts were removed by a custom-made MATLAB program with a linear interpolation algorithm. Briefly, a data segment of ∼1.0 ms around each artifact of stimulation pulse was replaced by a short line connecting the two end points of the artifact segment (Yu et al., 2016). Because the bipolar concentric stimulation electrode limited the stimulated area, the stimulation artifacts picked by the recording electrode did not induce substantial saturation in the amplifier. In addition, the detection and evaluation of PS waveforms were performed in the intervals of pulses directly on raw recording signals (0.3–5000 Hz) neither involving the removal of stimulation artifacts nor involving a low-frequency filter of field potentials.

RESULTS

Responses of Neuronal Populations to Antidromic-HFS With Random Inter-Pulse-Intervals

To compare the differences in neuronal responses to HFS with constant and random IPI in the same stimulation sequence, we utilized a HFS sequence starting with a constant pulse frequency and then switching to varying frequencies. Additionally, to focus on the reactions of neuronal axons and somata without involvement of synaptic transmissions, we firstly investigated the responses of CA1 neurons to the antidromic-HFS (A-HFS) in the efferent fibers, the alveus of hippocampal region. **Figure 1** shows a typical example of results that were repeated in five individual rat experiments with the same A-HFS paradigm.

At the onset of A-HFS with a constant pulse frequency (100 Hz), each stimulation pulse evoked a large antidromically evoked population spike (APS, ∼9 mV), indicating that synchronous action potentials propagated from the efferent fibers back to the somata of the neuronal populations in the upstream region of stimulation site (**Figures 1A,B**). The appearance of large APS potentials formed an abrupt change at the onset of stimulation. However, the amplitudes of APS decreased rapidly

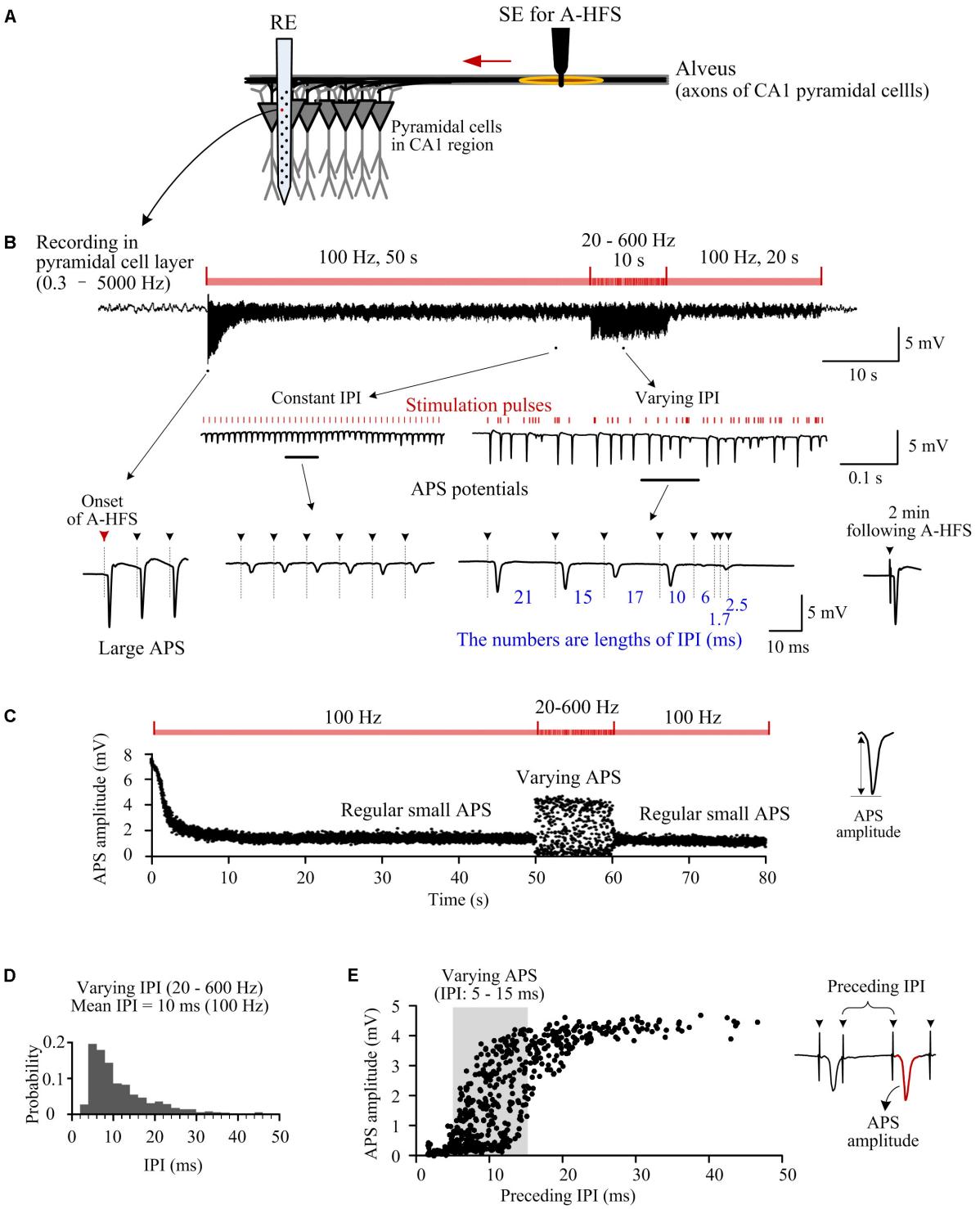

FIGURE 1 | Responses of neuron populations to A-HFS with random inter-pulse-intervals (IPI). **(A)** Schematic diagram of the locations of stimulation electrode (SE) for antidromic-HFS (A-HFS) in the alveus and recording electrode array (RE) in the CA1 region. **(B)** A recording of neuronal responses to 80-s A-HFS with constant IPI (100 Hz, during 0–50 s and 60–80 s) and random IPI (20–600 Hz, during 50–60 s), together with expanded plots of APS waveforms. Red bars denote the stimulation pulses. Dashed lines with arrows denote the locations of removed artifacts of stimulation pulses. **(C)** Scatter diagrams of the amplitudes of APS evoked by each pulse during the A-HFS in **(B)**. **(D)** Probability distribution of the random IPI (20–600 Hz) for the 10-s A-HFS period in **(B)** with a mean pulse frequency of 100 Hz. **(E)** Scatter diagrams of the amplitudes of APS potentials as a function of the lengths of IPI immediately preceding the APS during the 10-s period of A-HFS with random IPI.

in the initial period of stimulation. After tens of seconds of stimulation, the amplitudes of APS stabilized to a low level (∼20% of the initial APS amplitude, **Figures 1B,C**), indicating that the neuronal responses transformed from a transient phase to a steady-state phase with regular small APS evoked by each stimulation pulse. Previous studies have shown that the suppression of APS by prolonged HFS might be caused by axonal failures, a partial block of axonal activation (Jensen and Durand, 2009; Feng et al., 2013, 2014).

The small APS potentials continued with constant 100-Hz stimulation until the pulse frequency was switched into a varying pattern (20–600 Hz, mean 100 Hz) for 10 s. In this 10-s period, APS waveforms with varying amplitudes (0–4.5 mV) followed each stimulation pulse (**Figures 1B,C**). Afterward, when the stimulation was switched back to constant 100 Hz, regular small APS reappeared. Two minutes following the termination of the entire A-HFS, a single test pulse induced an APS waveform (in the lower right of **Figure 1B**) similar to that appeared at the onset of A-HFS, indicating reversibility of the stimulation effects. The recovery of neuronal responses after A-HFS was similar to previous studies with stimulations of pure constant IPI (Feng et al., 2013, 2014). To avoid redundancy, we omitted the details of recovery data.

During the 10-s A-HFS with random IPI, although the mean pulse frequency was still 100 Hz (see **Figure 1D**, a decline distribution was used to ensure a mean frequency of 100 Hz), the amplitudes of APS varied markedly (**Figure 1E**). APS amplitudes were larger ($>$ 4 mV) with a longer preceding IPI (25–50 ms); while APS amplitudes were smaller ($<$ 1 mV) with a shorter preceding IPI (1.7–5 ms) (note the expanded waveforms in **Figure 1B** and the scatter diagrams of APS amplitudes in **Figure 1E**). These data indicated that a longer pause of stimulation might facilitate the generation of a larger APS.

Surprisingly, however, the amplitude of evoked APS still varied in a relative large range of 0–4.5 mV with a preceding IPI in a relative short range of 5–15 ms (shadow area in **Figure 1E**). That is, an APS could also be large following a relative short IPI. This result implied that even if all of the lengths of IPI were short enough without longer pauses, small changes in IPI might also result in population activation of neurons with large APS that was different from the small APS induced by stimulations with constant IPI. Therefore, we next tested the hypothesis by changing the IPI in a smaller range.

Large Population Spikes Appeared During A-HFS With Small Changes in IPI

To investigate the effects of small differences in short IPI on the neuronal responses, we utilized an A-HFS sequence with random IPI only in a range of 5–10 ms (a corresponding frequency range of 100–200 Hz) following a 50-s period of constant frequency 100 or 200 Hz as a control (**Figure 2**).

For a 100 Hz control frequency, the mean pulse frequency (∼130 Hz) of the random-IPI uniformly distributed in 100–200 Hz was higher than the control frequency of constant 100 Hz. Furthermore, no random-IPI was greater than 10 ms (the IPI of constant 100 Hz). Nevertheless, during the period of random IPI, some of the pulses induced larger APS while some other pulses induced no APS (**Figures 2A,B**). To compare the neuronal responses to constant and random IPI, the distributions of APS amplitudes within two neighboring periods of 10-s stimulation were evaluated: 40–50 s of the A-HFS with constant 10 ms (**Figure 2C**) and 50–60 s of the A-HFS with random IPI (**Figure 2D**). The probability distribution of APS amplitudes during constant IPI was approximate to a normal distribution with a small range 0.83–1.90 mV and a mean amplitude 1.32 mV, while the probability distribution of APS amplitudes during random IPI was a decline distribution with a large range 0–3.22 mV and a mean amplitude 1.03 mV. Additionally, the decline distribution of APS amplitudes induced by random IPI was different from the uniform distribution of random IPI (in the upper right of **Figure 2D**), indicating a nonlinear relationship between the neuronal responses and the lengths of IPI.

Similar results were observed with a same stimulation paradigm but an increased control frequency of 200 Hz (**Figures 2E–H**). The increase in control frequency resulted in a decrease of the steady-state APS amplitude to a mean value 0.64 mV (with a smaller range 0.36–1.15 mV) during the 40–50 s of the A-HFS (**Figure 2G**). However, during the 50–60 s of the A-HFS when the stimulation was switched into the pattern of random IPI (still 100–200 Hz), the change of APS amplitudes again increased to a larger range 0–3.38 mV with a mean value 1.17 mV (**Figure 2H**), which were similar to the situation with a lower control frequency 100 Hz (**Figure 2D**).

The above stimulations (**Figure 2**) with both 100 and 200 Hz as a control frequency were repeated in nine rats. Statistical data of the nine experiments showed that with a similar initial APS amplitude induced by the very first pulse at the onset of A-HFS (**Figure 3A**), the mean steady-state APS amplitude of 200-Hz A-HFS was significantly smaller than the corresponding value of 100-Hz A-HFS during control periods of both 40–50 s and 60–70 s. This result was consistent with previous reports, indicating that constant A-HFS with a higher frequency can suppress APS more by inducing deeper failures in axonal conduction (Jensen and Durand, 2009; Feng et al., 2013, 2014). However, both the mean and the interquartile range of APS amplitudes during the 10-s periods of random IPI inserted in 200-Hz control A-HFS were not significantly different from the values with 100-Hz control A-HFS (**Figure 3B**). This result indicated that the neuronal responses to random IPI were not correlated with the preceding suppression level of APS.

More interestingly, despite the limited range of random IPI in 5–10 ms (200–100 Hz), the amplitude ranges of varying APS induced by the random IPI were far beyond the steady-state amplitudes of APS induced by constant IPI of 100 or 200 Hz. The maximum APS amplitudes induced in the periods of random IPI were significantly greater than the maximum APS amplitudes induced in the preceding control periods of both 100- and 200-Hz A-HFS (**Figure 3C**). Additionally, some pulses of random IPI failed to induce APS (amplitude = 0) whereas each pulse of constant IPI induced APS (**Figure 2**).

These results showed that although the range of random IPI was limited in the small range of 100 to 200 Hz, the APS amplitudes induced by random IPI were not limited

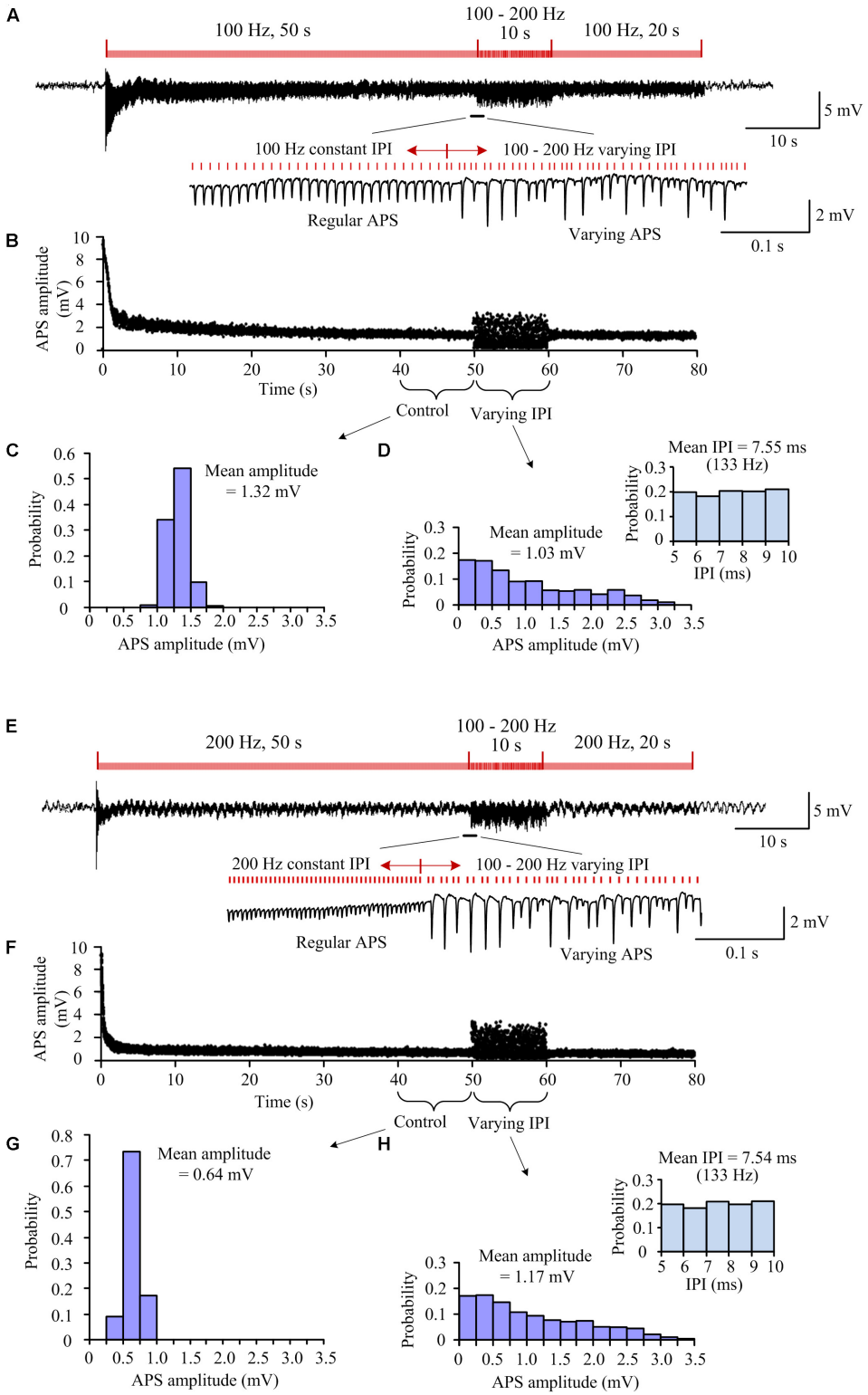

FIGURE 2 | Neuronal responses to A-HFS with constant and random IPI in the range of 100–200 Hz. **(A)** A recording of 80-s A-HFS with constant IPI (100 Hz, during 0–50 s and 60–80 s) and random IPI (100–200 Hz, during 50–60 s), together with expanded plots of APS waveforms. Red bars denote the stimulation pulses. **(B)** Scatter diagrams of the amplitudes of APS evoked by each pulse during the A-HFS in **(A)**. **(C)** Probability distribution of the APS amplitudes during the 10-s control period before the stimulation of random IPI. **(D)** Probability distribution of the APS amplitudes during the 10-s period with random IPI and the probability distribution of IPI (*upper right*). **(E–H)** Corresponding plots as **(A–D)** for A-HFS with a same order of the stimulation paradigms in **(A)** but constant IPI changed to 200 Hz.

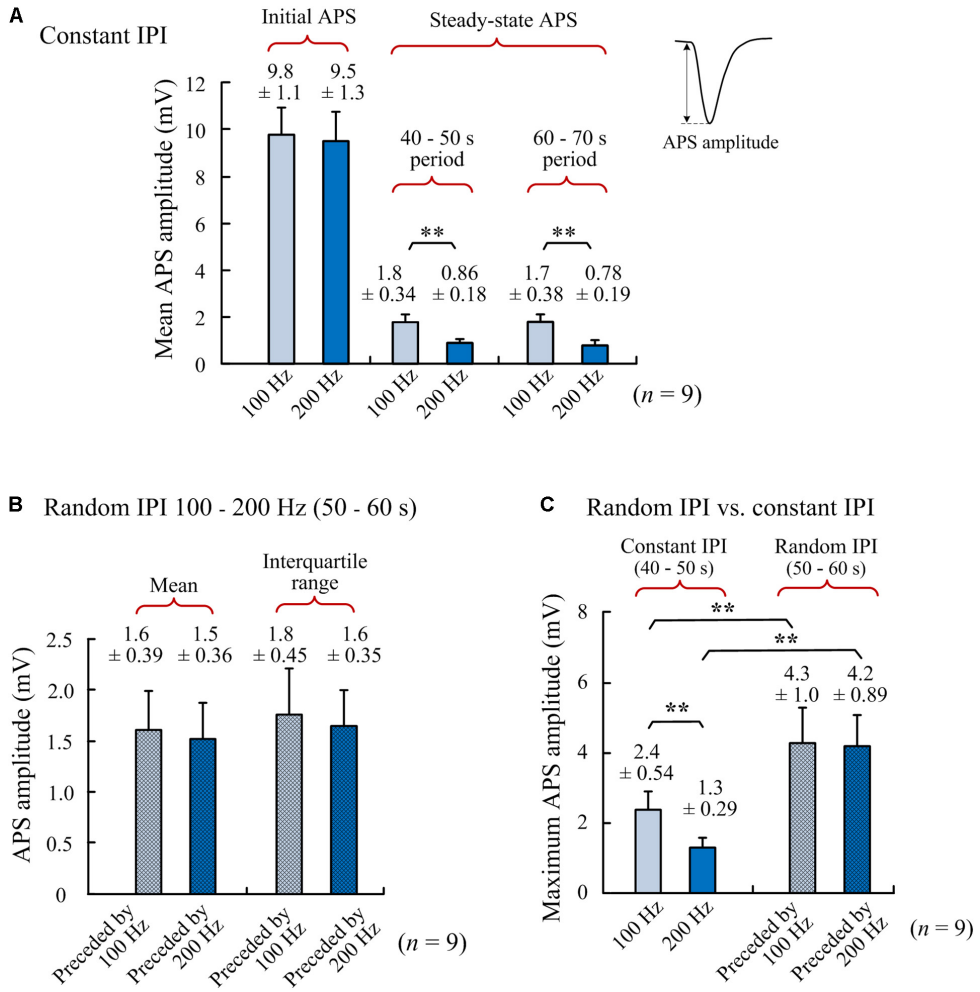

FIGURE 3 | Comparisons of APS amplitudes among different periods of A-HFS. **(A)** Amplitudes of the initial APS (evoked by the very first pulse at the onset of A-HFS) and the steady-state APS (mean amplitudes in 40–50 s and 60–70 s of stimulations) during A-HFS with constant IPI 100 and 200 Hz, respectively. **(B)** Mean APS amplitudes and interquartile ranges of APS amplitudes during 10-s A-HFS periods (50–60 s) with random IPI (100–200 Hz) preceded by 100- or 200-Hz constant stimulations, respectively. **(C)** Maximum APS amplitudes during A-HFS periods with constant IPI (steady-state) and with random IPI. $^{**}P < 0.01$, $n = 9$, *t*-test.

between the amplitude levels of the steady-state APS induced by constant 100 and 200 Hz. Because larger APS represents higher synchronization of action potential firing of neuronal populations, we next tested the hypothesis that irregularity of IPI could facilitate synchronous firing of neurons by reshaping firing timing without significantly changing the total amount of neuronal firing.

Reshaping the Neuronal Firing Timing by A-HFS With Random IPI

Area of an APS waveform can be used to represent the number of neurons that fire action potential synchronously to form the APS (Theoret et al., 1984). Therefore, we used the index of accumulative APS areas to compare the amounts of neuronal firing between the stimulation periods with constant and random IPI. To evaluate the neuronal firing under same amount of stimulation pulses (i.e., same amount of electrical charge injected), the frequency of control stimulation was set at 130 Hz, similar to the mean frequency (133 Hz) of the stimulation with random IPI uniformly distributed in the range 100–200 Hz. The accumulative APS areas per second were similar during the two 10-s periods: the control periods of constant IPI and the period of random IPI (**Figures 4A,B**; $P = 0.64$, $n = 6$, *t*-test). Nevertheless, the interquartile range of APS areas during random IPI was significantly greater than that during constant IPI (**Figure 4C**; $P < 0.01$, $n = 6$, *t*-test). These data indicated that the differences of IPI caused a redistribution of the neuronal firing without significantly altering the total amount of neuronal firing.

To further investigate the relationships between the synchronization of neuronal firing and the random IPI, we examined the correlations among the amplitude of current APS, the amplitude of preceding APS, and the length of preceding

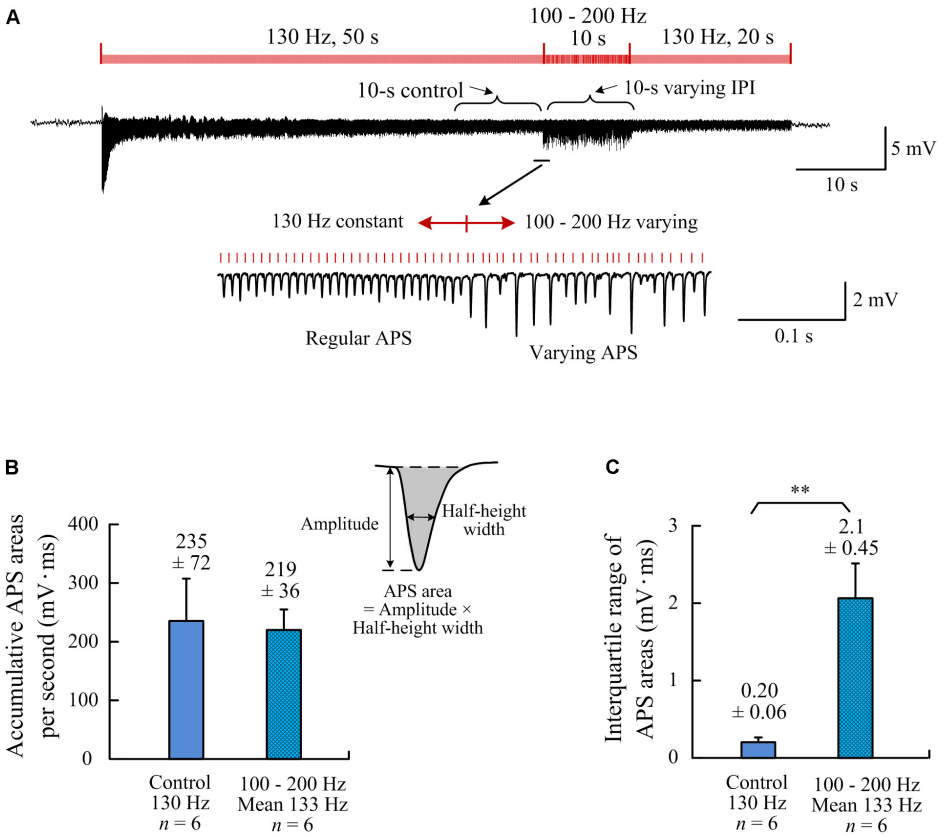

FIGURE 4 | Comparisons of neuronal firing amounts quantified by APS areas during the two different A-HFS periods with constant IPI (control) and with random IPI (but with same amount of pulses). **(A)** a recording of 80-s A-HFS with constant IPI (130 Hz, during 0–50 s and 60–80 s) and random IPI (100–200 Hz, mean ∼130 Hz, during 50–60 s), together with expanded plots of APS waveforms. Red bars denote the stimulation pulses. **(B)** Comparisons of the accumulative APS areas between the control period of constant IPI and the period of random IPI ($P = 0.64$, $n = 6$, t-test). **(C)** Comparisons of the interquartile ranges of APS areas during the two different periods (**$P < 0.01$, $n = 6$, t-test).

IPI (**Figure 5A**). During the 10-s A-HFS with random IPI in the small range of 5–10 ms, larger APS (> 1.8 mV) only followed longer IPI but not shorter IPI (5–7.5 ms, the shade area in **Figure 5B**). Although smaller APS also appeared following longer IPI, many of those smaller APS had a larger preceding APS (**Figures 5C,D**). Additionally, although two longer IPI could exist next to each other in the uniform distribution of random IPI (**Figure 5E**), two larger APS never appeared consecutively (see the shade area in **Figure 5C**). This indicated that a larger preceding APS could prevent a second larger APS immediately induced by the next pulse. As expected, the APS amplitudes did not correlate with current IPI since APS was induced by the preceding pulse but not by the succeeding one (**Figure 5F**). Similar results were obtained in all of the twenty rat experiments by applying A-HFS with the random IPI.

Additionally, to demonstrate the persistent of effects induced by random IPI, in five rat experiments, a stimulation sequence with random IPI (100–200 Hz) through a whole duration of 3 min (180 s) was applied (**Figure 6** upper row). In these same experiments, a control of 3-min stimulation with a constant IPI of 130 Hz frequency (**Figure 6** bottom row) was also applied. The APS events induced at the onsets of the two stimulation sequences were similar. However, during the late periods of stimulations, corresponding to the periods that steady small APS events were induced during A-HFS with constant IPI, large APS appeared irregularly during A-HFS with random IPI. Except the first few seconds of the stimulations, the differences of neuronal responses persisted through the remaining ∼3 min periods of the two separate stimulations. The results indicated that the distinct neuronal responses induced by small changes in IPI (5–10 ms) could last steadily, not transiently.

The above results were all obtained from antidromic stimulations without involving synaptic transmissions. They indicated that during axonal antidromic-HFS, despite the high enough mean-frequency of stimulation, small differences in IPI may significantly change the firing time of neurons to facilitate the generation of highly synchronized action potentials in upstream neuronal somata. Because the stimulation-induced activation of axons can conduct in both antidromic and orthodromic directions simultaneously (Udupa and Chen, 2015; Feng et al., 2017), we hypothesized that the same stimulation paradigms with random IPI applied orthodromically at the afferent fibers of CA1 region could also induce irregular population activity in the post-synaptic neurons downstream.

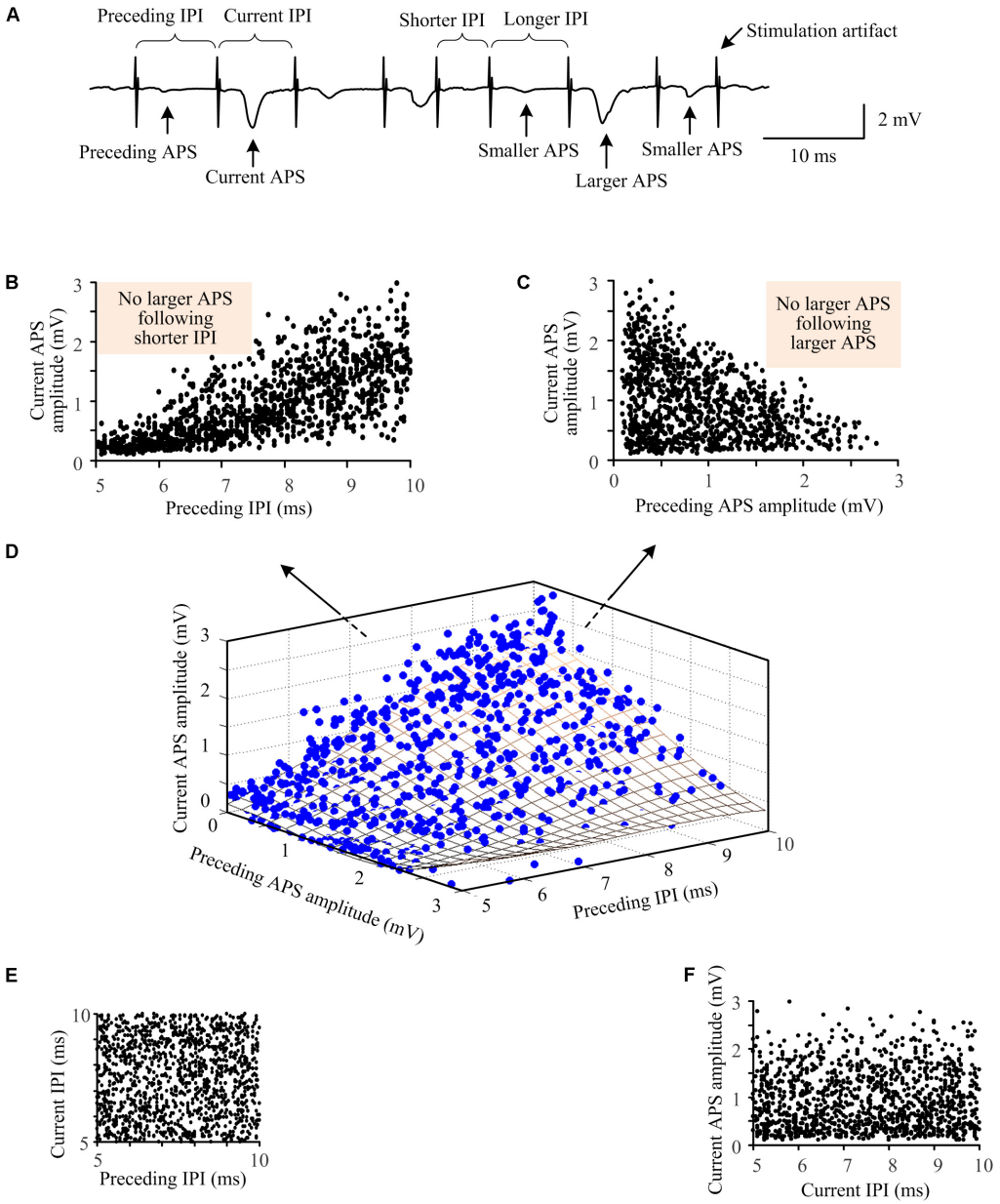

FIGURE 5 | Relationships among the amplitudes of neighboring APS waveforms and the lengths of IPI during A-HFS with random IPI. **(A)** A segment of signal illustrating the definitions of indexes. **(B)** The amplitudes of current APS as a function of the lengths of preceding IPI. **(C)** The amplitudes of current APS as a function of the amplitudes of preceding APS. **(D)** Three-dimensional plot of the amplitudes of current APS as a function of both the amplitudes of preceding APS and the lengths of preceding IPI. The fitting surface (grid surface) denotes the distribution trend of the relationship. **(E)** The length of current IPI did not correlate with the length of preceding IPI, resulting in a uniform distribution between neighboring IPI. **(F)** The amplitude of current APS did not correlate with the length of current IPI.

Thus, we next tested this hypothesis by applying orthodromic-HFS (O-HFS) at the Schaffer collaterals of hippocampal CA1 region (**Figure 7A**).

Synchronous Firing Induced by Orthodromic-HFS With Random IPI

To compare the neuronal responses to O-HFS with constant IPI and random IPI, a period of 50-s O-HFS with constant IPI (10 ms, 100 Hz) was firstly applied and then it was switched to 10-s O-HFS with random IPI (5–10 ms, 200–100 Hz). The identical stimulation paradigm repeated twice and was finally followed by a 20-s constant IPI to complete a total of 140-s stimulation. Consistent with previous reports (Feng et al., 2013, 2017), at the onset of O-HFS, the first pulse evoked a large orthodromically evoked population spike (OPS) followed by a period with PS potentials (**Figure 7B**). After seconds of continuous stimulation of 100 Hz, in the steady-state of neuronal responses, OPS activity

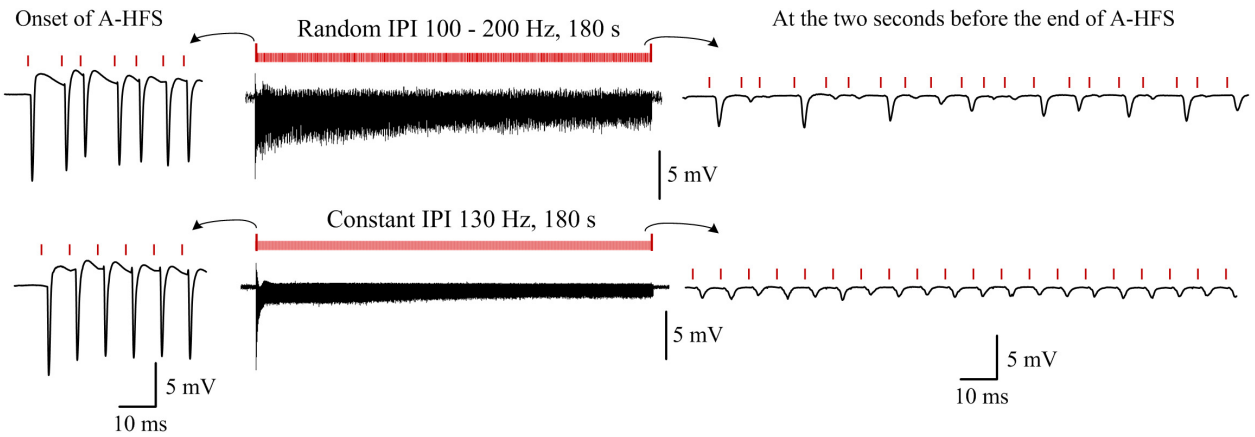

FIGURE 6 | Examples of typical responses of neuron populations to a 180-s A-HFS sequence with entire random IPI in a frequency range of 100–200 Hz (*upper row*) and to a 180-s A-HFS sequence with constant IPI of 130 Hz frequency (*bottom row*). Induced potentials at the onset of A-HFS and at seconds before the end of A-HFS are enlarged. Red bars denote the stimulation pulses.

disappeared. Nevertheless, in this steady-state period without OPS events, unit activity increased (see reference Feng et al., 2017 for details, similar data obtained in the present study are omitted here).

Once the stimulation was switched to O-HFS with random IPI (5–10 ms), OPS activity reappeared. Afterward, immediately following the stimulation switched back to constant IPI (10 ms), OPS disappeared again. The reappearance of OPS was repeated in the second turn of stimulation with random IPI (**Figure 7B**).

Changing the constant IPI from 100 to 200 Hz (5 ms IPI) and keeping the other parameters in the stimulation sequence unchanged, OPS activity also appeared during the two inserted periods with random IPI in the same range of 5–10 ms. No OPS appeared during the steady-state periods with 200-Hz constant IPI except the initial transient-period of O-HFS (**Figure 7C**). In four rat experiments applied by two stimulations with a 100 and 200 Hz control frequency separately (total 8 stimulation sequences), during the two periods of 10-s random IPI, the mean OPS rate was 10.1 ± 1.7 counts/s and the mean OPS amplitude was 4.1 ± 1.0 mV (n = 8 stimulation sequences in four rats; **Figure 7D**). The OPS waveforms were detected by a threshold of 0.5 mV.

These results indicated that during prolonged O-HFS at afferent fibers, pulses with random IPI could irregularly induce synchronized firing of action potentials in the neuronal populations downstream, while pulses with constant IPI did not.

DISCUSSION

The major findings of the present study are: (1) During antidromic stimulations of efferent axons (without involving synaptic transmissions), random IPIs in a high-frequency range of 100–200 Hz can generate highly synchronized firing in the neuronal somata, whereas stimulations with constant IPI cannot. (2) The synchronous firing may be generated by reshaping the timing of neuronal firing with the small changes of IPI rather than by increasing the amount of neuronal firing. (3) Similar to antidromic stimulations, during orthodromic stimulations of afferent axons, HFS with random IPI can also induce synchronous activity in downstream neurons through monosynaptic transmission. The possible mechanisms underlying these observations are discussed below.

Small Relative Differences in IPI Lengths Can Alter Neuronal Activity Markedly

The novel finding of our present study is that even if without long pauses, small changes in short enough IPI corresponding to HFS over 100 Hz can generate a pattern of neuronal activity markedly different from the activity induced by HFS of constant IPI. One could assume that the generation of highly synchronous firing of neurons by random IPI might be attributed to the fact that some of the lengths in random IPI were longer than constant IPI of control stimulation. However, even when all of the IPI (within 5–10 ms) of random stimulation were not longer than the constant IPI (e.g., 10 ms) of control stimulation (**Figures 2A–C**, **7B**), the random stimulation with a higher mean frequency (∼130 Hz) could still induce more synchronous neuronal firing than constant IPI with a lower frequency (100 Hz). The results clearly showed that the crucial stimulation parameter facilitating the generation of highly synchronized firing of neurons (i.e., the larger PS) is the relative differences in IPI lengths rather than the absolute lengths of IPI nor the average lengths of IPI. To our knowledge, this is a novel finding that has not been reported before.

The importance of temporal pattern of stimulation on DBS efficacy, not simply stimulation frequency, has been recognized in many reports (Montgomery, 2005; Baker et al., 2011; Hess et al., 2013). Previous studies have shown that DBS with varying IPI is less effective than with constant IPI (Dorval et al., 2010; Birdno et al., 2012). However, most of these studies have focused on the effects of long pauses that are at least longer than constant IPI of control stimulations (Birdno et al., 2012; Kuncel et al., 2012;

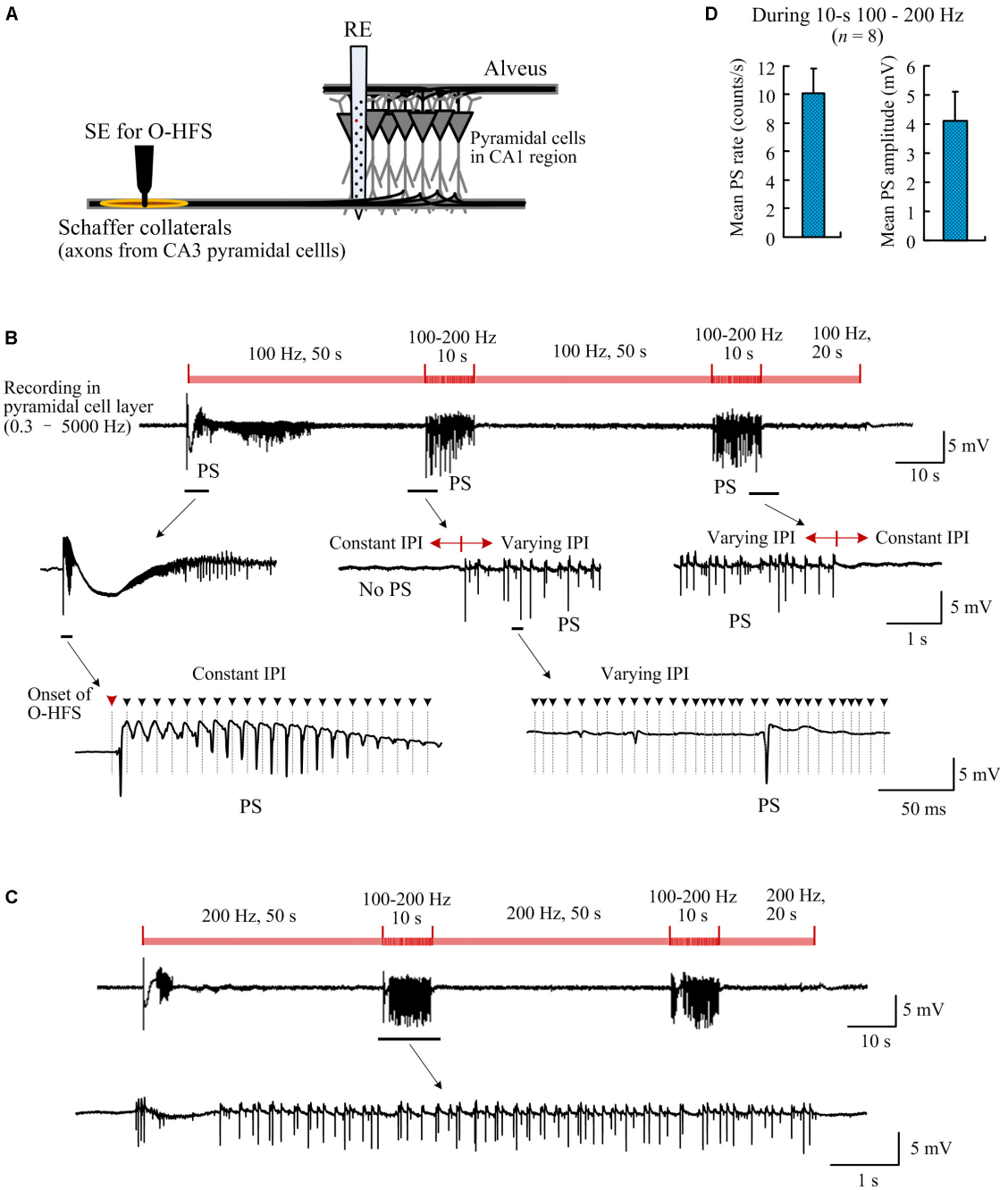

FIGURE 7 | Population spikes induced by orthodromic-HFS (O-HFS) with random IPI. **(A)** Schematic diagram of the locations of stimulation electrode (SE) for O-HFS in the Schaffer collaterals and recording electrode array (RE) in the hippocampal CA1 region. **(B)** A recording example of neuronal responses to 140-s O-HFS with constant IPI (100 Hz, during 0–50 s, 60–110 s, and 120–140 s) and two inserted periods of random IPI (100–200 Hz, during 50–60 s, and 110–120 s). Expanded plots show the orthodromically evoked population spikes (PS). Dashed lines with arrows denote the locations of removed stimulation artifacts. **(C)** A recording example of neuronal responses to a similar stimulation order as in **(B)** but with constant IPI increased to 200 Hz. **(D)** The mean PS rate and the mean PS amplitude during the two periods of 10-s random IPI in both **(B)** and **(C)**, *n* = 8 stimulation sequences in four rats.

McConnell et al., 2016). Long pauses could decrease the HFS effects of DBS in masking or suppressing the synchronous activity of pathological neurons in some disorders (Llinás et al., 1999; Birdno and Grill, 2008; McConnell et al., 2016; Swan et al., 2016). Nevertheless, the present study provides new clues to explain the efficacy decrease of DBS with varying IPI. That is, HFS with varying IPI could induce synchronous activity in target neurons rather than suppress synchronous activity. In addition, long pauses are not necessary to induce the synchronous activity. It might explain why even pauses far shorter than pathological

oscillations may destroy the DBS efficacy (Birdno et al., 2007; Swan et al., 2016). Nonlinear dynamics in neuronal responses to varying IPI might be an underlying mechanism.

Random IPI May Induce Synchronous Firing Through a Nonlinear Recovery Course of HFS-Induced Failures

During steady-state periods of axonal A-HFS with constant IPI, the antidromically evoked population spikes (APS) were suppressed (**Figures 1**, **2**, **3A**). Because the APS potentials are induced by the stimulation excitations traveling along axons antidromically to cell bodies, not involving synaptic transmission; only failures in axons or/and cell bodies can result in the APS suppression. Previous studies have shown that HFS-induced axonal failures may cause the APS decrease by preventing the stimulated axons from generating action potentials following every stimulation pulse (Jensen and Durand, 2009; Zheng et al., 2011; Feng et al., 2013; Rosenbaum et al., 2014). The axonal failures may be caused by potassium accumulation in the narrow space immediately outside the axon membrane that results in a depolarization block (Poolos et al., 1987; Shin et al., 2007; Bellinger et al., 2008). Additionally, the axonal block may be intermittent or partial (Jensen and Durand, 2009; Feng et al., 2017; Guo et al., 2018). That is, the blocked axons could recover in turn and fire an action potential every several pulses thereby generating small APS following each pulse (**Figures 2**, **3A**). Furthermore, the extent of axonal block depends on stimulation frequency. With a higher stimulation frequency, fewer axons can follow each stimulation pulse to generate an action potential (Feng et al., 2013, 2014; Guo et al., 2018). Thus, the APS amplitudes during steady-state periods of 200-Hz A-HFS were smaller than the values during 100-Hz A-HFS (**Figure 3A**).

This frequency-dependent block of axons implies that the amplitudes of evoked APS could be positively correlated to the length of preceding IPI. That is, if the IPI varies in a range of 5–10 ms, the APS amplitudes should be expected to vary in a range limited by the upper and lower limits of APS amplitudes induced by constant 100- and 200-Hz A-HFS, respectively. Surprisingly, our present study shows that the maximum APS amplitudes induced by random IPI were significantly larger than the limit values of corresponding A-HFS with constant IPI (**Figure 3C**).

In addition, for a similar mean frequency (i.e., same amount of stimulation pulses), the total amount of neuronal firing induced by random IPI was similar to that induced by constant IPI (**Figure 4B**). Therefore, randomization of IPI could only redistribute the firing time of neurons but not increase their firing amount. Presumably, a nonlinear time-course of recovery from HFS-induced axonal block could cause the redistribution of firing time by random IPI. The nonlinearity of recovery may be due to highly nonlinear dynamics of ionic-channel activations in cell membranes and their response to stimulations (Hodgkin and Huxley, 1952; Grill, 2015).

One can imagine that with constant IPI, every time a stimulation pulse arrives, a similar number of blocked axons would have recovered readily to respond to the pulse thereby generating APS with uniform and small amplitudes. In contrast, with random IPI, the number of ready axons for each coming pulse would be different due to multiple factors, such as the length of preceding IPI and the history of axon firing (**Figure 5**), that are determined by the nonlinear dynamics of axonal membranes. A pulse arriving "ahead of time", i.e., a relatively shorter IPI, could prevent some axons from firing and postpone their firing to follow the second incoming pulse, together with the firing of other available axons, thereby forming a larger APS. Because of the extension of refractory period of axons by HFS-induced depolarization block (Feng et al., 2014), the larger APS might prevent the third incoming pulse from inducing axonal firing, causing no APS following the third pulse. Thus, the random appearances of "extreme" large and "extreme" small APS would result in the large range of APS amplitudes (see **Figures 2–5**).

The APS potentials induced by A-HFS do not involve synaptic transmission. During O-HFS, the axonal excitations travel orthodromically to terminals and then through synapses to post-synaptic neurons. The additional effect of synaptic transmission in the orthodromic responses of neurons might further increase the timing variability in neuronal firing among random IPI thereby generating large population spikes in the post-synaptic neurons of downstream regions (**Figure 7**).

Taken together, a nonlinear recovery course of HFS-induced axonal block could be responsible substantially for producing highly synchronized firing during stimulation of random IPI even with a high enough mean frequency. The different neuronal responses were switched back and forth in seconds immediately following the switches between random IPI and constant IPI in the antidromic-HFS without involving synapses. Therefore, the changes of neuronal responses could hardly be caused by hippocampal plasticity that mainly generates in synapses and is characterized by long-term changes. Nevertheless, nonlinear dynamics in neuronal elements other than axons, such as cell bodies and synaptic transmissions might also contribute to the synchronous activity induced by varying IPI and await further studies.

Implication and Limitation

The distinct pattern of neuronal responses to the stimulations with random IPI provides clues for extending the DBS therapy to brain diseases other than movement disorders.

Previous studies have shown that conventional DBS with a constant pulse frequency can regularize neuronal firing patterns. The regularization of neuronal firing may be crucial for the clinical effectiveness of DBS in treating movement disorders (Kuncel et al., 2007; Birdno and Grill, 2008; Dorval et al., 2008). However, different brain diseases are caused by distinct pathological mechanisms thereby likely requiring different DBS patterns to obtain desirable efficacy. For example, DBS has been used to treat disorders of consciousness caused by severe traumatic brain injury to arouse patients from minimally conscious state (Schiff et al., 2007). Studies have shown that stimulations with random IPI might be more effective for increasing arousal than conventional constant IPI (Quinkert and Pfaff, 2012; Tabansky et al., 2014). The present study suggests that synchronous activation may be induced by random IPI, generating salient impulses to brain tissues. It seems reasonable

to speculate that the impulses may arouse an "inactive" brain more effectively than regular and mild inputs from constant IPI. Therefore, the irregular stimulation could be potential paradigms for advancing DBS therapy in treating more brain diseases, such as disorders of consciousness and memory decline (Schiff et al., 2007; Laxton et al., 2010).

Taking the advantage of the dense and lamellar distributions of hippocampal neurons to facilitate the evaluation of synchronization of neuronal firing, we performed the present study in the hippocampal region. Besides direct revelations for treating diseases generated in hippocampi such as epilepsy and Alzheimer's disease (Sankar et al., 2015; Udupa and Chen, 2015), the results of direct responses of hippocampal neurons to stimulations with random IPI may also extend to neurons in other brain regions based on general properties of most brain neurons. Nevertheless, brain regions other than hippocampus need to be investigated to finally verify the universality of the neuronal responses to stimulations of random IPI.

Although urethane was used in the *in vivo* experiments here, the influences of the anesthetic on neuronal activity in brain are slight (Shirasaka and Wasterlain, 1995; Sceniak and Maciver, 2006). Additionally, we used a control of constant IPI in the same stimulation sequence with random IPI. Therefore, a small potential decrease of background neuronal activity by the use of anesthetic should not affect the comparison of neuronal responses to the stimulations switched back and forth in seconds between constant IPI and random IPI. Nevertheless, further studies are needed to duplicate the results in awake animals. Finally, the therapeutic efficacies of random IPI await investigations in pathological models of animals other than normal animals.

CONCLUSION

Previous studies have shown that high-frequency pulse stimulation with constant IPI can desynchronize neuronal activity or generate asynchronous firing in target neurons (Medeiros and Moraes, 2014; Popovych and Tass, 2014; Feng et al., 2017), whereas the present study shows that small random changes of IPI can result in synchronous firing of population neurons even without long IPI. The results suggest that small changes of IPI can modulate the synchronization of neuronal activity during HFS. The novel finding provides clues for extending the DBS therapy widely to more brain diseases.

AUTHOR CONTRIBUTIONS

ZF and ZW designed the experiments and interpreted the data. WM, CQ, HH, and ZW performed the experiments and analyzed the data. ZF wrote the manuscript. All authors approved the final version of the manuscript to be published and agreed to be accountable for all aspects of the manuscript.

FUNDING

This work was supported by the National Natural Science Foundation of China (No. 30970753) and by Major Scientific Project of Zhejiang Lab (No. 2018DG0ZX01).

REFERENCES

Andersen, P., Morris, R., and Amaral, D. (2007). *The Hippocampus Book*. Oxford: Oxford University Press.

Andersen, P., Soleng, A. F., and Raastad, M. (2000). The hippocampal lamella hypothesis revisited. *Brain Res.* 886, 165–171. doi: 10.1016/S0006-8993(00)02991-7

Baker, K. B., Zhang, J., and Vitek, J. L. (2011). Pallidal stimulation: effect of pattern and rate on bradykinesia in the non-human primate model of Parkinson's disease. *Exp. Neurol.* 231, 309–313. doi: 10.1016/j.expneurol.2011.06.012

Bellinger, S. C., Miyazawa, G., and Steinmetz, P. N. (2008). Submyelin potassium accumulation may functionally block subsets of local axons during deep brain stimulation: a modeling study. *J. Neural Eng.* 5, 263–274. doi: 10.1088/1741-2560/5/3/001

Birdno, M. J., Cooper, S. E., Rezai, A. R., and Grill, W. M. (2007). Pulse-to-pulse changes in the frequency of deep brain stimulation affect tremor and modeled neuronal activity. *J. Neurophysiol.* 98, 1675–1684. doi: 10.1152/jn.00547.2007

Birdno, M. J., and Grill, W. M. (2008). Mechanisms of deep brain stimulation in movement disorders as revealed by changes in stimulus frequency. *Neurotherapeutics* 5, 14–25. doi: 10.1016/j.nurt.2007.10.067

Birdno, M. J., Kuncel, A. M., Dorval, A. D., Turner, D. A., Gross, R. E., and Grill, W. M. (2012). Stimulus features underlying reduced tremor suppression with temporally patterned deep brain stimulation. *J. Neurophysiol.* 107, 364–383. doi: 10.1152/jn.00906.2010

Brocker, D. T., Swan, B. D., So, R. Q., Turner, D. A., Gross, R. E., and Grill, W. M. (2017). Optimized temporal pattern of brain stimulation designed by computational evolution. *Sci. Transl. Med.* 9:eaah3532. doi: 10.1126/scitranslmed.aah3532

Cassar, I. R., Titus, N. D., and Grill, W. M. (2017). An improved genetic algorithm for designing optimal temporal patterns of neural stimulation. *J. Neural Eng.* 14:066013. doi: 10.1088/1741-2552/aa8270

Cury, R. G., Fraix, V., Castrioto, A., Pérez Fernández, M. A., Krack, P., Chabardes, S., et al. (2017). Thalamic deep brain stimulation for tremor in Parkinson disease, essential tremor, and dystonia. *Neurology* 89, 1416–1423. doi: 10.1212/WNL.0000000000004295

Dorval, A. D., Kuncel, A. M., Birdno, M. J., Turner, D. A., and Grill, W. M. (2010). Deep brain stimulation alleviates parkinsonian bradykinesia by regularizing pallidal activity. *J. Neurophysiol.* 104, 911–921. doi: 10.1152/jn.00103.2010

Dorval, A. D., Russo, G. S., Hashimoto, T., Xu, W., Grill, W. M., and Vitek, J. L. (2008). Deep brain stimulation reduces neuronal entropy in the MPTP-primate model of Parkinson's disease. *J. Neurophysiol.* 100, 2807–2818. doi: 10.1152/jn.90763.2008

Eusebio, A., Thevathasan, W., Gaynor, L. D., Pogosyan, A., Bye, E., Foltynie, T., et al. (2011). Deep brain stimulation can suppress pathological synchronisation in parkinsonian patients. *J. Neurol. Neurosurg. Psychiatry* 82, 569–573. doi: 10.1136/jnnp.2010.217489

Feng, Z., Wang, Z., Guo, Z., Zhou, W., Cai, Z., and Durand, D. M. (2017). High frequency stimulation of afferent fibers generates asynchronous firing in the downstream neurons in hippocampus through partial block of axonal conduction. *Brain Res.* 1661, 67–78. doi: 10.1016/j.brainres.2017.02.008

Feng, Z., Ying, Y., Guo, Z., Cao, J., and Durand, D. M. (2014). High frequency stimulation extends the refractory period and generates axonal block in the rat hippocampus. *Brain Stimul.* 7, 680–689. doi: 10.1016/j.brs.2014.03.011

Feng, Z., Zheng, X., Yu, Y., and Durand, D. M. (2013). Functional disconnection of axonal fibers generated by high frequency stimulation in the hippocampal CA1 region *in vivo*. *Brain Res.* 1509, 32–42. doi: 10.1016/j.brainres.2013.02.048

Fridley, J., Thomas, J. G., Navarro, J. C., and Yoshor, D. (2012). Brain stimulation for the treatment of epilepsy. *Neurosurg. Focus* 32:E13. doi: 10.3171/2012.1.FOCUS11334

Girgis, F., and Miller, J. P. (2016). White matter stimulation for the treatment of epilepsy. *Seizure* 37, 28–31. doi: 10.1016/j.seizure.2016.02.004

Gradinaru, V., Mogri, M., Thompson, K. R., Henderson, J. M., and Deisseroth, K. (2009). Optical deconstruction of parkinsonian neural circuitry. *Science* 324, 354–359. doi: 10.1126/science.1167093

Grill, W. M. (2015). Model-based analysis and design of waveforms for efficient neural stimulation. *Prog. Brain Res.* 222, 147–162. doi: 10.1016/bs.pbr.2015.07.031

Guo, Z., Feng, Z., Wang, Y., and Wei, X. (2018). Simulation study of intermittent axonal block and desynchronization effect induced by high-frequency stimulation of electrical pulses. *Front. Neurosci.* 12:858. doi: 10.3389/fnins.2018.00858

Herrington, T. M., Cheng, J. J., and Eskandar, E. N. (2016). Mechanisms of deep brain stimulation. *J. Neurophysiol.* 115, 19–38. doi: 10.1152/jn.00281.2015

Hess, C. W., Vaillancourt, D. E., and Okun, M. S. (2013). The temporal pattern of stimulation may be important to the mechanism of deep brain stimulation. *Exp. Neurol.* 247, 296–302. doi: 10.1016/j.expneurol.2013.02.001

Hodgkin, A. L., and Huxley, A. F. (1952). A quantitative description of membrane current and its application to conduction and excitation in nerve. *J. Physiol.* 117, 500–544. doi: 10.1113/jphysiol.1952.sp004764

Jensen, A. L., and Durand, D. M. (2009). High frequency stimulation can block axonal conduction. *Exp. Neurol.* 220, 57–70. doi: 10.1016/j.expneurol.2009.07.023

Kuncel, A. M., Birdno, M. J., Swan, B. D., and Grill, W. M. (2012). Tremor reduction and modeled neural activity during cycling thalamic deep brain stimulation. *Clin. Neurophysiol.* 123, 1044–1052. doi: 10.1016/j.clinph.2011.07.052

Kuncel, A. M., Cooper, S. E., Wolgamuth, B. R., Clyde, M. A., Snyder, S. A., Montgomery, E. B. Jr., et al. (2006). Clinical response to varying the stimulus parameters in deep brain stimulation for essential tremor. *Mov. Disord.* 21, 1920–1928. doi: 10.1002/mds.21087

Kuncel, A. M., Cooper, S. E., Wolgamuth, B. R., and Grill, W. M. (2007). Amplitude- and frequency-dependent changes in neuronal regularity parallel changes in tremor with thalamic deep brain stimulation. *IEEE Trans. Neural Syst. Rehabil. Eng.* 15, 190–197. doi: 10.1109/TNSRE.2007.897004

Laxton, A. W., Tang-Wai, D. F., McAndrews, M. P., and Lozano, A. M. (2010). A phase I trial of deep brain stimulation of memory circuits in Alzheimer's disease. *Ann. Neurol.* 68, 521–534. doi: 10.1002/ana.22089

Llinás, R. R., Ribary, U., Jeanmonod, D., Kronberg, E., and Mitra, P. P. (1999). Thalamocortical dysrhythmia: a neurological and neuropsychiatric syndrome characterized by magnetoencephalography. *Proc. Natl. Acad. Sci. U.S.A.* 96, 15222–15227. doi: 10.1073/pnas.96.26.15222

McConnell, G. C., So, R. Q., and Grill, W. M. (2016). Failure to suppress low-frequency neuronal oscillatory activity underlies the reduced effectiveness of random patterns of deep brain stimulation. *J. Neurophysiol.* 115, 2791–2802. doi: 10.1152/jn.00822.2015

Medeiros, D. C., and Moraes, M. F. (2014). Focus on desynchronization rather than excitability: a new strategy for intraencephalic electrical stimulation. *Epilepsy Behav.* 38, 32–36. doi: 10.1016/j.yebeh.2013.12.034

Montgomery, E. J. (2005). Effect of subthalamic nucleus stimulation patterns on motor performance in Parkinson's disease. *Parkinsonism Relat. Disord.* 11, 167–171. doi: 10.1016/j.parkreldis.2004.12.002

Poolos, N. P., Mauk, M. D., and Kocsis, J. D. (1987). Activity-evoked increases in extracellular potassium modulate presynaptic excitability in the CA1 region of the hippocampus. *J. Neurophysiol.* 58, 404–416. doi: 10.1152/jn.1987.58.2.404

Popovych, O. V., and Tass, P. A. (2014). Control of abnormal synchronization in neurological disorders. *Front. Neurol.* 5:268. doi: 10.3389/fneur.2014.00268

Quinkert, A. W., and Pfaff, D. W. (2012). Temporal patterns of deep brain stimulation generated with a true random number generator and the logistic equation: effects on CNS arousal in mice. *Behav. Brain Res.* 229, 349–358. doi: 10.1016/j.bbr.2012.01.025

Rizzone, M., Lanotte, M., Bergamasco, B., Tavella, A., Torre, E., Faccani, G., et al. (2001). Deep brain stimulation of the subthalamic nucleus in Parkinson's disease: effects of variation in stimulation parameters. *J. Neurol. Neurosurg. Psychiatry* 71, 215–219. doi: 10.1136/jnnp.74.8.1036

Rosenbaum, R., Zimnik, A., Zheng, F., Turner, R. S., Alzheimer, C., Doiron, B., et al. (2014). Axonal and synaptic failure suppress the transfer of firing rate oscillations, synchrony and information during high frequency deep brain stimulation. *Neurobiol. Dis.* 62, 86–99. doi: 10.1016/j.nbd.2013.09.006

Sankar, T., Chakravarty, M. M., Bescos, A., Lara, M., Obuchi, T., Laxton, A. W., et al. (2015). Deep brain stimulation influences brain structure in Alzheimer's disease. *Brain Stimul.* 8, 645–654. doi: 10.1016/j.brs.2014.11.020

Sceniak, M. P., and Maciver, M. B. (2006). Cellular actions of urethane on rat visual cortical neurons in vitro. *J. Neurophysiol.* 95, 3865–3874. doi: 10.1152/jn.01196.2005

Schiff, N. D., Giacino, J. T., Kalmar, K., Victor, J. D., Baker, K., Gerber, M., et al. (2007). Behavioural improvements with thalamic stimulation after severe traumatic brain injury. *Nature* 448, 600–603. doi: 10.1038/nature06041

Shin, D. S., Samoilova, M., Cotic, M., Zhang, L., Brotchie, J. M., and Carlen, P. L. (2007). High frequency stimulation or elevated K+ depresses neuronal activity in the rat entopeduncular nucleus. *Neuroscience* 149, 68–86. doi: 10.1016/j.neuroscience.2007.06.055

Shirasaka, Y., and Wasterlain, C. G. (1995). The effect of urethane anesthesia on evoked potentials in dentate gyrus. *Eur. J. Pharmacol.* 282, 11–17. doi: 10.1016/0014-2999(95)00244-F

Swan, B. D., Brocker, D. T., Hilliard, J. D., Tatter, S. B., Gross, R. E., Turner, D. A., et al. (2016). Short pauses in thalamic deep brain stimulation promote tremor and neuronal bursting. *Clin. Neurophysiol.* 127, 1551–1559. doi: 10.1016/j.clinph.2015.07.034

Tabansky, I., Quinkert, A. W., Rahman, N., Muller, S. Z., Lofgren, J., Rudling, J., et al. (2014). Temporally-patterned deep brain stimulation in a mouse model of multiple traumatic brain injury. *Behav. Brain Res.* 273, 123–132. doi: 10.1016/j.bbr.2014.07.026

Theoret, Y., Brown, A., Fleming, S. P., and Capek, R. (1984). Hippocampal field potential: a microcomputer aided comparison of amplitude and integral. *Brain Res. Bull.* 12, 589–595. doi: 10.1016/0361-9230(84)90178-3

Udupa, K., and Chen, R. (2015). The mechanisms of action of deep brain stimulation and ideas for the future development. *Prog. Neurobiol.* 133, 27–49. doi: 10.1016/j.pneurobio.2015.08.001

Wichmann, T., and DeLong, M. R. (2016). Deep brain stimulation for movement disorders of basal ganglia origin: restoring function or functionality? *Neurotherapeutics* 13, 264–283. doi: 10.1007/s13311-016-0426-6

Wilson, C. J., Beverlin, B. N., and Netoff, T. (2011). Chaotic desynchronization as the therapeutic mechanism of deep brain stimulation. *Front. Syst. Neurosci.* 5:50. doi: 10.3389/fnsys.2011.00050

Yu, Y., Feng, Z., Cao, J., Guo, Z., Wang, Z., Hu, N., et al. (2016). Modulation of local field potentials by high-frequency stimulation of afferent axons in the hippocampal CA1 region. *J. Integr. Neurosci.* 15, 1–17. doi: 10.1142/S0219635216500011

Zheng, F., Lammert, K., Nixdorf-Bergweiler, B. E., Steigerwald, F., Volkmann, J., and Alzheimer, C. (2011). Axonal failure during high frequency stimulation of rat subthalamic nucleus. *J. Physiol.* 589, 2781–2793. doi: 10.1113/jphysiol.2011.205807

Conflict of Interest Statement: The authors declare that the research was conducted in the absence of any commercial or financial relationships that could be construed as a potential conflict of interest.

frontiers in Neuroscience

ORIGINAL RESEARCH
published: 27 February 2019
doi: 10.3389/fnins.2019.00161

Motor Task-Dependent Dissociated Effects of Transcranial Random Noise Stimulation in a Finger-Tapping Task Versus a Go/No-Go Task on Corticospinal Excitability and Task Performance

Andreas Jooss[1], Linus Haberbosch[1], Arvid Köhn[1], Maria Rönnefarth[1], Rouven Bathe-Peters[1], Leonard Kozarzewski[1], Robert Fleischmann[1,2], Michael Scholz[3], Sein Schmidt[1†] and Stephan A. Brandt[1†]*

[1] Department of Neurology, Charité – Universitätsmedizin Berlin, Berlin, Germany, [2] Department of Neurology, Universitätsmedizin Greifswald, Greifswald, Germany, [3] Neural Information Processing Group, Technische Universität Berlin, Berlin, Germany

OPEN ACCESS

Edited by:
Mikhail Lebedev, Duke University, United States

Reviewed by:
Makii Muthalib, Université de Montpellier, France
Raffaella Ricci, University of Turin, Italy
Takashi Hanakawa, National Center of Neurology and Psychiatry, Japan

***Correspondence:**
Andreas Jooss
andreas.jooss@charite.de

† These authors have contributed equally to this work

Specialty section:
This article was submitted to Neural Technology, a section of the journal Frontiers in Neuroscience

Received: *30 October 2018*
Accepted: *12 February 2019*
Published: *27 February 2019*

Citation:
Jooss A, Haberbosch L, Köhn A, Rönnefarth M, Bathe-Peters R, Kozarzewski L, Fleischmann R, Scholz M, Schmidt S and Brandt SA (2019) Motor Task-Dependent Dissociated Effects of Transcranial Random Noise Stimulation in a Finger-Tapping Task Versus a Go/No-Go Task on Corticospinal Excitability and Task Performance. Front. Neurosci. 13:161. doi: 10.3389/fnins.2019.00161

Background and Objective: Transcranial random noise stimulation (tRNS) is an emerging non-invasive brain stimulation technique to modulate brain function, with previous studies highlighting its considerable benefits in therapeutic stimulation of the motor system. However, high variability of results and bidirectional task-dependent effects limit more widespread clinical application. Task dependency largely results from a lack of understanding of the interaction between externally applied tRNS and the endogenous state of neural activity during stimulation. Hence, the aim of this study was to investigate the task dependency of tRNS-induced neuromodulation in the motor system using a finger-tapping task (FT) versus a go/no-go task (GNG). We hypothesized that the tasks would modulate tRNS' effects on corticospinal excitability (CSE) and task performance in opposite directions.

Methods: Thirty healthy subjects received 10 min of tRNS of the dominant primary motor cortex in a double-blind, sham-controlled study design. tRNS was applied during two well-established tasks tied to diverging brain states. Accordingly, participants were randomly assigned to two equally-sized groups: the first group performed a simple motor training task (FT task), known primarily to increase CSE, while the second group performed an inhibitory control task (go/no-go task) associated with inhibition of CSE. To establish task-dependent effects of tRNS, CSE was evaluated prior to- and after stimulation with navigated transcranial magnetic stimulation.

Results: In an 'activating' motor task, tRNS during FT significantly facilitated CSE. FT task performance improvements, shown by training-related reductions in intertap intervals and increased number of finger taps, were similar for both tRNS and sham stimulation. In an 'inhibitory' motor task, tRNS during GNG left CSE unchanged while

inhibitory control was enhanced as shown by slowed reaction times and enhanced task accuracy during and after stimulation.

Conclusion: We provide evidence that tRNS-induced neuromodulatory effects are task-dependent and that resulting enhancements are specific to the underlying task-dependent brain state. While mechanisms underlying this effect require further investigation, these findings highlight the potential of tRNS in enhancing task-dependent brain states to modulate human behavior.

Keywords: random noise stimulation, transcranial electrical stimulation, task dependency, finger-tapping task, go/no-go task, corticospinal excitability, neuroplasticity

INTRODUCTION

Transcranial electrical stimulation applied to the primary motor cortex is a non-invasive, portable, and low-cost method shown to enhance motor function in healthy subjects and maximize recovery after stroke (Talelli and Rothwell, 2006; Hummel et al., 2008). In addition to tDCS, tRNS is emerging as a promising neuromodulatory tool (Terney et al., 2008; Schmidt et al., 2013b; Prichard et al., 2014). In contrast to the constant direct current of tDCS, tRNS uses a biphasic alternating current with a random amplitude and frequency, drawn from a frequency range between 0.1–640 Hz (full spectrum) or 100–640 Hz (high-frequency). While tDCS modulates resting membrane potential, tRNS is understood to facilitate transmission of existing subthreshold neural activity to increase neuron excitability (Terney et al., 2008; Schmidt et al., 2013b).

Transcranial random noise stimulation is reported to provide considerable benefits over tDCS including polarity independence of stimulation effects (Terney et al., 2008), more pronounced effect sizes (Fertonani et al., 2011) and possibly improved reliability (Antal et al., 2010). Interestingly, tRNS has been suggested to be a vital component in a patterned, individualized stimulation algorithm aiming to maximize recovery after stroke (Schmidt et al., 2013b). Together, these findings suggest that tRNS might be more reliable, safer and better suited for therapeutic stimulation of the motor system.

However, a major and largely unresolved challenge across all transcranial electrical stimulation methods is the high variability of results, limiting more widespread clinical application. Important factors influencing interindividual variability in transcranial electrical stimulation studies are the baseline neuronal level of motor and cognitive function, psychological factors, circadian rhythm, genetics, anatomy, age, and variability in assessment methods (e.g., TMS) (Li et al., 2015). Additionally, since the state of neuron populations during stimulation is likely to play a pivotal role for the final behavioral effect, a significant part of variability is understood to be related to the brain's task dependent activity state during stimulation (Silvanto et al., 2008; Li et al., 2015). The term brain state is used to describe characteristic changes in global brain activity dynamically adjusted to task demands (Gilbert and Sigman, 2007; Lee and Dan, 2012). Task dependency is a well-established phenomenon in non-invasive brain stimulation studies (Antal et al., 2007; Silvanto et al., 2008; Terney et al., 2008). It implies that the neuromodulatory effects of non-invasive brain stimulation might vary strongly dependent on the endogenous brain state both prior to as well as during stimulation.

In the motor system, CSE, acquired by TMS, is an electrophysiological parameter providing a direct, temporally and spatially precise readout to monitor task-dependent activation and inhibition via MEPs. CSE quantifies state changes of the stimulated motor cortex by probing post-synaptic corticospinal projections (Bestmann and Krakauer, 2015).

Studies aiming to modulate CSE and induce behavioral changes with tRNS highlight the controversial role of task-dependent brain states. tRNS was shown to have bidirectional task-dependent effects on CSE, which is associated with motor learning and recovery. tRNS applied *offline*, i.e., in idle subjects, was shown to increase CSE (Terney et al., 2008). Motor and cognitive tasks carried out *online*, i.e., during stimulation were shown to reduce CSE (Terney et al., 2008). Nevertheless, motor skill learning enhancements were found to be driven primarily by online effects during stimulation (Prichard et al., 2014). Saiote and colleagues investigated functional magnetic resonance imaging changes following a visuomotor task with online tRNS and found stimulation related blood-oxygen-level dependent changes only in regions related to the task, implying direct interaction of online tRNS with task related activity (Saiote et al., 2013). Results from these and other studies conducted in the visual- and cognitive domains (Fertonani et al., 2011; Pirulli et al., 2013; Snowball et al., 2013) suggest that the neuromodulatory effects of tRNS are dependent on *whether* a task and *what type* of task is performed online during stimulation, with enhancements specific to the engaged neural population or brain state.

The aim of this study was to investigate the task dependency of tRNS-induced neuromodulation in the motor system. The hypothesis of this study was that tRNS would modulate task effects in opposite directions, depending on the underlying brain state. Hence, for tRNS during a simple motor training task (FT task), known primarily to increase CSE, we hypothesize an increase in CSE and

Abbreviations: CSE, corticospinal excitability; FT, finger-tapping; GNG, go/no-go; ITI, intertap interval; MEP, motor evoked potential; nTMS, navigated transcranial magnetic stimulation; RT, reaction time; tDCS, transcranial direct current stimulation; TMS, transcranial magnetic stimulation; tRNS, transcranial random noise stimulation.

behavioral performance (Koeneke et al., 2006). For tRNS during an inhibitory control task (GNG task), associated with inhibition of CSE, we hypothesize a decrease in CSE and enhanced behavioral performance reflecting greater inhibition (Bestmann and Duque, 2016).

For this purpose, we closely monitored online as well as offline changes of behavioral and electrophysiological parameters that are established indicators of task-dependent brain states (Schmidt et al., 2013b). As the primary electrophysiological parameter, CSE was acquired via MEPs by nTMS. Compared to conventional, non-navigated TMS, nTMS uses an optical tracking system to control the physical variance related to the 3D parameters of the TMS coil in space. Since small divergences in TMS coil location and orientation can lead to significant variance in CSE estimates, nTMS is an often neglected, but essential prerequisite to reliably quantify changes of task-dependent brain states (Schmidt et al., 2009). Understanding the interaction between tRNS and task-dependent brain activity is imperative for increasing reliability, repeatability, and ultimately, therapeutic usefulness of this emerging neuromodulatory technique.

MATERIALS AND METHODS

Participants

Thirty healthy, right-handed individuals (18 females, mean age 22.8 $\pm$ 2.8 years) received tRNS as well as sham stimulation to the dominant (left) primary motor cortex. All participants were right handed as assessed with the Edinburgh handedness inventory. General exclusion criteria for non-invasive brain stimulation were applied (Brunoni et al., 2011). Specifically, none of the subjects had a history of neurological disease, including movement disorders or epilepsy (Brunoni et al., 2011). All participants gave written informed consent. The study was approved by the local ethics committee and adheres to the principles of good clinical practice of the Charité – Universitätsmedizin Berlin ("Grundsätze der Charité zur Sicherung guter wissenschaftlicher Praxis"), as well as "The Code of Ethics of the World Medical Association" (Declaration of Helsinki).

Experimental Paradigm

A double-blind sham-controlled design was used in this study. The participants were randomly divided into two groups according to the task they were to perform during tRNS or sham stimulation: one group (15 participants) performed an 'activating' task (FT task) during stimulation, known primarily to increase CSE. The other 15 participants performed an 'inhibitory' task (GNG task), associated with inhibition of CSE. Behavioral and electrophysiological measurements were acquired offline in a baseline condition prior to stimulation, and a post-stimulation condition following 10 min of stimulation. Offline measurements were complemented by online behavioral assessments during stimulation as described below and in **Figure 1**. In this context, it is important to note that tasks served two functions during stimulation: they are indicators of task performance changes in response to stimulation and utilized to induce a well-established task-dependent brain state (**Figure 1**).

Finger-Tapping Task (FT Task)

The experimental timeline for the FT task is depicted in **Figure 1A**. For the FT task, subjects were instructed to use the index finger of either hand to repeatedly exert a vertical force on a standard telegraph key as quickly and regularly as possible while receiving visual feedback on a screen. Visual feedback was provided with a live graphical display of ITIs on the x-axis and the corresponding number of taps on the y-axis. For the first block, the starting hand was randomly allocated and the tapping duration for one hand was 30 s before switching to the other hand for 30 s (Schulze et al., 2002). Two blocks for each hand (i.e., 4 $\times$ 30 s = 2 min) were followed by a 120 s pause (60 s pause during stimulation) to avoid excessive build-up of fatigue (Rönnefarth et al., 2018). As another precaution, the vertical force required to complete a tapping motion was adjusted to the lowest possible setting. Preventing excessive fatigue with regular pauses served to minimize its confounding influence on CSE (Terney et al., 2008). Prior to the experiment, participants were instructed and practiced the task for two blocks for each hand, resulting in a total of 1 min practice for each hand. The baseline condition consisted of two blocks for each hand, the stimulation condition (10 min) consisted of six blocks for each hand and the post-stimulation condition consisted of four blocks for each hand.

Go/No-Go Task (GNG Task)

The experimental timeline for the GNG task is depicted in **Figure 1B**. One GNG trial with a total duration of 2.5–3 s followed the following time course: first, a fixation cross was presented on a screen, which lasted 1 s and was followed by a 250 ms warning cue (yellow square) (Joundi et al., 2012). Subsequently, a 250 ms target cue was presented with a varied latency of 250–750 ms based on an underlying, linearly increasing hazard rate, in line with (Schoffelen et al., 2005). Subjects exerted a maximal horizontal force on the lever only when a "go" cue (green circle) appeared (91%), while 9% of target cues were "no-go" cues (red circle) (Schoffelen et al., 2005). The hazard rate and the low probability of "no-go" trials were utilized to ensure optimal inhibition-related activity (Schoffelen et al., 2005; Wessel, 2018). The response period was limited to 750 ms.

During the GNG task, when no response was required, subjects maintained a horizontal isometric force of 4% of maximum voluntary contraction, with the index finger of the dominant hand on a lever, in line with (Kristeva et al., 2007). A low force output was used since it was shown to effectively enable corticospinal interaction and recruit most neurons in M1 (Evarts et al., 1983; Kristeva et al., 2007). The predetermined force was monitored throughout task execution and verbal feedback was given in case of deviations.

Prior to the experiment, participants were instructed and practiced 10 GNG trials. One block consisted of 37 GNG trials

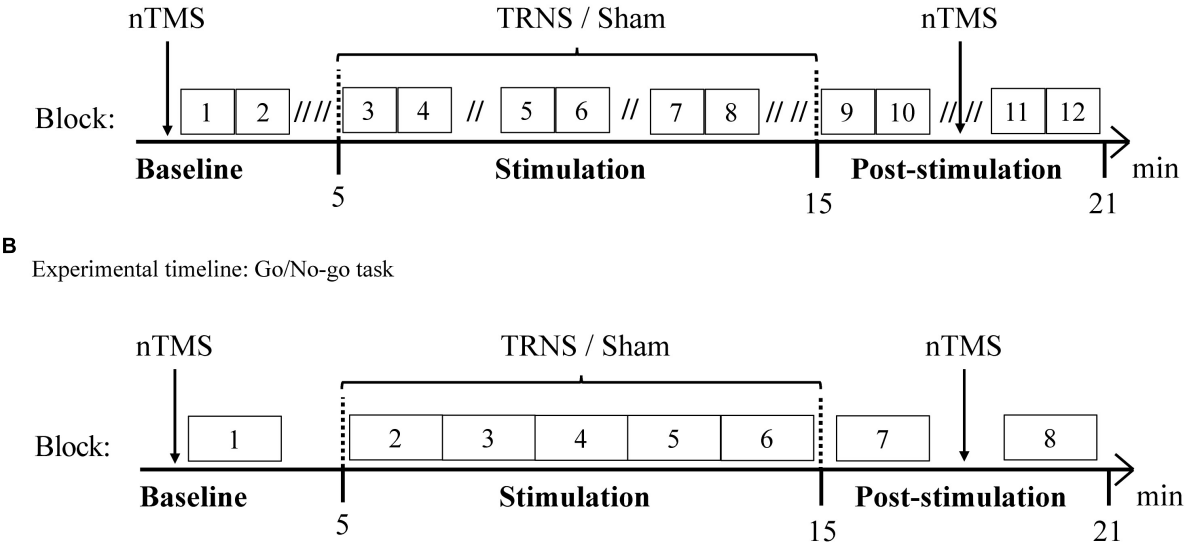

FIGURE 1 | Experimental timelines. Behavioral measurements of the FT task **(A)** and the GNG task **(B)** were conducted along with nTMS to evaluate CSE. Behavioral and electrophysiological measurements were acquired in a baseline condition and a post-stimulation condition. Offline measurements were complemented by online behavioral assessments during 10 min stimulation with tRNS or sham stimulation. **(A)** Experimental timeline of the FT task. 15 participants performed the FT task. During one block of 60 s, one hand was tapping for 30 s before switching to the other hand for 30 s. Double slashes ("//") denote a 60 s pause between blocks ("// //" = 120 s), to avoid excessive fatigue. **(B)** Experimental timeline of the GNG task. 15 participants performed the GNG task. One block consisted of 37 GNG trials and ended with a 15 s pause, resulting in 2 min per block.

and a 15 s pause, resulting in 2 min per block. The baseline condition consisted of one block, the stimulation condition (10 min) consisted of five consecutive blocks (i.e., a total of 5 × 37 trials = 185 trials) and the post-stimulation conditions consisted of two blocks.

Transcranial Random Noise Stimulation (tRNS)

Random noise stimulation was applied by a multi-channel low-voltage stimulation and EEG device certified for clinical use (NextWave, EBS Technologies GmbH, Kleinmachnow, Germany), which delivered weak random noise stimulation through conductive-rubber electrodes (NeuroConn GmbH, Ilmenau, Germany), placed in two saline-soaked sponges. One electrode (circular, 12.5 cm^2) was situated over the dominant motor cortex at the C3 EEG electrode position (since all subjects were right-handed), the other electrode (rectangular electrode, 30 cm^2) was placed over the contralateral frontopolar cortex (Moliadze et al., 2012). For tRNS, a peak-to-peak stimulation intensity of 1.51 mA (0.8 mA effective current intensity) was applied for 10 min with no DC offset. The random signal was drawn from a uniform probability density with a sample rate of 1280 Hz and digitally filtered to ensure a frequency distribution of 100–640 Hz, based on Terney et al. (2008). For sham stimulation, a 15 s ramp-up and 15 s ramp-down current was used in line with recommendations for tDCS (Nitsche et al., 2008; Schmidt et al., 2013a). Respective sessions of tRNS and sham stimulation were at least 7 days apart to avoid carry-over effects.

Navigated Transcranial Magnetic Stimulation (nTMS)

Single pulse nTMS (eXimia VR TMS, Nexstim, Helsinki, Finland) with optical tracking and subject-specific magnetic resonance images was used in combination with a biphasic figure-of-eight coil (70-mm wing diameter) to evaluate CSE with optimal control of physical parameters (Schmidt et al., 2015). Compared to conventional, non-navigated TMS, nTMS was shown to reduce MEP amplitude variance by 27% (Schmidt et al., 2009). Electromyography activity in response to nTMS was recorded from the dominant first dorsal interosseus muscle with Neuroline 700 surface electrodes (Ambu VR, Ballerup, Denmark) arranged in belly-tendon montage. MEP amplitude was defined by peak-to-peak measurement. The stimulation target was the "center of gravity" of the dominant first dorsal interosseus (Wassermann et al., 1992). Resting motor threshold was defined as the stimulation intensity required to elicit a 500 μV MEP appearing with 50% probability using the maximum-likelihood threshold detection method and a 95% confidence interval, ensuring an individually calibrated intensity prior to data acquisition in each session (Awiszus, 2003). CSE was then assessed with 20 MEPs

prior to and after electrical stimulation at the timepoints specified in **Figure 1**.

Analysis and Statistics

Two subjects withdrew consent to participate in the study before completion. The remaining 28 subjects (13 in the FT group, 15 in the GNG group) were included in the analysis and statistics.

CSE data was manually reviewed and outliers, defined as values above or below 2.2x the interquartile range, were identified in each session and removed (Hoaglin and Iglewicz, 1987). CSE was estimated by using an in-house algorithm that accounted for physiological and physical confounders, such that MEPs associated with confounding prestimulus muscle contraction (preinnervation) above 20 μV and 100 ms prior to stimulation were excluded and further physical and physiological covariance was partitioned out of CSE estimation with step-wise regression (Schmidt et al., 2015). Mean CSE data was then baseline normalized by subtracting baseline values from post-stimulation values. Normality of data was graphically confirmed with histograms and by using the Shapiro–Wilk test. Levene's test confirmed homogeneity of variances. Statistical analysis was conducted using a mixed model ANOVA to compare the main and interaction effects on CSE, with TASK (i.e., GNG, FT) as between-subjects factor and STIMULATION (i.e., tRNS, sham) as within-subjects factor.

Go/no-go task RTs, GNG task accuracy, FT ITI and FT taps were manually reviewed, which lead to exclusion of three subjects in the GNG group due to technical artifacts in the data. RTs and ITIs were outlier corrected, baseline normalized and z-transformed on a per subject basis over each session, in line with recommendations for within-subject designs and psychophysiological data (Bush et al., 1993). GNG accuracy data and FT taps were outlier corrected and baseline normalized for statistical analysis. Outlier correction involved trimming data by 5% of highest and lowest scores (Bush et al., 1993; Whelan, 2017). For GNG RTs specifically, trials without response and RTs below 100 ms after target cue presentation were rejected (Joundi et al., 2012). Baseline normalization required the mean of the baseline condition to be subtracted from the data. Z-transformation was used to increase power in comparison to raw means by accounting for intraindividual variability across subjects (Bush et al., 1993). A normal distribution could be confirmed both graphically as well as mathematically by the Shapiro–Wilk test. A linear mixed model for repeated measures was used to analyze the effect of tRNS on behavioral performance in the FT task and GNG task. It was used in favor of a repeated measures ANOVA due to its extended flexibility with regard to unbalanced data and precision in giving less biased estimates of fixed effects in repeated, correlated measurements (Cnaan et al., 1997; Krueger and Tian, 2004). As fixed effects, STIMULATION (i.e., tRNS/sham) and TIME (i.e., block) was entered into the model. SUBJECTS was entered as random effects. For a significant interaction of STIMULATION × TIME, *post hoc* tests for individual blocks were controlled for multiple comparisons using Bonferroni correction.

All digital signal processing was carried out with custom-made scripts within the MATLAB programming environment (MATLAB R2014a, The MathWorks, Inc., Natick, MA, United States). All statistical analysis was performed using SPSS Statistics with statistical significance level set at $\alpha = 0.05$ (IBM SPSS Statistics for Windows, Version 21.0. Armonk, NY, United States: IBM, Corp.). Results are presented as mean values and standard errors of the mean unless stated otherwise.

RESULTS

Corticospinal Excitability (CSE)

Effects of tRNS on CSE are depicted in **Figure 2**. Mean uncorrected baseline CSE for the FT group was similar for the tRNS (691 ± 89 μV) and the sham condition (FT, sham: 686 ± 125 μV) [$t(12) = 9.032$, $p = 0.975$]. Baseline CSE for the GNG group was also similar for the tRNS (530 ± 71 μV) and the sham condition (500 ± 105 μV) [$t(14) = 0.250$, $p = 0.806$]. In the mixed model ANOVA, there was no significant main effect of TASK [$F(1,26) = 1.961$, $p = 0.173$, $\eta_p^2 = 0.07$] and STIMULATION [$F(1,26) = 1.814$, $p = 0.19$, $\eta_p^2 = 0.05$] on CSE. However, there was a significance for the interaction STIMULATION × TASK [$F(1,26) = 5.474$, $p = 0.027$, $\eta_p^2 = 0.17$], indicating that excitability changes were dependent on the specific stimulation applied during task execution. Pairwise comparisons revealed that in the FT group, baseline corrected MEP responses were significantly facilitated following tRNS (381 ± 146 μV) compared to sham stimulation (14 ± 133 μV) ($p = 0.018$, $\eta_p^2 = 0.2$). In the GNG group, tRNS (−36 ± 97 μV) did not influence MEP responses compared to sham stimulation (−63 ± 93 μV) ($p = 0.473$, $\eta_p^2 = 0.02$). This shows that tRNS specifically increased CSE

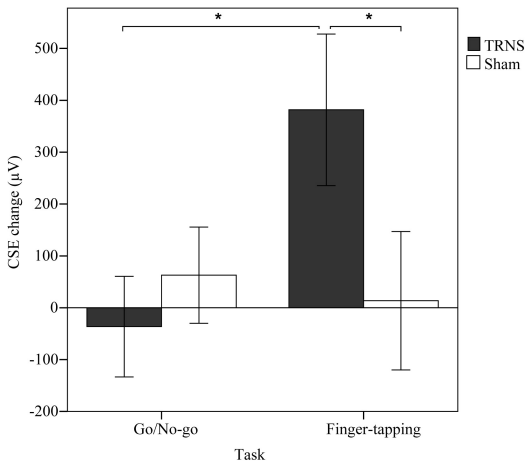

FIGURE 2 | Effects of tRNS on corticospinal excitability. Mean CSE change (μV) was calculated by subtracting baseline CSE measurements from post-stimulation measurements. CSE change is depicted for respective task type (GNG or FT) performed during 10 min of stimulation with either tRNS or sham stimulation. Error bars depict the standard error of the mean. In the FT group, MEP responses were significantly facilitated (*) after tRNS compared to sham stimulation and tRNS in the GNG group.

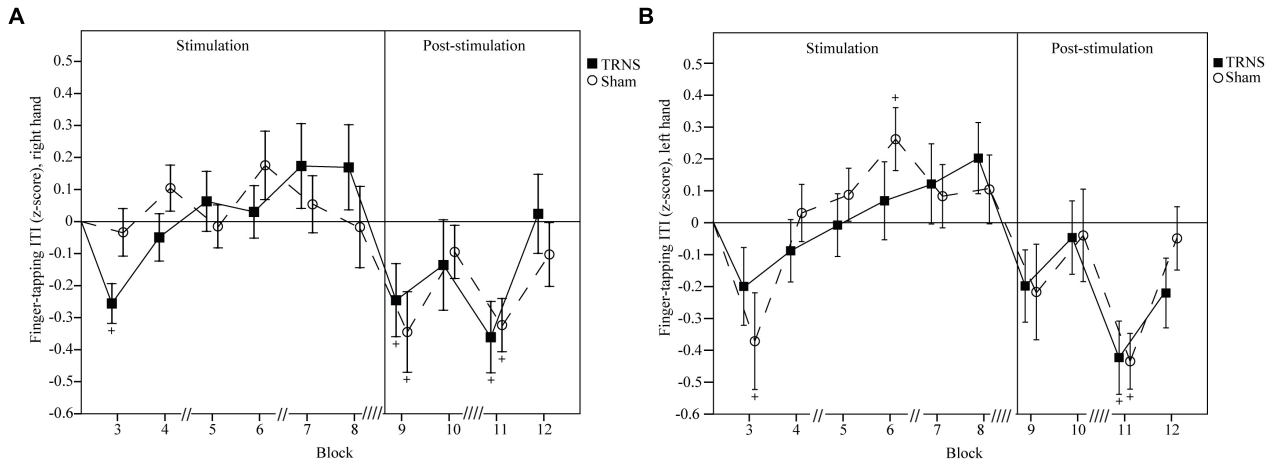

FIGURE 3 | Effects of tRNS on FT ITI. Mean FT ITIs are baseline corrected and z-transformed. Blocks 3–8 (30 s per block) depict ITIs during electrical stimulation, while blocks 9–12 present data post-stimulation. Double slashes ("//") denote a 60 s pause between blocks ("// //" = 120 s), to avoid excessive fatigue. Mean ITI is displayed with standard error of the mean. Significant changes from baseline are marked with "+." ITIs of the right hand **(A)** and the left hand **(B)** were not significantly different between the tRNS condition compared to the sham condition. For both hands, singular significant reductions in ITIs in block 3 of one condition likely represent a rebound effect after a prior pause. Reductions in ITIs post-stimulation for both the tRNS and sham conditions imply motor learning.

after the FT task but not after the GNG task (p = 0.022, η_p^2 = 0.19) (**Figure 2**).

FT: Intertap Interval (ITI)

Effects of tRNS on FT ITIs are depicted in **Figure 3A** (right hand) and **Figure 3B** (left hand). Uncorrected baseline ITIs were shorter for the right hand (tRNS, 148 ± 6 ms; sham, 149 ± 5 ms) compared to the left hand (tRNS, 170 ± 6 ms; sham, 170 ± 6 ms).

For the right hand, a linear mixed model did not show a significant main effect of STIMULATION on FT ITIs [$F(2)$ = 2.35, p = 0.6]. However, a significant interaction of STIMULATION × TIME could be observed [$F(20)$ = 3.03, $p < 0.001$]. *Post hoc* tests revealed significant reductions in ITIs after both tRNS (block 9, −0.246 ± 0.104, p = 0.02; block 11, −0.361 ± 0.101, $p < 0.001$) and sham stimulation (block 9, −0.345 ± 0.105, p = 0.001; block 11, −0.323 ± 0.101, p = 0.001). ITIs at the beginning of stimulation in block 3 were significantly faster only in the tRNS condition (−0.256 ± 0.101, p = 0.012). Bonferroni corrected pairwise comparisons between individual blocks and stimulation did not reach significant results (**Figure 3A**).

For the left hand, a linear mixed model did not show a significant main effect of STIMULATION on FT ITIs [$F(2)$ = 2.86, p = 0.58]. However, a significant interaction of STIMULATION × TIME could be observed [$F(20)$ = 3.29, $p < 0.001$]. *Post hoc* tests revealed significant reductions in ITIs after both tRNS (block 11, −0.423 ± 0.117, $p < 0.001$) and sham stimulation (block 3, −0.371 ± 0.112, p = 0.001; block 11, −0.434 ± 0.112, $p < 0.001$). There was a significant increase in ITIs the sham condition in block 6 (0.262 ± 0.112, p = 0.02) during stimulation. Bonferroni corrected pairwise comparisons between individual blocks and stimulation did not reach significant results (**Figure 3B**).

FT: Finger Taps

Effects of tRNS on FT taps are depicted in **Figure 4A** (right hand) and **Figure 4B** (left hand). Mean uncorrected baseline finger taps were higher for the right hand (tRNS, 171.62 ± 7.18; sham 173.65 ± 7.32) compared to the left hand (tRNS 150.81 ± 6.17; sham 154.23 ± 6.11).

For the right hand, a linear mixed model with baseline corrected data did not show a significant main effect of STIMULATION on FT taps [$F(2)$ = 1.98, p = 0.14]. However, a significant interaction of STIMULATION × TIME could be observed [$F(20)$ = 3.39, $p < 0.001$]. *Post hoc* tests revealed significant increases in the number of finger taps versus baseline for tRNS (block 3, 5.69 ± 2.34, p = 0.016; block 9, 5.54 ± 2.34, p = 0.019; block 11, 8.38 ± 2.34, $p < 0.001$) and sham stimulation (block 9, 7 ± 2.44, p = 0.004; block 11, 8.88 ± 2.33, $p < 0.001$). Additionally, toward the end of tRNS, the number of finger taps was significantly reduced versus baseline (block 7, −5.54 ± 2.34, p = 0.019; block 8, −4.77 ± 2.34, p = 0.043). Bonferroni corrected pairwise comparisons between individual blocks and stimulation did not reach significant results (**Figure 4A**).

For the left hand, a linear mixed model with baseline corrected data showed a significant main effect of STIMULATION on FT finger taps [$F(2)$ = 3.45, p = 0.03] with a significant increase in FT finger tap estimates of fixed effects for tRNS (2.06 ± 0.79) [$t(255)$ = −2.62, p = 0.09] but not for sham (0.16 ± 0.8) [$t(255)$ = 0.2, p = 0.84]. However, *post hoc* tests between tRNS and sham did not reveal a significant difference between stimulation conditions [$t(255)$ = −1.7, p = 0.09]. A significant interaction of STIMULATION × TIME could be observed [$F(20)$ = 2.63, $p < 0.001$]. *Post hoc* tests revealed significant increases in the number of finger taps versus baseline after both tRNS (block 9, 4.73 ± 2.37, p = 0.047; block 11, 8.58 ± 2.37, $p < 0.001$; block 12, 5.69 ± 2.34, p = 0.029) and sham stimulation (block 3, 5.69 ± 2.37, p = 0.017;

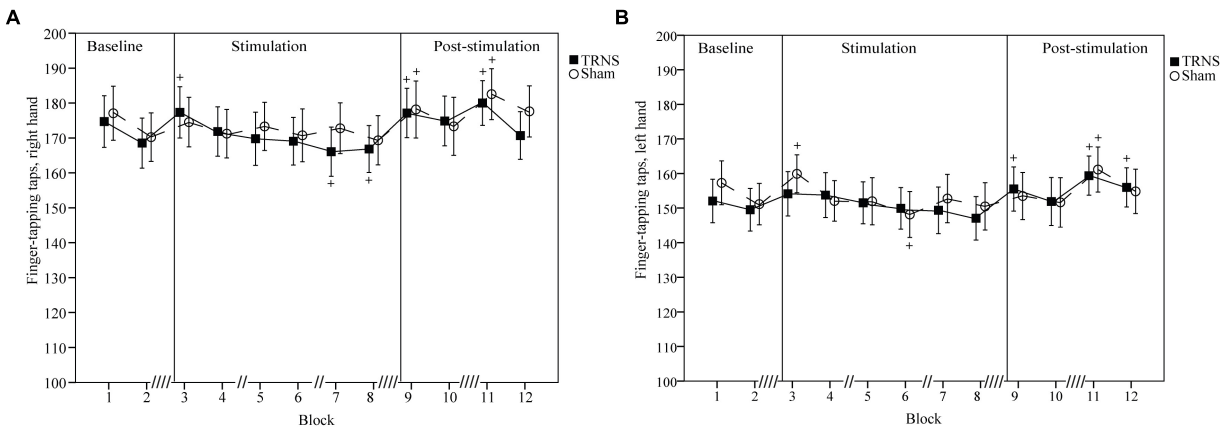

FIGURE 4 | Effects of tRNS on FT taps. Mean FT number of taps are shown which illustrate an overall higher tapping performance of the right hand **(A)** compared to the left hand **(B)** and complement changes in FT ITIs observed in **Figure 3**. Blocks 3–8 (30 s per block) depict finger taps during electrical stimulation, while blocks 9–12 present data post-stimulation. Double slashes ("//") denote a 60 s pause between blocks ("// //" = 120 s), to avoid excessive fatigue. Mean finger taps are displayed with standard error of the mean. Significant changes from baseline are marked with "+." **(A,B)** Number of finger taps for both hands were not significantly different between the tRNS condition compared to the sham condition. For both hands, singular significant increases in the number of finger taps in block 3 of one condition likely represent a rebound effect after a prior pause. Significant reductions during stimulation represent fatigue. Increased number of finger taps post-stimulation for both tRNS and sham conditions imply motor learning.

block 11, 6.92 ± 2.37, $p = 0.004$). Additionally, toward the end of sham stimulation, the number of finger taps was significantly reduced versus baseline (block 6, −6.08 ± 2.37, $p = 0.011$). Bonferroni corrected pairwise comparisons between individual blocks and stimulation did not reach significant results (**Figure 4B**).

GNG: Reaction Time (RT)

Effects of tRNS on GNG RT are depicted in **Figure 5A**. Mean uncorrected baseline RT for the tRNS condition was 303 ± 5 ms, and 313 ± 7 ms for the sham condition. A linear mixed model showed a significant main effect of STIMULATION on GNG RTs [$F(2) = 11.69$, $p < 0.001$] with a significant increase in estimates of fixed effects for tRNS (0.21 ± 0.045) [$t(160) = 4.65$, $p < 0.001$] but not for sham (0.06 ± 0.045) [$t(160) = 1.33$, $p = 0.19$]. Importantly, *post hoc* tests between tRNS and sham revealed a significant difference between stimulation conditions [$t(160) = -2.35$, $p = 0.019$]. Breaking down the main effect of STIMULATION into a stimulation period (blocks 2–6) and a post-stimulation period (blocks 7–8), the linear mixed model for RTs post-stimulation was significant [$F(2) = 5.48$, $p = 0.007$], with a significant difference in estimates of fixed effects: GNG RTs were attenuated after tRNS (0.24 ± 0.085, $p = 0.06$) compared to sham (−0.14 ± 0.085, $p = 0.107$) [$t(44) = -3.19$, $p = 0.002$]. There was no significant difference between tRNS and sham during the stimulation period [$t(114) = -0.79$, $p = 0.43$). A significant interaction of STIMULATION × TIME could also be observed [$F(14) = 2.57$, $p = 0.002$]. *Post hoc* tests showed attenuated RTs for tRNS in block 5 (0.284 ± 0.122, $p = 0.021$) and block 7 (0.32 ± 0.122, $p = 0.01$) and at the start of sham stimulation (block 2; 0.256, ± 0.117, $p = 0.031$). Bonferroni corrected pairwise comparisons between individual blocks and stimulation did not reach significant results. Together, these results show that tRNS specifically attenuated RTs in the GNG task in the post-stimulation period (**Figure 5A**).

GNG: Task Accuracy

Effects of tRNS on GNG task accuracy are depicted in **Figure 5B**. Mean uncorrected baseline GNG task accuracy for the tRNS condition was 96.88 ± 0.91 and 98.34 ± 0.58% for the sham condition. A linear mixed model showed a significant main effect of STIMULATION on baseline corrected GNG accuracy [$F(2) = 18.01$, $p < 0.001$] with a significant increase in estimates of fixed effects for tRNS (1.89 ± 0.32) [$t(173) = 5.94$, $p < 0.001$] but not for sham (0.29 ± 0.33) [$t(173) = 0.86$, $p = 0.39$]. Importantly, *post hoc* tests between tRNS and sham revealed a significant difference between stimulation conditions [$t(173) = -3.49$, $p < 0.001$]. Breaking down the main effect of STIMULATION into a stimulation period (blocks 2–6) and a post-stimulation period (blocks 7–8), the linear mixed model for GNG accuracy during stimulation was significant [$F(2) = 12$, $p < 0.001$], with a significant difference in estimates of fixed effects: GNG accuracy was increased during tRNS (1.74 ± 0.36, $p < 0.001$) compared to sham (0.37 ± 0.38, $p = 0.973$) [$t(123) = -2.62$, $p = 0.009$]. GNG accuracy was also significantly increased in the post-stimulation period [$F(2) = 5.97$, $p = 0.005$] with significant differences in estimates of fixed effects after tRNS (2.27 ± 0.66, $p = 0.001$) compared to sham (0.083 ± 0.68, $p = 0.904$) [$t(48) = -2.30$, $p = 0.023$). A significant interaction of STIMULATION × TIME could also be observed [$F(14) = 2.78$, $p = 0.001$]. *Post hoc* tests showed increased task accuracy during tRNS in block 3 (1.85 ± 0.86, $p = 0.033$), block 5 (2.69 ± 0.86, $p = 0.002$) and after tRNS in block 7 (2.69 ± 0.86, $p = 0.002$) and block 8 (1.85 ± 0.86, $p = 0.033$). The sham condition did not reach significant results. Bonferroni corrected pairwise comparisons between individual blocks and stimulation did not reach significant results. Together,

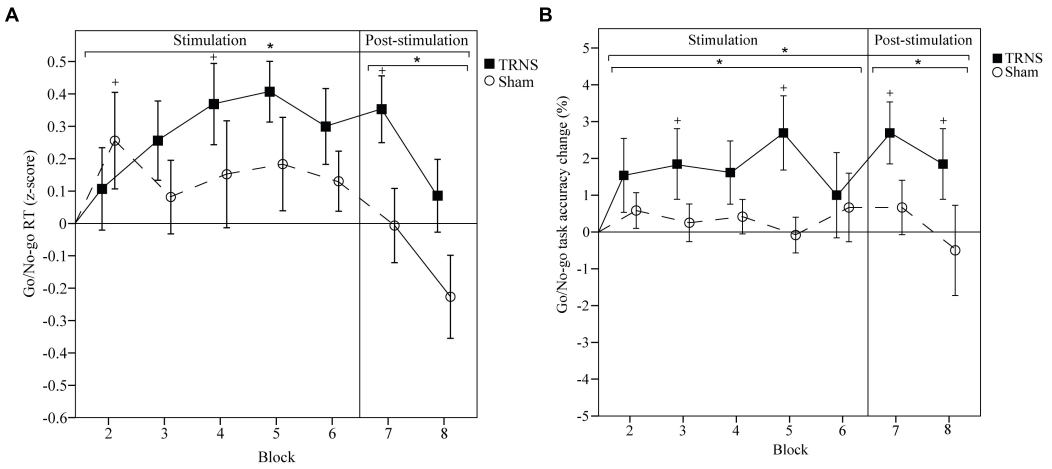

FIGURE 5 | Effects of tRNS on GNG RT and task accuracy. **(A,B)** Mean GNG RT and task accuracy are baseline corrected. RTs are z-transformed. Blocks 2–6 (2 min per block) depict RTs and task accuracy change during electrical stimulation, while blocks 7 and 8 present data post-stimulation. Means are displayed with standard error of the mean. Significant changes from baseline are marked with "+." Significant changes compared to sham are marked with "*." **(A)** RTs were significantly longer in the tRNS condition compared to sham. **(B)** Task accuracy was significantly improved during and after tRNS compared to sham. Together, these results suggest that tRNS specifically strengthened motor inhibition and inhibitory control in the GNG task.

these results show that tRNS specifically increased task accuracy in the GNG task during stimulation and in the post-stimulation period (**Figure 5B**).

DISCUSSION

The purpose of this study was to investigate the task dependency of tRNS-induced neuromodulation in the motor system. The main results of this study show task-dependent dissociated effects on CSE and behavioral performance following tRNS during a FT task versus a GNG task. After motor training (FT task), characterized by repetitive motor activation, tRNS led to significant facilitation of CSE compared to sham stimulation, while behavioral performance was not significantly different to sham stimulation. Conversely, in the inhibitory control task (GNG task), tRNS-enhanced inhibition led to an attenuation of RTs without effects on CSE. Together, these findings support the notion that tRNS enhances the predominant task-dependent brain state. Our results highlight the interaction between tRNS and task-dependent brain activity and provide further evidence for tRNS' proposed mechanisms of action.

Motor Activation

In the simple motor training task (FT), online tRNS significantly facilitated CSE as compared to sham stimulation. To our knowledge, we are the first to show CSE enhancements after task execution during tRNS. CSE enhancements after tRNS have been previously shown only in idling subjects. In idling subjects, reliable CSE increases lasting 60 min are possible (Terney et al., 2008). Additionally, with regards to tRNS parameters, high frequency tRNS (100–640 Hz) (Terney et al., 2008) at high current intensities (1 mA) (Moliadze et al., 2012) with a duration of at least 5 min (Chaieb et al., 2011) was also shown to reliably increase CSE. In contrast, online tRNS was previously reported to impede CSE enhancements: CSE was found to be slightly attenuated for a cognitive task and strongly attenuated for a motor task (Terney et al., 2008). Attenuation after the motor task was suggested to be associated with task-induced fatigue (Terney et al., 2008).

Results from this study suggest that CSE facilitation after the FT task with online tRNS reflects an enhancement of task-dependent activation, i.e., additional motor activation in primed neural populations. Simple tapping tasks are well-established as prototype tasks to study motor training-induced neuroplasticity in the primary motor cortex (for a review see, Ljubisavljevic, 2006; Bezzola et al., 2012). Maximal sequential movements of the FDI ensure a maximum task-related activation of its cortical representation in M1, minimizing a confounding influence from other brain areas (Bezzola et al., 2012). Motor activation is independent of the physical tapping speed of subjects, since the amount of neural effort determines maximal neurophysiological activation (Lutz et al., 2005). Motor training leads to larger muscle representations, specific to the muscles involved in the task, and increased CSE (Pascual-Leone et al., 1994; Muellbacher et al., 2001; Koeneke et al., 2006).

The observation of further enhancement of task-dependent activation with tRNS fits well in line with the current understanding of tRNS' proposed mechanism of action: increase of CSE via transmission of subthreshold neural signals – a phenomenon known as stochastic resonance (Terney et al., 2008). Stochastic resonance, i.e., the mechanism by which an optimal noise condition improves signal detection in non-linear systems, has been known in the physics community since at least the early 1980s and has been universally observed in various neural systems including the human brain (Moss et al., 2004; Schmidt et al., 2013b).

Unchanged CSE levels after sham stimulation suggest that the tapping training duration was not sufficiently long to increase functional recruitment in the absence of tRNS. Motor training studies typically last 30–60 min (Classen et al., 1998; Muellbacher et al., 2001; Koeneke et al., 2006). These studies highlight the crucial addition of online tRNS in our study to dramatically reduce the required time for motor training-induced neuroplasticity in the primary motor cortex.

Motor Fatigue and Motor Learning

The FT task is a simple motor training task involving motor fatigue and motor learning indexed by a change in ITIs. It has been utilized as a clinical tool to characterize motor deficits in Parkinson's disease, cerebellar dysfunction, stroke and as a result of aging (Shimoyama et al., 1990; Arias et al., 2012).

In the present study, a linear increase in mean ITIs and finger taps *during* electrical- and sham stimulation represents task-induced motor fatigue (Rönnefarth et al., 2018). Fatigue inevitably occurs within seconds of task initiation (Shimoyama et al., 1990; Aoki et al., 2003; Rönnefarth et al., 2018). It involves not only peripheral, but also central mechanisms (central motor fatigue) as evidenced by reduced CSE after a fatiguing task (Kluger et al., 2012). Therefore, fatigue is a potential confounder in brain stimulation studies aiming to enhance CSE levels and likely explains CSE disruptions previously observed after online tRNS in the motor system (Antal et al., 2007; Terney et al., 2008). Several measures were taken in our study to tune the FT task to reduce the influence of fatigue (see section "Finger-Tapping Task (FT Task)). These measures were effective in preventing fatigue outlasting the stimulation condition, since post-stimulation ITIs and finger taps were equal to or lower than baseline levels and CSE inhibition, typically seen after excessive fatigue, was absent. Reduced ITIs and increased number of finger taps compared to baseline in block 3 (right hand), at the beginning of tRNS were not significant compared to sham stimulation and likely represent a rebound effect after a prior pause of 120 s. This might also explain the analogous phenomenon in block 3 of the left hand, at the beginning of sham stimulation.

The significant ITI enhancements and increased number of finger taps *after* tRNS and sham stimulation (between blocks 9–12) show that the utilized FT task was efficient in inducing motor learning. These unspecific effects on motor learning gain special significance when interpreted with corresponding CSE results: although the FT task improvements in the right hand were also observed in the sham condition, facilitation of CSE occurred only after tRNS. This implies that electrical stimulation might be associated with an enhanced potential for learning (Koeneke et al., 2006). Motor learning is known to occur as a result of motor training (for a review see, Ljubisavljevic, 2006), and to be closely associated with CSE facilitation and ITI improvements in simple tapping tasks (Koeneke et al., 2006). Further studies also emphasize the robust relation between motor learning and excitability enhancements, e.g., CSE levels return to baseline once subjects overlearn a task (Muellbacher et al., 2001) and improvement retention is disrupted when CSE is specifically suppressed over M1 (Muellbacher et al., 2002).

The robust behavioral improvements in the FT task after stimulation could not be differentiated (i.e., tRNS, sham), possibly due to a ceiling effect. In the young, healthy participants of this study, underlying motor learning processes are likely to be already optimized. Additionally, maximum task-related activation of M1 is thought to leave no room for further performance gains, especially in early stages of motor learning (Bezzola et al., 2012). Other measures of FT task performance, e.g., force and tapping duration might expose tRNS-specific behavioral gains with higher sensitivity (Muellbacher et al., 2001; Rönnefarth et al., 2018). Providing evidence for neuromodulation of motor learning would be particularly relevant in the context of novel interventions following brain injury (Pascual-Leone et al., 2005).

Motor Inhibition

Unlike the simple motor training task, random noise stimulation in the inhibitory control task (GNG task) left CSE unchanged in both the tRNS and sham conditions, suggestive of an underlying inhibitory task-dependent brain state counteracting the facilitatory tRNS effects reported in idle subjects (Terney et al., 2008). We hypothesized a decrease in CSE after GNG and tRNS, reflecting enhanced motor inhibition. Methodological limitations and task complexity might have contributed to the absence of a clearer MEP decrease:

Firstly, CSE measurements after tRNS were not obtained on a trial-by-trial basis during GNG task execution and do not trace the time course of transient inhibitory state fluctuations per trial. The GNG task is a hallmark for motor inhibition encompassing periods of response preparation and response inhibition reflected by changes in CSE, for a review see Greenhouse et al. (2015) and Bestmann and Duque (2016). As subjects engage in the task and prepare to respond, motor inhibition, characterized by reduced MEPs, prevents a premature response (Greenhouse et al., 2015). The warning cue further enhances inhibitory processes (Boulinguez et al., 2009; Criaud et al., 2012) and the specificity of suppression to the muscles involved in the task (Greenhouse et al., 2012). If a "no-go" target cue appears, response inhibition acts as an active breaking process leading to global suppression of motor cortical activity with concurrent MEP suppression (Stinear et al., 2009; Greenhouse et al., 2012; MacDonald et al., 2014; Bestmann and Duque, 2016). Since CSE was investigated with single pulse nTMS *after* task execution, any potential transient enhancement of motor inhibition *during* the GNG task would not be detected in our paradigm.

Secondly, inhibition is interrupted by "go" cues requiring motor activation with concurrent brief facilitation of CSE (Stinear et al., 2009; MacDonald et al., 2014). These short but frequent motor responses might have contributed to the absence of a clear MEP suppression. Yet, rare "no-go" trials (<20%) are required to ensure sufficient inhibition-related activity and a 9% "no-go" probability has been shown to induce such activity (Schoffelen et al., 2005; Wessel, 2018). As becomes apparent, the inhibitory state associated with the GNG task is comparably more complex than the FT task. It includes the subcomponents response preparation, response inhibition,

response activation and poses the methodological challenge of tracking these dynamically overlapping state changes with sufficient temporal resolution.

Inhibitory Control

Considering limitations arising from using single pulse nTMS to measure CSE after task completion, RT and task accuracy data acquired online, during the GNG task, serve as an easily assessable, more adequate parameter. RT and task accuracy are behaviorally relevant and trace dynamic state changes with a higher temporal resolution. RTs were significantly slowed in the tRNS condition, especially after electrical stimulation, while task accuracy was enhanced. Slowing of RTs in "go" trials is commonly used as a surrogate parameter for motor inhibition and is positively correlated to task accuracy (Bezdjian et al., 2009; Leotti and Wager, 2010). Response slowing is associated with suppression of MEPs, very similar to mechanisms involved in response inhibition (Jahfari et al., 2010).

The speed-accuracy trade-off is modulated by intraindividual inhibitory control: patients with impulse control disorders such as attention deficit and hyperactivity disorder (ADHD) and in patients who stutter, the speed-accuracy trade-off is shifted toward deficient inhibitory control with faster RTs and lower task accuracy (Bezdjian et al., 2009; Eggers et al., 2013). In turn, longer RTs and better task accuracy as signs of enhanced inhibitory control are achieved in patients with ADHD by pharmacological agents such as Modafinil (Turner et al., 2004). This phenomenon can likewise be observed in healthy subjects depending on gender (enhanced in female) and motivation (Bezdjian et al., 2009; Leotti and Wager, 2010). Consequently, we propose slowed RTs and enhanced task accuracy during and after tRNS to result from strengthened motor inhibition and inhibitory control outlasting stimulation. Our data suggests that tRNS impedes movement initiation by stabilizing the existing task-dependent brain state and delaying response initiation (Schmidt et al., 2013b). Future tRNS studies could try to modulate and optimize the speed-accuracy-tradeoff via task difficulty and in patients with deficient inhibitory control.

CONCLUSION

We provide evidence that tRNS-induced neuromodulation in the motor system is dependent on the task during stimulation such that CSE is enhanced in a FT task and inhibitory control is improved in a GNG task. Results confirm our hypothesis that transcranially applied random noise stimulation enhances the endogenous task-dependent brain state of healthy subjects. To our knowledge, we are the first to show CSE facilitation after online tRNS during a FT task. We argue in favor of online tRNS to avoid contradictory results and expose task specific regulatory processes to be modulated by transcranial stimulation techniques. Further confirmation of tRNS' mechanism of action is required to limit variability as a result of task dependency and to potentiate its neuroplastic effects in health and disease.

DATA AVAILABILITY

The datasets generated for this study are available on request to the corresponding author.

AUTHOR CONTRIBUTIONS

SS, MS, and SB conceived the principle idea of the work. AJ, SS, MS, SB, LH, AK, MR, and RF designed the experiments. MS developed the software for experimental procedures and electrical stimulation. AJ, LH, and AK performed the measurements. AJ, SS, LH, LK, and RB-P conducted computational and statistical analyses of the data. All authors participated in the interpretation of the data. The manuscript was drafted by AJ and critically revised and approved by all authors.

FUNDING

This work was supported by the German Research Foundation, DFG grant BR 1691/8-1 and OB 102/22-1.

REFERENCES

Antal, A., Chaieb, L., Moliadze, V., Monte-Silva, K., Poreisz, C., Thirugnanasambandam, N., et al. (2010). Brain-derived neurotrophic factor (BDNF) gene polymorphisms shape cortical plasticity in humans. *Brain Stimul.* 3, 230–237. doi: 10.1016/j.brs.2009.12.003

Antal, A., Terney, D., Poreisz, C., and Paulus, W. (2007). Towards unravelling task-related modulations of neuroplastic changes induced in the human motor cortex. *Eur. J. Neurosci.* 26, 2687–2691. doi: 10.1111/j.1460-9568.2007.05896.x

Aoki, T., Francis, P. R., and Kinoshita, H. (2003). Differences in the abilities of individual fingers during the performance of fast, repetitive tapping movements. *Exp. Brain Res.* 152, 270–280. doi: 10.1007/s00221-003-1552-z

Arias, P., Robles-Garcia, V., Espinosa, N., Corral, Y., and Cudeiro, J. (2012). Validity of the finger tapping test in Parkinson's disease, elderly and young healthy subjects: Is there a role for central fatigue? *Clin. Neurophysiol.* 123, 2034–2041. doi: 10.1016/j.clinph.2012.04.001

Awiszus, F. (2003). TMS and threshold hunting. *Suppl. Clin. Neurophysiol.* 56, 13–23. doi: 10.1016/S1567-424X(09)70205-3

Bestmann, S., and Duque, J. (2016). Transcranial magnetic stimulation: decomposing the processes underlying action preparation. *Neuroscientist* 22, 392–405. doi: 10.1177/1073858415592594

Bestmann, S., and Krakauer, J. W. (2015). The uses and interpretations of the motor-evoked potential for understanding behaviour. *Exp. Brain Res.* 233, 679–689. doi: 10.1007/s00221-014-4183-7

Bezdjian, S., Baker, L. A., Lozano, D. I., and Raine, A. (2009). Assessing inattention and impulsivity in children during the Go/NoGo task. *Br. J. Dev. Psychol.* 27, 365–383. doi: 10.1348/026151008X314919

Bezzola, L., Mérillat, S., and Jäncke, L. (2012). Motor training-induced neuroplasticity. *GeroPsych* 25, 189–197. doi: 10.1024/1662-9647/a000070

Boulinguez, P., Ballanger, B., Granjon, L., and Benraiss, A. (2009). The paradoxical effect of warning on reaction time: demonstrating proactive response inhibition with event-related potentials. *Clin. Neurophysiol.* 120, 730–737. doi: 10.1016/j.clinph.2009.02.167

Brunoni, A. R., Amadera, J., Berbel, B., Volz, M. S., Rizzerio, B. G., and Fregni, F. (2011). A systematic review on reporting and assessment of adverse effects associated with transcranial direct current stimulation. *Int. J. Neuropsychopharmacol.* 14, 1133–1145. doi: 10.1017/S1461145710001690

Bush, L. K., Hess, U., and Wolford, G. (1993). Transformations for within-subject designs: a Monte Carlo investigation. *Psychol. Bull.* 113, 566–579. doi: 10.1037/0033-2909.113.3.566

Chaieb, L., Paulus, W., and Antal, A. (2011). Evaluating aftereffects of short-duration transcranial random noise stimulation on cortical excitability. *Neural Plast.* 2011:105927. doi: 10.1155/2011/105927

Classen, J., Liepert, J., Wise, S. P., Hallett, M., and Cohen, L. G. (1998). Rapid plasticity of human cortical movement representation induced by practice. *J. Neurophysiol.* 79, 1117–1123. doi: 10.1152/jn.1998.79.2.1117

Cnaan, A., Laird, N. M., and Slasor, P. (1997). Using the general linear mixed model to analyse unbalanced repeated measures and longitudinal data. *Statist. Med.* 16, 2349–2380. doi: 10.1002/(SICI)1097-0258(19971030)16:20<2349::AID-SIM667>3.0.CO;2-E

Criaud, M., Wardak, C., Ben Hamed, S., Ballanger, B., and Boulinguez, P. (2012). Proactive inhibitory control of response as the default state of executive control. *Front. Psychol.* 3:59. doi: 10.3389/fpsyg.2012.00059

Eggers, K., De Nil, L. F., and Van Den Bergh, B. R. (2013). Inhibitory control in childhood stuttering. *J. Fluency Disord.* 38, 1–13. doi: 10.1016/j.jfludis.2012.10.001

Evarts, E. V., Fromm, C., Kroller, J., and Jennings, V. A. (1983). Motor Cortex control of finely graded forces. *J. Neurophysiol.* 49, 1199–1215. doi: 10.1152/jn.1983.49.5.1199

Fertonani, A., Pirulli, C., and Miniussi, C. (2011). Random noise stimulation improves neuroplasticity in perceptual learning. *J. Neurosci.* 31, 15416–15423. doi: 10.1523/JNEUROSCI.2002-11.2011

Gilbert, C. D., and Sigman, M. (2007). Brain states: top-down influences in sensory processing. *Neuron* 54, 677–696. doi: 10.1016/j.neuron.2007.05.019

Greenhouse, I., Oldenkamp, C. L., and Aron, A. R. (2012). Stopping a response has global or nonglobal effects on the motor system depending on preparation. *J. Neurophysiol.* 107, 384–392. doi: 10.1152/jn.00704.2011

Greenhouse, I., Sias, A., Labruna, L., and Ivry, R. B. (2015). Nonspecific inhibition of the motor system during response preparation. *J. Neurosci.* 35, 10675–10684. doi: 10.1523/JNEUROSCI.1436-15.2015

Hoaglin, D. C., and Iglewicz, B. (1987). Fine-tuning some resistant rules for outlier labeling. *J. Am. Statist. Assoc.* 82, 1147–1149. doi: 10.1080/01621459.1987.10478551

Hummel, F. C., Celnik, P., Pascual-Leone, A., Fregni, F., Byblow, W. D., Buetefisch, C. M., et al. (2008). Controversy: noninvasive and invasive cortical stimulation show efficacy in treating stroke patients. *Brain Stimul.* 1, 370–382. doi: 10.1016/j.brs.2008.09.003

Jahfari, S., Stinear, C. M., Claffey, M., Verbruggen, F., and Aron, A. R. (2010). Responding with restraint: What are the neurocognitive mechanisms? *J. Cogn. Neurosci.* 22, 1479–1492. doi: 10.1162/jocn.2009.21307

Joundi, R. A., Jenkinson, N., Brittain, J. S., Aziz, T. Z., and Brown, P. (2012). Driving oscillatory activity in the human cortex enhances motor performance. *Curr. Biol.* 22, 403–407. doi: 10.1016/j.cub.2012.01.024

Kluger, B. M., Palmer, C., Shattuck, J. T., and Triggs, W. J. (2012). Motor evoked potential depression following repetitive central motor initiation. *Exp. Brain Res.* 216, 585–590. doi: 10.1007/s00221-011-2962-y

Koeneke, S., Lutz, K., Herwig, U., Ziemann, U., and Jancke, L. (2006). Extensive training of elementary finger tapping movements changes the pattern of motor cortex excitability. *Exp. Brain Res.* 174, 199–209. doi: 10.1007/s00221-006-0440-8

Kristeva, R., Patino, L., and Omlor, W. (2007). Beta-range cortical motor spectral power and corticomuscular coherence as a mechanism for effective corticospinal interaction during steady-state motor output. *Neuroimage* 36, 785–792. doi: 10.1016/j.neuroimage.2007.03.025

Krueger, C., and Tian, L. (2004). A comparison of the general linear mixed model and repeated measures ANOVA using a dataset with multiple missing data points. *Biol. Res. Nurs.* 6, 151–157. doi: 10.1177/1099800404267682

Lee, S. H., and Dan, Y. (2012). Neuromodulation of brain states. *Neuron* 76, 209–222. doi: 10.1016/j.neuron.2012.09.012

Leotti, L. A., and Wager, T. D. (2010). Motivational influences on response inhibition measures. *J. Exp. Psychol. Hum. Percept. Perform.* 36, 430–447. doi: 10.1037/a0016802

Li, L. M., Uehara, K., and Hanakawa, T. (2015). The contribution of interindividual factors to variability of response in transcranial direct current stimulation studies. *Front. Cell Neurosci.* 9:181. doi: 10.3389/fncel.2015.00181

Ljubisavljevic, M. (2006). Transcranial magnetic stimulation and the motor learning-associated cortical plasticity. *Exp. Brain Res.* 173, 215–222. doi: 10.1007/s00221-006-0538-z

Lutz, K., Koeneke, S., Wustenberg, T., and Jancke, L. (2005). Asymmetry of cortical activation during maximum and convenient tapping speed. *Neurosci. Lett.* 373, 61–66. doi: 10.1016/j.neulet.2004.09.058

MacDonald, H. J., Coxon, J. P., Stinear, C. M., and Byblow, W. D. (2014). The fall and rise of corticomotor excitability with cancellation and reinitiation of prepared action. *J. Neurophysiol.* 112, 2707–2717. doi: 10.1152/jn.00366.2014

Moliadze, V., Atalay, D., Antal, A., and Paulus, W. (2012). Close to threshold transcranial electrical stimulation preferentially activates inhibitory networks before switching to excitation with higher intensities. *Brain Stimul.* 5, 505–511. doi: 10.1016/j.brs.2011.11.004

Moss, F., Ward, L. M., and Sannita, W. G. (2004). Stochastic resonance and sensory information processing: a tutorial and review of application. *Clin. Neurophysiol.* 115, 267–281. doi: 10.1016/j.clinph.2003.09.014

Muellbacher, W., Ziemann, U., Boroojerdi, B., Cohen, L., and Hallett, M. (2001). Role of the human motor cortex in rapid motor learning. *Exp. Brain Res.* 136, 431–438. doi: 10.1007/s002210000614

Muellbacher, W., Ziemann, U., Wissel, J., Dang, N., Kofler, M., Facchini, S., et al. (2002). Early consolidation in human primary motor cortex. *Nature* 415, 640–644. doi: 10.1038/nature712

Nitsche, M. A., Cohen, L. G., Wassermann, E. M., Priori, A., Lang, N., Antal, A., et al. (2008). Transcranial direct current stimulation: state of the art 2008. *Brain Stimul.* 1, 206–223. doi: 10.1016/j.brs.2008.06.004

Pascual-Leone, A., Amedi, A., Fregni, F., and Merabet, L. B. (2005). The plastic human brain cortex. *Annu. Rev. Neurosci.* 28, 377–401. doi: 10.1146/annurev.neuro.27.070203.144216

Pascual-Leone, A., Grafman, J., and Hallett, M. (1994). Modulation of cortical motor output maps during development of implicit and explicit knowledge. *Science* 263, 1287–1289. doi: 10.1126/science.8122113

Pirulli, C., Fertonani, A., and Miniussi, C. (2013). The role of timing in the induction of neuromodulation in perceptual learning by transcranial electric stimulation. *Brain Stimul.* 6, 683–689. doi: 10.1016/j.brs.2012.12.005

Prichard, G., Weiller, C., Fritsch, B., and Reis, J. (2014). Effects of different electrical brain stimulation protocols on subcomponents of motor skill learning. *Brain Stimul.* 7, 532–540. doi: 10.1016/j.brs.2014.04.005

Rönnefarth, M., Bathe-Peters, R., Jooss, A., Haberbosch, L., Scholz, M., Schmidt, S., et al. (2018). Force increase in a repetitive motor task inducing motor fatigue. *J. Mot. Behav.* doi: 10.1080/00222895.2018.1495172 [Epub ahead of print].

Saiote, C., Polania, R., Rosenberger, K., Paulus, W., and Antal, A. (2013). High-frequency TRNS reduces BOLD activity during visuomotor learning. *PLoS One* 8:e59669. doi: 10.1371/journal.pone.0059669

Schmidt, S., Bathe-Peters, R., Fleischmann, R., Ronnefarth, M., Scholz, M., and Brandt, S. A. (2015). Nonphysiological factors in navigated TMS studies; confounding covariates and valid intracortical estimates. *Hum. Brain Mapp.* 36, 40–49. doi: 10.1002/hbm.22611

Schmidt, S., Cichy, R. M., Kraft, A., Brocke, J., Irlbacher, K., and Brandt, S. A. (2009). An initial transient-state and reliable measures of corticospinal excitability in TMS studies. *Clin. Neurophysiol.* 120, 987–993. doi: 10.1016/j.clinph.2009.02.164

Schmidt, S., Fleischmann, R., Bathe-Peters, R., Irlbacher, K., and Brandt, S. A. (2013a). Evolution of premotor cortical excitability after cathodal inhibition of the primary motor cortex: a sham-controlled serial navigated TMS study. *PLoS One* 8:e57425. doi: 10.1371/journal.pone.0057425

Schmidt, S., Scholz, M., Obermayer, K., and Brandt, S. A. (2013b). Patterned brain stimulation, what a framework with rhythmic and noisy components might tell us about recovery maximization. *Front. Hum. Neurosci.* 7:325. doi: 10.3389/fnhum.2013.00325

Schoffelen, J. M., Oostenveld, R., and Fries, P. (2005). Neuronal coherence as a mechanism of effective corticospinal interaction. *Science* 308, 111–113. doi: 10.1126/science.1107027

Schulze, K., Luders, E., and Jancke, L. (2002). Intermanual transfer in a simple motor task. *Cortex* 38, 805–815. doi: 10.1016/S0010-9452(08)70047-9

Shimoyama, I., Ninchoji, T., and Uemura, K. (1990). The finger-tapping test. A quantitative analysis. *Arch. Neurol.* 47, 681–684. doi: 10.1001/archneur.1990.00530060095025

Silvanto, J., Muggleton, N., and Walsh, V. (2008). State-dependency in brain stimulation studies of perception and cognition. *Trends Cogn. Sci.* 12, 447–454. doi: 10.1016/j.tics.2008.09.004

Snowball, A., Tachtsidis, I., Popescu, T., Thompson, J., Delazer, M., Zamarian, L., et al. (2013). Long-term enhancement of brain function and cognition using cognitive training and brain stimulation. *Curr. Biol.* 23, 987–992. doi: 10.1016/j.cub.2013.04.045

Stinear, C. M., Coxon, J. P., and Byblow, W. D. (2009). Primary motor cortex and movement prevention: where Stop meets Go. *Neurosci. Biobehav. Rev.* 33, 662–673. doi: 10.1016/j.neubiorev.2008.08.013

Talelli, P., and Rothwell, J. (2006). Does brain stimulation after stroke have a future? *Curr. Opin. Neurol.* 19, 543–550. doi: 10.1097/WCO.0b013e32801080d1

Terney, D., Chaieb, L., Moliadze, V., Antal, A., and Paulus, W. (2008). Increasing human brain excitability by transcranial high-frequency random noise stimulation. *J. Neurosci.* 28, 14147–14155. doi: 10.1523/JNEUROSCI.4248-08.2008

Turner, D. C., Clark, L., Dowson, J., Robbins, T. W., and Sahakian, B. J. (2004). Modafinil improves cognition and response inhibition in adult attention-deficit/hyperactivity disorder. *Biol. Psychiatry* 55, 1031–1040. doi: 10.1016/j.biopsych.2004.02.008

Wassermann, E. M., Mcshane, L. M., Hallett, M., and Cohen, L. G. (1992). Noninvasive mapping of muscle representations in human motor cortex. *Electroencephalogr. Clin. Neurophysiol.* 85, 1–8.

Wessel, J. R. (2018). Prepotent motor activity and inhibitory control demands in different variants of the go/no-go paradigm. *Psychophysiology* 55:e12871. doi: 10.1111/psyp.12871

Whelan, R. (2017). Effective analysis of reaction time data. *Psychol. Rec.* 58, 475–482. doi: 10.1007/BF03395630

Conflict of Interest Statement: The authors declare that the research was conducted in the absence of any commercial or financial relationships that could be construed as a potential conflict of interest.

frontiers in Neuroscience

SYSTEMATIC REVIEW
published: 28 February 2019
doi: 10.3389/fnins.2019.00084

A Systematic Review of Integrated Functional Near-Infrared Spectroscopy (fNIRS) and Transcranial Magnetic Stimulation (TMS) Studies

Adrian Curtin[1,2], *Shanbao Tong*[2], *Junfeng Sun*[2], *Jijun Wang*[3], *Banu Onaral*[1] *and Hasan Ayaz*[1,4,5]*

[1] Drexel University, School of Biomedical Engineering, Science and Health Systems, Philadelphia, PA, United States, [2] School of Biomedical Engineering, Shanghai Jiao Tong University, Shanghai, China, [3] Shanghai Mental Health Center, Shanghai Jiao Tong University School of Medicine, Shanghai, China, [4] Department of Family and Community Health, University of Pennsylvania, Philadelphia, PA, United States, [5] Center for Injury Research and Prevention, Children's Hospital of Philadelphia, Philadelphia, PA, United States

OPEN ACCESS

Edited by:
Mikhail Lebedev,
Duke University, United States

Reviewed by:
Ali Yadollahpour,
Ahvaz Jundishapur University of Medical Sciences, Iran
Daniel Richard Leff,
Imperial College London, United Kingdom

***Correspondence:**
Hasan Ayaz
hasan.ayaz@drexel.edu

Specialty section:
This article was submitted to Neural Technology, a section of the journal Frontiers in Neuroscience

Received: *05 October 2018*
Accepted: *25 January 2019*
Published: *28 February 2019*

Citation:
Curtin A, Tong S, Sun J, Wang J, Onaral B and Ayaz H (2019) A Systematic Review of Integrated Functional Near-Infrared Spectroscopy (fNIRS) and Transcranial Magnetic Stimulation (TMS) Studies. Front. Neurosci. 13:84. doi: 10.3389/fnins.2019.00084

Background: The capacity for TMS to elicit neural activity and manipulate cortical excitability has created significant expectation regarding its use in both cognitive and clinical neuroscience. However, the absence of an ability to quantify stimulation effects, particularly outside of the motor cortex, has led clinicians and researchers to pair noninvasive brain stimulation with noninvasive neuroimaging techniques. fNIRS, as an optical and wearable neuroimaging technique, is an ideal candidate for integrated use with TMS. Together, TMS+fNIRS may offer a hybrid alternative to "blind" stimulation to assess NIBS in therapy and research.

Objective: In this systematic review, the current body of research into the transient and prolonged effects of TMS on fNIRS-based cortical hemodynamic measures while at rest and during tasks are discussed. Additionally, studies investigating the relation of fNIRS to measures of cortical excitability as produced by TMS-evoked Motor-Evoked-Potential (MEP) are evaluated. The aim of this review is to outline the integrated use of TMS+fNIRS and consolidate findings related to use of fNIRS to monitor changes attributed to TMS and the relationship of fNIRS to cortical excitability itself.

Methods: Key terms were searched in PubMed and Web-of-Science to identify studies investigating the use of both fNIRS and TMS. Works from Google-Scholar and referenced works in identified papers were also assessed for relevance. All published experimental studies using both fNIRS and TMS techniques in the study methodology were included.

Results: A combined literature search of neuroimaging and neurostimulation studies identified 53 papers detailing the joint use of fNIRS and TMS. 22/53 investigated the immediate effects of TMS at rest in the DLPFC and M1 as measured by fNIRS. 21/22 studies reported a significant effect in [HbO] for 40/54 stimulation conditions with 14 resulting an increase and 26 in a decrease. While 15/22 studies also reported [HbR], only 5/37 conditions were significant. Task effects of fNIRS+TMS were detailed in 16 studies,

including 10 with clinical populations. Most studies only reported significant changes in [HbO] related measures. Studies comparing fNIRS to changes in MEP-measured cortical excitability suggest that fNIRS measures may be spatially more diffuse but share similar traits.

Conclusion: This review summarizes the progress in the development of this emerging hybrid neuroimaging & neurostimulation methodology and its applications. Despite encouraging progress and novel applications, a lack of replicated works, along with highly disparate methodological approaches, highlight the need for further controlled studies. Interpretation of current research directions, technical challenges of TMS+fNIRS, and recommendations regarding future works are discussed.

Keywords: non-invasive brain stimulation (NIBS), functional near-infrared spectroscopy (fNIRS), transcranial magnetic stimulation (TMS), neuromodulation, cognition, motor, functional neuroimaging, TMS+fNIRS

INTRODUCTION

Since its introduction in 1985 by Barker (Barker et al., 1985), Transcranial Magnetic Stimulation (TMS) has grown to be an effective tool in both research and in the clinic. With the use of an electromagnetic coil, TMS produces a brief but powerful magnetic field (1.5–2 Tesla) capable of inducing current and triggering action potentials within neurons of the superficial areas of the cerebral cortex (Valero-Cabré et al., 2017). In addition to transiently inducing or disrupting neural activity, the application of repeated TMS (rTMS) is capable of either facilitating cortical excitation or cortical inhibition via the mechanisms of Long-Term Potentiation (LTP) and Long-Term Depression (LTD), respectively (Pell et al., 2011). Certain rTMS paradigms have been shown to continue to influence neural behaviors over an hour after the stimulation period (Huang et al., 2005), while the behavioral effects of repeated stimulation have demonstrated the potential to last several weeks (Lefaucheur et al., 2014).

The prospect of manipulating not just instantaneous neural activities, but long-term behavior of neural populations is attractive to researchers who want to promote the recovery of damaged or disordered neural systems and enhance the function of existing networks. TMS therapy has already been approved by the FDA for use in unipolar depression (Major Depressive Disorder, MDD) (George et al., 2013) and a considerable amount of research effort is currently being devoted to identifying its utility in stroke rehabilitation (Langhorne et al., 2011), schizophrenia (Cole et al., 2015), phobia (Notzon et al., 2015), epilepsy (Kimiskidis, 2016), and many other conditions. TMS offers substantial promise as a cognitive probe and as a therapeutic technique. However, individuals may vary substantially in their responses to stimulation, and understanding of the explicit effects of TMS remains limited.

Current knowledge regarding the effects of TMS paradigms is based primarily on the physiological effect on an individual's resting motor threshold (RMT), i.e., the required TMS stimulation level in the Motor Cortex (M1) to elicit a motor evoked potential (MEP) 50% of the time. Identification of an individual's RMT is an important first step in calibrating TMS stimulation and changes in RMT which occur following repeated stimulation are thought to reflect changes in cortical excitability (Valero-Cabré et al., 2017). Trains of low frequency (1 Hz) stimulation have been shown to decrease cortical excitability (increase in RMT) and trains of high frequency stimulation (>5 Hz) have been shown to increase cortical excitability (decrease in RMT) (Fitzgerald et al., 2006). Theta burst stimulation (TBS) represents an additional paradigm in which short 3 pulse bursts of stimulation at 50 Hz are repeated at 5 Hz which is thought to have a more pronounced effect compared with High Frequency and Low Frequency stimulation (Huang et al., 2005). When stimulated in short intervals, intermittent TBS (iTBS) is thought to have a faciliatory action on cortical excitability and when stimulated continuously (cTBS), the paradigm is thought to be inhibitory. As a majority of accessible TMS measurements are produced from stimulation of the motor cortex, the principles learned from stimulation of this area are assumed to apply in other cortical regions.

Although studies certainly benefit from the knowledge of motor-cortex sensitivity to TMS stimulation, many regions of therapeutic and psychiatric interest are located in cortical regions which have no easily measured physiological response. In these regions, the efficacy of this "blind" neurostimulation can only be measured in terms of the behavioral changes induced, which may only be apparent after repeated stimulation sessions. It is here that neuroimaging techniques provide a practical solution to "close the loop" and evaluate the immediate (online) and integrated (offline) responses to TMS stimulation, potentially enabling the identification of optimal treatment paradigms through the measurement of individual responses and additional insight into the ways in TMS meaningfully affects behavior and cognition.

The combined use of TMS and neuroimaging has become an exciting new landscape on which to test theories of both low-level and complex cognitive functions as well as inform TMS-based therapies. The use of Electroencephalography (EEG), functional Magnetic Resonance Imaging (fMRI) and Positron Emission Tomography (PET) in multimodal TMS has been the subject of a number of comprehensive reviews (Bestmann et al., 2008; Reithler et al., 2011; Bortoletto et al., 2015; Hallett et al.,

2017). Researchers have also employed functional Near Infrared Spectroscopy (fNIRS), an optical brain imaging technique which offers a number of benefits over other approaches. While each of these modalities offers particular advantages and disadvantages in terms of cost, spatial, and temporal resolution, fNIRS-based measurements are not intrinsically subject to electromagnetic interference and represent an affordably scalable technique to study both the immediate and prolonged effects of TMS. Although works have detailed the challenges and methodological issues associated with the use of concurrent TMS-fNIRS (Parks, 2013) and a number of studies have been published employing this approach, no systematic synthesis of this research is currently available. The purpose of this review is to consolidate studies related to the use of fNIRS and TMS in order to provide an accessible summary of the paradigms used, research questions addressed, and the current consensus on findings.

TMS-fNIRS Integration and Challenges

fNIRS is a non-invasive brain imaging technique that takes advantage of the "optical window," the natural transparency of tissue to near-infrared light (650–900 nm), to provide measurement of the changes in cortical hemoglobin concentrations (Villringer et al., 1993). Deoxygenated hemoglobin [HbR] and Oxygenated hemoglobin [HbO] are among the largest varying absorbers of light in the near-infrared spectrum and therefore the changes in light intensity can be used to estimate changes in chromophore concentration via the modified Beer-Lambert Law. fNIRS measures neural activities through the hemodynamic changes which occur due to neurovascular coupling (Fuster et al., 2005) and increases in neuronal firing rates in cortical areas are typically observed together with proportional changes in hemodynamic response (Heeger and Ress, 2002). Although the immediate effect of TMS is electromagnetic stimulation, the relatively tight coupling of neural activation to hemodynamic changes allows fNIRS to measure the effects of TMS (Allen et al., 2007). Despite this, the effects of TMS on local neuronal populations may depend significantly on the parameters employed, the location of the stimulation and the type and angle of the coil (Pashut et al., 2011). Additionally, the mechanisms of how individual TMS parameters impact hemodynamic response via excitatory and inhibitory synaptic activity remain to be determined (Arthurs and Boniface, 2002).

Since fNIRS measurements are based on the optical properties of the investigated medium, they are not fundamentally subject to electromagnetic interference produced by TMS coil operation and additionally do not place any restrictions on the placement of the coil. Alongside compatibility with TMS, fNIRS systems may be easily integrated with electrical stimulation approaches such as transcranial direct current stimulation (tDCS) (McKendrick et al., 2015), and can employ probes which are portable, wireless, well-tolerated, cost-effective, and can be applied in many situations in which subject movement is generally unrestricted including outdoor environments (McKendrick et al., 2016) and even vehicle operation (Gateau et al., 2018).

Despite these advantages, fNIRS has several considerations that must be addressed when used with TMS. fNIRS-based systems measure at depths that are a function of the optode distance between the light source and detector used (typically 2.5–4 cm), which effectively restricts the use of fNIRS measurements to shallow cortical regions (Okada and Delpy, 2003). Although sufficient for use with TMS, the spatial resolution of fNIRS is not as high as fMRI and the temporal speed of the measured hemodynamic response is much slower to evolve than the electrophysiological response measured by EEG. Integration with TMS may also impose restrictions on how and which fNIRS sensors are used. Although optically-measured fNIRS signals are not susceptible to electromagnetic interference, care must be taken to ensure that individual fNIRS systems are not only noise-free under TMS operation, but critically that these systems are properly shielded so as to prevent hardware damage from electromagnetic interference. Since TMS electrical fields degrade very quickly with distance, these issues are most important with LED-based or wireless systems that feature electronics localized closely with the coil.

TMS stimulation is typically accompanied by a vibration of the coil and an iconic clicking sound. While the motion associated with the TMS vibration is very limited and brief, fNIRS optode arrangements that include a TMS coil with close proximity may introduce mechanical noise into the signal or displace a component entirely. Typical fNIRS arrangements are also sensitive to both voluntary and involuntary movement of the subject during experiments which may result as a natural response of the individual to stimulation. Both of these situations can induce potentially large changes in the measured signal which are non-cortical in nature. Finally, fNIRS-based measurements may be subject to changes in the scalp caused by either TMS-induced stimulation of musculature or direct effects of TMS on superficial microvasculature. A variety of fNIRS techniques such as short-separation detectors have been proposed to provide measures of superficial blood flow in an attempt to resolve these issues (Gagnon et al., 2011). Typically, experimenters attempting to take advantage of combined TMS-fNIRS have addressed these issues by either not colocalizing the coil with sensors (measuring at a location distant from the coil), placing the coil above the fNIRS montage and increasing the power substantially to account for the weakening of the magnetic field with distance, designing a custom coil or optode arrangement that can be closely integrated together without interference, or simply choosing to measure offline. For a well-written description of technical issues concerning fNIRS and TMS integration the reader is referred to Parks (2013).

While there are multiple technical challenges associated with the integration of fNIRS and TMS, the combined approach of the two techniques offers a practical and flexible approach to studying the dynamics of cortical neurostimulation. In addition to ongoing development of newer fNIRS sensor technology and methods to improve signal quality, there exists a need for well-controlled studies which can verify and characterize the response of TMS-fNIRS on cortical activity at rest or during task. This review attempts to organize the current body of published work to provide an overview of current approaches, findings, and the degree of agreement between them. Although considerable heterogeneity in application and approach make

direct comparison between individual studies difficult, we hope that the work here will encourage and contribute to future research directions. To this end, a systematic search has been conducted using Web Of Science and PubMed to collect, categorize, and consolidate multimodal TMS-fNIRS studies according to the primary stimulation sites investigated (M1 and DLPFC) and provide a narrative overview of this multimodal approach in the context of task and excitability applications.

MATERIALS AND METHODS

In order to provide a comprehensive and structured review of studies using fNIRS and TMS in combination, this review was conducted according to PRISMA recommendations (Liberati et al., 2009).

Eligibility Criteria

Articles which reported the use of fNIRS and TMS as experimental techniques in their protocol and results were included, provided the article was published in a peer-reviewed journal and available in English. Both controlled and exploratory studies were included as eligible for this work and no restrictions were placed on the publication date of the studies. Studies which investigated any population group were at any age or gender were considered in this work. Works were excluded if they were non-experimental in nature (review, commentary, or purely methodological works), did not pertain to neuroscience as a discipline (out of field), did not involve cortical TMS stimulation or fNIRS, or were not in English. Conference papers were not considered eligible.

Primary outcomes of interest in this work were the type (HbO/HbR/HbT) and direction (increase/decrease) of fNIRS-biomarkers in the ipsilateral and contralateral hemisphere in response to TMS/rTMS delivered at rest, or prior to tasks. Cortical excitability papers were collected and summarized but not assessed in this manner.

Information Sources

Research articles were located using the Pubmed MEDLINE and Web of Science, but additional works were referenced through the use of Google Scholar and a thorough study of the referenced works in other identified papers.

Literature Search and Data Extraction

All combinations of the following Medical Subject Headings (MeSH) were used in a Pubmed literature search, and the search was repeated as Subject Topics in a parallel Web Of Science search: ("fNIRS" OR "NIRS" OR "Near Infrared Spectroscopy" OR "Optical Topography" OR "Diffuse Optical Imaging") AND ("TMS" OR "rTMS" OR "Transcranial Magnetic Stimulation"). References within articles identified as relevant and additional studies gathered from Google Scholar using similar search queries were also included. Studies were limited to non-conference academic publications published in English. The PRISMA chart for the screening and selection process is shown in **Figure 1**. The results and limitations of each study were assessed. The last date for this literature search was November 28th, 2018.

Two researchers (AC and HA) screened potentially relevant records on the basis of their titles and abstracts. The full text of each candidate article was accessed and reviewed to determine its eligibility. Information was extracted from the work regarding the subject population, number of subjects recruited, employed task, stimulation parameters, sham type, and location, as well as measurement area and primary outcomes. Primary results and conclusion of articles were identified, and discrepancies were resolved through discussion. Studies were arranged according to publication date and are here divided into 'stimulation at rest' with subdivisions based on the area of stimulation, 'effects of rTMS on task' with subdivisions based on healthy or clinical populations, and investigations into 'fNIRS and cortical excitability' with subdivisions for functional mapping, task-related excitability changes, and the study of central fatigue during exercise.

All information collected in the process of this review was organized within spreadsheets which contain the extracted information pertaining to each group. Attributes of each study were extracted; however, extracted information differed between the categories used to organize their review. For works which involved stimulation at rest the following information was extracted: stimulation parameters used, stimulation areas that were targeted, areas measured with fNIRS, whether fNIRS was measured online or offline, the type of sham stimulation employed, number of subjects, and a summary of findings. Additionally, results per stimulation condition, where applicable, were assessed for qualitative direction of change for typical biomarkers [HbO], [HbR], and [HbT] in ipsilateral and contralateral M1 or DLPFC to allow for a quantitative summary of results (detailed in **Supplementary Table 1**). For studies investigating the use of fNIRS to monitor either the effects of rTMS on tasks (as part of a clinical or non-clinical application), similar information was extracted with the addition of applicable task information (detailed information provided in **Supplementary Table 2**). For studies using MEP as a functional measure, the following information was extracted: population measured in the study, task employed/monitored with fNIRS, stimulation parameters used, stimulation area that was targeted, areas measured with fNIRS, whether TMS-fNIRS was measured online, type of sham stimulation employed, number of subjects in each experimental group, and a summary of findings. As these studies did not examine the impact of TMS or rTMS on fNIRS measures, qualitative assessment of changes in fNIRS biomarkers was not performed.

Due to the high heterogeneity of works currently available, extraction of statistical results from individual studies was not performed. Individual works differed substantially in protocol design, signal processing, stimulation methods, fNIRS equipment, subject population, and statistical approaches.

Several studies in this work also feature the Active Motor Threshold (AMT), a measurement which is similar to RMT except that the muscle is tonically active at 10% maximum voluntary contraction during testing (Terao et al., 1998). For the purposes of comparison, AMT has been converted to an

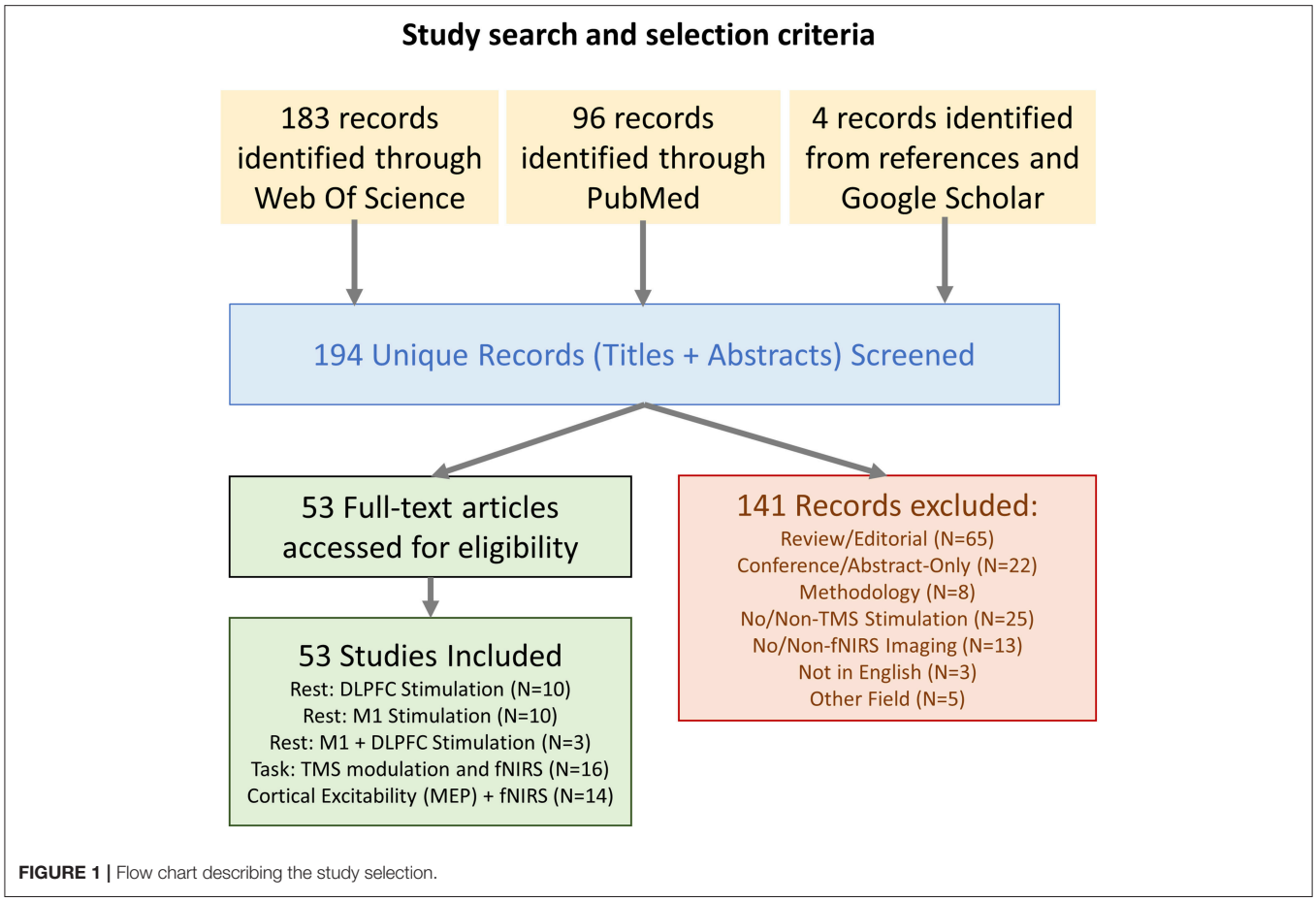

FIGURE 1 | Flow chart describing the study selection.

estimation of RMT using the conversion factor (100%RMT = 140%AMT) and noted using a tilde (∼) where this estimation has been performed.

RESULTS

Study Selection

A total of 194 unique articles were identified in the initial search query, and 4 additional works were introduced which did not appear in the initial search but were identified as relevant through supplementary searches in Google Scholar and examination of references in the identified studies. Of these works, 141 were excluded after reviewing the title and abstract. This list included 65 articles that were either review or editorials, 22 conference articles/abstracts, 8 articles describing methodologies with no experiment, 25 articles which did not use TMS as part of the methodology, 13 articles which did not feature fNIRS-based neuroimaging, 3 articles which were not available in English, and 5 articles which related to other disciplines.

In total, the 53 selected works were broadly categorized into four groups depending on their content: 10 works were categorized as Prefrontal Stimulation at rest, 10 works were categorized as Motor Cortex Stimulation at rest, 3 works were categorized as both Prefrontal and Motor stimulation at rest, and the remaining 30 publications were categorized as either fNIRS-measured effects of TMS on cognitive tasks or studies which related fNIRS-measures to TMS-measured cortical excitability (MEP). The trend of publication over time and distribution of categorized work is shown in **Figure 2**.

Review Organization

In the first section of this review, collected works were organized to investigate the effects of TMS on cortical activity as measured by fNIRS to compare the responses at different cortical regions at rest. Since the majority of publications involving TMS-fNIRS have focused on stimulation to the DLPFC and M1, these regions have been specifically discussed in separate sub-sections below.

In the second section of this review, the effects of TMS on task-evoked fNIRS measures is investigated and discussed within the study-specific contexts. These works feature studies in which rTMS may be applied just prior to a specific task or as stimuli within a task with the expectation that TMS will influence either task performance or cortical involvement in a manner measurable by fNIRS. As rTMS in these situations was often applied as part of a therapeutic strategy for clinical disorders, studies featuring healthy and clinical populations are described in separate sections.

In the final section, works focusing on the relationship of the cortical excitability measures and fNIRS are discussed. The first sub-section focuses on the works using a combination

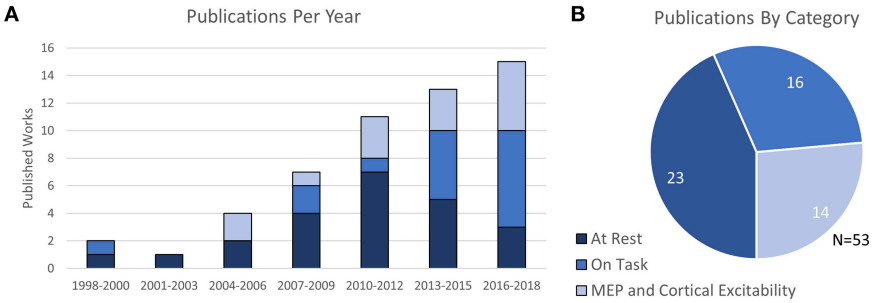

FIGURE 2 | Number and Type of TMS-fNIRS studies **(A)** over time and **(B)** as categorized.

of TMS measures and fNIRS as complementary techniques in functional motor mapping. The second sub-section introduces works discussing how TMS-measured cortical excitability may change during task performance and its relationship to similarly measured task-evoked fNIRS. Finally, works investigating the use of fNIRS and TMS-measured cortical excitability under the context of exercise physiology are presented. These studies primarily focus on the use of fNIRS as a measure of physiological influence on central fatigue due to hypoxia and other conditions.

EFFECTS OF TMS STIMULATION ON fNIRS MEASURES AT REST

Motor Cortex (M1)

Due in part to the availability a quantifiable response in the form of MEP measurement, motor cortex behavior provides an accessible means to understand the effects of transient and repeated stimulation by TMS. However, the application of TMS in this cortical area also has important clinical applications. Single pulses of TMS are approved by the FDA in the US as a prospective tool for neurosurgical planning in the primary motor cortex. In this procedure, physicians noninvasively disrupt active cortical circuits in patients preparing to undergo neurosurgery as an alternative to direct cortical stimulation which requires a craniotomy (Eldaief et al., 2013). These stimulations can help surgeons identify areas which may be preferentially avoided to prevent complications and disability resulting from neurosurgery. Additionally, rTMS methods have been proposed as a therapeutic technique for a number of motor-related disabilities including Parkinson's disease and stroke. Even with the accessibility of MEPs, passive neuroimaging offers a more continuous method of measuring cortical properties across multiple brain areas with the additional promise of sensitivity to stimulation which occurs below the motor threshold. Therefore, researchers continue to study the motor cortex in order to understand the influence of TMS on other neurophysiological metrics such as those measured by fNIRS. Details of each study targeting M1 including stimulation parameters, measurement area, primary findings, and other information are summarized in **Table 1** and visualized in **Figure 3**.

The first use of fNIRS and TMS together was reported by Oliviero et al. (1999). The authors examined the impact of 0.25 Hz stimulation repeated for 2 min (30 pulses) at maximum stimulator power (100% machine power) over the right motor cortex (M1) as well as the right DLPFC. While this stimulation strength is uncommonly high and unrelated to participant RMT, the authors reported that the effective stimulation strength was reduced by the added distance of the interceding fNIRS probe The authors observed a post-stimulation increase in [HbO] after 2 min of stimulation in both regions with a slightly larger magnitude of response in R-M1 than the R-DLPFC. However, the results of this first study may be incomparable to other works due to offline measurement, unknown effective stimulation strength, uncommon stimulation frequency, and in particular, a rather small subject size for the measure of M1 ($N = 4$). The first online work using fNIRS was reported in a conference paper by Nissilä et al. (2002), which examined the contralateral response to 30 s of 110%RMT stimulation at 0.5 Hz (15 pulses) over left-M1. Despite a limited number of subjects and the use of only a single NIR wavelength, the authors concluded that a decrease in absorption at 830 nm reflected an increase in [HbO] vs. sham and that the area of greatest increase during finger tapping matched the region of contralateral activation.

The first colocalized work with fNIRS was conducted by Noguchi et al. (2003), examining the effect of single pulses of TMS over left-M1 at various stimulation levels (∼50, ∼64, and ∼79%RMT) and observed that both 64 and 79%RMT resulted in an increase in [HbO]. This work was followed up by an additional sham-controlled experiment wherein subjects were in a relaxed state or tonically contracting the first dorsal interosseous muscle (FDI) (Mochizuki et al., 2006). Authors observed that stimulating at 50%RMT during contraction increased [HbO], but when relaxed, both 64 and 79% RMT resulted in large decreases in [HbR]. Using an integrated TMS-fNIRS coil, Furubayashi et al. (2013) replicated the work of Mochizuki et al. (2006) presenting stronger evidence for an increase in [HbO] associated with single pulse stimulation during relaxed and active conditions, representing an important verification of claims regarding single pulse stimulation in the motor cortex.

Hada et al. (2006) studied the response of fNIRS to short trains (10 pulses) of 0.5 and 2 Hz stimulation at 80% and 120%RMT in left-M1. The authors suggested that all conditions resulted in a decrease in [HbO] partnered with a slight increase in [HbR] and that changes increased with stimulation strength. Mochizuki

TABLE 1 | Studies investigating fNIRS-measured response to TMS stimulation of M1.

References	Stimulation parameters	Stimulation area	Measurement area	Sham	No. of subjects	Finding
Oliviero et al., 1999*	0.25 Hz, 100% Stimulator Power, 2 min	R-M1	R-M1 (Offline)	None	4	[HbO] increase vs. baseline after 30 stimulations
Noguchi et al., 2003	Single Pulse, {50%, 64%, 79%RMT} × 20 Trials	L-M1	L-M1	None	6	[HbO] increase for 79 and 64% RMT, no change for 50%RMT
Mochizuki et al., 2006	Single Pulse, {50%, 64%, 79%RMT} × 20 Trials {Active contraction, Relaxed}	L-M1	L-M1	Distant coil + electrical stimulus	8	[HbO] increase at 50% RMT when FDI contracted, decrease in [HbR] when 79%RMT [HbR] decrease at 64 and 79% RMT when at rest
Hada et al., 2006	{(0.5 Hz,20 s), (2 Hz,5 s)}, {80%, 120%RMT}, × 10 Trials	L-M1	L-M1	None	12	[HbO] decrease for 1 Hz and 2 Hz, larger decrease for 120% than 80%RMT
Mochizuki et al., 2007	2 s, iTBS (30 pulses), {57%, 71%RMT}	L-M1, L-S1, L-PM	R-PFC R-PM, R-M1, R-S1	Distant Coil	8	At 57%RMT: [HbO] decrease in contralateral PM when stimulated in PM, [HbO] decrease in contralateral S1 when M1 stimulated [HbO] decrease in contralateral M1 and S1 when S1 stimulated
Kozel et al., 2009*	1 Hz, 120%RMT, 10 s ×15 trials, 2 Days	L-M1	Bilateral M1	None	11	[HbO] decrease in ipsilateral and contralateral M1
Tian et al., 2012*	1 Hz, 120%RMT, 10 s ×15 trials, 2 Days	L-M1	Bilateral M1	None	11	Reliability Assessment of (Kozel et al., 2009)
Näsi et al., 2011	{0.5, 1, 2 Hz}, 75%RMT, 8 s × 25 trials	L-M1, Shoulder	Bilateral M1, Bilateral Shoulders	None	13	[HbT] decrease in bilateral M1, strongest at 2 Hz [HbT] decrease on stimulated shoulder, increase on opposite shoulder, correlations with PPG, HR
Hirose et al., 2011	{QPS-5,QPS50} at 0.2Hz, 79%RMT, 2 min X3 trials	L-M1	R-PM, R-M1, R-S1	Distant Coil	9	Decrease in contralateral [HbO] during stimulation for QPS-5 in measured areas and QPS-50 in M1
Groiss et al., 2013	Exp1: {QPS-5,QPS50} at 0.2Hz, 64%RMT, 2 min X3 trials Exp2: {QPS-5, QPS-50}, 64%RMT × 10 Trials	L-M1	L-M1,L-S1,L-PM, L-SMA,L-PFC	Distant Coil	Exp1:10 Exp2:7	[HbO] decrease in ipsilateral M1 for rQPS-5, single QPS-5 burst reduced [HbO] in M1 and PM, no change for QPS-50
Furubayashi et al., 2013	Single Pulse, {50%, 64%, 79%RMT} × 20 Trials {Active contraction, Relaxed}	L-M1	L-M1	Distant Coil	15	[HbO] increase during stimulation, increases with stimulation power in both active and relaxed condition [HbO] decrease 10s after stimulation in active condition, magnitude increases with stimulation power
Mesquita et al., 2013	1 Hz, 95%RMT, 20 min	L-M1	Bilateral M1	None	7	[HbO] increase ipsilaterally during stimulation, increase [CMRO2], no change contralaterally
Park et al., 2017	1 Hz, 90%RMT, 20 min	L-M1	R-M1, R-PM	Distant coil	11	[HbO] increase contralaterally in M1, PM1 and decrease in [HbR], smaller response in PM than M1

**Indicates that the study appears in both M1 and DLPFC tables.*

et al. (2007) measured the effects of 2 s of excitatory theta burst stimulation (iTBS, 30 pulses) at ∼57 and ∼71% RMT over the left premotor (PM), M1, and primary sensory (S1) areas. The authors observed that iTBS stimulation at 57%RMT typically decreased [HbO] in the contralateral region of stimulation, but that the response varied by region stimulated. Here, M1 showed a decrease in [HbO] when contralateral S1 was stimulated, but in S1, [HbO] decreased when either the contralateral M1 or S1 was stimulated. The authors attributed this to an increased interhemispheric directional connectivity between M1 and S1, relative to PFC, which did not change in response to any regional stimulation, and PM, which only responded when contralateral PM was targeted.

Further work by Kozel et al. (2009) examined the bilateral responses to stimulation at either the left-M1 or left-DLPFC using 10 pulse trains of 1 Hz stimulation at 120%RMT. The authors found that short 1 Hz trains resulted in a bilateral [HbO] decrease in M1 and found a similar bilateral response in the DLPFC when stimulating the left-DLPFC. In a later report, the authors examined the characteristics of these

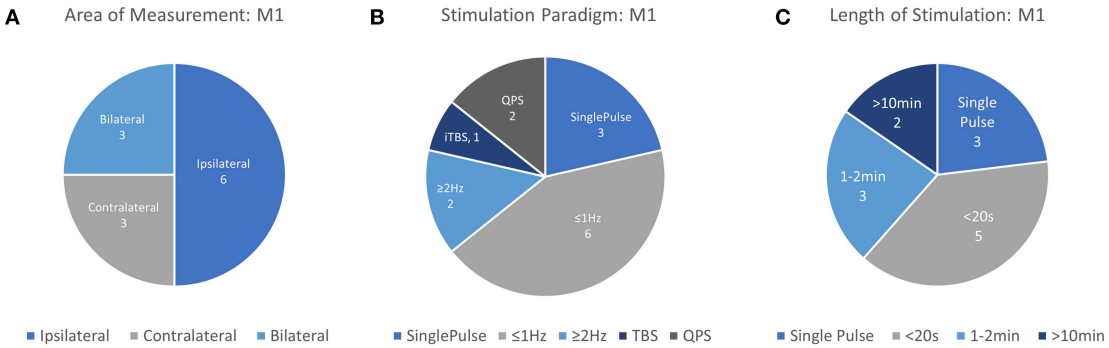

FIGURE 3 | Details of TMS-fNIRS studies applied at rest to M1 for **(A)** Hemisphere measured, **(B)** Stimulation paradigm, and **(C)** Length of stimulation.

responses and found that they had high spatial reproducibility (Tian et al., 2012).

Näsi et al. (2011) examined the contribution of physiological parameters to the fNIRS measured response of TMS by short trains of stimulation. The authors observed a bilateral decrease in [HbO] and [HbT] after 8 s of 75%RMT stimulation at 2 Hz over M1, but cast doubt that this change resulted from purely cerebral sources by pointing out strong correlations with photoplethysmogram (PPG) and heart rate (HR). In order to compare the changes attributed to cortical stimulation with systemic changes due to non-cortical stimulation, they conducted an experiment in which the fNIRS-measured TMS response was recorded again with stimulation and measurement occurring on the shoulders instead. In this set of experiments, they again observed that stimulation of the shoulder resulted in a decrease in [HbT] and an increase in the contralateral shoulder. Although measured in this case using fNIRS, the effect of TMS on systemic and autonomic processes has been observed in several forms, including changes to the vasomotor reactivity (Vernieri et al., 2014). These components must be taken into account in any interpretation of TMS and its effects on hemodynamic neurocorrelates. Although TMS has not been known to have any immediate impact on vasoconstriction itself, this does not bar changes attributable to autonomic intermediaries or systemic responses to the act of stimulation itself.

An investigation into the effects of Quadripulse Stimulation (QPS) and long trains of QPS bursts was examined by Hirose et al. (2011). QPS stimulation is suggested to induce powerful potentiation when four pulses of TMS are delivered with an interstimulus interval (ISI) of 5 ms, whereas a powerful neural depression is induced with an ISI of 50 ms (Hamada and Ugawa, 2010). The contralateral cortical response of these two paradigms (QPS-5 and QPS-50) was examined during 2 min of 78%RMT stimulation. While the the QPS-5 condition produced a measurable decrease in [HbO] in all contralaterally-measured areas (M1,PM,S1), changes associated with QPS-50 stimulation were only observed in contralateral M1. A further study by the same group (Groiss et al., 2013) monitored the ipsilateral response to QPS in these regions at 64%RMT and observed that a 2-min train of QPS-5 reduced [HbO] in ipsilateral M1 whereas a single burst of QPS-5 reduced [HbO] in both M1 and the PM. Under the same protocol, QPS-50 at 64%RMT produced no observable changes under either the 2-min train or single burst condition.

By and large, the previously studied works examined responses to stimulation based on TMS paradigms not typically featured in rTMS-based therapies. Stimulation using clinically relevant protocols have only been studied in two contexts. First, Mesquita et al. (2013) recorded the changes in bilateral M1 in response to clinically relevant 20 min, 95%RMT, 1 Hz stimulation trains over left-M1. During the course of stimulation, an increase in ipsilateral [HbO] was observed which resolved back to baseline following the protocol completion. Additionally, the authors reported that the estimated ipsilateral cerebral metabolic rate of oxygen consumption (CMRO2) increased during stimulation. No changes were noted in the contralateral side of stimulation for either measure. In the second case, Park et al. (2017) performed a similar stimulation paradigm at a slightly lower power level (90%RMT) while measuring contralateral changes in M1 and P1. Here, 20 min of 1 Hz stimulation were observed to produce contralateral increases in [HbO] in both measured regions. Although ipsilateral regions were not measured, these two works highlight the potential variability in response to even largely similar stimulation protocols.

In total, 12 unique studies were assessed for qualitative evaluation of the fNIRS-measured response to TMS in M1 and consistent findings are summarized here. Of these works, 3 publications studied Single Pulse effects at different subthreshold stimulation power levels with 9 different conditions. 8/9 of these conditions resulted in either an increase in [HbO] (5/9) or a decrease in [HbR] (3/9) in ipsilateral M1, suggesting that in most conditions, single pulse stimulation produced a measurable increase in Hemoglobin Difference ([HbDiff] = [HbO]–[HbR]) with sufficient stimulation power. Excitatory rTMS bursts applied to M1 have been studied in only 3 works, and currently, there is no overlap between areas measured, paradigm used, or length of stimulation to allow any preliminary conclusions to be drawn. Inhibitory rTMS was studied by 6 works either as a short train or burst (4 studies), short session (2 studies), or long session (2 studies). Short trains (8–10 s) of both subthreshold and suprathreshold rTMS stimulation ranging from 0.5 to 2 Hz were noted to induce ipsilateral decreases in [HbO] in 8/8

conditions across 4 independent works with bilateral reductions noted whenever measured (4/4 conditions). Response of M1 to a 20-min session of subthreshold 1 Hz stimulation has been suggested to produce an increase in ipsilateral [HbO] or an increase in contralateral [HbO], but more must be done to substantiate these findings. More work needs to be done to replicate and standardize protocols attempting to measure even similar rTMS paradigms so more direct comparisons between works can be drawn. Notably, the response to single pulse stimulation in contralateral M1, responses to suprathreshold single pulse stimulation in M1, the effects of high frequency rTMS (>5 Hz) have not been examined using fNIRS.

Dorsolateral Prefrontal Cortex (DLPFC)

The dorsolateral prefrontal cortex (DLPFC) is a critical area to many executive functions such as attention, working memory, response inhibition, problem solving. As an associative area and a key cortical area in many of the networks underlying complex cognitive function, the DLPFC is of great interest in the areas of cognitive science, neurology, and psychiatry. Apart from being a promising avenue of research, the use of rTMS targeting DLPFC for the treatment of MDD is currently the only FDA-approved use of rTMS in psychiatry. The therapeutic strategy for MDD prescribes the use of Low Frequency stimulation (∼1 Hz) on the right-DLPFC (near F4) or High Frequency Stimulation (>5 Hz) over the left-DLPFC (near F3), with both paradigms demonstrating somewhat equivalent clinical efficacy (George et al., 2013). Despite being the only cortical region with an approved application for rTMS treatment, the lack of peripherally evoked responses to TMS stimulation in the DLPFC has spawned significant interest in finding neurophysiological measurements which can guide the application of TMS therapy. Here, neuroimaging techniques offer a quantifiable response to stimulation which allows a deeper understanding of TMS and rTMS-induced cognitive modulation. Information from each study investigating the DLPFC including stimulation area, measurement area, primary findings and other details are summarized in **Table 2** and visualized in **Figure 4**.

Oliviero et al. (1999) first examined the effects of rTMS in the prefrontal region alongside the previously discussed results in M1. fNIRS was used to measure changes following 2 min of rTMS stimulation delivered at 0.25 Hz and 100% Machine power to Fp2. These results were contrasted with the effects of anodal transcranial electrical stimulation (TES) and rTMS to right-M1. Again, the use of full TMS power is atypical and may represent as much as 300% RMT, but TMS strength would be reduced by distance created by the presence of the fNIRS probe between the cortex and the coil. Authors observed that levels of [HbO] had significantly increased following stimulation, similar to results observed in M1, while anodal electrical stimulation resulted in no significant change. Results from this study are difficult to compare due to the use of offline measurement, an uncommon stimulation frequency (0.25 hz), and the unknown stimulation strength resulting from an uncertain scalp-coil distance and lack of adaptation to subject RMT.

In the first online studies of stimulation in the DLPFC, Hanaoka et al. (2007) measured the effect of 1 Hz stimulation on the right-DLPFC (5 cm anterior to M1) while using fNIRS to monitor the contralateral DLPFC. In the first study, healthy subjects were instructed to idly copy a cartoon image while receiving stimulation at an effective 50%RMT to the right-DLPFC, whereas a second study by Aoyama et al. (2009) reported the effect of varying stimulation power with the same paradigm. Both studies suggested that 50% RMT was sufficient to produce a contralateral decrease in [HbO] during stimulation, while lower levels of stimulation were insufficient to effect significant change. Further work by Kozel et al. (2009) performed the first online ipsilateral measurements of stimulation to the DLPFC using 10 s of stimulation at 1 Hz with 120%RMT power. Although this work featured no sham condition, the work was counterbalanced with additional stimulation over the motor cortex. The authors reported that 1 Hz stimulation over the left-DLPFC (5 cm anterior to M1) was associated with large decreases of [HbO] in the bilateral DLPFC and in a later publication assessed the spatial reliability of these responses as having high reproducibility (Tian et al., 2012).

A fourth set of studies by Thomson et al. (2011a,b); Thomson et al. (2012a,b); Thomson et al. (2013) represents an attempt to characterize the response of the left-DLPFC (F3) to cortical stimulation. As the framework for several of these studies is largely similar, it is likely that they featured a common control subject set and a degree of overlapping participants. The first of six studies published investigated the ipsilateral response to single pulses of TMS at varying amplitudes (Thomson et al., 2011b) and found that only 130%RMT stimulation resulted in a large decrease in [HbO] and that neither 90%RMT or 110%RMT sufficiently produced a response. A second study (Thomson et al., 2011a) attempted to discern if fNIRS captured measurable differences between single pulses and paired pulses spaced at 2 or 15 ms, denoting stimuli for intracortical inhibition (ICI) and intracortical facilitation (ICF) respectively, two phenomena which are demonstrated to be sensitive to glutamate and GABA neurotransmission (de Jesus et al., 2014). They reported that single pulses at 120% RMT, as well as both ICI and ICF paired pulses, decreased [HbO] and suggested differences in the temporal dynamics of this decrease between the stimuli types. An additional study (Thomson et al., 2012a) investigated the differential response to two or four suprathreshold (120%RMT) TMS pulses spaced at 5 s, finding that both decreased [HbO], but four pulses had a stronger effect. Altogether these studies imply a general role for decreased [HbO] in response to strong suprathreshold stimulation and suggest that increased stimuli dosage may increase and prolong this response.

Thomson et al. (2012b) also featured a work recording the response of the left-DLPFC to long trains (10 mins) of 1 Hz stimulation typical of rTMS therapy. Again recording and stimulating over the left-DLPFC, the authors reported that 1 Hz at 120%RMT for 10 min produced a sustained decrease in [HbO]. However, the authors also noted that both 80%RMT and 120%RMT stimulations increased [HbO] during the first minute of stimulation. In addition to these works, Thomson et al. (2013) investigated the effect of coil orientation on the effect of single pulse stimulation and short trains of rTMS (20 s), noting primarily that the commonly used 45-degree orientation

TABLE 2 | Studies investigating fNIRS-measured response to TMS stimulation of DLPFC.

References	Stimulation parameters	Stimulation area	Measurement Area	Sham	No. of subjects	Finding
Oliviero et al., 1999*	0.25 Hz, 100% Stimulator Power, 2 min	R-DLPFC	R-DLPFC (Offline)	None	10	[HbO] increase vs. baseline after 30 stimulations
Hanaoka et al., 2007	1 Hz, ~50%RMT, 60 s × 3 Trials	R-DLPFC	L-DLPFC	Distant Secondary Coil	11	[HbO] decrease during stimulation, subsequent increase
Aoyama et al., 2009	1 Hz, {28,41,58%}RMT, 60 s	R-DLPFC	L-DLPFC	Distant Secondary Coil	10	[HbO] decreases during rTMS when RMT > 50%
Kozel et al., 2009*	1 Hz, 120%RMT, 10 s × 15 trials, 2 Days	L-DLPFC	Bilateral DLPFC	None	11	[HbO] decrease in ipsilateral and contralateral PFC, [HbR] increased
Tian et al., 2012*	1 Hz, 120%RMT, 10 s × 15 trials, 2 Days	L-DLPFC	Bilateral DLPFC	None	11	Reliability Assessment of (Kozel et al., 2009)
Thomson et al., 2011a	Single Pulse, {90,110,130%} RMT × 15 trials	L-DLPFC	L-DLPFC	Distant Coil with electrical sham	12, 10 Sham	[HbO] decrease with 130%RMT, but not lower power
Thomson et al., 2011b	Single Pulse, 120%RMT Paired Pulse, (ICI,2 ms), (IFC 15 ms), 70%RMT conditioning, 120%RMT stimulus × 20 trials	L-DLPFC	L-DLPFC	Distant Coil with electrical sham	8, 10 Sham	[HbO] decrease with single pulse, SICF and SICI stimulation
Thomson et al., 2012a	{2 or 4 pulses}, 0.2 Hz, 130% RMT × 20 trials	L-DLPFC	L-DLPFC	Distant Coil with electrical sham	13, 10 Sham	[HbO] decrease for 2 pulses, larger decrease with 4 pulses
Thomson et al., 2012b	1 Hz, {80%, 120% RMT}, 10 min	L-DLPFC	L-DLPFC	None	6	Sustained [HbO] decrease for 10 min for 120%RMT Small increase in [HbO] during 1st min for both 80 and 120%RMT
Thomson et al., 2013	Single Pulse, 120%RMT, {45,135,225 deg} × 15 trials 1 Hz, 120%RMT, 20 s, {45, 225 deg} × 15 trials	L-DLPFC	Bilateral DLPFC	None	12 SP, 8 rTMS	Ipsilateral [HbO] decrease for single pulse at 45 deg, Bilateral [HbO] increase for 20 s 1 Hz at 45 degrees, 135 deg orientation does not elicit significant response
Cao et al., 2013	{1, 2, 5}, 120%RMT, 5s × 20 trials	L-DLPFC	Bilateral DLPFC	None	12	[HbO] decrease for 1 Hz stimulation, increase for 2 Hz and 5 Hz
Curtin et al., 2017	{(1 pulse, 110%RMT), (15 Hz, 110%RMT, 2 s), (iTBS, 90%RMT, 2 s)} × 10 Trials	L-DLPFC	Bilateral DLPFC	Flipped Coil with stimulation	17	[HbO] increase for 15 Hz suprathreshold stimulation
Shinba et al., 2018	10 Hz, 120%RMT, 4 s × 75 trains, × 30 Days	L-DLPFC	Bilateral DLPFC	None	15 MDD	Increased [HbO] during stimulation associated with continued therapeutic effect of rTMS

Indicates that the study appears in both M1 and DLPFC tables.

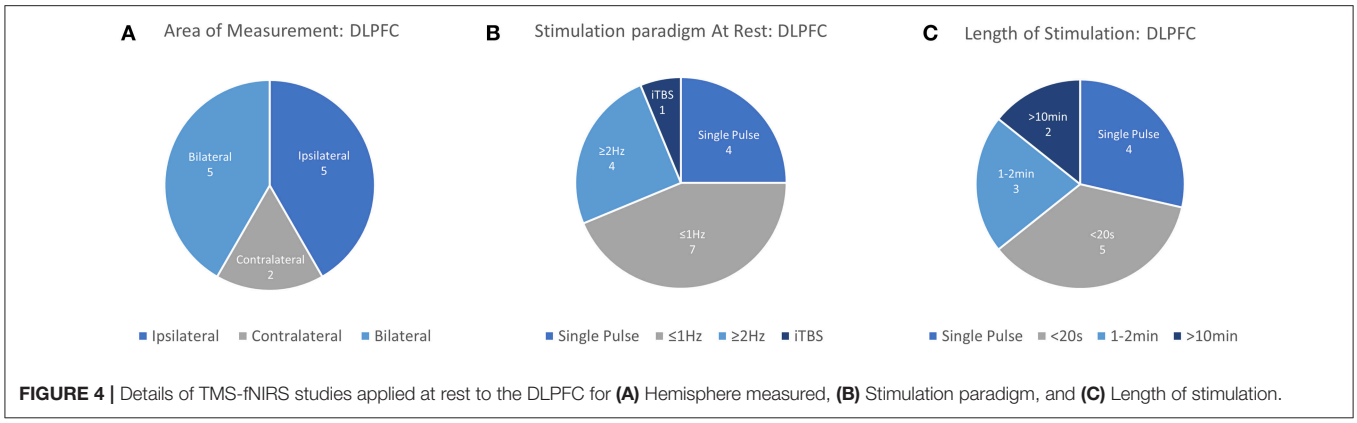

FIGURE 4 | Details of TMS-fNIRS studies applied at rest to the DLPFC for **(A)** Hemisphere measured, **(B)** Stimulation paradigm, and **(C)** Length of stimulation.

provided the strongest response and that a 135-degree coil orientation did not produce significant responses to stimulation. Similar to their previous findings, Single Pulses at 45 degree orientation and 120% RMT were again shown to have an ipsilateral decrease in [HbO]. However, 20 s of 1 Hz stimulation at 120%RMT was shown to instead increase [HbO] bilaterally. The authors noted that this increase in [HbO] may be an effect of cumulative stimulation as early rTMS trials showed decreased [HbO] and later trials showed larger increases.

The last work from this group, published by Cao et al. (2013), investigated the effect of 5 second trains of 1, 2, and 5 Hz stimulation at 120% RMT, showing again a decrease in [HbO] after 1 Hz and demonstrating an increase [HbO] after 2 and 5 Hz stimulation. In a recent publication, we similarly investigated the differential response to single pulses and short trains of rTMS (2 s) at 15 Hz conditions, as well as intermittent theta burst (iTBS) stimulation at 110%RMT and 90%RMT, respectively (Curtin et al., 2017). Our results suggested that single pulses at 110% RMT were not sufficient to elicit a response over the DLPFC, whereas 2-s trains of 15 Hz stimulation produced an increase in [HbO]. Subthreshold (90%RMT) trains of iTBS stimulation were not observed to introduce immediate changes in the area of stimulation despite claims of enhanced efficacy relative to high frequency stimulation.

Most recently, a clinical pilot study conducted by Shinba et al. (2018), reported significant increases in midline [HbO] during 10 Hz rTMS stimulation at 120%RMT to the left-DLPFC (5.5 cm anterior to M1) for treatment of drug-resistant individuals with MDD. Over the course of a 6-week treatment regime, the authors observed that the continued presence of [HbO] increase in response to stimulation was associated with clinical improvement as described by the Montgomery-Asberg Depression Rating Scale (MARDRS). Individuals who did not show positive changes associated with stimulation toward the end of the therapeutic regime did not show as strong clinical improvement.

In this review, 12 unique articles were identified which explored the effect of TMS on fNIRS-measured activation in the DLPFC. Of these articles, 4 works explored the effect of Single Pulse Stimulation in 6 conditions suggesting that single pulse stimulation of at least 120%RMT produce a measurable decrease in ipsilateral [HbO] (3/3 conditions). While the results of these works are in agreement with each other, the majority of these studies have been produced by one group and may not provide strong or independent evidence for this finding. The effects of inhibitory 1 Hz stimulation has been studied by 6 works, with 5/6 studies reporting a decrease in contralateral or ipsilateral [HbO] with sufficient stimulation power in at least one reported condition. Of these works, 2 early studies reported contralateral decreases in [HbO] with >50%RMT (while drawing), whereas suprathreshold 1 Hz stimulation at 110–120%RMT varied in reported effect. Here, short 5 and 10 s trains were independently reported to decrease ipsilateral or bilateral [HbO], while one study reported bilateral increase in [HbO] with 20 s stimulation. Only one study investigated longer clinically-relevant 1 Hz rTMS stimulation and reported [HbO] decrease only for suprathreshold (120%RMT) stimulation. Only 3 works investigated excitatory stimulation using rTMS, with two studies examining short (2–5 s) trains. These two independent studies suggest that short trains of suprathreshold high frequency stimulation produced either ipsilateral or a bilateral increase in [HbO]. While the remaining study measuring the clinical response of suprathreshold rTMS therapy in MDD provides some evidence for an expected increase in [HbO] and even a potential clinical correlate of treatment response, similar rTMS effects have not been described for healthy controls. In summary, despite evidence for decreased ipsilateral [HbO] in response to suprathreshold Single Pulse stimulation (3/4 studies), decreased ipsilateral or contralateral [HbO] in response to 1 Hz stimulation (5/6 studies), and increase [HbO] in response to suprathreshold excitatory high frequency stimulation (3/3 studies), a notable lack of consistency exists for specific parameters, protocols, precise stimulation target (F3 vs. 5 cm rule), and measurement areas used. This in combination with smaller subject sizes and a lack of well-controlled studies may limit interpretation of these results.

EFFECTS OF rTMS STIMULATION ON TASK-EVOKED fNIRS ACTIVITY

The ability of rTMS to modulate cortical excitability promises an accessible, non-invasive way to facilitate cognitive function and

treat disorders of brain function. To this end, researchers have become interested in the way rTMS paradigms effect changes on task performance and the associated neural activities involved, but also conversely, the way in which those activities may predict or reflect efficacy of rTMS itself. As changes in cortical excitability are largely inferred by effects on MEP (recorded while at rest in the motor region), it is often difficult to anticipate the way that rTMS paradigms will alter task-evoked measures of neural activity. Changes in functional measures during task-related activity are particularly important given interest in using rTMS to influence high-level cognitive function. Despite the potential utility of fNIRS for this purpose, this topic has been the subject of relatively few works. Although somewhat disparate in application and implementation, we summarize the list of known works. Their basic interpretations here are divided into clinical and healthy applications, such that they are accessible to interested readers. Details from each study including study population, task, stimulation parameters, measurement area, primary findings and other information are summarized in **Table 3** and visualized in **Figure 5**.

Effects in Healthy Populations

In one of the first studies to examine the effects of TMS on task-evoked fNIRS activity, Chiang et al. (2007) measured the effect of 20 min of 1 Hz stimulation at 115%RMT on evoked hemodynamic changes during a finger tapping task (involving the contralateral motor cortex) for up to 2 h after stimulation. The authors observed an increase in tapping-evoked [HbO] which lasted for up to 40 min after stimulation. While the employed paradigm is expected to induce inhibition in the targeted area, the authors noted that there is no consensus regarding changes to the contralateral motor region with both inhibitory and excitatory effects having been previously reported. The authors theorized that inhibition in the stimulated motor cortex may have increased excitation in the contralateral cortex. Despite the apparent simplicity of the task involved, these findings suggest a particular complexity in the effect of rTMS on task activity, with ostensibly inhibitory stimulation resulting in an increased level of activity in the contralateral cortex. This uncertainty regarding the local and regional effects of rTMS stimulation on fNIRS measures underlies some of the challenges which such studies face, particularly as the task and experimental questions involved increase in complexity.

TMS is commonly applied in neurophysiological studies as a method of interrupting active cognitive processing to understand the function of a particular region. The use of TMS in this context relies heavily on the particular area targeted and its theoretical role in the process investigated, along with when and how the region is stimulated. Here, the goal is primarily to provide causal/diagnostic information to inform further experimental and theoretical models. Regions stimulated with TMS may decrease or inhibit behavioral performance when the region is critical to task execution, or may increase task performance, either by potentiating a processing area, inhibiting an interfering process, or by some other possible pathway. Presently the use of fNIRS during intra-task TMS stimulation has only been investigated by one group under the context of spatial working memory. Yamanaka et al. (2010) studied whether short rTMS bursts of 5 Hz stimulation to the left parietal cortex (PC) during the retention period of a spatial working memory task (delayed match-to-sample) would increase performance. fNIRS was measured simultaneously on the bilateral-DLPFC while stimulation occurred in the adjacent left or right PC. While it was not observed that rTMS stimulation affected task accuracy, active rTMS applied to the right-PC appeared to decrease the reaction time during the working memory task. Active rTMS to the left-PC was also noted to result in [HbO] changes in the bilateral temporal regions. On the other hand, stimulation to the right-PC initially increased [HbO] in the left-precentral and marginal gyri and then shifted to the right gyri and finally the superior frontal gyrus during the response period. The authors described these changes as an asymmetric behavior of functional connectivity between the stimulated regions and suggested that this asymmetry was partially responsible for the effect observed in the right-PC which was not apparent in the left.

In a follow-up of this work, Yamanaka et al. (2014) explored the use of rTMS for cognitive enhancement in a healthy elderly population. However, after repeating the procedure in this population, right-PC rTMS did not significantly affect task reaction time or accuracy. When examining the fNIRS data, the authors observed that, in comparison with the young participants, older participants were observed to recruit more resources as evidenced by higher [HbO] during the working memory task. However, active rTMS had the effect of decreasing the task-evoked prefrontal [HbO] changes accompanying task performance. The authors suggest this is in line with reports that elderly individuals may require higher levels of neural resources in order to achieve similar performance outcomes and that active rTMS may have increased the neural efficiency of these systems. If the elderly participants were indeed engaging maximal cognitive resources, the ability of active TMS to further increase performance by increasing [HbO] may be hampered as the circuits may effectively be "at capacity." Importantly, the authors again noted a difference in the effect of left and right PC stimulation. While TMS to the right-PC appeared to result in little prefrontal change in elderly participants, TMS to the left-PC activated a similar number of channels, but with spatial differences. These results indicate not only the importance of TMS-fNIRS techniques in elucidating the differences between neural function among populations of interest, but also exemplify the more dynamic nature of stimulation responses during task activity.

As an exploration of rTMS to provide a clinical treatment for anxiety, Tupak et al. examined the Emotional Stroop task in healthy subjects after inhibitory cTBS application to the left or right DLPFC (Tupak et al., 2013). Here, the authors demonstrated that cTBS to the left-DLFPC (but not right-DLPFC or sham) bilaterally reduced task-evoked [HbO] to both neutral and anxiety words. This work appears to offer confirmation that inhibitory effects of cTBS as observed in the motor cortex may also inhibit task-evoked neural activity when applied to the left-DLPFC.

In another study examining a potential therapeutic avenue for anxiety and phobia, Guhn et al. (2014) applied high frequency

TABLE 3 | Effects of rTMS on fNIRS measures activity during task: clinical and Non-clinical applications.

	References	Population	Task	Stimulation Parameters	Stimulation area	Measurement area	Sham stimulation	No. of Subjects	Finding
Effect of rTMS on Task	Chiang et al., 2007	Healthy	Finger tapping	1 Hz, 115%RMT, 20 min	R-M1	L-M1	Distant secondary coil	5 HC	Task-Evoked [HbO] increase after contralateral TMS for up to 40 min
	Yamanaka et al., 2010	Healthy	Spatial match-to-sample	5 Hz, 100%RMT, 6 s × 10 Trials during Retention period	L/R-PC	Bilateral-DLPFC (Online)	Distant secondary coil	27 Left, 25 Right (HC)	Frontal [HbO] increase after stimulation to P4 during WM task and decreased RT, decrease in [HbO] during control
	Tupak et al., 2013	Healthy	Emotional Stroop	cTBS, 80%RMT, 10 min	L/R-DLPFC	Bilateral DLPFC	Placebo coil	16 Left, 16 Right, 19 Sham (HC)	Bilateral [HbO] decrease to left-PFC stimulation
	Guhn et al., 2014	Healthy	Conditioning stimuli	10 Hz, 110%RMT, 4 s × 40 trains	medial-PFC	Bilateral DLPFC	Placebo coil	40 Active, 45 Sham (HC)	Increased right-medial [HbO] during conditioning, early extinction for exploratory subgroup of strong responders ($N = 12$)
	Yamanaka et al., 2014	Elderly	Spatial Match-To-Sample	5 Hz, 100%RMT, 6 s × 10 Trials during Retention period	L/R-PC	Bilateral-DLPFC (Online)	Distant secondary coil	18 Left, 20 Right (Eld.)	Frontal [HbO] decrease during WM task and increase during Control Task (both P3, P4), no change in RT or accuracy
	Maier et al., 2018	Healthy	Ultimatum and Dictator Game	cTBS, 80%RMT, 40 s	R-DLPFC	Bilateral DLPFC	Placebo coil	19 HC	Reduced [HbO] and generosity during Dictator Game following verum stimulation
Clinical Applications (Task)	Eschweiler et al., 2000	Depression	Mirror Drawing, Mental Arithmetic	10Hz, 90%RMT, 10s × 20 trains, 5 Days	L-DLPFC	Bilateral DLPFC	Tilted coil	12 MDD	Pre-intervention [HbT] change at F3 during left-handed Mirror Drawing correlated with HAMD change
	Dresler et al., 2009	Panic disorder	Emotional Stroop	10Hz, 110%RMT, 4 s × 40 trains, 15 Days	L-DLPFC	Bilateral DLPFC	N/A	Case Study (PD)	Increased bilateral [HbO] to panic stimuli
	Schecklmann et al., 2014	Tinnitus	Audio Stimulation	cTBS, 30% Stimulator Output, 2 sessions × 600 pulses × 5 days	L-TPC	L/R-TPC	Flipped coil	23 Tinnitus (11 Sham), 12 HC	Trend significance toward increased [HbO] in Left-TPC after stimulation
	Deppermann et al., 2014	Panic disorder	Verbal Fluency	iTBS, 80%RMT, 2 s × 200 trains, 15 Days	L-DLPFC	Bilateral DLPFC	Flipped coil	44 PD (23 Sham), 23 HC	No change for real stimulation, [HbO] increase in left-IFG in PD Group following 15 session sham stimulation
	Deppermann et al., 2016	Phobia	Emotional Stroop	iTBS, 80%RMT, 2 s × 200 trains	L-DLPFC	Bilateral DLPFC	Tilted coil	41 Phobia (19Sham), 42 HC (19Sham)	Decreased [HbO] in left IFG for neutral words in phobia group independent of iTBS
	Sutoh et al., 2016	Bulimia nervosa	Food Presentation, Rock Paper Scissors	10Hz, 110%RMT, 5 s, × 15 trains, 5 Days	L-DLPFC	Bilateral DLPFC	N/A	8 BN	Decrease in Left-PFC [HbO] during RPS and neutral stimuli
	Deppermann et al., 2017	Panic disorder	Emotional Stroop	iTBS, 80%RMT, 2 s × 200 trains, 15 Days	L-DLPFC	Bilateral DLPFC	Flipped coil	44 PD (23 Sham), 23 HC	Increased [CBSI] following active stimulation for panic-stimuli
	Hara et al., 2017	Stroke-aphasia	Word repetition	{1 Hz, 40 min}, {10 Hz, 12 min}, 90%RMT, 10 Days	R-IFG	Bilateral-IFG	N/A	4 Left, 4 Right (Stroke)	LF stimulation reduced contralateral [HbO], HF stimulation increased bilateral [HbO]
	Urushidani et al., 2018	Stroke-paresis	Finger flexion/extension	1 Hz, 90%RMT, 20 min, 21 Sessions, 15 Days	Unaffected-M1	Bilateral-M1	N/A	Case study (Stroke)	Increased Lateralization Index (LI) toward lesional hemisphere
	Tamashiro et al., 2018	Stroke-paresis	Finger flexion/extension	1 Hz, 90%RMT, 20 min, 21 Sessions, 15 Days	Unaffected-M1	Bilateral-M1	N/A	59 Stroke patients	Pre-TMS Lateralization predicted changes in treatment lateralization and functional outcomes

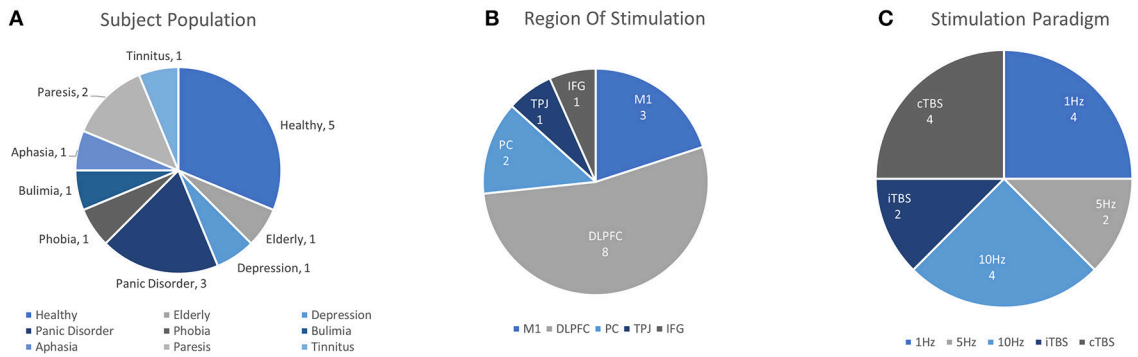

FIGURE 5 | Details of TMS-fNIRS studies applied before or during cognitive Tasks according to **(A)** Subject Population, **(B)** Region of Stimulation, and **(C)** Paradigm of Stimulation.

stimulation to the medial PFC following a fear conditioning session (audio of a scream) in healthy subjects. Active but not sham stimulation, reduced arousal in terms of fear-potentiated startle and skin conductance response during the extinction-learning phase, however, fNIRS measures were not significantly different between experimental groups. When authors selected an exploratory subset of participants who most strongly possessed a conditioned fear response, they identified that the active TMS group evoked a higher [HbO] response to early aversive stimuli in the medial prefrontal channels during the extinction-learning phase. They described these changes as an enhancement of self-regulatory inhibition in response to fear, hoping that such therapy may assist others in their ability to address the challenges of phobia.

Most recently, Maier et al. (2018) used inhibitory cTBS at 80%RMT applied to the right-DLPFC in order to reduce cognitive control over forgiveness. Based on previous studies which had implicated right-DLPFC activation in pro-social reactions to unfair situations, the authors replicated a protocol involving an ultimatum game against unfair or fair opponents, followed by a dictator game in which subjects were able to retaliate (Brüne et al., 2013). Following verum inhibitory rTMS, participants allocated less money to unfair opponents and showed reduced [HbO] in the right-DLPFC compared with sham stimulation. This work may serve as a useful example of how TMS-fNIRS may be used within cognitive neuroscience to investigate neural underpinnings of social interaction and behaviors.

Clinical Applications

A primary motivation to study the fNIRS-measured effects of rTMS during specific tasks is that fNIRS may offer a useful metric for treatment response, clinical status, or functional targeting for TMS therapies. In one of the earliest works employing both techniques, Eschweiler et al. (2000) reported that functional activation during mental tasks (mental arithmetic and left/right-handed mirror drawing) could serve as a predictor of TMS therapeutic effect in Major Depressive Disorder (MDD). Clinical improvement to 5-days of rTMS therapy (10 Hz, Left-DLPFC) was correlated with pretreatment [HbT] changes in the left-DLPFC during a left-handed mirror drawing task. Given the excitatory nature of high frequency rTMS and expected reduced left-PFC activity in depression, these results appear to confirm a general hypothesis that excitatory rTMS therapy could target regions of relative hypoactivity. As only pre-TMS task measurements were conducted, it was unknown what changes successful therapy may have had on fNIRS activity. However, this work establishes a precedent for functional targeting of TMS therapy using fNIRS-measured activity during tasks which have been identified as affected in a given disorder. Together with the recently published work by Shinba et al. (2018), these studies make a compelling case that the ability or inability of excitatory rTMS to evoke hemodynamic activity may serve to inform clinical status and predict treatment response to TMS therapies.

Dresler et al. reported a case study in which a patient with comorbid panic disorder (PD) and MDD was treated with high-frequency rTMS of the left-DLPFC over the course of 3 weeks (Dresler et al., 2009). fNIRS measures of an emotional Stroop task featuring panic-related and neutral words showed that therapy increased bilateral prefrontal recruitment in terms of [HbO] during exposure to the panic task-condition. These results inspired a larger clinical investigation into the replicability of hypofrontality in PD and the use of excitatory iTBS over the left-DLPFC as a potential treatment approach. In a double-blinded sham-controlled study with 44 patients, the authors separately confirmed fNIRS-measured prefrontal hypoactivity in PD during both a verbal fluency task (Deppermann et al., 2014) and the emotional Stroop task (Deppermann et al., 2017). Following 15 sessions of iTBS treatment and Cognitive Behavioral Therapy (CBT), results indicated that active rTMS did not impact pre-therapeutic activity on the fluency task, but in a confirmation of the original case study, increased the relative activation of panic-related stimuli to neutral stimuli during the emotional Stroop task. Although the work shows a promising indicator that TMS treatments can remediate clinically relevant functional deficits as measured by fNIRS, the link between this functional restoration and clinical effect is less clear due to lack of a significant difference in clinical improvement between sham and active iTBS therapies.

Deppermann et al. (2016) employed iTBS again as a potential remediation strategy in individuals with spider

phobia after identifying a hypofrontality in the left-DLPFC during neutral words during an emotional Stroop task in participants with phobia. However, following both active and sham iTBS targeting the left-DLPFC and a virtual reality phobia challenge, functional activation differences between control and phobia participants disappeared. The authors speculated that the mild phobia challenge may have helped recruit a compensatory prefrontal network which normalized activity in phobic participants.

TMS therapies also have the potential to address chronic neurophysiological conditions, such as tinnitus, which otherwise have no clear or effective treatment approach. Tinnitus is a perceptual auditory disorder which has been suggested to correlate with a hyperactivity in the left auditory cortex or abnormal lateralization in response to auditory stimuli. Following this proposed mechanism, TMS has been used as an approach to ameliorate symptoms by using rTMS paradigms thought to inhibit cortical excitability; however, individual variability to treatment remains high. In a sham-controlled exploratory work, Schecklmann et al. (2014) applied cTBS over the course of 5 days to the left Herschel's gyrus and monitored the fNIRS response to audio stimuli before and after the course of treatment. Subjects were exposed to speech noise in a block design paradigm as well as in an event-related paradigm. Overall, results from the study were somewhat contradictory, with active rTMS weakly increasing left-auditory [HbO] in the block design format, but slightly reducing [HbO] in the event-related design task. In addition, sham rTMS therapy exhibited essentially opposite trends in fNIRS activity. Finally, while tinnitus symptoms were successfully reduced after therapy, this reduction was independent of the sham/active condition (Schecklmann et al., 2016).

Clinicians view TMS therapies as a new avenue to improve or complement the efficacy of pharmaceutical and psychotherapeutic approaches, especially in applications where relapse rates are relatively high. Eating disorders represent one such area in which NIBS offer a new hope and fNIRS offers one method to understand the mechanisms behind TMS therapies designed to reduce cravings. In a small population of participants diagnosed with Bulimia Nervosa, Sutoh et al. (2016) measured the left and right DLPFC using fNIRS during a food photo task and a rock paper scissors task in which the participant was asked to intentionally win or lose. Subjects were measured 1 week before, and 4 h after, a single session of 10 Hz rTMS to the left-DLPFC. rTMS was successful at reducing subjective craving of high-calorie food stimuli with no effect on low-calorie or neutral stimuli. This effect was coupled by a reduction of [HbO] in the left-DLPFC to neutral photo stimuli during the latter half of the task. rTMS application prior to the lose/win rock papers scissors task appeared to reduce accuracy during the lose condition which was coupled with reduced [HbO] in the left-DLPFC channel. Although neural responses to desirable foods were not significantly different, the authors suggested that these results reflected an inefficient self-regulatory activity in the PFC which was improved by rTMS, resulting in decreased task [HbO] to neutral stimuli where such self-regulation was unnecessary. Such studies represent important efforts to understand how fNIRS provides insight into the treatment of mental disorders with complex etiologies.

Research into the use of fNIRS to guide and evaluate TMS treatment is still very much in an exploratory phase. However, the accumulation of evidence reviewed here and the increasingly practical application of the two techniques in combination has brought some aspects of this goal closer to reality, in particular, the use of fNIRS as a methodology for functional targeting. Recently, an exciting study used this approach to guide TMS intervention within a population of stroke patients who suffered from chronic aphasia. Hara et al. (2017) divided an exploratory aphasia population with exclusively left-hemisphere lesions into two groups based on the relative hemispheric activity during a word repetition task. Participants who exhibited higher left hemisphere activation were prescribed 1 Hz rTMS to the right inferior frontal gyrus (IFG), whereas subjects with right hemisphere activation were prescribed 10 Hz rTMS to the same location (rIFG). Following 11 sessions of TMS therapy and intensive speech therapy, participants showed significant improvement in language functions as well as differential effects of rTMS therapy depending on the assigned paradigm. Individuals receiving low-frequency stimulation showed a reduction in activation asymmetry, whereas individuals receiving high-frequency stimulation showed an increase in activation within the right hemisphere. Although it is not specifically possible to differentiate the effect of intensive therapy and that of rTMS, this study shows an exciting potential wherein fNIRS may be used to indicate effective TMS approaches and serve as a measure of effective treatment.

Two publications recently have continued this trend by examining the ability of fNIRS to influence or normalize the hemispheric balance after stroke. Described in one case study (Urushidani et al., 2018) as well as a clinical study with 59 participants (Tamashiro et al., 2018), fNIRS was used to evaluate effects of rTMS and occupational therapy on the balance of hemispheric involvement between the affected and unaffected motor cortices following stroke. Prior to and following a 15-day rTMS treatment regime consisting of 1 Hz at 90%RMT to the unaffected motor cortex, motor symmetry was assessed during a finger flexion/extension task. The case study described that 1 Hz rTMS was successful in increasing lateralization index (LI) in the direction of the lesioned hemisphere and the clinical study supported the beneficial nature of this by reporting that changes in LI were correlated with clinical improvement. However, it was also found that affected hemispheric dominance prior to treatment may affect the success of treatment. Despite individual variability in patient response to treatment, fNIRS here offers a clear approach for assessment of post-stroke cortical function as well as a measure of rTMS remediation of potentially deleterious functional asymmetry.

Altogether in this section 16 unique works addressed the ability of rTMS to effect changes on fNIRS activity. Of these, 6 works studied rTMS in tasks with healthy or aged populations. Excitatory rTMS paradigms were reported to increase ipsilateral [HbO] in 2/3 studies and inhibitory stimulation was reported to reduce evoked ipsilateral [HbO] in 2/2 studies. Additionally, 10 clinical works, including 2 case studies, reported the use

of rTMS in clinical conditions of depression, phobia, tinnitus, stroke, bulimia, and panic disorder. Currently, significant mismatch in clinical population, task design, stimulation conditions, and other methodological differences greatly restrict the interpretation of these observations. Studies evaluating the effects of rTMS on tasks using fNIRS all reported their findings as changes in [HbO] or as a corrected variant of [HbO] (4/16 studies, CBSI: see Cui et al., 2010), or in terms of hemispheric balance of [HbO] (Lateral Index, 2/16). However, only two studies reported any results in terms of [HbR] or [HbT]. While oftentimes it can be helpful in addressing complicated effects of stimulation on task by focusing on the changes in one biomarker, the absence of other reported measures may make it difficult to replicate and evaluate future findings.

RELATIONSHIP BETWEEN CORTICAL EXCITABILITY AND fNIRS MEASURES

Although much remains unknown about the relationship between the changes in cortical excitation observed with TMS and measured cortical responses by fNIRS, researchers have explored the use of TMS and fNIRS as complementary probes of neural function. While not considered a neuroimaging technique *per-se*, TMS can provide spatial mapping of cortical regions when tied to MEP amplitude. Mapping the motor region using TMS has been widely used as a way to test the functionality of the motor system in healthy situations and during recovery from traumatic injury such as stroke. Evoked MEP amplitudes are also known to change during task performance and have been proposed as an additional functional measure in some cases. Although these measures require active stimulation and cannot be easily obtained outside of the motor cortex, MEP changes offer an additional perspective on neurophysiological state during cognition. Finally, the combination of fNIRS measures and TMS have been popularized for the study of central fatigue, in particular the effect of hypoxic cerebral and peripheral conditions on exercise and muscle excitability. Although it is readily apparent that hypoxic conditions reduce athletic performance, especially in individuals unacclimated to such conditions, differentiating the causes of degraded performance has not been a straightforward task. Measurement of cerebral and peripheral oxygenation using fNIRS-based systems allows exercise physiologists to independently manipulate and verify the contributions of hypoxic conditions to fatigue under voluntary activity and TMS-evoked muscle movement. Studies describing the relation of fNIRS and cortical excitability are detailed in **Table 4** and broken down by the categorized methodological approaches.

TMS Motor Mapping and fNIRS Motor Mapping

In an early case study by Park et al. (2004), changes in the TMS motor map of a patient undergoing constraint-induced therapy for stroke alongside functional changes in a motor task activity as recorded by fNIRS and fMRI. Therapy was associated with bilaterally decreased task-evoked [HbO] and an increased laterality toward the hemisphere associated with the affected hand. These changes were also reflected in an increased TMS motor map area in the same hemisphere, suggesting that improvements in therapy were associated with improved cortical organization in both measures.

The specificity of TMS mapping has also been speculated as a useful way to inform neuroimaging. In particular, TMS has been proposed as one technique to identify areas that contain the peak fNIRS response which may be sensitive to individual variability. fNIRS sensor arrays can be positioned and arranged in many form factors, but most commonly, optode arrangements are placed based on rough anatomical locations such as 10–20 positions. Mismatches between individual anatomy, as well as functional differences within regions, may serve to reduce the sensitivity of specific measured channels to experimentally-relevant cortical changes by simple virtue of non-optimal placement. In one bid to enhance functional sensitivity, Akiyama et al. (2006) attempted to relate the evoked MEP Center of Gravity (CoG) for the Abductor pollicis brevis (APB) muscle with the functional response to a hand-grasping task using an optode arrangement centered on the CoG. The authors reported that the fNIRS oxygenation response was significantly lower in spatial specificity than the functional area estimated by TMS motor mapping but reported a specific spatial specificity for early-phase changes in [HbR] at the CoG. In a later study, Koenraadt et al. (2011) conducted a similar protocol, again mapping the CoG of the right APB and measuring fNIRS activity at the CoG as well as C3 on the 10-20 System. Although they confirmed that C3 was a poor estimation of CoG position with an average error of 19.2 mm, they were unable to identify any differences in the evoked hemodynamic changes during a thumb abduction/adduction task. The authors suggested that TMS-evoked MEP amplitudes and motor-evoked fNIRS may derive from a different physiological basis.

Changes in Cortical Excitability During Task: Functional MEP Measures

In a line of work attempting to compare MEP measures to task-evoked fNIRS, Lo et al. (2009) investigated the changes in TMS excitability and functional changes while subjects were engaged with overt reading or singing tasks. After identifying the CoG of the FDI muscle, experimenters identified 9 surrounding points at which, during separate sessions, either fNIRS measures or MEP amplitudes were evaluated during the speaking/singing tasks. Changes in the MEP amplitude were observed most strongly at the CoG, whereas fNIRS activation was observed as more distributed increases in [HbO]. The authors reported that maximum fNIRS activity did not occur at the CoG and fNIRS measures did not significantly correlate with the changes in MEP amplitude. Again, the authors claimed that the MEP and evoked [HbO] evaluated distinct neural dynamics involved in vocalization and that suggested that cortical excitability itself does not likely imply high metabolic demands.

Another work by Derosière et al. (2015) examined functional and motor excitability during sustained attention. Subjects were divided into two experimental groups, one group receiving

TABLE 4 | Relation of fNIRS and cortical excitability as measured by TMS: motor mapping, functional MEPs, and central fatigue.

	References	Population	Task	Stimulation Parameters	Stimulation Area	Measurement Area	No. of Subjects	Finding
Motor Mapping	Park et al., 2004	Stroke-Paresis	Key Turning	110%RMT for Motor Mapping	L/R-M1	Bilateral-M1	Case Study (Stroke)	Decreased [HbO], increased lateralization during task over therapy. Enlarged motor region after therapy.
	Akiyama et al., 2006	Healthy	Hand Grasping	120%RMT for Motor Mapping	L-M1	L-M1	10 HC	Biphasic [HbO] changes observed over MEP COG
	Koenraadt et al., 2011	Healthy	Thumb abduction	120%RMT for Motor Mapping	L-M1	L-M1	11 HC	No difference in [HbO] changes at MEP COG vs C3
MEP during Task	Lo et al., 2009	Healthy	Reading aloud, Singing	110%RMT, random MEP evaluation during task	L-M1	L-M1	5 HC	Changes in evoked MEP amplitude during vocalization at MEP COG, MEP changes not correlated with [HbO]
	Derosière et al., 2015	Healthy	Sustained Attention	MEP evaluated at 5min intervals	L-M1	PFC, L-M1, R-Parietal	15 TMS, 13 fNIRS, 4 Control	Increase in lateral PFC and right parietal [HbO], MEP amplitude increase over TOT
	Corp et al., 2018	Elderly	Dual Task [Tapping, N-Back]	MEP evaluated at 12.5s intervals	L-M1	Exp1: PFC (Online), Exp2: PFC, PM, M1	Exp1: 15 Young, 15 Eld. Exp2: 15 Eld.	Increased CSP during dual-tasks in elderly correlated with worse performance. fNIRS uncorrelated with dual-task performance
Exercise & Fatigue	Millet et al., 2012	Healthy	Isometric elbow contraction	MEP and CSP evaluation every 4th contraction	R-M1	L-DLPFC	Exp1: 12 HC, Exp2: 10 HC	Reduced performance and prefrontal oxygenation in hypoxia despite normoxia in muscle. Similar CSP and MEP responses
	Goodall et al., 2012	Healthy	Cycling	MEP, CSP, VA evaluation at 130%RMT before and after exercise	L-M1	L-DLPFC	9 HC	Reduced performance and prefrontal oxygenation in hypoxia and larger decrease in VA TMS after exercise
	Goodall et al., 2014	Healthy	Cycling	MEP, CSP, VA evaluation at 130%RMT before and after exercise	L-M1	L-DLPFC	7 HC	Greater decrease in prefrontal oxygenation in acute hypoxia, decrease in voluntary and potentiated force in both chronic and acute hypoxia. Doubled MEP size in chronic hypoxia.
	Rupp et al., 2015	Healthy	Isometric knee contraction	MEP, VA, CSP evaluated before and during contractions	L-M1	L-DLPFC	15 HC	Reduced performance in hypoxia, increased prefrontal oxygenation in hypoxia with CO2 clamping vs. w/o, VA TMS decrease greater in hypoxia w/o CO2 clamping
	Jubeau et al., 2017	Healthy	Cycling	MEP, VA, CSP evaluated before and 1,2,3 hours after exercise	L-M1	L-DLPFC, L-M1	10 HC	No performance difference, VA TMS or CSP after prolonged exercise in hypoxia conditions, reduced prefrontal oxygenation in hypoxia
	Marillier et al., 2017	Healthy	Isometric elbow contraction	MEP, VA, CSP evaluated before and during contractions	L-M1	L-DLPFC	11 HC	No performance differences between acute, chronic, or normoxia conditions or in VA TMS decline. Longer CSP in hypoxia conditions. No difference in prefrontal or muscle oxygenation
	Laurent et al., 2018	Healthy	Isometric knee extension	MEP, VA evaluated at 140% 'optimal' power, before and during extension, and after task failure	L-M1	L-DLPFC	14 Trained Athletes	No effect of salbutamol intake on VA TMS, prefrontal oxygenation, or task performance
	Solianik et al., 2018	Healthy	2 Hr Speed-Accuracy Motor task	MEP evaluation at 130%RMT before and after task	L-M1	DLPFC	10 HC	Increased MEP amplitude after prolonged activity, decrease in evoked left-prefrontal [Hb] in Stroop task vs. pre-task Stroop, no change for control activity

regular MEP measurement and one monitored using fNIRS. The authors worked to show how functional measures in different cortical areas and excitability in the motor region varied with the Time on Task (TOT). During a 30-min performance of a sustained attention task, increases in [HbO] in the lateral prefrontal regions and the right-parietal areas evolved after approximately 9 min of performance, whereas the left-M1 region exhibited these changes after 15 min. In the TMS group, increased MEP amplitude was also evidenced after 15 min of task performance, an effect not present in the non-task TMS control group. Together, the authors suggested that attentional areas including the lateral prefrontal regions and right parietal region may be more sensitive to prolonged attentional demands and that motor regions may become more involved in later stages of the task. Evidence of an increase in MEP amplitude following an extended attention-demanding task was also supported by a more recent study focusing on cognitive changes due to prolonged motor actives. Solianik et al. (2018) investigated changes to fNIRS-evoked cognitive activities and motor function following a 2 h speed-accuracy motor task compared with a non-demanding control task. Following the motor task, the authors noted increased prefrontal oxygenation (driven by decreased [HbR]) along with an increased resting MEP, whereas the non-demanding control task exhibited no changes on either cognitive biomarkers or cortical excitability. Most recently, MEP amplitudes and the cortical silent period (CSP) length were evaluated as a measure of engagement during dual-task performance in elderly and adult populations (Corp et al., 2018). While increased CSP length was associated with poor performance in elderly subjects, fNIRS measures were excessively noisy during an initial experiment and did not correlate with behavioral performance in a second experiment.

Although the preceding studies did not examine the effect of TMS on fNIRS measures but rather the relation between TMS measures and fNIRS, they still help inform works which do examine these approaches. In particular, these works emphasize the spatial dissimilarity between MEP measures and task-evoked fNIRS. In the context of motor mapping, observation of a broader fNIRS response may be interpreted as additional recruitment involved in voluntary muscle control as compared with TMS-evoked movement at rest. In the context of active vocalization, the dissimilarity in FDI excitability with the functional activity of the task itself may reflect different roles between motor control, planning, and cortical excitation during task execution. On the other hand, regional similarities in the emergence of time-on-task effects during prolonged attention suggest some common roles for the two cortical measures. Importantly, these works together suggest that TMS may activate more spatially specific areas than those recruited in voluntary activities which may be the result of more coordinated neural activities, even for relatively simple tasks.

Changes in Cortical Excitability During Exercise, Hypoxia, and Central Fatigue

In first work of this series, Millet et al. (2012) monitored muscle and cerebral hemodynamics using fNIRS under differing fixed inspired oxygen (FiO2) levels while the muscle performing contractions was occluded using an inflated cuff so that systemic hypoxia could be maintained during local normoxia. After occluding the arm, inspired oxygen was then administered for 5 min and afterwards subjects performed repeated isometric contractions until exhaustion. Electrical nerve stimulation (M wave) and TMS were used to generate muscle twitches during isometric contraction performance and assess the relation between spinal and cortical inhibition. Under severe hypoxia, muscle performance was decreased by 15% despite similar muscle hemodynamic conditions, but electrically and TMS-evoked MEP and CSP were unaltered by hypoxia, suggesting that reduced oxygenation in the brain may have a role in this performance reduction.

Extending this work by exploring the additional contribution of hypocapnia on central fatigue, Rupp et al. (2015) used the combination of TMS and fNIRS during knee extensions with CO_2 clamping to control end-tidal CO_2 concentrations. Reductions in exercise performance in terms of duration were again noted in hypoxic conditions regardless of the presence of CO_2 clamping conditions. However, CO_2 clamping appeared to increase both cerebral and muscular oxygenation. Additionally, maximal voluntary activation by TMS (VA_{tms}) at task failure during hypoxia was larger with CO_2 clamping. However, electrical muscle stimulation revealed that CO_2 clamping resulted in increased peripheral fatigue, suggesting that the control of expired CO_2 to prevent hypocapnia had shifted the balance of fatigue from central to peripheral mechanisms.

The most common environmental hypoxic situations are introduced by high-altitude conditions which can influence certain sports such as hiking and cycling. In two works, Goodall et al. (2012, 2014) examined the effect of hypoxia on cycling activity first by emulating high-altitude (3,800 m) conditions with changes in FiO_2 (Goodall et al., 2012), and then in individuals acclimatized to high-altitude conditions (14 days at 5,260 m) (Goodall et al., 2014). In the first study, hypoxia significantly reduced cycling duration as well as cerebral [HbO]. VA_{TMS} activation was further reduced after cycling compared with normoxia, but MEP amplitude was increased after hypoxia. The second work showed that while maximal contraction force, VA_{TMS}, and prefrontal oxygenation were decreased by the introduction of altitude-induced hypoxia, adaptation to the high-altitude environment appeared to normalize prefrontal hemodynamics and abolish the observed decrease in VA_{TMS}. Additionally, the authors observed that after altitude acclimatization, TMS-evoked MEP amplitudes were nearly twice as large, indicating that the central fatigue was attenuated by acclimatization, possibly through increased cerebral oxygenation or cortical excitability.

In contrast to these findings, Jubeau et al. (2017) studied the effects of hypoxia in cycling during prolonged (80 min) rather than strenuous conditions. During the performance of more moderate exercise, performance differences were not significant between the two conditions, including changes in TMS measures and electrical nerve stimulation. Although prefrontal and motor cortex oxygenation were reduced in hypoxic conditions, the authors suggested that low-intensity prolonged exercise does

not result in increased central fatigue. Similarly in another altitude acclimatization study (5 days at 4,350 m), Marillier et al. (2017) noted that exposure to hypoxia did not alter excercise duration, prefrontal hemodynamics, muscle hemodynamics, or voluntary contraction force after low intensity isometric elbow flexion. While electrical nerve stimulation showed increased peripheral fatigue, TMS showed decreased cortical excitability after 5 days at high-altitude, suggesting that despite increased central inhibition, performance of less intense isometric exercise may not be substantially affected by hypoxia-induced central fatigue.

In another inquiry into central fatigue, Laurent et al. (2018) explored the use of TMS and fNIRS to determine the effects of Salbutamol on central fatigue and prefrontal oxygenation in trained cyclists. Knee extensions were performed until task failure at a variety of intensities, however differences were not observed in prefrontal oxygenation, VA_{TMS}, or athletic performance after intake of oral or inhaled Salbutamol. This work, while reporting negative results, shows an interesting application of fNIRS-TMS in evaluation of athletic doping. Salbutamol, an asthma medication, has uncertain effects on exercise performance, unlike the often more dramatic changes created by hypoxic conditions, but this study opens the door toward further usage of this methodology in the study of pharmaceutical effects on central fatigue and cortical excitability.

LIMITATIONS

The work presented here attempts to address an absence of a collective discussion of the mechanisms and applications of fNIRS and TMS. The range of applications and uses of the techniques as well as differences between protocols, subject populations, stimuli locations, and stimuli parameters can further exacerbate the lack of standardization between study objectives and approaches. In spite of this, presentation of the unified body of works still allows for an accessible comparison of methodological approaches so that future studies can explore and expand on the results of these findings.

The breadth of topics covered in this review places restrictions on the ability to perform comparative analysis between all studies introduced here. In the first primary section, we grouped together studies in which participants were measured during TMS stimulation under both offline and online contexts, both of which may measure different post-stimulation phenomena attributable to differences in experimental setup. Studies in this section were grouped in a manner according to the location at which stimulation was performed; however, differences between TMS coils used, targeting approaches, statistical/preprocessing approaches, as well as fNIRS equipment and measurement locations could introduce significant variability to the results expressed in the reported studies. While it is difficult to provide a quantitative comparison between all studies presented here due to this, some similarity in works may allow for a preliminary generalization of findings for expected activity to the most common stimulation parameters in M1 and the DLPFC. To this end we have made a qualitative evaluation of ipsilateral and contralateral responses to stimulation available in **Supplementary Table 1**. Strict review of the studies presented here also shows that a large number of studies originate from only a few groups which may impair the independence of reported findings.

In the second section, fNIRS was primarily used to investigate changes during task performance which could be attributed to rTMS stimulation. Within this designation, fNIRS is at times used as either a method to detect changes in evoked measures during task performance due to rTMS therapy in clinical populations, or as a method for modulating cognition within healthy individuals. Studies such as these may depend largely on the types of the tasks employed, as well as the clinical condition being targeted. These interventions may also differ in terms of their targeted stimulation/measurement regions, parameters and the length or style of intervention. For this reason, quantitative comparison of studies cannot yet be made, but the current progress within the conjoined application of the two modalities is discussed.

The third section concerns the use of fNIRS and cortical excitability within a functional and physiological context. This section contains several novel approaches for the use of MEP as functional measure in itself, but also describes the relationship of cortical oxygenation to the central nervous system's role in neuromuscular fatigue. Work involving the functional MEP measures allows a general comparison of changes in MEP excitability with evoked functional measures. However, it is generally understood that the physiological basis of both measures is very different in nature and as such, experimental designs to compare these measures must be constructed in a manner which takes advantage of the unique aspects of each measurement approach.

The preliminary nature of many of the works included in this review, as well as the limited number of researchers investigating these topics, precludes a rigorous investigation of bias. It is not currently clear whether reports where fNIRS measures, or fails to measure, the effects of TMS may be due to the stimulation parameters or the methodology used. Apart from these mentioned limitations, there are many other variables which govern the influence of rTMS on normal neurophysiology including anatomical differences and subject variability in response to rTMS. The state-space of TMS effects on neurophysiology may have an incredible complexity and considerable work must be done in order to consolidate the effects of even simple paradigms.

SUMMARY AND FUTURE DIRECTIONS

The combination of TMS and fNIRS as paired techniques for the study of neurophysiology and cognition has expanded well beyond the work of a handful of researchers. Given the mutual advantages of the techniques and the individual proliferation of both technologies in terms of availability to clinicians and procurement by researchers, the convergence of the fNIRS-TMS is easily anticipated. Currently, scientists have only just begun to employ fNIRS-TMS and many areas of research

with rather rich application remain uninvestigated or under-investigated. This includes, but is not limited to, the basic responses to individual pulses in different cortical regions, short trains of rTMS stimulation, effects of prolonged therapies, and investigation in clinical populations. In order to encourage further research and formalize the available knowledge, this review attempts to consolidate current findings regarding the effect of TMS on fNIRS measures under conditions of both rest and task. Furthermore, this work aggregates research into the spatial and functional relationship between fNIRS and cortical excitability measures.

Effects of TMS at Rest: DLPFC & M1

Here we have discussed results from studies of stimulation broadly in multiple cortical regions and the effects observed from various rTMS patterns with the goal of strengthening core findings by aligning similar investigative works. Studies have most frequently examined either the DLPFC or M1 as candidates for online stimulation and measurement; however, there exist a number of inconsistencies in the results which may be attributed to methodological variations, experimental error, subject variability, and other issues. Studies have illustrated that stimulus intensity, subject state during stimulation, location, and frequency all have an influence on the measured hemodynamic response in different regions. Some consensus exists that short trains of 1 Hz stimulation may reduce [HbO] in both the DLPFC and M1 regions. However, differences between these regions may exist for Single Pulse stimulation responses. Several studies seem to support the finding that subthreshold single pulses to M1 can increase [HbO] in a state-dependent measure, and on the other hand, research into responses in the DLPFC seem to indicate that suprathreshold Single Pulse stimulation decreases [HbO] while subthreshold stimulation does not effect a measurable response. This effect has been previously attributed to either differences in physiology in between M1 and the DLPFC in response to stimulation (Bestmann et al., 2008), greater scalp-cortex distances, or increased sensitivity of M1 (Thomson et al., 2011b). While this dichotomy is intriguing, it should be taken with a grain of salt. Notably, due to the primarily exploratory nature of these studies, many typical stimulation conditions have not been evaluated in a balanced manner.

There is a need for improved experimental control and repeatability in these studies with distinct lack of replication by independent research groups. Fortunately, both rTMS and fNIRS have substantially changed and improved over the past decade, with refinements in hardware, signal processing, sensors, and neuronavigated targeting, allowing researchers and clinicians more fine grain control over their stimulation systems. It is especially important that these new tools are used to translate discoveries from the behavior of cortical excitability changes to improvements in actual clinical applications as rTMS response rates, while significant, average 30–40%. Future TMS-fNIRS studies should consider focusing on the relationship between cortical activities in the motor cortex and the DLPFC.

Effects of rTMS on Task: Clinical and Non-clinical Applications

As cognitive and clinical neuroscientists seek to employ brain stimulation as a research tool and therapeutic approach, a substantial need for objective and quantifiable measures of stimulation effects presents itself. Several studies have used fNIRS to monitor or describe changes in task activity following rTMS. In clinical and non-clinical studies, rTMS has been successfully used to enhance or suppress cortical involvement with the aim of altering behavioral performance and clinical outcomes. Recently promising studies have provided preliminary evidence that rTMS may guide a cortical reorganization of functional activity following disorders such as stroke. Here, fNIRS offers a technique to monitor the efficacy of rTMS therapy, but also potentially identify treatment targets and stimulation parameters. Unfortunately, the limited number of clinical studies currently available prevent clear interpretation on the measured effects of rTMS paradigms as well as the clinical implications of such effects due in part to lack of replicated works, as well as incomplete reporting of affected fNIRS biomarkers. Despite this, future works may build upon these studies to provide explicit treatment recommendations informed by neuroimaging.

fNIRS and Cortical Excitability

The study of fNIRS functional measures and TMS-evoked MEPs represent a different, but important role for hybrid TMS-fNIRS with particular utility in functional mapping and the role of central fatigue in exercise physiology. Although this topic represents a smaller portion of the research covered here, since the effects of rTMS are often assessed with respect to changes in RMT, the influence of rTMS on fNIRS measures may require a deeper understanding of the relationship between cortical excitability and neurovascular coupling. Primarily these works identify a broader fNIRS response to voluntary motor activities as compared to regional mapping with TMS. These differences may represent functional differences related to motor control, planning, and other component processes during task execution. While it is expected generally that the ability of TMS to excite specific motor pathways might be more localized than activity related to voluntary motor movements, observations reviewed here show some similar functional trends between MEP measures and fNIRS measures during task execution. These may suggest some common roles between the two measures which may merit further investigation.

CONCLUSION

TMS-fNIRS as a multimodal strategy for imaging and cortical interrogation compliments the perspectives offered by TMS in combination with fMRI and EEG for the study of cortical changes in excitability, inhibition, and connectivity. This multimodal approach may even be expanded such that TMS-fNIRS may be deployed alongside EEG or fMRI, or with additional stimulation approaches such as TES for more complex, but complete, assessment and treatment. While scientific works add to a growing body of knowledge, in parallel, technological

challenges may be remediated through improved sensor design, optode montages, signal processing, and coil design, altogether enhancing the power and utility of the technique. As works here have presented, fNIRS as a methodology is well-equipped to monitor both transient and prolonged effects of TMS, but as of yet, the available research is limited in its replication and scope. This need for further work should not be used to dismiss the opportunity and unique information which may yet be afforded by TMS-fNIRS for scientific investigation, adaptive therapy, as well as prognostic and diagnostic applications.

AUTHOR CONTRIBUTIONS

HA, ST, and JS designed the structure and scope of the review. AC aggregated reviewed articles and prepared the draft manuscript. All authors reviewed and revised the manuscript.

FUNDING

This study was funded in part by National Key R&D Program of China (No. 2017YFC0909201), Med-X Research Fund of Shanghai Jiao Tong University (No. YG2015ZD12, YG2016MS36), the Program of Shanghai Academic/Technology Research Leader (16XD1402400), and NSFC (No.61571295).

SUPPLEMENTARY MATERIAL

The Supplementary Material for this article can be found online at: https://www.frontiersin.org/articles/10.3389/fnins.2019.00084/full#supplementary-material

Supplementary Table 1 | Detailed list of stimulation parameters and qualitative results for all studies investigating stimulation at rest.

Supplementary Table 2 | Detailed list of stimulation parameters and qualitative results for all studies investigating the effects of stimulation on task.

REFERENCES

Akiyama, T., Ohira, T., Kawase, T., and Kato, T. (2006). TMS orientation for NIRS-functional motor mapping. *Brain Topogr.* 19, 1–9. doi: 10.1007/s10548-006-0007-9.

Allen, E., a, Pasley, B. N., Duong, T., and Freeman, R. D. (2007). Transcranial magnetic stimulation elicits coupled neural and hemodynamic consequences. *Science* 317, 1918–1921. doi: 10.1126/science.1146426.

Aoyama, Y., Hanaoka, N., Kameyama, M., Suda, M., Sato, T., Song, M., et al. (2009). Stimulus intensity dependence of cerebral blood volume changes in left frontal lobe by low-frequency rTMS to right frontal lobe: a near-infrared spectroscopy study. *Neurosci. Res.* 63, 47–51. doi: 10.1016/j.neures.2008.10.003

Arthurs, O. J., and Boniface, S. (2002). How well do we understand the neural origins of the fMRI BOLD signal? *Trends Neurosci.* 25, 27–31. doi: 10.1016/S0166-2236(00)01995-0

Barker, A. T., Jalinous, R., and Freeston, I. L. (1985). Non-invasive magnetic stimulation of human motor cortex. *Lancet* 1, 1106–1107. doi: 10.1016/S0140-6736(85)92413-4

Bestmann, S., Ruff, C. C., Blankenburg, F., Weiskopf, N., Driver, J., and Rothwell, J. C. (2008). Mapping causal interregional influences with concurrent TMS-fMRI. *Exp. Brain Res.* 191, 383–402. doi: 10.1007/s00221-008-1601-8

Bortoletto, M., Veniero, D., Thut, G., and Miniussi, C. (2015). The contribution of TMS–EEG coregistration in the exploration of the human cortical connectome. *Neurosci. Biobehav. Rev.* 49, 114–124. doi: 10.1016/j.neubiorev.2014.12.014

Brüne, M., Juckel, G., and Enzi, B. (2013). An eye for an eye? Neural correlates of retribution and forgiveness. *PLoS ONE* 8, 1–11. doi: 10.1371/journal.pone.0073519

Cao, T. T., Thomson, R. H., Bailey, N. W., Rogasch, N. C., Segrave, R. A., Maller, J. J., et al. (2013). A near infra-red study of blood oxygenation changes resulting from high and low frequency repetitive transcranial magnetic stimulation. *Brain Stimul.* 6, 922–924. doi: 10.1016/j.brs.2013.04.006

Chiang, T. C., Vaithianathan, T., Leung, T., Lavidor, M., Walsh, V., and Delpy, D. T. (2007). Elevated haemoglobin levels in the motor cortex following 1 Hz transcranial magnetic stimulation: a preliminary study. *Exp. Brain Res.* 181, 555–560. doi: 10.1007/s00221-007-0952-x

Cole, J., Bernacki, C. G., Helmer, A., Pinninti, N., and O'Reardon, J. (2015). Efficacy of Transcranial Magnetic Stimulation (TMS) in the Treatment of Schizophrenia : a Review. *Innov. Clin. Neurosci.* 12, 12–19.

Corp, D. T., Youssef, G. J., Clark, R. A., Gomes-Osman, J., Yücel, M. A., Oldham, S. J., et al. (2018). Reduced motor cortex inhibition and a 'cognitive-first' prioritisation strategy for older adults during dual-tasking. *Exp. Gerontol.* 113, 95–105. doi: 10.1016/j.exger.2018.09.018

Cui, X., Bray, S., and Reiss, A. L. (2010). Functional near infrared spectroscopy (NIRS) signal improvement based on negative correlation between oxygenated and deoxygenated hemoglobin dynamics. *Neuroimage* 49, 3039–3046. doi: 10.1016/j.neuroimage.2009.11.050

Curtin, A., Sun, J., Ayaz, H., Qian, Z., Onaral, B., Wang, J., et al. (2017). Evaluation of evoked responses to pulse-matched high frequency and intermittent theta burst transcranial magnetic stimulation using simultaneous functional near-infrared spectroscopy. *Neurophotonics* 4:041405. doi: 10.1117/1.NPh.4.4.041405

de Jesus, D. R., Favalli, G. P. S., Hoppenbrouwers, S. S., Barr, M. S., Chen, R., Fitzgerald, P. B., et al. (2014). Determining optimal rTMS parameters through changes in cortical inhibition. *Clin. Neurophysiol.* 125, 755–762. doi: 10.1016/j.clinph.2013.09.011

Deppermann, S., Notzon, S., Kroczek, A., Rosenbaum, D., Haeussinger, F. B., Diemer, J., et al. (2016). Functional co-activation within the prefrontal cortex supports the maintenance of behavioural performance in fear-relevant situations before an iTBS modulated virtual reality challenge in participants with spider phobia. *Behav. Brain Res.* 307, 208–217. doi: 10.1016/j.bbr.2016.03.028

Deppermann, S., Vennewald, N., Diemer, J., Sickinger, S., Haeussinger, F. B., Dresler, T., et al. (2017). Neurobiological and clinical effects of fNIRS-controlled rTMS in patients with panic disorder/agoraphobia during cognitive-behavioural therapy. *NeuroImage Clin.* 16, 668–677. doi: 10.1016/j.nicl.2017.09.013

Deppermann, S., Vennewald, N., Diemer, J., Sickinger, S., Haeussinger, F. B., Notzon, S., et al. (2014). Does rTMS alter neurocognitive functioning in patients with panic disorder/agoraphobia? An fNIRS-based investigation of prefrontal activation during a cognitive task and its modulation via sham-controlled rTMS. *Biomed Res. Int.* 2014:542526. doi: 10.1155/2014/542526

Derosière, G., Billot, M., Ward, E. T., and Perrey, S. (2015). Adaptations of motor neural structures' activity to lapses in attention. *Cereb. Cortex* 25, 66–74. doi: 10.1093/cercor/bht206

Dresler, T., Ehlis, A. C., Plichta, M. M., Richter, M. M., Jabs, B., Lesch, K. P., et al. (2009). Panic disorder and a possible treatment approach by means of high-frequency rTMS: a case report. *World J. Biol. Psychiatry* 10, 991–997. doi: 10.1080/15622970902898147

Eldaief, M. C., Press, D. Z., and Pascual-Leone, A. (2013). Transcranial magnetic stimulation in neurology A review of established and prospective applications. *Neurol. Clin. Pract.* 3, 519–526. doi: 10.1212/01.CPJ.0000436213.11132.8e

Eschweiler, G. W., Wegerer, C., Schlotter, W., Spandl, C., Stevens, a, Bartels, M., et al. (2000). Left prefrontal activation predicts therapeutic effects of repetitive transcranial magnetic stimulation (rTMS) in major depression. *Psychiatry Res.* 99, 161–172. doi: 10.1016/S0925-4927(00)00062-7

Fitzgerald, P. B., Fountain, S., and Daskalakis, Z. J. (2006). A comprehensive review of the effects of rTMS on motor cortical excitability and inhibition. *Clin. Neurophysiol.* 117, 2584–2596. doi: 10.1016/j.clinph.2006.06.712

Furubayashi, T., Mochizuki, H., Terao, Y., Arai, N., Hanajima, R., Hamada, M., et al. (2013). Cortical hemoglobin concentration changes underneath the coil after single-pulse transcranial magnetic stimulation:

a near-infrared spectroscopy study. *J. Neurophysiol.* 109, 1626–1637. doi: 10.1152/jn.00980.2011

Fuster, J., Guiou, M., Ardestani, A., Cannestra, A., Sheth, S., Zhou, Y., et al. (2005). Near-infrared spectroscopy (NIRS) in cognitive neuroscience of the primate brain. *Neuroimage* 26, 215–220. doi: 10.1016/j.neuroimage.2005.01.055

Gagnon, L., Perdue, K., Greve, D. N., Goldenholz, D., Kaskhedikar, G., and Boas, D. (2011). Improved recovery of the hemodynamic response in diffuse optical imaging using short optode separations and state-space modeling. *Neuroimage* 56, 1362–1371. doi: 10.1016/j.neuroimage.2011.03.001

Gateau, T., Ayaz, H., and Dehais, F. (2018). *In silico* vs. Over the Clouds: On-the-Fly Mental State Estimation of Aircraft Pilots, Using a Functional Near Infrared Spectroscopy Based Passive-BCI. *Front. Hum. Neurosci.* 12:187. doi: 10.3389/fnhum.2018.00187

George, M. S., Taylor, J. J., and Short, E. B. (2013). The expanding evidence base for rTMS treatment of depression. *Curr. Opin. Psychiatry* 26, 13–18. doi: 10.1097/YCO.0b013e32835ab46d

Goodall, S., González-Alonso, J., Ali, L., Ross, E. Z., and Romer, L. M. (2012). Supraspinal fatigue after normoxic and hypoxic exercise in humans. *J. Physiol.* 590, 2767–2782. doi: 10.1113/jphysiol.2012.228890

Goodall, S., Twomey, R., Amann, M., Ross, E. Z., Lovering, A. T., Romer, L. M., et al. (2014). AltitudeOmics: exercise-induced supraspinal fatigue is attenuated in healthy humans after acclimatization to high altitude. *Acta Physiol.* 210, 875–888. doi: 10.1111/apha.12241

Groiss, S. J., Mochizuki, H., Furubayashi, T., Kobayashi, S., Nakatani-Enomoto, S., Nakamura, K., et al. (2013). Quadri-pulse stimulation induces stimulation frequency dependent cortical hemoglobin concentration changes within the ipsilateral motor cortical network. *Brain Stimul.* 6, 40–48. doi: 10.1016/j.brs.2011.12.004

Guhn, A., Dresler, T., Andreatta, M., Müller, L. D., Hahn, T., Tupak, S. V., et al. (2014). Medial prefrontal cortex stimulation modulates the processing of conditioned fear. *Front. Behav. Neurosci.* 8:44. doi: 10.3389/fnbeh.2014.00044

Hada, Y., Abo, M., Kaminaga, T., and Mikami, M. (2006). Detection of cerebral blood flow changes during repetitive transcranial magnetic stimulation by recording hemoglobin in the brain cortex, just beneath the stimulation coil, with near-infrared spectroscopy. *Neuroimage* 32, 1226–1230. doi: 10.1016/j.neuroimage.2006.04.200

Hallett, M., Di Iorio, R., Rossini, P. M., Park, J. E., Chen, R., Celnik, P., et al. (2017). Contribution of transcranial magnetic stimulation to assessment of brain connectivity and networks. *Clin. Neurophysiol.* 128, 2125–2139. doi: 10.1016/j.clinph.2017.08.007

Hamada, M., and Ugawa, Y. (2010). Quadripulse stimulation–a new patterned rTMS. *Restor. Neurol. Neurosci.* 28, 419–424. doi: 10.3233/RNN-2010-0564

Hanaoka, N., Aoyama, Y., Kameyama, M., Fukuda, M., and Mikuni, M. (2007). Deactivation and activation of left frontal lobe during and after low-frequency repetitive transcranial magnetic stimulation over right prefrontal cortex: a near-infrared spectroscopy study. *Neurosci. Lett.* 414, 99–104. doi: 10.1016/j.neulet.2006.10.002

Hara, T., Abo, M., Kakita, K., Mori, Y., Yoshida, M., and Sasaki, N. (2017). The effect of selective transcranial magnetic stimulation with functional near-infrared spectroscopy and intensive speech therapy on individuals with post-stroke aphasia. *Eur. Neurol.* 77, 186–194. doi: 10.1159/000457901

Heeger, D. J., and Ress, D. (2002). What does fMRI tell us about neuronal activity? *Nat. Rev. Neurosci.* 3, 142–151. doi: 10.1038/nrn730

Hirose, M., Mochizuki, H., Groiss, S. J., Tanji, Y., Nakamura, K., Nakatani-Enomoto, S., et al. (2011). On-line effects of quadripulse transcranial magnetic stimulation (QPS) on the contralateral hemisphere studied with somatosensory evoked potentials and near infrared spectroscopy. *Exp. Brain Res.* 214, 577–586. doi: 10.1007/s00221-011-2855-0

Huang, Y. Z., Edwards, M. J., Rounis, E., Bhatia, K. P., and Rothwell, J. C. (2005). Theta burst stimulation of the human motor cortex. *Neuron* 45, 201–206. doi: 10.1016/j.neuron.2004.12.033

Jubeau, M., Rupp, T., Temesi, J., Perrey, S., Wuyam, B., Millet, G. Y., et al. (2017). Neuromuscular fatigue during prolonged exercise in hypoxia. *Med. Sci. Sports Exerc.* 49, 430–439. doi: 10.1249/MSS.0000000000001118

Kimiskidis, V. K. (2016). Transcranial magnetic stimulation (TMS) coupled with electroencephalography (EEG): Biomarker of the future. *Rev. Neurol.* 172, 123–126. doi: 10.1016/j.neurol.2015.11.004

Koenraadt, K. L. M., Munneke, M. A, Duysens, J., and Keijsers, N. L. W. (2011). TMS: a navigator for NIRS of the primary motor cortex? *J. Neurosci. Methods* 201, 142–148. doi: 10.1016/j.jneumeth.2011.07.024

Kozel, F. A., Tian, F., Dhamne, S., Croarkin, P. E., McClintock, S. M., Elliott, A., et al. (2009). Using simultaneous repetitive Transcranial Magnetic Stimulation/functional Near Infrared Spectroscopy (rTMS/fNIRS) to measure brain activation and connectivity. *Neuroimage* 47, 1177–1184. doi: 10.1016/j.neuroimage.2009.05.016

Langhorne, P., Bernhardt, J., and Kwakkel, G. (2011). Stroke rehabilitation. *Lancet* 377, 1693–1702. doi: 10.1016/S0140-6736(11)60325-5

Laurent, J., Guinot, M., Le Roux Mallouf, T., Marillier, M., Larribaut, J., and Verges, S. (2018). Effects of acute salbutamol intake on peripheral and central fatigue in trained men. *Med. Sci. Sport. Exerc.* 50, 1267–1276. doi: 10.1249/MSS.0000000000001565

Lefaucheur, J.-P., André-Obadia, N., Antal, A., Ayache, S. S., Baeken, C., Benninger, D. H., et al. (2014). Evidence-based guidelines on the therapeutic use of repetitive transcranial magnetic stimulation (rTMS). *Clin. Neurophysiol.* 125, 1–57. doi: 10.1016/j.clinph.2014.05.021

Liberati, A., Altman, D. G., Tetzlaff, J., Mulrow, C., Gøtzsche, P. C., Ioannidis, J. P. A., et al. (2009). The PRISMA statement for reporting systematic reviews and meta-analyses of studies that evaluate health care interventions: explanation and elaboration. *PLoS Med.* 6:1000100. doi: 10.1371/journal.pmed.1000100

Lo, Y. L., Zhang, H. H., Wang, C. C., Chin, Z. Y., Fook-Chong, S., Gabriel, C., et al. (2009). Correlation of near-infrared spectroscopy and transcranial magnetic stimulation of the motor cortex in overt reading and musical tasks. *Motor Control.* 13, 84–99. doi: 10.1123/mcj.13.1.84

Maier, M. J., Rosenbaum, D., Haeussinger, F. B., Brüne, M., Enzi, B., Plewnia, C., et al. (2018). Forgiveness and cognitive control–Provoking revenge via theta-burst-stimulation of the DLPFC. *Neuroimage* 183, 769–775. doi: 10.1016/j.neuroimage.2018.08.065

Marillier, M., Arnal, P. J., Le Roux Mallouf, T., Rupp, T., Millet, G. Y., and Verges, S. (2017). Effects of high-altitude exposure on supraspinal fatigue and corticospinal excitability and inhibition. *Eur. J. Appl. Physiol.* 117, 1747–1761. doi: 10.1007/s00421-017-3669-y

McKendrick, R., Parasuraman, R., and Ayaz, H. (2015). Wearable functional near infrared spectroscopy (fNIRS) and transcranial direct current stimulation (tDCS): expanding vistas for neurocognitive augmentation. *Front. Syst. Neurosci.* 9, 1–14. doi: 10.3389/fnsys.2015.00027

McKendrick, R., Parasuraman, R., Murtza, R., Formwalt, A., Baccus, W., Paczynski, M., et al. (2016). Into the Wild: neuroergonomic differentiation of hand-held and augmented reality wearable displays during outdoor navigation with functional near infrared spectroscopy. *Front. Hum. Neurosci.* 10:216. doi: 10.3389/fnhum.2016.00216.

Mesquita, R. C., Faseyitan, O. K., Turkeltaub, P. E., Buckley, E. M., Thomas, A., Kim, M. N., et al. (2013). Blood flow and oxygenation changes due to low-frequency repetitive transcranial magnetic stimulation of the cerebral cortex. *J. Biomed. Opt.* 18:067006. doi: 10.1117/1.JBO.18.6.067006

Millet, G. Y., Muthalib, M., Jubeau, M., Laursen, P. B., and Nosaka, K. (2012). Severe hypoxia affects exercise performance independently of afferent feedback and peripheral fatigue. *J. Appl. Physiol.* 112, 1335–1344. doi: 10.1152/japplphysiol.00804.2011

Mochizuki, H., Furubayashi, T., Hanajima, R., Terao, Y., Mizuno, Y., Okabe, S., et al. (2007). Hemoglobin concentration changes in the contralateral hemisphere during and after theta burst stimulation of the human sensorimotor cortices. *Exp. Brain Res.* 180, 667–675. doi: 10.1007/s00221-007-0884-5

Mochizuki, H., Ugawa, Y., Terao, Y., and Sakai, K. L. (2006). Cortical hemoglobin-concentration changes under the coil induced by single-pulse TMS in humans: a simultaneous recording with near-infrared spectroscopy. *Exp. brain Res.* 169, 302–310. doi: 10.1007/s00221-005-0149-0

Näsi, T., Mäki, H., Kotilahti, K., Nissil,ä, I., Haapalahti, P., and Ilmoniemi, R. J. (2011). Magnetic-stimulation-related physiological artifacts in hemodynamic near-infrared spectroscopy signals. *PLoS ONE* 6:0024002. doi: 10.1371/journal.pone.0024002

Nissilä, I., Kotilahti, K., Komssi, S., Kähkönen, S., Noponen, T., and Ilmoniemi, R. J. (2002). "Optical measurement of hemodynamic changes in the contralateral motor cortex induced by transcranial magnetic stimulation," in *Proceedings of the 13th International Conference on Biomagnetism (BIOMAG 2002),* Jena, Germany: VDE Verlag, 851–854.

Noguchi, Y., Watanabe, E., and Sakai, K. L. (2003). An event-related optical topography study of cortical activation induced by single-pulse transcranial magnetic stimulation. *Neuroimage* 19, 156–162. doi: 10.1016/S1053-8119(03)00054-5

Notzon, S., Deppermann, S., Fallgatter, A., Diemer, J., Kroczek, A., Domschke, K., et al. (2015). Psychophysiological effects of an iTBS modulated virtual reality challenge including participants with spider phobia. *Biol. Psychol.* 112, 66–76. doi: 10.1016/j.biopsycho.2015.10.003

Okada, E., and Delpy, D. T. (2003). Near-infrared light propagation in an adult head model. II. Effect of superficial tissue thickness on the sensitivity of the near-infrared spectroscopy signal. *Appl. Opt.* 42, 2915–22. doi: 10.1364/AO.42.002915

Oliviero, A., Di Lazzaro, V., Piazza, O., Profice, P., Pennisi, M. A., Delia Corte, F., et al. (1999). Cerebral blood flow and metabolic changes produced by repetitive magnetic brain stimulation. *J. Neurol.* 246, 1164–1168. doi: 10.1007/s004150050536

Park, E., Kang, M. J., Lee, A., Chang, W. H., Shin, Y.-I., and Kim, Y.-H. (2017). Real-time measurement of cerebral blood flow during and after repetitive transcranial magnetic stimulation: a near-infrared spectroscopy study. *Neurosci. Lett.* 653, 78–83. doi: 10.1016/j.neulet.2017.05.039

Park, S.-W., Butler, A. J., Cavalheiro, V., Alberts, J. L., and Wolf, S. L. (2004). Changes in Serial Optical Topography and TMS during Task Performance after Constraint-Induced Movement Therapy in Stroke: a Case Study. *Neurorehabil. Neural. Repair*. 18, 95–105. doi: 10.1177/0888439004265113

Parks, N. A. (2013). Concurrent application of TMS and near-infrared optical imaging: methodological considerations and potential artifacts. *Front. Hum. Neurosci.* 7:592. doi: 10.3389/fnhum.2013.00592

Pashut, T., Wolfus, S., Friedman, A., Lavidor, M., Bar-Gad, I., Yeshurun, Y., et al. (2011). Mechanisms of magnetic stimulation of central nervous system neurons. *PLoS Comput. Biol.* 7:1002022. doi: 10.1371/journal.pcbi.1002022

Pell, G. S., Roth, Y., and Zangen, A. (2011). Modulation of cortical excitability induced by repetitive transcranial magnetic stimulation: influence of timing and geometrical parameters and underlying mechanisms. *Prog. Neurobiol.* 93, 59–98. doi: 10.1016/j.pneurobio.2010.10.003

Reithler, J., Peters, J. C., and Sack, A. T. (2011). Multimodal transcranial magnetic stimulation: using concurrent neuroimaging to reveal the neural network dynamics of noninvasive brain stimulation. *Prog. Neurobiol.* 94, 149–165. doi: 10.1016/j.pneurobio.2011.04.004

Rupp, T., Le Roux Mallouf, T., Perrey, S., Wuyam, B., Millet, G. Y., and Verges, S. (2015). CO2 Clamping, peripheral and central fatigue during hypoxic knee extensions in men. *Med. Sci. Sports Exerc.* 47, 2513–2524. doi: 10.1249/MSS.0000000000000724

Schecklmann, M., Giani, A., Tupak, S., Langguth, B., Raab, V., Polak, T., et al. (2014). Functional near-infrared spectroscopy to probe state- and trait-like conditions in chronic tinnitus: a proof-of-principle study. *Neural Plast.* 2014, 1–8. doi: 10.1155/2014/894203

Schecklmann, M., Giani, A., Tupak, S., Langguth, B., Raab, V., Polak, T., et al. (2016). Neuronavigated left temporal continuous theta burst stimulation in chronic tinnitus. *Restor. Neurol. Neurosci.* 34, 165–175. doi: 10.3233/RNN-150518

Shinba, T., Kariya, N., Matsuda, S., Matsuda, H., and Obara, Y. (2018). Increase of frontal cerebral blood volume during transcranial magnetic stimulation in depression is related to treatment effectiveness: a pilot study with near-infrared spectroscopy. *Psychiatry Clin. Neurosci.* 72, 602–610. doi: 10.1111/pcn.12680

Solianik, R., Satas, A., Mickeviciene, D., Cekanauskaite, A., Valanciene, D., Majauskiene, D., et al. (2018). Task-relevant cognitive and motor functions are prioritized during prolonged speed–accuracy motor task performance. *Exp. Brain Res.* 236, 1–14. doi: 10.1007/s00221-018-5251-1

Sutoh, C., Koga, Y., Kimura, H., Kanahara, N., Numata, N., Hirano, Y., et al. (2016). Repetitive transcranial magnetic stimulation changes cerebral oxygenation on the left dorsolateral prefrontal cortex in bulimia nervosa: a near-infrared spectroscopy pilot study. *Eur. Eat. Disord. Rev.* 24, 83–88. doi: 10.1002/erv.2413

Tamashiro, H., Kinoshita, S., Okamoto, T., Urushidani, N., and Abo, M. (2018). Effect of baseline brain activity on response to low-frequency rTMS/intensive occupational therapy in poststroke patients with upper limb hemiparesis: a near-infrared spectroscopy study. *Int. J. Neurosci.* 26, 1–7. doi: 10.1080/00207454.2018.1536053

Terao, Y., Ugawa, Y., Sakai, K., Miyauchi, S., Fukuda, H., Sasaki, Y., et al. (1998). Localizing the site of magnetic brain stimulation by functional MRI. *Exp. brain Res.* 121, 145–52.

Thomson, R. H., Cleve, T. J., Bailey, N. W., Rogasch, N. C., Maller, J. J., Daskalakis, Z. J., et al. (2013). Blood oxygenation changes modulated by coil orientation during prefrontal transcranial magnetic stimulation. *Brain Stimul.* 6, 576–581. doi: 10.1016/j.brs.2012.12.001

Thomson, R. H., Daskalakis, Z. J., and Fitzgerald, P. B. (2011a). A near infra-red spectroscopy study of the effects of pre-frontal single and paired pulse transcranial magnetic stimulation. *Clin. Neurophysiol.* 122, 378–382. doi: 10.1016/j.clinph.2010.08.003

Thomson, R. H., Maller, J. J., Daskalakis, Z. J., and Fitzgerald, P. B. (2011b). Blood oxygenation changes resulting from suprathreshold transcranial magnetic stimulation. *Brain Stimul.* 4, 165–168. doi: 10.1016/j.brs.2010.10.003

Thomson, R. H., Maller, J. J., Daskalakis, Z. J., and Fitzgerald, P. B. (2012a). Blood oxygenation changes resulting from trains of low frequency transcranial magnetic stimulation. *Cortex* 48, 487–491. doi: 10.1016/j.cortex.2011.04.028

Thomson, R. H., Rogasch, N. C., Maller, J. J., Daskalakis, Z. J., and Fitzgerald, P. B. (2012b). Intensity dependent repetitive transcranial magnetic stimulation modulation of blood oxygenation. *J. Affect. Disord.* 136, 1243–1246. doi: 10.1016/j.jad.2011.08.005

Tian, F., Kozel, F. A., Yennu, A., Croarkin, P. E., McClintock, S. M., Mapes, K. S., et al. (2012). Test-retest assessment of cortical activation induced by repetitive transcranial magnetic stimulation with brain atlas-guided optical topography. *J. Biomed. Opt.* 17:116020. doi: 10.1117/1.JBO.17.11.116020

Tupak, S. V., Dresler, T., Badewien, M., Hahn, T., Ernst, L. H., Herrmann, M. J., et al. (2013). Inhibitory transcranial magnetic theta burst stimulation attenuates prefrontal cortex oxygenation. *Hum. Brain Mapp.* 34, 150–157. doi: 10.1002/hbm.21421

Urushidani, N., Kinoshita, S., Okamoto, T., Tamashiro, H., and Abo, M. (2018). Low-frequency rTMS and intensive occupational therapy improve upper limb motor function and cortical reorganization assessed by functional near-infrared spectroscopy in a subacute stroke patient. *Case Rep. Neurol.* 5143, 223–231. doi: 10.1159/000492381

Valero-Cabré, A., Amengual, J., Stengel, C., Pascual-Leone, A., and Coubard, O. A. (2017). Transcranial Magnetic Stimulation in basic and clinical neuroscience: a comprehensive review of fundamental principles and novel insights. *Neurosci. Biobehav. Rev.* 83, 381–404. doi: 10.1016/j.neubiorev.2017.10.006

Vernieri, F., Altamura, C., Palazzo, P., Altavilla, R., Fabrizio, E., Fini, R., et al. (2014). 1-Hz repetitive transcranial magnetic stimulation increases cerebral vasomotor reactivity: a possible autonomic nervous system modulation. *Brain Stimul.* 7, 281–286. doi: 10.1016/j.brs.2013.12.014

Villringer, A., Planck, J., Hock, C., Schleinkofer, L., and Dirnagl, U. (1993). Near infrared spectroscopy (NIRS): a new tool to study hemodynamic changes during activation of brain function in human adults. *Neurosci. Lett.* 154, 101–104.

Yamanaka, K., Tomioka, H., Kawasaki, S., Noda, Y., Yamagata, B., Iwanami, A., et al. (2014). Effect of parietal transcranial magnetic stimulation on spatial working memory in healthy elderly persons - Comparison of near infrared spectroscopy for young and elderly. *PLoS ONE* 9:e102306. doi: 10.1371/journal.pone.0102306

Yamanaka, K., Yamagata, B., Tomioka, H., Kawasaki, S., and Mimura, M. (2010). Transcranial magnetic stimulation of the parietal cortex facilitates spatial working memory: near-infrared spectroscopy study. *Cereb. Cortex* 20, 1037–1045. doi: 10.1093/cercor/bhp163

Conflict of Interest Statement: The authors declare that the research was conducted in the absence of any commercial or financial relationships that could be construed as a potential conflict of interest.

frontiers in Neuroscience

REVIEW
published: 18 March 2019
doi: 10.3389/fnins.2019.00223

Electromagnetic Brain Stimulation in Patients With Disorders of Consciousness

Pierre Bourdillon[1,2,3,4,5†], *Bertrand Hermann*[2,3,4,5,6†], *Jacobo D. Sitt*[3,4,5] *and Lionel Naccache*[2,3,4,5,7*]

[1] Department of Neurosurgery, Adolphe de Rothschild Foundation, Paris, France, [2] Sorbonne Université, Faculté de Médecine Pitié-Salpêtrière, Paris, France, [3] Institut du Cerveau et de la Moelle Épinière, ICM, PICNIC Lab, Paris, France, [4] Inserm U 1127, Paris, France, [5] CNRS, UMR 7225, Paris, France, [6] Department of Neurology, Neuro ICU, Groupe Hospitalier Pitié-Salpêtrière, AP-HP, Paris, France, [7] Department of Neurophysiology, Groupe Hospitalier Pitié-Salpêtrière, AP-HP, Paris, France

Severe brain injury is a common cause of coma. In some cases, despite vigilance improvement, disorders of consciousness (DoC) persist. Several states of impaired consciousness have been defined, according to whether the patient exhibits only reflexive behaviors as in the vegetative state/unresponsive wakefulness syndrome (VS/UWS) or purposeful behaviors distinct from reflexes as in the minimally conscious state (MCS). Recently, this clinical distinction has been enriched by electrophysiological and neuroimaging data resulting from a better understanding of the physiopathology of DoC. However, therapeutic options, especially pharmacological ones, remain very limited. In this context, electroceuticals, a new category of therapeutic agents which act by targeting the neural circuits with electromagnetic stimulations, started to develop in the field of DoC. We performed a systematic review of the studies evaluating therapeutics relying on the direct or indirect electro-magnetic stimulation of the brain in DoC patients. Current evidence seems to support the efficacy of deep brain stimulation (DBS) and non-invasive brain stimulation (NIBS) on consciousness in some of these patients. However, while the latter is non-invasive and well tolerated, the former is associated with potential major side effects. We propose that all chronic DoC patients should be given the possibility to benefit from NIBS, and that transcranial direct current stimulation (tDCS) should be preferred over repetitive transcranial magnetic stimulation (rTMS), based on the literature and its simple use. Surgical techniques less invasive than DBS, such as vagus nerve stimulation (VNS) might represent a good compromise between efficacy and invasiveness but still need to be further investigated.

Keywords: consciousness, disorders of consciousness, deep brain stimulation, vagus nerve stimulation, transcranial magnetic stimulation, transcranial electric stimulation, transcranial direct current stimulation, transcranial alternative current stimulation

OPEN ACCESS

Edited by:
Olivier David,
Institut National de la Santé et de la Recherche Médicale (INSERM), France

Reviewed by:
Christoph Guger,
g.tec Medical Engineering GmbH, Austria
Cunyi Fan,
Shanghai Jiao Tong University, China

***Correspondence:**
Lionel Naccache
lionel.naccache@aphp.fr;
lionel.naccache@gmail.com

† These authors have contributed equally to this work

Specialty section:
This article was submitted to Neural Technology, a section of the journal Frontiers in Neuroscience

Received: *30 December 2018*
Accepted: *26 February 2019*
Published: *18 March 2019*

Citation:
Bourdillon P, Hermann B, Sitt JD and Naccache L (2019) Electromagnetic Brain Stimulation in Patients With Disorders of Consciousness. Front. Neurosci. 13:223. doi: 10.3389/fnins.2019.00223

INTRODUCTION

Loss of consciousness and arousal are frequent after severe brain injuries. Usually, patients recover from this transient state of coma to a normal state of consciousness even though they can suffer from various cognitive deficits. However, in some cases, despite vigilance improvement, disorders of consciousness (DoC) persist. Several states of impaired consciousness have thus been defined, according to whether the patient exhibits only reflexive behaviors as in the vegetative

state/unresponsive wakefulness syndrome (VS/UWS) or purposeful behaviors distinct from reflexes as in the minimally conscious state (MCS) (Giacino et al., 2002). This latter category has been recently refined to distinguish MCS 'minus' (MCS−) patients from MCS 'plus' patients (MCS+) according to the absence/presence of command following and/or intelligible verbalizations (Bruno et al., 2011). While this MCS label leaves open the issue of conscious state in these patients, it indicates with certitude that, unlike in VS/UWS, cortical networks contribute overtly to the behavior. In other terms, MCS can be reinterpreted as a cortically mediated state (CMS), more prone to evolve to recovery of consciousness than VS/UWS (Naccache, 2018). According to current classifications, a patient emerges from MCS (exit-MCS or EMCS) whenever he is able to communicate or make functional use of objects. Importantly, DoC must be differentiated from the locked-in syndrome (LIS) in which patients are conscious but lack the ability to communicate due to a disruption of motor tracts in the brainstem.

The current gold standard to diagnose these states of consciousness is the behavioral examination using a dedicated scale, the Coma Recovery Scale - revised (Kalmar and Giacino, 2005). However, recent studies have shown that a wilful modulation of brain activity could be detected in some clinically unresponsive patients (Owen et al., 2006; Edlow et al., 2017), a situation referred to as cognitive-motor dissociation (CMD). This new concept has brought the need of new classifications integrating active and passive brain-imaging to tract purposeful behaviors/consciousness (Engemann et al., 2018).

In parallel, several theories of consciousness have been developed. While some authors postulate than consciousness stem from a brain-scale cortico-cortical communication (global workspace theory; Dehaene et al., 2006; Dehaene and Changeux, 2011), others claim that consciousness arises from the coordinated activity within thalamo-cortical as well as non-thalamic ascending reticular activating system (ARAS) pathways (Edlow et al., 2012; Jang and Kwon, 2015; Jang et al., 2018), or from fronto-pallido-thalamo-cortical loops (meso-circuit hypothesis, Schiff, 2010). According to all of these theories, the common feature in DoC pathophysiology would be the disruption of a complex and organized high-order activity among large-scale neural networks.

In spite of these progresses in our understanding of DoC pathophysiology, efficient therapeutics is still lacking. Except for the moderate acceleration of recovery of traumatic brain injury (TBI) with amantadine (Giacino et al., 2012) and the rare and transient paradoxical effect of zolpidem (Whyte and Myers, 2009; Whyte et al., 2014), neuropharmacological therapies are disappointing and, most of the time, neuro-rehabilitation, despite a limited impact (Giacino et al., 2013), is the only treatment. Within this context, 'electroceuticals,' relying on the direct or indirect electro-magnetic stimulation of the brain, may be promising tools to restore consciousness in DoC patients (**Figure 1**). We conducted a narrative review of the use of these techniques in DoC patients by conducting a Pubmed/MEDLINE literature search up to December 2018 with the terms: 'disorders of consciousness,' 'consciousness' AND 'non-invasive brain stimulation stimulation,' 'transcranial electrical stimulation,' 'transcranial direct current stimulation,' 'transcranial alternative current stimulation,' 'transcranial random noise stimulation,' 'transcranial magnetic stimulation,' 'invasive brain stimulation,' 'deep brain stimulation.' We selected original papers with patients data based on their importance in the field.

INVASIVE ELECTRIC STIMULATION

Deep Brain Stimulation

Stereotactic surgical methodology was first described in the late 19th century (Apra et al., 2016), but applications in neurological diseases on the basis of neurophysiological principles started only in the second half of the 20th century (Giller et al., 2017; Bourdillon et al., 2018). Performing a lesion on deep mesencephalic or diencephalic small structures with wide projections on large cortical areas was exciting perspectives in psychiatric and neurological fields and drastically reduced the morbidity of the surgical procedures (Miocinovic et al., 2013; Bourdillon et al., 2017). These lesional procedures were indicated in pathologies producing positive signs (like tremor or dystonia) but were useless in pathologies in which negative signs were preponderant, such as disorder of consciousness (DoC). In this context, electric stimulation in human patients by means of stereotactically placed intracranial deep electrodes was developed. DoC, which was then considered as a default of cortical activation consecutive to an interruption of the projections of the ARAS through the diencephalon to the cortex, was indeed one of the first pathologies in which deep brain stimulation (DBS) was used (McLardy et al., 1968; Hassler et al., 1969). Despite an exciting effect of these first reports of pallidal and thalamic stimulation on the arousal of vegetative patient, no other study was done until the DBS was democratized in the late 1980's by its use in Parkinson disease (Benabid et al., 1987).

Patients and Clinical Response

Since 1968, a systematic review of the literature (through Medline, Embase, and web of Science) found that ten studies reporting 78 unique DoC patients who underwent DBS have been published (**Table 1**) (McLardy et al., 1968; Tsubokawa et al., 1990; Cohadon and Richer, 1993; Schiff et al., 2007; Yamamoto et al., 2010; Wojtecki et al., 2014; Adams et al., 2016; Magrassi et al., 2016; Chudy et al., 2018; Lemaire et al., 2018).

A response was noticed in 30 of the 67 patients classified as VS/UWS and in 6 of the 11 MCS. The definition of "response" is highly variable throughout the studies as the outcome measures have dramatically evolved since the 1970's. Nevertheless, the clinical description provided in the oldest studies are all compatible with an improvement on the Coma Recovery Scale revised (CRS-R), the outcome measure systematically used nowadays.

Etiologies of DoC were traumatic brain injuries (27 patients), anoxic causes (12 patients) and vascular causes (13 patients) but were not reported in the largest series (Cohadon and Richer, 1993). Throughout the literature, it is unclear whether etiology is an outcome predictive factor (Vanhoecke and Hariz,

TABLE 1 | Deep brain stimulation studies in DoC patients.

Study	Design/ Control	Population	Target/Stimulation parameters	Behavioral effects	Electrophysiological/ metabolic effects	Side effects
McLardy et al., 1968	Case report/ None	1 (considered as) VS/UWS	Left thalamus; midbrain (intralaminar nuclei/reticular formation) / 250Hz, 1ms	No modifications of consciousness, left hand spontaneous movement	No post procedure electrophysiological nor metabolic evaluation available	None
Hassler et al., 1969	Case report/ None	1 (considered as) VS/UWS	Left ventral anterior thalamus; right pallidum / Left, 25-30Hz, 20V, 1-3ms; Right 8Hz, 30V, 1-3ms	"Improvement" of consciousness, vocalizations, left limbs spontaneous movement	EEG recordings showed a disappearance of a unilateral delta focus which is replaced by an alpha activity	None
Tsubokawa et al., 1990	Open-label/ None	8 patients (VS/UWS)	Central thalamic nuclei; nucleus cuneiformis (reticular formation)/50 Hz, 0–10 V	4 recoveries (PCS 2–4 = > 8-9) 1 responder (PCS 2–4 = > 7) 3 failures (PCS 2–4 = > 3-5)	Increase of spectral power and desynchronization on EEG in the 4 patients who recovered/Increase on the brain perfusion on MRI in these patients	None
Cohadon and Richer, 1993	Open-label/ None	25 patients (VS/UWS)	Central nucleus of the thalamus/50 Hz, 5–10 V, 5 ms	1 moderate disabilities (GOS) 10 severe disabilities (GOS) 12 no effect *(2 patients died before the endpoint)*	No post procedure electrophysiological nor metabolic evaluation available	2 died (unrelated to surgical procedure)
Schiff et al., 2007	Case report, Cross-over RCT/ Sham	1 MCS	Anterior intralaminar thalamic nuclei / 100Hz, 4V	Fluctuant increase in CRS-R subscales, better feeding and motor behaviors, restoration of communication	No post procedure electrophysiological nor metabolic evaluation available	None
Yamamoto et al., 2010 *(includes publications since 2002)*	Open-label/ None	21 patients (VS/UWS)	Centro-median nucleus of the thalamus; midbrain (reticular formation) / 25Hz, various intensities	8 became MCS or EMCS 13 remain VS/ UWS	The 8 patients who recovered from VS showed desynchronization on continuous EEG frequency analysis/Increase on the brain perfusion on MRI in these patients	None
Wojtecki et al., 2014	Case report/ None	1 MCS	Internal medullary lamina; nuclei reticularis thalami/70–250 Hz, various intensities	No modifications of consciousness	Modulation of oscillatory activity in the beta and theta band within the central thalamus accompanied by an increase in thalamocortical coherence in the theta band	None
Magrassi et al., 2016	Open-label/ None	3 patients (1 MCS, 2 VS/UWS)	Anterior intralaminar nuclei; paralaminar Areas/80–110 Hz, various intensities	Increase of CRS-R in all of the 3 patients: 14 = > c15 8 = > 11 6 = > 9	Increase of theta and gamma power spectrum in EEG after 1 month of stimulation. No modifications of the evoked potentials.	1 postoperative intraparenchymal hematoma
Adams et al., 2016	Case report/ None	1 MCS	Anterior intralaminar thalamic nuclei/100 Hz, 4 V	Variable increase of CRS-R (11–14)	Long term re-emergence of sleep patterns	None
Chudy et al., 2018	Open-label/ None	14 patients (4 MCS, 10 VS/UWS)	Central thalamic nuclei / 25 Hz, 2.5–3.5 V, 90 μs	3 MCS became EMCS; 1 VS became MCS; 7 had no improvement of consciousness *(3 patients died before the endpoint)*	No post procedure electrophysiological nor metabolic evaluation available	3 died (unrelated to surgical procedure)
Lemaire et al., 2018	Cross-over RCT/ Sham	5 patients (4 MCS, 1 VS/UWS)	Dual pallido-thalamic / 30-Hz, 6V, 60μs	1 VS/UWS and 1 MCS had an significant improvement of the CRS-R.	The metabolism of the medial cortices increased specifically in the two responders	1 postoperative bronchopulmonary infection

CRS-R, Coma Recovery Scale – Revised; DoC, disorders of consciousness; EEG, electroencephalogram; EMCS, Emergence from Minimally Conscious State; GOS, Glasgow Outcome Scale; MCS, Minimally Conscious State; PCS, Prolonged Coma Scale; RCT, randomized controlled trial; VS/UWS, vegetative state/unresponsive wakefulness syndrome.

2017). Severe side effects may occurs during DBS. The safety is reported in **Table 1**.

It is worth mentioning that two studies, totalizing 5 patients, were not taken into account as the included patients did not fit with the present definition of DoC patients (Sturm et al., 1979; Hosobuchi and Yingling, 1993).

Targets and Parameters of Stimulation

Multiple targets have been tested including the reticular formation (McLardy et al., 1968; Tsubokawa et al., 1990; Yamamoto et al., 2010), the central nucleus of the thalamus (McLardy et al., 1968; Tsubokawa et al., 1990; Cohadon and Richer, 1993; Schiff et al., 2007; Yamamoto et al., 2010; Wojtecki et al., 2014; Adams et al., 2016; Chudy et al., 2018), the anterior intralaminar nuclei and paralaminar areas (Magrassi et al., 2016). In two studies, pallidal stimulation was associated to thalamic targets (Hassler et al., 1969; Lemaire et al., 2018). The multiplicity of targets in the limited number of both VS/UWS and MCS patients makes it impossible to identify the superiority of a procedure among the others. However, all these targets correspond anatomically to the projections of the ARAS through the thalamus to the cortex. Consequently, despite an apparent heterogenicity of the DBS targets, all the published studies report observations of the modulation of the same pathway making the interpretation of the overall results easier. Low-frequency stimulation (up to 50 Hz) was mostly used (Hassler et al., 1969; Tsubokawa et al., 1990; Cohadon and Richer, 1993; Yamamoto et al., 2010; Chudy et al., 2018), but some studies reported results using high frequency stimulations (up to 100 Hz) (Schiff et al., 2007; Wojtecki et al., 2014; Adams et al., 2016; Magrassi et al., 2016). The impact of the parameters of stimulation on the clinical response remains unclear (Kundu et al., 2018).

Limitations

One of the most important criticisms on the published studies is about the time frame. The Multi Society Task Force on persistent VS/UWS has published that spontaneous recovery from non-anoxic VS/UWS lasting longer than 1 month occurs in 30% of patients at 6 months and in 43% at 12 months (Multi-Society Task Force on PVS, 1994; Vanhoecke and Hariz, 2017). This observation is not limited to VS as 83% of the patients emerged from MCS after 6 months (Lammi et al., 2005). Yet, most studies report DBS performed within the year following the brain injury (Hassler et al., 1969; Tsubokawa et al., 1990; Cohadon and Richer, 1993; Yamamoto et al., 2010; Chudy et al., 2018) so that, in the 29 out of the 41 patients who improved after DBS, spontaneous recovery cannot be excluded.

Another limitation is the selection of the patients on clinical criteria. Very different lesions in the central nervous system can lead to the same clinical presentation. For instance, VS/UWS may result from diffuse cortical lesions as well as from a very focal lesion in the brainstem of the ARAS. In the first situation, DBS will modulate a damaged cortex with altered capacity of long distance synchronization while, in the second, a modulation of the thalamus will have an effect on a preserved cortex. The most recent studies tend to take this into account by excluding anoxic causes (Lemaire et al., 2018) or trying to identify the potential connectivity that the DBS may restore (Schiff et al., 2007; Magrassi et al., 2016). Nonetheless, most of the studies mixed patients with similar clinical presentations but with a potentially great physio-pathological heterogenicity.

Perspectives

To avoid the methodological issues due to the study design of the initial studies, DBS should not be offered within the interval of 1 year of possible spontaneous recovery from DoC (Vanhoecke and Hariz, 2017). The double-blind design introduced in DBS for DoC by Schiff (Schiff et al., 2007) should lead to less biased clinical conclusions and to exclusion of spontaneous recovery.

To overcome the heterogenicity of the patients in terms of physiopathology and to choose the most appropriate target for a single patient, an option could be to take advantage of the recent advances in the description of the physiology and anatomy of DoC patients. The structural integrity of the white matter tracts (Weng et al., 2017; Zheng et al., 2017; Velly et al., 2018; Wang et al., 2018; Wu et al., 2018) and the functional connectivity assessed by electrophysiology (Bekinschtein et al., 2009; King et al., 2013; Sitt et al., 2014; El Karoui et al., 2015) or MRI (Owen et al., 2006; Cruse et al., 2011; Boly et al., 2012; Laureys and Schiff, 2012; Casali et al., 2013) are becoming routine practice in DoC patients evaluation so that patient level connectivity maps tend to become available. Definition of a minimal criterion of brain connectivity before trailing with DBS could be an interesting option to appropriately select patients in whom DBS may be beneficial. Moreover, DBS target could be personalized, in such selected patients, to restore long range connectivity in low frequency band through deep nuclei or tracts considered as damaged nodes in the network. Finally, DBS could be proposed in priority to patients in a CMS (Naccache, 2018) defined by the existence of substantial cortical functional networks revealed by behavioral examination (e.g., MCS patient and in particular MCS+ patients and/or by functional brain-imaging (including CMD patients). Indeed, such patients are predicted in theory to benefit the most from sub-cortical activation of residual cortical networks.

Vagus Nerve Stimulation

More recently, as a less invasive alternative to DBS, vagus nerve stimulation (VNS) has been tested in a DoC patient (Corazzol et al., 2017). The vagus nerve directly modulates activity in the brainstem and, through the nucleus of the solitary tract, reaches the dorsal raphe nuclei and the thalamus (Rutecki, 1990). Its positive effect on reticular formation, thalamus and forebrain metabolism has been established (Henry et al., 1999). In addition to this modulation of the ARAS, very similar to what is observed in DBS, VNS is known to enhance the releasing of norepinephrine in the thalamus through an enhancement of the neuronal firing of the locus coeruleus, a crucial pathway for arousal (Dorr and Debonnel, 2006).

The unique patient reported with this technique was a 35 years old man in a VS/UWS for 15 years after a severe TBI. The maximum effect was obtained with a 1 mA stimulation. The CRS-R increased, from a score of 5 at baseline to 10 and the patient was then classified as MCS. The pre and post stimulation high density

EEG showed a significant increase in theta band (4–7 Hz) and the 18F-FDG PET results corroborated these findings and reveal an increase of activity in fronto-parietal and basal ganglia regions. These results are coherent with an emergence of the patient from the VS/UWS to the MCS. This observation demonstrates the ability of vagus nerve stimulation to modulate large-scale connectivity and its therapeutic potential in DoC patients.

NON-INVASIVE ELECTRIC AND MAGNETIC STIMULATION

By analogy with DBS, the idea that externally applied electrical current on the scalp could be used to probe brain-behavior relationship arose around 40 years ago (Merton and Morton, 1980). However, the huge intensities used at this time (∼ 20 A) led to important side effects, and this breakthrough was not immediately pursued. Only since the end of the 1990s, non-invasive brain stimulation (NIBS) was refined and gained interest in neuroscience with the emergence of two main methods, transcranial electrical stimulation (tES) and transcranial magnetic stimulation (TMS). In the recent years, both have been proposed as therapeutic tools for various conditions, among which DoC, with the main advantage of being easier to implement and not invasive as compared to DBS and VNS. However, given the greater studies heterogeneity, their results will be presented separately.

Transcranial Magnetic Stimulation

Principle

Transcranial magnetic stimulation is a non-invasive stimulation technique modifying cortical excitability through the delivery of magnetic impulses generated by the flow of high-density electric current through a magnetic coil placed over the scalp. Single or short pulses of TMS can trigger firing of action potentials and allow to interact with the underlying brain activity with a high temporal resolution with excitatory or inhibitory effect depending on the modalities. These on-line TMS properties are mainly used in neuroscience to probe the function and connections of targeted brain regions. In DoC patients, such procedures have been employed to explore motor pathways' integrity and complexity of information processing and to index consciousness (Casali et al., 2013). Therapeutic studies rely on another type of TMS taking advantages of the neuromodulatory after-effects induced by repetitive stimulation (rTMS). These longer term effects are thought to be related to changes in synaptic plasticity by modulation of glutamatergic and GABAergic balance (Stagg et al., 2009) and non-synaptic pathways (Ardolino et al., 2005).

Clinical Studies

Despite several studies (**Table 2**), the level of evidence supporting the therapeutic use of rTMS in DoC patients is low (Lefaucheur et al., 2014). Indeed, most of them are uncontrolled trials targeting heterogeneous patients with small sample size and various stimulation protocols.

The first description of therapeutic TMS in DoC dates back to 2009, when Louise-Bender Pape et al. (2009) stimulated a VS patient daily for 6 weeks with 10 Hz rTMS over the right dorsolateral prefrontal cortex. While the patient presented some behavioral improvement followed by an improvement of amplitudes and latencies of brainstem auditory evoked potentials, these changes did not reach statistical significance. A second case reports an MCS patient found similar results with a transient augmentation of CRS-R score (up to 6 h) paralleled with spectral power changes on resting state EEG after two sessions of 20 Hz rTMS. This observation was latter matched by another similar case report (Bai et al., 2016).

While these first cases failed to show consistent behavioral effect on consciousness, they served as proof-of-concept supporting the safety of this procedure in DoC patients. They were thus followed by prospective open-label studies including at most 16 patients using either one session of 20 Hz stimulation over M1 (Manganotti et al., 2013), one (Naro et al., 2015b) or 30 sessions of 10 Hz rTMS over the right-DLPFC (Pape et al., 2014), or 28 sessions of 5 Hz rTMS over the same site (Xie et al., 2015). Only the latter yielded an improvement of CRS-R in 6 out of 10 patients stimulated, with a long-lasting effect persisting at 4 weeks. A more recent study by Xia et al. (2017) also seemed to show a potential benefit of DLPFC stimulation, albeit at higher frequency (10 Hz), with an increase in CRS-R scores in 5 out 5 MCS patients and 4 out of 11 VS/UWS, remaining 10 days after the end of the stimulation.

As for cross-over double-blind randomized controlled trials of rTMS in DoC, only four studies were conducted, between 2015 and 2018, with a total number of 34 patients included. They all assessed the efficacy of 20 Hz rTMS over the left M1 in comparison to a sham control condition. None of them demonstrated consciousness improvement by stimulation, regardless of whether the protocol consisted in a single session (Liu et al., 2016) or in daily sessions over 5 days (Cincotta et al., 2015; He et al., 2018; Liu et al., 2018). These studies only showed some minor EEG changes in power spectra or hemodynamic parameters monitored by transcranial doppler.

Regarding the safety of rTMS in DoC patients, these studies seemed to support its relative innocuity, even though epileptic seizures attributable to stimulation were reported in at least one subject (Louise-Bender Pape et al., 2009; Pape et al., 2014). Given the small number of patients included, this should be taken with caution, as it is known that seizures can be elicited by TMS in healthy subjects, with an increasing risk in brain-lesioned patients and with a history of seizures, two frequent conditions in DoC patients.

Although the great diversity of stimulation frequency (5, 10, 20 Hz), intensity (from 90 to 120% of resting motor threshold), site of stimulation (left or right prefrontal cortex or primary motor cortex) and number of sessions (single or repeated) makes it hard to draw definite conclusions, the few positive results demonstrating an impact of rTMS on patients' consciousness are casting shadow over potential of rTMS in this condition. Moreover, TMS protocols are not easy to implement at bedside and require a specialized expertise and dedicated material, which questions its accessibility in the many structures

TABLE 2 | Transcrania lmagnetic stimulation studies in DoC patients.

Study	Design/Control	Population	Target/ Stimulation parameters	Behavioral effects	Electrophysiological effects	Side effects
Louise-Bender Pape et al., 2009	Case report/ None	1 VS/UWS patient	Right DLPFC/30 sessions over 6 weeks of 10 Hz rTMS (300 paired-pulse) at 110% RMT	No significant (trend) improvement of DOC Scale	Improvement of latencies of auditory brainstem evoked potentials	None
Piccione et al., 2011	Case report/ Median nerve stimulation	1 MCS patient	Left M1/2 sessions of 20 Hz rTMS (10 trains of 100 stimuli) at 90% RMT	Increased CRS-R score lasting 6 h after stimulation	Increase of absolute and relative power in delta, alpha and gamma band	None
Manganotti et al., 2013	Open-label/ None	6 patients (3 VS/UWS and 3 MCS)	Left or right M1/1 session of 20 Hz rTMS (10 trains of 100 stimuli) at 120% RMT	Improvement of consciousness in only 1 patient	Increase of absolute and relative power in delta, alpha and gamma band and reactivity in the responding patient	None
Pape et al., 2014	Open-label/ None	2 patients	Right DLPFC/30 sessions over 6 weeks of 10 Hz rTMS (300 paired-pulse) at 110% RMT	Not assessed	Not assessed	One epileptic seizure
Xie et al., 2015	Open-label/ Case-control	20 patients (2 coma, 11 VS/UWS, 7 MCS) of which 10 were stimulated	Right DLPFC/28 sessions over 28 days of 5 Hz rTMS	6 out of 10 patients stimulated showed CRS-R improvement persisting at 4 weeks	Increase of alpha power and decrease of delta power	Not reported
Naro et al., 2015a	Not randomized/ Sham	10 patients (all VS/UWS) and 10 healthy controls	Right DLPFC/1 session of 10 Hz rTMS (1000 pulses) at 90% RMT	No significant group effect but small short-lasting improvement in 3 patients on the motor subscale of the CRS-R	No significant effect at the group level, but some short-lasting modulation of motor evoked potentials in the 3 responding patients	None
Cincotta et al., 2015	Cross-over RCT/ Sham	11 patients (all VS/UWS)	Left M1/5 sessions over 5 days of 20 Hz rTMS (1000 pulses) at 90% RMT	No significant differences in CRS-R scores between stimulation and sham	No significant changes on EEG (Synek classification)	None
Liu et al., 2016	Cross-over RCT/ Sham	10 patients (5 VS/UWS, 5 MCS)	Left M1/1 session of 20 Hz rTMS (1000 pulses) at 100% RMT	No behavioral effect	Significant changes in hemodynamic parameters (mean and peak velocity of middle cerebral artery) on transcranial doppler only in MCS	None
Bai et al., 2017	Case report/ None	1 MCS patient	Left DLPFC/ 20 sessions over 20 days of 10 Hz rTMS (1000 pulses) at 90% RMT	Improvement of CRS-R after 20 sessions	Concomitant improvement of perturbational complexity index, global mean field power and motor evoked potential.	None
Xia et al., 2017	Prospective/ Not controlled	16 patients (11 VS/UWS and 5 MCS)	Left DLPFC/ 20 sessions over 20 days of 10 Hz rTMS (1000 pulses) at 90% RMT	Improvement of CRS-R score in all MCS patients and 4/11 VS/UWS persisting 10 days after stimulation.	None	None
Xia et al., 2017	Prospective/ Not controlled	18 patients (12 had repeated sessions for 20 days)	Left DLPFC/ 20 sessions over 20 days of 10 Hz rTMS (1000 pulses) at 90% RMT	Overlapping population with the previous study. No statistical testing.	Decreased low-frequency band power and increased high-frequency band power, especially in MCS	None
He et al., 2018	Cross-over RCT/ Sham	6 patients (3 VS/UWS, 2 MCS and 1 EMCS)	Left M1/5 sessions over 5 days of 20 Hz rTMS (1000 pulses) at 100% RMT	No significant differences in CRS-R. One patient improved after real stimulation.	Increase delta, theta, alpha and beta power spectra in the responding patient.	Not reported
Liu et al., 2018	Cross-over RCT/ Sham	7 patients (2 VS/UWS and 5 MCS)	Left M1/5 sessions over 5 days of 20 Hz rTMS (1000 pulses) at 100% RMT	No significant changes of CRS-R scores	No significant changes in functional connectivity on EEG	None

CRS-R, Coma Recovery Scale – Revised; DLPFC, dorsolateral prefrontal cortex; DoC, disorders of consciousness; EEG, electroencephalogram; EMCS, Emergence from Minimally Conscious State; M1, primary motor cortex; MCS, Minimally Conscious State; RCT, randomized controlled trial; RMT, resting motor threshold; rTMS, repetitive transcranial magnetic stimulation; VS/UWS, vegetative state/unresponsive wakefulness syndrome.

(intensive care unit, neurology and rehabilitation facilities, nursing home or even at home) taking care of DoC patients. In respect to this, tES techniques are superior to TMS.

Transcranial Electric Stimulation

Transcranial Direct Current Stimulation

The most used tES technique is transcranial direct current stimulation (tDCS), which delivers a continuous and weak intensity current (1–2 mA) to the scalp through a bipolar montage (the current flowing from an anode to a cathode). Although some controversies are still hanging regarding the ability of these induced electric fields to elicit clinically relevant modification of the brain activity (Vöröslakos et al., 2018), considerable evidence shows that tDCS is able to modulate the neural resting state membrane potential polarization depending on both the polarity of stimulation (Nitsche and Paulus, 2001) and of the underlying brain activity by fine tuning of synaptic gains (Lafon et al., 2017). Interestingly, as for rTMS, tDCS stimulation lasting more than a few minutes is able to induce after-effects mediated mainly by synaptic pathways [modulation of LTP and LTD (Kronberg et al., 2017) through NMDA-dependent synaptic plasticity (Liebetanz et al., 2002; Nitsche et al., 2003)] and other non-synaptic pathways (Gellner et al., 2016). Initially, tDCS was mainly targeted to probe brain functions in healthy subjects and its first therapeutic use goes back to Hummel et al. (2005). Since then, numerous studies applied tDCS in various neurologic (Parkinson's disease, dystonia, post-stroke or primary progressive aphasia) and psychiatric conditions (depression, autism, addiction, schizophrenia, and attention disorders) with unequivocal efficacy (Lefaucheur, 2016). Studies of tDCS in DoC patients are presented in **Table 3**.

The first report of tDCS in DoC patients is from Angelakis et al. (2014), who showed an increase in CRS-R in 3 patients out of 10 with either a left DLPFC (L-DLPFC) or a left sensorimotor cortex repeated stimulation (5 sessions). However, this study was not controlled and the sham sessions were always performed before the repetitive sessions of active stimulation which doesn't prevent a confound with spontaneous recovery. These encouraging results were further supported by a double-blind randomized controlled trial against sham published by Thibaut et al. (2014). In this study, the authors found a significant effect on consciousness of a single 2 mA L-DLPFC tDCS stimulation only in the MCS group, with an improvement in CRS-R in 13/30 (43%) MCS patients and 2/25 (8%) VS/UWS. Retrospective analysis of PET-TDM and MRI data of these patients prior stimulation yielded that tDCS responsiveness was characterized by preserved brain metabolism and gray matter integrity in cortical and subcortical regions traditionally involved in consciousness (prefrontal cortex, precuneus and thalamus) (Thibaut et al., 2015). Responders were also characterized by a higher connectivity in regions belonging to the extrinsic/executive control network in fMRI (Cavaliere et al., 2016) and increase theta connectivity and network centrality in EEG (Thibaut et al., 2018).

However, subsequent studies of single-session stimulation failed to reproduce the behavioral effect of tDCS (Naro et al., 2015a; Bai et al., 2016, 2017). Note though, that the stimulation parameters differed from those of the previous study, either due to smaller electrodes (25 cm^2 vs. 35 cm^2) or due to a distinct montage (orbitofrontal stimulation with anode between, Fp1 and Fp2 and cathode in Cz; Naro et al., 2015a). Yet these studies provided insight into the mechanisms of action of tDCS in DoC patients by combining the stimulation with other electrophysiological techniques (electroencephalogram -EEG-, event-related potentials -ERP- and/or transcranial magnetic stimulation -TMS). Hence, in a study combining TMS-EEG and tDCS over the L-DLPFC, Bai et al. (2017) showed that tDCS could modulate the cortical global excitability assessed by TMS with different spatial and temporal patterns in VS/UWS and MCS. In another study, the same authors showed that tDCS stimulation led to an increased fronto-parietal coherence in the theta band (Bai et al., 2016). Taken together, these results suggest that tDCS is able to modify the functional connectivity of consciousness-related networks as can be seen in healthy volunteers (Kunze et al., 2016) and could restore partially preserved long-range connectivity inside cortico-thalamic networks, thus explaining the better response rate observed in MCS patients.

In contrast to these single-session studies, in which the effect of tDCS appears transient, the repetition of tDCS sessions seems to increase both the rate and the amplitude of consciousness improvement. Indeed, Thibaut et al. (2017) showed in a double-blind cross-over randomized controlled trial, that repetitive sessions of L-DLPFC tDCS over five consecutive days led not only to an increased rate of response after the end of the stimulation period [significant improvement of CRS-R in 9 out of 16 (56%) MCS], but also that this improvement of consciousness was persisting 1 week after the last session of simulation. In another study, Zhang et al. (2017) further supported the efficacy of repetitive sessions (20 sessions in 10 consecutive working days) using a parallel controlled design coupling behavioral assessment with event-related potentials elicited during an auditory oddball paradigm. Together with a significant improvement of CRS-R scores, the authors reported an increased P300 amplitude, only after real stimulation in MCS (Zhang et al., 2017). It should, however, be noted that another study, despite similar design and stimulation parameters failed to show behavioral effects of both single-session and repetitive tDCS (Estraneo et al., 2017). These differences could be partially explained by a more heterogeneous population (inclusion of VS/UWS) farther away from the brain injury (more than a year in median). Interestingly, repetitive stimulation has also been tested in a home-based setting (home and rehabilitation facilities), in order to evaluate the feasibility of prolonged stimulation protocols by non-expert caregivers or family members (Martens et al., 2018). In this cross-over study by Martens et al. (2018), 27 chronic MCS received 4 weeks of tDCS and sham with a wash-out period of 8 weeks between the two. Overall adherence to treatment was very good (94%), but 5 patients received less than 80% of the planned sessions. This resulted in the

TABLE 3 | Transcranial direct current stimulation studies in DoC patients.

Study	Design/ Control	Population	Stimulation parameters	Behavioral effect	Electrophysiological effect	Side effects
Angelakis et al., 2014	Prospective/ Sham	10 patients (7 VS/UWS, 3 MCS)	5 sessions (20 min) of sham, 1 and 2 mA anodal L-DLPFC or L-SMC tDCS (F3/C3- Fp2; 25 cm2-35cm2)	CRS-R increase in the 3 MCS patients	Not assessed	None
Thibaut et al., 2014	Cross-over RCT/ Sham	55 patients (25 VS/UWS, 30 MCS)	Single session (20 min) of 2 mA anodal L-DLPFC tDCS (F3-Fp2; 35 cm^2)	Significant increase of CRS-R only in MCS patients.	Not assessed	None
Naro et al., 2015a	Cross-over RCT/ Sham	25 patients (12VS/UWS, 10 MCS, 2 EMCS)	Single session (10 min) of 1 mA anodal orbito-frontal cortex (Fp-Cz; 25–35 cm^2)	No effect	Changes in M1 excitability and premotor-motor connectivity in some DoC patients assessed by TMS	None
Naro et al., 2016b	Cross-over RCT/ Sham	20 patients (10 VS/UWS and 10 MCS)	Single session (20 min) of 2 mA cerebellar 5 Hz oscillatory tDCS (medial cerebellum-left buccinator muscle; 16 cm^2)	Improvement of CRS-R in MCS patients.	Increase in fronto-parietal coherence and power in theta and gamma band in MCS patients	None
Bai et al., 2017	Cross-over RCT/ Sham	18 patients (9 VS/UWS, 9 MCS)	Single session (20 min) of 2 mA anodal L-DLPFC (F3-Fp2; 25 cm^2)	No effect	Changes in cortical excitability assessed by TMS-EEG	Not reported
Bai et al., 2017	Cross-over RCT/ Sham	17 patients (9 VS/UWS, 8 MCS)	Single session (20 min) of 2 mA anodal L-DLPFC (F3-Fp2; 25 cm^2)	No effect	Increase fronto-parietal coherence in the theta band in MCS	Not reported
Zhang et al., 2017	Parallel RCT/ Sham	26 patients (11 VS/UWS, 15 MCS)	20 sessions (20 min) of 2 mA anodal L-DLPFC (F3-Fp2; 35 cm2) over 10 consecutive days	Significant improvement in CRS-R in MCS patients	Increased P300 amplitude in MCS during an auditory oddball paradigm	None
Thibaut et al., 2017	Cross-over RCT/ Sham	16 patients (all MCS)	5 sessions (20 min) of 2 mA anodal L-DLPFC (F3-Fp2; 35 cm^2) over 5 days	Significant improvement of CRSR [in 9/16 (56%)] at 5 days, persisting at 12 days.	Not assessed	None
Huang w. et al., 2017	Cross-over RCT/ Sham	27 patients (all MCS)	5 sessions (20 min) of 2 mA anodal posterior parietal cortex tDCS (Pz-Fp2; unknown)	Significant improvement of CRS-R after 5 days of stimulation, but no persistence at 10 days.	Not assessed	None
Estraneo et al., 2017	Cross-over RCT/ Sham	13 patients (7 VS/UWS, 6 MCS)	5 sessions (20 min) of 2 mA anodal L-DLPFC F3-Fp2; 35 cm^2) over 5 days	No effect on CRS-R after single or repeated sessions	Improvement of background rhythm in some patients	None
Martens et al., 2018	Cross-over RCT/ Sham	27 patients (all MCS) in rehabilitation facilities or at home.	20 sessions (20 min) of 2 mA anodal L-DLPFC F3-Fp2; 35 cm^2) over 4 weeks	No significant effect, but trend toward CRS-R improvement after 4 weeks, lasting at 12 weeks	Not assessed	One epileptic seizure

Details of the montages are given as follow: target of the stimulation (electrodes positions according to the 10–20 international system; electrodes surface). CRS-R, Coma Recovery Scale – Revised; DoC, disorders of consciousness; MCS, Minimally Conscious State; EMCS, Emergence from Minimally Conscious State; L-DLPFC, left dorso-lateral prefrontal cortex; RCT, randomized controlled trial; SMC, sensory motor cortex; tDCS, transcranial direct current stimulation.

	Deep Brain Stimulation (DBS)	Vagus Nerve Stimulation (VNS)	Rythmic Transcranial Magnetic Stimulation (rTMS)	Transcranial Direct Current Stimulation (tDCS)
TYPE	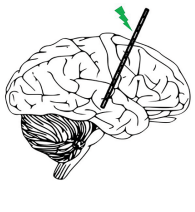	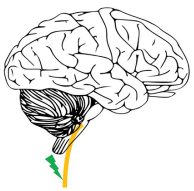	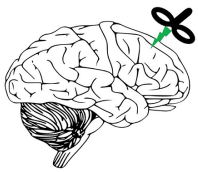	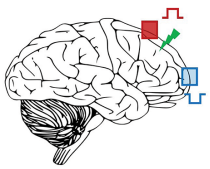
TARGET	Midbrain Thalamus Pallidum Striatum	Vagus Nerve	Right or left dorsolateral prefrontal cortex or Right or left primary motor cortex	Left dorsolateral prefrontal cortex or Posterior parietal cortex
CURRENT	Low (8-30 Hz) or high frequencies (50-250 Hz) 1-20 V voltages	30 Hz 1.5 mA intensity	Single or repeated sessions 5-20 Hz	20 minutes sessions (single or repeated) 1-2 mA intensities
INVASIVE	Yes	Moderately	No	No

FIGURE 1 | Different types of stimulation used in DoC patients. Schematic representation of the different types of invasive a non-invasive stimulation used in DoC patients. We listed the main targets and stimulation parameters (intensities, voltages, frequencies, and number of sessions) used in clinical studies. DBS, deep brain stimulation; Hz, Hertz; mA, milli-ampere; rTMS, rhythmic transcranial magnetic stimulation; tDCS, transcranial direct current stimulation; V, Volt; VNS, vagus nerve stimulation.

absence of significant effect on CRS-R on the intention to treat analysis, but significant effect at the end of the stimulation and a trend at 8 weeks after the stimulation in the per protocol analysis.

While previous studies targeted the L- DLPFC, some authors tested other sites of stimulation. Naro et al. (2016a) reported that cerebellar stimulation, using 5-Hz oscillatory tDCS (otDCS), elicited an increase in fronto-parietal coherence and spectral power in the theta and gamma band in MCS patients, paralleled with CRS-R improvement. Repetitive stimulation of the posterior parietal cortex also resulted in a consciousness improvement but with a smaller and less prolonged effect that prefrontal cortex stimulation (Huang w. et al., 2017). Both these results show that tDCS is a reliable tool to modulate activity within widespread networks distant from stimulation sites. However, the major involvement of prefrontal cortex in cortico-subcortical networks and especially its dense connections the thalamus seems to make it the better target of stimulation in DoC.

Importantly, except for a single epileptic seizure, the aforementioned studies did not report major side effects, strengthening previous evidence that tDCS is safe (Matsumoto and Ugawa, 2017). This point is of utmost importance considering the frailty of this population.

Transcranial Alternative Current Stimulation (tACS)

In contrast to tDCS, tACS delivers a sinusoidal current through the scalp able to elicit entrain underlying oscillatory activity and synchronize large scale neuronal networks. Only one study reported the use of tACS in DoC patients (Naro et al., 2016b). In this double-blind randomized cross-over study, two sites of gamma range (35–140 Hz) tACS stimulation were tested (right DLPFC and frontopolar cortex), against an active transcranial random noise stimulation (tRNS) control condition. No changes in CRS-R score were observed, but all MCS and some VS/UWS showed increased in theta and gamma relative power and fronto-parietal coherence in response to DLPFC stimulation.

Limitations and Perspectives of NIBS

While the therapeutic potential of rTMS in DoC patients seems limited so far, this review of the literature indicates a possible effect of tDCS in DoC patients. Indeed, several randomized controlled trials of tDCS in relatively large sample of DoC patients showed a significant behavioral improvement of consciousness, while rTMS studies failed to do so, maybe in part due to smaller sample sizes. Moreover, compared to rTMS, tDCS is together cheaper, less invasive, easier to use and more appropriate to repeated sessions, with consequently the potential of a wide availability for DoC patients, either during hospitalization or at home. However, please note that the current level of evidence is insufficient to issue recommendations on the use of both of these two techniques in DoC patients according to the latest guidelines on the therapeutic use of rTMS and tDCS (Lefaucheur et al., 2014, 2017) and further evidences from large-scale controlled studies

are needed. Indeed, substantial heterogeneity remains to be explained and many factors are known to account for the variability of behavioral and electrophysiological effects of NIBS (Polanía et al., 2018).

Regarding tES, despite encouraging results, some authors still doubt the ability of weak intensity currents to elicit changes in brain activity. The group of Buszaki showed that with conventional intensities, electric fields barely reached the threshold for resting membrane potential modification in rodents and humans cadaver brains (Vöröslakos et al., 2018), but intracranial recordings in human epileptic patients showed current densities consistent with neurophysiological effects (Huang Y. et al., 2017). Nonetheless, higher intensities (up to 4 mA) could lead to better or more robust clinical effect while staying safe (Chhatbar et al., 2017). On the other hand, the ability of TMS to induce changes in cortical excitability is not debated, yet its use in DoC patients is not supported by current evidence and further studies are needed to demonstrate a potential benefit. In addition, safety and logistic concerns may harden its development in this condition.

While increasing the number of sessions of tDCS led to a better and more sustained response, in accordance with potential cumulative effect of induced synaptic plasticity, the optimal number sessions is still unknown as well as the safety of prolonged or intensive stimulation. Furthermore, these lasting changes are allegedly underpinned by NMDA mediation and tDCS efficacy is known to be reduced in the presence of ion-channel blockers (Wischnewski et al., 2018). Future studies should systematically report the use of such treatments to better explain individual response.

As for now, all studies of NIBS in DoC patients used standardized montage and sites of stimulation, irrespective of the individual anatomy of patients. Despite a low spatial resolution, this one-size-fits-all approach is probably misleading given the variability of lesions (etiology, locations, severity). Moreover, most studies quantifying and modeling electric fields were done in healthy subjects (Huang Y. et al., 2017; Ciechanski et al., 2018). Recently, MRI-based models of current distribution inside the brain have been developed for tDCS [SimNIBS (Saturnino et al., 2015), ROAST (Huang et al., 2018)]. In addition, coming studies should couple behavioral assessment with detailed functional imaging of the brain (EEG, fMRI, PET) before, during and after stimulation. First, imaging residual functional connectivity and brain metabolism before stimulation, which are seemingly major determinants of tDCS efficacy, as suggested by the better response rate observed in MCS patients, will help better select patients that could benefit from stimulation. Second, assessing the changes in those measures according to stimulation will allow to further understand the mechanism of consciousness improvement by NIBS. Finally, the combination of stimulation with functional imaging techniques will allow to probe the underlying brain activity of patients, which is known to considerably influence the neuromodulation properties of both for tES and TMS (Silvanto et al., 2008). In these non-communicative and fluctuating patients (Wannez et al., 2017), the continuous recording of brain activity could pave the way to the development of closed-loop stimulation protocol (Berényi et al., 2012; Ngo et al., 2013; Kozák and Berényi, 2017; Kozák et al., 2018) to foster conscious patterns of brain activity. Taken together, these tools presumably hold the promise to substantially optimize tES stimulation in DoC patients.

CONCLUSION

Current evidence tends to support the efficacy of DBS and NIBS on consciousness in DoC patients (Thibaut and Schiff, 2018). However, while the latter is non-invasive and well tolerated, the former is associated with potential major side effects and should hence be reserved to selected patients. Less invasive techniques such as VNS are very promising and could represent a perfect trade-off between efficacy and invasiveness. Yet, evidence beyond the single-patient proof-of-concept study is needed to confirm its potential. Currently, we propose that all chronic DoC patients should be given the possibility to benefit from NIBS, and that tDCS should be preferred over rTMS given the evidence of the literature and its simpler use.

In any cases, future studies should systematically combine the stimulation with structural and functional brain-imaging, to (1) define patients who could benefit from the stimulation based on their residual brain activity (2) develop new stimulation protocols based on the understanding of the underlying mechanisms of consciousness improvement by electrical stimulation (3) tailor the stimulation to individual subjects based on their anatomy and/or functional brain-imaging through the use of computational modeling. This will also help define the relative place of each of these techniques in the treatment of DoC patients. One could imagine a progressive strategy, with a first-line use of NIBS to probe the possible response to stimulation followed by a second-line invasive stimulation to elicit sustained improvement of consciousness in carefully selected patients in which it is predicted to work. By then, some innovative and non-invasive stimulation techniques targeting deep brain structures, such as low intensity focused ultrasound pulsation (Monti et al., 2016), transcutaneous stimulation of the vagus nerve at the ear (Dietrich et al., 2008; Yu et al., 2017), or even indirect electrical brain stimulation through the olfactory receptors by using a nose-implanted electrode (Weiss et al., 2016) may turn to be efficient in DoC patients.

AUTHOR CONTRIBUTIONS

PB and BH reviewed the literature. PB and BH drafted the manuscript. All authors critically revised the manuscript for important intellectual content.

FUNDING

This work was funded by: "Institut National de la Santé et de la Recherche Médicale" (JS, LN), "Poste d'Accueil Inserm

program" (BH, PB), Sorbonne Université (LN), the James S. McDonnell Foundation (LN), FRM 2015 (LN), Académie des Sciences- Lamonica Prize 2016 (LN) and the FRM ('Equipe FRM 2015', LN). The research leading to these results has received funding from the program "Investissements d'Avenir" ANR-10- IAIHU-06.

ACKNOWLEDGMENTS

We would like to thank Pauline Pérez, Fédérico Raimondo, Benjamin Rohaut, and Mélanie Valente. We would also like to thank Caroline Apra for the help in editing the manuscript.

REFERENCES

Adams, Z. M., Forgacs, P. B., Conte, M. M., Nauvel, T. J., Drover, J. D., and Schiff, N. D. (2016). Late and progressive alterations of sleep dynamics following central thalamic deep brain stimulation (CT-DBS) in chronic minimally conscious state. *Clin. Neurophysiol.* 127, 3086–3092. doi: 10.1016/j.clinph.2016.06.028

Angelakis, E., Liouta, E., Andreadis, N., Korfias, S., Ktonas, P., Stranjalis, G., et al. (2014). Transcranial direct current stimulation effects in disorders of consciousness. *Arch. Phys. Med. Rehabil.* 95, 283–289. doi: 10.1016/j.apmr.2013.09.002

Apra, C., Bourdillon, P., and Lévêque, M. (2016). Surgical techniques: when brain bullets met crowdfunding. *Nature* 530, 160–160. doi: 10.1038/530160a

Ardolino, G., Bossi, B., Barbieri, S., and Priori, A. (2005). Non-synaptic mechanisms underlie the after-effects of cathodal transcutaneous direct current stimulation of the human brain. *J. Physiol.* 568, 653–663. doi: 10.1113/jphysiol.2005.088310

Bai, Y., Xia, X., Kang, J., Yang, Y., He, J., and Li, X. (2017). TDCS modulates cortical excitability in patients with disorders of consciousness. *Neuroimage Clin.* 15, 702–709. doi: 10.1016/j.nicl.2017.01.025

Bai, Y., Xia, X., Kang, J., Yin, X., Yang, Y., He, J., et al. (2016). Evaluating the effect of repetitive transcranial magnetic stimulation on disorders of consciousness by using TMS-EEG. *Front. Neurosci.* 10:473. doi: 10.3389/fnins.2016.00473

Bekinschtein, T. A., Dehaene, S., Rohaut, B., Tadel, F., Cohen, L., and Naccache, L. (2009). Neural signature of the conscious processing of auditory regularities. *Proc. Natl. Acad. Sci. U.S.A.* 106, 1672–1677. doi: 10.1073/pnas.0809667106

Benabid, A. L., Pollak, P., Louveau, A., Henry, S., and de Rougemont, J. (1987). Combined (thalamotomy and stimulation) stereotactic surgery of the VIM thalamic nucleus for bilateral Parkinson disease. *Appl. Neurophysiol.* 50, 344–346. doi: 10.1159/000100803

Berényi, A., Belluscio, M., Mao, D., and Buzsáki, G. (2012). Closed-loop control of epilepsy by transcranial electrical stimulation. *Science* 337, 735–737. doi: 10.1126/science.1223154

Boly, M., Massimini, M., Garrido, M. I., Gosseries, O., Noirhomme, Q., Laureys, S., et al. (2012). Brain connectivity in disorders of consciousness. *Brain Connect.* 2, 1–10. doi: 10.1089/brain.2011.0049

Bourdillon, P., Apra, C., and Lévêque, M. (2018). First clinical use of stereotaxy in humans: the key role of x-ray localization discovered by Gaston Contremoulins. *J. Neurosurg.* 128, 932–937. doi: 10.3171/2016.11.JNS161417

Bourdillon, P., Apra, C., Lévêque, M., and Vinckier, F. (2017). Neuroplasticity and the brain connectome: what can Jean Talairach's reflections bring to modern psychosurgery? *Neurosurg. Focus* 43:E11. doi: 10.3171/2017.6.FOCUS17251

Bruno, M.-A., Vanhaudenhuyse, A., Thibaut, A., Moonen, G., and Laureys, S. (2011). From unresponsive wakefulness to minimally conscious PLUS and functional locked-in syndromes: recent advances in our understanding of disorders of consciousness. *J. Neurol.* 258, 1373–1384. doi: 10.1007/s00415-011-6114-x

Casali, A. G., Gosseries, O., Rosanova, M., Boly, M., Sarasso, S., Casali, K. R., et al. (2013). A theoretically based index of consciousness independent of sensory processing and behavior. *Sci. Transl. Med.* 5:198ra105. doi: 10.1126/scitranslmed.3006294

Cavaliere, C., Aiello, M., Di Perri, C., Amico, E., Martial, C., Thibaut, A., et al. (2016). Functional connectivity substrates for tDCS response in minimally conscious state patients. *Front. Cell. Neurosci.* 10:257. doi: 10.3389/fncel.2016.00257

Chhatbar, P. Y., Chen, R., Deardorff, R., Dellenbach, B., Kautz, S. A., George, M. S., et al. (2017). Safety and tolerability of transcranial direct current stimulation to stroke patients - A phase I current escalation study. *Brain Stimul.* 10, 553–559. doi: 10.1016/j.brs.2017.02.007

Chudy, D., Deletis, V., Almahariq, F., Marčinković, P., Škrlin, J., and Paradžik, V. (2018). Deep brain stimulation for the early treatment of the minimally conscious state and vegetative state: experience in 14 patients. *J. Neurosurg.* 128, 1189–1198. doi: 10.3171/2016.10.JNS161071

Ciechanski, P., Carlson, H. L., Yu, S. S., and Kirton, A. (2018). Modeling transcranial direct-current stimulation-induced electric fields in children and adults. *Front. Hum. Neurosci.* 12:268. doi: 10.3389/fnhum.2018.00268

Cincotta, M., Giovannelli, F., Chiaramonti, R., Bianco, G., Godone, M., Battista, D., et al. (2015). No effects of 20 Hz-rTMS of the primary motor cortex in vegetative state: a randomised, sham-controlled study. *Cortex* 71, 368–376. doi: 10.1016/j.cortex.2015.07.027

Cohadon, F., and Richer, E. (1993). [Deep cerebral stimulation in patients with post-traumatic vegetative state. 25 cases]. *Neurochirurgie* 39, 281–292.

Corazzol, M., Lio, G., Lefevre, A., Deiana, G., Tell, L., André-Obadia, N., et al. (2017). Restoring consciousness with vagus nerve stimulation. *Curr. Biol.* 27, R994–R996. doi: 10.1016/j.cub.2017.07.060

Cruse, D., Chennu, S., Chatelle, C., Bekinschtein, T. A., Fernández-Espejo, D., Pickard, J. D., et al. (2011). Bedside detection of awareness in the vegetative state: a cohort study. *Lancet* 378, 2088–2094. doi: 10.1016/S0140-6736(11)61224-5

Dehaene, S., and Changeux, J.-P. (2011). Experimental and theoretical approaches to conscious processing. *Neuron* 70, 200–227. doi: 10.1016/j.neuron.2011.03.018

Dehaene, S., Changeux, J.-P., Naccache, L., Sackur, J., and Sergent, C. (2006). Conscious, preconscious, and subliminal processing: a testable taxonomy. *Trends Cogn. Sci.* 10, 204–211. doi: 10.1016/j.tics.2006.03.007

Dietrich, S., Smith, J., Scherzinger, C., Hofmann-Preiss, K., Freitag, T., Eisenkolb, A., et al. (2008). [A novel transcutaneous vagus nerve stimulation leads to brainstem and cerebral activations measured by functional MRI]. *Biomed. Tech.* 53, 104–111. doi: 10.1515/BMT.2008.022

Dorr, A. E., and Debonnel, G. (2006). Effect of vagus nerve stimulation on serotonergic and noradrenergic transmission. *J. Pharmacol. Exp. Ther.* 318, 890–898. doi: 10.1124/jpet.106.104166

Edlow, B. L., Chatelle, C., Spencer, C. A., Chu, C. J., Bodien, Y. G., O'Connor, K. L., et al. (2017). Early detection of consciousness in patients with acute severe traumatic brain injury. *Brain* 140, 2399–2414. doi: 10.1093/brain/awx176

Edlow, B. L., Takahashi, E., Wu, O., Benner, T., Dai, G., Bu, L., et al. (2012). Neuroanatomic connectivity of the human ascending arousal system critical to consciousness and its disorders. *J. Neuropathol. Exp. Neurol.* 71, 531–546. doi: 10.1097/NEN.0b013e3182588293

El Karoui, I., King, J.-R., Sitt, J., Meyniel, F., Van Gaal, S., Hasboun, D., et al. (2015). Event-related potential, time-frequency, and functional connectivity facets of local and global auditory novelty processing: an intracranial study in humans. *Cereb. Cortex* 25, 4203–4212. doi: 10.1093/cercor/bhu143

Engemann, D. A., Raimondo, F., King, J.-R., Rohaut, B., Louppe, G., Faugeras, F., et al. (2018). Robust EEG-based cross-site and cross-protocol classification of states of consciousness. *Brain* 141, 3179–3192. doi: 10.1093/brain/awy251

Estraneo, A., Pascarella, A., Moretta, P., Masotta, O., Fiorenza, S., Chirico, G., et al. (2017). Repeated transcranial direct current stimulation in prolonged disorders of consciousness: a double-blind cross-over study. *J. Neurol. Sci.* 375, 464–470. doi: 10.1016/j.jns.2017.02.036

Gellner, A.-K., Reis, J., and Fritsch, B. (2016). Glia: a neglected player in non-invasive direct current brain stimulation. *Front. Cell. Neurosci.* 10:188. doi: 10.3389/fncel.2016.00188

Giacino, J. T., Ashwal, S., Childs, N., Cranford, R., Jennett, B., Katz, D. I., et al. (2002). The minimally conscious state: definition and diagnostic criteria. *Neurology* 58, 349–353. doi: 10.1212/WNL.58.3.349

Giacino, J. T., Katz, D. I., and Whyte, J. (2013). Neurorehabilitation in disorders of consciousness. *Semin. Neurol.* 33, 142–156. doi: 10.1055/s-0033-1348960

Giacino, J. T., Whyte, J., Bagiella, E., Kalmar, K., Childs, N., Khademi, A., et al. (2012). Placebo-controlled trial of amantadine for severe traumatic brain injury. *N. Engl. J. Med.* 366, 819–826. doi: 10.1056/NEJMoa1 102609

Giller, C. A., Mornet, P., and Moreau, J.-F. (2017). The first formulation of image-based stereotactic principles: the forgotten work of Gaston Contremoulins. *J. Neurosurg.* 127, 1426–1435. doi: 10.3171/2016.10.JNS161966

Hassler, R., Ore, G. D., Bricolo, A., Dieckmann, G., and Dolce, G. (1969). EEG and clinical arousal induced by bilateral long-term stimulation of pallidal systems in traumatic vigil coma. *Electroencephalogr. Clin. Neurophysiol.* 27, 689–690. doi: 10.1016/0013-4694(69)91313-3

He, F., Wu, M., Meng, F., Hu, Y., Gao, J., Chen, Z., et al. (2018). Effects of 20Hz repetitive transcranial magnetic stimulation on disorders of consciousness: a resting-state electroencephalography study. *Neural Plast.* 2018:5036184. doi: 10.1155/2018/5036184

Henry, T. R., Votaw, J. R., Pennell, P. B., Epstein, C. M., Bakay, R. A., Faber, T. L., et al. (1999). Acute blood flow changes and efficacy of vagus nerve stimulation in partial epilepsy. *Neurology* 52, 1166–1173. doi: 10.1212/WNL.52.6.1166

Hosobuchi, Y., and Yingling, C. (1993). The treatment of prolonged coma with neurostimulation. *Adv. Neurol.* 63, 247–251.

Huang, W., Wannez, S., Fregni, F., Hu, X., Jing, S., Martens, G., et al. (2017). Repeated stimulation of the posterior parietal cortex in patients in minimally conscious state: a sham-controlled randomized clinical trial. *Brain Stimul.* 10, 718–720. doi: 10.1016/j.brs.2017.02.001

Huang, Y., Liu, A. A., Lafon, B., Friedman, D., Dayan, M., Wang, X., et al. (2017). Measurements and models of electric fields in the in vivo human brain during transcranial electric stimulation. *eLife* 6:e18834. doi: 10.7554/eLife.18834

Huang, Y., Datta, A., Bikson, M., and Parra, L. C. (2018). ROAST: an open-source, fully-automated, realistic volumetric-approach-based simulator for TES. *Conf. Proc. IEEE Eng. Med. Biol. Soc.* 2018, 3072–3075. doi: 10.1109/EMBC.2018.8513086

Hummel, F., Celnik, P., Giraux, P., Floel, A., Wu, W.-H., Gerloff, C., et al. (2005). Effects of non-invasive cortical stimulation on skilled motor function in chronic stroke. *Brain* 128, 490–499. doi: 10.1093/brain/awh369

Jang, S. H., and Kwon, H. G. (2015). The direct pathway from the brainstem reticular formation to the cerebral cortex in the ascending reticular activating system: a diffusion tensor imaging study. *Neurosci. Lett.* 606, 200–203. doi: 10.1016/j.neulet.2015.09.004

Jang, S. H., Park, J. S., Shin, D. G., Kim, S. H., and Kim, M. S. (2018). Relationship between consciousness and injury of ascending reticular activating system in patients with hypoxic ischaemic brain injury. *J. Neurol. Neurosurg. Psychiatry* doi: 10.1136/jnnp-2018-318366 [Epub ahead of print].

Kalmar, K., and Giacino, J. (2005). The JFK coma recovery scale—revised. *Neuropsychol. Rehabil.* 15, 454–460. doi: 10.1080/09602010443000425

King, J.-R., Sitt, J. D. D., Faugeras, F., Rohaut, B., El Karoui, I., Cohen, L., et al. (2013). Information sharing in the brain indexes consciousness in noncommunicative patients. *Curr. Biol.* 23, 1914–1919. doi: 10.1016/j.cub.2013.07.075

Kozák, G., and Berényi, A. (2017). Sustained efficacy of closed loop electrical stimulation for long-term treatment of absence epilepsy in rats. *Sci. Rep.* 7:6300. doi: 10.1038/s41598-017-06684-0

Kozák, G., Földi, T., and Berényi, A. (2018). Chronic transcranial electrical stimulation and intracortical recording in rats. *J. Vis. Exp.* 135:e56669. doi: 10.3791/56669

Kronberg, G., Bridi, M., Abel, T., Bikson, M., and Parra, L. C. (2017). Direct current stimulation modulates LTP and LTD: activity dependence and dendritic effects. *Brain Stimul.* 10, 51–58. doi: 10.1016/j.brs.2016.10.001

Kundu, B., Brock, A. A., Englot, D. J., Butson, C. R., and Rolston, J. D. (2018). Deep brain stimulation for the treatment of disorders of consciousness and cognition in traumatic brain injury patients: a review. *Neurosurg. Focus* 45:E14. doi: 10.3171/2018.5.FOCUS18168

Kunze, T., Hunold, A., Haueisen, J., Jirsa, V., and Spiegler, A. (2016). Transcranial direct current stimulation changes resting state functional connectivity: a large-scale brain network modeling study. *Neuroimage* 140, 174–187. doi: 10.1016/j.neuroimage.2016.02.015

Lafon, B., Rahman, A., Bikson, M., and Parra, L. C. (2017). Direct current stimulation alters neuronal input/output function. *Brain Stimul.* 10, 36–45. doi: 10.1016/j.brs.2016.08.014

Lammi, M. H., Smith, V. H., Tate, R. L., and Taylor, C. M. (2005). The minimally conscious state and recovery potential: a follow-up study 2 to 5 years after traumatic brain injury. *Arch. Phys. Med. Rehabil.* 86, 746–754. doi: 10.1016/j.apmr.2004.11.004

Laureys, S., and Schiff, N. D. (2012). Coma and consciousness: paradigms (re)framed by neuroimaging. *Neuroimage* 61, 478–491. doi: 10.1016/j.neuroimage.2011.12.041

Lefaucheur, J.-P. (2016). A comprehensive database of published tDCS clinical trials (2005–2016). *Neurophysiol. Clin. Neurophysiol.* 46, 319–398. doi: 10.1016/j.neucli.2016.10.002

Lefaucheur, J.-P., André-Obadia, N., Antal, A., Ayache, S. S., Baeken, C., Benninger, D. H., et al. (2014). Evidence-based guidelines on the therapeutic use of repetitive transcranial magnetic stimulation (rTMS). *Clin. Neurophysiol.* 125, 2150–2206. doi: 10.1016/j.clinph.2014.05.021

Lefaucheur, J.-P., Antal, A., Ayache, S. S., Benninger, D. H., Brunelin, J., Cogiamanian, F., et al. (2017). Evidence-based guidelines on the therapeutic use of transcranial direct current stimulation (tDCS). *Clin. Neurophysiol.* 128, 56–92. doi: 10.1016/j.clinph.2016.10.087

Lemaire, J.-J., Sontheimer, A., Pereira, B., Coste, J., Rosenberg, S., Sarret, C., et al. (2018). Deep brain stimulation in five patients with severe disorders of consciousness. *Ann. Clin. Transl. Neurol.* 5, 1372–1384. doi: 10.1002/acn3.648

Liebetanz, D., Nitsche, M. A., Tergau, F., and Paulus, W. (2002). Pharmacological approach to the mechanisms of transcranial DC-stimulation-induced after-effects of human motor cortex excitability. *Brain* 125, 2238–2247. doi: 10.1093/brain/awf238

Liu, P., Gao, J., Pan, S., Meng, F., Pan, G., Li, J., et al. (2016). Effects of high-frequency repetitive transcranial magnetic stimulation on cerebral hemodynamics in patients with disorders of consciousness: a sham-controlled study. *Eur. Neurol.* 76, 1–7. doi: 10.1159/000447325

Liu, X., Meng, F., Gao, J., Zhang, L., Zhou, Z., Pan, G., et al. (2018). Behavioral and resting state functional connectivity effects of high frequency rTMS on disorders of consciousness: a sham-controlled study. *Front. Neurol.* 9:982. doi: 10.3389/fneur.2018.00982

Louise-Bender Pape, T., Rosenow, J., Lewis, G., Ahmed, G., Walker, M., Guernon, A., et al. (2009). Repetitive transcranial magnetic stimulation-associated neurobehavioral gains during coma recovery. *Brain Stimul.* 2, 22–35. doi: 10.1016/j.brs.2008.09.004

Magrassi, L., Maggioni, G., Pistarini, C., Di Perri, C., Bastianello, S., Zippo, A. G., et al. (2016). Results of a prospective study (CATS) on the effects of thalamic stimulation in minimally conscious and vegetative state patients. *J. Neurosurg.* 125, 972–981. doi: 10.3171/2015.7.JNS15700

Manganotti, P., Formaggio, E., Storti, S. F., Fiaschi, A., Battistin, L., Tonin, P., et al. (2013). Effect of high-frequency repetitive transcranial magnetic stimulation on brain excitability in severely brain-injured patients in minimally conscious or vegetative state. *Brain Stimul.* 6, 913–921. doi: 10.1016/j.brs.2013.06.006

Martens, G., Lejeune, N., O'Brien, A. T., Fregni, F., Martial, C., Wannez, S., et al. (2018). Randomized controlled trial of home-based 4-week tDCS in chronic minimally conscious state. *Brain Stimul.* 11, 982–990. doi: 10.1016/j.brs.2018.04.021

Matsumoto, H., and Ugawa, Y. (2017). Adverse events of tDCS and tACS: a review. *Clin. Neurophysiol. Pract.* 2, 19–25. doi: 10.1016/j.cnp.2016.12.003

McLardy, T., Ervin, F., Mark, V., Scoville, W., and Sweet, W. (1968). Attempted inset-electrodes-arousal from traumatic coma: neuropathological findings. *Trans. Am. Neurol. Assoc.* 93, 25–30.

Merton, P. A., and Morton, H. B. (1980). Stimulation of the cerebral cortex in the intact human subject. *Nature* 285:227. doi: 10.1038/285227a0

Miocinovic, S., Somayajula, S., Chitnis, S., and Vitek, J. L. (2013). History, applications, and mechanisms of deep brain stimulation. *JAMA Neurol.* 70, 163–171. doi: 10.1001/2013.jamaneurol.45

Monti, M. M., Schnakers, C., Korb, A. S., Bystritsky, A., and Vespa, P. M. (2016). Non-invasive ultrasonic thalamic stimulation in disorders of consciousness after severe brain injury: a first-in-man report. *Brain Stimul.* 9, 940–941. doi: 10.1016/j.brs.2016.07.008

Multi-Society Task Force on PVS (1994). Medical aspects of the persistent vegetative state. *N. Engl. J. Med.* 330, 1572–1579. doi: 10.1056/NEJM199406023302206

Naccache, L. (2018). Minimally conscious state or cortically mediated state? *Brain* 141, 949–960. doi: 10.1093/brain/awx324

Naro, A., Bramanti, P., Leo, A., Russo, M., and Calabrò, R. S. (2016b). Transcranial alternating current stimulation in patients with chronic disorder of consciousness: a possible way to cut the diagnostic Gordian Knot? *Brain Topogr.* 29, 623–644. doi: 10.1007/s10548-016-0489-z

Naro, A., Calabrò, R. S., Russo, M., Leo, A., Pollicino, P., Quartarone, A., et al. (2015a). Can transcranial direct current stimulation be useful in differentiating unresponsive wakefulness syndrome from minimally conscious state patients? *Restor. Neurol. Neurosci.* 33, 159–176. doi: 10.3233/RNN-140448

Naro, A., Russo, M., Leo, A., Bramanti, P., Quartarone, A., and Calabrò, R. S. (2015b). A single session of repetitive transcranial magnetic stimulation over the dorsolateral prefrontal cortex in patients with unresponsive wakefulness syndrome: preliminary results. *Neurorehabil. Neural Repair* 29, 603–613. doi: 10.1177/1545968314562114

Naro, A., Russo, M., Leo, A., Cannavò, A., Manuli, A., Bramanti, A., et al. (2016a). Cortical connectivity modulation induced by cerebellar oscillatory transcranial direct current stimulation in patients with chronic disorders of consciousness: a marker of covert cognition? *Clin. Neurophysiol.* 127, 1845–1854. doi: 10.1016/j.clinph.2015.12.010

Ngo, H.-V. V., Martinetz, T., Born, J., and Mölle, M. (2013). Auditory closed-loop stimulation of the sleep slow oscillation enhances memory. *Neuron* 78, 545–553. doi: 10.1016/j.neuron.2013.03.006

Nitsche, M. A., Fricke, K., Henschke, U., Schlitterlau, A., Liebetanz, D., Lang, N., et al. (2003). Pharmacological modulation of cortical excitability shifts induced by transcranial direct current stimulation in humans. *J. Physiol.* 553, 293–301. doi: 10.1113/jphysiol.2003.049916

Nitsche, M. A., and Paulus, W. (2001). Sustained excitability elevations induced by transcranial DC motor cortex stimulation in humans. *Neurology* 57, 1899–1901. doi: 10.1212/WNL.57.10.1899

Owen, A. M., Coleman, M. R., Boly, M., Davis, M. H., Laureys, S., and Pickard, J. D. (2006). Detecting awareness in the vegetative state. *Science* 313, 1402–1402. doi: 10.1126/science.1130197

Pape, T. L.-B., Rosenow, J. M., Patil, V., Steiner, M., Harton, B., Guernon, A., et al. (2014). RTMS safety for two subjects with disordered consciousness after traumatic brain injury. *Brain Stimul.* 7, 620–622. doi: 10.1016/j.brs.2014.03.007

Piccione, F., Cavinato, M., Manganotti, P., Formaggio, E., Storti, S. F., Battistin, L., et al. (2011). Behavioral and neurophysiological effects of repetitive transcranial magnetic stimulation on the minimally conscious state: a case study. *Neurorehabil. Neural Repair* 25, 98–102. doi: 10.1177/1545968310369802

Polanía, R., Nitsche, M. A., and Ruff, C. C. (2018). Studying and modifying brain function with non-invasive brain stimulation. *Nat. Neurosci.* 21, 174–187. doi: 10.1038/s41593-017-0054-4

Rutecki, P. (1990). Anatomical, physiological, and theoretical basis for the antiepileptic effect of vagus nerve stimulation. *Epilepsia* 31(Suppl. 2), S1–S6. doi: 10.1111/j.1528-1157.1990.tb05843.x

Saturnino, G., Antunes, A., Stelzer, J., and Thielscher, A. (2015). "SimNIBS: a versatile toolbox for simulating fields generated by transcranial brain stimulation," in *Proceedings of the 21st Annual Meeting of the Organization for Human Brain Mapping (OHBM 2015)*, Honolulu, HI.

Schiff, N. D. (2010). Recovery of consciousness after brain injury: a mesocircuit hypothesis. *Trends Neurosci.* 33, 1–9. doi: 10.1016/j.tins.2009.11.002

Schiff, N. D., Giacino, J. T., Kalmar, K., Victor, J. D., Baker, K., Gerber, M., et al. (2007). Behavioural improvements with thalamic stimulation after severe traumatic brain injury. *Nature* 448, 600–603. doi: 10.1038/nature06041

Silvanto, J., Muggleton, N., and Walsh, V. (2008). State-dependency in brain stimulation studies of perception and cognition. *Trends Cogn. Sci.* 12, 447–454. doi: 10.1016/j.tics.2008.09.004

Sitt, J. D., King, J.-R., El Karoui, I., Rohaut, B., Faugeras, F., Gramfort, A., et al. (2014). Large scale screening of neural signatures of consciousness in patients in a vegetative or minimally conscious state. *Brain* 137, 2258–2270. doi: 10.1093/brain/awu141

Stagg, C. J., Best, J. G., Stephenson, M. C., O'Shea, J., Wylezinska, M., Kincses, Z. T., et al. (2009). Polarity-sensitive modulation of cortical neurotransmitters by transcranial stimulation. *J. Neurosci.* 29, 5202–5206. doi: 10.1523/JNEUROSCI.4432-08.2009

Sturm, V., Kühner, A., Schmitt, H. P., Assmus, H., and Stock, G. (1979). Chronic electrical stimulation of the thalamic unspecific activating system in a patient with coma due to midbrain and upper brain stem infarction. *Acta Neurochir.* 47, 235–244. doi: 10.1007/BF01406406

Thibaut, A., Bruno, M.-A., Ledoux, D., Demertzi, A., and Laureys, S. (2014). tDCS in patients with disorders of consciousness: sham-controlled randomized double-blind study. *Neurology* 82, 1112–1118. doi: 10.1212/WNL.0000000000000260

Thibaut, A., Chennu, S., Chatelle, C., Martens, G., Annen, J., Cassol, H., et al. (2018). Theta network centrality correlates with tDCS response in disorders of consciousness. *Brain Stimul.* 11, 1407–1409. doi: 10.1016/j.brs.2018.09.002

Thibaut, A., Di Perri, C., Chatelle, C., Bruno, M.-A., Bahri, M. A., Wannez, S., et al. (2015). Clinical response to tDCS depends on residual brain metabolism and grey matter integrity in patients with minimally conscious state. *Brain Stimul.* 8, 1116–1123. doi: 10.1016/j.brs.2015.07.024

Thibaut, A., and Schiff, N. (2018). "New therapeutic options for the treatment of patients with disorders of consciousness: the field of neuromodulation," in *Coma and Disorders of Consciousness*, eds C. Schnakers and S. Laureys (New York, NY: Springer International Publishing). doi: 10.1007/978-3-319-55964-3_12

Thibaut, A., Wannez, S., Donneau, A.-F., Chatelle, C., Gosseries, O., Bruno, M.-A., et al. (2017). Controlled clinical trial of repeated prefrontal tDCS in patients with chronic minimally conscious state. *Brain Inj.* 31, 466–474. doi: 10.1080/02699052.2016.1274776

Tsubokawa, T., Yamamoto, T., Katayama, Y., Hirayama, T., Maejima, S., and Moriya, T. (1990). Deep-brain stimulation in a persistent vegetative state: follow-up results and criteria for selection of candidates. *Brain Inj.* 4, 315–327. doi: 10.3109/02699059009026185

Vanhoecke, J., and Hariz, M. (2017). Deep brain stimulation for disorders of consciousness: systematic review of cases and ethics. *Brain Stimul.* 10, 1013–1023. doi: 10.1016/j.brs.2017.08.006

Velly, L., Perlbarg, V., Boulier, T., Adam, N., Delphine, S., Luyt, C.-E., et al. (2018). Use of brain diffusion tensor imaging for the prediction of long-term neurological outcomes in patients after cardiac arrest: a multicentre, international, prospective, observational, cohort study. *Lancet Neurol.* 17, 317–326. doi: 10.1016/S1474-4422(18)30027-9

Vöröslakos, M., Takeuchi, Y., Brinyiczki, K., Zombori, T., Oliva, A., Fernández-Ruiz, A., et al. (2018). Direct effects of transcranial electric stimulation on brain circuits in rats and humans. *Nat. Commun.* 9:483. doi: 10.1038/s41467-018-02928-3

Wang, L., Yang, Y., Chen, S., Ge, M., He, J., Yang, Z., et al. (2018). White matter integrity correlates with residual consciousness in patients with severe brain injury. *Brain Imaging Behav.* 12, 1669–1677. doi: 10.1007/s11682-018-9832-1

Wannez, S., Heine, L., Thonnard, M., Gosseries, O., Laureys, S., and Coma Science Group collaborators (2017). The repetition of behavioral assessments in diagnosis of disorders of consciousness. *Ann. Neurol.* 81, 883–889. doi: 10.1002/ana.24962

Weiss, T., Shushan, S., Ravia, A., Hahamy, A., Secundo, L., Weissbrod, A., et al. (2016). From nose to brain: un-sensed electrical currents applied in the nose alter activity in deep brain structures. *Cereb. Cortex* doi: 10.1093/cercor/bhw222 [Epub ahead of print].

Weng, L., Xie, Q., Zhao, L., Zhang, R., Ma, Q., Wang, J., et al. (2017). Abnormal structural connectivity between the basal ganglia, thalamus, and frontal cortex in patients with disorders of consciousness. *Cortex* 90, 71–87. doi: 10.1016/j.cortex.2017.02.011

Whyte, J., and Myers, R. (2009). Incidence of clinically significant responses to zolpidem among patients with disorders of consciousness: a preliminary placebo controlled trial. *Am. J. Phys. Med. Rehabil.* 88, 410–418. doi: 10.1097/PHM.0b013e3181a0e3a0

Whyte, J., Rajan, R., Rosenbaum, A., Katz, D., Kalmar, K., Seel, R., et al. (2014). Zolpidem and restoration of consciousness. *Am. J. Phys. Med. Rehabil.* 93, 101–113. doi: 10.1097/PHM.0000000000000069

Wischnewski, M., Engelhardt, M., Salehinejad, M. A., Schutter, D. J. L. G., Kuo, M.-F., and Nitsche, M. A. (2018). NMDA receptor-mediated motor cortex plasticity after 20 Hz transcranial alternating current stimulation. *Cereb. Cortex* doi: 10.1093/cercor/bhy160 [Epub ahead of print].

Wojtecki, L., Petri, D., Elben, S., Hirschmann, J., Yelnik, J., Eickhoff, S., et al. (2014). Modulation of central thalamic oscillations during emotional-cognitive processing in chronic disorder of consciousness. *Cortex* 60, 94–102. doi: 10.1016/j.cortex.2014.09.007

Wu, X., Zhang, J., Cui, Z., Tang, W., Shao, C., Hu, J., et al. (2018). White matter deficits underlying the impaired consciousness level in patients with disorders of consciousness. *Neurosci. Bull.* 34, 668–678. doi: 10.1007/s12264-018-0253-3

Xia, X., Bai, Y., Zhou, Y., Yang, Y., Xu, R., Gao, X., et al. (2017). Effects of 10 Hz repetitive transcranial magnetic stimulation of the left dorsolateral prefrontal cortex in disorders of consciousness. *Front. Neurol.* 8:182. doi: 10.3389/fneur.2017.00182

Xie, Y., Zhang, T., and Chen, A. C. N. (2015). Repetitive transcranial magnetic stimulation for the recovery of stroke patients with disturbance of consciousness. *Brain Stimul.* 8, 674–675. doi: 10.1016/j.brs.2015.01.406

Yamamoto, T., Katayama, Y., Kobayashi, K., Oshima, H., Fukaya, C., and Tsubokawa, T. (2010). Deep brain stimulation for the treatment of vegetative state. *Eur. J. Neurosci.* 32, 1145–1151. doi: 10.1111/j.1460-9568.2010.07412.x

Yu, Y.-T., Yang, Y., Wang, L.-B., Fang, J.-L., Chen, Y.-Y., He, J.-H., et al. (2017). Transcutaneous auricular vagus nerve stimulation in disorders of consciousness monitored by fMRI: the first case report. *Brain Stimul.* 10, 328–330. doi: 10.1016/j.brs.2016.12.004

Zhang, Y., Song, W., Du, J., Huo, S., Shan, G., and Li, R. (2017). Transcranial direct current stimulation in patients with prolonged disorders of consciousness: combined behavioral and event-related potential evidence. *Front. Neurol.* 8:620. doi: 10.3389/fneur.2017.00620

Zheng, Z. S., Reggente, N., Lutkenhoff, E., Owen, A. M., and Monti, M. M. (2017). Disentangling disorders of consciousness: insights from diffusion tensor imaging and machine learning. *Hum. Brain Mapp.* 38, 431–443. doi: 10.1002/hbm.23370

Conflict of Interest Statement: The authors declare that the research was conducted in the absence of any commercial or financial relationships that could be construed as a potential conflict of interest.

frontiers in Neuroscience

TECHNOLOGY REPORT
published: 12 April 2019
doi: 10.3389/fnins.2019.00266

Cerebellar Lobules Optimal Stimulation (CLOS): A Computational Pipeline to Optimize Cerebellar Lobule-Specific Electric Field Distribution

Zeynab Rezaee and Anirban Dutta*

Department of Biomedical Engineering, University at Buffalo, Buffalo, NY, United States

OPEN ACCESS

Edited by:
Michele Giugliano,
University of Antwerp, Belgium

Reviewed by:
Marta Parazzini,
Italian National Research Council (CNR), Italy
De-Lai Qiu,
Yanbian University, China

****Correspondence:***
Zeynab Rezaee
zeynabre@buffalo.edu

Specialty section:
This article was submitted to Neural Technology, a section of the journal Frontiers in Neuroscience

Received: *01 July 2018*
Accepted: *06 March 2019*
Published: *12 April 2019*

Citation:
Rezaee Z and Dutta A (2019) Cerebellar Lobules Optimal Stimulation (CLOS): A Computational Pipeline to Optimize Cerebellar Lobule-Specific Electric Field Distribution. Front. Neurosci. 13:266. doi: 10.3389/fnins.2019.00266

Objective: Cerebellar transcranial direct current stimulation (ctDCS) is challenging due to the complexity of the cerebellar structure which is reflected by the well-known variability in ctDCS effects. Therefore, our objective is to present a freely available computational modeling pipeline for cerebellar lobules' optimal stimulation (CLOS).

Methods: CLOS can optimize lobule-specific electric field distribution following finite element analysis (FEA) using freely available computational modeling pipelines. We modeled published ctDCS montages with 5 cm × 5 cm anode placed 3 cm lateral to inion, and the same sized cathode was placed on the: (1) contralateral supra-orbital area (called Manto montage), and (2) buccinators muscle (called Celnik montage). Also, a published (3) 4×1 HD-ctDCS electrode montage was modeled. We also investigated the effects of the subject-specific head model versus Colin 27 average head model on lobule-specific electric field distribution. Three-way analysis of variance (ANOVA) was used to determine the effects of lobules, montage, and head model on the electric field distribution. The differences in lobule-specific electric field distribution across different freely available computational pipelines were also evaluated using subject-specific head model. We also presented an application of our computational pipeline to optimize a ctDCS electrode montage to deliver peak electric field at the cerebellar lobules VII-IX related to ankle function.

Results: Eta-squared effect size after three-way ANOVA for electric field strength was 0.05 for lobule, 0.00 for montage, 0.04 for the head model, 0.01 for lobule*montage interaction, 0.01 for lobule* head model interaction, and 0.00 for montage*head model interaction. The electric field strength of both the Celnik and the Manto montages affected the lobules Crus I/II, VIIb, VIII, and IX of the targeted cerebellar hemisphere where Manto montage had a spillover to the contralateral cerebellar hemisphere. The 4×1 HD-ctDCS montage primarily affected the lobules Crus I/II of the targeted cerebellar

hemisphere. All three published ctDCS montages were found to be not optimal for ankle function (lobules VII-IX), so we presented a novel HD-ctDCS electrode montage.

Discussion: Our freely available CLOS pipeline can be leveraged to optimize electromagnetic stimulation to target cerebellar lobules related to different cognitive and motor functions.

Keywords: cerebellum, MRI, non-invasive brain stimulation (NIBS), neuromodulation, finite element analysis

INTRODUCTION

Transcranial direct current stimulation of the cerebellum (ctDCS) is a painless non-invasive technique where a weak direct current (i.e., up to 2 mA) is delivered through a scalp electrode overlying the cerebellum (van Dun et al., 2016) which is being explored as a viable intervention for patients with neurological conditions (Grimaldi et al., 2016). This is based on the evidence that cerebellar architecture supports the computations required by the feedforward prediction model from animal studies as well as from studies on patients with cerebellar dysfunction (Ebner, 2013). Specifically, Purkinje cell firing has several of the characteristics of a forward internal model (Ebner, 2013) which is the main target of ctDCS (Galea et al., 2009). For example, Galea and colleagues proposed that ctDCS produces polarity specific effects by polarizing the Purkinje cells thereby affecting the activity in the deep cerebellar output nuclei (Galea et al., 2009). Cerebellar role in modulating sensory processing has also been demonstrated (Popa et al., 2013), which can explain the ctDCS effects on distant plasticity in human cortical areas (i.e., the motor cortex) (Grimaldi et al., 2016). Besides the well-recognized role of the cerebellum in motor function, there is also a concurrent role in cognitive function (Koziol et al., 2014). Most recent works show that cerebellar lobules IV, V, VI, and only a part of VIII is related to motor functions (van Dun et al., 2018) while lobules VI, VII, VIIIa, Crus I and Crus II (Stoodley et al., 2012; Hartzell et al., 2016; Küper et al., 2016; Koppelmans et al., 2017; van Dun et al., 2018) are involved in non-motor functions. Also, Crus I and II have been shown to have no anatomical connections to motor cortex but show projections to the prefrontal cortex (Buckner et al., 2011). Therefore, as we explore ctDCS to affect motor control, cognition, learning and emotions (Ferrucci and Priori, 2014), computation of lobule-specific electric field distribution based on subject-specific head model is necessary for rational dosage considerations (Buckner et al., 2011; Mottolese et al., 2013) e.g., in cerebellar motor syndrome or cognitive performance (Stoodley and Schmahmann, 2009).

Rational dosing of ctDCS needs to account for the very high concentration of neurons with highly organized distribution in the cerebellar cortex. Here, modulation of the activity in the cerebellar neurons with the electric field is the goal (Ferrucci et al., 2015) but is very challenging due to the extreme folding of the cerebellar cortex. Therefore, ctDCS efficacy appears to be limited at present (Ferrucci et al., 2016). It is postulated that the efficacy can be improved significantly by optimizing the ctDCS electrode montage to align the electric field $\vec{E}$ parallel to the somatodendritic axis (usually radial to gray matter surface for Purkinje cells) that can modulate synaptic efficacy consistent with somatic polarization, with depolarization facilitating synaptic efficacy (Bikson, 2016). Such optimization will require determination of the lobule-specific electric field distribution, $\vec{E}$, concerning the cerebellar surface to optimize either radial (normal) or tangential components, as necessary. Furthermore, a systematic investigation of subject-specific lobule-specific electric field distribution based on a cerebellar atlas is necessary to investigate the effects of radial (normal) or tangential components of electric field on behavioral and neurophysiological test outcomes. Here, it is critical that the ctDCS electric field is limited to the cerebellar lobules under investigation without spillover to non-targeted regions. However, lobule-specific analysis of subject-specific electric field distribution during ctDCS was not found in the literature (Parazzini et al., 2014; Priori et al., 2014; Fiocchi et al., 2016).

Therefore, the main objective of this technology report is to present a freely available computational pipeline that allows visualization of the lobule-specific electric field distribution during ctDCS. Furthermore, we present an application where the pipeline can be used for the optimization of the lobule-specific electric field distribution which is important to specifically target the architecture of the cerebellar cortex (Stoodley and Schmahmann, 2009). Here, the earliest and the most studied mechanism based on the architecture of the cerebellar cortex is Marr-Albus-Ito hypothesis that assigns specific functions to the climbing fiber-Purkinje cell and the mossy fiber-granule cell-parallel fiber-Purkinje cell circuits (Popa et al., 2016). So, the relative magnitude of the electric field $\vec{E}$ needs to be quantified in the subject-specific head model (Rahman et al., 2013; Saturnino et al., 2018) to investigate the effects on the climbing fiber-Purkinje cell during ctDCS (Summers et al., 2018). Here, the challenges with lobule-specific targeting of ctDCS include high conductivity of the cerebrospinal fluid (CSF) and extreme folding of the cerebellar cortex (Fiocchi et al., 2017). The goal is an optimal electrode placement, e.g., with more focal high-definition (HD) ctDCS montages (Fiocchi et al., 2017), that can deliver the electric field toward deeper targets by taking advantage of the high conductivity of the CSF and the interhemispheric fissure. Moreover, computational modeling (Parazzini et al., 2014; Priori et al., 2014; Fiocchi et al., 2016) of lobule-specific electric field distribution is important to address the inter-subject variability in the ctDCS effects that is necessary to address for clinical translation (Ferrucci et al., 2016). This is also crucial since ctDCS effects were recently said to be mediated by mechanisms other

than cerebellar excitability changes (Grimaldi et al., 2016) where non-focal electric field with two-electrode montages was said to affect brain areas other than cerebellum.

In this technology report, we present a cerebellar lobule's optimal stimulation (CLOS) pipeline that creates a subject-specific head model based on magnetic resonance imaging (MRI) and then computes the electric field distribution in the cerebellar lobules. Our main contribution is in providing an approach for the isolation of the cerebellum and its lobules based on Spatially Unbiased Infratentorial Template for the Cerebellum (SUIT) atlas (Diedrichsen et al., 2009) that allowed us to investigate the lobule-specific electric fields following finite element analysis (FEA) using different freely available computational pipelines including SimNIBS (Saturnino et al., 2018) and ROAST (Huang et al., 2017). We have adapted the SUIT isolation and activation visualization scripts, which are commonly used to analyze functional MRI activation maps, to analyze the lobule-specific electric fields. Our SUIT–based approach to determine cerebellar lobule-specific electric field distribution can be applied to FEA results for transcranial magnetic stimulation (TMS) too. Here, we found it important to study the effects of subject-specific head model versus Colin 27 average head model on lobule-specific electric field distribution across different freely available computational (FEA) modeling pipelines. To show that visualization of cerebellar lobule-specific electric field distribution can provide further insights, we applied our pipeline to analyze previously published (Abadi and Dutta, 2017) healthy human experimental results during visuomotor learning of myoelectric visual pursuit. During our analysis, we found that the published ctDCS montages used in the study (Abadi and Dutta, 2017) were not optimal for the ankle motor task. For example, posterior and inferior cerebellum (i.e., lobules VI-VIII) is mainly susceptible to the available ctDCS montages (Grimaldi et al., 2016) which may be the reason why recent studies failed to demonstrate a significant association of motor performance and changes in neurophysiological measures after ctDCS (Summers et al., 2018). Therefore, we applied our CLOS pipeline to optimize multi-electrode ctDCS montage to target the cerebellar lobules shown related to ankle functions (Buckner et al., 2011; van Dun et al., 2018). Here, it is important to investigate the effects of the selection of the freely available computational (FEA) modeling pipeline on the lobule-specific electric field distribution across ctDCS montages which is presented in this technology report.

MATERIALS AND METHODS

We developed the cerebellar lobule's optimal stimulation (CLOS) pipeline using freely available software packages that are easily accessible worldwide to facilitate clinical translation of tDCS. Using our CLOS pipeline, we investigated two common ctDCS montages (Grimaldi et al., 2014, 2016) with the anode placed over the right cerebellum, and (1) the cathode placed over the right buccinator muscle – called Celnik montage henceforth, (2) the cathode placed on the contralateral supraorbital area – called Manto montage henceforth. We also investigated a recently published 4 × 1 high-definition (HD) ctDCS montage (Doppelmayr et al., 2016). Our computational pipeline leveraged SUIT, which is one of the automated algorithms developed explicitly for cerebellum segmentation (Diedrichsen, 2006), and is a freely available SPM [Statistical Parametric Mapping (SPM - Statistical Parametric Mapping)] toolbox for functional MRI data analysis. In this toolbox, a probabilistic atlas of the cerebellar nuclei, a cerebellar cortical parcellation atlas in MNI (Montreal Neurological Institute) space, and SUIT template are available. Therefore, we used SUIT SPM toolbox for isolation of cerebellar lobules where SUIT provided an improved and fine-grained exploration, registration and anatomical detail of the cerebellum for structural and electric field images. Since our SUIT–based approach can be applied to FEA results from different freely available FEA software so we compared the lobule-specific electric field results between the freely available SimNIBS pipeline (Opitz et al., 2015) and the Realistic volumetric-Approach to Simulate Transcranial Electric Stimulation (ROAST) pipeline (Huang et al., 2017) using subject-specific head model.

CLOS Pipeline

MRI Data Acquisition and Subject-Specific Head Model Creation

The first step in creating an anatomically accurate subject-specific head model is the segmentation of structural magnetic resonance images (MRI). The individual head model was constructed using MR images taken from a healthy volunteer in accordance with the Declaration of Helsinki - a statement of ethical principles for medical research involving humans. For research participation as well as for the publication of this case report including participant's identifiable information, written informed consent was obtained from the subject at the University at Buffalo. The subject did not have any history of neurological or psychiatric diseases. Images were taken from 3 Tesla Magnetic Resonance Imaging (MRI) system (Toshiba Vantage) at the University at Buffalo Clinical and Translational Science Institute using a sixteen multichannel receiver head coil. Two T1-weighted images (with and without fat suppression) were acquired for the subject (Windhoff et al., 2013). MR sequence consisted of the following parameters: MPRAGE, 192 slices, matrix size = 256 × 256, Flip/Flop angle = 8/0, TR/TE = 6.2/3.2. Also, two T2-weighted images (with and without fat suppression) were acquired for the subject with the sequence of 30 slices, matrix size of 256 × 256, flip/flop angle of 110/150 degree, and TR/TE = 11990/108. From these four MR images, a tetrahedral volume mesh of the head was created using "mri2mesh" script which is provided in the SimNIBS package (Windhoff et al., 2013). The "mri2mesh" is based on four open source software; FreeSurfer[1], FSL[2], Meshfix[3], and Gmsh[4]. This script integrates all these software into a single pipeline for mesh generation from MR images (Windhoff et al., 2013). After segmentation using FSL and FreeSurfer, five tissues were modeled by the volume mesh; Skin, Skull,

[1]https://surfer.nmr.mgh.harvard.edu/

[2]https://fsl.fmrib.ox.ac.uk/fsl/fslwiki

[3]https://github.com/MarcoAttene/MeshFix-V2.1

[4]http://gmsh.info/

Cerebrospinal Fluid, Gray Matter, and White Matter. Different brain tissues for the volume mesh components were modeled as different volume conductors in SimNIBS with their specific conductivity (Windhoff et al., 2013), as shown in **Table 1**. We also used Colin27 average brain (Holmes et al., 1998), which is the stereotaxic average of 27 T1-weighted MRI scans of the same individual, to create another head model (Guhathakurta and Dutta, 2016) for comparison.

Published Electrode Montages for ctDCS

In order to investigate lobule-specific electric field distribution from published ctDCS montages (Galea et al., 2009; Grimaldi and Manto, 2013; Doppelmayr et al., 2016), electrode positions were defined as follows:

(1) Celnik montage (Galea et al., 2009): 5 cm × 5 cm anode was placed over the right cerebellum, 1 cm below and 3 cm lateral to the inion (Iz, 10/10 EEG system), and the 5cm × 5cm cathode was placed over the right buccinator muscle for anodal ctDCS with 2 mA direct current.
(2) Manto montage (Grimaldi and Manto, 2013): 5 cm × 5 cm anode was placed over the right cerebellum, 1 cm below and 3 cm lateral to the inion (Iz, 10/10 EEG system), and the 5 cm × 5 cm cathode was placed on the contralateral supraorbital area (FP2, 10/10 EEG system) for anodal ctDCS with 2 mA direct current.
(3) HD-ctDCS 4×1 montage (Doppelmayr et al., 2016): 3.14 cm^2 anode was placed above the cerebellum 10% below Oz (10/10 EEG system) in the midline, and four 3.14 cm^2 cathodes were placed at Oz, O2, P8, and PO8 (10/10 EEG system) for anodal ctDCS with 1 mA direct current.

We investigated the lobule-specific electric field of anodal ctDCS due to the three electrode montages given above using the subject-specific head model as well as the Colin27 head model (Holmes et al., 1998; Guhathakurta and Dutta, 2016).

Finite Element Analysis of ctDCS Using SimNIBS

Finite element method was used to solve the quasistatic approximation for Maxwell's equation, $\nabla \cdot (\sigma \nabla \Phi) = 0$ in Ω [called the Laplace equation (Griffiths, 2017)], where $\Phi$is a potential and σ is the conductivity tensor in the volume conductor Ω. The solution to the Laplace equation is unique if the electric field (or, equivalently, the current density) is specified at all the locations. The applied ctDCS current density $\vec{J_e}$at the electrodes is normal ($\hat{n}$) to the boundary surface Γso ($\sigma \nabla \Phi \cdot \hat{n} = \vec{J}_e$) at the electrodes while ($\sigma \nabla \Phi \cdot \hat{n} = 0$) otherwise on Γ – a mixed boundary condition. Here, finite element analysis (FEA) was conducted on the subject-specific head model as well as the Colin27 average head model (Holmes et al., 1998; Guhathakurta and Dutta, 2016) to estimate the ctDCS induced electric field in the brain tissues. The anodal ctDCS was delivered using two 5 cm × 5 cm electrodes and a direct current of 2 mA. In all the simulations, the voxel size was 1 mm^3. The anode and the cathode injected the specified amount of current (source) in the volume conductor, i.e., the head model. The electrodes were modeled as a saline-soaked sponge placed at a given scalp location using 10/10 EEG system (Giacometti et al., 2014). We analyzed the head-model for electric field distribution using the SimNIBS pipeline (Windhoff et al., 2013). Following SimNIBS FEA, we used SUIT to isolate the cerebellum in SPM[5] package in Matlab (The Mathworks Inc., United States). Subject's T1 images were reoriented into LPI (Neurological) orientation. The isolation map was manually verified in an image viewer (MRIcron). After the isolation, the cerebellum was normalized to the SUIT atlas template using the cropped image and the isolation map. A non-linear deformation map to the SUIT template is the result of the normalization step. After the normalization, we could either resample the image into SUIT space or into the subject space. The latter was chosen for our subject-specific analysis to resample the probabilistic atlas of the cerebellum into the space of the individual subject. We customized msh2nifti script[6] to save the electric field distribution in the three direction – Ex, Ey, and Ez – from SimNIBS FEA results, as shown by the head model in **Figure 2**. The msh2nifti script created NIfTI (Neuroimaging Informatics Technology Initiative) images of the electric field distribution that were resliced using the individual mask and deformation matrix found in the previous step – see the workflow in the **Figure 1** using the SUIT toolbox to extract the cerebellar regions (or, lobules). The post-processing of the electric field distribution over the tetrahedral volume mesh and its visualization was performed in Gmsh (Geuzaine and Remacle, 2009). The volume of the cerebellar lobules, defined by the SUIT atlas (Diedrichsen, 2006), was used for the extraction of the lobule-specific electric field distribution in Matlab (The Mathworks Inc., United States). To visualize electric field distribution in cerebellar lobules, the flatmap script in SUIT toolbox was used in Matlab (The Mathworks Inc., United States), which provided a flat representation of the cerebellum after volume-based normalization as described by Diedrichsen (2006).

TABLE 1 | Electrical conductivity.

Component	Electrical conductivity (S m^{-1})
Scalp	0.465
Skull	0.010
CSF	1.654
Gray matter	0.276
White matter	0.126

Statistical Tests for the Effects of Lobules, Montage, and Head Model on the Lobule-Specific Electric Field Distribution

For group analysis of the lobule-specific electric field distribution, an averaging of the SUIT flatmap across subjects is possible. Here, the electric field distribution across lobules is important to determine the focality of different ctDCS montages. We performed the analysis of variance (ANOVA) of the cerebellar

[5]http://www.fil.ion.ucl.ac.uk/spm/
[6]https://github.com/ncullen93/mesh2nifti

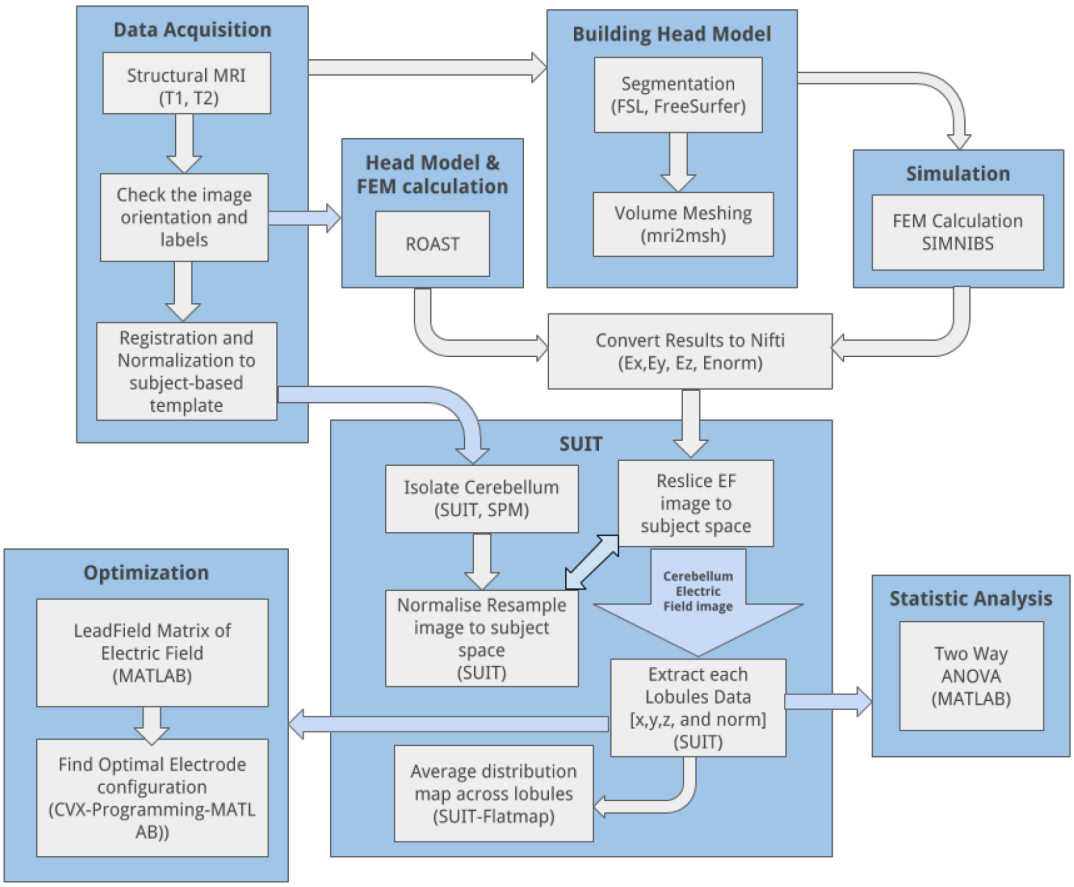

FIGURE 1 | CLOS pipeline: overall workflow to visualize and optimize the electric field distribution across cerebellar lobules during cerebellar transcranial direct current stimulation.

electric field distribution to investigate the factors of interest – lobules (28 from SUIT), montages (Celnik, Manto, HD-ctDCS), head model (Colin27, subject-specific), and their interactions. Also, two-way ANOVA of the cerebellar electric field distribution was conducted with the subject-specific head model to investigate the factors of interest – lobules (28 from SUIT), montages (Celnik, Manto, HD-ctDCS). Post-hoc multiple comparisons of the means (95% significance) were conducted with Bonferroni critical values. In the Generalized Linear Model (GLM), the proportion of the total variability in the dependent variable that is accounted for by the variation in the independent variable was found using the eta-squared effect size measure (Lakens, 2013).

Finite Element Analysis of ctDCS Using ROAST

We used another freely available FEA pipeline called Realistic volumetric Approach to Simulate Transcranial Electric Stimulation (ROAST) (Huang et al., 2018) to compare its lobule-specific electric field distribution with that from the SimNIBS pipeline (see Finite Element Analysis of ctDCS Using SimNIBS). We constructed a subject-specific head model using the same T1- and T2-weighted MRI from Section "Finite Element Analysis of ctDCS Using SimNIBS." The creation of the tetrahedral volume mesh of the head and solving the finite element model were implemented by ROAST. The pipeline is a Matlab script based on three open source software: Statistical Parametric Mapping (SPM) (Penny et al., 2011), Iso2mesh (Fang and Boas, 2009), and getDP (Dular et al., 1998). ROAST provided results for electric field distribution as NIfTI images which were processed in our pipeline to isolate the cerebellum for the analysis of the lobule-specific electric field distribution, as described in Section "Finite Element Analysis of ctDCS Using SimNIBS."

Application of the Computational Pipeline to Analyze Experimental Data From a Healthy Human Study

In our published healthy human study (Abadi and Dutta, 2017), 15 healthy volunteers participated in accordance with the Declaration of Helsinki. Ethics approval was obtained at the University Medical Center, Goettingen, Germany. In this study, two-electrode anodal ctDCS montages were investigated for the application of anodal transcranial direct current stimulation over the cerebellar hemisphere during visuomotor learning of myoelectric visual pursuit using the electromyogram (EMG) from ipsilateral gastrocnemius (GAS) muscle. This study was

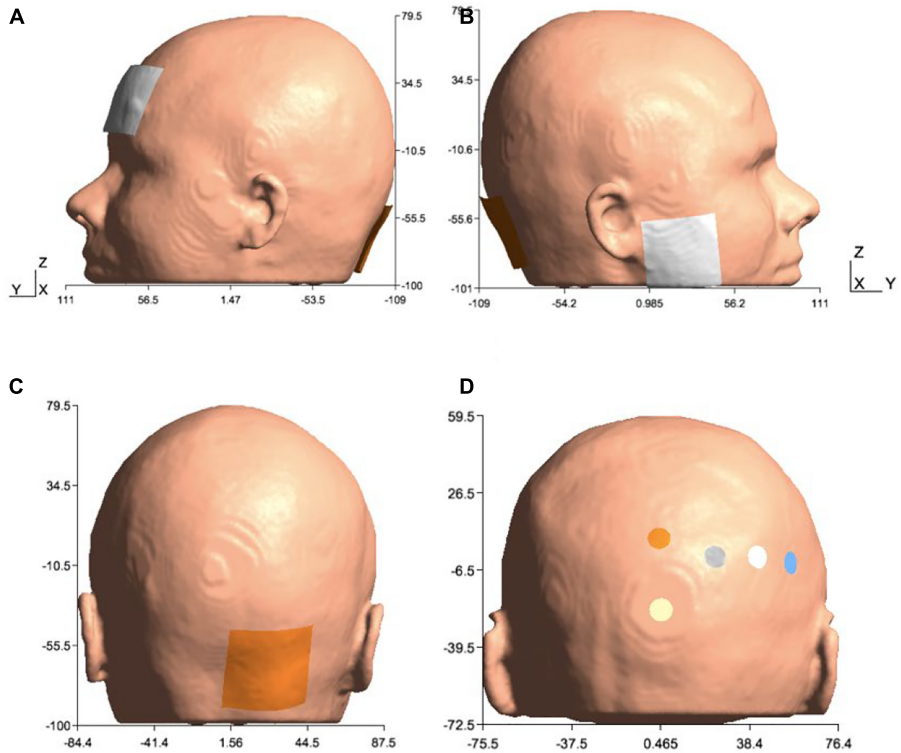

FIGURE 2 | Electrode configurations: **(A)** Manto montage: anode was placed over the right cerebellum, 1 cm below and 3 cm lateral to the inion (Iz, 10/10 EEG system), and the cathode was placed on the contralateral supraorbital area (FP2, 10/10 EEG system), **(B)** Celnik montage: anode was placed over the right cerebellum, 1 cm below and 3 cm lateral to the inion (Iz, 10/10 EEG system) and cathode was placed over the right buccinator muscle, **(C)** Anode was placed over the right cerebellum, 1 cm below and 3 cm lateral to the inion (Iz, 10/10 EEG system) for Manto and Celnik Montages, and **(D)** 4×1 HD-tDCS montage: anode was placed above the cerebellum 10% below Oz (10/10 EEG system) in the midline, and four cathodes were placed at Oz, O2, P8, and PO8 (10/10 EEG system).

conducted to investigate the effects of 15min of anodal ctDCS (current density = 0.526 A/m^2; electrode size 5 cm × 5 cm) using Celnik and Manto montage on the response time (RT) and root mean square error (RMSE) during isometric contraction of the dominant GAS for myoelectric visual pursuit, i.e., 'ballistic EMG control' (Dutta et al., 2014; see Abadi and Dutta, 2017 for further details). The EMG RT was computed offline as the duration from the instant of visual cursor target cue to the instant when the rectified EMG in a sliding window of 500 ms from the muscle jumped by more than three times of the standard deviation of the resting value. The response accuracy was computed as RMSE between the EMG driven cursor and the cursor target signals during cue presentation. 95% confidence intervals for the parameters were compared for overlap between post-intervention and baseline based on Student's *t*-distribution.

Application of the Computational Pipeline to Optimize ctDCS Montage for Cerebellar Lobules Related to Ankle Function

To calculate the optimal ctDCS electrode configuration to target the cerebellar lobules shown related to motor functions (van Dun et al., 2018), especially ankle function (Buckner et al., 2011), we applied convex optimization (Boyd and Vandenberghe, 2004) in MATLAB (The Mathworks Inc., United States). Convex optimization was previously used by Dmochowski et al. (2011) and Guler et al. (2016) for non-cerebellar targets. We leveraged our computational pipeline to first determine the 'transfer matrix' (or 'lead field matrix') from the electrodes on the scalp to the lobule-specific average electric field. Then, we applied convex optimization to find the electrode montage that minimizes the error from the specified lobule-specific average electric field at cerebellar lobules VII-IX (van Dun et al., 2018).

Computation of the 'Transfer Matrix' or 'Lead Field Matrix' in CLOS Pipeline

Any freely available computational modeling pipeline (see CLOS Pipeline) can be used to solve the quasistatic approximation for Maxwell's equation with a linear approximation of Ohm's law in a purely resistive medium Ω. So, we can write in a matrix form $\vec{E} = LI$ where $\vec{E}$ is the electric field in the brain generated by stimulation currents, I, applied to an electrode array and L is the 'transfer matrix' (or, 'leadfield matrix') that quantifies the electric field generated in the brain for a unit current applied to each of the stimulation electrodes (Dmochowski et al., 2011). Here, the problem of choosing an appropriate stimulation currents I for

the multi-electrode array to shape the induced electric field is similar to the 'beamforming' problem in array signal processing (Dmochowski et al., 2011). Specifically, we formulated a convex optimization problem (Boyd and Vandenberghe, 2004) where we minimized the Euclidean norm of the error between the desired brain activation (i.e., the electric field distribution $\vec{E}$ at cerebellar lobules VII-IX) and the one generated by the stimulation currents (see CLOS Pipeline), i.e., arg $\min_I || \vec{E} - LI||^2$. Due to safety and comfort considerations as well as due to restrictions on our tDCS device (StarStim 8, Neuroelectrics), we had constraints on the maximum injected current. Therefore, the 'leadfield matrix' or 'transfer matrix' is a forward model from the current injection at the scalp electrodes to the electric field in the brain that captured a reduced dimension head model as a Ohmic volume conductor (Dutta and Dutta, 2013). The individual head model in this study was constructed using MR images taken from a healthy volunteer (see MRI Data Acquisition and Subject-Specific Head Model Creation). From these MR images, a tetrahedral volume mesh of the head was created using "headreco" script which is provided in the SimNIBS package (Windhoff et al., 2013; Saturnino et al., 2018). The "headreco" is based on SPM[7] package in Matlab (The Mathworks Inc., United States). Here, all FEA simulations to compute the 'leadfield matrix' or 'transfer matrix' used circular electrodes (1 cm diameter) based on the EGI EEG net-based system[8] with a common cathode at the vertex (Cz) and a direct current of 1 mA. The anode was placed at the EEG locations one by one while the cathode stayed at the vertex (Cz). So, a series of 417 bipolar electrode montages were simulated using our CLOS pipeline (see CLOS Pipeline) and then the 'leadfield matrix' (Dutta and Dutta, 2013) was computed for the 'beamforming' (Dmochowski et al., 2011) to stimulate the cerebellar lobules VII-IX (Buckner et al., 2011; van Dun et al., 2018).

CLOS pipeline (see CLOS Pipeline) was used to compute the average electric field in the three directions (X, Y, Z) in each of the 28 SUIT lobules (Diedrichsen, 2006) as well as at the non-cerebellar brain. For the non-cerebellar brain, the cerebellum was masked, and the electric field across the rest of the brain was averaged. Then, the 'transfer matrix' or the 'lead field matrix' was computed for each direction of the electric field by combining 417 FEA simulations where the mapping was from the 417 scalp locations to the 28 SUIT lobules and the non-cerebellar brain. Here, the possible electrode positions were defined for the whole head coverage by combining the high-density 10-05 EEG locations (Oostenveld and Praamstra, 2001) with the EGI net-based system[9] and extra electrodes from ROAST (Huang et al., 2018). So, we identified a total of 417 scalp locations to consider in our optimization procedure.

Computation of the Optimal Electrode Montage Based on 'lead Field Matrix'

Consider a set of N bipolar electrode montages where the Ohmic relation from the electrode current array, *s* (anode positive current), to the average electric field at a certain lobule, *b*, can be written in a matrix form,

$b = LF \cdot s$ Equation (1)

where

$$b = \begin{bmatrix} b_1 \\ . \\ . \\ . \\ b_{29} \end{bmatrix}$$

and

$$LF = \begin{bmatrix} EF_{S_1,1} & \ldots & EF_{S_N,1} \\ . & . & . \\ . & . & . \\ . & . & . \\ EF_{S_1,29} & \ldots & EF_{S_N,29} \end{bmatrix}$$

Here, LF is the 'lead field matrix' and b_1 to b_{29} are the volume-average electric field at the 28 cerebellar lobules along with the non-cerebellum brain (b_{29}) due to all the N bipolar electrode montages. So, $EF_{S_N,M}$ in LF is the volume-average electric field at M^{th} lobule due to N^{th} anode delivering 1mA. Linear equation 1 allowed us to write the objective function viz. arg $\min_x$ ||LF · x-b||^2 that optimized an appropriate electrode current array, *x*, to minimize the L2-norm of the error, (LF. x-b), given a desired electric field distribution, *b*, across 28 cerebellar lobules and the non-cerebellar brain. The following constraints were considered for *x*:

o Total anodal current is equal to the cathodal current;

$$\sum_{n=1}^{N} x_n = 0$$

o Total anodal and cathodal current magnitude is below a set threshold of 4mA for safety and comfort (i.e., maximum total anodal or cathodal current is 2 mA);

$$\sum_{n=1}^{N} |x_n| \leq 4$$

The convex optimization problem (Boyd and Vandenberghe, 2004) was solved to get a uniform electric field at the cerebellar lobules related to ankle function (Buckner et al., 2011), a.k.a, lobules VII-IX.

RESULTS

Finite Element Analysis of ctDCS Using SimNIBS

Figure 3 shows a higher average electric field strength (magnitude or E_{norm}) at the targeted right cerebellar hemisphere than the left cerebellar hemisphere since the anode was placed over the right cerebellum (lateral to the inion) in both the Celnik and the Manto montages. FEA using SimNIBS showed that the ctDCS electric field magnitude for both the Celnik and the Manto montages could spread to neighboring structures, e.g., the right temporal lobe for the Celnik montage and the left prefrontal cortex for

[7]http://www.fil.ion.ucl.ac.uk/spm/

[8]https://www.egi.com

[9]https://www.egi.com

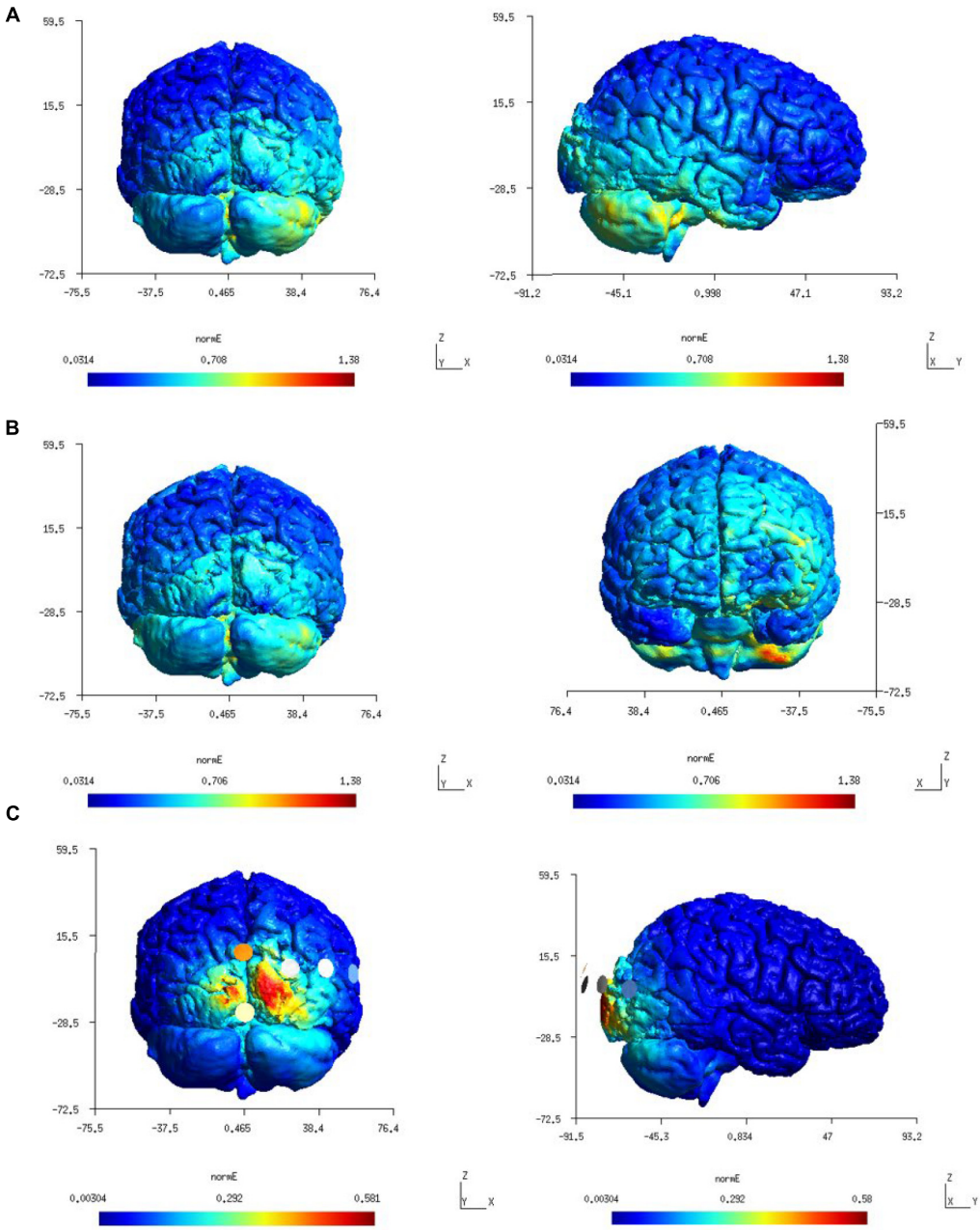

FIGURE 3 | (A) first-row panels (color scale: 0.0314–1.38 V/m) – electric field (Enorm) distribution for Celnik montage which was found confined to the right hemisphere. **(B)** second-row panels (color scale: 0.0314–1.38 V/m) – electric field (Enorm) distribution for the Manto montage at the right cerebellum and left prefrontal cortex. **(C)** third-row panels (color scale: 0.00304–0.581 V/m) – electric field (Enorm) distribution for the 4×1 HD-tDCS montage.

the Manto montage, as shown in **Figures 3A,B**. Moreover, ctDCS electric field strength for the 4×1 HD-ctDCS montage proposed by Doppelmayr et al. (2016) can spread to the occipital lobe, as shown in **Figure 3C**. Here, the central anode for 4×1 HD-ctDCS was placed 10% below the inion, but the cathodes were located at Oz, O2, P8, and PO8 which are partly on the right occipital lobe.

We further analyzed the SimNIBS FEA results using our SUIT-based computational pipeline to compute lobule-specific electric field distribution. The SUIT flat map results for E_x, E_y, E_z, and E_{norm} are shown in **Figure 4A** (and the volume-averaged quantitative values are presented in the **Supplementary Tables 1–3** of the **Supplementary Material**). E_y, which is approximately normal to the scalp surface at the anode, has the highest strength (maximum 0.6 V/m) while E_x and E_z have comparable strength (maximum 0.3 V/m). The SUIT flat map results for E_{norm} (in **Figure 4A**) showed that the Celnik and Manto montages primarily affected the Crus I/II, VIIb, VIII, and IX of the targeted right cerebellar hemisphere. However, Manto

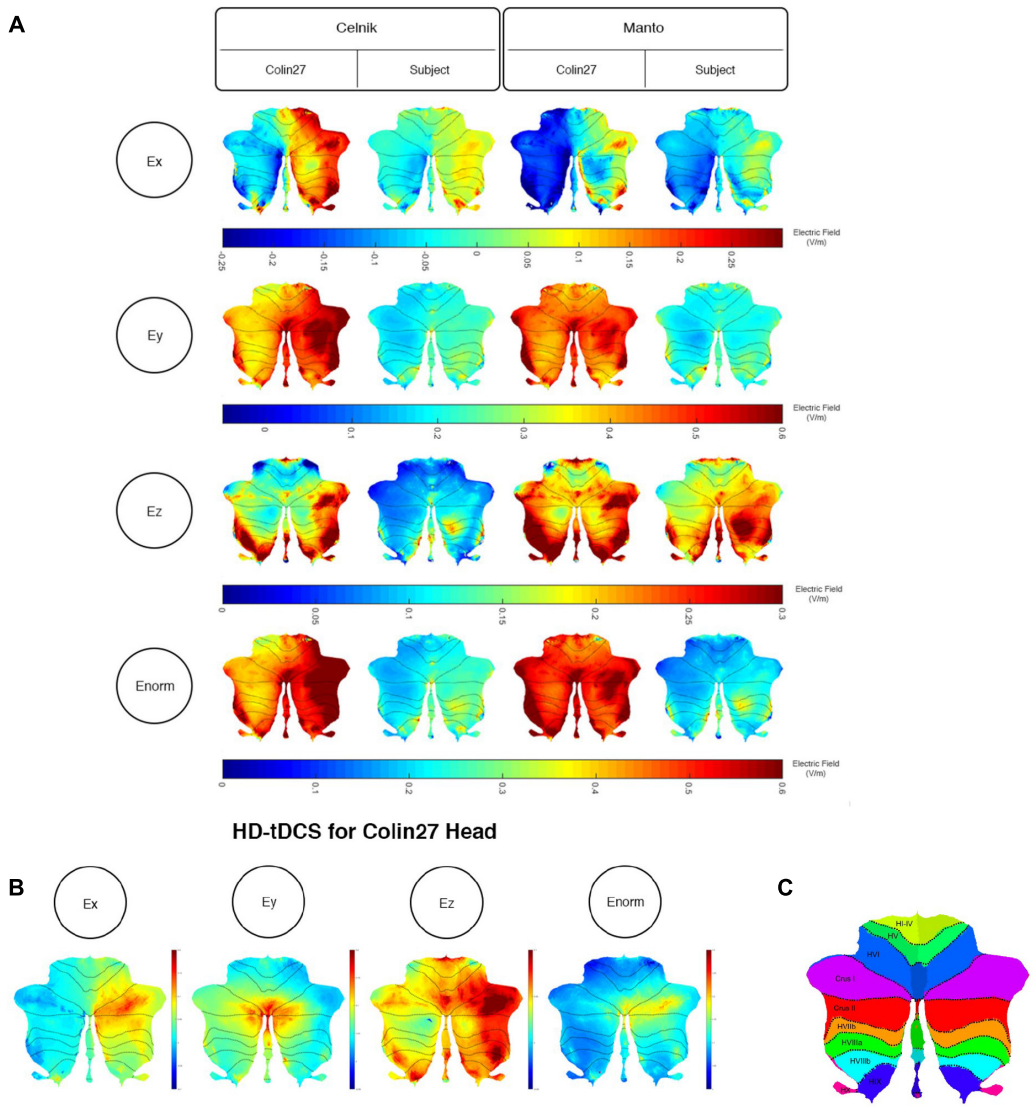

FIGURE 4 | (A) Comparison between the SimNIBS outcomes for Celnik and Manto Montages on Colin27 and subject-specific head model. Electric field distribution (Ex, Ey, Ez, and Enorm) of Celnik and Manto montages for Colin27 Head and Subject-specific head model were visualized in SUIT toolbox using flatmap. First row: Color Scale of –0.25–0.3 V/m – Electric field distribution (Ex); second row: Color Scale of –0.05–0.6 V/m – Electric field distribution (Ey); third row: Color Scale of 0–0.3 V/m – Electric field distribution (Ez); fourth row: Color Scale of 0–0.6 V/m – Electric field distribution (Enorm). **(B)** Electric field distribution of 4×1 HD-tDCS montage for Colin27 head model: Ex (color scale: –0.02 to 0.06 V/m), Ey (color scale: 0–0.18 V/m), Ez (color scale: 0–0.5 V/m), and Enorm (color scale: 0–0.15 V/m). **(C)** SUIT lobules (Diedrichsen et al., 2009).

montage had a more spillover to the contralateral left cerebellar hemisphere than the Celnik montage (see **Supplementary Tables 1–3** of the **Supplementary Material**). Also, When compared with the Colin27 head model, our subject-specific head model resulted in an overall lower magnitude for the electric field distribution – an effect of the head model shown in **Figure 4A**. Here, **Figure 4A** also shows the subject-specific differences in the lobule-specific electric field distribution when compared to the Colin27 head model. This demonstrated the importance of subject-specific optimization of the electrode montage. **Figure 4B** showed that the 4×1 HD-ctDCS montage led to more focal electric field strength (E_{norm}) at the Crus I, Crus II of the targeted right cerebellum (see also **Supplementary Table 3** of the **Supplementary Material**), however, the magnitude (E_{norm}) was much lower due to a smaller (1mA) direct current at the anode. Although the current intensity at the anode was lower for 4×1 HD-ctDCS, the current density at the electrode-skin interface was much higher at 0.32 mA/cm^2 when compared to only 0.08 mA/cm^2 for the Celnik and the Manto montages.

In order to investigate the effect of the head model, montage, and lobule on the electric field strength (E_{norm}), we computed

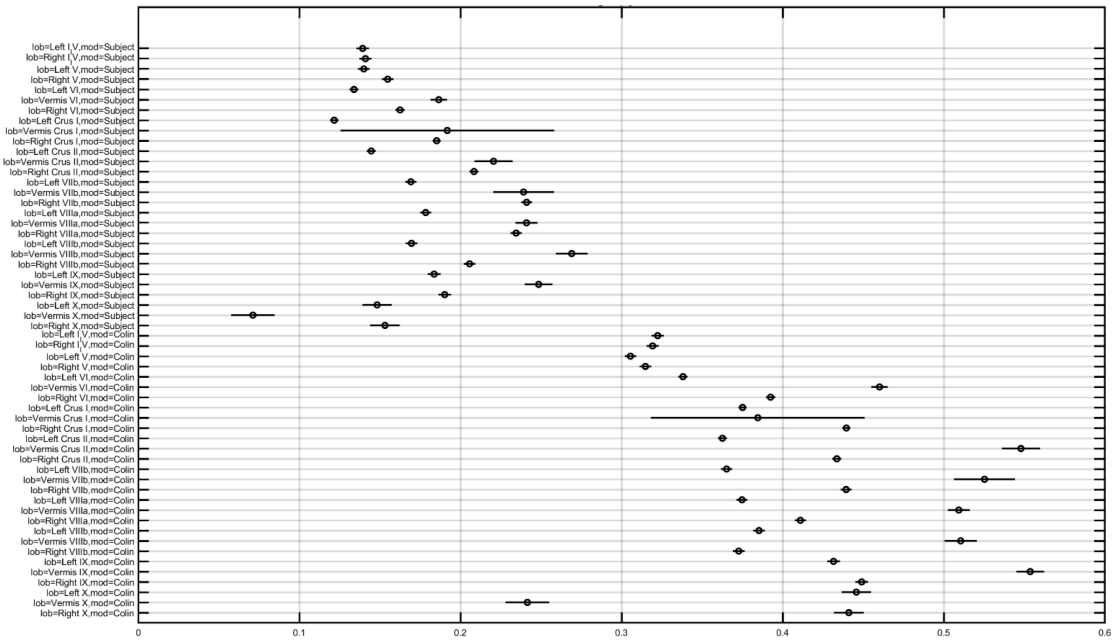

FIGURE 5 | Multiple comparison results for lobule*head model interaction for electric field strength (Enorm is the *X*-axis in the plot in V/m).

a three-way analysis of variance (ANOVA). The ANOVA results were evaluated for statistical significance using the eta-squared effect size measure. We found that the eta-squared effect size was 0.05 for lobule, 0.00 for montage, 0.04 for the head model, 0.01 for lobule*montage interaction, 0.01 for lobule* head model interaction, and 0.00 for montage*head model interaction in case of E_{norm}. The lobule*head model interaction for the electric field strength (Enorm) is shown in **Figure 5**, which shows that the magnitudes are different across head model while the overall electric field (E_{norm}) distribution is comparable. If we consider only the Colin27 head model then the two-way ANOVA of the electric field strength (E_{norm}) and the post-hoc multiple comparisons of the means (95% significance) with Bonferroni critical values showed that the Celnik and Manto montages primarily affected the lobules Crus I/II, VIIb, VIII, IX of the targeted right cerebellar hemisphere – see **Figures 4A**, **5** (and the volume-averaged quantitative values are presented in the **Supplementary Tables 1, 2** of the **Supplementary Material**). Post-hoc multiple comparisons of the means (95% significance) of the E_{norm}, E_x, E_y, and E_z are shown in **Supplementary Figure 1**. Here, the eta-squared effect size measure from two-way ANOVA results was 0.03 for lobule, 0.05 for montage, and 0.02 for interaction in case of E_{norm}; 0.38 for lobule, 0.02 for montage, and 0.07 for interaction in case of E_x; 0.03 for lobule, 0.05 for montage, and 0.02 for interaction in case of E_y; 0.09 for lobule, 0.04 for montage, and 0.04 for interaction in case of E_z. Here, the effect sizes are mostly small except for lobule*montage interaction for Ex and lobule for Ez, which were moderate. Manto montage was found to have a spillover to the contralateral cerebellar hemisphere when compared to Celnik montage. Electric field strength for 4×1 HD-ctDCS primarily affected the lobules Crus I, Crus II of the targeted right cerebellar hemisphere – see **Figure 4B** (also, **Supplementary Figure 1A**). An interesting finding is the mostly opposite direction of the E_x electric field in contralateral (non-targeted hemisphere) cerebellar lobules in the Manto montage when compared to the Celnik montage – see **Figure 4A** (also, **Supplementary Figure 1A** and **Supplementary Table 3**). *Post hoc* multiple comparisons on E_x, E_y, E_z (**Figures 1B–D** in the **Supplementary Material** respectively) also revealed that lobule-specific E_y distribution was different for the 4×1 HD-ctDCS montage when compared to Manto and Celnik montages (as shown in **Supplementary Figure 1C**) where E_y for 4×1 HD-ctDCS primarily targeted the vermis region. The average electric field strength (E_{norm}) across different lobules for Celnik, Manto, and 4×1 HD-ctDCS montages are listed in **Supplementary Tables 1–3**, respectively.

Effects of the Selection of the Freely Available Computational Pipeline on Lobule-Specific Electric Field Distribution Across Different ctDCS Montages

We compared the effect of the selection of freely available computational pipeline – SimNIBS (versions 2.0 and 2.1) and ROAST pipelines – on lobule-specific electric field strength across different ctDCS montages. Since VIIb, VIII, IX are related to the lower-limb movements (Buckner et al., 2011; Mottolese et al., 2013) so **Figure 6** shows that the electric field strength in those lobules can be affected by choice of the computational pipeline to compute the subject-specific electric field distribution. The lobular electric field strength for the same ctDCS montage can show a different up to ± 0.25 (shown by the color scale) for the lobules VIIb, VIII, IX. Here, SimNIBS version 2.0 (S2.0) took much more time (∼8–10 h) when compared to SimNIBS version

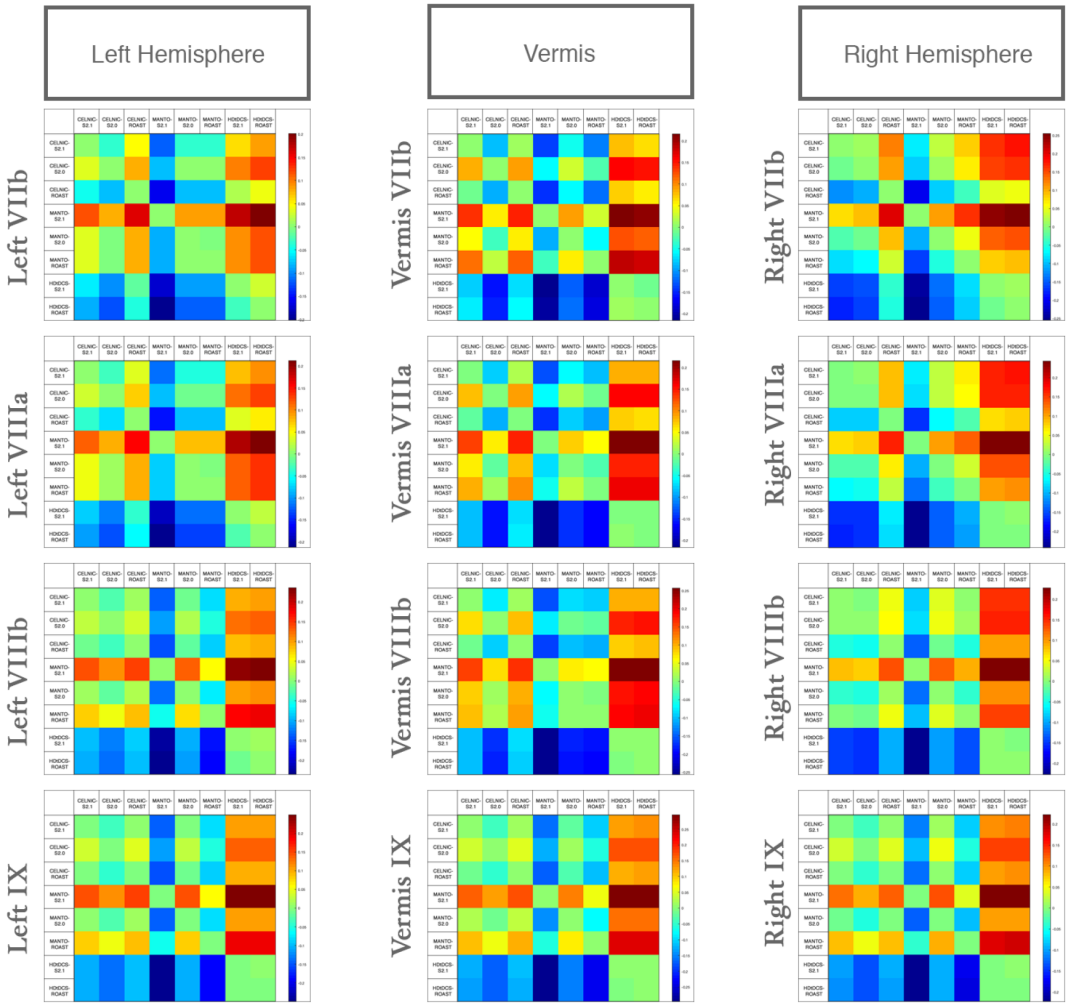

FIGURE 6 | Differences in the lobular electric field strength at VIIb, VIIIa, VIIIb, IX due to different computational pipelines (SimNIBS version 2.1, S2.1; SimNIBS version 2.0, S2.0, and ROAST) for Celnik, Manto, and 4×1 HD-ctDCS montages. Color scale shows the difference across different computational pipelines and ctDCS montages.

2.1 (S2.1) and ROAST (15–30 min) that leveraged the volumetric segmentation from SPM (Huang et al., 2017). Huang et al. (2017) have already shown a high deviation of SimNIBS version 2.0 generated electric field when compared to SPM-generated result in ROAST which was also found in the lobule-specific electric field distribution for the relevant lobules VIIb, VIII, IX shown in **Figure 6** (also see **Supplementary Figures 2**, **3**). Huang et al. (2017) postulated that this difference comes mainly from the two different segmentation approaches, and described the volumetric approach of segmentation in the ROAST pipeline being more realistic of the anatomy when compared to the surface-based segmentation in SimNIBS version 2.0. We found that the components with intersecting surfaces (e.g., gray matter and cerebellum) were better captured by ROAST and SimNIBS version 2.1which led to a better estimate of the bilateral electric field for the Manto montage (see **Supplementary Figures 2**, **3**). These indicate a genuine difference in these two categories of modeling methods where ROAST and SimNIBS version 2.1 performed better (also highlighted by Huang et al., 2017). Importantly, the limitation with SimNIBS version 2.0 is the difficulty in capturing the fine details of the cerebellum which is important for computing the lobule-specific electric field distribution despite the complexity of the cerebellar structure.

Application of the Computational Pipeline to Analyze Experimental Data From Healthy Human Study and Optimization of the ctDCS Montage for Ankle Function

The computational SUIT-based analysis presented in this technology report was used to investigate healthy human anodal ctDCS results during VMT performance (Foerster et al., 2015). Our prior experimental results (Abadi and Dutta, 2017) showed that Manto montage resulted in a statistically significant ($p < 0.05$) decrease in RT post-intervention than baseline when compared to the Celnik montage while Celnik montage resulted in a statistically significant ($p < 0.05$) decrease in RMSE

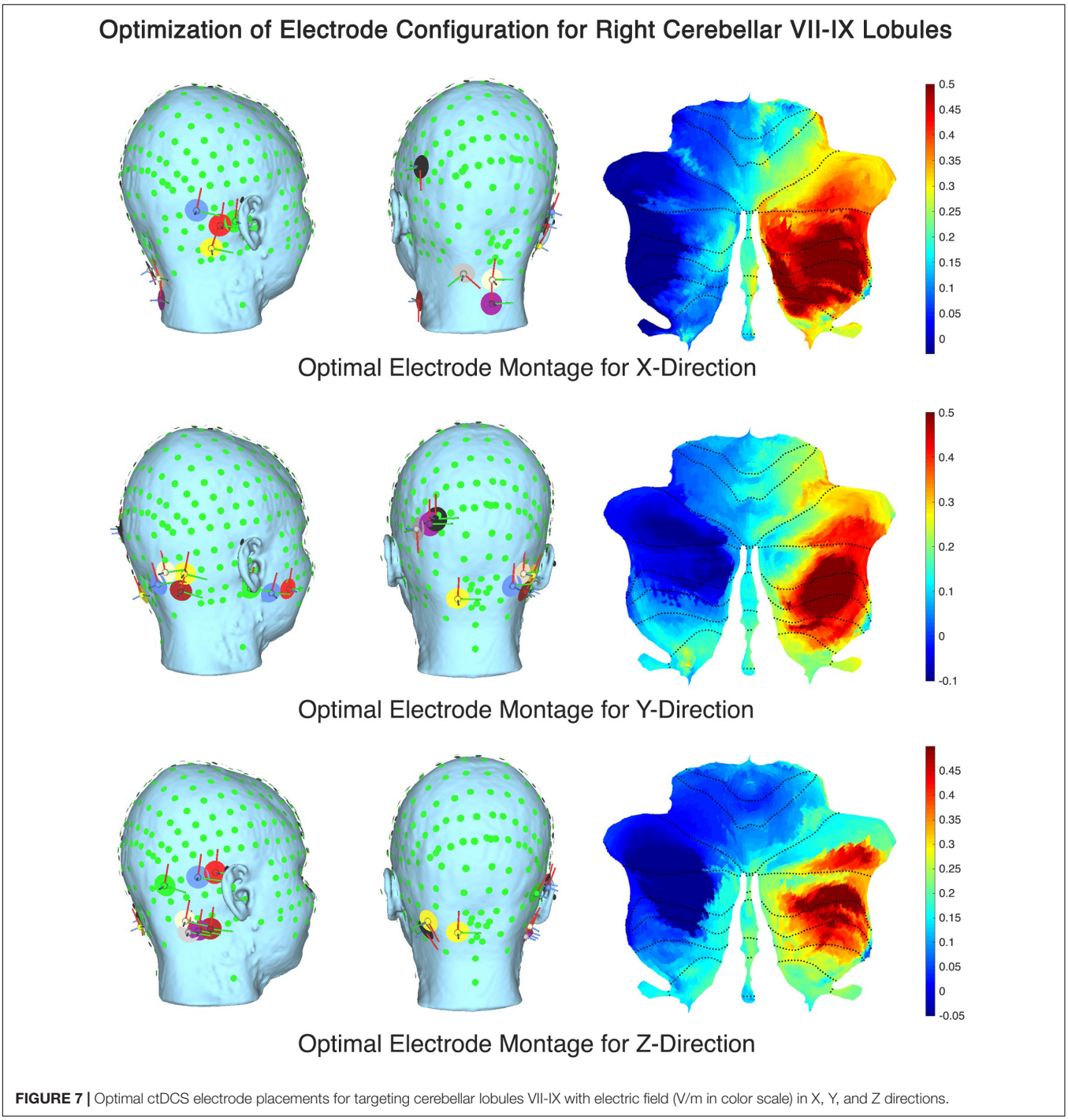

FIGURE 7 | Optimal ctDCS electrode placements for targeting cerebellar lobules VII-IX with electric field (V/m in color scale) in X, Y, and Z directions.

post-intervention than baseline when compared to the Manto montage. Also, ctDCS using Celnik montage has shown to affect the adaptation rate of spatial but not the temporal elements of walking (Jayaram et al., 2012) which is postulated to be related to electric field effects on different cerebellar regions, e.g., vermis (for spatial) versus adjacent hemispheres (for temporal elements) (Jahn et al., 2004). Indeed, we found in our analysis using CLOS pipeline that Celnik montage had a more unilateral effect of the electric field strength (E_{norm}) on the cerebellar hemispheres including vermis, as shown in **Figure 4**. Due to this limitation with published ctDCS montages, we aimed to optimize the ctDCS electrode locations to target ankle function during VMT (Abadi and Dutta, 2017), a.k.a, lobules VII-IX (Buckner et al., 2011). **Figure 7** shows the ctDCS electrode placements to target the cerebellar lobules VII-IX with an electric field (V/m in color scale) in X, Y, and Z directions. The flat map shown on the right panel demonstrates that CLOS optimization was successful where the hotspot with the peak electric field targeted the cerebellar

lobules VII-IX. **Supplementary Table 4** in the **Supplementary Material** presents the quantitative results of the current intensity at different electrode locations to align the electric field in X, Y, and Z directions to target different lobules (Right VIIb-VIII-IX, VIIb-VII-IX, Right CrusII-VIIb-VIII-IX).

DISCUSSION

Our freely available CLOS modeling approach to optimize lobule-specific electric field distribution based on subject-specific MRI provided an insight into healthy human anodal ctDCS results during a VMT performance (Foerster et al., 2015; Abadi and Dutta, 2017). The Celnik and Manto montages in the subject-specific head model affected primarily the lobules Crus II, VIIb, VIII, IX of the targeted cerebellar right hemisphere as shown in **Figure 4**. This was confirmed by the two-way ANOVA of the cerebellar electric field strength (E_{norm}) and the post-hoc multiple comparisons of the means (95% significance) with Bonferroni critical values. Specifically, in the E_x direction, Celnik montage performed better than Manto montage while in E_z direction, Manto montage performed better than Celnik montage (see **Figure 4** in the **Supplementary Material**). Therefore, the E_z electric field due to Manto montage is postulated to be responsible for a statistically significant ($p < 0.05$) decrease in RT post-intervention than baseline, i.e., temporal aspects (Jahn et al., 2004), while the E_x electric field due to Celnik montage is postulated to affect the spatial aspect of the target pursuit during VMT (Abadi and Dutta, 2017) and resulted in a statistically significant ($p < 0.05$) decrease in RMSE post-intervention than baseline. **Figure 4** also shows that the electric field in the mediolateral (X) direction changed direction across hemispheres for the Manto montage, going from a minimum of -0.25 V/m in the left cerebellum to a maximum of 0.3 V/m in the targeted right cerebellum, which is in contrast to that in the Celnik montage that was mostly positive from 0 to 0.3 V/m. Moreover, **Figure 4A** (also **Supplementary Figure 1A**) shows that Celnik montage affected the superior posterior cerebellar hemisphere more effectively than the Manto montage. This is important due to the existence of efferent projections from the superior posterior cerebellar hemisphere (specifically, lobule VI) to the foot area of the primary motor cortex (Lu et al., 2007). Therefore, the ctDCS effects on RMSE by Celnik montage may be the result of motor adaptation based on the ctDCS-modulation of the synaptic activity between parallel fiber and the dendritic tree of the Purkinje cells (i.e., the matrix memory) in the efferent pathways while the decrease in RT to unanticipated visual cue by Manto montage may be the result of ctDCS-enhanced responsiveness of the Purkinje cells in the lobules VIIb–IX related to the lower-limb movements (Buckner et al., 2011; Mottolese et al., 2013).

The electric field distribution in X, Y, Z directions for the lobules associated with the lower-limb movements (hemisphere VIIb–IX) (Mottolese et al., 2013) is shown in **Supplementary Figure 4**. Here, the effect of the selection of the computational pipeline on the lobule-specific electric field distribution can be up to $\pm$ 0.25 for the cerebellar lobules VIIb, VIII, IX for different ctDCS montages as shown in **Figure 6** (all the lobules are shown in **Supplementary Figure 3**). The multiple comparison results for lobule*head model interaction in the cerebellar electric field strength is shown in **Figure 5**. Since ctDCS montage for ankle function (Buckner et al., 2011), a.k.a, lobules VII-IX is important for an insight into healthy human anodal ctDCS results during a VMT performance (Foerster et al., 2015; Abadi and Dutta, 2017) so we optimized the ctDCS montage for lobules VII-IX as shown in **Figure 7**. This ctDCS montage is relevant for posture and gait which are sensorimotor actions that involve peripheral, spinal, and supraspinal structures (Jahn et al., 2004) related to motor function which is our future work. However, 4×1 HD-ctDCS montage primarily affected the lobules Crus I, Crus II, VIIb of the targeted cerebellar hemisphere that is linked to cognitive impairments (Stoodley and Schmahmann, 2010) with no anatomical connections to motor cortex. Therefore, 4×1 HD-tDCS montage presented by Doppelmayr et al. (2016) may be relevant for cognitive rehabilitation but not for lower limb motor rehabilitation.

Our optimized the ctDCS montage for lobules VII-IX, as shown in **Figure 7**, can facilitate rehabilitation of impaired standing balance which is a common problem in persons with multiple sclerosis (pwMS) (Bennett and Leavitt, 2018). Here, movement inefficiency and postural control impairment in pwMS may lead to falls and fatigue. Therefore, locomotor rehabilitation can address efficient sensory-motor integration with balance and eye movement exercises (BEEMS) (Hebert et al., 2018) in conjunction with ctDCS of lower limb function. Here, one should take into account the subcortical route besides the cortical route for the lower limb effects of ctDCS (and cerebellar TMS) where an obvious candidate for the subcortical route is the red nucleus (Mottolese et al., 2013) via superior cerebellar peduncle (SCP). Also, newly named endorestiform nucleus (Human Brainstem - 1st Edition) in the inferior cerebellar peduncle (ICP), at the junction between the brain and spinal cord, may be relevant for ctDCS (and cerebellar TMS) since Postural Assessment Scale for Stroke Patients (PASS) test scores could be predicted by the fractional anisotropy of the ICP (discussion with Dr. Jaillard, CHU Grenoble, France) (Abadi and Dutta, 2017). Indeed, this role of other pathways (ICP, SCP) need further investigation since cerebellar TMS using 110 mm double cone coil (Magstim, United Kingdom) with 1A/us current gradient at the right cerebellar cortex (3 cm lateral to the inion) showed the peak electric field strength at the Crus II (**Supplementary Figure 5**) which has been shown to have no anatomical connections to motor cortex (Buckner et al., 2011). Furthermore, prior work has suggested that cerebellar TMS has sufficient functional resolution to affect nodes of individual networks within the cerebellum which is also shown by our lobule-specific electric field modeling in **Figure 5** of the **Supplementary Material**. Such lobule specific electric field modeling using individual MRI is crucial for cerebellar TMS due to lack of a motor evoked response to find the "hotspot". NIBS of the cerebellum is postulated to modulate via thalamic connectivity to M1 since the feedback projections to the cerebral cortex from the cerebellum are conveyed from the deep cerebellar nuclei, principally the dentate nucleus, that terminate in the thalamus. Here, Crus II TMS has been

shown to alter default network connectivity within the thalamus while midline TMS was found to not alter default network functional connectivity. Therefore, SUIT high-resolution atlas template of the human cerebellum and brainstem is also crucial for systematic testing of cerebellar brain inhibition (CBI) protocols (Fernandez et al., 2018) using cerebellar TMS which is our future work.

One limitation of this technology report is the lack of neurophysiological testing of our optimized ctDCS montage for ankle function. For example, CBI is a physiological parameter of the connectivity strength between the cerebellum and the primary motor cortex (M1) that can be identified using TMS (Fernandez et al., 2018). Moreover, one may need to use *in vivo* intracranial cerebellar recordings in humans for experimental validation (Huang et al., 2017). Another limitation is an uncertain (anisotropic) conductivity profile for the cerebellum that can have a substantial influence on the prediction of optimal ctDCS montage, e.g., (Schmidt et al., 2015). Indeed, an individualized protocol for ctDCS that is verified with neurophysiological testing is necessary to reduce inter-individual variability (Iodice et al., 2017). Therefore, our freely available CLOS pipeline for cerebellum that is easily accessible worldwide is crucial to facilitate the clinical translation of ctDCS. Besides neurophysiological testing, behavioral system analysis using an error clamp design of the VMT (Kha et al., 2018) may further elucidate the behavioral mechanism of ctDCS. For example, when no visual feedback is presented after motor adaptation during 'error clamp' trials (Vaswani and Shadmehr, 2013). It has been postulated that motor memories show little decay in the absence of error if the brain is prevented from detecting a change in task conditions (Vaswani and Shadmehr, 2013). Therefore, during 'error clamp' trials, Celnik montage should have little effect on both RMSE and RT while Manto montage is postulated to have a significant effect on RT and little effect on RMSE. We have found RT effect of the primary motor cortex (M1) tDCS that changed the input-output function of the pyramidal cells (Lafon et al., 2017) leading to response time improvement post-tDCS when compared to pre-tDCS baseline performance (Kha et al., 2018). Furthermore, a systematic evaluation of more focal electrode montages, such as multi-anode (1 cm radius) tDCS (Otal et al., 2016), may elucidate the specificity of the ctDCS effects as shown computationally possible for lower limb function in **Figure 7**. Here, multi-anode (1 cm radius) tDCS may reach deeper into the cerebellum while limiting diffusion to neighboring structures (Fiocchi et al., 2017). From the Doppelmayr's study (Doppelmayr et al., 2016), we expected a more focal electric field distribution in 4×1 HD-ctDCS montage. However, we found diffusion to neighboring structures, e.g., the occipital lobe, as shown in **Figure 3B**. Therefore, the visual cortex effects of 4×1 HD-ctDCS (Doppelmayr et al., 2016) need to be evaluated using neurophysiological testing in future studies.

Here, we postulate that subject-specific ctDCS electric field orientation within the cerebellar lobules also needs to be optimized based on subject-specific head modeling where our CLOS pipeline can be useful (see **Figure 7**). The direction of the electric field vector requires investigation using multi-scale modeling (Seo and Jun, 2017) vis-à-vis Purkinje cell, climbing fiber, and parallel fiber orientations at each lobule, which is our future work. This is motivated by the differences in the electric field in the mediolateral (X) direction that may affect the parallel fibers differently between Celnik and Manto montages due to the difference in the E_x direction (see **Supplementary Figure 4**). Also, in this technology report, the top panel of **Figure 4** shows that the electric field in the mediolateral (X) direction is all negative for Manto montage when compared to Celnik montage for the targeted right hemisphere which may be relevant. Therefore, it can be postulated for the cerebellar lobules VII-IX related to ankle function based on our prior work that the E_x is primarily responsible for the RMSE post-intervention than baseline while the E_z is primarily responsible for the RT post-intervention than baseline, i.e., primarily the temporal aspects. Here, optimization using multi-anode (1cm radius) tDCS (Otal et al., 2016) instead of the single anode in 4×1 HD-ctDCS distributed the total current across the anode and provided a more focal targeting in different directions of the electric field vector (see **Figure 7**). Moreover, the direction of the electric field vector (shown in **Figure 7**) can be better controlled by current steering using multi-anode (1cm radius) tDCS (Otal et al., 2016), e.g., in aligning the major axis of the electric field gradient with the cerebellar peduncles, which may be relevant for motor neurorehabilitation (Dutta et al., 2014; Abadi and Dutta, 2017).

AUTHOR CONTRIBUTIONS

ZR conducted computational modeling under the guidance of AD. All the authors have drafted the work and revised it critically and have approved the final version before submission.

FUNDING

University at Buffalo SUNY funded this computational work.

ACKNOWLEDGMENTS

AD would like to acknowledge the help received from Dr. med. M.A. Nitsche at the University Medical Center, Goettingen, Germany for the data collection during visuo-myoelectric control study.

SUPPLEMENTARY MATERIAL

The Supplementary Material for this article can be found online at: https://www.frontiersin.org/articles/10.3389/fnins.2019.00266/full#supplementary-material

REFERENCES

Abadi, Z. R. H., and Dutta, A. (2017). "Optimizing cerebellar transcranial direct current stimulation for visuomotor learning - anterior versus posterior lobe of cerebellum," in *Proceedings of the 2017 8th International IEEE/EMBS Conference on Neural Engineering (NER)*, (Shanghai: IEEE). doi: 10.1109/NER.2017.8008381

Bennett, S., and Leavitt, V. M. (2018). An intervention to improve balance in persons with multiple sclerosis. *Neurology* 90, 403–404. doi: 10.1212/WNL.0000000000005038

Bikson, M. (2016). *Cellular Mechanisms of Transcranial Direct Current Stimulation*. Available at: http://www.dtic.mil/docs/citations/AD1012265 (accessed September 30, 2018).

Boyd, S., and Vandenberghe, L. (2004). *Convex Optimization*. Los Angeles: Cambridge University Press. doi: 10.1017/CBO9780511804441

Buckner, R. L., Krienen, F. M., Castellanos, A., Diaz, J. C., and Yeo, B. T. T. (2011). The organization of the human cerebellum estimated by intrinsic functional connectivity. *J. Neurophysiol.* 106, 2322–2345. doi: 10.1152/jn.00339.2011

Diedrichsen, J. (2006). A spatially unbiased atlas template of the human cerebellum. *NeuroImage* 33, 127–138. doi: 10.1016/j.neuroimage.2006.05.056

Diedrichsen, J., Balsters, J. H., Flavell, J., Cussans, E., and Ramnani, N. (2009). A probabilistic MR atlas of the human cerebellum. *NeuroImage* 46, 39–46. doi: 10.1016/j.neuroimage.2009.01.045

Dmochowski, J. P., Datta, A., Bikson, M., Su, Y., and Parra, L. C. (2011). Optimized multi-electrode stimulation increases focality and intensity at target. *J. Neural. Eng.* 8:046011. doi: 10.1088/1741-2560/8/4/046011

Doppelmayr, M., Pixa, N. H., and Steinberg, F. (2016). Cerebellar, but not motor or parietal, high-density anodal transcranial direct current stimulation facilitates motor adaptation. *J. Int. Neuropsychol. Soc.* 22, 928–936. doi: 10.1017/S1355617716000345

Dular, P., Geuzaine, C., Henrotte, F., and Legros, W. (1998). A general environment for the treatment of discrete problems and its application to the finite element method. *IEEE Trans. Magn.* 34, 3395–3398. doi: 10.1109/20.717799

Dutta, A., and Dutta, A. (2013). "Using electromagnetic reciprocity and magnetic resonance current density imaging to fit multi-electrode montage for non-invasive brain stimulation," in *Proceedings of the 2013 6th International IEEE/EMBS Conference on Neural Engineering (NER)*, (Shanghai: IEEE). doi: 10.1109/NER.2013.6695968

Dutta, A., Paulus, W., and Nitsche, M. A. (2014). Facilitating myoelectric-control with transcranial direct current stimulation: a preliminary study in healthy humans. *J. Neuroeng. Rehabil.* 11:13. doi: 10.1186/1743-0003-11-13

Ebner, T. J. (2013). "Cerebellum and Internal Models," in *Handbook of the Cerebellum and Cerebellar Disorders*, eds J. D. Schmahmann, and D. L. Gruol (Dordrecht: Springer).

Fang, Q., and Boas, D. A. (2009). "Tetrahedral mesh generation from volumetric binary and grayscale images," in *Proceedings of the 2009 IEEE International Symposium on Biomedical Imaging: From Nano to Macro*, (Boston, MA: IEEE). doi: 10.1109/ISBI.2009.5193259

Fernandez, L., Major, B. P., Teo, W.-P., Byrne, L. K., and Enticott, P. G. (2018). Assessing cerebellar brain inhibition (CBI) via transcranial magnetic stimulation (TMS): a systematic review. *Neurosci. Biobehav. Rev.* 86, 176–206. doi: 10.1016/j.neubiorev.2017.11.018

Ferrucci, R., Bocci, T., Cortese, F., Ruggiero, F., and Priori, A. (2016). Cerebellar transcranial direct current stimulation in neurological disease. *Cereb. Atax.* 3:16. doi: 10.1186/s40673-016-0054-2

Ferrucci, R., Cortese, F., and Priori, A. (2015). Cerebellar tDCS: how to do it. *Cerebellum* 14, 27–30. doi: 10.1007/s12311-014-0599-7

Ferrucci, R., and Priori, A. (2014). Transcranial cerebellar direct current stimulation (tcDCS): motor control, cognition, learning and emotions. *NeuroImage* 85(Pt 3), 918–923. doi: 10.1016/j.neuroimage.2013.04.122

Fiocchi, S., Chiaramello, E., Gazzola, V., Suttrup, J., Ravazzani, P., and Parazzini, M. (2017). "Assessment of the capability to target cerebellar sub-regions with high-definition transcranial direct current stimulation high-definition transcranial direct current stimulation (HD-tDCS) over the cerebellum," in *Proceedings of the 2017 IEEE 3rd International Forum on Research and Technologies for Society and Industry (RTSI)*, (Modena: IEEE). doi: 10.1109/RTSI.2017.8065894

Fiocchi, S., Ravazzani, P., Priori, A., and Parazzini, M. (2016). Cerebellar and spinal direct current stimulation in children: computational modeling of the induced electric field. *Front. Hum. Neurosci.* 10:522. doi: 10.3389/fnhum.2016.00522

Foerster, Á, Jacob, A., Dutta, A., and Nitsche, M. A. (2015). "Development of a brain computer interface for delivery of non-invasive brain stimulation during visuomotor task performance - a method study," in *Proceedings of the 2015 7th International IEEE/EMBS Conference on Neural Engineering (NER)*, (Montpellier: IEEE). doi: 10.1109/NER.2015.7146589

Galea, J. M., Jayaram, G., Ajagbe, L., and Celnik, P. (2009). Modulation of cerebellar excitability by polarity-specific non-invasive direct current stimulation. *J. Neurosci.* 29, 9115–9122. doi: 10.1523/JNEUROSCI.2184-09.2009

Geuzaine, C., and Remacle, J.-F. (2009). Gmsh: A 3-D finite element mesh generator with built-in pre- and post-processing facilities. *Int. J. Numer. Methods Eng.* 79, 1309–1331. doi: 10.1002/nme.2579

Giacometti, P., Perdue, K. L., and Diamond, S. G. (2014). Algorithm to find high density EEG scalp coordinates and analysis of their correspondence to structural and functional regions of the brain. *J. Neurosci. Methods* 229, 84–96. doi: 10.1016/j.jneumeth.2014.04.020

Griffiths, D. J. (2017). *Introduction to Electrodynamics*, 4 Edn. New York, NY: Cambridge University Press.

Grimaldi, G., Argyropoulos, G. P., Bastian, A., Cortes, M., Davis, N. J., Edwards, D. J., et al. (2016). Cerebellar transcranial direct current stimulation (ctDCS). *Neuroscientist* 22, 83–97. doi: 10.1177/1073858414559409

Grimaldi, G., Argyropoulos, G. P., Boehringer, A., Celnik, P., Edwards, M. J., Ferrucci, R., et al. (2014). Non-invasive cerebellar stimulation–a consensus paper. *Cerebellum* 13, 121–138. doi: 10.1007/s12311-013-0514-7

Grimaldi, G., and Manto, M. (2013). Anodal transcranial direct current stimulation (tDCS) decreases the amplitudes of long-latency stretch reflexes in cerebellar ataxia. *Ann. Biomed. Eng.* 41, 2437–2447. doi: 10.1007/s10439-013-0846-y

Guhathakurta, D., and Dutta, A. (2016). Computational pipeline for NIRS-EEG joint imaging of tDCS-evoked cerebral responses—an application in ischemic stroke. *Front. Neurosci.* 10:261. doi: 10.3389/fnins.2016.00261

Guler, S., Dannhauer, M., Erem, B., Macleod, R., Tucker, D., Turovets, S., et al. (2016). Optimizing stimulus patterns for dense array tDCS with fewer sources than electrodes using a branch and bound algorithm. *Proc. IEEE Int. Symp. Biomed. Imag.* 2016, 229–232. doi: 10.1109/ISBI.2016.7493251

Hartzell, J. F., Davis, B., Melcher, D., Miceli, G., Jovicich, J., Nath, T., et al. (2016). Brains of verbal memory specialists show anatomical differences in language, memory and visual systems. *NeuroImage* 131, 181–192. doi: 10.1016/j.neuroimage.2015.07.027

Hebert, J. R., Corboy, J. R., Vollmer, T., Forster, J. E., and Schenkman, M. (2018). Efficacy of balance and eye-movement exercises for persons with multiple sclerosis (BEEMS). *Neurology* 90, e797–e807. doi: 10.1212/WNL.0000000000005013

Holmes, C. J., Hoge, R., Collins, L., Woods, R., Toga, A. W., and Evans, A. C. (1998). Enhancement of MR images using registration for signal averaging. *J. Comput. Assist. Tomogr.* 22, 324–333.

Huang, Y., Datta, A., Bikson, M., and Parra, L. C. (2017). Realistic vOlumetric-approach to simulate transcranial electric stimulation – ROAST – a fully automated open-source pipeline. *bioRxiv* [Preprint]. doi: 10.1101/217331

Huang, Y., Datta, A., Bikson, M., and Parra, L. C. (2018). *ROAST?: An Open-Source, Fully-Automated, Realistic Volumetric-Approach-based Simulator for TES*. Available at: https://www.elsevier.com/books/human-brainstem/paxinos/978-0-12-814184-7 (accessed March 10, 2019).

Iodice, R., Manganelli, F., and Dubbioso, R. (2017). The therapeutic use of non-invasive brain stimulation in multiple sclerosis - a review. *Restor. Neurol. Neurosci.* 35, 497–509. doi: 10.3233/RNN-170735

Jahn, K., Deutschländer, A., Stephan, T., Strupp, M., Wiesmann, M., and Brandt, T. (2004). Brain activation patterns during imagined stance and locomotion in functional magnetic resonance imaging. *NeuroImage* 22, 1722–1731. doi: 10.1016/j.neuroimage.2004.05.017

Jayaram, G., Tang, B., Pallegadda, R., Vasudevan, E. V. L., Celnik, P., and Bastian, A. (2012). Modulating locomotor adaptation with cerebellar stimulation. *J. Neurophysiol.* 107, 2950–2957. doi: 10.1152/jn.00645.2011

Kha, V., Foerster, A. S., Bennett, S., Nitsche, M. A., Stefanovic, F., and Dutta, A. (2018). Systems analysis of human visuo-myoelectric control facilitated by anodal transcranial direct current stimulation in healthy humans. *Front. Neurosci.* 12:278. doi: 10.3389/fnins.2018.00278

Koppelmans, V., Hoogendam, Y. Y., Hirsiger, S., Mérillat, S., Jäncke, L., and Seidler, R. D. (2017). Regional cerebellar volumetric correlates of manual motor and cognitive function. *Brain Struct. Funct.* 222, 1929–1944. doi: 10.1007/s00429-016-1317-7

Koziol, L. F., Budding, D., Andreasen, N., D'Arrigo, S., Bulgheroni, S., Imamizu, H., et al. (2014). Consensus paper: the cerebellum's role in movement and cognition. *Cerebellum* 13, 151–177. doi: 10.1007/s12311-013-0511-x

Küper, M., Kaschani, P., Thürling, M., Stefanescu, M. R., Burciu, R. G., Göricke, S., et al. (2016). Cerebellar fMRI activation increases with increasing working memory demands. *Cerebellum* 15, 322–335. doi: 10.1007/s12311-015-0703-7

Lafon, B., Rahman, A., Bikson, M., and Parra, L. C. (2017). Direct current stimulation alters neuronal input/output function. *Brain Stimulat.* 10, 36–45. doi: 10.1016/j.brs.2016.08.014

Lakens, D. (2013). Calculating and reporting effect sizes to facilitate cumulative science: a practical primer for t-tests and ANOVAs. *Front. Psychol.* 4:863. doi: 10.3389/fpsyg.2013.00863

Lu, X., Miyachi, S., Ito, Y., Nambu, A., and Takada, M. (2007). Topographic distribution of output neurons in cerebellar nuclei and cortex to somatotopic map of primary motor cortex. *Eur. J. Neurosci.* 25, 2374–2382. doi: 10.1111/j.1460-9568.2007.05482.x

Mottolese, C., Richard, N., Harquel, S., Szathmari, A., Sirigu, A., and Desmurget, M. (2013). Mapping motor representations in the human cerebellum. *Brain* 136, 330–342. doi: 10.1093/brain/aws186

Oostenveld, R., and Praamstra, P. (2001). The five percent electrode system for high-resolution EEG and ERP measurements. *Clin. Neurophysiol.* 112, 713–719. doi: 10.1016/S1388-2457(00)00527-7

Opitz, A., Paulus, W., Will, S., Antunes, A., and Thielscher, A. (2015). Determinants of the electric field during transcranial direct current stimulation. *NeuroImage* 109, 140–150. doi: 10.1016/j.neuroimage.2015.01.033

Otal, B., Dutta, A., Foerster, Á, Ripolles, O., Kuceyeski, A., Miranda, P. C., et al. (2016). Opportunities for guided multichannel non-invasive transcranial current stimulation in poststroke rehabilitation. *Front. Neurol.* 7:21. doi: 10.3389/fneur.2016.00021

Parazzini, M., Rossi, E., Ferrucci, R., Liorni, I., Priori, A., and Ravazzani, P. (2014). Modelling the electric field and the current density generated by cerebellar transcranial DC stimulation in humans. *Clin. Neurophysiol.* 125, 577–584. doi: 10.1016/j.clinph.2013.09.039

Penny, W. D., Friston, K. J., Ashburner, J. T., Kiebel, S. J., and Nichols, T. E. (2011). *Statistical Parametric Mapping: The Analysis of Functional Brain Images*. Amsterdam: Elsevier.

Popa, L. S., Streng, M. L., Hewitt, A. L., and Ebner, T. J. (2016). The errors of our ways: understanding error representations in cerebellar-dependent motor learning. *Cerebellum* 15, 93–103. doi: 10.1007/s12311-015-0685-5

Popa, T., Velayudhan, B., Hubsch, C., Pradeep, S., Roze, E., Vidailhet, M., et al. (2013). Cerebellar processing of sensory inputs primes motor cortex plasticity. *Cereb. Cortex N. Y.* 1991, 305–314. doi: 10.1093/cercor/bhs016

Priori, A., Ciocca, M., Parazzini, M., Vergari, M., and Ferrucci, R. (2014). Transcranial cerebellar direct current stimulation and transcutaneous spinal cord direct current stimulation as innovative tools for neuroscientists. *J. Physiol.* 592, 3345–3369. doi: 10.1113/jphysiol.2013.270280

Rahman, A., Reato, D., Arlotti, M., Gasca, F., Datta, A., Parra, L. C., et al. (2013). Cellular effects of acute direct current stimulation: somatic and synaptic terminal effects. *J. Physiol.* 591, 2563–2578. doi: 10.1113/jphysiol.2012.247171

Saturnino, G. B., Puonti, O., Nielsen, J. D., Antonenko, D., Madsen, K. H. H., and Thielscher, A. (2018). SimNIBS 2.1: a comprehensive pipeline for individualized electric field modelling for transcranial brain stimulation. *bioRxiv* [Preprint]. doi: 10.1101/500314

Schmidt, C., Wagner, S., Burger, M., van Rienen, U., and Wolters, C. H. (2015). Impact of uncertain head tissue conductivity in the optimization of transcranial direct current stimulation for an auditory target. *J. Neural. Eng.* 12:046028. doi: 10.1088/1741-2560/12/4/046028

Seo, H., and Jun, S. C. (2017). Multi-scale computational models for electrical brain stimulation. *Front. Hum. Neurosci.* 11:515. doi: 10.3389/fnhum.2017.00515

Stoodley, C. J., and Schmahmann, J. D. (2009). Functional topography in the human cerebellum: a meta-analysis of neuroimaging studies. *NeuroImage* 44, 489–501. doi: 10.1016/j.neuroimage.2008.08.039

Stoodley, C. J., and Schmahmann, J. D. (2010). Evidence for topographic organization in the cerebellum of motor control versus cognitive and affective processing. *Cortex J. Dev. Study Nerv. Syst. Behav.* 46, 831–844. doi: 10.1016/j.cortex.2009.11.008

Stoodley, C. J., Valera, E. M., and Schmahmann, J. D. (2012). Functional topography of the cerebellum for motor and cognitive tasks: an fMRI study. *NeuroImage* 59, 1560–1570. doi: 10.1016/j.neuroimage.2011.08.065

Summers, R. L. S., Chen, M., Hatch, A., and Kimberley, T. J. (2018). Cerebellar transcranial direct current stimulation modulates corticospinal excitability during motor training. *Front. Hum. Neurosci.* 12:118. doi: 10.3389/fnhum.2018.00118

van Dun, K., Bodranghien, F. C. A. A., Mariën, P., and Manto, M. U. (2016). tDCS of the cerebellum: where do we stand in 2016? technical issues and critical review of the literature. *Front. Hum. Neurosci.* 10:199. doi: 10.3389/fnhum.2016.00199

van Dun, K., Mitoma, H., and Manto, M. (2018). Cerebellar cortex as a therapeutic target for neurostimulation. *Cerebellum* 17, 777–787. doi: 10.1007/s12311-018-0976-8

Vaswani, P. A., and Shadmehr, R. (2013). Decay of motor memories in the absence of error. *J. Neurosci.* 33, 7700–7709. doi: 10.1523/JNEUROSCI.0124-13.2013

Windhoff, M., Opitz, A., and Thielscher, A. (2013). Electric field calculations in brain stimulation based on finite elements: an optimized processing pipeline for the generation and usage of accurate individual head models. *Hum. Brain Mapp.* 34, 923–935. doi: 10.1002/hbm.21479

Conflict of Interest Statement: The authors declare that the research was conducted in the absence of any commercial or financial relationships that could be construed as a potential conflict of interest.

frontiers in Neuroscience

ORIGINAL RESEARCH
published: 12 April 2019
doi: 10.3389/fnins.2019.00307

Cognitive Training and Transcranial Direct Current Stimulation in Mild Cognitive Impairment: A Randomized Pilot Trial

*Namrata Das[1], Jeffrey S. Spence[1], Sina Aslan[1,2], Sven Vanneste[1], Raksha Mudar[3], Audette Rackley[1], Mary Quiceno[4] and Sandra Bond Chapman[1]**

[1] Center for BrainHealth, The University of Texas at Dallas, Dallas, TX, United States, [2] Advance MRI, LLC, Frisco, TX, United States, [3] Department of Speech and Hearing Science, University of Illinois at Urbana-Champaign, Champaign, IL, United States, [4] University of North Texas Health Science Center and Department of Internal Medicine and Geriatrics and TCU/UNTHSC, School of Medicine, Department of Medical Education, Fort Worth, TX, United States

Background: Transcranial direct current stimulation (tDCS), a non-invasive stimulation, represents a potential intervention to enhance cognition across clinical populations including Alzheimer's disease and mild cognitive impairment (MCI). This randomized clinical trial in MCI investigated the effects of anodal tDCS (a-tDCS) delivered to left inferior frontal gyrus (IFG) combined with gist-reasoning training (SMART) versus sham tDCS (s-tDCS) plus SMART on measures of cognitive and neural changes in resting cerebral blood flow (rCBF). We were also interested in SMART effects on cognitive performance regardless of the tDCS group.

Methods: Twenty-two MCI participants, who completed the baseline cognitive assessment (T1), were randomized into one of two groups: a-tDCS + SMART and s-tDCS + SMART. Of which, 20 participants completed resting pCASL MRI scan to measure rCBF. Eight SMART sessions were administered over 4 weeks with a-tDCS or s-tDCS stimulation for 20 min before each session. Participants were assessed immediately (T2) and 3-months after training (T3).

Results: Significant group × time interactions showed cognitive gains at T2 in executive function (EF) measure of inhibition [DKEFS- Color word (p = 0.047)], innovation [TOSL (p = 0.01)] and on episodic memory [TOSL (p = 0.048)] in s-tDCS + SMART but not in a-tDCS + SMART group. Nonetheless, the gains did not persist for 3 months (T3) after the training. A voxel-based analysis showed significant increase in regional rCBF in the right middle frontal cortex (MFC) (cluster-wise p = 0.05, k = 1,168 mm^3) in a-tDCS + SMART compared to s-tDCS + SMART. No significant relationship was observed between the increased CBF with cognition. Irrespective of group, the combined MCI showed gains at T2 in EF of conceptual reasoning [DKEFS card sort (p = 0.033)] and category fluency [COWAT (p = 0.055)], along with gains at T3 in EF of verbal fluency [COWAT (p = 0.009)].

OPEN ACCESS

Edited by:
Mikhail Lebedev,
Duke University, United States

Reviewed by:
Aurore Thibaut,
University of Liège, Belgium
Emilia Biffi,
Eugenio Medea (IRCCS), Italy

****Correspondence:***
Sandra Bond Chapman
schapman@utdallas.edu

Specialty section:
This article was submitted to Neural Technology, a section of the journal Frontiers in Neuroscience

Received: *19 December 2018*
Accepted: *18 March 2019*
Published: *12 April 2019*

Citation:
Das N, Spence JS, Aslan S, Vanneste S, Mudar R, Rackley A, Quiceno M and Chapman SB (2019) Cognitive Training and Transcranial Direct Current Stimulation in Mild Cognitive Impairment: A Randomized Pilot Trial. Front. Neurosci. 13:307. doi: 10.3389/fnins.2019.00307

Conclusion: One intriguing finding is a-tDCS to left IFG plus SMART increased blood flow to right MFC, however, the stimulation seemingly blocked cognitive benefits of SMART on EF (inhibition and innovation) and episodic memory compared to s-tDCS + SMART group. Although the sample size is small, this paper contributes to growing evidence that cognitive training provides a way to significantly enhance cognitive performance in adults showing memory loss, where the role of a-tDCS in augmenting these effects need further study.

Keywords: mild cognitive impairment, Alzheimer's disease, transcranial direct current stimulation, cerebral blood flow, fMRI, cognitive training, strategic memory advanced reasoning training, brain modulation

INTRODUCTION

Mild cognitive impairment (MCI) is a stage in which individuals endorse subtle changes in cognitive functions that are corroborated on objective assessments of cognition but have minimal changes in functional abilities (Weiner et al., 2013; Cohen and Klunk, 2014). The rate of conversion from MCI to a diagnosis of Alzheimer's disease (AD) is around 10–15% per year (Manly et al., 2008; Roberts et al., 2014). To date, pharmacological interventions have failed to show realizable benefits in mitigating cognitive decline in individuals with MCI and in preventing progression to AD (Andrieu et al., 2015). As a result, there is growing interest in exploring the benefits of non-pharmacological interventions such as lifestyle modifications (nutrition and exercise) (Morris, 2009; Erickson et al., 2011), cognitive training (Jean et al., 2010; Belleville et al., 2011; Chapman and Mudar, 2014; Chapman et al., 2017; Edward et al., 2017; Harvey et al., 2018), and repetitive non-invasive brain stimulation such as Transcranial Magnetic Stimulation (rTMS) and Transcranial Direct Current Stimulation (tDCS) (Flöel et al., 2012; Elder and Taylor, 2014).

Decades of research on the effectiveness of process-based and strategy-based cognitive training have shown that training protocols that target higher-order cognitive functions (e.g., reasoning) and are strategy-based yield broad cognitive benefits across clinical groups and in individuals with MCI, in particular (Edward et al., 2017). For instance, our group has shown that strategic memory and advanced reasoning training (SMART), previously referred to as gist reasoning training, improves top–down cognitive processes and associated training-related neural outcomes Specifically, benefits of SMART gains have been reported as increased executive functions and enhanced neural functions in cognitively normal older adults (Anand et al., 2011; Chapman et al., 2015, 2017; Motes et al., 2018) and in adults with traumatic brain injury (Vas et al., 2011, 2015; Cook et al., 2014; Han et al., 2017). Consistent findings of increased resting cerebral blood flow (rCBF) to specific areas of the brain were associated with cognitive gains following SMART in cognitively normal older adults (Chapman et al., 2016), adults with TBI (Vas et al., 2015), and adults with bipolar disorder (Venza et al., 2016). In our previous study with SMART training in healthy aging, we demonstrated increases in global and regional blood flow in bilateral medial orbital frontal cortex (mOFC), a part of inferior fontal gyrus (IFG), and posterior cingulate cortex (PCC) and associated cognitive gains (Chapman et al., 2015, 2017). The IFG is of particular interest because it purportedly supports a cognitive control network of complex mental processes associated with executive functions including reasoning, working memory, and inhibition of unwanted information required for goal-directed behavior (Rubia et al., 2003; Aron et al., 2004). In AD animal models, IFG is shown to aid in the maintenance of the cognitive performance, whereas in adults with genetic risk of AD, IFG seems to support the compensatory mechanism in the brain (Wishart et al., 2006; Filbey et al., 2010). Furthermore, functional imaging studies have associated greater BOLD activity of IFG to better cognitive outcomes (Diamond et al., 2007) and memory recovery success in AD patients (Grady, 2012).

Gist reasoning training has also shown to be beneficial in individuals with MCI (Mudar et al., 2017, 2019). In a separate but recently completed randomized pilot study, MCI individuals who underwent SMART improved in strategic processing and attention during a list learning task and on a concept abstraction measure relative to an active control group that received new learning of relevant facts about brain health (Mudar et al., 2017). Not only did the SMART trained group show significant improvement on cognitive and self-reported memory measures, but training-related modulations in neural functions were also noted. With regard to neural changes, MCI individuals who underwent SMART training showed enhanced event-related desynchronization in low-frequency alpha band (8–10 Hz) on response inhibition (NoGo) trials and high-frequency alpha band (11–13 Hz) on response execution (Go) trials relative to the active control group (Mudar et al., 2019).

Given the growing evidence of both cognitive and neural benefits of reasoning training (SMART), the next logical question to examine was whether benefits of SMART for individuals with MCI can be augmented using brain stimulation approaches such as tDCS when combined with cognitive training. tDCS is a non-invasive brain stimulation approach used to modulate cortical functioning by applying weak direct current over the scalp (Nitsche et al., 2007). Recent studies have begun to explore the cognitive benefits of tDCS alone in MCI (Biundo et al., 2015; Manenti et al., 2016; Yun et al., 2016). In a randomized clinical trial involving 16 individuals with MCI, Yun et al. (2016) investigated if anodal direct current stimulation (a-tDCS) over left dorsolateral prefrontal cortex (DLPFC) with reference electrode over right DLPFC for 30 min over nine sessions

in 3 weeks could enhance memory. Compared to the sham group, significant improvement was observed on a Multifactorial Memory Questionnaire (MMQ) with questions probing on how individual feel about their memory and mistakes. Similarly, Murugaraja et al. (2017) findings in 10 individuals with MCI demonstrated that 20 min of 2 mA anodal stimulation over the left DLPFC with a reference electrode on right supraorbital region for five consecutive sessions significantly improved immediate and delayed recall of pictures over an extended period of 1 month. A study by Meinzer et al. (2015) examined the effect of a-tDCS on brain function in individuals with MCI on semantic word-retrieval using fMRI. A 1 mA intensity over 20 min applied over left IFG showed improvement in semantic word retrieval task with a decrease in task-related prefrontal hyperactivity supporting enhanced processing efficacy.

The body of research supporting the cognitive benefits of a-tDCS in MCI, used alone, is growing; however, no study to our knowledge has yet examined the combined effects of tDCS and cognitive training in MCI. A study by Cotelli et al. (2014) in patients with mild to moderate AD provides support to motivate the present study. Their team examined the effects of combined tDCS applied to the DLPFC and individualized computerized (IC) memory training on memory improvements. Their findings of significant improvement in face-name association memory task suggest that there may be a value in exploring such combined therapies in individuals at earlier stages of dementia, specifically those with MCI.

The goals of this study were three-fold. First, we investigated whether anodal tDCS to left inferior frontal gyrus (IFG) combined with SMART training (a-tDCS + SMART) would show significant cognitive gains over an extended period (i.e., 3 months post-training) compared to the sham tDCS and SMART training group (s-tDCS + SMART). Based on evidence summarized above showing neural gains after SMART training in MCI and healthy controls combined with evidence for IFG vulnerability in AD, we chose to stimulate the region over the left IFG. We hypothesized that a-tDCS to left IFG delivered for 20 min just prior to participating in SMART training would enhance the cognitive benefits. The potential to enhance cognitive-training benefits with neuromodulation is based on a hypothesis that the brain's inherent neuroplasticity can be 'primed' to be more responsive to intervention protocols (Meinzer et al., 2015; Reinhart et al., 2017). Secondly, we examined whether a-tDCS + SMART significantly altered rCBF, a measure of neural function previously identified in clinical training trials involving other clinical populations, relative to s-tDCS + SMART. We focused on rCBF to measure neural health based on a series of cognitive training trials where fMRI findings revealed that rCBF was an early and sensitive measures of improved cognitive brain health following interventions (Chapman et al., 2015, 2016, Vas et al., 2016; Venza et al., 2016). We expected that the a-tDCS + SMART would bring about greater changes to rCBF as compared to the s-tDCS + SMART, given the enhanced potential to harness neural plasticity shown by previous tDCS trials (Yun et al., 2016). Finally, we wanted to explore whether SMART training improved cognitive functions irrespective of the a-tDCS or s-tDCS group. Based on prior results showing adults with MCI benefitted from SMART protocol (Mudar et al., 2017, 2019), we proposed that both groups would show cognitive gains.

MATERIALS AND METHODS

This blinded randomized clinical trial (ClinicalTrials.gov ID: NCT02588209) study using tDCS in individuals with MCI was approved by the Institutional Review Boards (IRB) of The University of Texas Southwestern Medical Center (UTSW IRB STU082015-031) and The University of Texas at Dallas (UTD IRB# 15-97). All eligible participants signed informed consent under the guidelines of UTSW and UTD IRBs under the Declaration of Helsinki 1975 revised in 1981.

Participants

Twenty-two (22) participants with a diagnosis of MCI based on either Petersen's (Petersen et al., 2001) or Alzheimer's disease neuroimaging initiative (ADNI, Aisen et al., 2010) criteria were included in the study from the Dallas Fort Worth community. The diagnosis of MCI was confirmed by the research team consisting of a neurologist, cognitive neuroscientist, and speech-language pathologist. The comprehensive Petersen's or ADNI criteria used for enrollment were: (1) subjective memory complaints; (2) objective memory loss measured by either logical memory subtest from Wechsler Memory Scale-III (WMS-III, Wechsler, 1997b) with delayed memory recall scores of 9–11 for 16 or more years of education, 5–9 for 8–15 years of educational and 3–6 for 0–7 years of education or California Verbal Learning Task (CVLT) delayed memory recall of −1.5 standard deviation below the mean; (3) preserved daily functional activities; (4) clinical dementia rating scale of 0.5 (CDR, Morris, 1993); (5) MMSE of 24–30 (Folstein et al., 1975); and (6) without symptoms of dementia. Subjective memory concerns of each participant were assessed using a Multifactorial Memory Questionnaire (MMQ, Troyer and Rich, 2002). The questionnaire included 57 items divided into three subscales: MMQ-Contentment (MMQ-C), MMQ-Ability (MMQ-A), and MMQ-Strategies (MMQ-S). MMQ-C assessed participants' self-satisfaction and concerns of their memory in which higher scores indicated greater satisfaction with one's memory. MMQ-A measured self-perception of memory ability with higher scores indicating better self-reported memory ability. Whereas, MMQ-S assessed individuals use of memory strategies in daily life with higher scores reflecting greater use of memory strategies. Irrespective of sex and ethnic groups other inclusion factors were right-handed individuals, age 50–80 years with a minimum of 12 years' education. All participants were assessed for signs of depression using the geriatric depression scale (GDS, Yesavage et al., 1982) and only participant with no or mild depression were in the study (see **Table 1**). The ability to read at the level of 12th grade was assessed using the Wide Range Achievement Test (WRAT4, Wilkinson and Robertson, 2006).

Exclusion criteria of the study were: less than 12th grade of education, left-handed, unable to speak, read, and write English; CDR value of 0 or >0.5, previous or present

TABLE 1 | Demographics and clinical characteristics (Cognitive Screening Measures).

Measures	Total group (Mean ± *SD*)	Anodal tDCS group (Mean ± *SD*)	Sham tDCS group (Mean ± *SD*)	*p*-values
Demographics				
Number	22	12	10	
Age	62.91 ± 7.79	62.58 ± 8.43	63.30+7.38	0.836
Education	17.14 ± 3.20	17.92 ± 3.94	16.20 ± 1.75	0.218
Sex (Females: Males)	15:7	8:4	8:2	0.300
Cognitive screening measures				
CDR	0.5	0.5	0.5	
MMSE	27.91 ± 1.34	28 ± 0.95	27.80 ± 1.75	0.737
GDS	2.05 ± 1.70	2 ± 1.65	2 ± 1.85	0.895
LM Immediate Recall	11.41 ± 2.64	11.17 ± 2.17	11.70 ± 3.20	0.647
LM Delayed Recall	10.36 ± 2.34	10.42 ± 2.11	10.30 ± 2.71	0.911
CVLT Immediate Recall	8.23 ± 3.56	6.75 ± 3.05	10 ± 3.43	0.029*
CVLT Delayed Recall	9.14 ± 3.33	7.83 ± 3.38	10.70 ± 2.63	0.041*

*CDR, Clinical Dementia Rating Scale; MMSE, Mini Mental Status Examination; GDS, Geriatric Depression Scale; LM, Logical Memory; CVLT, California Verbal Learning Task. There was no difference between the participants' demographics, $p > 0.05$. *Indicates significant at $p < 0.05$.*

diagnosis of neurological disorders such as stroke, brain tumor, cerebral hemorrhage; autoimmune diseases such as fibromyalgia, systemic lupus erythematosus (SLE), multiple sclerosis (MS) and rheumatoid arthritis (RA); uncontrolled metabolic disturbances such as uncontrolled diabetes mellitus, thyroid disorders; psychiatric disorders like bipolar disorder, major depressive disorder, pervasive developmental disorder, schizophrenia, and anxiety disorder; history of substance abuse; head injuries, cancer patients with a history of radiation or chemotherapy. Participants with metallic objects, permanent makeup, medical devices in the body were excluded from the study. Moreover, participants on antidepressants, sedatives, anxiolytics, neuroleptics medications were also denied to take part in the study as it interfered with tDCS stimulation.

All 22 participants completed baseline neurocognitive assessments of which 20 completed resting state pCASL MRI before training (T1). A research assistant, who was blinded to all the participant information and cognitive behavior, randomized the participants into one of two groups: either the a-tDCS or the s-tDCS group following by SMART training using random function on Microsoft excel sheet, after the initial baseline assessment. The research assistant was not involved in either the neurocognitive assessments or trainings. Post-SMART training (T2), 16 subjects completed the neurocognitive assessment of which 15 participants had the follow-up scan. Finally, at 3-month post-training (T3) follow-up, 15 individuals were assessed for neurocognitive behavior only. The complete breakdown of the participant enrollment and follow-up is summarized in **Figure 1**.

Neurocognitive Measures

A 3-h neurocognitive test battery was administered on a non-training day at three time points i.e., before training (T1), post-training (T2), and 3-month post training (T3). The measures included the cognitive domains of executive function, and memory summarized in **Table 2**. Twenty-two (22) participants completed the baseline cognitive assessment and sixteen (16) immediate post-training assessment. Fifteen (15) completed 3-month follow-up assessment. For details on the follow-up sessions see **Figure 1**.

tDCS Stimulation

Direct current was provided through a battery-driven stimulator (DC-Stimulator Plus, neuroConn GmbH). To insure consistency of electrode placement on each participant's skull over the left IFG brain region, the placement of the anodal electrode was calculated as 0.5 cm above the left eyebrow and 1cm on the left forehead away from the center of the nasal bridge. Research assistants were trained to maintain consistency of IFG area stimulation across all the participants. The localization of IFG was based on prior research wherein anodal electrode positions were defined according to the 10–20 EEG system (Iyer et al., 2005; Cattaneo et al., 2011; Meinzer et al., 2015). In the EEG simulating studies IFG anodal electrode was positioned at the center of line connecting between (a) and (b) wherein (a) the intersection of T3-F3 and F7-C3 and (b) is the midpoint between F7-F3 on the left side of the head. The stimulating electrode was inserted in a 3×5 cm^2 saline-soaked synthetic sponge, and was centered FG as previous studies found significantly improved semantic fluency with this electrode montage over IFG (Iyer et al., 2005; Cattaneo et al., 2011; Meinzer et al., 2015). The reference electrode (3×5 cm^2) was positioned over the contralateral shoulder. tDCS was delivered with a constant current of 2mA during resting-state. The a-tDCS group received the stimulation for 20 min (10 s fade-in and 10 s fade-out). The s-tDCS received stimulation for a total of 20 s (10 s fade-in and 10 s fade-out) to mimic the sensation of the stimulation. As the SMART training occurred in groups of 2–5 participants irrespective of the group assignment (a-tDCS versus s-tDCS) all individuals were attached to the machine with the electrode for a total of 20 min irrespective of the group assignment. Each SMART training session (total of 8 sessions spread over 4 weeks) was coupled with tDCS session just before the training. To maintain some consistency of mental processing during the tDCS sessions prior to training, everyone watched Planet Earth videos.

SMART: Cognitive Training Protocol

In previous MCI research, SMART training was labeled as gist reasoning training (Mudar et al., 2017, 2019). Detailed information about the specifics of the training can be found in Mudar et al. (2017, 2019). Training was delivered to all participants in both groups in sessions involving small groups of 2–5 individuals over 4 weeks, consisting of two 1-h sessions per week for a total of 8 h of training. The training is strategy-based rather than content-based so that the focus is not content specific or situation dependent, but hierarchical with each strategy building upon previous strategies to transform the concrete meaning into abstracted gist-based meanings through reasoning and inferencing. Participants received a-tDCS or

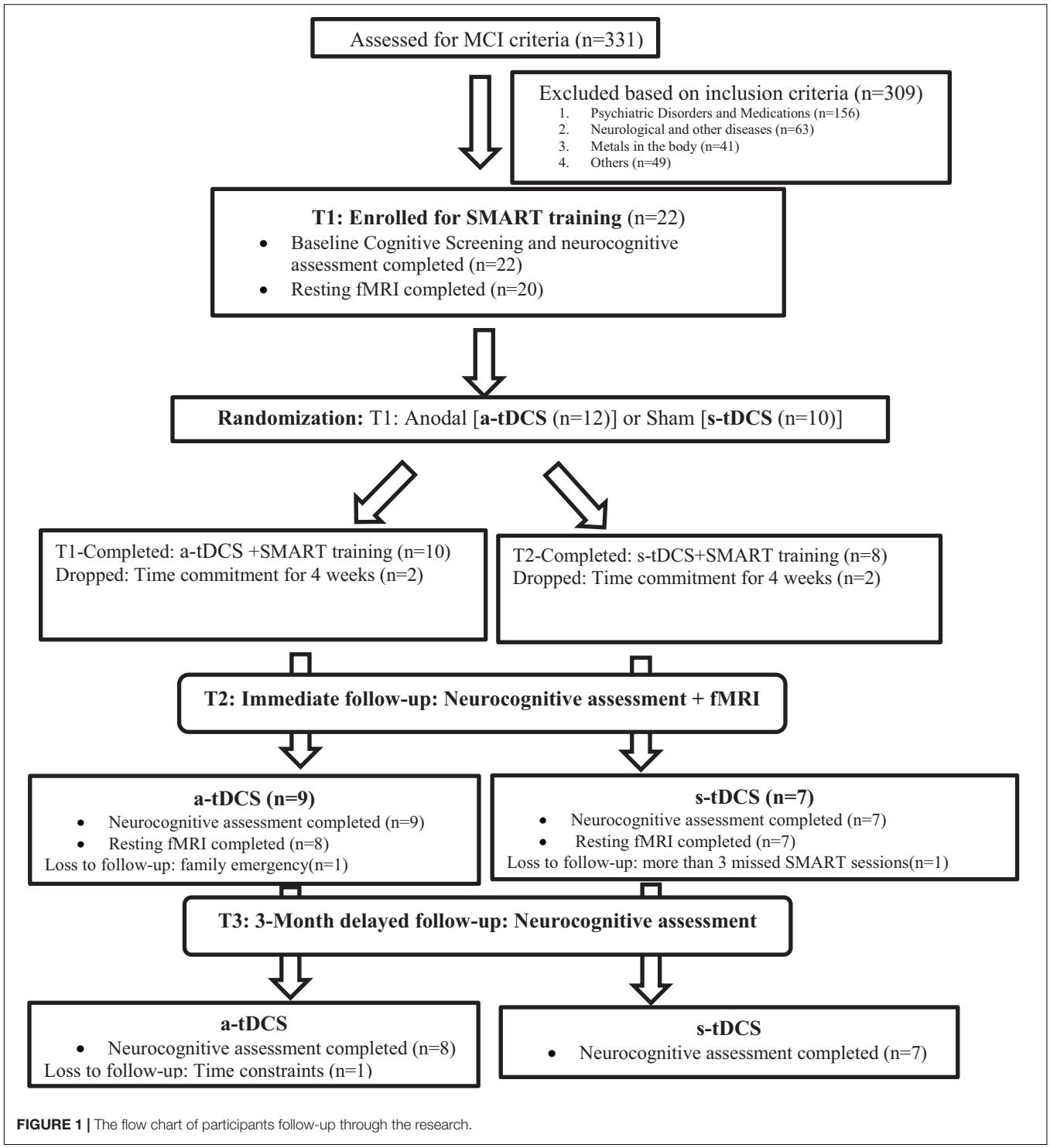

FIGURE 1 | The flow chart of participants follow-up through the research.

s-tDCS stimulation immediately prior to each of the SMART training sessions.

MRI Experiment

MRI scans were completed using 3-Tesla (Philips Medical System, Best, The Netherlands within one (1) week before (T1) and after SMART training (T2) but not at 3-month training (T3). A body coil was used for radiofrequency (RF) transmission and a 32-channel head coil with parallel imaging capability was used for signal reception. We used a pCASL (pseudo-Continuous Arterial Spin Labeling) sequence to measure cerebral blood flow (CBF) at rest. Additionally, a high-resolution T_1-weighted image was acquired as an anatomical reference. The details of imaging parameters and their processing techniques are provided below.

TABLE 2 | Neurocognitive measures, memory questionnaire and memory screening measures administered to the participants.

Cognitive Domain	Measures	Description
Executive Function		
(1) Complex abstraction	Test of Strategic Learning (TOSL) (Chapman et al., 2002)	Examined the ability to condense and synthesize lengthy information written as a summary from a complex text. Scores represents number of abstracted ideas.
(2) Innovation	Test of Strategic Learning (TOSL) (Chapman et al., 2002)	Assessed the ability to construct as many interpretations as possible from the same text above. Scores represent fluency of abstracted idea generation.
(3) Fluency: Verbal/ Category	Controlled Oral Word Association (COWAT) (Benton et al., 1994; Spreen and Strauss, 1998)	Examined the ability to generate as many words staring with a particular alphabet or a category in 1 min.
(4) Inhibition	Delis–Kaplan executive function system (DKEFS) color word interference test (Delis et al., 2001)	Examined the ability to inhibit from reading color of printed word instead of reading the word. Scored as time taken to complete the task.
(5) Conceptual Reasoning	Delis–Kaplan executive function system (DKEFS) card sort (Delis et al., 2001)	Examined the ability to draw similarities between two sets of cards by drawing reasons behind the selection of cards.
Memory		
(1) Episodic Memory: Memory for facts	Test of Strategic Learning (TOSL) (Chapman et al., 2002)	Examined the ability to recall details of a complex short story.
(2) Complex Memory	Selective Auditory learning task (Hanten et al., 2007)	Examined the ability to focus and pay attention to high-priority stimulus, while simultaneously blocking or inhibiting unwanted or low-priority information.
Subjective memory perception		
(1) Memory questionnaire	Multifactorial Memory Questions (MMQ) (Troyer and Rich, 2002)	Examined the individual's self-perception of memory in three subscales using 57 items questionnaire (1) MMQ-Contentment (MMQ-C): Self-satisfaction of memory (2) MMQ-Ability (MMQ-A): Self-perception of memory (3) MMQ-Strategy (MMQ-S): Using of memory strategies in daily life functions.
Screening Memory measures	(1) California Verbal Learning Task (Petersen et al., 2001)	Examined the ability to recall a list of sixteen (16) words in four categories immediately after the list was read followed by delayed recall after 20 min interval.
	(2) Logical Memory (ADNI Criteria, WMS-III, Wechsler, 1997b)	Examined the ability to recall a short story as it is read out immediately and after 20 min interval.

Imaging parameters for pCASL experiments were: single-shot gradient-echo EPI, field-of-view (FOV) = 240 × 240, matrix = 80 × 80, voxel size = 3 mm × 3 mm, 29 slices acquired in ascending order, slice thickness = 5 mm, no gap between slices, labeling duration = 1650 ms, post-labeling delay = 1525 ms, time interval between consecutive slice acquisitions = 35.5 ms, TR/TE = 4260/14 ms, SENSE factor 2.5, number of controls/labels = 45 pairs, RF duration = 0.5 ms, pause between RF pulses = 0.5 ms, labeling pulse flip angle = 90°, bandwidth = 2.7 kHz, echo train length = 35, and scan duration 6.5 min. The high-resolution T_1-weighted image parameters were magnetization prepared rapid acquisition of gradient-echo (MPRAGE) sequence, TR/TE = 8.3/3.8 ms, shot interval = 2100 ms, inversion time = 1100 ms, flip angle = 12°, 160 sagittal slices, voxel size = 1 mm × 1 mm × 1 mm, FOV = 256 mm × 256 mm × 160 mm, and duration 4 min.

pCASL image series were realigned to the first volume for motion correction (SPM8's realign function, University College London, United Kingdom). An in-house MATLAB (Mathworks, Natick, MA, United States) program was used to calculate the difference between averaged control and label images. Then, the difference image was corrected for imaging slice delay time to yield CBF-weight image, which was normalized to the Brain template from Montreal Neurological Institute (MNI). Last, the absolute CBF was estimated by using Alsop and Detre's equation in the units of mL blood/min/100 g of brain tissue (Aslan et al., 2010).

Statistical Analyses

For the behavioral outcomes, we modeled each respective dependent variable as a constrained linear mixed effects model$y_{ijk} = \mu_0 + \delta_{ij} + \varepsilon_{ijk}$, where μ_0 is the common baseline mean prior to randomization into i = 1, 2 groups (a-tDCS + SMART or s-tDCS + SMART); $\delta_{ij}$is mean change from baseline by j = 1,2 time periods (immediate (T2) or 3-month delay (T3)post-training); and ε_{ijk} are random errors, which are independent across the $k = 1, \ldots n_i$ subjects but positively correlated across the j = 0, 1, 2 time. We applied the Benjamini-Hochberg method (Benjamini and Hochberg, 1995) to control the false discovery rate (FDR) over the multiple tests.

For voxel-based analyses (VBA), the individual CBF maps were spatially smoothed with full-width half-maximum kernel of 6 mm, following the pre-processing of the images. Mixed linear effects models, as described above, were then applied to each voxel's rCBF measure, except for the fact that j = 0, 2 only (i.e., no T3 images were obtained). To control for multiple testing across voxels, we employed standard cluster extent inference, using the function *3dClustsim* (with –acf option) in AFNI (NIMH Scientific and Statistical Computing Core, Bethesda, MD, United States) and a voxel-level threshold of 0.005.

Our hypotheses concerned the two interaction effects from the mixed model, as well as the two time effects from the mixed model. Specifically, to test the effects of tDCS on both rCBF and behavioral measures, we derived *t*-statistics from the two interaction contrasts $\delta_{1j} - \delta_{2j}$ for $j = 1, 2$, corresponding to group differences between immediate- or 3-month-delay post-training mean changes from baseline, respectively To test the "main effect" of time (i.e., effects due to cognitive training, in the absence of an interaction) we derived t-statistics from the contrasts $(\delta_{1j} + \delta_{2j})/2$, the mean change from baseline, averaged over the two treatment groups for each of the post-training time periods.

Finally, at each voxel, we modeled change in rCBF as group-specific regressions on changes in behavioral measures to test for neural/behavioral relationships. Specifically, we used the linear model $\Delta z_{ik} = \beta_{0i} + \beta_{1i} \cdot \Delta y_{ik} + \in_{ik}$ and derived t-statistics from the contrasts $\beta_{11} - \beta_{12}$ to test whether the relationship depended on the tDCS treatment or from $\beta_{11} - \beta_{12}/2$ to test whether the relationship was common to both treatment groups.

RESULTS

Effect of tDCS on SMART

Overall, we observed three significant two-way interactions between groups and training effect over time. The s-tDCS + SMART group showed significant immediate cognitive gains (T2 to T1) in executive functions of inhibition [DKEFS-Color word interference *($t = -2.04$, $p = 0.047$)*] and innovation [TOSL ($t = -2.67$, $p = 0.010$)], and episodic memory as measured by retrieval of facts from a lengthy text [TOSL ($t = -2.03$, $p = 0.048$)]; whereas the a-tDCS + SMART training showed no such gains (**Table 4** and **Figure 2**). Nonetheless, the cognitive benefits did not last for over 3-months after training (T3 to T1).

Effect of tDCS on CBF

Figure 3 shows the interaction of VBA results between a-tDCS + SMART group versus s-tDCS + SMART group, testing the increase from T1 to T2 due to tDCS stimulation. A significantly larger increase in blood flow was observed at the right middle frontal cortex (MFC) in the a-tDCS + SMART compared to the s-tDCS + SMART, cluster-wise at $p = 0.05$, $k = 1{,}168$ mm^3. **Table 3** summarizes these findings for cluster-level inference as well as descriptive statistics for peak voxel within cluster. We did not find significant relationships between neurocognitive changes and rCBF changes between a-tDCS + SMART and s-tDCS + SMART groups.

Effect of Cognitive Training Averaged Over Groups

When we averaged both groups (a-tDCS and s-tDCS), we observed significant immediate cognitive improvement (T2 to T1) in executive functions of conceptual reasoning [DKEFS card sort ($p = 0.033$)] and category fluency ($p = 0.055$) along with later-emerging cognitive gains (T3 to T1) of verbal fluency ($p = 0.009$). Additionally, we showed immediate (T2 to T1) and persisted gains (T3 toT1) in self-evaluation of memory contentment and satisfaction(MMQ-C) e.g., confidence in remembering things [T2 to T1: MMQ-C ($p = 0.003$) and T3 to T1: MMQ-C ($p = 0.000$)], ability to make less mistakes on memory task (MMQ-A) e.g., *paying bills on time* [T2 to T1: MMQ-A *($p = 0.000$)* and T3to T1: MMQ-A ($p = 0.002$)] with significant improvement in applying memory strategies, e.g., organizing information one wants to remember at 3-month post training[T3 to T1: MMQ-S ($p = 0.044$)]. Finally, we observed improvement on an objective memory measure (CVLT), used also for screening purposes, immediately after training (T2 to T1) in immediate recall ($p = 0.002$) and delayed recall of words ($p = 0.001$) with the gains maintained after 3 months training (T3 to T1) in both immediate recall ($p < 0.001$), and delayed recall ($p = 0.020$) of words (**Table 5**).

DISCUSSION

The present randomized pilot trial represents a concerted effort to explore the potential benefits of a complementary

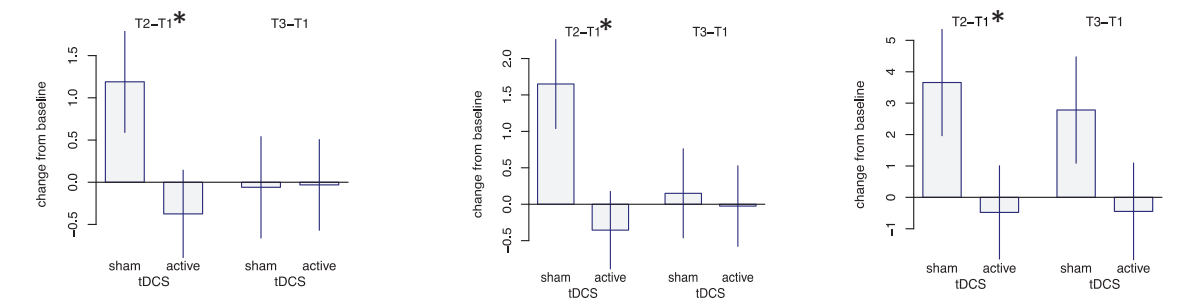

FIGURE 2 | Mixed Model Effects: Immediate cognitive gains (T2-T1) in s-tDCS + SMART group **(A)** Executive Function of Inhibition: DKEFS Color word interference ($p = 0.047$), **(B)** Executive Function of Innovation: TOSL ($p = 0.010$), and **(C)** Episodic Memory: Test of Strategic Learning (TOSL) ($p = 0.048$) relative to the a-tDCS + SMART group. *Indicates significant change (T2-T1) at $p < 0.05$.

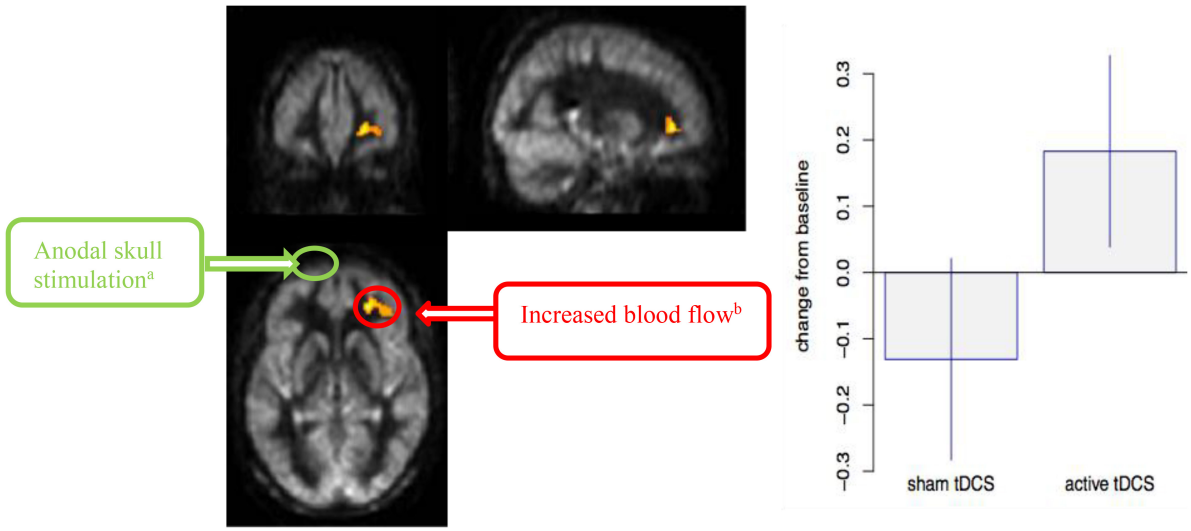

FIGURE 3 | Cerebral blood flow (CBF) voxel-based analysis for the interaction contrast, superimposed on average CBF map of all participants. Right Middle Frontal Cortex (MFC) was significant at a cluster *p*-value = 0.05 (k = 1,168 mm^3). Representation of the anodal stimulation site (green circle) and increased CBF. We illustrate the contralateral nature of the anodal stimulation from the CBF changes. **(A)** Anodal skull stimulation over *left* inferior frontal gyrus (IFG) for a total 8 sessions for 20 min prior to cognitive training over 4-week period. **(B)** Increased blood flow in *right* MFC after completing cognitive training sessions(T2-T1).

non-pharmacological treatment strategy of adding transcranial direct current stimulation prior to cognitive training sessions in MCI, a population at risk population for Alzheimer's disease. Our goal was to determine whether a-tDCS + SMART combined intervention protocol would work synergistically to increase gains above any benefits from a cognitive training protocol (i.e., SMART) alone, previously shown to benefit MCI in separate studies (Chapman and Mudar, 2014; Mudar et al., 2017). We examined post-intervention effects in cognitive abilities and neuronal health immediately after training (T2) and whether any gains would be maintained at 3 months post-training (T3) to motivate a larger trial. The study examined differences in neuronal health using measures of rCBF to better understand the neural mechanisms underlying changes resulting from a-tDCS + SMART versus s-tDCS + SMART. Additionally, the study examined the effects of cognitive training immediately (T2) and 3 months (T3) after training when both tDCS groups (a-tDCS + SMART, s-tDCS + SMART) were combined as single group for analyses.

Three findings emerged from this randomized pilot study. The primary hypothesis was that a-tDCS, delivered to the left frontal brain region for 20 min prior to each training session, would incrementally improve the effects of cognitive training over training alone (s-tDCS). This prediction was not supported. Instead, the group with a-tDCS stimulation to the left inferior frontal gyrus (IFG) prior to each training session failed to show significant gains on select measures of interest (i.e., inhibition, innovation and memory for facts)

TABLE 3 | Brain regions that showed significant cerebral blood flow (CBF) increase at rest in Active group compared to SHAM group.

			MNI			
Brain Regions	**BA**	**Cluster Size (mm^3)**	***X***	***Y***	***Z***	***T*-Value**
Sham < Active						
Right Middle Frontal Cortex	10	1,168	24	44	−2	6.1

The coordinates depict the peak of clusters.

TABLE 4 | Mixed Model: Interaction effects [Group (a-tDCS versus s-tDCS) × Time effect (SMART training)]: Immediate cognitive gains (T2-T1), and Delayed cognitive gains (T3-T1) changes in cognitive function in mild cognitive impairment (MCI).

Screening and Neurocognitive Measures	**Immediate cognitive gains (T2-T1)**		**Delayed cognitive gains (T3-T1)**	
	***t*-statistics**	***p*-value**	***t*-statistics**	***p*-value**
Executive Functions				
(1) Inhibition				
(a) *DKEFS-Colorword interference (Switching and Inhibition)*	−2.04	0.047*	0.04	0.971
(2) Complex abstraction				
(a) *TOSL*	−0.27	0.79	−1.01	0.315
(3) Innovation				
(a) *TOSL*	−2.67	0.010*	−0.23	0.820
Memory				
(1) *Episodic Memory: Memory for facts*				
(a) *TOSL*	−2.03	0.048*	−1.55	0.127

DKEFS, Delis–Kaplan Executive Function System^{TM}, TOSL, Test of Strategic Learning. p-values < 0.05(significant) specified tests of interaction contrasts.*

TABLE 5 | Mixed Model: Time Effect on cognitive measures irrespective of group assignment: Immediate cognitive gains (T2-T1), and Delayed cognitive gains (T3-T1) changes in cognitive function in mild cognitive impairment (MCI).

Neurocognitive Measures	Immediate cognitive gains (T2-T1)		Delayed cognitive gains (T3-T1)	
	t-statistics	*p*-value	*t*-statistics	*p*-value
Executive Functions				
(1) Conceptual Reasoning				
(a) DKEFS Card Sort	2.22	0.032*	1.54	0.015*
(2) Fluency				
(a) Verbal Fluency (COWAT)	0.88	0.385	2.82	0.009**
(b) Category Fluency (COWAT)	1.99	0.055*	1.38	0.176
3. Complex abstraction	0.96	0.343	0.89	0.379
Memory				
(1) Complex Memory				
(a) *Selective Auditory Learning* Task				
(i) Trial 1	−0.27	0.294	−0.50	0.620
(ii) Trial 2	0.56	0.580	1.68	0.101
(iii) Trial 3	0.49	0.624	1.07	0.292
Subjective Memory Evaluation (MMQ)				
(a) MMQ Contentment	3.29	0.003**	3.92	<0.001**
(b) MMQ Ability	5.17	<0.001**	3.39	0.002**
(c) MMQ Strategies	1.07	0.294	2.10	0.044*
Memory Screening Measures (CVLT)				
(a) CVLT: Immediate Recall	3.40	0.002**	4.22	0.000**
(b) CVLT: Delayed Recall	3.63	0.001**	2.43	0.020*

*DKEFS, Delis–Kaplan Executive Function System™; MMQ, Multifactorial Memory Questionnaire; COWAT, Controlled Oral Word Association Test; CVLT, California Verbal Learning Task. *p-values refers to the mixed model effects. **Significance at 5% false discovery rate (FDR) over the multiple tests.*

after training compared to the s-tDCS + SMART group at T2 or T3. In contrast, the s-tDCS + SMART group showed significant immediate gains (T2) on two measures of executive function, both inhibition and innovation, and on a memory for facts (episodic memory) measure as compared to the a-tDCS group. Second, our analyses of regional resting cerebral blood flow (rCBF) revealed a significant immediate increase in the right middle frontal cortex (MFC) (T2-T1) in the a-tDCS + SMART group when compared to the sham + SMART group. These two findings of between-group differences taken together, suggest that the a-tDCS did indeed modulate cognitive and neural plasticity, just not in the expected manner. The findings suggested that the a-tDCS served to 'block' certain higher-order cognitive performance gains on measures of inhibition, innovation, and memory for facts. Nonetheless, we did find evidence that participants, combined across groups, showed immediate (T2) cognitive gains in executive functions of conceptual reasoning and fluency (verbal and category fluency) as well as on a screening measure of memory (i.e., CVLT). On the latter screening measure (CVLT), both groups made comparable gains despite significantly different baseline means on CVLT. The combined groups also showed significant immediate (T2 to T1) and persisted (T3 to T1) improvement in subjective satisfaction in memory abilities [Multifactorial Memory questionnaire (MMQ)] reported via questionnaire.

To our knowledge, the present randomized pilot represents one of the first studies in MCI to compare a-tDCS directed toward left IFG versus s-tDCS, delivered before each cognitive training session. The contradictory findings to our expectations suggest that the anode and cathode placement sites we chose, i.e., left IFG and right arm respectively, failed to incrementally improve cognition above that achieved by SMART training alone, despite clear evidence that the tDCS altered rCBF. What is important to note is the higher rCBF at T2 (end of training period of eight sessions) was in the contralateral prefrontal cortex to the one stimulated, not the region beneath the stimulated left IFG.

The key question that emerges is why a-tDCS over left IFG 'blocked' rather than enhanced neuromodulation effects of cognitive training (SMART) on relevant cognitive measures in this MCI randomized pilot trial. We offer several possible explanations for our unexpected findings that should be explored in subsequent trials to better understand the underlying mechanisms contributing to or blocking additive benefits of tDCS to cognitive training. Transcranial direct current stimulation has shown to modulate cortical plasticity that can be manifested as either excitatory or inhibitory (Prehn and Flöel, 2015). A plausible explanation for why the a-tDCS did not enhance performance in this pilot trial could be that the direct current applied to left IFG may have modulated the resting membrane action potential (AP) inducing inhibitory hemostatic mechanism, and thereby reducing the neuroplasticity of subsequent learnings during cognitive training (Lang et al., 2003; Peters et al., 2013). A second alternative is that the multiple sessions of a-tDCS to left IFG perturbed the spontaneous firing rates of neural networks thereby blocking the consolidation of top-down learned strategies of SMART training (Peters et al., 2013). In order to explore the real-time neural changes induced by tDCS, future studies should evaluate neural response during stimulation with measures such as immediate changes in rCBF, alterations in resting-state functional connectivity or changes in EEG, to mention a few. Another possible explanation for the 'blocked' effects may be the a-tDCS triggered a reallocation of CBF to the contralateral side to the site stimulated, disrupting the underlying neural network subserving these higher-order cognitive abilities. Support for this possible explanation of the 'blocking effects' of the a-tDCS arises from prior evidence that disrupted right prefrontal cortical function interferes with holistic processing, such as that assessed by our innovation measure (Heilman et al., 2003; Siddiqui et al., 2008). Whether the detrimental impact of a-tDCS prior to cognitive training, implicated in this pilot project, is due to the fact that the brain was already compromised by MCI, or whether this would be the case for other populations, either healthy or those with more focal injuries, remains to be explored.

One pattern that remains equivocal is whether higher or lower rCBF represents positive or maladaptive neural changes (Chapman et al., 2016). Seemingly the increased rCBF was not linked to adaptive gains in the present study. However, it is

important to point out that we did not find a relationship between lower cognitive performance and either higher versus lower rCBF in the present study, possibly due to small sample size. Therefore, we interpret our findings that the increased rCBF in the right MFC may be a maladaptive response to stimulation of the left frontal area cautiously. The present pilot findings raise more questions than it answers and points to the importance of seeking converging patterns between cognitive and neural changes resulting from intervention protocols, to better understand the neural mechanisms related to both positive and negative effects. Whereas we had anticipated the neural changes to be more closely identified in the site of stimulation, (i.e., left prefrontal cortex), other work has shown remote changes from the stimulation site. Similar to our findings of increased CBF in alternate brain regions from the one stimulated, Yun's study (Yun et al., 2016) which measured glucose utilization a proxy for rCBF using resting 18-Fluorodeoxyglucose positron emission tomography (18FDG-PET) observed increased glucose uptake in non-stimulated area i.e., dorsolateral, ventrolateral, medial prefrontal cortices, the anterior and posterior insula, the hippocampal and parahippocampal areas, and the dorsal anterior cingulate but not in the stimulated region.

The present pilot trial provides data to glean insights to guide future endeavors which incorporate tDCS to test as a viable additive intervention option in MCI. The factors to consider that may help improve upon our current methodology include, but are not limited to: (1) the mechanism of action resulting from tDCS, (2) the electrode placement for stimulation (anodal and cathodal), (3) timing, length, and frequency of stimulation, (4) population under-study, and (5) measures adopted to examine effectiveness.

Mechanism of Action

An important finding from our study was that a-tDCS directed over the left IFG was associated with increased rCBF to the right MFC. We cannot ascertain whether the tDCS stimulation effect alone created the changes in right frontal brain region or whether it was a combination effect of the training + tDCS effects. Prior work has shown that the 'site of stimulation' is the general area beneath the anode site, however, the neural alterations can occur across a larger neural network than the stimulated region (Yun et al., 2016). Our findings support the growing evidence that the tDCS impact is not directly related to the specific brain region under the electrode (Polanía et al., 2011). Our preliminary data suggest that the tDCS served to modulate neuronal function across specific brain networks since the left and right frontal regions are highly interconnected (Greicius et al., 2003). Thus as implicated above, the inhibitory effects from left frontal cortex may represent a generalized network effect that spread to the right frontal cortex.

Whereas the tDCS stimulation attenuated cognitive training effects on select measures, i.e., inhibition, innovation and complex fact memory (episodic memory) or episodic memory; other processes of complex abstraction and memory were less affected. Thus, it is important to point out that tDCS did not have a global inhibitory effect on all cognitive domains. Nonetheless, tDCS did not enhance any of the cognitive gains over and above the levels accelerated by training alone in the present study. We recognize that the pattern of findings is limited by our methodology and sample size.

Montage Placement

The general anodal and cathodal placement that we utilized in the present study did not result in enhanced cognitive training effects. One next possible alternative methodology to test would be to stimulate the right frontal cortex to test whether this site of stimulation would increase rCBF to left frontal cortex. It is possible that stimulation to the contralateral frontal brain region may have enhanced, rather than attenuated, frontally mediated higher-order cognitive domains such as innovative thinking and complex inhibitory responses since prior evidence has supported left frontal cortex increased CBF associated with higher cognitive performance following training (Chapman and Mudar, 2014; Chapman et al., 2015). Additionally, the placement of the cathode electrode may impact the outcomes. A handful of other studies using tDCS in MCI applied the cathode stimulation to the right frontal polar cortex (Meinzer et al., 2015); whereas we chose to place the cathode on the right arm motivated by prior study in MCI and AD (Ferrucci et al., 2008; Boggio et al., 2012; Cotelli et al., 2014). The rationale for this cathode electrode placement was that we did not want to deactivate the opposite side of the brain region i.e., right frontal cortex, a hub for modulation of attention and creativity the summary of SMART training (Shruti et al., 2015).

Timing and Frequency

Another major difference between our methodology and the one used by Meinzer et al. (2015) in MCI was they stimulated during active task performance rather than prior to learning new cognitive strategies, as in our study. We chose to stimulate prior to training based on prior evidence that tDCS can enhance the brain's readiness to respond to subsequent learning (Prehn and Flöel, 2015). Subsequent trials should test whether anodal stimulation during training instead of just prior to training would enhance gains. We only provided stimulation and training twice a week. More intensive stimulation within shorter time intervals may be necessary to keep the brain primed to benefit from training.

Population

Overall, the results support prior evidence (Mudar et al., 2017, 2019) that individuals with MCI can benefit from cognitive training, which in this case was SMART, as manifested by cognitive gains in the s-tDCS + SMART and both groups combined (sham + a-tDCS) with SMART. The current finding of generalizability of SMART to non-trained cognitive gains to other domains such as fluency and daily life function as measured by the MMQ (subjective memory evaluation) is promising. Additionally, the emergence of gains in the perceived facility in using memory strategies MMQ-S, although not observed immediately, but rather at 3 months after the training ended, may be due to a strengthening of self-confidence persisting from training. Previous work has shown that individuals manifest gains after SMART training has ended, hypothesized to emerge as individuals continue to

utilize and habitually apply strategies learned during SMART in their daily life. Similar findings of SMART benefits were found across different studies in both healthy and clinical populations such as traumatic brain injury and bipolar disorders (Chapman et al., 2015; Vas et al., 2016; Venza et al., 2016). Not only does cognitive training strengthen cognitive and neural abilities but emerging evidence suggests that strategy-based cognitive training might be beneficial in mitigating dementia onset. The Advanced Cognitive Training for Independent and Vital Elderly (ACTIVE) RCT study in older cognitively normal adults, which implemented three cognitive training models targeting: memory, reasoning, and speed of processing, found that speed of processing training was able to decrease the rate of dementia by 29% over a 10 years' period (Edward et al., 2017). Thus, our findings add to the prior knowledge that cognitive training can help strengthen cognitive functions not only in cognitively normal elderly but also in individuals with MCI and perhaps even slow rate of cognitive losses.

Moreover, cognitive gains, when both groups were combined, showed not only gains in individual's subjective memory perception [Multifactorial-Memory Questionnaire(MMQ)] as noted above, but also on the objective measure of memory [California Verbal Learning Task (CVLT)], a test that was used to characterize MCI in participants as screening criteria. On this objective memory measure, the combined groups showed significantly higher scores immediately (T2) and over 3-months post-training (T3) period. Taken together, these results suggest that SMART impacted not only enhanced higher-order cognitive performance but also showed generalized effects on memory, both self-reported (MMQ) and measured (CVLT).

The failure to find significant group differences on the subjective and objective memory measures may be due to the small sample size as we were moderately powered for assessing the interaction effects, though well-powered for all neurocognitive tests assessing the SMART effect alone. The limitation of low power of the study could explain the discrepancy of our study findings from Yun's study (Yun et al., 2016) which showed substantial improvement in subjective memory rating (MMQ) only in a-tDCS group compared to the s- tDCS stimulation over left DLPFC. One more issue of consideration is where the individuals are along the MCI to Alzheimer's dementia continuum in terms of disease severity. For example, based on Cotelli's work (Cotelli et al., 2014) in 36 AD patients failed to show significant cognitive gains when computerized memory training was combined with a-tDCS stimulation to the left DLPFC with a constant current of 2 mA for a total of 10 sessions for 25 min per session over 2 weeks compared to sham group. Perhaps our participants were more impaired than those in Yun's study.

Measures

The majority of tDCS studies have investigated the benefit on primary motor cortex and isolated cognitive processes. Our results suggest that tDCS may have limited beneficial adjuvant effects in recruiting cortical plasticity to enhance higher-order cognitive processes in individuals who are at a greater risk of cognitive decline. In the current study, a-tDCS over left IFG served to attenuate gains of SMART on complex measures of inhibition, innovative cognition as measured by fluency of multiple interpretations, and episodic memory as measured by recall of facts from complex textual information. Nonetheless, even in a healthy aging group, the result supports that consolidation of visual learning could be blocked as soon as second day, using a-tDCS stimulation for 20 min and 2 mA current on primary visual cortex (Peters et al., 2013). In line with our work and similar other work on motor cortex and visual learning (Lang et al., 2003; Peters et al., 2013), one presumable hypothesis is that repeated stimulation to vulnerable region i.e., IFG blocked the consolidation of frontally mediated top–down learning strategies central to SMART training. Moreover, it is unclear to what extent these present findings are transferable to other methodological manipulations such as loci of stimulation and stimulation during or prior to trainings.

CONCLUSION

This study provides evidence that a-tDCS to the left frontal cortex does affect cognitive-neural changes in MCI, but not in a direction that supported a view that tDCS presented just prior to cognitive training elevated higher-order cognitive training benefits or served to ameliorate cognitive dysfunction. That is, the loci and timing of stimulation adopted in the present study did not replicate prior findings suggesting a potential modifying effect of tDCS on MCI (Meinzer et al., 2015; Yun et al., 2016; Murugaraja et al., 2017; Gonzalez et al., 2018). Future work is needed to examine precisely what happens to brain when tDCS is applied using fMRI studies to better understand the action of tDCS at the neuronal level. Strengths of the study are the randomized control design, the inclusion of broad-based cognitive measures, well-defined MCI population based on widely accepted criteria, and replication of prior findings that individuals with MCI can benefit from top–down cognitive training, namely SMART. Prior evidence has shown consistent data that cognitive training may be one of the most promising currently available interventions to impact disease progression (Edward et al., 2017).

Moreover, the most important contribution of the present study is that it adds to the growing body of compelling evidence that cognitive training provides an intervention option to benefit people today. Instead of feeling no options exist, this work supports prior evidence that being proactive about cognitive brain health may reap benefits in strengthening cognitive capabilities. Further studies are required to explore the short-term and long-term cognitive and neural benefits of combined non-pharmacological interventions in MCI with the goal to develop protocols that delay progression of MCI to AD. Indeed, keeping the mind stimulated may be a key aspect to mitigating some age-related aspects of cognitive decline or

MCI-specified deficits. This study motivates future work to test potential additive effects of tDCS stimulation during training and potentially different loci of stimulation. Nonetheless, this initial pilot supports the view that tDCS stimulation techniques are safe to apply to the human brain and do cross the bony protection of the skull into effect brain change.

AUTHOR CONTRIBUTIONS

ND has been the key player in the research, analysis of the data, and writing the complete manuscript. SC was the principal investigator of the study and has been an integral part in the completion of the manuscript. JS played a key role in analyzing the data. SA was involved in MRI analysis. SV and AR were an integral part in the development of tDCS research protocol and implementation of the research. AR involved in the recruitment of the participant. RM helped in reviewing the article and give valuable feedback. MQ is board certified neurologist that confirmed the diagnosis of MCI in the study.

FUNDING

This research project was supported by BvB Dallas, Sammons Enterprises, Barbara Wallace and Kelly King Charitable Foundation Trust, the AWARE fund of the Dallas Foundation, and the Golden Rule Family Foundation. ClinicalTrials.gov ID: NCT02588209.

ACKNOWLEDGMENTS

We would like to thank all of the participants in this study and the research team, especially Jennifer Kriegel (Research Coordinator), Erin Venza (Clinician), and Stacy Vernon (Clinician) for making this research possible.

REFERENCES

Aisen, P. S., Petersen, R. C., and Donohue, M. C. (2010). Clinical core of the Alzheimer's disease neuroimaging initiative: progress and plans. *Alzheimers Dement* 6, 239–246. doi: 10.1016/j.jalz.2010.03.006

Anand, R., Chapman, S. B., Rackley, A., Keebler, M., Zientz, J., and Hart, J. (2011). Gist reasoning training in cognitively normal seniors. *Int. J. Geriatr. Psychiatry* 26, 961–968. doi: 10.1002/gps.2633

Andrieu, S., Coley, N., Lovestone, S., Aisen, P. S., and Vellas, B. (2015). Prevention of sporadic alzheimer's disease: lessons learned from clinical trials and future directions. *Lancet Neurol.* 14, 926–944. doi: 10.1016/S1474-4422(15)00153-2

Aron, A. R., Robbins, T. W., and Poldrack, R. A. (2004). Inhibition and the right inferior frontal cortex. *Trends Cogn. Sci.* 8, 170–177. doi: 10.1016/j.tics.2004.02.010

Aslan, S., Xu, F., Wang, P. L., Uh, J., Yezhuvath, U. S., van Osch, M., et al. (2010). Estimation of labeling efficiency in pseudocontinuous arterial spin labeling. *Magn. Res. Med.* 63, 765–771. doi: 10.1002/mrm.22245

Belleville, S., Clement, F., Mellah, S., Gilbert, B., Fontaine, F., and Gauthier, S. (2011). Training-related brain plasticity in subjects at risk of developing Alzheimer's disease. *Brain* 134, 1623–1634. doi: 10.1093/brain/awr037

Benjamini, Y., and Hochberg, Y. (1995). Controlling the false discovery rate: a practical and powerful approach to multiple testing. *J. R. Stat. Soc. (Ser. B)* 57, 289–300. doi: 10.1111/j.2517-6161.1995.tb02031.x

Benton, A. L., Hamsher, K. D., and Sivan, A. B. (1994). *Multilingual Aphasia Examination: Manual of Instructions*. Iowa City, IA: AJA Associates Inc.

Biundo, R., Weis, L., Fiorenzato, E., and Gentile, E. (2015). Double-blind randomized trial of t-DCS versus sham in parkinson patients with mild cognitive impairment receiving cognitive training. *Brain Stimulat.* 8, 1223–1225. doi: 10.1016/j.brs.2015.07.043

Boggio, P. S., Ferrucci, R., and Mameli, F. (2012). Prolonged visual memory enhancement after direct current stimulation in Alzheimer's disease. *Brain Stimulat*. 5, 223–230. doi: 10.1016/j.brs.2011.06.006

Cattaneo, Z., Pisoni, A., and Papagno, C. (2011). Transcranial direct current stimulation over Broca's region improves phonemic and semantic fluency in healthy individuals. *Neuroscience* 183, 64–70. doi: 10.1016/j.neuroscience.2011.03.058

Chapman, S. B., Aslan, S., Spence, J. S., Hart, J. J. Jr., Bartz, E. K., Didehbani, N., et al. (2015). Neural mechanisms of brain plasticity with complex cognitive training in healthy seniors. *Cereb. Cortex* 25, 396–405. doi: 10.1093/cercor/bht234

Chapman, S. B., Aslan, S., Spence, J. S., Keebler, M. W., DeFina, L. F., Didehbani, N., et al. (2016). Distinct brain and behavioral benefits from cognitive vs. physical training: a randomized trial in aging adults. *Front. Hum. Neurosci.* 10:338. doi: 10.3389/fnhum.2016.00338

Chapman, S. B., and Mudar, R. A. (2014). Enhancement of cognitive and neural functions through complex reasoning training: evidence from normal and clinical populations. *Front. Syst. Neurosci.* 8:69. doi: 10.3389/fnsys.2014.00069

Chapman, S. B., Spence, J., Aslan, S., and Keebler, M.W. (2017). Enhancing innovation and underlying neural mechanisms via cognitive training in healthy older adults. *Front. Aging Neurosci.* 9:314. doi: 10.3389/fnagi.2017.00314

Chapman, S. B., Zientz, J., Weiner, M., Rosenberg, R., Frawley, W., and Burns, M. H. (2002). Discourse changes in early Alzheimer disease, mild cognitive impairment, and normal aging. *Alzheimer Dis. Assoc. Disord.* 16177–16186. doi: 10.1097/00002093-200207000-00008

Cohen, A. D., and Klunk, W. E. (2014). Early detection of Alzheimer's disease using PiB and FDG PET. *Neurobiol. Dis.* 72(Pt A), 117–122. doi: 10.1016/j.nbd.2014.05.001

Cook, L. G., Chapman, S. B., Elliott, A. C., Evenson, N. N., and Vinton, K. (2014). Cognitive gains from gist reasoning training in adolescents with chronic-stage traumatic brain injury. *Front. Neurol.* 5:87. doi: 10.3389/fneur.2014.00087

Cotelli, M., Manenti, R., and Brambilla, M. (2014). Anodal tDCS during face-name associations memory training in Alzheimer's patients. *Front. Aging Neurosci.* 6:38. doi: 10.3389/fnagi.2014.00038

Delis, D. C., Kaplan, E., and Kramer, J. H. (2001). *Delis-Kaplan Executive Function System (D-KEFS)*. San Antonio, TX: Psychological Corporation.

Diamond, E. L., Miller, S., Dickerson, B. C., Atri, A., Depeau, K., Fenstermacher, E., et al. (2007). Relationship of fMRI activation to clinical trial memory measures in Alzheimer disease. *Neurology* 69, 1331–1341. doi: 10.1212/01.wnl.0000277292.37292.69

Edward, J. D., Huiping, X., Daniel, O. C., Lin, T. G., Lesley, A. R., Frederick, W. U., et al. (2017). Speed of processing training results in lower risk of dementia. *Alzheimer's Dementia Transl.* 3, 603–611. doi: 10.1016/j.trci.2017.09.002

Elder, G. J., and Taylor, J. P. (2014). Transcranial magnetic stimulation and transcranial direct current stimulation: treatments for cognitive and neuropsychiatric symptoms in the neurodegenerative dementias? *Alzheimer's Res. Ther.* 6:74. doi: 10.1186/s13195-014-0074-1

Erickson, K. I., Voss, M. W., Prakash R. S., Basak, C., Szabo, A., Chaddock, L., et al. (2011). Exercise training increases size of hippocampus and improves memory. *Proc. Natl. Acad. Sci. U.S.A.* 108, 3017–3022. doi: 10.1073/pnas.1015950108

Ferrucci, R., Mameli, F., Guidi, I., Mrakic-Sposta, S., Vergari, M., Marceglia, S., et al. (2008). Transcranial direct current stimulation improves recognition memory in Alzheimer disease. *Neurology* 71, 493–498. doi: 10.1212/01.wnl.0000317060.43722.a3

Filbey, F. M., Chen, G., Sunderland, T., and Cohen, R. M. (2010). Failing compensatory mechanisms during working memory in older apolipoprotein E-epsilon4 healthy adults. *Brain Imag. Behav.* 4, 177–188. doi: 10.1007/s11682-010-9097-9

Flöel, A., Suttorp, W., Kohl, O., Kürten, J., Lohmann, H., Breitenstein, C., et al. (2012). Non-invasive brain stimulation improves object-location learning in the elderly. *Neurobiol. Aging* 33, 1682–1689. doi: 10.1016/j.neurobiolaging.2011.05.007

Folstein, M. F., Folstein, S. E., and McHugh, P. R. (1975). Minimentalstate: apractical method for grading the cognitive state of patients for the clinician. *J. Psychiatr. Res.* 12, 189–198. doi: 10.1016/0022-3956(75)90026-6

Gonzalez, P. C., Fong, K., Chung, R., Ting, K. H., Law, L., and Brown, T. (2018). Can transcranial direct-current stimulation alone or combined with cognitive training be used as a clinical intervention to improve cognitive functioning in persons with mild cognitive impairment and dementia? A systematic review and meta-analysis. *Front. Hum. Neurosci.* 12:416. doi: 10.3389/fnhum.2018.00416

Grady, C. (2012). The cognitive neuroscience of ageing. *Nat. Rev. Neurosci.* 13, 491–505. doi: 10.1038/nrn3256

Greicius, M. D., Krasnow, B., Reiss, A. L., and Menon, V. (2003). Functional connectivity in the resting brain: a network analysis of the default mode hypothesis. *Proc. Natl. Acad. Sci. U.S.A.* 100, 253–258. doi: 10.1073/pnas.0135058100

Han, K., Davis, R. A., Chapman, S. B., and Krawczyk, D. C. (2017). Strategy-based reasoning training modulates cortical thickness and resting-state functional connectivity in adults with chronic traumatic brain injury. *Brain Behav.* 7:e00687. doi: 10.1002/brb3.687

Hanten, G., Li, X., and Chapman, S. B. (2007). Development of verbal selective learning. *Dev. Neuropsychol.* 32, 585–596. doi: 10.1080/87565640701361112

Harvey, P. D., McGurk, S. R., Mahncke, H., and Wykes, T. (2018). Controversies in computerized cognitive training. *Biol. Psychiatry Cognit. Neurosci. Neuroimaging* 3, 907–915. doi: 10.1016/j.bpsc.2018.06.008

Heilman, K. M., Nadeau, S. E., and Beversdorf, D. O. (2003). Creative innovation: possible brain mechanisms. *Neurocase* 9, 369–379. doi: 10.1076/neur.9.5.369.16553

Iyer, M. B., Mattu, U., Grafman, J., Lomarev, M., Sato, S., and Wassermann, E. M. (2005). Safety and cognitive effect of frontal DC brain polarization in healthy individuals. *Neurology* 64, 872–875. doi: 10.1212/01.WNL.0000152986.07469.E9

Jean, M.-È., Bergeron, S., and Thivierge, M. (2010). Cognitive intervention programs for individuals with mild cognitive impairment: systematic review of the literature. *Am. J. Geriatr. Psychiatry* 18, 281–296. doi: 10.1097/JGP.0b013e3181c37ce9

Lang, N., Nitsche, M. A., Sommer, M., Tergau, F., and Paulus, W. (2003). Chapter 28 modulation of motor consolidation by external DC stimulation. *Suppl. Clin. Neurophysiol.* 56, 277–281. doi: 10.1016/S1567-424X(09)70231-4

Manenti, R., Brambilla, M., Benussi, A., Rosini, S., Cobelli, C., Ferrari, C., et al. (2016), Mild cognitive impairment in Parkinson's disease is improved by transcranial direct current stimulation combined with physical therapy. *Mov. Disord.* 31, 715–724. doi: 10.1002/mds.26561

Manly, J. J., Tang, M. X., Schupf, N., Stern, Y., Vonsattel, J. P., and Mayeux, R. (2008). Frequency and course of mild cognitive impairment in a multiethnic community. *Ann. Neurol.* 63, 494–506. doi: 10.1002/ana.21326

Meinzer, M., Lindenberg, R., Phan, M. T., Ulm, L., Volk, C., and Flöel, A. (2015). Transcranial direct current stimulation in mild cognitive impairment: behavioral effects and neural mechanisms. *Alzheimer Dement.* 11, 1032–1040. doi: 10.1016/j.jalz.2014.07.159

Morris, J. (1993). The clinical dementia rating (CDR): current version and scoring rules. *Neurology* 43, 2412–2414. doi: 10.1212/WNL.43.11.2412-a

Morris, M. C. (2009). The role of nutrition in Alzheimer's disease: epidemiological evidence. *Eur. J. Neurol.* 16(Suppl 1), 1–7. doi: 10.1111/j.1468-1331.2009.02735.x

Motes, M. A., Yezhuvath, U. S., Aslan, S., Spence, J. S., Rypma, B., and Chapman, S. B. (2018) Higher-order cognitive training effects on processing speed-related neural activity: a randomized trial. *Neurobiol. Aging* 62, 72–81. doi: 10.1016/j.neurobiolaging.2017.10.003

Mudar, R. A., Chapman, S. B., Rackley, A., Eroh, J., Chiang, H. S., Perez, A., et al. (2017). Enhancing latent cognitive capacity in mild cognitive impairment with gist reasoning training: a pilot study. *Int J Geriatr Psychiatry* 32, 548–555. doi: 10.1002/gps.4492

Mudar, R. A., Nguyen, L. T., Eroh, J., Chiang, H., Rackley, A., and Chapman, S. B. (2019). Event-related neural oscillation changes following reasoning training in individuals with mild cognitive impairment. *Brain Res.* 1704, 229–240. doi: 10.1016/j.brainres.2018.10.017

Murugaraja, V., Shivakumar, V., Sivakumar, P. T., Sinha, P., and Venkatasubramanian, G. (2017). Clinical utility and tolerability of transcranial direct current stimulation in mild cognitive impairment. *Asian J. Psychiatr.* 30, 135–140. doi: 10.1016/j.ajp.2017.09.001

Nitsche, M. A., Antal, A., Liebetanz, D., Lang, N., Tergau, F., and Paulus, W. (2007). "Induction and modulation of neuroplasticity by behavioural neurology 13 transcranial direct current stimulation," in *Transcranial Brain Stimulation for Treatment of Psychiatric Disorders*, eds M. A. Marcolin and F. Padberg, Vol. 23 (Basel: Karger).

Peters, M. A. K., Thompson, B., Merabet, L. B., Wu, A. D., and Shams, L. (2013) Anodal tDCS to V1 blocks visual perceptual learning consolidation. *Neuropsychologia* 51, 1234–1239. doi: 10.1016/j.neuropsychologia.2013.03.013

Petersen, R. C., Doody, R., and Kurz, A. (2001). Current concepts in mild cognitive impairment. *Arch. Neurol.* 58:1985. doi: 10.1001/archneur.58.12.1985

Polanía, R., Nitsche, M. A., and Paulus, W. (2011). Modulating functional connectivity patterns and topological functional organization of the human brain with transcranial direct current stimulation. *Hum. Brain Mapp.* 32, 1236–1249. doi: 10.1002/hbm.21104

Prehn, K., and Flöel, A. (2015). Potentials and limits to enhance cognitive functions in healthy and pathological aging by tDCS. *Front. Cell. Neurosci.* 9:355. doi: 10.3389/fncel.2015.00355

Reinhart, R. M., Cosman, J. D., Fukuda, K., and Woodman, G. F. (2017). Using transcranial direct-current stimulation (tDCS) to understand cognitive processing. *Attent. Percept. Psychophys.* 79, 3–23. doi: 10.3758/s13414-016-1224-2

Roberts, R. O., Knopman, D. S., Mielke, M. M., Cha, R. H., Pankratz, V. S., Christianson, T. J., et al. (2014). Higher risk of progression to dementia in mild cognitive impairment cases who revert to normal. *Neurology* 82, 317–325. doi: 10.1212/WNL.0000000000000055

Rubia, K., Smith, A. B., Brammer, M. J., and Taylor, E. (2003). Right inferior prefrontal cortex mediates response inhibition while mesial prefrontal cortex is responsible for error detection. *Neuroimage* 20, 351–358. doi: 10.1016/S1053-8119(03)00275-1

Shruti, J., Holiday, K., Satyshur, M., Mukai, I., and Ungerleider, L. G. (2015). A role of right middle frontal gyrus in reorienting of attention: a case study. *Front. Syst. Neurosci.* 9:23. doi: 10.3389/fnsys.2015.00023

Siddiqui, S. V., Chatterjee, U., Kumar, D., Siddiqui, A., and Goyal, N. (2008). Neuropsychology of prefrontal cortex. *Indian J. Psychiatry* 50, 202–208. doi: 10.4103/0019-5545.43634

Spreen, O., and Strauss, E. (1998). *A Compendium of Neuropsychological Tests: Administration, Norms, and Commentary*. New York, NY: Oxford University Press.

Troyer, A. K., and Rich, J. B. (2002). Psychometric properties of a new metamemory questionnaire for older adults. *J. Gerontol. B Psychol. Sci. Soc. Sci.* 57, P19–P27. doi: 10.1093/geronb/57.1.P19

Vas, A., Chapman, S., Aslan, S., Spence, J., Keebler, M., Rodriguez-Larrain, G., et al. (2016). Reasoning training in veteran and civilian traumatic brain injury with persistent mild impairment. *Neuropsychol. Rehabil.* 26, 502–531. doi: 10.1080/09602011.2015.1044013

Vas, A. K., Chapman, S. B., and Cook, L. G. (2015). Language impairments in traumatic brain injury: a window into complex cognitive performance. *Handb. Clin. Neurol.* 128, 497–510. doi: 10.1016/b978-0-444-63521-1.00031-5

Vas, A. K., Chapman, S. B., Cook, L. G., Elliott, A. C., and Keebler, M. (2011). Higher-order reasoning training years after traumatic brain injury in adults. *J. Head Trauma Rehabil.* 26, 224–239. doi: 10.1097/HTR.0b013e318218dd3d

Venza, E. E., Chapman, S. B., Aslan, S., Zientz, J. E., Tyler, D. L., and Spence, J. S. (2016). Enhancing executive function and neural health in bipolar disorder through reasoning training. *Front. Psychol.* 7:1676. doi: 10.3389/fpsyg.2016.01676

Wechsler, D. (1997a). *Wechsler Adult Intelligence Scale III*. San Antonio, TX: Harcourt Assessment.

Wechsler, D. (1997b). *Wechsler Memory Scale*, 3rd Edn. San Antonio, TX: The Psychological Corporation.

Weiner, M. W., Veitch, D. P., and Aisen, P. S. (2013). The alzheimer's disease neuroimaging initiative: a review of papers published since its inception. *Alzheimer's Dementia* 9:194. doi: 10.1016/j.jalz.2013.05.1769

Wilkinson, G. S., and Robertson, G. J. (2006). *WRAT4 Wide Range Achievement Test: Professional Manual*. Lutz, FL: PAR.

Wishart, H. A., Saykin, A. J., Rabin, L. A., Santulli, R. B., Flashman, L. A., Guerin, S. J., et al. (2006). Increased brain activation during working memory in cognitively intact adults with the APOE epsilon4 allele. *Am. J. Psychiatry* 163, 1603–1610. doi: 10.1176/appi.ajp.163.9.1603

Yesavage, J. A., Brink, T. L., and Rose, T. L. (1982). Development and validation of a geriatric depression screening scale: a preliminary report. *J. Psychiatr. Res.* 17, 37–49. doi: 10.1016/0022-3956(82)90033-4

Yun, K., Song, I.-U., and Chung, Y. -A. (2016). Changes in cerebral glucose metabolism after 3 weeks of noninvasive electrical stimulation of mild cognitive impairment patients. *Alzheimer. Res. Ther.* 8:49. doi: 10.1186/s13195-016-0218-6

Conflict of Interest Statement: The authors declare that the research was conducted in the absence of any commercial or financial relationships that could be construed as a potential conflict of interest.

frontiers in Neuroscience

REVIEW
published: 18 April 2019
doi: 10.3389/fnins.2019.00366

Beyond Emotions: Oscillations of the Amygdala and Their Implications for Electrical Neuromodulation

Lisa-Maria Schönfeld[1] *and Lars Wojtecki*[2,3,4]*

[1] Comparative Psychology, Institute of Experimental Psychology, Heinrich Heine University Düsseldorf, Düsseldorf, Germany, [2] Institute of Clinical Neuroscience and Medical Psychology, Medical Faculty, Heinrich Heine University Düsseldorf, Düsseldorf, Germany, [3] Department of Neurology, Center for Movement Disorders and Neuromodulation, Medical Faculty, Heinrich Heine University Düsseldorf, Düsseldorf, Germany, [4] Department of Neurology and Neurorehabilitation, Hospital zum Heiligen Geist, Kempen, Germany

The amygdala is a structure involved in emotions, fear, learning and memory and is highly interconnected with other brain regions, for example the motor cortex and the basal ganglia that are often targets of treatments involving electrical stimulation. Deep brain stimulation of the basal ganglia is successfully used to treat movement disorders, but can carry along non-motor side effects. The origin of these non-motor side effects is not fully understood yet, but might be altered oscillatory communication between specific motor areas and the amygdala. Oscillations in various frequency bands have been detected in the amygdala during cognitive and emotional tasks, which can couple with oscillations in cortical regions or the hippocampus. However, data on oscillatory coupling between the amygdala and motor areas are still lacking. This review provides a summary of oscillation frequencies measured in the amygdala and their possible functional relevance in different species, followed by evidence for connectivity between the amygdala and motor areas, such as the basal ganglia and the motor cortex. We hypothesize that the amygdala could communicate with motor areas through coherence of low frequency bands in the theta-alpha range. Furthermore, we discuss a potential role of the amygdala in therapeutic approaches based on electrical stimulation.

Keywords: amygdala, basal ganglia, neuromodulation, deep brain stimulation, oscillations

OPEN ACCESS

Edited by:
Giovanni Mirabella,
Sapienza University of Rome, Italy

Reviewed by:
Martina Ardizzi,
University of Parma, Italy
Fausto Caruana,
University of Parma, Italy

***Correspondence:**
Lars Wojtecki
wojtecki@uni-duesseldorf.de

Specialty section:
This article was submitted to Neural Technology, a section of the journal Frontiers in Neuroscience

Received: *19 December 2018*
Accepted: *01 April 2019*
Published: *18 April 2019*

Citation:
Schönfeld L-M and Wojtecki L (2019) Beyond Emotions: Oscillations of the Amygdala and Their Implications for Electrical Neuromodulation. Front. Neurosci. 13:366. doi: 10.3389/fnins.2019.00366

INTRODUCTION

The amygdala is one of the core regions associated with emotions and has gained broad interest for its role in emotional conditioning, especially fear conditioning (LeDoux et al., 1990). Besides conditioned fear responses, the amygdala plays an essential role in context-based acquisition of fear responses, PTSD, social anxiety and preparing the organism to react upon a threat (Phillips and LeDoux, 1992; Killgore and Yurgelun-Todd, 2005; Alvarez et al., 2008; Morey et al., 2012; O'Doherty et al., 2017; Engelen et al., 2018). Furthermore, the amygdala is receiving additional attention for its modulating role in social behavior, learning processes, addiction and mood

Abbreviations: BLA, basolateral amygdala; DBS, deep brain stimulation; GP, globus pallidus; GP_e, external globus pallidus; GP_i, internal globus pallidus; MCS, motor cortex stimulation; mPFC, medial prefrontal cortex; PD, Parkinson's disease; PTSD, posttraumatic stress disorder; SNr, substantia nigra pars reticulata; STN, subthalamic nucleus; tDCS, transcranial direct current stimulation; TMS, transcranial magnetic stimulation; VIM, ventral intermediate nucleus of the thalamus.

disorders (Langevin, 2012; Bickart et al., 2014; Janak and Tye, 2015). Several human studies also imply an influence of the amygdala on motor and autonomic responses. Bilateral amygdala lesions led to impaired recognition of fearful faces due to an inability of gaze fixation on the eyes (Adolphs et al., 2005; Kennedy and Adolphs, 2010). Also the amygdala is responsible for defensive behaviors in response to acute threats (Klumpers et al., 2017) and increased connectivity between the amygdala and cortical regions is predictive of heart rate variability in patients suffering from generalized anxiety disorder (Makovac et al., 2016). Abnormal functioning of the amygdala is observed in various psychiatric disorders such as generalized anxiety disorder, PTSD, specific phobias, depression, autism spectrum disorder and antisocial personality disorder (Baron-Cohen et al., 2000; Ferri et al., 2017; Fonzo and Etkin, 2017; Garcia, 2017; Kolla et al., 2017; Henigsberg et al., 2019). However, the amygdala might also play a role in psychiatric symptoms of movement disorders, as smaller amygdala volumes are linked to anxiety symptoms in early PD Vriend et al. (2016).

Parkinson's disease is a movement disorder that can be treated with DBS as stimulation of the STN, the internal GP_i, or the VIM can reduce core motor symptoms, such as hypokinesia, rigor, tremor, and dyskinesias, in patients that do not benefit from pharmacotherapy alone (Moldovan et al., 2015). In PD beta oscillatory neural activity is observed in the dorsolateral motor part of the STN, which is thought to be a mediator for motor symptoms associated with the disease (Accolla et al., 2016). DBS in PD is assumed to interfere with the pathological oscillations in the basal ganglia by superimposing another oscillatory stimulation pattern with a higher frequency, which paradoxically stops the entrainment of neurons to the pathological frequency and allows them to fire at a more irregular pattern (Wilson, 2014). For PD patients that are not suited to receive DBS, MCS, delivered via flat electrodes positioned epi- or subdurally, might pose an alternative treatment option (De Rose et al., 2012) although its effectiveness in PD is unclear (Tsubokawa et al., 1991; Moro et al., 2011; De Rose et al., 2012).

Besides severe motor disabilities, psychiatric symptoms such as depression, psychosis and anxiety often co-occur and severely impact the quality of life of PD patients (Aarsland et al., 1999). The effect of DBS treatment on non-motor symptoms of PD is not fully explored yet and there are indications that STN-DBS might lead to a significant reduction in anxiety (Witt et al., 2008; Fabbri et al., 2017). However, DBS treatment in itself can cause non-motor side effects, such as transient depressive episodes, pathological crying, laughter or mania (Bejjani et al., 1999; Krack et al., 2001; Herzog et al., 2003; Wojtecki et al., 2007). These side effects are assumed to occur either by stimulating the limbic connections of the STN (Wojtecki et al., 2007) or by current spread from the STN to neighboring areas. One of these areas might be the amygdala; however, current spread to other regions, such as the cingulate cortex might contribute to non-motor side effects as well.

Although there is evidence for structural and functional connections between the amygdala and motor areas, such as the basal ganglia or the motor cortex, premotor cortex and supplementary motor cortex (Peron et al., 2016; Markovic et al., 2017; Loonen and Ivanova, 2018), studies on oscillatory communication between motor areas and the amygdala are lacking. The aim of this review is first, to collect evidence that might hint toward oscillatory coupling of the amygdala with the basal ganglia and the motor cortex. In addition, potential frequency bands are proposed through which communication between regions could occur. Second, it will be discussed whether modulation of amygdala activity has any therapeutic relevance to treat movement disorders. Modulation of the amygdala could most likely occur through indirect stimulation via connected brain regions or even through DBS of the amygdala itself.

OSCILLATIONS IN THE AMYGDALA

Neural activity can fluctuate at a periodic interval, which leads to oscillations with a specific frequency and amplitude (Buzsaki, 2006). Oscillations can occur locally within a single brain region, but also synchronized between two or more brain regions. This "coupling" of oscillations is assumed to reflect information processing (Schnitzler and Gross, 2005) and arises through synchronizing oscillations in several ways. Neuronal populations can couple within a distinct frequency by oscillating in-phase, which can be quantified using coherence as a measure. Furthermore, coupling can also be calculated between two different frequencies (cross-frequency coupling). Classically, five categories of oscillation frequencies are defined: delta (0.5–4 Hz), theta (4–8 Hz), alpha (8–12 Hz), beta (12–30 Hz), and gamma (above 30 Hz; Buzsaki, 2006). The frequency specific functions of brain oscillators are complex. As Buzsaki and Draguhn (2004) explain with reference to multiple literature sources: "However, different oscillatory classes might carry different dimensions of brain integration [. . .]. Slow rhythms synchronize large spatial domains and can bind together specific assemblies by the appropriate timing of higher frequency localized oscillations [. . .]." In other words: "Higher frequency oscillations are confined to a small neuronal space, whereas very large networks are recruited during slow oscillations [. . .]. This relationship between anatomical architecture and oscillatory pattern allows brain operations to be carried out simultaneously at multiple temporal and spatial scales [. . .]." Besides that, a region specific or function specific interpretation of frequency bands is empirically described in various publications. In this review we list some of these findings of oscillations related to the amygdala.

A small number of human studies have been conducted where oscillations in the amygdala were measured. PTSD patients received fMRI-based neurofeedback and a successful lowering of alpha frequencies co-occurred with a shift in connectivity of the BLA from fear and memory-related structures, such as the hippocampus and the periaqueductal gray, toward prefrontal areas involved in emotion regulation (Nicholson et al., 2016). Oscillations in the alpha range have been associated with selective attention and information processing (for review see Klimesch, 2012). Furthermore, alpha desynchronization during a therapeutic session enabled connectivity changes between brain

regions (Ros et al., 2013), which might lead to decreases in oscillatory power in specific regions such as the amygdala. Epilepsy patients with electrodes implanted in the BLA and the hippocampus exhibited high gamma oscillations (70–180 Hz) in both regions upon viewing fearful faces. Moreover, gamma oscillations in the BLA preceded those in the hippocampus (Zheng et al., 2017). An entrainment of hippocampal gamma oscillations by the BLA might suggest a modulatory role of the BLA in the processing of fearful stimuli and retrieval of fearful memories.

In contrast to the sparse number of human studies, several animal experiments have been performed that led to mechanistic insights about oscillations in the amygdala. Consolidation and retrieval of fearful memories in mice led to theta oscillatory coherence between the BLA and the hippocampus (Seidenbecher et al., 2003; Narayanan et al., 2007). In the hippocampus theta oscillations are associated with memory consolidation and retrieval (Hasselmo, 2005) and again, its increased communication with the BLA might point at enhanced processing of emotional memories as opposed to more neutral ones. In the case of fear extinction learning in mice, interneurons in the BLA play a pivotal role, since they enable oscillations in the alpha range (here 6–12 Hz), which interfere with fear-associated oscillations in the low theta range (here 3–6 Hz; Davis et al., 2017). Increases in theta power in the BLA have also been measured while mice entered a non-social compartment instead of a social compartment in a spatial decision task. Interestingly, injections of the NMDA receptor antagonist Ketamine abolished differences in theta power when entering the compartments (Mihara et al., 2017). In another experiment, DBS in the infralimbic cortex in anesthetized rats caused increases in slow wave (<1.5 Hz), theta and fast gamma power in the BLA, coupling between slow waves with faster theta and beta frequencies within the BLA and coherence of slow waves and theta frequencies between the BLA and the hippocampus (Cervera-Ferri et al., 2016). The increase in oscillatory activity in the BLA and the enhanced coherence between the BLA and the hippocampus upon infralimbic cortex DBS might be relevant for the therapeutic effect of cingulate gyrus DBS. The cingulate gyrus in humans corresponds to the infralimbic cortex in rodents and DBS of the cingulate gyrus has been shown to reduce depressive symptoms (Uylings et al., 2003; Mayberg et al., 2005). During reward learning in cats, increased coherence of gamma oscillations between the BLA and rhinal cortices was observed, which was initiated by enhanced synchrony of BLA neurons (Bauer et al., 2007). In the mouse BLA, fast gamma oscillations were coupled to theta waves during states of fear, whereas coupling decreased during states of safety (Stujenske et al., 2014). Simultaneously to this decrease in local theta-gamma coupling during safety, gamma power increased in the BLA and a stronger coherence between the BLA and the mPFC was detected, which might reflect a suppression of learned feelings of fear (Stujenske et al., 2014). Avoidance of shock delivery to a fellow rat was linked to low gamma coherence between the insula, OFC and BLA, whereas choices, which resulted in another rat receiving a shock, were linked to increased gamma coherence between the same regions. Interestingly, high gamma oscillations in the BLA preceded those in the insula (Schaich Borg et al., 2017). In addition, stronger alpha power was observed in several brain regions, including the amygdala, and correlated positively with avoidance of shock delivery. Within the network of interest, the amygdala seemed to be the source of alpha oscillations as its activity preceded alpha oscillations measured in other brain areas (Schaich Borg et al., 2017). Theta oscillations that have been observed in rats in a social fearful context (Tendler and Wagner, 2015) were measured in the BLA and correlated negatively with the shock avoidance behavior described above (Schaich Borg et al., 2017).

CONNECTIONS OF THE AMYGDALA WITH MOTOR AREAS AND IMPLICATIONS FOR ELECTRICAL NEUROMODULATION

Several studies using tracing or imaging techniques have discovered structural connections between the amygdala and different motor areas in humans and animals. In this section "motor areas" encompass the STN, GP and the motor cortex, as these are the main clinically relevant targets to treat movement disorders such as PD or Huntington's disease; however, the amygdala also projects to other motor areas that are beyond the scope of this review.

In humans, diffusion tensor imaging provided evidence for structural connectivity between the dorsal part of the amygdala and the motor cortex through the external capsule, which grants the amygdala a significant influence on motor behavior (Grezes et al., 2014). More recently, the existence of a functional circuit between the amygdala and the sensorimotor cortex at rest was demonstrated in an fMRI study using a large number of participants, further supporting the assumption that the amygdala is a critical modulator of motor behavior (Toschi et al., 2017). Other imaging studies revealed functional connectivity between the STN and the amygdala (Peron et al., 2016) and the GP and the amygdala (Yang et al., 2017).

Tracing studies in animals have provided more detailed insights about anatomical links between the amygdala and motor regions by revealing monosynaptic connections between both. Primate and rodent studies have detected structural connections between the amygdala and the motor cortex (Kita and Kitai, 1990; McDonald, 1998). Anterograde tracing in rhesus monkeys showed projections from the BLA onto the motor cortex, the majority of which terminated in the face and arm representation (Morecraft et al., 2007). The latter finding is interesting, considering the role of the amygdala in processing and expressing emotions. Recently, projections from neurons positive for corticotropin-releasing factor in the central amygdala to the GP_e were discovered, indicating a novel circuit for stress-relevant information (Hunt et al., 2018). In rats, high frequency stimulation of the STN caused an increase in neural activity in the BLA (Hachem-Delaunay et al., 2015); however, proof of direct structural connections between the amygdala and the STN remains absent.

The connections between the basal ganglia and the motor cortex including their alterations in a typical movement disorder such as Huntington's disease have been described in detail (Wojtecki et al., 2016). Upon receiving cortical input, the striatum projects either directly to the GP_i and the SNr (*direct pathway*) or indirectly via the GP_e and the STN (*indirect pathway*). The GP_i and SNr in turn send inhibitory projections to the thalamus that provides excitatory input to the motor cortex (Calabresi et al., 2014). Moreover, projections from cortical layer V are assumed to target the STN via the *hyperdirect pathway*. These projections might originate in the primary motor cortex or neighboring cortical regions like the supplementary motor area and the dorsal and ventral divisions of the premotor cortex (Nambu et al., 2002). Interestingly, stimulation of cortical layer V neurons reduced Parkinsonian symptoms in mice (Gradinaru et al., 2009), indicating that the motor cortex might play a causal role in the pathogenesis of PD and that DBS of the STN might be effective through antidromic activation of the motor cortex via the hyperdirect pathway (Arbuthnott and Garcia-Munoz, 2017). The amygdala has the potential to influence all three pathways within the basal ganglia due to its connections to the STN, the GP and the motor cortex. In fact, it was recently shown that PD patients who suffer from freezing of gait have higher resting state connectivity between the amygdala and the striatum compared to PD patients that do not suffer from freezing of gait (Gilat et al., 2018), indicating that abnormal amygdala activity worsen the clinical picture of movement disorders.

Potential Oscillatory Interactions Between the Amygdala and Motor Regions

Abnormal amygdala activity has been associated with anxiety disorders for decades and recently became acknowledged for its role in pathological motor symptoms (Gilat et al., 2018). Due to connections with motor areas that are frequent targets of DBS, modulation of the amygdala might occur indirectly as a result of network changes induced by the stimulation and could account for emotional side effects that arise from DBS. Side effects linked to DBS of the STN include worsening of verbal fluency, cognitive deterioration, hypomania and impairment in affect regulation (Krack et al., 2003; Wojtecki et al., 2007; Witt et al., 2008; Kim et al., 2012). The STN and presumably also the GP_e have direct functional connections to the amygdala and a therapeutic alteration of oscillations within these nuclei could change the input to the amygdala, inducing potentially unwanted effects on learning, memory and emotions. Pathological beta oscillations in the STN are a major hallmark of PD and can be suppressed by DBS (Quinn et al., 2015). A decrease in these beta oscillations and an increase in theta-alpha power in the STN are associated with superior motor performance of PD patients (Anzak et al., 2012; Tan et al., 2013). Also an increase in theta-alpha frequencies in the STN during a verbal generation task was found with increased coherence between the STN and frontal cortical association areas (Wojtecki et al., 2017). However, theta oscillations in the amygdala have frequently been reported to co-occur with states of fear and anxiety (Narayanan et al., 2007; Davis et al., 2017). If theta oscillations by the STN would induce theta oscillations in the amygdala following DBS, improved motor performance might come with the cost of increased anxiety.

In the basal ganglia of PD patients, alpha frequencies are observed and while some researchers report an influence of dopaminergic medication (Gironell et al., 1997), others did not show any medication-induced change in alpha frequencies (Brittain and Brown, 2014). Furthermore decreases in alpha frequencies have been linked to PD-associated dementia (Cozac et al., 2016). In a rat study, the BLA has been the source of alpha oscillations during social decisions, entraining connected regions (Schaich Borg et al., 2017). Alpha frequency entrainment of motor regions by the amygdala would be an interesting mechanism to improve cognitive functions in PD patients suffering from dementia. However, inductions of oscillations at a specific frequency in the amygdala might require direct electrical stimulation, which has many drawbacks as discussed in the following section.

Beta frequencies represent the majority of oscillations in the motor cortex and were coupled to delta frequencies in a motor task that specifically requires attention and planning (Saleh et al., 2010). As the amygdala provides direct input to the motor cortex, it is also closely involved in the generation of motor behavior. Thereby, amygdala modulation might cause disturbances in psychomotor functioning, which have been observed in the form of pathological crying that occurred in the absence of adequate emotions (Wojtecki et al., 2007). Still, the exact role of the amygdala in the occurrence of non-motor side effects during DBS needs further investigation.

To reduce non-motor side effects of DBS, theta and alpha frequencies would be interesting candidate frequencies to modulate within an amygdala–basal ganglia network. Theta and alpha frequencies in the STN have been associated with improved motor functions in PD patients (Anzak et al., 2012; Tan et al., 2013) and have been observed during focused attention, potentially having a gating function in decision-making (Cavanagh et al., 2011; Wojtecki et al., 2017). Although theta oscillations in the BLA have been associated with fear responses (Davis et al., 2017), increases in theta power were measured also during social decision tasks, specifically when animals chose against the social option (Mihara et al., 2017; Schaich Borg et al., 2017). The latter might reflect a rather general, emotionless role of theta oscillations in choice behavior since increases in theta power have been linked to novel stimuli (Tendler and Wagner, 2015). Alpha oscillations are found in both the basal ganglia and the amygdala and are thought to act as an inhibitory filter in attention processes (Klimesch, 2012) and might have the potential to improve cognition. Lastly, slow theta-alpha frequencies might reflect information transfer over long distances across the brain (von Stein and Sarnthein, 2000), which makes them suitable of facilitating communication between the amygdala with the basal ganglia and the cortex. A simplified summary of connections between the amygdala and motor areas, the most common oscillatory frequencies found in each region and hypothetical shared oscillations are provided in **Figure 1**. In that scheme slower rhythms such as theta or alpha might synchronize the activity of distal neuronal networks

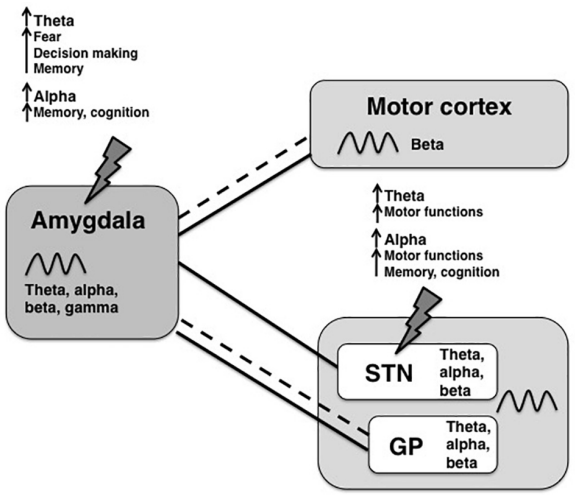

FIGURE 1 | Overview of oscillatory frequencies and connections between amygdala and motor areas. The amygdala is structurally (dashed lines) and functionally (solid lines) connected to motor areas, such as the motor cortex, the limbic part of the subthalamic nucleus (STN) and the globus pallidus (GP). For all shown regions, a broad spectrum of oscillation frequencies has been previously described, but the frequency bands that are used for information transfer between the amygdala and the basal ganglia are not known yet. In this review, we propose coherence of theta-alpha oscillations as a possible way of inter-regional communication with potential therapeutic value. Upon stimulation of the amygdala-motor circuit, for example by STN-DBS or amygdala-DBS (indicated by lightning bolts), theta and alpha frequencies might be increased within the circuit, where each frequency has different functional properties depending on the source region.

(e.g., between the amygdala and the basal ganglia) and couple to local higher frequencies (for ex., gamma within the amygdala).

Amygdala DBS: Worth the Risk?

Electrical stimulation of the amygdala possesses several potential obstacles, which make it a risky, if not unsuitable target for DBS in humans. First, segregating the specific nuclei within the amygdala is not possible with standard MRI-based localization approaches and amygdala anatomy varies substantially across subjects (Oya et al., 2009). Second, the amygdala is a known kindling site in animal studies, where electrical stimulation can lead to recurring after-discharges and seizures (Cleeren et al., 2016; Li et al., 2016; Wicker and Forcelli, 2016). In addition, structural changes occur in patients suffering from temporal lobe epilepsy (Reyes et al., 2017), which further complicates target localization at least in these patients.

Due to the associated risks, DBS of the amygdala has only been performed in a few cases. Seizure frequency could be reduced by amygdala DBS in patients suffering from refractory temporal lobe epilepsy, without causing behavioral alterations or stimulation-induced seizures (Vonck et al., 2002; Boon et al., 2007). Furthermore, brief electrical stimulation during a cognitive task improved declarative memory, potentially by increasing oscillations in the theta and gamma band between the amygdala, the hippocampus and the perirhinal cortex (Inman et al., 2018). DBS of the BLA in a child suffering from autism caused a decrease in self-directed aggression and improvements in cognitive, social and emotional functioning (Sturm et al., 2012). The BLA might be seen as a communication hub between different centers, for example the frontal cortex, sensory cortices and the basal ganglia, that are all involved in the generation of autistic symptoms and the improvement in symptoms could have been achieved by a reset of oscillatory activity in the BLA (Sinha et al., 2015). In a PTSD patient intraoperative microelectrode recordings showed an increased firing of the right BLA in the beta range, whereas predominant frequencies in the left BLA were in the theta-alpha range. DBS of the BLA led to a reduction of anxiety and improvements in sleeping pattern (Langevin et al., 2016). In PTSD patients, the amygdala is overactive in response to trauma-related stimuli, but also during unrelated emotional tasks and at rest (Reznikov and Hamani, 2017) and DBS might normalize its activity. Given the potential of amygdala DBS to treat PTSD, a larger clinical trial has been proposed, but results are not published yet (Koek et al., 2014).

A few studies have been conducted to specifically assess potential emotional alterations following amygdala stimulation, with a diverse outcome. Unilateral amygdala stimulation caused an increase in feelings of fear, regardless which hemisphere was stimulated (Meletti et al., 2006). Conversely, stimulation of the right BLA in a single case created a positive affective bias during the evaluation of emotional stimuli (Bijanki et al., 2014). In another study, stimulation of the right amygdala was associated with increased feelings of fear and sadness, whereas stimulation of the left amygdala could evoke both pleasant (happiness) and unpleasant (fear, sadness, and anxiety) states (Lanteaume et al., 2007).

Taken together, the body of evidence for DBS to treat psychiatric symptoms is growing, but given the risk associated with amygdala DBS and its potential to evoke a variety of negative emotions, this target needs further thorough investigation.

DISCUSSION

The amygdala is connected to brain regions such as the hippocampus, the ventral striatum and the cortex; therefore, it is embedded in a network involved in generating emotions and learning (Langevin, 2012; Gibson et al., 2017). Structural connections between the amygdala and motor areas, such as the STN, GP and motor cortex have been discovered in different animal species (Morecraft et al., 2007) and resting state connectivity between the amygdala and the basal ganglia has been shown recently in a subpopulation of PD patients (Gilat et al., 2018). In addition, stimulation of different subregions belonging to the cingulate cortex, which are connected to the amygdala, induced emotional motor responses (Caruana et al., 2015, 2018). In a recent study it was demonstrated that emotional stimuli induced an effect on motor behavior, potentially mediated by connections from the amygdala to motor areas. Interestingly, that behavioral effect was only evident when the emotional content of the stimuli was task-relevant (Mirabella, 2018).

Up to date, no simultaneous electrophysiological measurements have been performed in the amygdala and

motor areas. Based on structural connections between the amygdala and motor areas, we raised the question whether amygdala modulation could potentially alleviate psychiatric symptoms of PD or conversely could induce non-motor side effects that occur during DBS of the basal ganglia. Modulation of the amygdala might cause or exacerbate some non-motor side effects that occur during DBS of the basal ganglia, for example by alterations in theta and alpha frequencies. On the contrary, DBS of the BLA has been shown to decrease anxiety (Langevin et al., 2016), potentially by decreases in theta power, therefore direct or indirect modulation of the amygdala could support the management of anxiety associated with PD. As there is scarce feasibility of amygdala DBS without negative side effects it is worthwhile to consider non-invasive stimulation techniques, such as tDCS or TMS for indirect neuromodulation of the amygdala through a cortical network entry point. These techniques can induce short term or even chronic alterations in neuronal activity without the risk associated with implanted stimulation electrodes. However, these techniques only allow precise stimulation of superficial cortical regions. To gain insight into possible mechanisms of such an indirect amygdala modulation it is relevant to study amygdala oscillatory coupling with motor cortical regions.

Taken together, there is evidence for structural connections between the amygdala and motor areas, such as the basal ganglia and the motor cortex, that are functionally altered in movement disorders. We hypothesized that information transfer between the amygdala and motor areas occurs through oscillations in the alpha and theta frequencies, potentially having either beneficial or adverse effects. In the future, simultaneous electrophysiological measurements in the amygdala and motor regions are needed to specify oscillatory connections during cognitive and motor tasks. To obtain reliable behavioral effects, task-relevance of stimuli seems to be important, which should be investigated in relation to the amygdala and motor areas. Based on these findings, oscillation frequencies that show coherence between the amygdala and motor areas could be specified to prevent psychiatric side effects of DBS or even use secondary amygdala activation as an add-on for current DBS or MCS therapy.

AUTHOR CONTRIBUTIONS

L-MS wrote the first draft, which was revised by LW. Both authors conceptualized the topic and content of the review, and approved the manuscript.

FUNDING

This work was supported by a grant for Collaborative Research Centers (CRC 991, Grant No. INST 208/702-1) from the German Research Foundation (Deutsche Forschungsgemeinschaft; DFG) to Tobias Kalenscher from which the salary of L-MS is being paid, and by ERA-NET NEURON/BMBF Germany (TYMON, Grant No. 01EW1411) to LW.

REFERENCES

Aarsland, D., Larsen, J. P., Lim, N. G., Janvin, C., Karlsen, K., Tandberg, E., et al. (1999). Range of neuropsychiatric disturbances in patients with Parkinson's disease. *J. Neurol. Neurosurg. Psychiatry* 67, 492–496.

Accolla, E. A., Herrojo Ruiz, M., Horn, A., Schneider, G. H., Schmitz-Hubsch, T., Draganski, B., et al. (2016). Brain networks modulated by subthalamic nucleus deep brain stimulation. *Brain* 139, 2503–2515. doi: 10.1093/brain/aww182

Adolphs, R., Gosselin, F., Buchanan, T. W., Tranel, D., Schyns, P., and Damasio, A. R. (2005). A mechanism for impaired fear recognition after amygdala damage. *Nature* 433, 68–72. doi: 10.1038/nature03086

Alvarez, R. P., Biggs, A., Chen, G., Pine, D. S., and Grillon, C. (2008). Contextual fear conditioning in humans: cortical-hippocampal and amygdala contributions. *J. Neurosci.* 28, 6211–6219. doi: 10.1523/JNEUROSCI.1246-08.2008

Anzak, A., Tan, H., Pogosyan, A., Foltynie, T., Limousin, P., Zrinzo, L., et al. (2012). Subthalamic nucleus activity optimizes maximal effort motor responses in Parkinson's disease. *Brain* 135, 2766–2778. doi: 10.1093/brain/aws183

Arbuthnott, G. W., and Garcia-Munoz, M. (2017). Are the symptoms of parkinsonism cortical in origin? *Comput. Struct. Biotechnol. J.* 15, 21–25. doi: 10.1016/j.csbj.2016.10.006

Baron-Cohen, S., Ring, H. A., Bullmore, E. T., Wheelwright, S., Ashwin, C., and Williams, S. C. (2000). The amygdala theory of autism. *Neurosci. Biobehav. Rev.* 24, 355–364.

Bauer, E. P., Paz, R., and Pare, D. (2007). Gamma oscillations coordinate amygdalo-rhinal interactions during learning. *J. Neurosci.* 27, 9369–9379. doi: 10.1523/jneurosci.2153-07.2007

Bejjani, B. P., Damier, P., Arnulf, I., Thivard, L., Bonnet, A. M., Dormont, D., et al. (1999). Transient acute depression induced by high-frequency deep-brain stimulation. *N. Engl. J. Med.* 340, 1476–1480. doi: 10.1056/nejm199905133401905

Bickart, K. C., Dickerson, B. C., and Barrett, L. F. (2014). The amygdala as a hub in brain networks that support social life. *Neuropsychologia* 63, 235–248. doi: 10.1016/j.neuropsychologia.2014.08.013

Bijanki, K. R., Kovach, C. K., McCormick, L. M., Kawasaki, H., Dlouhy, B. J., Feinstein, J., et al. (2014). Case report: stimulation of the right amygdala induces transient changes in affective bias. *Brain Stimul.* 7, 690–693. doi: 10.1016/j.brs.2014.05.005

Boon, P., Vonck, K., De Herdt, V., Van Dycke, A., Goethals, M., Goossens, L., et al. (2007). Deep brain stimulation in patients with refractory temporal lobe epilepsy. *Epilepsia* 48, 1551–1560. doi: 10.1111/j.1528-1167.2007.01005.x

Brittain, J. S., and Brown, P. (2014). Oscillations and the basal ganglia: motor control and beyond. *Neuroimage* 85(Pt 2), 637–647. doi: 10.1016/j.neuroimage.2013.05.084

Buzsaki, G. (2006). *Rhythms of the Brain*. Oxford: Oxford University Press.

Buzsaki, G., and Draguhn, A. (2004). Neuronal oscillations in cortical networks. *Science* 304, 1926–1929. doi: 10.1126/science.1099745

Calabresi, P., Picconi, B., Tozzi, A., Ghiglieri, V., and Di Filippo, M. (2014). Direct and indirect pathways of basal ganglia: a critical reappraisal. *Nat. Neurosci.* 17, 1022–1030. doi: 10.1038/nn.3743

Caruana, F., Avanzini, P., Gozzo, F., Francione, S., Cardinale, F., and Rizzolatti, G. (2015). Mirth and laughter elicited by electrical stimulation of the human anterior cingulate cortex. *Cortex* 71, 323–331. doi: 10.1016/j.cortex.2015.07.024

Caruana, F., Gerbella, M., Avanzini, P., Gozzo, F., Pelliccia, V., Mai, R., et al. (2018). Motor and emotional behaviours elicited by electrical stimulation of the human cingulate cortex. *Brain* 141, 3035–3051. doi: 10.1093/brain/awy219

Cavanagh, J. F., Wiecki, T. V., Cohen, M. X., Figueroa, C. M., Samanta, J., Sherman, S. J., et al. (2011). Subthalamic nucleus stimulation reverses mediofrontal influence over decision threshold. *Nat. Neurosci.* 14, 1462–1467. doi: 10.1038/nn.2925

Cervera-Ferri, A., Teruel-Marti, V., Barcelo-Molina, M., Martinez-Ricos, J., Luque-Garcia, A., Martinez-Bellver, S., et al. (2016). Characterization of oscillatory changes in hippocampus and amygdala after deep brain stimulation of the infralimbic prefrontal cortex. *Physiol. Rep.* 4:e12854. doi: 10.14814/phy2.12854

Cleeren, E., Premereur, E., Casteels, C., Goffin, K., Janssen, P., and Van Paesschen, W. (2016). The effective connectivity of the seizure onset zone and ictal perfusion changes in amygdala kindled rhesus monkeys. *Neuroimage Clin.* 12, 252–261. doi: 10.1016/j.nicl.2016.05.020

Cozac, V. V., Gschwandtner, U., Hatz, F., Hardmeier, M., Ruegg, S., and Fuhr, P. (2016). Quantitative EEG and cognitive decline in Parkinson's disease. *Parkinsons Dis.* 2016:9060649. doi: 10.1155/2016/9060649

Davis, P., Zaki, Y., Maguire, J., and Reijmers, L. G. (2017). Cellular and oscillatory substrates of fear extinction learning. *Nat. Neurosci.* 20, 1624–1633. doi: 10.1038/nn.4651

De Rose, M., Guzzi, G., Bosco, D., Romano, M., Lavano, S. M., Plastino, M., et al. (2012). Motor cortex stimulation in Parkinson's disease. *Neurol. Res. Int.* 2012:502096. doi: 10.1155/2012/502096

Engelen, T., Zhan, M., Sack, A. T., and de Gelder, B. (2018). Dynamic interactions between emotion perception and action preparation for reacting to social threat: a combined cTBS-fMRI study. *eNeuro* 5:ENEURO.408-ENEURO.417. doi: 10.1523/ENEURO.0408-17.2018

Fabbri, M., Coelho, M., Guedes, L. C., Rosa, M. M., Abreu, D., Goncalves, N., et al. (2017). Acute response of non-motor symptoms to subthalamic deep brain stimulation in Parkinson's disease. *Parkinsonism Relat. Disord.* 41, 113–117. doi: 10.1016/j.parkreldis.2017.05.003

Ferri, J., Eisendrath, S. J., Fryer, S. L., Gillung, E., Roach, B. J., and Mathalon, D. H. (2017). Blunted amygdala activity is associated with depression severity in treatment-resistant depression. *Cogn. Affect. Behav. Neurosci.* 17, 1221–1231. doi: 10.3758/s13415-017-0544-6

Fonzo, G. A., and Etkin, A. (2017). Affective neuroimaging in generalized anxiety disorder: an integrated review. *Dialogues Clin. Neurosci.* 19, 169–179.

Garcia, R. (2017). Neurobiology of fear and specific phobias. *Learn. Mem.* 24, 462–471. doi: 10.1101/lm.044115.116

Gibson, W. S., Cho, S., Abulseoud, O. A., Gorny, K. R., Felmlee, J. P., Welker, K. M., et al. (2017). The impact of mirth-inducing ventral striatal deep brain stimulation on functional and effective connectivity. *Cereb. Cortex* 27, 2183–2194. doi: 10.1093/cercor/bhw074

Gilat, M., Ehgoetz Martens, K. A., Miranda-Dominguez, O., Arpan, I., Shine, J. M., Mancini, M., et al. (2018). Dysfunctional limbic circuitry underlying freezing of gait in Parkinson's disease. *Neuroscience* 374, 119–132. doi: 10.1016/j.neuroscience.2018.01.044

Gironell, A., Barbanoj, B., Anderer, P., Antonijoan, R., Massana, E., Kulisevsky, J., et al. (1997). EEG effects of levodopa in Parkinson's disease. *Electroencephalogr. Clin. Neurophysiol.* 103:1997.

Gradinaru, V., Mogri, M., Thompson, K. R., Henderson, J. M., and Deisseroth, K. (2009). Optical deconstruction of parkinsonian neural circuitry. *Science* 324, 354–359. doi: 10.1126/science.1167093

Grezes, J., Valabregue, R., Gholipour, B., and Chevallier, C. (2014). A direct amygdala-motor pathway for emotional displays to influence action: a diffusion tensor imaging study. *Hum. Brain Mapp.* 35, 5974–5983. doi: 10.1002/hbm.22598

Hachem-Delaunay, S., Fournier, M. L., Cohen, C., Bonneau, N., Cador, M., Baunez, C., et al. (2015). Subthalamic nucleus high-frequency stimulation modulates neuronal reactivity to cocaine within the reward circuit. *Neurobiol. Dis.* 80, 54–62. doi: 10.1016/j.nbd.2015.05.007

Hasselmo, M. E. (2005). What is the function of hippocampal theta rhythm?–Linking behavioral data to phasic properties of field potential and unit recording data. *Hippocampus* 15, 936–949. doi: 10.1002/hipo.20116

Henigsberg, N., Kalember, P., Petrovic, Z. K., and Secic, A. (2019). Neuroimaging research in posttraumatic stress disorder - Focus on amygdala, hippocampus and prefrontal cortex. *Prog. Neuropsychopharmacol. Biol. Psychiatry* 90, 37–42. doi: 10.1016/j.pnpbp.2018.11.003

Herzog, J., Reiff, J., Krack, P., Witt, K., Schrader, B., Muller, D., et al. (2003). Manic episode with psychotic symptoms induced by subthalamic nucleus stimulation in a patient with Parkinson's disease. *Mov. Disord.* 18, 1382–1384. doi: 10.1002/mds.10530

Hunt, A. J. Jr., Dasgupta, R., Rajamanickam, S., Jiang, Z., Beierlein, M., Chan, C. S., et al. (2018). Paraventricular hypothalamic and amygdalar CRF neurons synapse in the external globus pallidus. *Brain Struct. Funct.* 223, 2685–2698. doi: 10.1007/s00429-018-1652-y

Inman, C. S., Manns, J. R., Bijanki, K. R., Bass, D. I., Hamann, S., Drane, D. L., et al. (2018). Direct electrical stimulation of the amygdala enhances declarative memory in humans. *Proc. Natl. Acad. Sci. U.S.A.* 115, 98–103. doi: 10.1073/pnas.1714058114

Janak, P. H., and Tye, K. M. (2015). From circuits to behaviour in the amygdala. *Nature* 517, 284–292. doi: 10.1038/nature14188

Kennedy, D. P., and Adolphs, R. (2010). Impaired fixation to eyes following amygdala damage arises from abnormal bottom-up attention. *Neuropsychologia* 48, 3392–3398. doi: 10.1016/j.neuropsychologia.2010.06.025

Killgore, W. D., and Yurgelun-Todd, D. A. (2005). Social anxiety predicts amygdala activation in adolescents viewing fearful faces. *Neuroreport* 16, 1671–1675. doi: 10.1097/01.wnr.0000180143.99267.bd

Kim, J. S., Kim, H. J., Lee, J. Y., Kim, J. M., Yun, J. Y., and Jeon, B. S. (2012). Hypomania induced by subthalamic nucleus stimulation in a Parkinson's disease patient: does it suggest a dysfunction of the limbic circuit? *J. Mov. Disord.* 5, 14–17. doi: 10.14802/jmd.12004

Kita, H., and Kitai, S. T. (1990). Amygdaloid projections to the frontal cortex and the striatum in the rat. *J. Comp. Neurol.* 298, 40–49. doi: 10.1002/cne.902980104

Klimesch, W. (2012). alpha-band oscillations, attention, and controlled access to stored information. *Trends Cogn. Sci.* 16, 606–617. doi: 10.1016/j.tics.2012.10.007

Klumpers, F., Kroes, M. C. W., Baas, J. M. P., and Fernández, G. (2017). How human amygdala and bed nucleus of the stria terminalis may drive distinct defensive responses. *J. Neurosci.* 37, 9645–9656. doi: 10.1523/jneurosci.3830-16.2017

Koek, R. J., Langevin, J. P., Krahl, S. E., Kosoyan, H. J., Schwartz, H. N., Chen, J. W., et al. (2014). Deep brain stimulation of the basolateral amygdala for treatment-refractory combat post-traumatic stress disorder (PTSD): study protocol for a pilot randomized controlled trial with blinded, staggered onset of stimulation. *Trials* 15:356. doi: 10.1186/1745-6215-15-356

Kolla, N. J., Patel, R., Meyer, J. H., and Chakravarty, M. M. (2017). Association of monoamine oxidase-A genetic variants and amygdala morphology in violent offenders with antisocial personality disorder and high psychopathic traits. *Sci. Rep.* 7:9607. doi: 10.1038/s41598-017-08351-w

Krack, P., Batir, A., Van Blercom, N., Chabardes, S., Fraix, V., Ardouin, C., et al. (2003). Five-year follow-up of bilateral stimulation of the subthalamic nucleus in advanced Parkinson's disease. *N. Engl. J. Med.* 349, 1925–1934. doi: 10.1056/nejmoa035275

Krack, P., Kumar, R., Ardouin, C., Dowsey, P. L., McVicker, J. M., Benabid, A. L., et al. (2001). Mirthful laughter induced by subthalamic nucleus stimulation. *Mov. Disord.* 16, 867–875. doi: 10.1002/mds.1174

Langevin, J. P. (2012). The amygdala as a target for behavior surgery. *Surg. Neurol. Int.* 3, S40–S46. doi: 10.4103/2152-7806.91609

Langevin, J. P., Chen, J. W., Koek, R. J., Sultzer, D. L., Mandelkern, M. A., Schwartz, H. N., et al. (2016). Deep brain stimulation of the basolateral amygdala: targeting technique and electrodiagnostic findings. *Brain Sci.* 6:28. doi: 10.3390/brainsci6030028

Lanteaume, L., Khalfa, S., Regis, J., Marquis, P., Chauvel, P., and Bartolomei, F. (2007). Emotion induction after direct intracerebral stimulations of human amygdala. *Cereb. Cortex* 17, 1307–1313. doi: 10.1093/cercor/bhl041

LeDoux, J. E., Cicchetti, P., Xagoraris, A., and Romanski, L. M. (1990). The lateral amygdaloid nucleus: sensory interface of the amygdala in fear conditioning. *J. Neurosci.* 10, 1062–1069. doi: 10.1523/jneurosci.10-04-01062.1990

Li, J. J., Li, Y. H., Gong, H. Q., Liang, P. J., Zhang, P. M., and Lu, Q. C. (2016). The spatiotemporal dynamics of phase synchronization during epileptogenesis in amygdala-kindling mice. *PLoS One* 11:e0153897. doi: 10.1371/journal.pone.0153897

Loonen, A. J., and Ivanova, S. A. (2018). The evolutionary old forebrain as site of action to develop new psychotropic drugs. *J. Psychopharmacol.* 32, 1277–1285. doi: 10.1177/0269881118798617

Makovac, E., Meeten, F., Watson, D. R., Herman, A., Garfinkel, S. N., Critchley, H. D., et al. (2016). Alterations in amygdala-prefrontal functional connectivity

account for excessive worry and autonomic dysregulation in generalized anxiety disorder. *Biol. Psychiatry* 80, 786–795. doi: 10.1016/j.biopsych.2015.10.013

Markovic, V., Agosta, F., Canu, E., Inuggi, A., Petrovic, I., Stankovic, I., et al. (2017). Role of habenula and amygdala dysfunction in Parkinson disease patients with punding. *Neurology* 88, 2207–2215. doi: 10.1212/WNL.0000000000004012

Mayberg, H. S., Lozano, A. M., Voon, V., McNeely, H. E., Seminowicz, D., Hamani, C., et al. (2005). Deep brain stimulation for treatment-resistant depression. *Neuron* 45, 651–660.

McDonald, A. J. (1998). Cortical pathways to the mammalian amygdala. *Prog. Neurobiol.* 55, 257–332. doi: 10.1016/s0301-0082(98)00003-3

Meletti, S., Tassi, L., Mai, R., Fini, N., Tassinari, C. A., and Russo, G. L. (2006). Emotions induced by intracerebral electrical stimulation of the temporal lobe. *Epilepsia* 47(Suppl. 5), 47–51. doi: 10.1111/j.1528-1167.2006.00877.x

Mihara, T., Mensah-Brown, K., Sobota, R., Lin, R., Featherstone, R., and Siegel, S. J. (2017). Amygdala activity associated with social choice in mice. *Behav. Brain Res.* 332, 84–89. doi: 10.1016/j.bbr.2017.04.040

Mirabella, G. (2018). The weight of emotions in decision-making: how fearful and happy facial stimuli modulate action readiness of goal-directed actions. *Front. Psychol.* 9:1334. doi: 10.3389/fpsyg.2018.01334

Moldovan, A. S., Groiss, S. J., Elben, S., Sudmeyer, M., Schnitzler, A., and Wojtecki, L. (2015). The treatment of Parkinson's disease with deep brain stimulation: current issues. *Neural Regen. Res.* 10, 1018–1022. doi: 10.4103/1673-5374.160094

Morecraft, R. J., McNeal, D. W., Stilwell-Morecraft, K. S., Gedney, M., Ge, J., Schroeder, C. M., et al. (2007). Amygdala interconnections with the cingulate motor cortex in the rhesus monkey. *J. Comp. Neurol.* 500, 134–165. doi: 10.1002/cne.21165

Morey, R. A., Gold, A. L., LaBar, K. S., Beall, S. K., Brown, V. M., Haswell, C. C., et al. (2012). Amygdala volume changes in posttraumatic stress disorder in a large case-controlled veterans group. *Arch. Gen. Psychiatry* 69, 1169–1178. doi: 10.1001/archgenpsychiatry.2012.50

Moro, E., Schwalb, J. M., Piboolnurak, P., Poon, Y. Y., Hamani, C., Hung, S. W., et al. (2011). Unilateral subdural motor cortex stimulation improves essential tremor but not Parkinson's disease. *Brain* 134, 2096–2105. doi: 10.1093/brain/awr072

Nambu, A., Tokuno, H., and Takada, M. (2002). Functional significance of the cortico-subthalamo-pallidal 'hyperdirect' pathway. *Neurosci. Res.* 43, 111–117. doi: 10.1016/s0168-0102(02)00027-5

Narayanan, R. T., Seidenbecher, T., Sangha, S., Stork, O., and Pape, H. C. (2007). Theta resynchronization during reconsolidation of remote contextual fear memory. *Neuroreport* 18, 1107–1111.

Nicholson, A. A., Ros, T., Frewen, P. A., Densmore, M., Theberge, J., Kluetsch, R. C., et al. (2016). Alpha oscillation neurofeedback modulates amygdala complex connectivity and arousal in posttraumatic stress disorder. *Neuroimage Clin.* 12, 506–516. doi: 10.1016/j.nicl.2016.07.006

O'Doherty, D. C. M., Tickell, A., Ryder, W., Chan, C., Hermens, D. F., Bennett, M. R., et al. (2017). Frontal and subcortical grey matter reductions in PTSD. *Psychiatry Res.* 266, 1–9. doi: 10.1016/j.pscychresns.2017.05.008

Oya, H., Kawasaki, H., Dahdaleh, N. S., Wemmie, J. A., and Howard, M. A. III (2009). Stereotactic atlas-based depth electrode localization in the human amygdala. *Stereotact. Funct. Neurosurg.* 87, 219–228. doi: 10.1159/000225975

Peron, J., Fruhholz, S., Ceravolo, L., and Grandjean, D. (2016). Structural and functional connectivity of the subthalamic nucleus during vocal emotion decoding. *Soc. Cogn. Affect. Neurosci.* 11, 349–356. doi: 10.1093/scan/nsv118

Phillips, R. G., and LeDoux, J. E. (1992). Differential contribution of amygdala and hippocampus to cued and contextual fear conditioning. *Behav. Neurosci.* 106, 274–285. doi: 10.1037//0735-7044.106.2.274

Quinn, E. J., Blumenfeld, Z., Velisar, A., Koop, M. M., Shreve, L. A., Trager, M. H., et al. (2015). Beta oscillations in freely moving Parkinson's subjects are attenuated during deep brain stimulation. *Mov. Disord.* 30, 1750–1758. doi: 10.1002/mds.26376

Reyes, A., Thesen, T., Kuzniecky, R., Devinsky, O., McDonald, C. R., Jackson, G. D., et al. (2017). Amygdala enlargement: temporal lobe epilepsy subtype or nonspecific finding? *Epilepsy Res.* 132, 34–40. doi: 10.1016/j.eplepsyres.2017.02.019

Reznikov, R., and Hamani, C. (2017). Posttraumatic stress disorder: perspectives for the use of deep brain stimulation. *Neuromodulation* 20, 7–14. doi: 10.1111/ner.12551

Ros, T., Theberge, J., Frewen, P. A., Kluetsch, R., Densmore, M., Calhoun, V. D., et al. (2013). Mind over chatter: plastic up-regulation of the fMRI salience network directly after EEG neurofeedback. *Neuroimage* 65, 324–335. doi: 10.1016/j.neuroimage.2012.09.046

Saleh, M., Reimer, J., Penn, R., Ojakangas, C. L., and Hatsopoulos, N. G. (2010). Fast and slow oscillations in human primary motor cortex predict oncoming behaviorally relevant cues. *Neuron* 65, 461–471. doi: 10.1016/j.neuron.2010.02.001

Schaich Borg, J., Srivastava, S., Lin, L., Heffner, J., Dunson, D., Dzirasa, K., et al. (2017). Rat intersubjective decisions are encoded by frequency-specific oscillatory contexts. *Brain Behav.* 7:e00710. doi: 10.1002/brb3.710

Schnitzler, A., and Gross, J. (2005). Normal and pathological oscillatory communication in the brain. *Nat. Rev. Neurosci.* 6, 285–296. doi: 10.1038/nrn1650

Seidenbecher, T., Laxmi, T. R., Stork, O., and Pape, H. C. (2003). Amygdalar and hippocampal theta rhythm synchronization during fear memory retrieval. *Science* 301, 846–850. doi: 10.1126/science.1085818

Sinha, S., McGovern, R. A., and Sheth, S. A. (2015). Deep brain stimulation for severe autism: from pathophysiology to procedure. *Neurosurg. Focus* 38:E3. doi: 10.3171/2015.3.FOCUS1548

Stujenske, J. M., Likhtik, E., Topiwala, M. A., and Gordon, J. A. (2014). Fear and safety engage competing patterns of theta-gamma coupling in the basolateral amygdala. *Neuron* 83, 919–933. doi: 10.1016/j.neuron.2014.07.026

Sturm, V., Fricke, O., Buhrle, C. P., Lenartz, D., Maarouf, M., Treuer, H., et al. (2012). DBS in the basolateral amygdala improves symptoms of autism and related self-injurious behavior: a case report and hypothesis on the pathogenesis of the disorder. *Front. Hum. Neurosci.* 6:341. doi: 10.3389/fnhum.2012.00341

Tan, H., Pogosyan, A., Anzak, A., Foltynie, T., Limousin, P., Zrinzo, L., et al. (2013). Frequency specific activity in subthalamic nucleus correlates with hand bradykinesia in Parkinson's disease. *Exp. Neurol.* 240, 122–129. doi: 10.1016/j.expneurol.2012.11.011

Tendler, A., and Wagner, S. (2015). Different types of theta rhythmicity are induced by social and fearful stimuli in a network associated with social memory. *eLife* 4:e03614. doi: 10.7554/eLife.03614

Toschi, N., Duggento, A., and Passamonti, L. (2017). Functional connectivity in amygdalar-sensory/(pre)motor networks at rest: new evidence from the Human Connectome Project. *Eur. J. Neurosci.* 45, 1224–1229. doi: 10.1111/ejn.13544

Tsubokawa, T., Katayama, Y., Yamamoto, T., Hirayama, T., and Koyama, S. (1991). Treatment of thalamic pain by chronic motor cortex stimulation. *Pacing Clin. Electrophysiol.* 14, 131–134. doi: 10.1111/j.1540-8159.1991.tb04058.x

Uylings, H. B., Groenewegen, H. J., and Kolb, B. (2003). Do rats have a prefrontal cortex? *Behav. Brain Res.* 146, 3–17. doi: 10.1016/j.bbr.2003.09.028

von Stein, A., and Sarnthein, J. (2000). Different frequencies for different scales of cortical integration: from local gamma to long range alpha/theta synchronization. *Int. J. Psychophysiol.* 38, 301–313. doi: 10.1016/s0167-8760(00)00172-0

Vonck, K., Boon, P., Achten, E., De Reuck, J., and Caemaert, J. (2002). Long-term amygdalohippocampal stimulation for refractory temporal lobe epilepsy. *Ann. Neurol.* 52, 556–565. doi: 10.1002/ana.10323

Vriend, C., Boedhoe, P. S., Rutten, S., Berendse, H. W., van der Werf, Y. D., and van den Heuvel, O. A. (2016). A smaller amygdala is associated with anxiety in Parkinson's disease: a combined FreeSurfer-VBM study. *J. Neurol. Neurosurg. Psychiatry* 87, 493–500. doi: 10.1136/jnnp-2015-310383

Wicker, E., and Forcelli, P. A. (2016). Chemogenetic silencing of the midline and intralaminar thalamus blocks amygdala-kindled seizures. *Exp. Neurol.* 283, 404–412. doi: 10.1016/j.expneurol.2016.07.003

Wilson, C. J. (2014). Oscillators and oscillations in the basal ganglia. *Neuroscientist* 21, 530–539. doi: 10.1177/1073858414560826

Witt, K., Daniels, C., Reiff, J., Krack, P., Volkmann, J., Pinsker, M. O., et al. (2008). Neuropsychological and psychiatric changes after deep brain stimulation

for Parkinson's disease: a randomised, multicentre study. *Lancet Neurol.* 7, 605–614. doi: 10.1016/S1474-4422(08)70114-5

Wojtecki, L., Elben, S., Vesper, J., and Schnitzler, A. (2017). The rhythm of the executive gate of speech: subthalamic low-frequency oscillations increase during verbal generation. *Eur. J. Neurosci.* 45, 1200–1211. doi: 10.1111/ejn.13429

Wojtecki, L., Groiss, S. J., Hartmann, C. J., Elben, S., Omlor, S., Schnitzler, A., et al. (2016). Deep brain stimulation in huntington's disease-preliminary evidence on pathophysiology, efficacy and safety. *Brain Sci.* 6:E38. doi: 10.3390/brainsci6030038

Wojtecki, L., Nickel, J., Timmermann, L., Maarouf, M., Südmeyer, M., Schneider, F., et al. (2007). Pathological crying induced by deep brain stimulation. *Mov. Disord.* 22, 1314–1316. doi: 10.1002/mds.21266

Yang, J., Yin, Y., Svob, C., Long, J., He, X., Zhang, Y., et al. (2017). Amygdala atrophy and its functional disconnection with the cortico-striatal-pallidal-thalamic circuit in major depressive disorder in females. *PLoS One* 12:e0168239. doi: 10.1371/journal.pone.0168239

Zheng, J., Anderson, K. L., Leal, S. L., Shestyuk, A., Gulsen, G., Mnatsakanyan, L., et al. (2017). Amygdala-hippocampal dynamics during salient information processing. *Nat. Commun.* 8:14413. doi: 10.1038/ncomms14413

Conflict of Interest Statement: The authors declare that the research was conducted in the absence of any commercial or financial relationships that could be construed as a potential conflict of interest.

frontiers in Neuroscience

ORIGINAL RESEARCH
published: 08 May 2019
doi: 10.3389/fnins.2019.00418

Anti-inflammatory Effects of Abdominal Vagus Nerve Stimulation on Experimental Intestinal Inflammation

Sophie C. Payne[1,2], John B. Furness[3,4], Owen Burns[1], Alicia Sedo[3], Tomoko Hyakumura[1,2], Robert K. Shepherd[1,2] and James B. Fallon[1,2,5]*

[1] Bionics Institute, Fitzroy, VIC, Australia, [2] Medical Bionics Department, University of Melbourne, Parkville, VIC, Australia, [3] Florey Institute of Neuroscience and Mental Health, Parkville, VIC, Australia, [4] Department of Anatomy and Neuroscience, University of Melbourne, Parkville, VIC, Australia, [5] Department of Otolaryngology, University of Melbourne, Parkville, VIC, Australia

OPEN ACCESS

Edited by:
Giovanni Mirabella, Sapienza University of Rome, Italy

Reviewed by:
Ali Yadollahpour, Ahvaz Jundishapur University of Medical Sciences, Iran
Sonia Pellissier, Université Savoie Mont Blanc, France

***Correspondence:**
Sophie C. Payne
spayne@bionicsinstitute.org

Specialty section:
This article was submitted to Neural Technology, a section of the journal Frontiers in Neuroscience

Received: *05 February 2019*
Accepted: *11 April 2019*
Published: *08 May 2019*

Citation:
Payne SC, Furness JB, Burns O, Sedo A, Hyakumura T, Shepherd RK and Fallon JB (2019) Anti-inflammatory Effects of Abdominal Vagus Nerve Stimulation on Experimental Intestinal Inflammation. Front. Neurosci. 13:418. doi: 10.3389/fnins.2019.00418

Electrical stimulation of the cervical vagus nerve is an emerging treatment for inflammatory bowel disease (IBD). However, side effects from cervical vagal nerve stimulation (VNS) are often reported by patients. Here we hypothesized that stimulating the vagus nerve closer to the end organ will have fewer off-target effects and will effectively reduce intestinal inflammation. Specifically, we aimed to: (i) compare off-target effects during abdominal and cervical VNS; (ii) verify that VNS levels were suprathreshold; and (iii) determine whether abdominal VNS reduces chemically-induced intestinal inflammation in rats. An electrode array was developed in-house to stimulate and record vagal neural responses. In a non-recovery experiment, stimulation-induced off-target effects were measured by implanting the cervical and abdominal vagus nerves of anaesthetized rats (n = 5) and recording changes to heart rate, respiration and blood pressure during stimulation (10 Hz; symmetric biphasic current pulse; 320 nC per phase). In a chronic experiment, the efficacy of VNS treatment was assessed by implanting an electrode array onto the abdominal vagus nerve and recording *in vivo* electrically-evoked neural responses during the implantation period. After 14 days, the intestine was inflamed with TNBS (2.5% 2,4,6-trinitrobenzene sulphonic acid) and rats received therapeutic VNS (n = 7; 10 Hz; 320 nC per phase; 3 h/day) or no stimulation (n = 8) for 4.5 days. Stool quality, plasma C-reactive protein and histology of the inflamed intestine were assessed. Data show that abdominal VNS had no effect (two-way RM-ANOVA: $P \geq 0.05$) on cardiac, respiratory and blood pressure parameters. However, during cervical VNS heart rate decreased by 31 ± 9 beats/minute ($P \geq 0.05$), respiration was inhibited and blood pressure decreased. Data addressing efficacy of VNS treatment show that electrically-evoked neural response thresholds remained stable (one-way RM ANOVA: $P \geq 0.05$) and therapeutic stimulation remained above threshold. Chronically stimulated rats, compared to unstimulated rats, had improved stool quality (two-way RM ANOVA: $P < 0.0001$), no blood in feces ($P < 0.0001$), reduced plasma C-reactive

protein (two-way RM ANOVA: $P < 0.05$) and a reduction in resident inflammatory cell populations within the intestine (Kruskal–Wallis: $P < 0.05$). In conclusion, abdominal VNS did not evoke off-target effects, is an effective treatment of TNBS-induced inflammation, and may be an effective treatment of IBD in humans.

Keywords: vagus nerve stimulation, peripheral nerve stimulation, inflammatory bowel disease, medical device, bioelectric neuromodulation

INTRODUCTION

Inflammatory bowel diseases (IBDs), encompassing Crohn's disease and ulcerative colitis, are progressive debilitating immune-mediated disorders of the gastrointestinal tract (Ananthakrishnan, 2015b). The impact of the disease on patient quality of life is substantial due to its onset in young adulthood, fluctuating periods in which the disease is active (relapse and remission) and the lack of a cure (Abraham and Cho, 2009). The incidence of IBD is on the increase worldwide, with the prevalence of the disease highest in North America with an estimated 1.5 million people affected (Ananthakrishnan, 2015b).

The etiology of IBD is unknown, however, interactions between an individual's genetic makeup and external environment (i.e., diet, stress) play key roles in the emergence of IBD (Ananthakrishnan, 2015a). IBD is characterized by the over production of the key upstream pro-inflammatory mediator tumor-necrosis-factor-alpha (TNF-α) from macrophages, monocytes and differentiated T cells within the gastrointestinal tissue (Sanchez-Munoz et al., 2008). The production of TNF-α leads to the infiltration of inflammatory cells, which themselves further release pro-inflammatory cytokines, such as interleukin-1β (IL-1 β), IL-6, and interferon-gamma (IFN-γ) (Sanchez-Munoz et al., 2008; Neurath, 2014). Current gold standard immunosuppressant pharmacological therapies and anti-TNF-α biologicals, suppress the immune reaction and reduce the cascade of cytokine release by targeting TNF-α production (Rutgeerts et al., 2004; Nielsen and Munck, 2007). Although clinical management of such combined therapies has led to advancements in the control and prediction of the disease (Caprilli et al., 2006; De Cruz et al., 2015), adverse events in response to medication can be experienced in up to 20% of IBD patients when using these therapies (Chaparro et al., 2013; Gecse et al., 2016). Furthermore, despite the development of new anti-TNF-α therapies and clinical management strategies, surgical resection of the inflamed area of the gastrointestinal tract is necessary in 80% of ileocecal Crohn's disease patients (Caprilli et al., 2006). Therefore, an alternative therapy that keeps patients in remission is needed to more effectively treat IBD over the long-term.

A growing body of evidence has demonstrated that unilateral electrical stimulation of the left cervical vagus nerve is a feasible treatment in a rodent model of colitis (Meregnani et al., 2011; Sun et al., 2013). Following chemically-induced colitis in rats, cervical vagus nerve stimulation (VNS) improved the disease activity index (DAI: weight and stool quality), decreased histological damage and reduced inflammatory molecular markers expressed in colonic tissue (Meregnani et al., 2011). However, the effects of VNS therapy on histology and molecular markers were only seen in areas adjacent to, but not within, the inflammatory lesion. In a subsequent colitis study, inflammatory markers were only modestly reduced by cervical VNS, and inflammatory disease parameters (DAI, histology, inflammatory cytokine production) in VNS treated tissue did not return to control levels (Sun et al., 2013).

A first, small clinical trial demonstrated efficacy cervical VNS in ileocecal Crohn's disease patients (Bonaz et al., 2016) The majority of patients (5 of 7) responded to treatment and showed a reduction in clinical symptoms (Crohn's DAI), improvements in molecular markers (C-reactive protein and fecal calprotectin) and endoscopy DAI score. However, two patients experienced worsening of clinical symptoms and were removed from the study (Bonaz et al., 2016). Additionally, patients reported voice alterations (dysphonia) during stimulation (Bonaz et al., 2016). Other side effects, such as coughing, pain and labored/shortness of breath (dyspnea) are frequently reported following cervical VNS in patients treated with VNS for drug resistant epilepsy (Ben-Menachem et al., 2015). Studies in epileptic children fitted with a cervical VNS report more serious complications during sleep. Stimulation-induced effects on respiration and a reduction in overall oxygen saturation was seen in the majority of patients (87.5%, 8 patients; 100%, 10 patients, respectively) (Nagarajan et al., 2003; Zaaimi et al., 2005), while stimulus-induced changes to heart rate variability are reported in 50% of patients (10 patients) (Pruvost et al., 2006; Zaaimi et al., 2007). Another study reports stimulus-induced obstructive sleep apnea (15%; 26 patients) (Khurana et al., 2007). Such off-target affects are due to the activation of low threshold cervical vagal fibers to the larynx, pharynx, heart, and lungs (discussed in detail in the discussion), while the abdominal vagus nerve is at a site below these branches and its stimulation is predicted to results in fewer off-target effects.

Although evidence for VNS therapy to treat IBD is promising, the current approach of stimulating the cervical vagus nerve has a number of clinical limitations, including potentially an undesirable side-effect profile. To overcome the limitations of cervical VNS, we hypothesized that stimulating the sub-diaphragmatic abdominal vagus nerve (**Figure 1A**), which is below vagal branches to the lungs and heart and closer to the end organ, will improve the therapeutic effect of VNS and have fewer off-target effects. To address this hypothesis, in this study we first developed an electrode array (in house) that was able to stimulate and record neural responses from the vagus nerve of the rats. Using this electrode array in a non-recovery experiment, referred to as the "*VNS off-target experiment*," off-target effects to cardiac and respiratory rate were assessed during abdominal and cervical

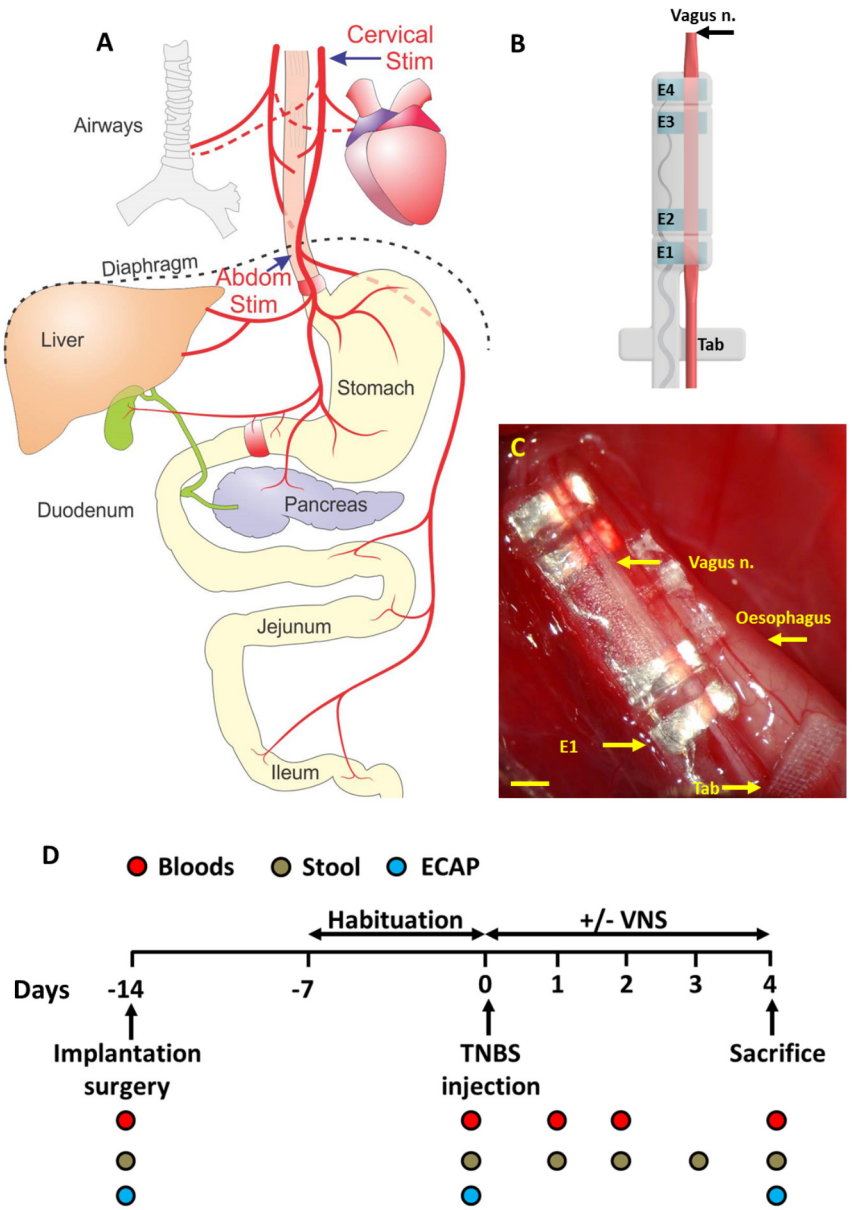

FIGURE 1 | Abdominal vagus nerve anatomy, electrode design and experimental schedule. **(A)** Schematic anatomical diagram shows the cervical and abdominal branches of the vagus nerve. Off-target effects in response to cervical stimulation (Cervical Stim indicated by arrow) and abdominal stimulation (Abdom Stim indicated by arrrow) were evaluated. For the VNS efficacy experiment, the electrode array was implanted onto the anterior abdominal vagus nerve, below the diaphragm and above the hepatic and celiac vagal branches. **(B)** The cuff electrode array had two platinum electrode pairs (E1–E2; E3–E4) that stimulated and recorded evoked neural responses. The array was anchored by suturing the Dacron tab to the esophagus. **(C)** Image of the abdominal vagus nerve electrode array *in vivo*. **(D)** Experimental schedule for the VNS efficacy experiment. Scale bar in **(C)** 1 mm.

VNS. In a recovery experiment, referred to as the "*VNS efficacy experiment,*" the efficacy of abdominal VNS was assessed using a rodent model of chemically-induced intestinal inflammation (**Figure 1A**). Behavioral, molecular and histological markers of inflammation were evaluated to determine the efficacy of abdominal VNS, and the histology of the implanted vagus nerve examined to confirm the safety of electrode array and stimulation delivered.

MATERIALS AND METHODS

This paper describes: (i) an acute (non-recovery) experiment that evaluated off-target effects during cervical and abdominal VNS. This is referred to as the "*VNS off-target experiment*"; and (ii) a chronic VNS efficacy experiment that evaluated the efficacy of abdominal VNS following chemically-induced intestinal inflammation, which is referred to as the "*VNS efficacy*

experiment" The methods section describes general procedures common to all experiments, followed by techniques specific to the VNS off-target and efficacy experiments.

General Methods

Animals and Anaesthesia

Sprague-Dawley rats (10–12 weeks old, Animal Resource Centre, Western Australia) were used, and all animal procedures were approved by the Animal Research and Ethics Committee of the Bionics Institute and complied with the Australian Code for the Care and Use of Animals for Scientific Purposes (National Health and Medical Research Council of Australia). Approval was also obtained from the United States Army Medical Research and Material Command Animal Care and Use Review Office, protocol SSC-7486.02. Animals were kept on a 12 h light (7 a.m.–7 p.m.)/dark cycle (7 p.m.–7 a.m.) and allowed *ad libitum* access to fresh food, standard chow and water. For all surgical interventions, rats were anaesthetized (2–3% isoflurane using an oxygen flow rate of 1–1.5 L/min) and breathing rate remained between 45 and 60 breaths per minute (Payne et al., 2018c). All procedures were performed under aseptic conditions and following recovery surgery, rats were monitored carefully, given an analgesic (Carprofen 5 mg/kg sub-cutaneous) and housed separately. At the conclusion of the experiment, rats were anaesthetized (2% isoflurane using an oxygen flow rate of 1–1.5 L/min), then euthanized (300 mg/kg Lethabarb, intracardial injection).

Design of the Vagus Nerve Electrode Array

The vagus nerve electrode array consisted of four platinum (99.95%) electrodes embedded in a medical grade silicone elastomer cuff. Each platinum electrode had an exposed surface area of 0.3 mm^2. The distance between adjacent electrodes (E1–E2, or E3–E4, center to center) was 1.2 mm, while the distance between electrode pairs (E1–E2 to E3–E4, center to center) was 4.7 mm (**Figure 1B**). A channel (0.55 mm wide × 0.2 mm deep) traversed the length of the array to position the vagus nerve in close contact with the electrodes without damaging the nerve. A silicone 'lid' completes the cuff, preventing the nerve from migrating from the channel. A Dacron embedded silicone tab adjacent to the electrode array was used to suture the array to the esophagus, when chronically implanted onto the abdominal vagus nerve, in order to provide mechanical stability (**Figure 1B**). Individually insulated 50 μm diameter platinum/iridium (90/10) wires were welded to each electrode and formed a helical cable which traversed to a percutaneous connector mounted on the lumbar region of the rat.

Abdominal Vagus Nerve Electrode Array Implantation Surgery

Rats were anaesthetized, the skin incised on the ventral abdominal midline and along the dorsal-lumbar aspect of the spine. The vagus nerve electrode array was tunneled subcutaneously from the dorsal-lumbar incision to exit through the ventral abdominal incision. The abdominal cavity was exposed and the liver retracted gently using sterile saline soaked gauze. Abdominal tissue was kept moist at all times using warm sterile saline. The sub-diaphragmatic anterior abdominal branch of the vagus nerve was dissected away from the esophagus and the array implanted rostral to the hepatic and celiac branches of the vagus (**Figures 1A,C**). The array was sutured (7-0 silk, Ethicon) to the esophagus to provide stabilization and the abdominal cavity and skin sutured closed. The rat was rotated to expose the dorsal aspect of the spine, the percutaneous connector was anchored to the connective tissue of the lumbar region of the spine, and the skin closed around it.

Electrode Impedance Testing and Electrophysiological Recordings

To test the functionality of electrodes, the impedance of electrodes was measured using biphasic current pulses passed between the electrode of interest and all other implanted electrodes (Fallon et al., 2009). The peak voltage at the end of the first phase (V_{total}) of the current pulse was measured following delivery of a 25 μs per phase current pulse and current of 931 μA (Richardson et al., 2009). The V_{total} value was then used to calculate total impedance (Z_{total}) using Ohm's law (Z = voltage/current).

Electrically-evoked compound action potentials (ECAPs) were recorded in anaesthetized rats using bipolar vagus nerve electrodes. Either pair of electrodes (E1–E2 or E3–E4) could be used to stimulate or record neural responses. Two sets of evoked electrophysiological recordings (averaged from a total of 50 responses) were made at currents from 0 to 2 mA in 0.1 mA steps using a biphasic pulse (width = 200 μs, 50 μs interphase gap) presented at a rate of 10 pulses per second. Recordings were sampled at a rate of 100 kHz and filtered (high pass: 200 Hz; low pass: 2000 Hz; voltage gain 10^3) (Payne et al., 2018a). The electrically-evoked neural response threshold was defined as the minimum stimulus intensity producing a response amplitude of at least 0.1 μV within a post-stimulus latency window of 4.0–7.0 ms (Payne et al., 2018a). All recorded neural responses had conduction velocities within the range of a C-fiber response (Castoro et al., 2011).

VNS Off-Target Effects Experiment

Acute experiments (n = 5) were performed in normal, isoflurane anaesthetized, freely respiring rats to assess changes to heart rate, respiration rate and blood pressure during cervical and abdominal VNS. *Vagus nerve implantation surgery*: The left cervical vagus nerve was exposed and identified (Childs et al., 2015), and a vagus nerve electrode array (**Figure 1B**) implanted around the nerve. In the same rat, a second vagus nerve electrode array was implanted onto the anterior abdominal vagus nerve (see section above for details). *Femoral artery cannulation and measurements*: To measure arterial blood pressure changes, the femoral artery was exposed and cannulated. The cannula was connected to a calibrated blood pressure transducer (World Precision Instruments (WPI), Canada), the signal amplified and waveforms recorded (Cerebus System 128 Channel Neural Stimulator, Blackrock Microsystems, Massachusetts). *Heart and respiration rate measurements*: Heart rate was measured by recording electrocardiograms (ECG) by placing needles (26 Gauge) across the thorax and a return in the left leg.

The ECG was amplified using a WPI Iso-80 bioamp (Gain: $\times 10^3$; high pass: 5 Hz; low pass 10 kHz) before being recorded via the Cerebus system. Respiration rate was measured by placing a PolyPower®stretch sensor (Danfoss PolyPower, Denmark) around the upper thorax. Care was taken to place the respiratory band sensor over the largest excursion point during respiration. *Stimulus-induced off-target testing*: Baseline recordings of heart rate, respiration rate or blood pressure were generated for 30 s during which no (cervical or abdominal) stimulation was applied. After baseline recordings were taken, the cervical or abdominal vagus nerve was stimulated (10 Hz, 50 repetitions) at 0 or 1.6 mA (200 μs pulse width) for 20 s. To confirm that 1.6 mA stimulation applied to the cervical or abdominal vagus nerve was suprathreshold, electrically-evoked neural responses were recorded (1.6 mA, 200 μs pulse width). Following this stimulation period, 30 s of recordings were taken to monitor the return of measurements to baseline. Heart rate, respiration rate and blood pressure changes from baseline were calculated from the waveforms using a detection algorithm in IGOR8 software. At the conclusion of the experiment, rats were euthanized. No tissue was taken for histology.

VNS Efficacy Experiment

Chronic experiments (n = 15) assessed the efficacy of abdominal VNS in reducing inflammatory markers following TNBS-induced inflammation of the small intestine (experimental overview shown in **Figure 1D**).

Experimental Groups

The primary experimental groups consisted of rats that were implanted with an electrode array onto the abdominal vagus, allowed to recover for 7 days, habituated for 6 days and injected with TNBS to inflame the small intestine (see below). At 4 h following the TNBS injection, rats were randomly selected to receive abdominal VNS (TNBS+VNS: n = 7) or no stimulation (TNBS: n = 8). Blood and stool samples were collected, and ECAPs were recorded on days -14, 0, and 4 (**Figure 1D**). Rats were euthanized 4.5 days after TNBS injection (T = 4) and tissue taken for histological analysis. Similar to previous experiments (Pontell et al., 2009), control tissue (n = 9) was taken 5 cm oral to the ligation for the TNBS injection from animals in the TNBS (n = 5) and TNBS+VNS (n = 4) groups. An additional cohort of animals were euthanized 4 h after TNBS injection (4 H TNBS; n = 3) in order to evaluate the degree of intestinal inflammation at the onset of stimulation (**Table 1**).

Inflammation of the Small Intestine

At 14 days following implantation of the electrode array onto the abdominal vagus nerve, rats were anaesthetized and under aseptic conditions the abdominal midline incised and an 8 cm segment of jejunum, clear of intra-luminal content, was selected and ligated between two sutures (2-0 silk, Ethicon; Nurgali et al., 2007). Inflammation was induced within this ligated area by slowly injecting 1 mL of TNBS (2.5% dilution in 50% ethanol, Sigma) at the oral end of the ligated small intestine over a course of 2 min. After 5 min the ligatures were removed, the intestine returned to the abdominal cavity and the skin and abdominal wall muscle sutured closed in two layers (Pontell et al., 2009). The small intestine was kept moist with sterile saline solution during the whole procedure.

Habituation and Vagus Nerve Stimulation

Rats were habituated for 6 consecutive days prior to the TNBS injection (T = -7 to -1) to ensure no additional stress to the animal during the testing period (T = 0–4). Animals were housed individually in Perspex boxes and percutaneous plugs connected to an external stimulator (Fallon et al., 2018), but no stimulation was delivered. Given that routine laboratory procedures can cause stress to the animal, every attempt to handle animals equally and as little as possible was made (Balcombe et al., 2004). Immediately prior to the TNBS injection (T = 0), ECAPs were generated in all implanted animals. At 4 h following TNBS injection, awake animals were randomly selected to receive VNS delivered at 1.6 mA and 200 μs/phase (i.e., 320 nC per phase) using a stimulus rate of 10 pulses/s with a 30 s ON 5 min OFF duty cycle for 3 h/day (1:30–4:30 p.m.) for 5 consecutive days (T = 0 to T = 4; 5 stimulation sessions in total). Unstimulated rats (TNBS group) were subjected to the same procedures as stimulated rats, but did not receive VNS. ECAPs were recorded on days -14, 0, and 4 (**Figure 1D**). Electrical stimulation was delivered using an external battery operated stimulator (Fallon et al., 2018) connected to the percutaneous connector. The stimulator delivered charge-balanced biphasic current pulses to the selected bipolar electrodes located on the nerve. Charge recovery was achieved via electrode shorting on completion of each current pulse.

Quantification of Disease Activity Index

Stool produced from implanted rats while being weighed (between 9 and 10 a.m. each day (T = 0 to T = 4) was assessed for consistency and signs of bleeding (**Table 2** and **Figure 1D**) (Sun et al., 2013).

TABLE 1 | Experimental cohorts in the efficacy of VNS experiment.

Experimental group	TNBS	VNS	Sample size
TNBS only (4H TNBS)	Yes	N/A	3
Unstimulated (TNBS)	Yes	No	8
Stimulated (TNBS+VNS)	Yes	Yes	7

Control tissue was taken from an oral segment of gut from implanted animals (control tissue from TNBS rats: n = 5 of 8; Control tissue from TNBS+VNS rats: n = 4 of 7).

TABLE 2 | Scoring system of stool quality following TNBS injection.

Variable	0	1	2
Stool consistency	Normal stool: hard pellet shaped form	Loose stools: Pellet is sticky and deforms under pressure	Diarrhea: No form; fecal matter adherent to fur
Signs of blood	No blood: Stool is a medium brown color	Mild bleeding: Stool is dark brown or black in appearance	Gross bleeding: Blood is visible on fur and bedding

Quantification of C-Reactive Protein

Blood was taken from the tail vein of implanted rats (**Figure 1D**). Blood taken prior to TNBS injection on day 0 served as a control. The final bleed was taken after the final round of stimulation. Whole blood (300 μL) was collected in K2-EDTA tubes (Starstedt) centrifuged (2000 g for 10 min) and plasma aliquoted and stored at −80°C. On the day of the assay, aliquots were thawed on ice and the C-reactive protein (CRP) ELISA conducted according to manufacturer instructions (Cusabio CSB-E07922r) and CRP levels determined via absorbance measurements using a Biorad BenchMark Plus microplate spectrophotometer.

Dissection, Histology, and Immunohistochemistry of Small Intestine Tissue

At the conclusion of the experiment, implanted rats were euthanized and the TNBS-inflamed segment of small intestine tissue dissected and processed as previously described (Payne et al., 2018c). In brief, a 2 cm segment of control tissue was removed spanning 5–7 cm oral to where the ligation limiting the inflamed site had been. As TNBS-induced inflammation is patchy, the 8 cm length of inflamed intestine was divided equally into four 2 cm long segments, and cut longitudinally along the mesenteric border and pinned out onto balsa boards (mucosa side up). One half was placed in fixative (2% formaldehyde plus 0.2% picric acid in 0.1 M sodium phosphate buffer, pH 7.4) overnight, embedded in paraffin, sectioned (5 μm) and stained with hematoxylin and eosin (H&E) (Pontell et al., 2009) or immunohistochemically stained with anti-CD3, a cytotoxic T cell marker (1:200; Cytomation, Dako E0432) (Payne et al., 2018c). The other half of the tissue was processed for frozen sections (14 μm) and myeloperoxidase (MPO) staining (Payne et al., 2018c). All sections were mounted with DPX.

Histopathology Scoring of Inflamed Tissue

Histopathologist (J.B.Furness), blinded to procedures, used H&E stained sections to evaluate the degree of inflammation in each segment of intestine. Histological changes were on a scale of 0–3 for the assessment of damage to the mucosa (villi architecture changes, including loss of height, pinching, clubbing, venous engorgement), and assessment of inflammatory changes (leukocyte infiltration) on a scale of 0–2 for assessment of the numbers of leukocytes within venules (adapted from Payne et al., 2018c; **Table 3**). Scores were out of a total of 9.

Inflammatory Cell Quantification in Transmural Small Intestine Tissue

Eosinophils, T cells (CD3+ cells) and neutrophils (MPO+ cells) were quantified using a Zeiss Axioplan II microscope, positive cells were counted (×40 objective) across three consecutive fields of view across the external smooth muscle layers, submucosal and mucosal layers. Cells were counted within the most inflamed area of the tissue. Images of the total field of view were generated (Axiovision, Zeiss, Germany). For MPO, eosinophil and T cell counts, cells per mm length of intestine were quantified.

Vagal Nerve Tissue Processing and Analysis

Immediately following dissection of small intestine tissue, implanted animals were perfused intracardially with 0.9% saline followed by fixative (4% paraformaldehyde in 0.1 M phosphate buffer, pH 7.4, room temperature). The esophagus and implanted vagus nerve array were dissected from the carcass. At the implanted region, the vagus nerve was dissected from the array and the region of the nerve adjacent to the electrodes (E1–E4) labeled using tissue dye (Davidson's Marking system, Bradley Products, MN, United States) (Villalobos et al., 2013). Tissue proximal to the implanted site was also taken and processed as an intra-animal, non-implanted control. The esophagus and attached vagus nerve were embedded in paraffin and serial sections (5 μm) taken. The tissue dye marked the area of vagus nerve that was adjacent to electrodes. Sections were stained for H&E and mounted with DPX. Sections were examined by an observer (S.C Payne), blinded to procedures, for signs of histopathological damage. At each location light microscope images were taken using a Zeiss Axioplan II microscope and Axiovision software (Zeiss, Germany). Using ImageJ, total fascicle area was quantified across one section per electrode position, per animal. The cross-sectional area of the vagus nerve was not measured as the boundary of the epineurium was difficult to define.

Statistics

Differences between normally distributed data were tested using a one- or two-way repeated measures (RM) ANOVA with Sidak or Tukey *post hoc* tests as appropriate. Differences between data that was not normally distributed was analyzed using a non-parametric Kruskal Wallis one-way ANOVA and Dunn's *post hoc* test. Details of each statistical test are stated in the relevant results section. Statistically significant differences were accepted

TABLE 3 | Histological parameters used to score tissue taken from the small intestine following TNBS injection.

	Variable	0	1	2	3
Mucosal damage	Extent of mucosal damage (including loss of height, pinching, clubbing, venous engorgement)	No damage	Damage affects less than 1/3 of villi	Damage affects between 1/3 and 2/3 of villi	Damage affects more than 2/3 of villi
	Shortening of villi	0–20% shortening	20–60% shortening	60–100% shortening	N/A
	Pinching of villi	Absent	Affecting < 50% of villi	Affecting > 50% of villi	N/A
Inflammatory changes	Leukocyte presence in large venules (avoiding capillaries and small venules or lymphatics)	<4 adherent leukocytes in venules	4–10 adherent leukocytes in venules	>10 adherent leukocytes in venules	N/A

Adapted from Payne et al. (2018c).

as P-values of < 0.05 and GraphPad Prism 4 (GraphPad Software, United States) was used for all analysis.

RESULTS

VNS Off-Target Effects Experiment

No Measurable Off Target Affects During Abdominal Vagus Nerve Stimulation

The average (standard error of mean, SEM) threshold for activation of C-fibers by cervical VNS was 0.25 ± 0.07 mA and abdominal VNS was 0.43 ± 0.11 mA, indicating the test stimulation of 1.6 mA was substantially suprathreshold for C-fibers at both stimulation sites in all animals. In the example shown in **Figure 2A**, cervical VNS resulted in an average heart rate drop of 43 beats per minute (bpm) from baseline (370 ± 15.4 bpm), a maximum decrease in blood pressure of 8.2 mmHg and an almost complete cessation of breathing (baseline respiration rate: 52 ± 7.0 cycles per minute, cpm). In contrast, the same level of abdominal VNS produced no change in heart rate (400 ± 31.4 bpm), repiration rate (54 ± 5.0 cpm) or blood pressure (**Figure 2B**).

Statistical analysis [two-way (Current × Location) RM ANOVA; $n = 5$] of the effects of VNS on heart rate revealed a significant effect of Current ($P = 0.06$), Location ($P = 0.04$) and a significant Interaction ($P = 0.02$). Tukey's *post hoc* analysis showed the average 31 ± 9 bpm (mean ± SEM) drop in heart rate during suprathreshold cervical VNS was significantly ($P = 0.02$) greater than suprathreshold abdominal VNS, which was not different to no stimulation ($P = 0.9$). Respiration recordings were noisy and difficult to quantify, however, severe disruptions to the regular respiration pattern were observed in 4 of 5 rats during the suprathreshold cervical VNS, while no changes in respiration were observed with abdominal VNS. Blood pressure changes were only assessed in $n = 2$ animals and therefore no statistical comparisons of the data were performed.

VNS Efficacy Experiment

Thresholds for Electrically-Evoked Neural Responses Remained Below Stimulation Levels

ECAPs were recorded to ensure stimulation levels were above neural threshold. The mean threshold of recorded ECAPs remained unchanged (one-way RM ANOVA (Time): $P = 0.8$) between day -14 (393 ± 74 μA; **Figure 3A**), day 0 (357 ± 65 μA; **Figure 3B**) and day 4 (325 ± 75 μA; **Figure 3C**) and substantially below the levels used to delivery therapeutic stimulation (1.6 mA, 200 μs/phase). The latency of ECAPs also remained unchanged (one-way RM ANOVA; $P = 0.16$) during the implantation period (T = -14: 5.43 ± 0.35 ms; T = 0: 6.69 ± 0.58 ms; T = 4: 5.52 ± 0.35 ms).

Impedance of Implanted Abdominal Vagus Nerve Electrodes

The mean electrode impedance (±SEM) in saline (prior to implantation) was 2308 ± 96 Ω (range: 1880–3340 Ω). Immediately following implantation, common ground impedance of electrodes increased to 5070 ± 246 Ω (range

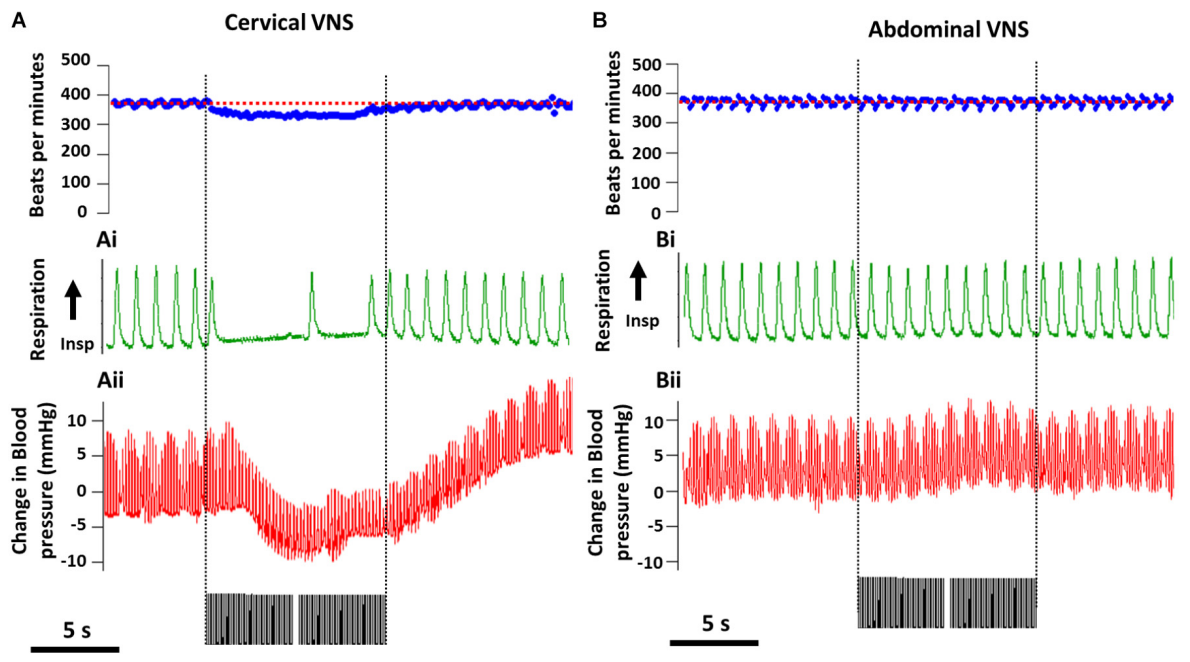

FIGURE 2 | Off-target effects during cervical and abdominal VNS. Representative recordings from from one animal show a decrease in heart rate (baseline heart rate indicated by red dotted line) **(A)**, respiratory rate **(Ai)** and blood pressure **(Aii)** during cervical VNS (1.6 mA, 200 μs/phase). **(B–Bii)** No changes in heart rate (baseline heart rate indicated by red dotted line) **(B)**, respiratory rate **(Bi)** and blood pressure **(Bii)** were seen during abdominal VNS (1.6 mA, 200 μs/phase). Scale bar in **(A,B)** represents 5 s.

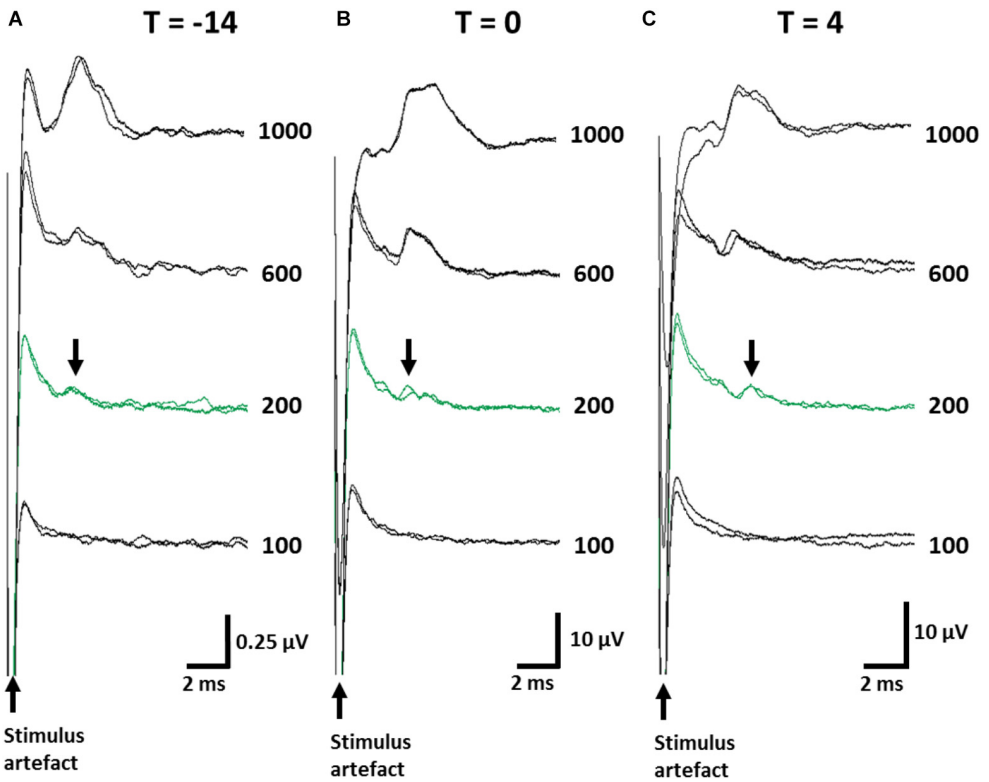

FIGURE 3 | Electrically-evoked C-fiber responses from the abdominal vagus nerve were recorded over the implantation period. Representative ECAPs from one animal are shown when taken immediately following implantation surgery (**A**, $T = -14$), prior to the injection of TNBS (**B**, $T = 0$) and at the conclusion of the experiment (**C**, $T = 4$). Note, the amplitude of the neural response recorded immediately post-implantation ($T = -14$) were consistently smaller than those at later time points green traces indicate the neural threshold (200 µA) and arrows indicate the elecrically evoked C-fiber response (Latency range: 5.3–5.6 ms). Current amplitude (in µA) is indicated to the right of each set of ECAPs.

between 3485 and 7194 Ω). At the conclusion of the experiment the *in vivo* impedances had increased to 8379 ± 269 Ω (5807–9650 Ω). During the implantation period, there were no short circuits, and only 4 out of 60 electrodes ($n = 4$ electrodes per rat; $n = 15$ implanted rats in total) became open circuit. These short circuits did not compromise the delivery of VNS.

Vagus Nerve Stimulation Improved Clinical Measurements of Inflammation

On day 0 (referred to as the "control"), prior to the TNBS injection, all implanted rats ($n = 15$) produced stools that were solid, dry pellets, with no signs of blood. Following TNBS injection, unstimulated rats (TNBS, $n = 8$) had significantly worse stool quality [two-way RM ANOVA (Time × Treatment): Time: $P < 0.0001$; Treatment $P = 0.0009$; Interaction: $P = 0.02$] than control (day 0) on day 1 (*Sidak post hoc* test: $P < 0.0001$), day 2 ($P < 0.0001$), day 3 ($P = 0.002$) and day 4 ($P = 0.015$; differences indicated by "*" in **Figure 4A**). The stool quality of stimulated rats (TNBS+VNS, $n = 7$) remained similar to control following TNBS injection ($P \geq 0.05$). Furthermore, stimulated rats (TNBS+VNS) had significantly better stool quality than unstimulated rats (TNBS) on day 1 ($P = 0.0002$), day 2 ($P = 0.012$), day 3 ($P = 0.04$), and day 4 ($P = 0.03$; differences indicated by a 'circle' in **Figure 4A**).

Following TNBS injection, the presence of blood in feces was observed (two-way RM ANOVA: Time: $P = 0.058$; Treatment $P < 0.0001$; Interaction: $P = 0.058$) in unstimulated rats (TNBS; $n = 5$) significantly more often, compared to control (day 0), on days 1 ($P = 0.0002$) and day 2 ($P = 0.006$; differences indicated by "*" in **Figure 4B**).

Unstimulated rats (TNBS; $n = 5$) were observed to have higher presence of blood in feces than stimulated rats (TNBS+VNS) on day 1 ($P = 0.001$) and day 2 ($P = 0.02$; differences indicated by a "circle" in **Figure 4B**). Stimulated rats (TNBS+VNS; $n = 4$) were not observed to have blood in feces at any time point following TNBS injection (**Figure 4B**).

Following TNBS treatment, plasma CRP levels in unstimulated rats (TNBS) were significantly increased [two-way RM ANOVA (Stimulation × Time); Treatment: $P = 0.005$; Time, $P < 0.0001$, Interaction, $P < 0.0001$] at day 1 (Sidak *post hoc*: $P < 0.0001$) and day 2 ($P = 0.0004$), compared to day 0 (indicated by "*" in **Figure 4C**). By day 4, CRP levels returned to baseline levels. CRP levels of stimulated rats (TNBS+VNS) were significantly higher than baseline only at day 1 ($P = 0.006$), and no different from control (day 0) on days 2 and 4 ($P \geq 0.05$). However, on day 1 CRP levels were still significantly lower ($P < 0.0001$) than unstimulated rats (TNBS, indicated by a "circle," **Figure 4C**).

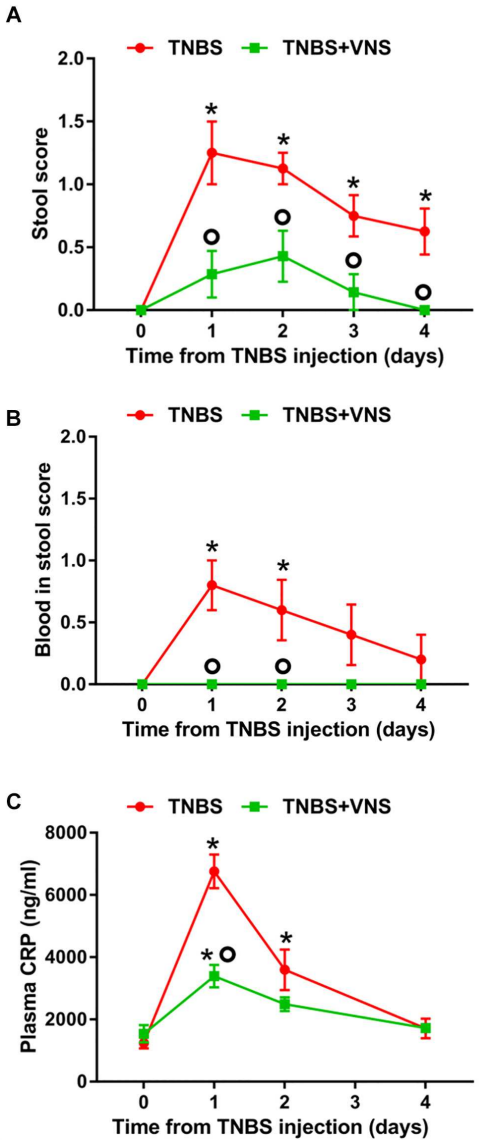

FIGURE 4 | (A) Vagus nerve stimulation improves clinical measurements of inflammation following TNBS injection. **(A)** The quality of stool produced from unstimulated (TNBS; $n = 8$) and stimulated (TNBS+VNS; $n = 7$) rats were scored following the TNBS injection. **(B)** Blood in stool produced from unstimulated (TNBS; $n = 5$) and stimulated (TNBS + VNS; $n = 4$) rats was scored following TNBS injection. **(C)** CRP content in blood plasma was measured in unstimulated (TNBS; $n = 6$) and stimulated (TNBS+VNS; $n = 6$) on day 0 (pre-TNBS control) and days 1, 2, and 4 following TNBS injection. All data show mean ± SEM. Significant differences from control (day 0, pre-TNBS) are indicated by "*", while significant differences between unstimulated (TNBS) and stimulated (TNBS+VNS) groups are indicated by "O".

TNBS-Induced Inflammatory Damage Improved Following VNS

In small intestine tissue 5–7 cm oral to the site of TNBS induced inflammation (i.e., control tissue), there was no damage to the epithelial cells of the villi along the length of the analyzed tissue, with villi exhibiting the normal long finger-like projections (**Figures 5A,Ai**). Few leukocytes (less than 4) were observed within venules of the lamina propria and within the circular and longitudinal muscle layers, while there was mild infiltration of leukocyte populations within the mucosa and submucosa layers. In acute TNBS tissue (4 h post-injection, at the time that active VNS was applied) extensive epithelial cell loss (**Figures 5B,Bi** indicated by arrows) and leukocyte infiltration (**Figures 5B,Bi**, indicated by circle) was observed. Leukocyte infiltration into the mucosa/submucosal layers was moderate. At 4 days following TNBS injection, tissue from unstimulated (TNBS) rats had extensive irregularities to villus epithelial cells (**Figures 5C,Ci**, indicated by arrows). Villi were shorter and had a blunted appearance, and leukocyte infiltration was severe within the mucosa, submucosa and venules (**Figures 5C,Ci**). Tissue from stimulated (TNBS+VNS) animals exhibited reduced inflammation-induced damage. Less damage or abnormalities to villi surface epithelium was observed (**Figures 5D,Di**), while villi architecture was sometimes indistinguishable from control small intestine tissue. However, some inflammation-induced irregularities, such as shortening of villi remained within tissue from stimulated animals (TNBS+VNS; **Figure 5D**).

The histological score measured from control tissue of unstimulated (TNBS; $n = 5$) and stimulated (TNBS+VNS; $n = 4$) rats were no different from each other ($P \geq 0.05$; unpaired T-test). Therefore the control groups were combined ($n = 9$). Statistical analysis of the histological score showed there was significant (Kruskal–Wallis one-way ANOVA: $P = 0.001$) histological damage in tissue from 4 h post-TNBS injection (Dunn's *post hoc*: $P = 0.002$) and in unstimulated rats (TNBS; $P = 0.0006$; **Figure 5E**). However, the histological score of tissue taken from stimulated animals (TNBS+VNS) was no different from control ($P = 0.17$), suggesting that VNS improved recovery from inflammation-induced damage (**Figure 5E**).

Numbers of Leukocytes in Mucosal and Submucosal Layers Was Reduced Following VNS

The numbers of leukocytes measured from the control mucosal, submucosal and muscle layers were no different from each other ($P \geq 0.05$; unpaired T-test). Thus the control groups were combined ($n = 9$). Tissue taken 4 h (4 H TNBS; $n = 3$) following TNBS is shown in **Figures 5B,Bi**, but was not included in the statistical cell count analysis, nor included in subsequent graphs (**Figure 6**), due to the low number of animals in this group. Four days following the TNBS injection, there was a significant increase in eosinophils within the mucosal layer (Kruskall–Wallis: one-way ANOVA: Treatment $P = 0.0002$), and a significant increase in the number of CD3+ cells (T cells) within both the mucosa ($P = 0.001$) and submucosa ($P = 0.01$) in unstimulated animals (TNBS, **Figures 6A–C**). In contrast, there was no significant elevation in the number of eosinophils, MPO+ cells or CD3+ cells in stimulated animals (TNBS+VNS; **Figures 6A–C**). Furthermore, eosinophil (Dunn's *post hoc*: $P = 0.03$) and T cells ($P = 0.02$) populations were significantly reduced in the mucosal layer of stimulated

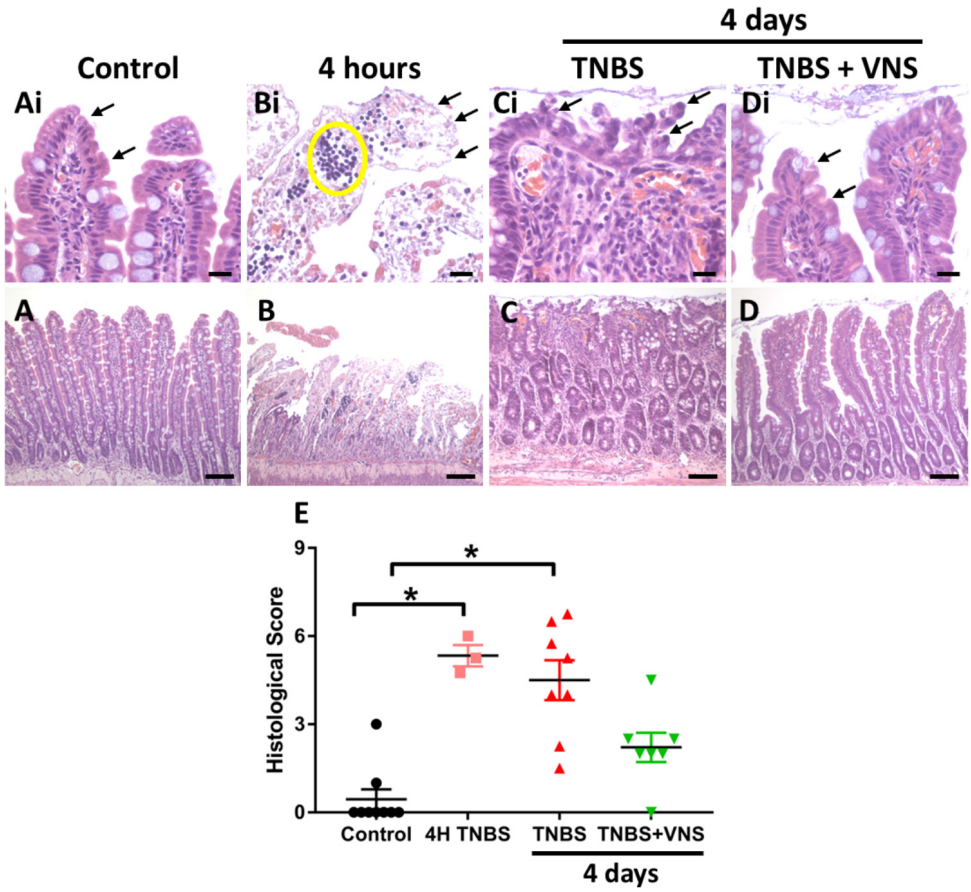

FIGURE 5 | Vagal nerve stimulation reduced histological damage of small intestine tissue following TNBS injection. **(A)** Control small intestine **(A,Ai)** had undamaged, intact surface epithelium (arrows, **Ai**). **(B,Bi)** At 4 h following TNBS injection (the time that VNS was applied), extensive epithelial cell loss (arrow, **Bi**) and leukocyte infiltration (yellow circle) was observed. **(C,Ci)** At 4 days following TNBS injection, there was extensive damage to villus architecture (**Ci**, arrows) and leukocyte infiltration in venules (circle) in tissue from unstimulated rats (TNBS). **(D,Di)** In tissue from stimulated rats (TNBS+VNS), histological damage was less severe than tissue taken from unstimulated (TNBS) rats. Surface epithelial cells were intact (arrows), and villi were mostly undamaged, although some inflammation-induced irregularities remained. **(E)** The histological score was quantified in tissue taken from control animals, at 4 h following TNBS injection, and from unstimulated (TNBS) and stimulated animals (TNBS+VNS). Data show raw histological score (0–9) of each animal, median and interquartile range. Significant differences of $P < 0.05$ are indicated by "*." Scale bars in **(A–D)**: 100 μm; in **(Ai–Di)**: 20 μm.

animals (TNBS+VNS), compared to unstimulated animals (TNBS; **Figures 6A,C**).

Leukocyte Infiltration Into External Muscle Layers Was Reduced Following VNS

Tissue taken 4 h (4 H TNBS; $n = 3$) following TNBS was not included in the statistical cell count analysis, nor included in subsequent graphs (**Figure 7**), due to the low number of animals in this group. In the circular and longitudinal muscle layers, there was an increase in eosinophils within tissue taken from unstimulated (TNBS; Kruskal–Wallis: $P = 0.001$) and stimulated rats (TNBS+VNS; $P = 0.012$), compared to control (**Figure 7D**). Numbers of MPO+ cells (representative images for control, TNBS and TNBS+VNS tissue shown in **Figures 7A–C**) (neutrophils) increased in tissue taken from unstimulated rats (TNBS; $P < 0.0001$), but was significantly less in tissue taken from stimulated rats (TNBS+VNS; $P = 0.048$; **Figure 7E**). Numbers of CD3+ cells (T cells) within the muscle layers of tissue taken from TNBS treated rats were greater than control ($P < 0.0001$). However, there were significantly fewer T cells in the muscle layer of tissue taken from stimulated rats ($P = 0.04$), compared to unstimulated rats treated with TNBS (**Figure 7F**).

Assessment of the Implanted Vagus Nerve

Chronically implanted abdominal vagus nerves ($n = 9$) were assessed for histopathological changes (**Figures 8A,Ai**) and changes in fascicle area (**Figure 8B**). We observed no tissue granulation or infiltration of acute inflammatory cells, however, a foreign body tissue response (**Figure 8Ai**, indicated by **) was seen within the electrode channel, surrounding the nerve (**Figure 8Ai**). No inflammatory cells were observed suggesting the foreign body response was likely benign. Furthermore, blood vessels (**Figure 8Ai**, indicated as "BV") were observed within the nerve. There were no observed differences between stimulated and unstimulated nerve histology.

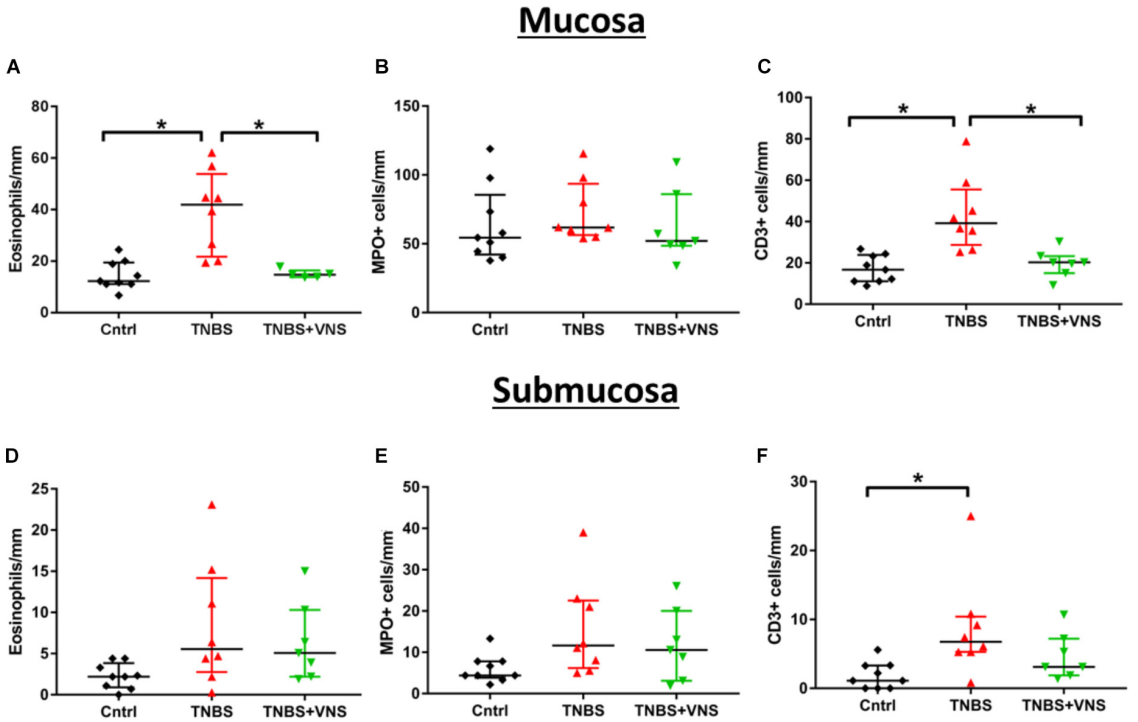

FIGURE 6 | VNS reduces resident leukocyte populations in mucosal and submucosal layers following TNBS injection. **(A–C)** Quantification of eosinophils **(A)**, MPO+ cells (neutrophils, **B**) and CD3+ cells (T cells; **C**) within the mucosal layer. **(D–F)** Quantification of eosinophils **(D)**, MPO+ cells **(E)** and CD3+ cells **(F)** within the submucosal layer. Data show raw data from each animal, median and interquartile range. Significant differences of $P < 0.05$ are indicated by "*."

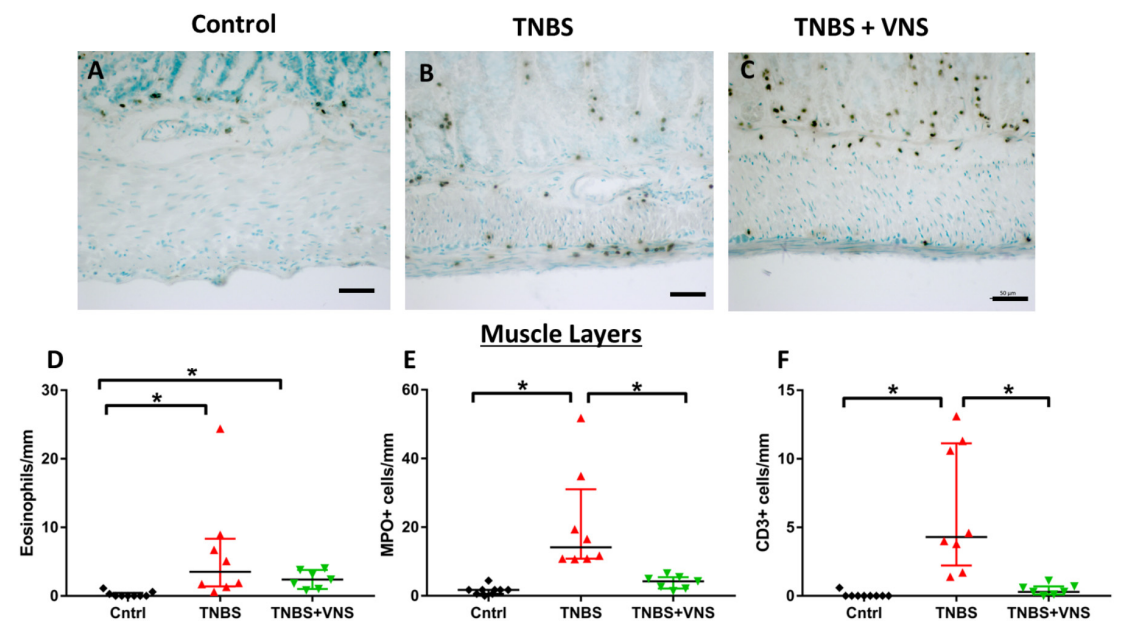

FIGURE 7 | VNS reduces resident leukocyte populations in muscle layers following TNBS injection. **(A–C)** Images show myeloperoxidase (MPO) positive cells (neutrophils) within circular and longitudinal muscle layers of tissue taken from control **(A)**, TNBS rats **(B)** and TNBS+VNS rats **(C)**. **(D–F)** Quantification of eosinophils **(D)**, MPO+ cells **(E),** and CD3+ cells **(F)** within the circular and longitudinal muscle layers. Data show mean count/animal, median and interquartile range. Significant differences of $P < 0.05$ are indicated by "*."

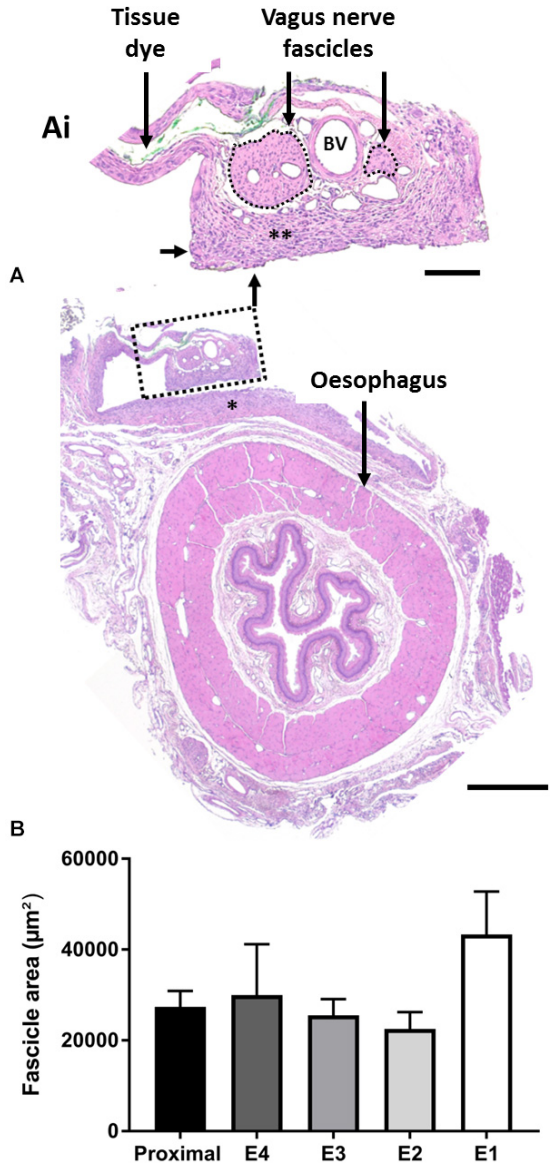

FIGURE 8 | Histopathology of the anterior abdominal vagus nerve following implantation. **(A,Ai)** H&E stained vagus nerve that was stimulated for 4 days shows a benign foreign body tissue response (**A**, indicated by *), which extended into the electrode channel (**Ai**, indicated by **). There were no acute inflammatory cells within the epineurium, the two fascicles of the vagus nerve (outlined by a dotted line) appeared undamaged, and blood vessels (example indicated by "BV") appeared patent. Tissue dye was used to identify the implanted nerve upon dissection. **(B)** Quantification of total fascicle area (example indicated by dotted lines in **Ai**) between non-implanted neural tissue, taken proximal to implantation site, and implanted tissue adjacent to electrodes E1–E4. Data show mean fascicle area (μm^2) + SEM, and there were no significant differences between locations. Scale bar in **(A)** 500 μm Scale bar in **(Ai)** 100 μm.

The fascicle area (indicated by dotted lines, **Figure 8Ai**) of the nerve adjacent to the electrodes E1-E4 was analyzed and compared to non-implanted vagus nerve tissue (taken proximal to the implantation site). There were no significant changes in fascicle area between implanted (E1–E4) and non-implanted (proximal) tissue (one-way RM ANOVA: $P = 0.9$; $n = 9$) (**Figure 8B**).

DISCUSSION

VNS was effective in improving a number of markers of inflammation, including stool quality, systemic inflammation and leukocyte infiltration within the small intestine. Furthermore, significant off-target cardiac and respiratory events occurred during suprathreshold cervical VNS, while in contrast, no measured off-target changes were seen during abdominal VNS. The absence of off-target effects and efficacy in reducing inflammation suggests that abdominal VNS is a suitable alternative to cervical VNS. Taken together, these findings support the use of this novel peripheral nerve array for abdominal VNS as a potential treatment for IBDs, such as Crohn's disease.

Stimulation of the cervical vagus nerve at higher frequencies (30 Hz) or lower frequencies (10 Hz) has the potential to activate fibers to the larynx, heart and lungs, in addition to the gastrointestinal tract and liver (Bonaz et al., 2013). In this study, cervical VNS (10 Hz, 1.6 mA, 200 μs) caused a decrease in heart rate and respiration. These changes can be attributed to the activation of large pulmonary stretch A-fibers and cardio-inhibitory vagal B fibers (McAllen et al., 2018). In a retrospective clinical study, a significant proportion of epileptic patients ($n = 95$) receiving cervical VNS (30 Hz, 0.25–3.5 mA, 500 μs) treatment reported stimulation-induced hoarseness of voice (63%), coughing (44%), and pain (37%) (Handforth et al., 1998; DeGiorgio et al., 2000). Similarly, ileocecal Crohn's disease patients treated with cervical VNS (10 Hz, 500 μs, 1.25 mA) also reported dysphonia during stimulation, although symptoms resolved over time (Bonaz et al., 2016). In humans, the effects on heart rate are less pronounced than that reported in rats, nevertheless, some clinical studies show disruptive effects to heart contractility and heart rate during stimulation of the left cervical and thoracic vagus nerve, i.e., above the vagal cardiac branches (Frei and Osorio, 2001; Lewis et al., 2001). Taken together, cervical VNS has a number of unwanted, albeit often mild, off-target effects. Such off-target effects potentially limit the intensity and duration of therapeutic stimulation delivered, thereby potentially compromising or limiting the effectiveness of the bioelectric neuromodulation treatment. In contrast abdominal VNS did not evoke changes in heart rate, respiration rate or blood pressure. These findings are in agreement with previous reports of abdominal VNS in anaesthetized pigs and humans for the treatment of post-operative ileus (Stakenborg et al., 2017), and is consistent with the known functional anatomy of the vagus.

Engaging the optimal nerve fiber population is essential for an effective bioelectric neuromodulation therapy (Payne et al., 2018b). The cervical vagus nerve consists of a mixed population of large, myelinated A-fibers, smaller myelinated B-fibers and small, unmyelinated C-fibers, which have different electrical activation thresholds (Castoro et al., 2011). This is problematic for cervical VNS for the treatment of intestinal

inflammation as activation of vagal C-fibers, thought to be involved in driving anti-inflammatory effects in the intestine (Martelli et al., 2014; Payne et al., 2018b), typically also activates A-fibers (Castoro et al., 2011; McAllen et al., 2018). Selective activation of C-fibers, while minimizing the activation of A- and B-fiber populations is very difficult to achieve long-term *in vivo* (reviewed in Guiraud et al., 2016). Some studies have demonstrated a partial preferential activation of C-fibers while suppressing A-fibers activation in the vagus nerve of pigs by delivering a non-rectangular pulse waveform (Tosato et al., 2007). However, this stimulation strategy requires high, often unsafe levels of charge to be delivered in order to be effective (Vuckovic et al., 2008; Qing et al., 2015). Targeting the abdominal vagus nerve overcomes this issue as the nerve consists primarily of C-fibers (rats: 99%; humans: 97%) (Hoffman and Schnitzlein, 1961; Prechtl and Powley, 1990). Furthermore, targeting this C-fiber dense segment of the vagus nerve might increase the clinical efficacy of stimulation in electrically-activating C-fibers. We measured the conduction velocity of the electrically-evoked neural responses elicited by abdominal VNS and they ranged between 0.55 and 0.84 m/s, which fits within the range of C-fiber conduction velocities (Castoro et al., 2011).

Abdominal VNS was effective in reducing TNBS-induced inflammation, as indicated by changes in several markers, including the stool quality, systemic CRP, histology and leukocyte infiltration into transmural layers. In contrast, previous studies on experimental colitis showed cervical VNS had no protective effects within the inflammatory lesion site (Meregnani et al., 2011), and all measured inflammatory markers of colitis (mucosal index damage index, disease activity index, histological score and colonic cytokine content) remained significantly higher in tissue taken from cervical VNS rats, compared to control ($P \geq 0.05$) (Sun et al., 2013). One explanation for this disparity is the differences in TNBS injections between studies. The concentration of TNBS administered here was 2.5% w/v, while others used higher concentrations of 40% (Sun et al., 2013) and ∼180% (Meregnani et al., 2011). Additionally, we injected TNBS into the small intestine, rather than the colon. Vagal innervation of the small intestine, specifically the jejunum, is denser than in the distal colon (Berthoud et al., 1990); therefore the therapeutic action of VNS may have had an increased potency.

The stimulation regime used in this study involved a charge density of ∼1 $\mu C/cm^2$/phase, delivered for 3 h at the same time each day (1:30–4:30 p.m.), with a duty cycle of 30 s ON, followed by 5 min OFF. This stimulation is well below the safety limit for platinum electrodes (Cogan et al., 2016). The stimulation timing and duty cycle were chosen to be similar to those used in the treatment of colitis (Sun et al., 2013) and ileocecal Crohn's disease (Bonaz et al., 2016), which in turn were based on VNS to treat patients with drug resistant epilepsy and depression (Sackeim et al., 2001; Cukiert et al., 2013). Therefore, it is quite likely that the timing and duty cycle used may not be optimal for the treatment of IBD; the optimization of stimulation parameters to those most appropriate for therapy has been poorly explored and remains a significant challenge for bioelectric neuromodulation therapies (Payne et al., 2018b). Testing of parameters, such as pulse durations, stimulation rate, duty cycles, and the duration and time of day that stimulation is applied, are essential to explore in appropriate animal models of the disease if bioelectric neuromodulation is to be successful long-term clinical treatment.

CONCLUSION

We have developed a stimulating and recording electrode array that effectively activates C-fibers in the abdominal vagus nerve, allowing for VNS to treat inflammation following TNBS injection to be applied closer to the end organ with no measurable off-target effects. Our work supports abdominal VNS as an effective approach to the treatment of IBD in humans.

ETHICS STATEMENT

All animal procedures were approved by the Animal Research and Ethics Committee of the Bionics Institute and complied with the Australian Code for the Care and Use of Animals for Scientific Purposes (National Health and Medical Research Council of Australia). Approval was also obtained from the United States Army Medical Research and Material Command Animal Care and Use Review Office, protocol SSC-7486.02.

AUTHOR CONTRIBUTIONS

All authors listed have made a substantial, direct and intellectual contribution to the work, and approved it for publication.

FUNDING

This work was funded by the Defense Advanced Research Projects Agency (DARPA) BTO, under the auspices of Dr. Doug Weber and Dr. Eric Van Gieson through the Space and Naval Warfare Systems Center (Contract No. N66001-15-2-4060). The Bionics Institute and the Florey Institute of Neuroscience and Mental Health acknowledge the support they receive from the Victorian Government through its Operational Infrastructural Support Program.

ACKNOWLEDGMENTS

We are grateful to Dr. Alex Thompson for his biomedical technical assistance and Ross Thomas for his assistance in designing the rat pedestals and Angel De Silva for manufacture of the electrode arrays. We also thank Dr. Martin J. Stebbing and Dr. Tyler Best for helpful comments on the manuscript.

REFERENCES

Abraham, C., and Cho, J. H. (2009). Inflammatory bowel disease. *N. Engl. J. Med.* 361, 2066–2078.

Ananthakrishnan, A. (2015a). "Why did this happen to me? epidemiology, genetics, and pathophysiology of IBD," in *Inflammatory Bowel Disease*, eds D. Stein and R. Shaker (Cham: International Publishing Springer).

Ananthakrishnan, A. N. (2015b). Epidemiology and risk factors for IBD. *Nat. Rev. Gastroenterol. Hepatol.* 12, 205–217. doi: 10.1038/nrgastro.2015.34

Balcombe, J. P., Barnard, N. D., and Sandusky, C. (2004). Laboratory routines cause animal stress. *Contemp. Top Lab. Anim. Sci.* 43, 42–51.

Ben-Menachem, E., Revesz, D., Simon, B. J., and Silberstein, S. (2015). Surgically implanted and non-invasive vagus nerve stimulation: a review of efficacy, safety and tolerability. *Eur. J. Neurol.* 22, 1260–1268. doi: 10.1111/ene.12629

Berthoud, H. R., Jedrzejewska, A., and Powley, T. L. (1990). Simultaneous labeling of vagal innervation of the gut and afferent projections from the visceral forebrain with dil injected into the dorsal vagal complex in the rat. *J. Comp. Neurol.* 301, 65–79. doi: 10.1002/cne.903010107

Bonaz, B., Picq, C., Sinniger, V., Mayol, J. F., and Clarencon, D. (2013). Vagus nerve stimulation: from epilepsy to the cholinergic anti-inflammatory pathway. *Neurogastroenterol. Motil.* 25, 208–221. doi: 10.1111/nmo.12076

Bonaz, B., Sinniger, V., Hoffmann, D., Clarencon, D., Mathieu, N., Dantzer, C., et al. (2016). Chronic vagus nerve stimulation in Crohn's disease: a 6-month follow-up pilot study. *Neurogastroenterol. Motil.* 28, 948–953. doi: 10.1111/nmo.12792

Caprilli, R., Gassull, M. A., Escher, J. C., Moser, G., Munkholm, P., Forbes, A., et al. (2006). European evidence based consensus on the diagnosis and management of Crohn's disease: special situations. *Gut* 55(Suppl. 1), i36–i58. doi: 10.1136/gut.2005.081950c

Castoro, M. A., Yoo, P. B., Hincapie, J. G., Hamann, J. J., Ruble, S. B., Wolf, P. D., et al. (2011). Excitation properties of the right cervical vagus nerve in adult dogs. *Exp. Neurol.* 227, 62–68. doi: 10.1016/j.expneurol.2010.09.011

Chaparro, M., Ordas, I., Cabre, E., Garcia-Sanchez, V., Bastida, G., Penalva, M., et al. (2013). Safety of thiopurine therapy in inflammatory bowel disease: long-term follow-up study of 3931 patients. *Inflamm. Bowel Dis.* 19, 1404–1410. doi: 10.1097/MIB.0b013e318281f28f

Childs, J. E., Alvarez-Dieppa, A. C., Mcintyre, C. K., and Kroener, S. (2015). Vagus nerve stimulation as a tool to induce plasticity in pathways relevant for extinction learning. *J. Vis. Exp.* 102:e53032. doi: 10.3791/53032

Cogan, S. F., Ludwig, K. A., Welle, C. G., and Takmakov, P. (2016). Tissue damage thresholds during therapeutic electrical stimulation. *J. Neural. Eng.* 13:021001. doi: 10.1088/1741-2560/13/2/021001

Cukiert, A., Cukiert, C. M., Burattini, J. A., Lima, A. M., Forster, C. R., Baise, C., et al. (2013). A prospective long-term study on the outcome after vagus nerve stimulation at maximally tolerated current intensity in a cohort of children with refractory secondary generalized epilepsy. *Neuromodulation* 16, 551–556;discussion556. doi: 10.1111/j.1525-1403.2012.00522.x

De Cruz, P., Kamm, M. A., Hamilton, A. L., Ritchie, K. J., Krejany, E. O., Gorelik, A., et al. (2015). Crohn's disease management after intestinal resection: a randomised trial. *Lancet* 385, 1406–1417. doi: 10.1016/S0140-6736(14)61908-5

DeGiorgio, C. M., Schachter, S. C., Handforth, A., Salinsky, M., Thompson, J., Uthman, B., et al. (2000). Prospective long-term study of vagus nerve stimulation for the treatment of refractory seizures. *Epilepsia* 41, 1195–1200.

Fallon, J. B., Irvine, D. R., and Shepherd, R. K. (2009). Cochlear implant use following neonatal deafness influences the cochleotopic organization of the primary auditory cortex in cats. *J. Comp. Neurol.* 512, 101–114. doi: 10.1002/cne.21886

Fallon, J. B., Senn, P., and Thompson, A. C. (2018). "A highly configurable neurostimulator for chronic pre-clinical stimulation studies," in *Proceedings of the Neural Interfaces Conferences*, (Minneapolis, MN).

Frei, M. G., and Osorio, I. (2001). Left vagus nerve stimulation with the neurocybernetic prosthesis has complex effects on heart rate and on its variability in humans. *Epilepsia* 42, 1007–1016. doi: 10.1046/j.1528-1157.2001.0420081007.x

Gecse, K. B., Lovasz, B. D., Farkas, K., Banai, J., Bene, L., Gasztonyi, B., et al. (2016). Efficacy and safety of the biosimilar infliximab CT-P13 treatment in inflammatory bowel diseases: a prospective, multicentre, nationwide cohort. *J. Crohns Colitis* 10, 133–140. doi: 10.1093/ecco-jcc/jjv220

Guiraud, D., Andreu, D., Bonnet, S., Carrault, G., Couderc, P., Hagege, A., et al. (2016). Vagus nerve stimulation: state of the art of stimulation and recording strategies to address autonomic function neuromodulation. *J. Neural Eng.* 13:041002. doi: 10.1088/1741-2560/13/4/041002

Handforth, A., DeGiorgio, C. M., Schachter, S. C., Uthman, B. M., Naritoku, D. K., Tecoma, E. S., et al. (1998). Vagus nerve stimulation therapy for partial-onset seizures: a randomized active-control trial. *Neurology* 51, 48–55. doi: 10.1212/wnl.51.1.48

Hoffman, H. H., and Schnitzlein, H. N. (1961). The numbers of nerve fibers in the vagus nerve of man. *Anat. Rec.* 139, 429–435. doi: 10.1002/ar.1091390312

Khurana, D. S., Reumann, M., Hobdell, E. F., Neff, S., Valencia, I., Legido, A., et al. (2007). Vagus nerve stimulation in children with refractory epilepsy: unusual complications and relationship to sleep-disordered breathing. *Childs Nerv. Syst.* 23, 1309–1312. doi: 10.1007/s00381-007-0404-8

Lewis, M. E., Al-Khalidi, A. H., Bonser, R. S., Clutton-Brock, T., Morton, D., Paterson, D., et al. (2001). Vagus nerve stimulation decreases left ventricular contractility in vivo in the human and pig heart. *J. Physiol.* 534, 547–552. doi: 10.1111/j.1469-7793.2001.00547.x

Martelli, D., Mckinley, M. J., and McAllen, R. M. (2014). The cholinergic anti-inflammatory pathway: a critical review. *Auton. Neurosci.* 182, 65–69. doi: 10.1016/j.autneu.2013.12.007

McAllen, R. M., Shafton, A. D., Bratton, B. O., Trevaks, D., and Furness, J. B. (2018). Calibration of thresholds for functional engagement of vagal A, B and C fiber groups in vivo. *Bioelectron. Med.* 1, 21–27. doi: 10.2217/bem-2017-0001

Meregnani, J., Clarencon, D., Vivier, M., Peinnequin, A., Mouret, C., Sinniger, V., et al. (2011). Anti-inflammatory effect of vagus nerve stimulation in a rat model of inflammatory bowel disease. *Auton. Neurosci.* 160, 82–89. doi: 10.1016/j.autneu.2010.10.007

Nagarajan, L., Walsh, P., Gregory, P., Stick, S., Maul, J., and Ghosh, S. (2003). Respiratory pattern changes in sleep in children on vagal nerve stimulation for refractory epilepsy. *Can. J. Neurol. Sci.* 30, 224–227. doi: 10.1017/s0317167100002638

Neurath, M. F. (2014). Cytokines in inflammatory bowel disease. *Nat. Rev. Immunol.* 14, 329–342. doi: 10.1038/nri3661

Nielsen, O. H., and Munck, L. K. (2007). Drug insight: aminosalicylates for the treatment of IBD. *Nat. Clin. Pract. Gastroenterol. Hepatol.* 4, 160–170. doi: 10.1038/ncpgasthep0696

Nurgali, K., Nguyen, T. V., Matsuyama, H., Thacker, M., Robbins, H. L., and Furness, J. B. (2007). Phenotypic changes of morphologically identified guinea-pig myenteric neurons following intestinal inflammation. *J. Physiol.* 583, 593–609. doi: 10.1113/jphysiol.2007.135947

Payne, S. C., Burns, O., Stebbing, M., Thomas, R., De Silva, A., Sedo, A., et al. (2018a). Vagus nerve stimulation to treat inflammatory bowel disease: a chronic, preclinical safety study in sheep. *Bioelectron. Med.* doi: 10.2217/bem-2018-0011 [Epub ahead on Print].

Payne, S. C., Furness, J. B., and Stebbing, M. J. (2018b). Bioelectric neuromodulation for gastrointestinal disorders: effectiveness and mechanisms. *Nat. Rev. Gastroenterol. Hepatol.* 16, 89–105. doi: 10.1038/s41575-018-0078-6

Payne, S. C., Shepherd, R. K., Sedo, A., Fallon, J. B., and Furness, J. B. (2018c). An objective in vivo diagnostic method for inflammatory bowel disease. *R. Soc. Open Sci.* 5:180107. doi: 10.1098/rsos.180107

Pontell, L., Castelucci, P., Bagyanszki, M., Jovic, T., Thacker, M., Nurgali, K., et al. (2009). Structural changes in the epithelium of the small intestine and immune cell infiltration of enteric ganglia following acute mucosal damage and local inflammation. *Virchows Arch.* 455, 55–65. doi: 10.1007/s00428-009-0795-x

Prechtl, J. C., and Powley, T. L. (1990). The fiber composition of the abdominal vagus of the rat. *Anat. Embryol.* 181, 101–115.

Pruvost, M., Zaaimi, B., Grebe, R., Wallois, F., Berquin, P., and Perlitz, V. (2006). Cardiorespiratory effects induced by vagus nerve stimulation in epileptic children. *Med. Biol. Eng. Comput.* 44, 338–347. doi: 10.1007/s11517-006-0041-5

Qing, K. Y., Ward, M. P., and Irazoqui, P. P. (2015). Burst-modulated waveforms optimize electrical stimuli for charge efficiency and fiber selectivity. *IEEE Trans. Neural Syst. Rehabil. Eng.* 23, 936–945. doi: 10.1109/TNSRE.2015.2421732

Richardson, R. T., Wise, A. K., Thompson, B. C., Flynn, B. O., Atkinson, P. J., Fretwell, N. J., et al. (2009). Polypyrrole-coated electrodes for the delivery of

charge and neurotrophins to cochlear neurons. *Biomaterials* 30, 2614–2624. doi: 10.1016/j.biomaterials.2009.01.015

Rutgeerts, P., Van Assche, G., and Vermeire, S. (2004). Optimizing anti-TNF treatment in inflammatory bowel disease. *Gastroenterology* 126, 1593–1610. doi: 10.1053/j.gastro.2004.02.070

Sackeim, H. A., Rush, A. J., George, M. S., Marangell, L. B., Husain, M. M., Nahas, Z., et al. (2001). Vagus nerve stimulation (VNS) for treatment-resistant depression: efficacy, side effects, and predictors of outcome. *Neuropsychopharmacology* 25, 713–728. doi: 10.1016/s0893-133x(01)00271-8

Sanchez-Munoz, F., Dominguez-Lopez, A., and Yamamoto-Furusho, J. K. (2008). Role of cytokines in inflammatory bowel disease. *World J. Gastroenterol.* 14, 4280–4288.

Stakenborg, N., Wolthuis, A. M., Gomez-Pinilla, P. J., Farro, G., Di Giovangiulio, M., Bosmans, G., et al. (2017). Abdominal vagus nerve stimulation as a new therapeutic approach to prevent postoperative ileus. *Neurogastroenterol. Motil.* 29, e13075–e13086. doi: 10.1111/nmo.13075

Sun, P., Zhou, K., Wang, S., Li, P., Chen, S., Lin, G., et al. (2013). Involvement of MAPK/NF-kappaB signaling in the activation of the cholinergic anti-inflammatory pathway in experimental colitis by chronic vagus nerve stimulation. *PLoS One* 8:e69424. doi: 10.1371/journal.pone.0069424

Tosato, M., Yoshida, K., Toft, E., and Struijk, J. J. (2007). Quasi-trapezoidal pulses to selectively block the activation of intrinsic laryngeal muscles during vagal nerve stimulation. *J. Neural Eng.* 4, 205–212. doi: 10.1088/1741-2560/4/3/005

Villalobos, J., Nayagam, D. A., Allen, P. J., Mckelvie, P., Luu, C. D., Ayton, L. N., et al. (2013). A wide-field suprachoroidal retinal prosthesis is stable and well tolerated following chronic implantation. *Invest. Ophthalmol. Vis. Sci.* 54, 3751–3762. doi: 10.1167/iovs.12-10843

Vuckovic, A., Tosato, M., and Struijk, J. J. (2008). A comparative study of three techniques for diameter selective fiber activation in the vagal nerve: anodal block, depolarizing prepulses and slowly rising pulses. *J. Neural Eng.* 5, 275–286. doi: 10.1088/1741-2560/5/3/002

Zaaimi, B., Grebe, R., Berquin, P., and Wallois, F. (2007). Vagus nerve stimulation therapy induces changes in heart rate of children during sleep. *Epilepsia* 48, 923–930. doi: 10.1111/j.1528-1167.2006.01019.x

Zaaimi, B., Heberle, C., Berquin, P., Pruvost, M., Grebe, R., and Wallois, F. (2005). Vagus nerve stimulation induces concomitant respiratory alterations and a decrease in SaO2 in children. *Epilepsia* 46, 1802–1809. doi: 10.1111/j.1528-1167.2005.00283.x

Conflict of Interest Statement: The authors declare that the research was conducted in the absence of any commercial or financial relationships that could be construed as a potential conflict of interest.

frontiers in Neuroscience

ORIGINAL RESEARCH
published: 17 May 2019
doi: 10.3389/fnins.2019.00447

Test–Retest Reliability of the Effects of Continuous Theta-Burst Stimulation

Ali Jannati[1], Peter J. Fried[1], Gabrielle Block[1†], Lindsay M. Oberman[2†], Alexander Rotenberg[1,3] and Alvaro Pascual-Leone[1,4]**

[1] Berenson-Allen Center for Noninvasive Brain Stimulation and Division of Cognitive Neurology, Department of Neurology, Beth Israel Deaconess Medical Center, Harvard Medical School, Boston, MA, United States, [2] Neuroplasticity and Autism Spectrum Disorder Program, Department of Psychiatry and Human Behavior, E.P. Bradley Hospital, Warren Alpert Medical School, Brown University, East Providence, RI, United States, [3] Neuromodulation Program and Division of Epilepsy and Clinical Neurophysiology, Department of Neurology, Boston Children's Hospital, Harvard Medical School, Boston, MA, United States, [4] Institut Guttman de Neurorehabilitació, Universitat Autónoma de Barcelona, Barcelona, Spain

OPEN ACCESS

Edited by:
Olivier David,
Institut National de la Santé et de la Recherche Médicale (INSERM), France

Reviewed by:
Silvia Casarotto,
University of Milan, Italy
Giuseppe D'Avenio,
Istituto Superiore di Sanità (ISS), Italy

***Correspondence:**
Ali Jannati
jannati@gmail.com;
ajannati@bidmc.harvard.edu
Alvaro Pascual-Leone
apleone@bidmc.harvard.edu

†Present address:
Gabrielle Block,
School of Medicine, New York Medical College, Valhalla, NY, United States
Lindsay M. Oberman,
Center for Neuroscience and Regenerative Medicine, Department of Medical and Clinical Psychology, Uniformed Services University of the Health Sciences, Bethesda, MD, United States

Specialty section:
This article was submitted to Neural Technology, a section of the journal Frontiers in Neuroscience

Received: 01 January 2019
Accepted: 18 April 2019
Published: 17 May 2019

Citation:
Jannati A, Fried PJ, Block G, Oberman LM, Rotenberg A and Pascual-Leone A (2019) Test–Retest Reliability of the Effects of Continuous Theta-Burst Stimulation. Front. Neurosci. 13:447. doi: 10.3389/fnins.2019.00447

Objectives: The utility of continuous theta-burst stimulation (cTBS) as index of cortical plasticity is limited by inadequate characterization of its test–retest reliability. We thus evaluated the reliability of cTBS aftereffects, and explored the roles of age and common single-nucleotide polymorphisms in the brain-derived neurotrophic factor (*BDNF*) and apolipoprotein E (*APOE*) genes.

Methods: Twenty-eight healthy adults (age range 21–65) underwent two identical cTBS sessions (median interval = 9.5 days) targeting the motor cortex. Intraclass correlation coefficients (ICCs) of the log-transformed, baseline-corrected amplitude of motor evoked potentials (ΔMEP) at 5–60 min post-cTBS (T5–T60) were calculated. Adjusted effect sizes for cTBS aftereffects were then calculated by taking into account the reliability of each cTBS measure.

Results: ΔMEP at T50 was the most-reliable cTBS measure in the whole sample (ICC = 0.53). Area under-the-curve (AUC) of ΔMEPs was most reliable when calculated over the full 60 min post-cTBS (ICC = 0.40). cTBS measures were substantially more reliable in younger participants (< 35 years) and in those with *BDNF* Val66Val and *APOE* ε4– genotypes.

Conclusion: cTBS aftereffects are most reliable when assessed 50 min post-cTBS, or when cumulative ΔMEP measures are calculated over 30–60 min post-cTBS. Reliability of cTBS aftereffects is influenced by age, and *BDNF* and *APOE* polymorphisms. Reliability coefficients are used to adjust effect-size calculations for interpretation and planning of cTBS studies.

Keywords: transcranial magnetic stimulation, continuous theta-burst stimulation, plasticity, reliability, *BDNF*, *APOE*

Abbreviations: %Δ, percent change from the baseline; Δ_{B-A}, visit-B *minus* visit-A; ΔMEP, natural log-transformed, baseline-corrected amplitude of motor evoked potentials; *APOE*, apolipoprotein E; AUC, area under-the-curve; *BDNF*, brain-derived neurotrophic factor; cTBS, continuous theta-burst stimulation; FDR, false discovery rate; GABA, gamma-aminobutyric acid; ICC, intraclass correlation coefficient; iTBS, intermittent theta-burst stimulation; LME, linear mixed-effects regression analysis; LTD, long-term depression; LTP, long-term potentiation; NMDA, *N*-Methyl-D-aspartic acid; PCR, polymerase chain reaction; Rm-ANOVA, repeated-measures analysis of variance; SNP, single-nucleotide polymorphism; T0–T*n*, over the first *n* minutes following cTBS; TMS, transcranial magnetic stimulation; T*n*, at *n* minutes post-cTBS.

INTRODUCTION

Transcranial magnetic stimulation (TMS) is a method for focal non-invasive stimulation of the brain through electromagnetic induction (Barker et al., 1985). Application of TMS within the recommended guidelines (Rossi et al., 2009; Rossini et al., 2015) is a safe means of triggering or modulating neural activity in a given brain region or network (Pascual-Leone et al., 2011; Fox et al., 2012; Valero-Cabré et al., 2017). A form of repetitive TMS (rTMS) known as continuous theta-burst stimulation (cTBS) consists of 50 Hz bursts of three TMS pulses repeated at 5 Hz for a total of 600 pulses over 40 s (Huang et al., 2005). The average amplitude of motor evoked potentials (MEPs) induced by single TMS pulses is reduced by approximately 25% for up to 50 min following cTBS of the primary motor cortex (M1) (Wischnewski and Schutter, 2015). This neuromodulatory effect is thought to involve mechanisms similar to long-term depression (LTD) (Pascual-Leone et al., 1994; Huang et al., 2005; Hallett, 2007). Therefore, the pattern of cTBS-induced changes in MEPs provides a neurophysiologic index of the mechanism of cortical plasticity (Pascual-Leone et al., 2005, 2011; Oberman et al., 2010, 2012, 2014, 2016; Suppa et al., 2016).

The neuromodulatory effect of cTBS applied to M1 or other brain regions has been investigated for its potential as a neurophysiological biomarker and a therapeutic intervention in several neurological and psychiatric disorders (Koch et al., 2009, 2012; Eberle et al., 2010; McClintock et al., 2011; Cazzoli et al., 2012; Oberman et al., 2012, 2014; Di Lazzaro et al., 2013, 2016; Mori et al., 2013; Cantone et al., 2014; Chuang et al., 2014; Forogh et al., 2014; Li et al., 2014; Suppa et al., 2014; Carrette et al., 2016). Despite its growing popularity, however, cTBS responses show large inter-individual (Hamada et al., 2013; Goldsworthy et al., 2014; López-Alonso et al., 2014; Vallence et al., 2015; Guerra et al., 2017; Heidegger et al., 2017; Hordacre et al., 2017; Jannati et al., 2017) and intra-individual variability (Vernet et al., 2014; Vallence et al., 2015) that can limit the utility of cTBS for assessing brain plasticity in clinical populations.

Only two published studies have assessed the reproducibility of cTBS aftereffects (Vernet et al., 2014; Vallence et al., 2015). The first (Vernet et al., 2014) used a relatively small sample size (n = 10) and did not report reliability coefficients of cTBS aftereffects, which can be compared with the reliability coefficients of other TMS measures (Carroll et al., 2001; Kimiskidis et al., 2004; Christie et al., 2007; Livingston and Ingersoll, 2008; Bastani and Jaberzadeh, 2012; Ngomo et al., 2012; Hinder et al., 2014; Liu and Au-Yeung, 2014; Sankarasubramanian et al., 2015; Schambra et al., 2015; Hermsen et al., 2016; Fried et al., 2017). The second study (Vallence et al., 2015) used an input–output curve approach that allowed assessment of cTBS aftereffects elicited over a range of stimulation intensities, but at the cost of fewer time-points. Specifically, assessments were only performed at 0, 15, and 30 min post-cTBS. This excluded the earliest time points, i.e., 5 and 10 min post-cTBS, which typically exhibit the maximal cTBS effects (Wischnewski and Schutter, 2015) and later time-points, i.e., 40–60 min post-cTBS, which capture the longer-lasting TBS effects and have been found to be useful in differentiating clinical populations such as individuals with Alzheimer's disease (Freitas et al., 2011), autism spectrum disorder (Oberman et al., 2012), diabetes (Fried et al., 2016), and schizophrenia (McClintock et al., 2011) from healthy individuals. For comparison, at least three studies have assessed the reliability of intermittent theta-burst stimulation (iTBS) aftereffects (Hinder et al., 2014; Fried et al., 2017; Schilberg et al., 2017).

Full characterization of the test–retest reliability of cTBS aftereffects is essential to properly interpret results and plan for future studies. We thus aimed to address this need by systematically assessing the test–retest reliability of cTBS aftereffects in 5- or 10-min intervals for 60 min post-cTBS in a sizeable sample of healthy adults. We also calculated adjusted effect sizes for cTBS aftereffects by taking into account the reliability (or lack thereof) of each cTBS measure (Friedman, 1968; Wright, 2014; Fried et al., 2017). In addition, we explored the effects of age group on the reproducibility of cTBS aftereffects, as well as of single-nucleotide polymorphisms (SNPs) in brain-derived neurotrophic factor (*BDNF*) and apolipoprotein E (*APOE*) genes, which have been found to influence neuroplasticity (White et al., 2001; Cheeran et al., 2008; Nichol et al., 2009; Antal et al., 2010; Peña-Gomez et al., 2012; Lee et al., 2013; Chang et al., 2014; Di Lazzaro et al., 2015; Jannati et al., 2017). Our results can improve the utility of cTBS as a neurophysiologic index of cortical plasticity in neurological and psychiatric disorders, help elucidate the sources of intra-individual variability in cTBS responses, and ensure adequate sample size and power in future cTBS studies in clinical populations.

MATERIALS AND METHODS

Participants

Twenty-eight healthy adults (25 males, age range: 21–65) participated in the study, which was approved by the local Institutional Review Board in accordance with the Declaration of Helsinki. All participants provided written informed consent prior to enrollment and received monetary compensation upon completion. None of the participants had any TMS contraindication (Rossi et al., 2009), and all had normal physical and neurological examinations. Individual and group-level demographics are presented in **Tables 1** and **2**, respectively.

Neuropsychological Testing

Mini-Mental State Examination (Folstein et al., 1975; Crum et al., 1993) and the Abbreviated Battery of Stanford–Binet IV intelligence scale (Thorndike et al., 1986), including Verbal Knowledge and Non-Verbal Fluid Reasoning subscores, were completed.

Genetic Analyses

Saliva samples from 22 participants were assessed for *BDNF* Val66Met polymorphism and the presence of *APOE* ε4 allele, as reported previously (Jannati et al., 2017). Aliquot (700 μL) extraction of genomic DNA was performed on saliva samples collected using the Oragene Discover OGR-250 Kit (DNA

TABLE 1 | Participants' demographics, neuropsychological measures, single-nucleotide polymorphisms, and inter-visit measures.

ID	Age range (years)	Race	Ethnicity	Education (year)	Handedness	*BDNF*	*APOE*	MMSE	IQ	Verbal KN	Non-verbal FR	Inter-visit interval (days)	Visit-A start time	Visit-B start time	$\lvert\Delta_{B-A}\rvert$ start time (min)
1	20–25	White	Non-Hispanic	16	R	Val/Met	ε3/ε3	30	130	17	13	10	10:20	11:18	58
2	26–30	Other	Non-Hispanic	19	R	Val/Val	ε3/ε4	30	121	17	10	8	13:50	13:50	0
3	20–25	Multiracial	Hispanic	16	R	Val/Val	ε2/ε4	30	106	11	11	33	14:50	14:52	2
4	20–25	Multiracial	Non-Hispanic	16	R	–	–	30	112	11	13	7	9:55	9:50	5
5	56–60	White	Non-Hispanic	16	R	Val/Met	ε3/ε3	30	109	13	10	7	9:36	9:25	11
6	56–60	Black	Non-Hispanic	14	R	–	–	30	97	9	10	28	10:50	11:43	53
7	46–50	White	Non-Hispanic	20+	R	Val/Val	ε3/ε3	30	133	17	14	9	14:38	13:57	41
8	20–25	Asian	Non-Hispanic	16	R	–	–	30	94	8	10	7	9:27	9:39	12
9	50–55	White	Non-Hispanic	16	R	Val/Val	ε3/ε4	30	106	13	9	9	14:00	14:01	1
10	50–55	White	Non-Hispanic	16	R	Val/Val	ε3/ε3	30	115	14	11	19	12:56	14:39	103
11	60–65	White	Non-Hispanic	16	R	Val/Met	ε3/ε4	30	118	12	14	7	11:25	11:22	3
12	20–25	White	Hispanic	15	R	Val/Val	ε3/ε4	30	109	14	9	10	9:42	9:52	10
13	20–25	White	Hispanic	17	R	Val/Val	ε2/ε3	30	112	10	14	7	9:47	9:39	8
14	30–35	White	Non-Hispanic	19	R	Val/Val	ε3/ε3	29	100	9	11	8	14:33	10:19	254
15	20–25	White	Non-Hispanic	17	R	–	–	30	118	13	13	8	9:46	9:28	18
16	45–50	White	Non-Hispanic	16	R	–	–	30	94	9	9	28	14:04	13:36	28
17	26–30	White	Hispanic	–	R	Val/Val	ε3/ε3	30	115	13	12	12	12:04	13:10	66
18	26–30	White	Hispanic	–	R	Val/Val	ε3/ε3	29	100	10	10	7	10:52	10:50	2
19	50–55	Black	Non-Hispanic	–	R	–	–	30	97	10	9	11	9:12	12:07	175
20	20–25	White	Non-Hispanic	17	R	Val/Val	ε2/ε3	30	127	16	13	7	14:14	14:15	1
21	20–25	Multiracial	Hispanic	17	R	Val/Met	ε2/ε3	28	115	12	13	7	9:50	10:14	24
22	45–50	Black	Non-Hispanic	18	R	Val/Val	ε3/ε4	29	118	16	10	14	11:29	14:09	160
23	20–25	Asian	Non-Hispanic	17	R	Val/Met	ε3/ε4	30	103	9	12	17	9:41	9:40	1
24	45–50	Black	Non-Hispanic	18	R	Val/Met	ε3/ε3	30	88	9	7	19	10:43	10:45	2
25	30–35	Asian	Non-Hispanic	20+	R	Val/Met	ε3/ε4	30	103	8	13	14	9:53	9:41	12
26	60–65	Asian	Non-Hispanic	20+	R	Val/Val	ε3/ε4	30	124	15	13	7	11:02	10:04	58
27	45–50	White	Non-Hispanic	13	R	Val/Val	ε3/ε4	30	88	9	7	19	11:47	13:02	75
28	30–35	White	Non-Hispanic	20+	L	Val/Met	ε3/ε4	29	97	10	9	20	13:55	13:48	7

$\lvert\Delta_{B-A}\rvert$, absolute inter-visit difference; APOE, apolipoprotein E; BDNF, brain derived neurotrophic factor; FR, fluid reasoning; IQ, intelligence quotient; KN, knowledge; Met, methionine; MMSE, Mini-Mental State Examination; Val, valine. Racial and ethnic categories were defined according to the National Institutes of Health policy and guidelines on the inclusion of minorities as subjects in clinical research (NIH Office of Extramural Research, 2001).

TABLE 2 | Participants' demographics, single-nucleotide polymorphisms, neuropsychological results, and neurophysiological measures for the total sample and for the age and genetic subgroups.

	All (N = 28)	Age < 35 (n = 16)	Age ≥ 45 (n = 12)	p	*BDNF* Met− (n = 14)†	*BDNF* Met+ (n = 8)†	p	*APOE* ε4− (n = 12)†	*APOE* ε4+ (n = 10)†	p
Age (year, mean ± SD)	36.8 ± 14.5	25.3 ± 4.3	52.1 ± 6.5	N/ A	36.6 ± 14.4	37.8 ± 15.4	0.86	33.8 ± 12.6	40.8 ± 16.1	0.27
Sex (M : F)	25 : 3	15 : 1	10 : 2	0.56	13 : 1	8 : 0	1.00	11 : 1	10 : 0	1
Race (White : non-White)	16 : 12	9 : 7	7 : 5	1.00	10 : 4	4 : 4	0.39	9 : 3	5 : 5	0.38
Ethnicity (Hispanic : non-Hispanic)	6 : 22	6 : 10	0 : 12	**0.02**	9 : 5	7 : 1	0.35	7 : 5	9 : 1	0.16
Education (year, mean ± SD)*	17.0 ± 2.3	17.4 ± 1.9	16.4 ± 2.8	–	17.3 ± 2.4	17.8 ± 2.1	0.69	17.3 ± 1.6	17.7 ± 2.8	–
BDNF (Met− : Met+)†	14 : 8	8 : 5	6 : 3	–	14 : 0	0 : 8	N/A	8 : 4	6 : 4	1.00
APOE (ε4− : ε4+)†	12 : 10	8 : 5	4 : 5	–	8 : 6	4 : 4	1.00	12 : 0	0 : 10	N/ A
Handedness (Right: Left)	27 : 1	15 : 1	12 : 0	1.00	14 : 0	7 : 1	0.36	12 : 0	9 : 1	0.46
MMSE score (mean ± SD)	29.8 ± 0.5	29.7 ± 0.6	29.9 ± 0.3	0.24	29.8 ± 0.4	29.6 ± 0.7	0.52	29.7 ± 0.7	29.8 ± 0.4	0.58
IQ (mean ± SD)	108.9 ± 12.3	110.1 ± 10.6	107.2 ± 14.7	0.55	112.4 ± 12.0	107.9 ± 13.1	0.42	112.5 ± 13.2	108.7 ± 11.5	0.49
Verbal KN score	11.9 ± 2.9	11.8 ± 3.0	12.2 ± 2.9	0.71	13.1 ± 2.9	11.3 ± 2.9	0.16	12.6 ± 2.9	12.3 ± 3.2	0.83
Non-verbal FR score	11.0 ± 2.0	11.6 ± 1.6	10.3 ± 2.4	0.08	11.0 ± 2.0	11.4 ± 2.4	0.70	11.6 ± 2.0	10.6 ± 2.3	0.30
RMT (% MSO, mean ± SD)										
Visit A	35.3 ± 7.6	35.4 ± 8.7	35.3 ± 6.4	0.97	32.4 ± 5.5	38.1 ± 9.7	0.09	31.2 ± 6.0	37.9 ± 8.2	0.054
Visit B	35.9 ± 7.7	35.9 ± 8.2	35.9 ± 7.4	0.99	33.6 ± 5.8	37.4 ± 10.1	0.27	32.4 ± 6.4	38.0 ± 8.3	0.09
AMT (% MSO, mean ± SD)										
Visit A	25.9 ± 5.2	26.6 ± 5.9	25.0 ± 4.0	0.44	24.3 ± 3.7	27.3 ± 6.2	0.18	24.6 ± 4.8	26.3 ± 5.1	0.42
Visit B	25.7 ± 4.6	25.9 ± 5.0	25.4 ± 4.3	0.78	24.3 ± 3.2	26.8 ± 5.9	0.21	24.3 ± 4.2	26.3 ± 4.6	0.29
Baseline MEP amplitude (mV, mean ± SD)										
Visit A	1.3 ± 1.5	1.1 ± 1.1	1.5 ± 1.9	0.42	1.2 ± 1.2	0.8 ± 0.5	0.45	1.1 ± 1.3	1.0 ± 0.5	0.75
Visit B	1.1 ± 1.0	1.2 ± 1.0	1.1 ± 1.0	0.82	1.4 ± 1.0	0.7 ± 0.4	0.08	1.2 ± 1.1	0.9 ± 0.5	0.43
Intervisit interval (days) (mean ± SD)	12.8 ± 7.4	11.4 ± 7.0	14.8 ± 7.8	0.24	12.1 ± 7.3	12.6 ± 5.6	0.86	12.1 ± 7.9	12.5 ± 5.0	0.89
$\lvert\Delta_{B-A}\rvert$ Start Time (min, mean ± SD)	42.5 ± 62.2	30.0 ± 62.9	59.2 ± 59.7	0.23	55.8 ± 74.6	14.8 ± 19.0	0.15	47.7 ± 72.6	32.7 ± 51.9	0.59

*Comparisons of proportions were conducted with Fisher's exact test. Education and single-nucleotide polymorphisms were not statistically compared between the subgroups because the data were not available for the total sample. The p-values were not adjusted for multiple comparisons. The p-value < 0.05 is highlighted in bold font. $\lvert\Delta_{B-A}\rvert$, absolute inter-visit difference; AMT, active motor threshold; APOE, apolipoprotein E; APOE ε4+, ε2/ε4 or ε3/ε4 genotype; APOE ε4–, ε2/ε3 or ε3/ε3; BDNF, brain-derived neurotrophic factor; BDNF Met–, Val66Val; BDNF Met+, Val66 Met; FR, fluid reasoning; IQ, intelligence quotient; KN, knowledge; MEP, motor evoked potential; Met, metionine; MMSE, Mini-Mental State Examination; MSO, maximum stimulator output; RMT, resting motor threshold; SD, standard deviation; Val, valine. *Education data were available for 26 participants. †BDNF and APOE results were available for 22 participants.*

Genotek Inc., Ottawa, ON, Canada). DNA was extracted from samples using standard methodology and the prepIT L2P reagent (DNA Genotek Inc., 2015). The rs6265 SNP of the *BDNF* gene, and the rs429358 and the rs7412 SNPs of the *APOE* gene were analyzed using a TaqMan single-tube genotyping assay, which uses polymerase chain reaction (PCR) amplification and a pair of fluorescent dye detectors that target the SNP. During PCR, the polymerase released the fluorescent probe into solution where it was detected using endpoint analysis in an 7900HT Real-Time instrument from Applied Biosystems, Inc. (Foster City, CA, United States).

Transcranial Magnetic Stimulation

Two identical TMS visits (7–33 days apart; median interval = 9.5 days) were conducted. The starting times of the two visits were 0–254 min apart (interquartile range = 1–103 min; median = 12 min). The inter-visit intervals and starting-time differences for individual subjects are presented in **Table 1**.

All TMS procedures followed the recommended guidelines endorsed by the International Federation of Clinical Neurophysiology (Rossi et al., 2009; Rossini et al., 2015). Participants were seated in a comfortable chair with the right arm and hand in a natural pronated ∼90° angle on a pillow in front of them. They were instructed to keep their right hand as still and relaxed as possible throughout the experiment. They were also monitored for drowsiness and were asked to keep their eyes open during the TMS application. Single TMS pulses and cTBS were applied to the left primary motor cortex (M1) at 120% of individual resting motor threshold (RMT) and 80% of active motor threshold (AMT), respectively, as biphasic pulses with an antero-posterior–postero-anterior (AP-PA) induced current direction using a MagPro X100 stimulator and a MC-B70 Butterfly Coil (outer diameter: 97 mm; MagPro, MagVenture A/S, Farum, Denmark). The coil was held tangentially to the participant's head surface, with the handle pointing occipitally and positioned at 45° relative to the mid-sagittal axis of the participant's head. The optimal spot for the maximal responses of the right first dorsal interosseous (FDI) muscle ("motor hotspot") was localized. A Polaris infrared-optical tracking system (Northern Digital Inc., Waterloo, ON, Canada) and a Brainsight TMS neuronavigation system (Rogue Research Inc., Montreal, QC, Canada) with a brain MRI template

(for 21 participants) or the participant's brain MRI (for the remaining 7 participants) was used to ensure consistent targeting throughout the experiment.

Surface electromyogram (EMG) was recorded from the right FDI with a PowerLab 4/25 data-acquisition device and LabChart 8 software (AD Instruments, Colorado Springs, CO, United States). Electrodes were placed over the FDI belly (negative) and the first interphalangeal joint of the second finger (positive). The ground electrode was placed over the ipsilateral ulnar styloid process. The TMS system delivered triggered pulses that synchronized the TMS and EMG systems. EMG signal was digitized at 1 kHz for 500 ms following each stimulus trigger and 100 ms pre-trigger, amplified with a range of ±10 mV (band-pass filter 0.3–1000 Hz).

Each TMS session began by localizing the motor hotspot for FDI and assessment of the RMT, defined as the lowest intensity of stimulation that elicited MEPs $\geq$ 50 μV in at least five of ten pulses in the relaxed right FDI. To assess pre-cTBS cortico-motor reactivity, three blocks of 30 single TMS pulses were applied to M1, with a 5–10 min inter-block interval and at a random 4–6 s inter-pulse interval. In each block, individual MEPs > 2.5 SD from the mean were excluded. Baseline MEP amplitude was calculated as the average of the peak-to-peak amplitude of MEPs in the three blocks. The AMT was then assessed as the lowest intensity that elicited MEPs $\geq$ 200 μV in at least five of ten pulses with the FDI slightly contracted. After a 5-min break, during which participants were instructed to maintain hand relaxation to control the effects of voluntary hand movements on cTBS responses (Iezzi et al., 2008), cTBS was applied as 200 bursts of three pulses at 50 Hz, repeated at 200-ms intervals for 40 s (for a total of 600 pulses). Cortico-motor reactivity was reassessed at 5, 10, 15, 20, 30, 40, 50, and 60 min post-cTBS (*T5–T60*).

Statistical Analyses

Stata software version 13.1 (StataCorp, College Station, TX, United States) and MATLAB and Statistics and Machine Learning Toolbox R2016b (The MathWorks, Natick, MA, United States) were used for data analysis. Data from each TMS visit included: (a) RMT and AMT, expressed as percentage of maximum stimulator output; (b) baseline MEP amplitude, calculated as the average of baseline MEP amplitude in 3 blocks of 30 single TMS pulses; and (c) percent change in the average amplitude of 30 MEPs at T5–T60 relative to baseline (%Δ) for each participant.

The Shapiro–Wilk test found significant deviations in MEP values from normal distribution; thus, natural log-transformed, baseline-corrected MEP amplitude at each post-cTBS time point (ΔMEP) was averaged over all participants separately for each visit. The following measures were also calculated: absolute MEP modulation at T5–T60 (|ΔMEP|), maximum suppression and maximum modulation of MEPs during 60 min post-cTBS, area under-the-curve (AUC) and the absolute AUC value (|AUC|) of ΔMEPs over T0–T10, . . . , and T0–T60 intervals. Cumulative AUC and |AUC| measures up to each time-point were calculated as the summed products of the average ΔMEP and the average |ΔMEP|, respectively, across each two consecutive time-points and the time in minutes between them.

Grand-average values for all cTBS measures were calculated separately for both visits and were compared against zero using one-sample *t*-tests. Visit-B *minus* visit-A difference (Δ_{B-A}) and $|\Delta_{B-A}|$ were calculated for each neurophysiological measure (**Table 3**). All analyses were two-tailed, and the α level was set to 0.05. When explicitly noted, false discovery rate (FDR) was used to adjust *p*-values for multiple testing (Benjamini and Hochberg, 1995; Benjamini and Yekutieli, 2001).

ΔMEPs at T10 and T40 were previously found to be the best predictors of *inter*-individual variability in cTBS aftereffects in visit-A (Jannati et al., 2017). Thus, to assess the effect of potential covariates on the *intra*-individual variability of cTBS aftereffects at T10 and T40, we conducted linear mixed-effects (LME) regression analyses with Δ*MEPs at T10* or *T40* as dependent variable, *Visit* (visit-A vs. visit-B) as a within-subject factor, and potential covariates including RMT, AMT, baseline MEP amplitude, number of days between the two visits (*Inter-visit Interval*), and the absolute inter-visit difference in starting time (in minutes) (*Time Difference*) as between-subject factors. Based on previous studies that found in many situations a regression model is likely to be reliable when the number of candidate predictors is smaller than one-tenth of the number of subjects (Harrell, 2015) (p. 72), up to three between-subjects predictors were considered for simultaneous inclusion in any regression model.

To assess test–retest reliability, intraclass correlation coefficients (ICCs) (Portney and Watkins, 2009) were calculated in the form of absolute agreement between the two visits for all neurophysiological measures. ICCs were calculated using a two-way mixed-effects model, with fixed column (C) effects and random row (R) effects (McGraw and Wong, 1996):

$$\mathrm{ICC(A,\,1)} = \frac{MS_{\mathrm{R}} - MS_{E}}{MS_{\mathrm{R}} + (k-1)MS_{\mathrm{E}} + \frac{k}{n}(MS_{\mathrm{C}} - MS_{\mathrm{E}})}$$

where ICC(A,1) represents the degree of absolute agreement of measurements made under the two fixed levels of the column factor. k = the number of raters/measurements per subject; MS_{R} = mean square for rows (representing the individual subjects); MS_{E} = mean square error; MS_{C} = mean square for columns (representing the two visits); n = the number of subjects.

Using this formula, ICC = 1 indicates maximum reliability and ICC $\leq$ 0 indicates no reliability [in the case that the within-group variance is equal to or higher than the between-groups variance (Kenny et al., 2002)]. ICC values were interpreted as follows (Portney and Watkins, 2009): (i) ICC < 0.25: very low to no reliability; (ii) 0.25 $\leq$ ICC < 0.50: low reliability; (iii) 0.50 $\leq$ ICC < 0.75: moderate reliability; and (iv) ICC $\geq$ 0.75: high reliability. ICC values were statistically compared using two-way mixed-effects *F* statistics (McGraw and Wong, 1996, Table 8). The effects on the ICCs of covariates that had a significant effect on ΔMEPs were assessed by including the covariate in the corresponding mixed-effects regression model and re-calculating the residual intraclass correlation.

Lack of reliability of a measure of interest attenuates the observed effect size compared to the population parameter

TABLE 3 | Neurophysiological measures (mean ± SD) and their test-retest reliability for the whole sample (N = 28).

	Visit A	Visit B	Δ_{B-A}	$\lvert\Delta_{B-A}\rvert$	ICC	p	Reproducibility-adjusted effect sizes		
							Cohen's d = 0.2	Cohen's d = 0.5	Cohen's d = 0.8
Motor threshold (% MSO)									
RMT	35.3 ± 7.6	35.9 ± 7.7	0.6 ± 2.2	1.8 ± 1.4	**0.96**	<0.001	0.20	0.50	0.79
AMT	25.9 ± 5.2	25.7 ± 4.6	−0.2 ± 1.8	1.5 ± 1.1	**0.93**	<0.001	0.20	0.49	0.78
Baseline MEP amplitude (mV)	1.3 ± 1.5	1.1 ± 1.0	−0.2 ± 1.0	0.6 ± 0.8	**0.70**	<0.001	0.18	0.46	0.72
Post-cTBS ΔMEP									
T5	−0.05 ± 0.3	−0.07 ± 0.4	−0.02 ± 0.5	0.41 ± 0.3	0.16	0.213	0.13	0.31	0.48
T10	−0.02 ± 0.4	0.08 ± 0.4	0.11 ± 0.5	0.42 ± 0.3	0.11	0.289	0.12	0.28	0.44
T15	0.09 ± 0.3	0.00 ± 0.3	−0.09 ± 0.5	0.40 ± 0.3	−0.16	0.791	–	–	–
T20	0.10 ± 0.3	0.03 ± 0.4	−0.07 ± 0.5	0.39 ± 0.3	0.20	0.157	0.13	0.33	0.51
T30	0.07 ± 0.4	−0.02 ± 0.5	−0.09 ± 0.5	0.36 ± 0.4	**0.37**	0.024	0.16	0.39	0.61
T40	0.07 ± 0.4	−0.06 ± 0.5	−0.14 ± 0.5	0.40 ± 0.3	0.26	0.076	0.14	0.35	0.55
T50	0.08 ± 0.4	0.07 ± 0.5	−0.01 ± 0.5	0.37 ± 0.3	**0.53**	0.002	0.17	0.42	0.67
T60	−0.04 ± 0.5	0.03 ± 0.6	0.08 ± 0.8	0.61 ± 0.5	−0.08	0.653	–	–	–
Maximum suppression	−0.50 ± 0.5	−0.53 ± 0.5	−0.03 ± 0.6	0.45 ± 0.3	**0.38**	0.024	0.16	0.39	0.61
Post-cTBS |ΔMEP|									
T5	0.29 ± 0.2	0.33 ± 0.2	0.04 ± 0.3	0.29 ± 0.2	−0.27	0.912	–	–	–
T10	0.31 ± 0.2	0.28 ± 0.2	−0.03 ± 0.4	0.27 ± 0.2	−0.18	0.815	–	–	–
T15	0.26 ± 0.2	0.26 ± 0.2	0.00 ± 0.3	0.21 ± 0.1	0.11	0.297	0.11	0.28	0.44
T20	0.29 ± 0.2	0.33 ± 0.3	0.03 ± 0.3	0.22 ± 0.1	0.29	0.068	0.15	0.36	0.57
T30	0.33 ± 0.3	0.37 ± 0.3	0.03 ± 0.3	0.20 ± 0.2	**0.50**	0.003	0.17	0.42	0.66
T40	0.32 ± 0.2	0.32 ± 0.3	0.00 ± 0.4	0.24 ± 0.3	0.17	0.190	0.13	0.32	0.49
T50	0.33 ± 0.3	0.35 ± 0.3	0.02 ± 0.4	0.29 ± 0.2	**0.34**	0.037	0.15	0.38	0.59
T60	0.37 ± 0.3	0.44 ± 0.4	0.07 ± 0.5	0.35 ± 0.3	−0.03	0.567	–	–	–
Maximum modulation (|ΔMEP|)	0.76 ± 0.4	0.86 ± 0.4	0.10 ± 0.4	0.35 ± 0.3	**0.31**	0.045	0.15	0.37	0.58
AUC of ΔMEPs									
T0–T10	−0.33 ± 2.3	−0.15 ± 2.4	0.18 ± 3.1	2.55 ± 1.6	0.13	0.257	0.12	0.29	0.46
T0–T15	−0.16 ± 3.6	0.05 ± 3.4	0.21 ± 4.6	3.94 ± 2.2	0.15	0.228	0.12	0.31	0.48
T0–T20	0.31 ± 4.7	0.10 ± 4.6	−0.20 ± 6.0	5.14 ± 2.9	0.18	0.183	0.13	0.32	0.50
T0–T30	1.13 ± 7.2	0.15 ± 8.0	−0.99 ± 9.2	7.41 ± 5.4	0.27	0.078	0.14	0.36	0.56
T0–T40	1.85 ± 10.2	−0.26 ± 11.9	−2.12 ± 13.2	10.28 ± 8.3	0.29	0.061	0.15	0.36	0.57
T0–T50	2.60 ± 13.3	−0.25 ± 15.4	−2.85 ± 16.2	12.70 ± 10.2	**0.36**	0.026	0.16	0.38	0.60
T0–T60	2.77 ± 16.5	0.26 ± 19.1	−2.51 ± 19.7	15.94 ± 11.5	**0.40**	0.018	0.16	0.39	0.62
|AUC| of ΔMEP									
T0–T10	2.22 ± 1.2	2.36 ± 1.4	0.14 ± 2.1	1.74 ± 1.2	−0.35	0.961	–	–	–
T0–T15	3.63 ± 1.7	3.70 ± 2.1	0.07 ± 3.1	2.51 ± 1.8	−0.32	0.946	–	–	–
T0–T20	5.02 ± 2.1	5.16 ± 2.7	0.14 ± 3.5	2.72 ± 2.2	−0.08	0.647	–	–	–
T0–T30	8.15 ± 3.3	8.64 ± 4.1	0.48 ± 4.4	3.48 ± 2.7	0.31	0.053	0.15	0.37	0.58
T0–T40	11.42 ± 5.0	12.05 ± 6.2	0.64 ± 6.2	4.66 ± 4.0	**0.39**	0.018	0.16	0.39	0.61
T0–T50	14.66 ± 6.7	15.37 ± 8.3	0.71 ± 7.9	5.96 ± 5.2	**0.45**	0.008	0.16	0.41	0.64
T0–T60	18.17 ± 8.1	19.33 ± 10.6	1.16 ± 9.9	6.00 ± 0.1	**0.46**	0.007	0.16	0.41	0.64

AUC and |AUC| of ΔMEPs were calculated as the summed products of the average ΔMEP and the average |ΔMEP|, respectively, across two consecutive time-points and the time in minutes between them. The ICC values with $p < 0.05$ are highlighted in bold font. Abbreviations: Δ_{B-A}, Visit B minus Visit A; $\lvert\Delta_{B-A}\rvert$, absolute inter-visit difference; AMT, active motor threshold; AUC, area under-the-curve; ΔMEP, natural log-transformed, baseline-corrected MEP amplitude; ICC, intraclass correlation coefficient; MEP, motor evoked potential; MSO, maximum stimulator output; RMT, resting motor threshold; T0–Tn, over the first n minutes following cTBS.

(Hunter and Schmidt, 1994). Following previously applied methodology (Friedman, 1968; Wright, 2014; Fried et al., 2017), we assessed how test–retest reliability (or lack thereof) of TMS measures would attenuate small, medium, and large effect sizes, i.e., Cohen's d values of 0.2, 0.5, and 0.8 (Cohen, 1992), respectively, which assume perfect reproducibility. First, each

idealized Cohen's *d* is converted to an *r* (Cohen, 1988) (p. 23):

$$r_{\text{IDEALIZED}} = \frac{d_{\text{IDEALIZED}}}{\sqrt{d^2_{\text{IDEALIZED}} + 4}}$$

This idealized *r* is then *adjusted* for unreliability using the ICC (Wright, 2014):

$$r^2_{\text{ADJUSTED}} = r^2_{\text{IDEALIZED}} * \sqrt{ICC}$$

Finally, the adjusted *r* is converted back to an adjusted *d* (Friedman, 1968) (p. 246):

$$d_{\text{ADJUSTED}} = \frac{2 * r_{\text{ADJUSTED}}}{\sqrt{1 - r^2_{\text{ADJUSTED}}}}$$

Exploratory Analyses

Though unintended, the age of our participants conformed to a bimodal distribution. Thus, to explore the impact of age on our reliability measures, the total sample was subdivided into two distinct age groups with a 10-year gap and a ∼27-year difference in mean age: a *Younger* group with age < 35 ($n = 16$; range: 21–34; mean ± SD, 25.3 ± 4.3) and an *Older* group with age ≥ 45 ($n = 12$; range: 45–65; mean ± SD, 52.1 ± 6.5). To explore the effect of age on the test–retest reliability of cTBS aftereffects: (i) the ICC values of TMS measures were calculated separately for the two age groups; (ii) separate repeated-measures analyses of variance (Rm-ANOVAs) were conducted with Δ*MEP at T10* or *T40* as dependent variable, *Age Group* as a between-subjects factor, *Visit* as a within-subject factor, and *Age Group* × *Visit* interaction. Because the proportion of Hispanic participants was significantly higher in the Younger group than in the Older group, we assessed the effect of *Ethnicity* as a categorical covariate in these Rm-ANOVAs. We also re-calculated all the ICCs for the Younger group while controlling for *Ethnicity*.

To explore the roles of *BDNF* and *APOE* SNPs in the reliability of TMS measures, we calculated the ICC values of neurophysiological measures over the two visits separately for participants with *BDNF* Val/Val (Met–; $n = 14$) and Val/Met (Met+; $n = 8$) genotypes as well as for those with *APOE* ε2/ε3 or ε3/ε3 (ε4–; $n = 12$) and *APOE* ε2/ε4 or ε3/ε4 (ε4+; $n = 10$) genotypes.

Because *BDNF* was previously found to influence the cTBS aftereffect at T10 (Jannati et al., 2017), we assessed the cTBS aftereffects separately for *BDNF* Met– and Met+ participants in each visit and conducted a Rm-ANOVA with Δ*MEP at T10* as dependent variable, *BDNF Status* (Met– vs. Met+) as a between-subjects factor, *Visit* (visit-A vs. visit-B) as a within-subject factor, and *BDNF Status* × *Visit* interaction. Further, we assessed the effect of *BDNF Status* as a covariate in the LME regression analyses at T10.

RESULTS

Demographics, neuropsychological measures, inter-visit interval, starting times of the two visits, and inter-visit differences in starting time for individual participants are presented in **Table 1**. Statistical comparisons of these measures between the two age groups are presented in **Table 2**.

Genetic Analyses

Available *BDNF* and *APOE* results and comparisons of all available measures between *BDNF*/*APOE* subgroups are presented in **Tables 1** and **2**, respectively.

Among 22 participants with available DNA results, the frequencies of *BDNF* Val/Val and Val/Met genotypes were 0.64 and 0.36, respectively, while the frequencies of *APOE* ε2/ε3, ε3/ε3, and ε3/ε4 genotypes were 0.14, 0.41, and 0.46, respectively. *BDNF* and *APOE* subgroups were comparable in all available measures (**Table 2**).

Baseline Neurophysiological Measures

The RMT, AMT, and baseline MEP amplitude in each visit and their inter-visit differences are summarized in **Tables 2** and **3**, respectively.

There were no significant differences in any of the baseline neurophysiological measures in either visit between age or genetic subgroups (**Table 2**). There was also no significant difference between the two visits in any of the baseline neurophysiological measures for the whole sample (p's > 0.14), for each age group (p's > 0.17), or for each *BDNF* (p's > 0.08) or *APOE* (p's > 0.28) subgroup.

The LME regression analyses of ΔMEP at T10 found a significant, negative effect of *Time Difference* in all models (p's < 0.025), but no significant effect of any of the baseline neurophysiological measures or *Visit* (p's > 0.21). LME regression analyses of ΔMEP at no other time point found a significant effect of *Time Difference* (p's > 0.41).

cTBS-Induced Plasticity Results

Grand-average ΔMEPs in visits A and B are shown in **Figure 1**. ΔMEP and |ΔMEP| values, maximum suppression and maximum modulation as well as their inter-visit differences

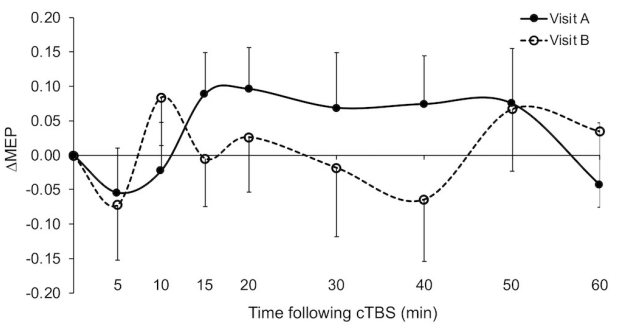

FIGURE 1 | Grand-average ΔMEPs recorded from the right FDI muscle at 5 to 60 min following cTBS of the left primary motor cortex in two identical visits. The ΔMEPs did not significantly differ from zero at any post-cTBS time point in either visit (p's > 0.11). Error bars represent standard error of the mean. cTBS, continuous theta-burst stimulation; ΔMEP, natural log-transformed, baseline-corrected amplitudes of the motor evoked potential; FDI, first dorsal interosseous.

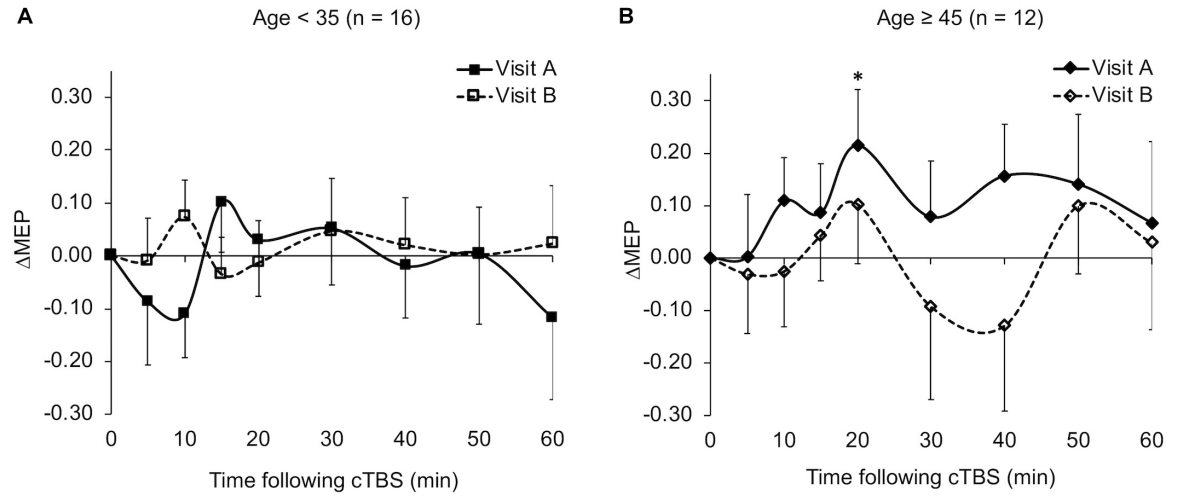

FIGURE 2 | Average ΔMEPs recorded from the right FDI muscle at 5 to 60 min following cTBS of the left primary motor cortex in two identical visits in the Younger **(A)** and Older **(B)** groups. The ΔMEPs did not significantly differ from zero at any time point in either visit in the Younger group (p's > 0.06). *The ΔMEPs in the Older group were significantly greater than zero at T20 in visit-A (P_{FDR} = 0.029), but not at any other time point in either visit (p's > 0.18). Error bars represent standard error of the mean. cTBS, continuous theta-burst stimulation; ΔMEP, natural log-transformed, baseline-corrected amplitudes of the motor evoked potential; FDI, first dorsal interosseous; FDR, false discovery rate.

are summarized in **Table 3**. Grand-average ΔMEPs did not significantly differ from zero at any time point in either visit (p's > 0.11). There was also no significant difference in grand-average ΔMEP or |ΔMEP| between the two visits at any time point (p's > 0.16).

The ΔMEPs in the Older group were significantly greater than zero at T20 in visit-A (P_{FDR} = 0.029), but not at any other time point in either visit (p's > 0.18). The ΔMEPs in the Younger group did not significantly differ from zero at any time point in either visit (p's > 0.06). The ΔMEPs in the *BDNF* Met– group were significantly less than zero at T10 in visit-A (P_{FDR} = 0.042), but not at any other time point in either visit (p's > 0.14). The ΔMEPs in the *BDNF* Met+ group were not significantly different from zero at any time point in either visit (P_{FDR}'s > 0.05). cTBS aftereffects in both visits for the two age subgroups and the two *BDNF* subgroups are presented in **Figures 2** and **4** respectively.

The Rm-ANOVA on the ΔMEP at T10 found a significant effect of *BDNF* status, $F(1, 20) = 8.28$, $p = 0.009$, $\eta_p^2 = 0.29$, but no significant effects of Visit or *BDNF* × *Visit* interaction (p's > 0.10). *BDNF* Met-carrier status had a significant positive effect in all LME regression analyses of ΔMEP at T10 ($\hat{B}$'s > 0.28, p's < 0.027). There was no other significant effect in any of the LME models (p's > 0.08).

To control for potential effects of gender, race/ethnicity, and handedness on cTBS-induced plasticity measures, we calculated ΔMEP's at T5–T60 in a subgroup of White, non-Hispanic, and right-handed males (n = 11, **Table 1**). In this smaller, but more-homogenous subsample, ΔMEPs did not significantly differ from zero at any time point in either visit (p's > 0.23).

Test–Retest Reliability of TMS Measures

Measures of inter-visit variability and test–retest reliability for RMT, AMT, baseline MEP amplitude and cTBS measures, as well as reliability-adjusted effect sizes for each TMS measure in the whole group are presented in **Table 3**.

The ICCs of baseline neurophysiological measures was not significantly different between the two age groups (p's > 0.19; **Figure 3**). In contrast, ΔMEPs in the Younger group were significantly more reliable than in the Older group at T10 and T60 (P_{FDR}'s < 0.015), but not at other individual time points (P_{FDR}'s > 0.058). Similarly, |AUC| measures were significantly more reliable in the Younger group than in the Older group over T0–T20 and beyond (P_{FDR}'s < 0.001; **Figure 3**). The reliability of other cumulative ΔMEP measures was not significantly different between the two age groups (p's > 0.058). After adjusting for *Ethnicity*, none of the ICCs in the Younger group crossed our pre-defined boundaries for interpretation of ICC values (see "Materials and Methods" section).

To control for potential effects of gender, race/ethnicity, and handedness on the test–retest reliability of cTBS aftereffects, we calculated the ICC values of baseline neurophysiological measures and ΔMEP's at T5–T60 among White, non-Hispanic, and right-handed males (n = 11, **Table 1**). The ICC values of RMT, AMT, and baseline MEP amplitude in this subgroup were 0.86 (p < 0.001), 0.96 (p < 0.001), and 0.75 (p = 0.003), respectively. The ICC values of ΔMEP at T5, T10, T15, T20, T30, T40, T50, and T60 in this subgroup were 0.54 (p = 0.031), –0.09 (p = 0.602), 0.18 (p = 0.297), 0.71 (p = 0.005), 0.86 (p < 0.001), 0.67 (p = 0.008), 0.79 (p = 0.001), and 0.17 (p = 0.309), respectively.

The ICCs of baseline neurophysiological measures were not significantly different between either the *BDNF* or the *APOE* subgroups (p's > 0.16; **Figure 5**). In contrast, ΔMEPs were significantly more reliable in *BDNF* Met– participants than in *BDNF* Met+ participants at T20–T40 (P_{FDR}'s < 0.023), but not at other time points (p's > 0.24). Maximum suppression, maximum modulation, and AUC of

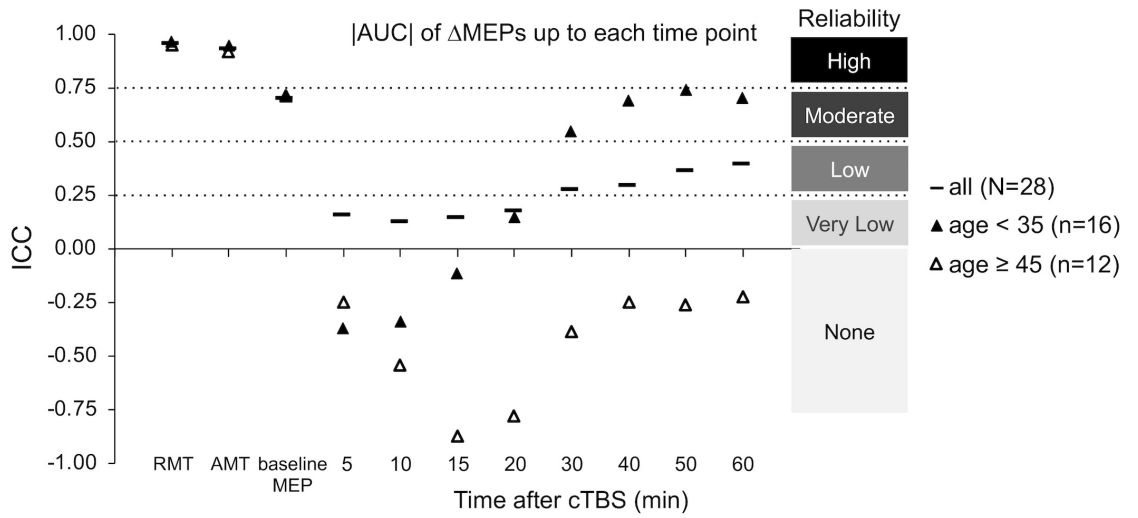

FIGURE 3 | Test–retest reliability of baseline neurophysiological measures and post-cTBS ΔMEP measures separately in the Younger (age < 35, *n* = 16) and Older (age ≥ 45, *n* = 12) groups. |AUC| of ΔMEPs were calculated as the summed products of the average |ΔMEP| across each two consecutive time-points and the time in minutes between them over T0–T10, T0–15, . . . , T0–T60 intervals (marked by their end time point on the abscissa). The ICCs of the RMT, AMT, and baseline MEP amplitude were not significantly different between the two age groups (*p*'s > 0.19). The |AUC| of ΔMEPs were significantly more reliable in the Younger group than in the Older group over T0–T15 and beyond (P_{FDR}'s < 0.001). The reliability of other cumulative ΔMEP measures was not significantly different between the two age groups (*p*'s > 0.058). AUC, area under-the-curve; cTBS, continuous theta-burst stimulation; FDR, false discovery rate; ΔMEP, natural log-transformed, baseline-corrected MEP amplitude; ICC, intraclass correlation coefficient; MEP, motor evoked potential; T0–T*n*, over the first *n* minutes post-cTBS.

ΔMEPs over T0–T30 and beyond were significantly more reliable in *BDNF* Met– participants than in *BDNF* Met+ participants (P_{FDR}'s < 0.032; **Figure 5**). The reliability of other cumulative ΔMEP measures was not significantly different between the two *BDNF* subgroups (P_{FDR} > 0.21).

ΔMEPs were significantly more reliable in *APOE* ε4– participants than in *APOE* ε4+ participants at T5 and T20–T40 (P_{FDR}'s < 0.024), but not at other time points (P_{FDR}'s > 0.07). All AUC measures were significantly more reliable in *APOE* ε4– participants than in *APOE* ε4+ participants (P_{FDR}'s < 0.021; **Figure 5**). There were no significant differences in the reliability of maximum suppression or maximum modulation between the two *APOE* subgroups (P_{FDR}'s > 0.27).

DISCUSSION

Test–retest reliability of TMS measures influences their utility as potential neurophysiologic biomarkers or targets for therapeutic intervention. As the use of plasticity-inducing rTMS protocols becomes more common, it is necessary to investigate the magnitude and sources of their inter- and intra-individual variability. While some of the factors that contribute to the inter-individual variability of these types of plasticity metrics among healthy individuals have been identified (Cheeran et al., 2008, 2009; Antal et al., 2010; Hamada et al., 2013; Goldsworthy et al., 2014; López-Alonso et al., 2014; Nettekoven et al., 2014, 2015; Vallence et al., 2015; Suppa et al., 2016; Hordacre et al., 2017; Jannati et al., 2017), few studies have assessed the intra-individual reliability of cTBS responses (Vernet et al., 2014; Vallence et al., 2015) and no study, to our knowledge, has systematically assessed the test–retest reliability of cTBS aftereffects during 60 min post-cTBS. The present study was designed to fill this gap by assessing the test–retest reliability of cTBS aftereffects at 5- or 10-minute intervals (T5–T60) and of cumulative cTBS aftereffects during 60 min post-cTBS in healthy adults. Furthermore, in order to provide guidance and reference for future studies, we calculated adjusted effect sizes that take into account the test–retest reliability of cTBS measures. Finally, we explored the influences of age group and common SNPs in *BDNF* and *APOE* genes on the reliability of cTBS aftereffects.

Overall Reliability of Baseline Neurophysiological Measures

Resting motor threshold had high test–retest reliability (**Table 3**), which was comparable with the ICC values reported in most previous studies (Carroll et al., 2001; Kimiskidis et al., 2004; Livingston and Ingersoll, 2008; Bastani and Jaberzadeh, 2012; Ngomo et al., 2012; Hinder et al., 2014; Schambra et al., 2015; Fried et al., 2017; Davila-Pérez et al., 2018) and somewhat higher than other studies that found RMT ICCs in the 0.75–0.80 range (Fleming et al., 2012; Liu and Au-Yeung, 2014; Sankarasubramanian et al., 2015; Hermsen et al., 2016). The AMT also had high test–retest reliability (**Table 3**), which was comparable with the results of previous studies (Ngomo et al., 2012; Hinder et al., 2014; Fried et al., 2017).

Baseline MEP amplitude had moderate test–retest reliability (**Table 3**). The ICC of baseline MEP amplitude found in the present study (ICC = 0.70) was moderate compared to the wide range of ICC values for baseline MEP amplitude (–0.16 to 0.87) reported in previous studies (Kamen, 2004; McDonnell et al.,

2004; Christie et al., 2007; Fleming et al., 2012; Ngomo et al., 2012; Hinder et al., 2014; Hermsen et al., 2016; Fried et al., 2017; Davila-Pérez et al., 2018). Variability of baseline MEP amplitude was previously found to be associated with variability of TBS aftereffects (Hordacre et al., 2017; Fried et al., 2017). The moderate reliability of baseline MEP amplitude in the present study suggests that such variability was not the main cause of the low reliability of some of the cTBS measures reported here.

Overall Reliability of cTBS Aftereffects

The finding that differences between the start times of the two visits influenced the cTBS aftereffects at T10 could be due to the effect of circadian rhythm on the neuromodulatory effects of rTMS arising from changes in cortical excitability and synaptic efficiency during the day (Cohen et al., 2005). While the present results cannot definitively conclude that circadian factors influenced the intra-individual variability in plasticity at T10, future studies could attempt to control for the time of day or, perhaps even better, to individualize visits to coincide with the same relative point in each subject's circadian cycle.

The finding that T5 had one of the lowest between-visit variabilities among post-cTBS time points is consistent with the findings of a previous study (Vernet et al., 2014). Importantly, however, the low between-visit variability of cTBS aftereffects at T5 and T50 at the group level in the present study did not translate to high test–retest reliability measures, which take into account both within-individual and between-individuals variability; while T50 was the most reliable post-cTBS time point (ICC = 0.53), T5 had very low reliability (ICC = 0.16). This pattern of results underlines the importance of calculating the ICCs of TMS measures rather than relying only on measures of inter-visit variability at the group level. Further, the low ICCs at T5 and T10 indicate that the time points expected to show maximal effects of cTBS (Wischnewski and Schutter, 2015) do not necessarily exhibit high test–retest reliability. This remained true for the cumulative measures of cTBS aftereffects over the first 20 min post-cTBS.

The very low test–retest reliability of ΔMEPs at T10 (ICC = 0.11) could be due to two factors: (1) The ΔMEPs at T10 in both visits could be the most influenced by *BDNF* polymorphism (Jannati et al., 2017). Consistent facilitation of MEPs, at least numerically, in *BDNF* Met+ participants in both visits may have resulted in higher test–retest reliability of T10 ΔMEP in that subgroup (**Figure 5**). (2) Despite the relatively long inter-visit interval in the present study, T10 seemed to exhibit a *metaplastic*-like effect similar to those reported with shorter intervals (Maeda et al., 2000; Gentner et al., 2008; Valero-Cabré et al., 2008; Oberman et al., 2016) in the overall results (**Figure 1**), as well in the Younger group (**Figure 2A**) and the *BDNF* Met– subgroup (**Figure 4A**). In all three cases, the direction of the neuromodulatory effect of cTBS at T10 was reversed, at least numerically, from inhibitory in visit-A to facilitatory in visit-B. Such reversals, when predominant at the individual level, would substantially reduce the test–retest reliability of cTBS aftereffects at T10. Although a previous iTBS study found only inter-visit intervals shorter than 7 days to be associated with metaplastic changes after iTBS in aging adults (Fried et al., 2017), the initial cTBS in the present study may have set into motion subtle changes that were still present when the second cTBS was applied. Further, it is possible that demographic, genetic, and state-dependent factors modulate the metaplastic(-like) effects of successive TBS sessions (Opie et al., 2017).

The low test–retest reliability of several cTBS aftereffects resulted in adjustment of large- and medium effect sizes to medium and small effect sizes, respectively (**Table 3**). While calculating the cumulative cTBS measures improved the overall ICCs over T0–T30 and beyond (**Figures 3**, **5**), the ICCs of the cumulative measures for the whole sample remained below 0.5. Attenuation of idealized effect sizes by this level of reproducibility indicates that detecting significant differences in cTBS responses between healthy and clinical populations may require sample sizes that are substantially larger than those used in most previous cTBS studies (Wischnewski and Schutter, 2015; Chung et al., 2016; Suppa et al., 2016), unless steps can be implemented to improve the reliability of this technique.

The finding that within White, non-Hispanic, and right-handed males (n = 11), none of the ΔMEPs at any time point in either visit differed significantly from zero suggests that controlling for demographic factors such as gender, race/ethnicity, and handedness is not enough to overcome the large inter-individual variability in cTBS responses in either visit. We found, despite comparable reliability of baseline neurophysiological measures, T5 and T20–T50 ΔMEPs were substantially more reliable in this more-homogenous subgroup, suggesting that heterogeneity of these demographic factors influence the reliability of cTBS aftereffects in the whole sample. While the small sample precludes definitive conclusions about the effects of gender, handedness, and race/ethnicity, these results nonetheless appear to suggest that demographic variation plays a role in the test–retest reliability of cTBS responses.

Age and Reliability of cTBS Aftereffects

The significant *Age Group* × *Visit* interaction effect on T10 ΔMEP indicates that cTBS aftereffects at T10 in the Younger group, but not in the Older group, switched from inhibitory in visit-A to facilitatory in visit-B (**Figure 2**). Such reversal could be due to metaplasticity or some other state-dependent factor. The distinct patterns of cTBS aftereffects at T10 among Younger and Older groups could be due to two factors: (i) Based on animal studies that have found an age-related reduction in the efficiency of gamma-aminobutyric acid- (GABA-) mediated inhibition (Milbrandt et al., 1994; Billard et al., 1995; McQuail et al., 2012), it is possible that older participants have less-efficient GABAergic synaptic transmission, which is presumed to be involved in cTBS-induced plasticity (Stagg et al., 2009; Trippe et al., 2009). The resulting reduced inhibitory effects of cTBS, potentially combined with cumulative facilitatory effects of successive single TMS pulses (Pellicciari et al., 2016), could have resulted in facilitation of MEPs in the Older group, at least in visit-A. (ii) The finding that the Younger group, but not the Older group, showed metaplastic-like changes at T10 could be due to age-related differences in the priming effect of TBS (Opie et al., 2017), i.e., a stronger priming effect of cTBS in visit-A among younger participants.

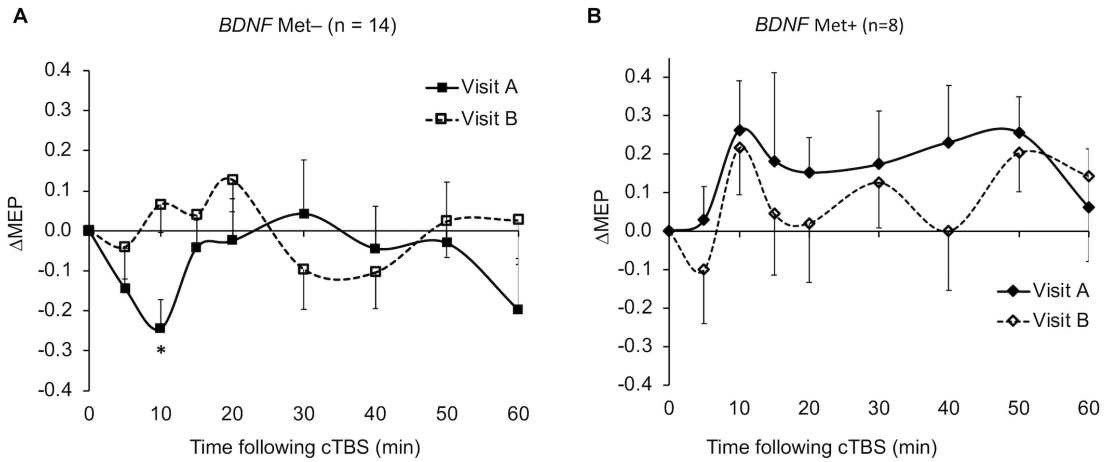

FIGURE 4 | Average ΔMEPs recorded from the right FDI muscle at 5 to 60 min following cTBS of the left primary motor cortex in two identical visits in the *BDNF* Met– **(A)** and Met+ **(B)** groups. *The ΔMEPs in the *BDNF* Met– group were significantly less than zero at T10 in visit-A (P_{FDR} = 0.042), but not at any other time point in either visit (*p*'s > 0.14). The ΔMEPs in the *BDNF* Met+ group were not significantly different from zero at any time point in either visit (P_{FDR}'s > 0.05). Error bars represent standard error of the mean. *BDNF*, brain-derived neurotrophic factor; *BDNF* Met–, Val66Val; *BDNF* Met+, Val66Met; cTBS, continuous theta-burst stimulation; FDR, false discovery rate; ΔMEP, natural log-transformed, baseline-corrected; MEP amplitude; MEP, motor evoked potential; Met, metionine; Val, valine.

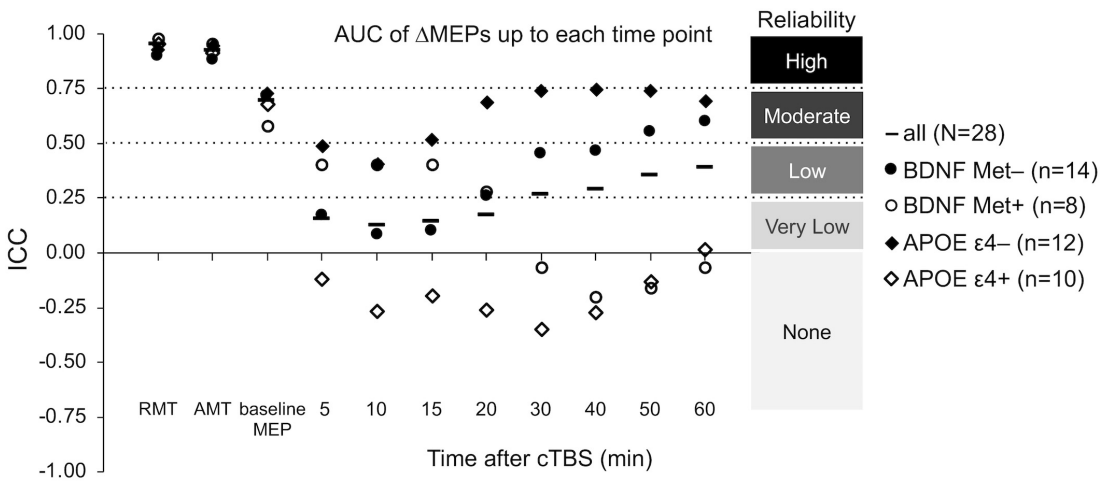

FIGURE 5 | Test–retest reliability of baseline neurophysiological measures and post-cTBS ΔMEP measures separately in the *BDNF* Met–/Met+ and *APOE* ε4–/ε4+ groups. AUC of ΔMEPs were calculated as the summed products of the average ΔMEP across each two consecutive time-points and the time in minutes between them over T0–T10, T0–15, . . . , T0–T60 intervals (marked by their end time point on the abscissa). The ICC values of RMT, AMT, and baseline MEP amplitude were not significantly different between the two *BDNF* groups (*p*'s > 0.19) or the two *APOE* groups (*p*'s > 0.16). Maximum suppression, maximum modulation, and the AUC of ΔMEPs over T0–T30 and beyond were significantly more reliable in the *BDNF* Met– group than in the *BDNF* Met+ group (P_{FDR}'s < 0.032). The reliability of other cumulative ΔMEP measures was not significantly different between the two *BDNF* groups (P_{FDR} > 0.208). All the AUC measures were significantly more reliable in the *APOE* ε4– group than in the *APOE* ε4+ group (P_{FDR}'s < 0.021). The maximum suppression, maximum modulation were not significantly different between the two *APOE* groups (P_{FDR}'s > 0.27). AMT, active motor threshold; *APOE*, apolipoprotein E; *APOE* ε4+, ε2/ε4 or ε3/ε4 genotype; *APOE* ε4–, ε2/ε3 or ε3/ε3 genotype; AUC, area under-the-curve; *BDNF*, brain-derived neurotrophic factor; *BDNF* Met–, Val66Val; *BDNF* Met+, Val66Met; cTBS, continuous theta-burst stimulation; FDR, false discovery rate; ICC, intraclass correlation coefficient; ΔMEP, natural log-transformed, baseline-corrected MEP amplitude; MEP, motor evoked potential; Met, metionine; RMT, resting motor threshold; T0–T*n*, over the first *n* minutes following cTBS; Val, valine.

Similarly, the finding that despite comparable ICCs of baseline neurophysiological measures in the two age groups, cTBS aftereffects were substantially less reliable in older participants (**Figure 3**) could be due to the age-related decrease in the efficiency of GABAergic synaptic transmission reported in animal studies (Milbrandt et al., 1994; Billard et al., 1995; McQuail et al., 2012). These results indicate that in order to retain adequate power to detect differences in cTBS measures of plasticity in future studies, it may be necessary to adjust effect sizes separately for younger and older age groups.

BDNF and *APOE* Polymorphisms and Reliability of cTBS Aftereffects

Despite comparable ICC values of RMT, AMT, and baseline MEP amplitude in *BDNF* Met– and Met+ groups, cTBS aftereffects at several time points and most cumulative measures of cTBS aftereffects were substantially more reliable in *BDNF* Met– participants than in Met+ participants (**Figure 5**). This pattern of results could be due to the following: *BDNF* Met carrier status is known to be associated with impaired *N*-Methyl-D-aspartic acid- (NMDA-)dependent LTD (Woo et al., 2005), aberrant GABAergic synaptic transmission (Abidin et al., 2008), reduced cTBS-induced inhibition of MEPs (Chung et al., 2016), and "paradoxical" cTBS-induced facilitation of MEPs in visit-A reported in our previous study (Jannati et al., 2017) and a few other studies (Gentner et al., 2008; Goldsworthy et al., 2012; Hellriegel et al., 2012; Brownjohn et al., 2014). The finding that *BDNF* Met+ participants showed MEP facilitation, at least numerically, at T10 in both visits (**Figure 4B**) supports an association between *BDNF* Met+ status and facilitatory response to cTBS at T10 in the present sample. The noticeably lower test–retest reliability of cTBS aftereffects in *BDNF* Met+ participants (**Figure 5**) could be due to the less-efficient cTBS-induced plasticity caused by aberrant GABAergic inhibition (Abidin et al., 2008), assumed to be involved in the LTD-like effects of cTBS (Stagg et al., 2009; Trippe et al., 2009).

Despite comparable ICC values of RMT, AMT, and baseline MEP amplitude in *APOE* ε4– and ε4+ participants, cTBS aftereffects at several time points and most cumulative measures of cTBS aftereffects were substantially more reliable in *APOE* ε4– participants than in *APOE* ε4+ participants (**Figure 5**). These results could be due to the influence of *APOE* ε4 on NMDA-mediated synaptic plasticity, which has been found to be involved in TBS aftereffects (Huang et al., 2007; Chen et al., 2010). These results are also consistent with the less-efficient rTMS-induced activation of brain networks in *APOE* ε4 carriers (Peña-Gomez et al., 2012).

The small number of participants in the *BDNF* and *APOE* subgroups study limits the generalizability of the present findings on genetic influences on the test–retest reliability of cTBS measures. Assuming that the noticeable differences in reliability of cTBS aftereffects in *BDNF* and *APOE* subgroups observed here (**Figure 5**) are confirmed in future studies, it would be advantageous to consider the expected proportions of *BDNF* and *APOE* subgroups and adjust effect sizes for each SNP subgroup accordingly. For example, the minor allele frequencies of rs6265 (*BDNF*), rs429358 (*APOE*), and rs7412 (*APOE*) SNPs in the admixed American population in the 1000 Genomes Project (Auton et al., 2015) are 0.1527, 0.1037, and 0.0476, respectively. As long as that the SNP frequencies among participants do not significantly deviate from Hardy–Weinberg equilibrium proportions (Guo and Thompson, 1992; Wigginton et al., 2005), these frequencies provide good approximations to the frequencies of minor *BDNF* and *APOE* alleles in future cTBS studies.

In comparisons of test–retest reliability of cTBS measures between age or genetic subgroups, the finding that the subgroups in each case were comparable in gender, race/ethnicity, handedness, and the reliability of baseline neurophysiological measures indicates that differences in heterogeneity of demographic factors and baseline cortical excitability did not play a major role in the observed differences in test–retest reliability of cTBS aftereffects.

In addition to considering age, genetic polymorphisms, inter-visit interval (Fried et al., 2017), the time of day (Cohen et al., 2005), and the use of neuronavigation (Julkunen et al., 2009), other factors that could improve the test–retest reliability of TMS measures include: ensuring comparable blood glucose levels and caffeine intake before and during each visit (Specterman et al., 2005; Cerqueira et al., 2006; Badawy et al., 2013), comparable amount and quality of sleep the night before each visit (Civardi et al., 2001; Kreuzer et al., 2011), comparable intensity and duration of exercise before each visit (Samii et al., 1997; Lentz and Nielsen, 2002), comparable phase of the menstrual cycle across visits (Smith et al., 1999; Hattemer et al., 2007), the use of robotic arms such as the TMS-Robot (Axilum Robotics, Schiltigheim, France), which can reduce trial-to-trial variability of MEP amplitude (Foucher et al., 2012), comparable baseline MEP amplitude across plasticity visits (Fried et al., 2017), and implementing closed-loop systems that trigger TMS pulses timed to real-time, EEG-defined indices of brain states (Zrenner et al., 2016, 2018).

CONCLUSION

The present study assessed the test–retest reliability of cTBS aftereffects in healthy adults. cTBS aftereffects at most individual time points had low to moderate reliability. Cumulative cTBS measures over the first 30 min and beyond were relatively more reliable. Effect sizes adjusted for reliability of cTBS aftereffects are provided to help future studies retain adequate power for comparing M1 cTBS responses between healthy and clinical populations. Those calculations resulted in adjustment of several large and medium effect sizes to medium and small effect sizes, respectively, thereby substantially increasing the estimates of the required sample size to detect a significant difference in cTBS responses between healthy and clinical populations. Exploratory analyses found cTBS aftereffects were substantially more reliable in younger participants (age < 35 years) and those with *BDNF* Met– and *APOE* ε4– genotypes.

ETHICS STATEMENT

This study was approved by the Institutional Review Board at Beth Israel Deaconess Medical Center in accordance with the Declaration of Helsinki. All participants provided written informed consent prior to enrollment and received monetary compensation upon completion.

AUTHOR CONTRIBUTIONS

AJ, AR, and AP-L conceived and designed the study. AJ and GB collected the data. AJ analyzed the data and drafted the manuscript. AJ, PF, AR, and AP-L interpreted the data.

All authors revised the manuscript, approved the final version, and agreed to be accountable for the content of the work.

FUNDING

This study was primarily funded by the National Institutes of Health (NIH R01 MH100186). AJ was further supported by postdoctoral fellowships from the Natural Sciences and Engineering Research Council of Canada (NSERC 454617) and the Canadian Institutes of Health Research (CIHR 41791). PF was supported in part by the NIH (R21 NS082970, R21 AG051846). LO was further supported by the Simons Foundation Autism Research Initiative (SFARI) and the Nancy Lurie Marks Family Foundation. AR was further supported by the NIH (R01 NS088583), The Boston Children's Hospital Translational Research Program, Autism Speaks, Massachusetts Life Sciences, The Assimon Family, Brainsway, CRE Medical, Eisai, Neuroelectrics, Roche, Sage Therapeutics and Takeda Medical. AP-L was further supported by the Sidney R. Baer Jr. Foundation, the NIH (R01 HD069776, R01 NS073601, R21 MH099196, R21 NS085491, R21 HD07616), the Football Players Health Study at Harvard University, and Harvard Catalyst | The Harvard Clinical and Translational Science Center (NIH NCRR and NCATS, UL1 RR025758). The content is solely the responsibility of the authors and does not necessarily represent the official views of Harvard Catalyst, Harvard University and its affiliated academic health care centers, or any of the listed granting agencies.

ACKNOWLEDGMENTS

We thank Stephanie Changeau, Aaron Boes, and Simon Laganiere (Beth Israel Deaconess Medical Center) for assistance with physical/neurological examinations, and Ann Connor and Joanna Macone (Beth Israel Deaconess Medical Center) for regulatory oversight and compliance, and for assistance with evaluation of participants' health and medical history.

REFERENCES

Abidin, I., Eysel, U. T., Lessmann, V., and Mittmann, T. (2008). Impaired GABAergic inhibition in the visual cortex of brain-derived neurotrophic factor heterozygous knockout mice: GABA release is impaired in visual cortex of BDNF heterozygous KO mice. *J. Physiol.* 586, 1885–1901. doi: 10.1113/jphysiol.2007.148627

Antal, A., Chaieb, L., Moliadze, V., Monte-Silva, K., Poreisz, C., Thirugnanasambandam, N., et al. (2010). Brain-derived neurotrophic factor (BDNF) gene polymorphisms shape cortical plasticity in humans. *Brain Stimul.* 3, 230–237. doi: 10.1016/j.brs.2009.12.003

Auton, A., Abecasis, G. R., Altshuler, D. M., Durbin, R. M., Abecasis, G. R., Bentley, D. R., et al. (2015). A global reference for human genetic variation. *Nature* 526, 68–74. doi: 10.1038/nature15393

Badawy, R. A. B., Vogrin, S. J., Lai, A., and Cook, M. J. (2013). Cortical excitability changes correlate with fluctuations in glucose levels in patients with epilepsy. *Epilepsy Behav.* 27, 455–460. doi: 10.1016/j.yebeh.2013.03.015

Barker, A. T., Jalinous, R., and Freeston, I. L. (1985). Non-invasive magnetic stimulation of human motor cortex. *Lancet* 325, 1106–1107. doi: 10.1016/S0140-6736(85)92413-4

Bastani, A., and Jaberzadeh, S. (2012). A higher number of TMS-elicited mep from a combined hotspot improves intra- and inter-session reliability of the upper limb muscles in healthy individuals. *PLoS One* 7:e47582. doi: 10.1371/journal.pone.0047582

Benjamini, Y., and Hochberg, Y. (1995). Controlling the false discovery rate: a practical and powerful approach to multiple testing. *J. R. Stat. Soc. B* 57, 289–300. doi: 10.1111%2Fj.2517-6161.1995.tb02031.x

Benjamini, Y., and Yekutieli, D. (2001). The control of the false discovery rate in multiple testing under dependency. *Ann. stat.* 29, 1165–1188. doi: 10.1186/1471-2105-9-114

Billard, J., Lamour, Y., and Dutar, P. (1995). Decreased monosynaptic GABAB-mediated inhibitory postsynaptic potentials in hippocampal CA1 pyramidal cells in the aged rat: pharmacological characterization and possible mechanisms. *J. Neurophysiol.* 74, 539–546. doi: 10.1152%2Fjn.1995.74.2.539

Brownjohn, P. W., Reynolds, J. N. J., Matheson, N., Fox, J., and Shemmell, J. B. H. (2014). The Effects of individualized theta burst stimulation on the excitability of the human motor system. *Brain Stimul.* 7, 260–268. doi: 10.1016/j.brs.2013.12.007

Cantone, M., Di Pino, G., Capone, F., Piombo, M., Chiarello, D., Cheeran, B., et al. (2014). The contribution of transcranial magnetic stimulation in the diagnosis and in the management of dementia. *Clin. Neurophysiol.* 125, 1509–1532. doi: 10.1016/j.clinph.2014.04.010

Carrette, S., Boon, P., Dekeyser, C., Klooster, D. C. W., Carrette, E., Meurs, A., et al. (2016). Repetitive transcranial magnetic stimulation for the treatment of refractory epilepsy. *Expert Rev. Neurother.* 16, 1093–1110. doi: 10.1080/14737175.2016.1197119

Carroll, T. J., Riek, S., and Carson, R. G. (2001). Reliability of the input–output properties of the cortico-spinal pathway obtained from transcranial magnetic and electrical stimulation. *J. Neurosci. Methods* 112, 193–202. doi: 10.1016/S0165-0270(01)00468-X

Cazzoli, D., Muri, R. M., Schumacher, R., von Arx, S., Chaves, S., Gutbrod, K., et al. (2012). Theta burst stimulation reduces disability during the activities of daily living in spatial neglect. *Brain* 135, 3426–3439. doi: 10.1093/brain/aws182

Cerqueira, V., de Mendonça, A., Minez, A., Dias, A. R., and de Carvalho, M. (2006). Does caffeine modify corticomotor excitability? *Neurophysiol. Clin.* 36, 219–226. doi: 10.1016/j.neucli.2006.08.005

Chang, W. H., Bang, O. Y., Shin, Y.-I., Lee, A., Pascual-Leone, A., and Kim, Y.-H. (2014). BDNF polymorphism and differential rTMS effects on motor recovery of stroke patients. *Brain Stimul.* 7, 553–558. doi: 10.1016/j.brs.2014.03.008

Cheeran, B. J., Ritter, C., Rothwell, J. C., and Siebner, H. R. (2009). Mapping genetic influences on the corticospinal motor system in humans. *Neuroscience* 164, 156–163. doi: 10.1016/j.neuroscience.2009.01.054

Cheeran, B. J., Talelli, P., Mori, F., Koch, G., Suppa, A., Edwards, M., et al. (2008). A common polymorphism in the brain-derived neurotrophic factor gene (BDNF) modulates human cortical plasticity and the response to rTMS: *BNDF* polymorphism modulates response to rTMS. *J. Physiol.* 586, 5717–5725. doi: 10.1113/jphysiol.2008.159905

Chen, Y., Durakoglugil, M. S., Xian, X., and Herz, J. (2010). ApoE4 reduces glutamate receptor function and synaptic plasticity by selectively impairing ApoE receptor recycling. *Proc. Natl. Acad. Sci. U.S.A.* 107, 12011–12016. doi: 10.1073/pnas.0914984107

Christie, A., Fling, B., Crews, R. T., Mulwitz, L. A., and Kamen, G. (2007). Reliability of motor-evoked potentials in the ADM muscle of older adults. *J. Neurosci. Methods* 164, 320–324. doi: 10.1016/j.jneumeth.2007.05.011

Chuang, W.-L., Huang, Y.-Z., Lu, C.-S., and Chen, R.-S. (2014). Reduced cortical plasticity and GABAergic modulation in essential tremor. *Mov. Disord.* 29, 501–507. doi: 10.1002/mds.25809

Chung, S. W., Hill, A. T., Rogasch, N. C., Hoy, K. E., and Fitzgerald, P. B. (2016). Use of theta-burst stimulation in changing excitability of motor cortex: a systematic review and meta-analysis. *Neurosci. Biobehav. Rev.* 63, 43–64. doi: 10.1016/j.neubiorev.2016.01.008

Civardi, C., Boccagni, C., Vicentini, R., Bolamperti, L., Tarletti, R., Varrasi, C., et al. (2001). Cortical excitability and sleep deprivation: a transcranial magnetic stimulation study. *J. Neurol. Neurosurg. Psychiatry* 71, 809–812. doi: 10.1136/jnnp.71.6.809

Cohen, D. A., Pascual-Leone, A., Press, D. Z., and Robertson, E. M. (2005). Off-line learning of motor skill memory: a double dissociation of goal and movement. *Proc. Natl Acad. Sci. U.S.A.* 102, 18237–18241. doi: 10.1073/pnas.0506072102

Cohen, J. (1988). *Statistical Power Analysis for the Behavioral Sciences*. Hilsdale. NJ: Lawrence Earlbaum Associates.

Cohen, J. (1992). A power primer. *Psychol. Bull.* 112, 155–159.

Crum, R. M., Anthony, J. C., Bassett, S. S., and Folstein, M. F. (1993). Population-based norms for the mini-mental state examination by age and educational level. *JAMA* 269, 2386–2391. doi: 10.1001/jama.1993.03500180078038

Davila-Pérez, P., Jannati, A., Fried, P. J., Cudeiro Mazaira, J., and Pascual-Leone, A. (2018). The effects of waveform and current direction on the efficacy and test–retest reliability of transcranial magnetic stimulation. *Neuroscience* 393, 97–109. doi: 10.1016/j.neuroscience.2018.09.044

Di Lazzaro, V., Capone, F., Di Pino, G., Pellegrino, G., Florio, L., Zollo, L., et al. (2016). Combining robotic training and non-invasive brain stimulation in severe upper limb-impaired chronic stroke patients. *Front. Neurosci.* 10:88. doi: 10.3389/fnins.2016.00088

Di Lazzaro, V., Pellegrino, G., Di Pino, G., Corbetto, M., Ranieri, F., Brunelli, N., et al. (2015). Val66Met BDNF gene polymorphism influences human motor cortex plasticity in acute stroke. *Brain Stimul.* 8, 92–96. doi: 10.1016/j.brs.2014.08.006

Di Lazzaro, V., Rothwell, J. C., Talelli, P., Capone, F., Ranieri, F., Wallace, A. C., et al. (2013). Inhibitory theta burst stimulation of affected hemisphere in chronic stroke: a proof of principle, sham-controlled study. *Neurosci. Lett.* 553, 148–152. doi: 10.1016/j.neulet.2013.08.013

DNA Genotek Inc. (2015). *Laboratory Protocol for Manual Purification of DNA from 0.5 mL of Sample*. Available at: http://www.dnagenotek.com/US/pdf/PD-PR-006.pdf (accessed January 12, 2016).

Eberle, M.-C., Wildgruber, D., Wasserka, B., Fallgatter, A. J., and Plewnia, C. (2010). Relief from chronic intractable auditory hallucinations after long-term bilateral theta burst stimulation. *Am. J. Psychiatry* 167, 1410–1410. doi: 10.1176/appi.ajp.2010.10070988

Fleming, M. K., Sorinola, I. O., Newham, D. J., Roberts-Lewis, S. F., and Bergmann, J. H. M. (2012). The effect of coil type and navigation on the reliability of transcranial magnetic stimulation. *IEEE Trans. Neural Syst. Rehabil. Eng.* 20, 617–625. doi: 10.1109/TNSRE.2012.2202692

Folstein, M. F., Folstein, S. E., and McHugh, P. R. (1975). Mini-mental state". A practical method for grading the cognitive state of patients for the clinician. *J. Psychiatr. Res.* 12, 189–198.

Forogh, B., Yazdi-Bahri, S.-M., Ahadi, T., Fereshtehnejad, S.-M., and Raissi, G. R. (2014). Comparison of two protocols of transcranial magnetic stimulation for treatment of chronic tinnitus: a randomized controlled clinical trial of burst repetitive versus high-frequency repetitive transcranial magnetic stimulation. *Neurol. Sci.* 35, 227–232. doi: 10.1007/s10072-013-1487-5

Foucher, J., Lorgouilloux, K., Turek, J., Pham, B.-T., Elowe, J., Bayle, B., et al. (2012). "Robotic assistance in coil positioning improves reliability and comfort," in *Proceedings of the 3rd Annual Conference of the German Society for Brain Stimulation - Modulating Emotions*, (Berlin).

Fox, M. D., Halko, M. A., Eldaief, M. C., and Pascual-Leone, A. (2012). Measuring and manipulating brain connectivity with resting state functional connectivity magnetic resonance imaging (fcMRI) and transcranial magnetic stimulation (TMS). *NeuroImage* 62, 2232–2243. doi: 10.1016/j.neuroimage.2012.03.035

Freitas, C., Mondragón-Llorca, H., and Pascual-Leone, A. (2011). Noninvasive brain stimulation in Alzheimer's disease: systematic review and perspectives for the future. *Exp. Gerontol.* 46, 611–627. doi: 10.1016/j.exger.2011.04.001

Fried, P. J., Jannati, A., Davila-Pérez, P., and Pascual-Leone, A. (2017). Reproducibility of single-pulse, paired-pulse, and intermittent theta-burst tms measures in healthy aging, type-2 diabetes, and alzheimer's disease. *Front. Aging Neurosci.* 9:263. doi: 10.3389/fnagi.2017.00263

Fried, P. J., Schilberg, L., Brem, A.-K., Saxena, S., Wong, B., Cypess, A. M., et al. (2016). Humans with type-2 diabetes show abnormal long-term potentiation-like cortical plasticity associated with verbal learning deficits. *J. Alzheimer's Dis.* 55, 89–100. doi: 10.3233/JAD-160505

Friedman, H. (1968). Magnitude of experimental effect and a table for its rapid estimation. *Psychol. Bull.* 70, 245–251. doi: 10.1037%2Fh0026258

Gentner, R., Wankerl, K., Reinsberger, C., Zeller, D., and Classen, J. (2008). Depression of human corticospinal excitability induced by magnetic theta-burst stimulation: evidence of rapid polarity-reversing metaplasticity. *Cereb. Cortex* 18, 2046–2053. doi: 10.1093/cercor/bhm239

Goldsworthy, M. R., Müller-Dahlhaus, F., Ridding, M. C., and Ziemann, U. (2014). Inter-subject variability of LTD-like plasticity in human motor cortex: a matter of preceding motor activation. *Brain Stimul.* 7, 864–870. doi: 10.1016/j.brs.2014.08.004

Goldsworthy, M. R., Pitcher, J. B., and Ridding, M. C. (2012). The application of spaced theta burst protocols induces long-lasting neuroplastic changes in the human motor cortex. *Eur. J. Neurosci.* 35, 125–134. doi: 10.1111/j.1460-9568.2011.07924.x

Guerra, A., López-Alonso, V., Cheeran, B., and Suppa, A. (2017). Variability in non-invasive brain stimulation studies: reasons and results. *Neurosci. Lett.* doi: 10.1016/j.neulet.2017.12.058 [Epub ahead of print],

Guo, S. W., and Thompson, E. A. (1992). Performing the exact test of Hardy-Weinberg proportion for multiple alleles. *Biometrics* 48, 361–372. doi: 10.2307/2532296

Hallett, M. (2007). Transcranial magnetic stimulation: a primer. *Neuron* 55, 187–199. doi: 10.1016/j.neuron.2007.06.026

Hamada, M., Murase, N., Hasan, A., Balaratnam, M., and Rothwell, J. C. (2013). The role of interneuron networks in driving human motor cortical plasticity. *Cereb. Cortex* 23, 1593–1605. doi: 10.1093/cercor/bhs147

Harrell, F. E. Jr. (2015). *Regression Modeling Strategies: with Applications to Linear Models, Logistic and Ordinal Regression, and Survival Analysis*. Berlin: Springer.

Hattemer, K., Knake, S., Reis, J., Rochon, J., Oertel, W. H., Rosenow, F., et al. (2007). Excitability of the motor cortex during ovulatory and anovulatory cycles: a transcranial magnetic stimulation study. *Clin. Endocrinol.* 66, 387–393. doi: 10.1111/j.1365-2265.2007.02744.x

Heidegger, T., Hansen-Goos, O., Batlaeva, O., Annak, O., Ziemann, U., and Lötsch, J. (2017). A data-driven approach to responder subgroup identification after paired continuous theta burst stimulation. *Front. Hum. Neurosci.* 11:382. doi: 10.3389/fnhum.2017.00382

Hellriegel, H., Schulz, E. M., Siebner, H. R., Deuschl, G., and Raethjen, J. H. (2012). Continuous theta-burst stimulation of the primary motor cortex in essential tremor. *Clin. Neurophysiol.* 123, 1010–1015. doi: 10.1016/j.clinph.2011.08.033

Hermsen, A., Haag, A., Duddek, C., Balkenhol, K., Bugiel, H., Bauer, S., et al. (2016). Test–retest reliability of single and paired pulse transcranial magnetic stimulation parameters in healthy subjects. *J. Neurol. Sci.* 362, 209–216. doi: 10.1016%2Fj.jns.2016.01.039

Hinder, M. R., Goss, E. L., Fujiyama, H., Canty, A. J., and Garry, M. I. (2014). Inter- and intra-individual variability following intermittent theta burst stimulation: implications for rehabilitation and recovery. *Brain Stimul.* 7, 365–371. doi: 10.1016/j.brs.2014.01.004

Hordacre, B., Goldsworthy, M. R., Vallence, A.-M., Darvishi, S., Moezzi, B., Hamada, M., et al. (2017). Variability in neural excitability and plasticity induction in the human cortex: a brain stimulation study. *Brain Stimul.* 10, 588–595. doi: 10.1016/j.brs.2016.12.001

Huang, Y.-Z., Chen, R.-S., Rothwell, J. C., and Wen, H.-Y. (2007). The after-effect of human theta burst stimulation is NMDA receptor dependent. *Clin. Neurophysiol.* 118, 1028–1032. doi: 10.1016/j.clinph.2007.01.021

Huang, Y.-Z., Edwards, M. J., Rounis, E., Bhatia, K. P., and Rothwell, J. C. (2005). Theta burst stimulation of the human motor cortex. *Neuron* 45, 201–206. doi: 10.1016/j.neuron.2004.12.033

Hunter, J. E., and Schmidt, F. L. (1994). "Correcting for sources of artificial variation across studies," in *The Handbook of Research Synthesis*, eds H. Cooper and L. V. Hedge (New York, NY: Russell Sage Foundation), 323–336.

Iezzi, E., Conte, A., Suppa, A., Agostino, R., Dinapoli, L., Scontrini, A., et al. (2008). Phasic voluntary movements reverse the aftereffects of subsequent theta-burst stimulation in humans. *J. Neurophysiol.* 100, 2070–2076. doi: 10.1152/jn.90521.2008

Jannati, A., Block, G., Oberman, L. M., Rotenberg, A., and Pascual-Leone, A. (2017). Interindividual variability in response to continuous theta-burst stimulation in healthy adults. *Clin. Neurophysiol.* 128, 2268–2278. doi: 10.1016/j.clinph.2017.08.023

Julkunen, P., Säisänen, L., Danner, N., Niskanen, E., Hukkanen, T., Mervaala, E., et al. (2009). Comparison of navigated and non-navigated transcranial magnetic stimulation for motor cortex mapping, motor threshold and motor evoked potentials. *NeuroImage* 44, 790–795. doi: 10.1016/j.neuroimage.2008.09.040

Kamen, G. (2004). Reliability of motor-evoked potentials during resting and active contraction conditions. *Med. Sci. Sports & Exercise* 36, 1574–1579. doi: 10.1249%2F01.mss.0000139804.02576.6a

Kenny, D. A., Mannetti, L., Pierro, A., Livi, S., and Kashy, D. A. (2002). The statistical analysis of data from small groups. *J. Personal. Soc. Psychol.* 83, 126–137. doi: 10.1037%2F%2F0022-3514.83.1.126

Kimiskidis, V. K., Papagiannopoulos, S., Sotirakoglou, K., Kazis, D. A., Dimopoulos, G., Kazis, A., et al. (2004). The repeatability of corticomotor threshold measurements. *Neurophysiol. Clin.* 34, 259–266. doi: 10.1016/j.neucli.2004.10.002

Koch, G., Bonni, S., Giacobbe, V., Bucchi, G., Basile, B., Lupo, F., et al. (2012). Theta-burst stimulation of the left hemisphere accelerates recovery of hemispatial neglect. *Neurology* 78, 24–30. doi: 10.1212/WNL.0b013e31823ed08f

Koch, G., Brusa, L., Carrillo, F., Lo Gerfo, E., Torriero, S., Oliveri, M., et al. (2009). Cerebellar magnetic stimulation decreases levodopa-induced dyskinesias in Parkinson disease. *Neurology* 73, 113–119. doi: 10.1212/WNL.0b013e3181ad5387

Kreuzer, P., Langguth, B., Popp, R., Raster, R., Busch, V., Frank, E., et al. (2011). Reduced intra-cortical inhibition after sleep deprivation: a transcranial magnetic stimulation study. *Neurosci. Lett.* 493, 63–66. doi: 10.1016/j.neulet.2011.02.044

Lee, M., Kim, S. E., Kim, W. S., Lee, J., Yoo, H. K., Park, K.-D., et al. (2013). Interaction of motor training and intermittent theta burst stimulation in modulating motor cortical plasticity: influence of BDNF Val66Met polymorphism. *PLoS One* 8:e57690. doi: 10.1371/journal.pone.0057690

Lentz, M., and Nielsen, J. F. (2002). Post-exercise facilitation and depression of M wave and motor evoked potentials in healthy subjects. *Clin. Neurophysiol.* 113, 1092–1098. doi: 10.1016/S1388-2457(02)00031-7

Li, C.-T., Chen, M.-H., Juan, C.-H., Huang, H.-H., Chen, L.-F., Hsieh, J.-C., et al. (2014). Efficacy of prefrontal theta-burst stimulation in refractory depression: a randomized sham-controlled study. *Brain* 137, 2088–2098. doi: 10.1093/brain/awu109

Liu, H., and Au-Yeung, S. S. Y. (2014). Reliability of transcranial magnetic stimulation induced corticomotor excitability measurements for a hand muscle in healthy and chronic stroke subjects. *J. Neurol. Sci.* 341, 105–109. doi: 10.1016/j.jns.2014.04.012

Livingston, S. C., and Ingersoll, C. D. (2008). Intra-rater reliability of a transcranial magnetic stimulation technique to obtain motor evoked potentials. *Int. J. Neurosci.* 118, 239–256. doi: 10.1080/00207450701668020

López-Alonso, V., Cheeran, B., Río-Rodríguez, D., and Fernández-del-Olmo, M. (2014). Inter-individual variability in response to non-invasive brain stimulation paradigms. *Brain Stimul.* 7, 372–380. doi: 10.1016/j.brs.2014.02.004

Maeda, F., Keenan, J. P., Tormos, J. M., Topka, H., and Pascual-Leone, A. (2000). Modulation of corticospinal excitability by repetitive transcranial magnetic stimulation. *Clin. Neurophysiol.* 111, 800–805. doi: 10.1016%2Fs1388-2457%2899%2900323-5

McClintock, S. M., Freitas, C., Oberman, L. M., Lisanby, S. H., and Pascual-Leone, A. (2011). Transcranial magnetic stimulation: a neuroscientific probe of cortical function in schizophrenia. *Biol. Psychiatry* 70, 19–27. doi: 10.1016/j.biopsych.2011.02.031

McDonnell, M. N., Ridding, M. C., and Miles, T. S. (2004). Do alternate methods of analysing motor evoked potentials give comparable results? *J. Neurosci. Methods* 136, 63–67. doi: 10.1016/j.jneumeth.2003.12.020

McGraw, K. O., and Wong, S. P. (1996). Forming inferences about some intraclass correlation coefficients. *Psychol. Methods* 1, 30–46. doi: 10.1037%2F1082-989x.1.1.30

McQuail, J. A., Bañuelos, C., LaSarge, C. L., Nicolle, M. M., and Bizon, J. L. (2012). GABAB receptor GTP-binding is decreased in the prefrontal cortex but not the hippocampus of aged rats. *Neurobiol. Aging* 33, 1124.e1–1124.e12. doi: 10.1016/j.neurobiolaging.2011.11.011

Milbrandt, J. C., Albin, R. L., and Caspary, D. M. (1994). Age-related decrease in GABAB receptor binding in the Fischer 344 rat i inferior colliculus. *Neurobiol. Aging* 15, 699–703.

Mori, F., Rossi, S., Piccinin, S., Motta, C., Mango, D., Kusayanagi, H., et al. (2013). Synaptic plasticity and PDGF signaling defects underlie clinical progression in multiple sclerosis. *J. Neurosci.* 33, 19112–19119. doi: 10.1523/JNEUROSCI.2536-13.2013

Nettekoven, C., Volz, L. J., Kutscha, M., Pool, E.-M., Rehme, A. K., Eickhoff, S. B., et al. (2014). Dose-dependent effects of theta burst rTMS on cortical excitability and resting-state connectivity of the human motor system. *J. Neurosci.* 34, 6849–6859. doi: 10.1523/JNEUROSCI.4993-13.2014

Nettekoven, C., Volz, L. J., Leimbach, M., Pool, E.-M., Rehme, A. K., Eickhoff, S. B., et al. (2015). Inter-individual variability in cortical excitability and motor network connectivity following multiple blocks of rTMS. *NeuroImage* 118, 209–218. doi: 10.1016/j.neuroimage.2015.06.004

Ngomo, S., Leonard, G., Moffet, H., and Mercier, C. (2012). Comparison of transcranial magnetic stimulation measures obtained at rest and under active conditions and their reliability. *J. Neurosci. Methods* 205, 65–71. doi: 10.1016/j.jneumeth.2011.12.012

Nichol, K., Deeny, S. P., Seif, J., Camaclang, K., and Cotman, C. W. (2009). Exercise improves cognition and hippocampal plasticity in APOE ε4 mice. *Alzheimers Dementia* 5, 287–294. doi: 10.1016/j.jalz.2009.02.006

NIH Office of Extramural Research (2001). *NIH Policy and Guidelines on the Inclusion of Women and Minorities as Subjects in Clinical Research*. Available at: https://grants.nih.gov/grants/funding/women_min/guidelines_amended_10_2001.htm (accessed February 1, 2016).

Oberman, L., Ifert-Miller, F., Najib, U., Bashir, S., Woollacott, I., Gonzalez-Heydrich, J., et al. (2010). Transcranial magnetic stimulation provides means to assess cortical plasticity and excitability in humans with fragile X syndrome and autism spectrum disorder. *Front. Synaptic Neurosci.* 2:26. doi: 10.3389/fnsyn.2010.00026

Oberman, L. M., Eldaief, M., Fecteau, S., Ifert-Miller, F., Tormos, J. M., and Pascual-Leone, A. (2012). Abnormal modulation of corticospinal excitability in adults with Asperger's syndrome: modulation of excitability in Asperger's. *Eur. J. Neurosci.* 36, 2782–2788. doi: 10.1111/j.1460-9568.2012.08172.x

Oberman, L. M., Ifert-Miller, F., Najib, U., Bashir, S., Gonzalez-Heydrich, J., Picker, J., et al. (2016). Abnormal mechanisms of plasticity and metaplasticity in autism spectrum disorders and fragile X syndrome. *J. Child Adoles. Psychopharmacol.* 26, 617–624. doi: 10.1089/cap.2015.0166

Oberman, L. M., Pascual-Leone, A., and Rotenberg, A. (2014). Modulation of corticospinal excitability by transcranial magnetic stimulation in children and adolescents with autism spectrum disorder. *Front. Hum. Neurosci.* 8:627. doi: 10.3389/fnhum.2014.00627

Opie, G. M., Vosnakis, E., Ridding, M. C., Ziemann, U., and Semmler, J. G. (2017). Priming theta burst stimulation enhances motor cortex plasticity in young but not old adults. *Brain Stimul.* 10, 298–304. doi: 10.1016/j.brs.2017.01.003

Pascual-Leone, A., Amedi, A., Fregni, F., and Merabet, L. B. (2005). The plastic human brain cortex. *Annu. Rev. Neurosci.* 28, 377–401. doi: 10.1146/annurev.neuro.27.070203.144216

Pascual-Leone, A., Freitas, C., Oberman, L., Horvath, J. C., Halko, M., Eldaief, M., et al. (2011). Characterizing brain cortical plasticity and network dynamics across the age-span in health and disease with TMS-EEG and TMS-fMRI. *Brain Topogr.* 24, 302–315. doi: 10.1007/s10548-011-0196-8

Pascual-Leone, A., Valls-Solé, J., Wassermann, E. M., and Hallett, M. (1994). Responses to rapid-rate transcranial magnetic stimulation of the human motor cortex. *Brain* 117, 847–858. doi: 10.1093%2Fbrain%2F117.4.847

Pellicciari, M. C., Miniussi, C., Ferrari, C., Koch, G., and Bortoletto, M. (2016). Ongoing cumulative effects of single TMS pulses on corticospinal excitability: an intra- and inter-block investigation. *Clin. Neurophysiol.* 127, 621–628. doi: 10.1016/j.clinph.2015.03.002

Peña-Gomez, C., Solé-Padullés, C., Clemente, I. C., Junqué, C., Bargalló, N., Bosch, B., et al. (2012). APOE status modulates the changes in network connectivity induced by brain stimulation in non-demented elders. *PLoS One* 7:e51833. doi: 10.1371/journal.pone.0051833

Portney, L. G., and Watkins, M. P. (2009). *Foundations of Clinical Research: Applications to Practice*, 3rd Edn. Upper Saddle River, NJ: Prentice Hall.

Rossi, S., Hallett, M., Rossini, P. M., and Pascual-Leone, A. (2009). Safety, ethical considerations, and application guidelines for the use of transcranial magnetic stimulation in clinical practice and research. *Clin. Neurophysiol.* 120, 2008–2039. doi: 10.1016/j.clinph.2009.08.016

Rossini, P. M., Burke, D., Chen, R., Cohen, L. G., Daskalakis, Z., Di Iorio, R., et al. (2015). Non-invasive electrical and magnetic stimulation of the brain, spinal cord, roots and peripheral nerves: basic principles and procedures for routine clinical and research application. An updated report from an I.F.C.N. Committee. *Clin. Neurophysiol.* 126, 1071–1107. doi: 10.1016/j.clinph.2015.02.001

Samii, A., Wassermann, E. M., and Hallett, M. (1997). Post-exercise depression of motor evoked potentials as a function of exercise duration. *Electroencephalogr. Clin. Neurophysiol.* 105, 352–356. doi: 10.1016/S0924-980X(97)00033-7

Sankarasubramanian, V., Roelle, S. M., Bonnett, C. E., Janini, D., Varnerin, N. M., Cunningham, D. A., et al. (2015). Reproducibility of transcranial magnetic stimulation metrics in the study of proximal upper limb muscles. *J. Electromyogr. Kinesiol.* 25, 754–764. doi: 10.1016/j.jelekin.2015.05.006

Schambra, H. M., Ogden, R. T., Martínez-Hernández, I. E., Lin, X., Chang, Y. B., Rahman, A., et al. (2015). The reliability of repeated TMS measures in older adults and in patients with subacute and chronic stroke. *Front. Cell Neurosci.* 9:335. doi: 10.3389/fncel.2015.00335

Schilberg, L., Schuhmann, T., and Sack, A. T. (2017). Interindividual variability and intraindividual reliability of intermittent theta burst stimulation-induced neuroplasticity mechanisms in the healthy brain. *J. Cogn. Neurosci.* 29, 1022–1032. doi: 10.1162/jocn_a_01100

Smith, M. J., Keel, J. C., Greenberg, B. D., Adams, L. F., Schmidt, P. J., Rubinow, D. A., et al. (1999). Menstrual cycle effects on cortical excitability. *Neurology* 53, 2069–2069. doi: 10.1212%2Fwnl.53.9.2069

Specterman, M., Bhuiya, A., Kuppuswamy, A., Strutton, P., Catley, M., and Davey, N. (2005). The effect of an energy drink containing glucose and caffeine on human corticospinal excitability. *Physiol. Behav.* 83, 723–728. doi: 10.1016/j.physbeh.2004.09.008

Stagg, C. J., Wylezinska, M., Matthews, P. M., Johansen-Berg, H., Jezzard, P., Rothwell, J. C., et al. (2009). Neurochemical effects of theta burst stimulation as assessed by magnetic resonance spectroscopy. *J. Neurophysiol.* 101, 2872–2877. doi: 10.1152/jn.91060.2008

Suppa, A., Huang, Y.-Z., Funke, K., Ridding, M. C., Cheeran, B., Di Lazzaro, V., et al. (2016). Ten years of theta burst stimulation in humans: established knowledge, unknowns and prospects. *Brain Stimul.* 9, 323–335. doi: 10.1016/j.brs.2016.01.006

Suppa, A., Marsili, L., Di Stasio, F., Berardelli, I., Roselli, V., Pasquini, M., et al. (2014). Cortical and brainstem plasticity in Tourette syndrome and obsessive-compulsive disorder. *Mov. Disord.* 29, 1523–1531. doi: 10.1002/mds.25960

Thorndike, R. L., Hagen, E. P., and Sattler, J. M. (1986). *The Stanford-Binet Intelligence Scale: Guide for Administering and Scoring*. Rolling Meadows, IL: Riverside Publishing Company.

Trippe, J., Mix, A., Aydin-Abidin, S., Funke, K., and Benali, A. (2009). Theta burst and conventional low-frequency rTMS differentially affect GABAergic neurotransmission in the rat cortex. *Exp. Brain Res.* 199, 411–421. doi: 10.1007/s00221-009-1961-8

Valero-Cabré, A., Amengual, J. L., Stengel, C., Pascual-Leone, A., and Coubard, O. A. (2017). Transcranial magnetic stimulation in basic and clinical neuroscience: a comprehensive review of fundamental principles and novel insights. *Neurosci. Biobehav. Rev.* 83, 381–404. doi: 10.1016/j.neubiorev.2017.10.006

Valero-Cabré, A., Pascual-Leone, A., and Rushmore, R. J. (2008). Cumulative sessions of repetitive transcranial magnetic stimulation (rTMS) build up facilitation to subsequent TMS-mediated behavioural disruptions. *Eur. J. Neurosci.* 27, 765–774. doi: 10.1111/j.1460-9568.2008.06045.x

Vallence, A.-M., Goldsworthy, M. R., Hodyl, N. A., Semmler, J. G., Pitcher, J. B., and Ridding, M. C. (2015). Inter- and intra-subject variability of motor cortex plasticity following continuous theta-burst stimulation. *Neuroscience* 304, 266–278. doi: 10.1016/j.neuroscience.2015.07.043

Vernet, M., Bashir, S., Yoo, W.-K., Oberman, L. M., Mizrahi, I., Ifert-Miller, F., et al. (2014). Reproducibility of the effects of theta burst stimulation on motor cortical plasticity in healthy participants. *Clin. Neurophysiol.* 125, 320–326. doi: 10.1016/j.clinph.2013.07.004

White, F., Nicoll, J. A. R., Roses, A. D., and Horsburgh, K. (2001). Impaired neuronal plasticity in transgenic mice expressing human apolipoprotein E4 compared to E3 in a model of entorhinal cortex lesion. *Neurobiol. Dis.* 8, 611–625. doi: 10.1006/nbdi.2001.0401

Wigginton, J. E., Cutler, D. J., and Abecasis, G. R. (2005). A note on exact tests of hardy-weinberg equilibrium. *Am. J. Hum. Genet.* 76, 887–893. doi: 10.1086/429864

Wischnewski, M., and Schutter, D. J. L. G. (2015). Efficacy and time course of theta burst stimulation in healthy humans. *Brain Stimul.* 8, 685–692. doi: 10.1016/j.brs.2015.03.004

Woo, N. H., Teng, H. K., Siao, C.-J., Chiaruttini, C., Pang, P. T., Milner, T. A., et al. (2005). Activation of p75NTR by proBDNF facilitates hippocampal long-term depression. *Nat. Neurosci.* 8, 1069–1077. doi: 10.1038/nn1510

Wright, K. (2014). "Adjusting effect sizes in light of reliability estimates," in *Paper Presented at the Annual Meeting of the Southwest Educational Research Association*, (New Orleans, LA).

Zrenner, C., Belardinelli, P., Müller-Dahlhaus, F., and Ziemann, U. (2016). Closed-loop neuroscience and non-invasive brain stimulation: a tale of two loops. *Front. Cell. Neurosci.* 10:92. doi: 10.3389/fncel.2016.00092

Zrenner, C., Desideri, D., Belardinelli, P., and Ziemann, U. (2018). Real-time EEG-defined excitability states determine efficacy of TMS-induced plasticity in human motor cortex. *Brain Stimul.* 11, 374–389. doi: 10.1016/j.brs.2017.11.016

Conflict of Interest Statement: AP-L serves on the scientific advisory boards for Neuronix, Starlab Neuroscience, Neuroelectrics, Constant Therapy, Cognito, NovaVision, and Neosync, and is listed as an inventor on several issued and pending patents on real-time integration of TMS with EEG and MRI. AR is a founder and advisor for Neuromotion, serves on the medical advisory board for NeuroRex, and is listed as an inventor on a patent related to integration of TMS and EEG.

The remaining authors declare that the research was conducted in the absence of any commercial or financial relationships that could be construed as a potential conflict of interest.

frontiers in Neuroscience

OPINION
published: 28 June 2019
doi: 10.3389/fnins.2019.00678

The Two-Fold Ethical Challenge in the Use of Neural Electrical Modulation

*Andrea Lavazza**

Centro Universitario Internazionale, Arezzo, Italy

Keywords: neuroethics, aging, enhancement, tDCS—transcranial direct current stimulation, inequalities

OPEN ACCESS

Edited by:
Olivier David,
Institut National de la Santé et de la Recherche Médicale (INSERM), France

Reviewed by:
Blaise Yvert,
Institut National de la Santé et de la Recherche Médicale (INSERM), France
Marianna Semprini,
Istituto Italiano di Tecnologia, Italy

***Correspondence:**
Andrea Lavazza
lavazza67@gmail.com

Specialty section:
This article was submitted to Neural Technology, a section of the journal Frontiers in Neuroscience

Received: *29 December 2018*
Accepted: *13 June 2019*
Published: *28 June 2019*

Citation:
Lavazza A (2019) The Two-Fold Ethical Challenge in the Use of Neural Electrical Modulation. Front. Neurosci. 13:678. doi: 10.3389/fnins.2019.00678

The use of electrical stimulation to influence biological functions and/or pathological processes in the body has been recently termed "electroceuticals." The most commonly used techniques are "neural electroceuticals," forms of electrical modulation of the brain that seem to represent the new frontier both to treat neurological and psychiatric diseases, when no other effective treatments are available, and to enhance cognitive functions (Kambouris et al., 2014; Reardon, 2014; Miller and Matharu, 2017).

These types of medical interventions have given rise to a wide ethical debate (Pickersgill and Hogle, 2015; Lavazza and Colzato, 2018; Packer et al., 2018). Here I wish to introduce two new challenges bearing important moral implications, which require the careful consideration of the scientific and philosophical community. These challenges can be co-present and can be placed in the same framework of human augmentation and the willingness to go beyond one's own physiological limits. However, it is possible to analytically distinguish them according to their initial conditions and their different scopes, as it will be explained.

The first challenge concerns a possible shift from a mainly therapeutic use of electroceuticals to a use aimed at enhancement. This potential shift is due to the fact that technology has now fulfilled a very ancient human aspiration, that of overcoming one's limits and improving indefinitely. And the effect of this shift could be a segmentation of society between enhanced and non-enhanced individuals, something that goes against the essentially egalitarian project of modern thought (Rawls, 1999; Mason, 2006).

The second challenge concerns the aging tendency and the demographic contraction that characterize European countries and Japan, and which may soon affect other economically developed countries (Lutz et al., 2008; Długosz, 2011; Murray et al., 2018). This trend, over time, will reduce the overall availability of cognitive skills and abilities in those populations, who will have to manage increasingly complex and diversified societies and environments. This mismatch between the needs arising from one's life context and the available resources could push people to resort to electroceuticals as means of strengthening their cognitive abilities, opening up scenarios in which ethical evaluations will have a role to play. Below, I will address these two challenges, giving more space to the first.

GOING BEYOND ONE'S LIMITS

Ever since the *Odyssey*, humans have always desired to alter their minds in a controlled manner through a mix of substances and to go beyond the limits established by brain physiology (Koops et al., 2013). In recent decades, important steps have been taken in this direction, both with new molecules able to act on brain chemistry and with instruments capable of electrically modulating brain activity (Dresler et al., 2018). Scientific consensus on the cognitive enhancement potential of the so-called Non-Invasive Brain Stimulation (NIBS) is not yet unanimous (see Horvath et al., 2015 on one side; Price and Hamilton, 2015 on the other side), but it is undeniable that there is a

great investment in research. A growing amount of research studies have produced at least some results in the field, even with different effects at an inter- and intra-individual level. For example, Transcranial Direct Current Stimulation (tDCS) is a form of neurostimulation that so far has been used on healthy subjects to enhance mathematical cognition, reading, memory, mood, learning, perception, decision making, creativity motivation, and moral reasoning (Chi and Snyder, 2012; Callaway, 2013; Meinzer et al., 2013; Snowball et al., 2013; Parkin et al., 2015). The use of NIBS is very often deemed effective by the public due to wide media coverage and Internet ads (Fitz and Reiner, 2015). However, the road to enhancement is now open and more relevant and consistent results may come both from more in-depth knowledge on the functioning of the nervous system and from more performing devices.

What are the consequences of a greater concentration of medical-scientific skills and resources in the field of cognitive neuroenhancement? Medicine is changing, suggests Harari (2016, ch 9), whose line of reasoning is useful here, even though he does not refer to electroceuticals. Somewhat oversimplifying, it can be said that the vocation of medicine, for most of its history, has been to treat the sick, to restore to a better condition those who saw their health deteriorate or were born with a congenital pathology or deficit. Classical Hippocratic medicine has then recently introduced the idea of disease prevention and the notion of combating the symptoms of aging (Bynum, 2008). This was a conceptual and clinical turning point, which has opened the door to the idea of improving the physical and cognitive status of healthy people, thus fulfilling the human aspiration I mentioned earlier, which had not yet been reflected in medical practice.

From an ethical point of view, caring for the sick—at least in principle—is an egalitarian project, because it envisions a level of health which each person can and should ideally reach, despite the limits of medical knowledge and of material resources. This project goes hand in hand with—and derives from—the social and political idea that Christianity and the Enlightenment have brought onto the Western world, according to which all human beings have equal dignity and rights and deserve the same treatment (despite the many exceptions due to material contingencies and the organization of life in society) (Hunt, 2007).

As Harari emphasizes, enhancing those in good health might instead be an elitist project, because it necessarily ignores universal levels of functioning or performance that are applicable to all (More and Vita-More, 2013). Every individual legitimately seeks to gain an advantage over others by exploiting the means made available by medical research to those who can pay for them. Once a certain level of enhancement has been achieved by the whole—or at least by the majority—of the population, the given technology will be available to everyone in terms of both diffusion and cost, and there will be demand for new and further forms of enhancement. These forms of enhancement will be sought by medical-scientific research within the dynamic that always pushes further the frontier of technical knowledge.

Harari's prediction is that the poorest people in the next 50 years will have much better healthcare than today, whereas the health inequality measured in functioning and physical-cognitive performance might get much worse. Strong inequalities have always been present in the history of mankind, even when enhancement was not even contemplated as a possibility. However, for reasons related to technical progress, today there may be no shared interest in ensuring healthcare to the entire population according to the best current standards.

In the twentieth century many states had an interest in, and the possibility of, integrating the masses in the social fabric, also by universally extending the benefits of modern medicine. In fact, there was the need to have millions of soldiers in good health and well-looked after when injured, while the industry benefited from millions of workers in good physical conditions and able to work in factories for many consecutive hours. These were the years when mass hygiene facilities and vaccination campaigns were introduced, and several epidemics were eradicated (cf. Pinker, 2018).

NEW POTENTIAL INEQUALITIES

The economic and military dynamics of the twenty-first century might be very different from the past. In the era of drones and remote or self-driving military vehicles, mass armies are no longer needed: what is needed are only a few selected super-experts in war technology (Scharre, 2018). The advent of robotics and the use of big data combined with evolving algorithms also make a large part of human work obsolete, so that production tasks can be performed by machines, leaving human beings in charge of more complex activities such as design and supervision (Ford, 2015).

These trends, of which we can already see some indications, could be accentuated and accelerated by the research on cognitive enhancement: the best performing individuals will be the ones to occupy positions of responsibility, as society will want to entrust the most important tasks to those with the best skills (Santoni de Sio et al., 2014). There are also scenarios that seem to come from a dystopian novel and, to the current state of knowledge, are certainly not realistic: such scenarios involve the emergence of superhumans with exceptional physical, emotional and intellectual abilities, which will stand out from the rest of the non-enhanced or less enhanced individuals, because the differences will become not only quantitative but also qualitative, leading to the creation of different groups distinguished by temperament and interests (Bess, 2015).

In fact, quantitative differences concern the increase of cognitive abilities, for example memory. Those who can access these forms of empowerment become high-performing people, who can succeed in the workplace and then improve their condition outperforming those who are not enhanced. Qualitative differences instead are brought on, for example, by genetic modifications thanks to recent techniques such as CRISPR-Cas9 (Lavazza, 2019a). In that case, genetically modified individuals could be different from non-modified individuals in the same way as adults and children or the most educated people and the illiterate ones are different. And social consequences would be predictably very relevant.

The equality project entailed by the material and moral progress of the world so far—which substantially amounts to defeating hunger, diseases and war—aims to guarantee decent living conditions for everyone, so that all people can equally pursue their own life project. Instead, the new goals aiming at overcoming our mortal and uncertain human condition, mainly thanks to technology, can hardly be within everyone's reach and, on the contrary, will often be linked to a privileged condition reserved for a few.

There has certainly been an increase in do-it-yourself use of simple transcranial direct current stimulation (tDCS) devices (Fitz and Reiner, 2015). However, dealing with the use of other latest generation electroceuticals and future more sophisticated devices we will have to address the challenge outlined above. Should we consider prohibiting the use of certain forms of enhancement or should we pursue egalitarian policies, allowing everyone to access electroceuticals? (Lavazza, 2019b). A possible (but debatable) solution is to try to enhance the moral abilities of individuals, to ensure the prevalence of pro-social motives and a general growth of the well-being of individuals and of whole society (Persson and Savulescu, 2012). If this was not possible, one could explore a use of cognitive enhancement according to Rawls's influential view that inequalities are acceptable if they benefit the whole society (Lavazza, 2016). In this sense, cognitively enhancing certain professional figures or public decision-makers will give them a benefit that others will not enjoy but will positively reverberate on the general functioning of society.

MANDATORY ENHANCEMENT?

The second challenge concerning electroceuticals is intertwined with the first, while it has a different scope. The processes of scientific and technological innovation on a global scale, along with the phenomena of social complexification, are undergoing continuous acceleration, which will require a greater availability of cognitive skills to manage this complexity and the associated problems (for example, those related to climate change and to the reduction of natural resources). According to Rindermann (2018), however, cognitive abilities in the Western world could go down due to demographic trends. In many nations, fewer births and a longer life expectancy result in a decline in memory, processing speed, attention, creativity and, therefore, in the capacity for innovation. Furthermore, the most educated and cognitively most capable people normally make fewer children.

It is difficult to quantify the phenomenon, both because it is new and because it is still little studied. However, it is plausible to assume that general aging will cause a decrease in the overall cognitive abilities of society. First, there will be more people over the age of 65, while people under the age of 65 will decrease in number. And it is established that "the normal aging process is associated with declines in certain cognitive abilities, such as processing speed and some aspects of memory, language, visuospatial function, and executive functions" (Harada et al., 2013; cf. also Reichman et al., 2010; Salthouse, 2012; Fechner et al., 2019). Secondly, with the number of elderly people increasing, even if the incidence rate remains fixed, the overall percentage of people suffering from diseases that affect cognition will increase. In the United States today there are about 6 million people with dementia; according to some estimates (Alzheimer's Association, 2019) the number will go up to 14 million in 2050, while the overall population will remain stable or grow slightly.

The idea of making enhancement (and cognitive improvement/rehabilitation for aged people) widespread and perhaps even mandatory also comes from arguments that underline how some emergencies cannot be faced with the cognitive and moral endowments that we have today (Lavazza and Reichlin, 2019). Persson and Savulescu (2012), for example, have stated that humans are ethically unfit to face the challenges of the present age. Their argument rests on the fact that today's humankind is facing two kind of threats "generated by the existence of modern scientific technology: the threats of weapons of mass destruction, especially in the hands of terrorist groups, and of climate change and environmental degradation" (Persson and Savulescu, 2012: 1). According to the authors, humans are not morally equipped to address such global problems within a democratic system, especially when it comes to environmental problems. Consequently, cognitive enhancement, understood as the basis of moral betterment, could become the object of policies that make it strongly recommended, encouraged, or mandatory.

In this framework, the classic suggestion is to increase the educational programs that allow for the enhancement of cognitive abilities, which constitute human capital. Specifically, reference is often made to cognitive training programs such as the reasoning training proposed by Klauer and Phye (2008). But if neurocognitive enhancement proves to be safe and effective, it promises to be quicker and more easily administrable to a greater percentage of the population compared to traditional programs, since it does not require the conscious and prolonged effort of the subject. In the case of a real decline in the cognitive abilities of a society as a whole, neurocognitive intervention via neural electrical modulation would become one of the viable options in order to improve the condition of the elderly and compensate for the loss of their cognitive skills and to partially rehabilitate people with degenerative diseases.

This would bring about some ethical questions, as well as the pressure to promote and spread forms of enhancement, and improvement for aged people (since they can only regain the previous performance). In this case, those who want to occupy relevant roles in society might be asked or even forced to undergo the enhancement to make up for the general decline in cognitive abilities. Ethical reflection will then be called to clarify the obligations to be enhanced and the rights of those who do not want to alter the functioning of their mind / brain.

This situation does not exclude the tendency linked to the first challenge that I have illustrated. On the one hand, medicine is concentrating on enhancing a lucky few, who could take advantage of the current dynamics to reverse the pursuit of equality that our societies have been implementing for some time (apart from temporary fluctuations in the distribution of income and wealth). On the other hand, demographic decline and aging may require that more people resort to cognitive

enhancement, improvement and rehabilitation to compensate for the decrease in the overall capabilities available to address the complex problems we are facing today.

CONCLUSION

These scenarios find their preconditions in trends that are already in place, but which will not be necessarily realized. However, they seem to deserve attention from all those working in the field of electroceuticals and from public decision-makers, that is, all those who can affect future situations. Philosophers and neuroethicists are entrusted with the task of thinking about these scenarios so as not to be unprepared in case they come true.

In the face of these challenges, however, some lines of intervention can already be hypothesized. Faced with the first challenge—that is, the possible shift from a mainly therapeutic use of electroceuticals to a use aimed at enhancement—a stricter regulation of devices must be promoted (Dubljević, 2015; Maslen et al., 2015). Secondly, scientists and clinicians could try to establish guidelines for the use of electroceuticals that should consider not only the safety features but also the possible social consequences of a widespread use of these enhancement techniques. Thirdly, research should be directed primarily at clinical applications, before moving toward the enhancement of healthy subjects.

As for the second challenge, the three recommendations set out above apply as well. More specifically, all operators engaged in medical practices involving electroceuticals should refer to the ethical codes of their respective professions and to international conventions (for example the Oviedo Convention) for the protection of human rights and dignity. All these rules already in force prevent the mandatory administration of medical treatments, except in extraordinary cases that are, or should be, well-specified. It would therefore be important to avoid defining electroceuticals as a non-medical treatment in order to use them only within a legal framework.

Faced with political decisions that could go toward the violation of the rules in force, the scientific community would have the responsibility to highlight the potential risks involved and to actively prevent them as well.

AUTHOR CONTRIBUTIONS

The author confirms being the sole contributor of this work and has approved it for publication.

REFERENCES

Alzheimer's Association (2019). *Alzheimer's Disease Facts and Figures*. Available online at: https://www.alz.org/alzheimers-dementia/facts-figures (accessed June 1, 2019).

Bess, M. (2015). *Our Grandchildren Redesigned: Life in the Bioengineered Society of the Near Future*. Boston, MA: Beacon Press.

Bynum, W. (2008). *The History of Medicine: A Very Short Introduction*. Oxford: Oxford University Press.

Callaway, N. (2013). Shocks to the brain improve mathematical abilities. *Nat. News*. doi: 10.1038/nature.2013.13012

Chi, R. P., and Snyder, A. W. (2012). Brain stimulation enables the solution of an inherently difficult problem. *Neurosci. Lett.* 515, 121–124. doi: 10.1016/j.neulet.2012.03.012

Długosz, Z. (2011). Population ageing in Europe. *Proced. Soc. Behav. Sci.* 19, 47–55. doi: 10.1016/j.sbspro.2011.05.106

Dresler, M., Sandberg, A., Bublitz, C., Ohla, K., Trenado, C., Mroczko-Wasowicz, A., et al. (2018). Hacking the brain: dimensions of cognitive enhancement. *ACS Chem. Neurosci.* 10, 1137–1148. doi: 10.1021/acschemneuro.8b00571

Dubljević, V. (2015). Neurostimulation devices for cognitive enhancement: toward a comprehensive regulatory framework. *Neuroethics* 8, 115–126. doi: 10.1007/s12152-014-9225-0

Fechner, H. B., Pachur, T., Schooler, L. J. (2019). How does aging impact decision making? The contribution of cognitive decline and strategic compensation revealed in a cognitive architecture. *J. Exper. Psychol. Learn. Mem. Cognit.* doi: 10.1037/xlm0000661 [Epub ahead of print].

Fitz, N. S., and Reiner, P. B. (2015). The challenge of crafting policy for do-it-yourself brain stimulation. *J. Med. Ethics* 41, 410–412. doi: 10.1136/medethics-2013-101458

Ford, M. (2015). *Technology and the Threat of a Jobless Future Rise of the Robots*. New York, NY: Basic Books.

Harada, C. N., Love, M. C. N., and Triebel, K. L. (2013). Normal cognitive aging. *Clin Geriatr. Med.* 29, 737–752. doi: 10.1016/j.cger.2013.07.002

Harari, Y. N. (2016). *Homo Deus: A Brief History of Tomorrow*. London: Harvill Secker.

Horvath, J. C., Forte, J. D., and Carter, O. (2015). Quantitative review finds no evidence of cognitive effects in healthy populations from single-session transcranial direct current stimulation (tDCS). *Brain Stimulat.* 8, 535–550. doi: 10.1016/j.brs.2015.01.400

Hunt, L. (2007). *Inventing Human Rights: A History*. New York, NY: W. W. Norton & Company.

Kambouris, M. E., Zagoriti, Z., Lagoumitzi, G., and Poulas, K. (2014). From therapeutic electrotherapy to electroceuticals: formats, applications and prospects of electrostimulation. *Ann. Res. Rev. Biol.* 4, 3054–3070. doi: 10.9734/ARRB/2014/10563

Klauer, K. J., and Phye, G. D. (2008). Inductive reasoning: a training approach. *Rev. Educ. Res.* 78, 85–123. doi: 10.3102/0034654307313402

Koops, B. J., Lüthy, C. H., Nelis, A., Sieburgh, C., Jansen J. P. M., Schmid, M. S., (eds.) (2013). *Engineering the Human: Human Enhancement Between Fiction and Fascination*. New York, NY; Heidelberg: Springer.

Lavazza, A. (2016). A Rawlsian version of the opportunity maintenance thesis. *Am. J. Bioethics* 16, 50–52. doi: 10.1080/15265161.2016.1170236

Lavazza, A. (2019a). Parental selective reproduction: genome-editing and maternal behavior as a potential concern. *Front. Genet.* 10:532. doi: 10.3389/fgene.2019.00532

Lavazza, A. (2019b). Transcranial electrical stimulation for human enhancement and the risk of inequality: prohibition or compensation? *Bioethics* 33, 122–131. doi: 10.1111/bioe.12504

Lavazza, A., and Colzato, L. S. (2018). Editorial special topic: neuroethical issues in cognitive enhancement. *J. Cognit. Enhanc.* 2, 319–322. doi: 10.1007/s41465-018-0117-9

Lavazza, A., Reichlin, M. (2019). Introduction: moral enhancement. *Topoi* 38:1. doi: 10.1007/s11245-019-09638-5

Lutz, W., Sanderson, W., and Scherbov, S. (2008). The coming acceleration of global population ageing. *Nature* 451, 716–719. doi: 10.1038/nature 06516

Maslen, H., Douglas, T., Cohen Kadosh, R., Levy, N., and Savulescu, J. (2015). The regulation of cognitive enhancement devices: refining Maslen et al.'s model. *J Law Biosci.* 2, 754–767. doi: 10.1093/jlb/lsv029

Mason, A. (2006). *Levelling the Playing Field: The Idea of Equal Opportunity and its Place in Egalitarian Thought*. New York, NY: Oxford University Press.

Meinzer, M., Lindenberg, R., Antonenko, D., Flaisch, T., and Flöel, A. (2013). Anodal transcranial direct current stimulation temporarily reverses age-associated cognitive decline and functional brain activity changes. *J. Neurosci.* 33, 12470–12478. doi: 10.1523/JNEUROSCI.5743-12.2013

Miller, S., and Matharu, M. S. (2017). "The use of electroceuticals and neuromodulation in the treatment of migraine and other headaches," in

Electroceuticals. Advances in Electrostimulation Therapies, ed A. Majid (Cham: Springer), 1–33.

More, M., and Vita-More, N. (eds.) (2013). *The Transhumanist Reader: Classical and Contemporary Essays on the Science, Technology, and Philosophy of the Human Future*. Hoboken, NJ: Wiley-Blackwell.

Murray, C. J., Callender, C. S., Kulikoff, X. R., Srinivasan, V., Abate, D., Abate, K. H., et al. (2018). Population and fertility by age and sex for 195 countries and territories, 1950–2017: a systematic analysis for the Global Burden of Disease Study 2017. *Lancet* 392, 1995–2051. doi: 10.1016/S0140-6736(18)32278-5

Packer, S., Mercado, N., and Haridat, A. (2018). Bioelectronic medicine—ethical concerns. *Cold Spring Harb. Perspect. Med.* doi: 10.1101/cshperspect.a034363. [Epub ahead of print].

Parkin, B. L., Ekhtiari, H., and Walsh, V. F. (2015). Non-invasive human brain stimulation in cognitive neuroscience: a primer. *Neuron* 87, 932–945. doi: 10.1016/j.neuron.2015.07.032

Persson, I., and Savulescu, J. (2012). *Unfit for the Future: The Need for Moral Enhancement*. Oxford: Oxford University Press.

Pickersgill, M., and Hogle, L. (2015). Enhancement, ethics and society: towards an empirical research agenda for the medical humanities and social sciences. *Med. Hum.* 41, 136–142. doi: 10.1136/medhum-2015-010718

Pinker, S. (2018). *Enlightenment Now: The Case for Reason, Science, Humanism, and Progress*. New York, NY: Viking.

Price, A. R., and Hamilton, R. H. (2015). A re-evaluation of the cognitive effects from single-session transcranial direct current stimulation. *Brain Stimul.* 8, 663–665. doi: 10.1016/j.brs.2015.03.007

Rawls, J. (1999). *A Theory of Justice, Revised, Edn*. Cambridge, MA: Belknap Press.

Reardon, S. (2014). Electroceuticals spark interest. *Nature* 511:18. doi: 10.1038/511018a

Reichman, W. E., Fiocco, A. J., and Rose, N. S. (2010). Exercising the brain to avoid cognitive decline: examining the evidence. *Aging Health* 6, 565–584. doi: 10.2217/ahe.10.54

Rindermann, H. (2018). *Cognitive Capitalism: Human Capital and the Wellbeing of Nations*. Cambridge: Cambridge University Press.

Salthouse, T. (2012). Consequences of age-related cognitive declines. *Ann. Rev. Psychol.* 63, 201–226. doi: 10.1146/annurev-psych-120710-100328

Santoni de Sio, F., Faulmüller, N., and Vincent, N. A. (2014). How cognitive enhancement can change our duties. *Front. Syst. Neurosci.* 8:131. doi: 10.3389/fnsys.2014.00131

Scharre, P. (2018). *Army of None: Autonomous Weapons and the Future of War*. New York, NY: W. W. Norton and Company.

Snowball, A., Tachtsidis, I., Popescu, T., Thompson, J., Delazer, M., and Zamarian, L., et al. (2013). Long-term enhancement of brain function and cognition using cognitive training and brain stimulation. *Curr. Biol.* 23, 987–992. doi: 10.1016/j.cub.2013.04.045

Conflict of Interest Statement: The author declares that the research was conducted in the absence of any commercial or financial relationships that could be construed as a potential conflict of interest.

frontiers in Neuroscience

ORIGINAL RESEARCH
published: 07 August 2019
doi: 10.3389/fnins.2019.00783

Safety Aspects, Tolerability and Modeling of Retinofugal Alternating Current Stimulation

Linus Haberbosch[1,2], Abhishek Datta[3], Chris Thomas[3], Andreas Jooß[1], Arvid Köhn[1], Maria Rönnefarth[1,4], Michael Scholz[5], Stephan A. Brandt[1] and Sein Schmidt[1,4]*

[1] Department of Neurology, Charité – Universitätsmedizin Berlin, Berlin, Germany, [2] Department of Endocrinology, Diabetes and Metabolism, Charité – Universitätsmedizin Berlin, Berlin, Germany, [3] Research and Development, Soterix Medical, New York, NY, United States, [4] Berlin Institute of Health (BIH), Berlin, Germany, [5] Neural Information Processing Group, Technical University of Berlin, Berlin, Germany

Background: While alternating current stimulation (ACS) is gaining relevance as a tool in research and approaching clinical applications, its mechanisms of action remain unclear. A review by Schutter and colleagues argues for a retinal origin of transcranial ACS' neuromodulatory effects. Interestingly, there is an alternative application form of ACS specifically targeting α-oscillations in the visual cortex via periorbital electrodes (retinofugal alternating current stimulation, rACS). To further compare these two methods and investigate retinal effects of ACS, we first aim to establish the safety and tolerability of rACS.

Objective: The goal of our research was to evaluate the safety of rACS via finite-element modeling, theoretical safety limits and subjective report.

Methods: 20 healthy subjects were stimulated with rACS as well as photic stimulation and reported adverse events following stimulation. We analyzed stimulation parameters at electrode level as well as distributed metric estimates from an ultra-high spatial resolution magnetic resonance imaging (MRI)-derived finite element human head model and compared them to existing safety limits.

Results: Topographical modeling revealed the highest current densities in the anterior visual pathway, particularly retina and optic nerve. Stimulation parameters and finite element modeling estimates of rACS were found to be well below existing safety limits. No serious adverse events occurred.

Conclusion: Our findings are in line with existing safety guidelines for retinal and neural damage and establish the tolerability and feasibility of rACS. In comparison to tACS, retinofugal stimulation of the visual cortex provides an anatomically circumscribed model to systematically study the mechanisms of action of ACS.

Keywords: retinofugal alternating current stimulation, electrical stimulation, feasibility, tolerability, safety, adverse events, finite element modeling

OPEN ACCESS

Edited by:
Mikhail Lebedev,
Duke University, United States

Reviewed by:
Till R. Schneider,
Universität Hamburg, Germany
Elena G. Sergeeva,
Boston Children's Hospital, Harvard Medical School, United States

****Correspondence:***
Linus Haberbosch
linus.haberbosch@charite.de

Specialty section:
This article was submitted to Neural Technology, a section of the journal Frontiers in Neuroscience

Received: *24 March 2019*
Accepted: *12 July 2019*
Published: *07 August 2019*

Citation:
Haberbosch L, Datta A, Thomas C, Jooß A, Köhn A, Rönnefarth M, Scholz M, Brandt SA and Schmidt S (2019) Safety Aspects, Tolerability and Modeling of Retinofugal Alternating Current Stimulation. Front. Neurosci. 13:783. doi: 10.3389/fnins.2019.00783

Abbreviations: EF, electrical field; NiBS: non-invasive brain stimulation; NRS, numeric rating scale; PS, photic stimulation; rACS: retinofugal alternating current stimulation; RPE, retinal pigment epithelium; tACS, transcranial alternating current stimulation.

INTRODUCTION

Non-invasive brain stimulation (NiBS) is an effective method for research, as well as a promising tool for therapy in cognitive and clinical neuroscience (Paulus, 2003; Hallett, 2007; Liew et al., 2014). Its effects range from direct brief modification of neural activity to long lasting recovery maximization following neural injury (Hallett, 2005; Talelli and Rothwell, 2006; Hummel et al., 2008; Sandrini and Cohen, 2013). Recently, transcranial alternating current stimulation (tACS), characterized by oscillatory low-voltage stimulation, showed promising effects on the motor system (Feurra et al., 2011, 2013), motor performance (Pogosyan et al., 2009; Joundi et al., 2012), memory (Marshall et al., 2006; Polania et al., 2012), higher order cognition (Santarnecchi et al., 2013, 2016) and tremor (Brittain et al., 2013). Despite these encouraging results, tACS' mechanisms of action remain unclear (Zaghi et al., 2010) and a retinal contribution to its effects on neural synchrony is still being discussed (Schutter, 2016).

Retinofugal alternating current stimulation (rACS) is a comparably novel form of alternating current stimulation (ACS). In contrast to tACS, rACS is characterized by transmission along retinofugal tracts terminating predominantly in cortical visual areas and neuromodulation of central rhythms (Gall et al., 2011; Schmidt et al., 2013a). While differing from other forms of NiBS in regard to stimulation site, rACS shares its use of alternating current and effects on the intrinsic frequencies of the visual system with tACS (Schmidt et al., 2013a; Haberbosch et al., 2019). Moreover, in comparison to other forms of NiBS (namely, most types of tES) with diffusely induced electric fields (EF) throughout large parts of the brain (Peterchev et al., 2012), rACS affects the well-defined retinofugal pathway (Rager and Singer, 1998) for stimulation confined to the visual system. Thus, rACS renders a unique means to study mechanisms underlying NiBS as it physiologically affects the circumscribed primary visual cortex with separate input from each eye.

Before any novel method can be employed to its full potential or compared with other methodologies, establishing its safety and tolerability is critically important (Bath et al., 2014). The lack of knowledge of safety parameters could culminate in ineffective or even hazardous use (Antal et al., 2008; Bath et al., 2014). While ineffective stimulation could lead to incoherent findings regarding stimulation effects, effective but hazardous use could possibly result in severe adverse events and lasting damages in stimulation subjects. As rACS is used for research purposes, its safety as well as tolerability has to be determined rigorously.

Refraining from potentially dangerous invasive measures, the safety of a novel NiBS montage should be assessed in several different ways.

Firstly, stimulation parameters can be compared to theoretical safety limits as established for NiBS and neural tissue damage in animal studies (Agnew and McCreery, 1987; Liebetanz et al., 2009; Jackson et al., 2017), which have since been used to assess NiBS safety in human studies (Poreisz et al., 2007; Bikson et al., 2009, 2016). The primarily employed metrics include current density (A/m^2) and charge density (C/m^2), although other parameters such as charge per phase (C/ph) have been proposed to account for the shifting polarity of AC stimulation (Nitsche et al., 2003; Merrill et al., 2005).

Secondly, these safety metrics can be modeled onto CNS structures (Datta et al., 2011; Bikson et al., 2016), to determine the possibility of damage at critical locations (Bikson et al., 2016) while accounting for anatomy and electrode position (Bikson et al., 2009; Bikson and Datta, 2012; Peterchev et al., 2012; Saturnino et al., 2015).

Finally, experimental validation of theoretical results by subjective reports of adverse events with validated questionnaires can be acquired (Brunoni et al., 2011). These reports are also instrumental in assessing the tolerability of the novel method.

In this study we hypothesized that rACS is to be considered safe if: (1) Stimulation parameters (current and charge densities at the electrode) are within theoretical safety limits, (2) finite element modeling data shows the same for EF estimates and current densities at eye, retina and cortex, and (3) adverse events do not exceed that of other established stimulation methods in rate as well as severity.

To address the primary hypothesis, the stimulation parameters of rACS were recorded during stimulation and employed for the calculation of safety limits. Ultra-high resolution topographical finite element modeling was performed to identify regions of critical interest and to calculate theoretical safety parameters. Adverse events were identified with an extended adverse events questionnaire developed for tDCS (Brunoni et al., 2011). For direct experimental comparison, we employed simple and safe photic stimulation (PS) (Walker et al., 1944) as the gold-standard method for stimulation of the retinofugal pathway regarding safety and clinical experience (Cobb, 1947; Trenite et al., 1999).

MATERIALS AND METHODS

To address the safety profile of rACS, we observed and questioned 20 test subjects during rACS and PS sessions. We assessed cutaneous, retinal and central adverse events and drew a comparison between PS and rACS.

Participants

We stimulated 20 healthy volunteers (10 men), mean age 25.9 $\pm$ 4.95, as part of a study investigating a common framework of action for NiBS. The subjects were interviewed prior to experimentation regarding their state of health. We applied established exclusion criteria for NiBS (Brunoni et al., 2012) and added evidence for photophobia and photosensitive epilepsy. Written informed consent was obtained from all individual participants included in the study. The subjects received financial compensation for their participation. All procedures were performed in accordance with the ethical standards of the Ethics Committee of the Charité – Universitätsmedizin Berlin ("Ethikkommission der Charité – Universitätsmedizin Berlin") and with the 1964 Declaration of Helsinki and its later amendments. This study adheres to the principles of good scientific practice of the Charité – Universitätsmedizin Berlin ("Grundsätze der Charité zur Sicherung guter wissenschaftlicher Praxis").

Retinofugal Alternating Current Stimulation (rACS)

Retinofugal alternating current stimulation was applied via a multi-channel low-voltage stimulation device certified for clinical use, which delivered weak oscillatory current sinus-pulses over four individual periorbital electrodes, respectively (NextWave, Eyetronic, Germany). The four superficial active stimulating electrodes (Grass SAFELEAD^{TM} gold electrodes, Astro-Med, Inc., RI, United States) were contained in foam-padded stimulation goggles and bilaterally made skin contact via small felt buffers (0.35 cm^2) superior and inferior to the eye. The return electrode (rectangular electrode, 30 × 30 mm polished stainless steel) was fastened on the back of the neck at the midline.

Alternating current was applied at 10 Hz, as ACS has shown robust effects at this frequency (Kanai et al., 2008; Helfrich et al., 2014; Vossen et al., 2015) and gold standard PS typically also employs 10 Hz stimulation (Photic driving) (Walker et al., 1944). Stimulation amplitude was set to 120% phosphene threshold (resulting in 351.69 μA (SD 63.95) peak-to-peak amplitude). The phosphene threshold was determined employing an ascending method of limits (Herrick, 1967) provided by the NextWave software. rACS was delivered in 30 s blocks followed by 30 s pauses over 10 min. The subjects were told to keep their eyes open and focus a fixed point on a white surface in 1 m distance for the duration of the experiment.

To assess the safety parameters of stimulation we additionally calculated the effective amplitude. The effective amplitude of the applied current is defined as the time normed integral of the signal, which simplifies to its mean value for discrete signals as is the case here, since the used stimulator receives an equidistant sampled discrete function as input. In the simplest case of a pure sine wave this simplifies to the following formula:

$$a(eff) = \frac{a_{\max}}{\sqrt{2}}$$

In the case of more complex stimuli such as noise + sine wave or signals with an additional amplitude modulation, the use of peak-to-peak "a(max)" values to describe the resulting electrical power of an electric current stimulation would be misleading.

Regarding charge, we decided to refrain from more complex line integral calculations, and instead used the following simple formula:

$$Q = I * t$$

This was done to ensure straightforward comparability of resulting values. It also adds to the rigidity of our safety considerations by rather over-than underestimating the injected charge.

Photic Stimulation

Photic Stimulation was applied via two 3 × 5 cm multi-color white LEDs contained in the stimulation goggles, which work via red, green and blue LEDs mixing their emissions to form white light. To be able to compare stimulation intensities with rACS, sinusoidal pulses of white light were applied at an intensity of 120% light threshold and with a frequency of 10 Hz. This threshold was also determined by an ascending method of limits and resulted in an average luminous intensity of 1.24 cd (±0.44) for stimulation.

The stimulation was also delivered in 30 s blocks followed by 30 s pauses over 10 min, and the subjects received the same instructions as for rACS.

Modeling

The ultra-high resolution head and neck model (MIDA: Multimodal Imaging-Based Detailed Anatomical Model) available through the IT'IS Foundation was used in this study (Iacono et al., 2015). The nifti (.nii) color masks from the MIDA model were first processed in MATLAB to re-create segmentation masks based on intensity values. These masks were then imported into Simpleware (Synopsys Ltd., CA, United States) and any errors in continuity and anatomical details were manually corrected for Datta et al. (2012). Masks with similar electrical conductivities were then merged to a single compartment barring the regions of interest (eye structures) in order to perform individual current flow analysis through them. For instance, mandible, teeth, vertebra, skull dipole, skull inner table, skull outer table, hyoid bone were combined with the skull mask but eye retina, choroid, and sclera were treated as individual masks.

The stimulation electrodes were created as CAD files mimicking the exact physical geometry and dimensions of the electrodes used in the experiments. The electrodes were positioned interactively within the image data simulating the electrode montage used for rACS (see **Figure 1C**). The adaptive meshes derived from the segmentation masks were then imported into COMSOL Multiphysics (Burlington, MA, United States) for finite element computation. The final model comprised >10 million elements with >15 million degrees of freedom.

The representative isotropic average electrical conductivities assigned to the different tissue compartments and the electrode materials (in S/m) are listed in **Table 1**.

The Laplace equation was solved and current densities corresponding to 350 μA total current were applied at the anode or active electrode (s). Ground was applied at the return electrode and all other external surfaces were treated as insulated. The linear iterative solver of conjugate gradients with a relative tolerance of 1E-6 was used.

Surface as well as cross-sectional EF magnitude maps on the gray matter, retina, and the optic nerve were obtained. For the scalp, the surface current density magnitude plot was obtained.

Questionnaire

The questionnaire we employed is based on the one proposed by Brunoni et al. (2011) and investigated the presence of headaches, difficulties in concentrating, acute mood changes, visual perceptual changes, fatigue and discomforting sensations tingling, itching and/or burning under the electrodes during and after rACS, as well as PS. The item "Difficulties in concentrating" was defined in accordance with Montgomery and Asberg (1979), while the item "Fatigue" was defined in accordance with Chaudhuri and Behan (2004).

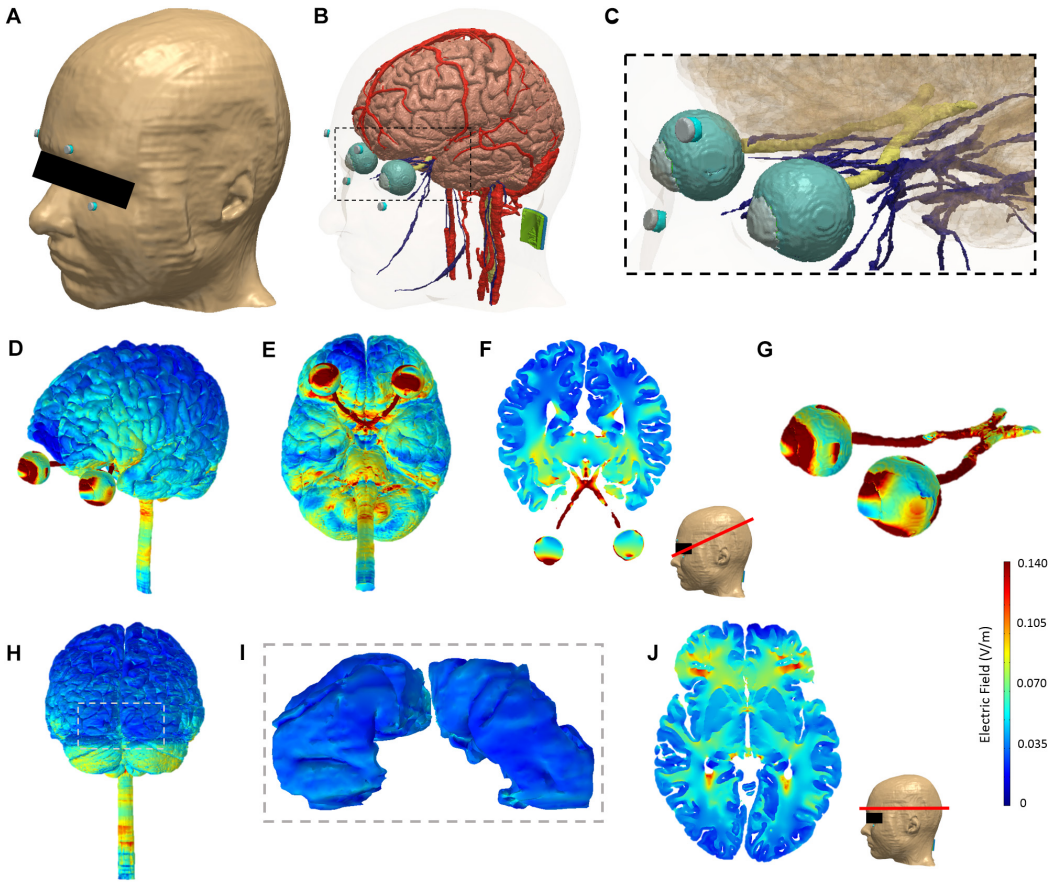

FIGURE 1 | Model segmentation and finite element analysis. The ultra-high resolution MIDA model was adapted for analysis in this study. **(A)** Skin tissue mask with periorbital electrodes (gray: electrode; blue: sponge). **(B)** The modeled brain, cranial nerves, blood vessels, eye structure, optic nerves, and electrodes (both active periorbital and the return inion electrode shown). **(C)** Zoomed view corresponding to the dashed section in panel **(B)** highlighting segmentation detail in the region of interest. Finite element analysis of current flow produced by rACS: Induced electric field magnitude plots on the cortical and eye level perspective **(D)** and bottom view **(E)**. A representative axial 2D cross-section view of electric field magnitude following the retinofugal tract was chosen and plotted **(F).** Panel **(G)** shows the induced electric field on the eyes and optic nerve. Panel **(H)** shows the rear view. Panel **(I)** shows the primary visual cortex (V1) corresponding to the dashed section in panel **(H)**. A representative 2D axial cross-section view of electric field magnitude taken at the level of half of the visual cortex along the superior–inferior plane is shown in panel **(J)**.

We modified the questionnaire by adding a description of phosphenes. Furthermore, to assess the overall tolerability, we defined the broad category of "Pain" as a summary of all discomforting sensations mentioned above and added a Numeric Rating Scale (NRS-11, 11 stages from 0 to 10, 10 being the strongest imaginable pain and 0 the absence of pain) (Farrar et al., 2001) as a more in-depth and reliable measurement (Downie et al., 1978). We discarded the four-point intensity rating for the other categories to avoid a "halo effect" bias (Streiner and Norman, 2008). We assumed that the foreign body feeling reported for physiologically similar transcorneal electrical stimulation (TCES) came from the electrode lying directly on the cornea (Gekeler et al., 2006) and therefore decided not to include it.

Three months after stimulation, the subjects received a second questionnaire to identify late and longer lasting after-effects.

As the data is not normally distributed and equal variance of residuals cannot be assumed, the severity of pain was analyzed in Wilcoxon Signed Ranks Tests for paired samples. The nominally scaled side effects were analyzed in Fishers Exact Tests, as expected values in several of the cells of a contingency table are below the recommended threshold for a classical Chi-Squared Test (Larntz, 1978). *P*-values of <0.05 were considered significant. All analyses were performed using IBM SPSS Statistics, Version 19.0.0.1 (IBM, United States).

RESULTS

Stimulation Parameters

An average 10 Hz phosphene threshold at 290.50 μV (SD 45.36), impedances at 12.05 kΩ (SD 2.89), and an average amplitude of 351.69 μA (SD 63.95) were noted. Calculated from peak-to-peak amplitude, the current density at electrode level amounted to a mean 1.00 mA/cm^2 (SD 0.28), and the charge density to 0.60 C/cm^2 (SD 0.11). As sine waves pulses were employed,

TABLE 1 | Assigned electrical conductivities.

Tissue compartment/Electrode material	Electrical conductivity (S/m)
Scalp	0.465
Muscle	0.35
Skull	0.01
CSF	1.65
Gray Matter	0.276
White Matter	0.126
Fat	0.04
Blood vessels	0.7
Eye Lens	0.32
Eye Retina/Choroid/Sclera	0.623
Eye Vitreous	1.55
Eye Cornea	0.5
Eye Aqueous	1.5
Optic Tract/Optic Chiasm/Cranial Nerve II	0.126
Air	1.00E−07
Sponge (felt buffer)	1.84
Periorbital electrode (gold electrodes)	4.10E+07
Inion electrode (stainless steel)	1.45E+06

The representative isotropic average electrical conductivities assigned to the different tissue compartments and the electrode materials (in S/m).

we additionally calculated the effective amplitude, resulting in a mean 248.68 μA (SD 47.0). Using effective amplitude, current density amounted to a mean 0.71 mA/cm^2 (SD 0.13), and the charge density to 0.42 C/cm^2 (SD 0.08). RACS was found to be well within safety limits and the findings comparable to other similar stimulation methods (see **Table 2**). Regarding stimulation amplitude, rACS (0.35 mA) was comparable to most TCES and tES montages (ranging from 0.08 to 1.2 mA). Electrosleep and the maximum intensity stimulation employed by Gekeler et al. (2006) were found to employ higher amplitudes (3–25 mA). The stimulated area (0.35 cm^2) is smaller than most tES montages (16–35 cm^2), comparable only to Electrosleep and TCES (0.35–1.25 cm^2). Regarding stimulation frequencies, rACS was compared to studies using similar frequencies (10–20 Hz), with the exceptions of Electrosleep, which is set at higher frequencies (100 Hz) as well as the non-oscillating tDCS and Gekeler's TCES. The calculations following these observations place the charge density of rACS just above the TCES of Ma et al. (2014) and far below the safety limit published by Liebetanz et al. (2009). This is consistent for charge per phase and charge density per phase. Regarding current density, rACS (1 mA/cm^2) ranks below Ma (1.2 mA/cm^2), well below the maximum intensity employed by Gekeler (8.57 mA/cm^2) and far below the safety limit proposed by McCreery (25 mA/cm^2). These findings are even more pronounced when using effective amplitude.

Finite Element Modeling

The EF distributed by rACS is strongest at the eye level, with the highest current density estimates at the retina. Further areas of elevated current densities are optic nerve and cortex (**Figures 1A,B**).

The calculated maximum current density at the retina amounted to a maximum of 1.24 A/m^2, while optic nerve (0.33 A/m^2) and cortex (0.13 A/m^2) were both subjected to less current flow. Regarding the EF, we estimated a maximum of 2.6 V/m in the optic nerve, followed by 1.99 V/m for the retina and 0.47 V/m for the cortex. Finally, current density at skin level underneath the active electrode amounted to a maximum induced value of 14.79 A/m^2 (**Figure 1C**), with the EF estimated at 31.80 V/m. It should be noted that due to edge effects, the observed values are higher than the current density toward the middle of the electrode which is simply the current injected over the contact area. For a detailed view, see **Table 3**.

TABLE 2 | Comparison of stimulation parameters.

	Amplitude	Area	Duration	Frequency	Current density	Charge density	Charge per phase	CD per phase
	(mA)	(cm^2)	(min)	(Hz)	(mA/cm^2)	(C/cm^2)	(C/ph)	(C/(cm^2*ph))
Safety limits (Agnew and McCreery, 1987)	–	–	–	–	25	–	–	0.000400
Safety limits (Liebetanz et al., 2009)	0.5	0.035	10	–	14.29	85.714 (52.400)	–	–
rACS	0.35	0.35	10	10	1	0.599	0.000035	0.0001
rACS (effective amplitude)	0.25	0.35	10	10	0.71	0.423	0.000025	0.000071
Electrosleep (Sergeev, 1963)	25	1.25	60	100	20	72	0.00025	0.0002
TCES (Ma et al., 2014)	1.2	1	5	20	1.2	0.36	0.00006	0.00006
TCES (Delbeke et al., 2001)	0.28	1.25	7	10	0.22	0.094	0.000028	0.000022
TCES (Gekeler et al., 2006) max	3	0.35	7	–	8.57	–	–	–
TCES (Gekeler et al., 2006) optimal	0.08	0.35	7	–	0.22	–	–	–
tACS (Antal et al., 2008)	0.4	16	5	10	0.03	0.008	0.00004	0.000003
tSDCS (Paulus et al., 2013)	0.25	16	4	10	0.02	0.004	0.000025	0.000002
tDCS (Nitsche et al., 2003)	1	35	9	–	0.03	–	–	–

Current density measures at electrode level employed for stimulation types employing continuous current (TCES (Gekeler) and tDCS), charge density, charge per phase and charge density (CD) per phase for oscillatory stimulation (rACS, Electrosleep, TCES (Ma and Delbeke), tACS and tSDCS).

TABLE 3 | Modeling data and comparison to safety limits.

		Current density	Electric field
		(mA/cm^2)	(V/m)
Safety limits	Liebetanz et al., 2009	14.29	42
rACS (retina)	Max	0.124	1.99
	Mean	0.007	0.11
	Median	0.005	0.08
rACS (optic nerve)	Max	0.033	2.6
	Mean	0.003	0.2
	Median	0.002	0.14
rACS (cortex)	Max	0.013	0.47
	Mean	0.001	0.05
	Median	0.001	0.04
rACS (V1)	Max	0.003	0.12
	Mean	0.001	0.03
	Median	0.001	0.03

This table presents the finite element modeling results for rACS: Current density and electric field estimates for retina, optic nerve, cortex and specifically the primary visual cortex (V1) in comparison to reported safety limits.

TABLE 4 | Adverse events for rACS and PS.

		rtACS		Photic Stim	
		n	%	*n*	%
Pain (overall)	During	8	40	4	20
	After	0	0	2	10
Fatigue	During	7	35	4	20
	After	7	35	4	20
Tingling	During	14	70	0	0
	After	0	0	0	0
Headache	During	0	0	3	15
	After	1	5	1	5
Itching	During	6	30	0	0
	After	5	25	0	0
Burning	During	6	30	0	0
	After	0	0	0	0
Difficulties in Concentrating	During	0	0	0	0
	After	0	0	2	10
Metallic Taste	During	3	15	0	0
	After	0	0	0	0
Muscle twitches	During	3	15	0	0
	After	0	0	0	0
Acute mood changes	During	0	0	0	0
	After	0	0	0	0
Nausea	During	0	0	0	0
	After	0	0	0	0

Reports of adverse events during and after stimulation in subjects and percent (data rounded to integers).

Adverse Events

Table 4 summarizes the adverse events in the 20 rACS and PS sessions in healthy participants. None of the subjects requested the stimulation to be terminated or required medical attention. In their subjective reports, rACS associated adverse events were predominant during stimulation, and PS associated adverse events were predominant following stimulation. More explicitly, a tingling sensation occurred in 70% of the subjects during but not after rACS. An itching sensation under the electrodes was reported by 30% of the subjects during rACS and 25% after rACS. A burning sensation was felt by 30% of the participants during but not after rACS. Fatigue occurred during, as well as after, stimulation in 35 and 20% of the rACS and PS group, respectively. Headaches were reported only by PS participants during stimulation (15%). After stimulation, it was reported by 5% for both PS, as well as rACS participants. Difficulties in concentrating were reported by 10% of the participants after PS, but not after rACS. There were no cases of acute mood changes, nausea and visual perceptual changes or lasting adverse events 3 months after stimulation.

Pain

Forty-percent of the subjects reported pain (**Figure 2A**) during rACS (mean intensity 2.5, SD 1.73) and 20% during PS (2.75, SD 0.83). While none of the participants reported pain after rACS, this was the case for 10% after PS (1.5, SD 0.5).

rACS vs. Photic Stimulation

In the statistical analyses, rACS and PS showed no significant effect of stimulation type (rACS versus PS) on pain intensity as assessed by Wilcoxon Signed Ranks Tests (**Figure 2A**), fatigue, headache and difficulties in concentrating as assessed by Fisher's Exact Tests (**Figure 2B**) during as well as after stimulation. PS and rACS significantly differed regarding skin sensations of tingling, itching and burning ($P < 0.05$, Fisher's Exact Tests), which all occurred exclusively in rACS. For a more detailed view, see **Tables 5**, **6**. The full dataset behind this comparison is available as **Supplementary Material**.

DISCUSSION

To address the safety profile of rACS, we assessed theoretical safety limits as well as finite-element modeling data and compared the reported adverse events for rACS and simple PS.

The primary findings are that rACS is safe based on the following observations: (1) stimulation parameters (current and charge densities at the electrode) are within theoretical safety limits, (2) finite element modeling data shows the same for EF estimates and current densities at eye, retina and cortex, and (3) adverse events are comparable to PS in direct experimental comparison (see **Tables 3**, **4**) and rate as well as severity of adverse events did not exceed that of other established brain stimulation methods (see **Table 2**).

Stimulation Parameters

To be efficacious and safe, a stimulation system must stimulate neural tissue without damaging tissue or electrode. Tissue damage is caused when excitable tissue is overstimulated and electrode damage ensues as metal oxidation occurs

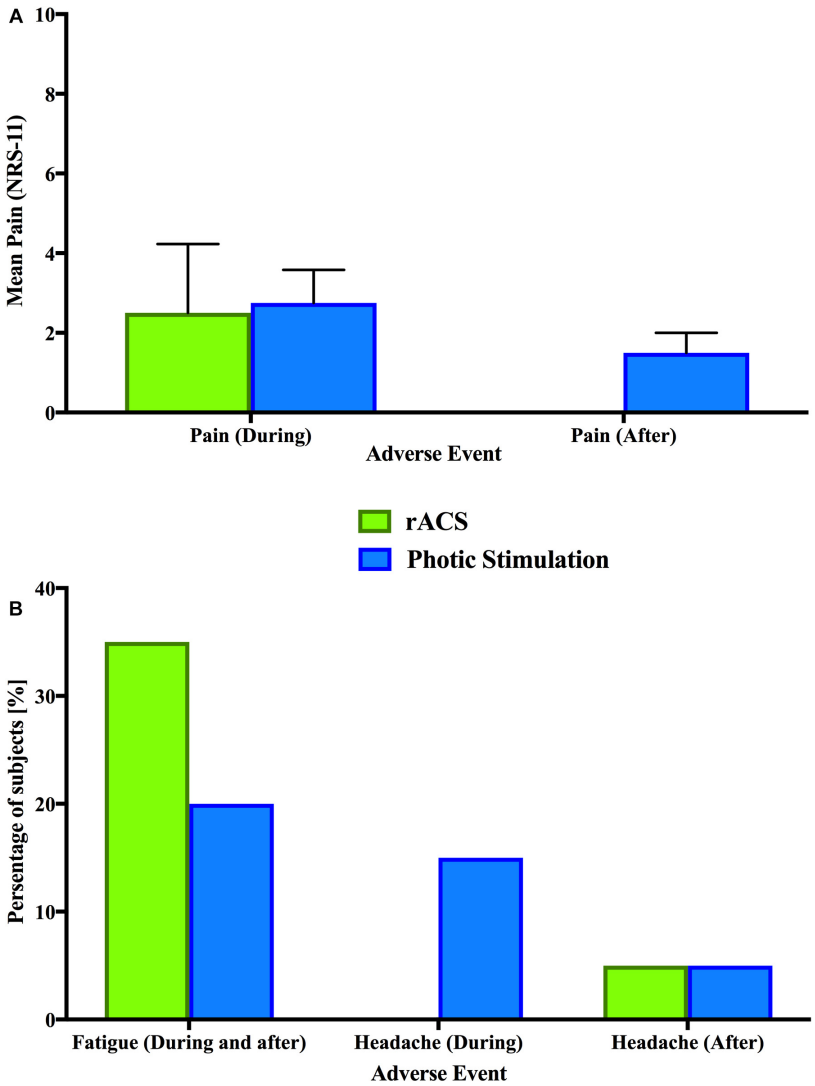

FIGURE 2 | Adverse events. A comparison of adverse events between rACS (green) and PS (blue). None of the depicted differences were significant in Bonferroni-corrected multiple comparisons. **(A)** Depicted is the mean rating (NRS-11) of overall pain and discomfort in affected subjects during and after stimulation. Error bars represent the standard deviation. **(B)** Comparison of shared adverse events (fatigue and headache) in percentage of subjects.

(Peterchev et al., 2012). Current density and charge density have been proposed as predictors for such damage (Bikson et al., 2016).

Current Density

Current density is the proposed optimal safety parameter for a constant current stimulation (Nitsche et al., 2003) and can be derived from the effective amplitude and compared to safety limits (Agnew and McCreery, 1987) as well as other similar stimulation paradigms (Gekeler et al., 2006; Ma et al., 2014).

We find that rACS current densities are within reported safety limits for tissue damage (Yuen et al., 1981; Lindenblatt and Silny, 2002; Liebetanz et al., 2009; Gellner et al., 2016).

TABLE 5 | Results of the Wilcoxon-signed ranks tests.

Source			Z	Asymp. Sig. (2-tailed)
Stimtype (rACS vs. PS)	Pain (overall)	During	–0.987[a]	0.323
		After	–1.342[b]	0.180

The results of the statistical analysis on overall pain during and after stimulation. [a]*Based on positive ranks.* [b]*Based on negative ranks.*

Charge Density and Charge per Phase

While current density is a well-established safety parameter, it is best suited for assessing the safety of constant current stimulation. ACS injects less charge than constant current stimulation of the same amplitude (Liebetanz et al., 2009; Schmidt et al., 2013a), dependent on stimulation frequency and duty cycle (Chaieb et al., 2014). The safety limits of charge balanced ACS, such as rACS, are therefore more precisely

TABLE 6 | Results of the Fisher's exact tests.

Source			Exact Sig. (2-tailed)
Stimtype (rACS vs. PS)	Fatigue	During	0.480
		After	0.480
	Difficulties in Concentrating	During	–
		After	0.487
	Headache	During	0.231
		After	1.000
	Itching	During	0.020*
		After	0.047*
	Burning	During	0.020*
		After	–
	Tingling	During	0.000*
		After	–

*The results of the statistical analysis on the nominally scaled adverse events presented in **Table 4**. The asterisk (*) marks significant results.*

determined by charge density and charge per phase (Nitsche et al., 2003; Merrill et al., 2005).

We find that rACS charge densities are also within reported safety limits for tissue damage (Yuen et al., 1981; Lindenblatt and Silny, 2002; Liebetanz et al., 2009; Gellner et al., 2016; Jackson et al., 2017).

Comparison to Other Stimulation Types

While stimulating at higher current and charge densities than most forms of tES, rACS stimulation parameters proved comparable to dose parameters reported for TCES using up to 10 mA per pulse to establish safety guidelines (Gekeler et al., 2011), well below early montage parameters for both stronger and longer stimulation used in early studies addressing Electrosleep therapy (Robinovitch, 1914; Knutson, 1967; Peterchev et al., 2012), and well below current densities reported for stimulation via implanted self-sizing spiral cuff electrodes in blind patients over the course of several years (Delbeke, 2011) (see **Table 2**).

Despite arguable differences between different stimulation techniques, there are remarkable similarities, e.g., comparably distant periorbital montage of electrodes, as well as modeling results for the serial resistance of the skin and eyelid (Delbeke et al., 2000; Merrill et al., 2005; Gekeler et al., 2006) to motivate this comparison.

This leads to the conclusion that the employed charge injection was safe with regards to possible tissue as well as electrode damage. In the future, studies addressing the calculation of rheobase and chronaxie and stimulation with variable pulse parameters might help to further reduce charge injection to the minimum necessary to efficaciously achieve a neuronal response (Irnich, 1980, 2010; Delbeke et al., 2001).

Finite Element Modeling

Electric Field Distribution

Expectedly, the EF distribution shows a clear focus on retina and optic nerve, while the cortical electric current flow is much weaker. Due to the electrode montage being superior–inferior, we see stronger EFs in the temporal regions and at the return electrode. While there is increased flow through the subcortical structures, brain stem and cerebellum, there appears to be no strong current flow to occipital areas, with a maximum current density of 0.033 A/m^2 and a maximum EF of 0.1208 V/m (**Table 3** and **Figure 1**).

This confirms the retinofugal pathway as the primary target of rACS. Still, stimulation intensity should be closely monitored, as strong over-threshold stimulation might lead to unwanted effects on subcortical structures.

Current Densities and EF Estimates

Evidence from relevant animal models indicates that brain injury by tDCS occurs at predicted brain current densities (14.9 A/m^2) (Liebetanz et al., 2009; Gellner et al., 2016; Jackson et al., 2017). Considering the well-established threshold proposed by Liebetanz et al. (2009), rACS maximum current densities rank two orders of magnitude (OOM) below lesion threshold for retina and optic nerve and three OOM below for the cortex.

Additionally, all of the EF estimates are at least one OOM below the safety threshold of 42 V/m (Liebetanz et al., 2009; Gellner et al., 2016; Jackson et al., 2017). It should be noted that, as mentioned above, ACS injects less charge than constant current stimulation of the same amplitude (Liebetanz et al., 2009; Schmidt et al., 2013a), and we calculated the current densities from peak-to-peak amplitude instead of effective amplitude. The risk of damage will consequently rather be over-than underestimated. We therefore conclude the rACS employed in this study should be safe from a modeling standpoint as well.

Adverse Events

No fatal or serious adverse events (Wester et al., 2008) were observed for rACS. The most notable adverse events in the present study were tingling, burning, itching and fatigue. The hazard rate for these adverse events is to be considered "very common" (>1/10 cases). This is comparable to results from other forms of tES (Brunoni et al., 2011), suggesting for tDCS that the type of adverse event is mild and their frequency of occurrence is "common." Direct experimental evidence shows significantly more cutaneous adverse events, but significantly less concentration deficits after stimulation for rACS as compared to PS (**Table 5**).

As the modeling results showed high maximum current densities and EF estimates at skin level, the presence of cutaneous adverse events during and after rACS comes as no surprise. Comparing rACS and PS regarding the summary category of pain, we have to note the complete lack of cutaneous sensations in PS and that multiple aversive sensations may be clustered and perceived in sum total as painful (Tuckett, 1982).

Skin Rashes and Damage

None of the subjects reported skin rashes or damage. Whereas the applied charge density is clearly strong enough to stimulate

C-nociceptors, it is too low and the duration is too short to induce skin damage (Dzhokic et al., 2008). For direct current stimulation, it has been shown that 1 mA via two 7 × 5 cm rubber electrodes in over 2000 stimulation sessions (Loo et al., 2011) can be applied for 20 min with no skin damage. Again, ACS is less likely than direct current stimulation to induce tissue or electrode damage. Although rACS is unlikely to induce skin damage, this study adhered to previous suggestions for avoiding cutaneous adverse events (Loo et al., 2011).

Tingling, Itching and Burning

Electrical stimulation of skin nociceptors is known to produce itching, burning and tingling sensations in the animal model, as well as in human subjects (Jarvis and Voita, 1971; Tuckett, 1982; Kellogg et al., 1989; Ledger, 1992). While even persisting shortly after stimulation due to central processes, these sensations are not necessarily indicative of local damage induced by stimulation (Tuckett, 1982).

Pain

One third of the subjects reported pain with a median strength of 2.5 NRS. The sensation of pain during and after electric stimulation is understood to be a combination of several factors, with the terminal branches of C-nociceptors of the stimulated skin acting as the primary central conductor (Magerl et al., 1987; Garnsworthy et al., 1988; Hakkinen et al., 1995). This matches subject descriptions of deep and spread pain associated with itch and burning sensations in this study (six cases) as well as anecdotal reports of painful perceptions that could not be attenuated by topical anesthetic and the lack of radiating pain sensations reported elsewhere (Hakkinen et al., 1995). Due to the common occurrence of cutaneous sensations, topical anesthesia might be preferential especially for placebo control or rACS versus PS studies. This study did not use topical anesthesia, as it might mask development of skin damage.

While the feeling of pain and discomfort should be monitored closely in future studies, it should be noted that we found no significant difference between rACS and well-established and tolerable PS regarding overall discomfort/pain (**Table 5**).

This pain during and after PS is most likely a form of "discomfort glare" associated with visual discomfort, annoyance, irritability or distraction without affecting the ability to see, but leading to symptoms of visual fatigue (Ticleanu and Littlefair, 2015).

Phosphenes

As we stimulated our subjects at 120% phosphene threshold, all subjects experienced phosphenes. These phosphenes induced by rACS were typically described as flickering at the edges of the field of view and not experienced as painful.

Historically, phosphenes induced by alternating current have been seen as a purely retinal phenomenon (Rohracher, 1935) resulting from the high susceptibility of the retina to electricity (Ziemssen, 1864). For rACS and other forms of tES the amount of confounding retinal or cortical stimulation following low-voltage stimulation is unknown or a matter of controversy (Paulus, 2010).

Yet, due to the respective montages there should be a magnitude of difference between methods (Peterchev et al., 2012) with TCES inducing the most, rACS with periorbital-occipital montages intermediate, and tES the least retinal stimulation (Delbeke et al., 2001; Thil et al., 2007; Paulus, 2010).

A previous tACS modeling effort indicated why transcranial stimulation may induce retinal phosphenes (Laakso and Hirata, 2013) by virtue of current density induced in the eyes exceeding phosphene thresholds. As different electrode montages result in different current flow patterns, whether a particular montage would result in retinal phosphenes would naturally depend on the montage being studied. Specifically they show that the threshold for retinal phosphenes for commonly used tACS montages is exceeded with stimulation current of 500–1000 μA (depending on the montage considered). Another prior tACS/tDCS modeling effort demonstrated that bilateral montages result in not only more focused current flow but higher current intensities than midline montages (Neuling et al., 2012). While no detailed analysis is performed on the eye regions, the authors state that the closer one of the stimulation electrodes is to the eye regions, the easier it is to perceive phosphenes.

Where exactly rACS phosphenes are generated remains subject to further investigation. While we find the highest EF estimates in the optic nerve, other authors (Brindley, 1955; Ma et al., 2014) suggested bipolar cells, or the parts of rod and cone cells lying inside the external limiting membrane as the main site of stimulation. In line with the flickering at the edges of the field of view as reported by our subjects for rACS at 120% phosphene threshold, it can be argued that inner retinal neurons are the most probable site at which an electrical stimulus exerts its primary effect, with predominant activation of the peripheral retina (Ma et al., 2014). This adds further support to previous findings suggesting that the primary location of the majority of retinal damage (the retinal pigment epithelium, RPE) induced by photochemical noxae is bypassed by electrical stimulation (Grützner et al., 1958). Besides fatigue and cutaneous effects, the participants described more phosphene or light related adverse events in association with well-known and safe PS applied at 120% light threshold than with rACS applied at 120% phosphene threshold.

Fatigue

Fatigue, reported by one third of the subjects after rACS, has been suggested in previous research to be an unspecific effect of tES. Similar to rACS, the early approaches to tES involved two "active" electrodes placed directly over the eyes, presumably to facilitate active current delivery through the optic foramina. These montages were first used in Electrosleep research initiated in Robinovitch (1914), with extensive research following (Obrosow, 1959; Sergeev, 1963; Brown, 1975). The consensus after about 60 years was that Electrosleep induces unspecific sleepiness and fatigue related to stimulation (Guleyupoglu et al., 2013).

The findings in this study, that rACS produces more fatigue than PS, support the notion of an indirect and unspecific central

(adverse) effect specific to electrical stimulation. This notion is in line with previous findings showing that action potentials induced by electrical stimulation of the retina can propagate directly to the visual cortex (Grützner et al., 1958), produce different evoked potentials (Potts et al., 1968) and modulate central rhythms (Schmidt et al., 2013a) as well as large scale networks of the brain (Bola et al., 2014).

CNS Damage and Seizure Risk

Beyond fatigue, the possibility of direct structural damage to central nervous structures by rACS seems low considering the distance between charge injection and brain tissue as well as stimulation strength. Yet, for rhythmic PS the danger of inducing an epileptic seizure is well established. Although not found in this study, for electrical stimulation the danger must also be assumed to be high due to neurophysiological similarities with intermittent photic stimulation (IPS) (Brindley, 1955) and proven effects on central processes and neural synchrony (Parra et al., 2003). Additionally, although no reports of seizures after comparable electrical stimulation sessions exist (Brunoni et al., 2012), we will continue to employ photosensitivity and epilepsy as exclusion criteria for future rACS studies.

CONCLUSION AND OUTLOOK

Having theoretically and experimentally characterized the relative safety profile of rACS, we believe future studies can further investigate retinal mechanisms of action for ACS effects, especially in comparison with tACS. Additionally, rACS allows for studies addressing the interaction of different signal types entering the visual system through two separate input channels (left and right eye) and converging at the level of the primary visual cortex. This provides an promising tool for studies aiming to address a common framework of action for NiBS with more than one input-signal, e.g., noise and oscillation (Schmidt et al., 2013b).

DATA AVAILABILITY

The datasets generated for this study are available on request to the corresponding author.

ETHICS STATEMENT

All protocols conformed to the Declaration of Helsinki, and were approved by the Ethics Committee of the Charité – Universitätsmedizin Berlin ("Ethikkommission der Charité – Universitätsmedizin Berlin"). Informed consent was obtained from all individual participants included in the study. This study adheres to the principles of good scientific practice of the Charité – Universitätsmedizin Berlin ("Grundsätze der Charité zur Sicherung guter wissenschaftlicher Praxis").

AUTHOR CONTRIBUTIONS

LH, AD, SS, MS, and SB conceived and designed the study. LH, AD, CT, AJ, and SS carried out data acquisition and analysis. LH, AD, and SS drafted the manuscript. CT, AJ, AK, MR, MS, and SB critically revised the manuscript. All authors participated in the interpretation of the data.

FUNDING

This work was supported by the German Research Foundation, DFG grant BR 1691/8-1 and OB 102/22-1.

SUPPLEMENTARY MATERIAL

The Supplementary Material for this article can be found online at: https://www.frontiersin.org/articles/10.3389/fnins.2019.00783/full#supplementary-material

REFERENCES

Agnew, W. F., and McCreery, D. B. (1987). Considerations for safety in the use of extracranial stimulation for motor evoked potentials. *Neurosurgery* 20, 143–147.

Antal, A., Boros, K., Poreisz, C., Chaieb, L., Terney, D., and Paulus, W. (2008). Comparatively weak after-effects of transcranial alternating current stimulation (tACS) on cortical excitability in humans. *Brain Stimul.* 1, 97–105. doi: 10.1016/j.brs.2007.10.001

Bath, P. M., Brainin, M., Brown, C., Campbell, B., Davis, S. M., Donnan, G. A., et al. (2014). Testing devices for the prevention and treatment of stroke and its complications. *Int. J. Stroke* 9, 683–695. doi: 10.1111/ijs.12302

Bikson, M., and Datta, A. (2012). Guidelines for precise and accurate computational models of tDCS. *Brain Stimul.* 5, 430–431. doi: 10.1016/j.brs.2011.06.001

Bikson, M., Datta, A., and Elwassif, M. (2009). Establishing safety limits for transcranial direct current stimulation. *Clin. Neurophysiol.* 120, 1033–1034. doi: 10.1016/j.clinph.2009.03.018

Bikson, M., Grossman, P., Thomas, C., Zannou, A. L., Jiang, J., Adnan, T., et al. (2016). Safety of transcranial direct current stimulation: evidence based update 2016. *Brain Stimul.* 9, 641–661. doi: 10.1016/j.brs.2016.06.004

Bola, M., Gall, C., Moewes, C., Fedorov, A., Hinrichs, H., and Sabel, B. A. (2014). Brain functional connectivity network breakdown and restoration in blindness. *Neurology* 83, 542–551. doi: 10.1212/WNL.0000000000000672

Brindley, G. S. (1955). The site of electrical excitation of the human eye. *J. Physiol.* 127, 189–200. doi: 10.1113/jphysiol.1955.sp005248

Brittain, J. S., Probert-Smith, P., Aziz, T. Z., and Brown, P. (2013). Tremor suppression by rhythmic transcranial current stimulation. *Curr. Biol.* 23, 436–440. doi: 10.1016/j.cub.2013.01.068

Brown, C. C. (1975). Electroanesthesia and electrosleep. *Am. Psychol.* 30, 402–410. doi: 10.1037/0003-066x.30.3.402

Brunoni, A. R., Amadera, J., Berbel, B., Volz, M. S., Rizzerio, B. G., and Fregni, F. (2011). A systematic review on reporting and assessment of adverse effects associated with transcranial direct current stimulation. *Int. J. Neuropsychopharmacol.* 14, 1133–1145. doi: 10.1017/S1461145710001690

Brunoni, A. R., Nitsche, M. A., Bolognini, N., Bikson, M., Wagner, T., Merabet, L., et al. (2012). Clinical research with transcranial direct current stimulation (tDCS): challenges and future directions. *Brain Stimul.* 5, 175–195. doi: 10.1016/j.brs.2011.03.002

Chaieb, L., Antal, A., Pisoni, A., Saiote, C., Opitz, A., Ambrus, G. G., et al. (2014). Safety of 5 kHz tACS. *Brain Stimul.* 7, 92–96. doi: 10.1016/j.brs.2013.08.004

Chaudhuri, A., and Behan, P. O. (2004). Fatigue in neurological disorders. *Lancet* 363, 978–988. doi: 10.1016/S0140-6736(04)15794-2

Cobb, S. (1947). Photic driving as a cause of clinical seizures in epileptic patients. *Arch. Neurol. Psychiatry* 58:70. doi: 10.1001/archneurpsyc.1947.02300300080008

Datta, A., Baker, J. M., Bikson, M., and Fridriksson, J. (2011). Individualized model predicts brain current flow during transcranial direct-current stimulation treatment in responsive stroke patient. *Brain Stimul.* 4, 169–174. doi: 10.1016/j.brs.2010.11.001

Datta, A., Truong, D., Minhas, P., Parra, L., and Bikson, M. (2012). Inter-individual variation during transcranial direct current stimulation and normalization of dose using MRI-derived computational models. *Front. Psychiatry* 3:91. doi: 10.3389/fpsyt.2012.00091

Delbeke, J. (2011). Electrodes and chronic optic nerve stimulation. *Biocybern. Biomed. Eng.* 31, 81–94. doi: 10.1016/s0208-5216(11)70021-3

Delbeke, J., Parrini, S., Andrien, A., Oozer, M., Legat, V., and Veraart, C. (2000). Modelling activation of visual structures through eyelid surface electrodes: preliminary result. *Pflügers Archiv. Eur. J. Physiol.* 440:R4.

Delbeke, J., Pins, D., Michaux, G., Wanet-Defalque, M. -C., Parrini, S., and Veraart, C. (2001). Electrical stimulation of anterior visual pathways in retinitis pigmentosa. *Invest. Ophthalmol. Vis. Sci.* 42, 291–297.

Downie, W., Leatham, P., Rhind, V., Wright, V., Branco, J., and Anderson, J. (1978). Studies with pain rating scales. *Ann. Rheum. Dis.* 37, 378–381.

Dzhokic, G., Jovchevska, J., and Dika, A. (2008). Electrical injuries: etiology, pathophysiology and mechanism of injury. *Macedonian J. Med. Sci.* 1, 54–58. doi: 10.3889/mjms.1857-5773.2008.0019

Farrar, J. T., Young J. P. Jr., LaMoreaux, L., Werth, J. L., and Poole, R. M. (2001). Clinical importance of changes in chronic pain intensity measured on an 11-point numerical pain rating scale. *Pain* 94, 149–158. doi: 10.1016/s0304-3959(01)00349-9

Feurra, M., Bianco, G., Santarnecchi, E., Del Testa, M., Rossi, A., and Rossi, S. (2011). Frequency-dependent tuning of the human motor system induced by transcranial oscillatory potentials. *J. Neurosci.* 31, 12165–12170. doi: 10.1523/JNEUROSCI.0978-11.2011

Feurra, M., Pasqualetti, P., Bianco, G., Santarnecchi, E., Rossi, A., and Rossi, S. (2013). State-dependent effects of transcranial oscillatory currents on the motor system: what you think matters. *J. Neurosci.* 33, 17483–17489. doi: 10.1523/JNEUROSCI.1414-13.2013

Gall, C., Sgorzaly, S., Schmidt, S., Brandt, S., Fedorov, A., and Sabel, B. A. (2011). Noninvasive transorbital alternating current stimulation improves subjective visual functioning and vision-related quality of life in optic neuropathy. *Brain Stimul.* 4, 175–188. doi: 10.1016/j.brs.2011.07.003

Garnsworthy, R. K., Gully, R. L., Kenins, P., and Westerman, R. A. (1988). Transcutaneous electrical stimulation and the sensation of prickle. *J. Neurophysiol.* 59, 1116–1127. doi: 10.1152/jn.1988.59.4.1116

Gekeler, F., Messias, A., Ottinger, M., Bartz-Schmidt, K. U., and Zrenner, E. (2006). Phosphenes electrically evoked with DTL electrodes: a study in patients with retinitis pigmentosa, glaucoma, and homonymous visual field loss and normal subjects. *Invest. Ophthalmol. Vis. Sci.* 47, 4966–4974.

Gekeler, F., Wrobel, W.G., and Messias, A. (2011). Method for treating an eye. United States patent application US 13/199,904. Washington, DC: U.S. Patent and Trademark Office.

Gellner, A. K., Reis, J., and Fritsch, B. (2016). Glia: a neglected player in non-invasive direct current brain stimulation. *Front. Cell. Neurosci.* 10:188. doi: 10.3389/fncel.2016.00188

Grützner, A., Grüsser, O. -J., and Baumgartner, G. (1958). Reaktionen einzelner Neurone im optischen Cortex der Katze nach elektrischer Reizung des Nervus opticus. *Arch. Psychiatrie Nervenkrankheiten* 197, 377–404. doi: 10.1007/bf00345845

Guleyupoglu, B., Schestatsky, P., Edwards, D., Fregni, F., and Bikson, M. (2013). Classification of methods in transcranial electrical stimulation (tES) and evolving strategy from historical approaches to contemporary innovations. *J. Neurosci. Methods* 219, 297–311. doi: 10.1016/j.jneumeth.2013.07.016

Haberbosch, L., Schmidt, S., Jooß, A., Köhn, A., Kozarzewski, L., Rönnefarth, M., et al. (2019). Rebound or entrainment? The influence of alternating current stimulation on individual alpha. *Front. Hum. Neurosci.* 13:43. doi: 10.3389/fnhum.2019.00043

Hakkinen, V., Eskola, H., Yli-Hankala, A., Nurmikko, T., and Kolehmainen, S. (1995). Which structures are sensitive to painful transcranial electric stimulation? *Electromyogr. Clin. Neurophysiol.* 35, 377–383.

Hallett, M. (2005). Neuroplasticity and rehabilitation. *J. Rehabil. Res. Dev.* 42, 17–22.

Hallett, M. (2007). Transcranial magnetic stimulation: a primer. *Neuron* 55, 187–199. doi: 10.1016/j.neuron.2007.06.026

Helfrich, R. F., Schneider, T. R., Rach, S., Trautmann-Lengsfeld, S. A., Engel, A. K., and Herrmann, C. S. (2014). Entrainment of brain oscillations by transcranial alternating current stimulation. *Curr. Biol.* 24, 333–339. doi: 10.1016/j.cub.2013.12.041

Herrick, R. M. (1967). Psychophysical methodology: comparison of thresholds of the method of limits and of the method of constant stimuli. *Percept. Mot. Skills* 24, 915–922. doi: 10.2466/pms.1967.24.3.915

Hummel, F. C., Celnik, P., Pascual-Leone, A., Fregni, F., Byblow, W. D., Buetefisch, C. M., et al. (2008). Controversy: noninvasive and invasive cortical stimulation show efficacy in treating stroke patients. *Brain Stimul.* 1, 370–382. doi: 10.1016/j.brs.2008.09.003

Iacono, M. I., Neufeld, E., Akinnagbe, E., Bower, K., Wolf, J., Vogiatzis Oikonomidis, I., et al. (2015). MIDA: a multimodal imaging-based detailed anatomical model of the human head and neck. *PloS One* 10:e0124126. doi: 10.1371/journal.pone.0124126

Irnich, W. (1980). The chronaxie time and its practical importance. *Pacing Clin. Electrophysiol.* 3, 292–301. doi: 10.1111/j.1540-8159.1980.tb05236.x

Irnich, W. (2010). The terms "chronaxie" and "rheobase" are 100 years old. *Pacing Clin. Electrophysiol.* 33, 491–496. doi: 10.1111/j.1540-8159.2009.02666.x

Jackson, M. P., Truong, D., Brownlow, M. L., Wagner, J. A., McKinley, R. A., Bikson, M., et al. (2017). Safety parameter considerations of anodal transcranial Direct Current Stimulation in rats. *Brain Behav. Immun.* 64, 152–161. doi: 10.1016/j.bbi.2017.04.008

Jarvis, C. W., and Voita, D. A. (1971). Low voltage skin burns. *Pediatrics* 48, 831–832.

Joundi, R. A., Jenkinson, N., Brittain, J. S., Aziz, T. Z., and Brown, P. (2012). Driving oscillatory activity in the human cortex enhances motor performance. *Curr. Biol.* 22, 403–407. doi: 10.1016/j.cub.2012.01.024

Kanai, R., Chaieb, L., Antal, A., Walsh, V., and Paulus, W. (2008). Frequency-dependent electrical stimulation of the visual cortex. *Curr. Biol.* 18, 1839–1843. doi: 10.1016/j.cub.2008.10.027

Kellogg, D. L. Jr., Johnson, J. M., and Kosiba, W. A. (1989). Selective abolition of adrenergic vasoconstrictor responses in skin by local iontophoresis of bretylium. *Am. J. Physiol.* 257(5 Pt 2), H1599-H1606.

Knutson, R.C. (1967). First international symposium on electrosleep therapy and electroanesthesia: a report. *Anesth. Analg.* 46, 333–339.

Laakso, I., and Hirata, A. (2013). Computational analysis shows why transcranial alternating current stimulation induces retinal phosphenes. *J. Neural. Eng.* 10:046009. doi: 10.1088/1741-2560/10/4/046009

Larntz, K. (1978). Small-sample comparisons of exact levels for chi-squared goodness-of-fit statistics. *J. Am. Stat. Assoc.* 73, 253–263. doi: 10.2307/2286650

Ledger, P. W. (1992). Skin biological issues in electrically enhanced transdermal delivery. *Adv. Drug Delivery Rev.* 9, 289–307. doi: 10.1016/0169-409X(92)90027-N

Liebetanz, D., Koch, R., Mayenfels, S., Konig, F., Paulus, W., and Nitsche, M. A. (2009). Safety limits of cathodal transcranial direct current stimulation in rats. *Clin. Neurophysiol.* 120, 1161–1167. doi: 10.1016/j.clinph.2009.01.022

Liew, S. L., Santarnecchi, E., Buch, E. R., and Cohen, L. G. (2014). Non-invasive brain stimulation in neurorehabilitation: local and distant effects for motor recovery. *Front. Hum. Neurosci.* 8:378. doi: 10.3389/fnhum.2014.00378

Lindenblatt, G., and Silny, J. (2002). Electrical phosphenes: on the influence of conductivity inhomogeneities and small-scale structures of the orbita on the current density threshold of excitation. *Med. Biol. Eng. Comput.* 40, 354–359. doi: 10.1007/bf02344219

Loo, C., Martin, D., Alonzo, A., Gandevia, S., Mitchell, P., and Sachdev, P. (2011). Avoiding skin burns with transcranial direct current stimulation: preliminary considerations. *Int. J. Neuropsychopharmacol.* 14, 425–426. doi: 10.1017/s1461145710001197

Ma, Z., Cao, P., Sun, P., Li, L., Lu, Y., Yan, Y., et al. (2014). Optical imaging of visual cortical responses evoked by transcorneal electrical stimulation with different

parameters. *Invest. Ophthalmol. Vis. Sci.* 55, 5320–5331. doi: 10.1167/iovs.14-14600

Magerl, W., Szolcsanyi, J., Westerman, R. A., and Handwerker, H. O. (1987). Laser Doppler measurements of skin vasodilation elicited by percutaneous electrical stimulation of nociceptors in humans. *Neurosci. Lett.* 82, 349–354. doi: 10.1016/0304-3940(87)90281-3

Marshall, L., Helgadottir, H., Molle, M., and Born, J. (2006). Boosting slow oscillations during sleep potentiates memory. *Nature* 444, 610–613. doi: 10.1038/nature05278

Merrill, D. R., Bikson, M., and Jefferys, J. G. (2005). Electrical stimulation of excitable tissue: design of efficacious and safe protocols. *J. Neurosci. Methods* 141, 171–198. doi: 10.1016/j.jneumeth.2004.10.020

Montgomery, S. A., and Asberg, M. (1979). A new depression scale designed to be sensitive to change. *Br. J. Psychiatry* 134, 382–389. doi: 10.1192/bjp.134.4.382

Neuling, T., Wagner, S., Wolters, C. H., Zaehle, T., and Herrmann, C. S. (2012). Finite-element model predicts current density distribution for clinical applications of tDCS and tACS. *Front. Psychiatry* 3:83. doi: 10.3389/fpsyt.2012.00083

Nitsche, M. A., Liebetanz, D., Lang, N., Antal, A., Tergau, F., and Paulus, W. (2003). Safety criteria for transcranial direct current stimulation (tDCS) in humans. *Clin. Neurophysiol.* 114, 2220–2222. doi: 10.1016/s1388-2457(03)00235-9

Obrosow, A. E. (1959). "Electrosleep therapy," in *Therapeutic Electricity and Ultraviolet Radiation*, ed. S. Licht (New Haven, CT: Imprint unknown), 169.

Parra, J., Kalitzin, S., Iriarte, J., Blanes, W., Velis, D., and Da Silva, F. L. (2003). Gamma-band phase clustering and photosensitivity: is there an underlying mechanism common to photosensitive epilepsy and visual perception? *Brain* 126, 1164–1172. doi: 10.1093/brain/awg109

Paulus, W. (2003). Transcranial direct current stimulation (tDCS). *Suppl. Clin. Neurophysiol.* 56, 249–254. doi: 10.1016/s1567-424x(09)70229-6

Paulus, W. (2010). On the difficulties of separating retinal from cortical origins of phosphenes when using transcranial alternating current stimulation (tACS). *Clin. Neurophysiol.* 121, 987–991. doi: 10.1016/j.clinph.2010.01.029

Paulus, W., Peterchev, A. V., and Ridding, M. (2013). Transcranial electric and magnetic stimulation: technique and paradigms. *Handbook Clin. Neurol.* 116, 329–342. doi: 10.1016/B978-0-444-53497-2.00027-9

Peterchev, A. V., Wagner, T. A., Miranda, P. C., Nitsche, M. A., Paulus, W., Lisanby, S. H., et al. (2012). Fundamentals of transcranial electric and magnetic stimulation dose: definition, selection, and reporting practices. *Brain Stimul.* 5, 435–453. doi: 10.1016/j.brs.2011.10.001

Pogosyan, A., Gaynor, L. D., Eusebio, A., and Brown, P. (2009). Boosting cortical activity at Beta-band frequencies slows movement in humans. *Curr. Biol.* 19, 1637–1641. doi: 10.1016/j.cub.2009.07.074

Polania, R., Paulus, W., and Nitsche, M. A. (2012). Noninvasively decoding the contents of visual working memory in the human prefrontal cortex within high-gamma oscillatory patterns. *J. Cogn. Neurosci.* 24, 304–314. doi: 10.1162/jocn_a_00151

Poreisz, C., Boros, K., Antal, A., and Paulus, W. (2007). Safety aspects of transcranial direct current stimulation concerning healthy subjects and patients. *Brain Res. Bull.* 72, 208–214. doi: 10.1016/j.brainresbull.2007.01.004

Potts, A. M., Inoue, J., and Buffum, D. (1968). The electrically evoked response of the visual system (EER). *Invest. Ophthalmol. Vis. Sci.* 7, 269–278.

Rager, G., and Singer, W. (1998). The response of cat visual cortex to flicker stimuli of variable frequency. *Eur. J. Neurosci.* 10, 1856–1877. doi: 10.1046/j.1460-9568.1998.00197.x

Robinovitch, L. (1914). "Electrical analgesia, sleep and resuscitation," in *Anesthesia*, ed. J.T. Gwathmey (New York, NY: D. Appleton and Company), 628–643.

Rohracher, H. (1935). Die gehirnelektrischen Erscheinungen bei geistiger Arbeit. *Zeitschrift für Psychologie und Charakterkunde* 136, 308–324.

Sandrini, M., and Cohen, L.G. (2013). "Noninvasive brain stimulation in neurorehabilitation," in *Handbook of Clinical Neurology*, eds A.M. Lozano & M. Hallett (Amsterdam: Elsevier), 499–524. doi: 10.1016/b978-0-444-53497-2.00040-1

Santarnecchi, E., Muller, T., Rossi, S., Sarkar, A., Polizzotto, N. R., Rossi, A., et al. (2016). Individual differences and specificity of prefrontal gamma frequency-tACS on fluid intelligence capabilities. *Cortex* 75, 33–43. doi: 10.1016/j.cortex.2015.11.003

Santarnecchi, E., Polizzotto, N. R., Godone, M., Giovannelli, F., Feurra, M., Matzen, L., et al. (2013). Frequency-dependent enhancement of fluid intelligence induced by transcranial oscillatory potentials. *Curr. Biol.* 23, 1449–1453. doi: 10.1016/j.cub.2013.06.022

Saturnino, G. B., Antunes, A., and Thielscher, A. (2015). On the importance of electrode parameters for shaping electric field patterns generated by tDCS. *Neuroimage* 120, 25–35. doi: 10.1016/j.neuroimage.2015.06.067

Schmidt, S., Mante, A., Ronnefarth, M., Fleischmann, R., Gall, C., and Brandt, S. A. (2013a). Progressive enhancement of alpha activity and visual function in patients with optic neuropathy: a two-week repeated session alternating current stimulation study. *Brain Stimul.* 6, 87–93. doi: 10.1016/j.brs.2012.03.008

Schmidt, S., Scholz, M., Obermayer, K., and Brandt, S. A. (2013b). Patterned brain stimulation, what a framework with rhythmic and noisy components might tell us about recovery maximization. *Front. Hum. Neurosci.* 7:325. doi: 10.3389/fnhum.2013.00325

Schutter, D. J. (2016). Cutaneous retinal activation and neural entrainment in transcranial alternating current stimulation: a systematic review. *Neuroimage* 140, 83–88. doi: 10.1016/j.neuroimage.2015.09.067

Sergeev, G. V. (1963). Electrosleep as a method of neurotropic therapy of patients with hypertensive disease. *Am. Heart J.* 66, 138–139. doi: 10.1016/0002-8703(63)90081-4

Streiner, D. L., and Norman, G. R. (2008). *Health Measurement Scales: A Practical Guide to their Development and Use*. Oxford: Oxford university press.

Talelli, P., and Rothwell, J. (2006). Does brain stimulation after stroke have a future? *Curr. Opin. Neurobiol.* 19, 543–550. doi: 10.1097/WCO.0b013e32801080d1

Thil, M.-A., Duy, D. T., Colin, I. M., and Delbeke, J. (2007). Time course of tissue remodelling and electrophysiology in the rat sciatic nerve after spiral cuff electrode implantation. *J. Neuroimmunol.* 185, 103–114. doi: 10.1016/j.jneuroim.2007.01.021

Ticleanu, C., and Littlefair, P. (2015). A summary of LED lighting impacts on health. *Int. J. Sustain. Light.* 17, 5–11. doi: 10.26607/ijsl.v17i0.11

Trenite, D. G., Binnie, C. D., Harding, G. F., Wilkins, A., Covanis, T., Eeg-Olofsson, O., et al. (1999). Medical technology assessment photic stimulation–standardization of screening methods. *Neurophysiol. Clin.* 29, 318–324. doi: 10.1016/s0987-7053(99)90045-x

Tuckett, R. P. (1982). Itch evoked by electrical stimulation of the skin. *J. Invest. Dermatol.* 79, 368–373. doi: 10.1111/1523-1747.ep12529734

Vossen, A., Gross, J., and Thut, G. (2015). Alpha power increase after transcranial alternating current stimulation at alpha frequency (alpha-tACS) reflects plastic changes rather than entrainment. *Brain Stimul.* 8, 499–508. doi: 10.1016/j.brs.2014.12.004

Walker, A. E., Woolf, J. I., Halstead, W. C., and Case, T. J. (1944). Photic driving. *Arch. Neurol. Psychiatry* 52, 117–125.

Wester, K., Jönsson, A. K., Spigset, O., Druid, H., and Hägg, S. (2008). Incidence of fatal adverse drug reactions: a population based study. *Br. J. Clin. Pharmacol.* 65, 573–579. doi: 10.1111/j.1365-2125.2007.03064.x

Yuen, T. G., Agnew, W. F., Bullara, L. A., Jacques, S., and McCreery, D. B. (1981). Histological evaluation of neural damage from electrical stimulation: considerations for the selection of parameters for clinical application. *Neurosurgery* 9, 292–299. doi: 10.1227/00006123-198109000-00013

Zaghi, S., Acar, M., Hultgren, B., Boggio, P. S., and Fregni, F. (2010). Noninvasive brain stimulation with low-intensity electrical currents: putative mechanisms of action for direct and alternating current stimulation. *Neuroscientist* 16, 285–307. doi: 10.1177/1073858409336227

Ziemssen, H. (1864). *Die Electricität in der Medicin*. Berlin: August Hirschwald.

Conflict of Interest Statement: The authors declare that the research was conducted in the absence of any commercial or financial relationships that could be construed as a potential conflict of interest.

frontiers in Neuroscience

ORIGINAL RESEARCH
published: 14 August 2019
doi: 10.3389/fnins.2019.00841

Determinants of Inter-Individual Variability in Corticomotor Excitability Induced by Paired Associative Stimulation

*Lora Minkova[1,2,3], Jessica Peter[1], Ahmed Abdulkadir[1], Lena V. Schumacher[4], Christoph P. Kaller[3,5], Christoph Nissen[2,6,7], Stefan Klöppel[1,8] and Jacob Lahr[2,3]**

[1] University Hospital of Old Age Psychiatry and Psychotherapy, University of Bern, Bern, Switzerland, [2] Department of Psychiatry and Psychotherapy, Medical Center – University of Freiburg, Faculty of Medicine, University of Freiburg, Freiburg, Germany, [3] Freiburg Brain Imaging, Medical Center – University of Freiburg, Freiburg, Germany, [4] Department of Medical Psychology and Medical Sociology, Faculty of Medicine, University of Freiburg, Freiburg, Germany, [5] Department of Neuroradiology, Medical Center – Faculty of Medicine, University of Freiburg, Freiburg, Germany, [6] University Hospital of Psychiatry and Psychotherapy, University Psychiatric Services, University of Bern, Bern, Switzerland, [7] Department of Neurology, University Hospital Bern, University of Bern, Bern, Switzerland, [8] Center for Geriatrics and Gerontology Freiburg, Medical Center – Faculty of Medicine, University of Freiburg, Freiburg, Germany

OPEN ACCESS

Edited by:
Julie Duque, Catholic University of Louvain, Belgium

Reviewed by:
Erika Kristine Ross, Mayo Clinic, United States
Virginia López-Alonso, Universidad Pontificia Comillas, Spain
Martin Victor Sale, The University of Queensland, Australia

***Correspondence:**
Jacob Lahr
jacob.lahr@uniklinik-freiburg.de

Specialty section:
This article was submitted to Neural Technology, a section of the journal Frontiers in Neuroscience

Received: *30 April 2019*
Accepted: *26 July 2019*
Published: *14 August 2019*

Citation:
Minkova L, Peter J, Abdulkadir A, Schumacher LV, Kaller CP, Nissen C, Klöppel S and Lahr J (2019) Determinants of Inter-Individual Variability in Corticomotor Excitability Induced by Paired Associative Stimulation. Front. Neurosci. 13:841. doi: 10.3389/fnins.2019.00841

Transcranial magnetic stimulation (TMS) is a well-established tool in probing cortical plasticity *in vivo*. Changes in corticomotor excitability can be induced using paired associative stimulation (PAS) protocol, in which TMS over the primary motor cortex is conditioned with an electrical peripheral nerve stimulation of the contralateral hand. PAS with an inter-stimulus interval of 25 ms induces long-term potentiation (LTP)-like effects in cortical excitability. However, the response to a PAS protocol tends to vary substantially across individuals. In this study, we used univariate and multivariate data-driven methods to investigate various previously proposed determinants of inter-individual variability in PAS efficacy, such as demographic, cognitive, clinical, neurophysiological, and neuroimaging measures. Forty-one right-handed participants, comprising 22 patients with amnestic mild cognitive impairment (MCI) and 19 healthy controls (HC), underwent the PAS protocol. Prior to stimulation, demographic, genetic, clinical, as well as structural and resting-state functional MRI data were acquired. The two groups did not differ in any of the variables, except by global cognitive status. Univariate analysis showed that only 61% of all participants were classified as PAS responders, irrespective of group membership. Higher PAS response was associated with lower TMS intensity and with higher resting-state connectivity within the sensorimotor network, but only in responders, as opposed to non-responders. We also found an overall positive correlation between PAS response and structural connectivity within the corticospinal tract, which did not differ between groups. A multivariate random forest (RF) model identified age, gender, education, IQ, global cognitive status, sleep quality, alertness, TMS intensity, genetic factors, and neuroimaging measures (functional and structural connectivity, gray matter (GM) volume, and cortical thickness as poor predictors of PAS response. The model resulted in low accuracy of the RF classifier

(58%; 95% CI: 42 – 74%), with a higher relative importance of brain connectivity measures compared to the other variables. We conclude that PAS variability in our sample was not well explained by factors known to influence PAS efficacy, emphasizing the need for future replication studies.

Keywords: TMS, paired associative stimulation, resting-state fMRI, sensorimotor network, DTI, corticospinal tract, random forest

INTRODUCTION

Transcranial magnetic stimulation (TMS) is a well-established non-invasive brain stimulation tool that can be used to probe cortical plasticity. Changes in corticomotor excitability can be induced using a paired associative stimulation (PAS; Stefan et al., 2000). This involves the repeated application of an electrical peripheral nerve stimulus (e.g., median nerve stimulation; MNS) paired with a single-pulse TMS to the primary motor cortex. The TMS leads to a contralateral muscle contraction that can be measured in the form of a motor evoked potential (MEP). PAS is related to Hebbian principle of activity-dependent long-term modification of synaptic plasticity (Hebb, 1949). Depending on the inter-stimulus intervals and stimulation duration, PAS may induce either long-term potentiation (LTP)-like or long-term depression (LTD)-like effects (Ziemann et al., 2008). Such shifts in corticomotor excitability are quantified by topographically specific changes in the MEP amplitudes.

The PAS protocol consists of a short pre-measurement period (i.e., baseline MEP), followed by the PAS intervention, and finally a post-measurement period to evaluate stimulation effects. PAS-induced LTP-like effects are associated with increased MEP amplitudes following stimulation. However, research shows that the PAS response is not always robustly elicited but is rather affected by considerable inter- and intra-individual variability (Müller-Dahlhaus et al., 2008; Ridding and Ziemann, 2010; Karabanov et al., 2016). For instance, a number of different studies have shown that PAS targeting the primary motor cortex elicited the expected effect in only 60% or less of all participants (for a review, see Karabanov et al., 2016). Due to this variability, the division into responders and non-responders has been used in previous works by applying a dichotomous cut-off (Müller-Dahlhaus et al., 2008; List et al., 2013b; López-Alonso et al., 2014; Klöppel et al., 2015; Lahr et al., 2016b). More specifically, the grand average of the post-stimulation sessions is calculated, normalized to the mean MEP at baseline. Participants are then divided into PAS responders (with post/baseline ratios above 1) and PAS non-responders (with post/baseline ratios equal to or below 1).

To date, fluctuations in post-stimulation effects among participants are poorly-understood. PAS-induced LTP-like effects have been reported to decrease with age (Müller-Dahlhaus et al., 2008) as well as in clinical populations, such as Alzheimer's patients (Battaglia et al., 2007) and Parkinson's patients (Morgante et al., 2006), among others. Other potential sources of intra-and inter-individual variability in responses to PAS include circadian fluctuations and time of day (Sale et al., 2007; López-Alonso et al., 2014), alertness (Kamke et al., 2012), attentional state (Stefan et al., 2004), sleep (Kuhn et al., 2016), stimulation intensity (Müller-Dahlhaus et al., 2008), as well as genetic traits (Missitzi et al., 2011), such as brain-derived neurotrophic factor (BDNF) polymorphism (Cheeran et al., 2008; Fried et al., 2017) and possibly also Apolipoprotein E (APOE) genotype (Peña-Gomez et al., 2012; Lahr et al., 2016b). Additionally, neuroanatomical determinants, such as cortical thickness (Conde et al., 2012; List et al., 2013b) and microstructural properties of white matter (WM) (Klöppel et al., 2008; List et al., 2013a), seem to influence cortical excitability, as well. Previously, it has been shown that resting-state functional connectivity patterns measured prior to repetitive TMS intervention in depression may also predict individual therapeutic response (Downar et al., 2014; Salomons et al., 2014).

All the various potential determinants of inter-individual variability in PAS efficiency have been investigated in isolation by different studies but have not been replicated systematically. Here, we propose a multivariate explorative approach to investigate to what extent PAS response rate can be predicted using different factors of variability, including demographic variables and factors (e.g., age, gender, education, IQ), genetic characteristics (e.g., BNDF, APOE), neuroanatomical measures (e.g., cortical thickness, structural and functional connectivity patterns), neurophysiological qualities (e.g., sleep quality, attention, alertness), and neuropsychological variables (cognitive status, depression). For this purpose, we used a Random Forest (RF) classifier, an ensemble machine learning algorithm, which consists of a collection of decision trees trained with different subsets of the original data (Breiman, 2001). Among the advantages of RF is that it is robust to noise, is invariant to the scaling of features, can handle high-dimensional, redundant data and can be used for ranking the importance of predictors by randomly permuting the values of each predictor at a time and estimating the decrease in prediction accuracy. The aim of our study is twofold. First, we hypothesize that a combination of different factors would be best suited to predict the efficiency of the PAS outcome, and, second, we aim to assess the hierarchical importance of these determinants of PAS variability, which could be used to inform future studies focusing on TMS-induced plasticity.

MATERIALS AND METHODS

Participants

A total of 48 participants were included in the original study (Lahr et al., 2016b). Among them, 24 were patients with amnestic MCI and 24 were age-, sex- and education-matched healthy

controls (HC). MCI were diagnosed as being amnestic if memory function was below 1.5 SD on verbal delayed recall (Petersen et al., 1999; Albert et al., 2011). One participant with Beck Depression Inventory (BDI-II; Beck et al., 1996) score of $\geq$13 and Geriatric Depression Scale (GDS; Yesavage and Sheikh, 1986) score $\geq$5 was excluded from the study, according to the cut-off score for a minor depressive syndrome. Further three participants were excluded due to corrupt or missing MRI scans, as well as three participants were excluded due to left-handedness, which was assessed using the Edinburgh Handedness Inventory (EHI; Oldfield, 1971). Further exclusion criteria included any history of severe neurological, psychiatric or other diseases, smoking, or any history of substance abuse. Thus, the final study sample comprised 41 participants (19 MCI and 22 HC). Patients were recruited from the Center for Geriatric Medicine and Gerontology of the Medical Center – University of Freiburg, Germany, while controls were recruited via newspaper advertisements and handouts circulated in Freiburg. The study was approved by the Ethics Commission of the Medical Center – University of Freiburg (Approval #227/12) and written informed consent was obtained from all participants prior to participation according to the Declaration of Helsinki.

Study Procedure

Each participant took part in the study on two consecutive days. Prior to testing, all participants were asked to complete the questionnaire of handedness (EHI; Oldfield, 1971), the Pittsburgh Sleep Quality Index (PSQI; Buysse et al., 1989) to assess sleep quality over the 4 weeks prior to testing, as well as BDI and GDS to assess depressive symptoms. The total BDI and GDS depression scores were transformed into z-scores using the sample statistics and combined into one single composite score (i.e., the average of the two scores) for subsequent analyses. On the first study day, participants completed a neuropsychological battery including diverse short tests assessing executive functioning, verbal and non-verbal learning, episodic memory, and visuo-constructive abilities, as reported elsewhere (Lahr et al., 2016b; Peter et al., 2016, 2018a,b). Global cognitive functioning was evaluated using the Montreal Cognitive Assessment (MoCA; Nasreddine et al., 2005). Structural and functional MRI scans were also acquired during the first day of testing (for more detail, see sections "MRI Data Acquisition" to "Diffusion MRI" below). On the following day, TMS was performed in the afternoon and sleep quality between day 1 and day 2 was assessed using the Sleep Questionnaire A (SFA; Görtelmeyer, 1985). Alertness and selective attention were evaluated using the WAF Perception and Attention Functions Battery (Sturm, 2006) as part of Vienna Test System[1]. Finally, blood samples were also collected from all participants in order to determine APOE allele ε4 genotype and BDNF Val66Met polymorphism.

PAS Protocol

The stimulation protocol was based on a previously published and widely used PAS paradigm (Stefan et al., 2000), in which TMS over the left primary motor cortex was conditioned by electrical stimulation of the right hand.

We performed TMS using a magnetic stimulator (Magstim 200; Magstim; Whitland, United Kingdom) with a figure-of-eight coil. The coil was positioned tangentially above the left primary motor cortex, with the handle pointing backward and rotated approximately 45° away from the midsagittal plane. The stimulation hotspot was defined as the optimal coil position to elicit motor responses in the contralateral abductor pollicis brevis (APB) muscle at suprathreshold stimulator intensity. The strength of the muscle contraction was recorded as motor evoked potentials (MEPs), the amplitude of which reflects cortical excitability from the targeted primary motor cortex. The stimulator intensity was adjusted in order to evoke a peak-to-peak MEP amplitude of 1 mV. MEPs were monitored online and amplified, bandpass-filtered (lowpass-filter: 8 kHz, time constant: 30 ms, corresponding to a cut-off frequency of 5.3 Hz) and digitized with an analog-to-digital converter at a sampling rate of 2 kHz (micro1401, Cambridge Electronic Designs, United Kingdom). Coil position and orientation were monitored and captured using an optical navigation system (Localite GmbH, Sankt Augustin, Germany).

Conditioning stimuli represented single pulses of electrical stimulation through bipolar electrodes applied to the median nerve at the right wrist, using a constant current stimulator (Digitimer DS7; Welwyn Garden City, United Kingdom). Electrical stimulation intensity was set to 300% of the individual perception threshold. The conditioning stimulus preceded the magnetic cortical stimulus by a time interval of 25 ms, which has been shown to result in facilitation of the MEP responses (Stefan et al., 2000). A total of 180 paired stimuli were applied at an interval of 5 s.

The PAS protocol consisted of three different conditions: one pre-measurement as a baseline (PRE), the intervention condition (PAS), and three post-measurement conditions: immediately after PAS (post1), after 8 min (post2), and after 15 min (post3), respectively. During the PRE and POST conditions, 20 TMS pulses were applied at an interval of 6 s and with a variability of 20% in order to prevent systematic MEP variability due to expectation. To keep participants attentive, they were presented landscape images on a screen during the PRE and POST conditions. When the PAS intervention started, they were asked to mentally count blue balls appearing on a computer screen. Ball counting was meant to ensure that participants did not close their eyes or fall asleep during PAS, but the total number of balls counted was not included in subsequent statistical analyses.

Trials with pre-facilitated activity were discarded manually, affecting on average 6.3 ± 1.8 out of 80 trials per individual. Based on previous literature, the three post-sessions were averaged and divided by the baseline amplitude in order to compute a marker of potentiation (Müller-Dahlhaus et al., 2008; List et al., 2013a,b). Based on the recommendations by a previous multicentric analysis (Lahr et al., 2016a), we used the logarithms of the MEP amplitude ratio (i.e., post/baseline quotient) for subsequent analyses to reduce the possibility that results are driven by few extreme MEP measurements. Furthermore, we divided participants into two categories: PAS responders (log

[1]https://www.schuhfried.at/test/WAF

of MEP-ratio above 0) and non-responders (log of MEP-ratio equal to or below 0).

Electric Field Simulation

The distribution of the electric field strength (i.e., the vector norm of the electric field E) induced by TMS was computed in SimNIBS (Version 2.1.1)[2], based on the finite element approach using individual head models derived from the structural T1 and T2 MR images (Windhoff et al., 2013; Thielscher et al., 2015). Following the approach by Antonenko et al. (2018), the middle layer of the cortex was estimated for each participant based on segmentation results of the Computational Anatomy Toolbox CAT12 r1355[3]. Then, the position of the maximum electric field strength within the middle cortex layer was calculated as the TMS hotspot for each individual separately.

MRI Data Acquisition

Scanning was performed on a 3 Tesla Siemens MAGNETOM TrioTim Syngo MR B17 scanner (Siemens Medical Systems, Erlangen, Germany) with a 12-channel phase array head coil. A high-resolution whole-brain T1-weighted anatomical image was acquired for each participant using the following magnetization-prepared rapid acquisition gradient echo (MPRAGE) sequence parameters: TR = 2200 ms, TE = 2.15 ms, FA = 12°, FOV = 256 mm, matrix size of 256 × 256 × 176 mm, and slice thickness of 1.0 × 1.0 × 1.0 mm, without a slice gap. Additionally, whole-brain T2*-weighted functional resting-state scans oriented along the AC-PC line were acquired for all participants using the following gradient echo-planar imaging (EPI) sequence: TR = 2610 ms, TE = 30 ms, FA = 80°, FOV = 192 mm, matrix size = 192 × 192 × 151 mm, 42 axially oriented slices acquired in a descending order, slice thickness of 3.0 × 3.0 × 3.0 mm, without a slice gap, and bandwidth of 2056 Hz/px. Resting-state scans consisted of 201 volumes. Participants were instructed to relax and passively stare at a fixation cross on a monitor display, keeping their eyes open during data acquisition. Diffusion-weighted images (DWI) were also acquired for each participant with the following acquisition parameters: TR = 10 s, TE = 94 ms, number of diffusion gradient directions = 61 (b = 1000 s/mm^2), one image without diffusion weighting (b = 0 s/mm^2), FOV = 208 mm, matrix size = 208 × 208 × 138 mm, slice thickness = 2.0 × 2.0 × 2.0 mm, and number of slices = 69.

Structural MRI

Raw T1-weighted scans were visually inspected to ensure proper data quality and the absence of brain pathology (e.g., stroke or subdural hematoma). One participant was excluded due to poor data quality. All images were preprocessed using SPM12 v.6685 (Statistical Parametric Mapping, Welcome Trust Centre for Neuroimaging[4]) and the CAT12 r1355 (see footnote 3), running on MATLAB R2015a (Mathworks, Natick, MA, United States). They were first segmented into gray matter (GM), WM, and cerebrospinal fluid (CSF) using the IXI550_MNI152 template and the tissue probability map based on the Unified Segmentation (Ashburner and Friston, 2005). The segmented images were used to create an improved anatomical scan for subsequent co-registration of the functional images. Using the DARTEL extension for high-dimensional registration approach (Ashburner, 2007), deformation parameters were extracted for normalization of the functional images. CAT12 was used for voxel-based morphometry (VBM) to calculate GM and total intracranial volumes as well as for surface-based morphometry (SBM) to estimate cortical thickness based on the project-based thickness method (Dahnke et al., 2013). Region-of-interest (ROI) was the left precentral gyrus (Brodmann area 4) based on the Desikan-Killiany atlas (Desikan et al., 2006), which corresponds to the primary motor cortex. Regional GM volume was corrected for total intracranial volume (TIV) to account for individual brain size.

Functional MRI

Preprocessing and functional connectivity of the resting-state fMRI data were completed using the CONN Toolbox v.18a (Whitfield-Gabrieli and Nieto-Castanon, 2012) in conjunction with SPM12. The first ten volumes were removed prior to preprocessing to avoid T1 equilibration effects. Preprocessing steps then included: slice-timing correction, realignment, coregistration to the anatomical image, normalization to MNI space, outlier detection (ART-based scrubbing), and smoothing with a Gaussian kernel (6 mm FWHM). None of the participants was excluded due to excessive head movement (motion artifact threshold: translation >3 mm, rotation >1°). One participant was excluded due to incomplete scans. A component-based noise correction (aCompCor) strategy (Behzadi et al., 2007) was used to remove the confounding effects of WM and CSF (five components each). Motion parameters were also regressed out (12 regressors: 6 motion parameters + 6 first-order temporal derivatives). Finally, the time-series were linearly detrended and band-pass filtered (0.01–0.08 Hz) to reduce noise effects and low-frequency drift.

Functional connectivity analysis was then performed using a whole-brain seed-to-voxel approach, where individual correlation maps were generated by extracting the mean resting-state BOLD time-series from the seed and calculating the correlation coefficients with the BOLD time-series of all other voxels. To compute the functional connectivity of the sensorimotor network, the left precentral gyrus based on the Desikan-Killiany atlas (Desikan et al., 2006) was used as a seed. The network was also replicated by replacing the seed with each individual's TMS hotspot region that resulted from the electric field simulation analysis. Bivariate correlation coefficients were calculated using the General Linear Model (GLM) and a Fisher's transformation was applied in order to normalize the data. Second-level (group) analysis within the CONN toolbox was used to compute and visualize the seed-based sensorimotor connectivity network across all

[2]https://simnibs.github.io/simnibs/build/html/index.html

[3]http://www.neuro.uni-jena.de/cat/

[4]http://www.fil.ion.ucl.ac.uk/spm

participants, with p-uncorrected value <0.001 before applying the False Discovery Rate (FDR) correction at the cluster level ($p_{FDR} < 0.05$). Connectivity strengths were then extracted for further statistical analysis.

Diffusion MRI

The DWI data were processed using standard FLS v.6.0 pipelines (Smith et al., 2004). The raw images were first corrected for eddy current distortions. The no-gradient (B0) image was skull-stripped using the Brain Extraction Tool (BET). Diffusion tensor fitting was completed using DTIFIT and fractional anisotropy (FA) values were derived from the tensors. Prior to fiber-tracking, crossing fibers within each voxel of the brain were estimated with a Bayesian method implemented in BEDPOSTX (Behrens et al., 2007). Probabilistic tractography of the corticospinal tract (CST) was computed in PROBTRACKX (Behrens et al., 2007) using pre-selected ROIs as seeds and targets based on previous literature (Wakana et al., 2004; Zhang et al., 2010; Chenot et al., 2018). More specifically, the left precentral gyrus was defined as a seed and the cerebral peduncle as a target. The internal capsule and the pons were defined as inclusion (i.e., waypoint) masks. In contrast, exclusion masks included the midline to remove pathways crossing into the other hemisphere. A WM termination mask was also used to ensure tracts stopped at the gray/white matter interface, thus discarding pathways extending into gray matter, CSF or dura. ROIs were created using the FSL Montreal Neurological Institute template and the Johns Hopkins University WM Labels Atlas (Mori et al., 2005). Connectivity distributions were generated from the seed regions in native space. The number of streamlines per voxel was set to 5000. The resulting images were then warped into diffusion space using the FMRIB's Linear Image Registration Tool (FLIRT) and overlaid onto the B0 image for quality control. Each participant's *FA* values were extracted from the CST for further statistical analysis. The tractography pathways of all participants were registered to FMRIB58_FA standard MNI space and averaged for visualization purposes.

Statistical Analysis and Machine Learning

Statistical analysis was completed using R version 3.5.2 (R Core Team, 2016). First, demographic, clinical, and imaging data were compared between PAS responders and non-responders. Previously, we found no significant differences between controls and MCI (Lahr et al., 2016b), but report results here for completeness. Data normality was assessed using the Shapiro–Wilk test. Univariate statistical analysis was conducted using ANOVA/ANCOVA or Mann–Whitney U tests for continuous variables, as appropriate. Kruskal–Wallis test was used for ordinal variables and Chi-square test for dichotomous variables. Our analysis focused on the PAS response rate (responders vs. non-responders), which is a dichotomized variable with less statistical power. Therefore, we also completed a correlation analysis (Spearman's rank correlation coefficient) using the log-transformed MEP ratio between the averaged post-measurements and baseline as a dependent variable. Correlation coefficients were converted to z-scores and compared between responders and non-responders. In all univariate analyses, a p-value < 0.05 (two-tailed) was considered significant. Adjustment for multiple comparisons was performed using the Benjamini–Hochberg method (Benjamini and Hochberg, 1995), controlling for FDR. Of note, due to the high number of variables and the relatively small sample size, the univariate analysis is exploratory in nature and may be affected by false-negative results.

Multivariate data analysis was conducted using a RF classifier, implemented in the *randomForest* R package (Liaw and Wiener, 2002). RF is an ensemble machine learning algorithm, which consists of a collection of decision trees trained with different subsets of the original data (Breiman, 2001). A detailed description of the algorithm is provided elsewhere (Liaw and Wiener, 2002). Briefly, the algorithm draws n_{tree} bootstrap samples from the original data and grows a classification tree for each of the bootstrap samples by sampling the predictors randomly (m_{try}) and choosing the best split among those variables. After a large number of trees are generated, each RF classifier casts a vote for the most popular class. At each bootstrap iteration, out-of-bag (OOB) predictions (i.e., predicting the data not in the bootstrap sample using the tree grown with the bootstrap sample) are aggregated. On average, each data point would be OBB around 36% of the times. An OBB estimate of error rate (i.e., misclassification rates) is computed representing the classifier's strength and dependence. RF also provides a measure of the importance of the predictor variables by looking at how much prediction error increases when OBB data for the variable is permuted, while all others are left unchanged.

We set the optimal number of trees (n_{tree}) to 500 and ran the model 10 times in order to choose the number of random variables used in each tree (mtry). We chose $m_{try} = 6$ for our model, where the OOB error rate showed to stabilize and reach a minimum. We assessed the accuracy of the RF model in classifying between PAS responders and non-responders (outcome variable) using the *caret* R package (Kuhn et al., 2019). The ROC curve for RF was created using the *ROCR* R package (Sing et al., 2005). The following predictive variables were included in the model: demographic (age, sex, education, and IQ), clinical (MCI vs. HC, composite depression score, and global cognitive status based on MoCA), neurophysiological (sleep quality, attention, and alertness), genetic (APOE and BDNF), and MRI measures (cortical thickness, GM volume, functional and structural connectivity). TMS intensity (i.e., percent of maximal stimulator output) was also included as a predictor in the model. The importance of each variable was assessed using the mean decrease of accuracy, representing how much removing each variable reduced the accuracy of the model, as well as the mean decrease in Gini impurity index used for the calculation of splits in trees. Loosely speaking, the higher the values of mean decrease in accuracy and decrease in Gini score, the higher the importance of the variable in the model.

TABLE 1 | Sample characteristics.

	N	Overall (*n* = 41)	HC (*n* = 22, 54%)	MCI (*n* = 19, 46%)	Responders (*n* = 25, 61%)	Non-responders (*n* = 16, 39%)
Demographic, cognitive and clinical data						
Groups						
HC	22	22 (54%)	–	–	11 (50%)	11 (50%)
MCI	19	19 (46%)	–	–	14 (74%)	5 (26%)
Age (years)	41	70.2 (5.5)	69.5 (5.9)	71.5 (4.9)	70.3 (5.0)	69.9 (6.5)
Gender (males)	41	24 (58%)	14 (63%)	10 (53%)	15 (60%)	9 (57%)
Education (years)	41	13.0 (7–20)	14.5 (7–20)	13.0 (8–20)	13.0 (7–20)	13.5 (9–20)
MWT-B IQ	41	124 (97–143)	127 (97–143)	121 (97–136)	118 (97–143)	124 (100–136)
MoCA score	40	26 (17–30)	27 (22–30)	23 (17–29)	25 (17–30)	27 (19–30)
BDI-GDS z-score	41	−0.07 (0.90)	−0.14 (0.81)	0.16 (0.98)	0.02 (0.95)	−0.03 (0.83)
Sleep, attention and alertness						
SFA-SQ score	40	4.1 (1.9–5.2)	4.2 (1.9–5.0)	3.9 (2.1–5.2)	4.2 (2.1–5.2)	3.9 (1.9–4.9)
PSQI score	40	6 (2–16)	5 (2–14)	6 (2–16)	6 (2–16)	5 (3–9)
WAF (RT in ms)						
Alertness (intrinsic)	40	236 (66)	212 (50)	263 (84)	232 (72)	243 (57)
Alertness (phasic)	41	221 (88)	207 (70)	237 (110)	216 (98)	228 (75)
Selective attention	39	355 (138)	342 (110)	371 (171)	332 (123)	390 (143)
Genetic traits						
BDNF (Val66Met)	39	15 (38%)	8 (36%)	7 (41%)	10 (41%)	5 (33%)
APOE4 ε4 carriers	35	17 (49%)	7 (37%)	10 (63%)	12 (55%)	5 (39%)
TMS data						
PAS response (log)	41	0.05 (0.2)	0.02 (0.1)	0.07 (0.2)	0.2 (0.2)	−0.2 (0.1)
TMS intensity (%)	41	50 (35–82)	54 (38–82)	49 (35–72)	49 (35–82)	54 (38–65)
PAS responders	41	25 (61%)	11 (44%)	14 (56%)	–	–
Imaging data						
CT of M1	41	2.1 (0.1)	2.1 (0.2)	2.1 (0.1)	2.1 (0.1)	2.0 (0.2)
GMV of M1 ($TIV_{corr.}$)	41	0.1 (1.1)	0.2 (1.3)	0.1 (0.1)	0.2 (0.9)	0.5 (1.3)
FA of CST	41	0.5 (0.2–0.5)	0.5 (0.4–0.5)	0.5 (0.2–0.5)	0.5 (0.3–0.5)	0.4 (0.2–0.5)
FC of M1-S1	41	0.1 (0.1)	0.2 (0.1)	0.1 (0.1)	0.2 (0.1)	0.1 (0.1)

Data are provided as mean (SD), median (IQR), or n (%). HC, healthy controls; MCI, mild cognitive impairment; MWT-B IQ, multiple-choice word intelligence test, version B; MoCA, Montreal Cognitive Assessment; BDI-GDS z-score, composite score of the beck depression inventory and the geriatric depression score; SFA-SQ, sleep questionnaire A – sleep quality; PSQI, Pittsburgh Sleep Quality Index; WAF, Perception and Attention Functions Battery; BDNF, brain derived neurotrophic factor; APOE4, apolipoprotein allele 4; PAS response, log-transformed MEP ratio between the averaged post-measurements and baseline; CT, cortical thickness; M1, primary motor cortex; S1, primary somatosensory cortex; GMV, gray matter volume; TIV, total intracranial volume; FA, fractional anisotropy; CST, corticospinal tract; FC, resting-state functional connectivity z-scores.

RESULTS

A detailed description of the cohort's demographic and clinical information is presented in **Table 1**.

Demographic, Cognitive and Clinical Data

Of the 41 participants included in the study, 22 (54%) were HC and 19 (46%) were MCI. The two groups did not differ in age ($F_{(1,39)} = 2.098$, $p = 0.156$), gender (HC: 14 males, MCI: 10 males; $X^2_{(1)} = 0.156$, $p = 0.693$), or education (Mann–Whitney $U = 243$, $p = 0.378$). No difference was also found between genetic factors such as the presence of APOE allele $\varepsilon 4$ genotype ($X^2_{(1)} = 0.138$, $p = 0.241$) or BDNF Val66mMet polymorphism ($X^2_{(1)} = 0$, $p = 1$). As expected per definition, controls had significantly higher MoCA scores than MCI ($U = 359$, $p_{FDR} < 0.001$), even after adding age, gender, and education as covariates, but no difference was found for the IQ score ($U = 258$, $p = 0.102$). In terms of sleep, alertness, and attention, groups differed only in intrinsic alertness ($F_{(1,38)} = 6.532$, $p_{-uncorr.} = 0.014$), but this effect did not survive the FDR correction.

TMS Data

The PAS intervention led to an increase in MEP amplitude in only 61% of all participants included in this study. Responder rate (responders vs. non-responders) did not differ according to group ($X^2_{(1)} = 1.511$, $p = 0.219$) or gender ($X^2_{(1)} = 0$, $p = 1$). Using 4 × 2 repeated-measures ANOVA analysis (TIME: Baseline (PRE), Post1, Post2, Post3 and GROUP: HC, MCI), we found no significant effect for TIME ($F_{(1,39)} = 0.154$, $p = 0.697$) or for the TIME x GROUP interaction ($F_{(3,117)} = 0.776$, $p = 0.510$), even if only responders were included in the analysis ($F_{(3,69)} = 2.34$, $p = 0.081$).

The correlation analysis revealed a weak, non-significant negative association between PAS response (i.e., the logarithm of the MEP amplitude ratio) and age (r_s = −0.22, p = 0.17), which did not differ between HC and MCI, or between responders and non-responders. In terms of stimulation strength, TMS intensity was negatively correlated with PAS response (**Figure 1A**), but only in responders (r_s = −0.52, p = 0.008) as opposed to non-responders (r_s = 0.12, p = 0.66). However, no association was found between TMS intensity and PAS response when dividing the groups into HC (r_s = −0.029, p = 0.9) and MCI (r_s = −0.35, p = 0.051).

Using the SimNIBS toolbox, we visualized the location of the TMS hotspot to verify that the hotspot was within the motor cortex. An exemplary TMS-induced field distribution is illustrated in **Figure 1B**, while each individual's coordinates in MNI space are provided in the **Supplementary Table S1**.

Functional and Structural Data

The seed-based functional connectivity analysis of the resting-state fMRI group data revealed a consistent sensorimotor network (SMN; **Figure 2A**). More specifically, the SMN comprised one large cluster that overlapped with the following brain regions (**Table 2**): bilateral precentral gyrus, corresponding to the primary motor cortex (M1), bilateral postcentral gyrus, including the primary sensorimotor cortex (S1), supplementary motor area (SMA), bilateral superior parietal lobule (SPL), and bilateral supramarginal cortex (SMG). PAS response and functional connectivity of M1-S1 were positively correlated in responders (r_s = 0.45, p = 0.023) and negatively correlated at trend levels in non-responders (r_s = −0.49, p = 0.055) and correlation coefficients differed between the groups (z = 2.918, p = 0.001; **Figure 2B**). This effect was not observed when dividing the groups into HC (r_s = 0.3, p = 0.18) and MCI (r_s = −0.032, p = 0.9).

Figure 3A illustrates the corticospinal tract (CST), averaged across all participants, resulting from the probabilistic fiber tractography analysis. The weighted average *FA* values did not differ between MCI and HC (U = 162, p = 0.224), and showed only trend significance between responders and non-responders (U = 127, p = 0.053). The correlation analysis showed a significant positive correlation between *FA* values and PAS response across all participants (**Figure 3B**; r_s = 0.39, p = 0.011), but no difference in the correlation coefficients between responders and non-responders (z = 0.741, p = 0.229). In terms of cortical thickness and GM volume of the primary motor cortex, no significant differences between groups or associations with PAS response were found.

Prediction of PAS Response Rate

A RF classifier was trained with n_{tree} = 500 and m_{try} = 6 using 19 different features in order to classify participants into two groups: PAS responders and non-responders. The RF classifier was not able to reliably predict the PAS response rate, showing a low estimated accuracy of 58% (95% CI: 42–72%). The results of the OBB estimations (i.e., confusion matrix) are shown in **Table 3**. We observed an estimated classification sensitivity [TP/(TP + FN)] of 65% and an estimated classification specificity [TN/(TN + FP)] of 50%, suggesting high susceptibility to large Type I error (false positives) of the model. The receiver operating characteristic (ROC) curve for the classifier is illustrated in **Figure 4A**. The area under the curve (AUC) was 0.49. The relative importance of variables is summarized in **Figure 4B**, showing that brain connectivity measures (i.e., microstructure of CST and functional connectivity of SMN) had the highest Gini impurity index. However, it should be noted that while RF can handle correlated variables well, multicollinearity may affect the relative importance of variables and should be interpreted with caution. The correlation matrix of all variables is provided in the **Supplementary Figure S1**.

DISCUSSION

Paired associative stimulation (PAS) is a well-established method to non-invasively probe cortical plasticity *in vivo*, but PAS effects tend to vary considerably among individuals. In this study, we addressed this issue by investigating the role of different

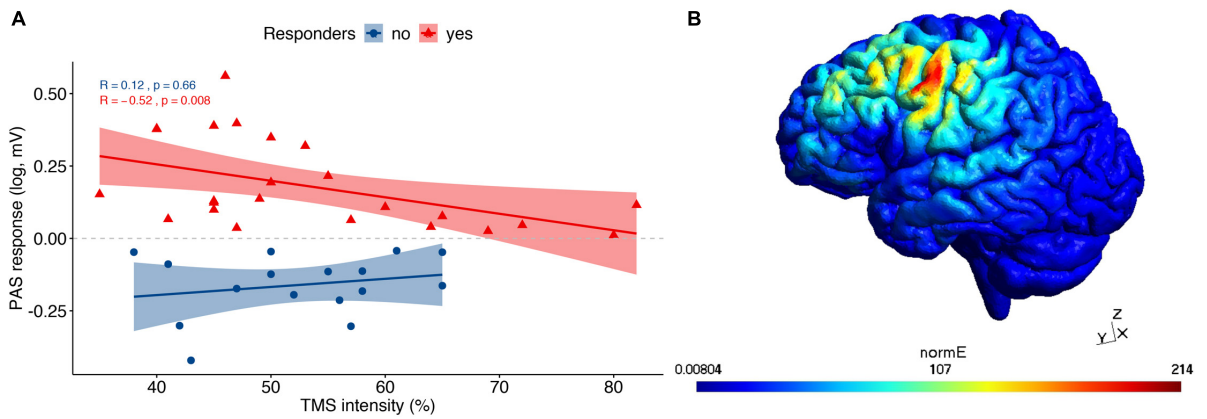

FIGURE 1 | TMS results: **(A)** Correlational analysis between TMS intensity and PAS response, divided into responders and non-responders. **(B)** An exemplary TMS-induced field distribution from the simulation computed in SimNIBS.

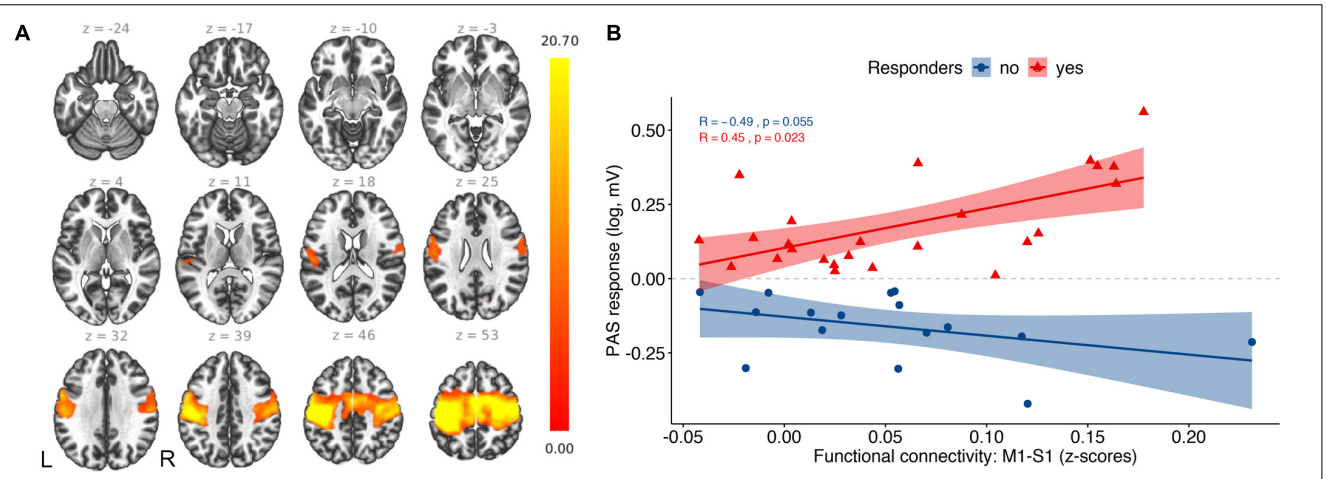

FIGURE 2 | Resting-state fMRI results: **(A)** Average functional connectivity map of the sensorimotor network with the TMS hotspot as a seed ($p_{-FDR} < 0.05$). The color bar represents *T*-values. **(B)** Correlation analysis between PAS response and functional connectivity between primary motor cortex (M1) and primary somatosensory cortex (S1).

TABLE 2 | Functional connectivity results: brain regions that positively correlated with the TMS hotspot seed.

Anatomical labels	Cluster size (voxels)	MNI coordinates			*T*	p_{-FDR}
		x	*y*	*z*		
Postcentral gyrus (S1) L	3708	−50	−22	52	20.70	<0.001
Precentral gyrus (M1) L	3548	−38	−10	62	19.36	<0.001
Precentral gyrus (M1) R	3413	24	−10	58	14.34	<0.001
Postcentral gyrus (S1) R	3065	52	−14	56	14.14	<0.001
Supplementary motor area (SMA)	1021	2	−6	52	16.46	<0.001
Superior Parietal Lobule (SPL) L	882	−38	−42	62	15.25	<0.001
Superior Parietal Lobule (SPL) R	650	24	−40	68	10.38	<0.001
Supramarginal gyrus (SMG) L	401	−60	−26	42	9.38	<0.001
Supramarginal gyrus (SMG) R	251	50	−26	44	7.66	<0.001

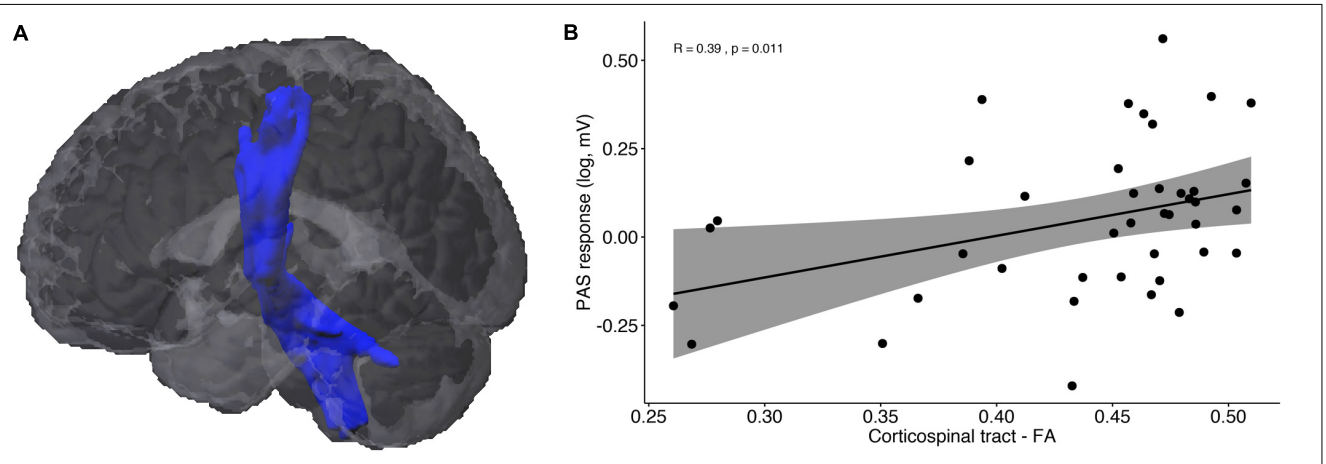

FIGURE 3 | DTI results: **(A)** Probabilistic fiber tractography of the corticospinal tract (CST). **(B)** Correlation analysis between PAS response and average fractional anisotropy (FA) of the CST.

TABLE 3 | OBB estimation confusion matrix.

		REFERENCE	
		PAS responders	**PAS non-responders**
PREDICTION	PAS responders	TP = 20	FP = 5
	PAS non-responders	FN = 11	TN = 5

TP, true positive; TN, true negative; FN, false negative; FP, false positive.

factors that may affect PAS efficacy. In line with previous reports (Müller-Dahlhaus et al., 2008; López-Alonso et al., 2014; Lahr et al., 2016a), we found that only 61% of all participants included in our study showed the expected MEP facilitation as a function of the PAS intervention. More importantly, responder rate was independent of whether participants were HC or MCI. Using uni- and multivariate data analyses, we sought to determine if the observed high inter-individual variability could be predicted by factors that have previously been reported to influence PAS response, such as demographic, clinical, genetic, neurophysiological or neuroanatomical ones. We hypothesized that no single variable would be sufficient to predict the PAS outcome but expected that a combination of different determinants would have a synergetic effect on the predictability of the PAS response. Contrary to our expectations, our multivariate model could not sufficiently predict PAS response rate using these previously proposed determinants of PAS variability. To our knowledge, this is the first study to attempt predicting PAS efficacy using a multivariate classifier.

Demographic, Clinical, and Genetic Factors

From the demographic data, age is considered a major factor that is known to influence LTP-like cortical plasticity and sensorimotor integration (for a review, see Bhandari et al., 2016). For instance, PAS-induced changes in MEP amplitude have previously been reported to be substantially smaller in elderly healthy individuals relative to young ones (Müller-Dahlhaus et al., 2008), while another study found only a trend toward a main effect of age, with young adults showing increases in MEP amplitude relative to older adults (Dickins et al., 2017). Here, we found only a trend for a negative association between age and PAS response, with no significant differences between HC and MCI, or between PAS responders and non-responders. However, it should be noted that the current study was not explicitly designed to investigate age-dependent effects on PAS-induced plasticity. Particularly, we included only older adults with a relatively narrow age range (60–77 years). While we agree that age should be regarded as an important confounding factor in TMS studies in general, we argue that PAS variability found in our study was not due to age differences. The same was also the case for other demographic determinants, such as sex, education, IQ, and global cognition.

The effects of clinical measures, including depression score and presence of cognitive impairment, were also considered in our analysis, motivated by previous findings. For instance, a recent study reported that depression may impair PAS-induced plasticity, with depressive patients showing lower PAS potentiation compared to HC (Noda et al., 2018). However, we found no correlation between depressive symptoms and PAS response, as well as no difference in depression scores between PAS responders relative to non-responders. This suggests that the inter-individual PAS variability observed in our sample could not be explained by depressive symptoms. Of note, depression symptoms were among the exclusion criteria in the current study in order to ensure that cognitive complaints in MCI were not due to depression. The initial goal of the study was to investigate whether PAS-induced plasticity differed between MCI and HC (Lahr et al., 2016b). Not only did we not confirm this hypothesis, but we also found that almost the same amount of HC were PAS non-responders, as observed in the MCI group. Since we found no main effect of group (except for MOCA) or interaction effects of group with any of the variables, we included the whole sample in the multivariate analysis. Limiting the analysis to controls only would have decreased statistical power without changing the conclusions of the study. Importantly, MCI is not a specific disease, but rather represents a "stage" along the aging continuum that does not necessarily need to progress to dementia. By definition, MCI participants present with mild

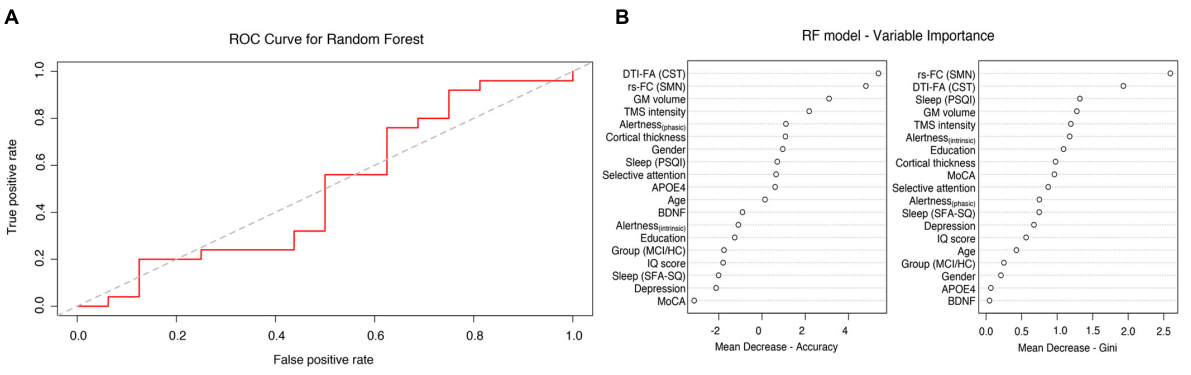

FIGURE 4 | Random forest analysis: **(A)** Receiver operating characteristic (ROC) curves for the RF model with 19 features (AUC 0.49). **(B)** Importance of single variables.

cognitive deficits that do not impair their abilities to carry out normal daily activities.

In general, there is only limited evidence supporting the clinical application of PAS, especially at prodromal stages of neurodegenerative diseases (Ziemann et al., 2008). So far, impaired M1 plasticity has been reported in Parkinson's disease (Morgante et al., 2006). Similarly, a previous study observed a PAS-induced increase in MEP amplitude in HC relative to patients with Parkinson's disease and essential tremor (Lu et al., 2016). In the cognitive domain, only a few studies have focused on TMS-induced plasticity in Alzheimer's disease (for a review, see Freitas et al., 2011), with some contradicting findings. More specifically, while most studies reported either no differences or decreased cortical excitability in AD (e.g., Battaglia et al., 2007), others suggested a short-term increase in post-intervention MEP amplitudes (Alagona et al., 2001). Interestingly, it has recently been suggested that a combination of different TMS paradigms may differentiate AD from frontotemporal dementia (Benussi et al., 2017).

The differences in findings among studies could be resulting from modulatory effects of potential pharmacological agents, as well as from the synergetic influence of genetic factors, such as APOE4 and BDNF. In particular, the impact of BDNF polymorphism on cortical excitability has been confirmed in mice (Fritsch et al., 2010) as well as in humans (for a review, see Chaieb et al., 2014). For instance, Kleim et al. (2006) showed in a TMS study that training-dependent facilitation of MEP amplitude was reduced in young healthy participants with a Val66Met polymorphism relative to those without the polymorphism. Moreover, Val/Val participants showed increased motor map areas of muscle representation, measured on T1-weighted images, relative to Val/Met and Met/Met participants, but this effect was only present after repeated training, suggesting that the physiological consequences of BDNF polymorphism may not manifest in the basal state but only occur in response to training-driven increases in neural activity, e.g., by reducing BDNF secretion in response to neuronal stimulation (Kleim et al., 2006). However, the small sample size (9 Val/Val, 11 Val/Met and 6 Met/Met participants) included in the study warrants some caution in interpreting these results. Here, we did not find a differential effect of BDNF polymorphism on PAS-induced plasticity but, possibly, the association between BDNF polymorphism and LTP-like facilitation may not manifest after a single PAS session.

Neurophysiological and Neuroanatomical Factors

Following previous recommendations (Sale et al., 2007), the PAS experiment was completed in the afternoon for all participants. In this way, we aimed to avoid potential effects of circadian rhythms and time of day effects, thus providing a greater reproducibility between sessions. Furthermore, we evaluated sleep quality within the past 4 weeks as well as during the night prior to testing to ensure that PAS after-effects were not dependent on sleep. Previously, it has been shown that sleep deprivation leads to decreases in TMS-induced plasticity (Kuhn et al., 2016). In the present study, sleep quality did not significantly differ between groups and was not associated with PAS response.

With regard to controlling for attention and alertness during the TMS session, there is currently no consensus on the optimal approach. Here, we used a simple visual task to ensure that participants kept attentive and did not fall asleep during the session. It has previously been shown that a low visual load had no modulatory effects on PAS (Kamke et al., 2012). In addition, selective attention and alertness were evaluated on the day before the TMS session and no correlation was found with PAS response, which is in contrast to a similar study investigating TMS-induced plasticity in young adults, where we showed that higher LTP-like plasticity, in both motor and visual system, was associated with higher subjective alertness (Klöppel et al., 2015). While sleep, attention, and alertness are undoubtedly important factors to control for in brain stimulation interventions, here we found no significant associations with PAS after-effects, lending support to the idea that PAS variability in our study was caused by different factors.

Among all the determinants of PAS variability investigated in our study, the most promising ones seemed to be functional and structural connectivity measures. Neuroanatomical determinants, including cortical thickness, GM volume and microstructural properties of WM have previously been proposed to affect cortical excitability (Klöppel et al., 2008; Conde et al., 2012; List et al., 2013a,b). Our findings suggested that only the microstructure of the CST had a small, albeit significant, contribution to PAS efficacy. However, other studies, using tract-based spatial statistics (TBSS) of the corticospinal tract (CST) in healthy adults (Hübers et al., 2012) and in patients with Parkinson's disease and essential tremor (Lu et al., 2016), showed that CST microstructure did not play a significant role in the generation of LTP-like plasticity. It is unclear whether these discrepancies are merely due to methodological differences among studies and, thus, warrants further examination. Considering that the CST is the major afferent pathway of the motor cortex, it is reasonable to expect that its anatomical integrity would be essential in defining the final motor output.

An advantage of functional connectivity measures over anatomical measures is their potential to provide useful insights into individual brain states as well as the effects of cortical excitability on neural processing. Although there is little understanding of the mechanisms underlying complex network organization and TMS-induced neuromodulation, available data highlight the utility of using task-based and resting-state fMRI to predict cortical excitability and TMS intervention outcomes (Fox et al., 2012, 2014; Cárdenas-Morales et al., 2014; Heba et al., 2017; Fiori et al., 2018; Ingemanson et al., 2019). For instance, a recent review on resting-state fMRI and treatment response in major depressive disorder reported that response to repetitive (rTMS) was consistently predicted by subcallosal cortex connectivity. Additionally, connectivity within default mode and cognitive control networks differed between treatment-resistant and treatment-sensitive patients (Dichter et al., 2015).

In our study, resting-state connectivity within the sensorimotor network was positively correlated with PAS-induced cortical plasticity, but only in responders relative to

non-responders. In contrast, a previous study investigating intermittent theta-burst stimulation (iTBS)-induced increases in MEP amplitude found that resting-state connectivity did not predict iTBS after-effects (Cárdenas-Morales et al., 2014). However, they showed that task-dependent effective connectivity between left premotor areas and M1 prior to stimulation was predictive of post-intervention M1 excitability, implying that plasticity-related changes seem to depend on brain connectivity within the task-dependent network.

Of note, our study showed a correlational effect of SMN connectivity, but limited predictive value of PAS efficacy, as evident from our multivariate analysis. In order to evaluate causal effects of stimulation protocols on changes in functional connectivity, we propose that studies should acquire fMRI data both prior and following TMS interventions. Moreover, task-based fMRI designs might be better suited to investigate specific task-dependent changes in network connectivity as well as the short-term transfer of TMS-induced plasticity. An alternative approach to study the neuronal communication within the sensorimotor network is the use of bifocal, cortico-cortical PAS protocols, in which an impulse over the target area (e.g., M1) is followed by a second impulse over an interconnected target area (e.g., premotor areas) in an inter-stimulus interval consistent with the activation of short-latency connections between the two target areas (Rizzo et al., 2009; Arai et al., 2011; Buch et al., 2011). Recently, it was shown that this kind of modified PAS protocol cannot only induce cortical plasticity but also improve performance on a motor task involving the stimulated pathway (Fiori et al., 2018).

Further Methodological Factors

An important consideration is whether the electrical field of the TMS indeed targeted the motor cortex with the intended direction and strength. In our study, we defined the stimulation hotspot as the optimal cortical location to elicit MEPs in the contralateral APB muscle. Furthermore, we used a neuronavigation system and each individual's anatomical scan to register and track the coil position during the whole TMS session. In this way, we effectively controlled for motion effects since minimal movements away from the optimal stimulation region may lead to attenuation of the MEP amplitude. Additionally, using the SimNIBS software, we examined the distribution of the electric field strength and the coordinates of the stimulation hotspot for each participant separately in order to ensure that we indeed targeted the motor cortex.

It can be argued that defining the optimal TMS hotspot by using brain stimulation might not be optimal. Indeed, this approach has both its strengths and limitations. One shortcoming is that the search for the optimal hotspot might take longer in some participants than others, leading to an unanticipated bias. An alternative approach would be to define a neuroanatomical hotspot by first segmenting the individual's T1 scan prior to the TMS session and then using an anatomical landmark, such as the left precentral gyrus. However, a limitation of this approach is that it does not take into account that the motor cortex consists of functionally and histologically distinct subregions and there is still no consensus which motor subregion should ideally be targeted (Bungert et al., 2017). In our study, we chose to functionally define the hotspot using the motor-evoked response and then inspect whether the coordinates of the TMS hotspot corresponded to the motor cortex.

Another methodological aspect is the choice of stimulation intensity. As generally recommended, we did not use a fixed intensity across all participants but, instead, defined it as the strength that evoked a peak-to-peak MEP amplitude of 1 mV, therefore ensuring that it was sufficient to induce the expected plasticity changes in each participant. Interestingly, our results suggest that higher TMS intensity does not lead to higher cortical excitability *per se*, emphasizing the importance of response-dose dependencies. Furthermore, TMS intensity can be influenced by (neuro-)anatomical features such as skull and cortical thickness, leading to individual differences in coil-to-cortex distance (McConnell et al., 2001; List et al., 2013b). To overcome this issue, we computed the distribution of the electric field strength (i.e., the vector norm of the electric field E) induced by TMS using the SimNIBS simulation approach, which takes into account neuroanatomical features such as CSF-skull boundaries and gyrification patterns, thus providing an anatomically more accurate modeling (Thielscher et al., 2015).

Implications and Future Directions

Taken together, our study suggests that inter-individual variability in responsiveness to PAS was present even if variables known to influence cortical excitability were controlled for, highlighting the need for further replication studies. A major limitation of our study is that several of the variables had a relatively small range since the initial design of the study aimed to control for potential confounders. Therefore, it could be argued that the low predictive value of our multivariate model in terms of the inter-individual variability in PAS response is not surprising. Still, our findings have important implications, as we show empirically that low PAS responders rates are still present, even after controlling for potential confounding variables. Therefore, the underlying sources of variability in PAS efficacy are not well-understood and warrant further investigation. We put a special emphasis on the importance of avoiding publication bias by encouraging authors to publish negative results as well as to report non-responders in their analyses. Additionally, the generalizability of findings can be improved by optimizing sample size in order to ensure sufficient statistical power. Alternatively, future studies may refine their selected population by first evaluating individual state-dependent measures in order to homogenize the study sample. Modifications of existing protocols, instead of applying protocols in a "one-size-fits-all" fashion, may improve intervention outcomes (Karabanov et al., 2016). If PAS is to be used as a biomarker of cortical plasticity, a better mechanistic understanding of the variability in the responsiveness to PAS, as well as to other non-invasive brain stimulation protocols in general, is necessary. In line with previous recommendations (Karabanov et al., 2016), we emphasize that future studies should further focus on the application of state-informed open-loop (i.e., offline feedback) stimulation protocols (e.g., by using fMRI data to assess changes in brain states prior to and following stimulation), as well as

the application of adaptive closed-loop (i.e., online feedback) approaches (e.g., by use of neurofeedback).

DATA AVAILABILITY

The data that support the findings of this study are available from the corresponding author upon reasonable request.

ETHICS STATEMENT

This study was approved by the Ethics Commission of the Medical Center – University of Freiburg (Approval #227/12) and written informed consent was obtained from all participants prior to the participation according to the Declaration of Helsinki.

AUTHOR CONTRIBUTIONS

LM acquired, analyzed, and interpreted the data, and drafted the manuscript. JP, SK, and JL designed the study, acquired, analyzed, and interpreted the data, and revised the manuscript. LS acquired the data and revised the manuscript. AA, CK, and CN interpreted the data and revised the manuscript. All authors read and approved the final manuscript.

FUNDING

This study was funded by an intramural grant from the Faculty of Medicine – University of Freiburg. The manuscript processing charges were funded by the German Research Foundation (DFG) and the University of Freiburg in the Open-Access Publishing Funding Program.

ACKNOWLEDGMENTS

The authors would like to thank Christian Münkel (Department of Neurology, Freiburg) for his help with genotyping, as well as Verena Landerer (Center for Geriatrics and Gerontology, Freiburg), Eliza Lauer (Department of Internal Medicine I, Freiburg), and Hansjörg Mast (Department of Neuroradiology, Freiburg) for assistance in data acquisition, and Volkmar Glauche (Department of Neurology, Freiburg) for his technical advice on data analysis.

SUPPLEMENTARY MATERIAL

The Supplementary Material for this article can be found online at: https://www.frontiersin.org/articles/10.3389/fnins.2019.00841/full#supplementary-material

REFERENCES

Alagona, G., Bella, R., Ferri, R., Carnemolla, A., Pappalardo, A., Costanzo, E., et al. (2001). Transcranial magnetic stimulation in Alzheimer disease: motor cortex excitability and cognitive severity. *Neurosci. Lett.* 314, 57–60. doi: 10.1016/S0304-3940(01)02288-1

Albert, M. S., DeKosky, S. T., Dickson, D., Dubois, B., Feldman, H. H., Fox, N. C., et al. (2011). The diagnosis of mild cognitive impairment due to Alzheimer's disease: recommendations from the national institute on aging-Alzheimer's Association workgroups on diagnostic guidelines for Alzheimer's disease. *Alzheimers Dement.* 7, 270–279. doi: 10.1016/j.jalz.2011.03.008

Antonenko, D., Nierhaus, T., Meinzer, M., Prehn, K., Thielscher, A., Ittermann, B., et al. (2018). Age-dependent effects of brain stimulation on network centrality. *NeuroImage* 176, 71–82. doi: 10.1016/j.neuroimage.2018.04.038

Arai, N., Müller-Dahlhaus, F., Murakami, T., Bliem, B., Lu, M.-K., Ugawa, Y., et al. (2011). State-dependent and timing-dependent bidirectional associative plasticity in the human SMA-M1 network. *J. Neurosci.* 31, 15376–15383. doi: 10.1523/JNEUROSCI.2271-11.2011

Ashburner, J. (2007). A fast diffeomorphic image registration algorithm. *NeuroImage*, 38, 95–113. doi: 10.1016/j.neuroimage.2007.07.007

Ashburner, J., and Friston, K. J. (2005). Unified segmentation. *NeuroImage*. 26, 839–851. doi: 10.1016/j.neuroimage.2005.02.018

Battaglia, F., Wang, H.-Y., Ghilardi, M. F., Gashi, E., Quartarone, A., Friedman, E., et al. (2007). Cortical plasticity in Alzheimer's disease in humans and rodents. *Biol. Psychiatry* 62, 1405–1412. doi: 10.1016/j.biopsych.2007.02.027

Beck, A. T., Steer, R. A., and Brown, G. K. (1996). *Manual for the Beck Depression Inventory-II*. San Antonio, TX: Psychological Corporation.

Behrens, T. E. J., Berg, H. J., Jbabdi, S., Rushworth, M. F. S., and Woolrich, M. W. (2007). Probabilistic diffusion tractography with multiple fibre orientations: what can we gain? *NeuroImage* 34, 144–155. doi: 10.1016/j.neuroimage.2006.09.018

Behzadi, Y., Restom, K., Liau, J., and Liu, T. T. (2007). A component based noise correction method (CompCor) for BOLD and perfusion based fMRI. *NeuroImage* 37, 90–101. doi: 10.1016/j.neuroimage.2007.04.042

Benjamini, Y., and Hochberg, Y. (1995). Controlling the false discovery rate: a practical and powerful approach to multiple testing. *J. R. Statist. Soc. B* 57, 289–300. doi: 10.1111/j.2517-6161.1995.tb02031.x

Benussi, A., Di Lorenzo, F., Dell'Era, V., Cosseddu, M., Alberici, A., Caratozzolo, S., et al. (2017). Transcranial magnetic stimulation distinguishes Alzheimer disease from frontotemporal dementia. *Neurology* 89, 665–672. doi: 10.1212/WNL.0000000000004232

Bhandari, A., Radhu, N., Farzan, F., Mulsant, B. H., Rajji, T. K., Daskalakis, Z. J., et al. (2016). A meta-analysis of the effects of aging on motor cortex neurophysiology assessed by transcranial magnetic stimulation. *Clin. Neurophysiol.* 127, 2834–2845. doi: 10.1016/j.clinph.2016.05.363

Breiman, L. (2001). Random forests. *Mach. Learn.* 45, 5–32. doi: 10.1023/A:1010933404324

Buch, E. R., Johnen, V. M., Nelissen, N., O'Shea, J., and Rushworth, M. F. S. (2011). Noninvasive associative plasticity induction in a corticocortical pathway of the human brain. *J. Neurosci.* 31, 17669–17679. doi: 10.1523/JNEUROSCI.1513-11.2011

Bungert, A., Antunes, A., Espenhahn, S., and Thielscher, A. (2017). Where does TMS stimulate the motor cortex? combining electrophysiological measurements and realistic field estimates to reveal the affected cortex position. *Cereb. Cortex* 27, 5083–5094. doi: 10.1093/cercor/bhw292

Buysse, D. J., Reynolds, C. F., Monk, T. H., Berman, S. R., and Kupfer, D. J. (1989). The Pittsburgh sleep quality index: a new instrument for psychiatric practice and research. *Psychiatry Res.* 28, 193–213. doi: 10.1016/0165-1781(89)90047-4

Cárdenas-Morales, L., Volz, L. J., Michely, J., Rehme, A. K., Pool, E.-M., Nettekoven, C., et al. (2014). Network connectivity and individual responses to brain stimulation in the human motor system. *Cereb. Cortex* 24, 1697–1707. doi: 10.1093/cercor/bht023

Chaieb, L., Antal, A., Ambrus, G. G., and Paulus, W. (2014). Brain-derived neurotrophic factor: its impact upon neuroplasticity and neuroplasticity inducing transcranial brain stimulation protocols. *Neurogenetics* 15, 1–11. doi: 10.1007/s10048-014-0393-1

Cheeran, B., Talelli, P., Mori, F., Koch, G., Suppa, A., Edwards, M., et al. (2008). A common polymorphism in the brain-derived neurotrophic factor gene (BDNF)

modulates human cortical plasticity and the response to rTMS. *J. Physiol.* 586, 5717–5725. doi: 10.1113/jphysiol.2008.159905

Chenot, Q., Tzourio-Mazoyer, N., Rheault, F., Descoteaux, M., Crivello, F., Zago, L., et al. (2018). A population-based atlas of the human pyramidal tract in 410 healthy participants. *Brain Struct. Funct.* 224, 599–612. doi: 10.1007/s00429-018-1798-7

Conde, V., Vollmann, H., Sehm, B., Taubert, M., Villringer, A., and Ragert, P. (2012). Cortical thickness in primary sensorimotor cortex influences the effectiveness of paired associative stimulation. *NeuroImage* 60, 864–870. doi: 10.1016/j.neuroimage.2012.01.052

Dahnke, R., Yotter, R. A., and Gaser, C. (2013). Cortical thickness and central surface estimation. *NeuroImage* 65, 336–348. doi: 10.1016/j.neuroimage.2012.09.050

Desikan, R. S., Ségonne, F., Fischl, B., Quinn, B. T., Dickerson, B. C., Blacker, D., et al. (2006). An automated labeling system for subdividing the human cerebral cortex on MRI scans into gyral based regions of interest. *NeuroImage* 31, 968–980. doi: 10.1016/j.neuroimage.2006.01.021

Dichter, G. S., Gibbs, D., and Smoski, M. J. (2015). A systematic review of relations between resting-state functional-MRI and treatment response in major depressive disorder. *J. Affect. Disord.* 172, 8–17. doi: 10.1016/j.jad.2014.09.028

Dickins, D. S. E., Kamke, M. R., and Sale, M. V. (2017). Corticospinal plasticity in bilateral primary motor cortices induced by paired associative stimulation to the dominant hemisphere does not differ between young and older adults. *Neural. Plast.* 2017:8319049. doi: 10.1155/2017/8319049

Downar, J., Geraci, J., Salomons, T. V., Dunlop, K., Wheeler, S., McAndrews, M. P., et al. (2014). Anhedonia and reward-circuit connectivity distinguish nonresponders from responders to dorsomedial prefrontal repetitive transcranial magnetic stimulation in major depression. *Biol. Psychiatry* 76, 176–185. doi: 10.1016/j.biopsych.2013.10.026

Fiori, F., Chiappini, E., and Avenanti, A. (2018). Enhanced action performance following TMS manipulation of associative plasticity in ventral premotor-motor pathway. *NeuroImage* 183, 847–858. doi: 10.1016/j.neuroimage.2018.09.002

Fox, M. D., Buckner, R. L., Liu, H., Chakravarty, M. M., Lozano, A. M., and Pascual-Leone, A. (2014). Resting-state networks link invasive and noninvasive brain stimulation across diverse psychiatric and neurological diseases. *PNAS* 111, E4367–E4375. doi: 10.1073/pnas.1405003111

Fox, M. D., Halko, M. A., Eldaief, M. C., and Pascual-Leone, A. (2012). Measuring and manipulating brain connectivity with resting state functional connectivity magnetic resonance imaging (fcMRI) and transcranial magnetic stimulation (TMS). *NeuroImage* 62, 2232–2243. doi: 10.1016/j.neuroimage.2012.03.035

Freitas, C., Mondragón-Llorca, H., and Pascual-Leone, A. (2011). Noninvasive brain stimulation in Alzheimer's disease: systematic review and perspectives for the future. *Exp. Gerontol.* 46, 611–627. doi: 10.1016/j.exger.2011.04.001

Fried, P. J., Jannati, A., Davila-Pérez, P., and Pascual-Leone, A. (2017). Reproducibility of single-pulse, paired-pulse, and intermittent theta-burst TMS measures in healthy aging, Type-2 diabetes, and Alzheimer's disease. *Front. Aging Neurosci.* 9:263. doi: 10.3389/fnagi.2017.00263

Fritsch, B., Reis, J., Martinowich, K., Schambra, H. M., Ji, Y., Cohen, L. G., et al. (2010). Direct current stimulation promotes BDNF-dependent synaptic plasticity: potential implications for motor learning. *Neuron* 66, 198–204. doi: 10.1016/j.neuron.2010.03.035

Görtelmeyer, R. (1985). "On the development of a standardized sleep inventory for the assessment of sleep," in *Methods of Sleep Research*, eds S. T. Kubicki and W. M. Herrmann (Stuttgart: Gustav Fisher Verlag), 93–98.

Heba, S., Lenz, M., Kalisch, T., Höffken, O., Schweizer, L. M., Glaubitz, B., et al. (2017). Regionally specific regulation of sensorimotor network connectivity following tactile improvement. *Neural. Plast.* 2017:5270532. doi: 10.1155/2017/5270532

Hebb, D. O. (1949). *The Organization of Behavior*. NewYork, NY: Wiley.

Hübers, A., Klein, J. C., Kang, J.-S., Hilker, R., and Ziemann, U. (2012). The relationship between TMS measures of functional properties and DTI measures of microstructure of the corticospinal tract. *Brain Stim.* 5, 297–304. doi: 10.1016/j.brs.2011.03.008

Ingemanson, M. L., Rowe, J. R., Chan, V., Wolbrecht, E. T., Reinkensmeyer, D. J., and Cramer, S. C. (2019). Somatosensory system integrity explains differences in treatment response after stroke. *Neurology* 92, e1098–e1108. doi: 10.1212/WNL.0000000000007041

Kamke, M. R., Hall, M. G., Lye, H. F., Sale, M. V., Fenlon, L. R., Carroll, T. J., et al. (2012). Visual attentional load influences plasticity in the human motor cortex. *J. Neurosci.* 32, 7001–7008. doi: 10.1523/JNEUROSCI.1028-12.2012

Karabanov, A., Thielscher, A., and Siebner, H. R. (2016). Transcranial brain stim: closing the loop between brain and stimulation. *Curr. Opin Neurol.* 29, 397–404. doi: 10.1097/WCO.0000000000000342

Kleim, J. A., Chan, S., Pringle, E., Schallert, K., Procaccio, V., Jimenez, R., et al. (2006). BDNF val66met polymorphism is associated with modified experience-dependent plasticity in human motor cortex. *Nat. Neurosci.* 9, 735–737. doi: 10.1038/nn1699

Klöppel, S., Bäumer, T., Kroeger, J., Koch, M. A., Büchel, C., Münchau, A., et al. (2008). The cortical motor threshold reflects microstructural properties of cerebral white matter. *NeuroImage* 40, 1782–1791. doi: 10.1016/j.neuroimage.2008.01.019

Klöppel, S., Lauer, E., Peter, J., Minkova, L., Nissen, C., Normann, C., et al. (2015). LTP-like plasticity in the visual system and in the motor system appear related in young and healthy subjects. *Front. Hum. Neurosci.* 9:506. doi: 10.3389/fnhum.2015.00506

Kuhn, M., Wing, J., Weston, S., WIlliams, A., Keefer, C., Engelhardt, A., et al. (2019). *caret: Classification and Regression Training. R package version 6.0-82*. Available at: https://CRAN.R-project.org/package=caret (accessed April 27, 2019).

Kuhn, M., Wolf, E., Maier, J. G., Mainberger, F., Feige, B., Schmid, H., et al. (2016). Sleep recalibrates homeostatic and associative synaptic plasticity in the human cortex. *Nat. Commun.* 7:12455. doi: 10.1038/ncomms12455

Lahr, J., Paßmann, S., List, J., Vach, W., Flöel, A., and Klöppel, S. (2016a). Effects of different analysis strategies on paired associative stimulation. a pooled data analysis from three research labs. *PLoS One* 11:e0154880. doi: 10.1371/journal.pone.0154880

Lahr, J., Peter, J., Minkova, L., Lauer, E., Reis, J., Heimbach, B., et al. (2016b). No difference in paired associative stimulation induced cortical neuroplasticity between patients with mild cognitive impairment and elderly controls. *Clin. Neurophysiol.* 127, 1254–1260. doi: 10.1016/j.clinph.2015.08.010

Liaw, A., and Wiener, M. (2002). Classification and regression by randomForest. *R News* 2, 18–22.

List, J., Duning, T., Kürten, J., Deppe, M., Wilbers, E., and Flöel, A. (2013a). Cortical plasticity is preserved in nondemented older individuals with severe ischemic small vessel disease. *Hum. Brain Mapp.* 34, 1464–1476. doi: 10.1002/hbm.22003

List, J., Kübke, J. C., Lindenberg, R., Külzow, N., Kerti, L., Witte, V., et al. (2013b). Relationship between excitability, plasticity and thickness of the motor cortex in older adults. *NeuroImage* 83, 809–816. doi: 10.1016/j.neuroimage.2013.07.033

López-Alonso, V., Cheeran, B., Río-Rodríguez, D., and Fernández-Del-Olmo, M. (2014). Inter-individual variability in response to non-invasive Brain Stim paradigms. *Brain Stim.* 7, 372–380. doi: 10.1016/j.brs.2014.02.004

Lu, M.-K., Chen, C.-M., Duann, J.-R., Ziemann, U., Chen, J.-C., Chiou, S.-M., et al. (2016). Investigation of motor cortical plasticity and corticospinal tract diffusion tensor imaging in patients with parkinsons disease and essential tremor. *PLoS One* 11:e0162265. doi: 10.1371/journal.pone.0162265

McConnell, K. A., Nahas, Z., Shastri, A., Lorberbaum, J. P., Kozel, F. A., Bohning, D. E., et al. (2001). The transcranial magnetic stimulation motor threshold depends on the distance from coil to underlying cortex: a replication in healthy adults comparing two methods of assessing the distance to cortex. *Biol. Psychiatry* 49, 454–459. doi: 10.1016/s0006-3223(00)01039-8

Missitzi, J., Gentner, R., Geladas, N., Politis, P., Karandreas, N., Classen, J., et al. (2011). Plasticity in human motor cortex is in part genetically determined. *J. Physiol.* 589, 297–306. doi: 10.1113/jphysiol.2010.200600

Morgante, F., Espay, A. J., Gunraj, C., Lang, A. E., and Chen, R. (2006). Motor cortex plasticity in Parkinson's disease and levodopa-induced dyskinesias. *Brain* 129, 1059–1069. doi: 10.1093/brain/awl031

Mori, S., Wakana, S., van Zijl, P. C. M., and Nagae-Poetscher, L. M. (2005). *MRI Atlas of Human White Matter*. Amsterdam: Elsevier.

Müller-Dahlhaus, J. F. M., Orekhov, Y., Liu, Y., and Ziemann, U. (2008). Interindividual variability and age-dependency of motor cortical plasticity induced by paired associative stimulation. *Exp. Brain Res.* 187, 467–475. doi: 10.1007/s00221-008-1319-7

Nasreddine, Z. S., Phillips, N. A., Bédirian, V., Charbonneau, S., Whitehead, V., Collin, I., et al. (2005). The Montreal Cognitive Assessment, MoCA: a brief

screening tool for mild cognitive impairment. *J. Am. Geriatr. Soc.* 53, 695–699. doi: 10.1111/j.1532-5415.2005.53221.x

Noda, Y., Zomorrodi, R., Vila-Rodriguez, F., Downar, J., Farzan, F., Cash, R. F. H., et al. (2018). Impaired neuroplasticity in the prefrontal cortex in depression indexed through paired associative stimulation. *Depress. Anxiety* 35, 448–456. doi: 10.1002/da.22738

Oldfield, R. C. (1971). The assessment and analysis of handedness: the edinburgh inventory. *Neuropsychologia* 9, 97–113. doi: 10.1016/0028-3932(71)90067-4

Peña-Gomez, C., Solé-Padullés, C., Clemente, I. C., Junqué, C., Bargalló, N., Bosch, B., et al. (2012). APOE status modulates the changes in network connectivity induced by Brain Stim in non-demented elders. *PLoS One* 7:e51833. doi: 10.1371/journal.pone.0051833

Peter, J., Kaiser, J., Landerer, V., Köstering, L., Kaller, C. P., Heimbach, B., et al. (2016). Category and design fluency in mild cognitive impairment: performance, strategy use, and neural correlates. *Neuropsychologia* 93, 21–29. doi: 10.1016/j.neuropsychologia.2016.09.024

Peter, J., Sandkamp, R., Minkova, L., Schumacher, L. V., Kaller, C. P., Abdulkadir, A., et al. (2018a). Real-world navigation in amnestic mild cognitive impairment: the relation to visuospatial memory and volume of hippocampal subregions. *Neuropsychologia* 109, 86–94. doi: 10.1016/j.neuropsychologia.2017.12.014

Peter, J., Schumacher, L. V., Landerer, V., Abdulkadir, A., Kaller, C. P., Lahr, J., et al. (2018b). Biological factors contributing to the response to cognitive training in mild cognitive impairment. *J. Alzheimers Dis.* 61, 333–345. doi: 10.3233/JAD-170580

Petersen, R. C., Smith, G. E., Waring, S. C., Ivnik, R. J., Tangalos, E. G., and Kokmen, E. (1999). Mild cognitive impairment. *Arch. Neurol.* 56:303. doi: 10.1001/archneur.56.3.303

R Core Team, (2016). *R: A Language and Environment for Statistical Computing*. Vienna: R Foundation for Statistical Computing.

Ridding, M. C., and Ziemann, U. (2010). Determinants of the induction of cortical plasticity by non-invasive Brain Stim in healthy subjects. *J. Physiol.* 588, 2291–2304. doi: 10.1113/jphysiol.2010.190314

Rizzo, V., Siebner, H. S., Morgante, F., Mastroeni, C., Girlanda, P., and Quartarone, A. (2009). Paired associative stimulation of left and right human motor cortex shapes interhemispheric motor inhibition based on a Hebbian mechanism. *Cereb. Cortex* 19, 907–915. doi: 10.1093/cercor/bhn144

Sale, M. V., Ridding, M. C., and Nordstrom, M. A. (2007). Factors influencing the magnitude and reproducibility of corticomotor excitability changes induced by paired associative stimulation. *Exp. Brain Res.* 181, 615–626. doi: 10.1007/s00221-007-0960-x

Salomons, T. V., Dunlop, K., Kennedy, S. H., Flint, A., Geraci, J., Giacobbe, P., et al. (2014). Resting-state cortico-thalamic-striatal connectivity predicts response to dorsomedial prefrontal rTMS in major depressive disorder. *Neuropsychopharmacology* 39, 488–498. doi: 10.1038/npp.2013.222

Sing, T., Sander, O., Beerenwinkel, N., and Lengauer, T. (2005). ROCR: visualizing classifier performance in R. *Bioinformatics* 21, 3940–3941. doi: 10.1093/bioinformatics/bti623

Smith, S. M., Jenkinson, M., Woolrich, M. W., Beckmann, C. F., Behrens, T. E. J., Johansen-Berg, H., et al. (2004). Advances in functional and structural MR image analysis and implementation as FSL. *NeuroImage* 23(Suppl. 1), S208–S219. doi: 10.1016/j.neuroimage.2004.07.051

Stefan, K., Kunesch, E., Cohen, L. G., Benecke, R., and Classen, J. (2000). Induction of plasticity in the human motor cortex by paired associative stimulation. *Brain* 123, 572–584. doi: 10.1093/brain/123.3.572

Stefan, K., Wycislo, M., and Classen, J. (2004). Modulation of associative human motor cortical plasticity by attention. *J. Neurophysiol.* 92, 66–72. doi: 10.1152/jn.00383.2003

Sturm, W. (2006). *Wahrnehnumgs- und Aufmerksamkeitsfunktionen*. Mödling: Schuhfried.

Thielscher, A., Antunes, A., and Saturnino, G. B. (2015). Field modeling for transcranial magnetic stimulation: a useful tool to understand the physiological effects of TMS? *Conf. Proc. IEEE Eng. Med. Biol. Soc.* 2015, 222–225. doi: 10.1109/EMBC.2015.7318340

Wakana, S., Jiang, H., Nagae-Poetscher, L. M., van Zijl, P. C. M., and Mori, S. (2004). Fiber tract-based atlas of human white matter anatomy. *Radiology* 230, 77–87. doi: 10.1148/radiol.2301021640

Whitfield-Gabrieli, S., and Nieto-Castanon, A. (2012). Conn: a functional connectivity toolbox for correlated and anticorrelated brain networks. *Brain Connect.* 2, 125–141. doi: 10.1089/brain.2012.0073

Windhoff, M., Opitz, A., and Thielscher, A. (2013). Electric field calculations in Brain Stim based on finite elements: an optimized processing pipeline for the generation and usage of accurate individual head models. *Hum. Brain Mapp.* 34, 923–935. doi: 10.1002/hbm.21479

Yesavage, J. A., and Sheikh, J. I. (1986). 9/Geriatric depression Scale (GDS). *Clin. Gerontol.* 5, 165–173. doi: 10.1300/J018v05n01_09

Zhang, Y., Zhang, J., Oishi, K., Faria, A. V., Jiang, H., Li, X., et al. (2010). Atlas-guided tract reconstruction for automated and comprehensive examination of the white matter anatomy. *NeuroImage* 52, 1289–1301. doi: 10.1016/j.neuroimage.2010.05.049

Ziemann, U., Paulus, W., Nitsche, M. A., Pascual-Leone, A., Byblow, W. D., Berardelli, A., et al. (2008). Consensus: motor cortex plasticity protocols. *Brain Stim.* 1, 164–182. doi: 10.1016/j.brs.2008.06.006

Conflict of Interest Statement: The authors declare that the research was conducted in the absence of any commercial or financial relationships that could be construed as a potential conflict of interest.

frontiers in Neuroscience

REVIEW
published: 20 August 2019
doi: 10.3389/fnins.2019.00808

Closed-Loop Implantable Therapeutic Neuromodulation Systems Based on Neurochemical Monitoring

Khalid B. Mirza, Caroline T. Golden, Konstantin Nikolic and Christofer Toumazou*

Department of Electrical and Electronic Engineering, Centre for Bio-Inspired Technology, Institute of Biomedical Engineering, Imperial College London, London, United Kingdom

OPEN ACCESS

Edited by:
Olivier David, Institut National de la Santé et de la Recherche Médicale (INSERM), France

Reviewed by:
Ali Yadollahpour, Ahvaz Jundishapur University of Medical Sciences, Iran
Maria Teresa Fiorenza, Sapienza University of Rome, Italy
Russell J. Andrews, Ames Associate (Smart Systems & Nanotechnology) at NASA Ames Research Center, United States
Hoon-Ki Min, Mayo Clinic, United States

***Correspondence:**
Khalid B. Mirza
k.mirza@imperial.ac.uk

Specialty section:
This article was submitted to Neural Technology, a section of the journal Frontiers in Neuroscience

Received: *10 December 2018*
Accepted: *19 July 2019*
Published: *20 August 2019*

Citation:
Mirza KB, Golden CT, Nikolic K and Toumazou C (2019) Closed-Loop Implantable Therapeutic Neuromodulation Systems Based on Neurochemical Monitoring. Front. Neurosci. 13:808. doi: 10.3389/fnins.2019.00808

Closed-loop or intelligent neuromodulation allows adjustable, personalized neuromodulation which usually incorporates the recording of a biomarker, followed by implementation of an algorithm which decides the timing (*when?*) and strength (*how much?*) of stimulation. Closed-loop neuromodulation has been shown to have greater benefits compared to *open-loop* neuromodulation, particularly for therapeutic applications such as pharmacoresistant epilepsy, movement disorders and potentially for psychological disorders such as depression or drug addiction. However, an important aspect of the technique is selection of an appropriate, preferably neural biomarker. Neurochemical sensing can provide high resolution biomarker monitoring for various neurological disorders as well as offer deeper insight into neurological mechanisms. The chemicals of interest being measured, could be ions such as potassium (K^+), sodium (Na^+), calcium (Ca^{2+}), chloride (Cl^-), hydrogen (H^+) or neurotransmitters such as dopamine, serotonin and glutamate. This review focusses on the different building blocks necessary for a *neurochemical*, *closed-loop* neuromodulation system including biomarkers, sensors and data processing algorithms. Furthermore, it also highlights the merits and drawbacks of using this biomarker modality.

Keywords: neurochemical monitoring, closed loop neuromodulation, deep brain stimulation (DBS), vagus nerve stimulation (VNS), FSCV, chemometrics

1. INTRODUCTION

The idea of treating intractable diseases with little or no known pharmacological interventions through the nervous system has led to a new area of therapeutic treatment, known as *electroceuticals* or *bio-electronic medicine* (Kristoffer et al., 2013). The therapeutic effects of *electroceutical* techniques are observed by modulating signals on the nervous system through external agents such as electrical stimulation. This process is known as neuromodulation. Current applications of electroceuticals target diseases such as Parkinson's disease (Tass, 2003; Benabid et al., 2009; Ebert et al., 2014), epilepsy (Amar et al., 2008), depression (Landau et al., 2015), diabetes (Shikora et al., 2013), inflammation (Borovikova et al., 2000; Tracey, 2002; Li et al., 2016), auto-immune diseases such as Crohn's disease (Bonaz et al., 2016), regulation of blood pressure (Hosokawa and Sunagawa, 2016) and obesity (Payne et al., 2018).

Closed-loop neuromodulation has been shown to be clinically more effective than open-loop neuromodulation (Sun and Morrell, 2014), under certain conditions. To implement a closed-loop neuromodulation paradigm, important aspects to consider are identifying the relevant neural *biomarker*, identifying the optimal *location(s)* for monitoring the biomarker and electrical stimulation, respectively, implementing the *sensing methodology* and instrumentation for the biomarker, followed by signal processing to differentiate the biomarker responses from background interferences, decision and dose tuning algorithms to determine *when* and *how much* to stimulate.

Traditional biomarkers for closed-loop neuromodulation include electrical neural signals such as action potentials (AP) or local field potentials (LFP), with many devices providing high channel count neural recording and processing (Zhou et al., 2019). There have also been recent efforts to incorporate high-resolution stimulation through optogenetic methods (Mickle et al., 2019). Non-neural biomarkers such as electrocardiography (ECG), electromyography (EMG) signals have also been used, particularly in epilepsy and movement disorders (Sun and Morrell, 2014), either as a direct or as an adjunctive biomarker.

For example, in Parkinson's disease, excessively synchronized neural activity is a crucial sign of Parkinson's. A technique, Coordinated Reset Stimulation (CRS) which seeks to desynchronize this abnormal synchronization by computationally modeling stimulation, is gaining traction. The unique advantage is that, the stimulus could be invasive electrical (Tass, 2003) or even non-invasive sensory stimulation such as somatosensory or vibrotactile stimulation. This review is primarily focussed on neurochemical biomarkers for closed-loop systems.

Neurochemical recording is an emerging form of neural recording, where ionic species or neurotransmitters, present inside neurological systems are monitored. Neurochemical monitoring has multiple advantages over traditional electrical neural recording including higher specificity in comparison to traditional electrical recording of neural activity, lesser interference from other signals such as EMG or heart rate (Cork et al., 2018) and possibility to detect inhibitory and excitatory neural activity by monitoring the concentration of specific neurotransmitters (Wightman et al., 1988).

In recent years, there has been significant traction in the pursuit of neurochemical closed-loop feedback in deep brain stimulation (DBS). A recent National Institute of Health (NIH) grant was aimed at exploring neurochemical recording for DBS applications (NIH, 2014). Another interdisciplinary seed grant was recently awarded by Stanford Bio-X, which is aimed at developing neurochemical closed-loop DBS system for treating psychiatric disorders (Stanford-Bio-X, 2018).

DBS is an invasive electrical stimulation therapy used to treat neurological disorders such as Parkinson's Disease (Krack et al., 2003; Bittar et al., 2005; Beuter et al., 2014), essential tremor (Koller et al., 1999; Rehncrona et al., 2003; Flora et al., 2010), chronic pain (Marchand et al., 2003; Owen et al., 2006; Boccard et al., 2015), and dystonia (Vidailhet et al., 2005, 2013). Although the therapeutic effects of DBS for symptomatic relief in Parkinson's is well appreciated, the inherent mechanisms are still not well understood.

The standard protocol in DBS is to follow a trial and error technique, whereby a given set of stimulation parameters are tested on-the-fly by the neurosurgeon during surgery (Volkmann et al., 2002). For instance, in the case of a patient with essential tremor, the feedback signal is to observe the amplitude of the tremor while the stimulation is on (Volkmann et al., 2002). Although numerous simulations have been performed in modeling the effect of stimulation on the surrounding neural tissue (Yousif et al., 2010, 2012; Golden et al., 2013), one cannot be sure of the nature of excitation or inhibition that is being introduced in the local neural network for a given therapeutic outcome *in vivo*. There are two potential feedback loops within DBS; electrical activity of the neural network, and neurochemical activity. In the former category, there are studies that are advancing the technology to a closed-loop system (Priori et al., 2013; Rosa et al., 2015), whereby the electrical activity of the surrounding population of neurons is used as a feedback signal. However, as this method relies on detecting electrical signals from surrounding neurons, it is highly susceptible to significant stimulation artifacts from the proximal stimulation electrode.

In comparison, a neurochemical feedback system measuring ions and neurotransmitters, has potential to gain a more nuanced picture of the effect of DBS, on the surrounding neural tissue. Indeed, efforts are being made in this endeavor, primarily in the development of the WINCS system (Chang et al., 2013; Grahn et al., 2014), a single channel, wireless, neurochemical feedback system for DBS. This technology has been advanced to a multichannel feedback loop in WINCS Harmoni (Lee et al., 2017), which has so far proven effective in rodents and swine.

Hence, this review is focused on describing the building blocks for a neurochemical closed-loop system. It describes briefly, the different neurochemical biomarkers that could be used in different neurological diseases and the sensing methodologies that have been used for these neurochemicals. It primarily focuses on processing algorithms for decision making and dose-tuning.

In this paper, section 2 describes various neurochemical biomarkers and respective optimal recording/stimulation loci for different neurological disorders. Section 3 describes different sensing methodologies that can be used to monitor various neurochemical biomarkers. The different steps required to implement an intelligent, implantable neuromodulation system are described in section 4. Discussion and Conclusions related to the above mentioned topics are presented in sections 5 and 6, respectively.

2. NEUROCHEMICAL BIOMARKERS

Both ions, such as Na^+, K^+, Ca^{2+}, Cl^- and, neurotransmitters can be used as biomarkers for various neurological disorders (**Figure 1**). This section describes activity dependent ion and neurotransmitter dynamics under various neurological disorders, which can be used as potential disease biomarkers for use in intelligent neuromodulation systems. The biomarkers

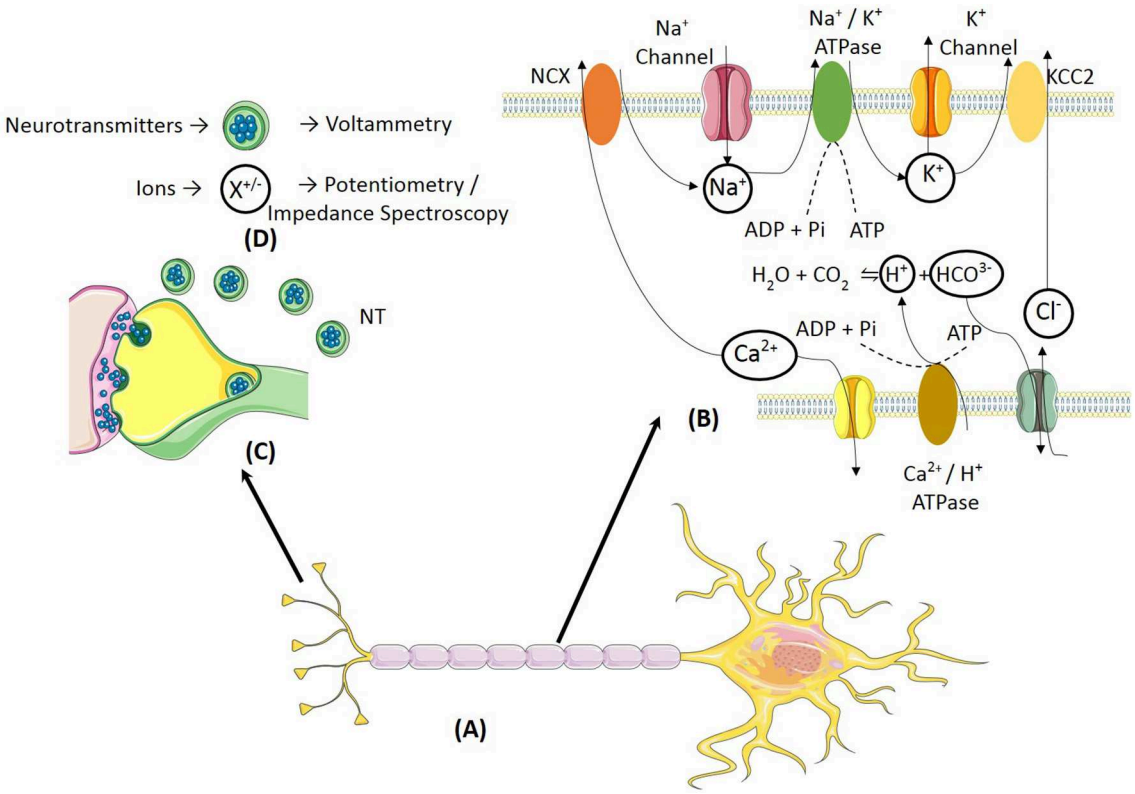

FIGURE 1 | (A) A typical neuron shows ionic and neurotransmitter transients induced due to neural activity. **(B)** The action potential propagation across the axon leads to ionic transients. The activation of the Na^+/ATPase and Ca^{2+}/ATPase leads to extracellular acidification and extracellular alkalinization, respectively. **(C)** Neurotransmitters are released into the synaptic cleft during propagation of neural response across neurons. **(D)** The two classes of neurochemicals i.e., neurotransmitters and ions can be detected using electrochemical methods such as voltammetry and potentiometry, respectively.

listed in **Table 1** were selected based on the following criteria, (a) a direct correlation between the biomarker and the clinical symptoms of the neurological disease has been observed, (b) the biomarker also reflects the effect of stimulation and hence can indicate the state of neurological disease after neural stimulation.

2.1. Ions

The brain is surrounded by extracellular fluid known as the cerebrospinal fluid (CSF), which nourishes the neural tissues with nutrients and performs waste removal. It is mainly composed of water, protein, glucose and ions such as Na^+, K^+ etc. A recent review has highlighted covered changes in ion dynamics during onset and duration of seizures (Raimondo et al., 2015). In addition to Na^+/K^+, changes in pH have also been detected in glial cells, astrocytes, the cerebellum and the retina in relation to neural activity and also due to electrical stimulation (Makani and Chesler, 2010).

Neurochemical studies in peripheral nerves are very rare, or are at a preliminary stage. They are primarily directed toward detection of ions only. This is because the PNS is composed primarily of axons with cell bodies elsewhere. The earliest known *in vitro* studies demonstrate the presence of extracellular pH change in unmylineated nerve fibers only (Bostock and Grafe, 1985; Bostock et al., 1998). The reported pH changes were in response to electrical stimulation. However, no such work was carried out *in vivo* and in response to physiological stimulation, such as the release of a specific hormone. Recently, we demonstrated *in vivo*, the presence of extracellular pH changes in response to intravenous injection of gut hormone cholecystokinin-8 (CCK) (Cork et al., 2018).

2.2. Neurotransmitters

Another viable class of neurochemical biomarkers are neurotransmitters. The following section will examine the neurotransmitters dopamine, serotonin, acetylcholine, and glutamate, each in brief, with respect to their links with neurological disorders.

2.2.1. Dopamine

Within the central nervous system (CNS), the dopaminergic system plays a key role in multiple functionalities including, working memory (Bubser and Schmidt, 1990; Sawaguchi et al., 1990; Sawaguchi and Goldman-Rakic, 1994; Zahrt et al., 1997, reward (Koob, 1992), and locomotion (Whishaw and Dunnett, 1985). The malfunction of this system is linked to a number of neurological disorders including Parkinson's Disease (Lotharius and Brundin, 2002), schizophrenia (Winterer

TABLE 1 | Summary of neurological diseases/conditions and their corresponding potential biomarkers.

Neurological condition	Neural biomarker	Recording site	References
Parkinson's Disease	Dopamine	SNc	Lotharius and Brundin, 2002
	Glutamate	SNc	Johnson et al., 2009,
	K^+, Na^+, Ca^{2+}, Cl^-	StN	Bittar et al., 2005
Schizophrenia	Dopamine	Prefrontal Cortex Mesolimbic Pathway	Winterer and Weinberger, 2004; Brisch et al., 2014
Cocaine Addiction	Dopamine	Nucleus Accumbens	Groppetti et al., 1973; Volkow et al., 2006
Amphetamine Addiction	Dopamine	Nucleus Accumbens	Groppetti et al., 1973
Stress	Dopamine	Ventral Hippocampus	Pani et al., 2000; Lodge and Grace, 2011
Essential Tremor	K^+, Na^+,Ca^{2+}, Cl^-	Ventral Intermediate Nucleus	Krack et al., 2003; Bittar et al., 2005
Chronic Pain	K^+, Na^+,Ca^{2+}, Cl^-	Ventral Posterolateral Nucleus Ventral Posteromedial Nucleus	Marchand et al., 2003
Dystonia	K^+, Na^+,Ca^{2+}, Cl^-	Globus Pallidus Internus	Krack et al., 2003; Bittar et al., 2005
Dementia	Serotonin	Prefrontal Cortex (Orbitofrontal, Frontal Medial and Cingulate cortices	Huey et al., 2006
Anxiety	Serotonin	*	Murphy et al., 2008
Migraine	Serotonin	†	Kowalska et al., 2016
Epilepsy	Serotonin	Raphe Nucleus Ipsilateral Thalamus (to epileptic foci)	Theodore, 2003
Multiple Sclerosis	Serotonin	Lumbar Cerebral Spinal Fluid	Hesse et al., 2014; Malinova et al., 2018
Amyotrophic Lateral Sclerosis	Serotonin	Thoracic Cerebral Spinal Fluid	Sandyk, 2006
Depression	Serotonin	‡	Manji et al., 2001
Alzheimer's Disease	Acetlycholine	Basal Forebrain	Mufson et al., 2008

(*) Current link between serotonin and anxiety is based on measurements of the transporter SERT or the effect of Serotonin Reuptake Inhibitors (SRIs) to ameliorate symptoms of anxiety. (†) Link with serotonin was through effect of serotonin receptor (specifically HT_{1B} and 5-HT_{1D}) inhibition on migraines and also links with genetic polymorphisms related to serotonin that correlate with migraine propensity. (‡) The link between serotonin and depression is through the therapeutic effects of anti-depressants that increase intrasynaptic serotonin and the fact that protocols that deplete monoamines (such as serotonin) have a tendency to precipitate depression . Hence more research is required in order to determine an isolated part of the brain, as yet to measure serotonin in order to provide a direct link.

and Weinberger, 2004; Brisch et al., 2014), and addiction (Koob, 1992; Volkow et al., 2006).

In Parkinsonian patients, the substantia pars compacta (SPc) experiences a substantial loss of dopaminergic neurons, which in turn, affects dopamine levels throughout brain regions that receive projections from this area (Lotharius and Brundin, 2002). Dopamine is also used as a reward signal in the brain (Ikemoto, 2007). This system is amplified in amphetamine and cocaine addiction. These substances block dopamine re-uptake and increase dopamine turnover. Furthermore, amphetamine has been shown to directly increase the release of dopamine (Groppetti et al., 1973). There has also been evidence for the role of the dopaminergic system in the stress response. During stress, there is a strong increase in dopaminergic activity (Pani et al., 2000; Lodge and Grace, 2011). Interestingly, a combination of evidence from the above neurological disorders shows a link between dopamine and gastric ulcers (Rasheed and Alghasham, 2012), possibly indicating a link between neurological conditions and the gut, through the gut brain axis. In incidences whereby dopaminergic activity is increased, such as schizophrenia, the incidence of gastric ulcers is significantly lower (Ozdemir et al., 2007).

2.2.2. Serotonin

Serotonin has a modulatory effect across numerous biophysical functions such as arousal (Trulson and Jacobs, 1979), stress (Carhart-Harris and Nutt, 2017), aggressiveness (Lucki, 1998). The malfunction of the serotonergic system has been linked to neurological disorders such as frontotemporal dementia (Huey et al., 2006), epilepsy (Theodore, 2003), multiple sclerosis (Davidson et al., 1977), amyotrophic lateral sclerosis (Sandyk, 2006), depression Manji et al., 2001), and migraines (Kowalska et al., 2016). These disorders are typically characterized by a decreased serotonin level. Interestingly, in cases of depression, the therapeutic effects of increasing the level of serotonin, through administration of serotonin re-uptake inhibitors (SRIs), are often only seen after chronic administration for weeks. This would indicate, that it is in fact, the downstream effects of increased serotonin that produce the therapeutic effect (Manji et al., 2001). There have also been links found between decreased serotonin levels and the pathogenesis of fronto-temporal dementia (Huey et al., 2006).

2.2.3. Glutamate

Glutamate is a key neurotransmitter in the basal ganglia motor circuit and as such, it has been linked with neurological disorders

associated with the malfunction of elements of the basal ganglia, such as Parkinson's Disease. Indeed, the administration of glutamatergic receptor antagonists have shown promising results in the treatment of Parkinson's Disease in animal models (Breysse et al., 2002, 2003; Ossowska et al., 2005). The therapeutic effect is thought to be due to two mechanisms; (i) the improvement of adverse motor symptoms of Parkinson's Disease through the direct effect on glutamatergic receptors in the basal ganglia, and (ii) the inhibition of glutamatergic transmission is thought to have a protective effect against neurodegeneration, which may slow down the loss of dopaminergic neurons in the substantia pars compacta (Johnson et al., 2009).

2.2.4. Acetylcholine

The cholinergic system has a key role in the modulation of inflammation in the body. As such, neurological disorders that exhibit inflammation such as multiple sclerosis (Mahad et al., 2015) and Alzheimer's Disease (AD) (Eikelenboom et al., 2000), are thought to be linked to abnormalities in the function of the cholinergic system. In post-mortem analysis of patients with Alzheimer's Disease, there is a clear loss of cholinergic neurons (Mufson et al., 2007), and a significant reduction in cholinergic enzymes, choline acetyltransferase (ChAT) and acetyl-cholinesterase (AChE) (DeKosky et al., 1992). Moreover, much of the cognitive decline that is seen in patients with AD has been attributed to the loss of cholinergic function across the CNS (Mufson et al., 2008).

3. NEUROCHEMICAL SENSORS

Neurochemical sensing methods employ primarily bio-electrochemical sensors which are easy to miniaturize and provide label free detection. The underlying chemical reaction involves a redox reaction at the electrode-electrolyte interface (EEI) or through impedance spectroscopy. If a redox reaction is involved, the redox current absorbed by the electrode provides a transduction pathway for the detection and measurement of various analytes. In sensors involving impedance spectroscopy, it involves adhesion or encapsulation of the target biomarker to the surface is needed, resulting in a change in impedance at the EEI.

Traditional chemical detection methods such as microdialysis have more specificity but are less feasible to implant and offer less temporal and spatial resolution (Rodeberg et al., 2017). The Carbon Fiber Microelectrodes (CFM), invented by Gonon et al. (1980), have been widely used in *in vivo* electrochemical recording and are also twenty times smaller than microdialysis probes. This results in less damage to the nervous system when CFM electrodes are inserted (Peters et al., 2004). Due to smaller electrode size, electrochemical techniques are able to offer higher temporal and spatial resolution. Additionally, smaller electrode size also leads to reduced signal distortion due to diffusion when dynamic events are being recorded (Wightman et al., 1988). For instance, it has been demonstrated that it is possible to detect non-evoked dopamine activity associated with electrical neural activity of dopaminergic fibrs (Robinson and Wightman, 2004). This was previously impossible to detect using microdialysis due to diffusion related loss of temporal resolution across the dialysis membrane (Michael and Borland, 2006). Recently, for smaller dimension neural tissue such as nerves, small dimension Iridium-Iridium Oxide (Ir/IrOx) electrodes have been used to perform potentiometric measurements for pH (Cork et al., 2018).

Hence, electrochemical detection of neurochemicals has the advantages of being a microscale, implantable electrode with high spatial and temporal resolution. The trade-off is low biomarker specificity compared to microdialysis techniques. Also, continuous *in vivo* recording is generally accompanied by drift and background activity which needs to be separated in order to extract the signal of interest.

It is important to note that electrochemical techniques are only able to measure change with respect to an unknown baseline. This is a common drawback in all electrochemical methods, as in a static environment, it is difficult to differentiate the contribution due to charging and faradaic currents. Next generation techniques are aiming to measure the basal dopamine level as highlighted in a recent review (Bucher and Wightman, 2015).

In this section, we review different electrochemical methods employed in measuring neurochemicals, shown in **Figure 2**, i.e., amperometry, cyclic voltammetry (CV), electrical impedance spectroscopy (EIS) and potentiometry. Amperometry and CV require three electrodes, consisting of a working electrode (WE), reference electrode (RE) and counter electrode (CE). Potentiometry requires two electrodes consisting only of WE and RE. EIS can be performed using two or more electrodes. The analog front-end circuits required to acquire electrochemical signals have been described in a recent review (Li et al., 2017).

3.1. Voltammetry

Voltammetric detection involves the measurement of redox current when a varying cyclic or periodic potential is applied between the WE and RE. The applied potential should be enough to trigger the redox reaction. The current between the RE and CE is proportional to the number of electrolysed molecules, which in turn is indicative of concentration.

3.1.1. Fast Scan Cyclic Voltammetry

In Fast Scan Cyclic Voltammetry (FSCV), a variable voltage, typically having a triangular waveform profile, is applied between the working and reference electrode. The voltage range and scan rate is dependant on the analyte of interest. For example, the parameters used for dopamine are −0.4V to +1.3V at a scan rate of 400 V/s, with a frequency of 10 Hz. The FSCV parameters used for detection of various neurochemicals are listed in **Table 2**.

The fast voltage scan leads to charging of the double layer capacitive-resistive interface at the electrode surface. This leads to large background current which needs to be subtracted in order to resolve the current generated due to the dopamine redox reaction. The cyclic voltammogram profile is unique to each neurotransmitter and the neurotransmitter concentration can be resolved based on current peaks and calibration factors obtained during the standardization process. Calibration could be done using a flow injection system for various analytes such as dompamine pre and post experiment (Venton et al.,

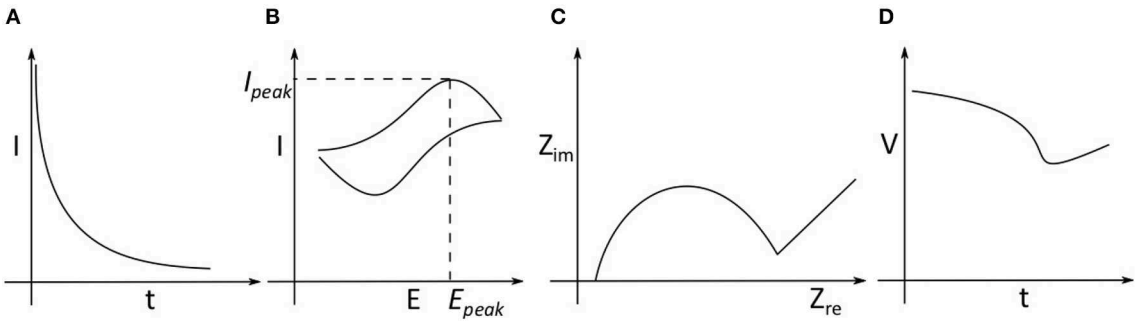

FIGURE 2 | Different electrochemical methods **(A)** Amperometry: where a constant potential difference is applied between the working electrode (WE) and reference electrode (RE). The current between the WE and counter electrode (CE) is monitored as is an indication of the analyte concentration as the reaction progresses. **(B)** Cyclic Voltammetry: The potential difference between the WE, RE is changed periodically and the current between WE and CE is monitored. **(C)** Impedance Spectroscopy: Based on the modality, the impedance of an analyte is measured based on voltage applied between WE, RE and the current through CE. **(D)** Potentiometry: The potential difference between WE and RE is measured without applying any external potential difference.

TABLE 2 | FSCV parameters for detecting various neurochemicals, performed usually at a frequency of 10 Hz.

Analyte	Resting potential (V)	Scan rate (V/s)	Voltage range (V)	References
Dopamine	−0.4	−0.4 − +1.0/+1.3	400	Venton et al., 2003; Park et al., 2011
Norepinephrine	−0.4	−0.4 − +1.3	400	Park et al., 2011
Serotonin	0	+1.2 −0.6	300	John and Jones, 2006
Oxygen	0	+0.8 −1.4	300	Venton et al., 2003

2003), to calculate electrode sensitivity. In addition to peak current, other features/parameters that can be used to distinguish voltammograms from different analytes, are rise time and half decay time.

CFM can be pre-treated so that oxidation currents can be resolved at different points under the potential axis. The selectivity of these electrodes can be further improved with the help of a polymer coating called Nafion, which is a sulfonated derivative of teflon (Gerhardt et al., 1984). Fixed anionic sites present in the Nafion membrane help in preventing anionic substances such as urate, ascorbate and acidic metabolites of monoamine neurotransmitters, from reaching the electrode surface and producing interference. This feature also reduces biofouling of the electrode (Turner et al., 1991).

3.1.2. High Speed Chronoamperometry

In chronoamperometry, the WE is held at a constant potential where no reaction is happening and the potential is stepped up to a different potential. This results in the initiation of an electrochemical reaction, upon which the current due to the reaction is measured. There are a variety of pulsed voltage techniques to detect neurotransmitter activity, some of which have been used to study kinetics and clearance mechanisms of serotonin (Daws et al., 2005), and dopamine (Gerhardt and Hoffman, 2001).

3.1.3. Amperometry

In amperometry, the potential of the working electrode is held constant and the current due to the reaction is measured temporally. Amperometry is best suited for conditions where there is a high level of confidence regarding the identity of the analyte being detected (Michael and Borland, 2006). For this reason, it is also used with enzyme-modified electrodes to detect specific non-electroactive species such as glutamate (Kiyatkin et al., 2013), acetylcholine (Sarter et al., 2009) and choline. For nonelectroactive neurotransmitter detection, oxidase enzymes are immobilized on the electrode surface, which, in the presence of target neurochemical, eventually lead to production of an electroactive species. For example, detection of glutamate is performed with glutamate oxidase, where, glutamate is converted to α-ketoglutarate and hydrogen peroxide (H_2O_2) (Kiyatkin et al., 2013; Bucher and Wightman, 2015).

3.2. Potentiometry

Potentiometry is the measurement of the potential of a solution with the help of two different electrodes, the working electrode which detects the change in chemical reaction and a reference electrode whose potential is known in reference to a standard electrode, such as the Standard Hydrogen Electrode (SHE). In general, the measurement of pH or metal ions can be done using potentiometric methods. The standard, portable pH measurement electrode is the glass electrode.

Previous work in neurochemistry, involving the measurement of pH or ions, was performed using glass electrodes *in vitro* (Endres et al., 1986; Chesler and Kaila, 1992; Makani and Chesler, 2010). However, for *in vivo* measurements, especially in measuring ionic concentrations in PNS, characteristics such

as *invasiveness, robustness, small form factor, high sensitivity* and *resolution* are needed. Metal-Metal oxide surfaces such as Iridium oxide (IrOx) can be used to measure pH (Ng and O'Hare, 2015). It can also be fashioned into microelectrodes or microwire electrode and can be used to measure extracellular ionic concentrations *in vivo* in the peripheral nervous system (PNS), such as the vagus nerve (Cork et al., 2018).

3.3. Impedance Spectroscopy

Recent work has also shown the potential of using Impedance spectroscopy as a means to detect ionic concentration in the CNS (Machado et al., 2016; De La Franier et al., 2017). A gold substrate is coated with anti-biofouling material to prevent the accumulation of blood or cells. On top of the anti-biofouling layer, 18-6-crown-ether and monoethyleneglycolthiol (MEG-SH) in a 1:10 ratio, respectively, is placed to capture potassium ions (Machado et al., 2016). Another methodology consists of using an oxide layer. This oxide layer is coated with a layer of anti-biofouling material, 3-(3-(trichlorosilyl)propoxy)propanoyl chloride (MEG- Cl). A common issue present in both works is interference from ionic species with similar size such as sodium (Na^+).

4. CLOSED-LOOP: SIGNAL PREPROCESSING, DECISION MAKING, AND STIMULATION DOSE SELECTION

The goal of closed-loop neuromodulation is to determine *when?* and *how much?* to stimulate, on the basis of information received directly or indirectly from the neuromodulatory target. Closed-loop neuromodulation can be performed for *prosthetic* or *therapeutic* neurological conditions. This review primarily focusses on *therapeutic* applications, with a focus on using neurochemicals as target biomarkers.

In this Section, different steps involved in implementing a neurochemical based closed-loop neuromodulation system are presented. The first step described is signal pre-processing which is useful in removing baseline drift and identifying symptomatic neurochemical change. This is followed by steps to determine the relationship between symptoms and neurochemical change performed by training set construction and cross validation. It will help the system determine *when* to initiate stimulation. The final step is determining the relationship between electrical stimulation and neurochemical change i.e., stimulation model selection. This will help the system to determine *how much* to stimulate.

Based on functionality and type of control feedback, neuromodulation systems can broadly be divided into five types : *continuous*, *scheduled intermittent*, *responsive*, *adaptive* and *complete closed-loop*, as classified in a recent review by Hoang et al. (2017). *Continuous* neuromodulation is an *open-loop* neuromodulation system, where the stimulation dose is delivered continuously. Adjustments to stimulation dosage is performed by clinicians or care-providers. The feedback in this case are external physiological symptoms and stimulation decisions are made by clinicians. *Scheduled Intermittent* neuromodulation is also a type of *open-loop* where the stimulation is intermittent and no feedback symptom is monitored over time. The stimulations dosage frequency and other parameters such as amplitude, pulsewidth (PW), waveform and frequency are pre-set based on empirical evidence from clinical trials. *Responsive* neuromodulation is a form of partial closed-loop neuromodulation system where the stimulation is initiated automatically based on a physiological biomarker threshold. The stimulation dosage are still pre-set and not tuned in real time. *Adaptive* stimulation is also a form of closed-loop neuromodulation where a single biomarker is monitored. Thresholds and scales on the biomarker are used to determine *when* and *how much* to stimulate. *Complete closed-loop* system consists of monitoring multiple biomarkers answer *when* and *how much* to stimulate.

Both decision making and stimulation dose selection algorithms have to undergo a training phase to enable autonomous operation. The training phase can be conducted on *in vivo* data (Behrend et al., 2009; Trevathan et al., 2015; Bozorgzadeh et al., 2016; Mirza et al., 2019), by recording the neurochemical response to different stimulation parameters. This is followed by cross validation to judge the precision of decision making and stimulation model control algorithms. Prior to *in vivo* training, bench testing using a flow injection system and target analytes may be performed to test electronics and processing system used for data readout and processing (Bozorgzadeh et al., 2016).

An overview of the different elements in a neurochemical, closed-loop neuromodulation system is shown in **Figure 3**. As shown in **Table 3**, there are very limited number of implantable, neurochemical closed-loop systems, as the field is still at a nascent stage. Furthermore, most of the previous work are either *responsive* or *adaptive* closed-loop system with only one biomarker under consideration.

4.1. Signal Pre-processing

The chemical signal acquired needs to be pre-processed. Different pre-processing techniques include low pass filtering, downsampling and the removal of drift due to faradaic or background activity. The specifications of different pre-processing elements vary according to the sensing modality and signal characteristics.

4.1.1. Filtering and Downsampling

Chemical signals are low pass filtered to remove high frequency noise. In FSCV recordings for dopamine, the low pass cut-off is typically set at approximately 100 Hz (Grahn et al., 2014), 1 kHz (Lee et al., 2017), 4 kHz (Bozorgzadeh et al., 2014). In our experiments, where we record pH changes in the sub-diaphragmatic vagus nerve, the pH change induced by CCK (potentiometric measurements) takes about 1–2 min to return to baseline (**Figure 4**). Hence, in this case, a low pass filter with a -3dB cut-off frequency of 0.1 Hz is enough to remove any high frequency interference including any line interference (50Hz/60Hz). In order to maintain high resolution, some solutions implement sigma-delta ($\Sigma\Delta$) analog

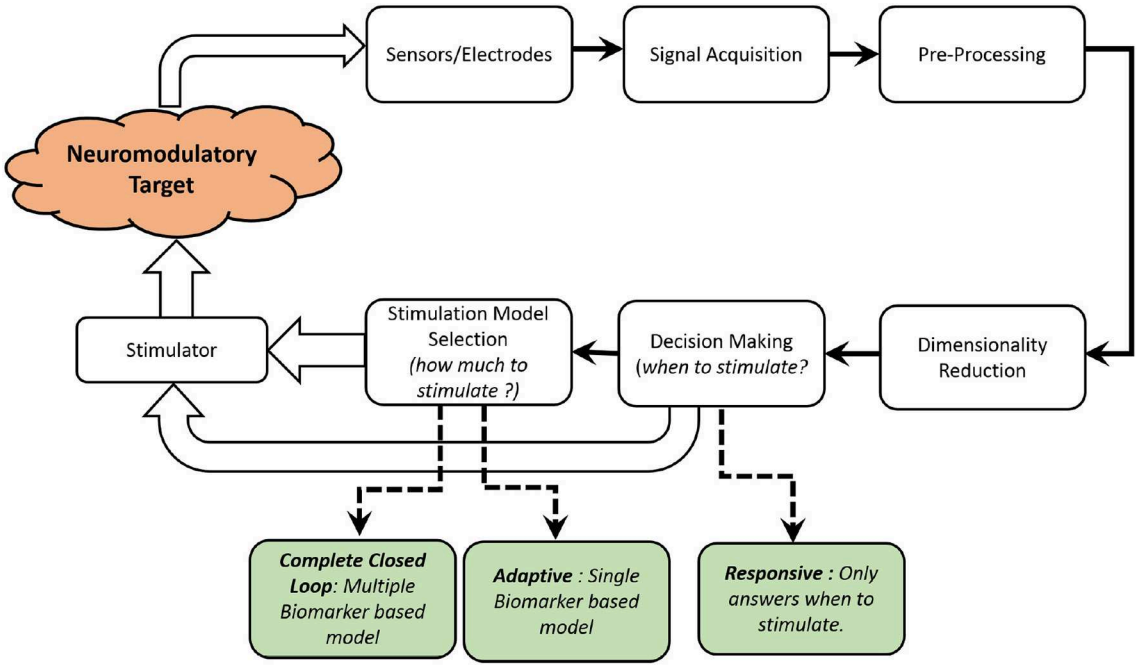

FIGURE 3 | A functional block diagram of a typical closed-loop neurochemical neuromodulation system is shown.

TABLE 3 | Review of existing technical platforms for neurochemical closed-loop neuromodulation.

References	Year	Neuromodulation target application (CNS/PNS)	Biomarker (*when?*)	Biomarker (*how much?*)	Sensor type (Neural)	Algorithm	Outcome
Cork et al., 2018	2018	VNS (PNS)	pH	–	Potentiometry using IrOx	Linear Regression	Non-implantable *in vivo* research device *Responsive* operation in animal models only
Lee et al., 2017	2017	DBS (CNS)	Neurotransmitter (Dopamine, Serotonin, Adenosine)	Neurotransmitter (Dopamine, Serotonin, Adenosine)	FSCV using CFM	ANN†	Non-implantable *in vivo* research device *Adaptive* operation in animal models only
Bozorgzadeh et al., 2016	2016	DBS (CNS)	Neurotransmitter (Dopamine)	–	FSCV using CFM	PCR*	Implantable research device *Responsive* operation in animal models only
Grahn et al., 2014	2014	DBS (CNS)	Neurotransmitter (Dopamine)	Neurotransmitter (Dopamine)	FSCV using CFM	ANN†	Non-implantable *in vivo* research device *Adaptive* operation in animal models only
Behrend et al., 2009	2009	DBS (CNS)	Neurotransmitter (Glutamate)	Neurotransmitter (Glutamate)	FSCV using CFM	ANN†	Non-implantable *in vivo* research device *Adaptive* operation in animal models only

† *Artificial Neural Networks.*
* *Principal Component Regression.*

to digital converters (ADC) (Bozorgzadeh et al., 2016; Lee et al., 2017). This results in oversampling of data which is further sampled down using Cascaded Integrator-Comb (CIC) filter as in Bozorgzadeh et al. (2016), to reduce data throughput.

4.1.2. Background Subtraction and Drift Removal

The current recorded whilst recording FSCV to sense neurotransmitters, is a combination of faradaic and background current. Similarly, during potentiometric recording, there is interference from background potentiometric changes and also

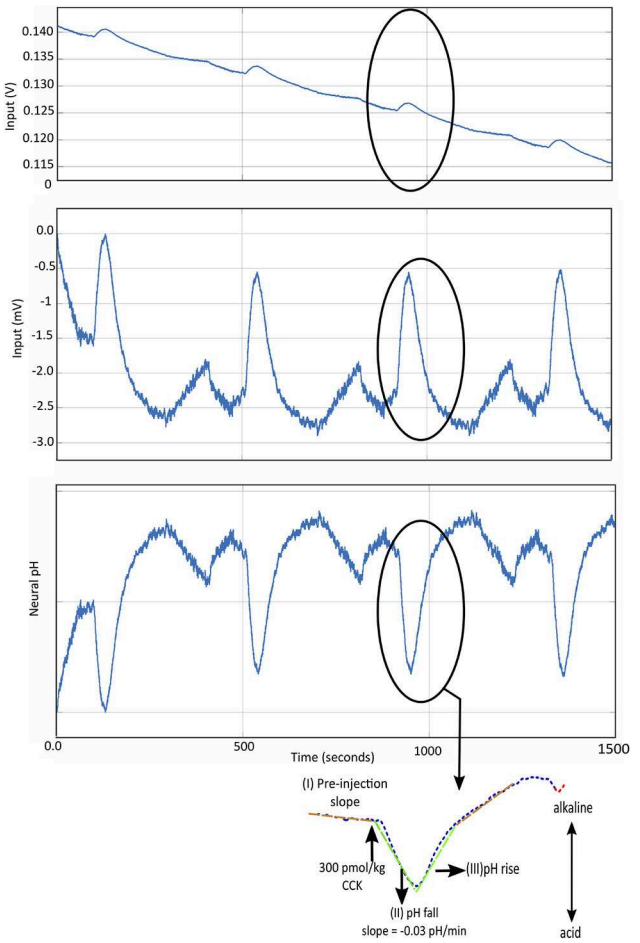

FIGURE 4 | (Top) The potentiometric *pH* data recorded using IrOx electrodes, *in vivo*, in the subdiaphragmatic vagus nerve of male Wistar rats. The changes due to CCK are highlighted. **(Middle)** The recorded potentiometric waveform is pre-processed to remove drift using the technique described in Ahmed et al. (2018). **(Bottom)** The ΔpH is determined using the sensitivity of the IrOx pH electrodes, followed by simple linear regression to determine CCK-induced change in neural pH (Cork et al., 2018). This is a demonstration of *responsive* type of intelligent neuromodulation.

a consistent, sometimes unidirectional drift, due to changes in Open Circuit Potential (OCP) of the potentiometric electrode. Hence, it is essential to remove large changes in background signal, before performing dimensionality reduction or pattern recognition, to identify signatures related to the neural activity being monitored.

A common technique in FSCV drift reduction is the subtraction of recorded current with a short recorded window of the previous current. This is possible because it has been observed during *in vivo* recordings, that FSCV current signatures due to dopamine transients occur in the range of 2–3 ms. Secondly, it has been observed that background current is typically stable over few seconds (Bozorgzadeh et al., 2016). Hence, the background current can be recorded, averaged over few scans (two or four scans) and then subtracted to remove any background activity as described in Bozorgzadeh et al. (2014) and Bozorgzadeh et al. (2016). Other solutions such as the WINCS Harmoni platform also implement background subtraction (Lee et al., 2017). For pre-processing of CCK induced pH changes, a resource efficient architecture was recently described, where the recorded data is down-sampled and slow, non-linear drift was removed in real-time (Ahmed et al., 2018).

4.2. Dimensionality Reduction

Data collected during neurochemical recordings are highly complex with multiple variables affecting readings, hence a multivariate dimensionality reduction technique needs to be utilized in order to ensure accurate analysis of the data and for detection of target neurochemical signature. Principal Component Analysis (PCA) has been widely used as a preferred technique for dimensionality reduction in a number of neurochemical FSCV applications (Keithley et al., 2010). PCA combined with inverse-least squares regression, known as Principal Component Regression (PCR), is used to make predictions regarding the concentration of target neurochemical analyte (Heien et al., 2004, 2005; Keithley et al., 2005, 2010; Keithley and Wightman, 2011; Bucher et al., 2013; Bozorgzadeh et al., 2016). PCA is a mathematical technique which, from a dataset of possibly correlated variables, identifies a set of vectors which are linearly uncorrelated (mutually orthogonal), called "principal components" (PCs). The application of PCA to *chemometrics* involves a four step procedure: (a) signal identification (b) training set construction, (c) generation and selection of relevant PCs, (d) cross validation of PCs.

4.2.1. Signal Identification

Signal identification consists of determining the signal characteristics which are directly correlated to changes in the target neurochemical analyte. The steps involved in signal identification may consist of *in vivo* experiments, followed by signal processing and statistical steps such as ANOVA to ensure reproducibility (Keithley et al., 2005; Cork et al., 2018). After identification of the neurochemical response, it is crucial to model the relationship between (a) the neurochemical response and physiological symptom under study, (b) the relationship between the electrical stimulation and the neurochemical response to it. This is achieved through a combination of mathematical modeling and machine learning techniques described later in this section.

4.2.2. Training Set Construction

The training matrix is generated by combining the temporal signatures of changes in target analyte that were observed electrochemically. For multivariate classification, background changes due to electrode drift or changes in interferring neurochemicals are also considered (Bozorgzadeh et al., 2016).

In **Figure 5**, where the interferents are not known, the pre-injection and post injection waveforms could be used as two types of background signal, in addition to the response to generate a training matrix (Mirza et al., 2017).

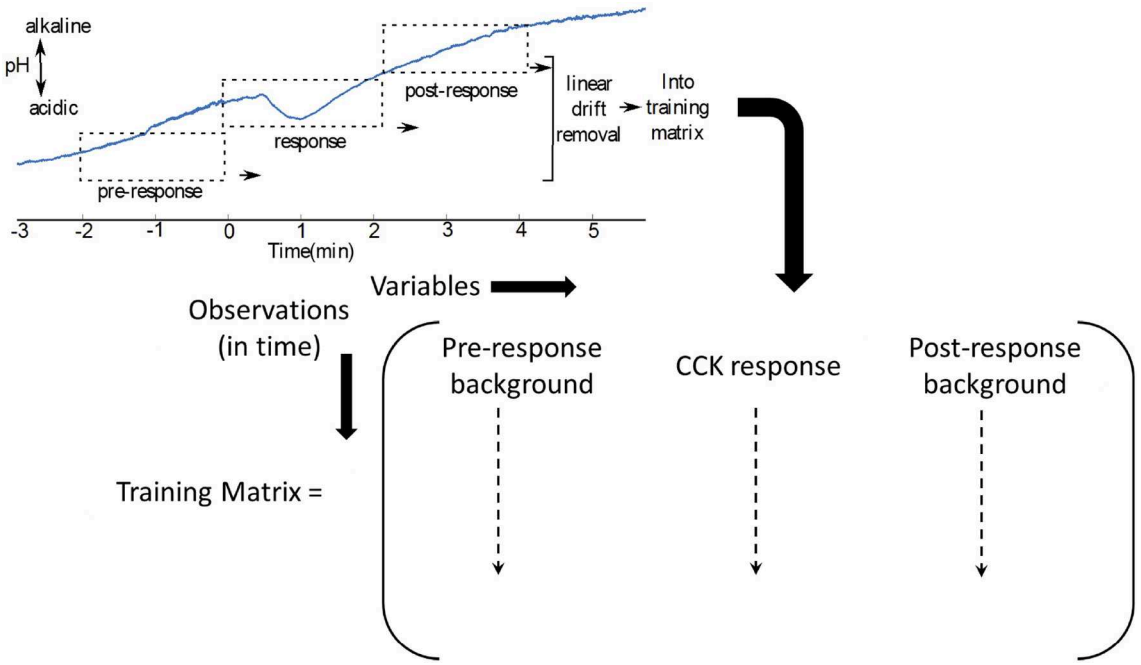

FIGURE 5 | The training matrix can be constructed for as shown, for CCK induced pH changes in the vagus nerve (Mirza et al., 2017).

4.2.3. Generation and Selection of Relevant PCs

The PCs are generated using Single Value Decomposition (SVD) (Equation 1). The commands listed in MATLAB are listed below.

$$[U, S, V] = svd(A) \tag{1}$$

A *scree* plot can be used to determine the variance captured by each PC. The PCs which capture maximum variance are relevant and hence, are retained.

$$Uc = U(:, 1:k) \tag{2}$$

where k is the number of relevant PCs. The decision to retain relevant PCs can be used to generate projections (A_{proj}) of the training matrix (A) onto the PCs:

$$A_{proj} = A \times Uc \tag{3}$$

where U is the PC matrix, composed of PCs generated from the training matrix. If PCR is used, then a regression matrix based on the dose response nature of the analyte is also generated as shown in Equation (11). After the PC matrix is calculated, the next step is cross validation.

4.2.4. Cross Validation of PCs

Cross validation involves determining the robustness and applicability of the training set. This is required to ensure the PCs are sufficient to perform dimensionality reduction in real time. There are a number of methodologies which can be utilized to cross-validate PCs (Keithley et al., 2005, 2010), one such method being residual analysis, which is described below. The residual of a data set is defined as the difference between actual data and data projected using the PCs. A parameter Q_t is defined as the difference in the square value of the actual and projected sample values, a_i and $\tilde{a}_i$, respectively.

$$Q_t = \sum_{i=1}^{N} (a_i^2 - \tilde{a}_i^2) = (a_1^2 - \tilde{a}_1^2) + \ldots + (a_N^2 - \tilde{a}_N^2) \tag{4}$$

where N is the total number of datapoints. a_i and $\tilde{a}_i^2$ are actual and projected data values, respectively, for the i^{th} sample. A significance threshold, Q_α, is set so that the residual for each dataset, Q_t, does not exceed Q_α. For the training set to be considered robust, Q_t must be less than Q_α for all data in the validation set. When Q_t is greater than Q_α, for a specific dataset, it indicates that the variance in the input data is not appropriately captured in the training set. It can indicate the data is non-deterministic and can lead to false positives. Q_α is calculated using the following formula (Keithley et al., 2010) :

$$Q_\alpha = \ominus_1 \left[\frac{c_\alpha \sqrt{2 \ominus_2 h_0^2}}{\ominus_1} + 1 + \frac{\ominus_2 h_0 (h_0 - 1)}{\ominus_1^2} \right] \tag{5}$$

where *k+1* to *n* is the number of discarded PCs, k is number of retained PCs and n is the total number of PCs generated.

$$\gamma = S^2 \tag{6}$$

where γ is the sum of the square of the projected datapoints from the training matrix and S is the singular value matrix generated

from Equation (1).

$$\ominus_i = \sum_{j=k+1}^{n} \gamma_j^i \tag{7}$$

$$h_0 = 1 - \frac{2 \ominus_1 \ominus_3}{\ominus_2^2} \tag{8}$$

where, Q_α denotes an upper limit on the random error to be tolerated. In Equation (5), for c_α = 1.645 or 2.326 Q_t will be greater than Q_α if 95% or 99%, respectively, of the dataset are due to random noise. More details are provided in Keithley et al. (2010).

4.3. Decision Making

This step involves determining *when* to stimulate. The decision when to stimulate could be based on a number of criteria. It could be (a) *threshold based*: stimulation is initiated when a specific neurochemical signature is detected and the response has reached a specific threshold (Bozorgzadeh et al., 2016) or (b) *response based*: where only the presence of a response is enough to trigger stimulation (Cork et al., 2018). In order to implement this, various statistical techniques could be utilized. Techniques such as Simple Linear Regression can be used in *response based*, univariate, decision making. Inverse least square regression in combination with PCA can be used to perform multivariate analyte concentration and a decision regarding *when* to stimulate can be made, based on the threshold of analyte concentration. In this section, we describe a multi-variate decision making model (Bozorgzadeh et al., 2016).

4.3.1. Simple Linear Regression

As shown in **Figure 4**, certain characteristics of the recorded neurochemical signal can be extracted and a simple linear regression model can be fitted on it to extract and identify a signature. This is a type of *univariate* detection method where only one variable is considered to affect the neurochemical signal. This technique was successfully demonstrated to implement a responsive closed-loop neuromodulation technique in an *in vivo* experimental setup. However, since this technique is a univariate approach, it is sometimes susceptible to false positives, hence it is best to limit this to stable *in vivo* experimental environment and not to extend it in an implant.

4.3.2. Inverse Least-Squares Regression

In this process, the regression matrix generated is used to estimate the concentration of the analyte. Different concentrations of analyte can result in different amplitude of neurochemical response peaks. Based on a preset threshold for analyte concentration, stimulation can be initiated. This process was first described in Keithley et al. (2005), followed by an implementation on a System-On-Chip (SoC) in Bozorgzadeh et al. (2016).

The regression matrix is based on the dose response to the analyte concentration (Bozorgzadeh et al., 2016). The regression matrix, in combination with the projected data set from PCA, can be used to predict the concentration of the analyte. This is described in the equation below :

$$F = C \times A_{proj} \times (A'_{proj} \times A_{proj}) \tag{9}$$

$$D_{proj} = D_u \times U_c \tag{10}$$

$$[C_A C_{B1} C_{B2}] = D_{proj} \times F \tag{11}$$

where C is the concentration matrix i.e., a diagonal matrix with concentration values of each analyte considered in a multivariate model, A_{proj} is the projection matrix defined in Equation (3), D_u is the real time data, D_{proj} is the projection of the real time data on the PCs, U_c is defined in Equation (2). F is the projection matrix and C_A, C_{B1}, C_{B2} are the projected concentrations based on inverse least-squares regression.

4.4. Model Selection

The primary goal of model selection is to determine optimal electrical stimulation parameters based on the relationship between stimulation parameters and the target neurochemical biomarker. It is a crucial step toward *adaptive* or *complete closed-loop* neuromodulation to determine the stimulation dose. The relationship between stimulation parameters and neurochemical biomarkers is established based on experimental data and mathematical modeling. Various linear (Behrend et al., 2009) and non linear (Grahn et al., 2014; Lee et al., 2017) modeling techniques have been utilized previously to develop stimulation models. The model selection could be different based on whether the neuromodulatory target is located in the CNS or PNS. In this section, we will describe briefly, one linear and two non-linear stimulation models.

4.4.1. CNS: Stimulation Evoked Release and Uptake of Neurotransmitters

DBS of specific areas in the brain is considered an effective therapy for the treatment of Parkinson's disease. For CNS disorders, the neurochemical biomarkers generally under consideration are dopamine, serotonin (Grahn et al., 2014; Lee et al., 2017) and glutamate (Behrend et al., 2009). In closed-loop DBS, the goal is to maintain a specific concentration of neurotransmitters (Lee et al., 2017). Several publications demonstrate possible techniques for choosing appropriate stimulation parameters (Wu et al., 2001; Behrend et al., 2009; Grahn et al., 2014; Walters et al., 2014; Lee et al., 2017). Behrend et al. (2009) use model equations, whereas Artificial Neural Network (ANN) is used in Lee et al. (2017)and Grahn et al. (2014). In this paper, we principally describe stimulation model selection based on linear or non-linear modeling techniques described in Behrend et al. (2009), Lee et al. (2017), and Grahn et al. (2014), respectively.

In Behrend et al. (2009), the concentration of glutamate recorded close to the sub-thalamic nucleus (StN) was modeled as a function of electrical stimulation. The parameters of electrical stimulation used in Behrend et al. (2009), were fixed (stimulation current $\approx$ 100 μA, a stimulation pulsewidth of 1 ms for 100 Hz stimulation frequency and 0.67 ms for 150 Hz stimulation frequency). A second order model equation, based on Auto Regressive eXogenous (ARX) fitting was developed, shown in

Equation (12). This was validated using cross correlation between simulated and recorded concentrations of glutamate, for varying stimulation durations in a rat model.

$$A(q) \times y(t) = B(q)u(t) + \varepsilon(t) \quad (12)$$

where, y(t) represents the glutamate concentration, u(t) corresponds to the input stimulation parameters and ε(t) corresponds to the stochastic error. For each set of stimulation parameters (i.e., two different sets of stimulation pulsewidth and frequency), the stimulation was switched on randomly to accurately capture the dynamic response of the system (Behrend et al., 2009).

The limitations of the stimulation model included limited visibility into the effects of changing stimulation currents, which is a crucial parameter to consider in DBS. Also, the model will benefit by selecting a wider range of pulsewidths and frequency. Furthermore, in order to further develop the therapy, the effects of stimulation on concentrations of other neurotransmitters such as dopamine and GABA are not modeled. The model itself is univariate, hence it does not consider interference from other neurochemicals with similar oxidation potential. The model also does not take the non-linear nature of neurochemical responses, into consideration. The univariate and linear transfer function, described in this model, needs to be expanded to ensure the model is applicable in a long-term implant.

The stimulation model, described in Behrend et al. (2009), is based on normalized values of glutamate concentration across animals. This was due to large variance in absolute glutamate concentrations across animals and also partly due to the limitation of neurochemical measurement based on electrochemical methods, which are only able to measure the change in analyte concentration only. However, the range of control on a normalized analyte concentration, in this case glutamate, is crucial. In Behrend et al. (2009), results suggest a normalized concentration range between 0.4 and 1.0 were set as control thresholds.

In Lee et al. (2017), the stimulation model was adopted from Trevathan et al. (2015). It is based on modeling dopamine kinetics due to electrical stimulation, using two different frameworks, ANN and time-series approach using Volterra kernels. Volterra kernels are particularly useful to capture the short-term and long-term effect of stimulation parameters (input) on neurochemical responses (output), in non-linear systems. Hence, they are useful in capturing the hysteresis effect i.e., effect of previous electrical stimulation events on present neurochemical responses (Trevathan et al., 2015). On the contrary, ANNs are better suited for compartmental modeling of input/output relationship between stimulation parameters and stimulation-evoked neurochemical release (Walters et al., 2014, 2015). The experimental data was obtained by stimulating the medial forebrain bundle (MFB) in rats and recording neurochemical data (Trevathan et al., 2015). A similar method was also adopted in the striatal and ventrotegmental area / substantia nigra pars compacta (VTA/SNc) of swine and non-human primate (NHP) (Trevathan et al., 2015). The stimulation parameters under consideration were stimulation amplitude (current) and pulsewidth. The stimulation duration was randomly selected to be either 0.5 or 2.0 s, to capture the dynamics of dopamine, while attempting to avoid hysteresis.

In Grahn et al. (2014), a combination of non-linear regression, computational modeling and constrained optimization was used for linking stimulation parameters with stimulation evoked dopamine responses during the experimental phase. The target stimulation electrode was placed in the medial forebrain bundle (MFB), the FSCV recording electrode was placed in the striatum and a reference silver-silver chloride electrode was placed in the contralateral cortex, to record dopamine concentration. The stimulation parameters (current, pulsewidth, frequency) were varied to record evoked dopamine responses. This dataset consisting of the stimulation parameters and their corresponding evoked dopamine responses were modeled as a combination of a 7th degree polynomial and 2nd order exponential mathematical models. The parameters in the model i.e., 8 for polynomial, 4 for exponential, and corresponding stimulation parameters were presented to an ANN. The ANN was a double feedforward ANN with sigmoidal and linear transfer funtions (Lujan and Crago, 2009). Later, in order to demonstrate closed-loop neuromodulation, the stimulation parameters required for sustaining dopamine responses at desired levels were predicted using ANN. Hence, to summarize the build-up of ANN, the inputs consisted of three stimulation parameters (stimulation frequency, pulsewidth and stimulus amplitude/current) and system outputs consisted of 12 model parameters.

The ANN consisted of 150 hidden neurons, the initial weights and biases are based on 10 different initial conditions and 10 corresponding ANNs were trained on 80% of the data (Levenberg-Marquardt algorithm). The remaining 20% of the data were used to simulate ANNs and identify those with the lowest generalization error. Constrained optimization was added to the ANN model to minimize stimulation energy and to eliminate mathematical redundancies. In order to determine the accuracy of the model, the predicted stimulation parameters and the measured dopamine levels evoked due to predictive stimulation was compared with the desired simulation results. The root mean squared error between measured and desired dopamine levels was determined, followed by least-squares regression analysis to determine dependencies between actual and desired dopamine levels were theni used in order to identify sources of error such as drift. Results in Grahn et al. (2014), from four rats, suggest that the computational and predictive models of stimulation-evoked dopamine levels can be adjusted using predicted stimulation parameters ($R^2 = 0.8$).

4.4.2. PNS: Neurochemical Recordings and Stimulation Evoked Compound Nerve Action Potentials (CNAPs)

The goal of stimulation model selection in PNS neuromodulatory therapeutic applications is to either inhibit or enhance nerve fiber activity. Peripheral nerve activity can be classified into (a) neural mass activity, (b) CNAPs and (c) Neurochemical ionic activity. Neurochemical recording can be utilized reliably to detect specific physiological events and initiate stimulation (Cork et al., 2018). However, stimulation dose tuning can

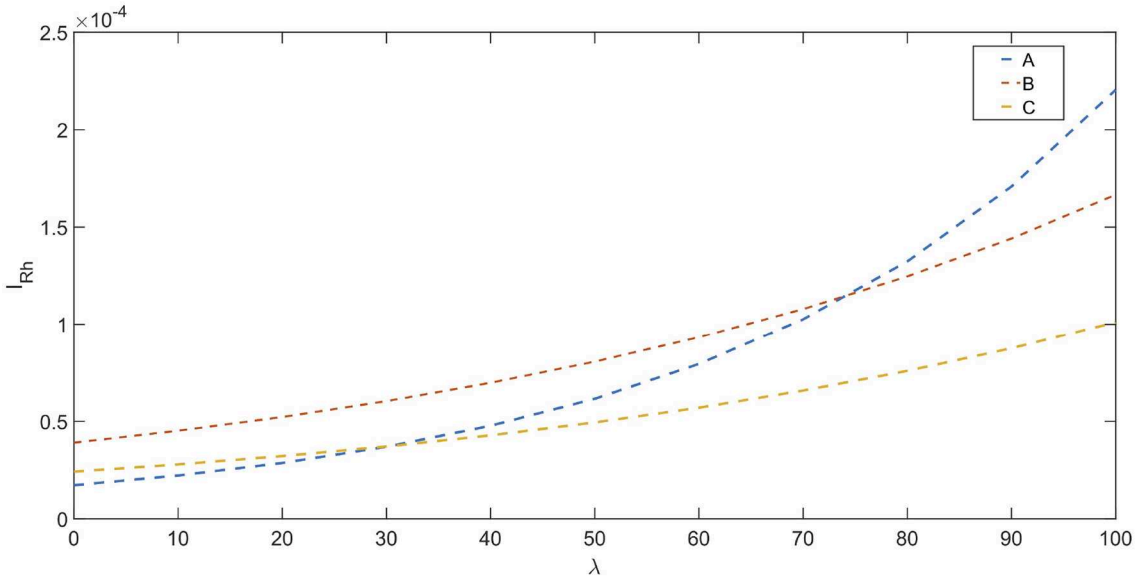

FIGURE 6 | NAP profiles for different fiber types : A, B, and C based on Ward et al. (2015), the rheobase current (I_{Rh} in A) is depicted vs. the percentage fiber activation(λ).

be achieved through monitoring electrical activity alone. A method to estimate the properties of individual fibers is through interrogative stimulation and recording. A stimulation protocol and method for high resolution CNAP recording on vagus nerve is described in Mirza et al. (2018).

In Ward et al. (2015), an effort has been made to determine stimulation dosage based on CNAPs. This involves determining a *nerve activation profile* (NAP) for each fiber type. The nerve activation potential is based on an exponential relation between rheobase current and normalized CNAP amplitude. Stimulation dosage (stimulation current) can be chosen appropriately based on NAPs. The relationships are shown below (Ward et al., 2015) :

$$I_{Rh_A} = e^{0.0255\lambda - 10.97} \tag{13}$$

$$I_{Rh_B} = e^{0.0145\lambda - 10.15} \tag{14}$$

$$I_{Rh_C} = e^{0.0143\lambda - 10.63} \tag{15}$$

where, I_{Rh} is the rheobase current. $\lambda = \frac{V_{cnap}}{V_{cnap\_max}} \times 100$, which represents the percent maximal activation of nerve fibers. The NAP for different fibers are shown in **Figure 6**.

In existing solutions, such as Behrend et al. (2009), Grahn et al. (2014), and Lee et al. (2017), model selection was performed using ANN. Implementation of ANN on-chip or SoCs can be resource and power intensive. To enable on-chip implementation of *model selection*, it is important to consider simplification of the stimulation control model by balancing the trade-off between complexity of the model and stimulation goals.

Alternatively, a better approach to develop implantable solutions, especially for PNS applications, will be to determine a mathematical model as described in Ward and Irazoqui (2010) and Behrend et al. (2009). Linear or polynomial models can be implemented on-chip and optimized to be resource and power efficient. Another approach will be to design stimulators which can perform selective activation of fibers by modifying the traditional stimulation waveforms (Joseph and Butera, 2011; Patel and Butera, 2015).

5. DISCUSSION

Closed-loop neuromodulation is likely to improve system performance and clinical outcomes. However, the challenges involved in implementing closed-loop neuromodulation consists of identification of appropriate biomarkers, identifying the recording and stimulation loci and the choice of neuromodulatory paradigm i.e., excitation/inhibition of neural activity or regulation of neurotransmitter concentration. A neurochemical monitoring modality for closed-loop neuromodulation is promising, as it provides higher resolution in terms of neural events, better Signal-to-Noise ratio and less interference in comparison to electrical recordings of neural signals.

This review highlights that, neurochemical closed-loop neuromodulation systems benefit from higher specificity and less interference for *therapeutic* neuromodulation applications. However, there is a clear lack of implantable, closed-loop neurochemical neuromodulation systems that are available commercially. The lack of neurochemical closed-loop neuromodulation is due to various reasons.

One of the limitations of neurochemical monitoring is ensuring direct contact between the neurochemical sensor and neurochemical molecules. For this reason, the sensors need to be inserted into neural tissue and hence have greater

susceptibility to bio-fouling. It is a long standing challenge to produce neurochemical sensors whose sensitivity lasts longer *in vivo*. CFM has been widely used to perform neurochemical voltammetric measurements and has been shown to work reliably up to 4 months after chronic implantation (Clark et al., 2010). Carbon fiber microelectrodes can also be coated with CNTs (Swamy and Venton, 2007), which increases its resistance to the adhesion of common biofouling agents such as 5-HIAA. CNT-based microelectrodes are able to increase selectivity and sensitivity of FSCV measurements at high speeds (Bucher and Wightman, 2015). Especially, polyamide-coated fused silica CFM electrode have been shown to last *in vivo* for approximately 25 days without any loss in sensitivity, albeit a small loss in temporal resolution (Clark et al., 2010). Efforts to tackle this challenge further include developing anti-biofouling coatings on the sensor (Blaszykowski et al., 2015; Machado et al., 2016). However, the lifetime of *in vivo* ion-selective electrodes needs to be investigated further.

A very promising line of research has been pursued by Thompson's group at the University of Toronto, who are developing anti-biofouling coatings for *in vivo* sensor applications (Sheikh et al., 2012, 2015). Furthermore, the same group have developed an anti-biofouling coating for potassium sensors, which will include neuro-chemical recording (Thompson, 2017).

Another important effort in sensor fabrication is directed toward reducing the size of the array while increasing recording locations. This will increase spatial resolution leading to better recording of neurotransmitter concentrations within the extracellular/intracellular environment. In this direction, research is progressing to explore the development of carbon-nanotube (CNTs) or carbon-nanofiber (CNF) based microelectrode array (MEA) which are compatible to be used for neurochemical measurements (Bucher and Wightman, 2015). In order to capture neurotransmitter activity from extracellular or exocytotic neural environment in the brain, the microelectrode array (MEA) pitch needs to be between $\sim 10 - 20\mu m$ to enable interfacing with individual neurons (Kishida et al., 2011). The latest neurochemical MEA consists of 36 microelectrodes within an area of 40 μm $\times$ 40 μm (Bucher and Wightman, 2015).

The majority of neurochemical recording in the CNS, reported earlier, is focussed on neurotransmitters. However, the relationship between stimulation parameters and stimulation-induced change in neurochemical concentration, may vary over time. This change could be due to neuro-plasticity or change in electrode-electrolyte interface, leading to re-adjustment of stimulation models on a regular basis, to adjust stimulation dosage accurately.

An important aspect of neurochemical recording is the interference from other neurochemicals. One of the common interferents is pH change, which produces similar profile of voltammograms to dopamine. Hence, it is important to subtract contribution due to pH in order to identify dopamine specific cyclic voltammogram. Another common interferent is ascorbate, which also has similar oxidation potential as dopamine but different voltammogram profile. A multivariate classification model can be used for distinguishing signal contribution due to target neurochemical signals and interferents. Furthermore, electrode design can also be utilized to reduce cross-talk between different neurochemical signals. It was shown that CNF performs better than glass carbon electrode in isolating signal contributions due to different neurotransmitters (Rand et al., 2013). Different neurotransmitters which show similar oxidation potentials using glass carbon electrodes, show different oxidation potentials when CNF is used.

Also, in diseases where there isn't a clear relationship between neurotransmitters and disease symptoms, there may exist a clear relationship between electrical neural signals and symptoms. In such cases, it is better to monitor neural ionic concentrations, such K+, Na+, or H+ which are also directly correlated with electrical neural signals (Makani and Chesler, 2010). This will ensure high specificity biomarker recording. Another fact to note is that the recent work in neurochemical monitoring mostly focusses on healthy animal models (Chang et al., 2012; Lee et al., 2017) and very limited work has been done in humans. Two human studies were performed by Kasasbeh et al. (2013) and Chang et al. (2012), in which no adverse effects to patient health were reported in the short-term. Also, no short-term reduction in DBS treatment efficiency was observed.

In existing neurochemical neuromodulation systems, the training step and in some cases, the entire *decision making* and *model selection* algorithm is implemented off-chip. Although, this works for research applications, it restricts patient mobility in a future implantable solution. In order to achieve local or on-chip machine learning capabilities, it is important to reduce complexity of the neuromodulation algorithm without sacrificing stimulation goals. Commercial solutions, such as those from ARM and Qualcomm, are also focussed on developing resource efficient, artificial intelligence on SoC (Desoli et al., 2017; Moons et al., 2017).

Another important aspect of achieving therapeutic efficiency is stimulating at the optimal location. When DBS is used for treating Parkinson's, the stimulation locus is generally the sub-thalamic nucleus/globus palliadus internus (StN/Gpi) (Hitti et al., 2019). For VNS, various locations have been used for different applications such as stimulation of left or right cervical vagus nerve for epilepsy (Boon et al., 2001), subdiaphragmatic vagus nerve for obesity (Ikramuddin et al., 2014), auricular branch of the vagus nerve (Clancy et al., 2014).

The WINCS platform has demonstrated that it is possible to develop an adaptive neuromodulation system based on a single neurochemical biomarker. However, the long term efficacy of a single biomarker based solution needs to be determined. A solution to better understand the success and, ultimately, improve closed-loop neuromodulation therapy is the addition of electrophysiological recording. Recently, an electrode was developed by Vajari et al. (2018), which incorporates the ability to record both neurochemical, neuro-electrical recording and electrical stimulation. This is a desirable addition for CNS based therapy, but is necessary for complete closed-loop in a PNS based closed-loop neuromodulation system (Mirza et al., 2017, 2019).

6. CONCLUSION

This review is focused on highlighting the benefits and challenges of using a neurochemical biomarker for intelligent neuromodulation. It has also outlined the different elements required to implement neurochemical closed-loop neuromdoulation as an implantable solution. The first step toward developing an intelligent neuromodulation system is identifying an appropriate biomarker, such as a neurochemical biomarker and a corresponding stimulation/recording site. The second step is to develop a reliable sensing methodology, sensor and data acquisition system. The third challenge is to implement the pre-processing and intelligent neuromodulation algorithms on-chip or locally in a single integrated SoC.

For CNS based applications, where neurotransmitters are the target biomarkers, FSCV is often chosen as a reliable detection technique and CFM is the preferred electrode for this application. Emerging techniques include impedimetery and potentiometry for detection of ionic concentrations, in both CNS and PNS. For potentiometric sensing, IrOx sensors can be used reliably for sensing pH. The sensitivity, selectivity and longevity of the sensors described in this paper can be improved through coatings such as, Nafion-CNT.

There are primarily two technical challenges that need to be addressed in order develop a neurochemical closed-loop system for long-term, chronic therapeutic efficacy studies. The first is development of an implantable chemical sensor, with a reliable sensitivity and resolution in the long term. The second challenge is implementing processing algorithms on-chip for stimulation decision making (*when?* to stimulate) and stimulation model selection (*how much?* to stimulate).

AUTHOR CONTRIBUTIONS

KM and CG wrote the manuscript. KN and CT supervised and reviewed the manuscript.

FUNDING

This work was supported by the European Research Council (Synergy Grant No. 319818, i2MOVE), UK EPSRC grant EP/N002474/1, and EPSRC-Imperial Impact Acceleration Award (2018).

REFERENCES

Ahmed, T., Mirza, K. B., and Nikolic, K. (2018). "Resource efficient pre-processor for drift removal in neurochemical signals," in *Circuits and Systems (ISCAS), 2018 IEEE International Symposium on* (Florence: IEEE), 1–5.

Amar, A. P., Levy, M. L., Liu, C. Y., and Apuzzo, M. L. J. (2008). Vagus nerve stimulation. *Proc. IEEE* 96, 1142–1151.

Behrend, C. E., Cassim, S. M., Pallone, M. J., Daubenspeck, J. A., Hartov, A., Roberts, D. W., et al. (2009). Toward feedback controlled deep brain stimulation: dynamics of glutamate release in the subthalamic nucleus in rats. *J. Neurosci. Methods* 180, 278–289. doi: 10.1016/j.jneumeth.2009.04.001

Benabid, A. L., Chabardes, S., Mitrofanis, J., and Pollak, P. (2009). Deep brain stimulation of the subthalamic nucleus for the treatment of parkinson's disease. *Lancet Neurol.* 8, 67–81. doi: 10.1016/S1474-4422(08)70291-6

Beuter, A., Lefaucheur, J. P., and Modolo, J. (2014). Closed-loop cortical neuromodulation in Parkinson's disease: an alternative to deep brain stimulation? *Clin. Neurophysiol.* 125, 874–885. doi: 10.1016/j.clinph.2014.01.006

Bittar, R. G., Burn, S. C., Bain, P. G., Owen, S. L., Joint, C., Shlugman, D., et al. (2005). Deep brain stimulation for movement disorders and pain. *J. Clin. Neurosci.* 12, 457–463. doi: 10.1016/j.jocn.2004.10.005

Blaszykowski, C., Sheikh, S., and Thompson, M. (2015). A survey of state-of-the-art surface chemistries to minimize fouling from human and animal biofluids. *Biomater. Sci.* 3, 1335–1370. doi: 10.1039/c5bm00085h

Boccard, S. G., Pereira, E. A., and Aziz, T. Z. (2015). Deep brain stimulation for chronic pain. *J. Clin. Neurosci.* 22, 1537–1543. doi: 10.1016/j.jocn.2015.04.005

Bonaz, B., Sinniger, V., Hoffmann, D., Clarençon, D., Mathieu, N., Dantzer, C., et al. (2016). Chronic vagus nerve stimulation in crohn's disease: a 6-month follow-up pilot study. *Neurogastroenterol. Motil.* 28, 948–953. doi: 10.1111/nmo.12792

Boon, P., Vonck, K., Reuck, J. D., and Caemaert, J. (2001). Vagus nerve stimulation for refractory epilepsy. *Seizure* 10, 448–455. doi: 10.1053/seiz.2001.0626

Borovikova, L. V., Ivanova, S., Zhang, M., Yang, H., Botchkina, G. I., Watkins, L. R., et al. (2000). Vagus nerve stimulation attenuates the systemic inflammatory response to endotoxin. *Nature* 405, 458–462. doi: 10.1038/35013070

Bostock, H., Cikurel, K., and Burke, D. (1998). Threshold tracking techniques in the study of human peripheral nerve. *Muscle Nerve* 21, 137–158.

Bostock, H., and Grafe, P. (1985). Activity-dependent excitability changes in normal and demyelinated rat spinal root axons. *J. Physiol.* 365, 239–257.

Bozorgzadeh, B., Covey, D. P., Heidenreich, B. A., Garris, P. A., and Mohseni, P. (2014). "Real-time processing of fast-scan cyclic voltammetry (FSCV) data using a field-programmable gate array (FPGA)," in *Annual International Conference of the IEEE Engineering in Medicine and Biology Society (IEEEMBC)* (Chicago, IL: IEEE Engineering in Medicine and Biology Society), 2036–2039.

Bozorgzadeh, B., Schuweiler, D. R., Bobak, M. J., Garris, P. A., and Mohseni, P. (2016). Neurochemostat: a neural interface SoC with integrated chemometrics for closed-loop regulation of brain dopamine. *IEEE Trans. Biomed. Circuits Syst.* 10, 654–667. doi: 10.1109/TBCAS.2015.2453791

Breysse, N., Amalric, M., and Salin, P. (2003). Metabotropic glutamate 5 receptor blockade alleviates akinesia by normalizing activity of selective basal-ganglia structures in parkinsonian rats. *J. Neurosci.* 23, 8302–8309. doi: 10.1523/JNEUROSCI.23-23-08302.2003

Breysse, N., Baunez, C., Spooren, W., Gasparini, F., and Amalric, M. (2002). Chronic but not acute treatment with a metabotropic glutamate 5 receptor antagonist reverses the akinetic deficits in a rat model of parkinsonism. *J. Neurosci.* 22, 5669–5678. doi: 10.1523/JNEUROSCI.22-13-05669.2002

Brisch, R., Saniotis, A., Wolf, R., Bielau, H., Bernstein, H.-G., Steiner, J., et al. (2014). Corrigendum: the role of dopamine in schizophrenia from a neurobiological and evolutionary perspective: old fashioned, but still in vogue. *Front. Psychiatry* 5:110. doi: 10.3389/fpsyt.2014.00110

Bubser, M., and Schmidt, W. J. (1990). 6-hydroxydopamine lesion of the rat prefrontal cortex increases locomotor activity, impairs acquisition of delayed alternation tasks, but does not affect uninterrupted tasks in the radial maze. *Behav. Brain Res.* 37, 157–168.

Bucher, E. S., Brooks, K., Verber, M. D., Keithley, R. B., Owesson-White, C., Carroll, S., et al. (2013). Flexible software platform for fast-scan cyclic voltammetry data acquisition and analysis. *Anal. Chem.* 85, 10344–10353. doi: 10.1021/ac402263x

Bucher, E. S., and Wightman, R. M. (2015). Electrochemical analysis of neurotransmitters. *Annu. Rev. Anal. Chem.* 8, 239–261. doi: 10.1146/annurev-anchem-071114-040426

Carhart-Harris, R. L. and Nutt, D. J. (2017). Serotonin and brain function: a tale of two receptors. *J. Psychopharmacol.* 31, 1091–1120. doi: 10.1177/0269881117725915

Chang, S.-Y., Kim, I., Marsh, M. P., Jang, D. P., Hwang, S.-C., Van Gompel, J. J., et al. (2012). Wireless fast-scan cyclic voltammetry to monitor adenosine in patients with essential tremor during deep brain stimulation. *Mayo Clin. Proc.* 87, 760–765. doi: 10.1016/j.mayocp.2012.05.006

Chang, S.-Y., Kimble, C. J., Kim, I., Paek, S. B., Kressin, K. R., Boesche, J. B., et al. (2013). Development of the mayo investigational neuromodulation control system: toward a closed-loop electrochemical feedback system for deep brain stimulation. *J. Neurosurg.* 119, 1556–1565. doi: 10.3171/2013.8.JNS122142

Chesler, M., and Kaila, K. (1992). Modulation of pH by neuronal activity. *Trends Neurosci.* 15, 396–402.

Clancy, J. A., Mary, D. A., Witte, K. K., Greenwood, J. P., Deuchars, S. A., and Deuchars, J. (2014). Non-invasive vagus nerve stimulation in healthy humans reduces sympathetic nerve activity. *Brain Stimul.* 7, 871–877. doi: 10.1016/j.brs.2014.07.031

Clark, J. J., Sandberg, S. G., Wanat, M. J., Gan, J. O., Horne, E. A., Hart, A. S., et al. (2010). Chronic microsensors for longitudinal, subsecond dopamine detection in behaving animals. *Nat. Methods* 7, 126–129. doi: 10.1038/nmeth.1412

Cork, S. C., Eftekhar, A., Mirza, K. B., Zuliani, C., Nikolic, K., Gardiner, J. V., et al. (2018). Extracellular pH monitoring for use in closed-loop vagus nerve stimulation. *J. Neural Eng.* 15:016001. doi: 10.1088/1741-2552/aa8239

Davidson, D., Pullar, I. A., Mawdsley, C., Kinloch, N., and Yates, C. M. (1977). Monoamine metabolites in cerebrospinal fluid in multiple sclerosis. *J. Neurol. Neurosurg. Psychiatry* 40, 741–745. doi: 10.1136/jnnp.40.8.741

Daws, L. C., Montañez, S., Owens, W. A., Gould, G. G., Frazer, A., Toney, G. M., et al. (2005). Transport mechanisms governing serotonin clearance *in vivo* revealed by high-speed chronoamperometry. *J. Neurosci. Methods* 143, 49–62. doi: 10.1016/j.jneumeth.2004.09.011

De La Franier, B., Jankowski, A., and Thompson, M. (2017). Functionalizable self-assembled trichlorosilyl-based monolayer for application in biosensor technology. *Appl. Surf. Sci.* 414, 435–441. doi: 10.1016/j.apsusc.2017.04.111

DeKosky, S. T., Harbaugh, R. E., Schmitt, F. A., Bakay, R. A., Chui, H. C., Knopman, D. S., et al. (1992). Cortical biopsy in alzheimer's disease: diagnostic accuracy and neurochemical, neuropathological, and cognitive correlations. *Ann. Neurol.* 32, 625–632. doi: 10.1002/ana.410320505

Desoli, G., Chawla, N., Boesch, T., Singh, S.-p., Guidetti, E., De Ambroggi, F., et al. (2017). "14.1 a 2.9 tops/w deep convolutional neural network soc in fd-soi 28nm for intelligent embedded systems," in *2017 IEEE International Solid-State Circuits Conference (ISSCC)* (San Francisco, CA: IEEE), 238–239.

Ebert, M., Hauptmann, C., and Tass, P. A. (2014). Coordinated reset stimulation in a large-scale model of the stn-gpe circuit. *Front. Comput. Neurosci.* 8:154. doi: 10.3389/fncom.2014.00154

Eikelenboom, P., Rozemuller, A. J., Hoozemans, J. J., Veerhuis, R., and van Gool, W. A. (2000). Neuroinflammation and alzheimer disease: clinical and therapeutic implications. *Alzheimer Dis. Assoc. Disord.* 14, S54–S61. doi: 10.1097/00002093-200000001-00009

Endres, W., Grafe, P., Bostock, H., and ten Bruggencate, G. (1986). Changes in extracellular pH during electrical stimulation of isolated rat vagus nerve. *Neurosci. Lett.* 64, 201–205. doi: 10.1016/0304-3940(86)90100-X

Flora, E. D., Perera, C. L., Cameron, A. L., and Maddern, G. J. (2010). Deep brain stimulation for essential tremor: a systematic review. *Mov. Disord.* 25, 1550–1559. doi: 10.1002/mds.23195

Gerhardt, G. A., and Hoffman, A. F. (2001). Effects of recording media composition on the responses of nafion-coated carbon fiber microelectrodes measured using high-speed chronoamperometry. *J. Neurosci. Methods* 109, 13–21. doi: 10.1016/S0165-0270(01)00396-X

Gerhardt, G. A., Oke, A. F., Nagy, G., Moghaddam, B., and Adams, R. N. (1984). Nafion-coated electrodes with high selectivity for cns electrochemistry. *Brain Res.* 290, 390–395. doi: 10.1016/0006-8993(84)90963-6

Golden, C. T., Nandi, D., Bain, P., and Yousif, N. (2013). Deep brain stimulation induced effects in a network of ventral intermediate neurons. *BMC Neurosci.* 14:P427. doi: 10.1186/1471-2202-14-S1-P427

Gonon, F., Buda, M., Cespuglio, R., Jouvet, M., and Pujol, J.-F. (1980). *In vivo* electrochemical detection of catechols in the neostriatum of anaesthetized rats: dopamine or dopac? *Nature* 286:902. doi: 10.1038/286902a0

Grahn, P. J., Mallory, G. W., Khurram, O. U., Berry, B. M., Hachmann, J. T., Bieber, A. J., et al. (2014). A neurochemical closed-loop controller for deep brain stimulation : toward individualized smart neuromodulation therapies. *Front. Neurosci.* 8:169. doi: 10.3389/fnins.2014.00169

Groppetti, A., Zambotti, F., Biazzi, A., and Mantegazza, P. (1973). "Amphetamine and cocaine on amine turnover," in *Frontiers in Catecholamine Research* (Starsbourg: Elsevier), 917–925.

Heien, M. L. A. V., Johnson, M. A., and Wightman, R. M. (2004). Resolving neurotransmitters detected by fast-scan cyclic voltammetry. *Anal. Chem.* 76, 5697–5704. doi: 10.1021/ac0491509

Heien, M. L. A. V., Khan, A. S., Ariansen, J. L., Cheer, J. F., Phillips, P. E., Wassum, K. M., et al. (2005). Real-time measurement of dopamine fluctuations after cocaine in the brain of behaving rats. *Proc. Natl. Acad. Sci. U.S.A.* 102, 10023–10028. doi: 10.1073/pnas.0504657102

Hesse, S., Moeller, F., Petroff, D., Lobsien, D., Luthardt, J., Regenthal, R. et al. (2014). Altered serotonin transporter availability in patients with multiple sclerosis. *Eur. J. Nucl. Med. Mol. Imaging.* 41, 827–835. doi: 10.1007/s00259-013-2636-z

Hitti, F. L., Ramayya, A. G., McShane, B. J., Yang, A. I., Vaughan, K. A., and Baltuch, G. H. (2019). Long-term outcomes following deep brain stimulation for parkinson's disease. *J. Neurosurg.* 1, 1–6. doi: 10.3171/2018.8.JNS182081

Hoang, K. B., Cassar, I. R., Grill, W. M., and Turner, D. A. (2017). Biomarkers and stimulation algorithms for adaptive brain stimulation. *Front. Neurosci.* 11:564. doi: 10.3389/fnins.2017.00564

Hosokawa, K., and Sunagawa, K. (2016). Closed-loop neuromodulation technology for baroreflex blood pressure control. *Proc. IEEE* 104, 432–443. doi: 10.1109/JPROC.2015.2496290

Huey, E. D., Putnam, K. T., and Grafman, J. (2006). A systematic review of neurotransmitter deficits and treatments in frontotemporal dementia. *Neurology* 66, 17–22. doi: 10.1212/01.wnl.0000191304.55196.4d

Ikemoto, S. (2007). Dopamine reward circuitry: two projection systems from the ventral midbrain to the nucleus accumbens–olfactory tubercle complex. *Brain Res. Rev.* 56, 27–78. doi: 10.1016/j.brainresrev.2007.05.004

Ikramuddin, S., Blackstone, R. P., Brancatisano, A., Toouli, J., Shah, S. N., Wolfe, B. M., et al. (2014). Effect of reversible intermittent intra-abdominal vagal nerve blockade on morbid obesity: the ReCharge randomized clinical trial. *JAMA* 312, 915–922. doi: 10.1001/jama.2014.10540

John, C. E., and Jones, S. R. (2006). "Fast scan cyclic voltammetry of dopamine and serotonin in mouse brain slices," in *Electrochemical Methods for Neuroscience,* eds A. C. Michael and L. M. Borland (Boca Raton, FL: CRC Press/Taylor & Francis). doi: 10.1201/9781420005868

Johnson, K. A., Conn, P. J., and Niswender, C. M. (2009). Glutamate receptors as therapeutic targets for parkinson's disease. *CNS Neurol. Disord. Drug Targets)* 8, 475–491. doi: 10.2174/187152709789824606

Joseph, L., and Butera, R. J. (2011). High-frequency stimulation selectively blocks different types of fibers in frog sciatic nerve. *IEEE Trans. Neural Syst. Rehabil. Eng.* 19, 550–557. doi: 10.1109/TNSRE.2011.2163082

Kasasbeh, A., Lee, K., Bieber, A., Bennet, K., and Chang, S.-Y. (2013). Wireless neurochemical monitoring in humans. *Stereotact. Funct. Neurosurg.* 91, 141–147. doi: 10.1159/000345111

Keithley, R. B., Carrelli, R. M., and Wightman, R. M. (2005). Rank estimation and the multivariate analysis of *in vivo* fast-scan cyclic voltammetric data. *Biophys. Chem.* 257, 2432–2437. doi: 10.1016/j.immuni.2010.12.017

Keithley, R. B., Heien, M. L., and Wightman, R. M. (2010). Multivariate concentration determination using principal component regression with residual analysis. *Trends Anal. Chem.* 28, 1127–1136. doi: 10.1016/j.trac.2009.07.002

Keithley, R. B., and Wightman, R. M. (2011). Assessing principal component regression prediction of neurochemicals detected with fast-scan cyclic voltammetry. *ACS Chem. Neurosci.* 2, 514–525. doi: 10.1021/cn200035u

Kishida, K. T., Sandberg, S. G., Lohrenz, T., Comair, Y. G., Sáez, I., Phillips, P. E., et al. (2011). Sub-second dopamine detection in human striatum. *PLoS ONE* 6:e23291. doi: 10.1371/journal.pone.0023291

Kiyatkin, E. A., Wakabayashi, K. T., and Lenoir, M. (2013). Physiological fluctuations in brain temperature as a factor affecting electrochemical evaluations of extracellular glutamate and glucose in behavioral experiments. *ACS Chem. Neurosci.* 4, 652–665. doi: 10.1021/cn300232m

Koller, W. C., Lyons, K. E., Wilkinson, S. B., and Pahwa, R. (1999). Efficacy of unilateral deep brain stimulation of the vim nucleus of the thalamus for essential head tremor. *Mov. Disord.* 14, 847–850. doi: 10.1002/1531-8257(199909)14:5<847::AID-MDS1021>3.0.CO;2-G

Koob, G. F. (1992). Dopamine, addiction and reward. *Semin. Neurosci.* 4, 139–148. doi: 10.1016/1044-5765(92)90012-Q

Kowalska, M., Prendecki, M., Kozubski, W., Lianeri, M., and Dorszewska, J. (2016). Molecular factors in migraine. *Oncotarget* 7:50708. doi: 10.18632/oncotarget.9367

Krack, P., Batir, A., Van Blercom, N., Chabardes, S., Fraix, V., Ardouin, C., et al. (2003). Five-year follow-up of bilateral stimulation of the subthalamic nucleus in advanced parkinson's disease. *N. Engl. J. Med.* 349, 1925–1934. doi: 10.1056/NEJMoa035275

Kristoffer, F., Litt, B., Tracey, K. J., Boyden, E. S., and Slaoui, M. (2013). A jump-start for electroceuticals. *Nature* 496, 159–161. doi: 10.1038/496159a

Landau, A. M., Dyve, S., Jakobsen, S., Alstrup, A. K., Gjedde, A., and Doudet, D. J. (2015). Acute vagal nerve stimulation lowers $\alpha 2$ adrenoceptor availability: possible mechanism of therapeutic action. *Brain Stimul.* 8, 702–707. doi: 10.1016/j.brs.2015.02.003

Lee, K. H., Lujan, J. L., Trevathan, J. K., Ross, E. K., Bartoletta, J. J., Park, H. O., et al. (2017). WINCS Harmoni: closed-loop dynamic neurochemical control of therapeutic interventions. *Sci. Rep.* 7:46675. doi: 10.1038/srep46675

Li, H., Liu, X., Li, L., Mu, X., Genov, R., and Mason, A. J. (2017). CMOS electrochemical instrumentation for biosensor microsystems: a review. *Sensors* 17:E74. doi: 10.3390/s17010074

Li, P., Liu, H., Sun, P., Wang, X., Wang, C., Wang, L., et al. (2016). Chronic vagus nerve stimulation attenuates vascular endothelial impairments and reduces the inflammatory profile via inhibition of the nf-κb signaling pathway in ovariectomized rats. *Exp. Gerontol.* 74, 43–55. doi: 10.1016/j.exger.2015.12.005

Lodge, D. J., and Grace, A. A. (2011). Developmental pathology, dopamine, stress and schizophrenia. *Int. J. Dev. Neurosci.* 29, 207–213. doi: 10.1016/j.ijdevneu.2010.08.002

Lotharius, J., and Brundin, P. (2002). Pathogenesis of parkinson's disease: dopamine, vesicles and α-synuclein. *Nat. Rev. Neurosci.* 3:932. doi: 10.1038/nrn983

Lucki, I. (1998). The spectrum of behaviors influenced by serotonin. *Biol. Psychiatry* 44, 151–162. doi: 10.1016/S0006-3223(98)00139-5

Lujan, J. L., and Crago, P. E. (2009). Automated optimal coordination of multiple-dof neuromuscular actions in feedforward neuroprostheses. *IEEE Trans. Biomed. Eng.* 56, 179–187. doi: 10.1109/TBME.2008.2002159

Machado, R., Soltani, N., Dufour, S., Salam, M. T., Carlen, P. L., Genov, R., et al. (2016). Biofouling-resistant impedimetric sensor for array high-resolution extracellular potassium monitoring in the Brain. *Biosensors* 6, 1–12. doi: 10.3390/bios6040053

Mahad, D. H., Trapp, B. D., and Lassmann, H. (2015). Pathological mechanisms in progressive multiple sclerosis. *Lancet Neurol.* 14, 183–193. doi: 10.1016/S1474-4422(14)70256-X

Makani, S., and Chesler, M. (2010). Rapid rise of extracellular pH evoked by neural activity is generated by the plasma membrane calcium ATPase. *J. Neurophysiol.* 103, 667–676. doi: 10.1152/jn.00948.2009

Malinova, T. S., Dijkstra, C. D., de Vries, H. E. (2018). Serotonin: a mediator of the gut-brain axis in multiple sclerosis. *Mult. Scler.* 24, 1144–1150. doi: 10.1177/1352458517739975

Manji, H. K., Drevets, W. C., and Charney, D. S. (2001). The cellular neurobiology of depression. *Nat. Med.* 7:541. doi: 10.1038/87865

Marchand, S., Kupers, R. C., Bushnell, M. C., and Duncan, G. H. (2003). Analgesic and placebo effects of thalamic stimulation. *Pain* 105, 481–488. doi: 10.1016/S0304-3959(03)00265-3

Michael, A. C., and Borland, L. (2006). *Electrochemical Methods for Neuroscience*. Boca Raton, FL: CRC Press.

Mickle, A. D., Won, S. M., Noh, K. N., Yoon, J., Meacham, K. W., Xue, Y., et al. (2019). A wireless closed-loop system for optogenetic peripheral neuromodulation. *Nature* 565, 361–365. doi: 10.1038/s41586-018-0823-6

Mirza, K. B., Alenda, A., Eftekhar, A., Grossman, N., Nikolic, K., Bloom, S. R., et al. (2018). Influence of cholecystokinin-8 on compound nerve action potentials from ventral gastric vagus in rats. *Int. J. Neural Syst.* 28:1850006. doi: 10.1142/S0129065718500065

Mirza, K. B., Kulasekeram, N., Liu, Y., Nikolic, K., and Toumazou, C. (2019). "System on chip for closed loop neuromodulation based on dual mode biosignals," in *2019 IEEE International Symposium on Circuits and Systems (ISCAS)* (Sapporo: IEEE), 1–5.

Mirza, K. B., Wildner, K., Kulasekeram, N., Cork, S. C., Bloom, S. R., Nikolic, K., et al. (2017). "Live demo: platform for closed loop neuromodulation based on dual mode biosignals," in *IEEE 2017 Biomedical Circuits and Systems Conference, BioCAS 2017 - Proceedings* (Milan).

Moons, B., Uytterhoeven, R., Dehaene, W., and Verhelst, M. (2017). "14.5 envision: A 0.26-to-10tops/w subword-parallel dynamic-voltage-accuracy-frequency-scalable convolutional neural network processor in 28nm fdsoi," in *2017 IEEE International Solid-State Circuits Conference (ISSCC)* (San Francisco, CA: IEEE), 246–247.

Mufson, E. J., Counts, S. E., Fahnestock, M., and Ginsberg, S. D. (2007). Cholinotrophic molecular substrates of mild cognitive impairment in the elderly. *Curr. Alzheimer Res.* 4, 340–350. doi: 10.2174/156720507781788855

Mufson, E. J., Counts, S. E., Perez, S. E., and Ginsberg, S. D. (2008). Cholinergic system during the progression of alzheimer's disease: therapeutic implications. *Expert Rev. Neurother.* 8, 1703–1718. doi: 10.1586/14737175.8.11.1703

Murphy, D. L., Fox, M. A., Timpano, K. R., Moya, P. R., Ren-Patterson, R., Andrews, A. M., et al. (2008). How the serotonin story is being rewritten by new gene-based discoveries principally related to slc6a4, the serotonin transporter gene, which functions to influence all cellular serotonin systems. *Neuropharmacology* 55, 932–960. doi: 10.1016/j.neuropharm.2008.08.034

Ng, S. R., and O'Hare, D. (2015). An iridium oxide microelectrode for monitoring acute local pH changes of endothelial cells. *Analyst* 140, 4224–4231. doi: 10.1039/C5AN00377F

NIH (2014). *Neurochemical Closed-Loop Controller For Smart DBS*. Project No: 5R01NS084975-02.

Ossowska, K., Konieczny, J., Wolfarth, S., and Pilc, A. (2005). Mtep, a new selective antagonist of the metabotropic glutamate receptor subtype 5 (mglur5), produces antiparkinsonian-like effects in rats. *Neuropharmacology* 49, 447–455. doi: 10.1016/j.neuropharm.2005.04.002

Owen, S. L., Green, A. L., Stein, J. F., and Aziz, T. Z. (2006). Deep brain stimulation for the alleviation of post-stroke neuropathic pain. *Pain* 120, 202–206. doi: 10.1016/j.pain.2005.09.035

Ozdemir, V., Jamal, M. M., Osapay, K., Jadus, M. R., Sandor, Z., Hashemzadeh, M., et al. (2007). Cosegregation of gastrointestinal ulcers and schizophrenia in a large national inpatient discharge database: revisiting the "brain-gut axis" hypothesis in ulcer pathogenesis. *J. Invest. Med.* 55, 315–320. doi: 10.2310/6650.2007.00014

Pani, L., Porcella, A., and Gessa, G. (2000). The role of stress in the pathophysiology of the dopaminergic system. *Mol. Psychiatry* 5:14. doi: 10.1038/sj.mp.4000589

Park, J., Takmakov, P., and Wightman, R. M. (2011). *In vivo* comparison of norepinephrine and dopamine release in rat brain by simultaneous measurements with fast-scan cyclic voltammetry. *J. Neurochem.* 119, 932–944. doi: 10.1111/j.1471-4159.2011.07494.x

Patel, Y. A., and Butera, R. J. (2015). Differential fiber-specific block of nerve conduction in mammalian peripheral nerves using kilohertz electrical stimulation. *J. Neurophysiol.* 113, 3923–3929. doi: 10.1152/jn.00529.2014

Payne, S. C., Furness, J. B., and Stebbing, M. J. (2018). Bioelectric neuromodulation for gastrointestinal disorders: effectiveness and mechanisms. *Nat. Rev. Gastroenterol. Hepatol.* 16, 89–105. doi: 10.1038/s41575-018-0078-6

Peters, J. L., Miner, L. H., Michael, A. C., and Sesack, S. R. (2004). Ultrastructure at carbon fiber microelectrode implantation sites after acute voltammetric measurements in the striatum of anesthetized rats. *J. Neurosci. Methods* 137, 9–23. doi: 10.1016/j.jneumeth.2004.02.006

Priori, A., Foffani, G., Rossi, L., and Marceglia, S. (2013). Adaptive deep brain stimulation (adbs) controlled by local field potential oscillations. *Exp. Neurol.* 245,77–86. doi: 10.1016/j.expneurol.2012.09.013

Raimondo, J. V., Burman, R. J., Katz, A. A., and Akerman, C. J. (2015). Ion dynamics during seizures. *Front. Cell. Neurosci.* 9:419. doi: 10.3389/fncel.2015.00419

Rand, E., Periyakaruppan, A., Tanaka, Z., Zhang, D. A., Marsh, M. P., Andrews, R. J., et al. (2013). A carbon nanofiber based biosensor for simultaneous detection of dopamine and serotonin in the presence of ascorbic acid. *Biosensors Bioelectron.* 42, 434–438. doi: 10.1016/j.bios.2012.10.080

Rasheed, N., and Alghasham, A. (2012). Central dopaminergic system and its implications in stress-mediated neurological disorders and gastric ulcers: short review. *Adv. Pharmacol. Sci.* 2012:182671. doi: 10.1155/2012/182671

Rehncrona, S., Johnels, B., Widner, H., Törnqvist, A.-L., Hariz, M., and Sydow, O. (2003). Long-term efficacy of thalamic deep brain stimulation for tremor: double-blind assessments. *Mov. Disord.* 18, 163–170. doi: 10.1002/mds.10309

Robinson, D. L., and Wightman, R. M. (2004). Nomifensine amplifies subsecond dopamine signals in the ventral striatum of freely-moving rats. *J. Neurochem.* 90, 894–903. doi: 10.1111/j.1471-4159.2004.02559.x

Rodeberg, N. T., Sandberg, S. G., Johnson, J. A., Phillips, P. E., and Mark Wightman, R. (2017). Hitchhiker's guide to voltammetry: acute and chronic electrodes for *in vivo* fast-scan cyclic voltammetry graphical abstract. *ACS Chem. Neurosci* 8, 221–234. doi: 10.1021/acschemneuro.6b00393

Rosa, M., Arlotti, M., Ardolino, G., Cogiamanian, F., Marceglia, S., Di Fonzo, A., et al. (2015). Adaptive deep brain stimulation in a freely moving parkinsonian patient. *Mov. Disord.* 30, 1003–1005. doi: 10.1002/mds.26241

Sandyk, R. (2006). Serotonergic mechanisms in amyotrophic lateral sclerosis. *Int. J. Neurosci.* 116, 775–826. doi: 10.1080/00207450600754087

Sarter, M., Parikh, V., and Howe, W. M. (2009). Phasic acetylcholine release and the volume transmission hypothesis: time to move on. *Nat. Rev. Neurosci.* 10, 383–390. doi: 10.1038/nrn2635

Sawaguchi, T., and Goldman-Rakic, P. S. (1994). The role of d1-dopamine receptor in working memory: local injections of dopamine antagonists into the prefrontal cortex of rhesus monkeys performing an oculomotor delayed-response task. *J. Neurophysiol.* 71, 515–528. doi: 10.1152/jn.1994.71.2.515

Sawaguchi, T., Matsumura, M., and Kubota, K. (1990). Effects of dopamine antagonists on neuronal activity related to a delayed response task in monkey prefrontal cortex. *J. Neurophysiol.* 63, 1401–1412. doi: 10.1152/jn.1990.63.6.1401

Sheikh, S., Blaszykowski, C., Nolan, R., Thompson, D., and Thompson, M. (2015). On the hydration of subnanometric antifouling organosilane adlayers: A molecular dynamics simulation. *J. Colloid Interface Sci.* 437, 197–204. doi: 10.1016/j.jcis.2014.09.025

Sheikh, S., Yang, D. Y., Blaszykowski, C., and Thompson, M. (2012). Single ether group in a glycol-based ultra-thin layer prevents surface fouling from undiluted serum. *Chem. Commun.* 48, 1305–1307. doi: 10.1039/C2CC15692J

Shikora, S., Toouli, J., Herrera, M. F., Kulseng, B., Zulewski, H., Brancatisano, R., et al. (2013). Vagal blocking improves glycemic control and elevated blood pressure in obese subjects with type 2 diabetes mellitus. *J. Obes.* 2013:245683. doi: 10.1155/2013/245683

Stanford-Bio-X (2018). *Closed-Loop Neurochemical Sensing and Modulation System for Treating Psychiatric Disorders*.

Sun, F. T., and Morrell, M. J. (2014). Closed-loop neurostimulation: the clinical experience. *Neurotherapeutics* 11, 553–563. doi: 10.1007/s13311-014-0280-3

Swamy, B. E., and Venton, B. J. (2007). Subsecond detection of physiological adenosine concentrations using fast-scan cyclic voltammetry. *Anal. Chem.* 79, 744–750. doi: 10.1021/ac061820i

Tass, P. A. (2003). A model of desynchronizing deep brain stimulation with a demand-controlled coordinated reset of neural subpopulations. *Biol. Cybern.* 89, 81–88. doi: 10.1007/s00422-003-0425-7

Theodore, W. H. (2003). Does serotonin play a role in epilepsy? *Epilepsy Curr.* 3, 173–177. doi: 10.1046/j.1535-7597.2003.03508.x

Thompson, M. (2017). Neurophysiological monitoring of potassium. in *Compendium of in vivo Monitoring in Real-Time Molecular Neuroscience* (World Scientific).

Tracey, K. J. (2002). The inflammatory reflex. *Nature* 420, 853. doi: 10.1038/nature01321

Trevathan, J. K., Yousefi, A., Park, H. O., Bartoletta, J. J., Ludwig, K. A., Lee, K. H., et al. (2015). Computational modeling of neurotransmitter release evoked by electrical stimulation: nonlinear approaches to predicting stimulation-evoked dopamine release. *ACS Chem. Neurosci.* 18, 386–392. doi: 10.1038/nn.3945

Trulson, M. E., and Jacobs, B. L. (1979). Raphe unit activity in freely moving cats: correlation with level of behavioral arousal. *Brain Res.* 163, 135–150.

Turner, R. F., Harrison, D. J., and Rojotte, R. V. (1991). Preliminary *in vivo* biocompatibility studies on perfluorosulphonic acid polymer membranes for biosensor applications. *Biomaterials* 12, 361–368.

Vajari, D. A., Vomero, M., Erhardt, J. B., Sadr, A., Ordonez, J. S., Coenen, V., et al. (2018). Integrity assessment of a hybrid DBS probe that enables neurotransmitter detection simultaneously to electrical stimulation and recording. *Micromachines*. 9:510. doi: 10.3390/mi9100510

Venton, B. J., Michael, D. J., and Wightman, R. M. (2003). Correlation of local changes in extracellular oxygen and pH that accompany dopaminergic terminal activity in the rat caudate-putamen. *J. Neurochem.* 84, 373–381. doi: 10.1046/j.1471-4159.2003.01527.x

Vidailhet, M., Jutras, M.-F., Roze, E., and Grabli, D. (2013). "Deep brain stimulation for dystonia," in *Handbook of Clinical Neurology*, Vol. 116, eds P. Vinken and G. Bruyn (Elsevier), 167–187. doi: 10.1016/B978-0-444-53497-2.00014-0

Vidailhet, M., Vercueil, L., Houeto, J.-L., Krystkowiak, P., Benabid, A.-L., Cornu, P., et al. (2005). Bilateral deep-brain stimulation of the globus pallidus in primary generalized dystonia. *N. Engl. J. Med.* 352, 459–467. doi: 10.1056/NEJMoa042187

Volkmann, J., Herzog, J., Kopper, F., and Deuschl, G. (2002). Introduction to the programming of deep brain stimulators. *Mov. Disord.* 17, S181–s187. doi: 10.1002/mds.10162

Volkow, N. D., Wang, G.-J., Telang, F., Fowler, J. S., Logan, J., Childress, A.-R., et al. (2006). Cocaine cues and dopamine in dorsal striatum: mechanism of craving in cocaine addiction. *J. Neurosci.* 26, 6583–6588. doi: 10.1523/JNEUROSCI.1544-06.2006

Walters, S. H., Robbins, E. M., and Michael, A. C. (2015). Modeling the kinetic diversity of dopamine in the dorsal striatum. *ACS Chem. Neurosci.* 6, 1468–1475. doi: 10.1021/acschemneuro.5b00128

Walters, S. H., Taylor, I. M., Shu, Z., and Michael, A. C. (2014). A novel restricted diffusion model of evoked dopamine. *ACS Chem. Neurosci.* 5, 776–783. doi: 10.1021/cn5000666

Ward, M. P., and Irazoqui, P. P. (2010). Evolving refractory major depressive disorder diagnostic and treatment paradigms: toward closed-loop therapeutics. *Front. Neuroeng.* 3:7. doi: 10.3389/fneng.2010.00007

Ward, M. P., Qing, K. Y., Otto, K. J., Worth, R. M., John, S. W., and Irazoqui, P. P. (2015). A flexible platform for biofeedback-driven control and personalization of electrical nerve stimulation therapy. *IEEE Trans. Neural Syst. Rehabil. Eng.* 23, 475–484. doi: 10.1109/TNSRE.2014.2351271

Whishaw, I. Q., and Dunnett, S. B. (1985). Dopamine depletion, stimulation or blockade in the rat disrupts spatial navigation and locomotion dependent upon beacon or distal cues. *Behav. Brain Res.* 18, 11–29. doi: 10.1016/0166-4328(85)90165-2

Wightman, R. M., Amatorh, C., Engstrom, R. C., Hale, P. D., Kristensen, E. W., Kuhr, W. G., et al. (1988). Real-time characterization of dopamine overflow and uptake in the rat striatum. *Neuroscience* 25, 513–523. doi: 10.1016/0306-4522(88)90255-2

Winterer, G., and Weinberger, D. R. (2004). Genes, dopamine and cortical signal-to-noise ratio in schizophrenia. *Trends Neurosci.* 27, 683–690. doi: 10.1016/j.tins.2004.08.002

Wu, Q., Reith, M. E., Wightman, R. M., Kawagoe, K. T., and Garris, P. A. (2001). Determination of release and uptake parameters from electrically evoked dopamine dynamics measured by real-time voltammetry. *J. Neurosci. Methods* 112, 119–133. doi: 10.1016/S0165-0270(01)00459-9

Yousif, N., Borisyuk, R., Pavese, N., Nandi, D., and Bain, P. (2012). Spatiotemporal visualization of deep brain stimulation-induced effects in the subthalamic nucleus. *Eur. J. Neurosci.* 36, 2252–2259. doi: 10.1111/j.1460-9568.2012.08086.x

Yousif, N., Purswani, N., Bayford, R., Nandi, D., Bain, P., and Liu, X. (2010). Evaluating the impact of the deep brain stimulation induced electric field on subthalamic neurons: a computational modelling study. *J. Neurosci. Methods* 188, 105–112. doi: 10.1016/j.jneumeth.2010.01.026

Zahrt, J., Taylor, J. R., Mathew, R. G., and Arnsten, A. F. (1997). Supranormal stimulation of d1 dopamine receptors in the rodent prefrontal cortex impairs spatial working memory performance. *J. Neurosci.* 17, 8528–8535. doi: 10.1523/JNEUROSCI.17-21-08528.1997

Zhou, A., Santacruz, S. R., Johnson, B. C., Alexandrov, G., Moin, A., Burghardt, F. L., et al. (2019). A wireless and artefact-free 128-channel neuromodulation device for closed-loop stimulation and recording in non-human primates. *Nat. Biomed. Eng.* 3, 15–26. doi: 10.1038/s41551-018-0323-x

Conflict of Interest Statement: CT holds a patent on chemical monitoring of the vagus nerve (US9055875 B2).

The remaining authors declare that the research was conducted in the absence of any commercial or financial relationships that could be construed as a potential conflict of interest.

frontiers in Neuroscience

METHODS
published: 27 August 2019
doi: 10.3389/fnins.2019.00877

An Effective Method for Acute Vagus Nerve Stimulation in Experimental Inflammation

April S. Caravaca[1], Alessandro L. Gallina[1], Laura Tarnawski[1], Kevin J. Tracey[2], Valentin A. Pavlov[2], Yaakov A. Levine[3] and Peder S. Olofsson[1,2]*

[1] Laboratory of Immunobiology, Center for Bioelectronic Medicine, Department of Medicine, Solna, Karolinska Institutet, Stockholm, Sweden, [2] Center for Biomedical Science and Bioelectronic Medicine, The Feinstein Institute for Medical Research, Manhasset, NY, United States, [3] Setpoint Medical, Inc., Valencia, CA, United States

Neural reflexes regulate inflammation and electrical activation of the vagus nerve reduces inflammation in models of inflammatory disease. These discoveries have generated an increasing interest in targeted neurostimulation as treatment for chronic inflammatory diseases. Data from the first clinical trials that use vagus nerve stimulation (VNS) in treatment of rheumatoid arthritis and Crohn's disease suggest that there is a therapeutic potential of electrical VNS in diseases characterized by excessive inflammation. Accordingly, there is an interest to further explore the molecular mechanisms and therapeutic potential of electrical VNS in a range of experimental settings and available genetic mouse models of disease. Here, we describe a method for electrical VNS in experimental inflammation in mice.

Keywords: Bioelectronic Medicine, vagus nerve stimulation, neural reflex, inflammation, inflammatory reflex, peripheral nerve, neural control

OPEN ACCESS

Edited by:
Olivier David,
Institut National de la Santé et de la Recherche Médicale (INSERM), France

Reviewed by:
Erika Kristine Ross,
Mayo Clinic, United States
Kevin J. Otto,
University of Florida, United States

****Correspondence:***
April S. Caravaca
april.caravaca@ki.se

Specialty section:
This article was submitted to Neural Technology, a section of the journal Frontiers in Neuroscience

Received: *15 May 2019*
Accepted: *05 August 2019*
Published: *27 August 2019*

Citation:
Caravaca AS, Gallina AL, Tarnawski L, Tracey KJ, Pavlov VA, Levine YA and Olofsson PS (2019) An Effective Method for Acute Vagus Nerve Stimulation in Experimental Inflammation. Front. Neurosci. 13:877. doi: 10.3389/fnins.2019.00877

INTRODUCTION

Excessive inflammation plays an important role in the pathogenesis of a range of common and debilitating acute and chronic diseases, including septic shock, rheumatoid arthritis, inflammatory bowel disease, and cardiovascular disease (Nathan and Ding, 2010). Therapeutic interventions to reduce cytokine levels and attenuate inflammation significantly improves symptoms and outcomes in many of these diseases (Feldmann, 2002; Ridker et al., 2017). Anti-cytokine drugs have shown success in clinical trials, but are costly and not always effective and/or suitable for patients that suffer from diseases characterized by excessive inflammation (Hansel et al., 2010; Li et al., 2017; Lin et al., 2019).

Discoveries on the neural reflex control of inflammation, particularly the neurophysiological and molecular mechanisms of vagus nerve regulation of systemic cytokine levels in the "*inflammatory reflex*" (Tracey, 2015), have made it possible to consider electrical vagus nerve stimulation (VNS) in the treatment of inflammation and inflammatory diseases (Pavlov and Tracey, 2015; Eberhardson et al., 2019). This neuro-immune reflex mechanism has an afferent arc that senses inflammation and injury, and an efferent arc that regulates cytokine production and release (Olofsson et al., 2012). The first clinical trials implementing these discoveries using implanted nerve stimulators to activate the inflammatory reflex and treat chronic inflammation have reported encouraging results on amelioration of disease activity score (Koopman et al., 2016). Based on these observations,

further exploration of the effects of electrical VNS on the immune system in the many available mouse models of inflammatory diseases is of great interest.

The vagus nerve is a cranial nerve and contains sensory and motor fibers wrapped in a sheath of connective tissue. Establishing an electrical interface with the vagus nerve that produces consistent stimulation in mouse models of inflammatory diseases requires standardization in dissection, electrode placement, and charge delivery. The methods for VNS in mouse models of inflammation used in published studies vary significantly, which may complicate interpretation of reported findings (Inoue et al., 2016; Meneses et al., 2016; Le Maître, Revathikumar et al., 2017). Sources of variation include differences in the dissection method, the physical interface with the nerve, charge delivery, sham treatment, anesthesia and stimulation monitoring (Borovikova et al., 2000; Huston et al., 2006; Rosas-Ballina et al., 2008).

Wide-spread availability of a simple, consistent, reproducible method for VNS would likely facilitate progress in the field (Kwan et al., 2016). Here, we describe a method for performing VNS for study of experimental inflammation that in the experience of the authors yields consistent and reproducible results across laboratories (Olofsson et al., 2015; Caravaca et al., 2017; Tarnawski et al., 2018).

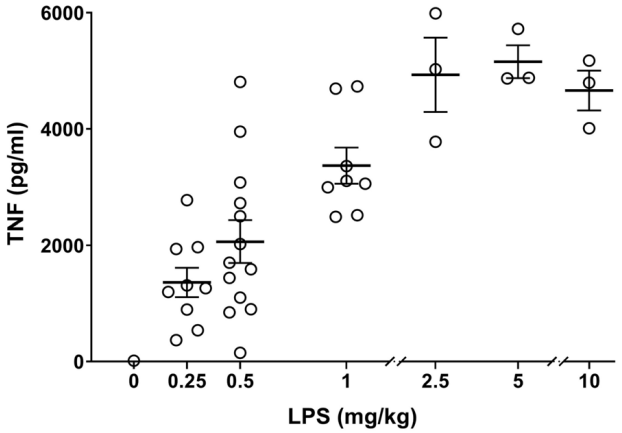

FIGURE 1 | Establishing TNF dose response in endotoxemia. Alert mice were injected intraperitoneally with 0–10 mg/kg of endotoxin and blood was collected by cardiac puncture 90 min later. Serum TNF levels, measured by ELISA, are plotted as mean ± SEM. n = 3–13 mice per group.

METHODS AND RESULTS

Ethics Statement

This study and all experimental protocols were approved by the Stockholm Regional Board for Animal Ethics (Stockholm, Sweden).

Animals

We used male BALB/c and C57Bl/6J mice purchased from Charles River Laboratories (median age was 10 weeks and the range 10–40 weeks). The animals were housed in a laboratory environment on a 12 h light/dark cycle, with *ad libitum* access to food and water.

Statistical Analysis

Differences between experimental groups were analyzed using unpaired two-tailed Student's *t*-test or one-way ANOVA as appropriate. Data are presented as mean ± SEM. $p \leq 0.05$ was considered significant. Prism 8 (GraphPad software, San Diego, CA, United States) was used for analyses.

Titration of Inflammatory Insult

For each batch of lipopolysaccharide (LPS), the dose was titrated for endotoxemia experiments. Bacterial LPS from *Escherichia coli*, O111:B4 (Manufacturer #L2640, Lot # 097M4041V) (Sigma-Aldrich, MO, United States) was prepared to a concentration of 5 mg/ml (0.5% of LPS in MilliQ water) and aliquots were stored at –20°C. Prior to use, aliquots were thawed and then sonicated (Branson B200, Connecticut, United States) for 30 min to dissolve and disaggregate LPS in the solvent (Ogawa and Kanoh, 1984). Mice were injected intraperitoneally with 0, 0.25, 0.5, 1, 2.5, 5, and 10 mg/kg of LPS and then euthanized using carbon dioxide asphyxiation 90 min after LPS injection (Rosas-Ballina et al., 2008). This time point was chosen because in rodent endotoxemia, serum TNF reaches its maximum concentration of TNF between 60 and 90 min after LPS injection (Huston et al., 2006). Blood was immediately collected via cardiac puncture. Samples were incubated at 1 h at room temperature and then centrifuged at 2700 × g for 7 min (Eppendorf, Hamburg, Germany). To remove cells from the serum, the supernatant was transferred to a new tube and centrifuged a second time at 10,600 × g for 1 min, and serum was retained. TNF levels in serum were analyzed by an enzyme-linked immunoabsorbant assay (ELISA) kit (R&D Systems, MN, United States). In this experiment, TNF levels reached a plateau at endotoxin doses ≥ 2.5 mg/kg. Accordingly, using this specific batch of endotoxin, approx. 0.25 – 1 mg/kg LPS was considered suitable for studying effects of interventions on serum TNF levels in the physiological range (**Figure 1**). Of note, in our previous studies with a different batch of endotoxin (Tarnawski et al., 2018), up to 8 mg/kg of LPS was used (Borovikova et al., 2000; Huston et al., 2007) and suppression of serum TNF levels was observed.

Equipment Setup

The setup for mouse VNS is shown in **Figure 2** and includes a computer (CAN ICES-3(B)/NMB-3(B), HP, California, United States) (**Figure 2A**) and a digital-to-analog interface for pulse generation (RME Fireface UFX or RME Babyface Pro, Audio AG, Haimhausen, Germany) (**Figure 2B**), a voltage-to-current converter (STIMSOLA, Biopac, CA, United States) (**Figure 2C**), an oscilloscope (Tektronix, Oregon, United States) (**Figure 2D**) to observe and record electrical signals, and a custom-built electrode for interfacing with the nerve (**Figure 2E**).

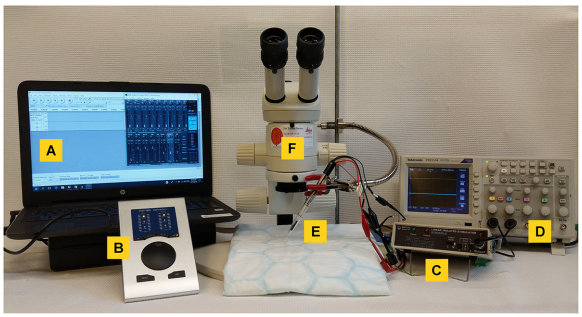

FIGURE 2 | Equipment setup for mouse vagus nerve stimulation. **(A)** A computer with a waveform editing program, connected to **(B)** a digital-to-analog interface to deliver the pulse output and a **(C)** voltage-to-constant current converter. To visualize voltage output an **(D)** oscilloscope was used. **(E)** A custom-built bipolar electrode was used to connect to the vagus nerve. Surgery was performed under a **(F)** stereotactic microscope.

A stereo microscope, preferably on a balanced swivel and arm, is recommended for surgery.

Different equipment and stimulator setups were evaluated, including a number of commercially available devices for nerve stimulation. In our experience, systems capable of delivering a suitable pulse at sufficiently high constant current work well to activate the inflammatory reflex (data not shown). Here, we used open source software (Audacity)[1] and a high-quality audio interface to generate the desired voltage. The voltage was fed through a voltage-to-constant current interface. The electrical output of the setup at a range of resistive loads was recorded (**Supplementary Figure 1**) to verify the performance of the setup.

Electrode Construction

The hook-type electrode described here was made from 0.25 mm platinum-iridium (Pt:Ir; 90:10%) (**Figure 3**). We connected a bipolar hook electrode with two pairs of connecting wires to the stimulator and oscilloscope, respectively (**Figure 3**). The spacing between the two electrode tips was fabricated to approximately 0.5 mm (Olofsson et al., 2015).

Platinum–iridium and silver electrodes enable low-impedance electrical interfaces to the vagus nerve with limited toxicity to cells and tissues (Geddes and Roeder, 2003; Navarro et al., 2007). Silver electrodes can be used in the experimental setup described here as a cost efficient alternative to platinum–iridium (**Supplementary Figure 2**).

Surgical Tools

Isolation of the vagus nerve requires delicate surgical manipulations, and appropriate instruments are key. Here, fine serrated micro dissection scissors (Agntho's #14058-09) (**Figure 4A**) and curved dressing forceps with serrated tips (Agntho's #11051-10) (**Figure 4B**) for handling skin were used. A pair of curved hemostatic forceps (Agntho's #13013-14) (**Figure 4C**) were used to retract skin and expose the surgical site. We used a pair of non-serrated standard curved forceps (Agntho's, #0303-7-PS) (**Figure 4D**) to dissect apart salivary glands, and surrounding tissues. We then used a pair of fine curved surgical dissection forceps (Agntho's, #0208-7-PS) (**Figure 4E**) for manipulations involving the carotid artery and vagus nerve. Instruments were cleaned and disinfected before and after use between experiments. Extra care is required for fine tools as the tips are very fragile. Damaged tips can affect the quality of the isolation and cause injury to the nerve.

Surgical Procedure: Isolation of the Vagus Nerve

An absorbent mat with plastic backing was placed over the surgical area. Anesthesia was induced using isoflurane at 3% in a 1:1 mixture of oxygen and air. Following induction of anesthesia, mice were placed on the surgical mat in the supine position (**Figure 5A**), and maintained at 1.5% isoflurane in a 1:1 oxygen:air mixture. The neck area was shaved and the loose fur removed with a gauze or adhesive tape. Masking tape was used to secure the paws in a fixed position to the surgical mat. The shaved neck area was swabbed with 70% ethanol. A ventral midline cervical incision was made between the mandible and sternum (**Figure 5B**). Subcutaneous tissues were separated using blunt dissection and retracted laterally with hemostatic forceps to expose the salivary glands (**Figure 5C**). The two lobes of the salivary glands were separated by simultaneously pulling them apart, away from the midline, to reveal the sternomastoid and sternohyoid muscles along the trachea (**Figure 5D**). Blunt dissection to either the right or left revealed the common carotid artery and the cervical vagus nerve forming a neurovascular bundle, or carotid sheath (**Figure 5E**). The vagus nerve was isolated away from the carotid artery and the surrounding connective sheath tissue (**Figure 5F**). A 1–2 cm piece of polypropylene suture was placed under the nerve to facilitate electrode placement (**Figure 5G**).

For sham surgery, the ventral midline cervical incision was performed, subcutaneous tissues were separated using blunt dissection, and salivary glands were separated (**Figures 5A–C**). It has been reported that mechanical stimulation of the vagus nerve reduces serum TNF levels compared to sham in mouse endotoxemia (Huston et al., 2004). To study whether the described isolation method and manipulation of the vagus nerve reduces TNF in mouse endotoxemia *per se*, we compared serum TNF levels between animals where the isolated vagus nerve was suspended on the electrode without electrical stimulation (**Figures 5A–G** + nerve suspension on hook) or left untouched on the carotid artery (**Figures 5A–D**). We observed no significant difference in serum TNF between these two groups (**Figure 6**). We observed no significant difference in serum TNF level in the sham surgery mice with or without vagus nerve isolation from the sheath (**Figure 6**). This observation suggests that manipulation of the vagus nerve in a careful manner does not necessarily elicit activation of the cholinergic anti-inflammatory pathway.

After stimulation, the electrode was removed, and in both the stimulation and sham surgery group, tissues were restored to their original position, and the incision sutured (Silk, 4-0,

[1] www.audacityteam.org

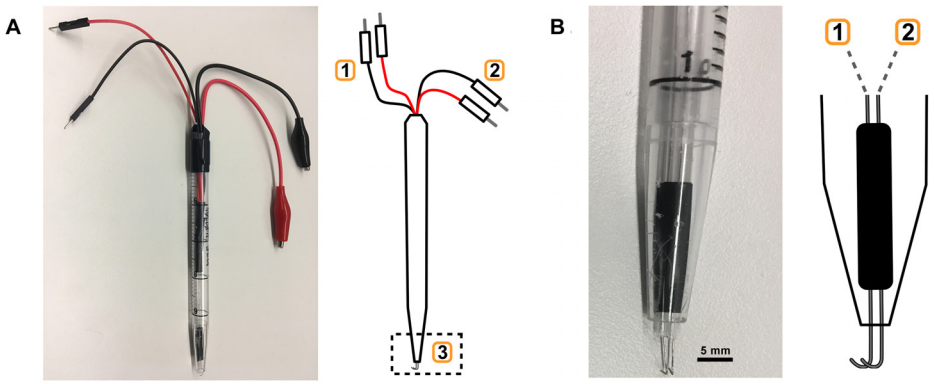

FIGURE 3 | Electrode fabrication. **(A)** Custom-built bipolar electrode with monitoring (1) and stimulation (2) leads, and the hook electrode (3). **(B)** Close-up of hook electrode (3) with connections to (1) and (2).

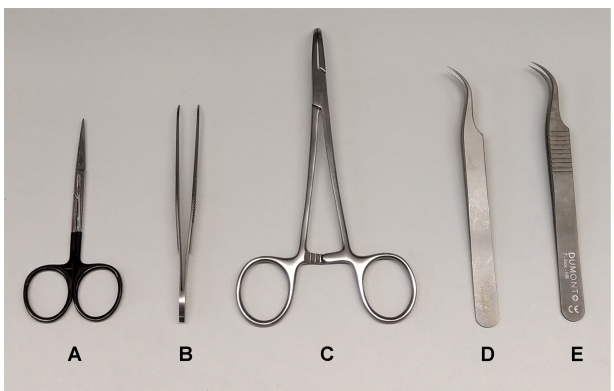

FIGURE 4 | Surgical tools for vagus nerve isolation. **(A)** Serrated micro dissection scissors. **(B)** Curved dressing forceps. **(C)** Curved hemostatic forceps. **(D)** Non-serrated standard curved forceps. **(E)** Non-serrated fine curved forceps.

FS-2 needle) or stapled with wound clips (stainless steel, 9 mm). During prolonged anesthesia, it is advisable to maintain core temperature at a physiological level using a rectal temperature probe and heating pad under the absorbent surgical mat during surgery, to prevent hypothermia. It is also recommended to place a heating pad under a clean cage for the mouse during recovery, however, precautions should be taken to ensure the animals are not overheated during recovery by covering a portion of the bottom of the cage so animals can move away from heated areas as they desire.

Vagus Nerve Stimulation

Constant current stimulation was applied to the nerve at 1 mA, 250 μs biphasic pulse, 50 μs interphase delay, at 10 Hz for 5 min (**Figure 7A**) (Olofsson et al., 2015). A charge-balanced biphasic square waveform for stimulation was used (Lilly et al., 1955). A charge-balanced pulse generates less tissue and electrode surface damage compared to unbalanced charge delivery (Harnack et al., 2004). Mice in the sham group were subjected to surgery, but not to electrical stimulation. Constant current was maintained by the constant current stimulator setup, as visualized using the voltage output on an oscilloscope (**Figures 7B,C**). In our stimulations, we visualized the output from the stimulator (**Figure 7B**; blue tracing represents voltage output from digital to analog interface), and the voltage across the electrodes at the tissue interface (**Figure 7B**; orange tracing represents electrode-nerve interface).

Voltage drop across the resistance was calculated from the oscilloscope tracing and is based on Ohm's Law ($Z = V/I$). Z is the impedance in ohms (Ω), V is the observed voltage across the electrodes, and I is the programed current delivered by the stimulator.

First phase cathodic stimulation was used because nerve activation occurs at lower current than during anodic stimulation (McIntyre and Grill, 1999; Basser and Roth, 2000). We have previously reported constant current levels sufficient to activate the inflammatory reflex and reduce TNF in acute experimental endotoxemia (Olofsson et al., 2015).

Consistent current delivery requires that the electrical path is confined to the nerve and isolated from the surrounding tissues. Even with insulated wiring the curvature of the hook wires may be exposed to surrounding tissue and extracellular liquid, offering an alternative electrical path. Caution must be exercised when suspending the nerve on the hook electrodes (**Figure 7D**) to avoid mechanical stretch injury that may cause aberrant or adverse effect.

Visual Observations

Non-specific muscle activation is a sign of unwanted current delivery to tissues outside the nerve. The vagus nerve and the electrode need to be sufficiently separated from surrounding tissues and fluids to avoid current leakage. Of note, twitching of specific laryngeal muscles is observed during stimulation, as the vagus nerve supplies motor nerve fibers to this area.

An oscilloscope was used during stimulation to continuously measure the electrical output as it fluctuates with variations in impedance. Changes in the oscilloscope tracings during

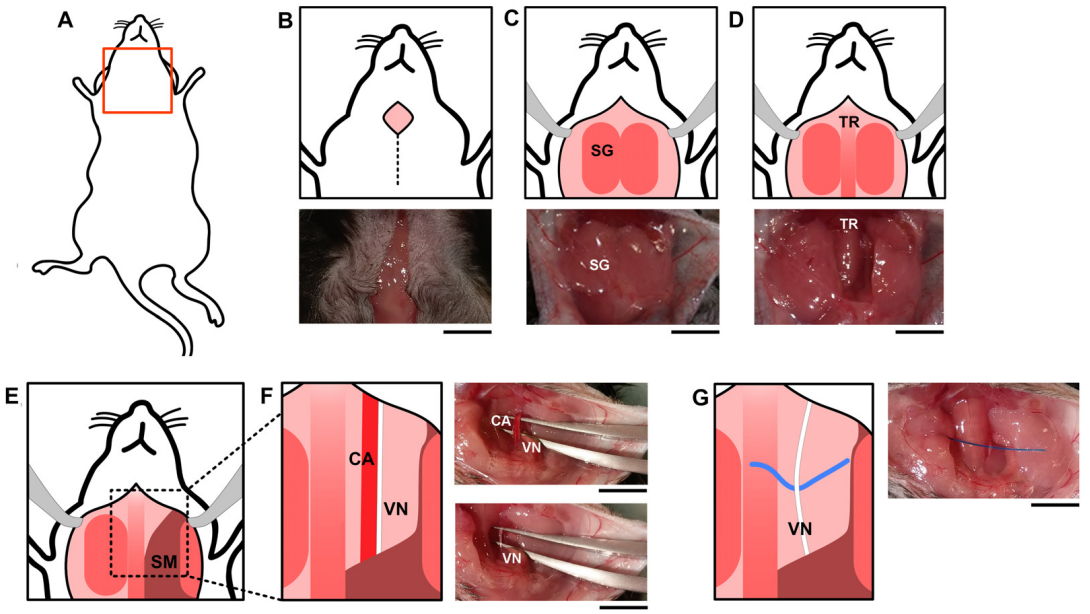

FIGURE 5 | Surgical vagus nerve isolation for electrical stimulation. **(A)** The neck area of the mouse was shaved and swabbed with ethanol. **(B)** A midline cervical incision was made, exposing the **(C)** salivary glands (SG) and **(D)** trachea (TR). Subcutaneous tissues between the **(E)** sternomastoid (SM) and sternohyoid muscles along the trachea were separated using blunt dissection which reveals the **(F)** common carotid artery (CA) and the cervical vagus nerve (VN). The vagus nerve and the carotid artery **(F)** are located parallel to each other and were separated using curved forceps with tips facing upward. One set held both the vagus nerve and carotid artery, and the other was used to separate the two structures. The forceps were then carefully opened and closed repeatedly to progressively detach the vagus nerve from the carotid artery. **(G)** A piece of polypropylene suture was placed under the nerve to facilitate electrode placement. The black scale bar indicates 5 mm.

stimulation should be observed and noted, as large deviations in the expected voltage tracing can reflect current leaks, faulty electrodes, problems with nerve-electrode contact, and other reasons for suboptimal charge delivery.

Vagotomy

Disruption of vagus nerve signaling aggravates systemic inflammation in experimental models of disease (Borovikova et al., 2000; van Westerloo et al., 2006; van Maanen et al., 2009). To study disruption of vagus nerve signaling, unilateral cervical vagotomy can be used. The surgical procedure is similar to the approach for VNS, as previously described herein. After isolation of the vagus nerve, a piece of 1–2 cm polypropylene suture was placed under the nerve. Forceps were used to carefully and gently lift and hold the nerve suspended. Cuts were made above and below the forceps grip in order to remove a segment of nerve approximately 2–3 mm in length. 2–3 mm is a minor discrepancy in terms of measurement used in vagotomy, and in our experience it is sufficient for acute experiments as the nerve remains severed (data not shown). After resection, salivary glands and tissues were restored to position and the skin was sutured (Silk, 4-0, FS-2 needle) or stapled with wound clips (stainless steel, 9 mm).

Endotoxemia

The endotoxin model of systemic inflammation is commonly used, and experimental murine endotoxemia is well established (Fink and Heard, 1990; Remick et al., 2000; Lewis et al., 2016). LPS binds to toll-like receptor 4 (TLR4) which is present on a number of cells such as monocytes and macrophages and promotes the secretion of pro-inflammatory cytokines such as TNF. Mice were allowed to recover for a minimum of 1 h from anesthesia and surgery before intraperitoneal administration of endotoxin, and longer recovery periods can be used (Tarnawski et al., 2018). The half-life of ketamine and xylazine in rodents can be as long as 2 h (Veilleux-Lemieux et al., 2013). Anesthesia has been reported to delay the inflammatory response (Fuentes et al., 2006). It is important for experimental consistency in the inflammatory response that mice recover from anesthesia before the inflammatory agent is administered.

Sample Processing and Cytokine Measurement

There are multiple steps involved in blood collection and sample processing, so we investigated whether delayed separation of whole blood and serum concentrations of TNF varied for up to 120 min. Mice were euthanized 90 min after injection of endotoxin and blood was collected via cardiac puncture using a 1 mL syringe fitted with a 23 gauge needle. The needle was then removed from the syringe to prevent hemolysis and the blood from each mouse was dispensed into three aliquots. Subsequently, the aliquots were left for 10, 30, or 120 min at room temperature before centrifugation. After the two-step centrifugation process as previously mentioned, the serum was transferred to Eppendorf tubes, frozen on dry ice, and transferred to −80°C for long term storage. Cytokine

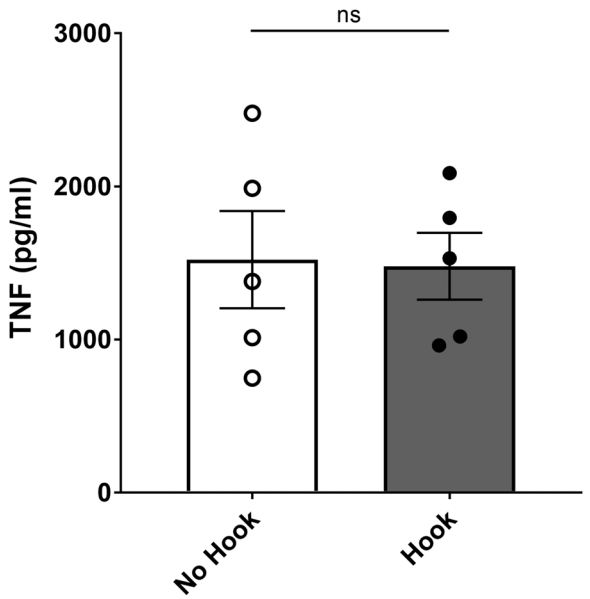

FIGURE 6 | No significant effect on endotoxemic serum TNF level by application of hook electrode. Mice were subjected to sham surgery with or without physical suspension of the vagus nerve on the hook electrode. After full recovery from anesthesia, mice were injected with endotoxin and blood collected 90 min later. Serum TNF was analyzed by ELISA. Results are shown as mean ± SEM, $n = 5$ mice per group from three distinct experiments; ns, not significant (unpaired, two-tailed Student's *t*-test).

levels were measured in serum by ELISA or multiplex assay kit (Meso Scale Discovery, MD, United States) according to manufacturer protocols. There was no significant difference in TNF levels between the groups from the different incubation times (**Figure 8**). The serum TNF level in samples from individual mice was stable across the incubation period at room temperature (**Figure 8**). However, in our experiments, we do standardize the time between collection and serum/plasma collection for each batch of samples. In line with previous observations (Borovikova et al., 2000; Olofsson et al., 2015), serum TNF levels were significantly reduced in endotoxemic mice subjected to electrical VNS, while unilaterally vagotomized endotoxemic mice showed significantly elevated serum TNF levels compared to sham (**Figure 9**).

DISCUSSION

Here, we define a method for VNS in experimental mouse endotoxemia. The significance of endotoxin titration, electrode fabrication, surgical vagus nerve isolation, and electrical stimulation and monitoring is described, as well as key points in experimental procedures.

There is an increasing interest in neural reflex control of inflammation, and electrical VNS in the context of experimental inflammation. However, the details in implementation of VNS for activating the inflammatory reflex vary considerably in the literature. In our experience, certain key features in the procedures are important to avoid inconsistent results across experiments and laboratories. Specifically, the induction of inflammatory insult should be kept within a physiological range, dissection of the vagus nerve must be uniform, and charge delivery to the nerve controlled. In addition, the particulars of sample processing are important.

It is crucial to be aware that even minor trauma to the vagus nerve, which can easily occur during the surgical isolation and suspension of the nerve on the electrode, can significantly affect physiology. Of note, stretching and compression during handling can cause physical stress that interferes with nerve function. Trauma may cause firing of action potentials or impairment of electrical activation with obvious significant effects on the consistency of experimental results. In our experience, the quality and condition of surgical tools are paramount along with proper training of the animal surgeon.

It is necessary to titrate the endotoxin to determine a suitable dose within the dynamic range of TNF response. In the case of endotoxin, there is commonly a significant lot-to-lot variation

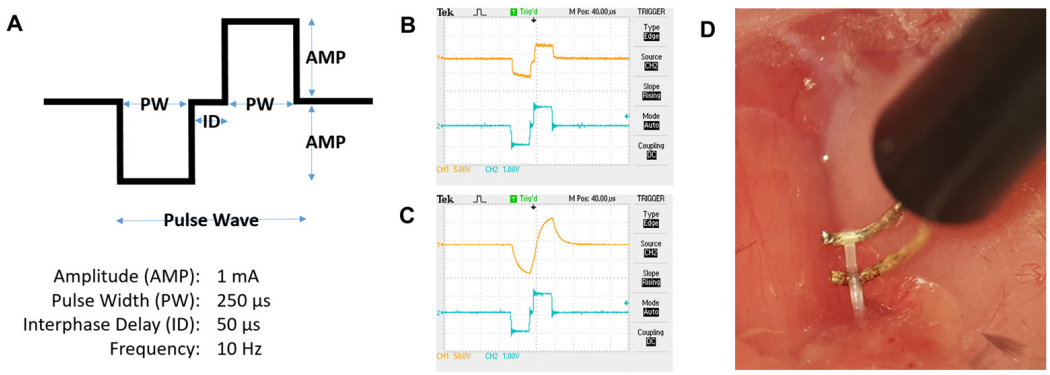

FIGURE 7 | Electrical stimulation of the cervical vagus nerve. **(A)** Schematic representation of a pulse wave. **(B)** Oscilloscope tracing of voltage output from the digital to analog interface (blue tracing, scale 1 V/square) at the desired impedance and voltage measured over the electrode leads (orange tracing, scale 5 V/square). **(C)** Example of tracing with electrode-nerve interface with a high impedance level (orange tracing, scale 50 V/square). **(D)** The isolated vagus nerve segment resting on custom-built hook electrodes.

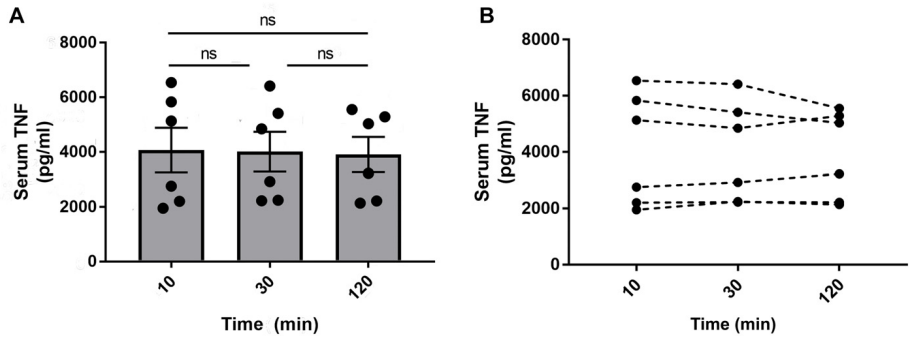

FIGURE 8 | Serum TNF in blood stored at room temperature for 10, 30, or 120 min. Alert mice were injected intraperitoneally with 0.25 mg/kg endotoxin. Mice were euthanized after 90 min and blood was collected via cardiac puncture. The blood was aliquoted in three separate tubes and stored at room temperature for 10, 30, or 120 min before centrifugation to isolate serum. TNF was then measured by ELISA and **(A)** plotted as mean ± SEM and **(B)** as individual TNF values for each mouse, $n = 6$ per group from one experiment; ns, not significant, one-way ANOVA followed by Tukey's test.

in potential to induce inflammation. Each batch must therefore be evaluated to find suitable dosing that produces sufficient inflammation within reasonable physiological limits (Thompson and Chesher, 2018). In this study, we found that the serum TNF level 90 min after endotoxin administration plateaued above 2.5 mg entodoxin/kg body weight for the used lot of endotoxin. Accordingly, doses from 0.25 to 1 mg/kg bodyweight produced a significant TNF response within the physiological range. Different strains of animals and animal species may vary in tolerance and measurable TNF response to LPS, which is another reason to titrate the suitable LPS dose for each specific experimental setup (Thomas et al., 2014).

A key component of consistent VNS is the integrity of the electrode interface with the vagus nerve, and a reliably stable charge delivery by a high-quality voltage-to-constant current converter. For electrode fabrication, a range of materials are suitable, including platinum–iridium (Olofsson et al., 2015), silver (Inoue et al., 2016), and tungsten–titanium (Caravaca et al., 2017). The goal is to create a non-toxic, efficient and stable interface between the stimulation equipment and the nerve. Electrodes may oxidize with use, so it is important to monitor the integrity of the interface over time. Long-term exposure to phosphate buffered saline (PBS) of various metal contacts can also influence electrode integrity (Howlader et al., 2015). A convenient way to monitor interface integrity is to measure interface impedance during the electrical stimulation. This can be achieved by connecting an oscilloscope and measuring the voltage across the electrode continually through the stimulation. Here, we observed voltages over the electrode around 5 V which at 1 mA current corresponds to an impedance of 5 kΩ, which in our experience is suitable for electrical VNS to activate the inflammatory reflex.

Optimal electrical stimulation parameters for activation of the inflammatory reflex are not known, but some empirical data on suitable stimulation settings are available. We have previously investigated a range of constant current stimulus parameters in both mice and rats, which we used to select the stimulation settings in this study, i.e., 1 mA current, 250 us pulse width at 10 Hz for 5 min (Olofsson et al., 2015). Going forward, it will be important to further optimize stimulation parameters for activation of the inflammatory reflex in experimental inflammation.

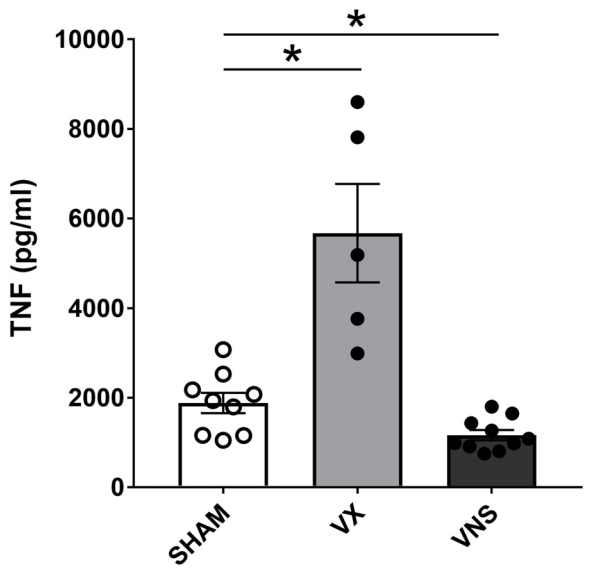

FIGURE 9 | Stimulation or ablation of cervical vagus nerve signaling alters serum TNF in endotoxemia. Vagus nerve stimulation (VNS) or vagotomy (VX) was performed under anesthesia. Mice were allowed to recover fully and then injected with LPS intraperitoneally. Blood was collected 90 min post-injection and serum TNF was analyzed by ELISA. $n = 5$–10 mice per group from five distinct experiments. *$p = 0.05$, one-way ANOVA followed by Dunnett's *post-hoc* test.

In line with previous observations (Borovikova et al., 2000; Olofsson et al., 2015; Tarnawski et al., 2018), serum TNF levels were significantly reduced in endotoxemic mice subjected to electrical VNS, while unilaterally vagotomized endotoxemic mice showed significantly elevated serum TNF levels compared to sham. Interestingly, it has been observed by others that physical manipulation of the vagus nerve may activate the inflammatory reflex (Huston et al., 2006). In itself, the careful physical

placement of the cervical vagus nerve on the electrodes in this study did not significantly change serum TNF levels in endotoxemia. This is achieved by employing a deliberately careful surgical technique to reduce the physical perturbation of the nerve, suggesting that mechanical manipulation of the vagus nerve does not necessarily elicit activation of the inflammatory reflex.

We observed that blood incubated between 10 and 120 min at room temperature did not significantly affect levels of measured TNF in this study, at least not in the range $\approx 2–6 \times 10^3$ pg/mL. While this observation may tempt investigators to streamline the sample handling process by reducing the need for careful timing of the serum isolation procedure, we still advocate to practice consistent timing of sample processing until more data is available.

In conclusion, we provide a method for electrical stimulation of the vagus nerve in experimental inflammation in mice.

DATA AVAILABILITY

The datasets generated for this study are available on request to the corresponding author.

AUTHOR CONTRIBUTIONS

AC, YL, AG, VP, KT, and PO contributed to the conception and design of the study. AC and AG performed the experiments, analyzed the data, and wrote the manuscript with supervision from YL, PO, VP, and LT. LT designed the figures. All authors provided the critical feedback, and edited and finalized the manuscript.

FUNDING

This work was supported by the Knut and Alice Wallenberg Foundation 20140212, Swedish Research Council 2017-03366, and Heart-Lung Foundation Grants 20170708 and 20170880.

SUPPLEMENTARY MATERIAL

The Supplementary Material for this article can be found online at: https://www.frontiersin.org/articles/10.3389/fnins.2019.00877/full#supplementary-material

REFERENCES

Basser, P. J., and Roth, B. J. (2000). New currents in electrical stimulation of excitable tissues. *Annu. Rev. Biomed. Eng.* 2, 377–397. doi: 10.1146/annurev.bioeng.2.1.377

Borovikova, L. V., Ivanova, S., Zhang, M., Yang, H., Botchkina, G. I., Watkins, L. R., et al. (2000). Vagus nerve stimulation attenuates the systemic inflammatory response to endotoxin. *Nature* 405, 458–462. doi: 10.1038/35013070

Caravaca, A. S., Tsaava, T., Goldman, L., Silverman, H., Riggott, G., Chavan, S. S., et al. (2017). A novel flexible cuff-like microelectrode for dual purpose, acute and chronic electrical interfacing with the mouse cervical vagus nerve. *J. Neural Eng.* 14:066005. doi: 10.1088/1741-2552/aa7a42

Eberhardson, M., Hedin, C. R. H., Carlson, M., Tarnawski, L., Levine, Y. A., and Olofsson, P. S. (2019). Towards improved control of inflammatory bowel disease. *Scand. J. Immunol.* 89:e12745. doi: 10.1111/sji.12745

Feldmann, M. (2002). Development of anti-TNF therapy for rheumatoid arthritis. *Nat. Rev. Immunol.* 2, 364–371. doi: 10.1038/nri802

Fink, M. P., and Heard, S. O. (1990). Laboratory models of sepsis and septic shock. *J. Surg. Res.* 49, 186–196.

Fuentes, J. M., Talamini, M. A., Fulton, W. B., Hanly, E. J., Aurora, A. R., and De Maio, A. (2006). General anesthesia delays the inflammatory response and increases survival for mice with endotoxic shock. *Clin. Vaccine Immunol.* 13, 281–288. doi: 10.1128/cvi.13.2.281-288.2006

Geddes, L. A., and Roeder, R. (2003). Criteria for the selection of materials for implanted electrodes. *Ann. Biomed. Eng.* 31, 879–890. doi: 10.1114/1.1581292

Hansel, T. T., Kropshofer, H., Singer, T., Mitchell, J. A., and George, A. J. T. (2010). The safety and side effects of monoclonal antibodies. *Nat. Rev. Drug Discov.* 9, 325–338. doi: 10.1038/nrd3003

Harnack, D., Winter, C., Meissner, W., Reum, T., Kupsch, A., and Morgenstern, R. (2004). The effects of electrode material, charge density and stimulation duration on the safety of high-frequency stimulation of the subthalamic nucleus in rats. *J. Neurosci. Methods* 138, 207–216. doi: 10.1016/j.jneumeth.2004.04.019

Howlader, M. M. R., Ul Alam, A., Sharma, R. P., and Deen, M. J. (2015). Materials analyses and electrochemical impedance of implantable metal electrodes. *Phys. Chem. Chem. Phys.* 17, 10135–10145. doi: 10.1039/c4cp05899b

Huston, J. M., Gallowitsch-Puerta, M., Ochani, M., Ochani, K., Yuan, R., Rosas-Ballina, M., et al. (2007). Transcutaneous vagus nerve stimulation reduces serum high mobility group box 1 levels and improves survival in murine sepsis. *Crit. Care Med.* 35, 2762–2768. doi: 10.1097/00003246-200712000-00014

Huston, J. M., Ochani, M., Ochani, K., Czura, C. J., Amella, C. A., and Tracey, K. J. (2004). Mechanical stimulation of the vagus nerve is sufficient for activation of the cholinergic anti-inflammatory pathway in mice. *Shock* 21:32. doi: 10.1097/00024382-200406002-00092

Huston, J. M., Ochani, M., Rosas-Ballina, M., Liao, H., Ochani, K., Pavlov, V. A., et al. (2006). Splenectomy inactivates the cholinergic antiinflammatory pathway during lethal endotoxemia and polymicrobial sepsis. *J. Exp. Med.* 203, 1623–1628. doi: 10.1084/jem.20052362

Inoue, T., Abe, C., Sung, S. J., Moscalu, S., Jankowski, J., Huang, L., et al. (2016). Vagus nerve stimulation mediates protection from kidney ischemia-reperfusion injury through α7nAChR+ splenocytes. *J. Clin. Invest.* 126, 1939–1952. doi: 10.1172/jci83658

Koopman, F. A., Chavan, S. S., Miljko, S., Grazio, S., Sokolovic, S., Schuurman, P. R., et al. (2016). Vagus nerve stimulation inhibits cytokine production and attenuates disease severity in rheumatoid arthritis. *Proc. Natl. Acad. Sci. U.S.A.* 113, 8284–8289. doi: 10.1073/pnas.1605635113

Kwan, H., Garzoni, L., Liu, H. L., Cao, M., Desrochers, A., Fecteau, G., et al. (2016). Vagus nerve stimulation for treatment of inflammation: systematic review of animal models and clinical studies. *Bioelectron. Med.* 3, 1–6. doi: 10.15424/bioelectronmed.2016.00005

Le Maître, E., Revathikumar, P., Estelius, J., and Lampa, J. (2017). Increased recovery time and decreased LPS administration to study the vagus nerve stimulation mechanisms in limited inflammatory responses. *J. Vis. Exp.* 121:54890. doi: 10.3791/54890

Lewis, A. J., Seymour, C. W., and Rosengart, M. R. (2016). Current murine models of sepsis. *Surg. Infect.* 17, 385–393. doi: 10.1089/sur.2016.021

Li, P., Zheng, Y., and Chen, X. (2017). Drugs for autoimmune inflammatory diseases: from small molecule compounds to anti-TNF biologics. *Front. Pharmacol.* 8:460. doi: 10.3389/fphar.2017.00460

Lilly, J. C., Hughes, J. R., Alvord, E. C., and Galkin, T. W. (1955). Brief, noninjurious electric waveform for stimulation of the brain. *Science* 121, 468–469. doi: 10.1126/science.121.3144.468

Lin, Y.-S., Cheng, S.-W., Wang, Y.-H., Chen, K.-H., Fang, C.-J., and Chen, C. (2019). Systematic review with meta-analysis: risk of post-operative complications associated with pre-operative exposure to anti-tumour necrosis

factor agents for Crohn's disease. *Aliment. Pharmacol. Ther.* 49, 966–977. doi: 10.1111/apt.15184

McIntyre, C. C., and Grill, W. M. (1999). Excitation of central nervous system neurons by nonuniform electric fields. *Biophys. J.* 76, 878–888. doi: 10.1016/s0006-3495(99)77251-6

Meneses, G., Bautista, M., Florentino, A., Diaz, G., Acero, G., Besedovsky, H., et al. (2016). Electric stimulation of the vagus nerve reduced mouse neuroinflammation induced by lipopolysaccharide. *J. Inflamm.* 13:33. doi: 10.1186/s12950-016-0140-5

Nathan, C., and Ding, A. (2010). Nonresolving Inflammation. *Cell* 140, 871–882. doi: 10.1016/j.cell.2010.02.029

Navarro, X., Lago, N., Vivo, M., Yoshida, K., Koch, K. P., Poppendieck, W., et al. (2007). "Neurobiological evaluation of thin-film longitudinal intrafascicular electrodes as a peripheral nerve interface," in *Proceedings of the IEEE 10th International Conference on Rehabilitation Robotics*, (Noordwijk: IEEE), 643–649.

Ogawa, Y., and Kanoh, S. (1984). Enhancement of endotoxicity and reactivity with carbocyanine dye by sonication of lipopolysaccharide. *Microbiol. Immunol.* 28, 1313–1323. doi: 10.1111/j.1348-0421.1984.tb00789.x

Olofsson, P. S., Levine, Y. A., Caravaca, A., Chavan, S. S., Pavlov, V. A., Faltys, M., et al. (2015). Single-pulse and unidirectional electrical activation of the cervical vagus nerve reduces TNF in endotoxemia. *Bioelectron. Med.* 2, 37–42. doi: 10.15424/bioelectronmed.2015.00006

Olofsson, P. S., Rosas-Ballina, M., Levine, Y. A., and Tracey, K. J. (2012). Rethinking inflammation: neural circuits in the regulation of immunity. *Immunol. Rev.* 248, 188–204. doi: 10.1111/j.1600-065X.2012.01138.x

Pavlov, V. A., and Tracey, K. J. (2015). Neural circuitry and immunity. *Immunol. Res.* 63, 38–57. doi: 10.1007/s12026-015-8718-1

Remick, D. G., Newcomb, D. E., Bolgos, G. L., and Call, D. R. (2000). Comparison of the mortality and inflammatory response of two models of sepsis: lipopolysaccharide vs. cecal ligation and puncture. *Shock* 13, 110–116. doi: 10.1097/00024382-200013020-00004

Ridker, P. M., Everett, B. M., Thuren, T., MacFadyen, J. G., Chang, W. H., Ballantyne, C., et al. (2017). Antiinflammatory therapy with canakinumab for atherosclerotic disease. *N. Engl. J. Med.* 377, 1119–1131. doi: 10.1056/NEJMoa1707914

Rosas-Ballina, M., Ochani, M., Parrish, W. R., Ochani, K., Harris, Y. T., Huston, J. M., et al. (2008). Splenic nerve is required for cholinergic antiinflammatory pathway control of TNF in endotoxemia. *Proc. Natl. Acad. Sci. U.S.A.* 105, 11008–11013. doi: 10.1073/pnas.0803237105

Tarnawski, L., Reardon, C., Caravaca, A. S., Rosas-Ballina, M., Tusche, M. W., Drake, A. R., et al. (2018). Adenylyl cyclase 6 mediates inhibition of TNF in the inflammatory reflex. *Front. Immunol.* 9:2648. doi: 10.3389/fimmu.2018.02648

Thomas, R. C., Bath, M. F., Stover, C. M., Lambert, D. G., and Thompson, J. P. (2014). Exploring LPS-induced sepsis in rats and mice as a model to study potential protective effects of the nociceptin/orphanin FQ system. *Peptides* 61, 56–60. doi: 10.1016/j.peptides.2014.08.009

Thompson, S., and Chesher, D. (2018). Lot-to-lot variation. *Clin. Biochem. Rev.* 39, 51–60.

Tracey, K. J. (2015). Approaching the next revolution? Evolutionary integration of neural and immune pathogen sensing and response. *Cold Spring Harb. Perspect. Biol.* 7:a016360. doi: 10.1101/cshperspect.a016360

van Maanen, M. A., Lebre, M. C., van der Poll, T., LaRosa, G. J., Elbaum, D., Vervoordeldonk, M. J., et al. (2009). Stimulation of nicotinic acetylcholine receptors attenuates collagen-induced arthritis in mice. *Arthritis Rheum.* 60, 114–122. doi: 10.1002/art.24177

van Westerloo, D. J., Giebelen, I. A., Florquin, S., Bruno, M. J., LaRosa, G. J., Ulloa, L., et al. (2006). The vagus nerve and nicotinic receptors modulate experimental pancreatitis severity in mice. *Gastroenterology* 130, 1822–1830. doi: 10.1053/j.gastro.2006.02.022

Veilleux-Lemieux, D., Castel, A., Carrier, D., Beaudry, F., and Vachon, P. (2013). Pharmacokinetics of ketamine and xylazine in young and old Sprague-Dawley rats. *J. Am. Assoc. Lab. Anim. Sci.* 52, 567–570.

Conflict of Interest Statement: YL is employed by SetPoint Medical, Inc., Valencia, CA, United States.

The remaining authors declare that the research was conducted in the absence of any commercial or financial relationships that could be construed as a potential conflict of interest.

frontiers in Neuroscience

REVIEW
published: 04 September 2019
doi: 10.3389/fnins.2019.00911

Vagus Nerve Stimulation in Rodent Models: An Overview of Technical Considerations

Crystal M. Noller[1,2,3], Yaakov A. Levine[4], Timur M. Urakov[5,6], Joshua P. Aronson[2,3] and Mark S. Nash[1,5,7]*

[1] The Miami Project to Cure Paralysis, Miller School of Medicine, University of Miami, Miami, FL, United States, [2] Section of Neurosurgery, Department of Surgery, Dartmouth-Hitchcock Medical Center, Lebanon, NH, United States, [3] Geisel School of Medicine, Dartmouth College, Hanover, NH, United States, [4] SetPoint Medical Corporation, Valencia, CA, United States, [5] Department of Neurological Surgery, Miller School of Medicine, University of Miami, Miami, FL, United States, [6] Jackson Memorial Hospital, Miami, FL, United States, [7] Department of Physical Medicine and Rehabilitation, Miller School of Medicine, University of Miami, Miami, FL, United States

Over the last several decades, vagus nerve stimulation (VNS) has evolved from a treatment for select neuropsychiatric disorders to one that holds promise in treating numerous inflammatory conditions. Growing interest has focused on the use of VNS for other indications, such as heart failure, rheumatoid arthritis, inflammatory bowel disease, ischemic stroke, and traumatic brain injury. As pre-clinical research often guides expansion into new clinical avenues, animal models of VNS have also increased in recent years. To advance this promising treatment, however, there are a number of experimental parameters that must be considered when planning a study, such as physiology of the vagus nerve, electrical stimulation parameters, electrode design, stimulation equipment, and microsurgical technique. In this review, we discuss these important considerations and how a combination of clinically relevant stimulation parameters can be used to achieve beneficial therapeutic results in pre-clinical studies of sub-acute to chronic VNS, and provide a practical guide for performing this work in rodent models. Finally, by integrating clinical and pre-clinical research, we present indeterminate issues as opportunities for future research.

Keywords: vagus nerve stimulation, vagus nerve, neuromodulation, nerve cuff electrode, electrical stimulation

OPEN ACCESS

Edited by:
Mikhail Lebedev,
Duke University, United States

Reviewed by:
Stefan Kampusch,
Vienna University of Technology, Austria
Ivan N. Pigarev,
Institute for Information Transmission Problems (RAS), Russia
Ilknur Ay,
Harvard Medical School, United States

****Correspondence:***
Crystal M. Noller
Crystal.M.Noller@dartmouth.edu

Specialty section:
This article was submitted to Neural Technology, a section of the journal Frontiers in Neuroscience

Received: *20 March 2019*
Accepted: *16 August 2019*
Published: *04 September 2019*

Citation:
Noller CM, Levine YA, Urakov TM, Aronson JP and Nash MS (2019) Vagus Nerve Stimulation in Rodent Models: An Overview of Technical Considerations. Front. Neurosci. 13:911. doi: 10.3389/fnins.2019.00911

INTRODUCTION

Vagus nerve stimulation (VNS) is an FDA-approved treatment for select neurological and psychiatric conditions including epilepsy, treatment-resistant depression, and cluster headache (Heck et al., 2002; Ruffoli et al., 2011; Conway et al., 2016; Pisapia and Baltuch, 2016; Lainez and Guillamon, 2017; Kumar et al., 2019). There is also growing interest in using VNS to treat other conditions, such as heart failure, rheumatoid arthritis, inflammatory bowel disease, ischemic stroke, and traumatic brain injury (Zhang et al., 2009; Bonaz et al., 2013; Cai et al., 2014; Levine et al., 2014a,b, Levine et al., 2018a,b; Dawson et al., 2016; Guiraud et al., 2016; Koopman et al., 2016; Pruitt et al., 2016; Kanashiro et al., 2018), many of which are characterized by inflammation. Extensive pre-clinical evidence has demonstrated the utility of VNS in treating inflammatory conditions (Huston et al., 2006, 2007; Rosas-Ballina et al., 2008; Levine et al., 2014a,b; Olofsson et al., 2015),

and a recent clinical study of rheumatoid arthritis (Koopman et al., 2016) further supports this treatment for widespread application. As VNS is applied to a broader range of conditions, it is important to recognize factors that influence study outcomes, such as stimulation settings, vagus nerve physiology, anatomical location of the target nerve branch, and electrode design. However, in many reports published thus far, these factors are often either not discussed, or are described as "customized" (i.e., as in the case of electrode design). A comprehensive discussion is therefore needed to inform the scientific design and reproducible execution of VNS studies.

The current review will provide a stepwise overview to inform the administration of VNS in rodent models, which often form the basis for higher-order study models. Key experimental conditions are discussed, including vagus nerve physiology, electrode design, stimulation equipment, microsurgical technique, and electrical stimulation parameters. Each step includes a detailed rationale to help inform modifications. Although a recent article outlined the surgical procedure for acute rodent VNS (Le Maitre et al., 2017), that method involved only a single stimulation and subsequent removal of the electrode. The current protocol will extend this work by outlining all of the steps necessary to conduct a full-scale sub-acute to chronic VNS study with an implanted cuff electrode. Here, we offer a practical guide to support pre-clinical VNS testing, anticipating the application of VNS for new clinical indications.

TARGETED STIMULATION OF THE VAGUS NERVE

Vagus Nerve Physiology

The vagus nerve is the tenth and longest cranial nerve and the primary mediator of the parasympathetic branch of the autonomic nervous system (Tracey, 2002; Bonaz et al., 2013). It also regulates immune system homeostasis through an intrinsic "cholinergic anti-inflammatory pathway" (Tracey, 2002; Bonaz et al., 2013). The vagus is a mixed nerve, largely composed of afferent sensory (∼80%) and efferent motor (∼20%) nerve fibers (George et al., 2003, 2004; Groves and Brown, 2005), the composition differing depending on the anatomical location of the nerve (Prechtl and Powley, 1990). The vagus nerve contains three main fiber types: A-, B-, and C-fibers, which are distinguished by fiber diameter, myelination, and activation thresholds (Heck et al., 2002; Groves and Brown, 2005; Ruffoli et al., 2011). A-fibers are large and myelinated (5–20 μm in diameter) and are activated by the lowest amount of current (0.01–0.2 mA) (Schnitzlein et al., 1958; Groves and Brown, 2005; Vuckovic et al., 2008; Ruffoli et al., 2011). B-fibers are mid-sized and myelinated (∼1–3 μm in diameter) and are also activated by low currents (0.04–0.6 mA) (Schnitzlein et al., 1958; Groves and Brown, 2005; Vuckovic et al., 2008; Ruffoli et al., 2011). C-fibers, which constitute the majority of vagus nerve fibers (∼65–80% of afferent fibers), are small and unmyelinated (0.4–2 μm in diameter) and require the highest activation currents (greater than 2.0 mA) (Schnitzlein et al., 1958; Heck et al., 2002; Groves and Brown, 2005; Vuckovic et al., 2008; Ruffoli et al., 2011; Yoo et al., 2013). Although the distribution of the vagus nerve has been shown to be comparable in some species (Mackay and Andrews, 1983; Asala and Bower, 1986), the morphology of the nerve changes depending on the anatomical location (Agostoni et al., 1957; Hoffman and Schnitzlein, 1961; McAllen and Spyer, 1978; Mei et al., 1980; Jammes et al., 1982; Powley et al., 1983; Prechtl and Powley, 1990; Henry, 2002; Ruffoli et al., 2011; Clancy et al., 2013; Hammer et al., 2015, 2018; Verlinden et al., 2015; Bonaz et al., 2016; Yuan and Silberstein, 2016; Planitzer et al., 2017).

Anatomical Considerations

Choosing an appropriate anatomical location to deliver stimulation is important when designing a VNS study. In most cases, VNS is delivered to the cervical vagus nerve (George et al., 2004; Howland, 2014) using an implanted electrode. Clinically, this anatomical location is the most common site for immune-modulation and treating epilepsy and depression (Lomarev et al., 2002; Nemeroff et al., 2006; Ben-Menachem et al., 2015; Koopman et al., 2016; Giordano et al., 2017). The left and right cervical branches differentially innervate the heart (O'Toole et al., 1986; Berthoud and Neuhuber, 2000; Ruffoli et al., 2011), where the right vagus nerve has more direct projections to the cardiac atria (Henry, 2002; Groves and Brown, 2005) and thus has a greater influence on heart rate. For this reason, left-sided VNS has been recommended to avoid adverse cardiovascular effects in humans (Henry, 2002; Groves and Brown, 2005; Van Leusden et al., 2015), even though equivalent anti-seizure effects are observed with either left, or right cervical VNS (Krahl et al., 2003; Navas et al., 2010). In rodent models, this lateral difference is not as clear and may differ depending on the stimulation parameters used (Stauss, 2017).

Anatomical differences in vagus innervation may be useful to help researchers adjust stimulation parameters to achieve specific, clinically relevant outcomes. Although most clinical applications target the left cervical vagus nerve, certain conditions may benefit from targeting different anatomical branches. For example, VNS applied to the right cervical vagus nerve is currently being explored to treat heart failure, where direct cardiac effects are desired (Li et al., 2004; Howland, 2014). Morphological differences in the right and left cervical vagus nerve branches (Verlinden et al., 2015) may also explain different clinical effects. Specifically, it was recently reported that both cervical nerve branches contain tyrosine hydroxylase- and dopamine β-hydroxylase-positive nerve fibers, but that the right cervical branch has a larger surface area and double the number of tyrosine hydroxylase-positive nerve fibers (Verlinden et al., 2015). These findings may inform the use of VNS for select cholinergic or adrenergic effects (Onkka et al., 2013; Seki et al., 2014; Verlinden et al., 2015).

Anatomical differences between the cervical vagus nerves may be less important in the treatment of other conditions, likely due to the abundant crossover of fibers between branches of the vagus nerve (Berthoud and Neuhuber, 2000). For example, in a recent study, no significant differences in inflammatory cytokines were found in animals receiving unilateral VNS to the left cervical

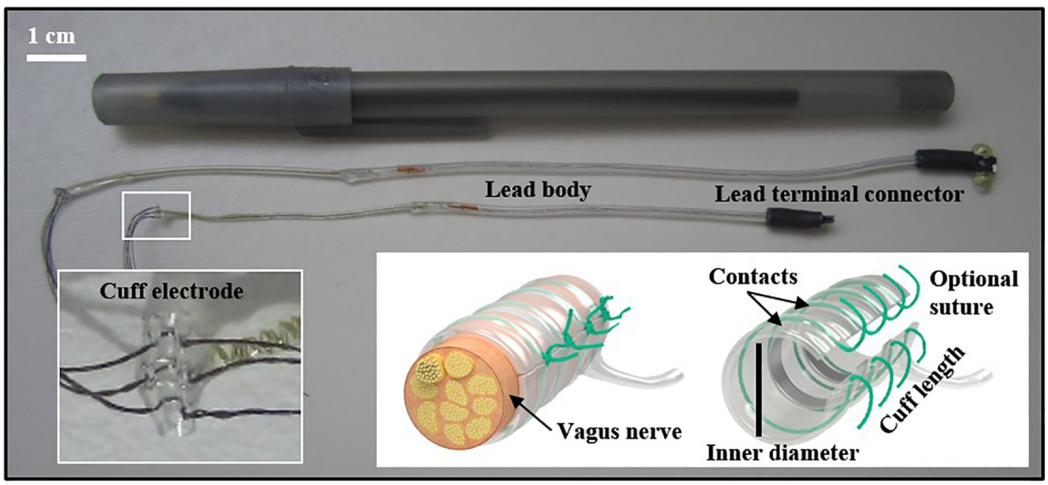

FIGURE 1 | Different sized (0.3 and 0.5 mm) cuff electrodes with connectors. Embedded sutures on the electrode can facilitate the surgical implant (inset). Other important electrode elements described in the text are identified. Cuff image reproduced with permission from MicroProbes for Life Science (Gaithersburg, MD).

vagus nerve compared to those receiving bilateral stimulation (VNS applied to the right and left nerve branches) (Olofsson et al., 2015). Laterality concerns may also be less pertinent for the emergent interest in transcutaneous VNS at the auricular or cervical branch (Howland, 2014; Ben-Menachem et al., 2015) and subdiaphragmatic VNS (Greenway and Zheng, 2007; de Lartigue, 2016). It remains to be determined whether the same stimulation parameters can be used for different vagus nerve branches or implanted vs. non-implanted modalities. Further research is needed to elucidate stimulation parameters for each clinical indication and comparative efficacy for implanted vs. non-implanted approaches. Here, the current review will focus on the most common clinical and pre-clinical stimulation site, the left cervical vagus nerve (Howland, 2014), using an implanted electrode. As rodents are commonly used in physiological studies with clinical relevance and form the basis for higher-order models, this overview will discuss specifications pertinent to mouse and rat models in a clinically relevant context, starting with electrode design and implantation, and concluding with stimulation parameters.

ELECTRODE DESIGN

The electrode design is an important factor to consider when planning a VNS study. In the most common clinical deployment using a can-and-lead system, the cervical vagus nerve is encircled with bipolar helical electrodes, and a pulse generator is implanted in the chest wall (Bonaz et al., 2013; Giordano et al., 2017). The electrode configuration consists of two spiral electrodes placed around the vagus nerve: the cathode is placed cranial and the anode caudal. A third helical tethering anchor is also placed around the nerve, directly caudal to the anode to provide strain relief (Pisapia and Baltuch, 2016; Giordano et al., 2017).

Electrodes used in rodents may differ, depending on the research objectives and study length (ranging from acute to chronic stimulation). The electrode configuration can include many designs (e.g., cuff or hook, and the inclusion of recording electrodes). A recent VNS methods paper described a needle electrode that was placed under the left cervical vagus nerve during a single stimulation (Le Maitre et al., 2017). For research involving multiple stimulation treatments, we implanted a bipolar cuff electrode with embedded sutures around the nerve (see **Figure 1**). Cuff electrodes are used in acute and chronic implantation to prevent current leakage into the surrounding tissue. We applied a strain-relieving suture close to the deployment site (detailed below), and the attached lead and pin connector was then tunneled under the skin and externalized at the base of the neck. **Figure 2** depicts the externalized connector and an awake animal receiving stimulation. Stimulation was delivered with a commercially available external pulse generator and current-controlled stimulus isolator (see **Figure 2**), described below.

For control conditions (unstimulated), a sham electrode can be made by implanting a silicon tube that is the same size as the electrode. This relatively inexpensive inactive design is helpful for feasibility testing, as it compensates for the mechanical stimulation that occurs when the nerve is manipulated (Huston et al., 2007). However, other variables (e.g., the weight of the electrode and tension from the connecting wire-embedded lead) may influence study outcomes, and it is best to have a control condition that consists of an identical implanted electrode that does not receive electricity or a cuff and lead constructed without wires.

In animal experimentation, placement of the cathode and anode are typically not reported. Animal research often includes study factors not relevant to clinical practice, such as stimulation of the distal nerve trunk of a vagotomized animal (Borovikova et al., 2000; de Jonge et al., 2005). In a recent rodent study, no significant differences in inflammatory cytokines were found with either rostral or caudal placement of the cathodic lead (Olofsson et al., 2015), likely because

FIGURE 2 | Left panel (top to bottom): Biphasic current-controlled stimulus isolator and biphasic pulse generator (BSI-1A, BPG-1P, respectively; Bak Electronics Incorporated, Umatilla, FL, United States). **Right panel** (top to bottom): Omnetics mating plug for the externalized connector and awake animal receiving stimulation. All procedures described and animal photography was performed with approval by the Institutional Animal Care and Use Committee (IACUC) at the University of Miami.

action potentials are generated in both directions when an axon is depolarized. Additional research is needed to understand how cathodic placement and pulse parameters can be modified for specific treatment indications, a topic that is currently being explored (Ardell et al., 2017; Patel et al., 2017; Stauss, 2017).

Electrode Specifications for Mice and Rats

Although many research groups construct their own electrodes, they can also be purchased and customized through commercial vendors. Nerve cuff electrodes can be made from several conductive materials, including platinum, platinum-iridium, and stainless steel. These electrodes are typically designed with monopolar, bipolar, or tripolar configurations, referring to the number of independent electrical contacts within the cuff. The tradeoff is generally increased control over current flow with a greater number of contacts, but also greater cost and cuff length. Monopolar electrodes are cheaper but require a return or ground, and current paths are less controllable. Bipolar electrodes are more expensive but allow better control over current flow than monopolar, as most of the current will flow directly between the two adjacent contacts. Bipolar cuff electrodes may be more practical and are widely used in pre-clinical research when the cost is a determining factor, especially in pilot studies. Tripolar electrodes may be connected in a pseudo-tripolar configuration (the two external electrodes linked together to form a common anode), which prevents current from leaking out of the cuff.

The size of the target nerve will determine the size of the electrode, as the inner diameter of the cuff should be approximately 1.4 times the outer diameter of the nerve. Use of a cuff that is too small could damage the nerve, and one that is too large could lead to insufficient surface contact or excessive current leakage (Agnew and McCreery, 1990; Yoshida and Riso, 2004). We used nerve cuffs with an inner diameter of 0.3 mm for both mice and small rats and 0.5 mm for larger rats. These sizes were informed by our experience and by published reports (Olofsson et al., 2015).

Besides inner diameter, other modifications include the number of contacts, the distance between contacts, and distance from the contacts to the end of the cuff. The number of contacts is determined by the stimulation paradigm desired. The distance between contacts ("inter-electrode spacing") we used was 0.5 mm for mice and small rats and 1 mm for larger rats. The distance from the last contact to the end of the cuff is typically three times the distance between contacts to prevent significant current leakage outside the cuff. This distance can be much smaller in pseudo-tripolar electrode configuration. Other custom modifications can be made to suit the research experiment, for example, using an angled cuff design, a multichannel omnetics connector on the externalized cuff lead, embedded suture material on the cuff for convenient closure, suture rings exiting from the base of the connector, and protective silicone tubing around the wiring. A deep review of electrode design is beyond the scope of the current article, but has been reviewed extensively elsewhere (Loeb and Peck, 1996; Merrill et al., 2005; Foldes et al., 2011; Dweiri et al., 2016; Caravaca et al., 2017).

Finally, stimulation conditions in acute vs. chronic studies may differ, as it has been shown that connective tissue forms around the cuff within the first 2 months of implantation (Agnew and McCreery, 1990; Helmers et al., 2012). While this scar tissue will bind the nerve and cuff together and prevent movement abrasion, it can also increase the impedance, causing an increase in the amount of stimulation voltage required to excite the nerve (Agnew and McCreery, 1990; Helmers et al., 2012). Furthermore, it was recently shown that chronic cuffing of the vagus nerve changes the integrity of the nerve fibers, likely due to the inflammatory response to the foreign material (Somann et al., 2018). Although the inflammatory response should resolve upon the formation of fibrous tissue, in some instances, it can negatively affect the integrity of the nerve, including demyelination (Tyler and Durand, 2003; Thil et al., 2007; Somann et al., 2018). It is currently unknown whether this process affects afferent and efferent vagus nerve fibers equally, but it is a potential source of study variability that should be considered when planning a chronic VNS study (Somann et al., 2018). Recent advancements in cuff design show promise in addressing some of these concerns (Caravaca et al., 2017).

STIMULATION EQUIPMENT

Commercially available equipment can be used to deliver a charge-balanced, biphasic square-wave pulse to a bipolar cuff electrode (Levine et al., 2014b; Olofsson et al., 2015). For investigators wanting readily available equipment, we have outlined the specifications related to one vendor, Bak Electronics Incorporated (Umatilla, FL, United States), but many of these specifications are also relevant to other vendors. For our studies, we delivered biphasic (cathodic-leading) stimulation (Levine et al., 2014b; Olofsson et al., 2015) using an external biphasic pulse generator and current-controlled biphasic stimulus isolator

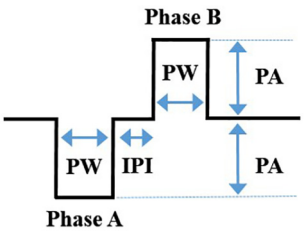

FIGURE 3 | A depiction of the waveform of one charge-balanced, biphasic, cathodic-leading square pulse cycle, showing pulse width (PW), inter-phase interval (IPI), and pulse amplitude (PA). These components have been explained in detail elsewhere (Merrill et al., 2005). Image adapted with permission (Levine et al., 2014b; Olofsson et al., 2015) under the Creative Commons Attribution License.

(BPG-1P and BSI-1A, respectively). Gently restrained rodents (without anesthesia) were connected to the equipment with a mating plug for stimulation delivery (De Herdt et al., 2009; Zhang et al., 2009). See **Figure 2** for equipment configuration and stimulation. Stimulation can be delivered for a specific period (e.g., 60 s) using the manual trigger or it can be digitally triggered or gated to a particular stimulus with a laptop configuration. The waveform design of one charge-balanced, biphasic, cathodic-leading square pulse cycle is represented in **Figure 3**.

The delivery specifications of each VNS "treatment" will depend on the physiological outcome measure to be studied. For example, in the context of anti-inflammatory effects, it has been shown that VNS delivered 24–48 h prior to endotoxin exposure resulted in a significant reduction in tumor necrosis factor (TNF) cytokine upon exposure (Huston et al., 2007). This period of therapeutic effects suggests that for certain indications (e.g., conditions characterized by an exaggerated inflammatory response to stimuli), VNS may be administered prophylactically or at specific intervals. As VNS treatment will likely be tailored to clinical symptoms, additional work is needed to determine the temporal response of VNS for other indications. Finally, it is important to include a measurable variable to determine stimulation effectiveness and rule out potential sources of study variability, such as incorrect placement or faulty electrodes, or mechanical damage to the nerve. One option is to record evoked potentials from the vagus nerve after VNS, for example, by stimulating the cervical branch and recording from the subdiaphragmatic branch (Olofsson et al., 2015). This approach can be taken just prior to euthanasia, or immediately after implantation; however, recording from the vagus nerve is technically challenging to perform in rodents (Silverman et al., 2018). To circumvent some of these challenges, investigators can record in a smaller cohort of animals, use electrodes that perform both stimulation and recording, or obtain electromyography (EMG) recordings of the laryngeal muscles that are innervated by the vagus. Another common option is to use heart rate to verify effective cuff placement, where stimulation is increased until a change in heart rate is observed (Levine et al., 2019). At a minimum, we recommend to visually inspect the nerve at euthanasia to ensure that it is still within the cuff and, when possible, to perform histology on the excised nerve to verify axon integrity.

MICROSURGICAL TECHNIQUE: ELECTRODE PLACEMENT

The stepwise surgical procedure detailed below involves the placement of an electrode on the LEFT cervical vagus nerve. The lateral configuration will change if implanting on the RIGHT nerve branch. All survival surgeries should be performed with aseptic technique while the animal is anesthetized, as recommended by the local Institutional Animal Care and Use Committee. Standard post-operative care should also be administered, including hydration and analgesia. With the animal lying prone, make a small opening (∼2 mm) in the skin at the craniovertebral junction, then place the animal in supine position. Palpate the sternal notch. Using scissors, carefully make a vertical incision at the neck, 3 mm caudal to the sternal notch. Dissect the subcutaneous space and extend the midline opening toward the jaw. Identify the inferior border of the thyroid tissue ("V" shaped distinct white line at the cervico-sternal junction). Blunt dissect the thyroid tissue along this line and reflect rostrally. Using a curved, narrow hemostat, create a subcutaneous tunnel toward the opening made at the craniovertebral junction. Bring the electrode through the tunnel and secure to the side of the incision site with tape or weighted instruments. Using blunt-tipped surgical hooks or modified needle syringes as hooks, reflect the thyroid superiorly and the left sternocleidomastoid inferiorly to expose the carotid fossa. No cutting of subcutaneous tissue should be done at any time.

Isolate the left carotid sheath from the connective tissue using pickup forceps and gentle opening-closing movements parallel to the vessels. Identify the nerve (white in appearance) located directly behind or adjacent to the carotid artery. Note, gentle dissection can be accomplished with small, blunt-tipped forceps, minimizing the risk of vessel puncture; however, sharp forceps can also be carefully used to separate the nerve from the carotid artery. Gently dissect the nerve circumferentially taking care not to damage the vessels or tug on the nerve, and place background material under the nerve (a small piece of sterile glove will serve this purpose). Feed the suture strings from the same side of the electrode cuff under the nerve. Advance the electrode cuff under the nerve. Open the cuff by pulling on the opposing sutures, allow the nerve to slide into the open cuff, and secure the cuff by tying the suture strings (see **Figure 4**). If the visualized nerve is very thin, it is also possible to encircle the entire carotid sheath in mice without isolating the nerve (Olofsson et al., 2015). Attach the lead body to the subcutaneous tissue with a non-absorbable suture (e.g., 4–0 Webcryl) placed approximately 5 mm away from the cuff. This suture will secure the electrode and provide strain relief. With the animal lying prone, feed the excess encased wires evenly into the subcutaneous space (if necessary, create a pocket with forceps by gentle opening-closing movements). Secure the connector to the skin with non-absorbable suture (using embedded suture rings or suture carefully placed through

FIGURE 4 | Surgical preparation of the electrode implant. Close up (inset), where the white dotted line lies parallel to the nerve lying inside the cuff. All procedures described and animal photography was performed with approval by the Institutional Animal Care and Use Committee (IACUC) at the University of Miami.

the rubber encasement) and close the skin opening. Before closing the neck incision, place the animal back in a supine position to inspect the electrode and ensure the cuff is encircling the nerve without twisting or pulling. Close the incision on the neck. During surgery, care should be taken to avoid excessive manipulation of the nerve to prevent axonal damage, and, as has been reported, mechanical activation of neuroimmune reflexes (Huston et al., 2007).

ELECTRICAL STIMULATION PARAMETERS

Current FDA-Approved Clinical VNS Guidelines

Many of the lessons learned in the application of VNS to treat epilepsy are generalizable to other VNS applications, although stimulation should be optimized to the specific treatment condition. Several important parameters can be adjusted when delivering stimulation to the vagus nerve: output current, pulse width, pulse frequency, and duty cycle (i.e., "ON" and "OFF" time) (Heck et al., 2002; Groves and Brown, 2005; Wheless et al., 2018). Collectively, these parameters determine the total amount of electrical energy delivered to the vagus nerve during treatment (Heck et al., 2002). Current guidelines in epilepsy include output currents between 0.25 and 3.5 mA and pulse frequencies ranging between 20 and 30 Hz (Heck et al., 2002; Groves and Brown, 2005; Ruffoli et al., 2011). Continuously applied, high-frequency (50–100 Hz) current leads to irreversible axonal injury, which can be avoided by reducing the frequency to 20 Hz (Agnew and McCreery, 1990). These findings and others showing optimal pulse frequencies for seizure reduction ranging from 10 to 30 Hz (Woodbury and Woodbury, 1990; Zabara, 1992) led to current FDA-approved guidelines (Groves and Brown, 2005). These settings also correspond with stimulation parameters reported in clinical trials of depression (Rush et al., 2000, 2005a,b) and a recent clinical study of rheumatoid arthritis (Koopman et al., 2016). Once a target fiber type is identified, stimulation can be adjusted within approved limits.

The output current is the stimulation parameter typically adjusted first (Heck et al., 2002). A tolerable range of current can be used to target specific nerve fibers and achieve clinical efficacy. Initially, VNS treatment for clinical epilepsy was thought to activate C-fibers, an approach that coincided with observations of progressive anti-epileptic effects with increasing current (Heck et al., 2002). This approach was not without consequence, as elevated currents are less tolerable and increase adverse effects, such as bradycardia, dyspnea, and throat tightness (Heck et al., 2002). The need to increase output current to achieve clinical efficacy (DeGiorgio et al., 2000, 2001) has been questioned and may have been influenced by the high currents used for non-responders (Heck et al., 2002). It has since been shown that C-fiber activation is not required for anticonvulsant effects (Krahl et al., 2001; Henry, 2002; Ruffoli et al., 2011) and that currents above 2 mA may be unnecessary for most patients (Heck et al., 2002).

The second parameter to consider is the pulse width, the duration of a single stimulation pulse (Labiner and Ahern, 2007), which can be adjusted to avoid the neural damage associated with continuous stimulation (Agnew and McCreery, 1990). Rodent seizure models report optimal pulse widths as high as 1,000 μs; however, the pulse width is inversely related to tolerance in people (Heck et al., 2002). Fortunately, this parameter can be adjusted to improve tolerance without loss of efficacy, for example, by shortening the pulse width from 500 μs to 250 μs (Heck et al., 2002). Pulse width is inversely related to the current required to stimulate a nerve (Heck et al., 2002; Labiner and Ahern, 2007; Levine et al., 2019), and together these two parameters determine the total charge per pulse (Labiner and Ahern, 2007; Levine et al., 2019). Although shorter and longer pulse durations may be preferred in different clinical applications (Agnew and McCreery, 1990), this is an area of active investigation (Mu et al., 2004; Kong et al., 2012; Aaronson et al., 2013; Loerwald et al., 2018). Thus, adjusting pulse width in concert with output current can meet stimulation requirements and reduce the risks of excessive stimulation current, while achieving a balance of clinical efficacy and tolerability.

A third parameter, pulse frequency (number of pulses per second), is less often varied in studies compared to other stimulation settings. Pulse frequencies that are generally used in rodent seizure models are similar to those used clinically, ranging from 10 to 30 Hz (Heck et al., 2002). For treatment indications besides epilepsy, the utility of specific pulse frequencies remains under investigation. In clinical practice, it may be helpful to use the natural firing rates of specific fiber types to guide pulse frequency (Bonaz et al., 2013). For example, it has been reported that the physiological firing frequency of A- and C-fibers is above and below 10 Hz, respectively (Binks et al., 2001). It is currently unclear whether pulse frequency can be used to preferentially stimulate afferent vs. efferent fibers without the use of chemical or electrical nerve block (Osharina et al., 2006; Bonaz et al., 2013; Olofsson et al., 2015; Patel et al., 2017; Patel and Butera, 2018), as generally, when an axon is depolarized beneath a cathodic electrode, action potentials travel in both directions.

To date, pulse frequencies that are responsible for specific clinical effects remain to be determined; however, as more studies are performed, we will better understand whether a combination of stimulation settings will be useful in targeting specific nerve fibers within efferent and afferent pathways [e.g., motor A-type or sensory group I, II, and III fibers (Yoo et al., 2013)]. The use of different stimulation paradigms to selectively target different fiber types remains an area of active investigation (Vuckovic et al., 2004, 2008; Howland, 2014; Peclin and Rozman, 2014; Guiraud et al., 2016; Patel et al., 2017; Nuntaphum et al., 2018; Patel and Butera, 2018).

A final parameter that affects stimulation is the duty cycle (ON/OFF cycle) (Heck et al., 2002; Labiner and Ahern, 2007). The standard duty cycle to treat persons with epilepsy is 30 s ON/5 min OFF (Heck et al., 2002). Although shorter OFF times can improve clinical efficacy, rapid cycling (i.e., very short duty cycles) is much more energy intensive and may not be necessary for effective treatment (Heck et al., 2002), at least for anti-seizure use. A more in-depth discussion on considerations regarding electrical stimulation can be found in previous reviews (Merrill et al., 2005; Mortimer and Bhadra, 2009; Cogan et al., 2018; Grill, 2018). As an example using our equipment setup (**Figure 2**), a stimulation "treatment" consisting of symmetrical biphasic square pulses with current intensity of 500 μA, 250 μs pulse width, and 50 μs inter-phase interval at 10 Hz for 60 s (Olofsson et al., 2015) can be delivered with the following settings. *Stimulus isolator*: 100 μA of constant current, AC coupling, continuous stimulation, and an input gain of 1. *Pulse generator*: 5.0 amplitude (5 × 100 μA × gain of 1), 250 μs pulse width, 100 ms period. It should be noted that the pulse period is the inverse of the desired frequency (i.e., 100 ms = 1/10 Hz × 1000 ms/s). To summarize, the stimulation "treatment" using the parameters from our previous example will consist of a 550 μs pulse (250 μs for each phase of the pulse, plus 50 μs inter-phase interval), and a 99,450 μs inter-pulse interval (total of 100,000 μs period).

Adverse Effects Associated With VNS

Commonly reported VNS adverse effects include cough, throat tightening or discomfort, shortness of breath, voice alterations, and cardiovascular symptoms, such as bradycardia (Ben-Menachem, 2001; Heck et al., 2002; Ben-Menachem et al., 2015; Jacobs et al., 2015). These transient effects are limited to when the device is actively stimulating and are proportional to increases in output current, pulse width, frequency, and duty cycle (Heck et al., 2002; Jacobs et al., 2015; Olofsson et al., 2015). Pulmonary effects are mainly associated with C-fiber activation (Banzett et al., 1999; Heck et al., 2002; Henry, 2002), which were previously associated with cardiovascular effects. However, it has been shown that cardioinhibitory effects can be attributed to activation of B-fibers (Jones et al., 1995; Banzett et al., 1999; Yoo et al., 2016; McAllen et al., 2018; Qing et al., 2018). Importantly, no evidence of "clinically relevant" bradycardia has been reported for stimulation within FDA-approved guidelines (Heck et al., 2002). It is also notable that anti-inflammatory and cardioinhibitory effects are separable (Huston et al., 2007), further indicating that stimulation parameters can be tailored for precise, clinically relevant outcomes.

Tailoring VNS for Specific Conditions

Early anti-epileptic work targeted C-fibers under the assumption that these abundant afferent fibers mediate the clinical effects of VNS (George et al., 2003, 2004; Groves and Brown, 2005; Yoo et al., 2013). As such, early VNS treatment utilized the high output currents needed to stimulate C-fibers (Heck et al., 2002). As A-, B-, and C-fibers are successively recruited with increased electrical current (Woodbury and Woodbury, 1990; Yoo et al., 2013), subsequent research demonstrated anticonvulsant effects without specifically targeting C-fibers, thus allowing for smaller amounts of current (Krahl et al., 2001; Henry, 2002; Ruffoli et al., 2011). The activation thresholds of A- and B-fibers overlap, but both require substantially less current than C-fibers (Groves and Brown, 2005; Castoro et al., 2011), which, when activated, are associated with most of the reported adverse effects (Heck et al., 2002; Henry, 2002).

As the field has progressed, this iterative process of associating specific fiber types with therapeutic effects has occurred in the use of VNS for other indications, where anti-inflammatory effects have been attributed to A-fibers (Huston et al., 2007) and B-fibers (Olofsson et al., 2015). Importantly, recent research shows that minimal stimulation can achieve beneficial therapeutic outcomes. A seminal pre-clinical study demonstrated that a minimal amount of current (0.5 mA) activated the inflammatory reflex in both mice and rats (Olofsson et al., 2015), effects of which were observed up to 2.5 mA. These output currents remain below FDA-approved levels (Heck et al., 2002) and are similar to currents used clinically for rheumatoid arthritis (Koopman et al., 2016). Thus, minimized stimulation may provide therapeutic benefits while avoiding the adverse effects associated with higher output currents (Heck et al., 2002).

CONCLUSION

Decades of research has brought extensive progress to the field of neuromodulation, and specifically to the clinical use of techniques such as VNS. Although VNS is a promising neuromodulation tool, it has been challenging to incorporate study findings from clinical and pre-clinical research. Pre-clinical VNS work often involves mechanistic study aspects not employed in clinical settings, such as the use of lidocaine to block efferent or afferent signaling or electrical stimulation of nerve stumps after vagotomy (Borovikova et al., 2000; de Jonge et al., 2005; Niederbichler et al., 2009; Olofsson et al., 2015). In clinical VNS application, decisions regarding stimulation parameters may not be explicitly defined, such as the number of treatment sessions; similarly, a clear rationale for pulse-design modifications are often not addressed. In addition to pulse frequencies, several other key stimulation parameters can influence study outcomes and reproducibility; however, selection of specific treatment parameters are often not detailed or are simply reported as "customized." Furthermore, as activation thresholds may differ depending on conditions of stimulation, it is critical that study conditions are outlined in ongoing research efforts.

These issues highlight the challenge of translating rodent work to clinical application. The inflammatory reflex appears to be conserved across species; where anti-inflammatory effects are observed with similar stimulation parameters in rodents with endotoxemia (Olofsson et al., 2015), rodents with collagen-induced arthritis (Levine et al., 2014b), and persons with rheumatoid arthritis (Koopman et al., 2016). However, it is unknown whether specific fiber types that mediate the reflex are similarly conserved. Additionally, as disease-related factors may influence VNS pathways, stimulation may be most effective if delivered at specific time points of disease progression. These and other questions remain to be determined and highlight the importance of translating pre-clinical findings to heterogeneous clinical populations.

The current review aims to advance VNS research by providing a comprehensive discussion on performing pre-clinical VNS studies in rodent models. We have provided a microsurgical technique, discussed stimulation equipment, and provided a rationale for choosing electrode design and electrical stimulation settings. We outlined how a combination of clinically relevant stimulation parameters can be adjusted to achieve selected therapeutic effects. Indeterminate issues are discussed and presented as avenues for future research.

AUTHOR CONTRIBUTIONS

CN, YL, TU, JA, and MN conceived, structured, and participated in writing and revising the review.

FUNDING

This work was supported in part by a project grant from the State of Florida to The Miami Project to Cure Paralysis (W. Dalton Dietrich, PI), a pilot grant from the Morton Cure Paralysis Fund awarded to CN, and an individual NIDILRR Mary Switzer Fellowship awarded to CN (90SFGE0006).

ACKNOWLEDGMENTS

We acknowledge Dr. Alexander Marcillo for his surgical assistance and April Mann for her assistance in the technical review of the manuscript.

REFERENCES

Aaronson, S. T., Carpenter, L. L., Conway, C. R., Reimherr, F. W., Lisanby, S. H., Schwartz, T. L., et al. (2013). Vagus nerve stimulation therapy randomized to different amounts of electrical charge for treatment-resistant depression: acute and chronic effects. *Brain Stimul.* 6, 631–640. doi: 10.1016/j.brs.2012.09.013

Agnew, W. F., and McCreery, D. B. (1990). Considerations for safety with chronically implanted nerve electrodes. *Epilepsia* 31(Suppl. 2), S27–S32.

Agostoni, E., Chinnock, J. E., De Daly, M. B., and Murray, J. G. (1957). Functional and histological studies of the vagus nerve and its branches to the heart, lungs and abdominal viscera in the cat. *J. Physiol.* 135, 182–205. doi: 10.1113/jphysiol.1957.sp005703

Ardell, J. L., Nier, H., Hammer, M., Southerland, E. M., Ardell, C. L., Beaumont, E., et al. (2017). Defining the neural fulcrum for chronic vagus nerve stimulation: implications for integrated cardiac control. *J. Physiol.* 595, 6887–6903. doi: 10.1113/JP274678

Asala, S. A., and Bower, A. J. (1986). An electron microscope study of vagus nerve composition in the ferret. *Anat. Embryol.* 175, 247–253. doi: 10.1007/bf00389602

Banzett, R. B., Guz, A., Paydarfar, D., Shea, S. A., Schachter, S. C., and Lansing, R. W. (1999). Cardiorespiratory variables and sensation during stimulation of the left vagus in patients with epilepsy. *Epilepsy Res.* 35, 1–11. doi: 10.1016/s0920-1211(98)00126-0

Ben-Menachem, E. (2001). Vagus nerve stimulation, side effects, and long-term safety. *J. Clin. Neurophysiol.* 18, 415–418. doi: 10.1097/00004691-200109000-00005

Ben-Menachem, E., Revesz, D., Simon, B. J., and Silberstein, S. (2015). Surgically implanted and non-invasive vagus nerve stimulation: a review of efficacy, safety and tolerability. *Eur. J. Neurol.* 22, 1260–1268. doi: 10.1111/ene.12629

Berthoud, H. R., and Neuhuber, W. L. (2000). Functional and chemical anatomy of the afferent vagal system. *Auton. Neurosci.* 85, 1–17. doi: 10.1016/s1566-0702(00)00215-0

Binks, A. P., Paydarfar, D., Schachter, S. C., Guz, A., and Banzett, R. B. (2001). High strength stimulation of the vagus nerve in awake humans: a lack of cardiorespiratory effects. *Respir. Physiol.* 127, 125–133. doi: 10.1016/s0034-5687(01)00252-3

Bonaz, B., Picq, C., Sinniger, V., Mayol, J. F., and Clarencon, D. (2013). Vagus nerve stimulation: from epilepsy to the cholinergic anti-inflammatory pathway. *Neurogastroenterol. Motil.* 25, 208–221. doi: 10.1111/nmo.12076

Bonaz, B., Sinniger, V., and Pellissier, S. (2016). Anti-inflammatory properties of the vagus nerve: potential therapeutic implications of vagus nerve stimulation. *J. Physiol.* 594, 5781–5790. doi: 10.1113/JP271539

Borovikova, L. V., Ivanova, S., Zhang, M., Yang, H., Botchkina, G. I., Watkins, L. R., et al. (2000). Vagus nerve stimulation attenuates the systemic inflammatory response to endotoxin. *Nature* 405, 458–462. doi: 10.1038/35013070

Cai, P. Y., Bodhit, A., Derequito, R., Ansari, S., Abukhalil, F., Thenkabail, S., et al. (2014). Vagus nerve stimulation in ischemic stroke: old wine in a new bottle. *Front. Neurol.* 5:107. doi: 10.3389/fneur.2014.00107

Caravaca, A. S., Tsaava, T., Goldman, L., Silverman, H., Riggott, G., Chavan, S. S., et al. (2017). A novel flexible cuff-like microelectrode for dual purpose, acute and chronic electrical interfacing with the mouse cervical vagus nerve. *J. Neural. Eng.* 14:066005. doi: 10.1088/1741-2552/aa7a42

Castoro, M. A., Yoo, P. B., Hincapie, J. G., Hamann, J. J., Ruble, S. B., Wolf, P. D., et al. (2011). Excitation properties of the right cervical vagus nerve in adult dogs. *Exp. Neurol.* 227, 62–68. doi: 10.1016/j.expneurol.2010.09.011

Clancy, J. A., Deuchars, S. A., and Deuchars, J. (2013). The wonders of the wanderer. *Exp. Physiol.* 98, 38–45. doi: 10.1113/expphysiol.2012.064543

Cogan, S. F., Hara, S., and Ludwig, K. A. (2018). "Chapter 7 - the safe delivery of electrical currents and neuromodulation," in *Neuromodulation*, 2 Edn, eds E. S. Krames, P. H. Peckham, and A. R. Rezai, (Cambridge, MA: Academic Press), 83–94. doi: 10.1016/b978-0-12-805353-9.00007-3

Conway, C. R., Gott, B. M., and Azhar, N. H. (2016). "Vagus nerve stimulation for treatment-refractory depression," in *Neuromodulation in Psychiatry*, eds C. Hamani, P. Holtzheimer, A. M. Lozano, and H. Mayberg, (Hoboken: John Wiley & Sons), 335–352. doi: 10.1002/9781118801086.ch18

Dawson, J., Pierce, D., Dixit, A., Kimberley, T. J., Robertson, M., Tarver, B., et al. (2016). Safety, feasibility, and efficacy of vagus nerve stimulation paired with upper-limb rehabilitation after ischemic stroke. *Stroke* 47, 143–150. doi: 10.1161/STROKEAHA.115.010477

De Herdt, V., Puimege, L., De Waele, J., Raedt, R., Wyckhuys, T., El Tahry, R., et al. (2009). Increased rat serum corticosterone suggests immunomodulation by stimulation of the vagal nerve. *J. Neuroimmunol.* 212, 102–105. doi: 10.1016/j.jneuroim.2009.04.013

de Jonge, W. J., van der Zanden, E. P., The, F. O., Bijlsma, M. F., van Westerloo, D. J., Bennink, R. J., et al. (2005). Stimulation of the vagus nerve attenuates macrophage activation by activating the Jak2-STAT3 signaling pathway. *Nat. Immunol.* 6, 844–851. doi: 10.1038/ni1229

de Lartigue, G. (2016). Role of the vagus nerve in the development and treatment of diet-induced obesity. *J. Physiol.* 594, 5791–5815. doi: 10.1113/JP271538

DeGiorgio, C. M., Schachter, S. C., Handforth, A., Salinsky, M., Thompson, J., Uthman, B., et al. (2000). Prospective long-term study of vagus nerve stimulation for the treatment of refractory seizures. *Epilepsia* 41, 1195–1200.

DeGiorgio, C. M., Thompson, J., Lewis, P., Arrambide, S., Naritoku, D., Handforth, A., et al. (2001). Vagus nerve stimulation: analysis of device parameters in 154 patients during the long-term XE5 study. *Epilepsia* 42, 1017–1020. doi: 10.1046/j.1528-1157.2001.0420081017.x

Dweiri, Y. M., Stone, M. A., Tyler, D. J., McCallum, G. A., and Durand, D. M. (2016). Fabrication of high contact-density, flat-interface nerve electrodes for recording and stimulation applications. *J. Vis. Exp.* 116:54388. doi: 10.3791/54388

Foldes, E. L., Ackermann, D. M., Bhadra, N., Kilgore, K. L., and Bhadra, N. (2011). Design, fabrication and evaluation of a conforming circumpolar peripheral nerve cuff electrode for acute experimental use. *J. Neurosci. Methods* 196, 31–37. doi: 10.1016/j.jneumeth.2010.12.020

George, M. S., Nahas, Z., Bohning, D. E., Mu, Q., Andrew Kozel, F., Borckhardt, J., et al. (2004). Mechanisms of action of vagus nerve stimulation (VNS). *Clin. Neurosci. Res.* 4, 71–79. doi: 10.1016/j.cnr.2004.06.006

George, M. S., Rush, A. J., Sackeim, H. A., and Marangell, L. B. (2003). Vagus nerve stimulation (VNS): utility in neuropsychiatric disorders. *Int. J. Neuropsychopharmacol.* 6, 73–83. doi: 10.1017/s1461145703003250

Giordano, F., Zicca, A., Barba, C., Guerrini, R., and Genitori, L. (2017). Vagus nerve stimulation: surgical technique of implantation and revision and related morbidity. *Epilepsia* 58(Suppl. 1), 85–90. doi: 10.1111/epi.13678

Greenway, F., and Zheng, J. (2007). Electrical stimulation as treatment for obesity and diabetes. *J. Diabetes Sci. Technol.* 1, 251–259. doi: 10.1177/193229680700100216

Grill, W. M. (2018). "Chapter 8 - waveforms for neural stimulation," in *Neuromodulation*, 2Edn Edn, eds E. S. Krames, P. H. Peckham, and A. R. Rezai, (Cambridge, MA: Academic Press), 95–102. doi: 10.1016/b978-0-12-805353-9.00008-5

Groves, D. A., and Brown, V. J. (2005). Vagal nerve stimulation: a review of its applications and potential mechanisms that mediate its clinical effects. *Neurosci. Biobehav. Rev.* 29, 493–500. doi: 10.1016/j.neubiorev.2005.01.004

Guiraud, D., Andreu, D., Bonnet, S., Carrault, G., Couderc, P., Hagege, A., et al. (2016). Vagus nerve stimulation: state of the art of stimulation and recording strategies to address autonomic function neuromodulation. *J. Neural. Eng.* 13:041002. doi: 10.1088/1741-2560/13/4/041002

Hammer, N., Glatzner, J., Feja, C., Kuhne, C., Meixensberger, J., Planitzer, U., et al. (2015). Human vagus nerve branching in the cervical region. *PLoS One* 10:e0118006. doi: 10.1371/journal.pone.0118006

Hammer, N., Loffler, S., Cakmak, Y. O., Ondruschka, B., Planitzer, U., Schultz, M., et al. (2018). Cervical vagus nerve morphometry and vascularity in the context of nerve stimulation - A cadaveric study. *Sci. Rep.* 8:7997. doi: 10.1038/s41598-018-26135-8

Heck, C., Helmers, S. L., and DeGiorgio, C. M. (2002). Vagus nerve stimulation therapy, epilepsy, and device parameters: scientific basis and recommendations for use. *Neurology* 59(6 Suppl. 4), S31–S37.

Helmers, S. L., Begnaud, J., Cowley, A., Corwin, H. M., Edwards, J. C., Holder, D. L., et al. (2012). Application of a computational model of vagus nerve stimulation. *Acta Neurol. Scand.* 126, 336–343. doi: 10.1111/j.1600-0404.2012.01656.x

Henry, T. R. (2002). Therapeutic mechanisms of vagus nerve stimulation. *Neurology* 59(6 Suppl. 4), S3–S14.

Hoffman, H. H., and Schnitzlein, H. N. (1961). The numbers of nerve fibers in the vagus nerve of man. *Anat. Rec.* 139, 429–435. doi: 10.1002/ar.1091390312

Howland, R. H. (2014). Vagus nerve stimulation. *Curr. Behav. Neurosci. Rep.* 1, 64–73.

Huston, J. M., Gallowitsch-Puerta, M., Ochani, M., Ochani, K., Yuan, R., Rosas-Ballina, M., et al. (2007). Transcutaneous vagus nerve stimulation reduces serum high mobility group box 1 levels and improves survival in murine sepsis. *Crit. Care Med.* 35, 2762–2768. doi: 10.1097/00003246-200712000-00014

Huston, J. M., Ochani, M., Rosas-Ballina, M., Liao, H., Ochani, K., Pavlov, V. A., et al. (2006). Splenectomy inactivates the cholinergic antiinflammatory pathway during lethal endotoxemia and polymicrobial sepsis. *J. Exp. Med.* 203, 1623–1628. doi: 10.1084/jem.20052362

Jacobs, H. I., Riphagen, J. M., Razat, C. M., Wiese, S., and Sack, A. T. (2015). Transcutaneous vagus nerve stimulation boosts associative memory in older individuals. *Neurobiol. Aging* 36, 1860–1867. doi: 10.1016/j.neurobiolaging.2015.02.023

Jammes, Y., Fornaris, E., Mei, N., and Barrat, E. (1982). Afferent and efferent components of the bronchial vagal branches in cats. *J. Auton. Nerv. Syst.* 5, 165–176. doi: 10.1016/0165-1838(82)90037-6

Jones, J. F., Wang, Y., and Jordan, D. (1995). Heart rate responses to selective stimulation of cardiac vagal C fibres in anaesthetized cats, rats and rabbits. *J. Physiol.* 489(Pt 1), 203–214. doi: 10.1113/jphysiol.1995.sp021042

Kanashiro, A., Shimizu Bassi, G., de Queiroz Cunha, F., and Ulloa, L. (2018). From neuroimunomodulation to bioelectronic treatment of rheumatoid arthritis. *Bioelectron. Med.* 1, 151–165. doi: 10.2217/bem-2018-0001

Kong, S. S., Liu, J. J., Hwang, T. C., Yu, X. J., Zhao, M., Zhao, M., et al. (2012). Optimizing the parameters of vagus nerve stimulation by uniform design in rats with acute myocardial infarction. *PLoS One* 7:e42799. doi: 10.1371/journal.pone.0042799

Koopman, F. A., Chavan, S. S., Miljko, S., Grazio, S., Sokolovic, S., Schuurman, P. R., et al. (2016). Vagus nerve stimulation inhibits cytokine production and attenuates disease severity in rheumatoid arthritis. *Proc. Natl. Acad. Sci. U.S.A.* 113, 8284–8289. doi: 10.1073/pnas.1605635113

Krahl, S. E., Senanayake, S. S., and Handforth, A. (2001). Destruction of peripheral C-fibers does not alter subsequent vagus nerve stimulation-induced seizure suppression in rats. *Epilepsia* 42, 586–589. doi: 10.1046/j.1528-1157.2001.09700.x

Krahl, S. E., Senanayake, S. S., and Handforth, A. (2003). Right-sided vagus nerve stimulation reduces generalized seizure severity in rats as effectively as left-sided. *Epilepsy Res.* 56, 1–4. doi: 10.1016/s0920-1211(03)00122-0

Kumar, A., Bunker, M. T., Aaronson, S. T., Conway, C. R., Rothschild, A. J., Mordenti, G., et al. (2019). Durability of symptomatic responses obtained with adjunctive vagus nerve stimulation in treatment-resistant depression. *Neuropsychiatr. Dis. Treat.* 15, 457–468. doi: 10.2147/NDT.S196665

Labiner, D. M., and Ahern, G. L. (2007). Vagus nerve stimulation therapy in depression and epilepsy: therapeutic parameter settings. *Acta Neurol. Scand.* 115, 23–33. doi: 10.1111/j.1600-0404.2006.00732.x

Lainez, M. J., and Guillamon, E. (2017). Cluster headache and other TACs: Pathophysiology and neurostimulation options. *Headache* 57, 327–335. doi: 10.1111/head.12874

Le Maitre, E., Revathikumar, P., Estelius, J., and Lampa, J. (2017). Increased Recovery time and decreased LPS administration to study the vagus nerve stimulation mechanisms in limited inflammatory responses. *J. Vis. Exp.* 121, 54890. doi: 10.3791/54890

Levine, Y. A., Faltys, M., and Chernoff, D. (2019). Harnessing the inflammatory reflex for the treatment of inflammation-mediated diseases. *Cold Spring Harb. Perspect. Med.* doi: 10.1101/cshperspect.a034330 [Epub ahead of print].

Levine, Y. A., Koopman, F., Faltys, M., Zitnik, R., and Tak, P.-P. (2014a). Neurostimulation of the cholinergic antiinflammatory pathway in rheumatoid arthritis and inflammatory bowel disease. *Bioelectron. Med.* 1, 34–43. doi: 10.15424/bioelectronmed.2014.00008

Levine, Y. A., Koopman, F. A., Faltys, M., Caravaca, A., Bendele, A., Zitnik, R., et al. (2014b). Neurostimulation of the cholinergic anti-inflammatory pathway ameliorates disease in rat collagen-induced arthritis. *PLoS One* 9:e104530. doi: 10.1371/journal.pone.0104530

Levine, Y. A., Faltys, M., and Zitnik, R. (2018a). "Chapter 126 - Activation of the inflammatory reflex in rheumatoid arthritis and inflammatory bowel disease; preclinical evidence, in Neuromodulation, 2nd Edn. eds. E. S.Krames, P. H. Peckham and A. R., Rezai, (Cambridge, MA: Academic Press), 1493–1502.

Levine, Y. A., Simon, J., Faltys, M., and Zitnik, R. (2018b). "Chapter 127 - Bioelectronic therapy for the treatment of rheumatoid arthritis and inflammatory bowel disease," in Neuromodulation, 2nd Edn. eds. E. S. Krames, P. H. Peckham and A. R. Rezai, (Cambridge, MA: Academic Press) 1503–1511.

Li, M., Zheng, C., Sato, T., Kawada, T., Sugimachi, M., and Sunagawa, K. (2004). Vagal nerve stimulation markedly improves long-term survival after chronic heart failure in rats. *Circulation* 109, 120–124. doi: 10.1161/01.cir.0000105721.71640.da

Loeb, G. E., and Peck, R. A. (1996). Cuff electrodes for chronic stimulation and recording of peripheral nerve activity. *J. Neurosci. Methods* 64, 95–103. doi: 10.1016/0165-0270(95)00123-9

Loerwald, K. W., Borland, M. S., Rennaker, R. L. II, Hays, S. A., and Kilgard, M. P. (2018). The interaction of pulse width and current intensity on the extent of cortical plasticity evoked by vagus nerve stimulation. *Brain Stimul.* 11, 271–277. doi: 10.1016/j.brs.2017.11.007

Lomarev, M., Denslow, S., Nahas, Z., Chae, J. H., George, M. S., and Bohning, D. E. (2002). Vagus nerve stimulation (VNS) synchronized BOLD fMRI suggests that VNS in depressed adults has frequency/dose dependent effects. *J. Psychiatr. Res.* 36, 219–227. doi: 10.1016/s0022-3956(02)00013-4

Mackay, T. W., and Andrews, P. L. (1983). A comparative study of the vagal innervation of the stomach in man and the ferret. *J. Anat.* 136(Pt 3), 449–481.

McAllen, R. M., Shafton, A. D., Bratton, B. O., Trevaks, D., and Furness, J. B. (2018). Calibration of thresholds for functional engagement of vagal A, B and C fiber groups in vivo. *Bioelectron. Med.* 1, 21–27. doi: 10.2217/bem-2017-0001

McAllen, R. M., and Spyer, K. M. (1978). Two types of vagal preganglionic motoneurones projecting to the heart and lungs. *J. Physiol.* 282, 353–364. doi: 10.1113/jphysiol.1978.sp012468

Mei, N., Condamin, M., and Boyer, A. (1980). The composition of the vagus nerve of the cat. *Cell Tissue Res.* 209, 423–431.

Merrill, D. R., Bikson, M., and Jefferys, J. G. (2005). Electrical stimulation of excitable tissue: design of efficacious and safe protocols. *J. Neurosci. Methods* 141, 171–198. doi: 10.1016/j.jneumeth.2004.10.020

Mortimer, J. T., and Bhadra, N. (2009). "Chapter 11 - fundamentals of electrical stimulation," in *Neuromodulation*, eds E. S. Krames, P. H. Peckham, and A. R. Rezai, (San Diego: Academic Press), 109–121. doi: 10.1016/b978-0-12-374248-3.00012-4

Mu, Q., Bohning, D. E., Nahas, Z., Walker, J., Anderson, B., Johnson, K. A., et al. (2004). Acute vagus nerve stimulation using different pulse widths produces varying brain effects. *Biol. Psychiatry* 55, 816–825. doi: 10.1016/j.biopsych.2003.12.004

Navas, M., Navarrete, E. G., Pascual, J. M., Carrasco, R., Nunez, J. A., Shakur, S. F., et al. (2010). Treatment of refractory epilepsy in adult patients with right-sided vagus nerve stimulation. *Epilepsy Res.* 90, 1–7. doi: 10.1016/j.eplepsyres.2010.04.007

Nemeroff, C. B., Mayberg, H. S., Krahl, S. E., McNamara, J., Frazer, A., Henry, T. R., et al. (2006). VNS therapy in treatment-resistant depression: clinical evidence and putative neurobiological mechanisms. *Neuropsychopharmacology* 31, 1345–1355. doi: 10.1038/sj.npp.1301082

Niederbichler, A. D., Papst, S., Claassen, L., Jokuszies, A., Steinstraesser, L., Hirsch, T., et al. (2009). Burn-induced organ dysfunction: vagus nerve stimulation attenuates organ and serum cytokine levels. *Burns* 35, 783–789. doi: 10.1016/j.burns.2008.08.023

Nuntaphum, W., Pongkan, W., Wongjaikam, S., Thummasorn, S., Tanajak, P., Khamseekaew, J., et al. (2018). Vagus nerve stimulation exerts cardioprotection against myocardial ischemia/reperfusion injury predominantly through its efferent vagal fibers. *Basic Res. Cardiol.* 113:22. doi: 10.1007/s00395-018-0683-0

Olofsson, P. S., Levine, Y. A., Caravaca, A., Chavan, S. S., Pavlov, V. A., Faltys, M., et al. (2015). Single-pulse and unidirectional electrical activation of the cervical vagus nerve reduces tumor necrosis factor in endotoxemia. *Bioelectron. Med.* 2, 37–42. doi: 10.15424/bioelectronmed.2015.00006

Onkka, P., Maskoun, W., Rhee, K. S., Hellyer, J., Patel, J., Tan, J., et al. (2013). Sympathetic nerve fibers and ganglia in canine cervical vagus nerves: localization and quantitation. *Heart Rhythm* 10, 585–591. doi: 10.1016/j.hrthm.2012.12.015

Osharina, V., Bagaev, V., Wallois, F., and Larnicol, N. (2006). Autonomic response and Fos expression in the NTS following intermittent vagal stimulation: importance of pulse frequency. *Auton. Neurosci.* 12, 72–80. doi: 10.1016/j.autneu.2006.03.011

O'Toole, M. F., Ardell, J. L., and Randall, W. C. (1986). Functional interdependence of discrete vagal projections to SA and AV nodes. *Am. J. Physiol.* 251(2 Pt 2), H398–H404.

Patel, Y. A., and Butera, R. J. (2018). Challenges associated with nerve conduction block using kilohertz electrical stimulation. *J. Neural. Eng.* 15:031002. doi: 10.1088/1741-2552/aaadc0

Patel, Y. A., Saxena, T., Bellamkonda, R. V., and Butera, R. J. (2017). Kilohertz frequency nerve block enhances anti-inflammatory effects of vagus nerve stimulation. *Sci. Rep.* 7:39810. doi: 10.1038/srep39810

Peclin, P., and Rozman, J. (2014). Alternative paradigm of selective vagus nerve stimulation tested on an isolated porcine vagus nerve. *Sci. World J.* 2014:310283. doi: 10.1155/2014/310283

Pisapia, J., and Baltuch, G. (2016). "Vagus nerve stimulation," in *Neuromodulation in Psychiatry*, eds C. Hamani, P. Holtzheimer, A. M. Lozano, and H. Mayberg, (Hoboken: John Wiley & Sons), 325–334.

Planitzer, U., Hammer, N., Bechmann, I., Glatzner, J., Loffler, S., Mobius, R., et al. (2017). Positional relations of the cervical vagus nerve revisited. *Neuromodulation* 20, 361–368. doi: 10.1111/ner.12557

Powley, T. L., Prechtl, J. C., Fox, E. A., and Berthoud, H. R. (1983). Anatomical considerations for surgery of the rat abdominal vagus: distribution, paraganglia and regeneration. *J. Auton. Nerv. Syst.* 9, 79–97. doi: 10.1016/0165-1838(83)90133-9

Prechtl, J. C., and Powley, T. L. (1990). The fiber composition of the abdominal vagus of the rat. *Anat. Embryol.* 181, 101–115.

Pruitt, D. T., Schmid, A. N., Kim, L. J., Abe, C. M., Trieu, J. L., Choua, C., et al. (2016). Vagus nerve stimulation delivered with motor training enhances recovery of function after traumatic brain injury. *J. Neurotrauma.* 33, 871–879. doi: 10.1089/neu.2015.3972

Qing, K. Y., Wasilczuk, K. M., Ward, M. P., Phillips, E. H., Vlachos, P. P., Goergen, C. J., et al. (2018). B fibers are the best predictors of cardiac activity during Vagus nerve stimulation. *Bioelectron. Med.* 4, 5.

Rosas-Ballina, M., Ochani, M., Parrish, W. R., Ochani, K., Harris, Y. T., Huston, J. M., et al. (2008). Splenic nerve is required for cholinergic antiinflammatory pathway control of TNF in endotoxemia. *Proc. Natl. Acad. Sci. U.S.A.* 105, 11008–11013. doi: 10.1073/pnas.0803237105

Ruffoli, R., Giorgi, F. S., Pizzanelli, C., Murri, L., Paparelli, A., and Fornai, F. (2011). The chemical neuroanatomy of vagus nerve stimulation. *J. Chem. Neuroanat.* 42, 288–296. doi: 10.1016/j.jchemneu.2010.12.002

Rush, A. J., George, M. S., Sackeim, H. A., Marangell, L. B., Husain, M. M., Giller, C., et al. (2000). Vagus nerve stimulation (VNS) for treatment-resistant depressions: a multicenter study**see accompanying editorial, in this issue. *Biol. Psychiatry* 47, 276–286. doi: 10.1016/s0006-3223(99)00304-2

Rush, A. J., Marangell, L. B., Sackeim, H. A., George, M. S., Brannan, S. K., Davis, S. M., et al. (2005a). Vagus nerve stimulation for treatment-resistant depression: a randomized, controlled acute phase trial. *Biol. Psychiatry* 58, 347–354. doi: 10.1016/j.biopsych.2005.05.025

Rush, A. J., Sackeim, H. A., Marangell, L. B., George, M. S., Brannan, S. K., Davis, S. M., et al. (2005b). Effects of 12 months of vagus nerve stimulation in treatment-resistant depression: a naturalistic study. *Biol. Psychiatry* 58, 355–363. doi: 10.1016/j.biopsych.2005.05.024

Schnitzlein, H. N., Rowe, L. C., and Hoffman, H. H. (1958). The myelinated component of the vagus nerves in man. *Anat. Rec.* 131, 649–667. doi: 10.1002/ar.1091310404

Seki, A., Green, H. R., Lee, T. D., Hong, L., Tan, J., Vinters, H. V., et al. (2014). Sympathetic nerve fibers in human cervical and thoracic vagus nerves. *Heart Rhythm* 11, 1411–1417. doi: 10.1016/j.hrthm.2014.04.032

Silverman, H. A., Stiegler, A., Tsaava, T., Newman, J., Steinberg, B. E., Masi, E. B., et al. (2018). Standardization of methods to record Vagus nerve activity in mice. *Bioelectron. Med.* 4:3.

Somann, J. P., Albors, G. O., Neihouser, K. V., Lu, K. H., Liu, Z., Ward, M. P., et al. (2018). Chronic cuffing of cervical vagus nerve inhibits efferent fiber integrity in rat model. *J. Neural. Eng.* 15:036018. doi: 10.1088/1741-2552/aaa039

Stauss, H. M. (2017). Differential hemodynamic and respiratory responses to right and left cervical vagal nerve stimulation in rats. *Physiol. Rep.* 5, e13244. doi: 10.14814/phy2.13244

Thil, M.-A., Duy, D. T., Colin, I. M., and Delbeke, J. (2007). Time course of tissue remodelling and electrophysiology in the rat sciatic nerve after spiral cuff electrode implantation. *J. Neuroimmunol.* 185, 103–114. doi: 10.1016/j.jneuroim.2007.01.021

Tracey, K. J. (2002). The inflammatory reflex. *Nature* 420, 853–859. doi: 10.1038/nature01321

Tyler, D. J., and Durand, D. M. (2003). Chronic response of the rat sciatic nerve to the flat interface nerve electrode. *Ann. Biomed. Eng.* 31, 633–642. doi: 10.1114/1.1569263

Van Leusden, J. W., Sellaro, R., and Colzato, L. S. (2015). Transcutaneous vagal nerve stimulation (tVNS): a new neuromodulation tool in healthy humans? *Front. Psychol.* 6:102.

Verlinden, T. J., Rijkers, K., Hoogland, G., and Herrler, A. (2015). Morphology of the human cervical vagus nerve: implications for vagus nerve stimulation treatment. *Acta Neurol. Scand.* 133, 173–182. doi: 10.1111/ane.12462

Vuckovic, A., Rijkhoff, N. J., and Struijk, J. J. (2004). Different pulse shapes to obtain small fiber selective activation by anodal blocking–a simulation study. *IEEE Trans. Biomed. Eng.* 51, 698–706. doi: 10.1109/tbme.2004.826663

Vuckovic, A., Tosato, M., and Struijk, J. J. (2008). A comparative study of three techniques for diameter selective fiber activation in the vagal nerve: anodal block, depolarizing prepulses and slowly rising pulses. *J. Neural. Eng.* 5, 275–286. doi: 10.1088/1741-2560/5/3/002

Wheless, J. W., Gienapp, A. J., and Ryvlin, P. (2018). Vagus nerve stimulation (VNS) therapy update. *Epilepsy Behav.* 88s, 2–10. doi: 10.1016/j.yebeh.2018.06.032

Woodbury, D. M., and Woodbury, J. W. (1990). Effects of Vagal stimulation on experimentally induced seizures in rats. *Epilepsia* 31, S7–S19.

Yoo, P. B., Liu, H., Hincapie, J. G., Ruble, S. B., Hamann, J. J., and Grill, W. M. (2016). Modulation of heart rate by temporally patterned vagus nerve stimulation in the anesthetized dog. *Physiol. Rep.* 4:e12689. doi: 10.14814/phy2.12689

Yoo, P. B., Lubock, N. B., Hincapie, J. G., Ruble, S. B., Hamann, J. J., and Grill, W. M. (2013). High-resolution measurement of electrically-evoked vagus nerve activity in the anesthetized dog. *J. Neural. Eng.* 10:026003. doi: 10.1088/1741-2560/10/2/026003

Yoshida, K., and Riso, R. (2004). "Peripheral nerve recording electrodes and techniques," in *Neuroprosthetics - Theory And Practice*, eds K. W. Horch, and G. S. Dhillon, (Singapore: World Scientific), 683–744. doi: 10.1142/9789812561763_0021

Yuan, H., and Silberstein, S. D. (2016). Vagus nerve and vagus nerve stimulation, a comprehensive review: part I. *Headache* 56, 71–78. doi: 10.1111/head.12647

Zabara, J. (1992). Inhibition of experimental seizures in canines by repetitive vagal stimulation. *Epilepsia* 33, 1005–1012. doi: 10.1111/j.1528-1157.1992.tb01751.x

Zhang, Y., Popovic, Z. B., Bibevski, S., Fakhry, I., Sica, D. A., Van Wagoner, D. R., et al. (2009). Chronic vagus nerve stimulation improves autonomic control and attenuates systemic inflammation and heart failure progression in a canine high-rate pacing model. *Circ. Heart Fail.* 2, 692–699. doi: 10.1161/CIRCHEARTFAILURE.109.873968

Conflict of Interest Statement: YL is an employee of SetPoint Medical Corporation, a company that is developing bioelectronic devices to target the vagus nerve in humans.

The remaining authors declare that the research was conducted in the absence of any commercial or financial relationships that could be construed as a potential conflict of interest.

frontiers in Neuroscience

MINI REVIEW
published: 06 September 2019
doi: 10.3389/fnins.2019.00952

Modulation of Neural Activity for Myelination in the Central Nervous System

*Elliot H. Choi[1,2], Agata Blasiak[3], Joonho Lee[4] and In Hong Yang[5]**

[1] Department of Pharmacology, School of Medicine, Case Western Reserve University, Cleveland, OH, United States, [2] Department of Ophthalmology, School of Medicine, Gavin Herbert Eye Institute, University of California, Irvine, Irvine, CA, United States, [3] Department of Biomedical Engineering, National University of Singapore, Singapore, Singapore, [4] School of Medicine and Dentistry, University of Rochester, Rochester, NY, United States, [5] Department of Mechanical Engineering and Engineering Science, Center for Biomedical Engineering and Science, University of North Carolina at Charlotte, Charlotte, NC, United States

Electrical stimulation has been playing a significant role in revealing various functions and mechanisms of the nervous system. It is no different for myelination, a process in which oligodendrocytes in the central nervous system (CNS) or Schwann Cells in the peripheral nerve system (PNS) wrap around axons to provide an insulating layer *in vitro* and *in vivo*. It has been widely recognized that the myelin sheath accelerates axon signal conduction and provides neuroprotection. Recent studies have begun to reveal its role in plasticity. The major mechanism that enables this process is activity-dependent myelination – the phenomenon where neuronal activity supports oligodendrocyte maturation and myelin sheath formation. In light of recent discoveries, a better understanding of this phenomenon has a potential to provide therapeutic targets for not only demyelinating diseases, but also psychiatric disorders. There is a growing need for experimental platforms capable of dissecting the effect of neural activity on myelination in health and disease. The effect of neural activity is commonly studied by comparing the myelination levels in cultures with neurons of low and high activity. Electrical stimulation is particularly well suited as a method of inducing neural activity in these systems. In this review, we describe *in vitro* platforms for studying activity-dependent myelination, which utilize neuron stimulation via electrical field. We also discuss stimulation profiles, as well as the alternatives to electrical stimulation in the context of regular, compartmentalized, and organotypic co-cultures.

Keywords: electrical stimulation, optogenetic stimulation, magnetic stimulation, myelination, neural activity, oligodendrocyte, Schwann cells

OPEN ACCESS

Edited by:
Alberto Priori,
University of Milan, Italy

Reviewed by:
Maria Teresa Fiorenza,
Sapienza University of Rome, Italy
Takashi D. Y. Kozai,
University of Pittsburgh, United States

***Correspondence:**
In Hong Yang
inhong.yang@uncc.edu;
iyangbio@gmail.com

Specialty section:
This article was submitted to Neural Technology, a section of the journal Frontiers in Neuroscience

Received: *01 April 2019*
Accepted: *23 August 2019*
Published: *06 September 2019*

Citation:
Choi EH, Blasiak A, Lee J and Yang IH (2019) Modulation of Neural Activity for Myelination in the Central Nervous System. Front. Neurosci. 13:952. doi: 10.3389/fnins.2019.00952

INTRODUCTION

Neuromodulation is an emerging technique for treating neurological diseases and psychiatric disorders in the field of medicine. This technique was first introduced by Merton and Morton (1980) who employed a high-voltage electrical stimulator to stimulate the primary cortex in humans through the intact scalp. Upon stimulation, a weak muscle twitch on the contralateral hand was

Abbreviations: BDNF, brain-derived neurotrophic factor; CNS, central nervous system; DRG, dorsal root ganglion; LIF, leukemia inhibitory factor; OPC, oligodendrocyte progenitor cell; PNS, peripheral nervous system; TES, transcranial electrical stimulation; TMS, transcranial magnetic stimulation; TTX, tetrodotoxin.

generated (Merton and Morton, 1980). It became apparent that the stimulation could activate muscle fibers by inducing upper motor neuron activities. This observation provided the evidence that non-invasive brain stimulation would be useful in both research and medicine. Over the past 30 years, numerous clinical studies have been performed with different techniques including transcranial electrical stimulation (TES) and transcranial magnetic stimulation (TMS). TES applies constant, oscillating or randomly alternating currents through two or more electrodes to modulate brain activity. The predominant direction of the current is radial to the brain surface. For TMS, stimulation is produced by a brief, high-intensity magnetic field, which is generated by an electric current passing through a magnetic coil. In contrast to TES, the predominant direction of the current is tangential to the brain surface. In recent years the application of neuromodulation has been extensively expanding as more studies demonstrate its therapeutic potential for treating a host of maladies, including major depressive disorders, obsessive-compulsive disorder, stroke, epilepsy, Parkinson's disease, and Alzheimer's disease (Tergau et al., 1999; George et al., 2010; Khedr et al., 2010; Mantovani et al., 2010; Rabey et al., 2013; Torres et al., 2015). The therapeutic effect mainly results from modulating neural activity. Low frequency stimulation reduces neural activity while high frequency stimulation excites neural activity (Hallett, 2007). It is clear that the effect of electrical stimulation is not limited to neurons. Multiple studies have suggested that electrical stimulation affects oligodendrocytes or Schwann cells which support neural conduction in the nervous system.

The nervous system of vertebrates requires rapid propagation of action potentials to integrate signals from the external environment. This rapid propagation is possible because of the myelination of axons, a process by which oligodendrocytes in the central nervous system (CNS) or Schwann cells in the peripheral nervous system wrap the axon. During the embryonic period, myelination begins with the proliferation of oligodendrocytes and Schwann cells followed by the establishment of glia-axon contacts (Jessen and Mirsky, 2005; Nave and Werner, 2014). Upon contact with the axonal membrane, OPCs and newly differentiated oligodendrocytes extend and retract their processes (Kirby et al., 2006). When contact is established, several molecular rearrangements result in a polarization of myelinating cells toward the axonal membrane (Baron and Hoekstra, 2010; Ozcelik et al., 2010; Nave and Werner, 2014). Longitudinal expansion of myelin segments coincides with secondary axon elongation during postnatal development (Hildebrand et al., 1993, 1994). After the peak of myelination in early life, remodeling of mature myelin membranes slows down. However, OPCs continue to proliferate and differentiate (Young et al., 2013) while Schwann cells retain high plasticity (Young et al., 2013; Jessen et al., 2015).

The mature myelin sheath is interrupted at regular intervals by unmyelinated regions where the membrane of the axon is exposed to the extracellular space. This arrangement of myelination allows for the generation of action potentials at short, unmyelinated axonal segments, and increases the velocity at which the action potentials are conducted. As such, small changes in myelin structure can lead to substantial changes in conduction velocity (Waxman and Bennett, 1972). In addition, myelin provides metabolic and trophic factors, which play a critical role in development of axons and viability of neurons (Wilkins et al., 2001, 2003; Funfschilling et al., 2012). Therefore, developmental failure of myelination in the nervous system in early life or loss of myelin have debilitating consequences in the remaining axons. It has been intriguing to examine whether modulating the activity of axons could induce myelination and hold therapeutic promise in demyelinating diseases. Interestingly, converging evidence has demonstrated that neural activity promotes oligodendrogenesis and myelination (Demerens et al., 1996; Stevens et al., 2002; Gibson et al., 2014; Mitew et al., 2018). Early support for this hypothesis emerged from the finding that transection of the developing optic nerve by axotomy or blockade of activity in the developing optic nerve by tetrodotoxin (TTX) dramatically reduces the rate of OPC proliferation (Barres and Raff, 1993) and the degree of optic nerve myelination (Demerens et al., 1996). In accordance with these studies, it was demonstrated that increasing neural activity with α-scorpion toxin enhances myelination (Demerens et al., 1996). Much of the *in vitro* work investigating the mechanisms by which neural activity regulates myelination has focused on the instructive roles of neurotransmitters and soluble factors. For instance, several studies have suggested that glutamate or acetylcholine released from depolarized neurons induces the synthesis of myelin (Gallo et al., 1996; Gudz et al., 2006; De Angelis et al., 2012). In dorsal root ganglion (DRG) neurons and OPC co-culture, adenosine was released from the neurons in an activity-dependent manner, promoting OPC differentiation, and myelination (Stevens et al., 2002). Moreover, brain-derived neurotrophic factor (BDNF) released from neurons has been shown to enhance myelin formation from oligodendrocytes and Schwann cells (Wan et al., 2010; Xiao et al., 2010). Building on these studies, development of new technologies has uncovered a rich experimental landscape for understanding neural activity-dependent myelination. Specifically, the compartmentalized microfluidic platform has become a valuable tool due to its applicability and flexibility (Campenot, 1977; Taylor et al., 2005; Wu et al., 2005; Park et al., 2006, 2014; Cox et al., 2008). The integration of co-cultures in the compartmentalized platform has enabled the physical separation of axons and oligodendrocytes from the neuronal soma (Yang et al., 2012; Malone et al., 2013; Lee et al., 2016; Prasad et al., 2017; Blasiak et al., 2018). In the present review, we discuss the role of neural activity in myelination and induction of myelination *in vitro* through stimulation of neurons with different technologies.

EARLY STUDIES ELUCIDATING THE ROLE OF AXONS IN MYELINATION

Oligodendrocytes in the CNS have the unique ability to form myelin. Although there is close interaction between oligodendrocytes and neurons, early evidence that neurons

directly influence the formation of myelin was lacking. Several studies have suggested that cultured oligodendrocytes express proteins necessary for myelination and develop myelin-like structures even in the absence of neurons (Mirsky et al., 1980; Dubois-Dalcq et al., 1986). Moreover, oligodendrocytes isolated from rodent brain could extend their tips to form myelin-like structures (Sarlieve et al., 1980; Szuchet et al., 1986). However, contradictory lines of evidence called into question the validity of myelination in the absence of axons. Analysis of the myelin-like structures by electron microscopy demonstrated that these structures were not compactly organized compared to the myelin that wrap axons (Althaus et al., 1984; Lubetzki et al., 1993). Ultrastructural analysis showed that the processes of oligodendrocytes folded up on themselves rather than winding around themselves. Moreover, primary oligodendrocytes cultured with astrocytes and neurons specifically myelinated axons but not astrocyte processes or dendrites. This exclusive myelination of axons suggested that a molecular cue from axons may recruit oligodendrocyte processes (Lubetzki et al., 1993). Later, it became evident that the factors released from axons play a trophic role in the proliferation of oligodendrocyte progenitor cells (OPCs) and subsequent differentiation (Wood and Bunge, 1986; Lubetzki et al., 1992). Following axotomy of the optic nerve, oligodendrocytes clustered without their longitudinal orientation, developed fewer processes, and eventually failed to form myelin in the transected optic nerve (Ueda et al., 1999). These results suggested that viable axons are essential for three-dimensional organization of oligodendrocytes and myelination. Taken together, these pioneer reports strongly argued that axons play a role in myelination. However, conclusive evidence of whether neural activity could influence myelination remained elusive.

INDUCTION OF MYELINATION BY NEURAL ACTIVITY

Myelination is a finely orchestrated process that involves interactions of oligodendrocytes or Schwann cells with other cells through extracellular signaling and physical contacts. Thus, it would be logical to speculate that these myelinating cells synchronize their differentiation according to neural development and activity. In the 1960s, Gyllensten and Malmfors introduced the idea that neural activity could influence the function of oligodendrocytes. Their study demonstrated that mice reared in the dark developed fewer myelinated axons in the optic nerve compared with control mice (Gyllensten and Malmfors, 1963). Lack of myelination was also observed in the optic nerve of blind rats, whereas myelination was accelerated in the optic nerve by pre-mature eye opening (Tauber et al., 1980; Omlin, 1997). These findings were further supported by a similar study showing that blockade of action potentials with 10^{-6} M TTX inhibited myelination, whereas increase in duration and frequency of action potentials with 10^{-9} M α-scorpion toxin enhanced myelination (Demerens et al., 1996). The idea that neural activity can induce myelination has been further advanced by a number of recent studies that employed powerful genetic and imaging tools. For instance, channelrhodopsin 2 (ChR2) has been utilized as an optogenetic tool to manipulate neural activity since its discovery. ChR2 is a light-gated cation channel derived from photoreceptors in microalgae (Nagel et al., 2003). Because ChR2 can depolarize neurons within milliseconds with 470-nm light, expression of ChR2 in a specific group of neurons allows spatial and temporal regulation of neuronal activity (Boyden et al., 2005; Arenkiel et al., 2007). Optogenitic stimulation (cycles of 30 s on, 2 min off, 10 min/d for 7 days) of the premotor circuit in Thy1:ChR2 mice resulted in newly generated oligodendrocytes and increased thickness of the associated myelin sheath (Gibson et al., 2014). In accordance with this result, pharmacogenetic stimulation of somatosensory axons in the mouse brain almost doubled the number of mature oligodendrocytes capable of myelination (Mitew et al., 2018). Conversely, the study also demonstrated that attenuation of neural activity reduces myelination. Neural activity modulates myelination not only by directly stimulating oligodendrocytes but also by activating microglia and astrocytes (Ishibashi et al., 2006). Studies in both visual and auditory systems have demonstrated that neural activity induces the activation of microglia (Tremblay et al., 2010; Rosskothen-Kuhl et al., 2018). The activated microglia could promote myelination through clearance of the cellular debris that could potentially to interfere with myelination processes (Kotter et al., 2006; Church et al., 2017). In line with this, *Cx3cr1*$^{-/-}$ mice exhibiting severe deficiency of microglia phagocytosis have impaired myelination (Lampron et al., 2015). Microglia also directly regulate proliferation, differentiation, and migration of OPCs (Miron, 2017). Taken together, recent studies strongly suggest that neural activity potentiates myelination. In line with the *in vivo* studies, several studies have elucidated potential molecular mechanisms mediating neural activity-dependent myelination. For instance, ATP released from DRGs in an activity-dependent manner is hydrolyzed to adenosine. Subsequently, adenosine binds to adenosine receptors on the OPC and promotes myelination (Stevens et al., 2002). There is also mounting evidence that neural activity triggers release of BDNF from axons and microglia (Trang et al., 2009; Parkhurst et al., 2013), which can subsequently induce myelination formation through the TrkB/Erk signaling pathway (Wan et al., 2010; Xiao et al., 2010; Ishii et al., 2012, 2013). Leukemia inhibitory factor (LIF) released from astrocytes in response to neural activity also appears to promote myelination (Ishibashi et al., 2006). Thus, it is clear that neural activity is an external regulator of myelination with important functional implications.

ENHANCEMENT OF MYELINATION FOLLOWING MODULATION OF NEURAL ACTIVITY *IN VITRO*

The therapeutic effect of TES and TMS has been attributed to its ability to modulate neural activity, which provides hope that TES and TMS can restore myelination via neural activity modulation. Although studies conducted over the past

two decades collectively demonstrated that neural activity promotes myelination, a more complete understanding of activity-dependent myelination is essential for the development of activity-based therapies to treat demyelinating diseases. Moreover, there are very limited findings regarding the response of oligodendrocytes to TES or TMS. It is critical to carefully examine the influence of TES or TMS on oligodendrocytes, especially when they are simultaneously stimulated with neurons. To address the cellular and molecular mechanisms, *in vitro* models allowing electrical or optogenetic stimulation in neuron/oligodendrocyte co-culture have been developed (Ishibashi et al., 2006; Yang et al., 2012; Lee et al., 2016, 2017; Blasiak et al., 2018). These models benefit from a compartmentalized microfluidic platform which allows the isolation of neuronal cell bodies from axons and oligodendrocytes. The features of the compartmentalized microfluidic platform were leveraged for myelination studies to more accurately mimic the *in vivo* microenvironment, to stimulate neurons exclusively and to study the effect of a focal stimulation on different subcellular locations. When 10 Hz electrical stimulation was applied to DRGs for 7 days (1 h/day), the formation of myelin segments was increased by fivefold compared to the non-stimulated groups (Yang et al., 2012). The formation of myelin was also enhanced following electrical stimulation of DRGs (10 Hz, 1 h/day for 7 days) prior to introducing oligodendrocytes in the culture (Malone et al., 2013). This study also demonstrated 10 Hz to be the most effective stimulation frequency in the range of 1 to 100 Hz, and 7 days to be the most effective length of the stimulation course. These findings were consistent with previous studies showing an active role of neurons in myelination of their axons. The optimized stimulation parameters were also used to demonstrate that electrical stimulation enhances myelination independent of subcellular location (Lee et al., 2017). When electrical stimulation (10 Hz, 1 h/day for 3–14 days) was delivered to soma, proximal axons, or distal axons, the degree of myelination was similar regardless of the stimulation site, but higher than in non-stimulated neurons (Lee et al., 2017). Similarly, subcellular optogenetic stimulation was applied to study the effect of neural stimulation on myelination (Lee et al., 2016; Blasiak et al., 2018). In line with previous studies, focal stimulation (10 Hz, 1 h/day for 3–14 days) on neurons was sufficient to promote myelination of axons. Based on these findings, it is reasonable to speculate that neural stimulation of distal axons innervating muscles could be as effective as neural stimulation of soma in the spinal cord as a treatment for demyelinating diseases.

PERSPECTIVES, UNANSWERED QUESTIONS AND CONCLUDING REMARKS

In summary, we have provided an overview of the role of neural activity in myelination, with an emphasis on myelination via modulation of neural activity. The pioneering efforts in the field have unraveled the complex interactions between oligodendrocytes and neurons. Particularly, recent *in vivo* studies employing optogenetics and pharmacogenetics have provided strong evidence that stimulation of neural activity promotes myelination (Gibson et al., 2014; Mitew et al., 2018). Interestingly, stimulation of demyelinated axons could enhance oligodendrocyte differentiation and remyelination (Ortiz et al., 2019). While the role of neural activity in myelin formation has become apparent, many mechanistic details remain to be filled in through further investigations. Perhaps most important is the identification of factors involved in activity-dependent myelination, which will enable choosing targets for remyelination and lesion repair. Because stimulation of neural activity could enhance myelination in co-culture of neurons and OPCs, molecular mechanisms linking neural activity and myelin formation should be further studied with *in vitro* models.

As transcranial electrical stimulation and transcranial magnetic stimulation allow modulation of neuronal firing pattern, they could induce activity-dependent myelination. However, it is still unclear how the interaction between oligodendrocytes and neurons will be influenced when both cell types are simultaneously stimulated. It is conceivable that external stimuli might change the contents of soluble factors released from both oligodendrocytes and neurons, which in turn activate numerous signaling pathways. In addition, the external stimuli could abruptly change the cellular membrane potential of both oligodendrocytes and neurons, which does not occur in the brain. The stimuli parameters, such as duration, current input, and frequency, need to be optimized for each disease condition. Therefore, it is crucial to carefully evaluate the advantages and disadvantages of TES and TMS using well-established models. In this review, we introduce *in vitro* models employing the compartmentalized microfluidic platform. Despite their unique advantages, these models also have limitations such as gliosis following electrical stimulation and requirement of a transient transfection prior to optogenetic stimulation (Williams et al., 1999; Zhong and Bellamkonda, 2008). Regarding this, there is an urgent need for the development of new tools and models that will become useful in investigating activity-dependent myelination. With a clearer understanding of molecular mechanisms, the modulation of neural activity has the potential to become as a novel therapeutic strategy for treating demyelinating diseases.

AUTHOR CONTRIBUTIONS

All authors listed have made a substantial, direct and intellectual contribution to the work, and approved it for publication.

FUNDING

EC was supported by the Medical Scientist Training Program T32GM007250 and Predoctoral Training in Molecular Therapeutics Program T32GM008803.

REFERENCES

Althaus, H. H., Montz, H., Neuhoff, V., and Schwartz, P. (1984). Isolation and cultivation of mature oligodendroglial cells. *Naturwissenschaften* 71, 309–315. doi: 10.1007/bf00396614

Arenkiel, B. R., Peca, J., Davison, I. G., Feliciano, C., Deisseroth, K., Augustine, G. J., et al. (2007). In vivo light-induced activation of neural circuitry in transgenic mice expressing channelrhodopsin-2. *Neuron* 54, 205–218. doi: 10.1016/j.neuron.2007.03.005

Baron, W., and Hoekstra, D. (2010). On the biogenesis of myelin membranes: sorting, trafficking and cell polarity. *FEBS Lett.* 584, 1760–1770. doi: 10.1016/j.febslet.2009.10.085

Barres, B. A., and Raff, M. C. (1993). Proliferation of oligodendrocyte precursor cells depends on electrical activity in axons. *Nature* 361, 258–260. doi: 10.1038/361258a0

Blasiak, A., Nag, S., and Yang, I. H. (2018). Subcellular optogenetic stimulation platform for studying activity-dependent axon myelination in vitro. *Methods Mol. Biol.* 1791, 207–224. doi: 10.1007/978-1-4939-7862-5_16

Boyden, E. S., Zhang, F., Bamberg, E., Nagel, G., and Deisseroth, K. (2005). Millisecond-timescale, genetically targeted optical control of neural activity. *Nat. Neurosci.* 8, 1263–1268. doi: 10.1038/nn1525

Campenot, R. B. (1977). Local control of neurite development by nerve growth factor. *Proc. Natl. Acad. Sci. U.S.A.* 74, 4516–4519. doi: 10.1073/pnas.74.10.4516

Church, J. S., Milich, L. M., Lerch, J. K., Popovich, P. G., and Mctigue, D. M. (2017). E6020, a synthetic TLR4 agonist, accelerates myelin debris clearance, chwann cell infiltration, and remyelination in the rat spinal cord. *Glia* 65, 883–899. doi: 10.1002/glia.23132

Cox, L. J., Hengst, U., Gurskaya, N. G., Lukyanov, K. A., and Jaffrey, S. R. (2008). Intra-axonal translation and retrograde trafficking of CREB promotes neuronal survival. *Nat. Cell Biol.* 10, 149–159. doi: 10.1038/ncb1677

De Angelis, F., Bernardo, A., Magnaghi, V., Minghetti, L., and Tata, A. M. (2012). Muscarinic receptor subtypes as potential targets to modulate oligodendrocyte progenitor survival, proliferation, and differentiation. *Dev. Neurobiol.* 72, 713–728. doi: 10.1002/dneu.20976

Demerens, C., Stankoff, B., Logak, M., Anglade, P., Allinquant, B., Couraud, F., et al. (1996). Induction of myelination in the central nervous system by electrical activity. *Proc. Natl. Acad. Sci. U.S.A.* 93, 9887–9892. doi: 10.1073/pnas.93.18.9887

Dubois-Dalcq, M., Behar, T., Hudson, L., and Lazzarini, R. A. (1986). Emergence of three myelin proteins in oligodendrocytes cultured without neurons. *J. Cell Biol.* 102, 384–392. doi: 10.1083/jcb.102.2.384

Funfschilling, U., Supplie, L. M., Mahad, D., Boretius, S., Saab, A. S., Edgar, J., et al. (2012). Glycolytic oligodendrocytes maintain myelin and long-term axonal integrity. *Nature* 485, 517–521. doi: 10.1038/nature11007

Gallo, V., Zhou, J. M., Mcbain, C. J., Wright, P., Knutson, P. L., and Armstrong, R. C. (1996). Oligodendrocyte progenitor cell proliferation and lineage progression are regulated by glutamate receptor-mediated K+ channel block. *J. Neurosci.* 16, 2659–2670. doi: 10.1523/jneurosci.16-08-02659.1996

George, M. S., Lisanby, S. H., Avery, D., Mcdonald, W. M., Durkalski, V., Pavlicova, M., et al. (2010). Daily left prefrontal transcranial magnetic stimulation therapy for major depressive disorder: a sham-controlled randomized trial. *Arch. Gen. Psychiatry* 67, 507–516. doi: 10.1001/archgenpsychiatry.2010.46

Gibson, E. M., Purger, D., Mount, C. W., Goldstein, A. K., Lin, G. L., Wood, L. S., et al. (2014). Neuronal activity promotes oligodendrogenesis and adaptive myelination in the mammalian brain. *Science* 344, 1252304. doi: 10.1126/science.1252304

Gudz, T. I., Komuro, H., and Macklin, W. B. (2006). Glutamate stimulates oligodendrocyte progenitor migration mediated via an alphav integrin/myelin proteolipid protein complex. *J. Neurosci.* 26, 2458–2466. doi: 10.1523/jneurosci.4054-05.2006

Gyllensten, L., and Malmfors, T. (1963). Myelinization of the optic nerve and its dependence on visual function–a quantitative investigation in mice. *J. Embryol. Exp. Morphol.* 11, 255–266.

Hallett, M. (2007). Transcranial magnetic stimulation: a primer. *Neuron* 55, 187–199. doi: 10.1016/j.neuron.2007.06.026

Hildebrand, C., Bowe, C. M., and Remahl, I. N. (1994). Myelination and myelin sheath remodelling in normal and pathological PNS nerve fibres. *Prog. Neurobiol.* 43, 85–141. doi: 10.1016/0301-0082(94)90010-8

Hildebrand, C., Remahl, S., Persson, H., and Bjartmar, C. (1993). Myelinated nerve fibres in the CNS. *Prog. Neurobiol.* 40, 319–384. doi: 10.1016/0301-0082(93)90015-k

Ishibashi, T., Dakin, K. A., Stevens, B., Lee, P. R., Kozlov, S. V., Stewart, C. L., et al. (2006). Astrocytes promote myelination in response to electrical impulses. *Neuron* 49, 823–832. doi: 10.1016/j.neuron.2006.02.006

Ishii, A., Furusho, M., and Bansal, R. (2013). Sustained activation of ERK1/2 MAPK in oligodendrocytes and schwann cells enhances myelin growth and stimulates oligodendrocyte progenitor expansion. *J. Neurosci.* 33, 175–186. doi: 10.1523/JNEUROSCI.4403-12.2013

Ishii, A., Fyffe-Maricich, S. L., Furusho, M., Miller, R. H., and Bansal, R. (2012). ERK1/ERK2 MAPK signaling is required to increase myelin thickness independent of oligodendrocyte differentiation and initiation of myelination. *J. Neurosci.* 32, 8855–8864. doi: 10.1523/JNEUROSCI.0137-12.2012

Jessen, K. R., and Mirsky, R. (2005). The origin and development of glial cells in peripheral nerves. *Nat. Rev. Neurosci.* 6, 671–682. doi: 10.1038/nrn1746

Jessen, K. R., Mirsky, R., and Lloyd, A. C. (2015). Schwann cells: development and role in nerve repair. *Cold Spring Harb. Perspect. Biol.* 7:a020487. doi: 10.1101/cshperspect.a020487

Khedr, E. M., Etraby, A. E., Hemeda, M., Nasef, A. M., and Razek, A. A. (2010). Long-term effect of repetitive transcranial magnetic stimulation on motor function recovery after acute ischemic stroke. *Acta Neurol. Scand.* 121, 30–37. doi: 10.1111/j.1600-0404.2009.01195.x

Kirby, B. B., Takada, N., Latimer, A. J., Shin, J., Carney, T. J., Kelsh, R. N., et al. (2006). In vivo time-lapse imaging shows dynamic oligodendrocyte progenitor behavior during zebrafish development. *Nat. Neurosci.* 9, 1506–1511. doi: 10.1038/nn1803

Kotter, M. R., Li, W. W., Zhao, C., and Franklin, R. J. (2006). Myelin impairs CNS remyelination by inhibiting oligodendrocyte precursor cell differentiation. *J. Neurosci.* 26, 328–332. doi: 10.1523/jneurosci.2615-05.2006

Lampron, A., Larochelle, A., Laflamme, N., Prefontaine, P., Plante, M. M., Sanchez, M. G., et al. (2015). Inefficient clearance of myelin debris by microglia impairs remyelinating processes. *J. Exp. Med.* 212, 481–495. doi: 10.1084/jem.20141656

Lee, H. U., Blasiak, A., Agrawal, D. R., Loong, D. T. B., Thakor, N. V., All, A. H., et al. (2017). Subcellular electrical stimulation of neurons enhances the myelination of axons by oligodendrocytes. *PLoS One* 12:e0179642. doi: 10.1371/journal.pone.0179642

Lee, H. U., Nag, S., Blasiak, A., Jin, Y., Thakor, N., and Yang, I. H. (2016). Subcellular Optogenetic stimulation for activity-dependent myelination of axons in a novel microfluidic compartmentalized platform. *ACS Chem. Neurosci.* 7, 1317–1324. doi: 10.1021/acschemneuro.6b00157

Lubetzki, C., Demerens, C., Anglade, P., Villarroya, H., Frankfurter, A., Lee, V. M., et al. (1993). Even in culture, oligodendrocytes myelinate solely axons. *Proc. Natl. Acad. Sci. U.S.A.* 90, 6820–6824. doi: 10.1073/pnas.90.14.6820

Lubetzki, C., Goujet-Zalc, C., Demerens, C., Danos, O., and Zalc, B. (1992). Clonal segregation of oligodendrocytes and astrocytes during in vitro differentiation of glial progenitor cells. *Glia* 6, 289–300. doi: 10.1002/glia.440060407

Malone, M., Gary, D., Yang, I. H., Miglioretti, A., Houdayer, T., Thakor, N., et al. (2013). Neuronal activity promotes myelination via a cAMP pathway. *Glia* 61, 843–854. doi: 10.1002/glia.22476

Mantovani, A., Simpson, H. B., Fallon, B. A., Rossi, S., and Lisanby, S. H. (2010). Randomized sham-controlled trial of repetitive transcranial magnetic stimulation in treatment-resistant obsessive-compulsive disorder. *Int. J. Neuropsychopharmacol.* 13, 217–227. doi: 10.1017/S1461145709990435

Merton, P. A., and Morton, H. B. (1980). Stimulation of the cerebral cortex in the intact human subject. *Nature* 285:227. doi: 10.1038/285227a0

Miron, V. E. (2017). Microglia-driven regulation of oligodendrocyte lineage cells, myelination, and remyelination. *J. Leukoc. Biol.* 101, 1103–1108. doi: 10.1189/jlb.3RI1116-494R

Mirsky, R., Winter, J., Abney, E. R., Pruss, R. M., Gavrilovic, J., and Raff, M. C. (1980). Myelin-specific proteins and glycolipids in rat Schwann cells and oligodendrocytes in culture. *J. Cell Biol.* 84, 483–494. doi: 10.1083/jcb.84.3.483

Mitew, S., Gobius, I., Fenlon, L. R., Mcdougall, S. J., Hawkes, D., Xing, Y. L., et al. (2018). Pharmacogenetic stimulation of neuronal activity increases myelination in an axon-specific manner. *Nat. Commun.* 9:306. doi: 10.1038/s41467-017-02719-2

Nagel, G., Szellas, T., Huhn, W., Kateriya, S., Adeishvili, N., Berthold, P., et al. (2003). Channelrhodopsin-2, a directly light-gated cation-selective membrane

channel. *Proc. Natl. Acad. Sci. U.S.A.* 100, 13940–13945. doi: 10.1073/pnas.1936192100

Nave, K. A., and Werner, H. B. (2014). Myelination of the nervous system: mechanisms and functions. *Annu. Rev. Cell Dev. Biol.* 30, 503–533. doi: 10.1146/annurev-cellbio-100913-013101

Omlin, F. X. (1997). Optic disc and optic nerve of the blind cape mole-rat (*Georychus capensis*): a proposed model for naturally occurring reactive gliosis. *Brain Res. Bull.* 44, 627–632. doi: 10.1016/s0361-9230(97)00283-9

Ortiz, F. C., Habermacher, C., Graciarena, M., Houry, P. Y., Nishiyama, A., Oumesmar, B. N., et al. (2019). Neuronal activity in vivo enhances functional myelin repair. *JCI Insight* 5:123434. doi: 10.1172/jci.insight.123434

Ozcelik, M., Cotter, L., Jacob, C., Pereira, J. A., Relvas, J. B., Suter, U., et al. (2010). Pals1 is a major regulator of the epithelial-like polarization and the extension of the myelin sheath in peripheral nerves. *J. Neurosci.* 30, 4120–4131. doi: 10.1523/JNEUROSCI.5185-09.2010

Park, J., Kim, S., Park, S. I., Choe, Y., Li, J., and Han, A. (2014). A microchip for quantitative analysis of CNS axon growth under localized biomolecular treatments. *J. Neurosci. Methods* 221, 166–174. doi: 10.1016/j.jneumeth.2013.09.018

Park, J. W., Vahidi, B., Taylor, A. M., Rhee, S. W., and Jeon, N. L. (2006). Microfluidic culture platform for neuroscience research. *Nat. Protoc.* 1, 2128–2136. doi: 10.1038/nprot.2006.316

Parkhurst, C. N., Yang, G., Ninan, I., Savas, J. N., Yates, J. R. III, Lafaille, J. J., et al. (2013). Microglia promote learning-dependent synapse formation through brain-derived neurotrophic factor. *Cell* 155, 1596–1609. doi: 10.1016/j.cell.2013.11.030

Prasad, A., Teh, D. B. L., Blasiak, A., Chai, C., Wu, Y., Gharibani, P. M., et al. (2017). Static Magnetic field stimulation enhances oligodendrocyte differentiation and secretion of neurotrophic factors. *Sci. Rep.* 7:6743. doi: 10.1038/s41598-017-06331-8

Rabey, J. M., Dobronevsky, E., Aichenbaum, S., Gonen, O., Marton, R. G., and Khaigrekht, M. (2013). Repetitive transcranial magnetic stimulation combined with cognitive training is a safe and effective modality for the treatment of Alzheimer's disease: a randomized, double-blind study. *J Neural Transm.* 120, 813–819. doi: 10.1007/s00702-012-0902-z

Rosskothen-Kuhl, N., Hildebrandt, H., Birkenhager, R., and Illing, R. B. (2018). Astrocyte Hypertrophy and microglia activation in the rat auditory midbrain is induced by electrical intracochlear stimulation. *Front. Cell Neurosci.* 12:43. doi: 10.3389/fncel.2018.00043

Sarlieve, L. L., Rao, G. S., Campbell, G. L., and Pieringer, R. A. (1980). Investigations on myelination in vitro: biochemical and morphological changes in cultures of dissociated brain cells from embryonic mice. *Brain Res.* 189, 79–90. doi: 10.1016/0006-8993(80)90008-6

Stevens, B., Porta, S., Haak, L. L., Gallo, V., and Fields, R. D. (2002). Adenosine: a neuron-glial transmitter promoting myelination in the CNS in response to action potentials. *Neuron* 36, 855–868.

Szuchet, S., Polak, P. E., and Yim, S. H. (1986). Mature oligodendrocytes cultured in the absence of neurons recapitulate the ontogenic development of myelin membranes. *Dev. Neurosci.* 8, 208–221. doi: 10.1159/000112254

Tauber, H., Waehneldt, T. V., and Neuhoff, V. (1980). Myelination in rabbit optic nerves is accelerated by artificial eye opening. *Neurosci. Lett.* 16, 235–238. doi: 10.1016/0304-3940(80)90003-8

Taylor, A. M., Blurton-Jones, M., Rhee, S. W., Cribbs, D. H., Cotman, C. W., and Jeon, N. L. (2005). A microfluidic culture platform for CNS axonal injury, regeneration and transport. *Nat. Methods* 2, 599–605. doi: 10.1038/nmeth777

Tergau, F., Naumann, U., Paulus, W., and Steinhoff, B. J. (1999). Low-frequency repetitive transcranial magnetic stimulation improves intractable epilepsy. *Lancet* 353, 2209. doi: 10.1016/s0140-6736(99)01301-x

Torres, F., Villalon, E., Poblete, P., Moraga-Amaro, R., Linsambarth, S., Riquelme, R., et al. (2015). Retrospective evaluation of deep transcranial magnetic stimulation as add-on treatment for Parkinson's Disease. *Front. Neurol.* 6:210. doi: 10.3389/fneur.2015.00210

Trang, T., Beggs, S., Wan, X., and Salter, M. W. (2009). P2X4-receptor-mediated synthesis and release of brain-derived neurotrophic factor in microglia is dependent on calcium and p38-mitogen-activated protein kinase activation. *J. Neurosci.* 29, 3518–3528. doi: 10.1523/JNEUROSCI.5714-08.2009

Tremblay, M. E., Lowery, R. L., and Majewska, A. K. (2010). Microglial interactions with synapses are modulated by visual experience. *PLoS Biol.* 8:e1000527. doi: 10.1371/journal.pbio.1000527

Ueda, H., Levine, J. M., Miller, R. H., and Trapp, B. D. (1999). Rat optic nerve oligodendrocytes develop in the absence of viable retinal ganglion cell axons. *J. Cell Biol.* 146, 1365–1374. doi: 10.1083/jcb.146.6.1365

Wan, L., Xia, R., and Ding, W. (2010). Short-term low-frequency electrical stimulation enhanced remyelination of injured peripheral nerves by inducing the promyelination effect of brain-derived neurotrophic factor on Schwann cell polarization. *J. Neurosci. Res.* 88, 2578–2587. doi: 10.1002/jnr.22426

Waxman, S. G., and Bennett, M. V. (1972). Relative conduction velocities of small myelinated and non-myelinated fibres in the central nervous system. *Nat. New Biol.* 238, 217–219. doi: 10.1038/newbio238217a0

Wilkins, A., Chandran, S., and Compston, A. (2001). A role for oligodendrocyte-derived IGF-1 in trophic support of cortical neurons. *Glia* 36, 48–57. doi: 10.1002/glia.1094

Wilkins, A., Majed, H., Layfield, R., Compston, A., and Chandran, S. (2003). Oligodendrocytes promote neuronal survival and axonal length by distinct intracellular mechanisms: a novel role for oligodendrocyte-derived glial cell line-derived neurotrophic factor. *J. Neurosci.* 23, 4967–4974. doi: 10.1523/jneurosci.23-12-04967.2003

Williams, J. C., Rennaker, R. L., and Kipke, D. R. (1999). Long-term neural recording characteristics of wire microelectrode arrays implanted in cerebral cortex. *Brain Res. Brain Res. Protoc.* 4, 303–313. doi: 10.1016/s1385-299x(99)00034-3

Wood, P. M., and Bunge, R. P. (1986). Evidence that axons are mitogenic for oligodendrocytes isolated from adult animals. *Nature* 320, 756–758. doi: 10.1038/320756a0

Wu, K. Y., Hengst, U., Cox, L. J., Macosko, E. Z., Jeromin, A., Urquhart, E. R., et al. (2005). Local translation of RhoA regulates growth cone collapse. *Nature* 436, 1020–1024. doi: 10.1038/nature03885

Xiao, J., Wong, A. W., Willingham, M. M., Van Den Buuse, M., Kilpatrick, T. J., and Murray, S. S. (2010). Brain-derived neurotrophic factor promotes central nervous system myelination via a direct effect upon oligodendrocytes. *Neurosignals* 18, 186–202. doi: 10.1159/000323170

Yang, I. H., Gary, D., Malone, M., Dria, S., Houdayer, T., Belegu, V., et al. (2012). Axon myelination and electrical stimulation in a microfluidic, compartmentalized cell culture platform. *Neuromolecular Med.* 14, 112–118. doi: 10.1007/s12017-012-8170-5

Young, K. M., Psachoulia, K., Tripathi, R. B., Dunn, S. J., Cossell, L., Attwell, D., et al. (2013). Oligodendrocyte dynamics in the healthy adult CNS: evidence for myelin remodeling. *Neuron* 77, 873–885. doi: 10.1016/j.neuron.2013.01.006

Zhong, Y., and Bellamkonda, R. V. (2008). Biomaterials for the central nervous system. *J. R. Soc. Interface* 5, 957–975. doi: 10.1098/rsif.2008.0071

Conflict of Interest Statement: The authors declare that the research was conducted in the absence of any commercial or financial relationships that could be construed as a potential conflict of interest.

frontiers in Neuroscience

TECHNOLOGY REPORT
published: 12 September 2019
doi: 10.3389/fnins.2019.00936

Proceedings of the Sixth Deep Brain Stimulation Think Tank Modulation of Brain Networks and Application of Advanced Neuroimaging, Neurophysiology, and Optogenetics

Adolfo Ramirez-Zamora[1], James Giordano[2], Edward S. Boyden[3,4,5], Viviana Gradinaru[6], Aysegul Gunduz[7], Philip A. Starr[8], Sameer A. Sheth[9], Cameron C. McIntyre[10], Michael D. Fox[11], Jerrold Vitek[12], Vinata Vedam-Mai[13], Umer Akbar[14], Leonardo Almeida[1], Helen M. Bronte-Stewart[15], Helen S. Mayberg[16], Nader Pouratian[17], Aryn H. Gittis[18], Annabelle C. Singer[19], Meaghan C. Creed[20], Gabriel Lazaro-Munoz[21], Mark Richardson[22], Marvin A. Rossi[23], Leopoldo Cendejas-Zaragoza[24], Pierre-Francois D'Haese[25], Winston Chiong[26], Ro'ee Gilron[8], Howard Chizeck[27], Andrew Ko[28], Kenneth B. Baker[29], Joost Wagenaar[30], Noam Harel[31], Wissam Deeb[1], Kelly D. Foote[13] and Michael S. Okun[1]*

[1] Department of Neurology, Fixel Institute for Neurological Diseases, University of Florida, Gainesville, FL, United States, [2] Neuroethics Studies Program, Department of Neurology and Department of Biochemistry, Georgetown University Medical Center, Washington, DC, United States, [3] Media Laboratory, Department of Biological Engineering, Massachusetts Institute of Technology, Cambridge, MA, United States, [4] Center for Neurobiological Engineering, Massachusetts Institute of Technology, Cambridge, MA, United States, [5] Department of Brain and Cognitive Sciences, Massachusetts Institute of Technology, Cambridge, MA, United States, [6] Division of Biology and Biological Engineering, California Institute of Technology, Pasadena, CA, United States, [7] Department of Neuroscience and Department of Biomedical Engineering and Department of Neurology, Fixel Institute for Neurological Diseases, University of Florida, Gainesville, FL, United States, [8] Graduate Program in Neuroscience, Department of Neurological Surgery, Kavli Institute for Fundamental Neuroscience, University of California, San Francisco, San Francisco, CA, United States, [9] Department of Neurological Surgery, Baylor College of Medicine, Houston, TX, United States, [10] Department of Biomedical Engineering, Case Western Reserve University, Cleveland, OH, United States, [11] Beth Israel Deaconess Medical Center, Harvard Medical School, Boston, MA, United States, [12] Department of Neurology, University of Minnesota, Minneapolis, MN, United States, [13] Department of Neurosurgery, Fixel Institute for Neurological Diseases, University of Florida, Gainesville, FL, United States, [14] Center for Neurorestoration and Neurotechnology, Rehabilitation R&D Service, Veterans Affairs Medical Center, Brown Institute for Brain Science, Brown University, Providence, RI, United States, [15] Department of Neurology and Department of Neurological Sciences and Department of Neurosurgery, Stanford University, Stanford, CA, United States, [16] Department of Neurology and Department of Neurosurgery, Icahn School of Medicine at Mount Sinai, New York, NY, United States, [17] Department of Neurosurgery, David Geffen School of Medicine at UCLA, Los Angeles, CA, United States, [18] Biological Sciences and Center for Neural Basis of Cognition, Carnegie Mellon University, Pittsburgh, PA, United States, [19] Coulter Department of Biomedical Engineering, Georgia Institute of Technology, Emory University School of Medicine, Atlanta, GA, United States, [20] Department of Pharmacology, University of Maryland School of Medicine, Baltimore, MD, United States, [21] Center for Medical Ethics and Health Policy, Baylor College of Medicine, Houston, TX, United States, [22] Center for the Neural Basis of Cognition, University of Pittsburgh School of Medicine, Pittsburgh, PA, United States, [23] Department of Diagnostic Radiology and Nuclear Medicine, Rush University Medical Center, Chicago, IL, United States, [24] Department of Biomedical Engineering, Illinois Institute of Technology, Chicago, IL, United States, [25] Electrical Engineering, Vanderbilt University, Nashville, TN, United States, [26] Department of Neurology, University of California, San Francisco, San Francisco, CA, United States, [27] Graduate Program in Neuroscience, Department of Electrical Engineering, University of Washington, Seattle, WA, United States, [28] Department of Neurological Surgery, University of Washington, Seattle, WA, United States, [29] Movement Disorders Program, Cleveland Clinic Foundation, Cleveland, OH, United States, [30] Department of Neurology, Center for Neuroengineering and Therapeutics, University of Pennsylvania, Philadelphia, PA, United States, [31] Center for Magnetic Resonance Research, University of Minnesota, Minneapolis, MN, United States

OPEN ACCESS

Edited by:
Olivier David, Institut National de la Santé et de la Recherche Médicale (INSERM), France

Reviewed by:
Patricia Limousin, University College London, United Kingdom
Veerle Visser-Vandewalle, University of Cologne, Germany

***Correspondence:**
Adolfo Ramirez-Zamora
Adolfo.Ramirez-Zamora@neurology.ufl.edu

Specialty section:
This article was submitted to Neural Technology, a section of the journal Frontiers in Neuroscience

Received: *05 February 2019*
Accepted: *21 August 2019*
Published: *12 September 2019*

Citation:
Ramirez-Zamora A, Giordano J, Boyden ES, Gradinaru V, Gunduz A, Starr PA, Sheth SA, McIntyre CC, Fox MD, Vitek J, Vedam-Mai V, Akbar U, Almeida L, Bronte-Stewart HM, Mayberg HS, Pouratian N, Gittis AH, Singer AC, Creed MC, Lazaro-Munoz G, Richardson M, Rossi MA, Cendejas-Zaragoza L, D'Haese P-F, Chiong W, Gilron R, Chizeck H, Ko A, Baker KB, Wagenaar J, Harel N, Deeb W, Foote KD and Okun MS (2019) Proceedings of the Sixth Deep Brain Stimulation Think Tank Modulation of Brain Networks and Application of Advanced Neuroimaging, Neurophysiology, and Optogenetics. Front. Neurosci. 13:936. doi: 10.3389/fnins.2019.00936

The annual deep brain stimulation (DBS) Think Tank aims to create an opportunity for a multidisciplinary discussion in the field of neuromodulation to examine developments, opportunities and challenges in the field. The proceedings of the Sixth Annual Think Tank recapitulate progress in applications of neurotechnology, neurophysiology, and emerging techniques for the treatment of a range of psychiatric and neurological conditions including Parkinson's disease, essential tremor, Tourette syndrome, epilepsy, cognitive disorders, and addiction. Each section of this overview provides insight about the understanding of neuromodulation for specific disease and discusses current challenges and future directions. This year's report addresses key issues in implementing advanced neurophysiological techniques, evolving use of novel modulation techniques to deliver DBS, ans improved neuroimaging techniques. The proceedings also offer insights into the new era of brain network neuromodulation and connectomic DBS to define and target dysfunctional brain networks. The proceedings also focused on innovations in applications and understanding of adaptive DBS (closed-loop systems), the use and applications of optogenetics in the field of neurostimulation and the need to develop databases for DBS indications. Finally, updates on neuroethical, legal, social, and policy issues relevant to DBS research are discussed.

Keywords: deep brain stimulation, neuromodulation, epilepsy, Parkinson's disease, tremor, optogenetics, Tourette syndrome, temporal dispersion

INTRODUCTION

Neuromodulation of brain structures and functions is an evolving field. Ongoing scientific and technological advancements have facilitated an improved understanding of brain networks and the neural signals involved in the signs and symptoms of a number of neuropsychiatric conditions. Novel methods of electrical current delivery have been recently applied to existing neuromodulation techniques in order to improve the understanding and the ability to more precisely affect mechanisms, function and to influence cortical and subcortical structures. The deep brain stimulation (DBS) Think Tank is an annual forum that facilitates discussion and debate about the latest scientific, technological, ethico-legal issues, social innovations, challenges, and opportunities in the field. The Sixth Annual DBS Think Tank was held in Atlanta, GA, United States from 6 to 8 May, 2018. The meeting focused on the use of novel modulation techniques and emerging areas of scientific, technological, ethical, and policy development. Specifically, the meeting addressed issues and possibilities of modulating different neuronal networks; expanding capabilities of responsive (closed-loop) DBS systems; and the therapeutic potential of targeted brain network modulation. Particular emphasis was placed upon advances and gaps in knowledge of and capabilities to affect brain electrophysiology, interface optogenetics and DBS, and on the multiple (technical, ethical, policy, and social) factors that can limit and/or de-limit these domains. We divided current proceedings in seven separate sections discussing advances in the field as follows: connectomic and network neuromodulation, advances in neurophysiological signals for DBS, new neuromodulation techniques, applications of optogenetic techniques in DBS, databases for DBS, and neuroethical, Legal and social issues in DBS.

Brain Network Neuromodulation and Connectomic DBS

Leveraging Human Brain Connectomics to Improve DBS

Different stereotactic techniques are commonly used to assure proper localization of subthalamic (STN-DBS) leads in Parkinson's disease (PD), including anatomical neuroimaging and indirect stereotactic methods. However, therapeutic benefits are likely the result of engagement and modulation of other brain regions that are interactive with specific stimulation sites and networks (Henderson, 2012; Fox et al., 2014). An improved understating of brain node and network connectivity could therefore be useful and of value to predicting and to optimizing DBS responses and outcomes (Horn et al., 2017). Using diffusion tractography, white matter tracts near the DBS electrode can be accurately identified (Coenen et al., 2011; Pouratian et al., 2011; Riva-Posse et al., 2014) and functional connectivity – a measure of the correlation in spontaneous activity – can be used to link subcortical DBS sites to effects in cortical regions (Anderson et al., 2011; Fox et al., 2014).

Recent works highlight the importance of modulating the hyperdirect pathway (connecting the STN to cortex) in the effectiveness of STN-DBS (Gradinaru et al., 2009; Accolla et al., 2016). Utilizing high-quality connectome datasets [diffusion tractography and functional connectivity from normal subjects (n = 1,030) and PD patients (n = 90)] Horn et al. (2017) were able to compute connectivity profiles of beneficial STN DBS for PD. There is a distinct pattern of connectivity with STN DBS electrodes, which directly correlated with clinical outcome. Importantly, structural and functional connectivity independently predicted DBS response.

Similarly, this technique can be used to explore or refine DBS targets and theoretically to avoid or reduce side effects of neuromodulation (Calabrese, 2016). Cognitive side effects are possible after STN-DBS. Witt et al. (2013) assessed the influence of cortical lead entry point, electrode path and position of stimulating electrode contacts on neuropsychological changes after surgery in patients with mild cognitive and semantic fluency decline. When trajectories intersected with the caudate nuclei, there was an increased risk of decline in cognition and decrements in working memory. However, these results need to be corroborated with additional larger and prospective studies. Additionally, subjects who showed a decline in semantic verbal fluency had the active electrode located outside the dorsolateral stimulation STN, and connectivity profiles showed clear differences between patients.

This technique can also be used in DBS treatment of other conditions. For example, chronic-progressive gait ataxia in patients with essential tremor (ET) can be reversed following prolonged DBS washout, and is likely due to a stimulation-induced vestibulo-cerebellar network dysfunction (Reich et al., 2016). Using volume of tissue activated (VTA) modeling, it was shown that stimulation of the more posteromedial and caudal zones of the thalamus might account for this side effect, and thus, avoiding a caudal and ventral placement might prevent such chronic side effects. Further validation of these datasets and findings is needed so that individualized DBS targets can be evermore precisely estimated using network assessments to minimize side effects.

Connectivity Underlies Antidepressant Response to Subcallosal Cingulate DBS

Deep brain stimulation of the subcallosal cingulate (SCC) has recently shown promise for the treatment of therapy-resistant depression (Mayberg et al., 2005; Holtzheimer et al., 2012; Puigdemont et al., 2012), acting via modulation of specific pathological circuits. However, one of the remaining challenges is a lack of biomarkers and feedback to enable confirmation of the intended brain target. Therefore, attempts to develop a biometric of signal propagation from a novel white matter target in the SCC region are ongoing by exploiting stimulation evoked potentials as a biomarker of effective connectivity. In a recent study, four subjects were implanted in the SCC with the aid of StimVision (Noecker et al., 2018). Electroencephalographic (EEG) recordings were performed with DBS that was directed to the SCC white matter region using 2 Hz settings at 6 V. The stimulation pulse width was 90 microseconds (μs) and current was placed in a monopolar configuration. Therapeutic stimulation of 130 Hz; 3–5 V; 90 μs was resumed after the recordings were collected. A SCC DBS evoked potential (p40) was consistently elicited and detected over a period of 14 months (at four time points) (**Figure 1**). These results indicated that it was feasible to obtain feedback on cortical responsivity by employing a stimulation evoked potential, which can be used as a signal of optimal targeting and test–retest reliability over time. This study indicated that the p40 feature may be an activation of the forceps minor, which was consistent with previous data that linked stimulation evoked response to white matter activation (Waters et al., 2018).

Targeting Identified Brain Connections With DBS

As previously stated, it is becoming increasingly evident that the benefits of DBS for disorders such as ET and PD depend on the connectivity of the site of stimulation with other brain networks and regions (Horn et al., 2017; Malekmohammadi et al., 2018b). Insights into the connectivity of effective therapeutic stimulation (in comparison to ineffective stimulation) will likely enhance the ability to target deep brain structures. This could also improve the ability to develop new DBS surgical methods (such as asleep image-guided implantation, although this procedure has been performed successfully without connectivity data in many centers for years), technologies (that more precisely produce network-based neuromodulation), and therapeutic indications (such as treatment-resistant depression and other neuropsychiatric disorders including addiction; as well as certain forms of intractable pain).

Methods for evaluating connectivity include both anatomical (diffusion tensor imaging and tractography) and functional techniques [EEG, functional MRI, and invasive neurophysiological techniques including microelectrode recordings, local field potentials (LFPs), and electrocorticography]. One of the earliest demonstrations of such DBS targeting was the application of connectivity-based thalamic segmentation, which revealed discrete thalamic regions with distinctive connectivity patterns with cortical regions (Pouratian et al., 2011). Subsequent reports have elaborated on the value of tractography for thalamic targeting, using methods to both directly target the region-of-interest in the thalamus (Sasada et al., 2017; Tsolaki et al., 2018) as well as for indirect targeting, in which adjacent tracts which should be avoided are delineated (Sammartino et al., 2016). An alternate method would entail mapping the pyramidal tracts and medial lemniscus, and targeting DBS placements that are medial and anterior to these tracts, respectively (Sammartino et al., 2016). The most efficacious DBS contact for tremor control is localized within the thalamic region connected to the premotor, rather than the primary motor cortex as would be predicted by traditional, preoperative, indirect targeting methods. In ET patients, diffusion tensor imaging (DTI) based fiber tractography can aid in determining the optimal target(s) to maximally achieve tremor suppression and to reduce the number of adverse events by avoiding stimulation or lesioning of other nearby tracts, respectively (Sasada et al., 2017). Analyzing four fiber tracts important for motor control, tractography revealed a strong role of the cerebello thalamic and pre motor cortex modulation in ET patients with thalamotomy or thalamic DBS. It was observed that those fiber afferents from the cerebellum that passed through ventral intermedius nucleus (VIM) and the area anterior to the VIM were likely connected to the pre motor or motor cortex. In another study, probabilistic tractography-guided thalamic targeting was employed to treat ET (Tsolaki et al., 2018): MR imaging and clinical outcomes following thalamotomy (MR guided- Focus ultrasound) were assessed. Thalamic connectivity to pre- and post-central gyral targets was evaluated and individual thalamic target maps were generated. Using receiver operating characteristic curves to define overlapping thalamic

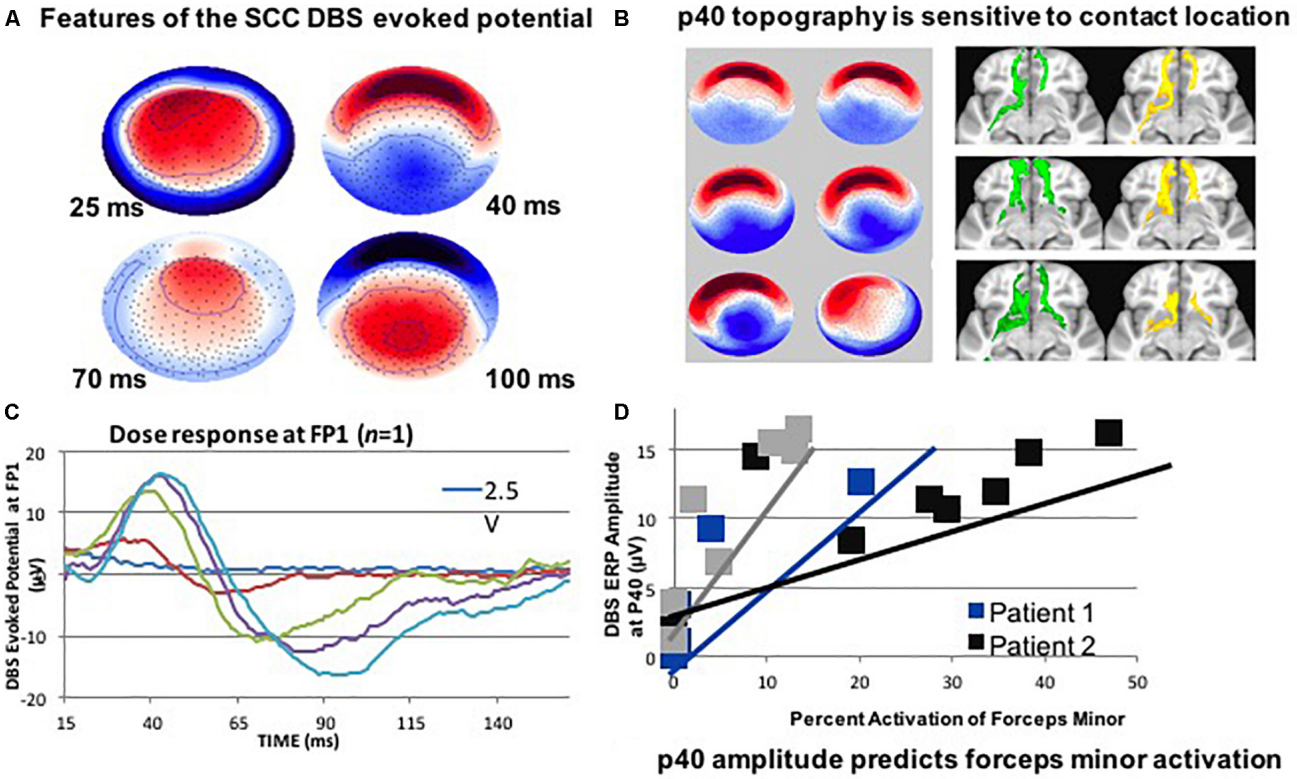

FIGURE 1 | (A) SCC DBS evoked potentials in patients with treatment resistant depression may also be useful. It is less important to hit the visible target; it is more about hitting the correct portion of the connectome. **(B)** Use DTI: to target structures intraoperatively. **(C)** Record LFP at the DTI-optimized target. **(D)** Use high-density EEG: to detect evoked cortical responses for stimulation. This figure adapted from Cho et al. (2017).

maps, the overlap between these thalamic target maps and the MR guided- Focus ultrasound lesion was systematically weighed with respect to clinical outcome, and the connectivity differences of best clinical outcomes were compared. These investigations demonstrated that the intersection between lesion and thalamic-connectivity mapped to motor areas, while sensory targets proved to be effective in predicting the response to therapy.

While the use of tractography-guided thalamic targeting for ET has been a powerful proof of concept, an additional practical utility lies in the potential of using such approaches to either optimize therapies that have been inconsistent to date, or to develop novel applications. For example, thalamic DBS for pain is associated with inconsistent efficacy, possibly due, in part, to the lack of optimized targeting. To gain insight to the potential value of tractography-guided thalamic DBS targeting for pain, a small retrospective analysis of five patients was performed. It was shown that the pain patients who derived benefit from thalamic DBS for their pain had DBS leads that co-localized with those thalamic regions with maximal connectivity with the post-central gyrus (Kim et al., 2016). Looking ahead, it may be important for the discipline to integrate knowledge about stimulation fields, therapeutic outcomes, and tractography in order to create clinically-weighted optimal connectivity maps with which to define optimal stimulation targets (rather than to identify and engage seed regions and targets based on predefined, potentially arbitrary, anatomic segmentations; Tsolaki et al., 2018). The idea of employing multiple methods to define target site represents something of a reversal: rather than starting with a hypothesis about the optimal network engagement, this approach allows data-driven outcome-weighted delineation of networks that may prove to be contributory to improved therapeutic outcomes.

Other studies have investigated DBS targets other than the thalamus. Investigators have mapped the hyperdirect pathway from the primary motor cortex to STN, based on the hypothesis that the optimal site of STN stimulation is the site of hyperdirect pathway input. To further explore this hypothesis, hyperdirect pathways and associated STN target maps generated by two different tractography approaches (i.e., tensor-based deterministic method, and an advanced probabilistic method) were compared (Petersen et al., 2017). Both identified connections between the ipsilateral motor cortex and STN, but defined different target regions in the STN. The probabilistic method, which is based on constrained spherical deconvolution, resulted in a reconstruction of motor cortical connections terminating in the dorsolateral STN, consistent with the optimal site

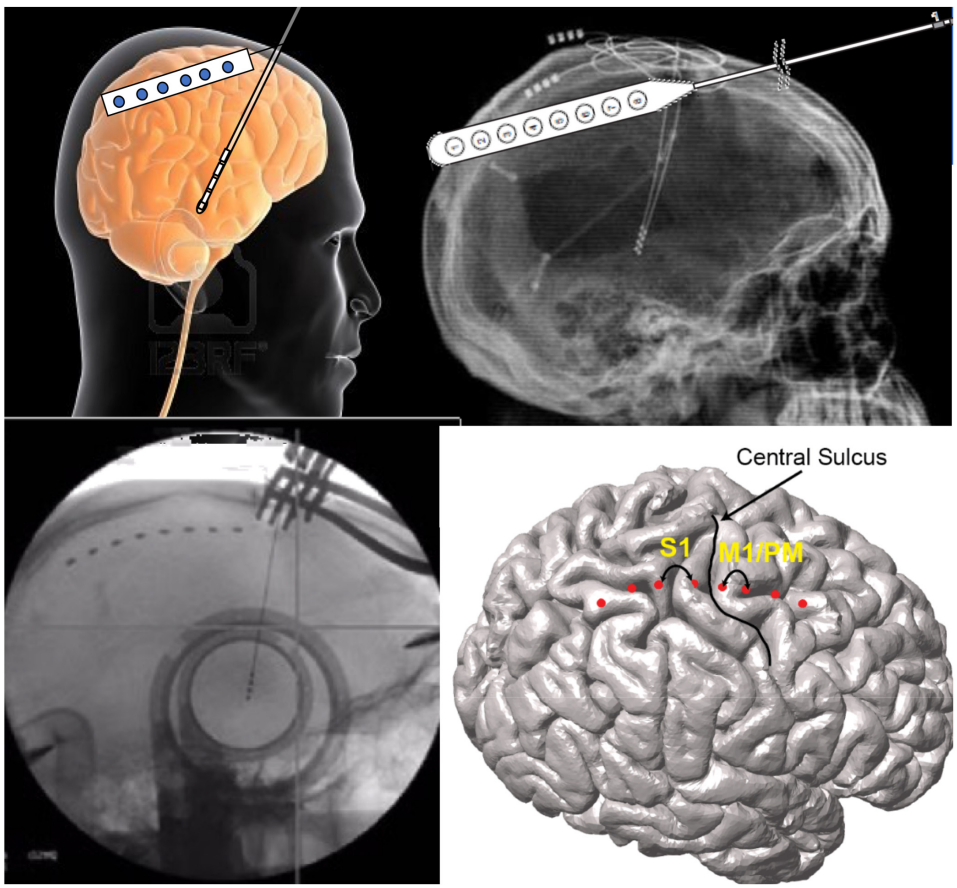

FIGURE 2 | Network-based measures can be recorded during DBS surgery via the same burr hole utilized for DBS lead implantation. In these illustrations, the use of an electrocorticography strip is shown. Simultaneous signals are recorded from the motor cortices while also recording through the DBS lead.

of stimulation. The tensor-based method resulted in a reconstruction of fewer, and more variable connections. Hence, the probabilistic method was considered to be more consistent for STN mapping.

Brain networks can also be evaluated using both non-invasive and invasive neurophysiologic methods (**Figure 2**). There have been several reports of either measuring biosignals in distinct nodes throughout a targeted network, or of evaluation of network-based biosignals. An example of the former is the detection of increased phase-amplitude coupling in the precentral gyrus of patients with PD, which is suppressed with therapeutic stimulation of both the STN (De Hemptinne et al., 2015) and the GPi (Malekmohammadi et al., 2018a). Another approach is to measure network connectivity by evaluating the coupling of signals in and across different nodes and to demonstrate modulation of these network-wide signals. Using such methods, two groups have recently demonstrated suppression of pallidocortical beta coherence with effective pallidal DBS and changes in cortico-subcortical functional connectivity were shown to be spatially exclusive to the motor cortex (Malekmohammadi et al., 2018b; Wang et al., 2018).

Individualized Network Interrogation and Targeted DBS

Neuropsychiatric disorders are increasingly being viewed as node and network-level brain dysfunctions. Apropos such a perspective, there is renewed enthusiasm for understanding the complex anatomical and functional bases of particular neuropsychiatric states and conditions. Extant, simplistic classifications of neuropsychiatric disorders based solely upon patient signs and symptoms have been limited, at best, and clinically ineffective and inefficient as worst, and therefore a taxonomy based on orthogonalized axes of psychological constructs and neural circuit dysfunction may be better suited (and of greater value) in affording a more rational (and testable) basis for developing new therapeutic methods and approaches, inclusive of DBS.

A number of brain networks have been implicated in depression, including those subserving the default mode, salience, and negative affect (Williams, 2017). The concept of targeting specific networks based on an individual biotype (e.g., neuropsychiatric phenotypes) remains an evolving construct, which may be advanced by the use of advanced neuroimaging to obtain neuroanatomical and neurophysiological information

about individual patients. This may facilitate improved clinical outcomes when using more saliently targeted DBS. In an ongoing study (NCT03437928), an innovative approach to assess patients with treatment refractory depression includes the use of subacute invasive neurophysiological monitoring (i.e., stereo-electroencephalography) to gain insight to the networks involved in depressive symptomatology. The goal is to demonstrate and to confirm the capability to selectively and predictably engage distinct brain networks that are contributory to the pathologic features of depression, and to demonstrate positive therapeutic changes in such signs and symptoms through the use of network-targeted stimulation.

The study included the use of directional current steering DBS and individualized network targeting; with the aims of demonstrating that this approach to targeting was feasible and safe, and could possibly reduce depressive symptoms. Targeting networks – instead of specific structures – might prove to be crucial to individualizing therapies aimed at modulating specific brain networks important to depression (and other neuropsychopathologies). In this light, specific network modulation may also be viable and of value in treating obsessive compulsive disorder (OCD) (Banks et al., 2015). Previously, a number of targets have been used to treat OCD. Recent tractographic data show network-level pathophysiology that can be targeted with DBS. It has been reported that subdivisions of the anterior limb of the internal capsule were found to vary substantially as viable targets for DBS in treating OCD. However, some loci did prove to be consistently useful targets, with the most notable effects being produced by stimulating regions most densely connected to the orbitofrontal cortex. Future studies are aimed at continuing these investigations to (1) develop new technologies to delineate symptomatic networks in neuropsychiatric disorders and (2) to assess the effect of neuromodulation that targets different networks and regions identified via advanced neuroimaging to be participatory in depressive (and other psychiatric disorders') signs and symptoms.

Network Assessment in Movement Disorders

Given mounting evidence to support the possibility of obtaining good clinical outcomes in the absence of neurophysiological mapping – and multi-dimensionally (e.g., clinically, technologically, economically); an important question is what the future of intracranial neurophysiology portends in an era of increasing use of real-time MRI-guided and CT-verified DBS implantation in asleep patients. One possibility is that network mapping, rather than mapping of a single target structure, will be important to improve the efficacy – and ultimate clinical effectiveness and value of DBS. For instance, as evidence emerges for separate networks that may be therapeutically responsive to differential stimulation (e.g., speech, gait, non-motor symptoms of PD) (Humphries and Gurney, 2012), techniques will be needed to identify the optimal locations within these networks for DBS placement. Additionally, if cortical sensors [e.g., electrocorticography (ECoG)] become an important component of closed-loop DBS systems, intraoperative functional connectivity mapping of the target network may be required for (optimized) placement of both sensing and stimulating electrodes.

Opportunities for multi-scale, high-resolution neurophysiological data collection are most robust intraoperatively, but assessments are limited by available time and by the physical constraints that restrict the complexity of behavioral tasks which can be engaged (**Figure 3**). The use of simultaneous ECoG during DBS implantation, however, can serve as a powerful tool for identifying optimal network nodes. Using this technique, single unit and LFP recordings from the target structure, as well as LFPs from functionally connected areas of the cortex can be simultaneously obtained (Panov et al., 2017). ECog has been used to map pathological and physiological networks in PD and dystonia. Additionally, (and perhaps of greater importance), these studies have elucidated processes of information transfer between the basal ganglia and cortex during limb movement and speech production, which may afford information about which signals are best suited for closed-loop DBS systems capable of adapting to specific behavioral signs and symptoms. Once a patient is implanted, intracranial neurophysiological recording locations and modalities are fixed, but the subject can participate in much longer trials of behavioral testing, either in a subacute setting with externalized leads, or chronically following implantation of a bi-directional pulse generator. Lastly, functional imaging modalities can be used in multiple settings facilitating longitudinal assessment. For example, pre-operative MEG or fMRI data can be compared to those data obtained in subacute or chronic post-operative periods in order to measure target network engagement and other network effects of stimulation over time.

Parametric Subtracted Post-ictal Diffusion Tensor Imaging for Guiding Direct Neurostimulation Therapy

New techniques in tractography are being investigated as methods which can be used to identify aberrant brain networks and potential foci of epilepsy (Sivakanthan et al., 2016). Using tractography to identify a specific ictal focus, implanting devices for white matter modulation might afford benefit to those epilepsy patients for whom other treatments are not viable. Currently, the goal is to capture ictal and post-ictal states via imaging tools in order to enable more individualized therapies. The development and use of newer techniques will allow greater precision in targeting domains of the refractory epileptogenic network(s) (Nemtsas et al., 2017; Rossi, 2017). This will optimize targeting and trajectories to access the involved network beyond simply an anatomical target, to more fully and specifically modulate the propagation pathway. Ongoing work aims to utilize parametric methods to subtract post-ictal DTI to identify such potential targets for modulation (Garibay-Pulido et al., 2018). This technique has been helpful both for studying ictal states and for identifying acute and chronic changes in network activity in epilepsy patients. There are statistical differences between pre- and post-seizure activity patterns that allow the visualization of the epileptic network. From this visualization, electrodes can be modeled into the DTI technique to reveal probabilistic stimulation-induced network activations. To be sure, these developments are promising, and additional steps and validation, including fiber "cable modeling" via the use of

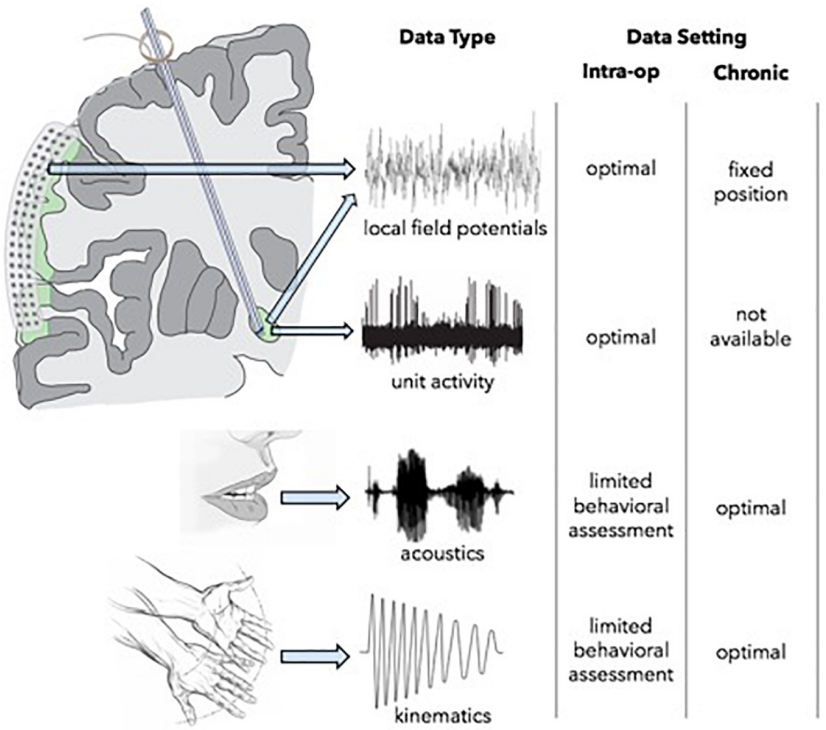

FIGURE 3 | Intracranial neurophysiology opportunities for network assessment.

Hodgkin-Huxley equations, will be necessary and important to validating and refining these methods.

Recent Advances in Neurophysiological Signals for DBS

STN Recordings to Inform Closed Loop DBS in Parkinson's Disease

Resting state LFP neural recordings from the PD STN in intra- or peri-operative studies have demonstrated exaggerated oscillatory neuronal activity and synchrony in both the alpha (8–12 Hz) and beta (13–30 Hz) bands (Maling et al., 2018). The extent of attenuation of resting state beta band power during therapeutic doses of both dopaminergic medication and high frequency (HF) DBS has been correlated with improvement in bradykinesia and rigidity. This suggests that STN resting state beta band power is a physiological marker of PD and could be a potential control variable for closed loop or adaptive (a)DBS. The resting state beta band is conserved over time and across different resting postures (Bronte-Stewart et al., 2009); it is similar between STN nuclei; of greater power in more affected STN (De Solages et al., 2010); it is a property of the functionally connected Parkinsonian sensorimotor network; and its phase is coupled with gamma band amplitude in the STN and M1 cortex (Whitmer et al., 2012). It is attenuated during HF DBS and after washout of chronic STN DBS (Whitmer et al., 2012; Trager et al., 2016); it is attenuated during tremor, but it is not highly correlated to PD motor signs (Shreve et al., 2017). Taken together, these findings prompt the question of whether resting state beta band power is a validly good control variable for aDBS in freely moving patients.

Apropos this question, it is now possible to record synchronized neural and kinematic signals from an implanted sensing neurostimulator and from wearable sensors respectively, in freely moving human subjects (Activa® PC + S, Medtronic, Inc., FDA IDE approved). It has been demonstrated that the transition from the resting state to a moving state (such as walking) is associated with a change in the LFP spectrum, which was more prominent in the akinetic rigid versus the tremor dominant PD phenotypes (Quinn et al., 2015), and in PD freezers as compared to non-freezers (Syrkin-Nikolau et al., 2017). Beta band power during movement was attenuated in a voltage dependent pattern during randomized presentations of differing voltages of STN DBS (Whitmer et al., 2012). Different beta sub-bands showed distinct sensitivities to attenuation during STN DBS. Based upon this, it was investigated whether the more or less sensitive sub-band was superior as a control variable for aDBS (Afzal et al., under review). Temporal fluctuations and the extent of unpredictable behavior of STN band neural activity during movement (i.e., movement band) differentiated PD freezers from non-freezers (**Figure 4**). Movement band burst durations and entropy (i.e., sample entropy) were longer and greater respectively in freezers compared to non-freezers during gait without FOG, and were longer/greater in freezers compared to non-freezers and during periods of FOG (Syrkin-Nikolau et al., 2017). Temporal properties of the resting state beta band did not differ between freezers and non-freezers. Longer movement

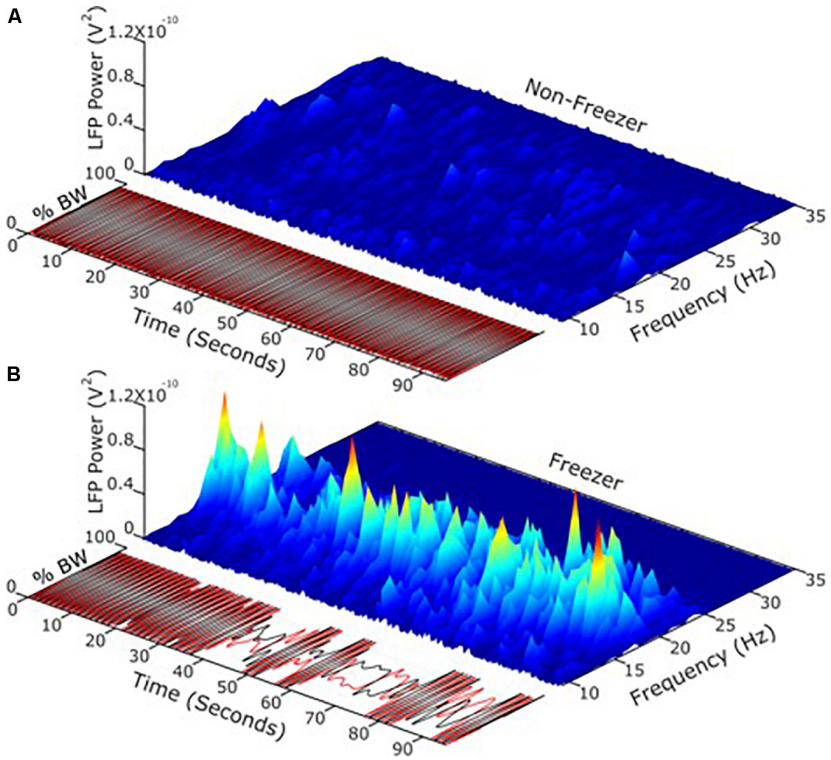

FIGURE 4 | (A) Using LFP's and neurophysiology to define and address freezing of gait in Parkinson's disease. **(B)** Temporal fluctuations and the extent of changeable behavior of STN band neural activity during movement differentiated PD freezers from non-freezers.

band burst durations and impaired gait improved during 60 and 140 Hz STN DBS in freezers, but short burst durations and normal gait in non-freezers were unchanged. These results suggest that gait impairment and FOG are characterized both by more prolonged periods of pathological neural synchrony and by unpredictability or chaos in STN beta rhythms, which disrupts normal sensorimotor processing. The effect of STN DBS was directed toward mitigating pathological neural activity related to gait, and toward restoring greater physiological information processing in the sensorimotor network, so as to improve gait and FOG in PD freezers. This information affords new neural control variables that may be more relevant in freely moving PD subjects than the resting state beta band.

Pallidal and Cortical Recordings in PD: Prospects for Pallidal Closed Loop DBS

There is increasing use of closed-loop DBS in PD, with most groups utilizing STN signals as the neurophysiological marker to enable aDBS. However, the globus pallidus interna (GPi) is also an important locus in the pathological network of PD, and is commonly targeted for the treatment of refractory motor symptoms (Ramirez-Zamora and Ostrem, 2018). Investigating potential pallidal and cortical signals might allow for reduction of adverse side effects. Cortical signals have greater signal to noise ratio than signals recorded from deep subcortical structures (De Hemptinne et al., 2015). However, recent work has been focusing on developing and characterizing pallidal interval recordings as potential markers that can be studied in advanced, adaptable DBS to improve tremor management in PD, reduce adverse effects (including brittle responses, tolerance), reduce current drain, and incorporate variability related to circadian rhythms (Swann et al., 2018). Prior work has validated exaggerated oscillatory neuronal activity and synchrony in the beta bands as a biomarker for aDBS.

Thus, current studies aim to improve the closed loop algorithm and to analyze smaller windows of data to test different refresh rates. Detector sophistication will be critical to acquiring and assessing signals, and several critical questions remain regarding whether to employ single threshold or center frequency; the ideal rate of signal updates; ramp and onset times, and the potential for energy savings, technical sources of variance, long term benefit and signal reliability and reproducibility afforded by this technique. Moreover, the increasing complexity of these signals will likely require computerized or algorithmic programing to mitigate long programing visits, and this prompts questions and concerns about capability and use of bio-informatic systems to facilitate these approaches (see also above, re: bio-informatic systems development, progress and challenges).

Adaptive Pedunculopontine Nucleus (PPN) DBS for Treatment of Freezing of Gait

FOG affects approximately 78% of PD patients and is a major cause of falls, and determinant of quality of life. Animal research suggests that the GPi and PPN contribute to the FOG in advanced PD (Thevathasan et al., 2018). Despite several clinical trials reporting improvement in PD motor

symptoms with DBS, treatment of FOG remains challenging. PPN and PPN + STN DBS trials have been attempted for management of refractory FOG, and have yielded mixed and inconclusive findings (Thevathasan et al., 2018). A recent study (NCT02318927) evaluated the feasibility and potential effectiveness of closed-loop PPN for medication-refractory FOG in patients with PD. Five (5) subjects with on-medication FOG were implanted with bilateral open-loop GPi DBS to address the cardinal PD motor symptoms. In addition, bilateral PPN DBS was used as an adaptive closed loop strategy to specifically address FOG. PPN recordings were precisely characterized and utilized for measuring neural correlates to deliver responsive stimulation. PPN low frequency power (1–8 Hz) tended to increase during gait, while GPi beta frequency tended to decrease during movement. Several challenges and complications were encountered during the study, as consistent with other studies in advanced PD patients. For example, recording signals were not consistent in all electrode contacts or across both hemispheres. But despite challenges, the study's primary goal of improving FOG was met, albeit with some limitation: the Closed loop-DBS protocol produced a greater than 40% improvement in FOG at 6 months in a minimum of 3/5 subjects. However, adverse events including scalp erosions and infections limited the feasibility of Closed loop-DBS in all patients, and disease progression led to worsening of motor and non-motor symptoms over time.

Thalamic and Cortical Signals for Development of Closed Loop DBS in Essential Tremor

Closed-loop stimulation has similar efficacy to open-loop, and in some contexts, closed-loop stimulation might be better than traditional DBS (Little et al., 2016). Chronically implanted sensing/stimulating devices (i.e., Activa RC + S) provide the capability to acquire large volumes of diverse data in real-life settings. These data can be useful in developing more sophisticated, accurate and reliable biomarkers than those that are currently available and used. Yet, closed loop-DBS also fosters a number of questions that are, and will be, important to consider; for example, is too much stimulation equally as problematic as too little stimulation – and if so, in what ways? For which diseases or disease states is closed loop-DBS best suited/most effective? Can closed loop-DBS afford more specific cortical biomarkers that can inform and guide improved modulation, clinical outcomes, and reduced side/adverse effects?

The Medtronic Activa PC + S device enables the use of a cortical strip for sensing/recording and a DBS electrode for stimulation in the treatment of patients with refractory tremor. The need for tremor control fluctuates greatly during the day and theoretically, a closed loop system could minimize concerns about side effects related to over- and/or under-stimulation (Kuo et al., 2018). Investigators have employed a cortical strip placed over M1, where beta power was used to trigger stimulation in the thalamus using a dual threshold method and machine learning in a subject-specific DBS model (Houston et al., 2019). Thresholds were set to optimize and minimize under-stimulation (at the relative calculated cost of over-stimulation). Assessments of three (3) subjects performed by blinded clinicians demonstrated that there was no significant difference in effectiveness between open-loop and closed loop stimulation, although at least one clinician evaluated spiral drawing by one subject to be better with closed-loop stimulation. Using machine learning tools, ongoing studies are attempting to define optimal parameters for open-loop stimulation for a given patient. A voluntary brain computer interface control method allows patients to control stimulation for patient-driven mitigation of side effects [depending on the function(s) being performed]. At present, it remains to be seen how accurate detection of movement and/or intention by cortical strips can be used to develop additional algorithms that can shift depending on a patient's functional state. Furthermore, exploratory assessment revealed that patients' feelings about their relative agency and/or autonomy may differ depending upon whether they have or do not have control over the level of DBS stimulation. Preliminary findings suggest that patients' sentiments vary widely (Gilbert, 2015).

Update on Brain Signals for Closed Loop DBS in Parkinson's Disease

Although DBS treatment of PD is an active field of research, many of the initial challenges and limitations of these treatments continue to be investigated. Meta-analysis of multiple DBS studies showed great variability in lead location (Perestelo-Perez et al., 2014). About one-third of implanted electrodes are revised or removed, and about 50% of these are due to suboptimal lead location. Lead localization and placement are integral to the success of DBS treatment, and this remains a challenge (Ellis et al., 2008). In part, this reflects varied anatomical preferences for DBS electrode implantation between neurosurgical practitioners and groups.

Thus, it becomes important to ask whether we really know where the target is, and if it is the "best" target. For example, in treating PD, tremor might be more responsive when the STN is stimulated in one subregion, and bradykinesia may improve more with stimulation of another subregion. In a recent study, researchers attempted beta-triggered closed- loop DBS in primates that were engaged in an acute reaching task. It was found that greater improvements in rigidity were obtained using closed- loop DBS (vs. traditional DBS), and that rigidity improved more during certain aspects of the movement (Hendrix et al., 2018). These results fortified the fact that biomarkers are dynamic and can fluctuate depending on functional state (e.g., sleep vs. awake), and that multiple algorithms might be needed to affect various target symptoms dependent on behavioral states. Biomarker detection using machine learning control algorithms might be required and may need to be adaptive over time to compensate for neuroplasticity. Data collected from cortical arrays implanted over M1 in primates showed that STN DBS reduced cortical-subcortical coupling (Wang et al., 2017). During off-DBS, the animal took longer to return to movement, but with GPi DBS-ON, there was a pattern of re-synchronization during the rest phase and de-synchronization during movement.

Evolving Neuromodulation Techniques

Temporal Interference and Deep Brain Stimulation

Boyden and Grossman recently developed a non-invasive approach to electrically stimulating neurons at depth

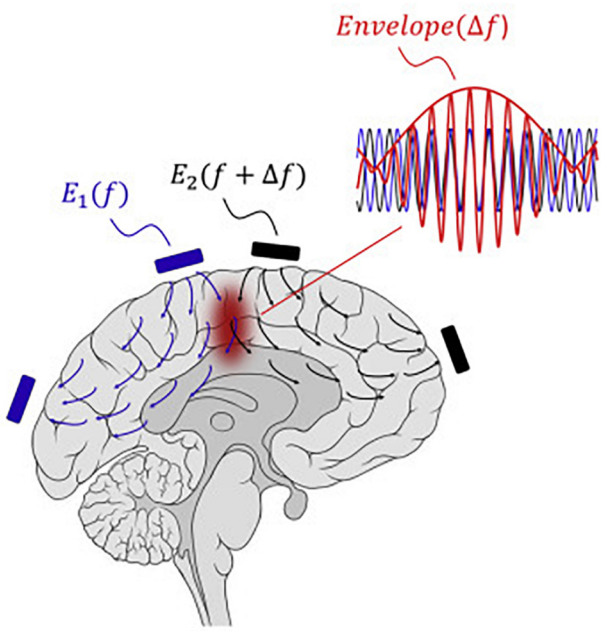

FIGURE 5 | Temporal interference as a non-invasive DBS technology.

(Grossman et al., 2017). By delivering multiple electric fields at frequencies too high to recruit neural firing, but which differ by a frequency within the dynamic range of neural firing, neurons could be stimulated throughout a region wherein interference between the multiple fields results in a prominent electric field envelope that is modulated at the difference frequency. This temporal interference (TI) was validated in modeling and physics experiments, and these studies verified that neurons in the living mouse brain could follow the electric field envelope (Grossman et al., 2017). The utility of TI stimulation was demonstrated *in vivo* by stimulating neurons in the mouse hippocampus without recruiting neurons of the overlying cortex. By altering the currents delivered to a set of immobile electrodes, different motor patterns in living mice could be 'steerably' evoked (**Figure 5**).

Update on Coordinated Reset

Increasingly, data from both preclinical models and direct recordings from patients undergoing DBS surgery support a mechanistic role for changes in the presence and dynamics of frequency-specific, synchronized oscillations across the dopamine-depleted basal ganglia thalamocortical 'motor' circuit (Nini et al., 1995; Brown et al., 2004; Mallet et al., 2008). Coordinated reset (CR) is an experimental neuromodulation paradigm engineered by Tass (2003) to desynchronize 'pathological' oscillatory activity across neuronal populations through the intermittent, pseudo-randomized delivery of brief, low-intensity, spatially-distributed pulse trains. A key advantage of CR relative to traditional DBS is that its effects should be achieved using lower individual pulse amplitudes (Tass, 2003), as the goal of the spatiotemporally-randomized stimuli is to break the otherwise hyper-synchronized target region into multiple, independent clusters. It is believed that an additional effect of this clustering phenomenon is to disrupt spike-timing-depending plasticity that may be reinforcing the persistence of the abnormal synaptic connectivity underlying the development and persistence of pathological activity. The end result being that even intermittent CR therapy may yield benefits that outlast cessation of stimulation by hours or days (Tass, 2003; Tass et al., 2012; Adamchic et al., 2014). From a therapeutic standpoint, a major benefit of CR DBS is that it may reduce the risk of provoking side-effects attributable either to the spread of electrical current outside of the target region or to chronic, continuous stimulation of the target itself (Ferraye et al., 2008; Moreau et al., 2008; Van Nuenen et al., 2008; Xie et al., 2012), and in these ways, reduce the overall duty-cycle of DBS delivery. Hence, a CR DBS approach that involves the intermittent delivery of low-intensity pulses may provide comparable motor benefit but be less disruptive to cognitive, affective, and even sensorimotor processing, while concomitantly reducing power consumption requirements.

At this time, the potential of CR stimulation to mitigate oscillatory activity is well-supported by theoretical models (Hauptmann et al., 2007; Hauptmann and Tass, 2009; Guo and Rubin, 2011; Lucken et al., 2013; Fan and Wang, 2015); however, *in vivo* preclinical or clinical evidence of its effects has been limited to three preliminary reports (Tass et al., 2012; Adamchic et al., 2014; Wang et al., 2016). On-going studies involve the use of the 1-methyl-4-phenyl-1,2,3,6-tetrahydropyridine (MPTP) non-human primate model of parkinsonism to better understand the acute, sub-acute and long-term efficacy profile of CR relative to traditional DBS, as well as to define its effects on neural activity across the basal ganglia thalamocortical motor circuit. The continuing goal is to acquire data that will facilitate the design of future human trials while further advancing an understanding of the role of synchronized oscillations in individual parkinsonian motor sign manifestation. The preliminary data acquired to date are extremely supportive of a potential role for CR in treating parkinsonian motor signs, but further point to potential interaction between its effects and baseline motor severity, lead localization, as well as the relative value of concurrent dopamine replacement therapy. To be sure, successful implementation of the CR DBS will require an effective re-dosing strategy to ensure long-term stability of its therapeutic effects. Potential options could range from open-loop strategies that involve applying CR at regimented dosing epochs, to more physiologically-dependent, demand-controlled approaches that are based on recordings derived either from the DBS lead itself or from secondary intracerebral recording arrays.

Advancing Applications of Optogenetic Techniques to DBS

Deep Brain Networks and Circuits for Multiple Behavioral States: Sleep, Arousal, Reward, Locomotion, and Addiction

As reports from previous DBS Think Tanks, and a growing body of international literature reveal, DBS can be a powerful

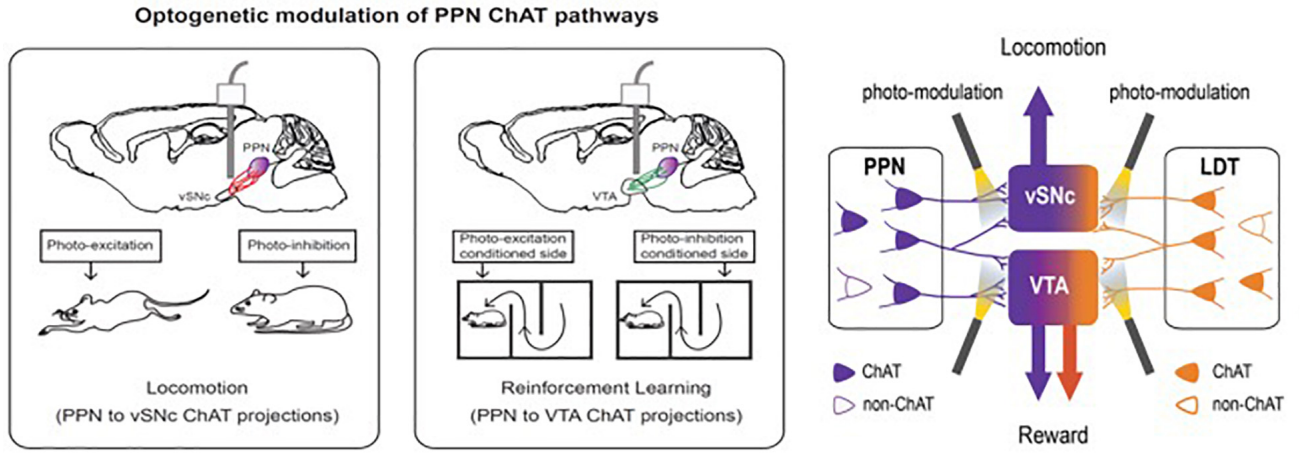

FIGURE 6 | Bidirectional manipulation of cholinergic cells in the PPN exert opposing effects on locomotor behavior and reinforcement learning via specific projections to the ventral substantia nigra pars compacta (vSNc) and the ventral tegmental area (VTA). This figure adapted from Cho et al. (2017).

therapeutic option for intractable movement and affective disorders, with benefits often being dramatic and manifested as instantaneous improvements in function and/or pathologic presentation. However, because electrical stimulation is non-specific, the mechanisms underlying or involved in the effects of DBS remain less than fully understood, and in some cases, are a source of controversy. The application of optogenetics to DBS challenged the traditional perception that DBS in the STN acts mainly by inhibiting local cell bodies at the stimulation site. Optogenetics uses genetically encoded, light-sensitive proteins to modulate or monitor the function of specific cell types within living heterogeneous tissue. In one of the first demonstrations of the power of optogenetics, we showed that control of axons in the stimulation area was sufficient to restore motor behavior in PD models (Gradinaru et al., 2009).

At least partly based upon these findings, a number of other targets for DBS are now being investigated for various indications. Examples include the neuromodulatory circuitry of two deep brain regions, the cholinergic mesopontine tegmentum [comprising the PPN and the laterodorsal tegmentum (LDT)] and the dopaminergic neurons of the dorsal raphe nucleus (DRN^{DA}) (Xiao et al., 2016). The use of neurotechnology revealed details of both circuits that may ultimately lead to new therapeutic targets for movement and addiction disorders (PPN circuits), and sleep/arousal disorders (DRN^{DA} circuits) (**Figure 6**). Bidirectional manipulation of cholinergic cells in the PPN exerts opposing effects on locomotor behavior and reinforcement learning via specific projections to the ventral substantia nigra pars compacta (vSNc) and the ventral tegmental area (vTA). Additionally, DRN^{DA} activity increases in response to salient stimuli irrespective of valence, is correlated with sleep–wake states, and can bi-directionally modulate arousal.

Sleep and arousal modulation

The ability to awaken in response to salient stimuli and to remain alert when awake, particularly upon perception of relevant environmental danger or crying offspring, holds obvious biological importance in terms of survival and fitness of self, kin, kith, and/or species. Our work using mouse models suggests that DRN^{DA} neurons play a key role in this process (Cho et al., 2017). Using simultaneous fiber photometry and polysomnography (EEG/EMG), time-delineated DRN^{DA} activity upon exposure to arousal-evoking salient cues, irrespective of hedonic valence, was observed. As well, fluctuations of DRN^{DA} activity across sleep–wake cycles were seen, with highest activity during wakefulness versus sleep states. Both endogenous and optogenetically driven DRN^{DA} firing were associated with arousal from sleep (**Figures 7**, **8**). Conversely, chemogenetic DRN^{DA} inhibition opposed wakefulness. Finally, time-locked DRN^{DA} inhibition reduced the probability of an immediate sleep-to-wake transition upon delivery of an unconditioned tonal stimulus.

Cumulatively, these data suggest that DRN^{DA} neurons modulate arousal and can promote awakening by salient stimuli. While the ability to rouse from sleep in response to alerting stimuli is an evolutionarily conserved survival strategy, it may have negative sequelae in modern human populations: insomnia or hypersomnia triggered by malfunctioning arousal-promoting circuits is a morbid societal burden (Roth, 2007). Going forward, strategies targeting DRN^{DA} activity may have utility both in the treatment of primary sleep–wake disorders and sleep/arousal disturbances secondary to myriad neuropsychiatric diseases, including depression, bipolar disorder, and schizophrenia.

Modulation of reward

The mesopontine tegmentum provides major cholinergic inputs to the midbrain and regulates locomotion and reward. To delineate underlying projection-specific circuit mechanisms, we employed optogenetics to control mesopontine cholinergic neurons at the somata and at divergent projections within distinct midbrain areas. Bidirectional manipulation of cholinergic cell bodies in the PPN exerted opposing effects on locomotor behavior and reinforcement learning. Motor and reward effects were separated by limiting photostimulation to PPN cholinergic terminals in the vSNc or in vTA, respectively. LDT cholinergic

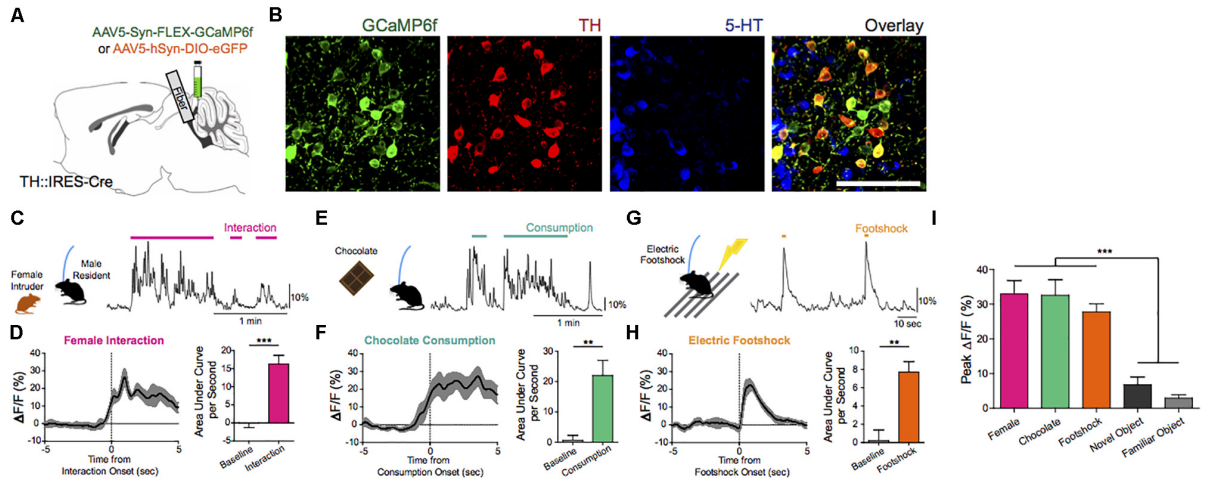

FIGURE 7 | Endogenous and optogenetically driven DRN^{DA} firing. **(A)** TH-Cre mice were injected with AAV5-Syn-FLEX-GCaMP6f or AAV5-hSyn-DIO-EGFP and implanted with an optical fiber into the DRN for fiber photometry. **(B)** Confocal images of GCaMP6f+ (green) neurons show co-localization with TH+ neurons (red), but no overlap with 5-HT+ neurons (blue). Scale bar, 100 μm. **(C)** Social interaction between a male DRN$^{DA\text{-}GCaMP6f}$ resident mouse and a female intruder were associated with increased DRNDA activity; the trace is a representative recording with interaction bouts indicated. **(D)** Left: female interaction caused an increase in fluorescence at the onset (first interactions only). Right: quantification of the area under the curve per second (AUC) during the interaction (0–5 s) shows that social interaction caused significant increase in DRNDA activity from baseline (−5 to 0 s) (n = 7 DRN$^{DA\text{-}GCaMP6f}$ mice; paired t test, t6 = 11.97, $^{***}p < 0.001$). **(E)** Chocolate consumption by a DRN$^{DA\text{-}GCaMP6f}$ mouse increased DRNDA activity; representative recording. **(F)** Left: DRNDA activity was increased upon chocolate consumption. Right: AUC quantification during consumption (0–5 s) compared with baseline (−5 to 0 s) shows that food consumption is associated with significant fluorescence increase (n = 7 DRN$^{DA\text{-}GCaMP6f}$ mice; paired t test, t6 = 4.273, $^{**}p < 0.01$). **(G)** Electric footshocks (0.25 mA, 1 s) were delivered; representative DRNDA trace during two consecutive footshocks. **(H)** Left: footshock induced phasic DRN^{DA} activation. Right: DRN^{DA} activity after footshock (0–5 s) was significantly increased relative to baseline (−5 to 0 s) (n = 7 DRN$^{DA\text{-}GCaMP6f}$ mice; paired t test, t6 = 5.763, $^{**}p < 0.01$). **(I)** Peak DRNDA fluorescence values during female interaction, chocolate consumption, and electric footshocks were significantly higher than those during novel and familiar object interaction (n = 7 DRN$^{DA\text{-}GCaMP6f}$ mice; one-way ANOVA, $F_{4,30}$ = 22.77, $p < 0.0001$, Bonferroni *post hoc* analysis, $^{***}p < 0.001$).

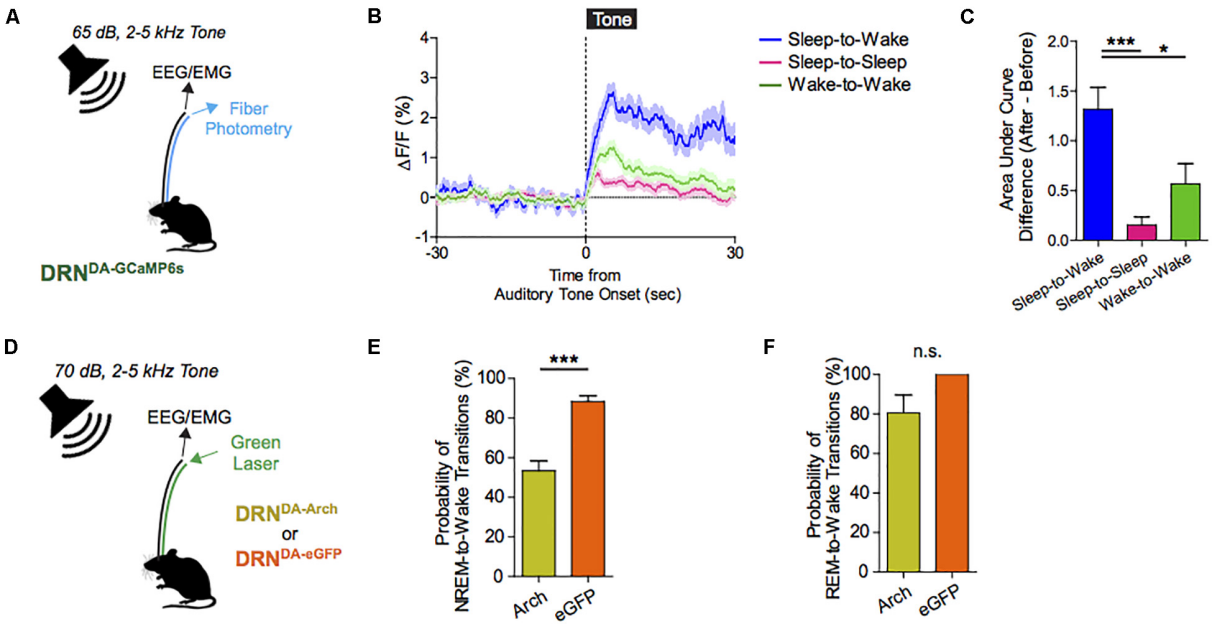

FIGURE 8 | Dorsal raphe nucleus dopaminergic (DRN^{DA}) activity escalates in response to salient stimuli irrespective of valence; correlates with sleep–wake states, and can bidirectionally modulate arousal. **(A)** Experimental paradigm. **(B)** Auditory cues are associated with time-locked increases in DRN^{DA} activity. **(C)** DRN^{DA} activity increase, as indexed by the difference in the area under the curve between before and after tone presentation, was larger when auditory tone induced sleep-to-wake transitions than when it was turned on while awake or when it failed to cause sleep-to-wake transitions (n = 7 DRN$^{DA-GCaMP6s}$; One-way ANOVA, $F_{2,18}$ = 10.79, $p < 0.001$, *Post hoc* Bonferroni analysis, $^{**}p < 0.01$). **(D)** Experimental paradigm. **(E)** Time-locked DRN^{DA} inhibition decreased the probability of NREM-to-wake transitions upon auditory cues (n = 6 DRN$^{DA-Arch}$, n = 4 DRN$^{DA-eGFP}$; Two-tailed, unpaired t-test, $^{***}p < 0.001$. **(F)** No significant change in the probability of REM-to-wake transitions (n = 6 DRN$^{DA-Arch}$, n = 4 DRN$^{DA-eGFP}$; Two-tailed, unpaired t-test, $p > 0.1$).

neurons also form connections with vSNc and vTA neurons; however, although photo-excitation of LDT cholinergic terminals in the vTAc aused positive reinforcement, LDT-to-vSNc modulation did not alter locomotion or reward. Therefore, the selective targeting of projection-specific mesopontine cholinergic pathways may offer increased benefits in treating movement and addiction disorders.

Optogenetic Techniques to Facilitate Modulation of Motor Circuits

The identification of distinct cell types in the basal ganglia has been critical to an understanding of basal ganglia function and the treatment of neurological disorders. The external globus pallidus (GPe) is a key contributor to motor suppressing pathways in the basal ganglia, yet its neuronal heterogeneity has not been engaged as a resource for therapeutic interventions. Optogenetic techniques may enable cell specific identification and stimulation of GPe networks that can be modulated by DBS (Gittis et al., 2014). The indirect pathway is overactive in PD and suppression of GPe neurons using these techniques might both increase activity in GPe and improve movement. However, experiments in mouse models failed to demonstrate a clear benefit in motor symptoms. In recent studies, optogenetic interventions that dissociate the activity of two neuronal populations in the GPe, elevating the activity of parvalbumin (PV)-expressing GPe neurons over that of Lim homeobox 6 (Lhx6)-expressing GPe neurons, reinstates movement in DA-depleted mice, and decreases pathological activity of basal ganglia output neurons for hours past stimulation (Mastro et al., 2017). These results establish the utility of cell-specific interventions in the GPe to target functionally distinct pathways, with the potential to induce long-lasting recovery of movement despite the continued absence of DA.

The Use of Optogenetics to Understand Addiction Circuitry

Addiction can be regarded – at least to some extent – as a neural circuit disorder; functional imaging has identified the cortico-accumbal-pallidal network as a locus of altered resting state connectivity in patients with addiction, and the nucleus accumbens (NAc) has been proposed as a target for DBS (**Figure 9**). NAc-DBS suppresses drug seeking and sensitization to drug-associated cues, although these behavioral effects are transient, and paradoxical increased substance consumption has been observed (Hadar et al., 2016; Creed, 2018). Moreover, a better understanding of the underlying mechanisms of the NAc-DBS may be useful for optimizating stimulation protocols.

Understanding mechanisms underlying altered functional connectivity in addiction could be leveraged to design targeted neuromodulation protocols to normalize circuit function and abolish behaviors associated with addiction. For example, cocaine exposure potentiates prefrontal cortical inputs to the NAc via the insertion of calcium-permeable AMPA receptors, and optogenetically driving these inputs between 10 and 15 Hz triggers a signaling cascade that reverses this synaptic potentiation and abolishes drug sensitization and seeking (Pascoli et al., 2011). Based on these observations, an optogenetically-inspired DBS (OiDBS) protocol was developed; this protocol combined 12 Hz stimulation with a D1 dopamine receptor antagonist (Creed et al., 2015). The D1R antagonist was necessary to prevent D1R-dependent signaling which inhibits de-potentiation. OiDBS normalized synaptic transmission and reduced locomotor sensitization following cocaine exposure. If translated to humans, an OiDBS protocol would have several advantages over traditional DBS protocols. It would significantly reduce stimulation time, which would extend battery life and/or could be instrumental to non-invasive stimulation methods. Stimulation protocols could also be tailored to normalize circuit function associated with diverse symptoms of addiction, such as craving vs. withdrawal-induced negative affect. To this end, neural signatures of behavioral symptoms would need to be identified. Recording from multiple sites and using altered synchrony across brain areas to trigger DBS in a closed-loop manner would represent a major therapeutic advance. Further, the use of OiDBS could extend beyond addiction to other disorders characterized by altered function of neural circuits, such as chronic pain, mood, and neurodevelopmental disorders.

Use of Optogenetics in Alzheimer's Disease Circuitry

While neural stimulation has opened up a new class of therapeutics for a number of neurological and psychiatric diseases, there has been little work to examine how such stimulation could be used to treat Alzheimer's disease (AD), the most common form of dementia. The lack of research on neural stimulation in AD likely stems from the fact that little is known about how neural activity fails in AD or how neural activity affects molecular pathology. Therefore, to determine how brain stimulation could potentially be used to treat AD, we identified deficits in neural activity in mouse models of AD and determined the effects of neural stimulation on molecular and cellular pathology (Iaccarino et al., 2016).

Because spatial navigation deficits are one of the earliest symptoms of AD and the hippocampus is one of the neuroanatomical areas first affected by the disease, we examined how hippocampal neural activity changes in AD (Fox et al., 1996; Deipolyi et al., 2007). Using a virtual reality behavior paradigm to record and manipulate neural activity in transgenic mice, the primary animal model of AD, deficits in hippocampal neural activity were revealed early in the progression of the disease. These deficits occurred in the same patterns of activity that we and others previously found to be involved in memory-guided decisions in spatial navigation tasks (Carr et al., 2012; Pfeiffer and Foster, 2013; Singer et al., 2013). Subsequently, we found that driving gamma activity, which is lacking in AD mice, mobilized the immune system to remove pathogenic proteins. Specifically, driving 40 Hz neural activity via optogenetic stimulation recruited microglia -the primary immune cells of the brain – to alter their morphology and increase engulfment of β amyloid, a protein thought to be involved (if not initiate) a series of neurotoxic events in AD (Iaccarino et al., 2016).

To achieve the same effects non-invasively, we harnessed the neural circuits' natural tendency to respond to sensory stimuli. While extensive prior work has shown that flickering

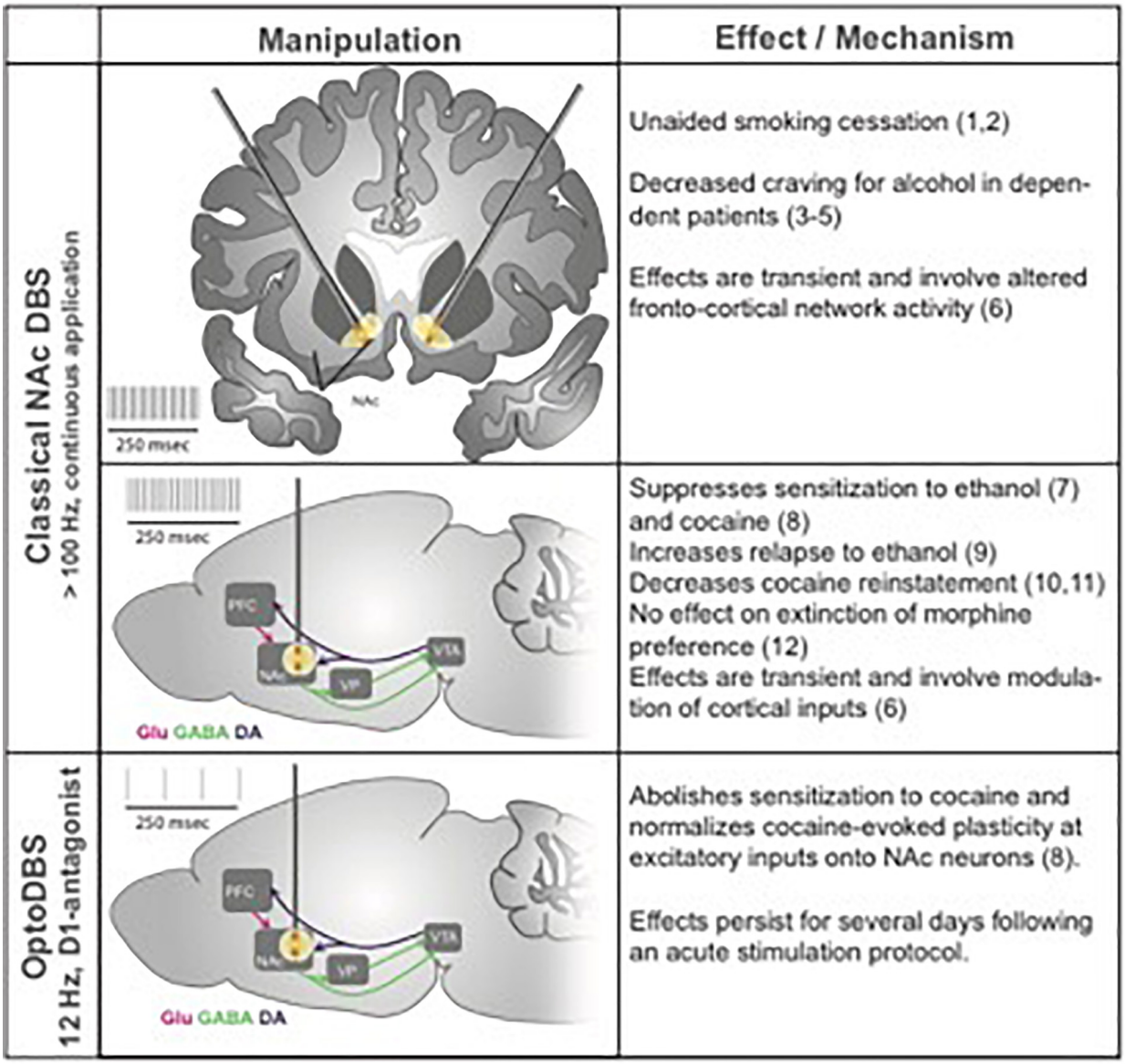

FIGURE 9 | Approaches to Addiction DBS.

lights and sound stimuli drive neural activity at specific frequencies in sensory cortices, we have found such flickering sensory stimuli can also drive specific frequencies of neural activity in deeper brain structures, including the hippocampus, albeit with more modulatory effects (Iaccarino et al., 2016). Using this approach, we demonstrated that flickering stimuli within gamma frequencies, 40 Hz in particular, drives gamma frequency neural activity in hippocampus and recruits microglia to engulf pathogenic proteins in mouse models of AD. Existing methods for stimulating neural circuits with temporal precision are either invasive (e.g., DBS), or only access superficial brain structures [e.g., transcranial electrical stimulation (tES)].

Thus, the demonstration that flickering sensory stimuli drives rhythmic neural activity in deep structures reveals a new, and potentially powerful non-invasive tool with which to modulate and/or manipulate neural activity. Moreover, the discovery that stimulating neural activity at specific frequencies can recruit immune cells in the brain to reduce molecular and immune cells may afford a new potential use of neural stimulation to treat certain forms of neuro-psychiatric disease.

Novel Databases for DBS and Neuroimaging Stereotactic Techniques

CranialCloud

The use of complex, heterogeneous, multi-level and -dimensional data is -and will increasingly be – crucial to realizing the potential of a number of neurotechnologies and their use in clinical practice (DiEuliis and Giordano, 2016). Rapidly advancing technology in healthcare informatics is providing increasing opportunities for innovative strategies in both the clinical management of patients, and the advancement of research. As informatic technology is more widely adopted into clinical practice, increasing opportunities – and challenges – arise in the collection, storage, analysis, interpretation, and use of ever larger and more multi-dimensional data resources. Many laboratories throughout the world are using varied imaging and neurophysiologic techniques to address research questions and the translation of positive experimental findings into clinically viable methods. Inter-institutional collaboration (on both intra- and inter-national scales) requires standardization of the data collection process and effective and efficient means of data sharing. However, much of the collected data is stored locally, and sharing capabilities are either expensive, inefficient, or unavailable. Therefore, it will be important to develop improved methods for facile exchange of information between large datasets and patient cohorts.

Cranial Cloud engages this opportunity by providing a platform to standardize data collection and storage (D'haese et al., 2015). This program is equipped with tools to process, analyze and share data in a de-identified manner. Similar in design to the *DropBox* model, the Cranial Cloud system is capable of integrating information with currently available and widely used electronic medical record systems (e.g., EPIC). Clinical assessments and anatomical/imaging data can be collected in a standardized method in order optimize compatibility with various atlases and programs. The overall goal is to maintain and advance normalized, consistent and efficient data collection, sharing and analysis soas to both reduce (if not eliminate) constraints imposed by existing systems, and to avoid the time and economic costs of duplicative analyses. Questions remain about the funding source of such an endeavor, but it will likely require collaboration between academic, corporate and government institutions. Concerns about data sharing with third parties will be a challenge for ensuing technologies.

Blackfynn

National Institutes of Health policy states that data should be widely and freely available, while still maintaining privacy and confidentiality[1]. In keeping with this policy, the Blackfynn Scientific Platform functions to standardize data collection in DBS patients, and to make these data more accessible in accordance with existing regulations for data sharing[2]. As well, this platform can maintain data that would otherwise be lost due to cessation of funding. Blackfynn aims to develop a strong business model to sustain the database independently of short-term funding. This database will enable improved workflow and medical record integration that will appeal to clinicians and researchers. A major feature of the program is its web-based, high performance computing capability, which allows users to maintain possession of their data while simultaneously using the platform for data analysis.

One example of such successful data collection, storage and sharing is the Parkinson's Progression Markers Initiative (PPMI), which facilitates rapid exploration and data-driven analysis, rather than exclusively utilizing a hypothesis-driven approach. This database can also be combined with other backgrounds and datasets to examine biomarker overlap and/or to integrate genetic or physiologic data, and can facilitate cooperation and collaboration between the academic and corporate sectors, and can positively impact and be implemented by a variety of stakeholders, including foundations and advocacy groups. These collaborations are – and will be ever more – essential given the resource demands for the sustenance and iterative expansion and improvement of such a large database.

Surgical Information Sciences

The neurosurgical implantation of DBS systems requires a high degree of accuracy in placing electrodes at the identified target sites, and clinical outcomes greatly depend upon the precise localization of special leads and contacts (Ellis et al., 2008). For example, suboptimal STN electrode placement has been associated with reduced clinical efficacy and the occurrence of adverse effects. At present, all candidates for DBS implantation surgery undergo 1.5 (i.e., structural) and/or 3 Tesla (T; functional) magnetic resonance imaging (MRI) as a component of the presurgical clinical workup. With the widespread availability of MRI devices for clinical use, direct targeting (i.e., targeting that is based on visually identifying the intended sites of electrode placement) has become more feasible. However, standard clinical MRI protocols are typically associated with low resolution, inadequate image contrast and relatively low signal to noise ratio (SNR), which make accurately identifying the intended anatomical targets difficult. As a result, it can be challenging to identify the exact borders of the intended targets, and differentiate DBS targets from adjacent anatomical structures.

Ultra-high field (UHF) MR acquires images using a generated magnetic field that is equal to or greater than 7T (Abosch et al., 2010). 7T MRI has proven to provide structural images of the human brain with rich informational content, higher contrast and resolution, and with the potential for use in clinical applications (Duchin et al., 2012, 2018; Gunalan et al., 2017).

[1]https://grants.nih.gov/grants/policy/data_sharing
[2]https://www.blackfynn.com

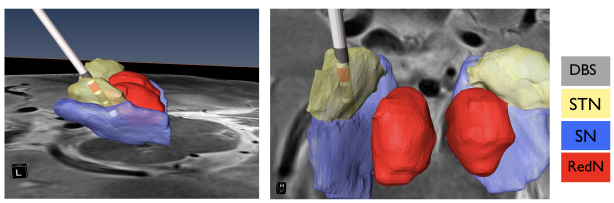

FIGURE 10 | Patient specific modeling for DBS.

The enhanced images acquired using 7T systems improve the ability to visualize subcortical structures, and to create patient-specific 3D anatomical models. This is important given that there is significant variability across individuals in the location, volume, length, depth, and width of a number of neuroanatomical structures (e.g., the STN). The use of patient-specific 3D anatomical models using pre-operatively acquired 7T MRI data can be combined with post-operative imaging (CT or MRI) to create computer-generated depictions of DBS electrode position and contacts (Duchin et al., 2018) (**Figure 10**). Additionally, the use of diffusion weighted images and structural connectivity-based parcelation protocols can enable depiction of STN connections to the motor, limbic, and associative cortical areas, which can be used to map the individual subdivisions of the nucleus (Plantinga et al., 2018). These new capabilities suggest that the use of 7T MR imaging may facilitate individualized and highly specific planning of DBS implantation of the STN, as well as other DBS targets (Patriat et al., 2018; Shamir et al., 2019). Our ongoing work is focused upon exploring these capabilities in further detail.

Neuroethical, Legal, and Social Issues (NELSI) in DBS

Continued Access to Investigational Brain Implants and Care

At the most fundamental level, the aim of development and use of brain implants has been to enable successful intervention against treatment-resistant neurological and psychiatric disorders. Although the underlying rationale and goals of invasive neuromodulation were and remain benevolent, implantation of these devices exposes patients to both the inherent risks of neurosurgery and to the burden and risks incurred through the use of novel technology (Giordano, 2015a). There is growing discourse about if and how DBS systems should be removed (i.e., explanted) if satisfactory or durable clinical outcomes are not achieved, or if deleterious/adverse effects are incurred. Most trials include plans for explantation for those patients who do not receive benefit or who may have adverse effects, but generally, the cost of explantation surgery is not covered. This is not unique or surprising, given that other incurred costs (e.g., unscheduled visits to the clinical specialists, battery replacement, device repairs, salvage procedures due to infection) may – and often – also are not covered (Rossi et al., 2017).

To date, such issues have been addressed on a case-by-case basis. In the United States there is no legal obligation to provide continued access to DBS devices or resources. Yet, given that the majority of DBS implantation is undertaken as either a large scale clinical trial, or as a component of investigator initiated research (IIR) studies, the constructs of the Declaration of Helsinki could be utilized to support and reinforce continuity of care under as a component obligation of protecting the best interests of the patient/subject – both during and as a consequence of the research study – as constituent to the conduct of responsible research (Giordano, 2015b, 2016). The strength of the moral obligation to provide continued provision of, and access to care depends on the vulnerability of patients, the burden placed on them by the research protocol (e.g., lack of treatment options, and imperatives to advance these technologies), and the feasibility of providing continued clinical care without unnecessarily impairing or impeding ongoing or future research.

Indeed, costs of establishing, and supporting continued care could substantially constrain certain sponsors' ability to pursue research. In turn, such constraints could negatively impact both a sponsor's engagement in and support of further research, and the potential benefits that such research could provide to the extant and future recipient patient populations at-large. Recent requests for proposals (RFPs) issued via the National Institutes of Health's programs within the US Brain Research through Advancing Innovative Neurotechnologies (BRAIN) Initiative have mandated that researchers describe the plan for the patient at the end of the study period, and the ethical principles supporting an extended (albeit) limited duty of care beyond the research protocol. More specific language is being considered for incorporation into current and future RFPs. But any meaningful discussion of ethics must acknowledge and address economic issues, and so consideration of continued care as a constituent of responsible research must be inclusive of cots and coverage of provision and access, time period of extended care, availability of treatment options and alternatives, development of novel treatments, and the systems in place and operational in order to accommodate the fiscal burdens of such needs and demands.

Toward Ethical Integration in the Development and Use of DBS

Perhaps one of the more provocative, if not contentious ethico-legal questions is whether DBS "changes" personality, the "self" and in these ways, impairs patient individual autonomy (Jotterand and Giordano, 2011; Giordano, 2015b). As well, there are concerns about patients' and families' psychological effects and reactions to living with the device; the effect of DBS on patients' social relationships; and to broader influence that DBS – and other neuromodulatory technologies – will incur upon and within society and culture. The question of whether stimulating brains is a form of "mind control" and "creating new selves" is gaining prominence as a focus of discourse, both within medicine and the social sciences, as these technologies and techniques are being both considered for the treatment of a broader palette of neurological and psychiatric disorders, and viewed toward the potential to modify cognition, emotion

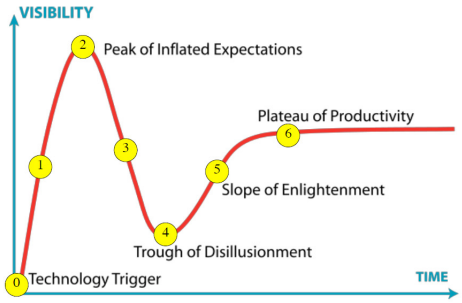

Indication/Use	Weighted average	Last year's score		Relative Change
DBS for Parkinson's	5.34	5.43	0	-1.66%
DBS for Essential Tremor	5.33	5.14	1	3.70%
Cochlear Implant	5.32	4.86	2	9.43%
VNS for Epilepsy	4.68	4.50	3	4.07%
Imaging Post DBS Implant	3.97	3.70	4	7.33%
Spinal Cord Stimulation for Pain Management	3.97	4.18	5	-5.14%
Imaging to Guide Surgical Targeting	3.91	3.96	6	-1.18%
MRI Safety of Neurotechnology Implants	3.59	3.51		2.33%
DBS for Depression	3.57	3.42		4.51%
DBS for Epilepsy	3.19	3.27		-2.49%
DBS for OCD	3.12	3.10		0.73%
Sacral Nerve Stimulation for Overactive Bladder	3.12	3.32		-6.16%
DBS for Tourette's	3.11	3.00		3.77%
Transcranial Magnetic Stimulation	3.10	2.87		8.01%
Modeling to Guide Surgical Targeting	2.64	2.43		8.70%
PNS Stimulation for Chronic Pain	2.55	2.71		-5.95%
FES for Foot Drop	2.51	2.61		-3.74%
EEG for Decoding Limb Movement (Chronic Use)	2.30	2.53		-9.27%
DBS for Chronic Pain	2.17	2.40		-9.59%
FES for SCI - Bladder Control	2.13	3.14		-32.03%
Closed-Loop Feedback	2.06	2.15		-4.19%
Retinal Implant	1.99	2.24		-11.25%
FES for SCI - Limb Control	1.91	2.00		-4.61%
Neural Stimulation for Stroke Symptoms	1.88	1.94		-2.90%
Microelectrodes in the CNS for Decoding Limb Movement (Chronic Use)	1.85	2.04		-9.55%
ECoG for Decoding Limb Movement (Chronic Use)	1.83	2.35		-21.99%
DBS for Alzheimer's	1.80	1.91		-5.66%
Microelectrodes in the PNS for Decoding Limb Movement (Chronic Use)	1.80	1.54		16.73%
Bi-Directional Wireless Telemetry	1.77	1.98		-10.84%
Wireless Power for Implants	1.71	1.78		-3.69%
Telemetric Cortical Recording and Stimulation	1.70	2.00		-15.10%
VNS for Heart Failure	1.63	1.11		46.69%
ECoG for Encoding Sensory Feedback (Chronic Use)	1.50	1.59		-5.66%
VNS for Obesity	1.49	1.54		-3.43%
Microelectrodes in the PNS for Encoding Sensory Feedback (Chronic Use)	1.41	1.41		0.18%
DBS for Addiction	1.39	1.15		20.59%
Reliable Implantable High-Channel Count Connectors (>=100 Channels)	1.38	1.68		-18.00%
Low-Intensity Focused Ultrasound	1.36	1.58		-13.92%
Neuromagnetic Interfaces	1.32	1.30		1.76%
Microelectrodes in the CNS for Encoding Sensory Feedback (Chronic Use)	1.31	1.45		-9.81%
VNS for Rheumatoid Arthritis	1.23	1.13		8.92%
DBS for Obesity	1.20	1.54		-22.20%
Optogenetics for Clinical Neural Interfaces	0.98	1.16		-15.55%
DBS for PTSD	0.93	1.00		-6.60%
DBS for TBI	0.93	1.27		-26.56%

FIGURE 11 | Perspectives and Attitudes Toward DBS. An anonymous 40 question poll was sent online to assess participants' perspectives and attitudes toward the current and near-term future developments and applications in the DBS field. Sixty six participants responded.

and behavior in "cosmetic," socio-politically and/or military contexts and ways. Looking – and moving – ahead, qualitative and behavioral studies in natural environments will likely be increasingly necessary to more fully elucidate the ways that DBS (and other neuromodulatory technologies) can, should, or should not be developed and used to mitigate or prevent the effects of disease and injury, and/or improve the quality of life.

Moreover, defining "advancement" and "improvement" to establish the groundwork for ongoing research, development and use-in-practice will be essential to a prudent approach to DBS in this era of personalized medicine, global health initiatives, healthcare and technological inequalities, and the expansion of multi-national research and medical tourism opportunities. In this light, such discourse must be international and sensitive, if not responsive, to differing cultural perspectives, needs, philosophies, values, and capabilities (Stein and Giordano, 2015; Giordano, 2018). We have previously advocated for "no new neuroscience without neuroethics" and "no neuroethics without neuroscience" (Giordano and Shook, 2015), as ethico-legal and social discourse and decisions must be based upon and proceed from the realistic capabilities conferred by the science and technology. Here, we widen our invocation to appeal for a multi-cultural lens, discourse and engagement soas to fortify scientific and technological developments with a fuller depiction and consideration of the socio-cultural contexts and realties that may shape and be shaped by the use of DBS on the world stage.

SUMMARY AND CONCLUSION

The field of neuromodulation continues to evolve and ongoing research will shape the scientific landscape. This manuscript represents the views of the participants of the think tank and does not consider all the literature on the topics discussed. As in prior years' meetings, an anonymous 40 question poll was sent online to evaluate participants' perspectives and attitudes toward the current and near-term future developments and applications in neuromodulation. Sixty six participants responded. **Figure 11** summarizes these responses and compares them to last year's responses. It is notable that some applications moved to the trough of disillusionment (e.g., DBS for depression), others moved to the peak of inflated expectations (e.g., Vagus nerve stimulator for heart failure), and others remained on the slope of enlightenment (DBS for Parkinson's, DBS for essential tremor, cochlear implants, and VNS for epilepsy). Consistently, the use of DBS for movement indications has reached the plateau of productivity and among most Think Tank participants there was cautious optimism regarding the use of larger network based modulation. There was also cautious optimism for advancing neurophysiological and anatomical signals to improve neuromodulation for several neuropsychiatric conditions, non-neurological indications. There was clear optimism for the development of novel technologies.

ETHICS STATEMENT

Individual studies were approved by the local Institutional Review Board of participating institutions in this technical report and written informed consent was obtained from all participants.

AUTHOR CONTRIBUTIONS

AR-Z, JG, EB, VG, AG, PS, SS, CM, MF, JV, VV-M, UA, LA, HB-S, HM, NP, AHG, AS, MC, GL-M, MR, MAR, LC-Z, P-FD, WC, RG, HC, AK, KB, JW, WD, NH, WD, KF, and MO fulfilled the authorship criteria by substantial contributions to the conception of the work, providing data for the work, revisiting it critically for important intellectual content, approving the final version, and agreeing to be accountable for all aspects of the work in ensuring that questions related to the accuracy or integrity of any part of the work are appropriately investigated and resolved.

FUNDING

AR-Z serves as a consultant for the National Parkinson Foundation, and has received consulting honoraria from Medtronic, Boston Scientific, and Wilson Therapeutics and has participated as a site PI and/or co-PI for several NIH, foundation, and industry sponsored trials over the years but has not received honoraria. JG work was supported in part by the European Union's Horizon 2020 Research and Innovation Programme under grant agreement 720270: HBP SGA1; by federal funds UL1TR001409 from the National Center for Advancing Translational Sciences (NCATS), National Institutes of Health, through the Clinical and Translational Science Awards Program (CTSA), a trademark of the Department of Health and Human Services, part of the Roadmap Initiative, "Re-Engineering the Clinical Research Enterprise"; by funding from the AEHS Foundation, in conjunction with Project Neuro-HOPE; and from the Austin and Ann O'Malley Visiting Chair in Bioethics of Loyola Marymount University. EB was supported by J. Doerr, the HHMI-Simons Faculty Scholars Program, the Open Philanthropy Project, Human Frontier Science Program (RGP0015/2016), US Army Research Laboratory and the US Army Research Office (W911NF1510548), US-Israel Binational Science Foundation (2014509), and NIH (2R01-DA029639 and 1R01-GM104948). VG work was primarily supported by the National Institutes of Health (NIH) Director's New Innovator grant DP2NS087949 and PECASE, National Institute on Aging grant R01AG047664, BRAIN grant U01NS090577, SPARC grant OT2OD023848-01, and the Defense Advanced Research Projects Agency (DARPA) Biological Technologies Office. Additional funding included the NSF NeuroNex Technology Hub grant 1707316 and funds from the Curci Foundation, the Beckman Institute, and the Rosen Center at Caltech. AG is supported by the NIH/NCATS Clinical and Translational Science Awards to the University of Florida UL1TR001427, KL2TR001429, and TL1TR001428. PS is a recipient of funding from the National Institutes of Health (R01 NS090913 and UH3 NS 100544) and from the Defense Advanced Research Projects Agency (DARPA). SS acknowledges support from the DARPA Restoring Active Memory (RAM) program (Co-operative Agreement N66001-14-2-4032) and NIH Grants MH104606 and 1S10OD018211-01. CM work was supported by the National Institutes of Health Grants R01 MH106173 and R01 NS086100. CM is a paid consultant for Boston Scientific Neuromodulation and Kernel, as well as a shareholder in the following companies: Surgical Information Sciences, Autonomic Technologies, Cardionomic, Enspire DBS, and Neuros Medical. MF work was supported by the NIH National Institute of Neurological Disorders and Stroke (K23NS083741) and Dystonia Medical Research Foundation. HB-S work was supported by the NINDS Grant 5 R21 NS096398-02, the Michael J. Fox Foundation, the Robert and Ruth Halperin Foundation, the John A. Blume Foundation, the Helen M. Cahill Award for Research in Parkinson's Disease, and Medtronic, Inc., who provided the devices used in this study but no additional financial support. HM work was supported by the NIH Brain Research through Advancing Innovative Neurotechnologies (BRAIN) Initiative (UH3NS103550) and the Hope for Depression Research Foundation. NP reports support by grants UH3NS103549, R01NS097782, and U01NS098961 from the National Institute of Neurological Disorders and Stroke (NINDS). AHG work was supported by grants from the Brain and Behavior Research Foundation (National Alliance for Research on Schizophrenia and Depression Young Investigator Grant), the Parkinson's Disease Foundation, and the NIH Intramural Research Program. MC work was funded by a Whitehall Research grant (Grant ID# 2017-12-54). GL-M work has been funded by the National Institutes of Health (NIH) grant R00HG008689. MR work has been supported by the National Institutes of Health through Grant Number UL1-TR-001857. P-FD acknowledges the National Institutes of Health (NIH) for their support of Neurotargetting LLC and their CranialSuite clinical software (R01-EB006136 and R01-NS095291). NH is a shareholder of Surgical Information Sciences, Inc. and holds a patent related to high-resolution brain image system (U.S. Patent 9600778). This study was partially supported by the National Institutes of Health (R01-NS085188, P41 EB015894, and P30 NS076408) and the University of Minnesota Udall center (P50NS098573). JW acknowledges grant support by NIH 1K01ES025436. KB reports support from NIH NINDS NS092730. AK and HC work was supported by National Institutes of Health grant T90 DA032436, National Science Foundation grant EEC-1028725, the Department of Defense through the National Defense and Engineering Graduate Fellowship program, and a donation by Medtronic. RG work was supported by NIH grants (NS090913-01 and NS100544-02) and the UC President's Postdoctoral Fellowship. MO serves as a consultant for the National Parkinson Foundation, and has received research grants from NIH, NPF, the Michael J. Fox Foundation, the Parkinson Alliance, Smallwood Foundation, the Bachmann-Strauss Foundation, the Tourette Syndrome Association, and the UF Foundation. MO's DBS research is supported by grants R01 NR014852 and R01NS096008 from the National Institutes of Health. MO has previously received honoraria, but in the past >60 months has received no support from

industry. MO has received royalties for publications with Demos, Manson, Amazon, Smashwords, Books4Patients, and Cambridge (movement disorders books). MO is an associate editor for New England Journal of Medicine Journal Watch Neurology. MO has participated in CME and educational activities on movement disorders (in the last 36 months) sponsored by PeerView, Prime, QuantiaMD, WebMD, Medicus, MedNet, Henry Stewart, and by Vanderbilt University. The institution and not MO receives grants from Medtronic, Abbvie, Allergan, and ANS/St. Jude, and the PI has no financial interest in these grants. MO has participated as a site PI and/or co-PI for several NIH, foundation, and industry sponsored trials over the years but has not received honoraria.

ACKNOWLEDGMENTS

MO acknowledges the support of Tyler's Hope for a Dystonia Cure and the Parkinson's Foundation Center of Excellence. AS acknowledges the Packard Foundation, Friends and Alumni of Georgia Tech, and the Lane Family.

REFERENCES

Abosch, A., Yacoub, E., Ugurbil, K., and Harel, N. (2010). An assessment of current brain targets for deep brain stimulation surgery with susceptibility-weighted imaging at 7 tesla. *Neurosurgery* 67, 1745–1756; discussion 1756. doi: 10.1227/NEU.0b013e3181f74105

Accolla, E. A., Herrojo Ruiz, M., Horn, A., Schneider, G. H., Schmitz-Hubsch, T., Draganski, B., et al. (2016). Brain networks modulated by subthalamic nucleus deep brain stimulation. *Brain* 139, 2503–2515. doi: 10.1093/brain/aww182

Adamchic, I., Hauptmann, C., Barnikol, U. B., Pawelczyk, N., Popovych, O., Barnikol, T. T., et al. (2014). Coordinated reset neuromodulation for Parkinson's disease: proof-of-concept study. *Mov. Disord.* 29, 1679–1684. doi: 10.1002/mds.25923

Anderson, J. S., Dhatt, H. S., Ferguson, M. A., Lopez-Larson, M., Schrock, L. E., House, P. A., et al. (2011). Functional connectivity targeting for deep brain stimulation in essential tremor. *AJNR Am. J. Neuroradiol.* 32, 1963–1968. doi: 10.3174/ajnr.A2638

Banks, G. P., Mikell, C. B., Youngerman, B. E., Henriques, B., Kelly, K. M., Chan, A. K., et al. (2015). Neuroanatomical characteristics associated with response to dorsal anterior cingulotomy for obsessive-compulsive disorder. *JAMA Psychiatry* 72, 127–135. doi: 10.1001/jamapsychiatry.2014.2216

Bronte-Stewart, H., Barberini, C., Koop, M. M., Hill, B. C., Henderson, J. M., and Wingeier, B. (2009). The STN beta-band profile in Parkinson's disease is stationary and shows prolonged attenuation after deep brain stimulation. *Exp. Neurol.* 215, 20–28. doi: 10.1016/j.expneurol.2008.09.008

Brown, P., Mazzone, P., Oliviero, A., Altibrandi, M. G., Pilato, F., Tonali, P. A., et al. (2004). Effects of stimulation of the subthalamic area on oscillatory pallidal activity in Parkinson's disease. *Exp. Neurol.* 188, 480–490. doi: 10.1016/j.expneurol.2004.05.009

Calabrese, E. (2016). Diffusion tractography in deep brain stimulation surgery: a review. *Front. Neuroanat.* 10:45. doi: 10.3389/fnana.2016.00045

Carr, M. F., Karlsson, M. P., and Frank, L. M. (2012). Transient slow gamma synchrony underlies hippocampal memory replay. *Neuron* 75, 700–713. doi: 10.1016/j.neuron.2012.06.014

Cho, J. R., Treweek, J. B., Robinson, J. E., Xiao, C., Bremner, L. R., Greenbaum, A., et al. (2017). Dorsal raphe dopamine neurons modulate arousal and promote wakefulness by salient stimuli. *Neuron* 94, 1205–1219.e8. doi: 10.1016/j.neuron.2017.05.020

Coenen, V. A., Allert, N., and Madler, B. (2011). A role of diffusion tensor imaging fiber tracking in deep brain stimulation surgery: DBS of the dentato-rubro-thalamic tract (drt) for the treatment of therapy-refractory tremor. *Acta Neurochir.* 153, 1579–1585; discussion 1585. doi: 10.1007/s00701-011-1036-z

Creed, M. (2018). Current and emerging neuromodulation therapies for addiction: insight from pre-clinical studies. *Curr. Opin. Neurobiol.* 49, 168–174. doi: 10.1016/j.conb.2018.02.015

Creed, M., Pascoli, V. J., and Luscher, C. (2015). Addiction therapy. Refining deep brain stimulation to emulate optogenetic treatment of synaptic pathology. *Science* 347, 659–664. doi: 10.1126/science.1260776

De Hemptinne, C., Swann, N. C., Ostrem, J. L., Ryapolova-Webb, E. S., San Luciano, M., Galifianakis, N. B., et al. (2015). Therapeutic deep brain stimulation reduces cortical phase-amplitude coupling in Parkinson's disease. *Nat. Neurosci.* 18, 779–786. doi: 10.1038/nn.3997

De Solages, C., Hill, B. C., Koop, M. M., Henderson, J. M., and Bronte-Stewart, H. (2010). Bilateral symmetry and coherence of subthalamic nuclei beta band activity in Parkinson's disease. *Exp. Neurol.* 221, 260–266. doi: 10.1016/j.expneurol.2009.11.012

Deipolyi, A. R., Rankin, K. P., Mucke, L., Miller, B. L., and Gorno-Tempini, M. L. (2007). Spatial cognition and the human navigation network in AD and MCI. *Neurology* 69, 986–997. doi: 10.1212/01.wnl.0000271376.19515.c6

D'haese, P. F., Konrad, P. E., Pallavaram, S., Li, R., Prassad, P., Rodriguez, W., et al. (2015). CranialCloud: a cloud-based architecture to support trans-institutional collaborative efforts in neurodegenerative disorders. *Int. J. Comput. Assist. Radiol. Surg.* 10, 815–823. doi: 10.1007/s11548-015-1189-y

DiEuliis, D., and Giordano, J. (2016). "Neurotechnological convergence and "big data": a force-multiplier toward advancing neuroscience," in *Ethical Reasoning in Big Data: An Exploratory Analysis*, eds J. Collman, and S. A. Matei, (New York NY: Springer).

Duchin, Y., Abosch, A., Yacoub, E., Sapiro, G., and Harel, N. (2012). Feasibility of using ultra-high field (7 T) MRI for clinical surgical targeting. *PLoS One* 7:e37328. doi: 10.1371/journal.pone.0037328

Duchin, Y., Shamir, R. R., Patriat, R., Kim, J., Vitek, J. L., Sapiro, G., et al. (2018). Patient-specific anatomical model for deep brain stimulation based on 7 Tesla MRI. *PLoS One* 13:e0201469. doi: 10.1371/journal.pone.0201469

Ellis, T. M., Foote, K. D., Fernandez, H. H., Sudhyadhom, A., Rodriguez, R. L., Zeilman, P., et al. (2008). Reoperation for suboptimal outcomes after deep brain stimulation surgery. *Neurosurgery* 63, 754–760; discussion 760–751. doi: 10.1227/01.NEU.0000325492.58799.35

Fan, D., and Wang, Q. (2015). Improving desynchronization of parkinsonian neuronal network via triplet-structure coordinated reset stimulation. *J. Theor. Biol.* 370C, 157–170. doi: 10.1016/j.jtbi.2015.01.040

Ferraye, M. U., Debu, B., Fraix, V., Xie-Brustolin, J., Chabardes, S., Krack, P., et al. (2008). Effects of subthalamic nucleus stimulation and levodopa on freezing of gait in Parkinson disease. *Neurology* 70, 1431–1437. doi: 10.1212/01.wnl.0000310416.90757.85

Fox, M. D., Buckner, R. L., Liu, H., Chakravarty, M. M., Lozano, A. M., and Pascual-Leone, A. (2014). Resting-state networks link invasive and noninvasive brain stimulation across diverse psychiatric and neurological diseases. *Proc. Natl. Acad. Sci. U.S.A.* 111, E4367–E4375. doi: 10.1073/pnas.1405003111

Fox, N. C., Warrington, E. K., Freeborough, P. A., Hartikainen, P., Kennedy, A. M., Stevens, J. M., et al. (1996). Presymptomatic hippocampal atrophy in Alzheimer's disease. A longitudinal MRI study. *Brain* 119(Pt 6), 2001–2007. doi: 10.1093/brain/119.6.2001

Garibay-Pulido, D., Cendejas-Zaragoza, L., Dawe, R., and Rossi, M. A. (2018). Parametric subtracted post-ictal diffusion tensor imaging for guiding direct neurostimulation therapy. *Hippocampus* 29, 468–478. doi: 10.1002/hipo.23061

Gilbert, F. (2015). A threat to autonomy? The intrusion of predictive brain implants. *AJOB Neurosci.* 6, 4–11. doi: 10.1080/21507740.2015.1076087

Giordano, J. (2015a). A preparatory neuroethical approach to assessing developments in neurotechnology. *Virtual Mentor* 17, 56–61. doi: 10.1001/virtualmentor.2015.17.01.msoc1-1501

Giordano, J. (2015b). Conditions for consent to the use of neurotechnology: a preparatory neuroethical approach to risk assessment and reduction. *AJOB Neurosci.* 6, 12–14. doi: 10.1080/21507740.2015.1094557

Giordano, J. (2016). Commentary: the value of patient benefit: consideration of framing contingencies to guide the ethical use of DBS-a case analysis. *Camb. Q. Healthc. Ethics* 25, 755–758. doi: 10.1017/S0963180116000530

Giordano, J. (2018). Looking ahead: the importance of views, values, and voices in neuroethics-now. *Camb. Q. Healthc. Ethics* 27, 728–731. doi: 10.1017/S096318011800021X

Giordano, J., and Shook, J. R. (2015). Minding brain science in medicine: on the need for neuroethical engagement for guidance of neuroscience in clinical contexts. *Ethics Biol. Eng. Med.* 6, 37–42.

Gittis, A. H., Berke, J. D., Bevan, M. D., Chan, C. S., Mallet, N., Morrow, M. M., et al. (2014). New roles for the external globus pallidus in basal ganglia circuits and behavior. *J. Neurosci.* 34, 15178–15183. doi: 10.1523/jneurosci.3252-14.2014

Gradinaru, V., Mogri, M., Thompson, K. R., Henderson, J. M., and Deisseroth, K. (2009). Optical deconstruction of parkinsonian neural circuitry. *Science* 324, 354–359. doi: 10.1126/science.1167093

Grossman, N., Bono, D., Dedic, N., Kodandaramaiah, S. B., Rudenko, A., Suk, H. J., et al. (2017). Noninvasive deep brain stimulation via temporally interfering electric fields. *Cell* 169, 1029–1041.e6. doi: 10.1016/j.cell.2017.05.024

Gunalan, K., Chaturvedi, A., Howell, B., Duchin, Y., Lempka, S. F., Patriat, R., et al. (2017). Creating and parameterizing patient-specific deep brain stimulation pathway-activation models using the hyperdirect pathway as an example. *PLoS One* 12:e0176132. doi: 10.1371/journal.pone.0176132

Guo, Y., and Rubin, J. E. (2011). Multi-site stimulation of subthalamic nucleus diminishes thalamocortical relay errors in a biophysical network model. *Neural Netw.* 24, 602–616. doi: 10.1016/j.neunet.2011.03.010

Hadar, R., Vengeliene, V., Barroeta Hlusicke, E., Canals, S., Noori, H. R., Wieske, F., et al. (2016). Paradoxical augmented relapse in alcohol-dependent rats during deep-brain stimulation in the nucleus accumbens. *Transl. Psychiatry* 6:e840. doi: 10.1038/tp.2016.100

Hauptmann, C., Popovych, O., and Tass, P. A. (2007). Desynchronizing the abnormally synchronized neural activity in the subthalamic nucleus: a modeling study. *Expert Rev. Med. Devices* 4, 633–650. doi: 10.1586/17434440.4.5.633

Hauptmann, C., and Tass, P. A. (2009). Cumulative and after-effects of short and weak coordinated reset stimulation: a modeling study. *J. Neural Eng.* 6:016004. doi: 10.1088/1741-2560/6/1/016004

Henderson, J. M. (2012). "Connectomic surgery": diffusion tensor imaging (DTI) tractography as a targeting modality for surgical modulation of neural networks. *Front. Integr. Neurosci.* 6:15. doi: 10.3389/fnint.2012.00015

Hendrix, C. M., Campbell, B. A., Tittle, B. J., Johnson, L. A., Baker, K. B., Johnson, M. D., et al. (2018). Predictive encoding of motor behavior in the supplementary motor area is disrupted in parkinsonism. *J. Neurophysiol.* 120, 1247–1255. doi: 10.1152/jn.00306.2018

Holtzheimer, P. E., Kelley, M. E., Gross, R. E., Filkowski, M. M., Garlow, S. J., Barrocas, A., et al. (2012). Subcallosal cingulate deep brain stimulation for treatment-resistant unipolar and bipolar depression. *Arch. Gen. Psychiatry* 69, 150–158.

Horn, A., Reich, M., Vorwerk, J., Li, N., Wenzel, G., Fang, Q., et al. (2017). Connectivity predicts deep brain stimulation outcome in Parkinson disease. *Ann. Neurol.* 82, 67–78. doi: 10.1002/ana.24974

Houston, B., Thompson, M., Ko, A., and Chizeck, H. (2019). A machine-learning approach to volitional control of a closed-loop deep brain stimulation system. *J. Neural Eng.* 16:016004. doi: 10.1088/1741-2552/aae67f

Humphries, M. D., and Gurney, K. (2012). Network effects of subthalamic deep brain stimulation drive a unique mixture of responses in basal ganglia output. *Eur. J. Neurosci.* 36, 2240–2251. doi: 10.1111/j.1460-9568.2012.08085.x

Iaccarino, H. F., Singer, A. C., Martorell, A. J., Rudenko, A., Gao, F., Gillingham, T. Z., et al. (2016). Gamma frequency entrainment attenuates amyloid load and modifies microglia. *Nature* 540, 230–235. doi: 10.1038/nature20587

Jotterand, F., and Giordano, J. (2011). Transcranial magnetic stimulation, deep brain stimulation and personal identity: ethical questions, and neuroethical approaches for medical practice. *Int. Rev. Psychiatry* 23, 476–485. doi: 10.3109/09540261.2011.616189.2011.616189

Kim, W., Chivukula, S., Hauptman, J., and Pouratian, N. (2016). Diffusion tensor imaging-based thalamic segmentation in deep brain stimulation for chronic pain conditions. *Stereotact. Funct. Neurosurg.* 94, 225–234. doi: 10.1159/000448079

Kuo, C. H., White-Dzuro, G. A., and Ko, A. L. (2018). Approaches to closed-loop deep brain stimulation for movement disorders. *Neurosurg. Focus* 45:E2. doi: 10.3171/2018.5.FOCUS18173

Little, S., Beudel, M., Zrinzo, L., Foltynie, T., Limousin, P., Hariz, M., et al. (2016). Bilateral adaptive deep brain stimulation is effective in Parkinson's disease. *J. Neurol. Neurosurg. Psychiatry* 87, 717–721. doi: 10.1136/jnnp-2015-310972

Lucken, L., Yanchuk, S., Popovych, O. V., and Tass, P. A. (2013). Desynchronization boost by non-uniform coordinated reset stimulation in ensembles of pulse-coupled neurons. *Front. Comput. Neurosci.* 7:63. doi: 10.3389/fncom.2013.00063

Malekmohammadi, M., Auyong, N., Ricks-Oddie, J., Bordelon, Y., and Pouratian, N. (2018a). Pallidal deep brain stimulation modulates excessive cortical high beta phase amplitude coupling in Parkinson disease. *Brain Stimul.* 11, 607–617. doi: 10.1016/j.brs.2018.01.028

Malekmohammadi, M., Shahriari, Y., Auyong, N., O'keeffe, A., Bordelon, Y., Hu, X., et al. (2018b). Pallidal stimulation in Parkinson disease differentially modulates local and network beta activity. *J. Neural Eng.* 15:056016. doi: 10.1088/1741-2552/aad0fb

Maling, N., Lempka, S. F., Blumenfeld, Z., Bronte-Stewart, H., and Mcintyre, C. C. (2018). Biophysical basis of subthalamic local field potentials recorded from deep brain stimulation electrodes. *J. Neurophysiol.* 120, 1932–1944. doi: 10.1152/jn.00067.2018

Mallet, N., Pogosyan, A., Sharott, A., Csicsvari, J., Bolam, J. P., Brown, P., et al. (2008). Disrupted dopamine transmission and the emergence of exaggerated beta oscillations in subthalamic nucleus and cerebral cortex. *J. Neurosci.* 28, 4795–4806. doi: 10.1523/JNEUROSCI.0123-08.2008

Mastro, K. J., Zitelli, K. T., Willard, A. M., Leblanc, K. H., Kravitz, A. V., and Gittis, A. H. (2017). Cell-specific pallidal intervention induces long-lasting motor recovery in dopamine-depleted mice. *Nat. Neurosci.* 20, 815–823. doi: 10.1038/nn.4559

Mayberg, H. S., Lozano, A. M., Voon, V., Mcneely, H. E., Seminowicz, D., Hamani, C., et al. (2005). Deep brain stimulation for treatment-resistant depression. *Neuron* 45, 651–660.

Moreau, C., Defebvre, L., Destee, A., Bleuse, S., Clement, F., Blatt, J. L., et al. (2008). STN-DBS frequency effects on freezing of gait in advanced Parkinson disease. *Neurology* 71, 80–84. doi: 10.1212/01.wnl.0000303972.16279.46

Nemtsas, P., Birot, G., Pittau, F., Michel, C. M., Schaller, K., Vulliemoz, S., et al. (2017). Source localization of ictal epileptic activity based on high-density scalp EEG data. *Epilepsia* 58, 1027–1036. doi: 10.1111/epi.13749

Nini, A., Feingold, A., Slovin, H., and Bergman, H. (1995). Neurons in the globus pallidus do not show correlated activity in the normal monkey, but phase-locked oscillations appear in the MPTP model of parkinsonism. *J. Neurophysiol.* 74, 1800–1805. doi: 10.1152/jn.1995.74.4.1800

Noecker, A. M., Choi, K. S., Riva-Posse, P., Gross, R. E., Mayberg, H. S., and Mcintyre, C. C. (2018). StimVision software: examples and applications in subcallosal cingulate deep brain stimulation for depression. *Neuromodulation* 21, 191–196. doi: 10.1111/ner.12625

Panov, F., Levin, E., De Hemptinne, C., Swann, N. C., Qasim, S., Miocinovic, S., et al. (2017). Intraoperative electrocorticography for physiological research in movement disorders: principles and experience in 200 cases. *J. Neurosurg.* 126, 122–131. doi: 10.3171/2015.11.JNS151341

Pascoli, V., Turiault, M., and Luscher, C. (2011). Reversal of cocaine-evoked synaptic potentiation resets drug-induced adaptive behaviour. *Nature* 481, 71–75. doi: 10.1038/nature10709

Patriat, R., Cooper, S. E., Duchin, Y., Niederer, J., Lenglet, C., Aman, J., et al. (2018). Individualized tractography-based parcellation of the globus pallidus pars interna using 7T MRI in movement disorder patients prior to DBS surgery. *Neuroimage* 178, 198–209. doi: 10.1016/j.neuroimage.2018.05.048

Perestelo-Perez, L., Rivero-Santana, A., Perez-Ramos, J., Serrano-Perez, P., Panetta, J., and Hilarion, P. (2014). Deep brain stimulation in Parkinson's disease: meta-analysis of randomized controlled trials. *J. Neurol.* 261, 2051–2060. doi: 10.1007/s00415-014-7254-6

Petersen, M. V., Lund, T. E., Sunde, N., Frandsen, J., Rosendal, F., Juul, N., et al. (2017). Probabilistic versus deterministic tractography for delineation of the cortico-subthalamic hyperdirect pathway in patients with Parkinson disease selected for deep brain stimulation. *J. Neurosurg.* 126, 1657–1668. doi: 10.3171/2016.4.JNS1624

Pfeiffer, B. E., and Foster, D. J. (2013). Hippocampal place-cell sequences depict future paths to remembered goals. *Nature* 497, 74–79. doi: 10.1038/nature12112

Plantinga, B. R., Temel, Y., Duchin, Y., Uludag, K., Patriat, R., Roebroeck, A., et al. (2018). Individualized parcellation of the subthalamic nucleus in patients with Parkinson's disease with 7T MRI. *Neuroimage* 168, 403–411. doi: 10.1016/j.neuroimage.2016.09.023

Pouratian, N., Zheng, Z., Bari, A. A., Behnke, E., Elias, W. J., and Desalles, A. A. (2011). Multi-institutional evaluation of deep brain stimulation targeting

using probabilistic connectivity-based thalamic segmentation. *J. Neurosurg.* 115, 995–1004. doi: 10.3171/2011.7.JNS11250

Puigdemont, D., Perez-Egea, R., Portella, M. J., Molet, J., De Diego-Adelino, J., Gironell, A., et al. (2012). Deep brain stimulation of the subcallosal cingulate gyrus: further evidence in treatment-resistant major depression. *Int. J. Neuropsychopharmacol.* 15, 121–133. doi: 10.1017/S1461145711001088

Quinn, E. J., Blumenfeld, Z., Velisar, A., Koop, M. M., Shreve, L. A., Trager, M. H., et al. (2015). Beta oscillations in freely moving Parkinson's subjects are attenuated during deep brain stimulation. *Mov. Disord.* 30, 1750–1758. doi: 10.1002/mds.26376

Ramirez-Zamora, A., and Ostrem, J. L. (2018). Globus pallidus interna or subthalamic nucleus deep brain stimulation for parkinson disease: a review. *JAMA Neurol.* 75, 367–372. doi: 10.1001/jamaneurol.2017.4321

Reich, M. M., Brumberg, J., Pozzi, N. G., Marotta, G., Roothans, J., Astrom, M., et al. (2016). Progressive gait ataxia following deep brain stimulation for essential tremor: adverse effect or lack of efficacy? *Brain* 139, 2948–2956. doi: 10.1093/brain/aww223

Riva-Posse, P., Choi, K. S., Holtzheimer, P. E., Mcintyre, C. C., Gross, R. E., Chaturvedi, A., et al. (2014). Defining critical white matter pathways mediating successful subcallosal cingulate deep brain stimulation for treatment-resistant depression. *Biol. Psychiatry* 76, 963–969. doi: 10.1016/j.biopsych.2014.03.029

Rossi, M. A. (2017). Localizing the ictal onset: visualizing the epileptogenic target. *Epilepsy Curr.* 17, 361–362. doi: 10.5698/1535-7597.17.6.361

Rossi, P. J., Giordano, J., and Okun, M. S. (2017). The problem of funding off-label deep brain stimulation: bait-and-switch tactics and the need for policy reform. *JAMA Neurol.* 74, 9–10.

Roth, T. (2007). Insomnia: definition, prevalence, etiology, and consequences. *J. Clin. Sleep Med.* 3, S7–S10.

Sammartino, F., Krishna, V., King, N. K., Lozano, A. M., Schwartz, M. L., Huang, Y., et al. (2016). Tractography-Based ventral intermediate nucleus targeting: novel methodology and intraoperative validation. *Mov. Disord.* 31, 1217–1225. doi: 10.1002/mds.26633

Sasada, S., Agari, T., Sasaki, T., Kondo, A., Shinko, A., Wakamori, T., et al. (2017). Efficacy of fiber tractography in the stereotactic surgery of the thalamus for patients with essential tremor. *Neurol. Med. Chir.* 57, 392–401. doi: 10.2176/nmc.oa.2016-0277

Shamir, R. R., Duchin, Y., Kim, J., Patriat, R., Marmor, O., Bergman, H., et al. (2019). Microelectrode recordings validate the clinical visualization of subthalamic-nucleus based on 7T magnetic resonance imaging and machine learning for deep brain stimulation surgery. *Neurosurgery* 84, 749–757. doi: 10.1093/neuros/nyy212

Shreve, L. A., Velisar, A., Malekmohammadi, M., Koop, M. M., Trager, M., Quinn, E. J., et al. (2017). Subthalamic oscillations and phase amplitude coupling are greater in the more affected hemisphere in Parkinson's disease. *Clin. Neurophysiol.* 128, 128–137. doi: 10.1016/j.clinph.2016.10.095

Singer, A. C., Carr, M. F., Karlsson, M. P., and Frank, L. M. (2013). Hippocampal SWR activity predicts correct decisions during the initial learning of an alternation task. *Neuron* 77, 1163–1173. doi: 10.1016/j.neuron.2013.01.027

Sivakanthan, S., Neal, E., Murtagh, R., and Vale, F. L. (2016). The evolving utility of diffusion tensor tractography in the surgical management of temporal lobe epilepsy: a review. *Acta Neurochir.* 158, 2185–2193. doi: 10.1007/s00701-016-2910-5

Stein, D. J., and Giordano, J. (2015). Global mental health and neuroethics. *BMC Med.* 13:44. doi: 10.1186/s12916-015-0274-y

Swann, N. C., De Hemptinne, C., Thompson, M. C., Miocinovic, S., Miller, A. M., Gilron, R., et al. (2018). Adaptive deep brain stimulation for Parkinson's disease using motor cortex sensing. *J. Neural Eng.* 15:046006. doi: 10.1088/1741-2552/aabc9b

Syrkin-Nikolau, J., Koop, M. M., Prieto, T., Anidi, C., Afzal, M. F., Velisar, A., et al. (2017). Subthalamic neural entropy is a feature of freezing of gait in freely moving people with Parkinson's disease. *Neurobiol. Dis.* 108, 288–297. doi: 10.1016/j.nbd.2017.09.002

Tass, P. A. (2003). A model of desynchronizing deep brain stimulation with a demand-controlled coordinated reset of neural subpopulations. *Biol. Cybern.* 89, 81–88. doi: 10.1007/s00422-003-0425-7

Tass, P. A., Qin, L., Hauptmann, C., Dovero, S., Bezard, E., Boraud, T., et al. (2012). Coordinated reset has sustained aftereffects in Parkinsonian monkeys. *Ann. Neurol.* 72, 816–820. doi: 10.1002/ana.23663

Thevathasan, W., Debu, B., Aziz, T., Bloem, B. R., Blahak, C., Butson, C., et al. (2018). Pedunculopontine nucleus deep brain stimulation in Parkinson's disease: a clinical review. *Mov. Disord.* 33, 10–20. doi: 10.1002/mds.27098

Trager, M. H., Koop, M. M., Velisar, A., Blumenfeld, Z., Nikolau, J. S., Quinn, E. J., et al. (2016). Subthalamic beta oscillations are attenuated after withdrawal of chronic high frequency neurostimulation in Parkinson's disease. *Neurobiol. Dis.* 96, 22–30. doi: 10.1016/j.nbd.2016.08.003

Tsolaki, E., Downes, A., Speier, W., Elias, W. J., and Pouratian, N. (2018). The potential value of probabilistic tractography-based for MR-guided focused ultrasound thalamotomy for essential tremor. *Neuroimage Clin.* 17, 1019–1027. doi: 10.1016/j.nicl.2017.12.018

Van Nuenen, B. F., Esselink, R. A., Munneke, M., Speelman, J. D., Van Laar, T., and Bloem, B. R. (2008). Postoperative gait deterioration after bilateral subthalamic nucleus stimulation in Parkinson's disease. *Mov. Disord.* 23, 2404–2406. doi: 10.1002/mds.21986

Wang, D. D., De Hemptinne, C., Miocinovic, S., Ostrem, J. L., Galifianakis, N. B., San Luciano, M., et al. (2018). Pallidal deep-brain stimulation disrupts pallidal beta oscillations and coherence with primary motor cortex in Parkinson's Disease. *J. Neurosci.* 38, 4556–4568. doi: 10.1523/JNEUROSCI.0431-18.2018

Wang, J., Johnson, L. A., Jensen, A. L., Baker, K. B., Molnar, G. F., Johnson, M. D., et al. (2017). Network-wide oscillations in the parkinsonian state: alterations in neuronal activities occur in the premotor cortex in parkinsonian nonhuman primates. *J. Neurophysiol.* 117, 2242–2249. doi: 10.1152/jn.00011.2017

Wang, J., Nebeck, S., Muralidharan, A., Johnson, M. D., Vitek, J. L., and Baker, K. B. (2016). Coordinated reset deep brain stimulation of subthalamic nucleus produces long-lasting, dose-dependent motor improvements in the 1-Methyl-4-phenyl-1,2,3,6-tetrahydropyridine non-human primate model of parkinsonism. *Brain Stimul.* 9, 609–617. doi: 10.1016/j.brs.2016.03.014

Waters, A. C., Veerakumar, A., Choi, K. S., Howell, B., Tiruvadi, V., Bijanki, K. R., et al. (2018). Test-retest reliability of a stimulation-locked evoked response to deep brain stimulation in subcallosal cingulate for treatment resistant depression. *Hum. Brain Mapp.* 39, 4844–4856. doi: 10.1002/hbm.24327

Whitmer, D., De Solages, C., Hill, B., Yu, H., Henderson, J. M., and Bronte-Stewart, H. (2012). High frequency deep brain stimulation attenuates subthalamic and cortical rhythms in Parkinson's disease. *Front. Hum. Neurosci.* 6:155. doi: 10.3389/fnhum.2012.00155

Williams, L. M. (2017). Defining biotypes for depression and anxiety based on large-scale circuit dysfunction: a theoretical review of the evidence and future directions for clinical translation. *Depress Anxiety* 34, 9–24. doi: 10.1002/da.22556

Witt, K., Granert, O., Daniels, C., Volkmann, J., Falk, D., Van Eimeren, T., et al. (2013). Relation of lead trajectory and electrode position to neuropsychological outcomes of subthalamic neurostimulation in Parkinson's disease: results from a randomized trial. *Brain* 136, 2109–2119. doi: 10.1093/brain/awt151

Xiao, C., Cho, J. R., Zhou, C., Treweek, J. B., Chan, K., Mckinney, S. L., et al. (2016). Cholinergic mesopontine signals govern locomotion and reward through dissociable midbrain pathways. *Neuron* 90, 333–347. doi: 10.1016/j.neuron.2016.03.028

Xie, T., Kang, U. J., and Warnke, P. (2012). Effect of stimulation frequency on immediate freezing of gait in newly activated STN DBS in Parkinson's disease. *J. Neurol. Neurosurg. Psychiatry* 83, 1015–1017. doi: 10.1136/jnnp-2011-302091

Conflict of Interest Statement: The authors declare that the research was conducted in the absence of any commercial or financial relationships that could be construed as a potential conflict of interest.

The reviewer VV-V declared a past co-authorship with one of the authors MO to the handling Editor.

frontiers in Neuroscience

ORIGINAL RESEARCH
published: 14 November 2019
doi: 10.3389/fnins.2019.01181

Effect of Theta Transcranial Alternating Current Stimulation and Phase-Locked Transcranial Pulsed Current Stimulation on Learning and Cognitive Control

*Farrokh Mansouri[1], Alaa Shanbour[2,3], Frank Mazza[4], Peter Fettes[3], José Zariffa[1,5,6,7] and Jonathan Downar[3,8,9,10]**

[1] Institute of Biomaterials and Biomedical Engineering, University of Toronto, Toronto, ON, Canada, [2] Department of Psychiatry, Central Michigan University, Mount Pleasant, MI, United States, [3] Institute of Medical Science, University of Toronto, Toronto, ON, Canada, [4] Department of Physiology, University of Toronto, Toronto, ON, Canada, [5] KITE, Toronto Rehab, University Health Network, Toronto, ON, Canada, [6] Rehabilitation Sciences Institute, University of Toronto, Toronto, ON, Canada, [7] Edward S. Rogers Sr. Department of Electrical and Computer Engineering, University of Toronto, Toronto, ON, Canada, [8] Department of Psychiatry, University of Toronto, Toronto, ON, Canada, [9] Centre for Mental Health, University Health Network, Toronto, ON, Canada, [10] Krembil Research Institute, University Health Network, Toronto, ON, Canada

OPEN ACCESS

Edited by:
Mikhail Lebedev, Duke University, United States

Reviewed by:
Leandro Da Costa Lane Valiengo, University of São Paulo, Brazil
Maarten A. Frens, Sophia Children's Hospital, Netherlands
Anthony Terrence O'Brien, Massachusetts Institute of Technology, United States

***Correspondence:**
Jonathan Downar
jonathan.downar@uhn.ca

Specialty section:
This article was submitted to Neural Technology, a section of the journal Frontiers in Neuroscience

Received: *06 May 2019*
Accepted: *18 October 2019*
Published: *14 November 2019*

Citation:
Mansouri F, Shanbour A, Mazza F, Fettes P, Zariffa J and Downar J (2019) Effect of Theta Transcranial Alternating Current Stimulation and Phase-Locked Transcranial Pulsed Current Stimulation on Learning and Cognitive Control. Front. Neurosci. 13:1181. doi: 10.3389/fnins.2019.01181

Non-invasive brain stimulation (NIBS) is emerging as a robust treatment alternative for major depressive disorder, with a potential for achieving higher remission rates by providing targeted stimulation to underlying brain networks, such as the salience network (SN). Growing evidence suggests that these therapeutic effects are dependent on the frequency and phase synchrony between SN oscillations and stimulation as well as the task-specific state of the SN during stimulation. However, the development of phase-synchronized non-invasive stimulation has proved challenging until recently. Here, we use a phase-locked pulsed brain stimulation approach to study the effects of two NIBS methods: transcranial alternating current stimulation (tACS) versus phase-locked transcranial pulsed current stimulation (tPCS), on the SN during an SN activating task. 20 healthy volunteers participated in the study. Each volunteer partook in four sessions, receiving one stimulation type at random (theta-tACS, peak tPCS, trough tPCS or sham) while undergoing a learning game, followed by an unstimulated test based on learned material. Each session lasted approximately 1.5 h, with an interval of at least 2 days to allow for washout and to avoid cross-over effects. Our results showed no statistically significant effect of stimulation on the event related potential (ERP) recordings, resting electroencephalogram (EEG), and the performance of the volunteers. While stimulation effects were not apparent in this study, the nominal performance of the phase-locking algorithm offers a technical foundation for further research in determining effective stimulation paradigms and conditions. Specifically, future work should investigate stronger stimulation and true task-specific stimulation of SN nodes responsible for the task as well as their recording. If refined, NIBS could offer an effective, homebased treatment option.

Keywords: brain stimulation, transcranial alternating current stimulation, transcranial pulsed current stimulation, transcranial electrical stimulation, phase-locked brain stimulation, closed-loop brain stimulation, salience network

INTRODUCTION

Non-invasive brain stimulation (NIBS) is an emerging alternative when conventional treatment approaches for Major Depressive Disorder (MDD) fail (Fregni and Pascual-Leone, 2007; Daskalakis et al., 2008; Ferrucci et al., 2009; Dayan et al., 2013). It is estimated that one in three MDD patients suffers from Treatment Resistant Depression (TRD), with failure to respond to at least two courses of antidepressant treatment (Nemeroff, 2007). NIBS technologies such as Food and Drug Administration (FDA)-approved repetitive transcranial magnetic stimulation (rTMS) and transcranial direct current stimulation (tDCS) have shown efficacy in helping with TRD in a large number of clinical trials, achieving 15–32% (O'Reardon et al., 2007; Berlim et al., 2014; Gaynes et al., 2014) and 7–43% (Berlim et al., 2013; Shiozawa et al., 2014) remission rates, respectively. There is a potential for achieving higher remission rates by providing a more targeted stimulation to the brain networks involved in MDD. Growing evidence (reviewed below) suggests that this can be achieved by first applying the stimulation at the same oscillatory profile as the underlying brain oscillation, and second by applying the stimulation during the time when the brain network of interest is in the most suitable state to receive the stimulation.

In contrast to tDCS, transcranial alternating current stimulation (tACS) and transcranial pulsed current stimulation (tPCS) use oscillatory waveforms with sinusoidal and square pulses that better match the underlying natural physiological brain activity. In a recent study, it has been shown that tACS can have an effect in spike timing of single neurons elucidating the mechanism of action for these types of NIBS and opening the opportunity for future research into the effects of timing of the stimulation waveform with respect to the underlying brain activity (Krause et al., 2019).

Multiple studies have shown the importance of achieving synchrony between the target brain oscillation and the stimulation frequencies and phase in order to increase the effect of the stimulation. A recent study has shown that adjusting rTMS pulse frequency to individual gamma oscillation resulted in a significant mood elevation compared to unadjusted rTMS stimulation at slightly higher or lower frequencies than their individual gamma oscillation (Chung et al., 2018). In another example, TMS phase-specific modulation of motor evoked potentials has been shown by applying pulses at the peak or trough of the μ-rhythm of the motor cortex (Zrenner et al., 2017). Similarly, the brain stimulation modalities that use energies below the threshold for induction of an action potential (e.g., transcranial electrical stimulation), are more effective when delivered at similar oscillation frequencies as the underlying brain target (Fröhlich and McCormick, 2010; Reato et al., 2013). For example, tACS has been shown effective to modulate alpha power only when delivered at alpha frequency (Zaehle et al., 2010; Vossen et al., 2015). Further, tACS delivered at a specific phase with respect to the underlying brain oscillation modulated the intensity of the tremor when applied to the motor cortex (Brittain et al., 2013) and changed the hearing thresholds when applied to the auditory cortex (Riecke et al., 2015; Wilsch et al., 2018).

The effects of brain stimulation have also consistently been shown to depend on the brain state at the time of stimulation (Silvanto et al., 2008). Current models of brain function posit that brain regions operate as integrated networks bound by coherent activity, and task-specific activation of these networks is seen across various brain states (Seager et al., 2002; Park and Friston, 2013; Pessoa, 2014). The state of the brain during the stimulation can change the outcome of the intervention; an elementary example would be the observation that the active motor threshold is substantially lower than the resting motor threshold for stimulation of the primary motor cortex (Hallett, 2007).

A useful stimulation target is the Salience Network (SN), which is activated when there is a transition between a cognitive task and sensory information (Downar et al., 2000, 2001). SN dysfunction is associated with a wide range of neuropsychiatric disorders, including MDD, post-traumatic stress disorder (PTSD), and schizophrenia (Peters et al., 2016). Targeting the SN has been proven successful when using rTMS for treating MDD (Peters et al., 2016). Considering the importance of brain state during brain stimulation, applying the stimulation during an SN-activating task may potentially improve the effect of the stimulation.

Providing a more targeted brain stimulation may help discover more effective treatments for MDD patients. A closed-loop system enabling phase-locked stimulation could potentially allow more precise control of the stimulation frequency and phase. Such system could achieve a more consistent treatment effect overall, given the findings pointing at the importance of brain state during the stimulation and the synchrony of the stimulation with the underlying brain oscillation. Here, we conducted an experiment to study the effect of two NIBS methods: tACS and transcranial phase-locked pulsed current stimulation (tPCS), on the SN during an SN activating task. The effects of these types of stimulation have previously been shown to be: spectral power density changes in specific frequency bands during rest EEG (Zaehle et al., 2010; Helfrich et al., 2014; Vossen et al., 2015), changes in task-specific activation of the brain (Meinzer et al., 2012; Jaušovec and Jaušovec, 2014; Cabral-Calderin et al., 2016), and behavioral or task-specific performance changes (Santarnecchi et al., 2013; Voss et al., 2014). We, therefore, hypothesized that by providing stimulation in synchrony with the underlying brain activity during an SN activating task, we would achieve more effective stimulation of the SN, as reflected by increases in these previously established electrophysiological and behavioral effects. We further hypothesized that tACS would strengthen the SN activity resulting in faster reaction time and better performance during the task, while producing an increase in resting theta power and ERP.

In this work we attempted to engage the SN by using tACS at theta frequency or phase-locked tPCS synchronized to the frontal theta when the volunteers were engaged in a SN activating task. Successful implementation of tACS in a closed-loop system with electroencephalography (EEG) recording is currently an unsolved problem, because the artifact generated by the stimulation obscures the recording (Neuling et al., 2017;

Noury and Siegel, 2017). To study the phase- and frequency-locked brain stimulation method, we previously have developed a phase-locked tPCS brain stimulation technique that can extract phase and frequency of the EEG signal and deliver the stimulation pulses at specific phase and frequency of the EEG signal in real-time (Mansouri et al., 2018). Here we applied this technique to phase-lock tPCS to the activity of the SN recorded through theta EEG. The electrical pulses were delivered either at peak or trough of the recording, with the expected result of generating opposite effects – as was previously shown when using rTMS over motor cortex (Zrenner et al., 2017), electrical stimulation of hippocampal brain slices (Hyman et al., 2003), and electrical stimulation of the somatosensory cortex in monkeys (Zanos et al., 2018). We hypothesized that trough tPCS would strengthen the SN activity, while peak tPCS would have the opposite effect, and that these effects would be exhibited through an increase or decrease of theta power and ERP recording, alongside changes in behavioral performance during the task.

MATERIALS AND METHODS

Participants and Visits

Twenty healthy adult (older than 18) volunteers free of neurological or psychiatric illnesses participated in the study. All participants gave written informed consent, and the study was approved by the Research Ethics Board of the University Health Network. For each of the four visits, volunteers received one of the stimulation types at random (theta-tACS, peak tPCS, trough tPCS or sham). The order of the visits was assigned at random using a random generator with the participants not informed of the order of the visits; only the experimenter knew the type of stimulation at each visit. The visits were scheduled at least 2 days apart to allow for washout and to avoid cross-over effects. Each session took approximately 1 h and a half.

Study Visit and Computer Task

During each visit, volunteers sat in front of a computer and performed a decision-making task described by Frank et al. (2004, 2005). Each visit consisted of a learning and a test period (**Figure 1**). During the learning period, the volunteers were presented with three pairs of randomly assigned Japanese characters (AB, CD, and EF) that were not easily verbalized. In each pair, one of the characters was more likely to win a reward (A:80%-B:20%, C:70%-D:30% and E:60%-F:40%). For each trial, the volunteers were presented with one pair (each character was displayed on an image of a jar) and within 1 sec had to select a character by pressing the left or the right arrow keys on a keyboard. Next, the volunteers were presented with a feedback to tell them whether they "won", "lost", or were too late to respond. This game continued for 1 h, with 1 min breaks every 4 min.

After completing the learning game, volunteers took a short test with same pairs as the learning game (AB, CD, and EF) and also pairs that they had not previously seen (AC, AE, CE, BD, BE, and DE). During the test, no feedback was presented, to avoid further learning effects.

The same task was performed during each of the four sessions. For each session, six new randomly selected Japanese characters were used. At each session, during the learning task, the volunteers received one of the 4 stimulation types. No stimulation was delivered during the test task.

Phase-Locked Transcranial Pulsed Current Stimulation

A similar method to Mansouri et al. (2018) was used to provide square wave 5 ms pulses of 2 mA amplitude at either peak (90 degree phase) or trough (270 degree phase) of the theta oscillation (4–8 Hz) recorded from the midfrontal part of the scalp. First, the stimulation electrodes (2 cm × 2 cm) were placed on the scalp at F3 (anode) and F4 (cathode); Ten20 conductive gel (Weaver

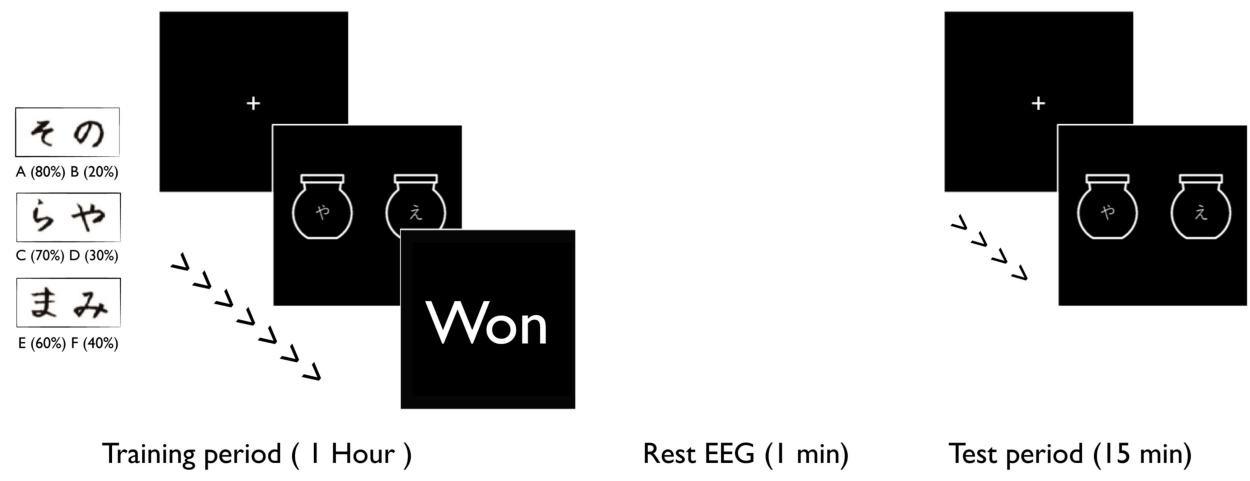

FIGURE 1 | Volunteers were presented with six pairs of Japanese characters. In each pair, one character had a higher probability of "winning". During the training period, the volunteers were presented with these pairs to learn their probabilities through reinforcement learning. The training task was continued for 1 h. The volunteers completed 1 min of rest EEG recording after the training period. During the test period volunteers, were presented with two Japanese characters but not necessarily paired in the same way, to create conflicting scenarios (win/win or lose/lose).

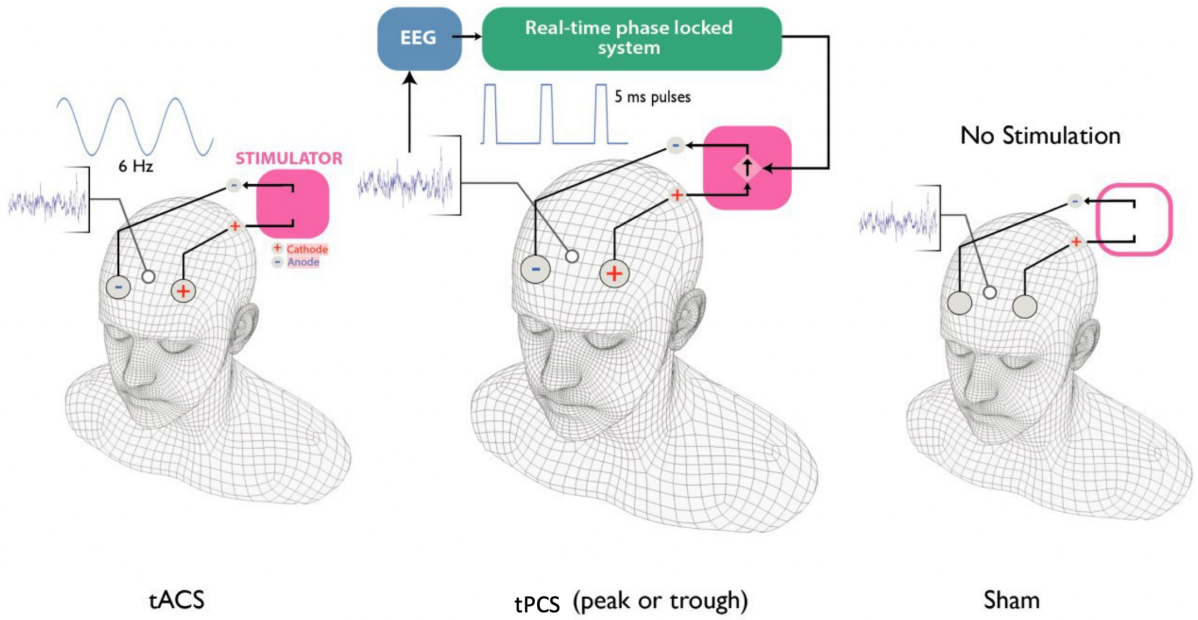

FIGURE 2 | Four different stimulation types were used in this study: tACS, tPCS peak, tPCS trough and sham. During tACS stimulation, a 6 Hz sinusoidal stimulation was applied over F3 and F4. During the tPCS at peak or trough, 5 ms pulses were delivered at peak or trough of the theta oscillation recorded from Fz. During the sham session, no stimulation was delivered.

and Company, Aurora, CO., United States) was applied to reduce the impedances of the electrodes to below 5 kΩ. Next, a 16-channel passive-electrode EEG cap (EasyCap GmbH, Germany) was worn by the volunteers on top of the stimulation electrodes and HiCL Abrasive EEG Gel (EasyCap GmbH, Germany) was applied to Fz (recording electrode), Pz (Reference electrode) and right tragus (Ground) to reduce the impedance of each of the recording electrodes to below 5 kΩ (**Figure 2**).

As previously described in Mansouri et al. (2017), the recorded EEG from Fz using V-AMP16 (Brain Products GmbH, Munich, Germany) was analyzed in MATLAB (MATLAB version 7.9.0) using a Fast Fourier Transform-based forecasting method (Mansouri et al., 2017) to provide the timing of the pulses and this timing was communicated to the ANT Neuro stimulator through an Arduino interface. The stimulation was applied for 1 h during the learning task; no stimulation was delivered during the test task.

Transcranial Alternating Current Stimulation (tACS) Procedure

First, the stimulation electrodes (2 cm × 2 cm) were placed on the scalp at F3 (anode) and F4 (cathode); Ten20 conductive gel (Weaver and Company, Aurora, CO., United States) was applied to reduce the impedances of the electrodes to below 5 kΩ. Then, the stimulation was set to provide a 6 Hz sinusoidal current stimulation with amplitude of 2 mA peak to peak and zero direct current. The stimulation was initiated with a 30-s ramp up from zero to 2 mA amplitude. As in the tpES case, the stimulation was applied for 1 h during the learning task and no stimulation was delivered during the test task.

Sham Stimulation Procedure

The stimulation electrodes were placed in a similar way to the pulsed stimulation and tACS stimulation. An initial tACS for 1 min with 30 s ramp up to 2 mA and 30 s ramp down stimulation was applied to help with the blinding of the participants. No further stimulation was applied during this visit. The participants completed both the learning and the test task.

Resting-State EEG and ERP Recording

The same EEG setup was used for rest EEG and ERP recordings. Pz was used as the reference and right tragus as the ground electrodes. Rest EEG was recorded before the test task for 1 min as the volunteers sat in front of the computer and the recording continued to capture the event-related potential (ERP) during the test task. Trigger signals were provided to the amplifier to capture the events during the game.

Resting-State EEG and ERP Analysis

All the analysis was done in MATLAB (MATLAB R2016b) and EEGLAB EEG analysis toolbox (Delorme and Makeig, 2004) was used for specific analysis. First, the channels were manually inspected and bad channels (large noise or poor connection) were identified and removed from the analysis. An average reference transformation was applied to the data to minimize the effect of reference site. Next a zero-phase 1 Hz high-pass FIR filter was used to remove the baseline drift. We applied a threshold to identify and remove large movement and eyeblink artifacts. Further, a zero-phase shift 1–50 Hz FIR bandpass filter was applied to the data. Response-locked ERP measures were extracted and a zero-phase shift 1–14 Hz bandpass IIR filter was

applied to avoid bifurcation (Frank et al., 2005). Welch's power spectral density estimate with a Hanning window was used to generate the spectral density of the rest EEG.

Analysis

Statistical Methods and Analysis

Considering the design of the study, a repeated-measure method to investigate the variability within the factors (subjects) is suitable for testing the effect of the stimulation. Previous publications, that employed the same task with a larger group of participants, used a parametric test for their statistical evaluations (Frank et al., 2004, 2005). We performed a Shapiro–Wilk test, which refuted that our data is from a normally distributed population. Thus, instead of the parametric repeated-measure analysis of variance (ANOVA), the non-parametric repeated-measure Friedman's test was used to assess the effect of the stimulation type over the outcome measures. Significance p-value level was set at 0.05 for rejecting the null hypothesis (no effect of stimulation). Considering the 15 statistical tests performed on the data, the significance p-value level with multiple comparison Bonferroni correction was adjusted to 0.003.

Phase Locking Value (PLV) was used to evaluate the performance of the phase-locked tPCS. PLV is a value between 0 and 1; higher PLV shows better phase locking.

Sample Size Justification

A power analysis for repeated-measure ANOVA test within factors was conducted using G*Power (Faul et al., 2007) assuming an intermediate effect size ($f = 0.5$) based on previously published tDCS studies (Minarik et al., 2016; Aleman et al., 2018), 95% power and alpha error probability of 5%. This analysis suggested the total sample size of at least 20 participants. We assumed there were no carryover effects between the four sessions.

RESULTS

Recruitment

Twenty volunteers (10/10 male/female; mean age 31.7 ± SD 8.6 years, range 23–53) were recruited to complete four visits. There were no complications after the stimulation sessions; minor tingling was reported during tACS stimulation. Pulsed stimulation was felt only during the beginning of the session as a tapping sensation on the head; the volunteers gradually acclimatized to these effects and reported no sensation of the stimulation afterward.

Closed-Loop Brain Stimulation

Both peak and trough tPCS were applied successfully in terms of phase-locking performance. A minimum of 0.31 PLV and maximum of 0.70 PLV and average of 0.50 ± 0.13 was achieved for peak stimulation. A minimum of 0.32 PLV and maximum of 0.80 PLV and average of 0.53 ± 0.14 was achieved for trough stimulation. The average error in the peak stimulation was 2.5° ± 16° and for trough was 5.2° ± 17°.

Task-Specific Findings

All participants learned the probabilistic reward associations of the task successfully and were able to score more than 65% on AB cases, 60% on CD cases and 50% on EF cases during the learning task in all four visits. However, when comparing learning performance across the four stimulation conditions, no significant effect was apparent: there was no effect of stimulation type on decision of the players to choose A over B (Friedman's test $\chi^2_F(3) = 1.49$, $p = 0.68$), C over D (Friedman's test $\chi^2_F(3) = 4.02$, $p = 0.26$), and E over F (Friedman's test $\chi^2_F(3) = 5.84$, $p = 0.12$).

Next, we examined at the probability of selecting A over all the other characters and probability of avoiding B over all the characters. "Positive learners", as described by Frank et al., 2004 have stronger tendency to select A, while "negative learners" have stronger tendency to avoid B (Frank et al., 2004). We did not find any statistical effect of stimulation on probability of choosing A (Friedman's test $\chi^2_F(3) = 1.76$, $p = 0.62$), or avoiding B (Friedman's test $\chi^2_F(3) = 1.49$, $p = 0.68$). Also the ratio of probability of choosing A over avoiding B was not affected by the type of stimulation (Friedman's test $\chi^2_F(3) = 0.85$, $p = 0.84$).

In addition, we evaluated the reaction times in no conflict cases where there was winning character paired with a losing character (i.e., AB), lose/lose conflict cases where there was a losing character paired with another losing character (i.e., BD) and win/win conflict cases where a winning character was paired with another winning character (i.e., AC). There was no significant effect of stimulation type on reaction time for no conflict cases (Friedman's test $\chi^2_F(3) = 3.03$, $p = 0.39$), lose/lose conflict cases (Friedman's test $\chi^2_F(3) = 0.52$, $p = 0.92$), or win/win conflict cases (Friedman's test $\chi^2_F(3) = 3.43$, $p = 0.33$) (**Figure 3**).

ERP Recording

Next, similarly to Frank et al., 2004, we investigated the event-related potentials when time-locked to response (Frank et al., 2004). The analysis showed similar ERPs as previously reported (Frank et al., 2004, 2005). There was no effect of stimulation in negativity amplitude in win/win ERP voltages (Friedman's test $\chi^2_F(3) = 1.03$, $p = 0.79$) and negativity amplitude in lose/lose ERP voltages (Friedman's test $\chi^2_F(3) = 0.34$, $p = 0.95$) (**Figure 4**).

EEG Spectral Power

Power spectral analysis of the resting EEG signal also did not show any difference among the 4 stimulation types. There was no statistical significance when measuring the power in delta (1–4 Hz) (Friedman's test $\chi^2_F(3) = 1.12$, $p = 0.77$), theta (4–8 Hz) (Friedman's test $\chi^2_F(3) = 4.54$, $p = 0.21$), alpha (8–13 Hz) (Friedman's test $\chi^2_F(3) = 1.78$, $p = 0.62$), or beta (13–30 Hz) (Friedman's test $\chi^2_F(3) = 1.71$, $p = 0.64$) EEG frequency bands (**Figure 5**).

DISCUSSION

In this work we have attempted to modulate SN activity differentially, by applying theta tACS or phase-locked tPCS synchronized to the frontal theta when the volunteers were

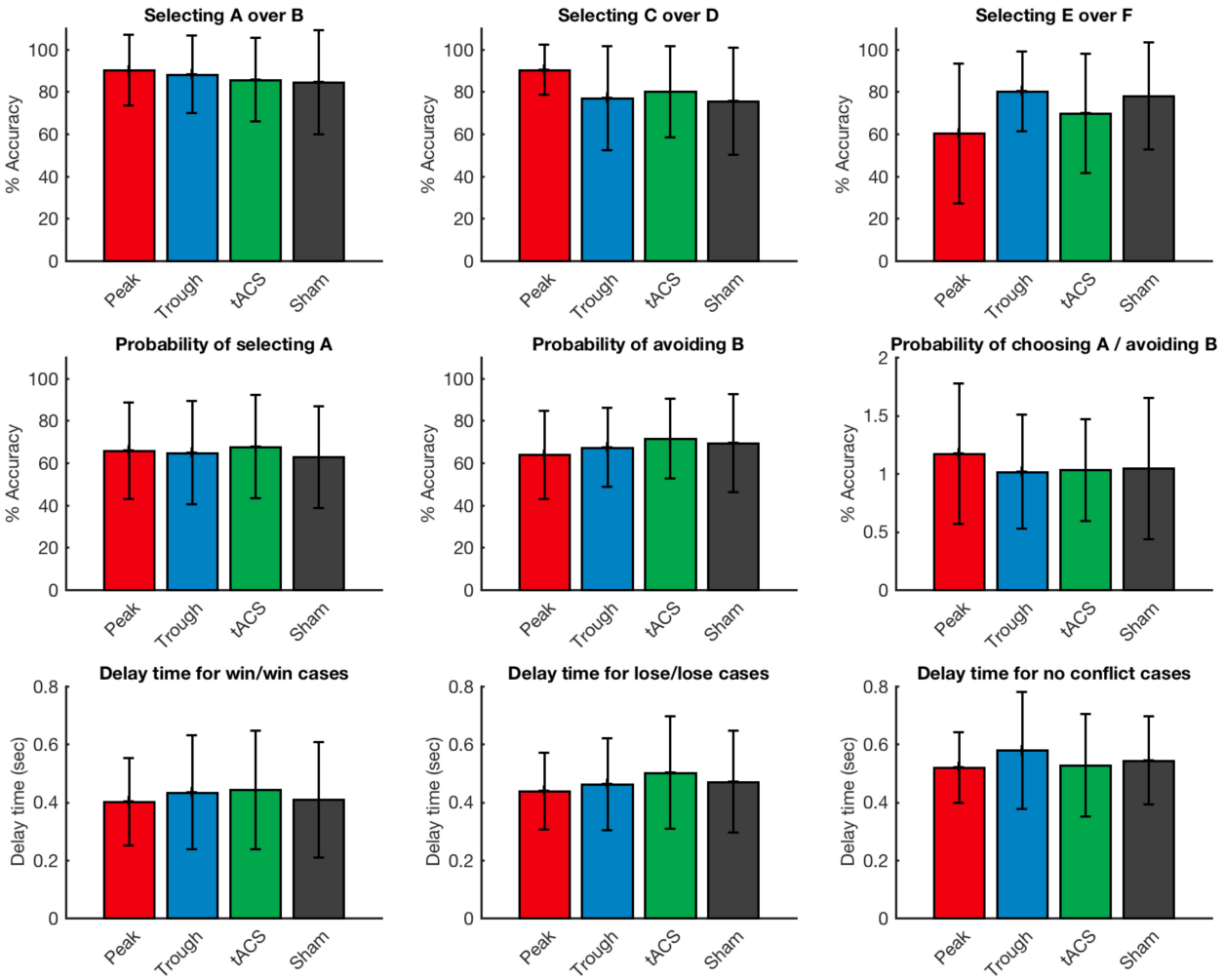

FIGURE 3 | Accuracy and response timing of the volunteers during the test period of the game during the various possible choice scenarios on the task. Error bars represent standard deviation.

engaged in a SN activating task. However, the results of the present study did not demonstrate differential effects of any of the 4 stimulation types on either electrophysiological or behavioral measures. Indeed, no significant effects were observed for any of the active stimulation conditions compared to sham stimulation in this investigation.

Previously, theta tACS applied during rest has been shown to be an effective modulator of frontal theta power (Pahor and Jaušovec, 2014); however, its effects have not been studied when the stimulation is applied during a task. In another study, theta tACS applied over parietal brain regions before a working memory task resulted in increased working memory storage; however, the same stimulation over frontal region had no effect (Jaušovec and Jaušovec, 2014). Cognitive effects of theta tPCS have been shown to be very small and specific to complex mathematical tasks (Morales-Quezada et al., 2015). In a more recent study, theta tACS applied over frontal region showed a decrease in nodal efficiency of dorsal anterior cingulate cortex (dACC) – one of the nodes of SN (Onoda et al., 2017).

The lack of any effect for any of the active stimulation conditions in the present study raises the question of whether the stimulation parameters were adequate to achieve neurophysiological effects in general, notwithstanding the role of phase-locking. Recent publications suggest that stronger transcranial electrical stimulation currents (i.e., >2 mA) may be required in some circumstances to have detectable effects on brain activity and behavior (Vöröslakos et al., 2018). In our study we respected the stimulation limits imposed by the hardware and what has been conventionally used and considered safe for these types of stimulation, which is 2 mA of current. However, it has been shown that in order to produce effective fields in the brain, currents as high as 6 mA are sometimes needed (Vöröslakos et al., 2018). Considering the thickness of the skull and the layers of dura protecting the brain, it is reasonable that stimulation may require higher currents to achieve the desired effect. Previously, other studies have shown that stimulation intensities as low as 2 mA can achieve sufficiently strong fields in the brain through computer

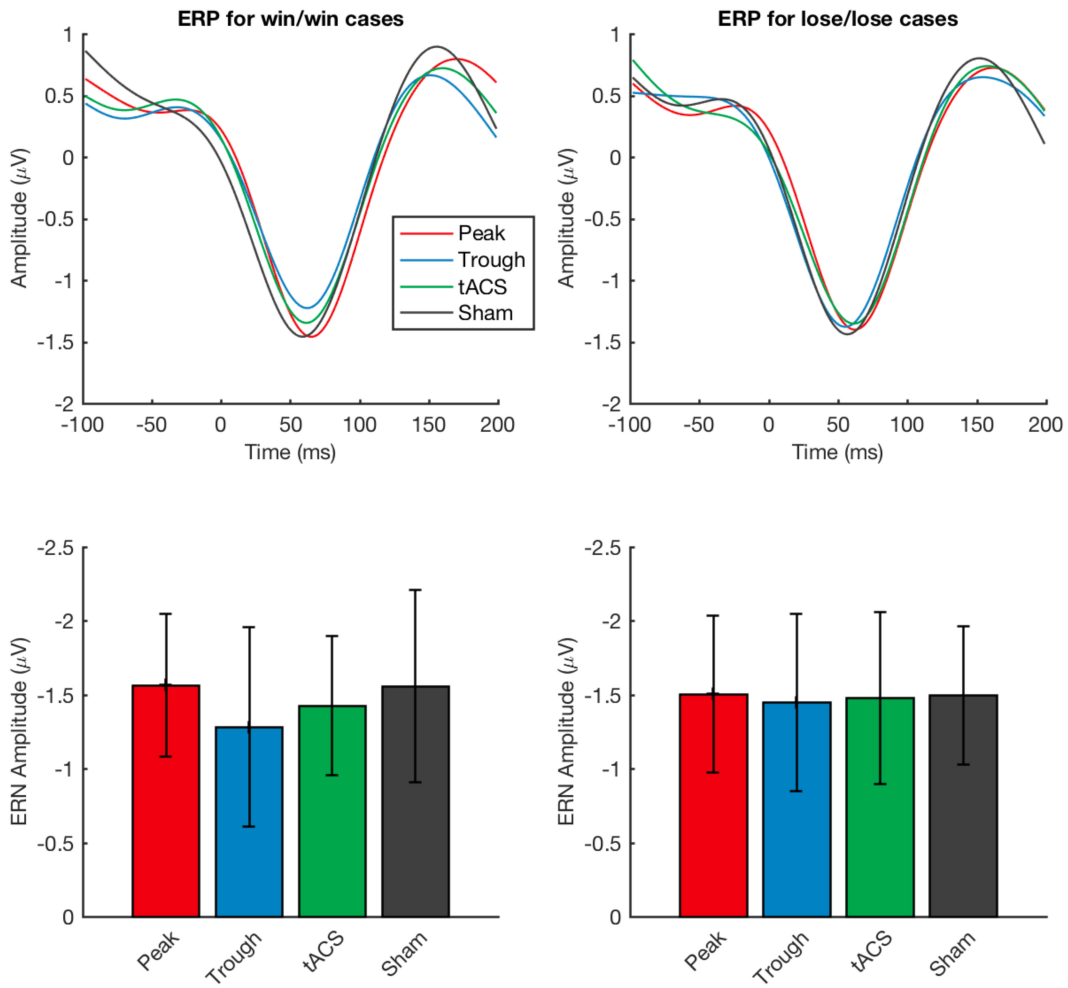

FIGURE 4 | Event-related potential recordings obtained during the test task under the four types of stimulation applied. Waveforms for event-related positive (ERP) and amplitudes for event-related negative (ERN) potentials are shown for tACS applied under the sham, active non-phase-locked, active peak-phase-locked, and active trough phase-locked stimulation conditions are compared. No significant differences were detected across any of the four stimulation types. Error bars represent standard deviation.

simulations (Wagner et al., 2007), and studies using tDCS and tACS have been proven effective (Zaghi et al., 2010; Stagg and Nitsche, 2011; Reato et al., 2013; Kuo et al., 2014); however, these experiments have used different electrode montages and targeted other brain networks rather than SN itself. Moreover, brain stimulation in these studies was generally applied during rest, while in our study the stimulation was applied during a task. Further, some studies could only detect improvement in MDD patients after multiple sessions of tDCS (Brunoni et al., 2011; Alonzo et al., 2012), multiple sessions of stimulations should be considered for future trials. Finally, and importantly, most previous work regarding effective current amplitude applied either ongoing transcranial direct current stimulation (tDCS) or else sinusoidal tACS. In contrast, the present study's phase-locked stimulation applied short pulses of 5 ms rather than sinusoidal pulses – a feature that may have precluded measurable effects on brain activity due to the short duty cycle of stimulation.

Considering the small sample size and the variability in the outcome measure, we speculate that the methods we used here (specifically, the 2 mA amplitude and brief-pulse waveform of phase-locked stimulation) may have had smaller effects than anticipated, and that the natural variability between the experimental sessions could have been larger than the effects of stimulation. In future work, using a larger sample size, increasing the stimulation intensity, or applying a longer duty cycle for the phase-locked tPCS could possibly lead to unveiling the effect of these types of NIBS.

As an additional factor to consider, the stimulation techniques used in this work may not have been suitable to modulate SN activity due to their low power and low spatial focality. Even though there is evidence of effectiveness of tACS in other models, modulation of SN has been mainly shown using rTMS, which is a much stronger type of brain stimulation in terms of both field intensity and depth. Body tissues have nearly uniform magnetic permeability and do not significantly distort the magnetic field

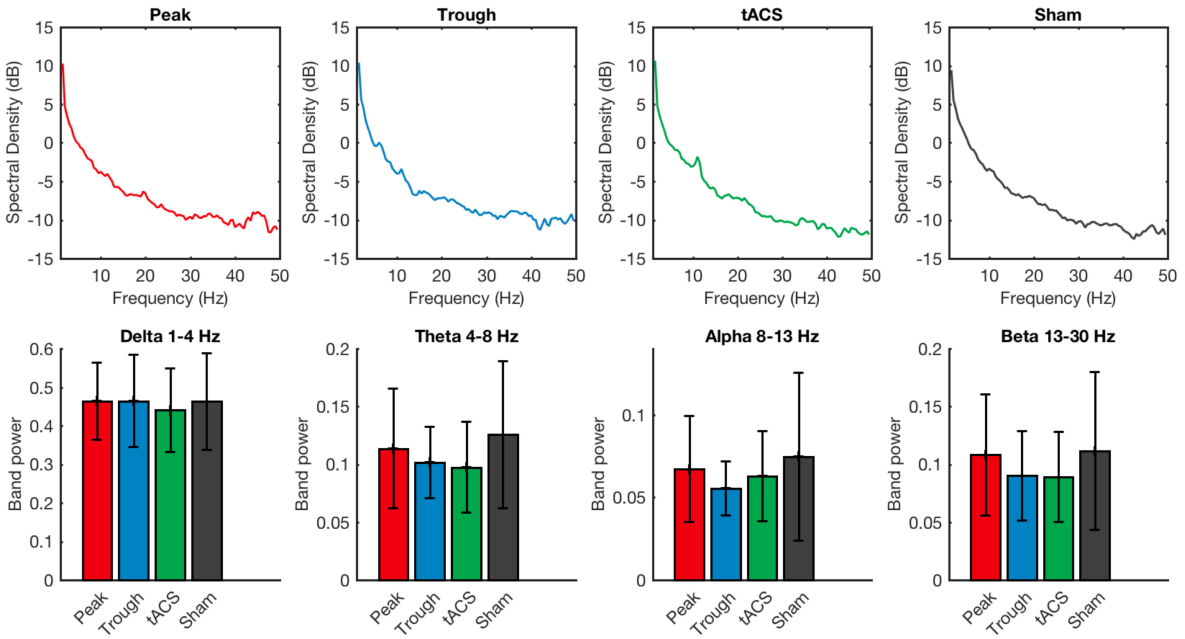

FIGURE 5 | Power spectral densities of the resting EEG recorded after the training session are compared for tACS applied under the sham, active non-phase-locked, active peak-phase-locked, and active trough phase-locked stimulation conditions. No significant differences were detected across any of the four stimulation types. Error bars represent standard deviation.

produced by rTMS, allowing effective focusing of the stimulation to a restricted target at higher intensity than tES (Wagner et al., 2004). On the other hand, for non-invasive electrical stimulation, the large differences in electrical conductivity of the various tissues in the overlying scalp and skull not only blocks most of the current from reaching brain tissue, but also disperses the fields, thereby precluding effective focusing of the stimulation. Some work has been done to use multiple electrodes in a high density (HD) fashion to improve the focality of the stimulation (Kuo et al., 2013), which potentially could improve the effectiveness of the stimulation in future work.

It is believed that the electrical stimuli of tES affect the ongoing activity of the brain; thus, task-specific activation of the SN was used as means to assess the effect of the stimulation. However, the task used in our paper has not yet been used in the context of brain stimulation, and thus, perhaps other tasks should be studied with a similar stimulation protocol. While we know that the presently employed task activates SN and produces increased theta oscillation – a hallmark of SN activity – it is possible that in this case the task did not activate the specific nodes of the SN where the stimulation was delivered, or that the activation was not reflected in the outcome measures we studied in this experiment. We have selected these specific outcome measures based on the previous findings (resting EEG power changes, ERPs specific to the task and task specific behavioral changes). The effects of these types of stimulation has previously been shown to result in spectral power density changes in specific frequency bands during rest EEG (Zaehle et al., 2010; Helfrich et al., 2014; Vossen et al., 2015), changes in task specific activation of the brain (Meinzer et al., 2012; Jaušovec and Jaušovec, 2014; Cabral-Calderin et al., 2016), and behavioral or task specific performance changes (Santarnecchi et al., 2013; Voss et al., 2014). It therefore would be valuable to test our methods, tACS and phase-locked tPCS, in a sensorimotor model so we can check for changes in motor or sensory evoked potentials as a result of the stimulation.

Translationally, the search for novel NIBS approaches is much needed, as the current treatment options for TRD are very limited. Electroconvulsive therapy (ECT) has conventionally been the treatment of choice for TRD; however, it is associated with high costs, significant stigma, and cognitive side effects that deter many patients (Gangadhar, 2005). rTMS is a potential alternative; however, its limited availability, higher costs, and requirement for in-clinic rather than at-home application are the main limitations restricting its widespread adoption. A cost-effective, home-based brain stimulation technique may potentially resolve those limitations and provide an alternative treatment option for TRD patients. tPCS/tACS can potentially be made available as a home-based treatment, and the application of the stimulating currents in an oscillatory, phase-locked fashion could provide an opportunity to improve its efficacy by attempting to engage specific brain networks. Primarily, the past few decades of neuropsychiatric and neuroimaging research points toward the SN as the main target for treating MDD and TRD. However, tDCS and other simple electrical stimulation protocols can become more effective when integrated in a closed-loop system (Zrenner et al., 2016). Future work in this direction may potentially help develop a closed-loop electrical based brain stimulation technique.

To summarize, in this study we have tested novel approaches, tACS and phase-locked tPCS, to stimulate the SN network with hopes that such stimulation could be used for

therapeutic purposes. If found effective, these techniques could potentially open doors for new treatments of MDD and other neuropsychiatric disorders linked to the SN. Although our results showed no statistically significant effect of stimulation on the ERP recordings, resting EEG recordings, and the performance of the volunteers in a SN activating task, future work will reveal whether such effects could be obtained by either modifying the amplitude or waveform of electrical stimulation, or else applying the same phase-locking algorithm to a more powerful stimulation modality, such as rTMS. Success could lead to more successful outcomes for patients undergoing treatment for TRD and other medically refractory neuropsychiatric illnesses.

DATA AVAILABILITY STATEMENT

The datasets generated for this study are available on request to the corresponding author.

ETHICS STATEMENT

Twenty healthy volunteers free of neurological or psychiatric illnesses participated in the study. All participants gave informed consent, and the study was approved by the Research Ethics Board of the University Health Network.

AUTHOR CONTRIBUTIONS

All authors listed have made a substantial, direct, and intellectual contribution to the work, and approved it for publication.

FUNDING

This work was supported by the MITACS Accelerate Grant (#IT05799) FM.

REFERENCES

Aleman, A., Enriquez-Geppert, S., Knegtering, H., and Dlabac-de Lange, J. J. (2018). Moderate effects of noninvasive brain stimulation of the frontal cortex for improving negative symptoms in schizophrenia: meta-analysis of controlled trials. *Neurosci. Biobehav. Rev.* 89, 111–118. doi: 10.1016/j.neubiorev.2018.02.009

Alonzo, A., Brassil, J., Taylor, J. L., Martin, D., and Loo, C. K. (2012). Daily transcranial direct current stimulation (tDCS) leads to greater increases in cortical excitability than second daily transcranial direct current stimulation. *Brain Stimul.* 5, 208–213. doi: 10.1016/j.brs.2011.04.006

Berlim, M. T., Van den Eynde, F., and Daskalakis, Z. J. (2013). Clinical utility of transcranial direct current stimulation (tDCS) for treating major depression: a systematic review and meta-analysis of randomized, double-blind and sham-controlled trials. *J. Psychiatr. Res.* 47, 1–7. doi: 10.1016/j.jpsychires.2012.09.025

Berlim, M. T., Van Den Eynde, F., Tovar-Perdomo, S., and Daskalakis, Z. J. (2014). Response, remission and drop-out rates following high-frequency repetitive transcranial magnetic stimulation (rTMS) for treating major depression: a systematic review and meta-analysis of randomized, double-blind and sham-controlled trials. *Psychol. Med.* 44, 225–239. doi: 10.1017/S0033291713000512

Brittain, J. S., Probert-Smith, P., Aziz, T. Z., and Brown, P. (2013). Tremor suppression by rhythmic transcranial current stimulation. *Curr. Biol.* 23, 436–440. doi: 10.1016/j.cub.2013.01.068

Brunoni, A. R., Ferrucci, R., Bortolomasi, M., Vergari, M., Tadini, L., Boggio, P. S., et al. (2011). Transcranial direct current stimulation (tDCS) in unipolar vs. *bipolar depressive disorder*. *Prog. Neuro- Psychopharmacology. Biol. Psychiatry* 35, 96–101. doi: 10.1016/j.pnpbp.2010.09.010

Cabral-Calderin, Y., Anne Weinrich, C., Schmidt-Samoa, C., Poland, E., Dechent, P., Bähr, M., et al. (2016). Transcranial alternating current stimulation affects the BOLD signal in a frequency and task-dependent manner. *Hum. Brain Mapp.* 37, 94–121. doi: 10.1002/hbm.23016

Chung, S. W., Sullivan, C. M., Rogasch, N. C., Hoy, K. E., Bailey, N. W., Cash, R. F. H., et al. (2018). The effects of individualised intermittent theta burst stimulation in the prefrontal cortex: a TMS-EEG study. *Hum. Brain Mapp.* 40, 608–627. doi: 10.1002/hbm.24398

Daskalakis, Z. J., Levinson, A. J., and Fitzgerald, P. B. (2008). Repetitive transcranial magnetic stimulation for major depressive disorder: a review. *Can. J. Psychiatry.* 53, 555–566. doi: 10.1177/070674370805300902

Dayan, E., Censor, N., Buch, E. R., Sandrini, M., and Cohen, L. G. (2013). Noninvasive brain stimulation: from physiology to network dynamics and back. *Nat. Neurosci.* 16, 838–844. doi: 10.1038/nn.3422

Delorme, A., and Makeig, S. (2004). EEGLAB: an open source toolbox for analysis of single-trial EEG dynamics including independent component analysis. *J. Neurosci. Methods.* 134, 9–21. doi: 10.1016/j.jneumeth.2003.10.009

Downar, J., Crawley, A. P., Mikulis, D. J., and Davis, K. D. (2000). A multimodal cortical network for the detection of changes in the sensory environment. *Nat. Neurosci.* 3, 277–283. doi: 10.1038/72991

Downar, J., Crawley, A. P., Mikulis, D. J., and Davis, K. D. (2001). The effect of task relevance on the cortical response to changes in visual and auditory stimuli: an event-related fMRI study. *Neuroimage* 14, 1256–1267. doi: 10.1006/nimg.2001.0946

Faul, F., Erdfelder, E., Lang, A. G., and Buchner, A. (2007). G*Power 3: a flexible statistical power analysis program for the social, behavioral, and biomedical sciences. *Behavior. Research. Methods.* 39, 175–191. doi: 10.3758/BF03193146

Ferrucci, R., Bortolomasi, M., Vergari, M., Tadini, L., Salvoro, B., Giacopuzzi, M., et al. (2009). Transcranial direct current stimulation in severe, drug-resistant major depression. *J. Affect. Disord.* 118, 215–219. doi: 10.1016/j.jad.2009.02.015

Frank, M. J., Seeberger, L. C., and O'Reilly, R. C. (2004). By carrot or by stick: cognitive reinforcement learning in parkinsonism. *Science* 306, 1940–1943. doi: 10.1126/science.1102941

Frank, M. J., Woroch, B. S., and Curran, T. (2005). Error-related negativity predicts reinforcement learning and conflict biases. *Neuron* 47, 495–501. doi: 10.1016/j.neuron.2005.06.020

Fregni, F., and Pascual-Leone, A. (2007). Technology insight: noninvasive brain stimulation in neurology-perspectives on the therapeutic potential of rTMS and tDCS. *Nat. Clin. Pract. Neurol.* 3, 383–393. doi: 10.1038/ncpneuro0530

Fröhlich, F., and McCormick, D. A. (2010). Endogenous electric fields may guide neocortical network activity. *Neuron* 67, 129–143. doi: 10.1016/j.neuron.2010.06.005

Gangadhar, B. N. (2005). The ECT handbook. *Indian J. Psychiatry* 47, 179–180.

Gaynes, B. N., Lloyd, S. W., Lux, L., Gartlehner, G., Hansen, R. A., Brode, S., et al. (2014). Repetitive transcranial magnetic stimulation for treatment-resistant depression: a systematic review and meta-analysis. *J. Clin. Psychiatry.* 75, 477–489. doi: 10.4088/JCP.13r08815

Hallett, M. (2007). Transcranial magnetic stimulation: a primer. *Neuron* 55, 187–199. doi: 10.1016/j.neuron.2007.06.026

Helfrich, R. F., Schneider, T. R., Rach, S., Trautmann-Lengsfeld, S. A., Engel, A. K., and Herrmann, C. S. (2014). Entrainment of brain oscillations by transcranial alternating current stimulation. *Curr. Biol.* 24, 333–339. doi: 10.1016/j.cub.2013.12.041

Hyman, J. M., Wyble, B. P., Goyal, V., Rossi, C. A., and Hasselmo, M. E. (2003). Stimulation in hippocampal region CA1 in behaving rats yields long-term potentiation when delivered to the peak of theta and long-term depression when delivered to the trough. *J. Neurosci.* 23, 11725–11731. doi: 10.1523/jneurosci.23-37-11725.2003

Jaušovec, N., and Jaušovec, K. (2014). Increasing working memory capacity with theta transcranial alternating current stimulation (tACS). *Biol. Psychol.* 96, 42–47. doi: 10.1016/j.biopsycho.2013.11.006

Krause, M. R., Vieira, P. G., Csorba, B. A., Pilly, P. K., and Pack, C. C. (2019). Transcranial alternating current stimulation entrains single-neuron activity in the primate brain. *Proc. Natl. Acad. Sci. U. S. A.* 116, 5747–5755. doi: 10.1073/pnas.1815958116

Kuo, H., Bikson, M., Datta, A., Minhas, P., Paulus, W., Kuo, M. F., et al. (2013). Comparing cortical plasticity induced by conventional and high-definition 4 × 1 ring tDCS: a neurophysiological study. *Brain Stimul.* 6, 644–648. doi: 10.1016/j.brs.2012.09.010

Kuo, M.-F., Paulus, W., and Nitsche, M. A. (2014). Therapeutic effects of non-invasive brain stimulation with direct currents (tDCS) in neuropsychiatric diseases. *Neuroimage* 85, 948–960. doi: 10.1016/j.neuroimage.2013.05.117

Mansouri, F., Dunlop, K., Giacobbe, P., Downar, J., and Zariffa, J. (2017). A fast EEG forecasting algorithm for phase-locked transcranial electrical stimulation of the human brain. *Front. Neurosci.* 11:401. doi: 10.3389/fnins.2017.00401

Mansouri, F., Fettes, P., Schulze, L., Giacobbe, P., Zariffa, J., and Downar, J. (2018). A real-time phase-locking system for non-invasive brain stimulation. *Front. Neurosci.* 12:877. doi: 10.3389/fnins.2018.00877

Meinzer, M., Antonenko, D., Lindenberg, R., Hetzer, S., Ulm, L., Avirame, K., et al. (2012). Electrical brain stimulation improves cognitive performance by modulating functional connectivity and task-specific activation. *J. Neurosci.* 32, 1859–1866. doi: 10.1523/JNEUROSCI.4812-11.2012

Minarik, T., Berger, B., Althaus, L., Bader, V., Biebl, B., Brotzeller, F., et al. (2016). The importance of sample size for reproducibility of tDCS effects. *Front. Hum. Neurosci.* 10:453. doi: 10.3389/fnhum.2016.00453

Morales-Quezada, L., Cosmo, C., Carvalho, S., Leite, J., Castillo-Saavedra, L., Rozisky, J. R., et al. (2015). Cognitive effects and autonomic responses to transcranial pulsed current stimulation. *Exp. Brain Res.* 233, 701–709. doi: 10.1007/s00221-014-4147-y

Nemeroff, C. B. (2007). Prevalence and management of treatment-resistant depression. *J. Clin. Psychiatry* 68(Suppl. 8), 17–25. doi: 10.1186/1471-2288-11-29

Neuling, T., Ruhnau, P., Weisz, N., Herrmann, C. S., and Demarchi, G. (2017). Faith and oscillations recovered: on analyzing EEG/MEG signals during tACS. *Neuroimage* 147, 960–963. doi: 10.1016/j.neuroimage.2016.11.022

Noury, N., and Siegel, M. (2017). Phase properties of transcranial electrical stimulation artifacts in electrophysiological recordings. *Neuroimage* 158, 406–416. doi: 10.1016/j.neuroimage.2017.07.010

Onoda, K., Kawagoe, T., Zheng, H., and Yamaguchi, S. (2017). Theta band transcranial alternating current stimulations modulates network behavior of dorsal anterior cingulate cortex. *Sci. Rep.* 7:, 3607. doi: 10.1038/s41598-017-03859-3857

O'Reardon, J. P., Solvason, H. B., Janicak, P. G., Sampson, S., Isenberg, K. E., Nahas, Z., et al. (2007). Efficacy and safety of transcranial magnetic stimulation in the acute treatment of major depression: a multisite randomized controlled trial. *Biol. Psychiatry.* 62, 1208–1216. doi: 10.1016/j.biopsych.2007.01.018

Pahor, A., and Jaušovec, N. (2014). The effects of theta transcranial alternating current stimulation (tACS) on fluid intelligence. *Int. J. Psychophysiol.* 93, 322–331. doi: 10.1016/j.ijpsycho.2014.06.015

Park, H.-J., and Friston, K. (2013). Structural and functional brain networks: from connections to cognition. *Science* 80:, 342. doi: 10.1126/science.1238411

Pessoa, L. (2014). Understanding brain networks and brain organization. *Phys. Life Rev.* 11, 400–435. doi: 10.1016/j.plrev.2014.03.005

Peters, S. K., Dunlop, K., and Downar, J. (2016). Cortico-Striatal-Thalamic loop circuits of the salience network: a central pathway in psychiatric disease and treatment. *Front. Syst. Neurosci.* 10:104. doi: 10.3389/fnsys.2016.00104

Reato, D., Rahman, A., Bikson, M., and Parra, L. C. (2013). Effects of weak transcranial alternating current stimulation on brain activity—a review of known mechanisms from animal studies. *Front. Hum. Neurosci.* 7:687. doi: 10.3389/fnhum.2013.00687

Riecke, L., Formisano, E., Herrmann, C. S., and Sack, A. T. (2015). 4-Hz transcranial alternating current stimulation phase modulates hearing. *Brain Stimul.* 8, 777–783. doi: 10.1016/j.brs.2015.04.004

Santarnecchi, E., Polizzotto, N. R., Godone, M., Giovannelli, F., Feurra, M., Matzen, L., et al. (2013). Frequency-dependent enhancement of fluid intelligence induced by transcranial oscillatory potentials. *Curr. Biol.* 23, 1449–1453. doi: 10.1016/j.cub.2013.06.022

Seager, M. A., Johnson, L. D., Chabot, E. S., Asaka, Y., and Berry, S. D. (2002). Oscillatory brain states and learning: impact of hippocampal theta-contingent training. *Proc. Natl. Acad. Sci. U.S.A.* 99, 1616–1620. doi: 10.1073/pnas.032662099

Shiozawa, P., Fregni, F., Benseñor, I. M., Lotufo, P. A., Berlim, M. T., Daskalakis, J. Z., et al. (2014). Transcranial direct current stimulation for major depression: an updated systematic review and meta-analysis. *Int. J. Neuropsychopharmacol.* 17, 1443–1452. doi: 10.1017/S1461145714000418

Silvanto, J., Muggleton, N., and Walsh, V. (2008). State-dependency in brain stimulation studies of perception and cognition. *Trends Cogn. Sci.* 12, 447–454. doi: 10.1016/j.tics.2008.09.004

Stagg, C. J., and Nitsche, M. A. (2011). Physiological basis of transcranial direct current stimulation. *Neuroscientist.* 17, 37–53. doi: 10.1177/1073858410386614

Vöröslakos, M., Takeuchi, Y., Brinyiczki, K., Zombori, T., Oliva, A., Fernández-Ruiz, A., et al. (2018). Direct effects of transcranial electric stimulation on brain circuits in rats and humans. *Nat. Commun.* 9:, 483. doi: 10.1038/s41467-018-02928-2923

Voss, U., Holzmann, R., Hobson, A., Paulus, W., Koppehele-Gossel, J., Klimke, A., et al. (2014). Induction of self awareness in dreams through frontal low current stimulation of gamma activity. *Nat. Neurosci.* 17, 810–814. doi: 10.1038/nn.3719

Vossen, A., Gross, J., and Thut, G. (2015). Alpha power increase after transcranial alternating current stimulation at alpha frequency (a-tACS) reflects plastic changes rather than entrainment. *Brain Stimul.* 8, 499–508. doi: 10.1016/j.brs.2014.12.004

Wagner, T., Fregni, F., Fecteau, S., Grodzinsky, A., Zahn, M., and Pascual-Leone, A. (2007). Transcranial direct current stimulation: a computer-based human model study. *Neuroimage* 35, 1113–1124. doi: 10.1016/j.neuroimage.2007.01.027

Wagner, T., Zahn, M., Grodzinsky, A. J., and Pascual-Leone, A. (2004). Three-dimensional head model simulation of transcranial magnetic stimulation. *IEEE Trans. Biomed. Eng.* 51, 1586–1598. doi: 10.1109/TBME.2004.827925

Wilsch, A., Neuling, T., Obleser, J., and Herrmann, C. S. (2018). Transcranial alternating current stimulation with speech envelopes modulates speech comprehension. *Neuroimage* 172, 766–774. doi: 10.1016/j.neuroimage.2018.01.038

Zaehle, T., Rach, S., and Herrmann, C. S. (2010). Transcranial alternating current stimulation enhances individual alpha activity in human EEG. *PLoS One* 5:e13766. doi: 10.1371/journal.pone.0013766

Zaghi, S., Acar, M., Hultgren, B., Boggio, P. S., and Fregni, F. (2010). Noninvasive brain stimulation with low-intensity electrical currents: putative mechanisms of action for direct and alternating current stimulation. *Neuroscientist* 16, 285–307. doi: 10.1177/1073858409336227

Zanos, S., Rembado, I., Chen, D., and Fetz, E. E. (2018). Phase-locked stimulation during cortical beta oscillations produces bidirectional synaptic plasticity in awake monkeys. *Curr. Biol.* 28, 2515.e–2526.e4. doi: 10.1016/j.cub.2018.07.009

Zrenner, C., Belardinelli, P., Müller-Dahlhaus, F., and Ziemann, U. (2016). Closed-Loop neuroscience and non-invasive brain stimulation: a tale of two loops. *Front. Cell. Neurosci.* 10:92. doi: 10.3389/fncel.2016.00092

Zrenner, C., Desideri, D., Belardinelli, P., and Ziemann, U. (2017). Real-time EEG-defined excitability states determine efficacy of TMS-induced plasticity in human motor cortex. *Brain Stimul.* 11, 374–389. doi: 10.1016/j.brs.2017.11.016

Conflict of Interest: The authors declare that the research was conducted in the absence of any commercial or financial relationships that could be construed as a potential conflict of interest.

frontiers in Neuroscience

ORIGINAL RESEARCH
published: 26 November 2019
doi: 10.3389/fnins.2019.01269

Modulation of Theta-Band Local Field Potential Oscillations Across Brain Networks With Central Thalamic Deep Brain Stimulation to Enhance Spatial Working Memory

Ching-Wen Chang[1†], Yu-Chun Lo[2†], Sheng-Huang Lin[3,4], Shih-Hung Yang[5], Hui-Ching Lin[6], Ting-Chun Lin[1], Ssu-Ju Li[1], Christine Chin-jung Hsieh[1,7], Vina Ro[1], Yueh-Jung Chung[6], Yun-Chi Chang[6], Chi-Wei Lee[2,6], Chao-Hung Kuo[1,8,9], Shin-Yuan Chen[10,11] and You-Yin Chen[1,2,7*]*

[1] Department of Biomedical Engineering, National Yang Ming University, Taipei, Taiwan, [2] The Ph.D. Program for Neural Regenerative Medicine, College of Medical Science and Technology, Taipei Medical University, Taipei, Taiwan, [3] Department of Neurology, Hualien Tzu Chi Hospital, Buddhist Tzu Chi Medical Foundation, Hualien City, Taiwan, [4] Department of Neurology, School of Medicine, Tzu Chi University, Hualien City, Taiwan, [5] Department of Mechanical Engineering, National Cheng Kung University, Tainan, Taiwan, [6] Department and Institute of Physiology, National Yang Ming University, Taipei, Taiwan, [7] Taiwan International Graduate Program in Interdisciplinary Neuroscience, National Yang Ming University, Academia Sinica, Taipei, Taiwan, [8] Department of Neurosurgery, Taipei Veterans General Hospital, Neurological Institute, Taipei, Taiwan, [9] Department of Neurological Surgery, University of Washington, Seattle, WA, United States, [10] Department of Neurosurgery, Hualien Tzu Chi Hospital, Buddhist Tzu Chi Medical Foundation, Hualien City, Taiwan, [11] Department of Surgery, School of Medicine, Tzu Chi University, Hualien City, Taiwan

Deep brain stimulation (DBS) is a well-established technique for the treatment of movement and psychiatric disorders through the modulation of neural oscillatory activity and synaptic plasticity. The central thalamus (CT) has been indicated as a potential target for stimulation to enhance memory. However, the mechanisms underlying local field potential (LFP) oscillations and memory enhancement by CT-DBS remain unknown. In this study, we used CT-DBS to investigate the mechanisms underlying the changes in oscillatory communication between the CT and hippocampus, both of which are involved in spatial working memory. Local field potentials (LFPs) were recorded from microelectrode array implanted in the CT, dentate gyrus, cornu ammonis (CA) region 1, and CA region 3. Functional connectivity (FC) strength was assessed by LFP–LFP coherence calculations for these brain regions. In addition, a T-maze behavioral task using a rat model was performed to assess the performance of spatial working memory. In DBS group, our results revealed that theta oscillations significantly increased in the CT and hippocampus compared with that in sham controls. As indicated by coherence, the FC between the CT and hippocampus significantly increased in the theta band after CT-DBS. Moreover, Western blotting showed that the protein expressions of the dopamine D1 and α4-nicotinic acetylcholine receptors were enhanced, whereas that of the dopamine D2 receptor decreased in the DBS group. In conclusion, the use of CT-DBS resulted in elevated theta oscillations, increased FC between the CT and hippocampus, and altered synaptic plasticity in the hippocampus, suggesting that CT-DBS is an effective approach for improving spatial working memory.

Keywords: central thalamus, deep brain stimulation, spatial working memory, synaptic plasticity, hippocampal theta oscillation

OPEN ACCESS

Edited by:
Olivier David,
Institut National de la Santé et de la Recherche Médicale (INSERM), France

Reviewed by:
Michal Zochowski,
University of Michigan, United States
Veronique Coizet,
INSERM U1216 Grenoble Institut des Neurosciences (GIN), France

****Correspondence:***
Sheng-Huang Lin
shlin355@gmail.com
You-Yin Chen
irradiance@so-net.net.tw

† These authors have contributed equally to this work

Specialty section:
This article was submitted to Neural Technology, a section of the journal Frontiers in Neuroscience

Received: *13 June 2019*
Accepted: *08 November 2019*
Published: *26 November 2019*

Citation:
Chang C-W, Lo Y-C, Lin S-H, Yang S-H, Lin H-C, Lin T-C, Li S-J, Hsieh CC-j, Ro V, Chung Y-J, Chang Y-C, Lee C-W, Kuo C-H, Chen S-Y and Chen Y-Y (2019) Modulation of Theta-Band Local Field Potential Oscillations Across Brain Networks With Central Thalamic Deep Brain Stimulation to Enhance Spatial Working Memory. Front. Neurosci. 13:1269. doi: 10.3389/fnins.2019.01269

INTRODUCTION

Deep brain stimulation (DBS) is a well-established neurosurgical technique applied during treatment for movement and psychiatric disorders. A medical device known as a neurostimulator is involved, with which local stimulation is performed on patients through electrodes implanted in specific brain regions to send electrical impulses to particular brain targets (Jacobs et al., 2016; Kuhn and Volkmann, 2017). In clinical applications, DBS has been used to treat a variety of neurological disorders by targeting nuclei in different brain regions. For instance, patients with Parkinson's disease (PD) demonstrated improved motor symptoms after the application of DBS in the subthalamic nucleus, which is a key node in the functional control of motor activity in basal ganglia (Benabid, 2003; Duncan et al., 2018). Also, after DBS in the nucleus accumbens (NAc) in patients with autism spectrum disorders, the patients' social communication skills were enhanced, and decreased metabolism in the prefrontal and frontal cortex were observed through fluorodeoxyglucose-positron emission tomography (Park et al., 2016). Furthermore, patients with major depressive disorder (MDD) treated with DBS in medial forebrain bundle had exhibited an improvement in their depression score due to the DBS-induced modulation of the mesolimblic reward system (Temel et al., 2015).

Recently, it has been reported that DBS has the ability to activate local and network-wide electrical effects and modulate oscillatory activities (Chiken and Nambu, 2014; Herrington et al., 2016). Additionally, several studies have revealed that DBS may modulate local field potentials (LFPs) by phase synchronization and rhythmic oscillations (de Hemptinne et al., 2015; Lin et al., 2015; Stefani et al., 2018). In humans, beta LFP oscillations appear to be related to motor function and gamma LFP oscillations related to sensory perception (Luo and Guan, 2018). In PD patients, DBS in the basal ganglia has been shown to inhibit beta LFP oscillations in the motor cortex, thereby improving cortical functions (de Hemptinne et al., 2015). In the Tourette syndrome (TS) patients, DBS in the centromedian nucleus (CM) of thalamus has been shown to increase the gamma LFP oscillations in the CM and also to ameliorate the TS symptoms (Maling et al., 2012). Furthermore, theta and alpha LFP oscillations are associated with memory (Colgin, 2013) and cognitive function (Klimesch, 2012), respectively. In MDD patients, DBS in the ventral internal capsule/ventral striatum increases theta oscillations in the prefrontal cortex, leading to enhanced performance of cognitive control tasks (Widge et al., 2019). In PD patients, DBS of caudal, and rostral pedunculopontine nucleus has been shown to inhibit alpha oscillations and improve gait (Thevathasan et al., 2012).

A number of studies have attempted to enhance memory and cognitive function by stimulating different DBS targets in humans and rodents. In humans, stimulation of the entorhinal cortex served to enhance spatial memory and increase theta oscillations in the hippocampus (Suthana et al., 2012). In rodents, theta oscillations in the hippocampus were restored by stimulating the fornix, and spatial working memory task performance was improved (Bick and Eskandar, 2016). Also, after application of DBS in the infralimbic cortex fin rodents, the cognitive function and memory were improved, and theta oscillations in the hippocampus were restored (Cervera Ferri et al., 2016). An improvement in working memory was found after electrical stimulation of the central thalamus (CT) in object recognition memory tasks in rodents (Mair and Hembrook, 2008). Moreover, forniceal DBS in Rett syndrome mice rescued spatial learning and memory, and restored *in vivo* hippocampal synaptic plasticity and hippocampal neurogenesis (Hao et al., 2015).

Enhancements of cognitive function and memory have been indicated through synaptic plasticity modification induced by DBS in the CT (Lin et al., 2015; Tsai et al., 2016; Wang et al., 2017). Restoration of consciousness and enhancement of cognitive function were demonstrated in patients with traumatic brain injury and disorders of consciousness after the implication of CT-DBS (Shah and Schiff, 2010; Tabansky et al., 2014; Schiff, 2016; Carlton and Murad, 2018). The activation of *c-Fos* and Zif268 in the cortical region and hippocampus has been shown to be modulated by DBS in the CT, which significantly improved behavioral performance associated with cognitive memory function in rodents (Shirvalkar et al., 2006). Application of DBS promotes the release of striatal dopamine and hippocampal acetylcholine (Figee et al., 2014; Posporelis et al., 2018). In human studies, DBS targeting of the NAc was indicated to be related to the dopaminergic system in the striatum. Patients with obsessive-compulsive disorder treated with DBS in the NAc were found to exhibit an increase in the dopamine release in the striatum, further increasing dopamine neurotransmission, leading to an improvement in their clinical symptoms (Figee et al., 2014). DBS in the medial septum applied in an Alzheimer's rodent models indicated an increase in acetylcholine release in the hippocampus and possible reversal of spatial memory impairments (Posporelis et al., 2018). Both dopaminergic and acetylcholine-mediated signaling are important for synaptic plasticity modification (Di Filippo et al., 2008).

The central thalamus comprises the central lateral nucleus, mediodorsal nucleus, parafascicular nucleus, CM and nucleus reuniens (Saalmann, 2014). In a previous study, the CT was revealed to play a critical role in the extra-hippocampal network in terms of spatial working memory consolidation (Lopez et al., 2009). The known anatomical projection of the CT includes the dentate gyrus (DG) (Shirvalkar et al., 2006), which is a subregion of the hippocampus. The hippocampus has been reported to receive dense innervation by cholinergic neurons, which serve to mediate the formation of memory; on the other hand, the acetylcholine has not only been shown to play a critical role in the hippocampus as a modulator of cognitive function, but has also aroused significant attention for its extensive effects on recovery of impaired memory (Haam and Yakel, 2017; Maurer and Williams, 2017). In rodent studies, an increase in acetylcholine in the DG was observed after the application of electrical stimulation to the hippocampus in intact mice, leading to an improvement in learning and memory performance (Matsuyama et al., 2000). A previous study showed that dopaminergic neurons innervate the hippocampus,

and hippocampal dopamine signaling has been indicated as strongly involved in spatial memory and cognitive function (Edelmann and Lessmann, 2018). Rodent models that had received the neurosurgical treatment of electrical stimulation have been observed to demonstrate the activation of dopamine in hippocampus and enhancement of behavioral performance (Li et al., 2003). The hippocampus comprises two characteristic interlocking C-shaped layers of cells, including the cornu ammonis (CA) region 1 (CA1), CA region 3 (CA3), and DG, also known as the trisynaptic circuit (Yeckel and Berger, 1990). It has been suggested that the above-mentioned regions serve different roles and exhibit distinct functions in the mediation of memory; e.g., the projection of the DG to CA3, which is essential for the process of spatial information encoding (Kesner et al., 2004). In contrast, the function of CA3 involves the rapid acquisition of novel information (Kesner, 2007), whereas that of CA1 is associated with temporal pattern separation (Gilbert et al., 2001). Previous studies have indicated that lesions in the DG and CT may result in neural activity inhibition and spatial working memory impairment based on the observation of delayed match-to-position tasks (Mizumori et al., 1994; Kesner et al., 2004; Mair et al., 2011).

Although structural and functional connections between the CT and hippocampus have been reported, memory enhancement and oscillatory communication between the two regions remain largely unknown. In this study, we investigated changes in both LFP oscillations and functional connectivity (FC) among four specific brain regions, including the CT, CA1, CA3, and DG after the application of CT-DBS. In addition, a T-maze behavioral task was employed to evaluate the effect of CT-DBS on spatial working memory. We hypothesized that increased FC between the CT and hippocampus induced by CT-DBS indicates an alteration of structural neuroplasticity. Therefore, Western blotting was used to examine CT-DBS-induced protein expression changes in dopamine and acetylcholine receptors.

MATERIALS AND METHODS

Animal Subjects and Grouping

In total, 30 male adult SD rats weighing between 250 and 350 g were used in this study. All rats were kept in an animal research facility under well-controlled laboratory conditions (12:12 light: dark cycle with lights kept on at 7 AM; 20°C ± 3°C) and fed *ad libitum*. All procedures followed the National Institute of Health's guidelines for animal care and procedures and were approved by the Institutional Animal Care and Use Committee of Tzu Chi General Hospital (IACUC Approval No.: 106-35).

The rats were equally divided into three groups (N = 10 per group): sham controls (sham stimulation), DBS group and DBS *wo.* T-maze group. Rats in sham controls (sham stimulation) and DBS group with implanting a microelectrode array and then received the T-maze behavioral test following CT-DBS (or sham stimulation), which was used to compare the improvement in spatial working memory using CT-DBS. To exclude the effects of T-maze behavioral training on LFP oscillation changes, rats in the DBS *wo.* T-maze group only received the CT-DBS treatment without T-maze test, which confirm the presence of CT-DBS-evoked LFP oscillation changes in **Supplementary Figure S1** and **Supplementary Table S1** (see **Supplementary Note S1**).

The experimental timeline is shown in **Figure 1**. The rats were allowed to recover for 7 days following implantation before the start of CT-DBS (or sham stimulation). Implanted rats in sham controls and DBS group performed a 30-min LFP recording twice, i.e., on the 8th and 16th day at 9:00–9:30 AM. The first LFP recording was used to establish a baseline before starting the T-maze behavioral task, whereas the second recording was used to evaluate the altered LFP oscillations and LFP–LFP coherence between the two brain regions with CT-DBS. From the 9th to 15th day, each rat in sham controls and DBS group was placed in a plastic cage for 30 min/day (9:00–9:30 AM) with/without CT-DBS, and then the rats performed the T-maze behavioral task (9:30–9:45 AM). Following the second LFP recording, rats in sham controls and DBS group were sacrificed for protein analysis by Western blotting on the 17th day. For only demonstration of the CT-DBS-evoked LFP oscillation changes in the DBS *wo.* T-maze group, all aspects of the experimental procedures were the same as described for sham controls and DBS group, except that the rats were excluded from T-maze behavioral testing and the Western blotting.

Animal Surgical Procedures for Neural Implantation

Surgeries were performed on both groups. The rats were anesthetized with intramuscular administration of 40 mg/kg zolazepam and tiletamine (Zoletil 50, Virbac, Corros, France) and 8 μg/kg dexmedetomidine hydrochloride (Dexdomitor®, Pfizer Inc., New York, NY, United States).

A 16-channel stainless microwire electrode array (product #M415050, 20-μm diameter, California Fine Wire Co., Grover Beach, CA, United States) was implanted into the bilateral CT [anterior/posterior (AP): −2.7 mm, medial/lateral (ML): ±1.6 mm, dorsal/ventral (DV): 5.5 mm], DG (AP: −4.0 mm, ML: ±2.0 mm, DV: 3.6 mm), CA1 (AP: −4.0 mm, ML: ±2.4 mm, DV: 1.9 mm), and CA3 (AP: −4.0 mm, ML: ±3.0 mm, DV: 1.9 mm), and each brain region contained two channels as shown in **Figure 2**. A stainless screw (BiFu Screw Parts Co., Ltd., Hsinchu, Taiwan) was secured to the skull over the cerebellum using dental cement (Coltene/Whaledent Inc., Cuyahoga Falls, OH, United States) as a reference electrode. After 7-day surgical recovery, the implanted rats received bilateral CT-DBS, LFP recordings were performed in the bilateral brain regions (CT, DG, CA3, and CA1), and the T-maze behavioral task was performed.

LFP Recordings and Data Analysis

Local field potentials were bilaterally recorded in the CT, DG, CA1, and CA3 to investigate changes in neural oscillations and FC using the Cerebus data acquisition system (Blackrock Microsystems LLC, Salt Lake, UT, United States). The sampling rate was 1 kHz, and the signal was bandpass analog filtered at cut-off frequencies of 0.3 and 250 Hz. Data analysis was post-processed with MATLAB (R2018b, MathWorks Inc., Natick, MA, United States). The comparison of LFP oscillations and coherence between the two groups were further performed.

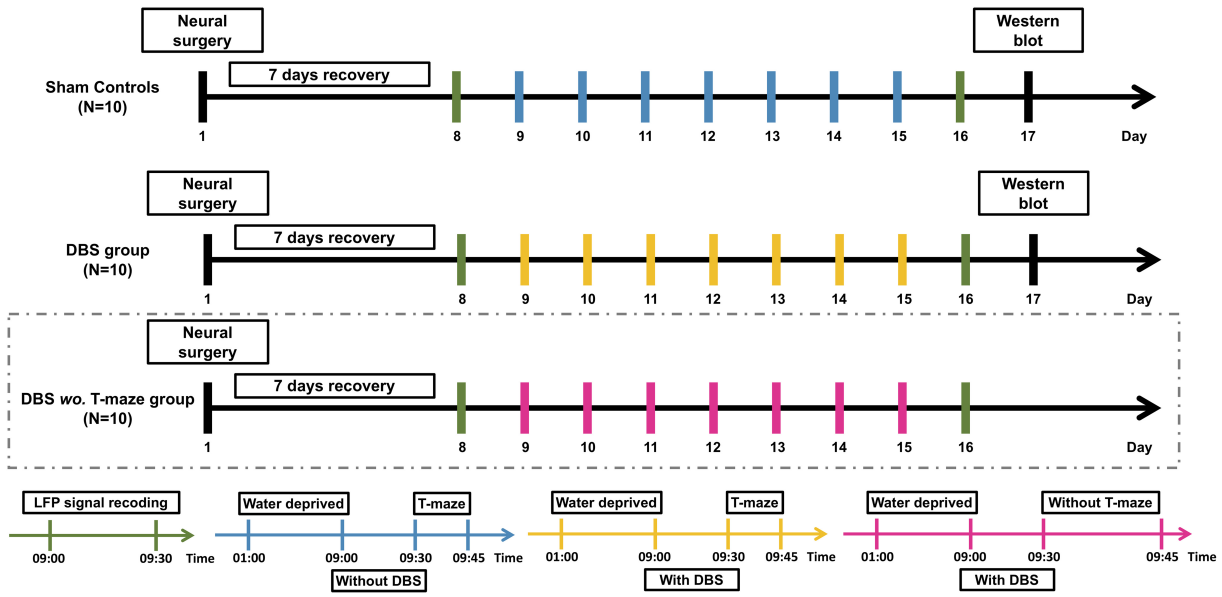

FIGURE 1 | Experimental procedure of CT-DBS evaluation. Thirty rats were divided into sham controls (*N* = 10), DBS group (*N* = 10), and DBS *wo.* T-maze group (*N* = 10). After a 7-day surgical recovery, implanted rats in sham controls and DBS group received CT-DBS (or sham stimulation) and underwent T-maze behavioral task training and LFP recording. For confirmation of CT-DBS-induced dynamic changes in LFP oscillatory activity in different hippocampal regions, to exclude confounding effects of T-maze behavioral training, we added a group of DBS *without* T-maze task (DBS *wo.* T-maze group, marked by dashed box). LFP recording (green bar): LFP recording was performed twice, i.e., on the 8th day for baseline and before Western blotting on the 16th day. Sham CT-DBS (blue bar): rats were placed in a plastic cage without 30-min CT-DBS and then trained for the T-maze behavioral task for 7 days. For CT-DBS (yellow bar): rats were placed in the same plastic cage with 30-min CT-DBS and then trained for the T-maze behavioral task for 7 days. Rats in sham controls and DBS group were sacrificed for protein level analysis by Western blotting on the 17th day (black bar).

Power spectral density (PSD) was calculated using the LFP data for delta (1–4 Hz), theta (4–7 Hz), alpha (7–13 Hz) and beta (13–20 Hz) bands using Welch's method (see **Supplementary Note S2**). Then, the PSD results for each frequency band were normalized using the following formula:

$$PSD\ \% = \frac{PSD^{post-treament}}{PSD^{baseline}} \times 100\% \quad (1)$$

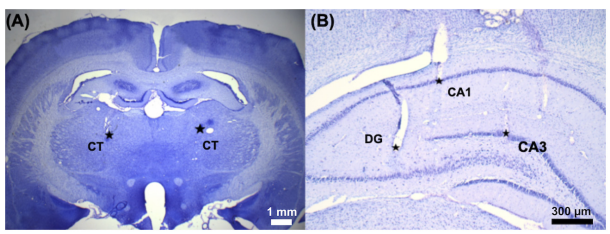

FIGURE 2 | The implantation sites of the microelectrode array was confirmed by Nissl staining. A 16-channel stainless microwire electrode array was used to perform CT-DBS and multi-site LFP recordings. **(A)** The representative coronal brain slice shows two small electrolytic lesions made around the tip of the electrode by passing 50 μA DC for 30 s in the bilateral CT (AP, −2.7 mm; ML, ±1.6 mm; and DV, 5.5 mm) marked with two star-symbols (*). **(B)** Three electrolytic lesions marked with three star-symbols (*): left hippocampal DG (AP, −4.0 mm; ML, −2.0 mm; and DV, 3.6 mm), CA1 (AP, −4.0 mm; ML, −2.4 mm; and DV, 1.9 mm), and CA3 (AP, −4.0 mm; ML, −3.0 mm; and DV, 1.9 mm).

where $PSD^{baseline}$ and $PSD^{post-treatment}$ were obtained from LFP PSD for each frequency band before (baseline) and after CT-DBS treatment or sham stimulation, respectively, in the CT, DG, CA1, and CA3.

To quantify the FC changes induced by CT-DBS, coherence (magnitude-squared coherence) was used to measure of linear association between two LFPs between two brain regions as a function of frequency as shown in the following equation:

$$Coh_{regionA,B}(f) = \frac{|PSD_{regionA,B}(f)|^2}{PSD_{regionA,A}(f) \times PSD_{regionB,B}(f)} \quad (2)$$

where $PSD_{regionA,A}(f)$ and $PSD_{regionB,B}(f)$ represent the averages of the spectral powers of the LFP time series of region A and region B, respectively. $PSD_{regionA,B}(f)$ is the average cross-spectral power. The magnitude-squared coherence values for the two brain regions were computed using Welch's method, a modified periodogram method. The magnitude-squared coherence estimate is a function of frequency with values ranging from 0 to 1, where a coherence of 0 indicates that the LFPs are unrelated and coherence of 1 indicates that the LFPs have a constant phase relationship. Data were analyzed offline using the custom-built MATLAB software (R2018b, MathWorks Inc., Natick, MA, United States). Magnitude-squared coherence measurement parameters include coherence frequency segment size (5,000 data points), Hanning window overlap (50%) and tapering, and sampling rate (1 kHz).

To compare the FC changes caused by CT-DBS, the measured FC between the distinct brain regions was normalized to the percentage coherence (*Coh*%), which was calculated using the post-treatment coherence by dividing the baseline coherence as shown in the following equation:

$$Coh_{(regionA-regionB)}\ \% = \frac{Coh^{post-treatment}_{(regionA-regionB)}}{Coh^{baseline}_{(regionA-regionB)}} \times 100\% \quad (3)$$

where $Coh^{baseline}_{(regionA-regionB)}$ and $Coh^{post-treatment}_{(regionA-regionB)}$ were the chosen coherences between the two brain regions before (baseline) and after CT-DBS (or sham stimulation), respectively.

Bilateral CT-DBS Protocol

The rats in the DBS group received 30-min bilateral CT-DBS in a plastic cage of 30-cm diameter and 38-cm height and were then trained for the T-maze behavioral task once a day for 7 days. Bipolar electrical stimulation with a pulse width of 25 μs/phase was administered to the bilateral CT using an isolated stimulator (Model 2100, A-M System Inc., Sequim, WA, United States). The intensity of the electrical stimulation was 250 μA at a frequency of 100 Hz. The sham controls were placed in the same plastic cage without CT-DBS for 30 min and then trained for the T-maze behavioral task once a day for 7 days.

T-Maze Behavioral Task

The T-maze was mainly prepared using polyvinyl chloride plastic. The maze comprised an approach alley (90 cm × 10 cm, height: 10 cm) and two goal arms (50 cm × 10 cm, height: 10 cm) covered with a T-shaped transparent polymethyl methacrylate sheet to prevent the rats from slipping off the maze. Animal movement was recorded with a video camera (NeuroMotive^{TM}, Blackrock Microsystems LLC, Salt Lake, UT, United States) positioned above the T-maze, and behavioral performance was analyzed by an open-source toolbox (Ben Shaul, 2017).

In this study, each rat underwent 5 trials daily in the T-maze behavioral tasks from the 9th to 15th day after 30-min CT-DBS or sham stimulation. Each trial was measured in 60 s, followed by a 30–90 s inter-trial interval for resting. The T-maze was wiped with alcohol between trials to remove any olfactory cues. For each trial, each rat was placed at the base of the T-maze and rewarded with water at one end of the goal arm. In this study, the water reward was always placed in the same goal arm. To evaluate the effects of CT-DBS on the behavioral performance in the T-maze behavioral task, the latency time to reach the water reward placed at the end of the goal arm and spatial working memory index (SWMI) (Bezu et al., 2017) was calculated:

$$SWMI\ (\%) = \frac{number\ of\ correct\ choices}{number\ of\ total\ trials} \times 100\% \quad (4)$$

Western Blotting

The DG, CA1, and CA3 were dissected from the brain tissues of the 10 study rats. Protein samples were extracted in ice-cold lysis buffer (50 mM Tris–HCl, pH = 7.5, 0.3 M sucrose, 0.5 mM EDTA, 2 mM sodium pyrophosphate, 1 mM sodium orthovanadate, 1 mM PMSF, 20 μg/mL leupeptin, and 4 μg/mL aprotinin) and then separated (30 μg) by SDS-PAGE. Gels were then transferred onto polyvinylidene difluoride membranes (Millipore, Billerica, MA, United States). The membranes were hybridized with the anti-dopamine D2 receptor (DRD2, 1:1000 dilution; ADR-002-50UL, Alomone Labs, Jerusalem, Israel) or anti-dopamine D1 receptor (DRD1, 1:1000 dilution; DR001AN03, Alomone Labs, Jerusalem, Israel) antibodies or anicotinic acetylcholine receptor alpha 4 (α4-nAChR, 1:1000 dilution; ANC-004-50UL, Alomone Labs, Jerusalem, Israel) antibodies. Next, the membranes were washed and incubated with HRP-conjugated goat anti-rabbit IgG antibody (1:1000 dilution; Jackson ImmunoResearch Inc., West Grove, PA, United States) and developed using the Luminata Forte Western HRP substrate (Millipore, Billerica, MA, United States). Images were recorded using a luminescence imaging system (LAS-4000, Fujifilm, Tokyo, Japan), and a gel analysis plug-in for the *ImageJ* software[1] (ver. 1.47, National Institutes of Health, Bethesda, MD, United States) was used to quantify the intensity of the protein bands.

Statistical Analysis

The normalized percentage of LFP PSD and FC analyses with the coherence between brain region pairs were compared before and after CT-DBS (or sham stimulation) by non-parametric statistical analysis, Wilcoxon signed-rank test, in each frequency band and FC for the two groups. In addition, the behavioral performances in terms of latency time and SWMI as well as protein expression levels of DRD1, DRD2, and α4-nAChR were analyzed by Wilcoxon two-sample *t*-test for comparing the differences between the two groups. A probability value of <0.05 was used as the criterion for determining statistical significance. All data are presented as the mean ± standard error of the mean (SEM). All statistical analyses mentioned above were performed using SPSS version 20.0 (SPSS Inc., Chicago, IL, United States) and their corresponding powers and effect sizes (Rosnow and Rosenthal, 1996; Rosnow et al., 2000) were determined using open source toolbox, G*Power (version 3, Institut fürExperimentelle Psychologie, Dusseldorf, Germany) (Cacioppo et al., 2007; Faul et al., 2007), and Cohen's *d* equation (Shavelson, 1988; Cohen, 1992), respectively. According to the results of power analyses and effect size test, sufficient statistical powers (>0.8) and medium to large effect sizes were shown in **Supplementary Tables S2–S5** (see **Supplementary Note S3**).

RESULTS

Behavioral Task Performance: Sham Controls vs. DBS Group

In the T-maze behavioral task, the rats were required to explore the routes for the water reward, and the behavioral performance indicators, i.e., latency time and SWMI, were analyzed to compare the CT-DBS effects on behavioral performance between the two groups. Latency time was significantly shorter to reach the criterion from the 13th to 15th day in the DBS group [13th

[1] http://imagej.nih.gov/ij/

day: 27.81 ± 0.29 s (**p = 0.00658), 14th day: 20.48 ± 0.23 s (***p = 0.00053), and 15th day: 13.54 ± 0.25 s (***p = 0.00075)] than that in the sham controls (13th day: 37.51 ± 0.47 s, 14th day: 29.26 ± 0.69 s, 15th day: 23.14 ± 0.21 s) as shown in **Figure 3A**. As shown in **Figure 3B**, the SWMI values were significantly higher from the 12th to 15th day in the DBS group [12th day: 66.72 ± 2.57% (***p = 0.00045), 13th day: 76.24 ± 0.65% (***p = 0.00057), 14th day: 87.87 ± 0.46% (***p = 0.00036), and 15th day: 97.56 ± 0.14% (***p = 0.00029)] than those in the sham controls (12th day: 54.33 ± 0.43%, 13th day: 67.91 ± 0.32%, 14th day: 77.50 ± 0.34%, and 15th day: 83.54 ± 0.21%).

Neural Oscillation: Before (Baseline) vs. After CT-DBS (or Sham Stimulation)

Neural oscillations in the studied brain regions after CT-DBS may be directly associated with the enhancement in T-maze behavioral task performance. To evaluate this further, LFPs were also recorded in the CT, CA1, CA3, and DG. The detailed PSD traces of the sham controls and DBS group are presented in **Supplementary Figure S2** (**Supplementary Note S2**). Furthermore, LFP oscillations were examined in the alpha, beta, delta, and theta bands. In **Figure 4A**, no significant differences were found in terms of the frequency bands of LFP oscillations in the four brain regions in the sham controls (sham stimulation) between before (baseline) and after the T-maze behavioral task (Wilcoxon signed-rank test). In the DBS group, there were significant increases in the LFP theta- and alpha-band oscillations in the CT [theta: 297.68 ± 15.58% (***p = 0.00034) and alpha: 213.79 ± 6.30% (***p = 0.00025)], DG [theta: 155.01 ± 15.85% (*p = 0.03572) and alpha: 174.20 ± 4.17% (***p = 0.00037)], CA1 [theta: 245.56 ± 5.89% (***p = 0.00041) and alpha: 229.59 ± 5.65% (***p = 0.00036)], and CA3 [theta: 264.50 ± 5.57% (***p = 0.00024) and alpha: 186.75 ± 13.59%, (**p = 0.00307)] following the T-maze behavioral task compared with the baseline values as shown in **Figure 4B**.

Brain Connectivity: Before (Baseline) vs. After CT-DBS (or Sham Stimulation)

To compare CT-DBS effects on brain connectivity between groups, LFP–LFP coherences between brain region pairs were used to perform FC analyses in the two groups. As shown in **Figure 5A**, the sham controls were not significantly different from the DBS group in terms of the theta- and alpha-band FC (Wilcoxon signed-rank test). As seen in **Figure 5B**, the DBS group showed significant increases in the theta-band FC strength for $Coh_{(CT-DG)}$[176.02 ± 8.03% (***p = 0.00048)], $Coh_{(CT-CA1)}$ [166.14 ± 5.19% (***p = 0.00078)], $Coh_{(CT-CA3)}$ [116.42 ± 4.10% (*p = 0.02407)], $Coh_{(DG-CA1)}$ [117.28 ± 4.27% (**p = 0.00792)], $Coh_{(DG-CA3)}$ [163.76 ± 6.37% (***p = 0.00038)], and $Coh_{(CA1-CA3)}$ [167.63 ± 2.12% (***p = 0.00054)] following the T-maze behavioral task. In addition, the alpha-band FC strength for $Coh_{(CT-DG)}$ [181.49 ± 5.12% (***p = 0.00057)], $Coh_{(CT-CA1)}$ [145.13 ± 6.10% (***p = 0.00042)], $Coh_{(CT-CA3)}$ [120.46 ± 7.05% (*p = 0.03104)], $Coh_{(DG-CA3)}$ [135.81 ± 8.54% (**p = 0.002537)] and $Coh_{(CA1-CA3)}$ [145.23 ± 4.76% (***p = 0.00067)] significantly increased in the DBS group. However, there were non-significant increases in the beta- and delta-band FC strengths in both groups as shown in **Supplementary Figure S3** (see **Supplementary Note S4**).

Western Blotting: Sham Controls vs. DBS Group

To confirm the CT-DBS-induced synaptic plasticity changes in the hippocampus, we evaluated the expressions of DRD1, DRD2, and α4-nAChR receptors in CA1, CA3 and DG, which are known to play key roles in synaptic plasticity. The results were calculated as the ratio of DRD1, DRD2 and α4-nAChR to

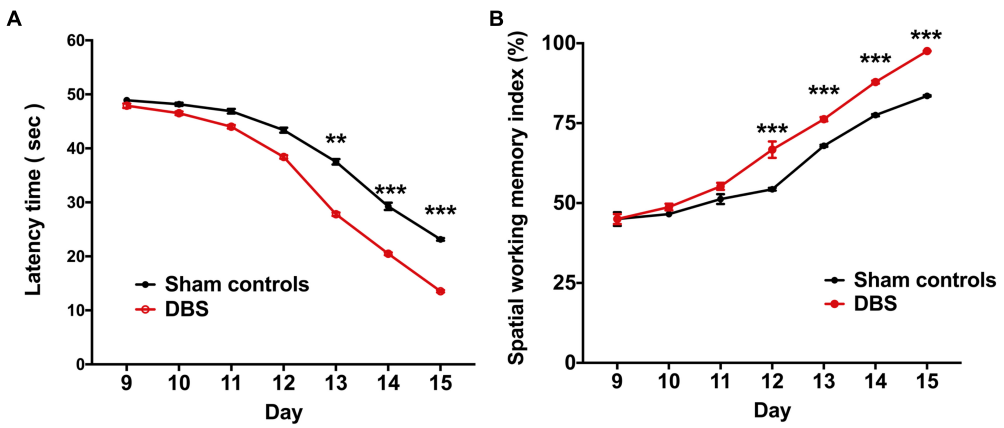

FIGURE 3 | Comparsion of behavioral performances in the T-maze behavioral task between the groups following CT-DBS (or sham stimulation). **(A)** Curves of latency time (s) to reach the correct T-maze goal arm was plotted against the sessions, i.e., one session/day and five trials/session. There were significantly shorter learning periods found in the DBS group from the 13th to 15th day compared with those in the sham controls during T-maze behavioral task training. **(B)** SWMI showed the percentage of the mean correct ratio to reach the correct T-maze goal arm against the sessions as **(A)**. SWMI also was found to significantly increase from the 12th to 15th day in the DBS group. **, and *** indicate significant differences in terms of latency time and SWMI with $p < 0.01$ and $p < 0.001$, respectively, analyzed by Wilcoxon two-sample t-tests (mean ± SEM).

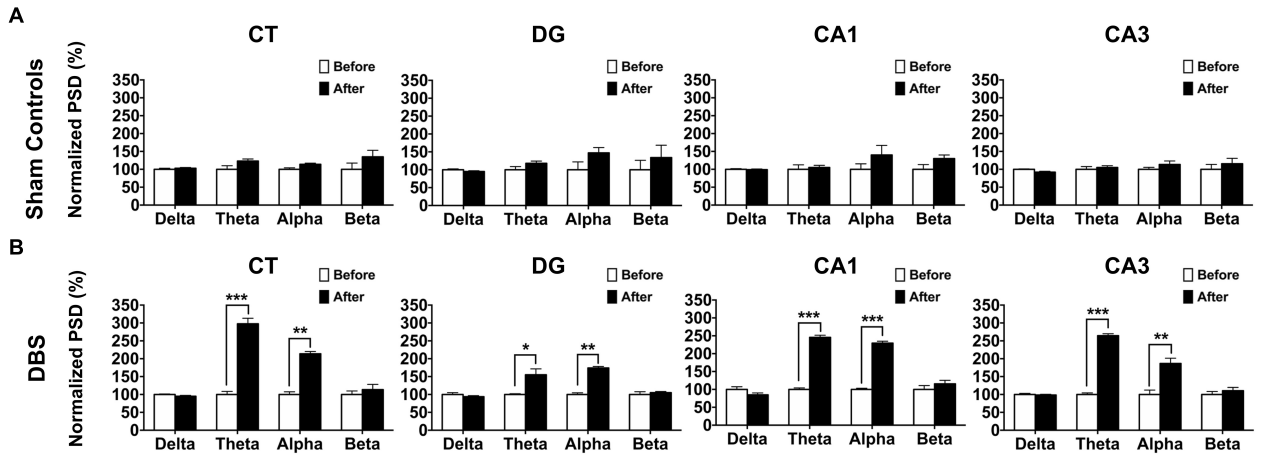

FIGURE 4 | Comparsion of LFP oscillatory changes before (baseline) and after CT-DBS (or sham stimulation) in both groups. The normalized percentage of the LFP PSD was calculated as the ratio of the original PSD before CT-DBS or sham stimulation (baseline) to that after CT-DBS or sham stimulation in the CT, DG, CA1, and CA3. **(A)** In the sham controls, there were no significant differences in terms of delta, theta, alpha and beta bands at each site. **(B)** In the DBS group, LFP PSD showed significant enhancements for the theta and alpha bands in the CT, DG, CA1, and CA3 following CT-DBS. *, **, and *** indicate significant differences in terms of PSD with $p < 0.05$, $p < 0.01$, and $p < 0.001$, respectively, analyzed by Wilcoxon signed-rank tests (mean ± SEM).

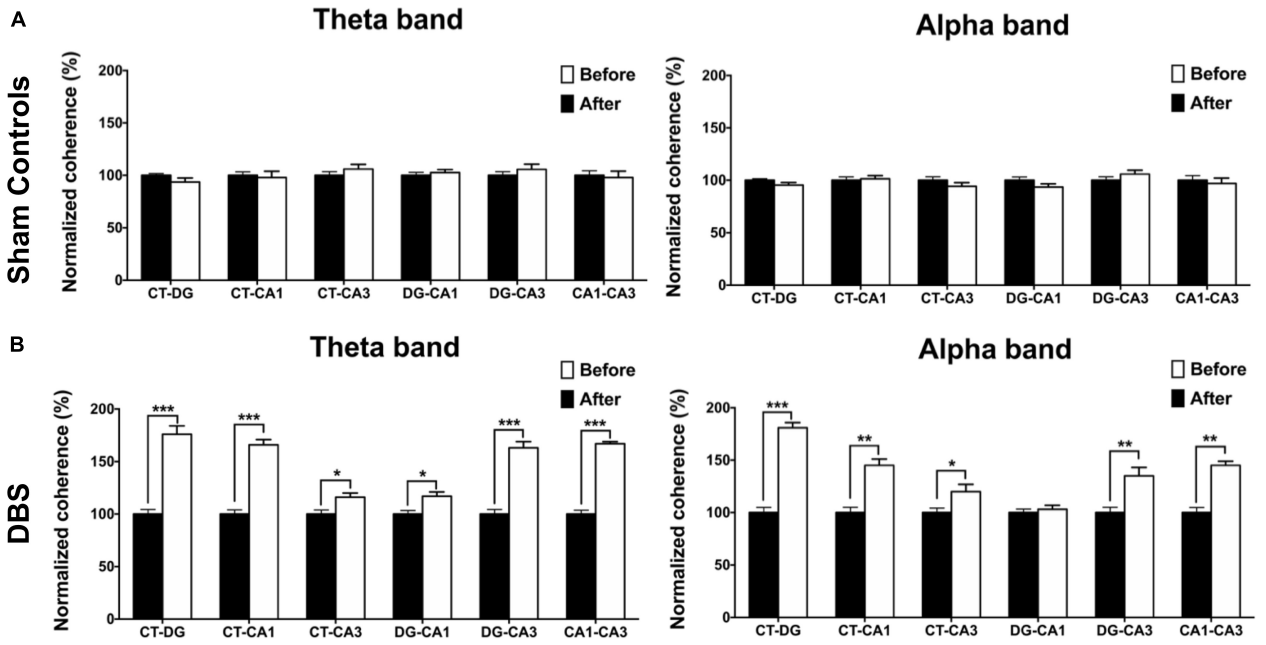

FIGURE 5 | Statistical comparison of FC changes before (baseline) and after CT-DBS (or sham stimulation). FC analyses were used to estimate the normalized coherence between the pairs of brain regions at LFP recording sites (CT, DG, CA1, and CA3) in the two group. **(A)** The strengths of theta- and alpha-band coherences in FC showed no significant differences before and after sham stimulation in the sham controls. **(B)** In DBS group, FC strengths between the brain region pairs CT–DG, CT–CA1, CT–CA3, DG–CA1, DG–CA3, and CA1–CA3 significantly increased with theta-band coherences following 7-day CT-DBS. Further, the FC strengths between the brain region pairs CT–DG, CT–CA1, CT–CA3, DG–CA3, and CA1–CA3 showed significant increases for alpha-band coherences following 7-day CT-DBS. *, **, and *** indicate significant differences in terms of coherence with $p < 0.05$, $p < 0.01$, and $p < 0.001$, respectively, relative to CT-DBS (baseline), analyzed by Wilcoxon signed-rank tests (mean ± SEM).

GAPDH. GAPDH levels were consistent across both groups. Our results demonstrated that significantly higher protein expressions of DRD1 and α4-nAChR and lower protein expression of DRD2 were associated with CT-DBS in the DBS group compared with those in sham controls in CA1, CA3, and DG (**Figure 6A**).

Statistical analyses further revealed that the normalized protein expression levels of DRD1 in CA1, CA3 and DG were significantly higher [CA1: 129.44 ± 10.03% (**p = 0.00683), CA3: 133.67 ± 11.45% (*p = 0.04702), DG: 138.55 ± 10.43% (*p = 0.02048)], α4-nAChR [CA1: 125.34 ± 8.59% (*p = 0.02607),

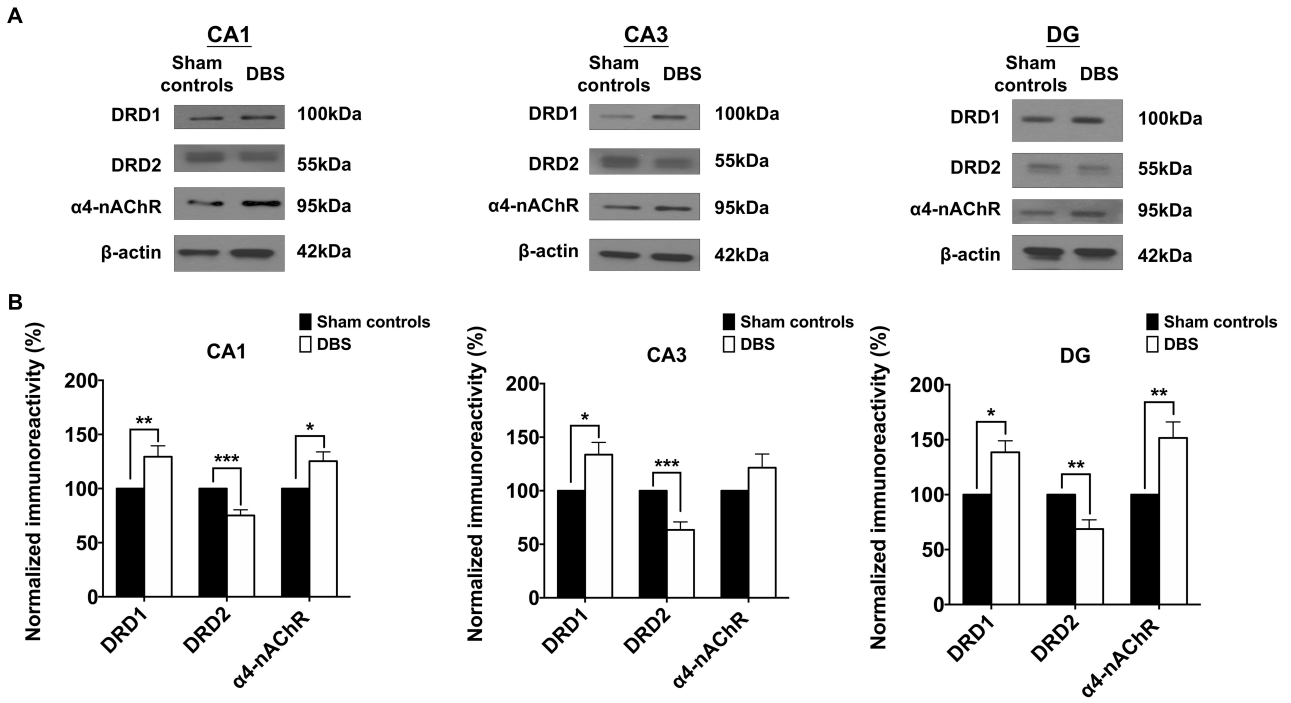

FIGURE 6 | Comparsion of the two groups based on Western blotting results of the protein expressions of the DRD1, DRD2, and α4-nAChR receptors in the CA1, CA3, and DG. **(A)** The protein expressions of the DRD1, DRD2, and α4-nAChR receptors in the CA1, CA3, and DG in both sham controls and DBS group. **(B)** The mean normalized protein expression levels of the DRD1, DRD2, and α4-nAChR receptors in the CA1, CA3, and DG in the two groups. The CA1, CA3, and DG in the DBS group show significant increases in the protein expression levels of the DRD1 receptor but significant decreases in the levels of the DRD2 receptor compared with those in the sham controls. The CA1 and DG in the DBS group exhibited significant increases in the protein expression levels of the α4-nAChR receptor compared with those in the sham controls. *, **, and *** indicated significant differences in terms of protein expression with $p < 0.05$, $p < 0.01$ and $p < 0.001$, respectively, relative to the sham controls, analyzed by Wilcoxon two-sample *t*-tests (mean ± SEM).

DG: 151.64 ± 114.52% (**p = 0.00760)] in the DBS group than in the sham controls (**Figure 6B**). Moreover, in the DBS group, CA1, CA3, and DG showed significantly lower protein expression levels of DRD2 [CA1: 75.15 ± 5.26% (***p = 0.00034), CA3: 63.42 ± 7.44% (***p = 0.00039), DG: 68.66 ± 8.42% (**p = 0.00435)] than in the sham controls. The results demonstrated the regulation of DRD1, DRD2, and α4-nAChR expression in the CA1, CA3, and DG with CT-DBS treatment.

DISCUSSION

CT-DBS Increased Theta Oscillations Associated With Spatial Working Memory as the Biomarker

In this study, CT-DBS enhanced both theta and alpha oscillations in the CT, CA1, CA3, and DG and improved T-maze behavioral task performance in a rat model related to spatial working memory. In a human study, hippocampal theta oscillation was related to spatial working memory or episodic memory (Klimesch et al., 1997). In humans, hippocampal alpha oscillations may be correlated to spatial working memory and likely with long-term memory engrams (Başar et al., 1999). However, in the majority of animal studies, the alpha band has been classified as a part of the theta band (Nerad and Bilkey, 2005).

In previous studies, hippocampal theta oscillation (4–13 Hz) has been shown to possibly modulate memory (Vertes, 2005; Suthana et al., 2012; Luo and Guan, 2018). In addition, hippocampal theta oscillation can be activated by sensory stimuli, which is related to spatial working memory (Givens, 1996). Other animal studies have also reported that DBS of the fornix and medial septal nucleus can improve spatial working memory and enhance hippocampal theta oscillations (Williams and Givens, 2003; Lee et al., 2012; Suthana and Fried, 2014). Thus, improvement in the performance of T-maze behavioral task by CT-DBS was characterized by increased hippocampal theta oscillation, which serve as a potential biomarker for enhancement of spatial working memory.

CT-DBS Enhanced FC Related to Neurotransmitter Receptors

Increased local theta rhythmic activity synchronized between each two regions of the trisynaptic circuit has indicated that excited projections functionally serve to couple CT and hippocampal connections (Everling et al., 2010; Reinhart and Nguyen, 2019). The FC between the CT and hippocampus consistent with previous studies, including the anatomical

mechanisms (Shirvalkar et al., 2006) and neural processing for the modulation of memory (Lee et al., 2017). We examined the synaptic neurotransmitter mechanisms underlying CT-DBS-induced FC changes and performance in the T-maze behavioral task. Our findings revealed increased expression of DRD1 by CT-DBS modulation but decreased expression of DRD2 in the CA1, CA3, and DG.

In rodents, the hippocampus has been extensively studied as one of the brain regions responsible for spatial memory and navigation. The first discovery of synaptic plasticity, known as long-term potentiation (LTP), occurred in the hippocampus, which consolidates the experience to memory (Bliss and Collingridge, 1993; Larkman and Jack, 1995). The trisynaptic circuit has generally been used to study LTP, including the connections from the DG to CA3 and CA3 to CA1 (Madison et al., 1991). In these synapses, dopamine may influence the induction of LTP through specific changes in the levels of cyclic adenosine monophosphate (cAMP), which is a critical regulator of LTP in the hippocampus (Jay, 2003). The activation of DRD2 as a presynaptic receptor serves to inhibit cAMP levels, which in turn inhibits the release of dopamine. DRD1, as a postsynaptic receptor, increases cAMP levels, which subsequently activates the release of dopamine (Nasehi et al., 2018). In addition, the α4-nAChR receptor in the nicotinic cholinergic system plays a role in attention and spatial working memory in the hippocampus, with activation of the α4-nAChR enhancing memory acquisition, consolidation, and information by increasing synaptic modification (Levin et al., 2006).

Increased dopamine and acetylcholine levels enhanced FC in the trisynaptic circuit. DBS may increase DRD1 and decrease DRD2 receptor expressions, contributing to increased activity of the dopamine synthesis enzyme and increasing dopamine neurotransmission in the hippocampus. Moreover, another study confirmed that increased release of acetylcholine enhances spatial working memory (Fadda et al., 1996). The application of CT-DBS contributed to the regulation of DRD1, DRD2 and α4-nAChR receptor expressions in the CA1, CA3 and DG, indicating that enhancement of performance in the T-maze behavioral task may be due to decreasing DRD2 activity and increasing DRD1and α4-nAChR activities. Thus, CT-DBS potentially modulates synaptic plasticity by altering the expression of dopaminergic and cholinergic receptors, resulting in the enhancement of FC in the trisynaptic circuit for spatial working memory.

CONCLUSION

In this study, CT-DBS revealed the enhancement of T-maze behavioral task performance, which was related to spatial working memory and elevated hippocampal theta oscillations. Meanwhile, CT-DBS promoted the FC between the CT and subregions (DG, CA3, and CA1) in the hippocampus due to neuroplasticity modulation (possibly due to altered expressions of the DRD1, DRD2, and α4-nAChR receptors). Therefore, our data may provide insights into the importance of CT-DBS in novel therapeutic approaches to improve memory.

DATA AVAILABILITY STATEMENT

The datasets generated for this study are available on request to the corresponding author.

ETHICS STATEMENT

The animal study was reviewed and approved by the Institutional Animal Care and Use Committee of Tzu Chi General Hospital (IACUC Approval No. 106-35).

AUTHOR CONTRIBUTIONS

C-WC, S-HL, S-YC, and Y-YC designed the project and organized the entire research. Y-CL, S-HY, and H-CL conceived the experiments. Y-CL, T-CL, S-JL, CH, VR, and C-HK conducted the experiments. C-WC, S-HY, T-CL, and S-JL analyzed the results. H-CL, Y-JC, Y-CC, and C-WL performed the immunohistochemistry and Western blot studies. C-WC, CH, S-HL, and Y-YC wrote the manuscript. All authors discussed the results and reviewed on the manuscript.

FUNDING

This work was financially supported by the Ministry of Science and Technology of Taiwan under contract numbers of MOST 108-2321-B-010-008-MY2, 108-2636-E-006-010, 107-2221-E-010-021-MY2, 107-2221-E-010-011, 107-2314-B-303-004, 107-2221-E-035-083-MY2, 107-2314-B-038-098-MY3, and 106-2314-B-038-021. We are grateful for support from Master Cheng Yen, President of the Tzu-Chi Foundation. This work was partially supported by the Buddhist Tzu Chi General Hospital Intramural Project (TCRD 107-29), and Buddhist Tzu Chi Medical Foundation (TCMF-MP 108-01-03).

SUPPLEMENTARY MATERIAL

The Supplementary Material for this article can be found online at: https://www.frontiersin.org/articles/10.3389/fnins.2019.01269/full#supplementary-material

REFERENCES

Başar, E., Başar-Eroğlu, C., Karakaş, S., and Schürmann, M. (1999). Are cognitive processes manifested in event-related gamma, alpha, theta and delta oscillations in the EEG? *Neurosci. Lett.* 259, 165–168. doi: 10.1016/S0304-3940(98)00934-3

Ben Shaul, Y. (2017). OptiMouse: a comprehensive open source program for reliable detection and analysis of mouse body and nose positions. *BMC Biol.* 15:41. doi: 10.1186/s12915-017-0377-3

Benabid, A. L. (2003). Deep brain stimulation for Parkinson's disease. *Curr. Opin. Neurobiol.* 13, 696–706. doi: 10.1016/j.conb.2003.11.001

Bezu, M., Maliković, J., Kristofova, M., Engidawork, E., Höger, H., Lubec, G., et al. (2017). Spatial working memory in male rats: pre-experience and task dependent roles of dopamine D1- and D2-like receptors. *Front. Behav. Neurosci.* 11:196. doi: 10.3389/fnbeh.2017.00196

Bick, S. K. B., and Eskandar, E. N. (2016). Neuromodulation for restoring memory. *Neurosurg. Focus* 40:E5. doi: 10.3171/2016.3.Focus162

Bliss, T. V. P., and Collingridge, G. L. (1993). A synaptic model of memory: long-term potentiation in the hippocampus. *Nature* 361, 31–39. doi: 10.1038/361031a0

Cacioppo, J. T., Tassinary, L. G., and Berntson, G. (2007). *Handbook of Psychophysiology*. Cambridge: Cambridge University Press.

Carlton, W. R. Y., and Murad, G. J. A. (2018). *Functional Neurosurgery for Sequelae of Traumatic Brain Injury*. Hershey, PA: Controversies in Severe Traumatic Brain Injury Management.

Cervera Ferri, A., Teruel Marti, V., Barcelo Molina, M., Martinez Ricos, J., Luque Garcia, A., Martinez Bellver, S., et al. (2016). Characterization of oscillatory changes in hippocampus and amygdala after deep brain stimulation of the infralimbic prefrontal cortex. *Physiol. Rep.* 4:e12854. doi: 10.14814/phy2.12854

Chiken, S., and Nambu, A. (2014). Disrupting neuronal transmission: mechanism of DBS? *Front. Syst. Neurosci.* 8:33. doi: 10.3389/fnsys.2014.00033

Cohen, J. (1992). A power primer. *Psychol. Bull.* 112, 155–159. doi: 10.1037/0033-2909.112.1.155

Colgin, L. L. (2013). Mechanisms and functions of theta rhythms. *Annu. Rev. Neurosci.* 36, 295–312. doi: 10.1146/annurev-neuro-062012-170330

de Hemptinne, C., Swann, N. C., Ostrem, J. L., Ryapolova-Webb, E. S., San Luciano, M., Galifianakis, N. B., et al. (2015). Therapeutic deep brain stimulation reduces cortical phase-amplitude coupling in Parkinson's disease. *Nat. Neurosci.* 18, 779–786. doi: 10.1038/nn.3997

Di Filippo, M., Tozzi, A., Costa, C., Belcastro, V., Tantucci, M., Picconi, B., et al. (2008). Plasticity and repair in the post-ischemic brain. *Neuropharmacology* 55, 353–362. doi: 10.1016/j.neuropharm.2008.01.012

Duncan, R. P., Van Dillen, L. R., Garbutt, J. M., Earhart, G. M., and Perlmutter, J. S. (2018). Physical therapy and deep brain stimulation in Parkinson's Disease: protocol for a pilot randomized controlled trial. *Pilot Feasibil. Stud.* 4:54. doi: 10.1186/s40814-018-0243-2

Edelmann, E., and Lessmann, V. (2018). Dopaminergic innervation and modulation of hippocampal networks. *Cell Tissue Res.* 373, 711–727. doi: 10.1007/s00441-018-2800-7

Everling, S., Leung, L. S., Vinck, M., and Womelsdorf, T. (2010). Selective theta-synchronization of choice-relevant information subserves goal-directed behavior. *Front. Human Neurosci.* 4:210. doi: 10.3389/fnhum.2010.00210

Fadda, F., Melis, F., and Stancampiano, R. (1996). Increased hippocampal acetylcholine release during a working memory task. *Eur. J. Pharmacol.* 307, R1–R2. doi: 10.1016/0014-2999(96)00289-0

Faul, F., Erdfelder, E., Lang, A.-G., and Buchner, A. (2007). G*Power 3: a flexible statistical power analysis program for the social, behavioral, and biomedical sciences. *Behav. Res. Methods* 39, 175–191. doi: 10.3758/bf03193146

Figee, M., de Koning, P., Klaassen, S., Vulink, N., Mantione, M., van den Munckhof, P., et al. (2014). Deep brain stimulation induces striatal dopamine release in obsessive-compulsive disorder. *Biol. Psychiatry* 75, 647–652. doi: 10.1016/j.biopsych.2013.06.021

Gilbert, P. E., Kesner, R. P., and Lee, I. (2001). Dissociating hippocampal subregions: double dissociation between dentate gyrus and CA1. *Hippocampus* 11, 626–636. doi: 10.1002/hipo.1077

Givens, B. (1996). Stimulus-evoked resetting of the dentate theta rhythm: relation to working memory. *Neuro. Rep.* 8, 159–163. doi: 10.1097/00001756-199612200-00032

Haam, J., and Yakel, J. L. (2017). Cholinergic modulation of the hippocampal region and memory function. *J. Neurochem.* 142(Suppl. 2), 111–121. doi: 10.1111/jnc.14052

Hao, S., Tang, B., Wu, Z., Ure, K., Sun, Y., Tao, H., et al. (2015). Forniceal deep brain stimulation rescues hippocampal memory in rett syndrome mice. *Nature* 526:430. doi: 10.1038/nature15694

Herrington, T. M., Cheng, J. J., and Eskandar, E. N. (2016). Mechanisms of deep brain stimulation. *J. Neurophysiol.* 115, 19–38. doi: 10.1152/jn.00281.2015

Jacobs, J., Miller, J., Lee, S. A., Coffey, T., Watrous, A. J., Sperling, M. R., et al. (2016). Direct electrical stimulation of the human entorhinal region and hippocampus impairs memory. *Neuron* 92, 983–990. doi: 10.1016/j.neuron.2016.10.062

Jay, T. M. (2003). Dopamine: a potential substrate for synaptic plasticity and memory mechanisms. *Prog. Neurobiol.* 69, 375–390. doi: 10.1016/s0301-0082(03)00085-6

Kesner, R. P. (2007). Behavioral functions of the CA3 subregion of the hippocampus. *Learn. Mem.* 14, 771–781. doi: 10.1101/lm.688207

Kesner, R. P., Lee, I., and Gilbert, P. (2004). A behavioral assessment of hippocampal function based on a subregional analysis. *Rev. Neurosci.* 15, 333–351.

Klimesch, W. (2012). alpha-band oscillations, attention, and controlled access to stored information. *Trends Cogn. Sci.* 16, 606–617. doi: 10.1016/j.tics.2012.10.007

Klimesch, W., Doppelmayr, M., Pachinger, T., and Ripper, B. (1997). Brain oscillations and human memory: EEG correlates in the upper alpha and theta band. *Neurosci. Lett.* 238, 9–12. doi: 10.1016/S0304-3940(97)00771-4

Kuhn, A. A., and Volkmann, J. (2017). Innovations in deep brain stimulation methodology. *Mov. Disord.* 32, 11–19. doi: 10.1002/mds.26703

Larkman, A. U., and Jack, J. J. B. (1995). Synaptic plasticity: hippocampal LTP. *Curr. Opin. Neurobiol.* 5, 324–334. doi: 10.1016/0959-4388(95)80045-X

Lee, D. J., Gurkoff, G. G., Izadi, A., Berman, R. F., Ekstrom, A. D., Muizelaar, J. P., et al. (2012). Medial septal nucleus theta frequency deep brain stimulation improves spatial working memory after traumatic brain injury. *J. Neuro.* 30, 131–139. doi: 10.1089/neu.2012.2646

Lee, S. H., Huh, N. J., Lee, J. W., Ghim, J. W., Lee, I., and Jung, M. W. (2017). Neural signals related to outcome evaluation are stronger in CA1 than CA3. *Front. Neural Circ.* 11:40. doi: 10.3389/fncir.2017.00040

Levin, E. D., McClernon, F. J., and Rezvani, A. H. (2006). Nicotinic effects on cognitive function: behavioral characterization, pharmacological specification, and anatomic localization. *Psychopharmacology* 184, 523–539. doi: 10.1007/s00213-005-0164-7

Li, S., Cullen, W. K., Anwyl, R., and Rowan, M. J. (2003). Dopamine-dependent facilitation of LTP induction in hippocampal CA1 by exposure to spatial novelty. *Nat. Neurosci.* 6, 526–531. doi: 10.1038/nn1049

Lin, H. C., Pan, H. C., Lin, S. H., Lo, Y. C., Shen, E. T., Liao, L. D., et al. (2015). Central thalamic deep-brain stimulation alters striatal-thalamic connectivity in cognitive neural behavior. *Front. Neural Circ.* 9:87. doi: 10.3389/fncir.2015.00087

Lopez, J., Wolff, M., Lecourtier, L., Cosquer, B., Bontempi, B., Dalrymple-Alford, J., et al. (2009). The intralaminar thalamic nuclei contribute to remote spatial memory. *J. Neurosci.* 29, 3302–3306. doi: 10.1523/JNEUROSCI.5576-08.2009

Luo, W. H., and Guan, J. S. (2018). Do brain oscillations orchestrate memory? *Brain Sci. Adv.* 4, 16–33. doi: 10.26599/bsa.2018.9050008

Madison, D. V., Malenka, R. C., and Nicoll, R. A. (1991). Mechanisms underlying long-term potentiation of synaptic transmission. *Annu. Rev. Neurosci.* 14, 379–397. doi: 10.1146/annurev.ne.14.030191.002115

Mair, R. G., and Hembrook, J. R. (2008). Memory enhancement with event-related stimulation of the rostral intralaminar thalamic nuclei. *J. Neurosci.* 28, 14293–14300. doi: 10.1523/JNEUROSCI.3301-08.2008

Mair, R. G., Onos, K. D., and Hembrook, J. R. (2011). Cognitive activation by central thalamic stimulation: the yerkes-dodson law revisited. *Dose Response J.* 9, 313–331. doi: 10.2203/dose-response.10-017.Mair

Maling, N., Hashemiyoon, R., Foote, K. D., Okun, M. S., and Sanchez, J. C. (2012). Increased thalamic gamma band activity correlates with symptom relief following deep brain stimulation in humans with tourette's syndrome. *PLoS One* 7:e44215. doi: 10.1371/journal.pone.0044215

Matsuyama, S., Matsumoto, A., Enomoto, T., and Nishizaki, T. (2000). Activation of nicotinic acetylcholine receptors induces long-term potentiation *in vivo* in the intact mouse dentate gyrus. *Eur. J. Neurosci.* 12, 3741–3747. doi: 10.1046/j.1460-9568.2000.00259.x

Maurer, S. V., and Williams, C. L. (2017). The cholinergic system modulates memory and hippocampal plasticity via its interactions with non-neuronal cells. *Front. Immunol.* 8:1489–1489. doi: 10.3389/fimmu.2017.01489

Mizumori, S. J. Y., Miya, D. Y., and Ward, K. E. (1994). Reversible inactivation of the lateral dorsal thalamus disrupts hippocampal place representation and impairs spatial learning. *Brain Res.* 644, 168–174. doi: 10.1016/0006-8993(94)90361-1

Nasehi, M., Hasanvand, S., Khakpai, F., and Zarrindast, M. R. (2018). The effect of CA1 dopaminergic system on amnesia induced by harmane in mice. *Acta Neuro. Belgica.* 119, 369–377. doi: 10.1007/s13760-018-0926-8

Nerad, L., and Bilkey, D. K. (2005). Ten- to 12-Hz EEG oscillation in the rat hippocampus and rhinal cortex that is modulated by environmental familiarity. *J. Neurophysiol.* 93, 1246–1254. doi: 10.1152/jn.00199.2004

Park, H. R., Kim, I. H., Kang, H., Lee, D. S., Kim, B.-N., Kim, D. G., et al. (2016). Nucleus accumbens deep brain stimulation for a patient with self-injurious behavior and autism spectrum disorder: functional and structural changes of the brain: report of a case and review of literature. *Acta Neurochir.* 159, 137–143. doi: 10.1007/s00701-016-3002-2

Posporelis, S., David, A. S., Ashkan, K., and Shotbolt, P. (2018). Deep brain stimulation of the memory circuit: improving cognition in Alzheimer's disease. *J. Alzheimers Dis.* 64, 337–347. doi: 10.3233/jad-180212

Reinhart, R. M. G., and Nguyen, J. A. (2019). Working memory revived in older adults by synchronizing rhythmic brain circuits. *Nat. Neurosci.* 22, 820–827. doi: 10.1038/s41593-019-0371-x

Rosnow, R. L., and Rosenthal, R. (1996). Computing contrasts, effect sizes, and counternulls on other people's published data: general procedures for research consumers. *Psychol. Methods* 1:331. doi: 10.1037//1082-989x.1.4.331

Rosnow, R. L., Rosenthal, R., and Rubin, D. B. (2000). Contrasts and correlations in effect-size estimation. *Psychol. Sci.* 11, 446–453. doi: 10.1111/1467-9280.00287

Saalmann, Y. B. (2014). Intralaminar and medial thalamic influence on cortical synchrony, information transmission and cognition. *Front. Syst. Neurosci.* 8:83. doi: 10.3389/fnsys.2014.00083

Schiff, N. D. (2016). Central thalamic deep brain stimulation to support anterior forebrain mesocircuit function in the severely injured brain. *J. Neural. Transm.* 123, 797–806. doi: 10.1007/s00702-016-1547-0

Shah, S. A., and Schiff, N. D. (2010). Central thalamic deep brain stimulation for cognitive neuromodulation - a review of proposed mechanisms and investigational studies. *Eur. J. Neurosci.* 32, 1135–1144. doi: 10.1111/j.1460-9568.2010.07420.x

Shavelson, R. J. (1988). *Statistical Reasoning for the Behavioral Sciences*. Hoboken, NJ: Wiley.

Shirvalkar, P., Seth, M., Schiff, N. D., and Herrera, D. G. (2006). Cognitive enhancement with central thalamic electrical stimulation. *Proc. Natl. Acad. Sci. U.S.A.* 103, 17007–17012. doi: 10.1073/pnas.0604811103

Stefani, A., Grandi, L. C., and Galati, S. (2018). Deep brain stimulation of the pedunculopontine nucleus modulates subthalamic pathological oscillations. *Neurobiol. Dis.* 233, 233–242. doi: 10.1016/j.nbd.2018.11.006

Suthana, N., and Fried, I. (2014). Deep brain stimulation for enhancement of learning and memory. *Neuroimage* 85(Pt 3), 996–1002. doi: 10.1016/j.neuroimage.2013.07.066

Suthana, N., Haneef, Z., Stern, J., Mukamel, R., Behnke, E., Knowlton, B., et al. (2012). Memory enhancement and deep-brain stimulation of the entorhinal area. *New Engl. J. Med.* 366, 502–510. doi: 10.1056/NEJMoa1107212

Tabansky, I., Quinkert, A. W., Rahman, N., Muller, S. Z., Lofgren, J., Rudling, J., et al. (2014). Temporally-patterned deep brain stimulation in a mouse model of multiple traumatic brain injury. *Behav. Brain Res.* 273, 123–132. doi: 10.1016/j.bbr.2014.07.026

Temel, Y., Kocabicak, E., Hoellig, A., Falkenburger, B., and Tan, S. (2015). Current perspectives on deep brain stimulation for severe neurological and psychiatric disorders. *Neuropsychiatr. Dis. Treat.* 11, 1051–1066. doi: 10.2147/ndt.S46583

Thevathasan, W., Pogosyan, A., Hyam, J. A., Jenkinson, N., Foltynie, T., Limousin, P., et al. (2012). Alpha oscillations in the pedunculopontine nucleus correlate with gait performance in parkinsonism. *Brain* 135, 148–160. doi: 10.1093/brain/awr315

Tsai, S. T., Chen, L. J., Wang, Y. J., Chen, S. Y., and Tseng, G. F. (2016). Rostral intralaminar thalamic deep brain stimulation triggered cortical and hippocampal structural plasticity and enhanced spatial memory. *Stereotactic Funct. Neurosurg.* 94, 108–117. doi: 10.1159/000444759

Vertes, R. P. (2005). Hippocampal theta rhythm: a tag for short-term memory. *Hippocampus* 15, 923–935. doi: 10.1002/hipo.20118

Wang, C. F., Yang, S. H., Lin, S. H., Chen, P. C., Lo, Y. C., Pan, H. C., et al. (2017). A proof-of-principle simulation for closed-loop control based on preexisting experimental thalamic DBS-enhanced instrumental learning. *Brain Stimulat.* 10, 672–683. doi: 10.1016/j.brs.2017.02.004

Widge, A. S., Zorowitz, S., Basu, I., Paulk, A. C., Cash, S. S., Eskandar, E. N., et al. (2019). Deep brain stimulation of the internal capsule enhances human cognitive control and prefrontal cortex function. *Nat. Commun.* 10:1536. doi: 10.1038/s41467-019-09557-4

Williams, J. M., and Givens, B. (2003). Stimulation-induced reset of hippocampal theta in the freely performing rat. *Hippocampus* 13, 109–116. doi: 10.1002/hipo.10082

Yeckel, M. F., and Berger, T. W. (1990). Feedforward excitation of the hippocampus by afferents from the entorhinal cortex: redefinition of the role of the trisynaptic pathway. *Proc. Natl. Acad. Sci. U.S.A.* 87:5832. doi: 10.1073/pnas.87.15.5832

Conflict of Interest: The authors declare that the research was conducted in the absence of any commercial or financial relationships that could be construed as a potential conflict of interest.

frontiers in Neuroscience

HYPOTHESIS AND THEORY
published: 13 December 2019
doi: 10.3389/fnins.2019.01346

Explainable Artificial Intelligence for Neuroscience: Behavioral Neurostimulation

*Jean-Marc Fellous[1,2], Guillermo Sapiro[3], Andrew Rossi[4], Helen Mayberg[5] and Michele Ferrante[1,6]**

[1] Theoretical and Computational Neuroscience Program, National Institute of Mental Health, National Institutes of Health, Bethesda, MD, United States, [2] Department of Psychology and Biomedical Engineering, University of Arizona, Tucson, AZ, United States, [3] Department of Electrical and Computer Engineering, Duke University, Durham, NC, United States, [4] Executive Functions and Reward Systems Program, National Institute of Mental Health, National Institutes of Health, Bethesda, MD, United States, [5] Center for Advanced Circuit Therapeutics, Icahn School of Medicine at Mount Sinai, New York, NY, United States, [6] Computational Psychiatry Program, National Institute of Mental Health, National Institutes of Health, Bethesda, MD, United States

The use of Artificial Intelligence and machine learning in basic research and clinical neuroscience is increasing. AI methods enable the interpretation of large multimodal datasets that can provide unbiased insights into the fundamental principles of brain function, potentially paving the way for earlier and more accurate detection of brain disorders and better informed intervention protocols. Despite AI's ability to create accurate predictions and classifications, in most cases it lacks the ability to provide a mechanistic understanding of how inputs and outputs relate to each other. Explainable Artificial Intelligence (XAI) is a new set of techniques that attempts to provide such an understanding, here we report on some of these practical approaches. We discuss the potential value of XAI to the field of neurostimulation for both basic scientific inquiry and therapeutic purposes, as well as, outstanding questions and obstacles to the success of the XAI approach.

Keywords: explain AI, closed-loop neurostimulation, computational psychiatry, behavioral paradigms, machine learning, neuro-behavioral decisions systems, data-driven discoveries of brain circuit theories

OPEN ACCESS

Edited by:
Giovanni Mirabella, University of Brescia, Italy

Reviewed by:
Vassiliy Tsytsarev, University of Maryland, College Park, United States
Andrea Brovelli, Centre National de la Recherche Scientifique (CNRS), France

***Correspondence:**
Michele Ferrante
ferrantem@nih.gov

Specialty section:
This article was submitted to Neural Technology, a section of the journal Frontiers in Neuroscience

Received: *11 August 2019*
Accepted: *29 November 2019*
Published: *13 December 2019*

Citation:
Fellous J-M, Sapiro G, Rossi A, Mayberg H and Ferrante M (2019) Explainable Artificial Intelligence for Neuroscience: Behavioral Neurostimulation. Front. Neurosci. 13:1346. doi: 10.3389/fnins.2019.01346

INTRODUCTION

One of the greatest challenges to effective brain-based therapies is our inability to monitor and modulate neural activity in real time. Moving beyond the relatively simple open-loop neurostimulation devices that are currently the standard in clinical practice (e.g., epilepsy) requires a closed-loop approach in which the therapeutic application of neurostimulation is determined by characterizing the moment-to-moment state of the brain (Herron et al., 2017). However, there remain major obstacles to progress for such a closed-loop approach. For one, we do not know how to objectively characterize mental states or even detect pathological activity associated with most psychiatric disorders. Second, we do not know the most effective way to improve maladaptive

Abbreviations: AI, Artificial Intelligence; ADHD, Attention Deficit and Hyperactivity Disorder; ANN, artificial neural networks; BMI, brain machine interface; CNN, convolutional neural networks; DBS, deep brain stimulation; ECoG, electro corticogram; EEG, electro encephalogram; FDA, Food and Drug Administration; fMRI, functional magnetic resonance imaging; MDD, major depression disorder; ML, machine learning; MVPA, multi variate pattern analysis; OCD, obsessive compulsive disorder; PD, Parkinson's disease; RDoC, Research Domain Criteria; SR, slow release; SVM, support vector machine; t-SNE, t-Stochastic Neighbor Embedding; UMAP, Uniform Manifold Approximation and Projection; XAI, Explainable Artificial Intelligence.

behaviors by means of neurostimulation. The solutions to these problems require innovative experimental frameworks leveraging intelligent computational approaches able to sense, interpret, and modulate large amount of data from behaviorally relevant neural circuits at the speed of thoughts. New approaches such as computational psychiatry (Redish and Gordon, 2016; Ferrante et al., 2019) or ML are emerging. However, current ML approaches that are applied to neural data typically do not provide an understanding of the underlying neural processes or how they contributed to the outcome (i.e., prediction or classifier). For example, significant progress has been made using ML to effectively classify EEG patterns, but the understanding of brain function and mechanisms derived from such approaches still remain relatively limited (Craik et al., 2019). Such an understanding, be it correlational or causal, is key to improving ML methods and to suggesting new therapeutic targets or protocols using different techniques. Explainable Artificial Intelligence (XAI) is a relatively new set of techniques that combines sophisticated AI and ML algorithms with effective explanatory techniques to develop explainable solutions that have proven useful in many domain areas (Core et al., 2006; Samek et al., 2017; Yang and Shafto, 2017; Adadi and Berrada, 2018; Choo and Liu, 2018; Dosilovic et al., 2018; Holzinger et al., 2018; Fernandez et al., 2019; Miller, 2019). Recent work has suggested that XAI may be a promising avenue to guide basic neural circuit manipulations and clinical interventions (Holzinger et al., 2017b; Vu et al., 2018; Langlotz et al., 2019). We will develop this idea further here.

Explainable Artificial Intelligence for neurostimulation in mental health can be seen as an extension in the design of BMI. BMI are generally understood as combinations of hardware and software systems designed to rapidly transfer information between one or more brain area and an external device (Wolpaw et al., 2002; Hatsopoulos and Donoghue, 2009; Nicolelis and Lebedev, 2009; Andersen et al., 2010; Mirabella and Lebedev, 2017). While there is a long history of research in the decoding, analyses and production of neural signal in non-human primates and rodents, a lot of progress has recently been made to develop these techniques for the human brain both invasively and non-invasively, unidirectionally or bi-directionally (Craik et al., 2019; Martini et al., 2019; Rao, 2019). Motor decision making for example, has been shown to involve a network of brain areas, before and during movement execution (Mirabella, 2014; Hampshire and Sharp, 2015), so that BMI intervention can inhibit movement up to 200 ms after its initiation (Schultze-Kraft et al., 2016; Mirabella and Lebedev, 2017). The advantage of this type of motor-decision BMI is that it is not bound to elementary motor commands (e.g., turn the wheel of a car), but rather to the high-level decision to initiate and complete a movement. That decision can potentially be affected by environmental factors (e.g., AI vision system detecting cars on the neighboring lane) and internal state (e.g., AI system assessing the state of fatigue of the driver). The current consensus is that response inhibition is an emergent property of a network of discrete brain areas that include the right inferior frontal gyrus and that leverage basic widespread elementary neural circuits such a local-lateral-inhibition (Hampshire and Sharp, 2015; Mirabella and Lebedev, 2017). This gyrus, as with many other cortical structures, is dynamically recruited so that individual neurons may code for drastically different aspects of the behavior, depending of the task at hand. Consequently, designing a BMI targeting such an area requires the ability for the system to rapidly switch its decoding and stimulation paradigms as a function of environmental or internal state information. Such online adaptability needs of course to be learned and personalized to each individual patient, a task that is ideally suited for AI/ML approaches. In the sensory domain, some have shown that BMI can be used to generate actionable entirely artificial tactile sensations to trigger complex motor decisions (O'Doherty et al., 2012; Klaes et al., 2014; Flesher et al., 2017). Most of the BMI research work has, however, focused on the sensory motor system because of the relatively focused and well-defined nature of the neural circuits. Consequently, most of the clinical applications are focused on neurological disorders. Interestingly, new generations of BMIs are emerging that are focused on more cognitive functions such as detecting and manipulating reward expectations using reinforcement learning paradigms (Mahmoudi and Sanchez, 2011; Marsh et al., 2015; Ramkumar et al., 2016), memory enhancement (Deadwyler et al., 2017) or collective problem solving using multi-brain interfacing in rats (Pais-Vieira et al., 2015) or humans (Jiang et al., 2019). All these applications can potentially benefit from the adaptive properties of AI/ML algorithms and, as mentioned, explainable AI approaches have the promise of yielding basic mechanistic insights about the neural systems being targeted. However, the use of these approaches in the context of psychiatric or neurodevelopmental disorders has not been realized though their potential is clear.

In computational neuroscience and computational psychiatry there is a contrast between theory-driven (e.g., reinforcement learning, biophysically inspired network models) and data-driven models (e.g., deep-learning or ensemble methods). While the former models are highly explainable in terms of biological mechanisms, the latter are high performing in terms of predictive accuracy. In general, high performing methods tend to be the least explainable, while explainable methods tend to be the least accurate. Mathematically, the relationship between the two is still not fully formalized or understood. These are the type of issues that occupy the ML community beyond neuroscience and neurostimulation. XAI models in neuroscience might be created by combining theory- and data-driven models. This combination could be achieved by associating explanatory semantic information with features of the model; by using simpler models that are easier to explain; by using richer models that contain more explanatory content; or by building approximate models, solely for the purpose of explanation.

Current efforts in this area include: (1) identify how explainable learning solutions can be applied to neuroscience and neuropsychiatric datasets for neurostimulation, (2) foster the development of a community of scholars working in the field of explainable learning applied to basic neuroscience and clinical neuropsychiatry, and (3) stimulate an open exchange of data and theories between investigators in this nascent field. To frame the scope of this article, we lay out some of the major key open questions in fundamental and clinical neuroscience

research that can potentially be addressed by a combination of XAI and neurostimulation approaches. To stimulate the development of XAI approaches the National Institute of Mental Health (NIMH) has released a funding opportunity to apply XAI approaches for decoding and modulating neural circuit activity linked to behavior[1].

INTELLIGENT DECODING AND MODULATION OF BEHAVIORALLY ACTIVATED BRAIN CIRCUITS

A variety of perspectives for how ML and, more generally AI could contribute to closed-loop brain circuit interventions are worth investigating (Rao, 2019). From a purely signal processing stand point, an XAI system can be an active stimulation artifact rejection component (Zhou et al., 2018). In parallel, the XAI system should have the ability to discover – in a data-driven manner – neuro-behavioral markers of the computational process or condition under consideration. Remarkable efforts are currently underway to derive biomarkers for mental health, as is the case for example for depression (Waters and Mayberg, 2017). Once these biomarkers are detected, and the artifacts rejected, the XAI system can generate complex feedback stimulation patterns designed and monitored (human in-the loop) to improve behavioral or cognitive performance (**Figure 1**). XAI approaches have also the potential to address outstanding biological and theoretical questions in neuroscience, as well as to address clinical applications. They seem well-suited for extracting actionable information from highly complex neural systems, moving away from traditional correlational analyses and toward a causal understanding of network activity (Yang et al., 2018). However, even with XAI approaches, one should not assume that understanding the statistical causality of neural interactions is equivalent to understanding behavior; a highly sophisticated knowledge of neural activity and neural connectivity is not generally synonymous with understanding their role in causing behavior.

Fundamental neuroscientific questions that XAI could address

- What are the biological mechanisms of memory storage and retrieval?
- What is the neural code and how is information transmitted between brain areas?
- What is the relationship between patterns of activity and behavior?
- Are there emergent properties of networks which are necessary for behavior?
- What are the relevant temporal and spatial scales necessary for decoding and modulating a given behavior?
- How should models account for the relationship between neurostimulation and physiological response, especially when that transfer function changes over time?

[1]https://grants.nih.gov/grants/guide/pa-files/PAR-19-344.html

Potential applications of XAI in computational psychiatry

- Real time, closed-loop stimulation for DBS: ML algorithms could be trained to identify electrophysiological patterns that correspond to pathological states and apply patterned DBS to achieve a normative state.
- Development of inexpensive computerized assessments for diagnosing or characterizing prodromal risk for neuropsychiatric conditions such as psychosis, depression, PTSD, ADHD or autism.
- Personalized medicine approach: XAI could provide automated identification of sub-clusters of patients through analysis of multimodal data (e.g., imaging, behavioral) to enable individualized interventions and forecasting.
- Identifying clinical diagnostic groups; discovering individualized biomarkers for treatment selection; tracking and quantifying treatment response over time.

Requirements to apply XAI approaches to neural circuit modulation

- Analytic modeling of behavior to define precision targets for ML.
- Statistically robust brain metrics to dimensionally differentiate along the normative-to-aberrant continuum of activity.
- Methods for discovering potential causal relationships between neurons and between neural activity and behavior using large data sets.
- The inclusion of both central and peripheral nervous system dynamics (e.g., Vagal nerve stimulation or closed loop control of visceral organ systems).
- Linking of analytical models: For example, classification/brain-decoding models (SVM/MVPA) to theoretically-driven, encoding models or biological multiscale modeling.
- Technology required to determine the level of resolution (e.g., number of neurons) associated with a specific behavior. Technology required to monitor populations of cells across several brain regions chronically and simultaneously, while decoding the relevant biomarkers and delivering a modifying signal in real time.

Beyond closed-loop neuro-behavioral modulation, unanswered questions relevant to the theoretical and practical applications of XAI:

- How much data is needed to build/train an accurate and generalizable model?
- Can we build robust models to predict cognition for every possible describable cognitive function? For each cognitive function, can we build an effective neurostimulation strategy? If such models behave as predicted, how do we test their combinatorial properties? How to include the known multidimensional aspects of complex neuropsychiatric disorders into these emerging models. Will combinatorial models follow single behavior models? Will such models predict behaviors reliably trans-diagnostically?

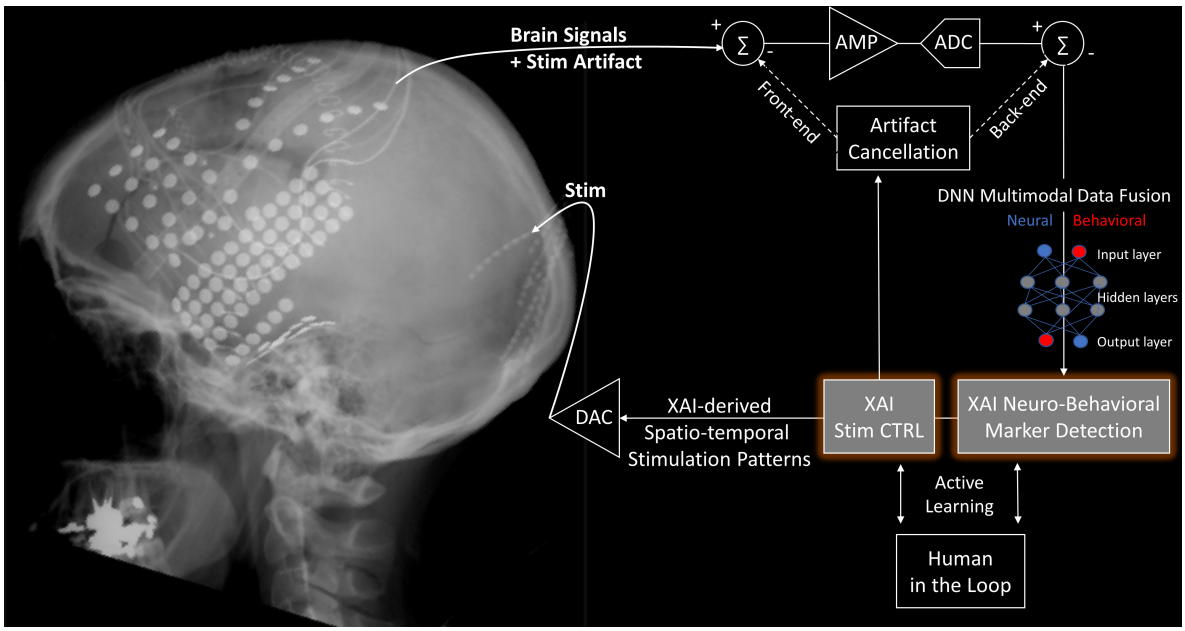

FIGURE 1 | An XAI-enabled closed-loop neurostimulation process can be described in four phases: (1) System-level recording of brain signals (e.g., spikes, LFPs, ECoG, EEG, neuromodulators, optical voltage/calcium indicators), (2) Multimodal fusion of neural data and dense behavioral/cognitive assessment measures. (3) XAI algorithm using unbiasedly discovered biomarkers to provide mechanistic explanations on how to improve behavioral/cognitive performance and reject stimulation artifacts. (4) Complex XAI-derived spatio-temporal brain stimulation patterns (e.g., TMS, ECT, DBS, ECoG, VNS, TDCS, ultrasound, optogenetics) that will validate the model and affect subsequent recordings. ADC, Analog to Digital Converter; AMP, Amplifier; CTRL, Control; DAC, Digital to Analog Converter; DNN, Deep Neural Network. XRay picture courtesy Ned T. Sahin. Diagram modified from Zhou et al. (2018).

- How do downstream neurons (i.e., reader/decoding mechanisms) interpret patterns of activity?
- Is it even possible to stimulate the brain exogenously in a manner that mimics endogenous activity?
- How best to move away from neo-phrenology and how to incorporate in our computational models the notion that the brain is a dynamical system, with all the significant computational challenges that this notion implies?
- What are the ethical considerations related to AI-assisted closed-loop stimulation?
- What are the legal considerations (e.g., FDA approval, liability) related to considering a continuously evolving AI-assisted closed-loop system a 'medical device'?

CAN AI SOLUTIONS BE EXPLAINABLE/INTERPRETABLE?

The field is split about the potential and need for AI to be explainable and/or interpretable (Holzinger et al., 2017a; Jones, 2018). Some view AI as a tool for solving a technical problem but not necessarily useful for answering a scientific question. Others think it may indeed be possible for AI actions to be interpreted and/or understood by humans, but it depends on the level of understanding being sought. Decoding techniques are typically used to test whether sampled neural data contains information that allow prediction of a dependent variable. For example, if a decoder is reducible to a set of independent contributions from the signals of individual cells, then it may be entirely possible to map the population signal back to descriptive statistics of the individual neurons (e.g., firing rate). In this case, the decoder is interpretable within our understanding of neurophysiology. On the other hand, a solution derived from a decoder may be abstract and not map onto our understanding of the neural system. For this more likely scenario, an iterative process for interpretability may be required to force ML methods to fit models with specific interpretations. This could conceivably be achieved by incorporating data visualization techniques and statistical tools that would allow neuroscientists to assess the validity of data characteristics that were used to solve the problem.

A related question is whether AI solutions can be explainable to the point of providing mechanistic insights into how the brain is accomplishing a particular function or a set of complex behaviors. Presently, there is a significant gap between the performance of explainable biophysical models for prediction and that of more opaque ANNs. Is it reasonable to expect that the synthetic algorithms and architecture that AI systems use be informative of the underlying biological process? Can we assume the decoder is using the same information as the biological network (downstream brain areas)? Perhaps the parsimonious AI process is not the same as the brain process. It may be that AI solutions are explainable (in abstraction) but inherently uninterpretable in the context of the underlying biology. Irrespective,

explanations can at a minimum give insights and help improve the AI performance.

WHAT ARE THE NEXT STEPS TOWARD A BREAKTHROUGH? WHAT ARE THE MAJOR CHALLENGES?

Three major areas in need of advancement can be identified: the need for richer datasets, more sophisticated models and methods, and cultural changes to further encourage collaborative efforts across scientific disciplines.

One of the challenges to building a durable theory of neural computation is that the foundational empirical data are limited or incomplete and, in the case of neural data, often sub-sampled (spatially and temporally). There is a general need for large, high-dimensional data sets to create models with a high degree of predictability. For example, such datasets could include quantitative data from specific multimodal signals (e.g., neural activity, neurotransmitter release, receptor activation, immune, endocrine or behavioral responses) for long periods of time. Data acquisition should be expanded to capture the developmental trajectory of an organism and contextually relevant environmental factors (e.g., naturalistic settings). Technological advances in acquisition systems will be necessary for monitoring and modulating brain function continuously, over long timescales. In addition, an important next step is to achieve more accurate and higher resolution measures of behavioral states (e.g., perceptual, social, affective, motor). Improvements in data accessibility and ease of sharing will be critical for these efforts to succeed.

A second critical step to move the field forward is the advancement of models and methods. Currently, most models operate at a single level of analysis (e.g., cell biophysics). Multi-level modeling has been a notoriously hard task to achieve using classical methods (e.g., analytically linking biophysical models to neural mass models). To accurately represent the complexity of neural systems, there is a need for XAI models to bridge from cellular level mechanisms to behavior. To reach this goal, we need heuristics and methods for quantifying the performance of these models and tools that will help us understand the nature of input-output transformations between interacting brain networks. These could include new methods for unsupervised learning from multiple modalities of data, and both statistical and analytical methods for understanding the relationships discovered in these data at multiple levels of description. The potential of these models for both basic neuroscience and clinical applications will rely on the development of tools to improve their construct validity and interpretability.

Finally, there needs to be a cultural change in the scientific enterprise itself. There is a need for more opportunities that enable meaningful and enduring collaborations between neuroscientists, clinicians, theorist, and ML experts. Interdisciplinary collaborative efforts need to be recognized and supported by academic institutions and funding agencies (Vu et al., 2018). In addition, open sharing of data and code will be important for moving this field forward. Modelers, theoreticians, and data scientists need unfettered access to well-annotated datasets. It may also be useful to adopt industry approaches like crowdsourcing, "use case" proof-of-concept studies, and grand challenges to attract interest to this area of science and technology development.

LEARNING FROM FAILURES AND SETTING EXPECTATIONS

It is interesting that we often publish and report our successes, but very seldom our no-less valuable failures, a phenomenon sometimes referred to as the 'file drawer problem' (Rosenthal, 1979; Song et al., 2009). These failures often become known if they are either catastrophic or if they became failures after a period of being considered a success. Interesting examples of past failures and lessons learned come to mind. For instance, the 2008 financial crisis taught us that domain knowledge is important when applying sophisticated data-driven algorithms to complex systems. Other examples can be found in robotics (Sheh and Monteath, 2017). Closer to home, the mental health translational pipeline is hindered by our inability as a field to produce animal models of polygenic diseases that accurately reflect any human psychopathological condition (Monteggia et al., 2018; Arguello et al., 2019; Bale et al., 2019). Or vice versa, by our inability to back translate human pathophysiological findings into animal models to gain more mechanistic insights. Significant obstacles need to be overcome to understand the role of the brain in behavior, to understand disease mechanisms and to obtain sets of biomarkers capable of characterizing a mental disease state and monitor the progress of its treatment.

On the computational front, early attempts using ANNs were successfully used to provide a data-driven way to map symptoms to diagnoses of depression (Nair et al., 1999), and in a second example to predict the effect of adinazolam SR in panic disorder with agoraphobia (Reid et al., 1996). While both studies produced interesting results, neither provided any mechanistic insights into depression or panic disorder (Cohen and Servan-Schreiber, 1992). Toward this goal, we might next look to combinations of biophysically informed models with traditional deep learning methods such as CNNs. For a variety of reasons, however, for-profit companies (the most important designers and users of ML) might not want or need to create interpretable models, so the bulk of the effort may need to come from academia or public-private partnerships.

XAI might be easier to deploy in applications such as computer vision where sensory constructive hierarchies are more clearly defined and key features for classification can be found. In radiology (medical imaging), explainability is gaining interest, including in systems that learn from expert's notes (Laserson et al., 2018). Perhaps, our desire to achieve a comprehensive theory of how brain and behavior relate to each other in more naturalistic settings might be unnecessarily ambitious, whereas well-defined and controlled experimental conditions may be as instructive of general principles.

As an initial step, new XAI projects should provide proof of concepts for new technology relevant to mental health with

very narrow focus rather than immediately aiming at longer-term goals such as curing schizophrenia or major depressive disorder. They will likely focus on key behavioral components which can be improved relatively quickly. The advent of new neurotechnology (computational or not) will allow us to answer new and more interesting questions. Even with current technologies, and limited data, we can still do a lot to generate new levels of understanding by shifting current ML paradigms. Technology development is important, but alone, it will not solve the problem of intelligent and explainable neurobehavioral modulation. We also need guiding theoretical/hypothesis-driven approaches that interact with the development and implementation of data-driven technologies. There is a need for more partnership opportunities between scientific domain experts in new or established theories and ML experts. Specifically, engaging users (e.g., clinical providers, patients, researchers) is a challenging problem that highlights that cultural normalization of these approaches is at least as important as statistical normalization (e.g., collecting reference ranges for various novel metrics). Actual "Big Data" in neuropsychiatry (as in an astounding number of individuals representative of natural heterogeneity) might not be the only path forward for AI to address behavioral health issues; but, "Deep-Data" (multimodal signals collected over time within single individuals) might be more feasible now (Vu et al., 2018). One concern is that current and very successful ML tools, such as deep learning, might seem precise in classifying and predicting within a specific learned dataset, but their results are often not robust and may not generalize to other datasets. These models can indeed be easily fooled (so-called 'adversarial attacks') when a new source of noise is added in the system or applied to data-sets that are out of sample (Finlayson et al., 2019).

HOW DO WE OPERATIONALLY DEFINE THE "EXPLAINABLE" PART OF XAI? WHAT ARE THE BEST STRATEGIES FOR USING SUCCESSFUL AI MODEL CONSTRUCTS TO IDENTIFY CONCRETE CAUSES (IN CONTRAST TO CORRELATIONS) AND (ACTIONABLE) VARIABLES?

There are no standard textbooks on XAI yet, but public repositories of implemented XAI models[2] and papers[3] are available. Similarly, attempts have been made to define explainability (Lipton, 2016; Gilpin et al., 2018; Murdoch et al., 2019) and propose practical steps that can be taken to develop an XAI system (see **Figure 2**, Khaleghi, 2019) and evaluate it (Doshi-Velez and Kim, 2017). The first step is to increase the information about the input datasets (**Figure 2**, left column). This can be achieved by preprocessing the data to extract information about its dimensionality, perhaps leading to some human-interpretable *a priori* partition (e.g., principal component analyses of input EEG channels, separation of artifacts, t-SNE (van der Maaten, 2014) or UMAP (McInnes et al., 2018) techniques). Various data visualization techniques can also be used to identify latent structures beyond those that can be obtained by straightforward statistics (Matejka and Fitzmaurice, 2017; Sarkar, 2018). Characterization of the input data can also be done by annotating and standardizing them, using for example documentation approaches such as datasheets (Gebru et al., 2018). Input data can also be embedded into a larger space in which additional dimensions are explainable features of the data (e.g., add spike burst occurrence dimension, because they may constitute privileged windows of synaptic plasticity). Such feature engineering can be done using expert knowledge in the field, or in a more principled manner using analytical approaches such as LIME (Locally Interpretable Model-Agnostic Explanations) or Contextual Explanation Networks (Al-Shedivat et al., 2018) or more general model-based techniques (Higgins et al., 2018; Murdoch et al., 2019). Finally, the explainability of the input data can be enhanced by the identification of subset of input data that are simultaneously representative of subclasses of the entire datasets and interpretable (e.g., prototypical spike waveforms sufficient for differentiating principal cells from inhibitory interneurons). Such prototypical data may serve to summarize the input dataset, and the assessment of their contributions to the model outputs can serve, at least in part, of an explanation (Bien and Tibshirani, 2011). This concept is closely related to the important topic of causality in AI (Pearl, 2009; Hernan and Robins, 2020). Equally useful to understand the data is the identification of input data that are meaningfully different from the majority of the inputs (what the data is NOT), sometime referred to as criticisms of the data (Been et al., 2016).

In addition to characterizing the data, explainability can be provided by the AI algorithm itself. Many AI models are inherently designed to potentially provide explainability, and include linear models (Ustun and Rudin, 2016), decision trees (Podgorelec et al., 2002; Geurts et al., 2009), rule sets (Jung et al., 2017), decision sets (Lakkaraju et al., 2016), Generalized additive models (Hastie and Tibshirani, 1987), and case-based reasoning systems (Lamy et al., 2019). Though potentially more explainable, these models do not guarantee explainability. High dimensionality or co-dependence of input data may make explanations difficult, if not impossible, and additional processing may be needed (Khaleghi, 2019). At least four classes of systems have been proposed that address the issue of explainability, while simultaneously attempting to maintain performance (**Figure 2** middle column and Khaleghi, 2019) including Hybrid explainable models (e.g., deep weighted averaging classifier, Card et al., 2018), joint prediction-explanation models (e.g., Teaching Explanation for Decision, Hind et al., 2018), architectural explainability models (e.g., explainable convolutional networks, Zhang et al., 2018; Tang et al., 2019) and models using regularization (e.g., Tree regularization, Wu et al., 2017).

Finally, explainability can be attributed *post hoc*, by analyzing the pattern of outputs of the algorithm. Recently, Khaleghi (2019) proposed a taxonomy of post-modeling explainability approaches that we summarize next (**Figure 2**, right column). The first class of approaches tailors *post hoc* explanations to the

[2]https://github.com/topics/xai

[3]https://github.com/anguyen8/XAI-papers

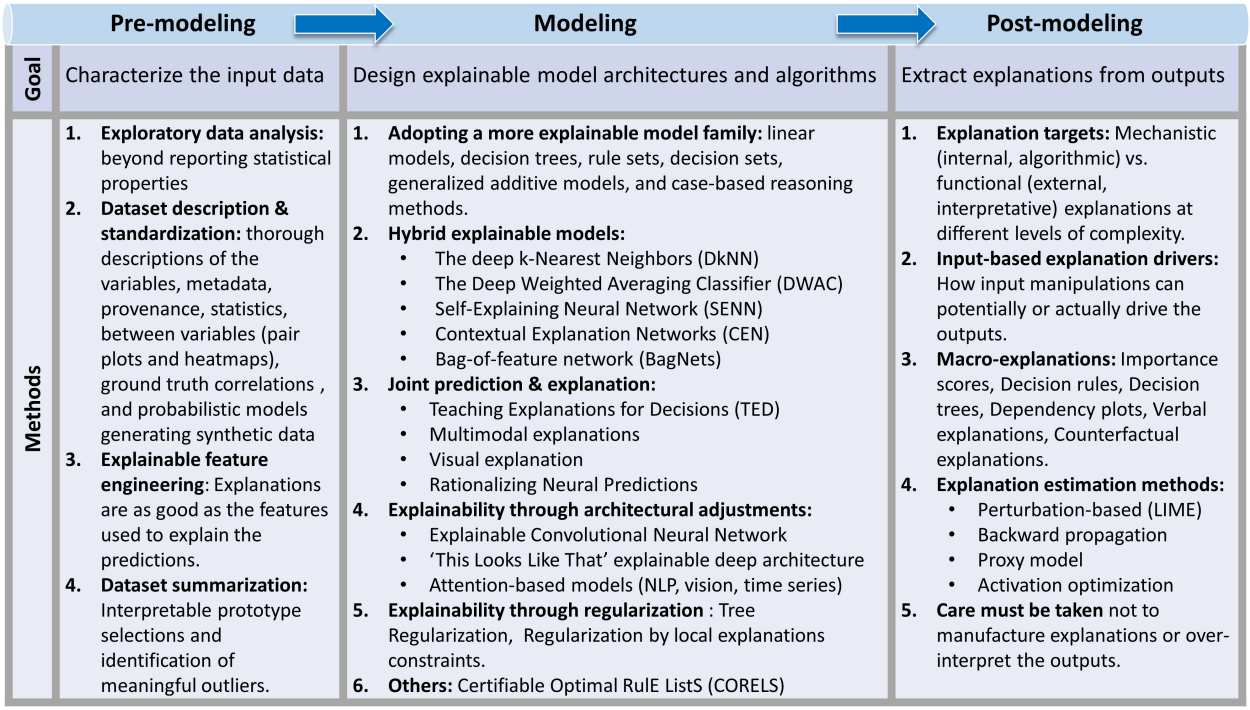

	Pre-modeling	Modeling	Post-modeling
Goal	Characterize the input data	Design explainable model architectures and algorithms	Extract explanations from outputs
Methods	1. **Exploratory data analysis:** beyond reporting statistical properties 2. **Dataset description & standardization:** thorough descriptions of the variables, metadata, provenance, statistics, between variables (pair plots and heatmaps), ground truth correlations , and probabilistic models generating synthetic data 3. **Explainable feature engineering**: Explanations are as good as the features used to explain the predictions. 4. **Dataset summarization:** Interpretable prototype selections and identification of meaningful outliers.	1. **Adopting a more explainable model family:** linear models, decision trees, rule sets, decision sets, generalized additive models, and case-based reasoning methods. 2. **Hybrid explainable models:** • The deep k-Nearest Neighbors (DkNN) • The Deep Weighted Averaging Classifier (DWAC) • Self-Explaining Neural Network (SENN) • Contextual Explanation Networks (CEN) • Bag-of-feature network (BagNets) 3. **Joint prediction & explanation:** • Teaching Explanations for Decisions (TED) • Multimodal explanations • Visual explanation • Rationalizing Neural Predictions 4. **Explainability through architectural adjustments:** • Explainable Convolutional Neural Network • 'This Looks Like That' explainable deep architecture • Attention-based models (NLP, vision, time series) 5. **Explainability through regularization** : Tree Regularization, Regularization by local explanations constraints. 6. **Others:** Certifiable Optimal RulE ListS (CORELS)	1. **Explanation targets:** Mechanistic (internal, algorithmic) vs. functional (external, interpretative) explanations at different levels of complexity. 2. **Input-based explanation drivers:** How input manipulations can potentially or actually drive the outputs. 3. **Macro-explanations:** Importance scores, Decision rules, Decision trees, Dependency plots, Verbal explanations, Counterfactual explanations. 4. **Explanation estimation methods:** • Perturbation-based (LIME) • Backward propagation • Proxy model • Activation optimization 5. **Care must be taken** not to manufacture explanations or over-interpret the outputs.

FIGURE 2 | The XAI Pipeline. Explainability can be achieved at various stages of the design of a system by characterizing the input data, developing explainable architectures and algorithms, or by implementing *post hoc* algorithms. Adapted from Khaleghi (2019). Similarly, see an up-to-date public repository of implemented XAI models (https://github.com/topics/xai) and papers (https://github.com/anguyen8/XAI-papers).

target group to which these explanations are aimed: explanations that are aimed at understanding the inner workings of the algorithm (mechanistic explanations) are different from those used to inform policy makers (functional explanations and interpretations of the outputs) (Tulio Ribeiro et al., 2016; Gilpin et al., 2019). A second class of output explanation includes algorithms that rely on understanding how input manipulations can potentially or in fact drive the outputs. They include input feature section (e.g., explainable feature engineering of the inputs, above), an analysis of how specific inputs affect outputs (e.g., influence function, Koh and Liang, 2017), or an analysis of how a specific class of inputs influence the outputs (e.g., Concept activation vectors, Kim et al., 2017). A third class of algorithms are holistic in nature and includes explanatory methods that abstract or summarize the system in terms that are understandable by the user. This type of Macro-level explanations includes methods such as saliency maps (Lundberg and Lee, 2017) or Decision rules (Guidotti et al., 2018). Finally, the fourth class of *post hoc* explanatory models includes algorithms that aim at estimating (rather than providing) an explanation. These methods include generally applicable algorithms such as LIME (Tulio Ribeiro et al., 2016) or Quantitative Input influence measures (Datta et al., 2017) which uses controlled and limited perturbations of the inputs to understand how the output vary. Overall, as with the methods targeted to input data, these algorithms address the general notion of causality in AI (Pearl, 2009; Hernan and Robins, 2020).

Importantly, and perhaps similarly to many other fields, interpretation of the outputs and of the general outcomes of an AI algorithm must be checked against bias and overall exaggeration (Lipton and Steinhardt, 2018). An important issue to keep in mind when designing an XAI system is contrasting explanation, causation, and correlation. Correlation is not necessarily causal because it may be mediated by a latent, common, factor. For example, in the case that A is correlated with B because C causes A and B with some probability, C would be a partial explanation for A and B, but A and B would bear no mutual explanatory link. XAI systems should handle such differentiation, or at the very least should quantify the extent to which they occur. This issue is even more relevant in non-linear (e.g., complex recurrent) systems such as the brain. A second related outcome to such differentiation stems from the fact that the input dimensions of an XAI system are likely not independent and feature a large amount of redundancies and co-dependencies. An XAI system should be able to pair a specific explanation with a subset of the input dimensions that caused it, therefore pointing to the important dimensions to use for further study, targeted experimental manipulations, or additional focused data collection. Human-in-the-loop approaches may also be beneficial, especially in eliminating trivial correlations that may bias the system toward un-interesting solutions (Zanzotto, 2019). It is likely in fact that the process of developing explanatory power may rely on an iterative approach whereby the human would evaluate the explanation of a previous cycle, inject his/her knowledge into

the XAI system, and improve the nature or accuracy of the explanation in the next cycle (**Figure 1**). There may be value in querying the field of Psychology of Interpretations. What makes an explanation a *good* explanation? Perhaps is it a matter of length and number of outputs explained? The more concise the explanation and the more outputs it explains, the better? Of course, explanations should be human-understandable as well ('42' is certainly concise and explains 'life, the universe and everything,' but it is hardly understandable, Adams, 1980).

Current AI can be made more explainable by using more appropriate research designs. For example, one can ask ML specific questions about brain or behavior while accounting for underlying (labeled) variables. But even the best and latest input pattern detectors, trained with multidimensional datasets will not inform us about the underlying mechanisms if we only ask how well they do at detecting the overt phenomenon. However, these detectors, when coupled to dimensionality reduction and feature extraction techniques could help identify mechanisms of action and actionable variables. Iterative feature selection and dimension reduction are methods to identify relevant features and the role played by their interactions. Another strategy could be identifying the 'useful' weights that contribute to the success of an AI neural-network-based algorithm and understanding what they mean in neuroscience terms and what they are doing to affect the neural circuitry. This method can address the issue of explainability as well as that of mechanism controllability. But ultimately, closed loop/perturbation experiments offer the best hope of moving beyond correlational findings. Eventually, direct and systematic mechanistic modulation of a given set of variables may be necessary to understand how the ML model reacts to each variable and each combination of variables, both in aggregate and for individual input examples. DBS systems for psychiatric disorders (e.g., OCD, MDD, Goodman and Alterman, 2012), which are first built in the clinic, will face additional challenges in the ambulatory environments. As ML takes place in these increasingly more complex environment-dependent situations, analyses of correct actions as well as errors would benefit from XAI. As an example, visual Case-Based Reasoning (CBR) – a form of analog reasoning in which the solution for a new query case is determined using a database of previous known cases with their solutions could be an effective approximation of an XAI solution that has not been employed in psychiatry (Lamy et al., 2019).

How can we determine what neural features are important to modulate behavior? The answer is likely to be different for each domain of applicability (neurostimulation or others). In general, before effective explanations can be generated, ML models should be validated (and cross-validated) on data sets not used for model-fitting, should be tested for generalizability across contexts/conditions and should incorporate strategies to avoid overfitting. The field needs to:

- Provide better analytical and statistical tools for characterizing dynamical systems within the constraints a given biological/ethological context;
- Provide models of compensation, adaptation or plasticity facilitated by exogenous modulatory inputs that might enhance (or interfere) with intended outputs and outcomes;
- Explore manifolds of parameters in unbiased ways that allow for the discovery of relevant sub-spaces where information that is biologically relevant to the organism's existence.

WHAT CONCEPTUAL AND TECHNICAL ADVANCES ARE NECESSARY FOR XAI TO BE A VIABLE COMPONENT OF NEUROSTIMULATION STRATEGIES?

Perhaps the first type of advances required to make XAI a viable tool in understanding the relationships between neural circuits and behavior is an improvement in the quality and amount of the input data. The field needs more simultaneous recordings from multiple cell types within multiple brain regions comprising all putative neural circuits and a wide range of quantitative behaviors. If XAI is to find subtle and more interesting ways to understand the interaction between neural circuits and behavior, we need to find more and better way to measure them. The temporal and spatial requirements of recordings depend on the specific clinical/physiological question being asked and more, and better, data are needed for optimal explainable AI results. Temporal precision at the millisecond level and spatial resolution down to the single-neuron or microcircuit-level are likely to be necessary. Hundreds more electrodes, covering both cortical and sub-cortical areas would provide crucial information, especially in the determination of the timing and intensity of neurostimulation, in quasi-autonomous systems. Continuous data collection that enables greater sampling of key behaviors in different contexts is also likely to be able to improve the performance of such systems.

Importantly, XAI needs to be able to effectively handle multi-modal data (e.g., visual, auditory, clinical). It should provide inherently non-linear computational algorithms that will be able to combine large datasets such as those provided by modern calcium imaging techniques [>1000 of neurons recorded simultaneously (Soltanian-Zadeh et al., 2019; Stringer et al., 2019)] and voltage sensitive dye techniques (Grinvald et al., 2016; Chemla et al., 2017) with smaller but highly meaningful datasets such as those describing behavior. These improvements would result, in turn, in better ways to 'close the loop' and devise effective algorithms for neurostimulation. Additional advances in real-time encoding of the environment and real time classification of behavioral states would give rise to a new generation of neurofeedback systems that could be used for therapeutic purposes, greatly expanding on the current trends for adaptive neurostimulation (Provenza et al., 2019). Another challenge is to quantify behavior and neural activity at multiple levels of complexity and multiple time scales and use new statistical and analytical tools to link and compare the different levels. At each of these levels, effort should be made to differentiate externally generated influences and internally generated computations. Finally, efforts need to be made to understand the organism's response to more naturalistic environments and stimuli. This is crucial in cases

where social interactions are known to play a major role, since much of the neuroscientific data is usually collected in single subjects, or in impoverished social or cognitive environments. Finally, advances in the quality and type of data should be accompanied with advances in AI/XAI theories and ML techniques (Greenwald and Oertel, 2017).

An interesting avenue to explore is the mapping between the XAI system and the neural systems, perhaps even designing such a system from scratch, with the brain as a starting point. In the specific context of neurostimulation, better models are needed to understand how neurostimulation actually affects the neural tissue (neuron, glial cells, synapse). A challenge will be for XAI to provide explanations for phenomena known to have none (consensually at least).

In general, XAI models should be scalable to bridge animal research and human clinical applications and be sufficiently computationally efficient to allow for implementations on actual small-scale devices that can be used clinically. Improvements in sustainable high-density recording devices for humans, mirroring those already available in animals, is desirable.

Moving forward, what types of initial steps can be taken to link XAI to the field of closed-looped neurostimulation? One can certainly imagine simply applying existing or novel XAI techniques to a known neurostimulation paradigm to provide explanatory power to close-loop neurobehavioral modulation (e.g., counter-factual probes). Other avenues may involve active modulations of complex neural circuits pertaining to mental disorders. Such manipulations may involve electrical or magnetic stimulations, optogenetics, genome editing or pharmacological compounds and may include dynamic automatic adjustments of closed-loop parameters as the neural substrate adapts to the manipulations.

BEYOND MENTAL HEALTH, WHAT OTHER DISEASES COULD BENEFIT FROM AN XAI SOLUTION?

There is potentially a variety of medical conditions that could be informed by XAI. Biomarkers, broadly defined as biological measurements that give the ability to predict, detect, and diagnose, can be key targets of XAI approaches. Specific clinical domains such as epilepsy have already benefited from relatively simple closed loop paradigms (so called 'responsive neurostimulation' techniques). Other domains such as cardiovascular illness, infectious disease, and epidemiology could also significantly benefit. Mental health conditions, and the RDoC are of particular interest, because they focus on understanding the nature of mental illness in terms of varying degrees of dysfunctions in general psychological/biological systems (Kozak and Cuthbert, 2016; Sanislow et al., 2019). Indeed, in the absence of a very large number of behaviors and comprehensive cell-type specific measurements, we can reasonably start with chunks of behavior as conceptualized and cataloged by RDoC which does allow for a systematic approach for XAI models and experiments. Research needs to be both rigorous and pragmatic about whether supervised or unsupervised XAI models are used but should remain realistic about the level of spatial and temporal resolution possible with the current generations of human recording and stimulating devices. The ability to utilize XAI results in a closed-loop fashion can make major contributions to epilepsy treatment, for example, by preventing seizure activity using XAI-based predictions to activate an implanted neurostimulator in real time. XAI can improve the efficacy of brain stimulation devices by allowing an in-depth dissection of the networks and nodes underlying brain-based disorders, and by providing an avenue of translation between recording and stimulation architectures.

Another area most amenable to XAI approaches includes computer vision approaches to radiological imaging interpretation. This area has already seen important progress, including FDA approved tools, see for example (Topol, 2019) for a recent review, which includes important caveats. XAI can further contribute to the difficult problem of data fusion of heterogeneous multimodal measurements including, for example, simultaneously sampled imaging, neurophysiological and behavioral data.

There is a strong desire to build what is already known into models and to start from simpler scenarios. Prior data could be used to design the model, provide initial constraints, and provide error refinement. Insights from biology, such as reafference/corollary discharge and statistical models of neural firing are certainly a source of useful design information. Seeking insights from development (e.g., differences in learning during childhood vs. adulthood) can also be used as a means to inform the XAI system. Whatever the prior information, its origin should be quantitatively and objectively measured and be based on continuous behavior and neural data. Moreover, it must be kept in mind that not all cognitive measures include relevant information and care should be taken when selecting them for processing to avoid potential issues affecting interpretability Also, summary or composite measures such as those related to emotional state or context could help differentiate normal from abnormal responses and should be considered as well. Finally, the ability to handle and benefit from incomplete or uncertain data may be a major contribution of XAI approaches.

In general, XAI has the potential to contribute to the integration of data-driven and theory driven models (e.g., integrating Deep Learning models with biophysically informed models), to label existing model features with semantic information that is understandable by users, to allow ML algorithms to unbiasedly discover the governing principles of a complex dynamical system by analyzing covarying multimodal data or to estimate the influence of a given feature on a model prediction by leveraging causal statistical methods.

CONCLUDING REMARKS

One key proposed approach to stimulate the field is the establishment of competitions on existing (curated) datasets, an approach that has been very successful in other disciplines (e.g., computer vision and ML). Other disciplines have shown multiple benefits of this type of activity, including the possibility

to compare and merge results and outcomes from multiple teams, the opportunity to show and evaluate progress, and the motivation experienced by atypical contributors that enjoy such competition and enter a field. Areas such as closed loop-neurostimulation provide multiple challenges, and openly sharing data via competitions can bring together multiple disciplines addressing problems ranging from signal synchronization to optimal outcome analysis and stimulation settings. Initial attempts in this direction in neuroscience recently started, and include a number of EEG competitions[4] and spike inference for calcium imaging (Berens et al., 2018).

It is important to note the need to harmonize different types of data and the necessity of longitudinal multimodal data. There is a large amount of existing data that can be tapped for secondary analyses, including the aforementioned competitions (e.g., the ENIGMA project)[5]. Aggregation needs to happen across scales, time (longitudinal), and individuals. The potential value of explainability in this challenge is clear; it is expected that the more explainable the data and analyses are, the easier it will be to combine disparate sources.

Following the trend of using and sharing existing data, there is a need to study "hybrid models" which use AI approaches to fit a biologically driven model – does AI converge on the same solution as expected? A recent example has been published (Banino et al., 2018; Cueva and Wei, 2018). Neurostimulation is a good sandbox where ML and biology are starting to interact (Kim et al., 2019; Shamir et al., 2019), and for which the need of explainability of biomarkers and interventions is critical.

It is important for researchers to be aware of the pitfalls inherent to the translation of results and models from animals to humans and the need to collect data with multiple tools and open technologies, staying away as much as possible from proprietary tools. This "closed" practice can lead to fitting to correlated noise in datasets/variation that is not biologically/clinically meaningful and to limit reproducibility and validation. The above mentioned openly shared and combined datasets is an important contribution to the development of better XAI.

Unsurprisingly, explainable AI in neuroscience and neurostimulation suffer from the 'curse of dimensionality' (data of very high dimensions), and partially driven by this challenge, show the need to consider simpler models, including variable selection. While this is an example of a technical/computational problem, clinical failures from the past need to be addressed as well, in particular the need to avoid the expectation that neurostimulation must have immediate effects (as in DBS for PD), but rather has complex and mixed acute and chronic effects, possibly involving long term synaptic plasticity. Using a single outcome measure, as was often done in the past, can lead to incorrect conclusions about models and interventions; there is a need to incorporate measures at multiple time scales, to use derivative-based metrics, to measure rate of change and to build characterization of normative data so as to measure deviations from it. It is interesting to note that these issues, here mentioned as failures from the past, connect to the above identified need to integrate data from multiple sources, time resolutions, and spatial scales, which is a recurring concern and for which explainability can be of significant help.

In addition, explainability may be valuable for building trust in the algorithms, for understanding risk and side effects, for aiding in the identification of therapeutic targets, for understanding the evolution or progression of disease and response to treatments, for understanding and supporting decisions, for closed-loop control, and for the design of the "safety parameter box" – FDA's bound on therapies. Although explainability may lead to improved trustworthiness, transparency and fairness, these are distinct but related concepts. The predisposition of scientists and healthcare professionals to accept the validity and reliability of ML results, given changes in the input or in the algorithmic parameters, without necessarily knowing how the results were derived has to do with trustworthiness. Trust relies on five key factors: the data, the system, the workflow, the outputs, and the ability to communicate the results of the algorithm clearly. Users need to be able to probabilistically determine when some results might be incorrect and ensure that results are interpreted correctly without needing to know the inner workings of the algorithm. Transparency and Fairness relate to the right to know and to understand the aspects of a dataset/input that could influence outputs (e.g., clinical decision support from AI algorithms or neurostimulation protocols). Transparency and fairness should lead to a reduction of bias perpetuation that can be produced by humans (e.g., tracking and education regarding biases in language), by AI algorithms (e.g., developing AI approaches able to identify bias in results), by better data collection (e.g., utilize more representative data sets).

It is of course critical to keep in mind that explainability can be beneficial but is not mandatory (e.g., detecting amyloid plaques in Alzheimer's Disease imaging data). In other words, non-explainable (or non-explainable yet) predictions can still have value as biomarkers. Importantly, explainability might be different for different audiences (Tomsett et al., 2018; Gilpin et al., 2019). For example, what needs to be explainable for the FDA might be different than for scientists or even patients (Murdoch et al., 2019), and these discrepancies raise regulatory issues related to the 'right to explanation' (Goodman and Flaxman, 2016). Finally, the incorporation of explainable ML in clinical trials, for example, to optimize neurostimulation parameters in a patient specific fashion instead of the common use of fixed protocols, can be a novel direction of research. This brings us to the important current area of AI in drug design, a very active topic of research in the academic and even more in the industrial community (Simm et al., 2018).

In sum, XAI applied to the domain of closed-loop neurostimulation may yield important new insights both at the fundamental research level and at the clinical therapeutic level and is ideally positioned to generate a new set of translational approaches capable of using increasingly larger multi-modal datasets to discover basic principles about normal and abnormal brain functions.

[4]https://www.kaggle.com

[5]http://enigma.ini.usc.edu/

ETHICS STATEMENT

Written informed consent was obtained from the individual(s) for the publication of any potentially identifiable images or data included in this article.

AUTHOR CONTRIBUTIONS

All authors contributed to manuscript conception, design, writing, literature review, and revision. All authors read and approved the submitted version.

ACKNOWLEDGMENTS

This manuscript is linked to a companion NIMH funding opportunity[6] and is partly based on the outcome of a NIH workshop held November 10, 2017 in Washington DC entitled 'Explainable Artificial Intelligence Solutions Applied to Neural and Behavioral Data'[7]. This workshop was partially informed by a DARPA program in eXplainable AI (Gunning and Aha, 2019) that seeks to develop general explainable models[8] not directly linked to the field of behavioral neurostimulation. See also the Computational Psychiatry Program and the Theoretical and Computational Neuroscience Program at NIMH, the 'Machine Intelligence in Healthcare: Perspectives on Trustworthiness, Explainability, Usability and Transparency' workshop at NIH/NCATS[9], and the SUBNETS program[10] and GARD programs[11] at DARPA for additional material, related activities and funding opportunities. We thank Dr. Sarah Morris, Dr. Aleksandra Vicentic and Dr. David McMullen for helpful comments on the manuscript.

[6] https://grants.nih.gov/grants/guide/pa-files/PAR-19-344.html

[7] https://www.nimh.nih.gov/news/events/2017/explainable-artificial-intelligence-solutions-applied-to-neural-and-behavioral-data.shtml

[8] https://www.darpa.mil/program/explainable-artificial-intelligence

[9] https://ncats.nih.gov/expertise/machine-intelligence#workshop

[10] https://www.darpa.mil/program/systems-based-neurotechnology-for-emerging-therapies

[11] https://www.darpa.mil/news-events/2019-02-06

REFERENCES

Adadi, A., and Berrada, M. (2018). Peeking Inside the Black-Box: A Survey on Explainable Artificial Intelligence (XAI). *IEEE Access* 6, 52138–52160. doi: 10.1109/access.2018.2870052

Adams, D. (1980). *The Hitchhiker's Guide to the Galaxy*. New York, NY: Harmony Books.

Al-Shedivat, M., Dubey, A., and Xing, E. P. (2018). The Intriguing Properties of Model Explanations. *arXiv* [Preprints] Available at: https://ui.adsabs.harvard.edu/abs/2018arXiv180109808A (accessed January 01, 2018).

Andersen, R. A., Hwang, E. J., and Mulliken, G. H. (2010). Cognitive neural prosthetics. *Annu. Rev. Psychol.* 61, 169–190.

Arguello, A. P., Addington, A., Borja, S., Brady, L., Dutka, T., Gitik, M., et al. (2019). From genetics to biology: advancing mental health research in the Genomics ERA. *Mol. Psychiatry* 24, 1576–1582. doi: 10.1038/s41380-019-0445-x

Bale, T. L., Abel, T., Akil, H., Carlezon, W. A. Jr., Moghaddam, B., Nestler, E. J., et al. (2019). The critical importance of basic animal research for neuropsychiatric disorders. *Neuropsychopharmacology* 44, 1349–1353. doi: 10.1038/s41386-019-0405-9

Banino, A., Barry, C., Uria, B., Blundell, C., Lillicrap, T., Mirowski, P., et al. (2018). Vector-based navigation using grid-like representations in artificial agents. *Nature* 557, 429–433. doi: 10.1038/s41586-018-0102-6

Been, K., Khanna, R., and Koyejo, O. (2016). "Examples are not enough, learn to criticize! criticism for interpretability," in *Proceedings of the Advances in Neural Information Processing Systems (NIPS 2016)*, Barcelona.

Berens, P., Freeman, J., Deneux, T., Chenkov, N., Mccolgan, T., Speiser, A., et al. (2018). Community-based benchmarking improves spike rate inference from two-photon calcium imaging data. *PLoS Comput. Biol.* 14:e1006157. doi: 10.1371/journal.pcbi.1006157

Bien, J., and Tibshirani, R. (2011). Prototype selection for interpretable classification. *Ann. Appl. Stat.* 5, 2403–2424. doi: 10.1214/11-aoas495

Card, D., Zhang, M., and Smith, N. A. (2018). Deep Weighted Averaging Classifiers. *arXiv* [Preprints] Available at: https://ui.adsabs.harvard.edu/abs/2018arXiv181102579C (accessed November 01, 2018).

Chemla, S., Muller, L., Reynaud, A., Takerkart, S., Destexhe, A., and Chavane, F. (2017). Improving voltage-sensitive dye imaging: with a little help from computational approaches. *Neurophotonics* 4:031215. doi: 10.1117/1.NPh.4.3.031215

Choo, J., and Liu, S. X. (2018). Visual Analytics for Explainable Deep Learning. *IEEE Comput. Graph. Appl.* 38, 84–92. doi: 10.1109/MCG.2018.042731661

Cohen, J. D., and Servan-Schreiber, D. (1992). Introduction to neural networks models in psychatry. *Psychiatr. Ann.* 22, 113–118.

Core, M. G., Lane, H. C., Van Lent, M., Gomboc, D., Solomon, S., and Rosenberg, M. (2006). "Building explainable artificial intelligence systems," in *Proceedings of the 18th Conference on Innovative Applications of Artificial Intelligence*, Palo Alto, CA: The AAAI Press, 1766.

Craik, A., He, Y., and Contreras-Vidal, J. L. (2019). Deep learning for electroencephalogram (EEG) classification tasks: a review. *J. Neural Eng.* 16:031001. doi: 10.1088/1741-2552/ab0ab5

Cueva, C. J., and Wei, X.-X. (2018). Emergence of grid-like representations by training recurrent neural networks to perform spatial localization. *arXiv* [Preprints] Available: https://ui.adsabs.harvard.edu/abs/2018arXiv180307770C (accessed March 01, 2018).

Datta, A., Sen, S., and Zick, Y. (2017). "Algorithmic transparency via quantitative input influence," in *Transparent Data Mining for Big and Small Data*, eds T. Cerquitelli, D. Quercia, and F. Pasquale, (Cham: Springer).

Deadwyler, S. A., Hampson, R. E., Song, D., Opris, I., Gerhardt, G. A., Marmarelis, V. Z., et al. (2017). A cognitive prosthesis for memory facilitation by closed-loop functional ensemble stimulation of hippocampal neurons in primate brain. *Exp. Neurol.* 287, 452–460. doi: 10.1016/j.expneurol.2016.05.031

Doshi-Velez, F., and Kim, B. (2017). Towards A Rigorous Science of Interpretable Machine Learning. *arXiv* [Preprints] Available at: ttps://ui.adsabs.harvard.edu/abs/2017arXiv170208608D (accessed February 01, 2017).

Dosilovic, F. K., Brcic, M., and Hlupic, N. (2018). "Explainable artificial intelligence: a survey," in *Proceedings of the 41st International Convention on Information and Communication Technology, Electronics and Microelectronics (MIPRO)*, Opatija.

Fernandez, A., Herrera, F., Cordon, O., Del Jesus, M. J., and Marcelloni, F. (2019). Evolutionary Fuzzy Systems for Explainable Artificial Intelligence: Why, When, What for, and Where to? *IEEE Comput. Intell. Mag.* 14, 69–81. doi: 10.1109/mci.2018.2881645

Ferrante, M., Redish, A. D., Oquendo, M. A., Averbeck, B. B., Kinnane, M. E., and Gordon, J. A. (2019). Computational psychiatry: a report from the 2017 NIMH workshop on opportunities and challenges. *Mol. Psychiatry* 24, 479–483. doi: 10.1038/s41380-018-0063-z

Finlayson, S. G., Bowers, J. D., Ito, J., Zittrain, J. L., Beam, A. L., and Kohane, I. S. (2019). Adversarial attacks on medical machine learning. *Science* 363, 1287–1289. doi: 10.1126/science.aaw4399

Flesher, S., Downey, J., Collinger, J., Foldes, S., Weiss, J., Tyler-Kabara, E., et al. (2017). Intracortical Microstimulation as a Feedback Source for Brain-Computer Interface Users. *Brain Comput. Interf. Res.* 6, 43–54. doi: 10.1007/978-3-319-64373-1_5

Gebru, T., Morgenstern, J., Vecchione, B., Wortman Vaughan, J., Wallach, H., Daumeé, H. III, et al. (2018). Datasheets for Datasets. *arXiv* [Preprints] Available at: https://ui.adsabs.harvard.edu/abs/2018arXiv180309010G (accessed March 01, 2018),

Geurts, P., Irrthum, A., and Wehenkel, L. (2009). Supervised learning with decision tree-based methods in computational and systems biology. *Mol. Biosyst.* 5, 1593–1605. doi: 10.1039/b907946g

Gilpin, L. H., Bau, D., Yuan, B. Z., Bajwa, A., Specter, M., and Kagal, L. (2018). Explaining explanations: an overview of interpretability of machine learning. *arXiv* [Preprints] Available at: https://ui.adsabs.harvard.edu/abs/2018arXiv180600069G (accessed May 01, 2018).

Gilpin, L. H., Testart, C., Fruchter, N., and Adebayo, J. (2019). Explaining explanations to society. *arXiv* [Preprints] Available at: https://ui.adsabs.harvard.edu/abs/2019arXiv190106560G (accessed January 01, 2019).

Goodman, B., and Flaxman, S. (2016). European Union regulations on algorithmic decision-making and a "right to explanation". *arXiv* [preprints] Available at: https://ui.adsabs.harvard.edu/abs/2016arXiv160608813G (accessed June 01, 2016).

Goodman, W. K., and Alterman, R. L. (2012). Deep brain stimulation for intractable psychiatric disorders. *Annu. Rev. Med.* 63, 511–524. doi: 10.1146/annurev-med-052209-100401

Greenwald, H. S., and Oertel, C. K. (2017). Future Directions in Machine Learning. *Front. Robot. AI* 3:79. doi: 10.3389/frobt.2016.00079

Grinvald, A., Omer, D. B., Sharon, D., Vanzetta, I., and Hildesheim, R. (2016). Voltage-sensitive dye imaging of neocortical activity. *Cold Spring Harb. Protoc.* 2016:pdb.top089367. doi: 10.1101/pdb.top089367

Guidotti, R., Monreale, A., Ruggieri, S., Turini, F., Pedreschi, D., and Giannotti, F. (2018). A Survey Of Methods For Explaining Black Box Models. *arXiv* [Preprints] Available at: https://ui.adsabs.harvard.edu/abs/2018arXiv180201933G (accessed February 01, 2018).

Gunning, D., and Aha, D. W. (2019). DARPA's Explainable Artificial Intelligence Program. *AI Mag.* 40, 44–58. doi: 10.1609/aimag.v40i2.2850

Hampshire, A., and Sharp, D. J. (2015). Contrasting network and modular perspectives on inhibitory control. *Trends Cogn. Sci.* 19, 445–452. doi: 10.1016/j.tics.2015.06.006

Hastie, T., and Tibshirani, R. (1987). Generalized additive-models - some applications. *J. Am. Stat. Assoc.* 82, 371–386.

Hatsopoulos, N. G., and Donoghue, J. P. (2009). The science of neural interface systems. *Annu. Rev. Neurosci.* 32, 249–266. doi: 10.1146/annurev.neuro.051508.135241

Hernan, M., and Robins, J. (2020). *Causal Inference: What If*. Boca Raton: Chapman & Hall/CRC.

Herron, J. A., Thompson, M. C., Brown, T., Chizeck, H. J., Ojemann, J. G., and Ko, A. L. (2017). Cortical brain-computer interface for closed-loop deep brain stimulation. *IEEE Trans. Neural. Syst. Rehabil. Eng.* 25, 2180–2187. doi: 10.1109/TNSRE.2017.2705661

Higgins, I., Amos, D., Pfau, D., Racaniere, S., Matthey, L., Rezende, D., et al. (2018). Towards a definition of disentangled representations. *arXiv* [Preprints] Available at: https://ui.adsabs.harvard.edu/abs/2018arXiv181202230H (accessed December 01, 2018).

Hind, M., Wei, D., Campbell, M., Codella, N. C. F., Dhurandhar, A., Mojsilović, A., et al. (2018). TED: Teaching AI to explain its decisions. *arXiv* [preprints] Available at: https://ui.adsabs.harvard.edu/abs/2018arXiv181104896H (accessed November 01, 2018).

Holzinger, A., Biemann, C., Pattichis, C. S., and Kell, D. B. (2017a). What do we need to build explainable AI systems for the medical domain? *arXiv* [Preprints] Available at: https://ui.adsabs.harvard.edu/abs/2017arXiv171209923H (accessed December 01, 2017).

Holzinger, A., Malle, B., Kieseberg, P., Roth, P. M., Müller, H., Reihs, R., et al. (2017b). Towards the Augmented Pathologist: Challenges of Explainable-AI in Digital Pathology. *arXiv* [Preprints] Available at: https://ui.adsabs.harvard.edu/abs/2017arXiv171206657H (accessed December 01, 2017).

Holzinger, A., Kieseberg, P., Weippl, E., and Tjoa, A. M. (2018). "Current advances, trends and challenges of machine learning and knowledge extraction: from machine learning to explainable AI," in *Machine Learning and Knowledge Extraction, Cd-Make*, eds A. Holzinger, P. Kieseberg, A. Tjoa, and E. Weippl, (Cham: Springer),

Jiang, L., Stocco, A., Losey, D. M., Abernethy, J. A., Prat, C. S., and Rao, R. P. N. (2019). BrainNet: A Multi-Person Brain-to-Brain Interface for Direct Collaboration Between Brains. *Sci. Rep.* 9:6115. doi: 10.1038/s41598-019-41895-7

Jones, H. (2018). *Geoff Hinton Dismissed The Need For Explainable AI: 8 Experts Explain Why He's Wrong*. Available at: https://www.forbes.com/sites/cognitiveworld/2018/12/20/geoff-hinton-dismissed-the-need-for-explainable-ai-8-experts-explain-why-hes-wrong (accessed March 12, 2019).

Jung, J., Concannon, C., Shroff, R., Goel, S., and Goldstein, D. G. (2017). Simple rules for complex decisions. *arXiv* [Preprint] Available at: https://ui.adsabs.harvard.edu/abs/2017arXiv170204690J (accessed February 01, 2017).

Khaleghi, B. (2019). *The How of Explainable AI: Pre-modelling Explainability*. Available at: https://towardsdatascience.com/the-how-of-explainable-ai-pre-modelling-explainability-699150495fe4 (accessed March 12, 2019).

Kim, B., Wattenberg, M., Gilmer, J., Cai, C., Wexler, J., Viegas, F., et al. (2017). Interpretability Beyond Feature Attribution: Quantitative Testing with Concept Activation Vectors (TCAV). *arXiv* [Preprints] Available at: https://ui.adsabs.harvard.edu/abs/2017arXiv171111279K (accessed November 01, 2017).

Kim, J., Duchin, Y., Shamir, R. R., Patriat, R., Vitek, J., Harel, N., et al. (2019). Automatic localization of the subthalamic nucleus on patient-specific clinical MRI by incorporating 7 T MRI and machine learning: application in deep brain stimulation. *Hum. Brain Mapp.* 40, 679–698. doi: 10.1002/hbm.24404

Klaes, C., Shi, Y., Kellis, S., Minxha, J., Revechkis, B., and Andersen, R. A. (2014). A cognitive neuroprosthetic that uses cortical stimulation for somatosensory feedback. *J. Neural Eng.* 11:056024. doi: 10.1088/1741-2560/11/5/056024

Koh, P. W., and Liang, P. (2017). Understanding Black-box Predictions via Influence Functions. *arXiv* [Preprints] . Available at: https://ui.adsabs.harvard.edu/abs/2017arXiv170304730K (accessed March 01, 2017).

Kozak, M. J., and Cuthbert, B. N. (2016). The NIMH research domain criteria initiative: background, issues, and pragmatics. *Psychophysiology* 53, 286–297. doi: 10.1111/psyp.12518

Lakkaraju, H., Bach, S. H., and Leskovec, J. (2016). "Interpretable decision sets: a joint framework for description and prediction," in *Proceedings of the 22nd ACM SIGKDD International Conference on Knowledge Discovery and Data Mining*, San Francisco, CA: ACM.

Lamy, J. B., Sekar, B., Guezennec, G., Bouaud, J., and Seroussi, B. (2019). Explainable artificial intelligence for breast cancer: a visual case-based reasoning approach. *Artif. Intell. Med.* 94, 42–53. doi: 10.1016/j.artmed.2019.01.001

Langlotz, C. P., Allen, B., Erickson, B. J., Kalpathy-Cramer, J., Bigelow, K., Cook, T. S., et al. (2019). A Roadmap for Foundational Research on Artificial Intelligence in Medical Imaging: From the 2018 NIH/RSNA/ACR/The Academy Workshop. *Radiology* 291, 781–791. doi: 10.1148/radiol.2019190613

Laserson, J., Lantsman, C. D., Cohen-Sfady, M., Tamir, I., Goz, E., Brestel, C., et al. (2018). TextRay: Mining Clinical Reports to Gain a Broad Understanding of Chest X-rays. *arXiv* [Preprints] Available at: https://ui.adsabs.harvard.edu/abs/2018arXiv180602121L (accessed June 01, 2018).

Lipton, Z. C. (2016). The Mythos of model interpretability. *arXiv* [Preprints] Available at: https://ui.adsabs.harvard.edu/abs/2016arXiv160603490L (accessed June 01, 2016).

Lipton, Z. C., and Steinhardt, J. (2018). Troubling trends in machine learning scholarship. *arXiv* [Preprints] Available at: https://ui.adsabs.harvard.edu/abs/2018arXiv180703341L (accessed July 01, 2018).

Lundberg, S., and Lee, S.-I. (2017). "A unified approach to interpreting model predictions," in *Proceedings of the 31st International Conference on Neural Information Processing Systems*, Long Beach, CA.

Mahmoudi, B., and Sanchez, J. C. (2011). Symbiotic Brain-Machine Interface through Value-Based Decision Making. *PLoS One* 6:e14760. doi: 10.1371/journal.pone.0014760

Marsh, B. T., Tarigoppula, V. S., Chen, C., and Francis, J. T. (2015). Toward an autonomous brain machine interface: integrating sensorimotor reward

modulation and reinforcement learning. *J. Neurosci.* 35, 7374–7387. doi: 10.1523/JNEUROSCI.1802-14.2015

Martini, M. L., Oermann, E. K., Opie, N. L., Panov, F., Oxley, T., and Yaeger, K. (2019). Sensor modalities for brain-computer interface technology: a comprehensive literature review. *Neurosurgery* doi: 10.1093/neuros/nyz286 [Epub ahead of print],

Matejka, J., and Fitzmaurice, G. (2017). "Same stats, different graphs: generating datasets with varied appearance and identical statistics through simulated annealing," in *Proceedings of the 2017 CHI Conference on Human Factors in Computing Systems*, Denver, CO: ACM.

McInnes, L., Healy, J., and Melville, J. (2018). UMAP: uniform manifold approximation and projection for dimension reduction. *arXiv* [Preprints] Available at: https://ui.adsabs.harvard.edu/abs/2018arXiv180203426M (accessed February 01, 2018).

Miller, T. (2019). Explanation in artificial intelligence: Insights from the social sciences. *Artif. Intell.* 267, 1–38. doi: 10.1016/j.artint.2018.07.007

Mirabella, G. (2014). Should I stay or should I go? conceptual underpinnings of goal-directed actions. *Front. Syst. Neurosci.* 8:206. doi: 10.3389/fnsys.2014.00206

Mirabella, G., and Lebedev, M. A. (2017). Interfacing to the brain's motor decisions. *J. Neurophysiol.* 117, 1305–1319. doi: 10.1152/jn.00051.2016

Monteggia, L. M., Heimer, H., and Nestler, E. J. (2018). Meeting Report: Can We Make Animal Models of Human Mental Illness? *Biol. Psychiatry* 84, 542–545. doi: 10.1016/j.biopsych.2018.02.010

Murdoch, W. J., Singh, C., Kumbier, K., Abbasi-Asl, R., and Yu, B. (2019). Interpretable machine learning: definitions, methods, and applications. *arXiv* [Preprints] Available at: https://ui.adsabs.harvard.edu/abs/2019arXiv190104592M (accessed January 01, 2019).

Nair, J., Nair, S. S., Kashani, J. H., Reid, J. C., Mistry, S. I., and Vargas, V. G. (1999). Analysis of the symptoms of depression–a neural network approach. *Psychiatry Res.* 87, 193–201. doi: 10.1016/s0165-1781(99)00054-2

Nicolelis, M. A., and Lebedev, M. A. (2009). Principles of neural ensemble physiology underlying the operation of brain-machine interfaces. *Nat. Rev. Neurosci.* 10, 530–540. doi: 10.1038/nrn2653

O'Doherty, J. E., Lebedev, M. A., Li, Z., and Nicolelis, M. A. (2012). Virtual active touch using randomly patterned intracortical microstimulation. *IEEE Trans. Neural. Syst. Rehabil. Eng.* 20, 85–93. doi: 10.1109/TNSRE.2011.2166807

Pais-Vieira, M., Chiuffa, G., Lebedev, M., Yadav, A., and Nicolelis, M. A. (2015). Building an organic computing device with multiple interconnected brains. *Sci. Rep.* 5:11869. doi: 10.1038/srep11869

Pearl, J. (2009). *Causality: Models, Reasoning and Inference*. New York, NY: Cambridge University Press.

Podgorelec, V., Kokol, P., Stiglic, B., and Rozman, I. (2002). Decision trees: an overview and their use in medicine. *J. Med. Syst.* 26, 445–463.

Provenza, N. R., Matteson, E. R., Allawala, A. B., Barrios-Anderson, A., Sheth, S. A., Viswanathan, A., et al. (2019). The Case for Adaptive Neuromodulation to Treat Severe Intractable Mental Disorders. *Front. Neurosci.* 13:152. doi: 10.3389/fnins.2019.00152

Ramkumar, P., Dekleva, B., Cooler, S., Miller, L., and Kording, K. (2016). Premotor and motor cortices encode reward. *PLoS One* 11:e0160851. doi: 10.1371/journal.pone.0160851

Rao, R. P. (2019). Towards neural co-processors for the brain: combining decoding and encoding in brain-computer interfaces. *Curr. Opin. Neurobiol.* 55, 142–151. doi: 10.1016/j.conb.2019.03.008

Redish, A. D., and Gordon, J. A. (2016). *Computational Psychiatry : New Perspectives on Mental Illness*. Cambridge, MA: The MIT Press.

Reid, J. C., Nair, S. S., Mistry, S. I., and Beitman, B. D. (1996). Effectiveness of Stages of Change and Adinazolam SR in Panic Disorder: A Neural Network Analysis. *J. Anxiety Disord.* 10, 331–345. doi: 10.1016/0887-6185(96)00014-x

Rosenthal, R. (1979). The file drawer problem and tolerance for null results. *Psychol. Bull.* 86, 638–641. doi: 10.1037/0033-2909.86.3.638

Samek, W., Wiegand, T., and Müller, K.-R. (2017). Explainable artificial intelligence: understanding, visualizing and interpreting deep learning models. *arXiv* [Preprints] Available at: https://ui.adsabs.harvard.edu/abs/2017arXiv170808296S (accessed August 01, 2017).

Sanislow, C. A., Ferrante, M., Pacheco, J., Rudorfer, M. V., and Morris, S. E. (2019). Advancing translational research using NIMH research domain criteria and computational methods. *Neuron* 101, 779–782. doi: 10.1016/j.neuron.2019.02.024

Sarkar, D. (2018). *Effective Visualization of Multi-Dimensional Data — A Hands-on Approach*. Available at: https://medium.com/swlh/effective-visualization-of-multi-dimensional-data-a-hands-on-approach-b48f36a56ee8 (accessed March 12, 2019).

Schultze-Kraft, M., Birman, D., Rusconi, M., Allefeld, C., Gorgen, K., Dahne, S., et al. (2016). The point of no return in vetoing self-initiated movements. *Proc. Natl. Acad. Sci. U.S.A* 113, 1080–1085. doi: 10.1073/pnas.1513569112

Shamir, R. R., Duchin, Y., Kim, J., Patriat, R., Marmor, O., Bergman, H., et al. (2019). Microelectrode recordings validate the clinical visualization of subthalamic-nucleus based on 7T magnetic resonance imaging and machine learning for deep brain stimulation surgery. *Neurosurgery* 84, 749–757. doi: 10.1093/neuros/nyy212

Sheh, R., and Monteath, I. (2017). "Introspectively assessing failures through explainable artificial intelligence," in *Proceedings of the 18th International Conference on Autonomous Agents and MultiAgent Systems*, Montreal QC.

Simm, J., Klambauer, G., Arany, A., Steijaert, M., Wegner, J. K., Gustin, E., et al. (2018). Repurposing high-throughput image assays enables biological activity prediction for drug discovery. *Cell. Chem. Biol.* 25, 611.e3–618.e3. doi: 10.1016/j.chembiol.2018.01.015

Soltanian-Zadeh, S., Sahingur, K., Blau, S., Gong, Y., and Farsiu, S. (2019). Fast and robust active neuron segmentation in two-photon calcium imaging using spatiotemporal deep learning. *Proc. Natl. Acad. Sci. U.S.A.* 116, 8554–8563. doi: 10.1073/pnas.1812995116

Song, F., Parekh-Bhurke, S., Hooper, L., Loke, Y. K., Ryder, J. J., Sutton, A. J., et al. (2009). Extent of publication bias in different categories of research cohorts: a meta-analysis of empirical studies. *BMC Med. Res. Methodol.* 9:79. doi: 10.1186/1471-2288-9-79

Stringer, C., Pachitariu, M., Steinmetz, N., Carandini, M., and Harris, K. D. (2019). High-dimensional geometry of population responses in visual cortex. *Nature* 571, 361–365. doi: 10.1038/s41586-019-1346-5

Tang, Z. Q., Chuang, K. V., Decarli, C., Jin, L. W., Beckett, L., Keiser, M. J., et al. (2019). Interpretable classification of Alzheimer's disease pathologies with a convolutional neural network pipeline. *Nat. Commun.* 10:2173.

Tomsett, R., Braines, D., Harborne, D., Preece, A., and Chakraborty, S. (2018). Interpretable to whom? A role-based model for analyzing interpretable machine learning systems. *arXiv* [Preprints] Available at: https://ui.adsabs.harvard.edu/abs/2018arXiv180607552T (accessed June 01, 2018).

Topol, E. J. (2019). High-performance medicine: the convergence of human and artificial intelligence. *Nat. Med.* 25, 44–56. doi: 10.1038/s41591-018-0300-7

Tulio Ribeiro, M., Singh, S., and Guestrin, C. (2016). "Why Should I Trust You?" Explaining the Predictions of Any Classifier. *arXiv* [Preprints] Available at: https://ui.adsabs.harvard.edu/abs/2016arXiv160204938T (accessed February 01, 2016).

Ustun, B., and Rudin, C. (2016). Supersparse linear integer models for optimized medical scoring systems. *Mach. Learn.* 102, 349–391. doi: 10.1007/s10994-015-5528-6

van der Maaten, L. (2014). Accelerating t-SNE using Tree-Based Algorithms. *J. Mach. Learn. Res.* 15, 3221–3245.

Vu, M. T., Adali, T., Ba, D., Buzsaki, G., Carlson, D., Heller, K., et al. (2018). A shared vision for machine learning in neuroscience. *J. Neurosci.* 38, 1601–1607. doi: 10.1523/JNEUROSCI.0508-17.2018

Waters, A. C., and Mayberg, H. S. (2017). Brain-based biomarkers for the treatment of depression: evolution of an idea. *J. Int. Neuropsychol. Soc.* 23, 870–880. doi: 10.1017/S1355617717000881

Wolpaw, J. R., Birbaumer, N., Mcfarland, D. J., Pfurtscheller, G., and Vaughan, T. M. (2002). Brain-computer interfaces for communication and control. *Clin. Neurophysiol.* 113, 767–791.

Wu, M., Hughes, M. C., Parbhoo, S., Zazzi, M., Roth, V., and Doshi-Velez, F. (2017). Beyond sparsity: tree regularization of deep models for interpretability. *arXiv* [Preprints] Available at: https://ui.adsabs.harvard.edu/abs/2017arXiv171106178W (accessed November 01, 2017).

Yang, S. C.-H., and Shafto, P. (2017). "Explainable artificial intelligence via Bayesian Teaching," in *Proceedings of the Conference on Neural Information Processing Systems*, Long Beach, CA: Long Beach Convention Center.

Yang, Y., Connolly, A. T., and Shanechi, M. M. (2018). A control-theoretic system identification framework and a real-time closed-loop clinical simulation testbed

for electrical brain stimulation. *J. Neural Eng.* 15:066007. doi: 10.1088/1741-2552/aad1a8

Zanzotto, F. M. (2019). Viewpoint: human-in-the-loop artificial intelligence. *J. Artif. Intell. Res.* 64, 243–252. doi: 10.1613/jair.1.11345

Zhang, Q. S., Wu, Y. N., and Zhu, S. C. (2018). "Interpretable convolutional neural networks," in *Proceedings of the 2018 IEEE/Cvf Conference on Computer Vision and Pattern Recognition (CVPR)*, Long Beach, CA, 8827–8836.

Zhou, A., Johnson, B. C., and Muller, R. (2018). Toward true closed-loop neuromodulation: artifact-free recording during stimulation. *Curr. Opin. Neurobiol.* 50, 119–127. doi: 10.1016/j.conb.2018.01.012

Conflict of Interest: The authors declare that the research was conducted in the absence of any commercial or financial relationships that could be construed as a potential conflict of interest.

frontiers in Neuroscience

OPINION
published: 28 February 2020
doi: 10.3389/fnins.2020.00160

Probable Mechanism of Antiepileptic Effect of the Vagus Nerve Stimulation in the Context of the Recent Results in Sleep Research

Ivan N. Pigarev[1]*, *Marina L. Pigareva*[2] and *Ekaterina V. Levichkina*[1,3]

[1] *Institute for Information Transmission Problems (Kharkevich Institute), Russian Academy of Sciences, Moscow, Russia,* [2] *Institute of Higher Nervous Activity and Neurophysiology, Russian Academy of Sciences, Moscow, Russia,* [3] *Department of Optometry and Vision Sciences, The University of Melbourne, Parkville, VIC, Australia*

Keywords: epilepsy, vagus nerve, electric stimulation, antiepileptic effect, visceral theory of sleep

The goal of this article is to discuss the possible contribution to antiepileptic effects of the vagus nerve stimulation (VNS) from the functional connectivity between the cortex and internal organs. According to our previous work, this connectivity is particularly prominent during sleep, the brain state when epileptic activity is prominent, as well. As such, the relationship between the brain and the viscera needs to be put into the equation when considering VNS as a treatment for epilepsy.

Vagus nerve stimulation is widely used as a seizure-preventive action in many types of otherwise incurable epilepsy and is extensively studied for treating other conditions ranging from rheumatoid arthritis to depression (Vonck et al., 2001; Groves and Brown, 2005; Yuan and Silberstein, 2016; Dibue-Adjei et al., 2019; Noller et al., 2019). It is well-known that vagus nerve is engaged in the bidirectional information transfer between the internal organs and the brain, but how changes in activity going along visceral pathways may be related to paroxysmal events occurring in various brain areas remained unclear. The available literature describe several ideas proposed to explain possible seizure preventing action of VNS, which mainly based on molecular mechanisms of synaptic transmission in the central nervous system. Although neuronal desynchronization, hippocampal plasticity, anti-inflammatory immune changes, and changes in neurotransmitter concentrations are all currently considered as possibly involved in its antiepileptic effects (Yuan and Silberstein, 2016), none of the existing theories explains the impressive variety of demonstrated effects of VNS. We are offering for discussion another suggestion, based on the role of the vagus nerve in autonomic regulation and on the recent results of sleep studies.

In this opinion article we do not present any new experimental results, but only aim to provide a possible link between four seemingly unrelated clusters of well-established physiological observations, which, being considered together, might offer new directions for thinking and investigation of VNS mechanisms.

First, there is a well-established connection between epileptic seizures and the state of sleep (e.g., Shouse et al., 1996; Herman et al., 2001; Dinner, 2002; Combi et al., 2004; Pavlova et al., 2004; Durazzo et al., 2008; Hofstra and de Weerd, 2009; Kothare and Kaleyias, 2010; Mirzoev et al., 2012). Ictal activity is generally most frequent in slow-wave sleep and during transition from wakefulness to sleep, but is very rarely present in REM-sleep. Approximately half of all recorded seizures are happening during slow wave sleep while this state occupies less than one third of circadian cycle in humans. In addition, it is highly likely that some seizures happening during sleep may stay undetected. We group these observations in the first cluster of the data.

A second cluster of observations to consider involves another generally recognized feature of many types of epilepsy—the epileptogenic effects of rhythmic stimulations delivered

OPEN ACCESS

Edited by:
Mikhail Lebedev,
Duke University, United States

Reviewed by:
Haiteng Jiang,
Carnegie Mellon University,
United States

****Correspondence:***
Ivan N. Pigarev
pigarev@iitp.ru

Specialty section:
This article was submitted to Neural Technology, a section of the journal Frontiers in Neuroscience

Received: *08 April 2019*
Accepted: *11 February 2020*
Published: *28 February 2020*

Citation:
Pigarev IN, Pigareva ML and Levichkina EV (2020) Probable Mechanism of Antiepileptic Effect of the Vagus Nerve Stimulation in the Context of the Recent Results in Sleep Research. Front. Neurosci. 14:160. doi: 10.3389/fnins.2020.00160

to various sensory systems (see e.g., Kaplan, 2003; Guerrini and Genton, 2004; Hirsch et al., 2004; Michelucci et al., 2004; Wilkins et al., 2004; Parra et al., 2005). Ictal activity provoked by rhythmic exteroceptive stimulation may have similar mechanism to physical resonance systems. Theoretically, any circuit with positive feedback has its own internal resonance frequency. Rhythmic external stimulation, even relatively weak, would initiate strong oscillations if the frequency of this stimulation approaches this resonance frequency. In the nervous system, it would manifest as paroxysmal activity. Neuronal circuits with feedback are common features at all levels of the nervous system, and resonance effects in the nervous system were indeed demonstrated (see e.g., Hutcheon and Yarom, 2000; Herrmann, 2001). In addition, widely accepted mechanism of pathologically elevated excitability in epileptic focus can be a part of this mechanism as it would be able to increase probability of the weak rhythmic afferent signal to reach thresholds for such resonant oscillations.

Resonant model of epileptogenesis implies the presence of two components. The first component is the local neuronal network with positive feedback, which has the fundamental frequency of oscillation and is susceptible to paroxysmal activity. The second component is the rhythmic afferent flow directed to that network that may cause the resonant activation. Neither of these two components can provoke an ictal activity alone.

Anticonvulsant drugs can elevate the activation thresholds of the resonant network, diminishing responses to the afferent signals, but are not able to eliminate the incoming signals driving the network into ictal activity.

It might seem that resonance evoked by afferent inputs cannot be a mechanism of the previously mentioned epileptic activity during sleep. In classical neuroscience paradigm, sleep is considered as the state when brain is sensory deprived and any external rhythmic stimulation is excluded. However, recent sleep studies offer an alternative source of rhythmic sensory afferent signals directed to cerebral cortex, that are not attenuated, but likely to be enhanced during sleep. We previously demonstrated that during sleep cortical sensory areas begin receiving information coming from various visceral organs (Pigarev, 1994, 2013; Pigarev et al., 2013; Pigarev and Pigareva, 2014, 2018). Experiments that demonstrated propagation of the visceral afferent signals to the cerebral cortex during sleep, were performed on gastrointestinal and cardio-respiratory systems, and their work is inherently rhythmical (Pigarev, 1994; Pigarev et al., 2013; Lavrova, 2019; Lavrova et al., 2019). Thus, nervous signals in the involved sensory pathways would be rhythmically organized during sleep. These results of sleep studies comprise the third block of the relevant observations.

Observable rhythmic motility of the visceral organs generally has relatively low frequencies in comparison to frequencies of exteroceptive sensory stimulation reported as epileptogenic (10–50 Hz). However, nervous signals from these organs transferring along the nerves might have another organization in time, and more complicated frequency spectrums. Namely, these nervous signals can interfere with resonant frequencies of different brain regions leading to ictal events. In addition to that, one should remember that not only the exact correspondence of frequencies leads to a resonance, as resonance is possible for both the fundamental frequency and for its harmonics and sub harmonics. Afferent information flow from some internal organs may have frequency pattern close to the resonant frequency of a particular brain circuit susceptible to paroxysmal events. In our opinion, during sleep epileptic activity could be initiated in such area by the rhythmical visceral afferentation, similarly to generation of such events by rhythmical exterosensory stimulation in wakefulness. Indeed, registration of vagal electrical activity during natural sleep in cat demonstrated synchronized appearance of spindle-like activity in vagus itself and in a range of cortical and subcortical regions receiving vagal input (Leichnetz, 1972).

Assuming that in some cases epileptic events are generated in response to resonant frequencies of visceral afferentation, antiepileptic effect of VNS may have a simple explanation. For therapeutic purpose, stimulation usually is applied to the left cervical vagal trunk that contains fibers from the recurrent laryngeal, cardiopulmonary, and subdiaphragmatic vagal branches. At this level, roughly 80% of the vagal fibers are afferent, and 20% are efferent (Krahl, 2012). With such fiber composition, VNS would change the pattern of visceral activity transmitted to the brain by the vagus nerve, and is likely to cause prominent reorganization of activities within the crucial structures receiving vagal afferentation and altering further visceral input, such as nucleus tractus solitarius, parabrachial nucleus, and hypothalamus.

The role of VNS as disrupting the afferent flow to the regions susceptible for convulsive activity is in good accordance with the ability of a surprisingly wide range of frequencies of VNS to reduce epileptic activity. Frequencies from 1 to 143 Hz were used for this purpose, although frequencies above 50 Hz are not recommended in clinical practice as potentially damaging to the vagus nerve itself (for details see Terry, 2014). It was also proposed that stimulation of the afferent vagus nerve fibers can change the fundamental resonant frequencies of the brain circuits itself (Fanselow, 2012).

Furthermore, stimulation of the efferent vagal fibers also alters the frequencies of rhythmically working visceral organs, such as heart, stomach and intestine (e.g., Martinson, 1965; Chang et al., 2003; Osharina et al., 2006; Tong et al., 2010; Bonaz et al., 2016; Frøkjaer et al., 2016). Changes of rhythmicity of the various visceral organs elicited by stimulation of the vagus efferent fibers and altering activity of the visceral organs should modify the frequency composition of the visceral afferent signals coming to the brain areas not only by vagal, but also by spinal cord pathways. All of the changes described above are expected to move visceral afferent frequencies out of the resonance range, thereby blocking paroxysmal activity. These visceral effects of VNS we present as the fourth cluster of the relevant observations.

Taking all the above mentioned into account it seems important to study background spike firing in the vagus nerve during wakefulness and sleep, and the effect of VNS on this firing. The former subject was actually investigated in one study in cat. It was shown that during natural sleep activity in vagus nerve itself and in a range of cortical and subcortical regions receiving vagal input demonstrated spindle-like synchronized

pattern, and prominent amplitude and frequency differences were noted between wakefulness, slow wave and REM sleep states (Leichnetz, 1972). However, the technique used at that time (ink electroencephalography) did not allow observing single spikes and only the integrated power of spike activity was recorded. Nevertheless, the results obtained by Leichnetz revealed that circadian dynamic is indeed present in vagal activity. Ramet et al. (1992) also indirectly observed increased vagal activity during sleep in humans. However, to the best of our knowledge, this topic has not been studied in detail using contemporary techniques. Such studies would be instrumental in finding the optimal parameters of VNS.

This opinion may meet disagreement based on a doubt concerning the increased involvement of the cerebral cortex in the processing of visceral information during sleep. Our view is based on electrophysiological experiments performed in rabbits, cats, and monkeys (see for review, e.g., Pigarev, 2014; Pigarev and Pigareva, 2014). However, results of these studies are not widely known yet, most likely because their subject, being located between three very different disciplines—classical sensory physiology, physiology of the visceral systems and sleep research, usually slips attention of the corresponding three groups of researchers. Recently several independent laboratories started demonstrating similar results. Lecci et al. (2017) found the relationship between slow periodicity in the cortical EEG during sleep and heart rate variability. In experiments combining functional MRI and electrogastroscopy the reflection of slow gastric rhythms in cortical sensory areas was observed in humans (Rebollo et al., 2018). There is also a growing body of evidence pointing to the link between visceral abnormalities and psychiatric disorders. For example, it was proposed that degeneration of cells in the intestinal enteric nervous system might have causal link with the following appearance of Parkinson disease (for a review see e.g., Smith and Parr-Brownlie, 2019). Fatal familiar insomnia syndrome, which leads to progressive inability to sleep, also results in severe autonomic dysfunction finally finishing by death (Lugaresi and Provini, 2007). It is generally believed that insular, orbitofrontal and medial prefrontal areas are directly involved in autonomic regulation (Neafsey, 1990; Ongür et al., 1998; Ongür and Price, 2000; Nieuwenhuys, 2012), but at the same time they are known to take part in regulation of the sleep-wake cycle (Saper et al., 2010; Chen et al., 2016). Significant increase in neuronal activity associated with slow waves during sleep was found in the inferior frontal, medial prefrontal, posterior cingulate areas and the precuneus (Dang-Vu et al., 2008). The overall, it was found that reorganization of the interneuronal connections during wake to sleep transition leads to formation of new cortical neuronal networks (Larson-Prior et al., 2011).

One may argue that VNS is also efficient in wakefulness. Influence of VNS in wakefulness can be understood taking into account that seizures often start in the high order associative cortical areas. It is known that local or partial sleep also starts developing from these cortical areas (Pigarev et al., 1997). According to the visceral theory of sleep (Pigarev and Pigareva, 2014) development of the local sleep in limited parts of the cerebral cortex indicates the onset of visceral information transfer to those cortical areas while behaviorally this state correspond to wakefulness or drowsiness. In addition, it was reported that epileptic attacks often happen during developing drowsiness (Mirzoev et al., 2012).

On the other hand, some cortical areas receiving vagal input, such as the insular cortex, are involved in the processing of visceral information in wakefulness as well. The role of the insular cortex in mediating bodily feelings—"interoceptive awareness"—has been discussed by Craig (Craig, 2011; for a review of the insula functions see Nieuwenhuys, 2012). Thus, rhythmic visceral afferentation definitely reaches insular cortex in wakefulness, and "visceral" mechanism of epileptogenesis may work through the insular network not only during sleep. However, we have recently reported the prevalence of insular neurons responding to non-noxious intestinal electrostimulation in slow wave sleep in comparison to wakefulness (Levichkina and Pigarev, 2016), and it is therefore expected that responses of the insular cortex to VNS can be more prominent in sleep as well.

Finally, it was hypothesized (Morchiladze et al., 2018) that some mental disorders can be associated with pathological chronic inactivation of the mechanisms blocking the propagation of visceral information toward the central nervous system in wakefulness. As a result, these visceral signals could be added to the normal exterosensory information flows as noise, disrupting their normal analysis. If this "noise" has rhythmic structure, it would be able to evoke seizers in a similar way to the exterosensory rhythmic signals.

In the context of the probable role of the visceral rhythmic afferentation in genesis of paroxysmal events it might be important to analyze the noted comorbidity of epilepsy to a number of visceral issues such as gastrointestinal bleed, chronic diseases of cardio- and respiratory systems, pneumonia and diabetes (Gaitatzis et al., 2004). It is not excluded that described positive effect of the ketogenic diet for treatment of epilepsy (e.g., D'Andrea Meira et al., 2019) also can be related to probable change of some rhythms in gastro-intestinal system and consequently of frequencies in the visceral afferent messages in response to the changed food content.

We do not intend to present this "visceral" mechanism of seizure generation and proposed mechanism of VNS antiepileptic effect as the only possibility. Obviously different types of epilepsy are likely to have other mechanisms of seizure initiation. The goal of our comment is to draw attention to the additional factor, which has not been considered yet. Important and unexpected feature of the proposed mechanism is that theoretically paroxysmal activity may start in a healthy brain. A deviation from normal activity of, e.g., organs of the gastro-intestinal or cardio-respiratory systems would lead to an emergence of signals with pathologic frequency composition directed to the central nervous system during sleep, with a possibility to cause epileptic events if these signals happen to be within the resonant ranges of the particular brain circuits. In light of that, it seems reasonable, especially in the pharmacoresistent cases, when no obvious morphological deviations in the brain tissue were found, to consider paying special attention to the visceral state of a patient, and particularly to the visceral systems with clearly rhythmic patterns of activity.

AUTHOR CONTRIBUTIONS

All authors listed have made a substantial, direct and intellectual contribution to the work, and approved it for publication.

FUNDING

This study was partly supported by Russian Foundation for Basic Research grants No. 19-04-00215 and 17-04-00594 A.

REFERENCES

Bonaz, B., Sinniger, V., and Pellissier, S. (2016). Vagal tone: effects on sensitivity, motility, and inflammation. *Neurogastroenterol. Motil.* 28, 455–462. doi: 10.1111/nmo.12817

Chang, H. Y., Mashimo, H., and Goyal, R. K. (2003). Musings on the wanderer: what's new in our understanding of vago-vagal reflex? IV. current concepts of vagal efferent projections to the gut. *Am. J. Physiol. Gastrointest. Liver Physiol.* 284, 357–366. doi: 10.1152/ajpgi.00478.2002

Chen, M. C., Chiang, W. Y., Yugay, T., Patxot, M., Özçivit, I. B., Hu, K., et al. (2016). Anterior insula regulates multiscale temporal organization of sleep and wake activity. *J. Biol. Rhythms*. 31, 182–193. doi: 10.1177/0748730415627035

Combi, R., Dalprà, L., Tenchini, M. L., and Ferini-Strambi, L. (2004). Autosomal dominant nocturnal frontal lobe epilepsy—a critical overview. *J. Neurol.* 251, 923–934. doi: 10.1007/s00415-004-0541-x

Craig, A. D. (2011). Significance of the insula for the evolution of human awareness of feelings from the body. *Ann. N. Y. Acad. Sci.* 1225, 72–82. doi: 10.1111/j.1749-6632.2011.05990.x

D'Andrea Meira, I., Romão, T. T., Pires do Prado, H. J., Krüger, L. T., Pires, M. E. P., and da Conceição, P. O. (2019). Ketogenic diet and epilepsy: what we know so far. *Front. Neurosci.* 13:5. doi: 10.3389/fnins.2019.00005

Dang-Vu, T. T., Schabus, M., Desseilles, M., Albouy, G., Boly, M., Darsaud, A., et al. (2008). Spontaneous neural activity during human slow wave sleep. *Proc. Natl. Acad. Sci. U. S. A.* 105, 15160–15165. doi: 10.1073/pnas.0801819105

Dibue-Adjei, M., Brigo, F., Yamamoto, T., Vonck, K., and Trinka, E. (2019). Vagus nerve stimulation in refractory and super-refractory status epilepticus—a systematic review. *Brain Stimul.* 12, 1101–1110 doi: 10.1016/j.brs.2019.05.011

Dinner, D. S. (2002). Effect of sleep on epilepsy. *J. Clin. Neurophysiol.* 19, 504–513. doi: 10.1097/00004691-200212000-00003

Durazzo, T. S., Spencer, S. S., Duckrow, R. B., Novotny, E. J., Spencer, D. D., and Zaveri, H. P. (2008). Temporal distributions of seizure occurrence from various epileptogenic regions. *Neurology* 70, 1265–1271. doi: 10.1212/01.wnl.0000308938.84918.3f

Fanselow, E. E. (2012). Central mechanisms of cranial nerve stimulation for epilepsy. *Surg. Neurol. Int.* 3(Suppl.4), S247–S254. doi: 10.4103/2152-7806.103014

Frøkjaer, J. B., Bergmann, S., Brock, C., Madzak, A., Farmer, A. D., Ellrich, J., et al. (2016). Modulation of vagal tone enhances gastroduodenal motility and reduces somatic pain sensitivity. *Neurogastroenterol. Motil.* 28, 592–598. doi: 10.1111/nmo.12760

Gaitatzis, A., Carroll, K., Majeed, A., and Sander, J. W. (2004). The epidemiology of the comorbidity of epilepsy in the general population. *Epilepsia* 45, 1613–1622. doi: 10.1111/j.0013-9580.2004.17504.x

Groves, D. A., and Brown, V. J. (2005). Vagal nerve stimulation: a review of its applications and potential mechanisms that mediate its clinical effects. *Neurosci. Biobehav. Rev.* 29, 493–500. doi: 10.1016/j.neubiorev.2005.01.004

Guerrini, R., and Genton, P. (2004). Epileptic syndromes and visually induced seizures. *Epilepsia* 45, 14–18. doi: 10.1111/j.0013-9580.2004.451011.x

Herman, S. T., and Walczak, T. S., Bazil, C. W. (2001). Distribution of partial seizures during the sleep-wake cycle: differences by seizure onset site. *Neurology* 56, 1453–1459. doi: 10.1212/WNL.56.11.1453

Herrmann, C. S. (2001). Human EEG responses to 1–100 Hz flicker: resonance phenomena in visual cortex and their potential correlation to cognitive phenomena. *Exp. Brain Res.* 137, 346–353. doi: 10.1007/s002210100682

Hirsch, L. J., Claassen, J., Mayer, S. A., and Emerson, R. G. (2004). Stimulus-induced rhythmic, periodic, or ictal discharges (SIRPIDs): a common EEG phenomenon in the critically ill. *Epilepsia* 45, 109–123. doi: 10.1111/j.0013-9580.2004.38103.x

Hofstra, W. A., and de Weerd, A. W. (2009). The circadian rhythm and its interaction with human epilepsy: a review of literature. *Sleep Med. Rev.* 13, 413–420. doi: 10.1016/j.smrv.2009.01.002

Hutcheon, B., and Yarom, Y. (2000). Resonance, oscillation and the intrinsic frequency preferences of neurons. *Trends Neurosci.* 23, 216–222. doi: 10.1016/S0166-2236(00)01547-2

Kaplan, P. W. (2003). Musicogenic epilepsy and epileptic music: a seizures song. *Epilepsy Behav.* 4, 464–473. doi: 10.1016/S1525-5050(03)00172-0

Kothare, S. V., and Kaleyias, J. (2010). Sleep and epilepsy in children and adolescents. *Sleep Med.* 11, 674–685. doi: 10.1016/j.sleep.2010.01.012

Krahl, S. E. (2012). Vagus nerve stimulation for epilepsy: a review of the peripheral mechanisms. *Surg. Neurol. Int.* 3(Suppl.S1), 47–52. doi: 10.4103/2152-7806.91610

Larson-Prior, L. J., Power, J. D., Vincent, J. L., Nolan, T. S., Coalson, R. S., Zempel, J., et al. (2011). Modulation of the brain's functional network architecture in the transition from wake to sleep. *Prog. Brain Res.* 193, 277–294. doi: 10.1016/B978-0-444-53839-0.00018-1

Lavrova, V. D. (2019). Heartbeat-related responses of frontal cortical neurons in the sleep-wake cycle in cats. *Sleep Med.* 64:S213. doi: 10.1016/j.sleep.2019.11.594

Lavrova, V. D., Busygina, I. I., and Pigarev, I. N. (2019). Heartbeat-evoked responses on EEG in slow wave sleep in cats. *Sensornie Systemi* 33, 70–76. doi: 10.1134/S0235009219010086

Lecci, S., Fernandez, L. M. J., Weber, F. D., Cardis, R., Chatton, J.-Y., et al. (2017). Coordinated infraslow neural and cardiac oscillations mark fragility and offline periods in mammalian sleep. *Sci. Adv.* 3:e1602026. doi: 10.1126/sciadv.1602026

Leichnetz, G. R. (1972). Relationship of spontaneous vagal activity to wakefulness and sleep in the cat. *Exp. Neurol.* 35, 194–210. doi: 10.1016/0014-4886(72)90069-6

Levichkina, E., and Pigarev, I. N. (2016). "Insula cortical responses to gut stimulation in sleep and wakefulness," in *Abstracts in Proceedings of Australasian Neuroscience Society Annual Scientific Meetings*. (Hobart, TAS).

Lugaresi, E., and Provini, F. (2007). Fatal familial insomnia and agrypnia excitata. *Rev. Neurol. Dis.* 4, 145–152.

Martinson, J. (1965). The effect of graded vagal stimulation on gastric motility, secretion and blood flow in the cat. *Acta Physiol. Scand.* 65, 300–309. doi: 10.1111/j.1748-1716.1965.tb04277.x

Michelucci, R., Gardella, E., de Haan, G.-J., Bisulli, F., Zaniboni, A., Cantalupo, G., et al. (2004). Telephone-induced seizures: a new type of reflex epilepsy. *Epilepsia* 45, 280–283. doi: 10.1111/j.0013-9580.2004.39703.x

Mirzoev, A., Bercovici, E., Stewart, L. S., Cortez, M. A., Snead, O. C. 3rd, and Desrocher, M. (2012). Circadian profiles of focal epileptic seizures: a need for reappraisal. *Seizure* 21, 412–416. doi: 10.1016/j.seizure.2012.03.014

Morchiladze, M. M., Silagadze, T. K., and Silagadze, Z. K. (2018). Visceral theory of sleep and origins of mental disorders. *Med. Hypothests.* 120, 22–27. doi: 10.1016/j.mehy.2018.07.023

Neafsey, E. J. (1990). Prefrontal cortical control of the autonomic nervous system: anatomical and physiological observations. *Prog. Brain Res.* 85, 147–165. doi: 10.1016/S0079-6123(08)62679-5

Nieuwenhuys, R. (2012). The insular cortex: a review. *Prog. Brain Res.* 195, 123–163. doi: 10.1016/B978-0-444-53860-4.00007-6

Noller, C. M., Levine, Y., Urakov, T., Aronson, J., and Nash, M. (2019). Vagus nerve stimulation in rodent models: an overview of technical considerations. *Front. Neurosci.* 13:911. doi: 10.3389/fnins.2019.00911

Ongür, D., An, X., and Price, J. L. (1998). Prefrontal cortical projections to the hypothalamus in macaque monkeys. *J. Comp. Neurol.* 401, 480–505. doi: 10.1002/(SICI)1096-9861(19981130)401:4<480::AID-CNE4>3.0.CO;2-F

Ongür, D., and Price, J. L. (2000). The organization of networks within the orbital and medial prefrontal cortex of rats, monkeys and humans. *Cereb. Cortex*. 10, 206–219. doi: 10.1093/cercor/10.3.206

Osharina, V., Bagaev, V., Wallois, F., and Larnicol, N. (2006). Autonomic response and Fos expression in the NTS following intermittent vagal stimulation: importance of pulse frequency. *Auton. Neurosci.* 126–127, 72–80. doi: 10.1016/j.autneu.2006.03.011

Parra, J., Kalitzin, S. N., and Lopes da Silva, F. H. (2005). Photosensitivity and visually induced seizures. *Curr. Opin. Neurol.* 18, 155–159. doi: 10.1097/01.wco.0000162857.52520.68

Pavlova, M. K., Shea, S. A., and Bromfield, E. B. (2004). Day/night patterns of focal seizures. *Epilepsy Behav.* 5, 44–49. doi: 10.1016/j.yebeh.2003.10.013

Pigarev, I. N. (1994). Neurons of visual cortex respond to visceral stimulation during slow wave sleep. *Neuroscience* 62, 1237–1243. doi: 10.1016/0306-4522(94)90355-7

Pigarev, I. N. (2013). The visceral theory of sleep. *Zh. Vyssh. Nervn. Deyat. Im. IP. Pavlova* 63, 86–104.

Pigarev, I. N. (2014). The visceral theory of sleep. *Neurosci. Behav. Physiol.* 44, 421–434. doi: 10.1007/s11055-014-9928-z

Pigarev, I. N., Bagaev, V. A., Levichkina, E. V., Fedorov, G. O., and Busigina, I. I. (2013). Cortical visual areas process intestinal information during slow-wave sleep. *Neurogastroenterol. Motil.* 25, 268–275. doi: 10.1111/nmo.12052

Pigarev, I. N., Nothdurft, H. C., and Kastner, S. (1997). Evidence for asynchronous development of sleep in cortical areas. *Neuroreport* 8, 2557–2560. doi: 10.1097/00001756-199707280-00027

Pigarev, I. N., and Pigareva, M. L. (2014). Partial sleep in the context of augmentation of brain function. *Front. Syst. Neurosci.* 8:75. doi: 10.3389/fnsys.2014.00075

Pigarev, I. N., and Pigareva, M. L. (2018). Therapeutic effects of electrical stimulation: interpretations and predictions based on the visceral theory of sleep. *Front. Neurosci.* 12:65. doi: 10.3389/fnins.2018.00065

Ramet, J., Hauser, B., Waldura, J., and De Prins, J. (1992). Circadian rhythm of cardiac responses to vagal stimulation tests. *Pediatr. Neurol.* 8, 91–96 doi: 10.1016/0887-8994(92)90027-V

Rebollo, I., Devauchelle, A.-D., Béranger, B., and Tallon- Baudry, C. (2018). Stomach-brain synchrony reveals a novel, delayed-connectivity resting-state network in humans. *Elife* 7:e33321 doi: 10.7554/eLife.33321.023

Saper, C. B., Fuller, P. M., Pedersen, N. P., Lu, J., and Scammell, T. E. (2010). Sleep state switching. *Neuron* 68, 1023–1042. doi: 10.1016/j.neuron.2010.11.032

Shouse, M. N., da Silva, A. M., and Sammaritano, M. (1996). Circadian rhythm, sleep, and epilepsy. *J. Clin. Neurophysiol.* 13, 32–50. doi: 10.1097/00004691-199601000-00004

Smith, L. M., and Parr-Brownlie, L. C. (2019). A neuroscience perspective of the gut theory of parkinson's disease. *Eur. J. Neurosci.* 49, 817–823. doi: 10.1111/ejn.13869

Terry, R. S. (2014). "Vagus nerve stimulation therapy for epilepsy," in *Epilepsy Topics,* eds D. Mark and Holmes (IntechOpen). doi: 10.5772/58332

Tong, V. D., Ridolfi, T. J., Kosinski, L., Ludvig, K., and Takahashi, T. (2010). Effects of autonomic nerve stimulation on colorectal motility in rats. *Neurogastroenterol. Motil.* 22, 688–693. doi: 10.1111/j.1365-2982.2009.01461.x

Vonck, K., Van Laere, K., Dedeurwaerdere, S., Caemaert, J., de Reuck, J., and Paul Boon, P. (2001). The mechanism of action of vagus nerve stimulation for refractory epilepsy. *J. Clin. Neurophysiol.* 18, 394–401. doi: 10.1097/00004691-200109000-00002

Wilkins, A. J., Bonanni, P., Porciatti, V., and Guerrini, R. (2004). Physiology of human photosensitivity. *Epilepsia* 45, 7–13. doi: 10.1111/j.0013-9580.2004.451009.x

Yuan, H., and Silberstein, S. D. (2016). Vagus nerve and vagus nerve stimulation, a comprehensive review: part III. *Headache* 56, 479–490. doi: 10.1111/head.12649

Conflict of Interest: The authors declare that the research was conducted in the absence of any commercial or financial relationships that could be construed as a potential conflict of interest.

frontiers in Neuroscience

ORIGINAL RESEARCH
published: 27 March 2020
doi: 10.3389/fnins.2020.00237

Predicting Long-Term After-Effects of Theta-Burst Stimulation on Supplementary Motor Network Through One-Session Response

Gong-Jun Ji[1†], Jinmei Sun[1,2,3,4†], Pingping Liu[1,3,4], Junjie Wei[1,3,4], Dandan Li[1,3,4], Xingqi Wu[1,3,4], Lei Zhang[2,3,4], Fengqiong Yu[2,3,4], Tongjian Bai[1,3,4], Chunyan Zhu[2,3,4], Yanghua Tian[1,3,4] and Kai Wang[1,2,3,4]*

[1] Department of Neurology, The First Affiliated Hospital of Anhui Medical University, Hefei, China, [2] Department of Medical Psychology, Chaohu Clinical Medical College, Anhui Medical University, Hefei, China, [3] Anhui Province Key Laboratory of Cognition and Neuropsychiatric Disorders, Hefei, China, [4] Collaborative Innovation Centre of Neuropsychiatric Disorder and Mental Health, Hefei, China

To understand the neural mechanism of repetitive transcranial magnetic stimulation (rTMS), the after-effects following one session or multiple days of stimulation have been widely investigated. However, the relation between the short-term effect (STE) and long-term effect (LTE) of rTMS is largely unknown. This study aims to explore whether the after-effects of 5-day rTMS on supplementary motor area (SMA) network could be predicted by one-session response. A primary cohort of 38 healthy participants underwent five daily sessions of real or sham continuous theta-burst stimulation (cTBS) on the left SMA. Resting-state functional magnetic resonance imaging (fMRI) data were acquired at the first (before and after the first stimulation) and sixth experimental day. The SMA connectivity changes after the first cTBS and after 5 days of stimulation were defined as STE and LTE, respectively. Compared to the baseline, significant STE and LTE were found in the bilateral paracentral gyrus (ParaCG) after real stimulation, suggesting shared neural correlates of short- and long-term stimulations. Region-of-interest analysis indicated that the resting-state functional connectivity between SMA and ParaCG increased after real stimulation, while no significant change was found after sham stimulation. Leave-one-out cross-validation indicated that the LTE in ParaCG could be predicted by the STE after real but not sham stimulations. In an independent cohort, the after-effects of rTMS on ParaCG and short- to long-term prediction were reproduced at the region-of-interest level. These imaging evidences indicate that one-session rTMS can aid to predict the regions responsive to long-term stimulation and the individualized response degree.

Keywords: continuous theta-burst stimulation, functional connectivity, magnetic resonance imaging, transcranial magnetic stimulation, supplementary motor area

OPEN ACCESS

Edited by:
Giovanni Mirabella, University of Brescia, Italy

Reviewed by:
Emilio Chiappini, University of Vienna, Austria
Lorenzo Rocchi, University College London, United Kingdom

****Correspondence:***
Kai Wang
wangkai1964@126.com;
jigongjun@163.com

† These authors have contributed equally to this work

Specialty section:
This article was submitted to Neural Technology, a section of the journal Frontiers in Neuroscience

Received: *07 November 2019*
Accepted: *03 March 2020*
Published: *27 March 2020*

Citation:
Ji G-J, Sun J, Liu P, Wei J, Li D, Wu X, Zhang L, Yu F, Bai T, Zhu C, Tian Y and Wang K (2020) Predicting Long-Term After-Effects of Theta-Burst Stimulation on Supplementary Motor Network Through One-Session Response. Front. Neurosci. 14:237. doi: 10.3389/fnins.2020.00237

INTRODUCTION

Repetitive transcranial magnetic stimulation (rTMS) is a powerful technique that could non-invasively modulate neural activity in human brain (Allen et al., 2007). It has been widely used to map brain function of healthy subjects or alleviate clinical symptoms for neuropsychological patients. However, high variability of rTMS after-effects has also been reported in both

neuroscientific and clinical studies (Hamada et al., 2013; Yesavage et al., 2018). For instance, although continuous theta-burst stimulation (cTBS) was initially proposed as an inhibitory protocol (Huang et al., 2005), a study with a larger sample size (n = 52) indicated that only 42% subjects respond to the stimulation as expected (Hamada et al., 2013). But notably, the variability may change with the readout measures. Electroencephalography might represent a more thorough reflection of cortical excitability than motor evoked potentials (MEP) (Rocchi et al., 2018). Consistent with this variability in healthy subjects, another study observed that less than half of patients with major depression could achieve symptom remission after days of rTMS treatment (Yesavage et al., 2018). Here, we defined the after-effects induced by days of rTMS as long-term effect (LTE). Before rTMS could be recommended as a conventional therapy, more investigations are required to elucidate the neural mechanism and individualized after-effect prediction.

Based on the Faraday's law of electromagnetic induction, TMS could induce an electrical field in the underlying brain tissues by generating a strong time-varying magnetic field. This electrical field drives currents in the cortical surface directly modulating electrical neuronal activation (Neggers et al., 2015). At the macro "neural systems" level, neuroimaging studies indicated that rTMS-induced effect can influence the activity of brain regions distant to the stimulation target (Valchev et al., 2015, 2016; Ji et al., 2017), suggesting a network mechanism (Bestmann and Feredoes, 2013; Sale et al., 2015; Hallett et al., 2017). By mapping whole-brain activity with high spatial resolution, functional magnetic resonance imaging (fMRI) provides a powerful approach to investigate rTMS effect in a network perspective (Sale et al., 2015; Bergmann et al., 2016). For brain disorders, the therapeutic mechanism of rTMS could be directly elucidated by comparing fMRI data before and after treatment. However, this paradigm requires a good combination of scientific and clinical resources. Alternatively, more studies turned to indirectly infer the treatment mechanism by assessing one-session rTMS effect on brain function. For instance, in a study on Parkinson's disease (PD), meta-analysis on random control trials (RCTs) indicated that inhibitory rTMS on supplementary motor area (SMA) may improve the motor symptoms (Chou et al., 2015), but few fMRI studies investigated the functional changes after clinical treatment. On the contrary, numerous studies focused on the after-effects of one-session rTMS on motor network (Reithler et al., 2011; Di Lazzaro and Rothwell, 2014; Ji et al., 2017), which could be termed as short-term effect (STE). For instance, resting-state fMRI (RS-fMRI) study indicated that cTBS significantly decreased the functional connectivity of SMA target (Ji et al., 2017). Nevertheless, it is largely unknown whether this STE could be used to predict LTE, which is critical to bridge the findings of basic neuroscience and clinic treatment.

Although both STE and LTE indicated high inter-individual variability, few studies directly compared them. Using fMRI and MEP, Nettekoven et al. (2015) found that individuals who did not respond to one-session stimulation cannot be transformed into responders by increasing stimulation dose. In this study, we hypothesized that the responsiveness to rTMS is a reflection of the participant's inherent and reliable traits (Hinder et al., 2014), and the LTE can be inferred from STE. To test this hypothesis, this study collected two resting-state fMRI datasets after one-session and 5 consecutive days of stimulations on the left SMA, respectively. We selected SMA as target because of its critical role in movement control. It was a potential effective rTMS target for alleviating symptoms of movement disorders (Shirota et al., 2013; Fox et al., 2014). We predicted that STE and LTE in SMA network have similar spatial distribution, and the LTE in functional connectivity could be individually predicted by their STE. Furthermore, independent data were collected to show the reproducibility of the relation between STE and LTE.

MATERIALS AND METHODS

Subjects

A total of 54 participants without any neurological or psychiatric diseases were initially recruited in this study. Ultimately, 33 and 16 subjects completed the primary and secondary experiments, respectively. This study protocol was reviewed and approved by the Medical Ethics Committee of Anhui Medical University. All participants provided informed, written consent.

Study Design

The primary experiment was designed as a single-blinded and between-subjects-based study (**Figure 1**). The participants were randomly assigned to real (n = 16) or sham (n = 17) groups, receiving cTBS for 5 days. At the first experiment day, one (T1) and two RS-fMRI (T2 and T3) sessions were performed before and after cTBS, respectively. STE would be estimated by comparing the data of T2/T3 to T1, while the LTE was estimated by comparing the RS-fMRI data at the sixth experiment day (T4) to T1. Structure images were acquired at the first and sixth experiment day as well. After 4 to 5 months, resting-state functional and structural images were collected to show the follow-up changes.

The second experiment was designed to reproduce the findings of the primary experiment. All participants (n = 16) received real cTBS for 5 consecutive days. Imaging data were acquired using the same parameters as the primary experiment.

Neuronavigated Transcranial Magnetic Stimulation

Transcranial magnetic stimulation was performed using a MagStim Rapid^2 stimulator (Magstim Company Ltd.) with a 70-mm air-cooled figure-of-eight coil. High-resolution anatomical images were acquired in the sagittal orientation using a three-dimensional brain-volume sequence (repetition/echo time, 8.16/3.18 ms; flip angle, 12°; field of view, 256 mm × 256 mm; 256 × 256 matrix; section thickness, 1 mm, without intersection gap; voxel size, 1 mm × 1 mm × 1 mm; 188 sections) for neuronavigation. The left SMA was defined as the target in the current study because of its potential in rTMS treatment for movement disorders (Le et al., 2013; Shirota et al., 2013; Chou et al., 2015; Eggers et al., 2015;

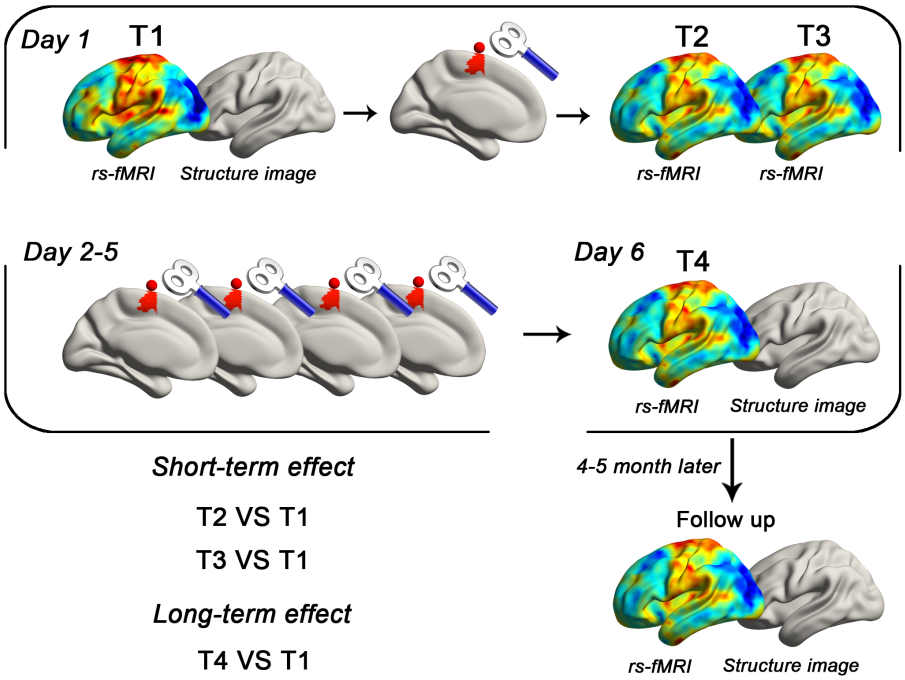

FIGURE 1 | Schematic of the primary experiment. Using a between-subject design, each subject received real or sham cTBS for 5 consecutive days. The target area was defined as the superficial central point (MNI coordinates: −6, −6, 77; radius = 6 mm) of the left SMA proper in the Automated Anatomical Labeling template. RS-fMRI data were collected in five time points (T1, T2, T3, T4, and follow-up). T1 images were also obtained in the first and sixth day.

Landeros-Weisenberger et al., 2015). A spherical image centered at the superficial central point (MNI coordinates: -6, -6, 77; radius = 6 mm) of the left SMA proper was transformed into each subject's individual space by SPM12[1] and TMStarget software (Ji et al., 2017). Then, the individualized target was imported into a frameless neuronavigation system (Brainsight; Rogue Research, Montreal, Canada). The coil was maintained horizontally pointing leftward, with the center of the coil positioned over the target (Zenon et al., 2015; Ji et al., 2017).

The cTBS protocol lasted 40 s and consisted of a burst of three pulses delivered at 50 Hz, which was repeated every 200 ms (at 5 Hz) for a total of 600 pulses. This 40-s protocol was repeated three times (1800 pulses in total) with two 15-min breaks (controlled by a stopwatch) (Nettekoven et al., 2014; Ji et al., 2017; Chen et al., 2018). cTBS was performed in a triple way to achieve accumulative after-effects (Nettekoven et al., 2014). Pulses were delivered at 70% of the resting motor threshold (RMT) (Nettekoven et al., 2014) that was defined as the lowest-intensity evoking MEP amplitudes of the first dorsal interosseus (>50 μV) in more than 5 of 10 consecutive trials. During RMT test, the coil was held approximately at a 45° angle away from the midline with the handle pointing backward and laterally. The electromyography signal was recorded using Ag/AgCl surface electrodes, amplified, digitized, and displayed by the Rogue EMG device.

[1]www.fil.ion.ucl.ac.uk/spm

Participants in the sham group received the same rTMS protocol and duration as the real rTMS group. The only difference was the usage of a sham coil (Magstim Company Ltd.) that produced a similar feeling on the participant's scalp as the real coil but did not induce a current in the cortex. To assess the integrity of blinding, subjects were asked which intervention they had received at T4.

RS-fMRI Data Acquisition

All MRI datasets were obtained at University of Science and Technology of China with a 3-T scanner (Discovery 750; GE Healthcare, Milwaukee, WI, United States). Foam padding and earplugs were applied to minimize head motion and scanner noise for all subjects. Participants were instructed to rest with their eyes closed without falling asleep during resting-state fMRI scanning. Functional images (217 volumes) were acquired using a single-shot gradient-recalled echo planar imaging sequence (repetition/echo time, 2400/30 ms; flip angle, 90°). Images of 46 transverse sections (field of view, 192 mm × 192 mm; 64 × 64 in-plane matrix; section thickness without intersection gap, 3 mm; voxel size, 3 mm × 3 mm × 3 mm) were acquired parallel to the anteroposterior commissure line. Each subject received MRI scanning for five times (T1, T2, T3, T4, and follow up). In the first experiment day, the stimulation and scanning (T1, T2, and T3) were performed in the morning. Immediately after stimulation, subjects were pushed into the MRI room for T2 and T3 by a compatible wheeled stretcher. The transfer time was recorded using a stopwatch.

RS-fMRI Data Processing

Functional images were processed using the DPARSF[2] (Chao-Gan and Yu-Feng, 2010), TMStarget[3], REST[4] (Song et al., 2011), and SPM12[5]. For preprocessing, we deleted the first five functional volumes, and then performed slice timing and realignment for the rest of the images. Structural images were then co-registered with these preprocessed functional images, and segmented into GM, WM, and cerebrospinal fluid (CSF) by Diffeomorphic Anatomical Registrations through Exponentiated Lie Algebra (DARTEL) (Ashburner, 2007). Normalized functional images were smoothed with a 4-mm full-width at half-maximum isotropic Gaussian kernel. Sources of spurious variance from each voxel's time series were removed by (a) filtering temporal bandpass (0.01–0.1 Hz) and (b) regressing out nuisance signals including 24 head-motion parameters, and mean signals in the whole brain, white matter, and CSF. No subject had head motion exceeding 3 mm of translation or 3° of rotation during the fMRI acquisition.

STATISTICAL ANALYSIS

Group-Level rTMS After-Effects

The SMA network was defined by performing a seed-to-whole-brain functional connectivity analysis. The seed was the rTMS target in the left SMA (MNI coordinates −6, −6, 77; radius = 6 mm). Positive correlations were converted to z scores using the Fisher r-to-z transformation and tested by the one-sample t test. Both real and sham groups were included for producing between-group comparison mask. Specifically, we conducted one-sample t tests for each group (four conditions in total). Voxels that survived either test (uncorrected voxel level $P < 0.05$) were included as mask for between-group comparisons (paired t tests). This comparison was performed through a toolbox in SPM12, Statistic non-Parametric Mapping (SnPM) (Nichols and Holmes, 2002). To control the family-wise error (FWE) in multiple comparisons, we first set a voxel level threshold $P < 0.01$. Then, only clusters larger than a given volume would be reported as having survived the cluster-level correction, $P_{corr} < 0.05$.

Individualized LTE Prediction

The predicting value of STE for LTE was estimated by leave-one-out cross-validation. Briefly, we sequentially selected one subject as a test, and the others as training data. In the training data, resting-state functional connectivity (RSFC) changes of the target (i.e., STE) were estimated by comparing the post- and pre-rTMS conditions. Voxels with significant STE ($P_{corr} < 0.05$) were defined as ROIs. RSFC alterations in these ROIs were correlated between short-term (T2/T3 minus T1) and long-term (T4 minus T1) conditions. Based on the information of the voxel with the highest correlation coefficient, a linear function between STE and LTE could be established. Then, predicted LTE of the test subject could be computed through the function and STE. Finally, Pearson's correlation was performed between the real and predicted LTE across subjects.

[2]http://rfmri.org/DPARSF

[3]http://www.brainhealthy.net

[4]www.restfmri.net

[5]http://www.fil.ion.ucl.ac.uk/spm

RESULTS

Characteristics of Participants

Five measures (age, gender, education, RMT, and interval) at baseline were compared within the primary cohort (real vs. sham), and no significant difference was found (**Table 1**). The interval refers to the period from the end of cTBS to the beginning of fMRI scanning at the first experiment day. These measures were also compared between the real groups of the primary and secondary cohorts. No significant difference was found either (**Table 1**).

In the primary cohort, around half of the participants in the real (50%, 8 in 16) and sham (41%, 7 in 17) group correctly guessed which group they belong to (*Fisher's* exact test, $P = 0.73$). This ratio in the second cohort is 41% (7 in 17), similar to the real group in the primary cohort (*Fisher's* exact test, $P = 0.72$).

Group-Level After-Effects in the Primary Cohort

To show the SLE and LTE, we firstly analyzed the after-effects of rTMS at T2, T3, and T4, respectively. Compared to the pre-rTMS state (T1), the real group showed decreased RSFC in the bilateral cerebellum at T2 (**Table 2** and **Figures 2A,B**), and increased RSFC in the bilateral paracentral gyrus (ParaCG) at T3 and T4 (**Table 2** and **Figures 2A,B**). The Dice value for clusters at T3 and T4 was 0.4 (**Figure 2C**). Notably, the peak voxel in T4 was significant at T3 ($t = 4.03$, $P = 0.001$), and vice versa ($t = 2.11$, $P = 0.05$).

The aim of this study was to predict LTE. To this end, we should first demonstrate that the findings in T4 were not induced by placebo effect. Although no significant functional alteration was found in sham group at T4, a direct real-sham comparison was still necessary. This was performed in both voxel and ROI level.

The voxel-wise ANOVA showed significant interaction effect (group [real and sham] by time [T1 and T4]) within significant regions at T4 in the real group. A significant RSFC increase was found in the real group, but not the sham group (see **Supplementary Material**).

For ROI-level analysis, a sphere ROI at the ParaCG (centered at the peak voxel at T4, radius = 3 mm) was used for the following sham-control analyses. We compared the RSFC of ParaCG ROI between real and sham groups at four time points (T1, T3, T4, and follow-up) using two-way ANOVA. Main effect was significant for time ($F = 4.51$, $P < 0.01$) but not group ($F = 0.72$, $P = 0.40$). Interaction effect between group and time was significant ($F = 4.67$, $P = 0.004$). Compared to the baseline at T1, a higher RSFC between the ParaCG ROI and SMA was found at T3 ($t = 4.61$, $P < 0.0001$), T4 (T1, $t = 2.85$, $P = 0.005$), but not follow-up ($t = 1.17$, $P = 0.25$) in the real group (**Figure 3A**). No significant changes were found in the sham group (T3 vs. T1,

TABLE 1 | Characteristics of participants in the primary and second cohorts.

	Primary cohort			Second cohort	
	Real (*n* = 16)	**Sham (*n* = 17)**	**Statistics/*P* [a]**	**Real (*n* = 16)**	**Statistics/*P*[b]**
Age (years)	21.6 ± 0.48	20.9 ± 0.71	0.78/0.44[c]	20.4 ± 0.51	1.68/0.10[c]
Gender (male/female)	6/10	11/6	0.17[d]	11/5	0.16[d]
Education (years)	15.4 ± 0.52	14.5 ± 0.50	1.25/0.22[c]	14.7 ± 0.44	1.09/0.28[c]
RMT (%)	58.4 ± 1.58	59.4 ± 1.26	0.49/0.63	58.4 ± 1.94	0.0/>0.99[c]
Interval [e]	192.9 ± 5.42	194.9 ± 7.16	0.22/0.83[c]	193.2 ± 2.72	0.052/0.96[c]
Follow-up (days)	140.1 ± 4.61	138.8 ± 4.33	0.20/0.85[c]	133.4 ± 2.87	1.23/0.23[c]

Data are represented as mean ± SEM. [a]The analysis was performed between the two groups of the primary cohort. [b]The analysis was performed between the real groups of the primary and secondary cohorts. [c]Two-sample t test. [d]Fisher's exact test. [e]Interval depicts the period from the end of cTBS to the beginning of functional MRI scanning at the first experiment day.

TABLE 2 | Functional connectivity alterations after real cTBS in the primary cohort.

Contrast	Brain regions	MNI coordinates	Brodmann area	Voxel number	Peak *t* value
T2 vs. T1	Cere B.	15 -75 -18	–	128	5.55
T3 vs. T1	ParaCG B.	-15 -15 72	4	410	6.36
T4 vs. T1	ParaCG B.	9 -21 72	4	126	4.91

Cere B., bilateral cerebellum; MNI, Montreal Neurological Institute; ParaCG B., bilateral paracentral gyrus.

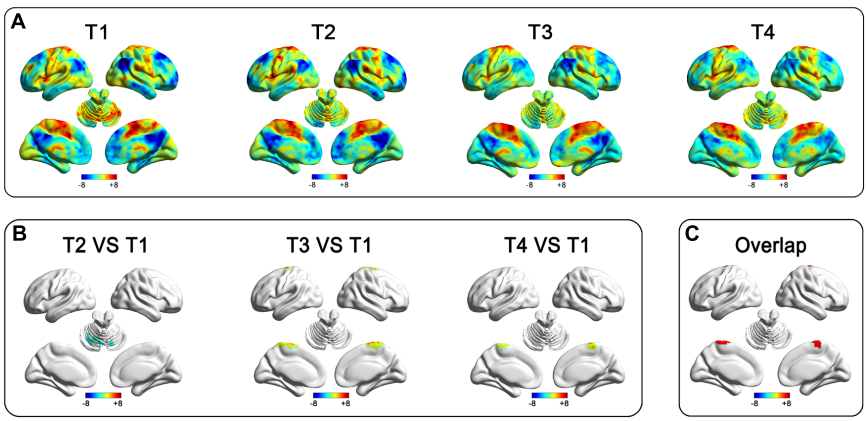

FIGURE 2 | After-effect of rTMS on functional connectivity in the real group of the primary cohort. Functional connectivity patterns of the target (left SMA) before and after stimulation **(A)**. Functional connectivity decreased in the bilateral cerebellum at T2 and increased in the bilateral paracentral gyrus at T3 and T4 after stimulation **(B)**. The rTMS after-effect at T3 and T4 have a spatial overlap at the bilateral ParaCG **(C)**.

$t = 0.51$, $P = 0.61$; T4 vs. T1, $t = 0.09$, $P = 0.93$; follow up vs. T1, $t = 1.46$, $P = 0.15$; **Figure 3B**).

Individual After-Effect Prediction in the Primary Cohort

The after-effect at T3 and T4 spatially overlapped at the bilateral ParaCG (**Figure 2C**), suggesting that STE and LTE have similar regions in responding. To predict the individualized RSFC changes at the T4, leave-one-out cross-validation was used. At each time of leave-one-out, a significant cluster at ParaCG was identified (T3 vs. T1, cluster level $P_{corr} < 0.05$). The linear function between STE and LTE in this cluster was used to predict LTE of the test subject. Correlation analysis indicated that the predicted LTE values were positively correlated with the real values ($r = 0.81$, $P = 0.0001$; **Figure 3A**).

Since voxel-level analysis for the sham group did not show significant RSFC change at T3 or T4 (cluster level $P_{corr} < 0.05$), the leave-one-out prediction was performed with predefined ParaCG ROI from the real group. The predicted and real LTE did not show significant correlation ($r = 0.38$, $P = 0.14$; **Figure 3B**).

Independent Validation

For the analysis of the primary cohort, we compared the SMA-to-whole brain RSFC between post- and pre-rTMS conditions. Neither T3 nor T4 showed significant alteration at the voxel level (cluster level $P_{corr} < 0.05$). However, analysis on the ParaCG ROI (from the primary cohort) indicated significant findings. As

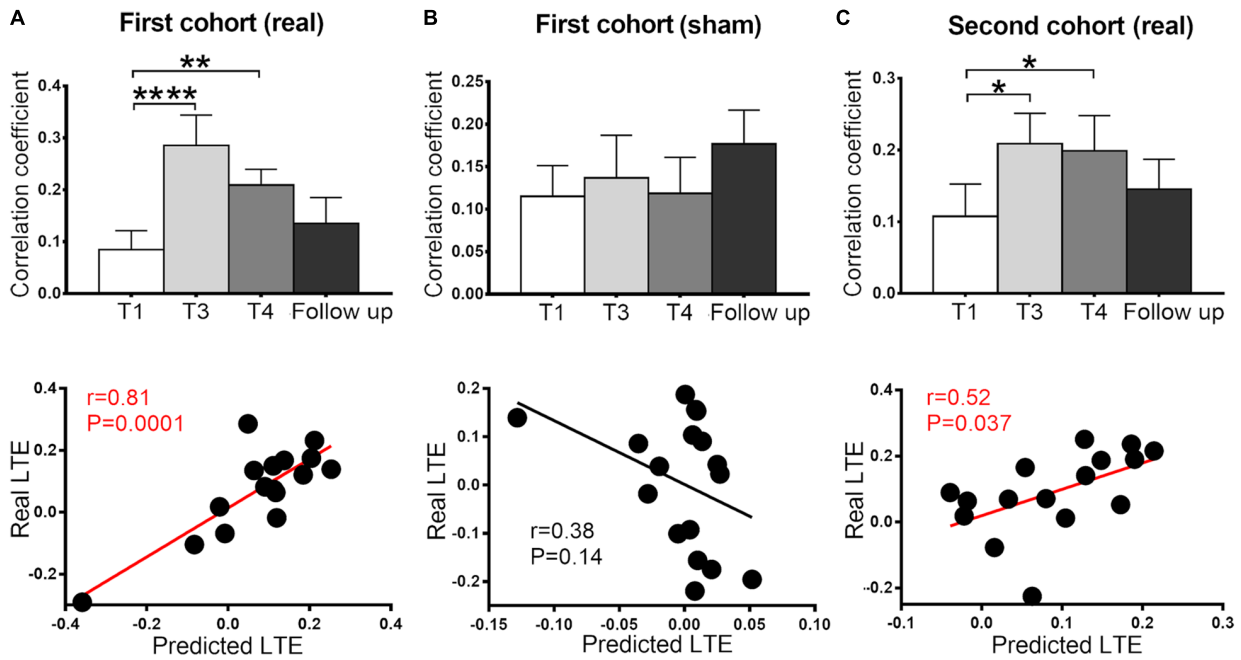

FIGURE 3 | Functional connectivity between SMA and ParaCG at four time points (T1, T3, T4, and follow-up) and cross-time prediction in the two cohorts. In the primary cohort, the connectivity significantly increased at T3 and T4 in the real **(A)** but not sham **(B)** group. This alteration was reproduced in the second cohort **(C)**. No significant difference was found between the baseline and follow-up in all three groups. The predicted LTE was positively correlated with the real values in real groups **(A,C)**, but not sham group **(B)**. Error bars indicate SEM. *$P < 0.05$, **$P < 0.01$, and ****$P < 0.0001$. None of the values were outliers that exceeded three standard deviations of the mean.

compared to T1, RSFC of the ParaCG was significantly higher in T3 ($t = 2.64$, $P = 0.02$) and T4 ($t = 2.93$, $P = 0.01$), but not in the follow up ($t = 1.02$, $P = 0.32$). By leave-one-out approach, we computed the predicted RSFC value of ParaCG in each subject. Correlation analysis indicated a positive correlation between predicted and real LTE in this second cohort ($r = 0.52$, $P = 0.037$) (**Figure 3C**).

DISCUSSION

To investigate the association between the after-effects of short- and long-term rTMS, this study collected resting-state fMRI data for participants around one-session and 5 days of rTMS. In the primary cohort, we found that both short- and long-term stimulations increased the RSFC between the SMA target and bilateral ParaCG. Leave-one-out cross-validation indicated that the LTE predicted by STE was significantly correlated with the real values. These findings were not significant in the sham group, but reproduced in the validation cohort receiving real rTMS. In summary, this study suggests that the region responsive to long-term rTMS and the individualized response degree could be predicted by that of one-session stimulation.

Group-Level After-Effects

Functional MRI studies for TMS could be roughly categorized into three classes that focused on immediate (Chen et al., 2013), short-term (Ji et al., 2017), and long-term (Chen et al., 2018) after-effects, respectively. Interleaved TMS and fMRI acquisition could reveal the immediate after-effect seconds after stimulations. By this approach, Vink et al. (2018) found that stimulations of the dorsal prefrontal cortex could trigger the activity of subgenual anterior cingulate cortex, which is a critical region in rTMS treatment for depression (Fox et al., 2012). It suggests that immediate effect of TMS may explain the mechanism of long-term treatment.

Here, we directly associated the short- and long-term after-effects of rTMS on SMA network. Using the same cTBS sequence, a previous study identified decreased RSFC in the inferior frontal gyrus and SMA regions (Ji et al., 2017), while the current study found increased RSFC in the ParaCG. Two factors may explain this discrepancy in STE. Firstly, the current study overcame previous limitations. All participants were transferred into the MRI room by an MRI-compatible wheeled stretcher to avoid movement-induced interference. Secondly, the interval between rTMS and fMRI scanning is 5.1 min in a previous study (Ji et al., 2017), while that in the current study, it is 3.2 and 11.9 min for T2 and T3, respectively. Different response patterns among these three intervals implicate that nodes in the target network may have distinct response time to rTMS.

Similar to the STE, increased RSFC was found at the ParaCG after 5 days of active stimulation. This cross-time similarity in response region is consistent to the findings on immediate and long-term after-effects (Vink et al., 2018) and may be helpful in developing clinical therapies. The gold standard for novel treatment usually requires long-term clinical trial with large

samples. This is a resource-intensive approach for demonstrating novel rTMS protocols. Although this step cannot be omitted before clinical application, our findings suggest that a simple test for the STE may screen out protocols with effective LTE. More specifically, the STE of novel rTMS protocols may predict whether their long-term application could restore the RSFC biomarker and ultimately alter clinical symptoms. Our follow-up findings indicated that the LTE in RSFC changes was transient and decreased to baseline a few months later. Further studies are required to show the shortest washout period of long-term rTMS.

Individual Prediction

Although rTMS protocols may stably increase or decrease the neural excitability at the group level, high variability of the after-effect was also reported across subjects (Hamada et al., 2013; Yesavage et al., 2018). In these studies, MEP is frequently used as a readout measure. However, MEP was also affected by factors except cortical excitability, such as spinal motoneuron excitability. In contrast, measures originated from cortices may be a better readout than MEP, such as EEG and fMRI (Rocchi et al., 2018). In this study, we associated the STE and LTE using functional connectivity. By leave-one-out cross-validation, we found a significantly positive correlation between STE and LTE in the real group, but not the sham group. Given the poor reproducibility of most neuroimaging findings (Eklund et al., 2016), we additionally performed the prediction analysis in an independent cohort. The correlation between predicted and real LTE was well reproduced. This positive prediction is consistent to previous findings that the responsiveness of subjects to rTMS is similar between one and three sessions of TBS (Nettekoven et al., 2015). This within-subject consistency may be explained by the stability of the interneuron networks that were recruited during stimulation (Hamada et al., 2013). Thus, these neuroimaging findings may be generalized to clinical prediction. The symptom improvement after long-term rTMS therapy may be inferred at the beginning of treatment, such as the response to the first stimulation session.

Limitations

Several limitations of the current study should be noted. Firstly, this is a neuroimaging study without behavior estimation. It would be interesting to investigate which kind of motor ability would be modulated with the RSFC alteration. Secondly, the rTMS after-effect in the primary cohort was validated in the second cohort by ROI-based analysis but not voxel-wise comparison. This is probably related to the small sample size and high after-effect variability between subjects (Nettekoven et al., 2015). Larger sample size is necessary to clarify the baseline characteristics and short-term response variability (Hamada et al., 2013). Thirdly, the figure-of-eight coil can successfully stimulate the superior part of SMA, while the medial part of SMA was largely unaffected. For future study, it would be interesting to test whether stimulating the medial part using a double cone coil can induce different after-effects (Georgiev et al., 2016; Mendez et al., 2017). Fourthly, the duration of our long-term stimulation is shorter than clinical rTMS treatment. For instance, guideline for depression treatment is 6 to 8 weeks (Blumberger et al., 2018). The number of response regions may be increased with the dose of stimulations. As a result, the STE may only predict part of the response region after long-term treatment. Because of the potential risk of applying longer stimulation for healthy subjects, this issue can only be addressed in patients that need rTMS treatment. Finally, the voxel with the highest LTE at T4 was close to the cortical target. The Euclidean distances between target and the two ParaCG peak points at T3/T4 were 13 and 22 mm, respectively. Although single stimulation with high strength (>RMT) only induced activation within 1-mm distance (Romero et al., 2019), the spatial extent of cTBS is still undetermined. Addressing this issue is important to explain to what extent the LTE in ParaCG was induced directly by cTBS.

CONCLUSION

This study associated the after-effects of short- and long-term rTMS on SMA network. At the group level, both one-session and 5-day stimulations exclusively increased the RSFC between SMA and ParaCG. At the individual level, the 5-day after-effects could be predicted by an individual's alteration after one-session stimulation. These imaging evidences indicated that one-session rTMS findings could predict the region's response to long-term stimulations, as well as the individualized response degree. It suggests shared neural mechanisms between short- and long-term rTMS. Future rTMS studies on patients may further investigate whether the STE in neuroimaging could be a predictor for screening rTMS-sensitive subjects before the end of long-term treatment.

DATA AVAILABILITY STATEMENT

The datasets generated for this study are available on request to the corresponding author.

ETHICS STATEMENT

The studies involving human participants were reviewed and approved by the Anhui Medical University. The patients/participants provided their written informed consent to participate in this study.

AUTHOR CONTRIBUTIONS

G-JJ and KW: full access to all the data in the study and take responsibility for the integrity of the data and the accuracy of the data analysis. G-JJ, JS, LZ, DL, and JW: study concept and design, acquisition, analysis, or interpretation of data. G-JJ, FY, CZ, XW, and TB: administrative, technical, or material support. CZ, YT, and KW: study supervision and obtained funding. All authors listed have made substantial, direct, and intellectual contribution to the work, and approved it for publication.

FUNDING

This work was supported by the Doctoral Foundation of Anhui Medical University, Grant/Award Number: XJ201532; the National Basic Research Program of China, Grant/Award Number: 2015CB856405; the National Key R&D Plan of China, Grant/Award Number: 2016YFC1300604; the National Natural Science Foundation of China, Grant/Award Numbers: 31970979, 81971689, 91432301, 81671354, 31571149, 91232717, 31771222, and 81771456; the Science Fund for Distinguished Young Scholars of Anhui Province, Grant/Award Number: 1808085J23; the Collaborative Innovation Center of Neuropsychiatric Disorders and Mental Health of Anhui Province; and the Youth Top-notch Talent Support Program of Anhui Medical University.

SUPPLEMENTARY MATERIAL

The Supplementary Material for this article can be found online at: https://www.frontiersin.org/articles/10.3389/fnins.2020.00237/full#supplementary-material

REFERENCES

Allen, E. A., Pasley, B. N., Duong, T., and Freeman, R. D. (2007). Transcranial magnetic stimulation elicits coupled neural and hemodynamic consequences. *Science* 317, 1918–1921. doi: 10.1126/science.1146426

Ashburner, J. (2007). A fast diffeomorphic image registration algorithm. *Neuroimage* 38, 95–113. doi: 10.1016/j.neuroimage.2007.07.007

Bergmann, T. O., Karabanov, A., Hartwigsen, G., Thielscher, A., and Siebner, H. R. (2016). Combining non-invasive transcranial brain stimulation with neuroimaging and electrophysiology: current approaches and future perspectives. *Neuroimage* 140, 4–19. doi: 10.1016/j.neuroimage.2016.02.012

Bestmann, S., and Feredoes, E. (2013). Combined neurostimulation and neuroimaging in cognitive neuroscience: past, present, and future. *Ann. N. Y. Acad. Sci.* 1296, 11–30. doi: 10.1111/nyas.12110

Blumberger, D. M., Vila-Rodriguez, F., Thorpe, K. E., Feffer, K., Noda, Y., Giacobbe, P., et al. (2018). Effectiveness of theta burst versus high-frequency repetitive transcranial magnetic stimulation in patients with depression (THREE-D): a randomised non-inferiority trial. *Lancet* 391, 1683–1692. doi: 10.1016/S0140-6736(18)30295-2

Chao-Gan, Y., and Yu-Feng, Z. (2010). DPARSF: a MATLAB toolbox for "pipeline" data analysis of resting-state fMRI. *Front. Syst. Neurosci.* 4:13. doi: 10.3389/fnsys.2010.00013

Chen, A. C., Oathes, D. J., Chang, C., Bradley, T., Zhou, Z. W., Williams, L. M., et al. (2013). Causal interactions between fronto-parietal central executive and default-mode networks in humans. *Proc. Natl. Acad. Sci. U.S.A.* 110, 19944–19949. doi: 10.1073/pnas.1311772110

Chen, X., Ji, G. J., Zhu, C., Bai, X., Wang, L., He, K., et al. (2018). Neural correlates of auditory verbal hallucinations in schizophrenia and the therapeutic response to theta-burst transcranial magnetic stimulation. *Schizophr. Bull.* 45, 474–483. doi: 10.1093/schbul/sby054

Chou, Y. H., Hickey, P. T., Sundman, M., Song, A. W., and Chen, N. K. (2015). Effects of repetitive transcranial magnetic stimulation on motor symptoms in Parkinson disease: a systematic review and meta-analysis. *JAMA Neurol.* 72, 432–440. doi: 10.1001/jamaneurol.2014.4380

Di Lazzaro, V., and Rothwell, J. C. (2014). Corticospinal activity evoked and modulated by non-invasive stimulation of the intact human motor cortex. *J. Physiol.* 592, 4115–4128. doi: 10.1113/jphysiol.2014.274316

Eggers, C., Gunther, M., Rothwell, J., Timmermann, L., and Ruge, D. (2015). Theta burst stimulation over the supplementary motor area in Parkinson's disease. *J. Neurol.* 262, 357–364. doi: 10.1007/s00415-014-75728

Eklund, A., Nichols, T. E., and Knutsson, H. (2016). Cluster failure: why fMRI inferences for spatial extent have inflated false-positive rates. *Proc. Natl. Acad. Sci. U.S.A.* 113, 7900–7905. doi: 10.1073/pnas.1602413113

Fox, M. D., Buckner, R. L., Liu, H., Chakravarty, M. M., Lozano, A. M., and Pascual-Leone, A. (2014). Resting-state networks link invasive and noninvasive brain stimulation across diverse psychiatric and neurological diseases. *Proc. Natl. Acad. Sci. U.S.A.* 111, E4367–E4375. doi: 10.1073/pnas.1405003111

Fox, M. D., Buckner, R. L., White, M. P., Greicius, M. D., and Pascual-Leone, A. (2012). Efficacy of transcranial magnetic stimulation targets for depression is related to intrinsic functional connectivity with the subgenual cingulate. *Biol. Psychiatry* 72, 595–603. doi: 10.1016/j.biopsych.2012.04.028

Georgiev, D., Rocchi, L., Tocco, P., Speekenbrink, M., Rothwell, J. C., and Jahanshahi, M. (2016). Continuous theta burst stimulation over the dorsolateral prefrontal cortex and the Pre-SMA alter drift rate and response thresholds respectively during perceptual decision-making. *Brain Stimul.* 9, 601–608. doi: 10.1016/j.brs.2016.04.004

Hallett, M., Di Iorio, R., Rossini, P. M., Park, J. E., Chen, R., Celnik, P., et al. (2017). Contribution of transcranial magnetic stimulation to assessment of brain connectivity and networks. *Clin. Neurophysiol.* 128, 2125–2139. doi: 10.1016/j.clinph.2017.08.007

Hamada, M., Murase, N., Hasan, A., Balaratnam, M., and Rothwell, J. C. (2013). The role of interneuron networks in driving human motor cortical plasticity. *Cereb. Cortex* 23, 1593–1605. doi: 10.1093/cercor/bhs147

Hinder, M. R., Goss, E. L., Fujiyama, H., Canty, A. J., Garry, M. I, Rodger, J., et al. (2014). Inter- and Intra-individual variability following intermittent theta burst stimulation: implications for rehabilitation and recovery. *Brain Stimul.* 7, 365–371. doi: 10.1016/j.brs.2014.01.004

Huang, Y. Z., Edwards, M. J., Rounis, E., Bhatia, K. P., and Rothwell, J. C. (2005). Theta burst stimulation of the human motor cortex. *Neuron* 45, 201–206. doi: 10.1016/j.neuron.2004.12.033

Ji, G. J., Yu, F., Liao, W., and Wang, K. (2017). Dynamic aftereffects in supplementary motor network following inhibitory transcranial magnetic stimulation protocols. *Neuroimage* 149, 285–294. doi: 10.1016/j.neuroimage.2017.01.035

Landeros-Weisenberger, A., Mantovani, A., Motlagh, M. G., de Alvarenga, P. G., Katsovich, L., Leckman, J. F., et al. (2015). Randomized Sham controlled double-blind trial of repetitive transcranial magnetic stimulation for adults with severe tourette syndrome. *Brain Stimul.* 8, 574–581. doi: 10.1016/j.brs.2014.11.015

Le, K., Liu, L., Sun, M. L., Hu, L., and Xiao, N. (2013). Transcranial magnetic stimulation at 1 Hertz improves clinical symptoms in children with Tourette syndrome for at least 6 months. *J. Clin. Neurosci.* 20, 251–256. doi: 10.1016/j.jocn.2012.01.049

Mendez, J. C., Rocchi, L., Jahanshahi, M., Rothwell, J., and Merchant, H. (2017). Probing the timing network: a continuous theta burst stimulation study of temporal categorization. *Neuroscience* 356, 167–175. doi: 10.1016/j.neuroscience.2017.05.023

Neggers, S. F., Petrov, P. I., Mandija, S., Sommer, I. E., and van den Berg, N. A. (2015). Understanding the biophysical effects of transcranial magnetic stimulation on brain tissue: the bridge between brain stimulation and cognition. *Prog. Brain Res.* 222, 229–259. doi: 10.1016/bs.pbr.2015.06.015

Nettekoven, C., Volz, L. J., Kutscha, M., Pool, E. M., Rehme, A. K., Eickhoff, S. B., et al. (2014). Dose-dependent effects of theta burst rTMS on cortical excitability and resting-state connectivity of the human motor system. *J. Neurosci.* 34, 6849–6859. doi: 10.1523/JNEUROSCI.4993-13.2014

Nettekoven, C., Volz, L. J., Leimbach, M., Pool, E. M., Rehme, A. K., Eickhoff, S. B., et al. (2015). Inter-individual variability in cortical excitability and motor network connectivity following multiple blocks of rTMS. *Neuroimage* 118, 209–218. doi: 10.1016/j.neuroimage.2015.06.004

Nichols, T. E., and Holmes, A. P. (2002). Nonparametric permutation tests for functional neuroimaging: a primer with examples. *Hum. Brain Mapp.* 15, 1–25. doi: 10.1002/hbm.1058

Reithler, J., Peters, J. C., and Sack, A. T. (2011). Multimodal transcranial magnetic stimulation: using concurrent neuroimaging to reveal the neural network dynamics of noninvasive brain stimulation. *Prog. Neurobiol.* 94, 149–165. doi: 10.1016/j.pneurobio.2011.04.004

Rocchi, L., Ibanez, J., Benussi, A., Hannah, R., Rawji, V., Casula, E., et al. (2018). Variability and predictors of response to continuous theta burst stimulation: a TMS-EEG study. *Front. Neurosci.* 12:400. doi: 10.3389/fnins.2018.00400

Romero, M. C., Davare, M., Armendariz, M., and Janssen, P. (2019). Neural effects of transcranial magnetic stimulation at the single-cell level. *Nat. Commun.* 10:2642. doi: 10.1038/s41467-019-10638-7

Sale, M. V., Mattingley, J. B., Zalesky, A., and Cocchi, L. (2015). Imaging human brain networks to improve the clinical efficacy of non-invasive brain stimulation. *Neurosci. Biobehav. Rev.* 57, 187–198. doi: 10.1016/j.neubiorev.2015.09.010

Shirota, Y., Ohtsu, H., Hamada, M., Enomoto, H., Ugawa, Y., and Research Committee on rTMS Treatment of Parkinson's Disease (2013). Supplementary motor area stimulation for Parkinson disease: a randomized controlled study. *Neurology* 80, 1400–1405. doi: 10.1212/WNL.0b013e31828c2f66

Song, X. W., Dong, Z. Y., Long, X. Y., Li, S. F., Zuo, X. N., Zhu, C. Z., et al. (2011). REST: a toolkit for resting-state functional magnetic resonance imaging data processing. *PLoS One* 6:e25031. doi: 10.1371/journal.pone.0025031

Valchev, N., Curcic-Blake, B., Renken, R. J., Avenanti, A., Keysers, C., Gazzola, V., et al. (2015). cTBS delivered to the left somatosensory cortex changes its functional connectivity during rest. *Neuroimage* 114, 386–397. doi: 10.1016/j.neuroimage.2015.04.017

Valchev, N., Gazzola, V., Avenanti, A., and Keysers, C. (2016). Primary somatosensory contribution to action observation brain activity-combining fMRI and cTBS. *Soc. Cogn. Affect Neurosci.* 11, 1205–1217. doi: 10.1093/scan/nsw029

Vink, J. J. T., Mandija, S., Petrov, P. I., van den Berg, C. A. T., Sommer, I. E. C., and Neggers, S. F. W. (2018). A novel concurrent TMS-fMRI method to reveal propagation patterns of prefrontal magnetic brain stimulation. *Hum. Brain Mapp.* 39, 4580–4592. doi: 10.1002/hbm.24307

Yesavage, J. A., Fairchild, J. K., Mi, Z., Biswas, K., Davis-Karim, A., Phibbs, C. S., et al. (2018). Effect of repetitive transcranial magnetic stimulation on treatment-resistant major depression in US veterans: a randomized clinical trial. *JAMA Psychiatry* 75, 884–893. doi: 10.1001/jamapsychiatry.2018.1483

Zenon, A., Sidibe, M., and Olivier, E. (2015). Disrupting the supplementary motor area makes physical effort appear less effortful. *J. Neurosci.* 35, 8737–8744. doi: 10.1523/JNEUROSCI.3789-14.2015

Conflict of Interest: The authors declare that the research was conducted in the absence of any commercial or financial relationships that could be construed as a potential conflict of interest.

frontiers in Neuroscience

REVIEW
published: 02 April 2020
doi: 10.3389/fnins.2020.00264

Neuromodulation of the Pineal Gland via Electrical Stimulation of Its Sympathetic Innervation Pathway

Susannah C. Lumsden[1,2], *Andrew N. Clarkson*[1,3,4] *and Yusuf Ozgur Cakmak*[1,2,4,5]*

[1] *Department of Anatomy, University of Otago, Dunedin, New Zealand,* [2] *Brain Health Research Centre, Dunedin, New Zealand,* [3] *Brain Research New Zealand, Dunedin, New Zealand,* [4] *Medical Technologies Centre of Research Excellence, Auckland, New Zealand,* [5] *Centre for Health Systems and Technology, Dunedin, New Zealand*

Stimulation of the pineal gland via its sympathetic innervation pathway results in the production of N-acetylserotonin and melatonin. Melatonin has many therapeutic roles and is heavily implicated in the regulation of the sleep-wake cycle. In addition, N-acetylserotonin has recently been reported to promote neurogenesis in the brain. Upregulation of these indoleamines is possible via neuromodulation of the pineal gland. This is achieved by electrical stimulation of structures or fibres in the pineal gland sympathetic innervation pathway. Many studies have performed such pineal neuromodulation using both invasive and non-invasive methods. However, the effects of various experimental variables and stimulation paradigms has not yet been reviewed and evaluated. This review summarises these studies and presents the optimal experimental protocols and stimulation parameters necessary for maximal upregulation of melatonin metabolic output.

Keywords: pineal, stimulation, neuromodulation, SCG, NAS, melatonin, AANAT, sympathetic

OPEN ACCESS

Edited by:
Simone Rossi,
University of Siena, Italy

Reviewed by:
Victor Manuel Pulgar,
Wake Forest School of Medicine, United States
Yun Qian,
Shanghai Jiao Tong University, China
Maria Egle De Stefano,
Sapienza University of Rome, Italy
Stefan Reuss,
Johannes Gutenberg University Mainz, Germany

***Correspondence:**
Yusuf Ozgur Cakmak
yusuf.cakmak@otago.ac.nz

Specialty section:
This article was submitted to Neural Technology, a section of the journal Frontiers in Neuroscience

Received: *24 September 2019*
Accepted: *09 March 2020*
Published: *02 April 2020*

Citation:
Lumsden SC, Clarkson AN and Cakmak YO (2020) Neuromodulation of the Pineal Gland via Electrical Stimulation of Its Sympathetic Innervation Pathway. Front. Neurosci. 14:264. doi: 10.3389/fnins.2020.00264

INTRODUCTION

The pineal gland is an azygous, endocrine gland located in the midline of the brain. In humans, it is one solid structure situated deep within the brain between the habenular and posterior commissures, directly posterior to the third ventricle. In rodents, the gland is comprised of superficial, deep and stalk components. The superficial gland is found on the surface of the brain – anterior to the cerebellum and directly beneath the confluens sinuum. The pineal gland is comprised of a variety of cell types: pinealocytes, microglia, astrocytes, vascular and leptomeningeal cells, and endothelial cells. It is possible to distinguish between pinealocytes and other cell types using electrophysiological characteristics specific to each type. For example, astrocytes do not exhibit a biphasic positive-negative waveform composed of an initial segment-soma dendritic inflexion, whereas pinealocytes do. Pinealocytes are distributed uniformly throughout the gland and are predominantly responsible for the synthesis and secretion of melatonin in response to environmental lighting changes (Mays et al., 2018). Melatonin is considered the chemical expression of darkness and in the absence of light is secreted in response to signals from the suprachiasmatic nucleus (SCN). Melatonin is a systemically ubiquitous molecule and is also secreted from extrapineal sites including the Harderian gland, retina, and GI tract (for review see: Huether, 1993).

For melatonin synthesis (**Figure 1**), tryptophan is uptaken into the pinealocyte from the blood and converted into 5-hydroxytryptophan (5-HTP) via tryptophan-5-hydroxylase. 5-HTP is then converted into serotonin by 5-HTP decarboxylase, before serotonin is converted to N-acetylserotonin (NAS) by the enzyme aralkylamine N-acetyltransferase (AANAT). The enzyme, hydroxyindole-O-methyltransferase (HIOMT) then converts NAS into melatonin, which is secreted directly into the bloodstream or cerebrospinal fluid (CSF) (Tan et al., 2018). Circulating norepinephrine (NE) is unable to contribute to pineal innervation. This is because the postganglionic sympathetic nerves actively take up circulating catecholamines to prevent persistent activation of the pineal, and also maintain the gland's circadian rhythmicity (Wetterberg, 1979; Reiter, 1990).

The anatomical pathway providing sympathetic input to the pineal gland is the in-road for pineal modulation. The polysynaptic innervation pathway of the gland (**Figure 2**) is as follows: an absence of light is detected by the retina and this information is transmitted via the retinohypothalamic tract (RHT) to the master pacemaker of the brain – the suprachiasmatic nucleus (SCN) (Hendrickson et al., 1972; Moore and Lenn, 1972; Moore, 1973). Information from the SCN is then transmitted to the paraventricular nucleus (PVN) (Vrang et al., 1995; Kalsbeek et al., 2000; Munch et al., 2002) whose fibres descend to connect with the intermediolateral column of the thoracic spinal cord (IML). Projections from the IML then ascend to the superior cervical ganglia (SCG) and then SCG postganglionic sympathetic fibres ascend through the internal carotid canal (Bowers et al., 1984b), accompanied by the internal carotid artery and innervate pinealocytes (Bargmann, 1943; Kappers, 1960a). Postganglionic sympathetic fibres initially contact the pineal from the dorso-posterior aspect (Kappers, 1960b; Bowers et al., 1984b). These sympathetic fibres are generally arranged into two distinct bundles known as "nervi conarii," however, sometimes they become fused and reach the gland as one bundle (le Gros Clark, 1940; Kappers, 1960b). The nervi conarii form a plexus over the entirety of the pineal gland, with nerve fascicles originating from both left and right SCG intermingling on its surface (Bowers et al., 1984b). Each innervating nervi conarii provides equal innervation to both the ipsilateral and contralateral side of the gland (Lingappa and Zigmond, 1987). These fibres' terminals often end in perivascular spaces (Huang and Lin, 1984) where they release NE onto pinealocytes during the night to stimulate melatonin synthesis.

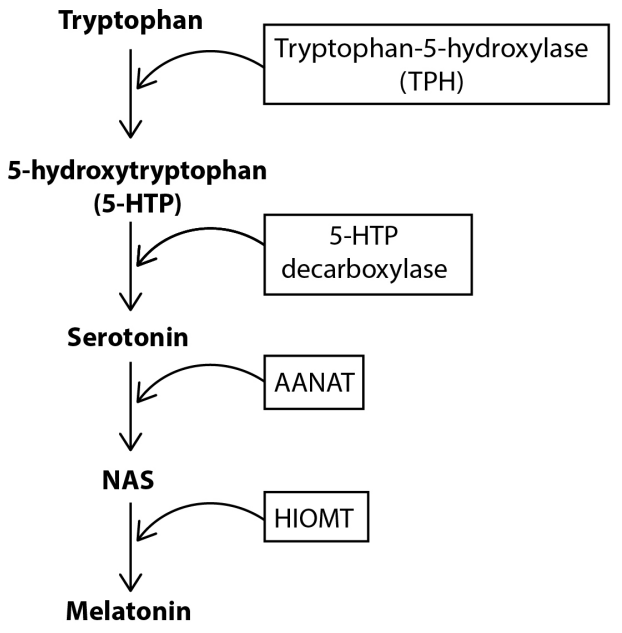

FIGURE 1 | Biosynthesis of melatonin. Tryptophan is converted to 5-hydroxytryptophan (5-HTP) by the enzyme tryptophan-5-hydroxylase (TPH). 5-HTP is then converted to serotonin via the enzyme 5-HTP decarboxylase. Serotonin is subsequently converted to NAS and then melatonin via the enzymes AANAT and HIOMT, respectively.

Inhibitory and excitatory responses have been recorded from pinealocytes. There may be specific groups of pinealocytes that become excited or inhibited depending upon the source of innervation i.e., whether innervated by fibres from the left, right, or both SCG (Reuss et al., 1985b). Regulation of pineal electrical responses might be also mediated by pinealocytes themselves, with the excitation of one pinealocyte causing the inhibition of another (Reuss, 1986). Yet, whilst it is generally accepted that hyperpolarisation of pinealocytes leads to melatonin synthesis (Sakai and Marks, 1972; Parfitt et al., 1975; Freschi and Parfitt, 1986), exactly how different types of electrical response regulate this process is unknown. One possible mechanism could be pinealocytes engaging in self-regulation through glutamate release following hyperpolarisation of the cell membrane. Glutamate may then act in an autocrine and/or paracrine manner via mGluR3 receptors which have been demonstrated on the pinealocyte cell membrane (Yamada et al., 1996a,b; Yatsushiro et al., 2000). The mGluR3 receptors are negatively coupled to adenylate cyclase (AC) through an inhibitory G-protein. This decreases AANAT activity which converts NAS into melatonin, thus decreasing melatonin synthesis (Yamada et al., 1998). Alternatively, pinealocytes may be involved in the formation of a tripartite synapse via the inclusion of astrocytes in the communication between the postganglionic sympathetic terminals and the pinealocyte membrane (Villela et al., 2013). Glutamate release may trigger an increase in astrocyte intracellular calcium levels ($[Ca^{2+}]_i$) and activation of nuclear factor kappa-light-chain-enhancer of activated β-cells (Villela et al., 2013). Astrocytes may then release particular gliotransmitters (e.g., tumour necrosis factor alpha TNFα) that act on receptors on the pinealocyte membrane, either alone or in conjunction with glutamate (Villela et al., 2013). These gliotransmitters may provide negative feedback to the presynaptic sympathetic terminal, preventing further release of NE (Parpura et al., 1994; Villela et al., 2013), or elicit inhibitory or excitatory responses in the post-synaptic pinealocyte membrane (Hassinger et al., 1995; Villela et al., 2013). Moreover, the number of AMPA receptors in the pinealocyte membrane may be upregulated through TNFα (Villela et al., 2013) – which may be the receptors through which TNFα and glutamate exert their effects. TNFα has also been shown to decrease NAS and serotonin

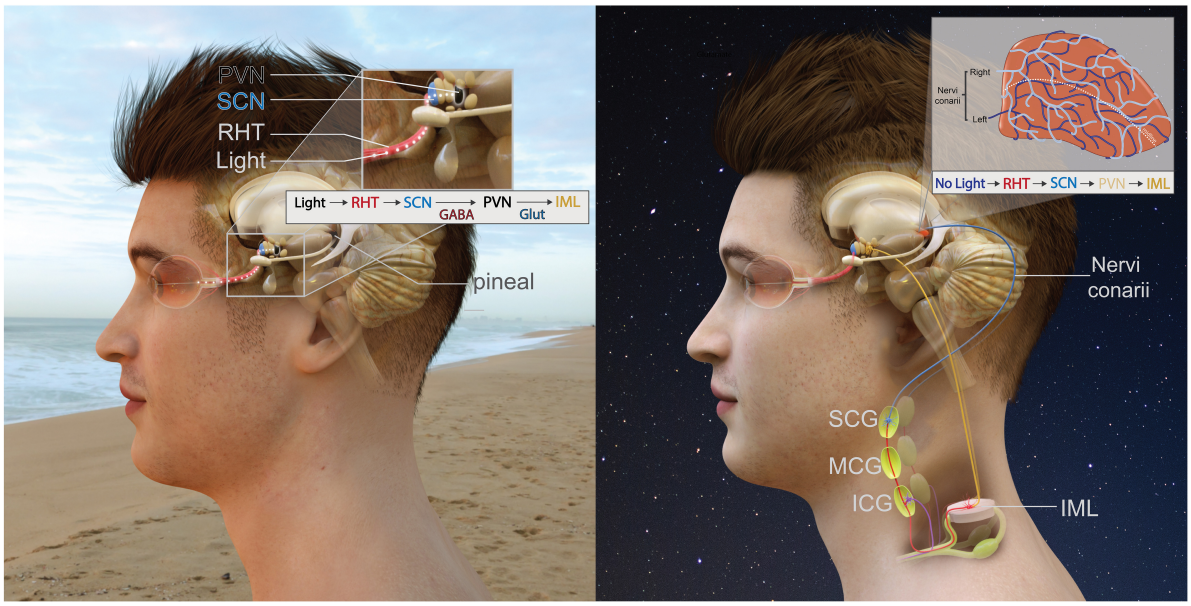

FIGURE 2 | Innervation of the pineal gland. The RHT which projects to the SCN followed by the PVN. The pineal pathway then descends down the spinal cord to the IML. Preganglionic sympathetic fibres ascend, pass through the inferior and middle cervical ganglia before terminating on the SCG. Postganglionic sympathetic fibres then ascend and innervate the pineal gland. **(A-left)** During the day, this pathway is inhibited due to light. **(B-right)** During the night, an absence of light activates this pathway and the pineal gland receives sympathetic input.

levels as well as AANAT mRNA expression (Tsai et al., 2001; Fernandes et al., 2006). Melatonin levels may be regulated via one, or a combination of the above mechanisms (see **Figure 3**).

The response of pinealocytes to adrenergic stimulation is complex, with an initial transient rapid hyperpolarisation followed by a sustained depolarisation (Zemkova et al., 2011). This hyperpolarisation is due in part to K^+ efflux from large-conductance Ca^{2+-}activated K^+ channels (BK_{Ca2+}) (Cena et al., 1991). An increase in $[Ca^{2+}]_i$ and cyclic adenosine monophosphate (cAMP) is necessary for the opening of these channels (Cena et al., 1991). This triggers a myriad of intracellular molecular cascades that eventually results in melatonin synthesis (see **Figure 3** and **Supplementary Material** for further details). However, it seems that the spontaneous electrical activity of all pinealocytes is not identical. Some researchers have grouped pinealocytes accordingly into 'clusters' of regularly firing cells (REG) and rhythmically firing cells (RHY), the latter forming the minority (Schenda and Vollrath, 1997; **Figure 4**). Each cluster is composed of 3–5 of one type and surrounded by 'silent' cells which exhibit no spontaneous firing (Schenda and Vollrath, 1997). The RHY clusters appear to interact with one another synaptically, with the firing of one cluster being linked to the firing of another (Schenda and Vollrath, 1999). This intrapineal network linkage may contribute to the regulation of extracellular substances known to stimulate or inhibit melatonin synthesis such as NE and acetylcholine, respectively (Yamada et al., 1996a,b; Schenda and Vollrath, 1999). Others have also suggested classifying pinealocytes into different categories due to morphological heterogeneity (Calvo and Boya, 1984; Al-Hussain, 2006), or differences in the quantitative presence of the HIOMT enzyme (Rath et al., 2016). However, at present there exists no definitive clarification for how such heterogeneity relates to melatonin metabolism.

The sympathetic innervation pathway of the pineal involving the PVN, SCN, and SCG is generally accepted to provide the only functional input to the gland. The SCG together with the middle and inferior cervical ganglia comprise the cervical sympathetic trunks (CSTs). Stimulation of the distal portion of the CST closest to the SCG invokes a significant increase in the rate of glucose metabolism in both the ipsilateral SCG and the pineal, but not elsewhere in the central nervous system (CNS) (Ito et al., 1988) reflecting the likely exclusivity of this pathway. However, other structures may also innervate the gland such as: the trigeminal ganglion (Yamamoto et al., 1983; Shiotani et al., 1986; Moller et al., 1993; Matsushima et al., 1994; Matsuura et al., 1994; Reuss, 1999), the lateral geniculate nucleus (Korf and Wagner, 1980; Mikkelsen and Moller, 1990), lateral hypothalamus (Fink-Jensen and Møller, 1990), the dorsal raphe nucleus (Leander et al., 1998; Moller and Hay-Schmidt, 1998), and fibres such as the habenular and posterior commissures (Moller, 1978; Moller and Korf, 1983; Reuss and Moller, 1986; Larsen et al., 1991), and the greater petrosal nerve (Kenny, 1967; Romijn, 1975). Wurtman et al. (1963) proposed that such pathways are crucial for providing information regarding chronic changes in lighting conditions i.e., seasonal changes. By contrast, Schapiro and Salas (1971) argue they provide an alternative sympathetic pathway, separate from the SCG, supplying the pineal with information regarding acute changes to photic stimuli. With regards to the commissural inputs, the linkage between the commissures and pineal gland are not surprising as they are topographically linked during

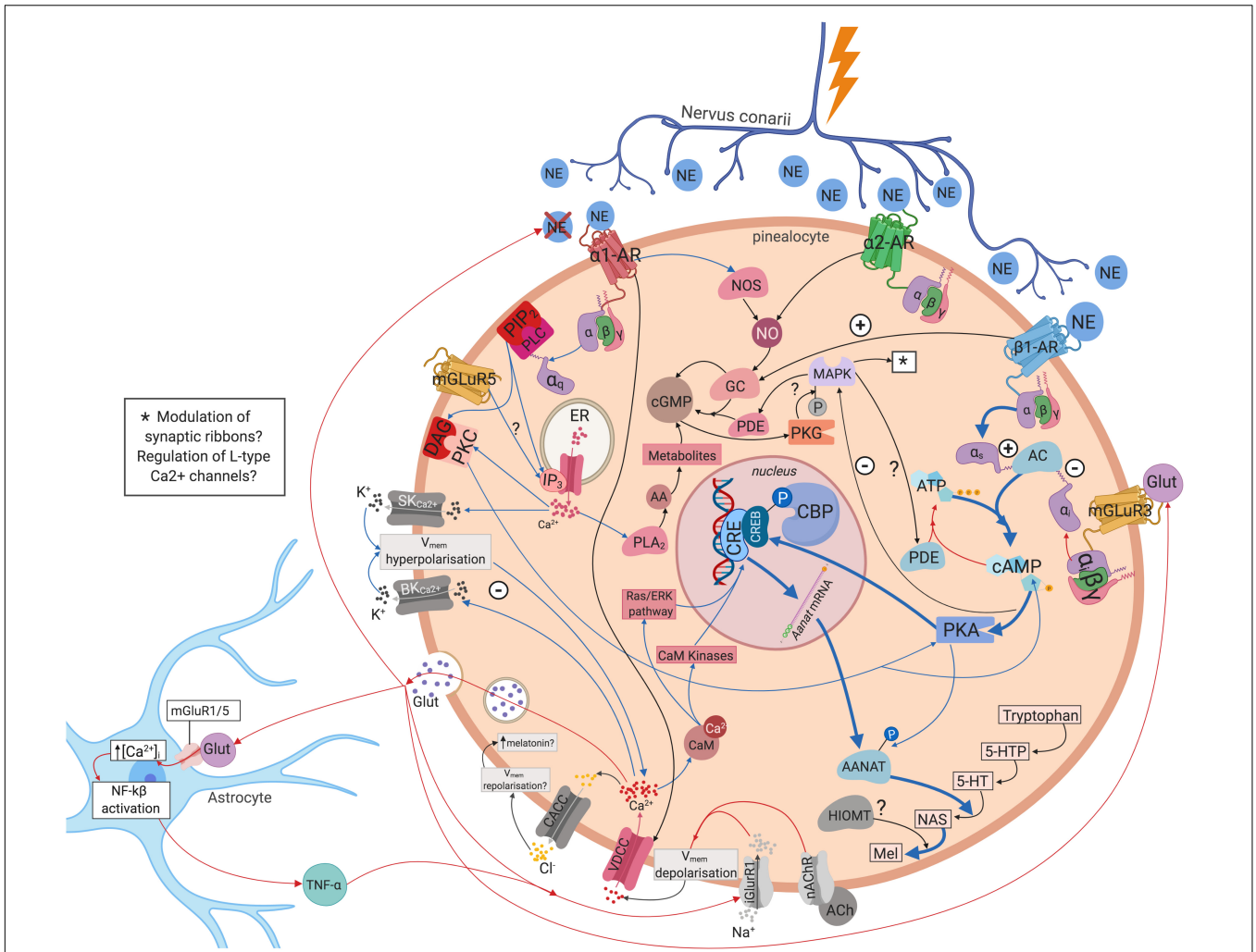

FIGURE 3 | Intra- and intercellular modulation of melatonin synthesis. NE binds to the α_1, α_2, and β_1 adrenergic receptors on pinealocytes triggering a complex myriad of intracellular molecular cascades that eventually regulate melatonin synthesis. Pinealocytes may engage in autocrine and/or paracrine regulation via glutamate release via mGluR3. Pinealocytes may also form a tripartite synapse with astrocytes and postganglionic sympathetic terminals. Blue arrows, upregulating melatonin synthesis; red arrows, downregulating melatonin synthesis; black arrows, mixed or unclear effects on melatonin synthesis. 5-HT, 5-hydroxytryptamine; 5-HTP, 5-hydroxytryptophan; AA, arachidonic acid; AANAT, aralkylamine N-acetyltransferase; AC, adenylate cyclase; AMPA, α-amino-3-hydroxy-5-methyl-4-isoxazolepropionic acid receptor; ATP, adenosine triphosphate; α_1-AR, α_1-adrenoreceptor; α_2-AR, α_2-adrenoreceptor; BK_{Ca2+}, large-conductance Ca^{2+}−activated K^+channel; CACC, Ca^{2+}activated Cl^- channels; CaM, calcium binding protein calmodulin; cAMP, cyclic guanosine monophosphate; CBP, CREB-binding protein; cGMP, cyclic guanosine monophosphate; CRE, cAMP response element; CREB, cAMP response element binding protein; DAG, diacylglycerol; ER, endoplasmic reticulum; GC, guanylate cyclase; Glut, glutamate; iGluR1, ionotropic glutamate receptor 1; IP_3, inositol trisphosphate; MAPK, mitogen-activated protein kinase MAPK; Mel, melatonin; mGluR3, metabotropic glutamate receptor 3; mGluR5, metabotropic glutamate receptor 5; nAChR, nicotinic acetylcholine receptor; NAS, N-acetylserotonin; NE, norepinephrine; NF-kβ, nuclear factor kappa-light-chain-enhancer of activated β cells; NO, nitric oxide; NOS, nitric oxide synthetase; PDE, phosphodiesterase; PKA, protein kinase A; PKC, protein kinase C; PKG, protein kinase G; PLA_2, phospholipase A_2; $SKCa^{2+}$, small-conductance Ca^{2+}−activated K^+ channel; TNF- α, tumour necrosis factor – α; VDCC, voltage-dependent Ca^{2+} channels; β1-AR, β1-adrenoreceptor.

ontological development. However, it may be that any projections from these structures to the pineal are aberrant and non-functional (le Gros Clark, 1940; Kappers, 1960b, 1965; Romijn, 1975). These projections remain a matter of great debate amongst researchers and further research is required to elucidate their exact relationship with the pineal gland.

Melatonin's therapeutic potential extends to a number of different mechanisms including: increasing neurogenesis in the hippocampus (Kim et al., 2004; Ramirez-Rodriguez et al., 2009; Rennie et al., 2009; Sotthibundhu et al., 2010; Crupi et al., 2011) and the induction, regulation, and prolonging of sleep (for review see: Dawson and Encel, 1993). Reduced melatonin levels are linked with chronic sleep disturbances (Haimov et al., 1994; Garfinkel et al., 1995) and advanced age in humans (Waldhauser et al., 1988). These observations have led to the development of the "melatonin replacement" hypothesis, which posits "(1) the age-related decline in melatonin, in some way, contributes to insomnia; and (2) replacement with

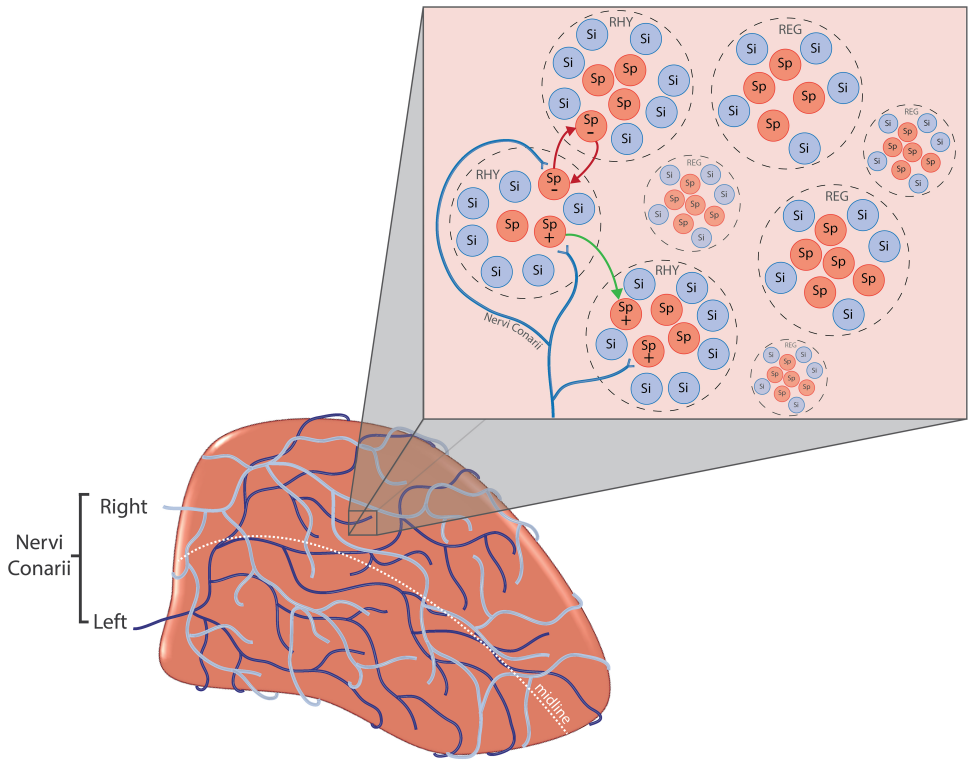

FIGURE 4 | (A-bottom left) Nervi conarii. The nervi conarii form an intermingling plexus of fibres over the pineal gland and release norepinephrine onto pinealocytes during the night to stimulate melatonin synthesis. **(B-top right)** Pinealocyte clusters. Spontaneously firing pinealocytes (Sp) are arranged into "clusters" of regularly firing cells (REG) and rhythmically firing cells (RHY). Clusters are surrounded by "silent" cells (Si) which exhibit no spontaneous firing. The firing of RHY cluster is synaptically linked to the firing of another (red arrows). The electrical response of pinealocytes is complex. Inhibitory and excitatory responses have been recorded from pinealocytes (+ and –). Specific groups of pinealocyte may become excited or inhibited depending upon the source of innervation i.e., left, right or both SCG. Regulation of pineal electrical responses might be also mediated by pinealocytes themselves, with the excitation of one pinealocyte causing the inhibition of another (green arrow).

high physiological doses of melatonin, will improve sleep" (Hughes et al., 1998). Consequently, oral administration of exogenous melatonin has been frequently utilised in clinical trials to upregulate melatonin levels and improve sleep. Oral administration of melatonin is temporally limited due to its quick absorption and relatively short plasma half-life (Waldhauser et al., 1984; Aldhous et al., 1985). Large doses of melatonin might maintain levels akin to endogenous levels, however, such large doses may place unnecessary strain on the liver, in addition to encouraging receptor desensitisation. Delivery of melatonin at regular intervals throughout the night to sustain endogenous levels has been suggested, however, this would require successive periods of waking, proving counterproductive in improving sleep. Further, modified release variants of melatonin have been investigated (Lemoine and Zisapel, 2012), but their efficacy is limited to elderly populations (Wade et al., 2010). Therefore, there exists demand for rapid-onset, long-lasting, non-pharmacological interventions addressing the problem of sleep disturbance via melatonin upregulation.

Neuromodulation is the "alteration of nerve activity through targeted delivery of a stimulus such as electrical stimulation. . ." (International Neuromodulation Society, 2018). Neuromodulation may be invasive or non-invasive. Invasive neuromodulation involves surgical intervention such as implantation of an electrical stimulation device directly into the body, which incurs risk and necessitates patient recovery time. Non-invasive techniques offer a safer alternative and include: stimulation of the scalp via transcranial electrical stimulation, transcutaneous electrical nerve stimulation (TENS) via stimulation of the skin that is not located on the scalp, and percutaneous electrical nerve stimulation (PENS) which may be considered a minimally invasive form of neuromodulation that involves stimulation delivered just under the skin e.g., electroacupuncture. Non-invasive techniques are often used to combat chronic neuropathic pain (Lefaucheur et al., 2001; Fregni et al., 2006a,b; Rossini et al., 2015), however, research indicates promising treatment avenues for other disorders such as tinnitus (Vanneste et al., 2010, 2013; Vanneste and De Ridder, 2011; De Ridder and Vanneste, 2012; Faber et al., 2012; Frank et al., 2012; Joos et al., 2014) and improving outcomes post-stroke (Fregni et al., 2005; Hummel et al., 2005, 2006; Khedr et al., 2005; Mansur et al., 2005; Takeuchi et al., 2005; Kim et al., 2006; Celnik et al., 2007, 2009).

Electrical stimulation paradigms targeting the pineal sympathetic pathway have been trialled in animal studies and show pineal neuromodulation is possible. This review will attempt to summarise the pertinent findings of both invasive and non-invasive stimulatory studies in addition to the various experimental procedures used (summarised in **Tables 1**, **2**). It is speculated that there exist differences of innervation mechanisms between mammals and birds. In birds, the melatonin synthesis pathway is not mediated via the sympathetic nervous system nor regulated by activation of β-adrenergic receptors. Therefore, this review will focus only on pineal stimulation studies involving mammals.

STIMULATION OF STRUCTURES IN THE PINEAL GLAND SYMPATHETIC INNERVATION PATHWAY

Invasive Stimulation

Evoked Cell Potentials

Experiments using electrical stimulation of the pineal sympathetic pathway have revealed significant heterogeneity pinealocyte response. Stimulation of the CSTs at 30 Hz (3 trains of 30 Hz for 1.25 s for 48 s per train) in rats was capable of evoking action potentials in the pineal gland (Brooks et al., 1975). In addition, use of 1 Hz frequency bilateral stimulation (0.2 ms pulse, 0.1–0.6 mA) of SCG postganglionic nerve fibres increased the firing rate of rat pineal cells (Reyes-Vazquez et al., 1986). Bowers and Zigmond (1982) bilaterally stimulated the CSTs in the rat at night-time and found a frequency dependent effect with temporal facilitation being observed in the postsynaptic potentials of the postganglionic fibres, with 10 Hz eliciting a greater effect compared with 1 Hz stimulation. The latter authors suggest that using higher frequencies allows for recruitment of a greater number of postganglionic fibres evoking action potentials that would otherwise remain "silent" if a continuous stimulus was used. These studies highlight that various frequencies are capable of influencing the pineal gland's sympathetic pathway.

An interaction between electrical pulse duration and current was discovered when a single electrical pulse of varying durations was delivered to the CSTs in order to examine the current required to produce an action potential in the internal carotid nerve (Bowers and Zigmond, 1982). It seems lower pulse durations (<3 ms) require a use of a greater current in order to elicit an action potential. Pulse durations of 3, 5, and 20 m appeared to require similarly low currents (∼5 μA) in order to elicit an action potential. This indicates pulse duration may be manipulated in experiments requiring use of low currents in order to prevent hyperpolarisation of postganglionic cell membranes. However, replication of these results is necessary in order to confirm this strength-duration relationship.

Brooks et al. (1975) first demonstrated that bilateral stimulation of the CSTs evoked discharges in pinealocytes. The response prevalence of pinealocytes following invasive stimulation of the SCG either bilaterally or unilaterally has been investigated in a handful of studies (see **Table 1**). One such study found approximately half (44.7–55.8%) of investigated cells elicited a significant electrical response following unilateral SCG stimulation during the daytime (Reuss et al., 1985b). This means that approximately half of cells investigated were unresponsive to innervation from just one ganglion. The authors note that the cells exhibited a preferential response for input from one ganglion. Whilst this could be attributed to factors such as submaximal stimulation, or investigated pinealocytes being too far away from innervating sympathetic fibres, this response rate is consistent with that previously reported (47%) (Pazo and Gonzalez, 1991). However, lower (28%) (Stehle et al., 1987), and much higher (62%) (Patel and Demaine, 1990) response rates are also reported. Interestingly, the latter authors report no difference in response prevalence between unilateral and bilateral SCG stimulation. Another study encountered a similar response prevalence in 55% of pinealocytes following bilateral stimulation of the postganglionic fibres of the SCG (Reyes-Vazquez et al., 1986). However, following bilateral SCG stimulation, Reuss et al. (1985b) found a higher response rate (73.1%). Interestingly, only 17.3% of these pinealocytes were responsive to input from both SCG, indicating only a small proportion of responding cells are influenced by contribution from both ganglia. This supports the notion that each ganglion provides innervation to the ipsilateral portion of the pineal gland, with only a small number of innervating fibres crossing the midline to innervate the contralateral portion of the gland simultaneously (Rodriguez-Perez, 1962). This view is now largely contested as recent research indicates equal innervation from both SCG and fibres intermingling to form a plexus over the gland (Bowers et al., 1984b; Lingappa and Zigmond, 1987).

The impact of unilateral vs. bilateral stimulation of the SCG remains poorly understood. Only two studies directly compare the response prevalence of pinealocytes following both unilateral and bilateral stimulation in rats and hamsters, respectively (Reuss et al., 1985b; Patel and Demaine, 1990). The contrasting response rates between unilateral and bilateral stimulation observed in these two studies may simply be due to interspecies differences between the hamster and the rat. In the rat, bilateral stimulation of the SCG evokes a greater response rate from pinealocytes (Reuss et al., 1985b) compared to unilateral stimulation, and the results from Pazo and Gonzalez (1991) seem to support this. The reason why Reyes-Vazquez et al. (1986) report a high response prevalence following unilateral stimulation similar to that reported for bilateral stimulation could be due to a number of reasons. Firstly, they stimulated the post-ganglionic fibres of the SCG whereas the other studies utilised stimulation of the SCG directly. This could have exaggerated the effect of stimulation delivered to the pineal. This could be because a purely excitatory response is being generated in the post-ganglionic fibres and this is translating to a greater response occurring in the pinealocytes. In contrast, when the SCG is stimulated directly, inhibitory signals being directed to the SCG could dampen the response of the SCG itself, which could in turn diminish any excitatory response being delivered to the post-ganglionic fibres, and therefore, the pinealocytes. Secondly, they utilised a stimulation frequency of 1 Hz whereas the other studies generally report use of higher frequencies. It has been observed that high and low

TABLE 1 | Summary of response rates from evoked potential studies.

							Percentage of responsive cells that were. . .					Percentage of total investigated cells that were. . .					
Authors	**Species**	**Structure Stimulated**	**Bilateral or Unilateral Stimulation?**	**Number of units investigated**	**Percentage of non-responsive cells**	**Percentage of responsive cells**	**Inhibited**	**Excited**	**Biphasic**	**Responsive to one ganglion only**	**Responsive to both ganglia**	**Inhibited**	**Excited**	**Biphasic**	**Responsive to one ganglion only**	**Responsive to both ganglia**	**Comments**
Reuss et al., 1984	Rat	Habenular nuclei	Bilateral	42	57.2% (*n* = 24)	42.8% (*n* = 18)	44.4% (*n* = 8)	55.6% (*n* = 10)	Not described	Not described	Not described	19% (*n* = 8)	23.8% (*n* = 10)	Not described	Not described	Not described	7 silent units were found. Confluens sinuum impaled with electrode.
Reuss et al., 1985b	Rat	SCG	Unilateral	94	55.3% (*n* = 52)	44.7% (*n* = 42)	57.1% (*n* = 24)	42.9% (*n* = 18)	Not described	Not described	Not described	25.6% (*n* = 24)	19.1% (*n* = 18)	Not described	N/A	N/A	13 silent units were found. Confluens sinuum impaled with electrode.
			Bilateral	52	26.9% (*n* = 14)	73.1% (*n* = 38)	Not described	Not described	Not described	76.3% (*n* = 29)	23.7% (*n* = 9)	Not described	Not described	Not described	55.8% (*n* = 29)	17.3% (*n* = 9)*	Confluens sinuum impaled with electrode.
Reyes-Vazquez et al., 1986	Rat	SCG	Bilateral	76	44.7% (*n* = 34)	55.3% (*n* = 42)	Not described	55.3% (*n* = 42)	Not described	Not described	Not described	Not described	55.3% (*n* = 42)	Not described	Not described	Not described	6 silent units were found. Sagittal sinus ligated.
Pazo and Gonzalez, 1991	Rat	SCG	Unilateral	19	53% (*n* = 10)	47% (*n* = 9)	56% (*n* = 5)	33% (*n* = 3)	11% (*n* = 1)	N/A	N/A	26.3% (*n* = 5)	26.3% (*n* = 5)	5.3% (*n* = 1)	N/A	N/A	In some animals, the sagittal sinus was ligated
		SCN	Unilateral	19	47% (*n* = 9)	53% (*n* = 10)	50% (*n* = 5)	30% (*n* = 3)	20% (*n* = 2)	N/A	N/A	26.3% (*n* = 5)	15.8% (*n* = 3)	10.5% (*n* = 2)	N/A	N/A	
Stehle et al., 1987	Hamster	SCG	Unilateral	48	72% (*n* = 35)	28% (*n* = 13)	61.5% (*n* = 8)	46.2% (*n* = 6)	Not described	N/A	N/A	16% (*n* = 8)	12% (*n* = 6)	Not described	N/A	N/A	Sagittal sinus ligated and cut. See notes**
Patel and Demaine, 1990	Hamster	SCG	Both	92	38% (*n* = 35)	62% (*n* = 57)	36.8% (*n* = 21)	36.8% (*n* = 21)	15.8% (*n* = 9)***	Not described	Not described	22.8% (*n* = 21)	29.3% (*n* = 27)	9.8% (*n* = 9)	Not described	Not described	No differences in form or magnitude of response found between unilateral vs bilateral or right vs left SCG stimulation. Confluens sinuum impaled with electrode.
Semm et al., 1981	Guinea-pig	Lateral habenular nuclei	Bilateral	128	56% (*n* = 72)	44% (*n* = 56)	44% (*n* = 56)	20% (*n* = 11)	Not described	Not described	Not described	35% (*n* = 45)	9% (*n* = 11)	Not described	Not described	Not described	No mention is made of the confluens sinuum in the methodology.

**7.7% (n = 4) of these cells showed different effects depending on whether left or right SCG was stimulated i.e., excitation or inhibition. Simultaneous stimulation showed no clear effects. **The number of units investigated in this study appears erroneous. This may possibly be due to a rounding error. ***This categorisation includes a population of cells which exhibited inconsistent responses following repeated stimulation.*

TABLE 2 | Summary of experimental procedures and stimulation parameters for reviewed studies concerning both invasive and non-invasive stimulation.

			Evoked Cell Potentials														
Authors	**Species**	**Strain**	**Type of Stimulation**	**Bilateral or Unilateral Stimulation?**	**Structures Stimulated**	**Time of Day of Stimulation**	**Overall Stimulation Time Period**	**Stimulus Pulse Duration**	**Stimulation Frequency/voltage**	**Stimulation Current**	**Lighting Conditions During Stimulation**	**Anaesthesia Used During Stimulation**	**Time of Sacrifice**	**Lighting Conditions During Sacrifice**	**Substance Measured**	**Collection Method**
Brooks et al., 1975	Rat	White	Invasive electrical	Bilateral	Cervical sympathetic trunks	Not described	48 s	1 every 1.25 s	30 Hz	Not described	Not described	Urethane	Not described	Not described	N/A	N/A
Ronnekleiv et al., 1980	Rat	Sprague Dawley	Invasive Electrical	Not described	Medial habenular nucleus	Usually > 18:00	Not described	50–200 μs	Up to 10 Hz	0.001–0.1 mA	Darkened room	Urethane	Following stimulation	Not described	N/A	N/A
Pazo, 1981	Rat	Wistar	Invasive electrical	Habenular complex: bilaterally, sciatic nerve: unilaterally, septal area: unclear, optic tract: unclear	Sciatic nerve, habenular complex and adjacent stria medullary, septal area, optic tract	10:00–18:00	Not described	0.5 ms	Not described	Variable intensity	Relatively dark room with no direct light on the animals	Ether	Not described	Not described	N/A	N/A
Semm et al., 1981	Guinea-pig	N/A	Invasive electrical	Bilateral	Lateral habenular nuclei	Daytime	50–100 ms (train)	0.5 ms	100 Hz	0.5 mA	Darkened room	Urethane, pentobarbitone. glucose, gallamine triethiodide mixture	Not described	Not described	N/A	N/A
Bowers and Zigmond, 1982	Rat	Sprague Dawley	Invasive Electrical	Bilateral	Cervical sympathetic trunks	Night-time	Not described	0.5, 1.0, 3.0, 5.0, and 20 ms	10 Hz	∼5 – 60 μA	Not described	Chloral Hydrate	Not described	Not described	N/A	N/A
Reuss et al., 1984	Rat	Not described	Invasive Electrical	Bilateral	Lateral habenular nuclei	Daytime	Not described	0.1–0.5 ms	1–10 Hz	0.1–0.5 mA (occasionally up to 5 mA)	Darkened room	Urethane and pentobarbital	Not described	Not described	N/A	N/A
Reuss et al., 1985b	Rat	Sprague Dawley	Invasive electrical	Both	SCG	09:00–18:00	Not described	0.2 ms	10 Hz	0.1–0.5 mA	"Natural lighting conditions"	Urethane	Not described	Not described	N/A	N/A
Reyes-Vazquez et al., 1986	Rat	Sprague Dawley	Invasive electrical	Bilateral	Postganglionic nerve fibres of the SCG	Not described	Not described	0.2 ms	1 Hz	0.1–0.6 mA	Ordinary room illumination during light cycle	Urethane	Following stimulation	Not described	N/A	N/A
Stehle et al., 1987	Hamster	Golden	Invasive electrical	SCG: unilateral, habenular nuclei: bilateral	SCG and lateral habenular nuclei	During the dark and light periods	<17 h	0.2ms	2–20 Hz	0.2 mA for habenular and optic but up to 2mA for the SCG	Not described	Urethane	Not described	Not described	N/A	N/A

(Continued)

TABLE 2 | Continued

Authors	Species	Strain	Type of Stimulation	Bilateral or Unilateral Stimulation?	Structures Stimulated	Time of Day of Stimulation	Overall Stimulation Time Period	Stimulus Pulse Duration	Stimulation Frequency/voltage	Stimulation Current	Lighting Conditions During Stimulation	Anaesthesia Used During Stimulation	Time of Sacrifice	Lighting Conditions During Sacrifice	Substance Measured	Collection Method
Evoked Cell Potentials																
Patel and Demaine, 1990	Hamster	Golden	Invasive electrical	Both	SCG	up to 6 h after 15:30	Not described	0.5–1 ms	10–20 Hz	0.5–1 mA	Artificial lab lighting	Urethane	Not described	Not described	N/A	N/A
Pazo and Gonzalez, 1991	Rat	Wistar	Invasive electrical	Unilateral	SCG and sciatic nerve	09:00–18:00	Not described	0.5 ms	Not described	Up to 0.5 mA	"Relatively dark room with no direct light on the animal during daylight"	Urethane	Not described	Not described	N/A	N/A
Indoleamine Output and Enzymatic Activity																
Brownstein and Heller, 1968	Rat	Holtzman	Invasive electrical	Unilateral	Preganglionic cervical sympathetic fibres	Not described	4 h	9 s on; 51 s off	10 Hz	3–5 mA	Not described but animals blinded	Ether	4-h post-op	Not described but animals blinded	HIOMT	Pineal homogenization
Volkman and Heller, 1971	Rat	Holtzman	Invasive electrical	Unilateral	Preganglionic cervical sympathetic trunk	Daytime/ light phase	1, 2, or 3 h	10 ms for 9 s every min	10 Hz	2x that required to produce maximal exophthalmos in the eye (2 × 0.23 mA)	Not described	Ether	Immediately or 1-h post-stimulation cessation	Not described	AANAT	Pineal homogenization
Bowers and Zigmond, 1980	Rat	Sprague Dawley	Invasive electrical	Bilateral	Cervical sympathetic trunks	>4 h after darkness onset	Animals were not stimulated past the time were lights would normally turn on	0.5 ms	5 Hz	0.4–2.0 mA	Exposed to light for 15 min prior to anaesthetic administration for SCG exposure to reduce night-time AANAT levels by more than 95%	Chloral hydrate	Immediately post-stimulation – before the onset of the light period	Dim red light	AANAT	Pineal homogenization
Heydorn et al., 1981	Rat (*ex vivo*)	Sprague Dawley	Invasive electrical	Bilateral	SCG	Not described	1 min	10 ms	10 Hz (10 V)	Not described	Not described	Not described	Not described	Not described	cAMP	Pineal homogenization

(Continued)

TABLE 2 | Continued

		Evoked Cell Potentials															
Authors	**Species**	**Strain**	**Type of Stimulation**	**Bilateral or Unilateral Stimulation?**	**Structures Stimulated**	**Time of Day of Stimulation**	**Overall Stimulation Time Period**	**Stimulus Pulse Duration**	**Stimulation Frequency/voltage**	**Stimulation Current**	**Lighting Conditions During Stimulation**	**Anaesthesia Used During Stimulation**	**Time of Sacrifice**	**Lighting Conditions During Sacrifice**	**Substance Measured**	**Collection Method**
Bowers and Zigmond, 1982	Rat	Sprague Dawley	Invasive electrical	Both	Cervical sympathetic trunks	Night (>4 h into night period) AND day (>4 h into light period)	0.5, 1, 1.5, and 2 h	0.5 ms	10 Hz	2x that require to produce maximal exophthalmos of the ipsilateral eye (values ranged for each nerve from 100–1000uA)	Not described	Chloral hydrate	Immediately following stimulation	Not described	AANAT	Pineal homogenization
Bowers et al., 1984a	Rat	Sprague Dawley	Invasive electrical	Bilateral	Cervical sympathetic trunks	>4 h into light period	3 h	Not described	5 Hz	2x that required to produce maximal exophthalmos in the ipsilateral eye	>4 h into light period	Chloral hydrate	>7 h into light period	Dimred light	AANAT	Pineal homogenization
Reuss et al., 1985a	Rats	Sprague Dawley	Invasive electrical	Bilateral	PVN	Daytime experiments: 11:00–13:00; Night-time experiments: 00:00–06:00	15, 30, 60 min	0.2 ms	10 Hz	0.1 mA	Normal artificial light	Urethane	Following stimulation	Normal artificial light but animals blinded for night-time experiments	AANAT, melatonin	Pineal homogenization
Olcese et al., 1987	Rat	Sprague Dawley	Invasive electrical	Bilateral	PVN	>02:00	2 min	0.2 ms	10 Hz	0.1 mA	Yes, but all animals blinded surgically	Urethane	30 min post-stimulation	Artificial light but animals are blinded	Melatonin, NE	Pineal homogenization
Reuss et al., 1989	Rat	Sprague Dawley	Invasive electrical	Bilateral	SCG	10:00–14:00	(1) 120 min; (2a + b) 15 min	(1) 0.5 ms; (2a) 0.5 ms; (2b) 1 ms	(1) 10 Hz; (2a) 10 Hz; (2b) 25 Hz	(1) 0.5 mA; (2a + b) 0.5 mA	Not described	Urethane	(1) 2 h after stimulation onset; (2) immediately following stimulation	Not described	AANAT	Pineal homogenization of 2/3 of each gland
Chan et al., 1989	Rabbit	New Zealand	Invasive electrical	Unilateral	Left preganglionic cervical sympathetic trunk	Light phase	24–60 min	60 ms every 2 s OR 7.5 s every 20 s	300 Hz	1–5 mA	Not described	Pentobarbital	Not described	Not described	Melatonin	Blood (plasma) sampling from the confluens sinuum
Lingappa and Zigmond, 2013	Rat	Sprague Dawley	Invasive electrical	Bilateral	Cervical sympathetic trunks	4–8 h into daytime	3 h	0.5 ms	10, 5, 2.5, and 1 Hz (10 Hz was considered optimal for AANAT stimulation)	0.2–0.8 mA	Not described	Chloral hydrate	Immediately after stimulation (stimulation carried out 4–8 h into daytime)	Not described	AANAT	Pineal homogenization

(Continued)

TABLE 2 | Continued

Authors	Subject	Species	Type of Stimulation	Bilateral or Unilateral Stimulation?	Structures Stimulated	Time of Day of Stimulation	Overall Stimulation Time Period	Stimulus Pulse Duration	Stimulation Frequency/voltage	Stimulation Current	Lighting Conditions During Stimulation	Anaesthesia Used During Stimulation	Time of Sacrifice	Lighting Conditions During Sacrifice	Substance Measured	Collection Method
Non-invasive Stimulation																
McIntyre and Oxenkrug, 1984	Rat	Sprague Dawley	Non-invasive electrical	Bilateral	Ears	Before 12:00	One shock every day for 7 days	0.75 s	130 V	Not described	Not described	Not described	2100h	Dim red light	5-HT, melatonin, NAS	Pineal homogenization
Nowak et al., 1988	Rat	Wistar	Non-invasive electrical	Bilateral	Ears	At the end of the light phase with the very final treatment being given at 22:00	A single electric sock or 10 shocks per day over 10 consecutive days	500 ms	50 Hz	70 mA (to induce tonic-clonic seizures)	Not described	Not described	1 or 2 h after the final stimulation	Light or dim-red light	AANAT, HIOMT	Pineal homogenization
Oxenkrug et al., 1991	Rat	Sprague Dawley	Non-invasive electrical	Bilateral	Ears	10:00	Not described	0.75 s	130 V	Not described	Not described	Not described	90 min after stimulation	Not described	Melatonin, serotonin, 5-HIAA. NAS	Pineal homogenization
Chao et al., 2001	Rat	Wistar	Percutaneous electrical nerve stimulation	N/A	Fengfu DU16 and Jinsuo DU8	Not described	30 or 60 min	Not described	80 Hz	1.7–2.5 mA	Not described	Sodium pentobarbital	After stimulation	Not described	Melatonin	Pineal homogenization
Spence et al., 2004	Humans	Humans with anxiety and insomnia (but no diagnosed anxiety disorder)	Acupuncture	Not described	Not described	Not described	2× a week for 5 weeks	1 hr per session	N/A	N/A	N/A	N/A	N/A	N/A	Melatonin	Measurement of urinary melatonin metabolite aMT6s
Kayumov et al., 2003	Humans	Humans with insomnia and anxiety	Acupuncture	Not described	Not described	Not described	2× a week for 5 weeks	N/A	N/A	N/A	Not described	N/A	N/A	N/A	Melatonin	Measurement of urinary melatonin metabolite aMT6s
Li et al., 2014	Rat	Zucker diabetic fatty and Zucker lean	Non-invasive electrical	Bilateral	Right side auricular concha region	14:00–17:00	30 min for 34 consecutive days	Not described	2 and 15 Hz alternating every sec	2 mA	Not described	Isoflurane	Not described	Not described	Melatonin	Blood (plasma) sampling from the tail vein
Wang et al., 2015	Rat	Zucker diabetic fatty	Non-invasive electrical	Bilateral	Right side auricular concha region	Afternoon	30 min	Not described	2 and 15 Hz switched every sec	2 mA	Not described	Isoflurane	Not described	Not described	Melatonin	Blood (plasma) sampling from the tail vein

frequency stimulation of various central structures, viscera, and vasculature can exert opposite effects (Ngai et al., 1999; Stener-Victorin et al., 2006; Cakmak et al., 2008; Zhao, 2008; Liu et al., 2012; Su et al., 2018). Therefore, it is likely a frequency dependent effect exists in the stimulation of the pineal gland.

Patel and Demaine (1990) report little difference in response rates following either bilateral and unilateral SCG stimulation (62%) in the hamster, yet a much lower response rate (28%) is alternatively reported in the same species using unilateral stimulation (Stehle et al., 1987). The differences in response rate following unilateral stimulation may be due to the latter authors ligating and separating the confluens sinuum, which exists in close proximity to the path of the nervi conarii that innervates the pineal gland (Kappers, 1960b). Such a practice may have inadvertently disrupted sympathetic innervation to the gland, resulting in a lower response rate than would otherwise be observed with the confluens sinuum intact. The current used to stimulate the SCG could also play a role in the response rate of pinealocytes, with higher currents resulting in hyperpolarisation of postganglionic cell membranes, and therefore, a lessened response from pinealocytes. This could explain why Stehle et al. (1987) report a lower response following bilateral stimulation of the SCG in hamsters compared to Patel and Demaine (1990), as the former used a slightly higher current.

Using unilateral SCG stimulation, the nature of augmentation in pineal cell firing was investigated in rats in the daytime (Pazo and Gonzalez, 1991). In this study, half (56%) of the responsive pinealocytes showed an inhibitory response, one third of the cells (33%) exhibited an excitatory response, and a biphasic response was observed in 11% of cells. In addition, two other studies note similar prevalence of inhibitory and excitatory responses (61.5% inhibitory and 46.2% excitatory[1], Stehle et al., 1987 vs. 42.9% excitatory and 57.1% inhibitory, Reuss et al., 1985b) following unilateral stimulation of the SCG in the hamster and rat, respectively. Patel and Demaine (1990) reported an increase in cell firing rate as the most prevalent response (47%) followed by a decrease in firing rate (37%), and a biphasic response in 16% of cells following SCG stimulation in the hamster. They also comment on the rapidness of the electrophysiological response to electrical stimulation of the SCG, commencing within 15 – 50 ms. In contrast, the pineal response to the onset of darkness is much slower, with increases in AANAT and melatonin not being apparent for several hours (Tamarkin et al., 1979, 1980) indicating that there exists a delay between the sympathetic pineal cell response and the intracellular melatonin upregulation. Similar response types and incidences were also reported following unilateral stimulation of the SCN using the same parameters (Pazo and Gonzalez, 1991). This implies that the pineal cellular responses are similar following stimulation of either the SCG or SCN. Contrary to this, unilateral stimulation of the sciatic nerve (Pazo and Gonzalez, 1991) resulted in mainly an inhibitory response, whilst stimulation of the lateral habenular nuclei elicited mainly an excitatory response in the pineal gland of guinea pigs (Semm et al., 1981). One study also found approximately one-quarter (26.9%) of spontaneously discharging cells tested to be unresponsive to SCG stimulation, indicating these cells may respond to innervation from other central or peripheral sources (Reuss et al., 1985b). This supports possible somatosensory and central inputs to the pineal gland, although further investigation to the exact nature of this input remains to be carried out.

Several authors (Reuss et al., 1985b; Reyes-Vazquez et al., 1986; Stehle et al., 1987) also note the presence of "silent units" within the pineal, in which no spontaneous electrical activity was initially observed. However, following stimulation, these silent cells showed discharge patterns similar to the spontaneously active cells. These "silent cells," first described by Brooks et al. (1975) and later by Reyes-Vazquez et al. (1986), have also been observed following stimulation of the habenular nuclei (Ronnekleiv et al., 1980; Reuss et al., 1984). This indicates that these cells likely only fire in response to deliberate input from structures contributing the pineal gland innervation, therefore, exhibiting no spontaneous input of their own. However, the exact function of these cells remains unknown. Therefore, further studies are required in order to uncover the purpose of these silent cells and the nature of their firing.

The experiments by Reuss et al. (1985b) indicate that certain pinealocytes exhibit a preferential response to specific forms of input from the SCG (see **Figure 4**). Further, the authors note a small number (7.7%) of the cells were either inhibited or augmented in their electrical discharge depending on whether stimulation was arising from the right or left ganglion, respectively, with their response following bilateral stimulation being unclear. These experiments show that sympathetic innervation of the pineal gland is not simply a case of recruiting excitation of all pinealocytes to the same degree, and that some pinealocytes serve different roles upon receiving sympathetic innervation. Whilst an excitatory response may facilitate synthesis of melatonin, an inhibitory response may prevent this. This could be mediated via astrocytes in close proximity to the pinealocytes releasing glutamate (Villela et al., 2013) or GABA (Minchin and Iversen, 1974), or even neighbouring pinealocytes releasing GABA, as both neurotransmitters are known to decrease melatonin synthesis (Rosenstein et al., 1989). Indeed, the presence of silent-cells that only respond to input from a specific structure support the notion of input-specific response pinealocytes (Ronnekleiv et al., 1980; Reuss et al., 1984, 1985b; Stehle et al., 1987). With this in mind, perhaps such response preferences of pineal cells exist but impart equal output, thus facilitating no overall difference in the magnitude of the total responses between unilateral and bilateral stimulation. It does appear that simultaneous input from both SCG is not additive (Patel and Demaine, 1990), and therefore the pineal cellular response of bilateral stimulation is not any greater than that of unilateral stimulation. This suggests that the cells recruited to fire following bilateral SCG stimulation are not the same populations recruited for unilateral stimulation, or are recruited to a lesser degree. It is also possible that interspecies differences between the rat and the hamster could be responsible for such inconsistencies in these findings. Finally, variation in stimulation frequencies used could also account for such

[1]The number of units investigated in this study appears erroneous. This may possibly be due to a rounding error by the authors.

differences. Frequency disparities include: 1 Hz (Reyes-Vazquez et al., 1986), 10–20 Hz (Patel and Demaine, 1990), whilst one did not describe the frequency used (Pazo and Gonzalez, 1991). Such differences in results may highlight the importance of the stimulation frequency used for such experiments.

The above studies show that modulation of the pineal gland is achievable on a cellular level, however, they also highlight the variability in response rate that can occur with different stimulation paradigms. It appears that significant thought should be given to the surgical approach and site(s) of invasive stimulation as well as the frequency and pulse durations used when attempting to exert a maximal modulatory cellular response in the gland.

Invasive Stimulation: Indoleamine Output and Enzymatic Activity of the Pineal Gland

Data obtained from single cell recordings in the pineal gland are important. However, knowledge of how stimulation of relevant anatomical structures impacts the indoleamine and enzymatic output of the gland provides more clinically translatable information. Such output of the pineal gland as a result of electrical stimulation of the sympathetic innervation pathway has been researched and will subsequently be summarised below.

The enzymatic activity of the pineal following stimulation of either the pre- or postganglionic neurons of the SCG was investigated (Bowers and Zigmond, 1982). Stimulation was delivered for 1 h at various frequencies. In both conditions, stimulation from 5–10 Hz produced maximal upregulation of AANAT activity when differences in length of time animals were in surgery and exposed to light were accounted for. Interestingly, stimulation at 1 Hz elicited a decrease in AANAT activity following pre-ganglionic stimulation, whereas AANAT activity remained unchanged following postganglionic stimulation at the same frequency. The authors offer that such a difference may be due to failure of synaptic transmission between pre- and post-synaptic neurons in the ganglia at low frequencies. The fact that no differences in AANAT activity was observed between pre- and postganglionic stimulation conditions at higher frequencies indicates that it is the lower frequency (1 Hz) enabling this transmission failure.

Volkman and Heller (1971) were amongst the first to demonstrate *in vivo* changes in rat pineal AANAT levels following direct, invasive stimulation of structures involved in the pineal sympathetic pathway during the day. Unilateral stimulation (10 Hz for 9 s every min for 1–3 h) of the pre-ganglionic CST was performed, which resulted in a duration-dependent increase in AANAT levels compared to control groups.

Following light-induced reduction of AANAT levels *in vivo* in rats, stimulation of the CSTs at 5 Hz during the night increased pineal AANAT levels in a linear fashion greater than what is observed during the night (Bowers and Zigmond, 1980). Volkman and Heller (1971) saw a lesser increase following their stimulation experiments. The latter stimulated the CSTs during the daytime, whereas the former stimulated during the night, which is claimed key to observing an immediate increase in AANAT levels comparable to those reached during the nightly peak (Bowers and Zigmond, 1980). It's postulated that stimulation during the daytime incurs a time delay in the physiological response of the pineal either to darkness, pharmacological stimulation, or electrical stimulation of the darkness signalling pathway (Bowers and Zigmond, 1980). However, it was later demonstrated that it is possible to maximally upregulate AANAT levels via stimulation during the day, disputing this theory (Bowers et al., 1984a). Following cessation of stimulation, Bowers and Zigmond (1980) also observed a rapid decline of pineal AANAT levels with a half-life of approximately 5 min, similar to that observed following exposure to light or administration of propranolol – a beta blockers that dampens sympathetic activity and, therefore, upregulation of AANAT. This indicates that continual stimulation would be required in order to maintain high pineal output for any significant length of time.

Bilateral stimulation of the SCG in rats *ex vivo* significantly elevated pineal cAMP levels compared to sham-stimulated controls (Heydorn et al., 1981). cAMP is a crucial component of the second messenger system mediating the upregulation of AANAT and is itself upregulated via NE released from postganglionic sympathetic terminals. Therefore, an increase in cAMP will result in an increase in AANAT, which facilitates the synthesis of melatonin. Although various stimulation parameters were investigated, those optimal for increasing cAMP levels were: 10 Hz, 20 V with a pulse duration of 10 ms for 1 min. The authors also found that this cAMP increase could be potentiated by more than 4-fold via the prior administration of desmethylimipramine – a tricyclic antidepressant that prevents reuptake of catecholamines including NE into sympathetic nerve terminals. This indicates that a surplus of NE allows for further increases in cAMP levels, however, it is not confirmed that such a surplus translates into greater increases in AANAT or melatonin levels.

Bowers and Zigmond (1982) compared the effects of bilateral stimulation of the rat CSTs in both day-time and night-time conditions at different frequencies. Prior to stimulation, exposure to light was used to reduce AANAT levels to levels encountered during the day. Stimulation for 2 h during the night-time at frequencies of 5 – 10 Hz induced maximal linear increases in AANAT activity. Stimulation at 2.5 Hz during the night increased AANAT levels linearly up to a point of 30 min before plateauing for the next 90 min. When elevated AANAT levels were achieved by 1 h of high frequency stimulation, stimulation at 2.5 Hz proved insufficient in maintaining these increased AANAT levels. Whilst stimulation frequencies of 2.5Hz and above induced an increase in AANAT activity, stimulation at 1 Hz produced a significant decrease in AANAT activity. Such results support the notion of frequency-dependent modulatory effects, although it is surprising that the point at which this effect switches from one of downregulation to upregulation is as low as 2.5 Hz.

Bowers and Zigmond (1982) stimulated at 10 Hz during the day, AANAT activity significantly increased during the first hour of stimulation but at a reduced rate compared to stimulation during the night-time. However, the rate of increase was significantly elevated with each passing hour of stimulation. This indicated that longer periods of stimulation facilitate greater increases in AANAT activity. Similar results were later reported

showing tripling of AANAT activity upon bilateral stimulation of the SCG at 10 Hz for 2 h during the day-time (Reuss et al., 1989). This was further confirmed when stimulation of the CSTs during the light period at 10 Hz for 3 h produced levels similar to that of peak night-time AANAT levels (Lingappa and Zigmond, 2013). However, Reuss et al. (1985b) did not find any significant change in enzyme levels following day-time stimulation at 10 Hz or 25 Hz for 15 min. This shows that stimulation periods must exceed 15 min in order to accommodate any significant elevation in AANAT activity.

Stimulation frequencies of 2.5 and 5 Hz, but not 1 Hz, were reported as capable of achieving submaximal AANAT levels to that seen during the night-time (Lingappa and Zigmond, 2013). This is in accordance with previously reported findings (Bowers and Zigmond, 1982). Taken together, findings suggest that whilst stimulation of the CSTs or SCG during the day-time at 10 Hz for 3 h can elicit significant upregulation of AANAT, stimulation during the night-time at a minimum frequency of 5 Hz for at least 2 h is optimal.

The effects of bilateral and unilateral stimulation of the CSTs using 10 Hz stimulation for 1 h at night were also examined (Bowers and Zigmond, 1982). Whilst there was no difference in AANAT activity as a result of left vs right CST unilateral stimulation, bilateral stimulation during the night-time produced a greater increase (>3-fold) in AANAT levels compared to unilateral stimulation. This suggests that there is equal input from both ganglia to the pineal, and bilateral CST stimulation is necessary in order to drive a maximal pineal sympathetic response.

Changes in the enzyme HIOMT in response to stimulation of structures in the pineal sympathetic pathway have not been fully investigated. This is likely because N-acylation of serotonin by the enzyme AANAT is generally considered to be the rate-limiting step in melatonin biosynthesis. Contrarily, it has been hypothesised that HIOMT is the true rate-limiting step in the pathway (Liu and Borjigin, 2005). This is due to high levels of pineal melatonin being apparent during the dark phase in rats despite chronic low levels of AANAT as a result of a point mutation in the *Aanat* gene. Following stimulation of the pre-ganglionic SCG fibres, one study (Reuss et al., 1989) observed no changes in the activity levels of the enzyme HIOMT when stimulating for 2 h, whereas another previously reported an 18% decrease in HIOMT when stimulating for 4 h (Brownstein and Heller, 1968). It is possible that this difference is due to insufficient stimulation time, yet, it has been previously shown that 2 h of stimulation is sufficient to maximally upregulate AANAT levels (Bowers and Zigmond, 1982). Such differences in results may be due to variations in stimulation paradigms and/or experimental protocols. Further differences pertaining to these two studies include enucleated vs blinded animals, unilateral vs bilateral stimulation, stimulation current, stimulation pulse duration, and type of anaesthetic used (for further details please see **Table 2**).

Most studies into pineal neuromodulation have been conducted in rats that are nocturnally active creatures. Mice appear to be disfavoured among studies investigating pineal output due to the fact that many commonly used strains of laboratory mice do not produce melatonin (Goto et al., 1989). Unilateral stimulation of the left SCG during the light period in the rabbit produced a significant increase (on average 15-fold) in plasma melatonin levels compared to pre-stimulation levels (Chan et al., 1989). Rabbits were stimulated at an unusually high frequency (300 Hz) at 5 mA for 7.5 s every 20 s for 24–60 min. Blood samples were collected from the confluens sinuum, where it is generally agreed that pineal melatonin is secreted (Quay, 1973). This means it is reasonable to assume the levels of plasma melatonin detected are not, in fact, secreted from extrapineal sources. As rabbits are crepuscular rather than nocturnal, such a study shows pineal output alteration can be achieved in different species despite their varying sleep/wake rhythms. The authors use of such a high frequency is curious as the other experiments reviewed do not use frequencies any higher than 80 Hz. Moreover, it has been previously shown that repetitive stimulation of the preganglionic SCG fibres at frequencies higher than 35 Hz in the rabbit results in a decline in successive action potential amplitude (Eccles, 1955). This suggests that although a pineal modulatory response may be elicited with stimulation at 300 Hz, a maximal response may be achieved with a much lower frequency.

The pattern of stimulation was an important determinant in the upregulation of AANAT despite the same average stimulation frequency (Bowers and Zigmond, 1982). 2-s bursts of 10 Hz bilateral CST stimulation every 20 s was amongst the most proficient to increase enzyme levels in comparison to constant 1 Hz stimulation for the same length of time (Bowers and Zigmond, 1982). This agrees with previous findings that documented successive episodes of bilateral stimulation produced a larger overall response from pineal cells compared to a single episode (Reuss et al., 1985b). In addition, it confirms that 1 Hz is incapable of upregulating pineal indoleamine/enzyme levels. However, it was found that 1 s bursts of 10 Hz every 10 s, and 4 s bursts of 5 Hz every 20 s did not significantly increase enzyme levels. Together, these findings indicate that whilst repeated episodes of bilateral stimulation at a frequency greater than 5 Hz are most effective for increasing sympathetic pineal output, the specific pattern of stimulation is important in order to exert an effect.

Fibres projecting from the SCN to the PVN are thought to be gamma-aminobutyric acid (GABA)-ergic in their output, ultimately resulting in inhibition of pineal melatonin synthesis (Teclemariam-Mesbah et al., 1999; Kalsbeek et al., 2000; Buijs et al., 2003). This aligns with the identity of the SCN as the master pacemaker, which exerts control over slave oscillators such as the pineal gland. The functional output of fibres arising from PVN is less clear. It has been previously speculated that the PVN provides inhibitory input to the pineal sympathetic pathway and experimental data at the time seemed to support this hypothesis (Gilbey et al., 1982a,b). However, recently the PVN is thought to be responsible for communicating excitatory glutamatergic signals to the IML (Yanovski et al., 1987; Kannan et al., 1989). Therefore, stimulation of the PVN is expected to result in an increase in pineal metabolic output. Variation of bilateral stimulation duration (10 Hz at 0.1 mA for 0.2 ms) of

the PVN resulted in a significant reduction in pineal AANAT levels following 60 min of PVN stimulation in rats during the day-time (Reuss et al., 1985a). During the night-time, a minimum of 30 min stimulation was necessary in order to significantly reduce AANAT levels, however, neither AANAT nor melatonin levels were reduced to that of day-time levels, but perhaps longer lengths of stimulation are necessary in order to elicit such results. Likewise, it was demonstrated that brief (2 min) invasive bilateral electrical PVN stimulation (10 Hz) is capable of inducing significant decreases in pineal melatonin, AANAT and NE in rats, compared to control levels – similar to the effect achieved with exposure to light during the night-time (Olcese et al., 1987). Given that the PVN is thought to provide excitatory input to the IML, this decrease in AANAT levels is somewhat unexpected. However, it has been previously noted that urethane anaesthesia can trigger a decrease in sympathetic output of the PVN (Kannan et al., 1987, 1989; Yamashita et al., 1987). Both Reuss et al. (1985a,b) and Olcese et al. (1987) used urethane as anaesthetic during their stimulation experiments, therefore it is possible that such use inflicted a confounding effect on their results, masking an otherwise excitatory sympathetic outflow of the PVN.

Placing potential confounding influences aside, Olcese et al. (1987) deduced that the observable changes in AANAT, melatonin and NE levels after such short stimulation periods were due to waiting at least 30 min before sacrifice. Previous experiments that euthanized animals immediately following cessation of the stimulation period reported significant changes in pineal AANAT, melatonin and NE levels only after much longer periods of stimulation (e.g., Reuss et al., 1985b). Therefore, they inferred that there exists a time delay between application of a stimulus and an effect on pineal melatonin and AANAT levels (Olcese et al., 1987). Whilst this may ring true for the mechanisms involved in decreasing pineal AANAT and melatonin levels, other experiments (Volkman and Heller, 1971) indicate this is not the case for inducing increasing pineal AANAT levels. In fact, it was found that AANAT levels were lower when waiting an hour post-stimulation prior to sacrificing as opposed to levels encountered upon immediate sacrifice.

Non-invasive Stimulation

Alongside experiments that directly stimulate structures in the pineal sympathetic innervation pathway, non-invasive stimulation methods have also been explored. The effects of unilateral transcutaneous auricular vagus nerve stimulation on pineal melatonin levels in Zucker lean and Zucker diabetic obese (ZDO) rats was investigated (Li et al., 2014). Stimulation was applied once during the day-time to the right auricular concha region via opposing magnetic electrodes. Stimulation frequency switched every second between 2 and 15 Hz at a current of 2 mA. Following 34 consecutive days of stimulation, plasma melatonin levels in stimulated ZDO rats was significantly higher compared to non-stimulated controls. Furthermore, this elevated concentration was detectable for over 20 h after the final stimulation session. Notably, the experimenters investigated the effect of transauricular vagus nerve stimulation (taVNS) on pinealectomised ZDO rats and were still able to observe acute increases in plasma melatonin levels similar to that seen in intact ZDO rats. Similar results were also achieved 1 year later using bilateral taVNS (Wang et al., 2015). As increases in melatonin were still observed despite removal of the pineal gland, this indicates that vagus nerve stimulation prompts secretion of melatonin from extrapineal sites rather than from the gland itself. However, since usual pinealectomy removes only the superficial portion of the gland, leaving the deep pineal intact, one cannot discount the possibility that circulating melatonin levels may be due to contribution from the deep portion of the gland. Yet, atrophy of the deep pineal is apparent following superficial pinealectomy in rats (Heidbuchel and Vollrath, 1983), which most likely results in impaired function, although this has not been confirmed. This is not surprising since the sympathetic fibres that innervate the gland first supply the superficial pineal before coursing down the stalk and supplying innervation to the deep pineal. This suggests that removal of the superficial pineal disrupts the sympathetic input to the deep pineal, which would account for the observed atrophy. If sympathetic input is disrupted, then one may speculate that the likelihood of the deep pineal contributing to systemic melatonin levels is low.

Studies into the antidepressant activity of electroconvulsive shock (ECS) therapy and its relation to pineal hormone levels are a less specific form of non-invasive pineal neuromodulation. No significant changes in pineal melatonin nor NAS levels following such stimulation were observed in rats (McIntyre and Oxenkrug, 1984). However, a significant decrease (40%) in serotonin levels in the pineal gland following seven days of single electroconvulsive stimulation at 130 V for 0.75 s was shown. Contrasting findings have been reported. Delivery of an ECS (130 V administered for 0.75 s) also via ear clip electrodes to rats during the day-time in order to induce tonic-clonic seizures lasting between 20–25 s resulted in pineal melatonin and serotonin levels had doubling, and 5-HIAA levels increased by 80% (Oxenkrug et al., 1991). However, NAS levels were below the detection limits in both groups, a finding that authors speculate could be due to all available NAS being rapidly converted into melatonin. Interestingly, serotonin levels were not significantly changed following stimulation, which contrasts with the previous findings (McIntyre and Oxenkrug, 1984). Given that both studies utilised the same stimulation parameters, the reasons underlying these differences remain unclear. It is possible that variation in experimental procedures are accountable. For example, Oxenkrug et al. (1991) extracted pineals for analysis 90 min following the cessation of stimulation whereas McIntyre and Oxenkrug (1984) performed extraction at 2100 h despite stimulating in the morning. This prolonged delay between stimulation and pineal extraction may have caused any pineal indoleamine increase to have dissipated. Consistent with this, invasive studies discussed in the above sections reinforce the notion that pineal modulatory effects are short-lived following cessation of the stimulus (Volkman and Heller, 1971; Bowers and Zigmond, 1980).

Nowak et al. (1988) examined AANAT levels following administration of trains of 10 ECS via ear clip electrodes to rats. Each train lasted 500 ms at a frequency of 50 Hz, and was delivered daily for ten consecutive days. No significant differences

were found in pineal AANAT levels in the experimental group following the course of stimulation compared to the control group. The authors also investigated the effect of ECS coupled with the β-adrenoreceptor agonist, isoproterenol. It was shown that treatment with this agonist in conjunction with a single ECS during the day-time produced a significant increase in AANAT compared to isoproterenol treatment alone. This increase was only apparent when tissue was collected 4 h after treatment onset, whereas no increase was observed when tissue was collected after 2 h. This is in contrast to findings that suggest a minimal delay between stimulation and analysis of the gland's contents is optimal for detection of pineal substances of interest (Volkman and Heller, 1971; Bowers and Zigmond, 1980; McIntyre and Oxenkrug, 1984; Oxenkrug et al., 1991). Interestingly, when isoproterenol was coupled with trains of ten ECSs over 10 days, no significant change in AANAT levels were observed compared to the treatment with the agonist alone, regardless of euthanasia time. This indicates that a single stimulation period is capable of upregulating enzyme levels but the mechanism by which this occurs takes over 2 h to yield a significant effect. It also suggests repeated sessions are not capable of modulating the enzymatic activity of the pineal gland. This may be due to saturation of the enzyme induction mechanism responsible for the upregulation of AANAT leading to enzyme depletion, desensitisation of the adrenergic receptors, or perhaps some form of negative feedback circuit that prevents excessive *Aanat* gene expression such as receptor downregulation. Such an explanation could provide clarification as to why McIntyre and Oxenkrug (1984) also found no significant modulation of melatonin nor NAS levels with repeated stimulation, whereas Oxenkrug et al. (1991), using single instances of stimulation, did.

The studies utilising ear clip electrodes may be stimulating the vagus nerve rather than the pineal sympathetic innervation pathway. This is because an auricular branch of the vagus nerve exists in the ear and stimulation of this part of the anatomy has been shown to successfully stimulate the vagus nerve (Lewy and Newsome, 1983; Kreuzer et al., 2012, 2014; Capone et al., 2015). Two studies explored this possibility by investigating plasma melatonin levels in both intact and pinealectomised rats (Li et al., 2014; Wang et al., 2015). It was found in both cases that increases in the hormone were still evident in the pinealectomised groups indicating melatonin release is facilitated from extrapineal sources. Nowak et al. (1988) did not investigate the effects in pinealectomised rats, however, AANAT levels were quantified following homogenisation of the pineal gland, confirming increased levels of the enzyme in the gland.

The release of melatonin has been suggested to be an endogenous, anticonvulsant (for review see Munoz-Hoyos et al., 1998). Indeed, studies have investigated this line of research in addition to exploring therapeutic interventions that aim to increase endogenous melatonin. Chao et al. (2001) induced seizures via injection of benzylpenicillin into the hippocampus of rats followed by administration of electroacupuncture to the acusites Fengfu (DU16) and Jinsuo (DU8). These acusites are located on the midline at the nape of the neck and between the ninth and tenth thoracic vertebrae, respectively. According to a dermatome mapping study, the nape of the neck is related with spinal nerves C2 and C3 in the rat (Takahashi and Nakajima, 1996). Following electroacupuncture, both central and peripheral melatonin levels were shown to be significantly elevated. At the level of C2 and C3, sympathetic input is supplied by the SCG, which is implicated in the pineal sympathetic innervation pathway (Netter, 1999; von Lanz and Wachsmuth, 2003; Lingford- Hughes and Kalk, 2012). Therefore, it is possible that electroacupuncture at this site stimulated this pathway directly to increase pineal metabolic output. Acupuncture increased nocturnal levels of the urinary melatonin metabolite 6-sulfatoxymelatonin (a6MTs) following ten bi-weekly acupuncture sessions in humans (Spence et al., 2004). In addition, increased nocturnal levels of the same urinary metabolite were found following a 5-week intervention consisting of two acupuncture treatments per week (Kayumov et al., 2003). Both studies do not note the acusites employed during the experiments, therefore no deduction can be made on which dermatomes were stimulated in order to facilitate increase in a6MT levels. Moreover, there is a possibility the myotomes or osteotomes were stimulated rather than dermatomes, which could exert different effects than those intended. Also, it is possible that the increase in the a6MT metabolite may be due to release of melatonin from extrapineal sites. In disagreement with this, a decrease in metabolite levels occurs in both humans (Neuwelt and Lewy, 1983) and rats (Lewy et al., 1980) following pinealectomy, supporting the notion of the pineal gland as the major source of circulating melatonin. Although these results support the idea that neuromodulation of pineal gland metabolic output may be achieved by less invasive stimulatory methods, further studies are required – perhaps utilising pinealectomy – in order to clarify whether increased melatonin is due to stimulation of the pineal gland and not other structures.

CLINICAL ASPECTS

Melatonin

Melatonin is a circadian rhythm synchroniser (Pfeffer et al., 2018) and disruptions in melatonin levels are linked to sleep disorders and chronic sleep deprivation (Zisapel, 2018). Sleep deprivation is a pervasive problem throughout society. A wide variety of reasons contribute to this problem such as: stress, prevalence of shift work, and prolonged working hours due to the advent of artificial light. In the short-term, sleep deprivation is associated with negative effects on memory, psychomotor skills, attention, and hyperalgesia (Zeitlhofer et al., 2000; Hoevenaar-Blom et al., 2011; Krause et al., 2019). Sleep deprivation is associated with a number of negative health repercussions, including suppression of the immune system (Dinges et al., 1995), acceleration of atherosclerosis (McAlpine et al., 2019), increased risk of developing obesity (Cappuccio et al., 2008), and development of certain cancers (Blask, 2009) (e.g., breast, Hansen, 2001; Mirick et al., 2001; Schernhammer et al., 2001, 2006), prostate (Kubo et al., 2006), endometrial (Viswanathan et al., 2007), and colorectal cancer (Schernhammer et al., 2003). In addition, one night of acute sleep deprivation is sufficient to increase DNA damage in otherwise healthy young adults (Cheung

et al., 2018). DNA damage, particularly double strand breaks, are especially hazardous to the genome. Disrepair upon replication leads to cell death, whilst misrepair can result in inappropriate end-joining events, which commonly underlies tumour development. As melatonin is a potent free-radical scavenger and powerful combatant against oxidative stress-induced damage, maintenance of optimal melatonin levels may be protective against DNA damage. This may be achieved through one or several of melatonin's known protective pathways such as: inhibiting pro-oxidative enzymes, activating antioxidant enzymes, and/or promoting DNA repair mechanisms.

Melatonin's antioxidant, anti-inflammatory, and free-radical scavenging properties may also be harnessed to promote tissue regeneration. When delivered via biomaterials that control its release, melatonin accelerates wound repair (Murali et al., 2016), promotes metabolic activity and proliferative capacity of mesenchymal stem cells (Çetin Altındal et al., 2019; Hu and Li, 2019), and enhances peripheral nerve regeneration (Qian et al., 2018). These actions are exerted through melatonin's regulation of the microenvironment and its antioxidant and anti-inflammatory properties. Melatonin and NAS also act as neuroprotective agents via several mechanisms (Luo et al., 2019) including: combating oxidative stress (Wang et al., 2009; Chern et al., 2012; Li et al., 2014; Wong et al., 2014), inhibiting cell death processes (Savaskan et al., 2007; Wang et al., 2009; Zhang et al., 2013; Zhou et al., 2014; Hoshino et al., 2017), and promotion of anti-inflammatory pathways (Wang et al., 2009, 2013; Carloni et al., 2016; Lin et al., 2016). Such findings indicate melatonin as a promising focus in regenerative and therapeutic medicine with potential benefits for sufferers of stroke, traumatic brain injury, and neurodegenerative diseases.

Sleep deprivation is also linked to an increased risk of developing neurodegenerative diseases such as Alzheimer's disease (AD) (for review see: Kumar and Chanana, 2014). It has been demonstrated via sampling CSF, that merely one night of sleep deprivation is sufficient to interfere with the normal physiological drop in β-amyloid (Aβ) protein levels (Ooms et al., 2014) and that disruption to slow-wave sleep is key to this effect (Zempel et al., 2017). This suggests that chronic slow-wave sleep deprivation may result in continuous elevation and accumulation of Aβ, which is theorised as the starting point for AD pathogenesis according the amyloid cascade hypothesis (Hardy and Higgins, 1992). Moreover, animal studies indicate that disruption to the sleep-wake cycle promotes excessive hyperphosphorylation of the tau protein in the brain (Rothman et al., 2013; Di Meco et al., 2014) leading to the formation of neurofibrillary tangles (NFTs), which are considered a neurological hallmark of AD. Interestingly, levels of melatonin in the CSF of AD patients progressively diminish as the disease progresses (Liu et al., 1999). Given that melatonin is a prominent regulator of the sleep-wake cycle, it has been suggested that this reduction in melatonin may at least partially drive the development of the disease. In this context, upregulation of endogenous melatonin may help slow the progression of AD. Indeed, melatonin has been shown to have beneficial effects both pre- and post-Aβ formation through transcriptional regulation of Aβ synthesis (Peng et al., 2013; Panmanee et al., 2015; Shukla et al., 2015; Mukda et al., 2016), acting as an antioxidant and free-radical scavenger to combat oxidative stress associated with Aβ-induced neurotoxicity (Rodriguez et al., 2004; Reiter et al., 2013; Zhang and Zhang, 2014) and, inhibition of Aβ fibrillogenesis (Pappolla et al., 1998; Bazoti et al., 2005) (for review see: Vincent, 2018).

Some sleep disorders are considered prodromal markers for such neurodegenerative diseases. For example, REM sleep behavior disorder (RBD) is a parasomnia that is characterised by an absence of muscle atonia during REM sleep. This results in sufferers acting out their dreams in a vigorous and often violent manner. RBD is strongly linked with α-synucleinopathies, and is considered a prodromal marker for dementia with Lewy Bodies, multiple system atrophy, and Parkinson's disease (Boeve et al., 2013). Melatonin is known to influence REM sleep latency and length (Cajochen et al., 1997; Kunz et al., 2004), and exogenous melatonin is currently used as a symptomatic treatment for RBD with clinical and neurophysiological benefits still observed up to 3 years following cessation of treatment (Kunz and Bes, 1999; Boeve et al., 2003; Kunz and Mahlberg, 2010; Schaefer et al., 2017). Further, as endogenous levels of melatonin decrease with age (Waldhauser et al., 1988; Garfinkel et al., 1995), which coincides with an increase in neurodegenerative disorders, it is possible that the age-associated decline in melatonin levels is causally linked to the development of neurodegenerative diseases (Reiter et al., 1994). Therefore, stimulating an increase in endogenous levels of melatonin may have beneficial protective, antioxidant and free-radical scavenging effects to dampen the progression of neurodegenerative diseases.

NAS

N-acetylserotonin, being an immediate precursor to melatonin and also showing circadian rhythmicity (Chattoraj et al., 2009), has naturally been investigated for its potential effects on sleep regulation. However, recent research is examining the role of NAS on neurogenesis, mood regulation and neuroprotection. Neurogenesis occurs throughout adulthood in humans and rats in the dentate gyrus of the hippocampus as well as along the rostral migratory stream (Eriksson et al., 1998; Gould et al., 1999; Curtis et al., 2007). Studies have shown voluntary exercise and environmental enrichment can increase neurogenesis, whereas both aging and sleep deprivation impair the neurogenic response (Ming and Song, 2005; Lledo et al., 2006; Zhao et al., 2008; Ma et al., 2009). It is possible that exogenous administration of NAS could play a role in stimulating an increase in neurogenesis, and therefore, infer a positive influence on aspects of memory, mood control, and mitigate the development of neurological conditions.

Early studies have found NAS and its associated enzyme, AANAT, present in areas of the CNS such as the hippocampus, olfactory bulb, spinal cord and cerebellum despite the absence of melatonin (Paul et al., 1974; Psarakis et al., 1982; Gaudet et al., 1991; Chae et al., 1999). Further, approximately 15% of synthesised melatonin is converted back into NAS (Leone and Silman, 1984; Young et al., 1985). NAS also shows a much higher affinity for the MT3 receptor than melatonin itself Nosjean et al. (2000) leading to some researchers pondering

whether the MT3 receptor should actually be reclassified as a NAS receptor (Jang et al., 2010; Oxenkrug and Ratner, 2012). Further, unlike melatonin, NAS is able to activate the tropomyosin receptor kinase B (TrkB) receptor, which is involved in mediating the effects of the neurotrophic factor, BDNF (brain derived neurotrophic factor) that plays a role in regulating neuronal activity and normal day-to-day function (Jang et al., 2010). BDNF-TrkB signaling is known to regulate a wide range of functions including: cell survival, neuronal differentiation and migration, neurite outgrowth, and facilitation of long-term potentiation and plasticity. Both BDNF and its high affinity receptor, TrkB, are widely produced throughout the CNS with high expression being observed in areas such as the neocortex, hypothalamus, and amygdala. Similar to melatonin, the expression of both BDNF and TrkB decrease with age, indicating neurons and glia yield a limited trophic ability to combat natural and pathological neurodegeneration (Berretta et al., 2014). In the absence of BDNF, NAS may act as an agonist for the TrkB receptor and enable circadian rhythmicity and also stimulate neurogenesis (Jang et al., 2010). Further, it seems that NAS is able to protect against sleep-deprivation-induced suppression of neurogenesis (Sompol et al., 2011). Whilst melatonin has previously been implicated in hippocampal neurogenesis (Ramirez-Rodriguez et al., 2009, 2011; Rennie et al., 2009; Manda and Reiter, 2010), further research indicates it does not increase the number of neuroblasts (Jang et al., 2010; Sompol et al., 2011), but may instead assist in neuroblast survival (Ramirez-Rodriguez et al., 2011). Taken together, these findings strongly indicate a melatonin-independent neuroregenerative role for NAS. Moreover, they suggest NAS is sufficient to induce hippocampal neurogenesis and mediate the negative effects chronic sleep deprivation imposes on hippocampal neurogenesis. Therefore, upregulation of pineal metabolic output may infer therapeutically beneficial effects via increasing systemic NAS levels in addition to melatonin levels. Given the interaction of NAS with TrkB, it remains to be determined if NAS-TrkB signalling has anti-brain aging and enhanced brain plasticity effects, similar to BDNF-TrkB signaling. The physiological and pathophysiological effects of NAS still remain poorly understood and much further work is required to investigate the role NAS plays in normal brain function.

EVALUATION OF STIMULATION PARAMETERS

Frequency

The frequency of stimulation appears to be particularly important when attempting to maximally influence pineal gland activity. A 10 Hz frequency appears capable of eliciting temporal facilitation whilst much lower frequencies are not. This suggests higher frequency stimulation exerts a greater effect on pineal sympathetic activity compared to lower frequency stimulation. Indeed, this finding from evoked potentials appears to concur with findings investigating pineal metabolic output. Stimulation at 5–10 Hz elicits the greatest increases in AANAT activity, whilst 1–2.5 Hz stimulation elicit subdued responses (Bowers and Zigmond, 1982; Lingappa and Zigmond, 2013). Frequencies below 5 Hz seem to produce submaximal upregulation of pineal metabolism, with 1 Hz capable of downregulating AANAT activity. This downregulation may occur due to failure in synaptic transmission and only occur following stimulation of pre-ganglionic fibres. A few studies investigated frequencies higher than 10 Hz, however the frequency effects are unclear as the majority of the literature only specifies frequency range (i.e., 10–20 Hz). One study (Brooks et al., 1975) used a stimulation frequency of 30 Hz and successfully recorded evoked potentials in the pineal gland. This suggests higher frequencies are capable of influencing the gland electrophysiologically, however, it is unclear how this affects melatonin metabolism. Therefore, further research is required in order to examine the effects of high frequency invasive stimulation on pineal gland metabolic output.

From the reviewed studies, stimulation at 10 Hz appears to be the most efficacious frequency for invasive stimulation. Higher frequencies are more commonly used in non-invasive stimulation literature. However, detailed stimulation parameter reporting in these studies is generally poor with only half reporting the frequency of stimulation used. This means it is difficult to ascertain the effects of different stimulation paradigms in the context of non-invasive stimulation. Two studies that do report the stimulation frequency used offer conflicting results, with one indicating upregulation of melatonin levels, and the other only reporting upregulation of such levels in the presence of a β-adrenergic agonist. This could be due to differences in current used, or other experimental variables that are again, poorly defined. The evidence presented suggests non-invasive stimulation is capable of modulating pineal gland metabolic output but further studies are necessary before definite conclusions can be made on the optimal stimulation parameters to be used.

Unilateral vs. Bilateral Stimulation

It appears that whilst unilateral stimulation is capable of evoking changes in pineal gland output, bilateral stimulation produces a more pronounced effect. This is particularly evident in the study conducted by Bowers and Zigmond (1982) that describes unilateral stimulation producing less than half the increase in pineal AANAT activity compared to bilateral stimulation. This study provides a useful comparison of the effects between these two variables due to the conservation of experimental and reporting methods between experiments. It proves difficult to compare the effects of other studies as many utilise different measurement units for quantifying the levels of AANAT or melatonin as the weight of pineal glands are not often detailed, making it impossible to accurately compare such levels. Moreover, even when units between studies align, other parameters such as frequency, or stimulation length are not aligned, so direct comparisons of pineal levels cannot be made. Interestingly, there are no differences in evoked potentials from pineal cells between unilateral and bilateral stimulation (Patel and Demaine, 1990). This indicates that the observed pineal cell firing does not equate with the enzymatic upregulation in the grand in response to sympathetic input.

Duration of Stimulation

The duration for which stimulation is administered appears to be critical. Stimulation for 15 min does not significantly increase AANAT levels, whereas stimulation for 2 h does (Reuss et al., 1989). This suggests that in order for stimulation at 5–10 Hz to produce optimal increases in AANAT activity, stimulation must be maintained for a sufficient length of time. Further, one study noted a decline in AANAT levels following cessation of 1 h at 5 Hz stimulation (Bowers and Zigmond, 1980). Another study reported that significant increases in AANAT activity persist following 2 h of stimulation at 10 Hz despite not sacrificing until 1 h following stimulation cessation (Volkman and Heller, 1971). This indicates that longer stimulation periods are likely to result in persisting pineal modulatory effects, whereas shorter periods of stimulation are not. Perhaps longer stimulation periods are required to alter AANAT levels due to transcription and translation of the *Aanat* gene being necessary before changes in the enzyme become apparent. Indeed, Nowak et al. (1988) reported that significant increases in AANAT levels were only apparent when sacrifice occurred 4 h following stimulation onset supporting the notion that such changes require some time before becoming apparent. In contrast, rapid changes in cAMP may be detected due to its relatively upstream position in the pineal sympathetic pathway. Rapid changes in pineal melatonin levels following PVN stimulation may be mediated via its theorised central input pathway to the gland, independent of the pathway incorporating the SCG.

Repetition, Pulse Duration, and Pattern of Stimulation

Successive bilateral SCG stimulation recruits a greater number of pinealocytes to fire, yet this is not the case for unilateral stimulation (Reuss et al., 1985b). This suggests a potential meta-modulatory effect, but only when input is sourced from both ganglia. This again supports the notion of pinealocyte response heterogeneity that is dependent upon the source of input. However, as only a subset of cells within the pineal have been investigated thus far, it is perhaps not wise to extrapolate the results of such small cell populations to the response of the gland as a whole.

Pulse duration of the stimulus delivered to the CSTs appears to affect the current threshold necessary to generate an action potential. A strength-duration relationship is evident, with lower pulse durations requiring a greater current to be used in order to elicit an evoked response in the postganglionic fibres. The data suggest a minimum pulse duration of 3 ms is necessary in order to accommodate a lower current and prevent potential hyperpolarisation of postganglionic cell membranes.

The pattern of the stimulation pulse also appears important in the optimal upregulation of pineal AANAT (Bowers and Zigmond, 1982). Strangely, patterns that correspond to similar relative durations of "on" stimulation and "off" stimulation appear to have significantly different upregulatory powers. It is unclear why certain patterns are more capable of exerting an upregulatory influence than others. Perhaps a minimum pulse duration of 2 s is necessary and perhaps these optimal patterns reflect the endogenous stimulation patterns delivered to the pineal. However, a limited number of stimulation patterns have been investigated, therefore, a stimulation pattern of greater upregulatory effect may exist. Further studies are necessary in order to clarify the effects of various stimulation patterns on the response of the pineal gland.

Light During Stimulation and Sacrifice

Although pineal modulation appears to be possible at any time of the day, stimulation of the CSTs during the night elicits the most rapid response. Night-time stimulation linearly increases pineal AANAT activity – reaching peak night-time levels within 2 h. In contrast, day-time stimulation has a variable rate of increase in AANAT activity, accelerating with passing time (Bowers and Zigmond, 1982). Stimulation of the PVN is equally effective in reducing AANAT levels when conducted during the day or night (Reuss et al., 1985a). However, such decreases during night-time stimulation are only significant when performed during the late portion of the dark phase (i.e., 0400–0600 h). This reduced effect of PVN stimulation does not seem to apply to stimulation of the CSTs, which proves capable of increasing AANAT activity during similar time periods (Bowers and Zigmond, 1980; Reuss et al., 1985b). It has been posited that the PVN provides inhibitory input to the pineal sympathetic pathway (Gilbey et al., 1982a,b). An explanation for this reduced response following PVN stimulation may be that inhibitory responses are themselves, in some way inhibited or dampened during the early and middle portions of the dark phase. Such dampening effects may help to maintain increased pineal indoleamine and enzyme levels during this time. However, more recently, the PVN is thought to be responsible for communicating excitatory glutamatergic rather than inhibitory GABA-ergic signals to the IML (Yanovski et al., 1987; Kannan et al., 1989). If this were true, one would expect PVN stimulation to increase AANAT levels. It has been previously noted that urethane anaesthesia can affect the sympathetic output of the PVN resulting in decreased sympathetic outflow (Kannan et al., 1987, 1989; Yamashita et al., 1987). Reuss et al. (1985a) used urethane anaesthesia during stimulation, therefore it is possible that such use inflicted a confounding effect on their results, masking an otherwise excitatory sympathetic outflow of the PVN.

Brief exposure to light during the dark phase is sufficient to rapidly decrease night-time AANAT levels to that of the day-time levels (Klein and Weller, 1972). It is therefore crucial that lighting conditions during night-time stimulations up to the point of sacrifice are carefully controlled. In the majority of the reviewed literature, the lighting conditions during such stimulation are not described. Lighting conditions during sacrifice are more often detailed as being carried out under dim-red light. Up until recently, dim-red "safe-light" with wavelengths above 600 nm was thought suitable for pineal-centred experiments due to the assumption that longer wavelengths of light exerted no influence on circadian rhythms. However, research in recent years strongly indicates that this is not the case. Dauchy et al. (2015) provided

compelling evidence that plasma melatonin levels of rodents housed with such "safe-lights" during the night were significantly lower ($p < 0.001$) than those of rodents housed in complete darkness during the night. Such findings undermine the validity of the results of studies conducted using dim-red light. It is possible that levels of any pineal substances measured are not in fact the true maximal levels achievable either during the nightly peak or via stimulation. One way to circumvent such confounding factors may be to use complete darkness during the subjective night-time of the animals in future experiments. However, this may not prove practicable as manipulations often need to be carried out during the dark period and use of complete darkness would prove dangerous for both the researcher and animal due to increased risk of injury. Another approach is to blind the animals via optic transection or enucleation as some of the authors in this review have opted to perform. This would ensure the animals are not exposed to any light stimulus and allows the researcher to perform manipulations unimpeded. However, consideration must be given as to whether possible melatonin desynchrony, as occurs following blindness in humans (Lewy and Newsome, 1983), is allowable. Researchers may consider the use of infrared goggles to be able to see in the dark and not disrupt animals' melatonin levels. Some of these goggles do emit light, therefore care must be taken to perform manipulations quickly in order to ensure minimal disruption to melatonin rhythms.

CONCLUSION

The pineal neuromodulatory response is thought to be mediated via upregulation of the enzyme AANAT, which in turn facilitates the increase of melatonin via its aforementioned biosynthetic pathway. Previously, the majority of studies investigated the potential benefits of upregulating pineal melatonin levels. Melatonin is undoubtedly a hormone with many potential therapeutic benefits. Its reported influences on physiology are vast and well documented including: its actions as a potent antioxidant and free-radical scavenger (for review see, Reiter et al., 2016), antiaging and anti-inflammatory properties (for reviews see: Hardeland, 2013; Mauriz et al., 2013), influence on reproductive behavior (for review see, Reiter et al., 2009) as well as sleep (for review see, Dawson and Encel, 1993). However, more recently, it is NAS that has been the subject of much investigation in other research areas.

Melatonin has been identified as a promising avenue of treatment for neurodegenerative disorders such as Parkinson's Disease (for review see, Mack et al., 2016). Comparatively, the potential therapeutic role of NAS has clearly been grossly underestimated in the past and therefore, much investigation in pineal stimulation studies is warranted. This may be considered a limitation of the research pertaining to the therapeutic effects of increasing pineal output discussed in this review, as most of the studies in this area of research have neglected NAS as a significant output of the gland.

The discussed findings in this review illustrate that invasive neuromodulation of the pineal is clearly possible. This is demonstrated through modulation pineal enzymatic activity and indolamine levels. There also exist encouraging results regarding the capability of non-invasive stimulation to produce similar effects. Unfortunately, many of the studies reviewed are lacking in detail regarding experimental protocol and stimulation paradigms. This makes it exceedingly difficult to draw accurate comparisons between the data. Where fair comparisons can be made are generally between data within the same study. It is therefore fortunate that a number of the reviewed pieces of literature were extensive and contain numerous experiments using the same methods. However, caution should be taken when generalising the findings from a handful of studies. Further, there exists little data correlating the electrical activity of pinealocytes with the regulation of melatonin synthesis. This is therefore a limitation of this review as assumptions must be made in order to connect the findings of the evoked cell potential with the indoleamine output and enzymatic activity research. However, the assumptions made have been previously postulated in previous literature and this review makes no attempt to offer novel assumptions in this regard. It is clear that further research is required in order to confirm the findings of previous research, but future studies should take care to conduct experiments using optimal stimulation parameters and be meticulous in detailing experimental variables when reporting results. According to the outcomes of this review, future studies should stimulate the SCG bilaterally at 10 Hz with a minimum pulse duration of 2 s and a minimum overall stimulation period of 2 h during the night-time in total darkness in order to exert optimal increases in pineal indoleamine levels and enzymatic activity. Further investigation is necessary in this field to uncover whether increases in NAS may result in physiological beneficial outcomes rather than the assumed melatonin, or at least partially.

AUTHOR CONTRIBUTIONS

YC developed the concept. SL performed the literature review and wrote the draft. SL, AC, and YC analyzed the literature and wrote and edited the main manuscript. SL and YC carried out the diagrams.

ACKNOWLEDGMENTS

Figure 3 was created with biorender.com. **Figure 2** was created by Ella Maru Studio, Inc., United States.

SUPPLEMENTARY MATERIAL

The Supplementary Material for this article can be found online at: https://www.frontiersin.org/articles/10.3389/fnins.2020.00264/full#supplementary-material

REFERENCES

Aldhous, M., Franey, C., Wright, J., and Arendt, J. (1985). Plasma concentrations of melatonin in man following oral absorption of different preparations. *Br. J. Clin. Pharmacol.* 19, 517–521. doi: 10.1111/j.1365-2125.1985.tb02679.x

Al-Hussain, S. M. (2006). The pinealocytes of the human pineal gland: a light and electron microscopic study. *Folia Morphol. (Warsz)* 65, 181–187.

Bargmann, W. (1943). "Die epiphysis cerebri," in *Handbuch der mikroskopischen Anatomie des Menschen*, ed. W. von Möllendorff, (Berlin: Springer).

Bazoti, F. M., Tsarbopoulos, A., Markides, K. E., and Bergquist, J. (2005). Study of the non-covalent interaction between amyloid-β-peptide and melatonin using electrospray ionization mass spectrometry. *J. Mass Spectrom.* 40, 182–192. doi: 10.1002/jms.738

Berretta, A., Tzeng, Y. C., and Clarkson, A. N. (2014). Post-stroke recovery: the role of activity-dependent release of brain-derived neurotrophic factor. *Expert Rev. Neurother.* 14, 1335–1344. doi: 10.1586/14737175.2014.969242

Blask, D. E. (2009). Melatonin, sleep disturbance and cancer risk. *Sleep Med. Rev.* 13, 257–264. doi: 10.1016/j.smrv.2008.07.007

Boeve, B. F., Silber, M. H., and Ferman, T. J. (2003). Melatonin for treatment of REM sleep behavior disorder in neurologic disorders: results in 14 patients. *Sleep Med.* 4, 281–284. doi: 10.1016/s1389-9457(03)00072-8

Boeve, B. F., Silber, M. H., Ferman, T. J., Lin, S. C., Benarroch, E. E., Schmeichel, A. M., et al. (2013). Clinicopathologic correlations in 172 cases of rapid eye movement sleep behavior disorder with or without a coexisting neurologic disorder. *Sleep Med.* 14, 754–762. doi: 10.1016/j.sleep.2012.10.015

Bowers, C. W., Baldwin, C., and Zigmond, R. E. (1984a). Sympathetic reinnervation of the pineal-gland after postganglionic nerve lesion does not restore normal pineal function. *J. Neurosci.* 4, 2010–2015. doi: 10.1523/jneurosci.04-08-02010.1984

Bowers, C. W., Dahm, L. M., and Zigmond, R. E. (1984b). The number and distribution of sympathetic neurons that innervate the rat pineal-gland. *Neuroscience* 13, 87–96. doi: 10.1016/0306-4522(84)90261-6

Bowers, C. W., and Zigmond, R. E. (1980). Electrical stimulation of the cervical sympathetic trunks mimics the effects of darkness on the activity of serotonin: N-acetyltransferase in the rat pineal. *Brain Res.* 185, 435–440. doi: 10.1016/0006-8993(80)91082-3

Bowers, C. W., and Zigmond, R. E. (1982). The influence of the frequency and pattern of sympathetic nerve activity on serotonin N-acetyltransferase in the rat pineal gland. *J. Physiol.* 330, 279–296. doi: 10.1113/jphysiol.1982.sp014341

Brooks, C. M., Ishikawa, T., and Koizumi, K. (1975). Automic system control of the pineal gland and the role of this complex in the integration of body function. *Brain Res.* 87, 181–190. doi: 10.1016/0006-8993(75)90414-X

Brownstein, M. J., and Heller, A. (1968). Hydroxyindole-O-methyl-transferase activity: effect of sympathetic nerve stimulation. *Science* 162, 367–368. doi: 10.1126/science.162.3851.367

Buijs, R. M., van Eden, C. G., Goncharuk, V. D., and Kalsbeek, A. (2003). The biological clock tunes the organs of the body: timing by hormones and the autonomic nervous system. *J. Endocrinol.* 177, 17–26. doi: 10.1677/joe.0.1770017

Cajochen, C., Krauchi, K., Mori, D., Graw, P., and Wirz-Justice, A. (1997). Melatonin and S-20098 increase REM sleep and wake-up propensity without modifying NREM sleep homeostasis. *Am. J. Physiol.* 272(4 Pt 2), R1189–R1196. doi: 10.1152/ajpregu.1997.272.4.R1189

Cakmak, Y. O., Akpinar, I. N., Ekinci, G., and Bekiroglu, N. (2008). Point- and frequency-specific response of the testicular artery to abdominal electroacupuncture in humans. *Fertil. Steril* 90, 1732–1738. doi: 10.1016/j.fertnstert.2007.08.013

Calvo, J., and Boya, J. (1984). Ultrastructure of the pineal gland in the adult rat. *J. Anat.* 138(Pt 3), 405–409.

Capone, F., Assenza, G., Di Pino, G., Musumeci, G., Ranieri, F., Florio, L., et al. (2015). The effect of transcutaneous vagus nerve stimulation on cortical excitability. *J. Neural Trans.* 122, 679–685. doi: 10.1007/s00702-014-1299-7

Cappuccio, F. P., Taggart, F. M., Kandala, N. B., Currie, A., Peile, E., Stranges, S., et al. (2008). Meta-analysis of short sleep duration and obesity in children and adults. *Sleep* 31, 619–626. doi: 10.1093/sleep/31.5.619

Carloni, S., Favrais, G., Saliba, E., Albertini, M. C., Chalon, S., Longini, M., et al. (2016). Melatonin modulates neonatal brain inflammation through endoplasmic reticulum stress, autophagy, and miR-34a/silent information regulator 1 pathway. *J. Pineal Res.* 61, 370–380. doi: 10.1111/jpi.12354

Celnik, P., Hummel, F., Harris-Love, M., Wolk, R., and Cohen, L. G. (2007). Somatosensory stimulation enhances the effects of training functional hand tasks in patients with chronic stroke. *Arch. Phys. Med. Rehabil.* 88, 1369–1376. doi: 10.1016/j.apmr.2007.08.001

Celnik, P., Paik, N. J., Vandermeeren, Y., Dimyan, M., and Cohen, L. G. (2009). Effects of combined peripheral nerve stimulation and brain polarization on performance of a motor sequence task after chronic stroke. *Stroke* 40, 1764–1771. doi: 10.1161/strokeaha.108.540500

Cena, V., Halperin, J. I., Yeandle, S., and Klein, D. C. (1991). Norepinephrine stimulates potassium efflux from pinealocytes: evidence for involvement of biochemical "AND" gate operated by calcium and adenosine 3',5'-monophosphate. *Endocrinology* 128, 559–569. doi: 10.1210/endo-128-1-559

Çetin Altındal, D., James, E. N., Kaplan, D. L., and Gümüşderelioğlu, M. (2019). Melatonin-induced osteogenesis with methanol-annealed silk materials. *J. Bioact. Compatible Polym.* 34, 291–305. doi: 10.1177/0883911519847489

Chae, H. D., Park, T. J., Lee, Y. K., Lee, T. G., and Kim, K. T. (1999). Rapid and simple measurement of serotonin N-acetyltransferase activity by liquid biphasic diffusion assay. *Neurochem. Int.* 35, 447–451. doi: 10.1016/s0197-0186(99)00086-8

Chan, Y. S., Cheung, Y. M., and Pang, S. F. (1989). Elevation of pineal melatonin secretion by electrical-stimulation of the cervical sympathetic trunk in rabbits. *Neurosci. Lett.* 105, 107–112. doi: 10.1016/0304-3940(89)90020-7

Chao, D. M., Chen, G., and Cheng, J. S. (2001). Melatonin might be one possible medium of electroacupuncture anti-seizures. *Acupunct. Electrother. Res.* 26, 39–48. doi: 10.3727/036012901816356027

Chattoraj, A., Liu, T., Zhang, L. S., Huang, Z., and Borjigin, J. (2009). Melatonin formation in mammals: in vivo perspectives. *Rev. Endocr. Metab. Disord.* 10, 237–243. doi: 10.1007/s11154-009-9125-5

Chern, C.-M., Liao, J.-F., Wang, Y.-H., and Shen, Y.-C. (2012). Melatonin ameliorates neural function by promoting endogenous neurogenesis through the MT2 melatonin receptor in ischemic-stroke mice. *Free Radic. Biol. Med.* 52, 1634–1647. doi: 10.1016/j.freeradbiomed.2012.01.030

Cheung, V., Yuen, V. M., Wong, G. T. C., and Choi, S. W. (2018). The effect of sleep deprivation and disruption on DNA damage and health of doctors. *Anaesthesia* 74, 434–440. doi: 10.1111/anae.14533

Crupi, R., Mazzon, E., Marino, A., La Spada, G., Bramanti, P., Spina, E., et al. (2011). Melatonin's stimulatory effect on adult hippocampal neurogenesis in mice persists after ovariectomy. *J. Pineal Res.* 51, 353–360. doi: 10.1111/j.1600-079X.2011.00897.x

Curtis, M. A., Kam, M., Nannmark, U., Anderson, M. F., Axell, M. Z., Wikkelso, C., et al. (2007). Human neuroblasts migrate to the olfactory bulb via a lateral ventricular extension. *Science* 315, 1243–1249. doi: 10.1126/science.1136281

Dauchy, R. T., Wren, M. A., Dauchy, E. M., Hoffman, A. E., Hanifin, J. P., Warfield, B., et al. (2015). The influence of red light exposure at night on circadian metabolism and physiology in sprague–dawley rats. *J. Am. Assoc. Labor. Anim. Sci.* 54, 40–50.

Dawson, D., and Encel, N. (1993). Melatonin and sleep in humans. *J. Pineal Res.* 15, 1–12. doi: 10.1111/j.1600-079X.1993.tb00503.x

De Ridder, D., and Vanneste, S. (2012). EEG Driven tDCS versus bifrontal tDCS for tinnitus. *Front. Psychiatry* 3:84. doi: 10.3389/fpsyt.2012.00084

Di Meco, A., Joshi, Y. B., and Pratico, D. (2014). Sleep deprivation impairs memory, tau metabolism, and synaptic integrity of a mouse model of Alzheimer's disease with plaques and tangles. *Neurobiol. Aging* 35, 1813–1820. doi: 10.1016/j.neurobiolaging.2014.02.011

Dinges, D. F., Douglas, S. D., Hamarman, S., Zaugg, L., and Kapoor, S. (1995). Sleep deprivation and human immune function. *Adv. Neuroimmunol.* 5, 97–110. doi: 10.1016/0960-5428(95)00002-J

Eccles, R. M. (1955). Intracellular potentials recorded from a mammalian sympathetic ganglion. *J. Physiol.* 130, 572–584. doi: 10.1113/jphysiol.1955.sp005428

Eriksson, P. S., Perfilieva, E., Bjork-Eriksson, T., Alborn, A. M., Nordborg, C., Peterson, D. A., et al. (1998). Neurogenesis in the adult human hippocampus. *Nat. Med.* 4, 1313–1317. doi: 10.1038/3305

Faber, M., Vanneste, S., Fregni, F., and De Ridder, D. (2012). Top down prefrontal affective modulation of tinnitus with multiple sessions of tDCS of dorsolateral prefrontal cortex. *Brain Stimul.* 5, 492–498. doi: 10.1016/j.brs.2011.09.003

Fernandes, P. A., Cecon, E., Markus, R. P., and Ferreira, Z. S. (2006). Effect of TNF-alpha on the melatonin synthetic pathway in the rat pineal gland: basis for a 'feedback' of the immune response on circadian timing. *J. Pineal Res.* 41, 344–350. doi: 10.1111/j.1600-079X.2006.00373.x

Fink-Jensen, A., and Møller, M. (1990). Direct projections from the anterior and tuberal regions of the lateral hypothalamus to the rostral part of the pineal complex of the rat. An anterograde neuron-tracing study by usingPhaseolus vulgaris leucoagglutinin. *Brain Res.* 522, 337–341. doi: 10.1016/0006-8993(90)91480-5

Frank, E., Schecklmann, M., Landgrebe, M., Burger, J., Kreuzer, P., Poeppl, T. B., et al. (2012). Treatment of chronic tinnitus with repeated sessions of prefrontal transcranial direct current stimulation: outcomes from an open-label pilot study. *J. Neurol.* 259, 327–333. doi: 10.1007/s00415-011-6189-4

Fregni, F., Boggio, P. S., Lima, M. C., Ferreira, M. J., Wagner, T., Rigonatti, S. P., et al. (2006a). A sham-controlled, phase II trial of transcranial direct current stimulation for the treatment of central pain in traumatic spinal cord injury. *Pain* 122, 197–209. doi: 10.1016/j.pain.2006.02.023

Fregni, F., Gimenes, R., Valle, A. C., Ferreira, M. J., Rocha, R. R., Natalle, L., et al. (2006b). A randomized, sham-controlled, proof of principle study of transcranial direct current stimulation for the treatment of pain in fibromyalgia. *Arthritis Rheum* 54, 3988–3998. doi: 10.1002/art.22195

Fregni, F., Boggio, P. S., Mansur, C. G., Wagner, T., Ferreira, M. J. L., Lima, M. C., et al. (2005). Transcranial direct current stimulation of the unaffected hemisphere in stroke patients. *Neuroreport* 16, 1551–1555. doi: 10.1097/01.wnr.0000177010.44602.5e

Freschi, J. E., and Parfitt, A. G. (1986). Intracellular recordings from pineal cells in tissue culture: membrane properties and response to norepinephrine. *Brain Res.* 368, 366–370. doi: 10.1016/0006-8993(86)90583-4

Garfinkel, D., Laudon, M., Nof, D., and Zisapel, N. (1995). Improvement of sleep quality in elderly people by controlled-release melatonin. *Lancet* 346, 541–544. doi: 10.1016/s0140-6736(95)91382-3

Gaudet, S., Palkovits, M., and Namboodiri, M. A. (1991). Regional distribution of arylamine and arylalkylamine N-acetyltransferase activities in the rat brain. *Brain Res.* 539, 355–357. doi: 10.1016/0006-8993(91)91645-h

Gilbey, M. P., Coote, J. H., Fleetwood-Walker, S., and Peterson, D. F. (1982a). The influence of the paraventriculo-spinal pathway, and oxytocin and vasopressin on sympathetic preganglionic neurones. *Brain Res.* 251, 283–290. doi: 10.1016/0006-8993(82)90745-4

Gilbey, M. P., Peterson, D. F., and Coote, J. H. (1982b). Some characteristics of sympathetic preganglionic neurones in the rat. *Brain Res.* 241, 43–48. doi: 10.1016/0006-8993(82)91226-4

Goto, M., Oshima, I., Tomita, T., and Ebihara, S. (1989). Melatonin content of the pineal gland in different mouse strains. *J. Pineal Res.* 7, 195–204. doi: 10.1111/j.1600-079x.1989.tb00667.x

Gould, E., Reeves, A. J., Fallah, M., Tanapat, P., Gross, C. G., and Fuchs, E. (1999). Hippocampal neurogenesis in adult Old World primates. *Proc. Natl. Acad. Sci. U.S.A.* 96, 5263–5267. doi: 10.1073/pnas.96.9.5263

Haimov, I., Laudon, M., Zisapel, N., Souroujon, M., Nof, D., Shlitner, A., et al. (1994). Sleep disorders and melatonin rhythms in elderly people. *Br. Med. J.* 309, 167–167. doi: 10.1136/bmj.309.6948.167

Hansen, J. (2001). Increased breast cancer risk among women who work predominantly at night. *Epidemiology* 12, 74–77. doi: 10.1097/00001648-200101000-00013

Hardeland, R. (2013). Melatonin and the theories of aging: a critical appraisal of melatonin's role in antiaging mechanisms. *J. Pineal Res.* 55, 325–356. doi: 10.1111/jpi.12090

Hardy, J. A., and Higgins, G. A. (1992). Alzheimer's disease: the amyloid cascade hypothesis. *Science* 256, 184–185.

Hassinger, T. D., Atkinson, P. B., Strecker, G. J., Whalen, L. R., Dudek, F. E., Kossel, A. H., et al. (1995). Evidence for glutamate-mediated activation of hippocampal neurons by glial calcium waves. *J. Neurobiol.* 28, 159–170. doi: 10.1002/neu.480280204

Heidbuchel, U., and Vollrath, L. (1983). Pineal complex of rats: effects of superficial pinealectomy on the deep pineal. *Acta Anat. (Basel)* 117, 165–169. doi: 10.1159/000145782

Hendrickson, A. E., Wagoner, N., and Cowan, W. M. (1972). Autoradiogrpahic and electron-microscopic study of retino-hypothalamic connections. *Z. Zellforschung Mikroskopische Anat.* 135:1. doi: 10.1007/bf00307084

Heydorn, W. E., Frazer, A., and Weiss, B. (1981). Electrical stimulation of sympathetic nerves increases the concentration of cyclic AMP in rat pineal gland. *Proc. Natl. Acad. Sci. U.S.A.* 78, 7176–7179. doi: 10.1073/pnas.78.11.7176

Hoevenaar-Blom, M. P., Spijkerman, A. M., Kromhout, D., van den Berg, J. F., and Verschuren, W. M. (2011). Sleep duration and sleep quality in relation to 12-year cardiovascular disease incidence: the MORGEN study. *Sleep* 34, 1487–1492. doi: 10.5665/sleep.1382

Hoshino, M., Kaneko, K., Miyamoto, Y., Yoshimura, K., Suzuki, D., Akaike, T., et al. (2017). 8-Nitro-cGMP promotes bone growth through expansion of growth plate cartilage. *Free Radic. Biol. Med.* 110, 63–71. doi: 10.1016/j.freeradbiomed.2017.05.022

Hu, C. X., and Li, L. J. (2019). Melatonin plays critical role in mesenchymal stem cell-based regenerative medicine in vitro and in vivo. *Stem Cell Res. Ther.* 10:11.

Huang, H. T., and Lin, H. S. (1984). Synaptic junctions between the adrenergic axon varicosity and the pinealocyte in the rat. *J. Pineal Res.* 1, 281–291. doi: 10.1111/j.1600-079X.1984.tb00219.x

Huether, G. (1993). The contribution of extrapineal sites of melatonin synthesis to circulating melatonin levels in higher vertebrates. *Experientia* 49, 665–670. doi: 10.1007/bf01923948

Hughes, R. J., Sack, R. L., and Lewy, A. J. (1998). The role of melatonin and circadian phase in age-related sleep-maintenance insomnia: assessment in a clinical trial of melatonin replacement. *Sleep* 21, 52–68.

Hummel, F., Celnik, P., Giraux, P., Floel, A., Wu, W. H., Gerloff, C., et al. (2005). Effects of non-invasive cortical stimulation on skilled motor function in chronic stroke. *Brain* 128, 490–499. doi: 10.1093/brain/awh369

Hummel, F. C., Voller, B., Celnik, P., Floel, A., Giraux, P., Gerloff, C., et al. (2006). Effects of brain polarization on reaction times and pinch force in chronic stroke. *BMC Neurosci.* 7:73. doi: 10.1186/1471-2202-7-73

International Neuromodulation Society (2018). *Welcome to the International Neuromodulation Society*. Available: https://www.neuromodulation.com/neuromodulation-defined [Accessed 14 November 2018 2018].

Ito, M., Kadekaro, M., and Sokoloff, L. (1988). Local glucose-utilization of the brain and pineal-gland during stimulation of the cervical sympathetic trunk. *J. Pineal Res.* 5, 51–62. doi: 10.1111/j.1600-079X.1988.tb00768.x

Jang, S. W., Liu, X., Pradoldej, S., Tosini, G., Chang, Q., Iuvone, P. M., et al. (2010). N-acetylserotonin activates TrkB receptor in a circadian rhythm. *Proc. Natl. Acad. Sci. U.S.A.* 107, 3876–3881. doi: 10.1073/pnas.0912531107

Joos, K., De Ridder, D., Van de Heyning, P., and Vanneste, S. (2014). Polarity specific suppression effects of transcranial direct current stimulation for tinnitus. *Neural Plast.* 2014:930860. doi: 10.1155/2014/930860

Kalsbeek, A., Garidou, M. L., Palm, I. F., van der Vliet, J., Simonneaux, V., Pevet, P., et al. (2000). Melatonin sees the light: blocking GABA-ergic transmission in the paraventricular nucleus induces daytime secretion of melatonin. *European Journal of Neuroscience* 12, 3146–3154. doi: 10.1046/j.1460-9568.2000.00202.x

Kannan, H., Hayashida, Y., and Yamashita, H. (1989). Increase in sympathetic outflow by paraventricular nucleus stimulation in awake rats. *Am. J. Physiol.* 256(6 Pt 2), R1325–R1330. doi: 10.1152/ajpregu.1989.256.6.R1325

Kannan, H., Niijima, A., and Yamashita, H. (1987). Inhibition of renal sympathetic nerve activity by electrical stimulation of the hypothalamic paraventricular nucleus in anesthetized rats. *J. Auton. Nerv. Syst.* 21, 83–86. doi: 10.1016/0165-1838(87)90094-4

Kappers, J. A. (1960a). Innervation of the epiphysis cerebri in the albino rat. *Anatom. Rec.* 136, 220–221.

Kappers, J. A. (1960b). The development, topographical relations and innervation of the epiphysis cerebri in the albino rat. *Z. Zellforschung Mikroskop. Anat.* 52, 163–215. doi: 10.1007/bf00338980

Kappers, J. A. (1965). Survey of the innervation of the epiphysis cerebri and the accessory pineal organs of vertebrates. *Prog. Brain Res.* 10, 87–153. doi: 10.1016/s0079-6123(08)63448-2

Kayumov, L., Spence, W., Lowe, A., Hawa, R., Koszorowska, M., Jain, U., et al. (2003). Acupuncture reduces depressive and insomnia symptoms, and increases nocturnal melatonin secretion. *Sleep* 26, A291–A292.

Kenny, G. C. (1967). Innervation of the mammalian pineal body. *Anat. Rec.* 157:269.

Khedr, E. M., Ahmed, M. A., Fathy, N., and Rothwell, J. C. (2005). Therapeutic trial of repetitive transcranial magnetic stimulation after acute ischemic stroke. *Neurology* 65, 466–468. doi: 10.1212/01.wnl.0000173067.84247.36

Kim, M. J., Kim, H. K., Kim, B. S., and Yim, S. V. (2004). Melatonin increases cell proliferation in the dentate gyrus of maternally separated rats. *J. Pineal Res.* 37, 193–197. doi: 10.1111/j.1600-079X.2004.00157.x

Kim, Y. H., You, S. H., Ko, M. H., Park, J. W., Lee, K. H., Jang, S. H., et al. (2006). Repetitive transcranial magnetic stimulation-induced corticomotor excitability and associated motor skill acquisition in chronic stroke. *Stroke* 37, 1471–1476. doi: 10.1161/01.Str.0000221233.55497.51

Klein, D. C., and Weller, J. L. (1972). Rapid light-induced decrease in pineal serotonin N-acetyltransferase activity. *Science* 177, 532–533. doi: 10.1126/science.177.4048.532

Korf, H. W., and Wagner, U. (1980). Evidence for a nervous connection between the brain and the pineal organ in the guinea-pig. *Cell Tissue Res.* 209, 505–510.

Krause, A. J., Prather, A. A., Wager, T. D., Lindquist, M. A., and Walker, M. P. (2019). The pain of sleep loss: a brain characterization in humans. *J. Neurosci.* 39, 2291. doi: 10.1523/JNEUROSCI.2408-18.2018

Kreuzer, P. M., Landgrebe, M., Husser, O., Resch, M., Schecklmann, M., and Geisreiter, F. (2012). Transcutaneous vagus nerve stimulation: retrospective assessment of cardiac safety in a pilot study. *Front. Psychiatry* 3:70. doi: 10.3389/fpsyt.2012.00070

Kreuzer, P. M., Landgrebe, M., Resch, M., Husser, O., Schecklmann, M., Geisreiter, F., et al. (2014). Feasibility, safety and efficacy of transcutaneous vagus nerve stimulation in chronic tinnitus: an open pilot study. *Brain Stimul.* 7, 740–747. doi: 10.1016/j.brs.2014.05.003

Kubo, T., Ozasa, K., Mikami, K., Wakai, K., Fujino, Y., Watanabe, Y., et al. (2006). Prospective cohort study of the risk of prostate cancer among rotating-shift workers: findings from the Japan collaborative cohort study. *Am. J. Epidemiol.* 164, 549–555. doi: 10.1093/aje/kwj232

Kumar, A., and Chanana, P. (2014). Sleep reduction: a link to other neurobiological diseases. *Sleep Biol. Rhythms* 12, 150–161. doi: 10.1111/sbr.12066

Kunz, D., and Bes, F. (1999). Melatonin as a therapy in REM sleep behavior disorder patients: an open-labeled pilot study on the possible influence of melatonin on REM-sleep regulation. *Mov. Disord.* 14, 507–511. doi: 10.1002/1531-8257(199905)14:3<507::aid-mds1021>3.0.co;2-8

Kunz, D., and Mahlberg, R. (2010). A two-part, double-blind, placebo-controlled trial of exogenous melatonin in REM sleep behaviour disorder. *J. Sleep Res.* 19, 591–596. doi: 10.1111/j.1365-2869.2010.00848.x

Kunz, D., Mahlberg, R., Muller, C., Tilmann, A., and Bes, F. (2004). Melatonin in patients with reduced REM sleep duration: two randomized controlled trials. *J. Clin. Endocrinol. Metab.* 89, 128–134. doi: 10.1210/jc.2002-021057

Larsen, P. J., Møller, M., and Mikkelsen, J. D. (1991). Efferent projections from the periventricular and medial parvicellular subnuclei of the hypothalamic paraventricular nucleus to circumventricular organs of the rat: a Phaseolus vulgaris-leucoagglutinin (PHA-L) tracing study. *J. Compar. Neurol.* 306, 462–479. doi: 10.1002/cne.903060310

le Gros Clark, W. E. (1940). The nervous and vascular relations of the pineal gland. *J. Anat.* 74(Pt 4), 471–492.

Leander, P., Vrang, N., and Moller, M. (1998). Neuronal projections from the mesencephalic raphe nuclear complex to the suprachiasmatic nucleus and the deep pineal gland of the golden hamster (*Mesocricetus auratus*). *J. Comp. Neurol.* 399, 73–93. doi: 10.1002/(sici)1096-9861(19980914)399:1<73::aid-cne6>3.0.co;2-7

Lefaucheur, J. P., Drouot, X., Keravel, Y., and Nguyen, J. P. (2001). Pain relief induced by repetitive transcranial magnetic stimulation of precentral cortex. *Neuroreport* 12, 2963–2965. doi: 10.1097/00001756-200109170-00041

Lemoine, P., and Zisapel, N. (2012). Prolonged-release formulation of melatonin (Circadin) for the treatment of insomnia. *Expert Opin. Pharmacother.* 13, 895–905. doi: 10.1517/14656566.2012.667076

Leone, R. M., and Silman, R. E. (1984). Melatonin can be differentially metabolized in the rat to produce N-acetylserotonin in addition to 6-hydroxy-melatonin. *Endocrinology* 114, 1825–1832. doi: 10.1210/endo-114-5-1825

Lewy, A. J., and Newsome, D. A. (1983). Different types of melatonin circadian secretory rhythms in some blind subjects. *J. Clin. Endocrinol. Metab.* 56, 1103–1107. doi: 10.1210/jcem-56-6-1103

Lewy, A. J., Tetsuo, M., Markey, S. P., Goodwin, F. K., and Kopin, I. J. (1980). Pinealectomy abolishes plasma melatonin in the rat. *J. Clin. Endocrinol. Metab.* 50, 204–205. doi: 10.1210/jcem-50-1-204

Li, S., Zhai, X., Rong, P., McCabe, M. F., Zhao, J., Ben, H., et al. (2014). Transcutaneous auricular vagus nerve stimulation triggers melatonin secretion and is antidepressive in zucker diabetic fatty rats. *PLoS ONE* 9:e111100. doi: 10.1371/journal.pone.0111100

Lin, C., Chao, H., Li, Z., Xu, X., Liu, Y., Hou, L., et al. (2016). Melatonin attenuates traumatic brain injury-induced inflammation: a possible role for mitophagy. *J. Pineal Res.* 61, 177–186. doi: 10.1111/jpi.12337

Lingappa, J. R., and Zigmond, R. E. (1987). A histochemical study of the adrenergic innervation of the rat pineal gland: evidence for overlap of the innervation from the two superior cervical ganglia and for sprouting following unilateral denervation. *Neuroscience* 21, 893–902. doi: 10.1016/0306-4522(87)90045-5

Lingappa, J. R., and Zigmond, R. E. (2013). Limited recovery of pineal function after regeneration of preganglionic sympathetic axons: evidence for loss of ganglionic synaptic specificity. *J. Neurosci.* 33, 4867–4874. doi: 10.1523/jneurosci.3829-12.2013

Lingford- Hughes, A., and Kalk, N. (2012). *Core Psychiatry*, 3rd Edn. London: Elsevier.

Liu, L. D., Prescott, I. A., Dostrovsky, J. O., Hodaie, M., Lozano, A. M., and Hutchison, W. D. (2012). Frequency-dependent effects of electrical stimulation in the globus pallidus of dystonia patients. *J. Neurophysiol.* 108, 5–17. doi: 10.1152/jn.00527.2011

Liu, R. Y., Zhou, J. N., van Heerikhuize, J., Hofman, M. A., and Swaab, D. F. (1999). Decreased melatonin levels in postmortem cerebrospinal fluid in relation to aging, Alzheimer's disease, and apolipoprotein E-epsilon 4/4 genotype. *J. Clin. Endocrinol. Metab.* 84, 323–327. doi: 10.1210/jc.84.1.323

Liu, T., and Borjigin, J. (2005). N-acetyltransferase is not the rate-limiting enzyme of melatonin synthesis at night. *J. Pineal Res.* 39, 91–96. doi: 10.1111/j.1600-079X.2005.00223.x

Lledo, P. M., Alonso, M., and Grubb, M. S. (2006). Adult neurogenesis and functional plasticity in neuronal circuits. *Nat. Rev. Neurosci.* 7, 179–193. doi: 10.1038/nrn1867

Luo, C., Yang, Q., Liu, Y., Zhou, S., Jiang, J., Reiter, R. J., et al. (2019). The multiple protective roles and molecular mechanisms of melatonin and its precursor N-acetylserotonin in targeting brain injury and liver damage and in maintaining bone health. *Free Radic. Biol. Med.* 130, 215–233. doi: 10.1016/j.freeradbiomed.2018.10.402

Ma, D. K., Kim, W. R., Ming, G. L., and Song, H. (2009). Activity-dependent extrinsic regulation of adult olfactory bulb and hippocampal neurogenesis. *Ann. N. Y. Acad. Sci.* 1170, 664–673. doi: 10.1111/j.1749-6632.2009.04373.x

Mack, J. M., Schamne, M. G., Sampaio, T. B., Pértile, R. A. N., Fernandes, P. A. C. M., Markus, R. P., et al. (2016). Melatoninergic system in Parkinson's disease: from neuroprotection to the management of motor and nonmotor symptoms. *Oxidat. Med. Cell. Longevity* 2016, 3472032–3472032. doi: 10.1155/2016/3472032

Manda, K., and Reiter, R. J. (2010). Melatonin maintains adult hippocampal neurogenesis and cognitive functions after irradiation. *Prog. Neurobiol.* 90, 60–68. doi: 10.1016/j.pneurobio.2009.10.019

Mansur, C. G., Fregni, F., Boggio, P. S., Riberto, M., Gallucci-Neto, J., Santos, C. M., et al. (2005). A sham stimulation-controlled trial of rTMS of the unaffected hemisphere in stroke patients. *Neurology* 64, 1802–1804. doi: 10.1212/01.Wnl.0000161839.38079.92

Matsushima, S., Sakai, Y., Hira, Y., Oomori, Y., and Daikoku, S. (1994). Immunohistochemical studies on sympathetic and non-sympathetic nerve fibers and neuronal cell bodies in the pineal gland of cotton rats, *Sigmodon hispidus*. *Arch. Histol. Cytol.* 57, 47–58. doi: 10.1679/aohc.57.47

Matsuura, T., Kumamoto, K., and Ebara, S. (1994). Nerve-fibers originating from the brain in the rat pineal complex. *J. Electron. Microsc.* 43, 255–263.

Mauriz, J. L., Collado, P. S., Veneroso, C., Reiter, R. J., and Gonzalez-Gallego, J. (2013). A review of the molecular aspects of melatonin's anti-inflammatory actions: recent insights and new perspectives. *J. Pineal Res.* 54, 1–14. doi: 10.1111/j.1600-079X.2012.01014.x

Mays, J. C., Kelly, M. C., Coon, S. L., Holtzclaw, L., Rath, M. F., Kelley, M. W., et al. (2018). Single-cell RNA sequencing of the mammalian pineal gland identifies two pinealocyte subtypes and cell type-specific daily patterns of gene expression. *PLoS ONE* 13:e0205883. doi: 10.1371/journal.pone.0205883

McAlpine, C. S., Kiss, M. G., Rattik, S., He, S., Vassalli, A., Valet, C., et al. (2019). Sleep modulates haematopoiesis and protects against atherosclerosis. *Nature* 566, 383–387. doi: 10.1038/s41586-019-0948-2

McIntyre, I. M., and Oxenkrug, G. F. (1984). Electroconvulsive shock: effect on pineal and hypothalamic indoles. *J. Pineal Res.* 1, 273–279. doi: 10.1111/j.1600-079x.1984.tb00218.x

Mikkelsen, J. D., and Moller, M. (1990). A direct neural projection from the intergeniculate leaflet of the lateral geniculate nucleus to the deep pineal gland of the rat, demonstrated with *Phaseolus vulgaris* leucoagglutinin. *Brain Res.* 520, 342–346. doi: 10.1016/0006-8993(90)91727-x

Minchin, M. C., and Iversen, L. L. (1974). Release of (3H)gamma-aminobutyric acid from glial cells in rat dorsal root ganglia. *J. Neurochem.* 23, 533–540. doi: 10.1111/j.1471-4159.1974.tb06056.x

Ming, G. L., and Song, H. (2005). Adult neurogenesis in the mammalian central nervous system. *Annu. Rev. Neurosci.* 28, 223–250. doi: 10.1146/annurev.neuro.28.051804.101459

Mirick, D. K., Stevens, R. G., and Davis, S. (2001). Night shift work, light at night, and risk of breast cancer. *J. Natl. Cancer Inst.* 93, 1557–1562. doi: 10.1093/jnci/93.20.1557

Moller, M. (1978). Presence of a pineal nerve (nervus pinealis) in the human fetus: a light and electron microscopical study of the innervation of the pineal gland. *Brain Res.* 154, 1–12. doi: 10.1016/0006-8993(78)91046-6

Moller, M., and Hay-Schmidt, A. (1998). Direct neuronal projection from the dorsal raphe nucleus to the pineal complex of the rat: a *Phaseolus vulgaris*-leucoagglutinin in vivo neuronal tracing study. *J. Pineal Res.* 25, 19–23. doi: 10.1111/j.1600-079x.1998.tb00381.x

Moller, M., and Korf, H. W. (1983). Central innervation of the pineal organ of the Mongolian gerbil. A histochemical and lesion study. *Cell Tissue Res.* 230, 259–272.

Moller, M., Phansuwan-Pujito, P., Govitrapong, P., and Schmidt, P. (1993). Indications for a central innervation of the bovine pineal gland with substance P-immunoreactive nerve fibers. *Brain Res.* 611, 347–351. doi: 10.1016/0006-8993(93)90525-r

Moore, R. Y. (1973). Retinohypothalamic projection in mammals – comparative study. *Brain Res.* 49, 403–409. doi: 10.1016/0006-8993(73)90431-9

Moore, R. Y., and Lenn, N. J. (1972). Retinohypothalamic projection in rat. *J. Compar. Neurol.* 146, 1–14. doi: 10.1002/cne.901460102

Mukda, S., Panmanee, J., Boontem, P., and Govitrapong, P. (2016). Melatonin administration reverses the alteration of amyloid precursor protein-cleaving secretases expression in aged mouse hippocampus. *Neurosci. Lett.* 621, 39–46. doi: 10.1016/j.neulet.2016.04.013

Munch, I. C., Moller, M., Larsen, P. J., and Vrang, N. (2002). Light-induced c-fos expression in suprachiasmatic nuclei neurons targeting the paraventricular nucleus of the hamster hypothalamus: phase dependence and immunochemical identification. *J. Compar. Neurol.* 442, 48–62. doi: 10.1002/cne.1421

Munoz-Hoyos, A., Sanchez-Forte, M., Molina-Carballo, A., Escames, G., Martin-Medina, E., Reiter, R. J., et al. (1998). Melatonin's role as an anticonvulsant and neuronal protector: experimental and clinical evidence. *J. Child Neurol.* 13, 501–509. doi: 10.1177/088307389801301007

Murali, R., Thanikaivelan, P., and Cheirmadurai, K. (2016). Melatonin in functionalized biomimetic constructs promotes rapid tissue regeneration in Wistar albino rats. *J. Mater. Chem. B* 4, 5850–5862. doi: 10.1039/c6tb01221c

Netter, F. H. (1999). *The Netter Collection of Medical Illustrations: Nervous System – Anatomy and Physiology*. Amsterdam: Elsevier.

Neuwelt, E. A., and Lewy, A. J. (1983). Disappearance of plasma melatonin after removal of a neoplastic pineal gland. *N. Engl. J. Med.* 308, 1132–1135. doi: 10.1056/nejm198305123081905

Ngai, A. C., Jolley, M. A., D'Ambrosio, R., Meno, J. R., and Winn, H. R. (1999). Frequency-dependent changes in cerebral blood flow and evoked potentials during somatosensory stimulation in the rat. *Brain Res.* 837, 221–228. doi: 10.1016/s0006-8993(99)01649-2

Nosjean, O., Ferro, M., Coge, F., Beauverger, P., Henlin, J. M., Lefoulon, F., et al. (2000). Identification of the melatonin-binding site MT3 as the quinone reductase 2. *J. Biol. Chem.* 275, 31311–31317. doi: 10.1074/jbc.M005141200

Nowak, J. Z., Przybysz, M., and Zurawska, E. (1988). The melatonin generating system in the rat retina and pineal gland: effect of single and repeated electroconvulsive shock (ECS). *Pol. J. Pharmacol. Pharm.* 40, 573–584.

Olcese, J., Reuss, S., and Steinlechner, S. (1987). Electrical stimulation of the hypothalamic nucleus paraventricularis mimics the effects of light on pineal melatonin synthesis. *Life Sci.* 40, 455–459. doi: 10.1016/0024-3205(87)90110-x

Ooms, S., Overeem, S., Besse, K., Rikkert, M. O., Verbeek, M., and Claassen, J. A. (2014). Effect of 1 night of total sleep deprivation on cerebrospinal fluid beta-amyloid 42 in healthy middle-aged men: a randomized clinical trial. *JAMA Neurol.* 71, 971–977. doi: 10.1001/jamaneurol.2014.1173

Oxenkrug, G., and Ratner, R. (2012). N-acetylserotonin and aging-associated cognitive impairment and depression. *Aging Dis.* 3, 330–338.

Oxenkrug, G. F., Requintina, P. J., McIntyre, I. M., and Davis, R. (1991). "Stimulation of rat pineal melatonin synthesis by a single electroconvulsive shock – chronobiological effect of antidepressant therapy," in *5-Hydroxytryptamine in Psychiatry: a Spectrum of Ideas*, eds M. Sandler, A. Coppen, and S. Harnett, (Oxford: Oxford University Press), 110–115. doi: 10.1093/acprof:oso/9780192620118.003.0009

Panmanee, J., Nopparat, C., Chavanich, N., Shukla, M., Mukda, S., Song, W., et al. (2015). Melatonin regulates the transcription of βAPP-cleaving secretases mediated through melatonin receptors in human neuroblastoma SH-SY5Y cells. *J. Pineal Res.* 59, 308–320. doi: 10.1111/jpi.12260

Pappolla, M., Bozner, P., Soto, C., Shao, H., Robakis, N. K., Zagorski, M., et al. (1998). Inhibition of Alzheimer beta-fibrillogenesis by melatonin. *J. Biol. Chem.* 273, 7185–7188. doi: 10.1074/jbc.273.13.7185

Parfitt, A., Weller, J. L., Klein, D. C., Sakai, K. K., and Marks, B. H. (1975). Blockade by ouabain or elevated potassium ion concentration of the adrenergic and adenosine cyclic 3',5'-monophosphate-induced stimulation of pineal serotonin N-acetyltransferase activity. *Mol. Pharmacol.* 11, 241–255.

Parpura, V., Basarsky, T. A., Liu, F., Jeftinija, K., Jeftinija, S., and Haydon, P. G. (1994). Glutamate-mediated astrocyte-neuron signalling. *Nature* 369, 744–747. doi: 10.1038/369744a0

Patel, S., and Demaine, C. (1990). Effects of stimulation of the superior cervical Ganglia and local application of noradrenaline on electrical activity of the Syrian hamster pineal gland. *J. Neuroendocrinol.* 2, 493–499. doi: 10.1111/j.1365-2826.1990.tb00438.x

Paul, S. M., Hsu, L. L., and Mandell, A. J. (1974). Extrapineal N-acetyltransferase activity in rat brain. *Life Sci.* 15, 2135–2143. doi: 10.1016/0024-3205(74)90030-7

Pazo, J. H. (1981). Electrophysiological study of evoked electrical activity in the pineal gland. *J. Neural Transm.* 52, 137–148. doi: 10.1007/bf01253105

Pazo, J. H., and Gonzalez, M. (1991). Effects of central and peripheral inputs on single pineal cell-activity in the rat. *Neuroscience* 43, 231–235. doi: 10.1016/0306-4522(91)90430-v

Peng, C.-X., Hu, J., Liu, D., Hong, X.-P., Wu, Y.-Y., Zhu, L.-Q., et al. (2013). Disease-modified glycogen synthase kinase-3β intervention by melatonin arrests the pathology and memory deficits in an Alzheimer's animal model. *Neurobiol. Aging* 34, 1555–1563. doi: 10.1016/j.neurobiolaging.2012.12.010

Pfeffer, M., Korf, H.-W., and Wicht, H. (2018). Synchronizing effects of melatonin on diurnal and circadian rhythms. *Gen. Compar. Endocrinol.* 258, 215–221. doi: 10.1016/j.ygcen.2017.05.013

Psarakis, S., Pulido, O. M., Brown, G. M., Grota, L. J., and Smith, G. K. (1982). Identification and quantification of n-acetylserotonin (NAS) in the developing hippocampus of the rat. *Prog. Neuropsychopharmacol. Biol. Psychiatry* 6, 439–442. doi: 10.1016/s0278-5846(82)80124-3

Qian, Y., Han, Q., Zhao, X., Song, J., Cheng, Y., Fang, Z., et al. (2018). 3D melatonin nerve scaffold reduces oxidative stress and inflammation and increases autophagy in peripheral nerve regeneration. *J. Pineal Res.* 65:e12516. doi: 10.1111/jpi.12516

Quay, W. B. (1973). Retrograde perfusions of the pineal region and the question of pineal vascular routes to brain and choroid plexuses. *Am. J. Anat.* 137, 387–401. doi: 10.1002/aja.1001370403

Ramirez-Rodriguez, G., Klempin, F., Babu, H., Benitez-King, G., and Kempermann, G. (2009). Melatonin modulates cell survival of new neurons in the hippocampus of adult mice. *Neuropsychopharmacology* 34, 2180–2191. doi: 10.1038/npp.2009.46

Ramirez-Rodriguez, G., Ortiz-Lopez, L., Dominguez-Alonso, A., Benitez-King, G. A., and Kempermann, G. (2011). Chronic treatment with melatonin stimulates dendrite maturation and complexity in adult hippocampal neurogenesis of mice. *J. Pineal Res.* 50, 29–37. doi: 10.1111/j.1600-079X.2010.00802.x

Rath, M. F., Coon, S. L., Amaral, F. G., Weller, J. L., Moller, M., and Klein, D. C. (2016). Melatonin synthesis: acetylserotonin o-methyltransferase (ASMT) is strongly expressed in a subpopulation of pinealocytes in the male rat pineal gland. *Endocrinology* 157, 2028–2040. doi: 10.1210/en.2015-1888

Reiter, R. J. (1990). *Biological Rhythms, Mood Disorders, Light Therapy, and the Pineal Gland*. Washington, DC: American Psychiatric Press.

Reiter, R. J., Mayo, J. C., Tan, D. X., Sainz, R. M., Alatorre-Jimenez, M., and Qin, L. L. (2016). Melatonin as an antioxidant: under promises but over delivers. *J. Pineal Res.* 61, 253–278. doi: 10.1111/jpi.12360

Reiter, R. J., Tan, D. X., Manchester, L. C., Paredes, S. D., Mayo, J. C., and Sainz, R. M. (2009). Melatonin and reproduction revisited. *Biol. Reprod.* 81, 445–456. doi: 10.1095/biolreprod.108.075655

Reiter, R. J., Tan, D. X., Poeggeler, B., Menendez-Pelaez, A., Chen, L. D., and Saarela, S. (1994). Melatonin as a free radical scavenger: implications for aging and age-related diseasesa. *Ann. N. Y. Acad. Sci.* 719, 1–12. doi: 10.1111/j.1749-6632.1994.tb56817.x

Reiter, R. J., Tan, D. X., Rosales-Corral, S., and Manchester, L. C. (2013). The universal nature, unequal distribution and antioxidant functions of melatonin and its derivatives. *Mini Rev. Med. Chem.* 13, 373–384. doi: 10.2174/1389557511313030006

Rennie, K., De Butte, M., and Pappas, B. A. (2009). Melatonin promotes neurogenesis in dentate gyrus in the pinealectomized rat. *J. Pineal Res.* 47, 313–317. doi: 10.1111/j.1600-079X.2009.00716.x

Reuss, S. (1986). Effects of chemical and surgical ganglionectomy on electrical activity of the pineal gland of male rats. *J. Pineal Res.* 3, 87–94. doi: 10.1111/j.1600-079x.1986.tb00729.x

Reuss, S. (1999). Trigeminal innervation of the mammalian pineal gland. *Microsc. Res. Tech.* 46, 305–309. doi: 10.1002/(sici)1097-0029(19990815/01)46:4/5<305::aid-jemt7>3.0.co;2-#

Reuss, S., and Moller, M. (1986). Direct projections to the rat pineal gland via the stria medullaris thalami. An anterograde tracing study by use of horseradish peroxidase. *Cell Tissue Res.* 244, 691–694.

Reuss, S., Concemius, W., Stehle, J., Seidel, A., Schröder, H., and Vollrath, L. (1989). Effects of electrical stimulation of the superior cervical ganglia on the number of "synaptic" ribbons and the activity of melatonin-forming enzymes in the rat pineal gland. *Anat. Embryol.* 179, 341–345. doi: 10.1007/bf00305060

Reuss, S., Olcer, S., and Vollrath, L. (1985a). Electrical stimulation of the hypothalamic paraventricular nuclei inhibits pineal melatonin synthesis in male rats. *Neuroendocrinology* 41, 192–196. doi: 10.1159/000124177

Reuss, S., Semm, P., and Vollrath, L. (1985b). Changes in the electrical activity of the rat pineal gland following stimulation of the cervical sympathetic ganglia. *J. Auton. Nerv. Syst.* 12, 281–288. doi: 10.1016/0165-1838(85)90043-8

Reuss, S., Semm, P., and Vollrath, L. (1984). Electrophysiological investigations on the central innervation of the rat and guinea-pig pineal gland. *J. Neural Trans.* 60, 31–43. doi: 10.1007/bf01254763

Reyes-Vazquez, C., Prieto-Gomez, B., Aldes, L. D., and Dafny, N. (1986). Rat pineal exhibits two electrophysiological patterns of response to microiontophoretic norepinephrine application. *J. Pineal Res.* 3, 213–222. doi: 10.1111/j.1600-079x.1986.tb00744.x

Rodriguez, C., Mayo, J. C., Sainz, R. M., Antolín, I., Herrera, F., Martín, V., et al. (2004). Regulation of antioxidant enzymes: a significant role for melatonin. *J. Pineal Res.* 36, 1–9. doi: 10.1046/j.1600-079X.2003.00092.x

Rodriguez-Perez, A. (1962). Contribución al conocimiento de la inervación de las glándulas endocrinas. IV. Primeros resultados experimentales en torno a la inervación de la epífisis. *Trab. Inst. Cajal Invest. Biol.* 54, 1–8.

Romijn, H. J. (1975). Structure and innervation of the pineal gland of the rabbit, oryctolagus cuniculus. *Cell Tissue Res.* 157, 25–51. doi: 10.1007/bf00223229

Ronnekleiv, O. K., Kelly, M. J., and Wuttke, W. (1980). Single unit recordings in the rat pineal gland: evidence for habenulo-pineal neural connections. *Exp. Brain Res.* 39, 187–192.

Rosenstein, R. E., Chuluyan, H. E., Pereyra, E. N., and Cardinali, D. P. (1989). Release and effect of gamma-aminobutyric acid (GABA) on rat pineal melatonin production in vitro. *Cell Mol. Neurobiol.* 9, 207–219. doi: 10.1007/bf00713029

Rossini, P. M., Burke, D., Chen, R., Cohen, L. G., Daskalakis, Z., Di Iorio, R., et al. (2015). Non-invasive electrical and magnetic stimulation of the brain, spinal cord, roots and peripheral nerves: basic principles and procedures for routine clinical and research application. An updated report from an IFCN Committee. *Clin. Neurophysiol.* 126, 1071–1107. doi: 10.1016/j.clinph.2015.02.001

Rothman, S. M., Herdener, N., Frankola, K. A., Mughal, M. R., and Mattson, M. P. (2013). Chronic mild sleep restriction accentuates contextual memory impairments, and accumulations of cortical Aβ and pTau in a mouse model of Alzheimer's disease. *Brain Res.* 1529, 200–208. doi: 10.1016/j.brainres.2013.07.010

Sakai, K. K., and Marks, B. H. (1972). Adrenergic effects on pineal cell membrane potential. *Life Sci. I* 11, 285–291. doi: 10.1016/0024-3205(72)90231-7

Savaskan, E., Jockers, R., Ayoub, M., Angeloni, D., Fraschini, F., Flammer, J., et al. (2007). The MT2 melatonin receptor subtype is present in human retina and decreases in Alzheimer's disease. *Curr. Alzheimer Res.* 4, 47–51. doi: 10.2174/156720507779939823

Schaefer, C., Kunz, D., and Bes, F. (2017). Melatonin effects in REM sleep behavior disorder associated with obstructive sleep apnea syndrome: a case series. *Curr. Alzheimer Res.* 14, 1084–1089. doi: 10.2174/1567205014666170523094938

Schapiro, S., and Salas, M. (1971). Effects of age, light and sympathetic innervation on electrical activity of rat pineal gland. *Brain Res.* 28, 47–55. doi: 10.1016/0006-8993(71)90523-3

Schenda, J., and Vollrath, L. (1997). Nitric oxide inhibits electrically active units in the rat pineal gland. *J. Neural Transm. (Vienna)* 104, 53–58. doi: 10.1007/bf01271293

Schenda, J., and Vollrath, L. (1999). An intrinsic neuronal-like network in the rat pineal gland. *Brain Res.* 823, 231–233. doi: 10.1016/s0006-8993(99)01199-3

Schernhammer, E. S., Kroenke, C. H., Laden, F., and Hankinson, S. E. (2006). Night work and risk of breast cancer. *Epidemiology* 17, 108–111.

Schernhammer, E. S., Laden, F., Speizer, F. E., Willett, W. C., Hunter, D. J., Kawachi, I., et al. (2001). Rotating night shifts and risk of breast cancer in women participating in the nurses' health study. *J. Natl. Cancer Inst.* 93, 1563–1568. doi: 10.1093/jnci/93.20.1563

Schernhammer, E. S., Laden, F., Speizer, F. E., Willett, W. C., Hunter, D. J., Kawachi, I., et al. (2003). Night-shift work and risk of colorectal cancer in the nurses' health study. *J. Natl. Cancer Inst.* 95, 825–828. doi: 10.1093/jnci/95.11.825

Semm, P., Schneider, T., and Vollrath, L. (1981). Morphological and electrophysiological evidence for habenular influence on the guinea-pig pineal gland. *J. Neural Transm.* 50, 247–266. doi: 10.1007/bf01249146

Shiotani, Y., Yamano, M., Shiosaka, S., Emson, P. C., Hillyard, C. J., Girgis, S., et al. (1986). Distribution and origins of substance-p (sp)-containing, calcitonin gene-related peptide (cgrp)-containing, vasoactive intestinal polypeptide (vip)-containing and neuropeptide-y (npy)-containing nerve-fibers in the pineal-gland of gerbils. *Neurosci. Lett.* 70, 187–192. doi: 10.1016/0304-3940(86)90461-1

Shukla, M., Htoo, H. H., Wintachai, P., Hernandez, J.-F., Dubois, C., Postina, R., et al. (2015). Melatonin stimulates the nonamyloidogenic processing of βAPP through the positive transcriptional regulation of ADAM10 and ADAM17. *J. Pineal Res.* 58, 151–165. doi: 10.1111/jpi.12200

Sompol, P., Liu, X., Baba, K., Paul, K. N., Tosini, G., Iuvone, P. M., et al. (2011). N-acetylserotonin promotes hippocampal neuroprogenitor cell proliferation in sleep-deprived mice. *Proc. Natl. Acad. Sci. U.S.A.* 108, 8844–8849. doi: 10.1073/pnas.1105114108

Sotthibundhu, A., Phansuwan-Pujito, P., and Govitrapong, P. (2010). Melatonin increases proliferation of cultured neural stem cells obtained from adult mouse subventricular zone. *J. Pineal Res.* 49, 291–300. doi: 10.1111/j.1600-079X.2010.00794.x

Spence, D. W., Kayumov, L., Chen, A., Lowe, A., Jain, U., Katzman, M. A., et al. (2004). Acupuncture increases nocturnal melatonin secretion and reduces insomnia and anxiety: a preliminary report. *J. Neuropsychiatry Clin. Neurosci.* 16, 19–28. doi: 10.1176/jnp.16.1.19

Stehle, J., Reuss, S., and Vollrath, L. (1987). Electrophysiological characterization of the pineal gland of golden hamsters. *Exp. Brain Res.* 67, 27–32. doi: 10.1007/bf00269449

Stener-Victorin, E., Fujisawa, S., and Kurosawa, M. (2006). Ovarian blood flow responses to electroacupuncture stimulation depend on estrous cycle and on site and frequency of stimulation in anesthetized rats. *J. Appl. Physiol. (1985)* 101, 84–91. doi: 10.1152/japplphysiol.01593.2005

Su, D., Chen, H., Hu, W., Liu, Y., Wang, Z., Wang, X., et al. (2018). Frequency-dependent effects of subthalamic deep brain stimulation on motor symptoms in Parkinson's disease: a meta-analysis of controlled trials. *Sci. Rep.* 8:14456.

Takahashi, Y., and Nakajima, Y. (1996). Dermatomes in the rat limbs as determined by antidromic stimulation of sensory C-fibers in spinal nerves. *Pain* 67, 197–202. doi: 10.1016/0304-3959(96)03116-8

Takeuchi, N., Chuma, T., Matsuo, Y., Watanabe, I., and Ikoma, K. (2005). Repetitive transcranial magnetic stimulation of contralesional primary motor

cortex improves hand function after stroke. *Stroke* 36, 2681–2686. doi: 10.1161/01.Str.0000189658.51972.34

Tamarkin, L., Reppert, S. M., and Klein, D. C. (1979). Regulation of pineal melatonin in the Syrian hamster. *Endocrinology* 104, 385–389. doi: 10.1210/endo-104-2-385

Tamarkin, L., Reppert, S. M., Klein, D. C., Pratt, B., and Goldman, B. D. (1980). Studies on the daily pattern of pineal melatonin in the Syrian hamster. *Endocrinology* 107, 1525–1529. doi: 10.1210/endo-107-5-1525

Tan, D. X., Xu, B., Zhou, X., and Reiter, R. J. (2018). Pineal calcification, melatonin production, aging, associated health consequences and rejuvenation of the pineal gland. *Molecules* 23:E301. doi: 10.3390/molecules23020301

Teclemariam-Mesbah, R., Ter Horst, G. J., Postema, F., Wortel, J., and Buijs, R. M. (1999). Anatomical demonstration of the suprachiasmatic nucleus-pineal pathway. *J. Compar. Neurol.* 406, 171–182. doi: 10.1002/(sici)1096-9861(19990405)406:2<171::aid-cne3>3.0.co;2-u

Tsai, S. Y., O'Brien, T. E., and McNulty, J. A. (2001). Microglia play a role in mediating the effects of cytokines on the structure and function of the rat pineal gland. *Cell Tissue Res.* 303, 423–431. doi: 10.1007/s004410000330

Vanneste, S., and De Ridder, D. (2011). Bifrontal transcranial direct current stimulation modulates tinnitus intensity and tinnitus-distress-related brain activity. *Eur. J. Neurosci.* 34, 605–614. doi: 10.1111/j.1460-9568.2011.07778.x

Vanneste, S., Plazier, M., Ost, J., van der Loo, E., Van de Heyning, P., and De Ridder, D. (2010). Bilateral dorsolateral prefrontal cortex modulation for tinnitus by transcranial direct current stimulation: a preliminary clinical study. *Exp. Brain Res.* 202, 779–785. doi: 10.1007/s00221-010-2183-9

Vanneste, S., Walsh, V., Van De Heyning, P., and De Ridder, D. (2013). Comparing immediate transient tinnitus suppression using tACS and tDCS: a placebo-controlled study. *Exp. Brain Res.* 226, 25–31. doi: 10.1007/s00221-013-3406-7

Villela, D., Atherino, V. F., Lima, L. D. S., Moutinho, A. A., do Amaral, F. G., Peres, R., et al. (2013). Modulation of pineal melatonin synthesis by glutamate involves paracrine interactions between pinealocytes and astrocytes through NF-κB activation. *BioMed Res. Int.* 2013, 618432–618432. doi: 10.1155/2013/618432

Vincent, B. (2018). Protective roles of melatonin against the amyloid-dependent development of Alzheimer's disease: a critical review. *Pharmacol. Res.* 134, 223–237. doi: 10.1016/j.phrs.2018.06.011

Viswanathan, A. N., Hankinson, S. E., and Schernhammer, E. S. (2007). Night shift work and the risk of endometrial cancer. *Cancer Res.* 67, 10618–10622. doi: 10.1158/0008-5472.can-07-2485

Volkman, P. H., and Heller, A. (1971). Pineal N-acetyltransferase activity: effect of sympathetic stimulation. *Science* 173, 839–840. doi: 10.1126/science.173.3999.839

von Lanz, T., and Wachsmuth, W. (2003). *Lanz/Wachsmuth Praktische Anatomie. Hals: Ein Lehr- und Hilfsbuch der anatomischen Grundlagen ärztlichen Handelns*. Berlin: Springer.

Vrang, N., Larsen, P. J., Moller, M., and Mikkelsen, J. D. (1995). Topographical organization of the rat suprachiasmatic-paraventricular projection. *J. Compar. Neurol.* 353, 585–603. doi: 10.1002/cne.903530409

Wade, A. G., Ford, I., Crawford, G., McConnachie, A., Nir, T., Laudon, M., et al. (2010). Nightly treatment of primary insomnia with prolonged release melatonin for 6 months: a randomized placebo controlled trial on age and endogenous melatonin as predictors of efficacy and safety. *BMC Med.* 8:51. doi: 10.1186/1741-7015-8-51

Waldhauser, F., Waldhauser, M., Lieberman, H. R., Deng, M. H., Lynch, H. J., and Wurtman, R. J. (1984). Bioavailability of oral melatonin in humans. *Neuroendocrinology* 39, 307–313. doi: 10.1159/000123997

Waldhauser, F., Weiszenbacher, G., Tatzer, E., Gisinger, B., Waldhauser, M., Schemper, M., et al. (1988). Alterations in nocturnal serum melatonin levels in humans with growth and aging. *J. Clin. Endocrinol. Metab.* 66, 648–652. doi: 10.1210/jcem-66-3-648

Wang, S. X., Zhai, X., Li, S. Y., McCabe, M. F., Wang, X., and Rong, P. J. (2015). Transcutaneous vagus nerve stimulation induces tidal melatonin secretion and has an antidiabetic effect in zucker fatty rats. *PLoS ONE* 10:12. doi: 10.1371/journal.pone.0124195

Wang, X., Figueroa Bryan, E., Stavrovskaya Irina, G., Zhang, Y., Sirianni Ana, C., Zhu, S., et al. (2009). Methazolamide and melatonin inhibit mitochondrial cytochrome C Release and are neuroprotective in experimental models of ischemic injury. *Stroke* 40, 1877–1885. doi: 10.1161/STROKEAHA.108.540765

Wang, Z., Wu, L., You, W., Ji, C., and Chen, G. (2013). Melatonin alleviates secondary brain damage and neurobehavioral dysfunction after experimental subarachnoid hemorrhage: possible involvement of TLR4-mediated inflammatory pathway. *J. Pineal Res.* 55, 399–408. doi: 10.1111/jpi.12087

Wetterberg, L. (1979). Clinical importance of melatonin. *Prog. Brain Res.* 52, 539–547. doi: 10.1016/s0079-6123(08)62962-3

Wong, C. S., Jow, G. M., Kaizaki, A., Fan, L. W., and Tien, L. T. (2014). Melatonin ameliorates brain injury induced by systemic lipopolysaccharide in neonatal rats. *Neuroscience* 267, 147–156. doi: 10.1016/j.neuroscience.2014.02.032

Wurtman, R. J., Axelrod, J., and Phillips, L. S. (1963). Melatonin synthesis in the pineal gland: control by light. *Science* 142, 1071–1073.

Yamada, H., Yamamoto, A., Takahashi, M., Michibata, H., Kumon, H., and Moriyama, Y. (1996a). The L-type Ca2+ channel is involved in microvesicle-mediated glutamate exocytosis from rat pinealocytes. *J. Pineal Res.* 21, 165–174. doi: 10.1111/j.1600-079x.1996.tb00284.x

Yamada, H., Yamamoto, A., Yodozawa, S., Kozaki, S., Takahashi, M., Morita, M., et al. (1996b). Microvesicle-mediated exocytosis of glutamate is a novel paracrine-like chemical transduction mechanism and inhibits melatonin secretion in rat pinealocytes. *J. Pineal Res.* 21, 175–191. doi: 10.1111/j.1600-079x.1996.tb00285.x

Yamada, H., Yatsushiro, S., Ishio, S., Hayashi, M., Nishi, T., Yamamoto, A., et al. (1998). Metabotropic glutamate receptors negatively regulate melatonin synthesis in rat pinealocytes. *J. Neurosci.* 18, 2056–2062. doi: 10.1523/jneurosci.18-06-02056.1998

Yamamoto, K., Matsuyama, T., Shiosaka, S., Inagaki, S., Senba, E., Shimizu, Y., et al. (1983). Overall distribution of substance-P containing nerves in the wall of the cerebral-arteries of the guinea-pig and its origins. *J. Compar. Neurol.* 215, 421–426. doi: 10.1002/cne.902150406

Yamashita, H., Kannan, H., Kasai, M., and Osaka, T. (1987). Decrease in blood pressure by stimulation of the rat hypothalamic paraventricular nucleus with L-glutamate or weak current. *J. Auton. Nerv. Syst.* 19, 229–234. doi: 10.1016/0165-1838(87)90069-5

Yanovski, J., Witcher, J., Adler, N., Markey, S. P., and Klein, D. C. (1987). Stimulation of the paraventricular nucleus area of the hypothalamus elevates urinary 6-hydroxymelatonin during daytime. *Brain Res. Bull.* 19, 129–133. doi: 10.1016/0361-9230(87)90175-4

Yatsushiro, S., Yamada, H., Hayashi, M., Yamamoto, A., and Moriyama, Y. (2000). Ionotropic glutamate receptors trigger microvesicle-mediated exocytosis of L-glutamate in rat pinealocytes. *J. Neurochem.* 75, 288–297. doi: 10.1046/j.1471-4159.2000.0750288.x

Young, I. M., Leone, R. M., Francis, P., Stovell, P., and Silman, R. E. (1985). Melatonin is metabolized to N-acetyl serotonin and 6-hydroxymelatonin in man. *J. Clin. Endocrinol. Metab.* 60, 114–119. doi: 10.1210/jcem-60-1-114

Zeitlhofer, J., Schmeiser-Rieder, A., Tribl, G., Rosenberger, A., Bolitschek, J., Kapfhammer, G., et al. (2000). Sleep and quality of life in the Austrian population. *Acta Neurol. Scand.* 102, 249–257.

Zemkova, H., Stojilkovic, S. S., and Klein, D. C. (2011). Norepinephrine causes a biphasic change in mammalian pinealocye membrane potential: role of alpha1B-adrenoreceptors, phospholipase C, and Ca2+. *Endocrinology* 152, 3842–3851. doi: 10.1210/en.2011-1180

Zempel, J. M., Zangrilli, M. A., Sutphen, C., Jerome, G., Macauley, S. L., Ju, Y.-E. S., et al. (2017). Slow wave sleep disruption increases cerebrospinal fluid amyloid-β levels. *Brain* 140, 2104–2111. doi: 10.1093/brain/awx148

Zhang, H.-M., and Zhang, Y. (2014). Melatonin: a well-documented antioxidant with conditional pro-oxidant actions. *J. Pineal Res.* 57, 131–146. doi: 10.1111/jpi.12162

Zhang, Y., Cook, A., Kim, J., Baranov, S. V., Jiang, J., Smith, K., et al. (2013). Melatonin inhibits the caspase-1/cytochrome c/caspase-3 cell death pathway, inhibits MT1 receptor loss and delays disease progression in a mouse model of amyotrophic lateral sclerosis. *Neurobiol. Dis.* 55, 26–35. doi: 10.1016/j.nbd.2013.03.008

Zhao, N., Zhong, C., Wang, Y., Zhao, Y., Gong, N., Zhou, G., et al. (2008). Impaired hippocampal neurogenesis is involved in cognitive dysfunction induced by thiamine deficiency at early pre-pathological lesion stage. *Neurobiol. Dis.* 29, 176–185. doi: 10.1016/j.nbd.2007.08.014

Zhao, Z. Q. (2008). Neural mechanism underlying acupuncture analgesia. *Prog. Neurobiol.* 85, 355–375. doi: 10.1016/j.pneurobio.2008.05.004

Zhou, H., Wang, J., Jiang, J., Stavrovskaya, I. G., Li, M., Li, W., et al. (2014). N-acetyl-serotonin offers neuroprotection through inhibiting mitochondrial death pathways and autophagic activation in experimental models of ischemic injury. *J. Neurosci.* 34, 2967–2978. doi: 10.1523/jneurosci.1948-13.2014

Zisapel, N. (2018). New perspectives on the role of melatonin in human sleep, circadian rhythms and their regulation. *Br. J. Pharmacol.* 175, 3190–3199. doi: 10.1111/bph.14116

Conflict of Interest: The authors declare that the research was conducted in the absence of any commercial or financial relationships that could be construed as a potential conflict of interest.

frontiers in Neuroscience

SYSTEMATIC REVIEW
published: 10 June 2021
doi: 10.3389/fnins.2021.671020

Self-Referential Processing Effects of Non-invasive Brain Stimulation: A Systematic Review

*Zhongjie Bao[1,2], Belal Howidi[1,2], Amer M. Burhan[1,3,4] and Paul Frewen[1,2]**

[1] Department of Psychiatry, Schulich School of Medicine and Dentistry, London, ON, Canada, [2] Interdisciplinary Program in Neuroscience, Western University, London, ON, Canada, [3] Ontario Shores Centre for Mental Health Sciences, Whitby, ON, Canada, [4] Department of Psychiatry, Temerty School of Medicine, University of Toronto, Toronto, ON, Canada

Systematic reviews of neuroimaging studies confirm stimulus-induced activity in response to verbal and non-verbal self-referential processing (SRP) in cortical midline structures, temporoparietal cortex and insula. Whether SRP can be causally modulated by way of non-invasive brain stimulation (NIBS) has also been investigated in several studies. Here we summarize the NIBS literature including 27 studies of task-based SRP comparing response between verbal and non-verbal SRP tasks. The studies differed in design, experimental tasks and stimulation parameters. Results support the role of left inferior parietal lobule (left IPL) in verbal SRP and for the medial prefrontal cortex when valenced stimuli were used. Further, results support roles for the bilateral parietal lobe (IPL, posterior cingulate cortex), the sensorimotor areas (the primary sensory and motor cortex, the premotor cortex, and the extrastriate body area) and the insula in non-verbal SRP (bodily self-consciousness). We conclude that NIBS may differentially modulate verbal and non-verbal SRP by targeting the corresponding brain areas.

Keywords: self-referential processing, neuromodulation, non-invasive brain stimulation (NIBS), systematic review, bodily self-consciousness

OPEN ACCESS

Edited by:
Giovanni Mirabella, University of Brescia, Italy

Reviewed by:
Sanjay Kumar, Oxford Brookes University, United Kingdom
Luca Falciati, University of Brescia, Italy

***Correspondence:**
Paul Frewen
pfrewen@uwo.ca

Specialty section:
This article was submitted to Neural Technology, a section of the journal Frontiers in Neuroscience

Received: *22 February 2021*
Accepted: *07 May 2021*
Published: *10 June 2021*

Citation:
Bao Z, Howidi B, Burhan AM and Frewen P (2021) Self-Referential Processing Effects of Non-invasive Brain Stimulation: A Systematic Review. Front. Neurosci. 15:671020. doi: 10.3389/fnins.2021.671020

INTRODUCTION

What constitutes our sense of self? This question has intrigued philosophers, psychologists, and neuroscientists alike for centuries. William James (1890) early subject-object framework distinguished the experience of self-referential processing (SRP) into its task vs. stimulus aspects, with the content or stimuli of SRP further categorizable into corporal (physical, somatic, non-verbal) versus non-corporal (spiritual, semantic, verbal) referents, and positive versus negative emotional valences (see also Legrand and Ruby, 2009). The distinction between verbal SRP (V-SRP) and non-verbal SRP (NV-SRP) bears significance in recent research topics (Frewen et al., 2020), including psychopathology (LeMoult et al., 2017; Lin et al., 2018; Yoon et al., 2019), neuroendocrinology (Li et al., 2018; van Buuren et al., 2020), and meditation (Katyal et al., 2020).

Researchers have also taken interest in the neurobiological basis of V-SRP and NV-SRP, with neuroimaging literature also providing a basis for distinguishing SRP into verbal (V-SRP) versus non-verbal (NV-SRP) domains (Frewen et al., 2020). Neuroimaging reviews suggested that SRP in general may be associated with activities in the default mode network (DMN) and its sub-systems. Within the DMN, the dorsomedial prefrontal cortex (DMPFC) subsystem consists of the DMPFC, inferior parietal lobule (IPL), the lateral temporal cortex, and the temporal poles, whereas the medial temporal lobe (MTL) subsystem consists of the ventromedial prefrontal cortex (VMPFC), posterior IPL, the retrosplenial cortex and the hippocampus, and the midline core subsystem can

be considered as the convergence of parts of the DMPFC and MTL subsystems (Andrews-Hanna et al., 2010; Wen et al., 2020). However, neuroimaging findings in response to SRP tasks further differentiate response among these ROIs. For example, V-SRP is known to be at least partially mediated by DMN activity in the medial prefrontal cortex (MPFC), posterior cingulate cortex (PCC), ventral precuneus, and the bilateral IPL (e.g., Araujo et al., 2015; Davey et al., 2016), although the response to different kinds of meditation practices suggest that it may be particularly the left more so than the right IPL that is associated with V-SRP (e.g., Fingelkurts et al., 2016; Fingelkurts et al., 2020). In contrast, NV-SRP emanating from the inner body (i.e., interoception; e.g., heartbeat) or the outer body (i.e., exteroception; e.g., touch) is assessed during tasks that engage attention toward bodily self-consciousness (BSC) (reviewed by Park and Blanke, 2019). Although interoception is typically associated with activity in the insula and cingulate cortex, exteroceptive aspects of BSC are typically associated with activity in the premotor cortex (PMC), intraparietal sulcus (IPS), and right IPL activity (Park and Blanke, 2019). Park and Blanke (2019) also suggested the existence of an integrated NV-SRP system centered in the IPS with the involvement of the PCC, IPL, PMC, and insula cortex. Further, both VMPFC and DMPFC may be important for valenced self-evaluation (Fingelkurts et al., 2016; Fingelkurts et al., 2020). However, although neuroimaging researchers can draw correlational inferences between SRP and response in various brain regions, causal evidence remains lacking.

One approach to arrive at causal evidence for the involvement of brain regions in SRP would be to modulate the activity of different brain regions and assess the outcomes of doing so for SRP. Emerging literature has therefore also investigated whether subjective and behavioral responses to SRP tasks can be modulated through non-invasive brain stimulation (NIBS) in the form of transcranial magnetic stimulation (TMS) and transcranial direct current stimulation (tDCS). TMS involves stimulating a region of the brain with a powerful magnetic field for a short period using a magnetic coil to induce a current in the cortical neurons parallel to the coil (Hallett, 2000; Barker and Shields, 2017). TMS can be applied phasically using an event-related approach correlated to the presentation of discrete stimuli during an SRP task or repeatedly (rTMS) and tonically over the course of an extended treatment session (e.g., measured in minutes). Typically, single or paired TMS pulses are applied within 500 milliseconds (ms) of stimulus onset during the event-related approach to affect the brain's response to that stimulus (Miniussi et al., 2013) whereas rTMS applied continuously can be used to affect task performance in general (Beynel et al., 2019), creating "carry-over" effects on neural excitability immediately during and after the stimulation session. As a rule of thumb, low frequency ($\leq$ 1Hz) rTMS reduces cortical excitability whereas high frequency ($\geq$ 5Hz) rTMS increases cortical excitability (Beynel et al., 2019). However, it is important to note that increases or decreases of cortical excitability do not necessarily equate to facilitation or inhibition of certain cognitive functions because the cascade of effects of cortical excitability is modulated by several factors before reaching the level of behavioral impacts (Bestmann et al., 2015).

Whereas TMS induces magnetic fields surrounding the skull to indirectly influence target electrical currents within the brain, tDCS uses a weak (typically $\leq$ 2.5 mA) direct current constantly applied to either increase or decrease neuronal excitability depending on the polarity. tDCS is almost always used tonically rather than phasically as single pulses to discrete stimuli, due to the weakness in tDCS current strength being unlikely to influence cognition in such fashion. Anodal tDCS is often thought to increase the likelihood of reaching the threshold of the action potential, while cathodal tDCS is thought to inhibit neural activity in the stimulated area (Inukai et al., 2016). However, depending on the distance between the electrodes used in various montages, the electrical field is increased either primarily under cortex positioned between the sites or underneath both sites (Sadleir et al., 2010). Similar to TMS, tDCS does not always yield effects in the desired direction, and "paradoxical" non-linear effects have been described (e.g., Kuo et al., 2013). Moreover, continuous stimulation might influence the mechanism of neurophysiological homeostasis in addition to cortical excitability (Fricke et al., 2011), thus rendering the outcome of the stimulation further uncertain.

With these precautions in mind, a number of NIBS studies show impacts for rTMS and tDCS in cognitive processes and psychopathologies (reviewed by Brunoni and Vanderhasselt, 2014; Dedoncker et al., 2020), suggesting that NIBS might also be used to study SRP. However, NIBS studies on SRP have been relatively scarce. Frewen et al. (2020) briefly overviewed studies whereby NIBS was used to modulate both on-task SRP and spontaneous SRP as it occurs during resting state. Further, Chaieb et al. (2019) systematically reviewed the effects of neuromodulation on mind-wandering which may be considered a form of spontaneous SRP during resting state due to the functional and anatomical overlap between the brain regions mediating mind-wandering and SRP (e.g., Qin and Northoff, 2011). In their review of the tDCS literature, Chaieb and colleagues (2019) identified the dorsolateral prefrontal cortex (DLPFC), ventrolateral prefrontal cortex, the MPFC, and the right IPL as regions involved in mind-wandering, and suggested that tDCS can potentially modulate activity within the MPFC and the right IPL, further suggesting possible applications of NIBS to SRP, although TMS studies were not included. Here, we undertook to what is in our knowledge the first systematic review of the effects of NIBS for on-task SRP that has considered both TMS and tDCS studies and theoretical differentiation between V-SRP and NV-SRP (BSC).

METHODS

We conducted a PsycInfo and PubMed search with the following terms on Apr 13th, 2021: (tDCS OR rTMS OR TMS OR tES) (self refer* OR self recog* OR self other OR rubber hand illusion), restricting our search to peer-reviewed journal articles with no restriction on publication time. This search yielded 217 results from PsycInfo and 391 results from PubMed, making a total of 608 results (**Figure 1**). After an initial screening of each article's abstract, 43 empirical studies were considered

potentially relevant and thus were passed for full-text screening. The screening process and methodological quality evaluation were carried out by two of the authors (ZB and PF) with discussions on each paper. Any uncertainty in agreement on the meeting of inclusion and exclusion criteria were taken up with a third co-author. The 566 excluded articles were either 1) focused on tasks unrelated to SRP or 2) focused on clinical populations or 3) lacked inclusion of a behavioral task. After reading the full texts of the 43 studies, 20 studies qualified for the review because they featured at least one task that required participants to explicitly attend to verbal or non-verbal (bodily) self-referential stimuli (i.e., involved on-task SRP). The 23 excluded studies either: 1) did not include an SRP task condition, or 2) only investigated spontaneous SRP without an explicit task (e.g., SRP occurring in the form of mind wandering during resting state). We decided not to include at-rest SRP studies because this literature was already recently reviewed by Chaieb et al. (2019). For this review, we focus on SRP tasks that required internal attention directed toward oneself in the verbal (V-SRP) or non-verbal sense (NV-SRP) (see Frewen et al., 2020). Comparably, tasks that primarily required attention being directed to other people (e.g., theory of mind tasks) or external stimuli were therefore excluded. Finally, seven new studies from the reference lists of the 20 qualified articles were identified and added to the review, resulting in 27 studies in total (**Figure 1**). By comparison, the excluded studies are listed in **Supplementary Table 1**.

From each article we extracted the most relevant experimental variables, that is, the (1) study design (rTMS vs. single-pulse TMS vs. tDCS), (2) NIBS parameters (stimulation site, duration, timing and strength), (3) sample size, (4) SRP task administered, (5) measurement (**Tables 1**, **2**), and (6) findings (**Tables 3**, **4**). We followed the guidelines and used the Cochrane risk-of-bias tool (Higgins et al., 2019) to assess the quality of study methods (**Table 5**).

The included studies are subcategorized into V-SRP or NV-SRP studies based on the broad nature of the task and further categorized based on specific task types. Studies that investigated responses to self-trait adjectives using self-referential encoding task (SRET) were considered within the V-SRP category. SRET studies were further subcategorized into those that used valenced words and therefore assessed the self-enhancement bias (SEB), defined as the tendency toward positive self-evaluation, or self-criticism, defined as the tendency toward negative self-evaluation, and those that selected primarily "neutral" trait adjectives and therefore assessed the self-processing effect (SPE), defined as one's tendency to process information differentially based on its degree of relevance toward oneself. In comparison, studies that broadly involved tasks involving BSC were categorized into the NV-SRP category (for a definition of BSC, see Park and Blanke, 2019). These NV-SRP tasks were further subcategorized into tasks that investigated one of two forms of exteroceptive NV-SRP or BSC, specifically, (1) visual self-other discrimination task (SODT) or the (2) rubber hand illusion (RHI), or involved (3) interoception in the form of heart-beat detection task (HBDT) or breath counting. In the visual self-other discrimination tasks, participants' faces were digitally morphed into another face (close others or famous persons) and participants were asked to react to the change of identity during the morphing process. For RHI tasks, studies introduced visual-tactile illusions where participants' real hand is stroked with a brush in synchrony with a rubber hand to create illusory tactile sensations measured by proprioceptive drift and subjective reports of a sense of ownership of the rubber hand (Botvinick and Cohen, 1998). Finally, HBDT objectively measured heart rate and/or respiration rate and determined participants' accuracies in self-monitoring these measures over a specified time (Dale and Anderson, 1978; Schandry, 1981; Brener and Kluvitse, 1988; Brener and Ring, 2016). The number of studies identified involving each of these tasks is noted in **Figure 2**, further categorized as to the form of NIBS that was employed.

RESULTS

Among the 27 studies, 10 were classified as V-SRP studies and 17 were NV-SRP studies. With regards to stimulation methods, 9 used single-pulse TMS (5 V-SRP, 4 NV-SRP), 9 used rTMS (1 V-SRP, 8 NV-SRP), and 9 used tDCS (4 V-SRP, 5 NV-SRP). The breakdown of the included studies by their method is summarized in **Figure 2**. The methodological details of each study are summarized in **Table 1**. Study findings are summarized in **Tables 1**, **3** for V-SRP and **Tables 2**, **4** for NV-SRP. Additionally, the studies excluded from this review and the detailed results of each study are described in the appendix (**Supplementary Material**).

The results of the methodological quality evaluation are listed in **Table 5**. In brief, the included studies have generally low levels of bias due to randomization, valid interventions, and appropriate use of missing data and outcome measurements. However, all studies received "some concerns" as the overall rating primarily due to the lack of pre-registered plans, albeit some of the papers were published before pre-registrations policies were available (**Table 5**).

V-SRP

Self-Processing Effect (SPE)

TMS studies

Two studies found that single-pulse TMS over the medial parietal region (Pz according to the 10-20 system) and the bilateral IPL reduced SPE (Lou et al., 2004, 2010; **Figure 3**). In comparison, neither study found involvement of the MPFC during trait-assignment tasks. In addition to behavioral measures, Lou and colleagues (2004) obtained participants' cerebral blood flow (CBF) with PET scan and showed that TMS application over Pz at 160 ms post-stimulus decreased the CBF in the left IPL more when the words presented were self-related rather than other-related (Lou et al., 2004).

tDCS studies

Only a single study investigated the effects of offline tDCS on V-SRP using neutral stimuli, thus examining the SPE (**Figure 3**). Here, Schäfer and Frings (2019) tested the effects

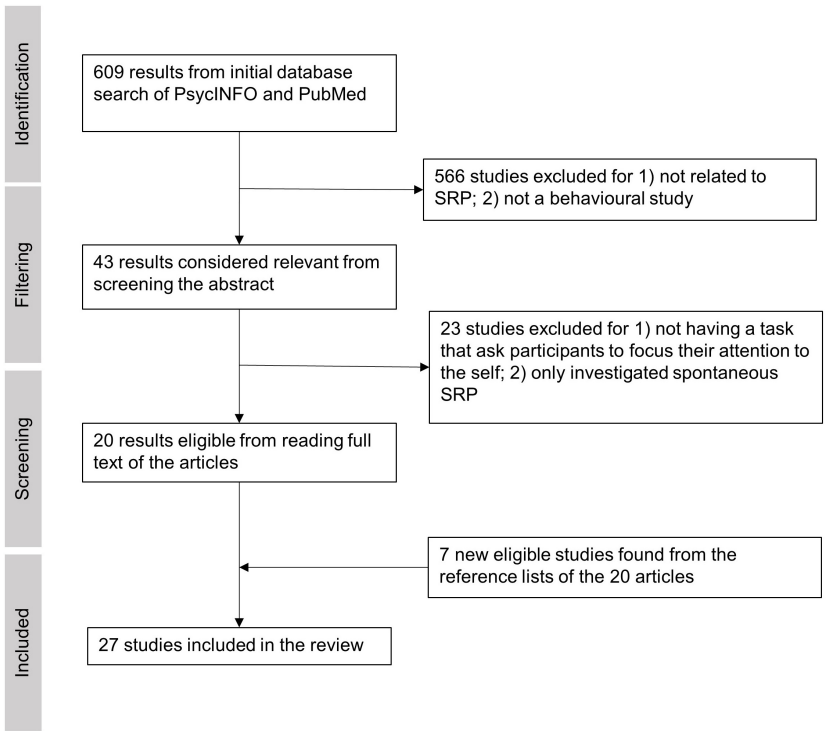

FIGURE 1 | The process of article inclusion and exclusion of the systematic literature review.

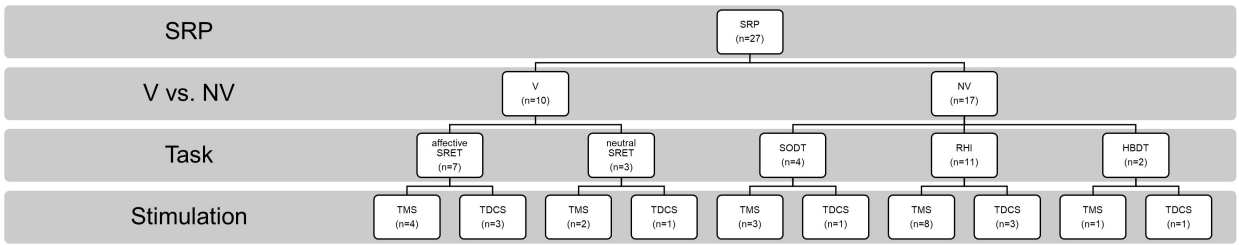

FIGURE 2 | Summary of the included studies by type, task, and stimulation modality. SRP, self-referential processing; V, verbal SRP; NV, non-verbal SRP; SRET, self-referential encoding task; SPE, self-processing effect; SODT, self-other discrimination task; RHI, rubber hand illusion; HBDT, heartbeat detection task.

of anodal stimulation over the ventral medial prefrontal cortex (VMPFC) (with cathode over the DLPFC) on participants' memory of emotionally neutral word associations but failed to identify any effect on V-SRP as the result of this stimulation.

Self-Enhancement Bias (SEB) and Self-Criticism

TMS studies

Four studies consistently found that TMS over the MPFC reduced SEB, supporting the MPFC's role in emotional SRP (single-pulse: Kwan et al., 2007; Barrios et al., 2008; Luber et al., 2012; rTMS: De Pisapia et al., 2019; **Figure 4**). Evaluating midline parietal cortex stimulation, Kwan et al. (2007) also found that stimulation applied to the Pz 10-20 EEG electrode site reduced SEB compared to TMS of the supplementary motor area (SMA), although the effect of Pz stimulation was not significantly different from sham stimulation. This complicates interpretation since we cannot conclude that SMA stimulation improved SEB based on the non-significance between SMA stimulation and sham stimulation, albeit this trending result may help future studies in power calculation. Additionally, De Pisapia et al. (2019) reported increased BOLD signal in the PCC in response to MPFC stimulation. However, no significant effect was found for left or right IPL stimulation on SEB (Luber et al., 2012).

tDCS studies

Among the three studies that used emotionally valenced stimuli, two studies targeting the left DLPFC reduced negative self-evaluation (De Raedt et al., 2017; Dedoncker et al., 2019; **Figure 4**) and, in terms of associated mood changes, participants

TABLE 1 | Summary of experimental paradigms of V-SRP studies.

Study	Experimental Task	Timing of Task	Design	Sham condition	Site of stimulation	*N(% females)*	Stimulation method, time and intensity	Dependent variable(s)
Schäfer and Frings, 2019	SRET - neutral	Offline	B	No	Anodal/cathodal VMPFC (Fpz), cathodal/anodal DLPFC (F3)	65(72%)	0.5-mA tDCS for 20 min. Target electrodes are 9 cm^2, reference electrodes are 35 cm^2	Accuracy and RT
Lou et al., 2004	SRET - neutral	Online	W	No	Oz, Pz, and Fz	25(54%)	Single-pulse TMS at 150% MEP of the feet, at 0∼480 ms post-stimulus	Accuracy and RT
Lou et al., 2010	SRET - neutral	Online	W	No	MPFC, left IPL, right IPL	15(39%)	Single-pulse TMS at 150% RMT, at 0∼480 ms post-stimulus	Accuracy and RT
Barrios et al., 2008	SRET - affective	Online	B	Yes	MPFC, Pz, and SMA	10(100%)	Single-pulse TMS at 90% RMT, 500 ms post-stimulus	Self-enhancement scores and RT
Mainz et al., 2020	SRET - affective	Offline	B	Yes	Anodal/cathodal Fpz (MPFC) and cathodal/anodal Oz (occipital)	75(0%)	2-mA tDCS for 20 min. Target and reference electrodes are 35 cm^2	Self-enhancement scores
Dedoncker et al., 2019	SRET - affective	Offline	B	Yes	Anodal Left DLPFC, cathodal right supraorbital area	41(100%)	1.5-mA tDCS or 20 mins. Target and reference electrodes are 25 cm^2	Perceived criticism, current mood, and resting FC
Kwan et al., 2007	SRET - affective	Online	W	Yes	MPFC, Pz, and SMA	12(83%)	Single-pulse TMS at 90% RMT, 500 ms post-stimulus	Self-enhancement scores and RT
Luber et al., 2012	SRET - affective	Online	W	No	MPFC, left IPL, right IPL	18(44%)	Single-pulse TMS at 150% RMT, 0∼480 ms post-stimulus	Self-enhancement scores and RT
De Raedt et al., 2017	SRET - affective	Offline	W	Yes	Anodal Left DLPFC, cathodal right supraorbital area	32(100%)	1.5-mA tDCS for 20 min. Target and reference electrodes are 35 cm^2	Ruminative thinking, current mood, implicit and explicit self-esteem
De Pisapia et al., 2019	SRET - affective	Offline	W	Yes	MPFC (Fpz)	14(50%)	1-Hz rTMS for 14 min at 100% of RMT	RT and fMRI BOLD signal

Abbreviations: W, within-subject design; B, between-subject design; RMT, resting motor threshold; RT, reaction time; TMS, transcranial magnetic stimulation; tDCS, transcranial direct current stimulation; rTMS, repetitive transcranial magnetic stimulation; cTBS, Continuous theta-burst stimulation; MPFC, medial prefrontal cortex; VMPFC, ventromedial prefrontal cortex; DLPFC, dorsolateral prefrontal cortex; IPL, inferior parietal lobule; BOLD, blood oxygen level dependant; SMA, supplementary motor area; PPC, posterior parietal cortex; HEP, heartbeat-evoked potential; MEP, motor-evoked potential; EBA, extrastriate body area; aIPS, anterior inferior pareital lobule; M1, primary motor cortex; SRET, self-referential encoding task; RHI, rubber hand illusion; SODT, self-other discrimination task; HBDT, heartbeat detection task.

in both studies reported feeling less vigorous and less cheerful after the stimulation. Moreover, Dedoncker et al. (2019) found that the reduction in negative self-evaluation was associated with reduced functional connectivity between the DLPFC and the left posterior insula. In contrast, the only study targeting the MPFC found no effect of offline tDCS on positive or negative self-evaluation (Mainz et al., 2020).

NV-SRP

Self-Other Discrimination

TMS studies

Three rTMS studies on self-other visual discrimination consistently found that right IPL stimulation increased participants' propensity to judge ambiguous faces to be their own (Uddin et al., 2006; Heinisch et al., 2011; Heinisch et al., 2012;

TABLE 2 | Summary of experimental paradigms of NV-SRP studies.

Study	Experimental Task	Timing of Task	Design	Sham condition	Site of stimulation	*N(% females)*	Stimulation method, time and intensity	Type of measure
Payne and Tsakiris, 2017	SODT	Offline	B	Yes	Right IPL (CP6), reference electrode over the Vertex	60(73%)	1-mA tDCS for 20 min. Target and reference electrodes are 3.5 cm^2	Proportion of morphing video judged "self"
Uddin et al., 2006	SODT	Offline	W	No	Left and Right IPL	8(75%)	1-Hz rTMS for 20 min at 100% RMT	Proportion of morphing pictures judged "self"
Heinisch et al., 2011	SODT	Offline	W	Yes	Left DLPFC (midpoint of triangle F3, F7, Fp1), right DLPFC (midpoint of triangle F4, F8, Fp2), left IPL (CP5), right IPL (CP6)	10(50%)	1-Hz rTMS for 20 min at 100% RMT	Proportion of morphing video judged "self", self-reported valence of self-recognition
Heinisch et al., 2012	SODT	Offline	W	Yes	Right IPL (CP6)	10(50%)	1-Hz rTMS for 20 min at 100% RMT	Proportion of morphing video that is judged to be the self, self-reported valence of self-recognition
Bassolino et al., 2018	RHI in Virtual reality	Online	Mixed design	No	M1, vertex, 80% RMT for subthreshold stimulation as control	32(50%)	Single-pulse TMS at 130% RMT	PD, MEP, subjective reports of body ownership
Convento et al., 2018	RHI	Online	B	Yes	Right PMC, right IPL	56(95%)	1.5-mA tDCS for 10 min. Target and reference electrodes are 25 cm^2	PD, subjective reports of body ownership
della Gatta et al., 2016	RHI	Online	B	No	Left M1, right M1 as control	52(64%)	Single-pulse TMS at 110% RMT	PD, MEP, subjective reports of body ownership
Tsakiris et al., 2008	RHI	Online	W	No	Right IPL, vertex	10(60%)	Single-pulse TMS with varying intensity (38-65% maximum stimulator output), 350 ms post-stimulus	PD
Kammers et al., 2009	RHI	Offline	W	Yes	Left IPL (TP3)	13(100%)	1-Hz rTMS for 20 min at 80% RMT	PD, subjective reports of sensations
Wold et al., 2014	RHI	Offline	W	No	Left EBA, 40% RMT stimulation as control	19(58%)	1-Hz rTMS for 20 min at 80% RMT	PD, subjective reports of body ownership
Karabanov et al., 2017	RHI	Online	W	No	Anterior IPS, M1	28(43%)	Single- and paired-pulse TMS at 100% RMT for M1, 90% RMT for aIPS, 500 ms post-stimulus	PD, MEP, subjective reports of body ownership
Fossataro et al., 2018	RHI	Offline	W	Yes	Left M1	48(79%)	1-Hz rTMS for 20 min at 90% RMT and single-pulse TMS at 100% RMT	PD, MEP, subjective reports of body ownership
Hornburger et al., 2019	RHI	Online	W	Yes	Anodal/cathodal S1(C3), reference electrode over right supraorbital region	30(60%)	1-mA tDCS for 20 min. Target and reference electrodes are 35 cm^2	PD, subjective reports of body ownership

(Continued)

TABLE 2 | Continued

Study	Experimental Task	Timing of Task	Design	Sham condition	Site of stimulation	*N(% females)*	Stimulation method, time and intensity	Type of measure
Lira et al., 2018	RHI	Online	W	Yes	Right PPC (35 cm^2, 2-mA, P4), right PMC (1-mA, fC4, 10-10 EEG system), reference electrode over contralateral supraorbital region (35 cm^2)	160(71%)	2- or 1-mA tDCS for 10 min. Target and reference electrodes are 35 or 21 cm^2	PD, subjective reports of body ownership
Peviani et al., 2018	RHI	Offline	W	No	PMC, vertex	24(79%)	1-Hz rTMS for 20 min at 100% RMT	PD, subjective reports of body ownership
Sagliano et al., 2019	HBDT	Offline	W	Yes	Anodal Left insula (midpoint of F7 and T3), cathodal left frontal pole (Fp2); anodal right insula (midpoint of F8 and T4), cathodal right frontal pole (Fp1)	16(56%)	1-mA tDCS for 15 min. Target electrode is 6.25 cm^2, reference electrode 25 cm^2	Heartbeat counting accuracy, self-reported state anxiety
Pollatos et al., 2016	HBDT	Offline	W	No	Right insula (FT8), somatosensory cortex (chest location, Cz), central occipital (Oz)	18(0%)	5-Hz cTBS for 40 sec at 80% RMT	Heartbeat and respiratory counting accuracy and confidence in judging accuracy, self-reported state anxiety, HEP

*Abbreviations: see the end of **Table 1** for abbreviations.*

Figure 5). Importantly, Heinisch and colleagues (2011, 2012) tested this effect to be self-other specific rather than simply about face-discrimination in general by controlling for face familiarity and other-other discrimination. Further, they found that rTMS over the right DLPFC reduced the judgment bias towards their faces in people who have negative attitudes toward their face, suggesting a role for valenced NV-SRP in the right DLPFC. As for studies that targeted the left IPL, neither Uddin et al. (2006) nor Heinisch et al. (2011) found a significant effect of left IPL stimulation on self-other discrimination.

tDCS studies

We identified only a single tDCS study on visual self-other discrimination that found that offline anodal stimulation to the right IPL increased the amount of self-face needed for self-recognition, effectively reducing participants' bias towards their face (Payne and Tsakiris, 2017; **Figure 5**).

Rubber Hand Illusion

TMS studies

The effect of TMS on RHI has been the most studied, with different targets of stimulation. Within these studies, two targeted the IPL and found that TMS reduced RHI-induced proprioceptive drift (single-pulse: Tsakiris et al., 2008; rTMS: Kammers et al., 2009; **Figure 6**), while one study targeting the extrastriate body area (EBA) found increased proprioceptive drift (rTMS: Wold et al., 2014). Another study using paired-pulse TMS targeting the anterior IPS (aIPS) and primary motor cortex (M1) found numerical but non-significant increases in proprioceptive drift when participants experienced agency and ownership over the rubber hand (Karabanov et al., 2017).

In comparison with the studies that targeted the right IPL, four studies targeted the M1 with TMS and consistently found increases in RHI strength measured by increased proprioceptive drift, sense of ownership and embodiment (single-pulse: della Gatta et al., 2016; Karabanov et al., 2017; Bassolino et al., 2018; rTMS: Fossataro et al., 2018; **Figure 6**). Interestingly, one study targeting the ventral premotor cortex (VPMC) also found reduced proprioceptive drift without changes in subjective ownership (rTMS: Peviani et al., 2018). These studies suggest that the RHI may be mediated by neural processes on different levels.

tDCS studies

Convento et al. (2018) showed that anodal stimulation to both the right IPL and the right PMC increased proprioceptive drift (**Figure 6**). Interestingly, in their experiment, the effects of tDCS on right PMC were indifferent to synchrony of stroking. Moreover, another study found that online anodal tDCS over the posterior parietal cortex (PPC) but not the PMC facilitated

TABLE 3 | Summary of results of the included V-SRP studies.

Study	Task	Main Results	Other Results
TMS studies			
Neutral			
Lou et al., 2004	Rate the applicability of personality traits to self, best friend, and the Danish Queen. Then indicate their previous choice as fast as they can	SPE was reduced by TMS to Pz applied 160ms post-stimulus (self > other)	No effect was found in the Fz stimulation condition
Lou et al., 2010	Same as Lou et al., 2004, but without the Danish Queen condition	SPE was reduced by TMS to both left and right IPL applied 160ms, 240ms, and 480 ms post-stimulus. The left IPL had a much stronger effects than right IPL.	No effect was found in the Fz stimulation condition
Affective			
Kwan et al., 2007	Assign positive, neutral and negative adjectives to either the self or their best friend	real stimulation over the MPFC reduced SEB compared to sham	Precuneus stimulation was also found to reduced SEB but only compared to the Supplementary motor area stimulation
Barrios et al., 2008	Assign egotistic or moralistic adjectives that are either positive or negative to the self or best friend	TMS to the MPFC significantly reduced SEB but only for egotistic words	No self-enhancement effect was found among their all-female samples
Luber et al., 2012	Assign desirable and undesirable adjectives to either the self or their best friend	real stimulation over the MPFC reduced SEB compared to sham	TMS over the parietal cortex did not affect the self-enhancement effect
De Pisapia et al., 2019	Assign positive and negative adjectives to the self, close other, and the Eiffel Tower or count the number of syllables.	rTMS to the MFPC resulted in inhibition of negative self-evaluation.	(1) TMS reduced the BOLD signal in the MPFC in other condition more than self; (2) TMS increased PCC BOLD signal in negative > positive; (3) TMS over the MPFC increased the BOLD signal in the bilateral IPL only for negative adjective assignment to the self
tDCS studies			
Neutral			
Schäfer and Frings, 2019	Recall previously learned word associations with the self, an other, and a neutral object	anodal VMPFC with cathodal DLPFC had no effect in all conditions	N/A
Affective			
De Raedt et al. (2017).	Respond "true" or "false" to positive or negative statements related to the self. Then listened to the negative statements in audio format	anodal tDCS over the DLPFC with cathodal r-SOA reduced negative self-evaluation compared to sham	participants reported being more tired, less vigorous, and less cheerful after both real and sham tDCS
Dedoncker et al. (2019).	Female participants listened to critical, neutral, and positive comments about them. Also reported their perceived level of criticism in their life.	Anodal left DLPFC stimulation reduced emotional responsiveness (measured by functional connectivity) toward criticisms in females with a high level of perceived criticism	Participants reported more fatigue, less vigor, and less cheerful after both real and sham tDCS Participants reported more anger and more depressed after being criticized
Mainz et al. (2020)	Respond descriptiveness of positive and negative adjectives related to the self. Then asked to recall the adjectives regardless of valence	anodal MPFC with cathodal near Oz had no effect for both conditions	Participants exhibited self-enhancement bias toward positive words

*Abbreviations: SPE, Self-processing effect; SEB, self-enhancement bias; SOA, supraorbital area; PCC, posterior cingulate cortex. See 'Abbreviations' under **Table 1** for missing abbreviations.*

proprioceptive drift and subjective ownership, further supporting the functional segregation between the parietal cortex and the PMC during RHI (Lira et al., 2018; **Figure 6**). Finally, a study found that online cathodal tDCS over the primary somatosensory cortex (S1) facilitated the subjective experience of RHI when compared to the anodal group but not on proprioceptive drift (Hornburger et al., 2019; **Figure 6**).

Interoception

TMS studies

We identified only one TMS study that investigated the effects of offline continuous theta-burst stimulation (cTBS) on interoception, focusing on right insula and S1 stimulation in comparison to occipital cortex stimulation as a control (Pollatos et al., 2016; **Figure 7**). The researchers found that right insula and S1 stimulation reduced interoceptive accuracy (IAc), IAc confidence, and interoceptive sensibility. Specifically, cTBS over S1 reduced cardiac IAc while cTBS over the right insula reduced both cardiac and respiratory IAc. Further, in terms of IAc confidence, right insula cTBS reduced confidence in respiration IAc compared specifically to occipital stimulation and reduced cardiac IAc confidence compared specifically to S1 stimulation. Additionally, both insula and S1 stimulation resulted in an increase in self-reported interoceptive sensibility compared to

TABLE 4 | Summary of results of the included NV-SRP studies.

Study	Task	Main Results	Other Results
TMS studies			
Self-other discrimination			
Uddin et al., 2006	Presented with pictures of their own face gradually morphed into a familiar other, then press a button to indicate a change of identity	rTMS over the right IPL increased propensity to judge faces to be one's own	No effect was found in the left IPL stimulation condition
Heinisch et al., 2011	Similar to Uddin et al., 2006 but: (1) used video morphing instead of pictures. (2) Added an unfamiliar face condition. (3) Added a questionnaire on perception of their own body.	rTMS over the right IPL and right DLPFC increased propensity to detect self-faces emerging from famous face but not unfamiliar face.	rTMS over the right DLPFC reduced self-recognition sensitivity in people who have negative attitudes toward their own face
Heinisch et al., 2012	Similar to Heinisch et al., 2011, but measured attention during the task	Replicated Uddin et al., 2006 and Heinisch et al., 2011. But rTMS over the right IPL have no effect on other-other discrimination	Attention had no impact on the effect of right IPL rTMS
Rubber hand illusion (RHI)			
Tsakiris et al., 2008	RHI, PD measurement	Single-pulse TMS over the r-IPL reduced PD when viewing the rubber hand, but increased drifts when viewing the neutral object	N/A
Kammers et al., 2009	RHI, PD measurement, and questionnaire about subjective RHI experience. Immediate and delayed effects were both measured	For immediate effects, rTMS over the left IPL reduced PD when viewing the rubber hand. No difference in subjective experience between real and sham TMS groups	No effect was found for delayed effects of rTMS
Wold et al., 2014	RHI with button clicking to indicate RHI onset, PD, subjective rating of RHI intensity	rTMS over the EBA increased PD during synchronous stroking compared to the asynchronous stroking	No rTMS effect on subjective reports of body ownership
della Gatta et al., 2016	RHI, PD measurement, and questionnaire about subjective ownership.	Single-pulse TMS over the M1 reduced MEP, increased PD, and increased sense of embodiment in the synchronous condition compared to the asynchronous condition	The reduction of MEP increased overtime
Karabanov et al., 2017	RHI procedure where the rubber hand can be anatomically implausible (ownership) and/or detached from real hand (agency). PD, subjective rating of agency and ownership, and the effective connectivity between brain regions were measured.	Single-pulse TMS over the M1 increased PD and ownership. No change of PD and subjective rating induced by paired-pulse stimulation (M1-aIPS)	TMS over the aIPS inhibited motor-evoked potential (MEP) from TMS-induced signals from M1. Such effect is dampened during sensorimotor conflicts
Bassolino et al., 2018	RHI procedure in virtual reality with PD, ownership, and agency measurement	Pulses of supra-threshold TMS over the M1 increased sense of ownership for synchronous stroking compared asynchronous Supra-threshold TMS over the M1 increased ownership and agency compared to sub-threshold for synchronous stroking	No effect was found for perceived agency, disownership, and location when compared the two supra-threshold conditions
Fossataro et al., 2018	RHI procedure in virtual reality with PD and embodiment questionnaire	rTMS over the M1 increased sense of embodiment and disembodiment for synchronous stroking	N/A
Peviani et al., 2018	RHI procedure in virtual reality with PD and ownership questionnaire	rTMS over the VPMC reduced PD without influencing the sense of ownership	N/A
Interoception			
Pollatos et al., 2016	Heartbeat and respiration counting task with interoceptive sensibility questionnaire before and after the task	cTBS over the S1 reduced cardiac IAc compared to occipital stimulation cTBS over the right insula reduced cardiac and respiratory IAc compared to occipital stimulation	Stimulation over the right insula reduced confidence in cardiac IAc compared to occipital stimulation Stimulation over the right insula reduced confidence in respiration IAc compared to S1 stimulation
tDCS studies			
Self-other discrimination			
Payne and Tsakiris, 2017	Similar to Heinisch et al., 2011, without the attention task	Anodal stimulation at CP6 with cathode at the vertex decreased propensity to judge faces to be one's own	N/A

(Continued)

TABLE 4 | Continued

Study	Task	Main Results	Other Results
Rubber hand illusion (RHI)			
Convento et al., 2018	RHI, PD measurement, and questionnaire about subjective RHI experience with an additional experiment with no stroking	Anodal stimulation over the right IPL increased PD in synchronous stroking compared to asynchronous stroking, while the effects of anodal right PMC stimulation on PD was indifferent of synchrony	Stimulation to the right IPL not the right PMC induced subjective feeling of "illusory touch" Anodal tDCS to right IPL and right PMC increased PD even without stroking
Hornburger et al., 2019	RHI procedure where location of rubber hand become increasingly anatomically implausible, PD, and subjective questionnaire measurements	Cathodal tDCS facilitated the subjective experience but not PD during RHI compared to the anodal group	Regardless of stimulation, RHI strength and PD exhibited gradual decreases as the rubber hand moved further away from the real hand
Lira et al., 2018	RHI, PD measurement, and questionnaire about subjective RHI experience	anodal tDCS over the PPC but not the PMC facilitated of RHI and subjective reports, regardless of synchrony.	PPC tDCS's strength of effect in PD is higher in synchronous condition compared to the asynchronous condition
Interoception			
Sagliano et al., 2019	Heartbeat counting task with ECG recordings before and after tDCS	sham tDCS over the left and right insula improved counting accuracy of heartbeats but not real stimulation.	No effect of tDCS on state anxiety

*Abbreviations: PMC, premotor cortex; VPMC, ventral premotor cortex; PD, proprioception drift; ECG, electrocardiogram; IAc, interoceptive accuracy; see 'Abbreviations' under **Table 1** for missing abbreviations.*

pre-stimulation. Note that one limitation of this study is that the cTBS targeting the insula would have an impact on the overlying frontotemporal cortices, complicating interpretation.

tDCS studies

We also identified only a single study that investigated interoception with tDCS. Specifically, Sagliano et al. (2019) found no effect of offline anodal tDCS over the left and right insula on heartbeat counting accuracy (**Figure 7**). However, sham tDCS facilitated counting accuracy when pre- and post-stimulation performances were compared. The authors suggested that this can be explained by real tDCS reducing the "practice effect" on interoceptive accuracy improvements, concluding that their study supports the role of the insula in IAc.

DISCUSSION

We systematically reviewed 27 studies that investigated the effect of NIBS on SRP, separated by verbal (V-SRP) vs. non-verbal (NV-SRP) domains. Within the context of V-SRP, studies examined neutral (SPE) vs. emotionally salient (SEB) trait characteristics with SRETs. As described in **Tables 1**, **3** referring to V-SRP and **Tables 2**, **4** referring to NV-SRP, the studies described in this review used diverse methods particularly in stimulation type (repetitive: rTMS or event-related: single or pair-pulse TMS) and strength (TMS strength and tDCS current density). In terms of experimental tasks, studies involved either self vs. non-self stimulus discrimination (V-SRP and NV-SRP), response to the rubber hand illusion (NV-SRP), or interoception (NV-SRP). Overall, the methodological quality of the studies reviewed has generally low biases but revealed some concerns. Despite such differences in methods, the results of the reviewed studies revealed some consistencies, albeit with some caveats.

Verbal SRP (V-SRP)

The results of NIBS on V-SRP were relatively consistent across the 10 reviewed studies in demonstrating a likely role for the cortical midline structures and particularly the left IPL in the self-processing effect (SPE) which, as a task involving self-endorsement responses to relatively neutral adjectives, negates the relevance of emotional valence (**Figure 3**). Moreover, although Lou et al. (2010) found that TMS to both the left and right IPL resulted in a reduction in SPE, the effect of left IPL stimulation was found to be greater than right IPL, which is in line with fMRI studies on V-SRP such as that of Davey et al. (2016) who found the involvement of the bilateral IPL in V-SRP with the left IPL showing increases in BOLD signal more than the right IPL. However, so far only two TMS studies have investigated the effects of IPL stimulation on V-SRP tasks, and therefore more studies are needed for further validation.

Further, whereas the IPL has been implicated in neutral V-SRP or the SPE, the MPFC demonstrates significance when studies considered emotional valence as a variable (**Figure 4**). In our review, three single-pulse TMS studies found that MPFC stimulation reduces self-enhancement bias (SEB), although one tDCS study failed to provide corroborative evidence. Additionally, other regions of interest (ROI) such as the precuneus and bilateral IPL received weak support (Kwan et al., 2007; Luber et al., 2012; De Pisapia et al., 2019). The effects of MPFC stimulation on SEB seem to be self-specific and egotistic, referring to an inflated sense of self-worth, status, and power, indicative of an increased SEB (Barrios et al., 2008). Importantly, three studies found that rTMS or anodal tDCS over the MPFC or the DLPFC also reduced negative self-evaluation (self-criticism), suggesting that activation of the prefrontal neurons could have resulted in an overall dampening of emotional response to V-SRP (De Raedt et al., 2017; Dedoncker et al., 2019; De Pisapia et al., 2019). However, Schäfer and Frings (2019) failed to find an effect of anodal VMPFC with cathodal DLPFC tDCS on neutral

TABLE 5 | Summary of methodological qualities of the included studies.

Study	Bias arising from the randomization process	Bias due to deviations from intended interventions	Bias due to missing outcome data	Bias in measurement of the outcome	Bias in selection of the reported result	Overall risk-of bias judgment
V-SRP						
Lou et al., 2004 (TMS portion)	L	SC	L	SC	SC	SC
Lou et al., 2010	L	L	SC	L	SC	SC
Schäfer and Frings, 2019	L	L	SC	L	SC	SC
Kwan et al., 2007	L	L	L	L	SC	SC
Barrios et al., 2008	L	L	L	SC	SC	SC
Luber et al., 2012	L	L	SC	L	SC	SC
Mainz et al., 2020	L	L	L	L	SC	SC
De Raedt et al., 2017	L	L	L	L	SC	SC
Dedoncker et al., 2019	L	L	L	SC	SC	SC
De Pisapia et al., 2019	L	L	L	L	SC	SC
NV-SRP						
Uddin et al., 2006	L	L	L	L	SC	SC
Heinisch et al., 2011	L	L	L	L	SC	SC
Heinisch et al., 2012	L	L	L	L	SC	SC
Payne and Tsakiris, 2017	L	L	L	L	SC	SC
Tsakiris et al., 2008	L	SC	L	L	SC	SC
Kammers et al., 2009	L	L	L	L	SC	SC
Wold et al., 2014	L	L	SC	L	SC	SC
Karabanov et al., 2017	L	SC	L	L	SC	SC
Convento et al., 2018	L	L	L	L	SC	SC
Bassolino et al., 2018	L	L	L	L	SC	SC
della Gatta et al., 2016	L	SC	L	L	SC	SC
Fossataro et al., 2018	L	L	L	L	SC	SC
Hornburger et al., 2019	L	L	L	L	SC	SC
Lira et al., 2018	L	L	L	L	SC	SC
Peviani et al., 2018	L	SC	L	L	SC	SC
Sagliano et al., 2019	L	L	L	L	SC	SC
Pollatos et al., 2016	L	L	L	L	SC	SC

SRP (i.e., the SPE), while Mainz et al. (2020) failed to find an effect of anodal MPFC with cathodal parietal cortex tDCS on emotional SRP.

Considering the V-SRP studies together, a pattern of functional segregation seems to emerge between the left IPL and the MPFC. Results suggest that the left IPL may be involved in determining the self-relevance of verbal information as primarily tested by the neutral V-SRP studies of SPE (**Figure 3**), while the MPFC might be more so involved in the affective evaluation of such information as tested primarily by the emotional SRP studies of SEB (**Figure 4**), consistent with several functional network models of SRP (Fingelkurts et al., 2016, 2020; Frewen et al., 2020). Further, considering the midline posterior cortex, Lou et al. (2004) and Kwan et al. (2007) applied TMS over Pz

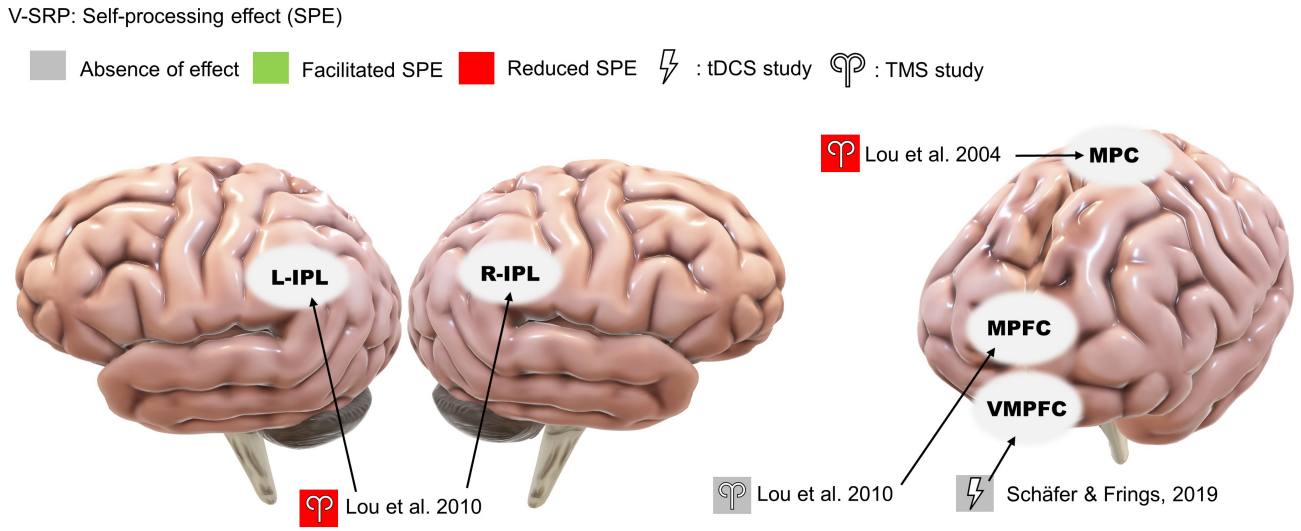

FIGURE 3 | Results of the reviewed studies on neutral SRP with tasks involving self-processing effect (SPE).

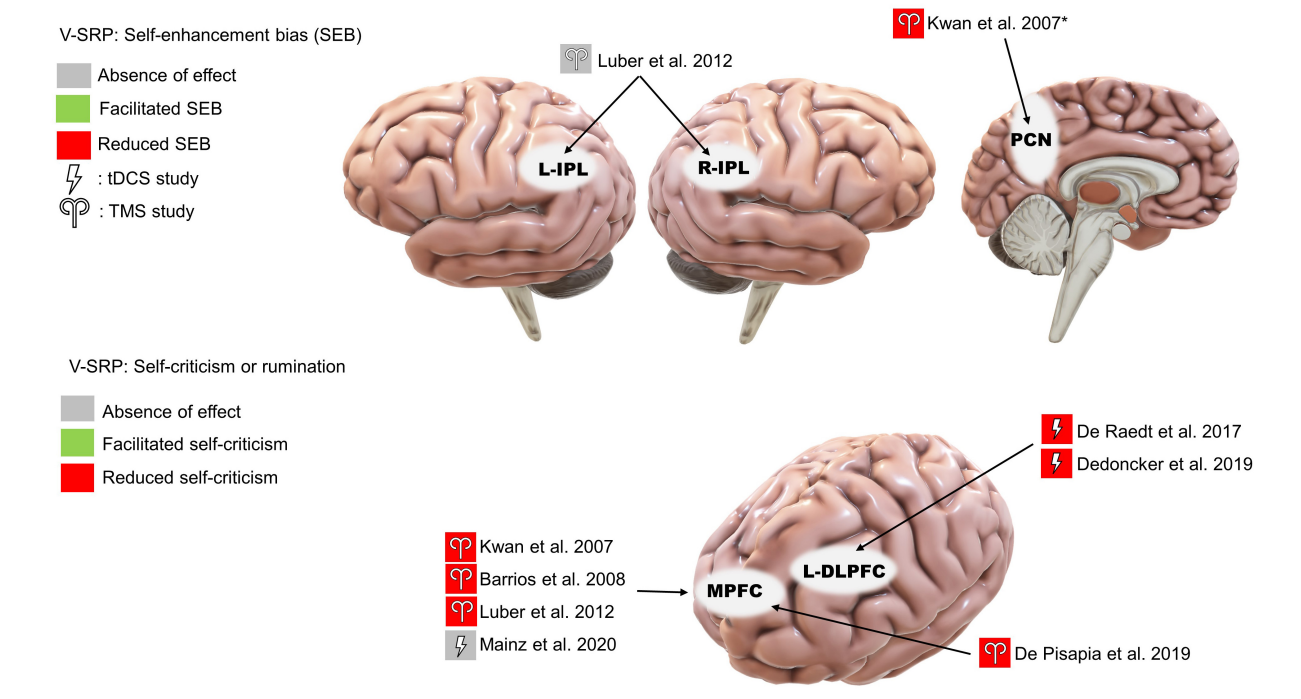

FIGURE 4 | Results of the reviewed studies on emotional SRP with tasks involving self-enhancement bias (SEB) and self-criticism or rumination. *Note: This result was only significant compared to supplementary motor area stimulation.

and found smaller degrees of impact on V-SRP compared to the MPFC, while De Pisapia et al. (2019) found that MPFC had an impact on both the PCC and the bilateral IPL BOLD signals during emotional V-SRP. Interestingly, the dynamic causal modeling conducted by Davey et al. (2016) suggested that the PCC may be the drive for self-related processes with the MPFC as the moderator. Taken together, this supports the notion that although the PCC might be the drive for SRP in general, V-SRP may be more closely related to the MPFC, especially when V-SRP is emotionally significant.

Non-Verbal SRP (NV-SRP)

Given our affinity to faces even from infancy, being able to distinguish one's face from others' faces can be considered as a basic form of NV-SRP, measured by SODTs. In this review, three TMS studies and one tDCS study supported the right

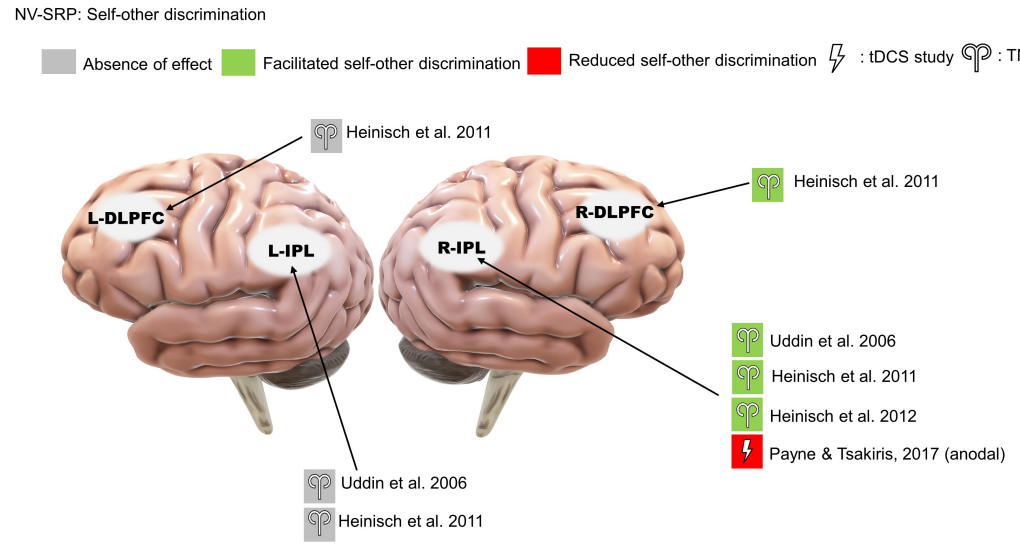

FIGURE 5 | Results of the reviewed studies on NV-SRP with tasks involving self-other discrimination.

IPL's causal role in self-other face discrimination (**Figure 5**), confirming the correlational findings from neuroimaging studies (Uddin et al., 2006; Heinisch et al., 2011, 2012; Payne and Tsakiris, 2017). On the contrary, stimulation over the left IPL did not yield any significant change in visual self-recognition. This pattern of lateralization in self-other discrimination in the right hemisphere is consistent with existing evidence (Uddin et al., 2005; Bukowski et al., 2020) but recent evidence also supported the involvement of the left hemisphere (Quesque and Brass, 2019). Furthermore, two studies in our review also found involvement of the right IPL in V-SRP, which suggests that the right IPL may be involved in both V-SRP and NV-SRP (Lou et al., 2010; De Pisapia et al., 2019). Interestingly, Heinisch et al. (2011) found that stimulation over the right DLPFC also reduced visual self-recognition but only in people who have pre-existing negative attitudes toward their own face, effectively reducing their negative self-evaluation. Therefore, there might be some degree of laterality in NV-SRP in the right hemisphere, although contrary evidence also exists. It is possible that NV-SRP is associated with multiple processes and therefore affected by stimulation to the right IPL primarily, and other regions such as the left IPL and the DLPFC to some degree. Considering the right IPL as part of the MTL subsystem of the DMN, one might postulate that NV-SRP partially overlaps with the functions of the MTL subsystem and interacts with affective processes in the PFC, which may explain the results of Heinisch et al. (2011). Given that most studies on emotional SRP have focused on V-SRP instead of NV-SRP, future studies could also investigate the effect of NIBS on emotional NV-SRP with MPFC stimulation, for example, in response to facial displays of emotion or using a priming methodology (Frewen et al., 2013, 2017, 2020).

Contrary to the possible right hemisphere dominance in visual self-other discrimination, NIBS over both the left and right hemispheres altered the effects of RHI for the contralateral hand (**Figure 6**). It is important to note that RHI strength has two dimensions: the change in perceived hand position measured by proprioceptive drift, and the change in subjective experiences such as embodiment and ownership of the rubber hand. As illustrated in **Figure 6**, stimulation over different areas had a differential impact on proprioceptive drift and subjective experience. We found that TMS over the M1 and the EBA facilitated subjective experience, whereas TMS over the left IPL and the left PMC reduced proprioceptive drift. Additionally, anodal tDCS over the right PMC and the right IPL facilitated proprioceptive drift, and cathodal tDCS over the S1 facilitated subjective experience (**Figure 6**). These results may offer support for hierarchical processing in the RHI wherein low-level somatosensory processing might be relayed to high-level multisensory integration to form feelings of ownership and agency over the body (Apps and Tsakiris, 2014). Consistent with this interpretation, paired-pulse TMS over the aIPS reduced the motor-evoked potentials from M1 (Karabanov et al., 2017) that was dampened by sensorimotor conflict, supporting the "comparator" mechanism that processes incoming sensory and proprioceptive inputs as proposed by Tsakiris (2010). In our review, areas shown to affect proprioceptive drift include the left VPMC, IPL, EBA, M1, and right IPL for proprioceptive drift, while areas shown to affect subjective experience included left M1, right PMC, S1, and the PPC. According to the hierarchical theory, the right IPL and the PPC might act as the integration area for proprioceptive drift and subjective experience respectively, but such assumptions need to be validated by further evidence.

As compared to the RHI, which involves the processing of one of the bodily extremities, interoception can be measured from a sensory perspective toward internal bodily sensations by IAc of heartbeat or respiration and a subjective perspective by interoceptive sensibility and IAc accuracy. With regards to accuracy, both of the reviewed NIBS studies supported

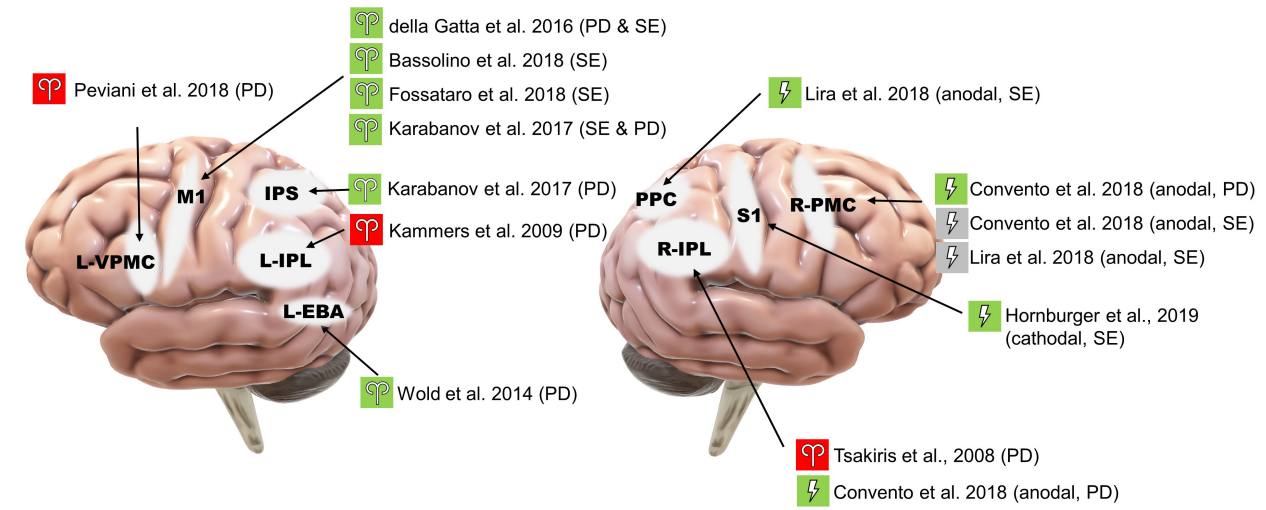

FIGURE 6 | Results of NV-SRP studies on RHI. PD, proprioceptive drift; SE, subjective embodiment of RHI.

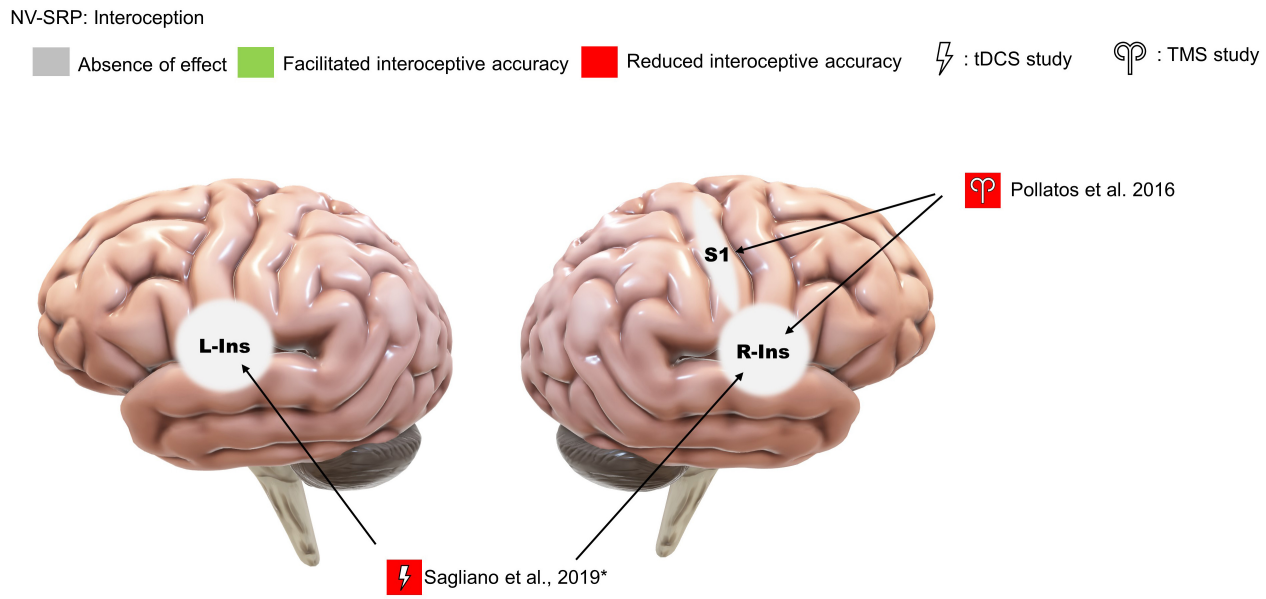

FIGURE 7 | Results of NV-SRP studies on interoception. *Note: This study found that sham but not real stimulation improved interoceptive accuracy.

the causal role of the left and right insula in both cardiac and respiratory interoception (**Figure 7**; for the right insula: Pollatos et al., 2016; and for the left and right insula: Sagliano et al., 2019). Further, with regards to subjective experience, Pollatos et al. (2016) found the involvement of the right S1 in both IAc and the awareness associated with IAc, suggesting that S1 may also be part of a neural system that links interoceptive sensory signals with awareness of such signals. These results provided support for the existence of Park and Blanke's (2019) integrative BSC system connecting multiple interoceptive sensory areas. Referring to meta-awareness as measured by IAc confidence, Pollatos et al. (2016) also argued that the decline might be related to disturbance of the sensory integrative processes in the anterior insula, resulting in mismatching between beliefs and sensory input. However, a more comprehensive picture of the brain areas involved still requires further evidence, as the NIBS literature on IAc and awareness is scarce.

Overall, our review provides causal support for brain regions discovered by neuroimaging studies in NV-SRP in the parietal cortex (including the IPL and PPC), the insula, and sensorimotor cortical areas (including the M1, S1, PMC, and EBA). More importantly, both interoception and BSC (observed in RHI studies) were able to show that stimulation to NV-SRP-related areas can induce changes in participants' perception of internal or external stimuli such as proprioceptive drift or IAc, and they can also alter participants' subjective experiences measured by self-reports, supporting the existence of a common NV-SRP system proposed by Park and Blanke (2019). In their theory, self-identification is associated with a PMC-IPS-insula network whereas self-location is associated with a PCC-IPS network. While a number of NIBS studies investigating the response to the RHI were able to alter self-location by stimulating the IPL, no reviewed NIBS studies on self-identification have chosen the PMC or the insula as the stimulation target, which can be of interest for future studies. Moreover, most of our reviewed NV-SRP NIBS studies have targeted the sensorimotor areas, which may be lower within the hierarchy of processes producing the subjective experiences associated with NV-SRP. In the study conducted by Karabanov et al. (2017), paired-pulse TMS was used to investigate the modulatory role of a higher-order integrative area (e.g., aIPS) toward the M1; future NIBS studies may use similar experimental paradigms to investigate the modulatory relationships between ROIs in NV-SRP.

However, as compared to the response to visual self-recognition tasks, we did not observe a strong right hemisphere dominance for RHI studies wherein left IPL, left EBA, and left VPMC stimulation all showed significant effects on proprioceptive drift (**Figure 6**). One explanation is that compared to self-identification and IAc which do not involve processing only of one side of the body, RHI tasks are more complex, involving multiple processes from raw sensorimotor processing and proprioception of one-sided bodily stimuli (e.g., left or right hand) to a higher-level integration into subjective experiences and BSC as a whole. However, these conclusions should be treated with caution since only two NIBS studies were found in the interoception category, one of which showed bilateral response in the insula (**Figure 7**; Sagliano et al., 2019). Therefore, future studies may investigate the effect of NIBS over higher-order parietal regions on NV-SRP and compare unilateral to bilateral montages.

Limitations and Future Directions

A quantitative meta-analysis was not possible for this review due to the large variability of study designs; thus, we relied on a qualitative and descriptive approach. Another limitation is that the quality of methodology utilized was judged to have some concerns for several of the included studies in this review; future studies are encouraged to utilize stronger methodology, ideally pre-registering their study and including double-blinded designs including both sham and active stimulation controls. Moreover, sample sizes in many studies were small and underpowered, and participant samples were frequently not well described such as for demographic characteristics, a problem that also requires attention in future studies.

In addition to the small number of NIBS studies that have investigated SRP, most reviewed studies have only investigated the effect of NIBS on subjective and behavioral outcomes. From a practical perspective, self-report and behavioral measures can have direct clinical applications, although the underlying brain mechanisms of NIBS on SRP remain a "black box" until the effects of NIBS are routinely simultaneously investigated not only for phenomenological and behavioral outcomes but also for neurobiological outcomes (e.g., EEG, fMRI). Moreover, the experimental tasks used in NIBS studies exhibit a clear verbal vs. non-verbal split between studies, while no studies have so far compared the response to both V-SRP and NV-SRP in the same study. Therefore, future studies may comparatively investigate both verbal and non-verbal aspects of SRP under one experimental design, and compare the effects of different stimulation sites, for example, inter-hemispherically within the IPL or the insula, or between posterior (e.g., IPL, PCC) and anterior (e.g., MPFC) sites, as well as by stimulation method (e.g., TMS vs. tDCS). Moreover, in so far as it is well known that many psychiatric and neurological disorders are associated with disturbances in SRP (e.g., reviewed by Frewen et al., 2020), it will be important to evaluate whether NIBS during SRP tasks would have any clinical significance in treatment, for example, for reducing self-criticism associated with affective disorders such as depression and posttraumatic stress.

AUTHOR CONTRIBUTIONS

ZB, BH, and PF contributed to the conception and design of the study. BH drafted the framework and the initial version of the article. ZB and PF revised and expanded on the article. AB edited and offered suggestions on the article. All authors contributed to the article and approved the submitted version.

FUNDING

This research project is funded by the Canadian Department of National Defense Innovation for Defence Excellence and Security (IDEaS) Program (IDEaS_CP-0555, W7714-196882).

SUPPLEMENTARY MATERIAL

The Supplementary Material for this article can be found online at: https://www.frontiersin.org/articles/10.3389/fnins.2021.671020/full#supplementary-material

REFERENCES

Andrews-Hanna, J. R., Reidler, J. S., Sepulcre, J., Poulin, R., and Buckner, R. L. (2010). Functional-anatomic fractionation of the brain's default network. *Neuron* 65, 550–562. doi: 10.1016/j.neuron.2010.02.005

Apps, M. A., and Tsakiris, M. (2014). The free-energy self: a predictive coding account of self-recognition. *Neurosci. Biobehav. Rev.* 41, 85–97. doi: 10.1016/j.neubiorev.2013.01.029

Araujo, H. F., Kaplan, J., Damasio, H., and Damasio, A. (2015). Neural correlates of different self domains. *Brain Behav.* 5:e00409.

Barker, A. T., and Shields, K. (2017). Transcranial magnetic stimulation: basic principles and clinical applications in migraine. *Headache: J. Head Face Pain* 57, 517–524. doi: 10.1111/head.13002

Barrios, V., Kwan, V. S., Ganis, G., Gorman, J., Romanowski, J., and Keenan, J. P. (2008). Elucidating the neural correlates of egoistic and moralistic self-enhancement. *Consciousness Cogn.* 17, 451–456. doi: 10.1016/j.concog.2008.03.006

Bassolino, M., Franza, M., Bello Ruiz, J., Pinardi, M., Schmidlin, T., Stephan, M. A., et al. (2018). Non−invasive brain stimulation of motor cortex induces embodiment when integrated with virtual reality feedback. *Eur. J. Neurosci.* 47, 790–799. doi: 10.1111/ejn.13871

Bestmann, S., de Berker, A. O., and Bonaiuto, J. (2015). Understanding the behavioural consequences of noninvasive brain stimulation. *Trends Cogn. Sci.* 19, 13–20. doi: 10.1016/j.tics.2014.10.003

Beynel, L., Appelbaum, L. G., Luber, B., Crowell, C. A., Hilbig, S. A., Lim, W., et al. (2019). Effects of online repetitive transcranial magnetic stimulation (rTMS) on cognitive processing: a meta-analysis and recommendations for future studies. *Neurosci. Biobehav. Rev.* 107, 47–58. doi: 10.1016/j.neubiorev.2019.08.018

Botvinick, M., and Cohen, J. (1998). Rubber hands 'feel'touch that eyes see. *Nature* 391, 756–756. doi: 10.1038/35784

Brener, J., and Ring, C. (2016). Towards a psychophysics of interoceptive processes: the measurement of heartbeat detection. *Philos. Transact. R. Soc. Lond. Ser. B Biol. Sci.* 371:20160015. doi: 10.1098/rstb.2016.0015

Brunoni, A. R., and Vanderhasselt, M. A. (2014). Working memory improvement with non-invasive brain stimulation of the dorsolateral prefrontal cortex: a systematic review and meta-analysis. *Brain Cogn.* 86, 1–9. doi: 10.1016/j.bandc.2014.01.008

Bukowski, H., Tik, M., Silani, G., Ruff, C. C., Windischberger, C., and Lamm, C. (2020). When differences matter: rTMS/fMRI reveals how differences in dispositional empathy translate to distinct neural underpinnings of self-other distinction in empathy. *Cortex* 128, 143–161. doi: 10.1016/j.cortex.2020.03.009

Brener, J., and Kluvitse, C. (1988). Heartbeat detection: judgments of the simultaneity of external stimuli and heartbeats. *Psychophysiology* 25, 554–561. doi: 10.1111/j.1469-8986.1988.tb01891.x

Chaieb, L., Antal, A., Derner, M., Leszczyński, M., and Fell, J. (2019). New perspectives for the modulation of mind-wandering using transcranial electric brain stimulation. *Neuroscience* 409, 69–80. doi: 10.1016/j.neuroscience.2019.04.032

Convento, S., Romano, D., Maravita, A., and Bolognini, N. (2018). Roles of the right temporo−parietal and premotor cortices in self−location and body ownership. *Eur. J. Neurosci.* 47, 1289–1302. doi: 10.1111/ejn.13937

Dale, A., and Anderson, D. (1978). Information variables in voluntary control and classical conditioning of heart rate: field dependence and heart-rate perception. *Percept. Mot. Skills* 47, 79–85.

Davey, C. G., Pujol, J., and Harrison, B. J. (2016). Mapping the self in the brain's default mode network. *Neuroimage* 132, 390–397. doi: 10.1016/j.neuroimage.2016.02.022

De Pisapia, N., Barchiesi, G., Jovicich, J., and Cattaneo, L. (2019). The role of medial prefrontal cortex in processing emotional self-referential information: a combined TMS/fMRI study. *Brain Imag. Behav.* 13, 603–614. doi: 10.1007/s11682-018-9867-3

De Raedt, R., Remue, J., Loeys, T., Hooley, J. M., and Baeken, C. (2017). The effect of transcranial direct current stimulation of the prefrontal cortex on implicit self-esteem is mediated by rumination after criticism. *Behav. Res. Ther.* 99, 138–146. doi: 10.1016/j.brat.2017.10.009

Dedoncker, J., Baeken, C., De Raedt, R., and Vanderhasselt, M. A. (2020). Combined transcranial direct current stimulation and psychological interventions: state of the art and promising perspectives for clinical psychology. *Biolog. Psychol.* 2020:107991. doi: 10.1016/j.biopsycho.2020.107991

Dedoncker, J., Vanderhasselt, M. A., Remue, J., De Witte, S., Wu, G. R., Hooley, J. M., et al. (2019). Prefrontal TDCS attenuates medial prefrontal connectivity upon being criticized in individuals scoring high on perceived criticism. *Brain Imag. Behav.* 13, 1060–1070. doi: 10.1007/s11682-018-9927-8

della Gatta, F., Garbarini, F., Puglisi, G., Leonetti, A., Berti, A., and Borroni, P. (2016). Decreased motor cortex excitability mirrors own hand disembodiment during the rubber hand illusion. *Elife* 5:e14972.

Fingelkurts, A. A., Fingelkurts, A. A., and Kallio-Tamminen, T. (2020). Selfhood triumvirate: From phenomenology to brain activity and back again. *Consciousn. Cogn.* 86:103031. doi: 10.1016/j.concog.2020.103031

Fingelkurts, A. A., Fingelkurts, A. A., and Kallio-Tamminen, T. (2016). Long-term meditation training induced changes in the operational synchrony of default mode network modules during a resting state. *Cogn. Proc.* 17, 27–37. doi: 10.1007/s10339-015-0743-4

Fossataro, C., Bruno, V., Giurgola, S., Bolognini, N., and Garbarini, F. (2018). Losing my hand. Body ownership attenuation after virtual lesion of the primary motor cortex. *Eur. J. Neurosci.* 48, 2272–2287. doi: 10.1111/ejn.14116

Frewen, P., Lundberg, E., Brimson-Théberge, M., and Théberge, J. (2013). Neuroimaging self-esteem: a fMRI study of individual differences in women. *Soc. Cogn. Affect. Neurosci.* 8, 546–555. doi: 10.1093/scan/nss032

Frewen, P., Schroeter, M. L., Riva, G., Cipresso, P., Fairfield, B., Padulo, C., et al. (2020). Neuroimaging the consciousness of self: Review, and conceptual methodological framework. *Neurosci. Biobehav. Rev.* 112, 164–212. doi: 10.1016/j.neubiorev.2020.01.023

Frewen, P., Thornley, E., Rabellino, D., and Lanius, R. (2017). Neuroimaging the traumatized self: fMRI reveals altered response in cortical midline structures and occipital cortex during visual and verbal self-and other-referential processing in women with PTSD. *Eur. J. Psychotraumat.* 8:1314164. doi: 10.1080/20008198.2017.1314164

Fricke, K., Seeber, A. A., Thirugnanasambandam, N., Paulus, W., Nitsche, M. A., and Rothwell, J. C. (2011). Time course of the induction of homeostatic plasticity generated by repeated transcranial direct current stimulation of the human motor cortex. *J. Neurophys.* 105, 1141–1149. doi: 10.1152/jn.00608.2009

Hallett, M. (2000). Transcranial magnetic stimulation and the human brain. *Nature* 406, 147–150.

Heinisch, C., Dinse, H. R., Tegenthoff, M., Juckel, G., and Brüne, M. (2011). An rTMS study into self-face recognition using video-morphing technique. *Soc. Cogn. Affect. Neurosci.* 6, 442–449. doi: 10.1093/scan/nsq062

Heinisch, C., Krüger, M. C., and Brüne, M. (2012). Repetitive transcranial magnetic stimulation over the temporoparietal junction influences distinction of self from famous but not unfamiliar others. *Behav. Neurosci.* 126:792. doi: 10.1037/a0030581

Higgins, J. P., Thomas, J., Chandler, J., Cumpston, M., Li, T., Page, M. J., et al. (eds) (2019). *Cochrane handbook for systematic reviews of interventions*. Hoboken, NJ: John Wiley & Sons.

Hornburger, H., Nguemeni, C., Odorfer, T., and Zeller, D. (2019). Modulation of the rubber hand illusion by transcranial direct current stimulation over the contralateral somatosensory cortex. *Neuropsychologia* 131, 353–359. doi: 10.1016/j.neuropsychologia.2019.05.008

Inukai, Y., Saito, K., Sasaki, R., Tsuiki, S., Miyaguchi, S., Kojima, S., et al. (2016). Comparison of three non-invasive transcranial electrical stimulation methods for increasing cortical excitability. *Front. Human Neurosci.* 10:668.

James, W. (1890). *The principles of psychology bd*. New York, NY: Henry Holt and Company.

Kammers, M. P., Verhagen, L., Dijkerman, H. C., Hogendoorn, H., De Vignemont, F., and Schutter, D. J. (2009). Is this hand for real? Attenuation of the rubber hand illusion by transcranial magnetic stimulation over the inferior parietal lobule. *J. Cogn. Neurosci.* 21, 1311–1320. doi: 10.1162/jocn.2009.21095

Karabanov, A. N., Ritterband−Rosenbaum, A., Christensen, M. S., Siebner, H. R., and Nielsen, J. B. (2017). Modulation of fronto−parietal connections during the rubber hand illusion. *Eur. J. Neurosci.* 45, 964–974. doi: 10.1111/ejn.13538

Katyal, S., Hajcak, G., Flora, T., Bartlett, A., and Goldin, P. (2020). Event-related potential and behavioural differences in affective self-referential processing in long-term meditators versus controls. *Cogn. Affect. Behav. Neurosci.* 2020, 1–14.

Kuo, H. I., Bikson, M., Datta, A., Minhas, P., Paulus, W., Kuo, M. F., et al. (2013). Comparing cortical plasticity induced by conventional and high-definition 4×

1 ring tDCS: a neurophysiological study. *Brain Stimulat.* 6, 644–648. doi: 10.1016/j.brs.2012.09.010

Kwan, V. S., Barrios, V., Ganis, G., Gorman, J., Lange, C., Kumar, M., et al. (2007). Assessing the neural correlates of self-enhancement bias: a transcranial magnetic stimulation study. *Exp. Brain Res.* 182, 379–385. doi: 10.1007/s00221-007-0992-2

Legrand, D., and Ruby, P. (2009). What is self-specific? Theoretical investigation and critical review of neuroimaging results. *Psycholog.Rev.* 116:252. doi: 10.1037/a0014172

LeMoult, J., Kircanski, K., Prasad, G., and Gotlib, I. H. (2017). Negative self-referential processing predicts the recurrence of major depressive episodes. *Clin. Psychol. Sci.* 5, 174–181. doi: 10.1177/2167702616654898

Li, G., Ji, G., Hu, Y., Xu, M., Jin, Q., Liu, L., et al. (2018). Bariatric surgery in obese patients reduced resting connectivity of brain regions involved with self−referential processing. *Human Brain Map.* 39, 4755–4765. doi: 10.1002/hbm.24320

Lin, Y., Callahan, C. P., and Moser, J. S. (2018). A mind full of self: Self-referential processing as a mechanism underlying the therapeutic effects of mindfulness training on internalizing disorders. *Neurosci. Biobehav. Rev.* 92, 172–186. doi: 10.1016/j.neubiorev.2018.06.007

Lira, M., Pantaleão, F. N., de Souza Ramos, C. G., and Boggio, P. S. (2018). Anodal transcranial direct current stimulation over the posterior parietal cortex reduces the onset time to the rubber hand illusion and increases the body ownership. *Exp. Brain Res.* 236, 2935–2943. doi: 10.1007/s00221-018-5353-9

Lou, H. C., Luber, B., Crupain, M., Keenan, J. P., Nowak, M., Kjaer, T. W., et al. (2004). Parietal cortex and representation of the mental Self. *Proc. Natl. Acad. Sci.U S A* 101, 6827L–6832.

Lou, H. C., Luber, B., Stanford, A., and Lisanby, S. H. (2010). Self-specific processing in the default network: A single-pulse TMS study. *Exp. Brain Res.* 207, 27–38. doi: 10.1007/s00221-010-2425-x

Luber, B., Lou, H. C., Keenan, J. P., and Lisanby, S. H. (2012). Self-enhancement processing in the default network: A single-pulse TMS study. *Exp. Brain Res.* 223, 177–187. doi: 10.1007/s00221-012-3249-7

Mainz, V., Britz, S., Drüke, B., and Gauggel, S. (2020). Transcranial Direct Current Stimulation of the Medial Prefrontal Cortex Has No Specific Effect on Self-referential Processes. *Front. Hum. Neurosci.* 14:56.

Miniussi, C., Harris, J. A., and Ruzzoli, M. (2013). Modelling non-invasive brain stimulation in cognitive neuroscience. *Neurosci. Biobehav. Rev.* 37, 1702–1712. doi: 10.1016/j.neubiorev.2013.06.014

Park, H. D., and Blanke, O. (2019). Coupling inner and outer body for self-consciousness. *Trends Cogn. Sci.* 23, 377–388. doi: 10.1016/j.tics.2019.02.002

Payne, S., and Tsakiris, M. (2017). Anodal transcranial direct current stimulation of right temporoparietal area inhibits self-recognition. *Cogn. Affect. Behav. Neurosci.* 17, 1–8. doi: 10.3758/s13415-016-0461-0

Peviani, V., Magnani, F. G., Ciricugno, A., Vecchi, T., and Bottini, G. (2018). Rubber hand illusion survives ventral premotor area inhibition: A rTMS study. *Neuropsychologia* 120, 18–24. doi: 10.1016/j.neuropsychologia.2018.09.017

Pollatos, O., Herbert, B. M., Mai, S., and Kammer, T. (2016). Changes in interoceptive processes following brain stimulation. *Philosop. Transac. R. Soc.B* 371:20160016. doi: 10.1098/rstb.2016.0016

Qin, P., and Northoff, G. (2011). How is our self related to midline regions and the default-mode network? *Neuroimage* 57, 1221–1233. doi: 10.1016/j.neuroimage.2011.05.028

Quesque, F., and Brass, M. (2019). The role of the temporoparietal junction in self-other distinction. *Brain Topogr.* 2019, 1–13. doi: 10.1097/wnr.0000000000000282

Sadleir, R. J., Vannorsdall, T. D., Schretlen, D. J., and Gordon, B. (2010). Transcranial direct current stimulation (tDCS) in a realistic head model. *Neuroimage* 51, 1310–1318. doi: 10.1016/j.neuroimage.2010.03.052

Sagliano, L., Magliacano, A., Parazzini, M., Fiocchi, S., Trojano, L., and Grossi, D. (2019). Modulating interoception by insula stimulation: A double-blinded tDCS study. *Neuroscience Letters* 696, 108–113. doi: 10.1016/j.neulet.2018.12.022

Schäfer, S., and Frings, C. (2019). Searching for the inner self: Evidence against a direct dependence of the self-prioritization effect on the ventro-medial prefrontal cortex. *Exp. Brain Res.* 237, 247–256. doi: 10.1007/s00221-018-5413-1

Schandry, R. (1981). Heart beat perception and emotional experience. *Psychophysiology* 18, 483–488.

Tsakiris, M. (2010). My body in the brain: a neurocognitive model of body-ownership. *Neuropsychologia* 48, 703–712. doi: 10.1016/j.neuropsychologia.2009.09.034

Tsakiris, M., Costantini, M., and Haggard, P. (2008). The role of the right temporo-parietal junction in maintaining a coherent sense of one's body. *Neuropsychologia* 46, 3014–3018. doi: 10.1016/j.neuropsychologia.2008.06.004

Uddin, L. Q., Molnar-Szakacs, I., Zaidel, E., and Iacoboni, M. (2006). rTMS to the right inferior parietal lobule disrupts self–other discrimination. *Soc. Cogn. Affect. Neurosci.* 1, 65–71. doi: 10.1093/scan/nsl003

Uddin, L. Q., Rayman, J., and Zaidel, E. (2005). Split-brain reveals separate but equal self-recognition in the two cerebral hemispheres. *Consciousness Cogn.* 14, 633–640. doi: 10.1016/j.concog.2005.01.008

van Buuren, M., Walsh, R. J., Sijtsma, H., Hollarek, M., Lee, N. C., Bos, P. A., et al. (2020). Neural correlates of self-and other-referential processing in young adolescents and the effects of testosterone and peer similarity. *Neuroimage* 219, 117060. doi: 10.1016/j.neuroimage.2020.117060

Wen, T., Mitchell, D. J., and Duncan, J. (2020). The functional convergence and heterogeneity of social, episodic, and self-referential thought in the default mode network. *Cereb. Cortex* 30, 5915–5929. doi: 10.1093/cercor/bhaa166

Wold, A., Limanowski, J., Walter, H., and Blankenburg, F. (2014). Proprioceptive drift in the rubber hand illusion is intensified following 1 Hz TMS of the left EBA. *Front. Hum. Neurosci.* 8:390.

Yoon, H. J., Seo, E. H., Kim, J. J., and Choo, I. H. (2019). Neural correlates of self-referential processing and their clinical implications in social anxiety disorder. *Clin. Psychopharm. Neurosci.* 17:12. doi: 10.9758/cpn.2019.17.1.12

Conflict of Interest: The authors declare that the research was conducted in the absence of any commercial or financial relationships that could be construed as a potential conflict of interest.

frontiers in Neuroscience

METHODS
published: 05 July 2021
doi: 10.3389/fnins.2021.687493

Functional Imaging to Guide Network-Based TMS Treatments: Toward a Tailored Medicine Approach in Alzheimer's Disease

Chiara Bagattini[1], Debora Brignani[1†], Sonia Bonnì[2], Giulia Quattrini[3,4], Roberto Gasparotti[5] and Michela Pievani[3]*

[1] Neurophysiology Lab, IRCCS Istituto Centro San Giovanni di Dio Fatebenefratelli, Brescia, Italy, [2] Non Invasive Brain Stimulation Unit/Department of Behavioral and Clinical Neurology, Santa Lucia Foundation IRCCS, Rome, Italy, [3] Laboratory Alzheimer's Neuroimaging and Epidemiology, IRCCS Istituto Centro San Giovanni di Dio Fatebenefratelli, Brescia, Italy, [4] Department of Molecular and Translational Medicine, University of Brescia, Brescia, Italy, [5] Neuroradiology Unit, ASST Spedali Civili Hospital, University of Brescia, Brescia, Italy

OPEN ACCESS

Edited by:
Olivier David, Institut National de la Santé et de la Recherche Médicale (INSERM), France

Reviewed by:
JeYoung Jung, University of Nottingham, United Kingdom
Farheen Syeda, Consultant, Baton Rouge, LA, United States

***Correspondence:**
Michela Pievani
mpievani@fatebenefratelli.eu

†Present address:
Debora Brignani, Department of Clinical and Experimental Sciences, University of Brescia, Brescia, Italy

Specialty section:
This article was submitted to Neural Technology, a section of the journal Frontiers in Neuroscience

Received: *29 March 2021*
Accepted: *09 June 2021*
Published: *05 July 2021*

Citation:
Bagattini C, Brignani D, Bonnì S, Quattrini G, Gasparotti R and Pievani M (2021) Functional Imaging to Guide Network-Based TMS Treatments: Toward a Tailored Medicine Approach in Alzheimer's Disease. Front. Neurosci. 15:687493. doi: 10.3389/fnins.2021.687493

A growing number of studies is using fMRI-based connectivity to guide transcranial magnetic stimulation (TMS) target identification in both normal and clinical populations. TMS has gained increasing attention as a potential therapeutic strategy also in Alzheimer's disease (AD), but an endorsed target localization strategy in this population is still lacking. In this proof of concept study, we prove the feasibility of a tailored TMS targeting approach for AD, which stems from a network-based perspective. Based on functional imaging, the procedure allows to extract individual optimal targets meanwhile accounting for functional variability. Single-subject resting-state fMRI was used to extract individual target coordinates of two networks primarily affected in AD, the default mode and the fronto-parietal network. The localization of these targets was compared to that of traditional group-level approaches and tested against varying degrees of TMS focality. The distance between individual fMRI-derived coordinates and traditionally defined targets was significant for a supposed TMS focality of 12 mm and in some cases up to 20 mm. Comparison with anatomical labels confirmed a lack of 1:1 correspondence between anatomical and functional targets. The proposed network-based fMRI-guided TMS approach, while accounting for inter-individual functional variability, allows to target core AD networks, and might thus represent a step toward tailored TMS interventions for AD.

Keywords: Alzheimer's disease, functional brain networks, resting-state fMRI, connectivity, tailored treatment, repetitive transcranial magnetic stimulation

INTRODUCTION

Through the repeated delivery of short-lived magnetic fields over the scalp, repetitive transcranial magnetic stimulation (rTMS) is able to induce long-lasting changes of cortical excitability, which resemble long-term potentiation or long-term depression-like mechanisms, depending on the stimulation parameters (Wassermann et al., 2008). Robust evidence proves that TMS acts beyond the site of stimulation, affecting the connectivity of the stimulated networks (Ruff et al., 2009; Siebner et al., 2009; Fox et al., 2012b), thus rising considerable interest for its therapeutic application

across a range of diseases with distributed network pathology (Fox et al., 2012a; Lefaucheur et al., 2014).

A growing number of studies have focused on brain connectivity as a promising approach to guide TMS treatment. Functional magnetic resonance imaging (fMRI)-based network connectivity has been already successfully used for the identification of TMS target in healthy young (Santarnecchi et al., 2018; Momi et al., 2020; Ozdemir et al., 2020) and elderly participants (Wang et al., 2014; Nilakantan et al., 2019), as well as in psychiatric patients (Hoffman et al., 2007; Fox et al., 2012a), but not in neurodegenerative disorders such as Alzheimer's Disease (AD).

While rTMS has gained increasing attention as a potential treatment for AD (Weiler et al., 2020), evidence regarding its clinical efficacy is feeble and key issues remain before its clinical application (Lefaucheur et al., 2020). The majority of previous rTMS studies individuated the target areas through coarse procedures, such as rule of thumb, EEG electrode system, group-averaged coordinates or anatomical landmarks (please refer to **Table 1** for an overview of methods adopted in previous studies).

These approaches, however, do not account for the functional organization of the brain and the synaptic dysfunction affecting specific networks in AD. In particular, AD is associated with the disruption of several large-scale networks, of which two play a central role in cognition, the Default Mode Network (DMN) and the Fronto-Parietal Network (FPN) (Agosta et al., 2012; Pievani et al., 2014). The DMN is medially anchored to the posterior cingulate cortex/precuneus and ventromedial prefrontal cortex, and to the bilateral parietal (inferior parietal lobule – IPL, which include the angular and inferior parietal gyri), temporal (lateral temporal cortex and hippocampi), and frontal cortex (dorsolateral prefrontal cortex – DLPFC, roughly corresponding to the superior frontal gyrus). The FPN includes the bilateral DLPFC (middle frontal gyrus) and parietal (superior parietal gyrus) cortex. Due to their crucial role in modulating cognition in AD, targeting these functional networks might represent a valid option for rTMS treatments in this population. The clinical promise of stimulating AD-core networks such as DMN is demonstrated by a recent study showing an improvement in memory by targeting the precuneus (Koch et al., 2018). Moreover, although some of the previous rTMS studies might have stimulated regions belonging to these networks (i.e., DLPFC node of the FPN, IPL node of the DMN; Lefaucheur et al., 2020), this remains speculative lacking a direct assessment with neuroimaging.

Given the potential value of tailored network-based rTMS intervention for neurocognitive and psychiatric diseases, here we demonstrate the feasibility of a TMS approach that uses resting-state fMRI to identify and target functionally, patho-physiologically and clinically relevant AD networks at the individual level. This strategy is compared to traditional approaches for target localization.

MATERIALS AND EQUIPMENT

Magnetic resonance imaging (MRI) scans were acquired on a 3T Siemens Skyra scanner equipped with a 64-channels head-neck coil at the Neuroradiology Unit, Spedali Civili Hospital (Brescia, Italy). Multiband accelerated resting-state fMRI (rs-fMRI) (TR = 1000 ms, TE = 27 ms, flip angle = 60°, voxel size = 2.1 mm isotropic, 70 slices, 600 volumes) and 3D T1-weighted (TR = 2300 ms, TE = 2 ms, flip angle = 9°, voxel size = 1 mm isotropic, 176 slices) scans were collected.

METHODS

We developed a pipeline to extract individual targets from rs-fMRI data for the stimulation of the DMN and FPN. We choose as targets the IPL node of the DMN and the DLPFC node of the FPN, since these targets are similar to those traditionally stimulated by previous rTMS studies in AD. The procedure, however, can be applied to other DMN and FPN regions as well (e.g., the lateral temporal node of the DMN, the DLPFC node of the DMN, the superior parietal gyrus of the FPN). Medial nodes such as the posterior cingulate cortex or the medial prefrontal cortex were not considered since these regions are difficult to reach with traditional coils. Moreover, we focused on the left hemisphere since a recent meta-analysis revealed that the effects of rTMS at the DLPFC are lateralized: high-frequency rTMS (i.e., the most adopted rTMS protocol) over the left hemisphere significantly improved memory functions (Chou et al., 2019). However, the procedure can be applied to extract contralateral targets as well. First, rs-fMRI data are pre-processed according to standard steps (removal of the first volumes for signal equilibrium, motion correction, susceptibility-induced distortions correction). Then, independent component analysis (ICA) is used to decompose the fMRI data into different spatial and temporal components. The spatial maps are transformed to standard MNI space to identify the networks of interest (in our case, the DMN and FPN) according to a template matching procedure. Alternatively, the components can be identified based on visual inspection. The ICA step is repeated multiple times to check for the reliability of the components and the most reliable components are selected. The resulting spatial maps are expressed as t-statistics or z-statistics, higher values indicating a higher degree of activation within the component or correlation with the time series. The spatial maps are decomposed into clusters; the largest clusters in the left IPL and left DLPFC areas are identified based on visual inspection; the cluster peaks (e.g., local maxima) are extracted as potential targets. The final individual TMS targets are selected according to the following criteria: (i) location specific to the network of interest, i.e., coordinates falling within the spatial maps of both DMN and FPN are excluded; (ii) being on a cortical gyrus and not on a sulcus (i.e., overlap with GM); (iii) representing the shortest perpendicular path between scalp and cortex. Finally, to stimulate the selected DMN and FPN coordinates, the TMS coil is positioned through a neuronavigation system. The entire procedure is summarized in **Figure 1**.

We tested this procedure in a sample of mild AD patients [$n = 13$; age: 73.54 years (min 56 – max 85); seven females; MMSE: 21.23 (min 17 – max 25)] (McKhann et al., 2011) recruited between June 2019 and April 2021 at the IRCCS Fatebenefratelli (Brescia, Italy) and at the IRCCS Santa Lucia (Rome, Italy) in

TABLE 1 | Summary of the target areas and localization methods adopted in previous rTMS interventions in AD patients.

Study	Target area(s)	Localization method
5-cm rule		
Ahmed et al., 2012	Left and right DLPFC	5 cm rostral to optimal site for motor threshold production in the first dorsal interosseous
Haffen et al., 2012	Left DLPFC	5 cm anterior and parasagittal from the hand area
Drumond Marra et al., 2015	Left DLPFC	5 cm in a parasagittal plane parallel to the point to maximum stimulation of the short abductor of the thumb
Electrode position(s) according to the International 10–20 EEG System		
Zhao et al., 2017	Left and right parietal and posterior-temporal areas	P3, P4, T5, T6
Alcalá-Lozano et al., 2018	Broca, Wernicke, right and left DLPFC, right and left pSAC	Left DLPFC: electrode not defined; other regions: localization method not defined
Turriziani et al., 2019	Right DLPFC	F4
Bagattini et al., 2020	Left DLPFC	F3
Group-average coordinates (mean Tailarach coordinates)		
Cotelli et al., 2010	Left DLPFC (BA 8/9)	$x = -35$, $y = 24$, $z = 48$
Cotelli et al., 2012	Left IPL	$x = -44$, $y = -51$, $z = 43$
Individual anatomical landmarks		
Bentwich et al., 2011	Broca, Wernicke, right and left DLPFC, right and left pSAC	Identified by neuroradiologist on individual MRI scans
Rabey et al., 2013	Broca, Wernicke, right and left DLPFC, right and left pSAC	Identified by neuroradiologist on individual MRI scans
Rabey and Dobronevsky, 2016	Broca, Wernicke, right and left DLPFC, right and left pSAC	Not better defined
Lee et al., 2016	Broca, Wernicke, right and left DLPFC, right and left pSAC	Identified by neuroradiologist on individual MRI scans
Nguyen et al., 2018	Broca, Wernicke, right and left prefrontal cortex, right and left parietal cortex	Identified by the Neuronix neuronavigation system based on the individual MRI.
Koch et al., 2018	Precuneus	Individual T1-weighted MRI volumes were used as anatomical reference
Sabbagh et al., 2020	Broca, Wernicke, right and left DLPFC, right and left parietal cortex	Brain regions were marked in individual MRI scan by projecting the relevant brain region onto the scalp

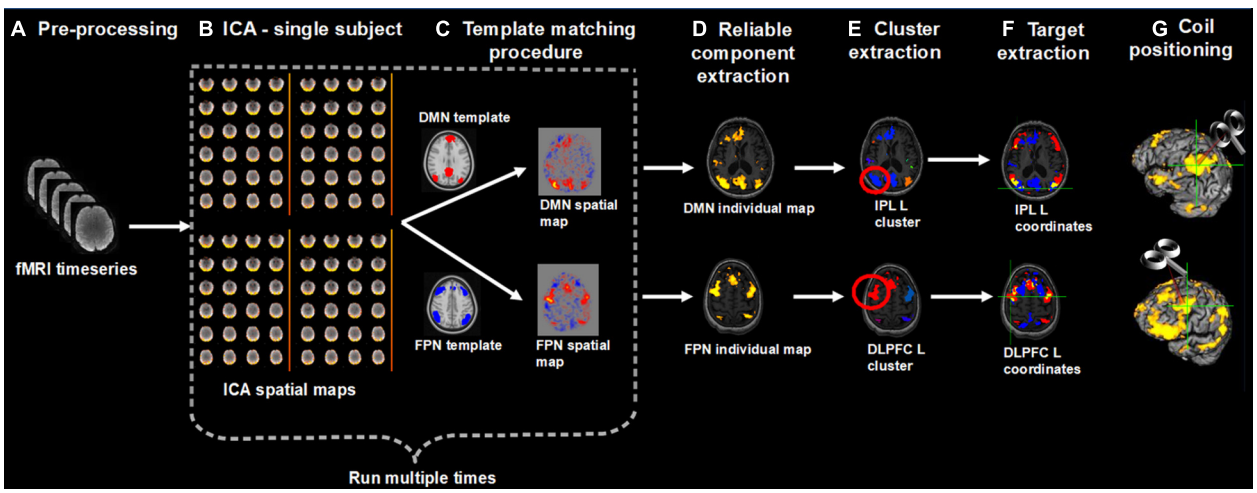

FIGURE 1 | Overview of the procedure for the identification and selection of individual DMN and FPN targets based on rs-fMRI; **(A)** Collected rs-fMRI data were pre-processed removing the first time-points, correcting motion, and susceptibility-induced distortions; **(B)** DMN and FPN were extracted from individual rs-fMRI scans using independent component analysis (ICA); **(C)** Networks of interest (in MNI space) were identified using a template matching procedure; **(B,C)** were repeated multiple times; **(D)** The most reliable components were identified and back-transformed to subjects' native T1 space; **(E)** Each network was decomposed into clusters and the largest cluster in the left IPL and left DLPFC was identified, for the DMN and FPN, respectively; **(F)** The peaks (local maxima) within these clusters were extracted and the final individual TMS targets were selected according to the following criteria: (i) location specific to the network of interest, i.e., coordinates falling within the spatial maps of both DMN and FPN (yellow areas) were excluded (blue = DMN, red = FPN); (ii) being on a cortical gyrus and not on a sulcus (i.e., overlap with GM); (iii) representing the shortest perpendicular path between scalp and cortex; **(G)** TMS coil was positioned through a neuronavigation system to target the selected DMN and FPN coordinates.

the context of an ongoing randomized controlled clinical trial (GR-2016-02364718; NCT04263194). The study was approved by the local ethics committee and participants signed a written informed consent.

rs-fMRI data pre-processing was carried out using the FMRIB's Software Library (FSL; Smith et al., 2004)[1]. After removal of the first ten time-points, motion correction was carried out with FLIRT (part of FSL) and correction of susceptibility-induced distortions with TOPUP (part of FSL) (Andersson et al., 2003). ICA was applied with Melodic (Beckmann and Smith, 2004)[2]. Melodic processing included high-pass temporal filtering (0.01 Hz), smoothing with a 4 mm FWHM filter, affine transformation of EPI images to native T1 images and non-linear warping of T1 images to standard MNI space. The number of components was automatically estimated by Melodic. The template matching procedure was applied using previously published templates (Shirer et al., 2012). For reliability assessment, Melodic was run 10 times and the spatial maps most frequently classified as "DMN" or "FPN" were retained. The selected DMN and FPN spatial maps were then back-transformed to subjects' native T1 space using Melodic transformations. FSL's *cluster* routine was used to decompose each network into clusters and to derive the peak (local maxima) within each cluster (left IPL and left DLPFC). The local maxima were overlaid onto the native T1 scan and the final targets were selected according to the above described criteria.

To check for the anatomical-functional correspondence of each target, the anatomical atlas label (AAL; Tzourio-Mazoyer et al., 2002) was used to label individual coordinates with the corresponding anatomical region.

The distance between individual rs-fMRI derived and traditional anatomical coordinates was computed as follows. Individual coordinates in native space were transformed to MNI space using the affine and non-linear warping estimated by Melodic. The Euclidean distance was used to compute the distance from group-level left IPL and DLPFC coordinates reported in previous TMS studies (Herwig et al., 2003; Cotelli et al., 2010, 2012; Fox et al., 2013). Coordinates in Talairach space were transformed to MNI space using a non-linear transformation (Lacadie et al., 2008). For studies using the Brett or Lancaster transformation to derive Talairach coordinates, we used the inverse Brett/Lancaster transformation to obtain the original MNI coordinates. One-sample Wilcoxon test was used to assess whether the distance between individual and traditional coordinates exceeded two threshold's levels, assuming a spatial extent of rTMS-induced activation of 12 mm (conservative threshold; Fox et al., 2013) and 20 mm (lenient threshold).

Finally, we compared the precision of our approach with traditional approaches testing (i) the sensitivity of group-level IPL and DLPFC coordinates to DMN and FPN spatial maps, respectively (i.e., how frequently group-level coordinates fell into the expected network), and (ii) the selectivity of this relationship (i.e., how frequently a coordinate falling into one network also fell into the other). Group-level coordinates were overlaid onto the individual spatial maps of the DMN and FPN before computing the above frequencies.

[1]http://www.fmrib.ox.ac.uk/fsl/

[2]https://fsl.fmrib.ox.ac.uk/fsl/fslwiki/MELODIC

Generalization to Healthy Elderly Population

In order to provide evidence on the generalization of the proposed individual network-based targeting approach to other populations, the same procedure applied in mild AD patients was tested in a sample of healthy elderly controls [n = 8; age: 66.38 years (min 60 – max 75); three females; MMSE: 29.75 (min 28 – max 30)] recruited at the IRCCS Fatebenefratelli (Brescia, Italy) between February 2021 and April 2021.

Validation With Seed-Connectivity Analysis

In order to assess the validity of the individual rs-fMRI coordinates obtained with our approach, seed connectivity analysis was computed. First, individual coordinates were used as seed for a whole-brain connectivity analysis. Thereafter, group-level coordinates were used as seeds. We then tested whether the seed-connectivity derived maps best matched to the individual DMN or FPN spatial map derived from ICA. For the seed-based correlation analysis, we created spherical ROIs (6 mm radius) centered on the target coordinates (in native T1 space for the TMS targets and in MNI space for the group-level coordinates) and transformed them to native EPI space. We then computed the correlation coefficients between the time-series within each seed and the time-series of all the other brain voxels. Finally, a template-matching procedure was used to test whether each seed-connectivity map best matched to the individual DMN or FPN spatial map ICA-derived.

RESULTS

Individual targets are shown relative to their network in **Figure 2A**, and their position is depicted in **Figure 2B** compared to the group-level coordinates (all coordinates are reported in MNI space). The median distance between individual IPL coordinates was 20.39 mm (interquartile range: 14.70–26.31 mm) and between individual DLPFC coordinates was 21.68 mm (interquartile range: 17.20–27.28 mm). When using the anatomical atlas label (AAL; Tzourio-Mazoyer et al., 2002) to localize our IPL coordinates, 5 out of 13 cases corresponded to or were close to the angular gyrus (AG), five to the middle occipital gyrus (MOG), two to the inferior parietal gyrus (IPL), and one was borderline between the latter two regions (**Table 2**). The median distance between individual fMRI-derived and group-level IPL coordinates was >20 mm for both the studies considered (Herwig et al., 2003; Cotelli et al., 2012). However, the distance between individual fMRI-derived and P3 coordinates (Herwig et al., 2003) significantly exceeded rTMS focality when considering the 12 mm threshold (p = 0.0002), but not the 20 mm threshold (p = 0.342; **Table 2**). When compared with the IPL coordinates used in Cotelli et al. (2012), the distance significantly exceeded both rTMS focalities (all p's < 0.05; **Table 2**).

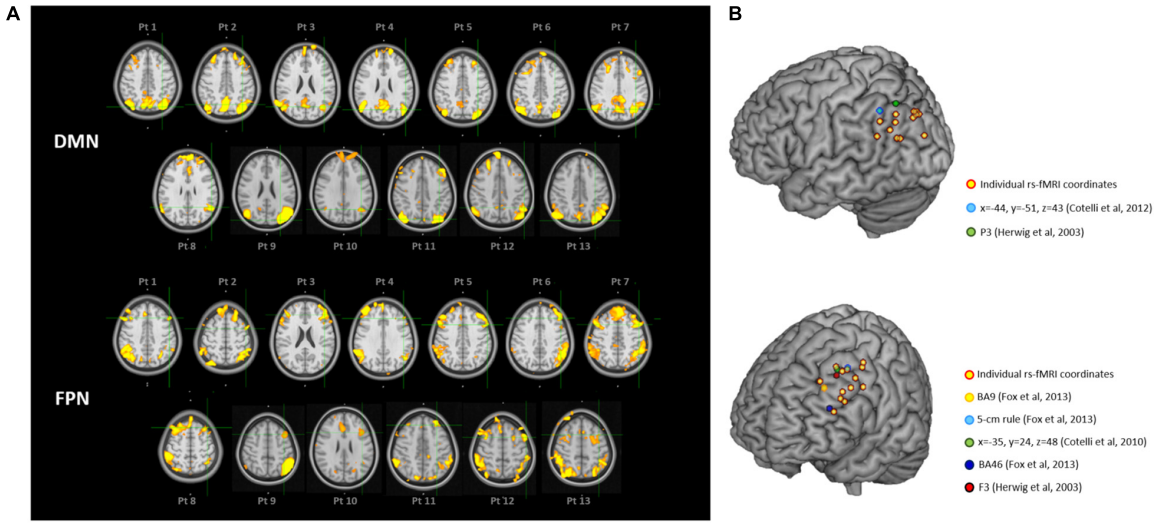

FIGURE 2 | (A) Location of the individual targets (overlaid onto the standard MNI template) for default mode network (DMN) stimulation **(top panel)** and frontoparietal network (FPN) stimulation **(bottom panel)** in thirteen AD patients. Images are shown in radiological convention (left denotes right). The individual targets (green cross) were extracted from each subject's 3T rs-fMRI data using ICA. The DMN targets correspond to the left IPL cluster, the FPN targets to the left DLPFC cluster. The individual DMN and FPN maps are shown in orange-yellow. The targets were defined in subjects' native T1 space and back-transformed to the standard MNI space for computation and visualization purposes; **(B)** 3D render showing the individual targets (red-yellow) overlaid onto the standard MNI template. For the DMN, green target corresponds to P3 (Herwig et al., 2003), and light-blue to IPL (Cotelli et al., 2012). For the FPN, yellow target corresponds to DLPFC BA9 (Fox et al., 2013), light-blue to DLPFC-5 cm rule (Fox et al., 2013), blue to DLPFC BA46 (Fox et al., 2013), red to F3 (Herwig et al., 2003), green to DLPFC BA8/9 (Cotelli et al., 2010). DMN, default mode network; FPN, fronto-parietal network; BA8/9, Broadmann areas 8 and 9; BA9, Broadmann area 9; BA46, Broadmann area 46; IPL, inferior parietal lobule; DLPFC, dorsolateral prefrontal cortex.

The sensitivity of group-level IPL coordinates to individual DMN spatial maps was 46% in the best case (Herwig et al., 2003) while selectivity was generally low (>67% of the coordinates falling into the DMN also fell within the FPN) (**Table 3**).

Dorsolateral prefrontal cortex coordinates were localized in the middle frontal gyrus (MFG) in 9 out of 13 cases (69.3% of cases), in the precentral gyrus (PCG) in one case, borderline between the two in two cases, and in the inferior frontal gyrus (IFG) in one case (**Table 2**). The distance between individual fMRI-derived and group-level DLPFC coordinates (Herwig et al., 2003; Cotelli et al., 2010; Fox et al., 2013) was significant for all group-level coordinates at the 12 mm threshold (all p's < 0.05), but not at the 20 mm threshold (all p's > 0.10), except for DLPFC BA46 (Fox et al., 2013) which significantly exceeded the threshold ($p = 0.024$; **Table 2**). Group-level DLPFC coordinates most sensitive to FPN spatial maps were F3 coordinates (62% of coordinates falling into the FPN), followed by 5 cm-rule (54%), and DLPFC BA8/9 (46%) coordinates. The selectivity of these coordinates, however, was relatively good only for the 5 cm rule (71% of the coordinates being specific for the FPN), and low for the remaining group level coordinates (50% for F3 and BA46 and 67% for BA8/9 and BA9 of cases also falling into the DMN) (**Table 3**).

Generalization to Healthy Elderly Population

Figure 3 depicts individual IPL and DLPFC targets relative to their network (**Figure 3A**), with their position compared to the coordinates reported in the literature (**Figure 3B**), in the sample of healthy elderly controls. Individual rs-fMRI coordinates and their comparison with group-level coordinates are shown in **Table 4**. The median distance between individual IPL coordinates was 21.35 mm (interquartile range: 13.24–30.30 mm) and between individual DLPFC coordinates was 15.75 mm (interquartile range: 10.84–21.32 mm). When using the anatomical atlas label (AAL; Tzourio-Mazoyer et al., 2002) to localize our IPL coordinates, four out of eight cases corresponded to the AG, two to the MTG, one to the IPL, and one was borderline between the MTG and the MOG (**Table 4**). The median distance between individual fMRI-derived and group-level IPL coordinates was >28 mm for both the studies considered (Herwig et al., 2003; Cotelli et al., 2012). Consistently with the results in AD patients, these distances significantly exceeded rTMS focality when considering both the conservative ($p = 0.012$ and $p = 0.008$, respectively) and the lenient threshold ($p = 0.054$ and $p = 0.027$, respectively; **Table 5**).

Dorsolateral prefrontal cortex coordinates were localized in the MFG in 87.5% of cases (seven out of eight cases) and in the PCG in one case (**Table 4**). The distance between individual fMRI derived and group-level coordinates (Herwig et al., 2003; Cotelli et al., 2010; Fox et al., 2013) was significant at the 12 mm threshold only for the BA9 ($p = 0.039$) and BA46 ($p = 0.004$) coordinates, the latter reaching significance also with the lenient threshold ($p = 0.004$; **Table 4**). No other significant differences emerged (all p's > 0.47).

TABLE 2 | Individual coordinates (reported in standard MNI space) of the two targets (the left IPL node of the DMN and the left DLPFC node of the FPN) obtained with the individual rs-fMRI guided approach in the sample of AD patients.

	DMN – left IPL				**FPN – left DLPFC**						
	Individual rs-fMRI coordinates	**AAL**	**Distance (mm) from P3**	**Distance (mm) from IPL**	**Individual rs-fMRI coordinates**	**AAL**	**Distance (mm) from BA9**	**Distance (mm) from BA46**	**Distance (mm) from 5 cm rule**	**Distance (mm) from F3**	**Distance (mm) from BA8/9**
Pt 1	−34 −80 44	IPL	16.16	27.93	−52 24 40	MFG	21.26	24.04	18.60	16.16	20.10
Pt 2	−38 −66 42	AG	9.00	14.00	−48 4 56	PCG	39.45	48.44	13.64	24.60	22.00
Pt 3	−44 −68 24	MOG	27.73	26.08	−46 38 22	MFG	20.59	4.69	38.13	30.15	35.44
Pt 4	−52 −72 26	AG	29.27	28.07	−48 32 32	MFG	15.62	12.08	27.17	20.12	25.38
Pt 5	−36 −82 42	MOG	18.47	29.39	−58 16 40	MFG/PCG	31.11	32.34	20.83	23.35	25.77
Pt 6	−34 −82 44	IPL/MOG	17.92	29.80	−50 32 38	MFG	15.36	16.91	23.79	17.12	22.18
Pt 7	−40 −66 36	AG	15.13	16.12	−50 16 46	MFG	26.76	33.20	10.86	15.13	16.37
Pt 8	−56 −54 28	AG	31.58	21.63	−40 28 56	MFG	19.29	33.85	13.64	8.77	8.25
Pt 9	−32 −88 24	MOG	35.34	42.24	−38 18 50	MFG	22.45	4.69	4.69	7.28	4.90
Pt 10	−42 −62 30	AG	21.75	18.00	−42 20 26	IFG	23.58	26.50	26.50	22,91	26.76
Pt 11	−38 −80 40	MOG	17.80	27.35	−30 36 44	MFG	7.48	25.02	25.02	14.18	17.20
Pt 12	−54 −56 40	IPL	21.84	11.83	−52 10 54	MFG/PCG	35.16	12.25	12.25	21.38	20.10
Pt 13	−34 −84 42	MOG	20.52	31.87	−38 12 50	MFG	27.93	4.69	4.69	13.15	10.39
Median (IQR)	**20.39 (14.70–26.31)**		**20.52 (17.80–27.73)**	**27.35 (18.00–29.39)**	**21.68 (17.20–27.28)**		**22.45 (19.29–27.93)**	**32.34 (21.12–34.50)**	**18.60 (12.25–25.02)**	**17.12 (14.18–22.91)**	**20.10 (16.37–25.38)**
p (12 mm threshold)	<0.0001*		0.0002*	0.0002*	<0.0001*		0.0006*	0.0006*	0.018*	0.005*	0.005*
p (20 mm threshold)	0.353		0.342	0.029*	0.018*		0.095	0.024*	0.758	0.863	0.472

*The corresponding anatomical region is provided based on the Anatomical atlas label (AAL), and the average distance between individual coordinates and group-level coordinates is provided. Results of one-sample Wilcoxon tests (p-values) assessing the null hypothesis that the distance between individual and group-level coordinates is below 12 mm and 20 mm are reported (*significant difference). DMN, default mode network; FPN, fronto-parietal network; BA8/9, Broadmann areas 8 and 9; BA9, Broadmann area 9; BA46, Broadmann area 46; IPL, inferior parietal lobule; DLPFC, dorsolateral prefrontal cortex; AG, angular gyrus; IFG, inferior frontal gyrus; MFG, middle frontal gyrus; MOG, middle occipital gyrus; PCG, precentral gyrus; IQR, interquartile range. Bold numbers depict median and IQR scores.*

TABLE 3 | Correspondence between group-level IPL and DLPFC coordinates and individual DMN and FPN maps.

Group-level coordinates	Sensitivity	Selectivity
DMN		
P3 (Herwig et al., 2003)	46%	33%
IPL (Cotelli et al., 2012)	31%	0%
FPN		
F3 (Herwig et al., 2003)	62%	50%
BA8/9 (Cotelli et al., 2010)	46%	33%
5-cm rule (Fox et al., 2013)	54%	71%
BA9 (Fox et al., 2013)	23%	33%
BA46 (Fox et al., 2013)	15%	50%

As a reference, individual fMRI-derived coordinates have a sensitivity and selectivity of 100%. DMN, default mode network; FPN, fronto-parietal network; BA8/9, Broadmann areas 8 and 9; BA9, Broadmann area 9; BA46, Broadmann area 46; IPL, inferior parietal lobule; DLPFC, dorsolateral prefrontal cortex.

Validation With Seed-Connectivity Analysis

Table 5 shows the correspondence between the individual ICA maps of the DMN and FPN and the seed connectivity maps obtained using individual rs-fMRI targets or the group-level coordinates as seeds. The template matching procedure revealed that the IPL individual targets matched the ICA-derived DMN individual map in all cases (100%), while the group-level targets matched the individual DMN maps only in 62% (Herwig et al., 2003) and 31% (Cotelli et al., 2012) of cases. For the DLPFC FPN target, the tailored fMRI-based targets showed a high correspondence with the ICA-derived FPN network (85% of cases), while correspondence was lower for the other group-level targets (matching in 69% of cases for the DLPFC BA9 target, 54% for DLPFC 5 cm-rule, 38% for the other DLPFC targets).

DISCUSSION

The combination of neuroimaging and neurostimulation techniques to design personalized protocols is an emerging research field, which may enhance the precision of rTMS (Cocchi and Zalesky, 2018). Here, we tested the feasibility of a tailored network-based rTMS protocol in a sample of AD patients, showing how to target AD relevant networks by extracting their hub coordinates from individual rs-fMRI.

The advantages of the proposed method over previous approaches become clear when the spatial extent of TMS-induced activation is considered. Although TMS focality is difficult to estimate because of technical and anatomical factors (Thielscher and Kammer, 2004), computational models (Fox et al., 2013)

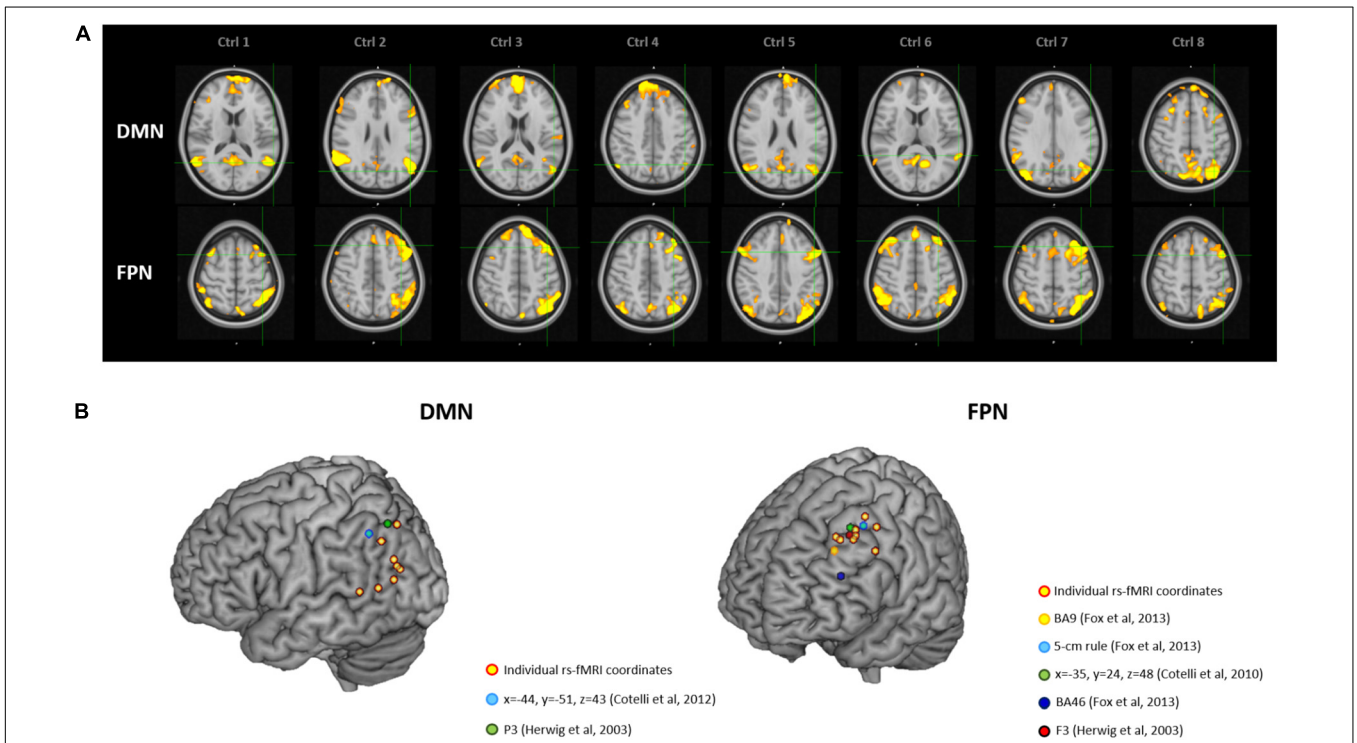

FIGURE 3 | (A) Location of the individual targets (overlaid onto the standard MNI template) for default mode network (DMN) stimulation **(top panel)** and frontoparietal network (FPN) stimulation **(bottom panel)** in eight healthy elderly controls. Images are shown in radiological convention (left denotes right). **(B)** 3D render showing the individual targets (red-yellow) overlaid onto the standard MNI template. For the DMN, green target corresponds to P3 (Herwig et al., 2003), and light-blue to IPL (Cotelli et al., 2012). For the FPN, yellow target corresponds to DLPFC BA9 (Fox et al., 2013), light-blue to DLPFC-5 cm rule (Fox et al., 2013), blue to DLPFC BA46 (Fox et al., 2013), red to F3 (Herwig et al., 2003), green to DLPFC BA8/9 (Cotelli et al., 2010). DMN, default mode network; FPN, fronto-parietal network; BA8/9, Broadmann areas 8 and 9; BA9, Broadmann area 9; BA46, Broadmann area 46; IPL, inferior parietal lobule; DLPFC, dorsolateral prefrontal cortex.

TABLE 4 | Individual coordinates (reported in standard MNI space) of the two targets (the left IPL node of the DMN and the left DLPFC node of the FPN) obtained with the individual rs-fMRI guided approach in the sample of healthy elderly controls.

	DMN – left IPL				**FPN – left DLPFC**						
	Individual rs-fMRI coordinates	**AAL**	**Distance (mm) from P3**	**Distance (mm) from IPL**	**Individual rs-fMRI coordinates**	**AAL**	**Distance (mm) from BA9**	**Distance (mm) from BA46**	**Distance (mm) from 5 cm rule**	**Distance (mm) from F3**	**Distance (mm) from BA8/9**
Ctrl 1	−60 −60 14	MTG	43.46	36.28	−40 12 58	MFG	31.87	44.11	6.78	16.52	12.33
Ctrl 2	−50 −72 26	AG	28.37	27.57	−42 26 46	MFG	14.70	25.88	12.57	4.58	9.38
Ctrl 3	−54 −72 26	AG	36.89	33.76	−42 24 48	MFG	17.20	28.67	9.90	4.12	7.48
Ctrl 4	−48 −62 42	AG	14.04	9.80	−36 32 46	MFG	8.49	24.21	18.71	7.55	11.66
Ctrl 5	−50 −74 24	MTG/MOG	30.61	30.33	−52 16 38	MFG	27.28	29.29	17.83	19.42	22.09
Ctrl 6	−62 −48 12	MTG	49.20	38.94	−34 34 48	MFG	9.17	26.04	20.64	9.85	12.81
Ctrl 7	−56 −70 32	AG	26.48	24.41	−42 24 52	MFG	19.39	31.97	9.06	5.74	6.32
Ctrl 8	−36 −72 50	IPL	6.40	20.10	−48 10 52	PCG	32.74	41.30	8.60	18.47	16.97
Median (IQR)	**21.35 (13.24–30.30)**		**29.49 (20.26–40.18)**	**28.95 (22.26–35.02)**	**15.75 (10.84–21.32)**		**18.30 (11.94–29.58)**	**28.98 (25.96–36.64)**	**11.23 (8.83–18.27)**	**8.70 (5.16–17.50)**	**12.00 (8.43–14.89)**
p (12 mm threshold)	<0.0001*		0.012*	0.008*	0.0098*		0.039*	0.004*	0.320	0.680	0.527
p (20 mm threshold)	0.172		0.054#	0.027*	0.997		0.473	0.004*	0.996	1.000	0.996

*The corresponding anatomical region is provided based on the Anatomical atlas label (AAL) and the average distance between individual coordinates and group-level coordinates is provided. Results of one-sample Wilcoxon tests (p-values) assessing the null hypothesis that the distance between individual and group-level coordinates is below 12 mm and 20 mm are reported (*significant difference; #trend toward significance). DMN, default mode network; FPN, fronto-parietal network; BA8/9, Broadmann areas 8 and 9; BA9, Broadmann area 9; BA46, Broadmann area 46; IPL, inferior parietal lobule; DLPFC, dorsolateral prefrontal cortex; AG, angular gyrus; IFG, inferior frontal gyrus; MFG, middle frontal gyrus; MTG, middle temporal gyrus; MOG, middle occipital gyrus; PCG, precentral gyrus; IQR, interquartile range. Bold numbers depict median and IQR scores.*

TABLE 5 | Correspondence between the individual ICA maps of the DMN and FPN and the seed connectivity maps obtained using (A) the individual TMS targets or (B) the group-level coordinates as seeds.

	DMN – left IPL			FPN – left DLPFC	
	Seed	**Match with individual DMN ICA**		**Seed**	**Match with individual FPN ICA**
A	Individual rs-fMRI coordinates	13/13 (100%)	A	Individual rs-fMRI coordinates	11/13 (85%)
B	IPL P3 (Herwig et al., 2003)	8/13 (62%)	B	5-cm rule (Fox et al., 2013)	7/13 (54%)
B	IPL (Cotelli et al., 2012)	4/13 (31%)	B	BA9 (Fox et al., 2013)	9/13 (69%)
			B	BA46 (Fox et al., 2013)	5/13 (38%)
			B	F3 (Herwig et al., 2003)	5/13 (38%)
			B	BA8/9 (Cotelli et al., 2010)	5/13 (38%)

Correspondence was assessed with a template matching procedure. DMN, default mode network; FPN, fronto-parietal network; BA8/9, Broadmann areas 8 and 9; BA9, Broadmann area 9; BA46, Broadmann area 46; IPL, inferior parietal lobule; DLPFC, dorsolateral prefrontal cortex.

indicate a physiological response to TMS within a spatial extent of 12 mm when considering the mostly used standard figure-of-eight coil. Our comparisons revealed a significant distance between functionally defined individual targets and anatomical group-level coordinates when assuming a stimulation field size <12 mm, thus favoring the spatial selectivity of our approach. This advantage is even more striking in the hypothesis that rTMS focality is <2 mm, as suggested by a recent study recording single-unit activity in the parietal cortex of rhesus monkeys (Romero et al., 2019). Even assuming a larger (e.g., 20 mm) focality for TMS, the proposed approach has important advantages. While at a 20 mm threshold the distance between individual and traditional coordinates might not exceed TMS focality, we observed a loss of precision in targeting. Indeed, the sensitivity of group-level coordinates was 54–62% at most, indicating that in 46–38% of cases other networks will be stimulated. Moreover, the selectivity of group-level coordinates was generally low, indicating that group-level coordinates would result in stimulation of both networks rather than in the selective targeting of the intended network. The best trade-off between sensitivity/selectivity was provided by the 5 cm rule for the DLPFC node (54–71%), however, these values are far less precise than our approach, which was designed to provide a sensitivity/selectivity of 100%.

The individual rs-fMRI targets of healthy elderly controls showed similar inter-subjects variability to that observed in AD patients for the IPL node of the DMN, whereas the tailored FPN targets showed lower variability in the group of healthy elderly controls. When considering the distance between functionally defined individual targets and group-level coordinates, results were similar in AD patients and healthy elderly controls for the DMN for both the conservative (i.e., 12 mm) and lenient (i.e., 20 mm) threshold. For the FPN targets, results were similar between groups only for the BA9 and BA46 areas, due to a lower variability in DLPFC coordinates between control subjects. These results suggest that the proposed approach may be advantageous in pathological aging, and even in healthy aging when targeting the DMN. The large variability observed between subjects' spatial maps and across individual targets is consistent with the knowledge that the brain's structure and function undergo substantial changes both in physiological aging and in AD, with a massive networks' reorganization (Dubovik et al., 2013; Edde et al., 2020; He et al., 2020; Pläschke et al., 2020). Our data suggest that this reorganization may be more pronounced in pathological than physiological aging, accounting for the remarkable importance of an individual targeting approach in this latter population.

Bearing this in mind, going beyond an anatomical approach might reveal crucial to increase rTMS clinical efficacy in patients. In our sample, the functional targets did not correspond to the expected anatomical region in 23–46% of cases, confirming a lack of function-anatomical correspondence that might explain the feeble evidence regarding clinical efficacy of rTMS in AD population. Consistently with this view, recent studies in depression showed that the efficacy of rTMS was higher when the target was selected on the basis of functional connectivity (Weigand et al., 2018; Cash et al., 2020).

The seed-connectivity analysis demonstrated the validity of our approach: seed-derived maps corresponded to the individual ICA maps obtained with our rs-fMRI tailored approach in 85–100% of cases. Moreover, this analysis confirmed the superiority of the proposed procedure compared to traditional group-level approaches, which showed a correspondence with individual maps in 70% of cases at best.

Notably, the proposed approach is not specific for a given TMS technique or protocol. Specifically, our strategy can be applied to both rTMS and theta burst stimulation techniques, and is not dependent on the type of stimulation protocol (i.e., inhibitory vs. excitatory). The choice of the type of stimulation to be delivered, while representing a key step in the design of TMS interventions, is outside the scope of this report. Here, we point out that TMS protocols for AD should take into account not only the localization of the target, but also the connectivity pattern (i.e., reduced vs. increased connectivity), the degree of pathology (i.e., affected vs. spared regions), and their interaction.

Furthermore, this approach was meant to be easily translated to other dementias and diseases affected by network dysfunction in order to design TMS disorder-specific protocols. Neurodegenerative and psychiatric diseases characterized by emotional and behavioral deficits such as the behavioral variant of frontotemporal dementia (Zhou et al., 2010) and borderline personality disorder (Quattrini et al., 2019) might benefit from stimulation of the DMN and salience network, while conditions characterized by language disturbances such as

primary progressive aphasia may be suited for stimulation of the language network (Ficek et al., 2019), whereas motor disorders such as Parkinson's disease may benefit from stimulation of the sensorimotor network (Göttlich et al., 2013).

Some possible limitations of the proposed approach should be mentioned. To be clinically usable, individualized coordinate extraction from rs-fMRI needs to be reliable. This requires (i) the definition of standard pre-processing procedure and (ii) that networks are reliable. For the first issue, while our procedure is relatively straightforward, it requires independent validation. Moreover, while we used ICA, seed-correlation analysis is a valid alternative that has already been applied in other studies (Nilakantan et al., 2019). Seed-based approaches typically use the hippocampus as seed region to derive the DMN parietal node, defined as the most functionally correlated region. While we used a different strategy (based on the local cluster maxima) that does not provide information on the strength of the correlation with the hippocampus or other DMN regions, our approach extracted the region most involved and active within the DMN component. Moreover, one advantage of ICA-based compared to seed-based approaches is that they enable to extract statistically independent sources, while the latter cannot distinguish whether a brain region is shared by multiple networks.

Furthermore, in our study we used relatively advanced fMRI sequences that may not be available at all centers (multiband, 600 volumes, 2 mm voxel resolution, TR = 1000 ms). Future studies might find appropriate to investigate whether this approach can be translated to other scanners and rs-fMRI protocols. For the second aspect, in our study we counterbalanced this issue by extracting the network 10-fold and ensuring that the same component was extracted reliably. Several automated tools are available to assess networks reliability (e.g., ICASSO; Himberg et al., 2004) and the use of these tools is recommended to ensure that the extracted networks are stable enough for rTMS targeting. Finally, while we might expect our approach to increase rTMS efficacy by increasing the precision of target localization, this was not formally tested and was not the objective of the present study. Forthcoming studies testing the differential impact of network-based versus traditional approaches on relevant clinical outcomes, such as memory performance, are needed to directly test this assumption.

In conclusion, based on a functional network perspective, we proposed a procedure for individual identification of TMS targets, paving the way for unprecedented personalized connectivity-based rTMS treatments for AD.

DATA AVAILABILITY STATEMENT

The datasets presented in this study can be found in online repositories. The names of the repository/repositories and accession number(s) can be found below: 10.17632/5zxyrvc5nz.2.

ETHICS STATEMENT

The studies involving human participants were reviewed and approved by the Local Ethics Committee of IRCCS Istituto Centro San Giovanni di Dio Fatebenefratelli, Brescia, Italy. The patients/participants provided their written informed consent to participate in this study.

AUTHOR CONTRIBUTIONS

CB, DB, SB, and MP designed the research. CB, DB, GQ, RG, and MP performed the research. GQ and MP analyzed the data. CB, DB, and MP drafted the article. SB, GQ, and RG revised the article critically. All authors contributed to the article and approved the submitted version.

FUNDING

This work was supported by a grant from the Italian Ministry of Health awarded to DB, SB, and MP (Bando Ricerca Finalizzata 2016 – grant number: GR-2016-02364718). The funder had no role in study design, data collection and analysis, decision to publish, or preparation of the manuscript.

REFERENCES

Agosta, F., Pievani, M., Geroldi, G., Copetti, M., Frisoni, G. B., and Filippi, M. (2012). Resting state FMRI in Alzheimer's disease: beyond the default mode network. *Neurobiol. Aging* 33, 1564–1578. doi: 10.1016/j.neurobiolaging.2011.06.007

Ahmed, M. A., Darwish, E. S., Khedr, E. M., El Serogy, Y. M., and Ali, A. M. (2012). Effects of low versus high frequencies of repetitive transcranial magnetic stimulation on cognitive function and cortical excitability in Alzheimer's Dementia. *J. Neurol.* 259, 83–92. doi: 10.1007/s00415-011-6128-4

Alcalá-Lozano, R., Morelos-Santana, E., Cortés-Sotres, J. F., Garza-Villarreal, E. A., Sosa-Ortiz, A. L., and González-Olvera, J. J. (2018). Similar clinical improvement and maintenance after RTMS at 5 Hz using a simple vs. Complex protocol in Alzheimer's Disease. *Brain Stimul.* 11, 625–627. . doi: 10.1016/j.brs.2017.12.011

Andersson, J. L., Skare, S., and Ashburner, J. (2003). How to correct susceptibility distortions in spin-echo echo-planar images: application to diffusion tensor imaging. *NeuroImage* 20, 870–888. doi: 10.1016/S1053-8119(03)00336-7

Bagattini, C., Zanni, M., Barocco, F., Caffarra, P., Brignani, D., Miniussi, C., et al. (2020). Enhancing cognitive training effects in Alzheimer's Disease: RTMS as an add-on treatment. *Brain Stimul.* 13, 1655–1664. doi: 10.1016/j.brs.2020.09.010

Beckmann, C. F., and Smith, S. M. (2004). Probabilistic independent component analysis for functional magnetic resonance imaging. *IEEE Trans. Med. Imaging* 23, 1169–1172.

Bentwich, J., Dobronevsky, E., Aichenbaum, S., Shorer, R., Peretz, R., Khaigrekht, M., et al. (2011). Beneficial effect of repetitive transcranial magnetic stimulation combined with cognitive training for the treatment of Alzheimer's Disease: a proof of concept study. *J. Neural Transm.* 118, 463–471. doi: 10.1007/s00702-010-0578-1

Cash, R. F. H., Cocchi, L., Lv, J., Fitzgerald, P. B., and Zalesky, A. (2020). Functional magnetic resonance imaging-guided personalization of transcranial magnetic

stimulation treatment for depression. *JAMA Psychiatry* 78, 337–339. doi: 10.1001/jamapsychiatry.2020.3794

Chou, Y. H., Ton That, V., and Sundman, M. (2019). A systematic review and meta-analysis of rtms effects on cognitive enhancement in mild cognitive impairment and Alzheimer's Disease. *Neurobiol. Aging* 86, 1–10. . doi: 10.1016/j.neurobiolaging.2019.08.020

Cocchi, L., and Zalesky, A. (2018). Personalized transcranial magnetic stimulation in psychiatry. *Biol. Psychiatry Cogn. Neurosci. Neuroimaging* 3, 731–741. doi: 10.1016/j.bpsc.2018.01.008

Cotelli, M., Calabria, M., Manenti, R., Rosini, S., Maioli, C., Zanetti, O., et al. (2012). Brain stimulation improves associative memory in an individual with amnestic mild cognitive impairment. *Neurocase* 18, 217–223. doi: 10.1080/13554794.2011.588176

Cotelli, M., Calabria, M., Manenti, R., Rosini, S., Zanetti, O., Cappa, S. F., et al. (2010). Improved language performance in alzheimer disease following brain stimulation. *J. Neurol. Neurosurg. Psychiatry* 82, 794–797. doi: 10.1136/jnnp.2009.197848

Drumond Marra, H. L., Myczkowski, M. L., Maia Memória, C., Arnaut, D., Leite Ribeiro, P., Sardinha, C. G., et al. (2015). Transcranial magnetic stimulation to address mild cognitive impairment in the elderly: a randomized controlled study. *Behav. Neurol.* 2015:287843. doi: 10.1155/2015/287843

Dubovik, S., Bouzerda-Wahlen, A., Nahum, L., Gold, G., Schnider, A., and Guggisberg, A. G. (2013). Adaptive reorganization of cortical networks in Alzheimer's Disease. *Clin. Neurophysiol.* 124, 35–43. doi: 10.1016/j.clinph.2012.05.028

Edde, M., Leroux, G., Altena, E., and Chanraud, S. (2020). Functional brain connectivity changes across the human life span: from fetal development to old age. *J. Neurosci. Res.* 99, 236–262. doi: 10.1002/jnr.24669

Ficek, B. N., Wang, Z., Zhao, Y., Webster, K. T., Desmond, J. E., Hillis, A. E., et al. (2019). The Effect of TDCS on Functional Connectivity in Primary Progressive Aphasia. *NeuroImage Clini.* 22:101734. doi: 10.1016/j.nicl.2019.101734

Fox, M. D., Buckner, R. L., White, M. P., Greicius, M. P., and Pascual-Leone, A. (2012a). Efficacy of transcranial magnetic stimulation targets for depression is related to intrinsic functional connectivity with the subgenual cingulate. *Biol. Psychiatry* 72, 595–603. doi: 10.1016/j.biopsych.2012.04.028

Fox, M. D., Halko, M. A., Eldaief, M. C., and Pascual-Leone, A. (2012b). Measuring and manipulating brain connectivity with resting state functional connectivity magnetic resonance imaging (FcMRI) and transcranial magnetic stimulation (TMS). *NeuroImage* 62, 2232–2243. doi: 10.1016/j.neuroimage.2012.03.035

Fox, M. D., Liu, H., and Pascual-Leone, A. (2013). Identification of reproducible individualized targets for treatment of depression with tms based on intrinsic connectivity. *NeuroImage* 66, 151–160. doi: 10.1016/j.neuroimage.2012.10.082

Göttlich, M., Münte, T. F., Heldmann, M., Kasten, M., Hagenah, J., and Krämer, U. M. (2013). Altered resting state brain networks in parkinson's disease. *PLoS One* 8:e77336. doi: 10.1371/journal.pone.0077336

Haffen, E., Chopard, G., Pretalli, J. B., Magnin, E., Nicolier, M., and Monnin, J. (2012). A case report of daily left prefrontal repetitive transcranial magnetic stimulation (RTMS) as an adjunctive treatment for Alzheimer Disease. *Brain Stimul.* 5, 264–266. doi: 10.1016/j.brs.2011.03.003

He, L., Wang, X., Zhuang, K., and Qiu, J. (2020). Decreased dynamic segregation but increased dynamic integration of the resting-state functional networks during normal aging. *Neuroscience* 437, 54–63. doi: 10.1016/j.neuroscience.2020.04.030

Herwig, U., Satrapi, P., and Schönfeldt-Lecuona, C. (2003). Using the international 10-20 EEG system for positioning of transcranial magnetic stimulation. *Brain Topogr.* 16, 95–99. ., doi: 10.1023/b:brat.0000006333.93597.9d

Himberg, J., Hyvarinen, A., and Esposito, F. (2004). Validating the independent components of neuroimaging time series via clustering and visualization. *NeuroImage* 22, 1214–1222. doi: 10.1016/j.neuroimage.2004.03.027

Hoffman, R. E., Hampson, M., Wu, K., Anderson, A. W., Gore, J. C., Buchanan, R. J., et al. (2007). Probing the pathophysiology of auditory/verbal hallucinations by combining functional magnetic resonance imaging and transcranial magnetic stimulation. *Cereb. Cortex* 17, 2733–2743. doi: 10.1093/cercor/bhl183

Koch, G., Bonnì, S., Pellicciari, M. C., Casula, E. P., Mancini, M., Esposito, R. V., et al. (2018). Transcranial magnetic stimulation of the precuneus enhances memory and neural activity in prodromal Alzheimer's Disease. *NeuroImage* 169, 302–311. doi: 10.1016/j.neuroimage.2017.12.048

Lacadie, C. M., Fulbright, R. K., Rajeevan, N., Constable, R. T., and Papademetris, X. (2008). More accurate talairach coordinates for neuroimaging using nonlinear registration. *Neuroimage* 42, 717–725. doi: 10.1016/j.neuroimage.2008.04.240

Lee, J., Choi, B. H., Oh, E., Sohn, E. H., and Lee, A. Y. (2016). Treatment of Alzheimer's Disease with repetitive transcranial magnetic stimulation combined with cognitive training: a prospective, randomized, double-blind, placebo-controlled study. *J. Clin. Neurol.* 12, 57–64. doi: 10.3988/jcn.2016.12.1.57

Lefaucheur, J. P., Aleman, A., Baeken, C., Benninger, D. H., Brunelin, J., Di Lazzaro, V., et al. (2020). Evidence-based guidelines on the therapeutic use of repetitive transcranial magnetic stimulation (RTMS). *Clin. Neurophysiol.* 131, 474–528. doi: 10.1016/j.clinph.2019.11.002

Lefaucheur, J. P., André-Obadia, N., Antal, A., Ayache, S. S., Baeken, C., Benninger, D. H., et al. (2014). Evidence-based guidelines on the therapeutic use of repetitive transcranial magnetic stimulation (RTMS). *Clin. Neurophysiol.* 125, 1–57.

McKhann, G. M., Knopman, D. S., Chertkow, H., Hyman, B. T., Jack, C. R., Kawas, C. H., et al. (2011). The diagnosis of dementia due to Alzheimer's disease: recommendations from the National Institute on Aging-Alzheimer's association workgroups on diagnostic guidelines for Alzheimer's disease. *Alzheimers Dement.* 7, 263–269.

Momi, D., Neri, F., Coiro, G., Smeralda, C., Veniero, D., Sprugnoli, S., et al. (2020). Cognitive enhancement via network-targeted cortico-cortical associative brain stimulation. *Cereb. Cortex* 30, 1516–1527. ., doi: 10.1093/cercor/bhz182

Nguyen, J. P., Suarez, A., Le Saout, E., Meignier, M., Nizard, J., and Lefaucheur, J. P. (2018). Combining cognitive training and multi-site RTMS to improve cognitive functions in Alzheimer's disease. *Brain Stimul.* 11, 651–652. . doi: 10.1016/j.brs.2018.02.013

Nilakantan, A. S., Mesulam, M. M., Weintraub, S., Karp, E. L., Vanhaerents, S., and Voss, J. L. (2019). Network-targeted stimulation engages neurobehavioral hallmarks of age-related memory decline. *Neurology* 92, E2349–E2354. doi: 10.1212/WNL.0000000000007502

Ozdemir, R. A., Tadayon, E., Boucher, P., Momi, D., Karakhanyan, K. A., and Fox, M. D. (2020). Individualized perturbation of the human connectome reveals reproducible biomarkers of network dynamics relevant to cognition. *Proc. Natl. Acad. Sci. U.S.A.* 117, 8115–8125. doi: 10.1073/pnas.1911240117

Pievani, M., Filippini, N., van den Heuvel, M. P., Cappa, S. F., and Frisoni, G. B. (2014). Brain connectivity in neurodegenerative diseases—from phenotype to proteinopathy. *Nat. Rev. Neurol.* 10, 620–633. doi: 10.1038/nrneurol.2014.178

Pläschke, R. N., Patil, K. R., Cieslik, E. C., Alessandra, C., Nostro, D., Varikuti, D. P., et al. (2020). Age differences in predicting working memory performance from network-based functional connectivity. *Cortex* 132, 441–459. . doi: 10.1016/j.cortex.2020.08.012

Quattrini, G., Pini, L., Pievani, M., Magni, L. R., Lanfredi, M., Ferrari, C., et al. (2019). Abnormalities in functional connectivity in borderline personality disorder: correlations with metacognition and emotion dysregulation. *Psychiatry Res. Neuroimaging* 283, 118–124. ., doi: 10.1016/j.pscychresns.2018.12.010

Rabey, J. M., Dobronevsky, E., Aichenbaum, S., Gonen, O., Marton, R. G., and Khaigrekht, M. (2013). Repetitive transcranial magnetic stimulation combined with cognitive training is a safe and effective modality for the treatment of Alzheimer's disease: a randomized, double-blind study. *J. Neural Transm.* 120, 813–819. doi: 10.1007/s00702-012-0902-z

Rabey, J. M., and Dobronevsky, E. (2016). Repetitive transcranial magnetic stimulation (RTMS) combined with cognitive training is a safe and effective modality for the treatment of Alzheimer's disease: clinical experience. *J. Neural Transm.* 123, 1449–1455. , doi: 10.1007/s00702-016-1606-6

Romero, M. C., Davare, M., Armendariz, M., and Janssen, P. (2019). Neural effects of transcranial magnetic stimulation at the single-cell level. *Nat. Commun.* 10, 1–11.

Ruff, C. C., Driver, J., and Bestmann, S. (2009). Combining TMS and FMRI: from 'virtual Lesions' to functional-network accounts of cognition. *Cortex* 45, 1043–1049. doi: 10.1016/j.cortex.2008.10.012

Sabbagh, M., Sadowsky, C., Tousi, B., Agronin, M. E., Alva, G., Armon, C., et al. (2020). effects of a combined transcranial magnetic stimulation (TMS) and cognitive training intervention in patients with Alzheimer's disease. *Alzheimers Dement.* 16, 641–650. doi: 10.1016/j.jalz.2019.08.197

Santarnecchi, E., Momi, D., Sprugnoli, G., Neri, F., Pascual-Leone, A., Rossi, A., et al. (2018). Modulation of network-to-network connectivity via spike-timing-dependent noninvasive brain stimulation. *Hu. Brain Mapp.* 39, 4870–4883. doi: 10.1002/hbm.24329

Shirer, W. R., Ryali, S., Rykhlevskaia, E., Menon, V., and Greicius, M. D. (2012). Decoding subject-driven cognitive states with whole-brain connectivity patterns. *Cereb. Cortex* 22, 158–165. doi: 10.1093/cercor/bhr099

Siebner, H. R., Bergmann, T. O., Bestmann, S., Massimini, M., Johansen-Berg, H., Mochizuki, H., et al. (2009). Consensus paper: combining transcranial stimulation with neuroimaging. *Brain Stimul.* 2, 58–80.

Smith, S. M., Jenkinson, M., Woolrich, M. W., Beckmann, C. F., Behrens, T. E., Johansen-Berg, H., et al. (2004). Advances in functional and structural MR image analysis and implementation as FSL. *NeuroImage* 23(Suppl. 1), 208–219.

Thielscher, A., and Kammer, T. (2004). Electric field properties of two commercial figure-8 coils in TMS: calculation of focality and efficiency. *Clin. Neurophysiol.* 115, 1697–1708. doi: 10.1016/j.clinph.2004.02.019

Turriziani, P., Smirni, D., Mangano, D. R., Zappalà, G., Giustiniani, A., Cipolotti, L., et al. (2019). Low-frequency repetitive transcranial magnetic stimulation of the right dorsolateral prefrontal cortex enhances recognition memory in Alzheimer's disease. *J. Alzheimers Dis.* 72, 1–10.

Tzourio-Mazoyer, N., Landeau, B., Papathanassiou, D., Crivello, F., Etard, O., Delcroix, N., et al. (2002). Automated anatomical labeling of activations in SPM using a macroscopic anatomical parcellation of the MNI MRI single-subject brain. *NeuroImage* 15, 273–289. doi: 10.1006/nimg.2001.0978

Wang, J. X., Rogers, L. M., Gross, E. Z., Ryals, A. J., Dokucu, M. E., Brandstatt, K. L., et al. (2014). Targeted enhancement of cortical-hippocampal brain networks and associative memory.". *Science* 345, 1054–1057. doi: 10.1126/science.1252900

Wassermann, E. M., Epstein, C. M., Ziemann, U., Walsh, V., Paus, T., and Lisanby, S. H. (eds) (2008). *The Oxford Handbook of Transcranial Stimulation*. First. New York: Oxford University Press, Inc.

Weigand, A., Horn, A., Caballero, R., Cooke, D., Stern, A. P., Taylor, S. F., et al. (2018). Prospective validation that subgenual connectivity predicts antidepressant efficacy of transcranial magnetic stimulation sites. *Biolo. Psychiatry* 84, 28–37. doi: 10.1016/j.biopsych.2017.10.028

Weiler, M., Stieger, K. C., Long, J. M., and Rapp, P. R. (2020). Transcranial magnetic stimulation in alzheimer's disease: are we ready? *eNeuro* 7, ENEURO.235–ENEURO.219. doi: 10.1523/ENEURO.0235-19.2019

Zhao, J., Li, Z., Cong, Y., Zhang, J., Tan, M., and Zhang, H. (2017). Repetitive transcranial magnetic stimulation improves cognitive function of Alzheimer's disease patients. *Oncotarget* 8, 33864–33871.

Zhou, J., Greicius, M. D., Gennatas, E. D., Growdon, M. E., Jang, J. Y., and Rabinovici, G. D. (2010). divergent network connectivity changes in behavioural variant frontotemporal dementia and Alzheimer's disease. *Brain* 133, 1352–1367. doi: 10.1093/brain/awq075

Conflict of Interest: The authors declare that the research was conducted in the absence of any commercial or financial relationships that could be construed as a potential conflict of interest.

frontiers in Neuroscience

ORIGINAL RESEARCH
published: 27 September 2021
doi: 10.3389/fnins.2021.705483

Recharging Difficulty With Pulse Generator After Deep Brain Stimulation: A Case Series of Five Patients

Hongyang Li[1,2†], Daoqing Su[3†], Yijie Lai[1,2], Xinmeng Xu[1,2], Chencheng Zhang[1,2], Bomin Sun[1,2], Dianyou Li[1,2*] and Yixin Pan[1,2*]*

[1] Department of Neurosurgery, Ruijin Hospital, Shanghai Jiao Tong University School of Medicine, Shanghai, China, [2] Center for Functional Neurosurgery, Ruijin Hospital, Shanghai Jiao Tong University School of Medicine, Shanghai, China, [3] Department of Neurosurgery, Liaocheng People's Hospital, Liaocheng Clinical School of Shandong First Medical University, Liaocheng, China

OPEN ACCESS

Edited by:
Giovanni Mirabella,
University of Brescia, Italy

Reviewed by:
Tipu Z. Aziz,
John Radcliffe Hospital,
United Kingdom
Olivier David,
Institut National de la Santé et de la Recherche Médicale (INSERM),
France

***Correspondence:**
Bomin Sun
sbm11224@rjh.com.cn
Dianyou Li
ldy11483@rjh.com.cn
Yixin Pan
pyx11725@rjh.com.cn

[†] These authors have contributed equally to this work

Specialty section:
This article was submitted to Neural Technology, a section of the journal Frontiers in Neuroscience

Received: 05 May 2021
Accepted: 31 May 2021
Published: 27 September 2021

Citation:
Li H, Su D, Lai Y, Xu X, Zhang C, Sun B, Li D and Pan Y (2021) Recharging Difficulty With Pulse Generator After Deep Brain Stimulation: A Case Series of Five Patients. Front. Neurosci. 15:705483. doi: 10.3389/fnins.2021.705483

Background: Deep brain stimulation (DBS) is a well-established treatment for a variety of movement disorders. Rechargeable cell technology was introduced to pulse generator more than 10 years ago and brought great benefits to patients. However, with the widespread use of rechargeable implanted pulse generators (r-IPGs), a new hardware complication, when charging the r-IPG has been difficult, was encountered.

Objective: The aims of this study were to report five cases confronted with r-IPG charging difficulty postoperatively and to explore the predisposing factors and treatment strategies for this rare complication.

Methods: We retrospectively reviewed our DBS patient database for those who were implanted with r-IPGs. From 2012, we identified a total of 1,226 patients, with five of them experiencing charging difficulties after surgery. Detailed patient profiles and clinical procedures were scrutinized and reviewed.

Results: All the charging problems were resolved by reoperation. Cases 1 and 2 required their r-IPGs to be anchored to the muscle and fascia. Cases 3 and 4 had their r-IPGs inserted in the wrong orientation at the initial surgery, which was resolved by turning around the r-IPGs at the revision surgery. Case 5, in which we propose that the thick subcutaneous fat layer blocked the connection between the r-IPG and the recharger, required a second operation to reposition the r-IPG in a shallow layer underneath the skin. For all cases, the charging problems were resolved without reoccurrences to date.

Conclusion: Our case series indicates a novel hardware complication of DBS surgery, which had been rarely reported before. In this preliminary study, we describe several underlying causes of this complication and treatment methods.

Keywords: hardware complication, deep brain stimulation, implanted pulse generator, rechargeable battery, Parkinson's disease

INTRODUCTION

Deep brain stimulation (DBS) has been shown to be a safe and effective treatment for a variety of movement disorders such as Parkinson's disease (Zhang et al., 2020b) and dystonia (Krauss et al., 2021) and neurobehavioral disorders like Tourette syndrome (Xu et al., 2020). The introduction of rechargeable implanted pulse generators (r-IPGs) in the 2000s has brought great benefits to DBS patients (Zhang et al., 2020a), including prolonging the life of the pulse generators and reducing the time of IPG replacement surgeries (Qiu et al., 2021), thereby alleviating the suffering of DBS patients and lowering the associated risks of potential infections (Thrane et al., 2014). Furthermore, a reduced long-term cost is achievable when investing in a r-IPG (Rizzi et al., 2015).

However, in clinical practice, a novel hardware-related complication wherein charging the r-IPGs had been difficult has been indicated. In this article, we describe five patients who presented with r-IPG charging difficulties postoperatively and anticipate discovering the underlying causes of and treatment methods for this complication.

MATERIALS AND METHODS

We retrospectively reviewed our DBS patient database at the Department of Functional Neurosurgery, Ruijin Hospital, between January 2012 and January 2021, which included 1,226 patients who were implanted with r-IPGs. Among the 1,226 patients, charging problems emerged in five of them and further revision surgeries were noted. Detailed medical records were collected and scrutinized. This study was approved by the Ethics Committee of the Ruijin Hospital, Shanghai Jiao Tong University School of Medicine. Written informed consent for the study was exempted by the Ethical Committee due to its retrospective nature and anonymous data presentation.

RESULTS

Clinical Characteristics

The clinical characteristics of the five cases included in our case series are summarized in **Table 1**. Three patients were diagnosed with Parkinson's disease (PD) and the other two with Tourette syndrome. The rechargeable implanted pulse generator (IPG) models in three patients were Activa RC (model 37612), manufactured by Medtronic (Minneapolis, MN, United States), and G102R, manufactured by PINS (Beijing, China), for the other two. The average time for the onset of complications was 13.8 (2–35) months following implantation.

Case 1 was a 32-year-old female with a long history of severe, medication-refractory Tourette syndrome. Eye blinking and vocal tics were predominant features and cannot be well controlled by optimal medication therapy. During a battery of preoperative neuropsychiatric tests, she reported a history of obsessive–compulsive disorder and anxiety. Bilateral globus pallidus internus (GPi) DBS surgery was recommended to her and implantation of the Activa RC in the right sub-clavicular pocket was performed. Good symptom control was achieved over a 1-year follow-up period. However, 18 months after DBS surgery, she reported experiencing difficulties in charging her r-IPG. When she attempted to use the charger located superficially on the r-IPG, one or two markers lit up on the charger's screen, implying that perfect coupling between the charger and the r-IPG was not remotely achieved. A plain X-ray (**Figure 1A**) examination revealed that the r-IPG was upside down inside the chest pocket. During the 18 months postoperative, she had lost more than 15 kg of weight and admitted intentional manipulation of her r-IPG. Manual manipulation by doctors failed to flip the r-IPG. She was then provided with revision surgery. During the operation, an excessively large pocket for the r-IPG was noted, and the r-IPG was found upside down inside the chest pocket. We anchored the r-IPG to the pectoralis fascia with 2–0 silk sutures and reduced the pocket size by stitching its inferior, medial, and lateral aspects. The postoperative period was uneventful. No charging difficulties occurred since then.

Case 2 was a 71-year-old woman who had a history of PD of more than 11 years. At the first visit, her symptoms were a prominent right-sided resting tremor and a gait disorder, wherein she presented with split steps and suffered great postural instability. Bilateral DBS surgery targeting the GPi was performed and the Activa RC was implanted in the right sub-clavicular pocket. No surgery-related complication was encountered. During the following 12 months of follow-up, she had good tremor control and was satisfied with the overall clinical outcome. However, at the 13-month post-operation, she complained of difficulties in charging her r-IPG. The issue of charging difficulty was similar to case 1, wherein one or two markers lit up on the charger's screen. A plain chest X-ray examination (**Figure 1B**) revealed an upside-down r-IPG, without evidence of twisting or breakage of the extension wire. Manual manipulation failed to flip the r-IPG. Surgery was recommended to detect any causes of this problem. Intraoperatively, we found that the anchoring wire had fallen and the r-IPG was upside down. We reimplanted the r-IPG and used two anchoring wires to attach it to the pectoralis fascia. She experienced a complication-free recovery.

Case 3 was a 66-year-old woman with a 15-year history of a right-side prominent PD. The preoperative levodopa equivalent daily dose (LEDD) was 600 mg/day, and she complained of peak dose dyskinesia and motor fluctuations. DBS surgery was performed and bilateral electrodes were implanted in the GPi and the G102R model in the sub-clavicular pocket. A test stimulation revealed satisfying outcome, and 3 days later, the dual-channel r-IPG was implanted in the right subcutaneous pocket. Impedance was within the normal range and she was discharged subsequently. However, 2 weeks after surgery, she complained of having difficulties charging her r-IPG. Initially, it was presumed that she did not spot the charger at the right place when charging her IPG, so a detailed explanation of the IPG charging procedure was given to her. However, 1 month later, she visited the clinic again and complained that the charging problem did not improve at all. A plain X-ray examination (**Figure 2A**) of the patient's chest, neck, and head revealed that the r-IPG

TABLE 1 | Clinical characteristics of the recharging difficulty presented by patients in this article, along with those presented in the literature for comparison.

Author and publication year	Indication	Sex/age (years)	DBS equipments	Etiology	Occurrence after initial surgery	Diagnosis	Treatment
Chelvarajah et al. (2012)	Hemidystonia	F, 19	Medtronic	Migration of the adaptor to lie superficially on the r-IPG	8 months	Palpation, X-ray	Manual manipulation, restoring the adaptor beneath the IPG, reducing the pocket size
	Generalized dystonia	F, 16	Medtronic		4 months	Palpation, X-ray	Manual manipulation
Case 1	Tourette syndrome	F, 32	Medtronic	Weight loss, intentional manipulation of the IPG	18 months	X-ray findings, patient history	Anchoring the IPG to the pectoralis fascia, reducing the pocket size
Case 2	Parkinson's disease	F, 71	Medtronic	Improper fixation of the IPG	12 months	X-ray findings, patient history	Anchoring the IPG to the pectoralis fascia, reducing the pocket size
Case 3	Parkinson's disease	F, 66	PINS	Wrong orientation of IPG insertion	2 months	X-ray findings, patient history	Reinsertion of the IPG at the correct orientation
Case 4	Parkinson's disease	F, 62	PINS	Wrong orientation of IPG insertion	3 days	X-ray findings, patient history	Reinsertion of the IPG at the correct orientation
Case 5	Tourette syndrome	M, 23	Medtronic	Excessively thick subcutaneous fat layer	35 months	Intraoperative findings, patient history	Creating a new subcutaneous pocket at a shallower layer

DBS, deep brain stimulation; r-IPG, rechargeable implanted pulse generator.

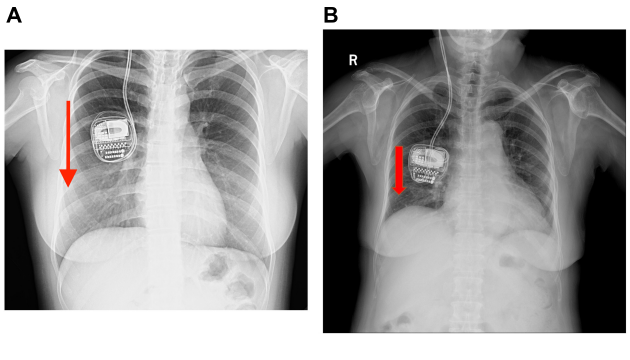

FIGURE 1 | (A,B) Plain chest X-rays of cases 1 and 2 showing the upside-down implanted pulse generators (IPGs) but with the extension wires still intact and no evidence of twisting observed. The red arrow means that the r-IPG was upside down.

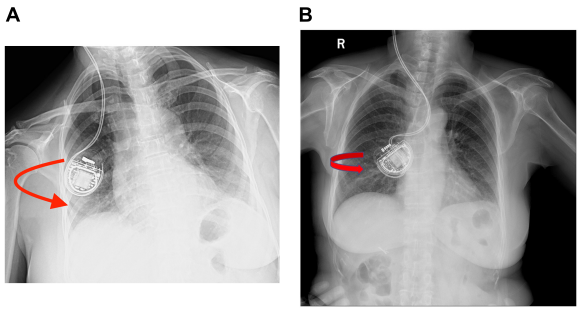

FIGURE 2 | (A,B) Plain chest X-rays showing that the rechargeable implanted pulse generators (r-IPGs) were inside out. No fracturing or twisting of the leads was observed. The red arrow means that the r-IPG was inside out.

was flipped around. Doctors tried to manipulate the IPG to its correct orientation, but failed because of less mobility. A revision surgery was provided. Intraoperatively, the r-IPG was found to be inside out, but the anchoring wires were in good condition. It is presumed that the r-IPG was implanted in the wrong orientation during the initial surgery. The r-IPG was reinserted and anchored with 2–0 wires. Subsequent follow-ups were free of any complications.

Case 4 was a 69-year-old woman with PD who had similar clinical characteristics and outcome to case 3. Bilateral DBS surgery targeting GPi was performed and the G102R was implanted in the right sub-clavicular pocket. She had an uneventful recovery and was discharged soon after surgery. However, 3 days after surgery, she complained of charging difficulties. A plain chest X-ray examination (**Figure 2B**) revealed the same result as that of case 2: the r-IPG was found inside out. Manual manipulation failed to flip the IPG. Revision surgery was performed and the r-IPG was reinserted in the correct orientation; no charging difficulties were encountered by the patient since then.

Case 5, the last patient, was a 25-year-old man with a long-standing history of Tourette syndrome. He was presented to our hospital in 2016. Before DBS surgery, he was 178 cm tall, weighed 87 kg, and had a body mass index of 27.4 kg/m^2. Bilateral globus pallidus internus was selected as the DBS target. Subsequently, the Activa RC was implanted in the right sub-clavicular pocket. In 2019, 3 years after the implantation of the DBS system, he began to experience difficulties with charging his r-IPG. He complained of extensive charging time and reduced charging efficiency. When he visited our hospital the second time, he weighed 106 kg and had a body mass index of 33.4 kg/m^2 (a body mass index $>$30 kg/m^2 is classified as obese). The r-IPG was in good position on chest X-ray examination (**Figure 3**). Revision surgery was then undertaken. During the operation, we found that the thickness of his thoracic subcutaneous fat layer was approximately 2 cm (**Figure 4**). We removed the r-IPG from the subcutaneous pocket and achieved good connection between the charger and the

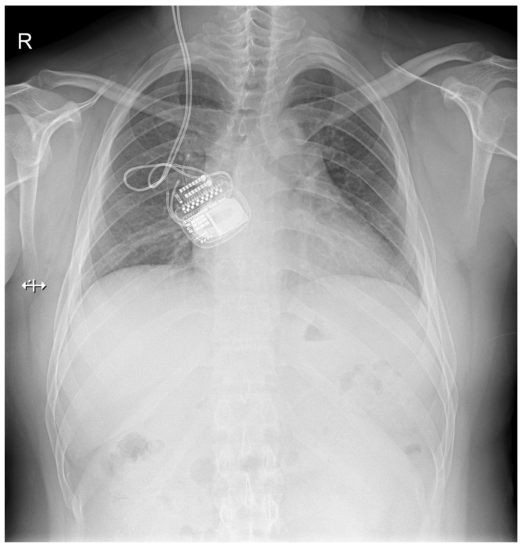

FIGURE 3 | Plain chest X-ray showing the normal view of the implanted pulse generator (IPG) and the extension wire. No fracturing or twisting of the wire was observed and the IPG was in the correct orientation.

FIGURE 4 | Intraoperative figure showing the thickness of the subcutaneous fat layer which is equal to the length of the index finger to the proximal interphalangeal joint.

r-IPG. A shallower pocket, 1 cm underneath the skin surface, was created to accommodate the r-IPG. The charging capability of the r-IPG was restored without complications to date.

DISCUSSION

The hardware complication was first described by Chelvarajah et al. (2012) when patients struggled to charge their r-IPGs after switching from non-rechargeable IPGs to r-IPGs. This problem arose when the adapter, which is used to connect the preexisting extension cable to the r-IPG, migrated to the surface of the r-IPG and acted as a physical barrier between the r-IPG and the charger, thus obstructing the wireless connection between them. This problem can be resolved either by manual manipulation, wherein the adapter is moved to the deep surface of the IPG, or surgical treatment when manual manipulation fails. **Table 1** summarizes two such cases presented in the literature along with the cases presented in this article.

From January 2012 to January 2021, we performed DBS surgeries on 1,226 patients, and charging difficulty occurred in five of them, which means that this complication did occur in 0.4% of patients with r-IPGs. The five cases presented with common characteristic features: reduced charging efficiency, prolonged charging time, and normal impedance under interrogation. Only one or two markers lit up on the charger's screen, indicating that a connection was not achieved. The complications in four out of five patients were evident under radiographs, presenting with an r-IPG with an incorrect orientation. Manual manipulation failed in the four patients whose r-IPGs were in the wrong orientation under X-ray examination.

To the best of our knowledge, this is the second report of the charging difficulties of r-IPG post-operation, but the first involving various causes such as obesity, weight loss, and wrong orientation of the r-IPG at insertion. Due to excessive weight loss postoperatively, the subcutaneous fat layer became thin and the pocket size enlarged, allowing overt mobility of the r-IPG, which has led to flipping inside the sub-clavicular pocket. Moreover, we presume that neuropsychological factors may also play a crucial role in the induction of this complication. Patient 1 admitted having manipulated her r-IPG multiple times because of feelings of itchiness and failed to move it back to the original position. Previous studies have also revealed that compulsive manipulation of the r-IPG caused rotation of the stimulator and hardware failure, which is called twiddler syndrome (Machado et al., 2005; Pourfar et al., 2015). For case 2, we propose that the r-IPG was improperly anchored during the initial surgery and the anchoring wire loosened after surgery, resulting in a r-IPG that flipped over unintentionally. An interesting observation was the phenomenon of the r-IPG inserted at the wrong orientation during the initial surgery, with the side engraved with the model number facing inward rather than outward. Charging difficulties were experienced when charging the r-IPG was not successful after the initial surgery. For case 5, we suppose that the sub-clavicular adipose layer has increased the physical distance between the r-IPG and the remote charger, thus making it difficult to charge the r-IPG. According to previous publications, obesity could also be a risk factor for twiddler syndrome (Boyle et al., 1998; Burdick et al., 2010; Gelabert-Gonzalez et al., 2010).

All of the patients who experienced charging difficulties were treated with a second surgery wherein the r-IPG was

reinserted with stronger fixing measures. To minimize the risk of such IPG-related complications, we propose strategies that use double-anchoring wires to attach the r-IPG to the pectoralis fascia. Attaching the r-IPG to the clavicle and the fat layer should be avoided. A previous study has suggested that single anchoring to attach the IPG may be a predisposing factor for excessive IPG mobility, which could be a risk factor for twiddler syndrome, and proposed that the r-IPG be anchored with double-fixing wires (Sobstyl et al., 2017). Moreover, a detailed explanation should be given to the patients and their caregivers that manual manipulation of the IPG should be strictly prohibited. We anticipate further advancements in r-IPG technology, and subsequently, the day when charging the r-IPG is possible regardless of its orientation.

CONCLUSION

The introduction of the new r-IPGs has resulted in a novel hardware complication, wherein charging the r-IPG has been difficult. We discussed five patients who presented with this complication, identified the underlying causes of this phenomenon, and described prevention strategies to reduce instances of this complication.

DATA AVAILABILITY STATEMENT

The original contributions presented in the study are included in the article/supplementary material, further inquiries can be directed to the corresponding authors.

ETHICS STATEMENT

The studies involving human participants were reviewed and approved by the Ruijin Hospital. Written informed consent was obtained from all participants for their participation in this study.

AUTHOR CONTRIBUTIONS

HL, DL, BS, and YP performed the surgery. HL, DS, XX, YL, and CZ wrote the manuscript. All authors contributed to the article and approved the submitted version.

FUNDING

YL was supported by the Shanghai Sailing Program (Grant No. 21YF1426700).

REFERENCES

Boyle, N. G., Anselme, F., Monahan, K. M., Beswick, P., Schuger, C. D., Zebede, J., et al. (1998). Twiddler's syndrome variants in ICD patients. *Pacing Clin. Electro.* 21, 2685–2687. doi: 10.1111/j.1540-8159.1998.tb00049.x

Burdick, A. P., Okun, M. S., Haq, I. U., Ward, H. E., Bova, F., Jacobson, C. E., et al. (2010). Prevalence of Twiddler's syndrome as a cause of deep brain stimulation hardware failure. *Stereotact. Funct. Neurosurg.* 88, 353–359. doi: 10.1159/000319039

Chelvarajah, R., Lumsden, D., Kaminska, M., Samuel, M., Hulse, N., Selway, R. P., et al. (2012). Shielded battery syndrome: a new hardware complication of deep brain stimulation. *Stereotact. Funct. Neurosurg.* 90, 113–117. doi: 10.1159/000336342

Gelabert-Gonzalez, M., Relova-Quinteiro, J.-L., and Castro-García, A. (2010). "Twiddler syndrome" in two patients with deep brain stimulation. *Acta Neurochir.* 152, 489–491. doi: 10.1007/s00701-009-0366-6

Krauss, J. K., Lipsman, N., Aziz, T., Boutet, A., Brown, P., Chang, J. W., et al. (2021). Technology of deep brain stimulation: current status and future directions. *Nat. Rev. Neurol.* 17, 75–87. doi: 10.1038/s41582-020-00426-z

Machado, A. G., Hiremath, G. K., Salazar, F., and Rezai, A. R. (2005). Fracture of subthalamic nucleus deep brain stimulation hardware as a result of compulsive manipulation: case report. *Neurosurgery* 57:E1318. doi: 10.1227/01.NEU.0000187566.01731.51

Pourfar, M. H., Budman, C. L., and Mogilner, A. Y. A. (2015). Case of deep brain stimulation for tourette's complicated by twiddler's syndrome. *Mov. Disord. Clin. Pract.* 2, 192–193. doi: 10.1002/mdc3.12132

Qiu, X., Wang, Y., Lin, Z., Wu, Y., Xu, W., Wu, Y., et al. (2021). Fixed-life or rechargeable batteries for deep brain stimulation: preference and satisfaction among patients with hyperkinetic movement disorders. *Front. Neurol.* 12:662383. doi: 10.3389/fneur.2021.662383

Rizzi, M., Messina, G., Penner, F., D'Ammando, A., Muratorio, F., and Franzini, A. (2015). Internal pulse generators in deep brain stimulation: rechargeable or not? *World Neurosurg.* 84, 1020–1029. doi: 10.1016/j.wneu.2015.05.028

Sobstyl, M. R., Ząbek, M., Brzuszkiewicz-Kuźmicka, G., and Pasterski, T. (2017). Dual anchor internal pulse generator technique may lower risk of twiddler's syndrome: a case series and literature review: twiddler's syndrome in parkinson's disease patients. *Neuromodulation* 20, 606–612. doi: 10.1111/ner.12581

Thrane, J. F., Sunde, N. A., Bergholt, B., and Rosendal, F. (2014). Increasing infection rate in multiple implanted pulse generator changes in movement disorder patients treated with deep brain stimulation. *Stereotact. Funct. Neurosurg.* 92, 360–364. doi: 10.1159/000365576

Xu, W., Zhang, C., Deeb, W., Patel, B., Wu, Y., Voon, V., et al. (2020). Deep brain stimulation for Tourette's syndrome. *Transl. Neurodegener.* 9:4. doi: 10.1186/s40035-020-0183-7

Zhang, C., Ramirez-Zamora, A., Meng, F., Lin, Z., Lai, Y., Li, D., et al. (2020a). An International Survey of deep brain stimulation utilization in asia and oceania: the DBS think tank east. *Front. Hum. Neurosci.* 14:162. doi: 10.3389/fnhum.2020.00162

Zhang, C., Wang, L., Hu, W., Wang, T., Zhao, Y., Pan, Y., et al. (2020b). Combined unilateral subthalamic nucleus and contralateral globus pallidus interna deep brain stimulation for treatment of parkinson disease: a pilot study of symptom-tailored stimulation. *Neurosurgery* 2020:nyaa201. doi: 10.1093/neuros/nyaa201

Conflict of Interest: The authors declare that the research was conducted in the absence of any commercial or financial relationships that could be construed as a potential conflict of interest.

Publisher's Note: All claims expressed in this article are solely those of the authors and do not necessarily represent those of their affiliated organizations, or those of the publisher, the editors and the reviewers. Any product that may be evaluated in this article, or claim that may be made by its manufacturer, is not guaranteed or endorsed by the publisher.

frontiers in Neuroscience

ORIGINAL RESEARCH
published: 26 November 2021
doi: 10.3389/fnins.2021.773792

Effect of Pulse Duration and Direction on Plasticity Induced by 5 Hz Repetitive Transcranial Magnetic Stimulation in Correlation With Neuronal Depolarization

Islam Halawa[1,2], Katharina Reichert[1], Aman S. Aberra[3], Martin Sommer[1,4,5], Angel V. Peterchev[3,6,7,8] and Walter Paulus[1,9]**

[1] Department of Clinical Neurophysiology, University Medical Center Göttingen, Göttingen, Germany, [2] Medical Research Division, National Research Center, Cairo, Egypt, [3] Department of Biomedical Engineering, Duke University, Durham, NC, United States, [4] Department of Neurology, University Medical Center Göttingen, Göttingen, Germany, [5] Department of Geriatrics, University Medical Center Göttingen, Göttingen, Germany, [6] Department of Psychiatry and Behavioral Sciences, Duke University, Durham, NC, United States, [7] Department of Electrical and Computer Engineering, Duke University, Durham, NC, United States, [8] Department of Neurosurgery, Duke University, Durham, NC, United States, [9] Department of Neurology, Ludwig-Maximilians University of Munich, Munich, Germany

OPEN ACCESS

Edited by:
Simone Rossi,
University of Siena, Italy

Reviewed by:
Domenica Veniero,
University of Nottingham,
United Kingdom
Antonio Suppa,
Sapienza University of Rome, Italy

***Correspondence:**
Islam Halawa
islam.halawa@med.uni-goettingen.de
Walter Paulus
walter.paulus@med.uni-muenchen.de

Specialty section:
This article was submitted to Neural Technology, a section of the journal Frontiers in Neuroscience

Received: 10 September 2021
Accepted: 28 October 2021
Published: 26 November 2021

Citation:
Halawa I, Reichert K, Aberra AS, Sommer M, Peterchev AV and Paulus W (2021) Effect of Pulse Duration and Direction on Plasticity Induced by 5 Hz Repetitive Transcranial Magnetic Stimulation in Correlation With Neuronal Depolarization. Front. Neurosci. 15:773792. doi: 10.3389/fnins.2021.773792

Introduction: High frequency repetitive transcranial magnetic stimulation applied to the motor cortex causes an increase in the amplitude of motor evoked potentials (MEPs) that persists after stimulation. Here, we focus on the aftereffects generated by high frequency controllable pulse TMS (cTMS) with different directions, intensities, and pulse durations.

Objectives: To investigate the influence of pulse duration, direction, and amplitude in correlation to induced depolarization on the excitatory plastic aftereffects of 5 Hz repetitive transcranial magnetic stimulation (rTMS) using bidirectional cTMS pulses.

Methods: We stimulated the hand motor cortex with 5 Hz rTMS applying 1,200 bidirectional pulses with the main component durations of 80, 100, and 120 μs using a controllable pulse stimulator TMS (cTMS). Fourteen healthy subjects were investigated in nine sessions with 80% resting motor threshold (RMT) for posterior-anterior (PA) and 80 and 90% RMT anterior-posterior (AP) induced current direction. We used a model approximating neuronal membranes as a linear first order low-pass filter to estimate the strength–duration time constant and to simulate the membrane polarization produced by each waveform.

Results: PA and AP 5 Hz rTMS at 80% RMT produced no significant excitation. An exploratory analysis indicated that 90% RMT AP stimulation with 100 and 120 μs pulses but not 80 μs pulses led to significant excitation. We found a positive correlation between the plastic outcome of each session and the simulated peak neural membrane depolarization for time constants >100 μs. This correlation was strongest for neural elements that are depolarized by the main phase of the AP pulse, suggesting the effects were dependent on pulse direction.

Conclusions: Among the tested conditions, only 5 Hz rTMS with higher intensity and wider pulses appeared to produce excitatory aftereffects. This correlated with the greater depolarization of neural elements with time constants slower than the directly activated neural elements responsible for producing the motor output (e.g., somatic or dendritic membrane).

Significance: Higher intensities and wider pulses seem to be more efficient in inducing excitation. If confirmed, this observation could lead to better results in future clinical studies performed with wider pulses.

Keywords: rTMS (repetitive transcranial magnetic stimulation), pulse duration and energy, direction of stimulation, rTMS intensity, MEPs

INTRODUCTION

The therapeutic use of repetitive transcranial magnetic stimulation (rTMS) has been shown to have level A efficacy in the treatment of depression and chronic pain (Lefaucheur et al., 2020). The main mechanism of its action is thought to be induction of synaptic plasticity producing either long term potentiation (LTP) or long term depression (LTD) (Huerta and Volpe, 2009; Vlachos et al., 2017). This is supported by the fact that responses to rTMS exhibit some properties of Hebbian synaptic plasticity (Hebb, 1949) depending on the different stimulation parameters, such as stimulation frequency and intensity (Bliss and Cooke, 2011; Pell et al., 2011).

The effects of key rTMS parameters, i.e., stimulation frequency, intensity, and number of pulses and sessions, on plastic aftereffects have been closely investigated (Rossini et al., 2015). However, there are few studies on the impact of pulse duration on rTMS outcome due to the scarcity of devices with adjustable pulse durations (Peterchev et al., 2011).

The controllable pulse parameter TMS device (cTMS3, Rogue Research Inc., Montreal, QC, Canada) allows varying the duration of its near-rectangular pulses using two capacitors and four transistors that alternate the current between the capacitors (Peterchev et al., 2014). The ratio of capacitor voltages is defined as the *M*-ratio, which determines the relative amplitudes of the different phases of the pulse waveform. Using $M = 0.2$ (lower values more unidirectional), the pulse duration of a single TMS pulse was recently found to bias the balance of excitation and inhibition (Hannah et al., 2020). We have already shown that with inhibitory 1 Hz rTMS ($M = 0.2$) only the widest pulse duration (120 μs) switched the 1 Hz inhibitory aftereffects to a significant increase in excitability, while 40 and 80 μs pulses produced the expected inhibition (Halawa et al., 2019).

In an early LTP experiment using high frequency stimulation of rat cortices and treating pulse duration as a surrogate for intensity, stimulation with wider pulses led to significant neuronal potentiation (McNaughton et al., 1978). The authors argued that increasing intensity and pulse durations stimulated more afferent inputs, which, in turn, enhanced their cooperativity and induced greater potentiation of synaptic transmission.

Here, we used cTMS to test the effect of increasing pulse durations on the aftereffects of 5 Hz rTMS, a protocol known to induce excitatory aftereffects (Ziemann et al., 2008; Rossi et al., 2009; Rothkegel et al., 2010). To interpret the effects of coil orientation, pulse duration, and pulse intensity on the neuromodulatory effects, we also simulated the relative membrane polarization induced by each pulse using a first-order linear model.

MATERIALS AND METHODS

Participants

As in our prior study, which showed a significant effect of pulse duration on neuromodulation with 1 Hz rTMS (Halawa et al., 2019), we recruited 15 subjects for this study. Of these, 14 subjects (4 men and 10 women with a mean age of 23.5 ± 2.6 SD years) completed the study. This sample would allow us to detect an effect size of $f = 0.29$ for alpha power of 0.05, beta power of 0.90, and the study design involving 9 within-subject measurements (estimated with G*Power). All participants were right-handed (Oldfield, 1971), free from any neurological or psychiatric disorders, taking no centrally acting medications, and had no contraindications to TMS (Rossi et al., 2009). A resting motor threshold (RMT) of more than 70% MSO for a Magstim 200^2 device was an exclusion criterion to prevent overheating the cTMS coil delivering the rTMS, particularly for the wider pulses.

We obtained written informed consent from each subject before participation. The local ethics committee of the University Medical Center Göttingen approved the study protocol, which conformed to the Declaration of Helsinki.

Recordings

Motor evoked potentials (MEPs) were recorded from the first dorsal interosseous (FDI) muscle of the right hand with surface Ag–AgCl electrodes in a belly-tendon montage. The electromyography signals were amplified, band-pass filtered (2 Hz–2 kHz), and digitized at a sampling rate of 5 kHz with a micro-1401 AD converter (Cambridge Electronic Design Ltd., Cambridge, United Kingdom). All signals were stored digitally for offline analysis. The peak-to-peak MEP amplitude served as an index for M1 excitability. The participants were requested to relax the right FDI during the measurements. Individual traces contaminated by voluntary muscle contraction before the MEP response were excluded from analysis.

Transcranial Magnetic Stimulation

For the pre- and post-rTMS MEP measurements, TMS was delivered over the M1 representation with a Magstim 200^2 (Magstim Co. Ltd., Whitland, United Kingdom). The 5-Hz rTMS protocol was delivered via a cTMS3 device.

Repeated, randomized sessions were performed, six for the 80% RMT anterior–posterior (AP) and posterior–anterior (PA) and three for the 90% RMT AP condition. They were separated by at least one week to avoid carry-over. Each session consisted of three steps as shown in **Figure 1**.

Step 1: Determining thresholds and baseline:

For each session, we used the Magstim 200^2 with the D70 coil to determine the RMT and the MSO intensity that gave a response of approximately 1 mV for the baseline measurement intensity in the PA direction with monophasic pulses. In addition, we determined the RMT for the cTMS pulse shape used in the interventions, both for the PA and the AP direction as a reference for the 5-Hz rTMS stimulation. The induced current direction was reversed by electronically switching the current pulse direction with the coil position fixed. The baseline measurements consisted of a 50-pulse series at 0.2 Hz using the previously determined MSO intensity that gave a 1-mV response in the PA direction with monophasic pulses.

Step 2: Interventional cTMS stimulation:

We used customized, bidirectional pulse shapes which could be generated at 5 Hz with no decay or variation of intensity, which we verified using an external electric field (E-field) probe coil (Koponen et al., 2020). We stimulated at 5 Hz using three durations of the second electric field phase, i.e., 80, 100, and 120 μs in the PA and the AP directions at 80% RMT and in the AP direction at 90%; the first phase was fixed at 60 μs (**Figure 2**).

In accordance with Rothkegel et al. (2010), we applied 1,200 pulses in six 200-pulse blocks separated by 15 MEP measurements at 0.2 Hz using the same intensity that produced 1 mV at baseline from the Magstim 200^2 device (the interval between the blocks thus lasted approximately 50 s).

Step 3: After the final rTMS pulse block, we applied 25 pulses at 0.2 Hz using the 1 mV baseline intensity and repeated the series every 5 min for 30 min using the Magstim 200^2 stimulator.

Statistical Analysis

For RMT, a two-way repeated measures ANOVA was used with the within-subject factors direction (PA and AP) and pulse duration (80, 100, and 120 μs) for the 80% PA and AP conditions. We conducted another repeated measures ANOVA for the AP condition with the within subject factors intensity (80 and 90%) and pulse duration to explore inter-session stability of RMT. For MEP amplitude changes, we first ran two one-way ANOVAs with the within-subject factor condition (across all direction, intensity, and pulse duration combinations) for the average of the 50 baseline MEP measurements and stimulation intensity needed to elicit 1 mV MEP, which were used for the baseline and post measurements, to exclude baseline differences between sessions. Then, for each session, MEP amplitudes for each subject were normalized by dividing the averaged in-between and post measurement values by the average of the subject's baseline measurement. Subsequent MEP measurements were binned together for the in-between, 0–15 min and 20–30 min measurements within each subject. A repeated measures ANOVA was used to test for the effect of the within-subject factors condition (PA 80%, AP 80%, and AP 90%), pulse duration (80, 100, and 120 μs), and time (baseline, in-between, 0–15 min, and 20–30 min) on the normalized MEP amplitude as a dependent variable. Sphericity violation was tested for by Mauchly's test and corrected for by Greenhouse-Geisser method if violated. Given the exploratory nature of the study, *post hoc t*-tests were conducted comparing the MEP amplitude change to the baseline for different pulse durations even though the pulse duration factor was not found significant in affecting MEP amplitudes in the ANOVA. Correction for multiple comparisons was done with the Bonferroni-Dunn method.

Neural Membrane Polarization Model

We recorded the cTMS pulse waveforms using the E-field probe coil sampled at a rate of 1 MHz. We then used a first-order low pass filter with time constant τ_m (Barker et al., 1991; Corthout et al., 2001; Peterchev et al., 2013) to approximate membrane polarization induced by each pulse waveform. We used this model to estimate both the strength–duration time constant from experimental motor threshold measurements (Peterchev et al., 2013; D'Ostilio et al., 2016; Aberra et al., 2020) as well as the peak depolarization for a range of time constants, representing different neuronal elements in cortex (cell bodies, axons, dendrites). For the former case, we estimated separate time constants for the PA and AP RMT measurements (D'Ostilio et al., 2016) and compared them using paired two-tailed *t*-tests. For the latter case, we extracted the peak depolarization for each pulse scaled by the mean stimulation intensity across subjects applied in each rTMS protocol, i.e., 80% RMT for the PA pulses and 80 and 90% RMT for the AP pulses. Since the linear membrane model has no spatial dimension or explicit direction, we tested two different definitions of pulse waveform polarity: (1) PA-directed E-field produced depolarization and AP-directed E-field produced hyperpolarization ("PA depolarizing") or (2) AP-directed E-field produced depolarization and PA-directed E-field produced hyperpolarization ("AP depolarizing"). These two definitions represent neural elements with opposite directions relative to the E-field. We then performed least-squares, linear regression for the peak depolarization and average normalized MEP amplitudes for both polarity definitions.

RESULTS

RMT

For the direction conditions, PA 80% and AP 80% there was a significant effect of direction [$F_{(1,13)} = 71.2743$, $p < 0.0001$] and pulse duration [$F_{(2,26)} = 99.374$, $p < 0.0001$] on RMT, but the interaction was not significant [$F_{(2,26)} = 0.209$, $p = 0.$

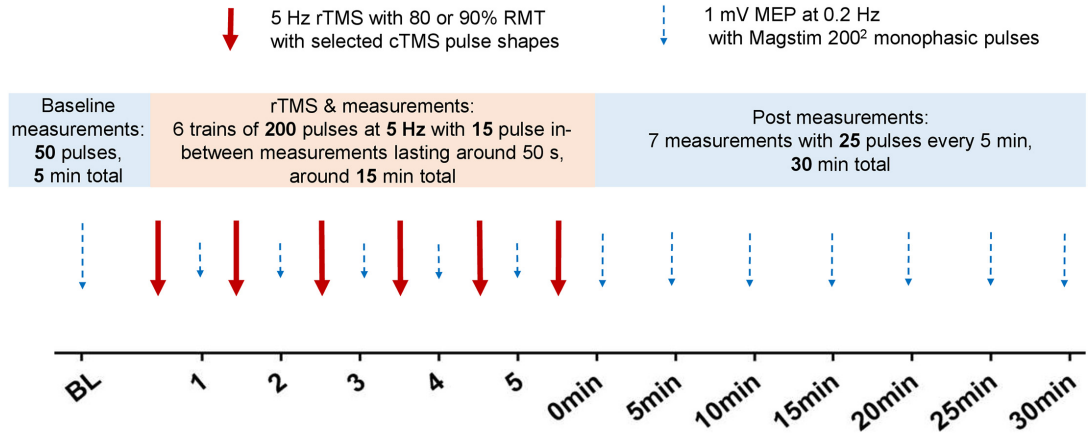

FIGURE 1 | Timeline of the experimental sessions. The sessions were randomized, and there was at least a 1-week pause between sessions to avoid possible carry-over effects.

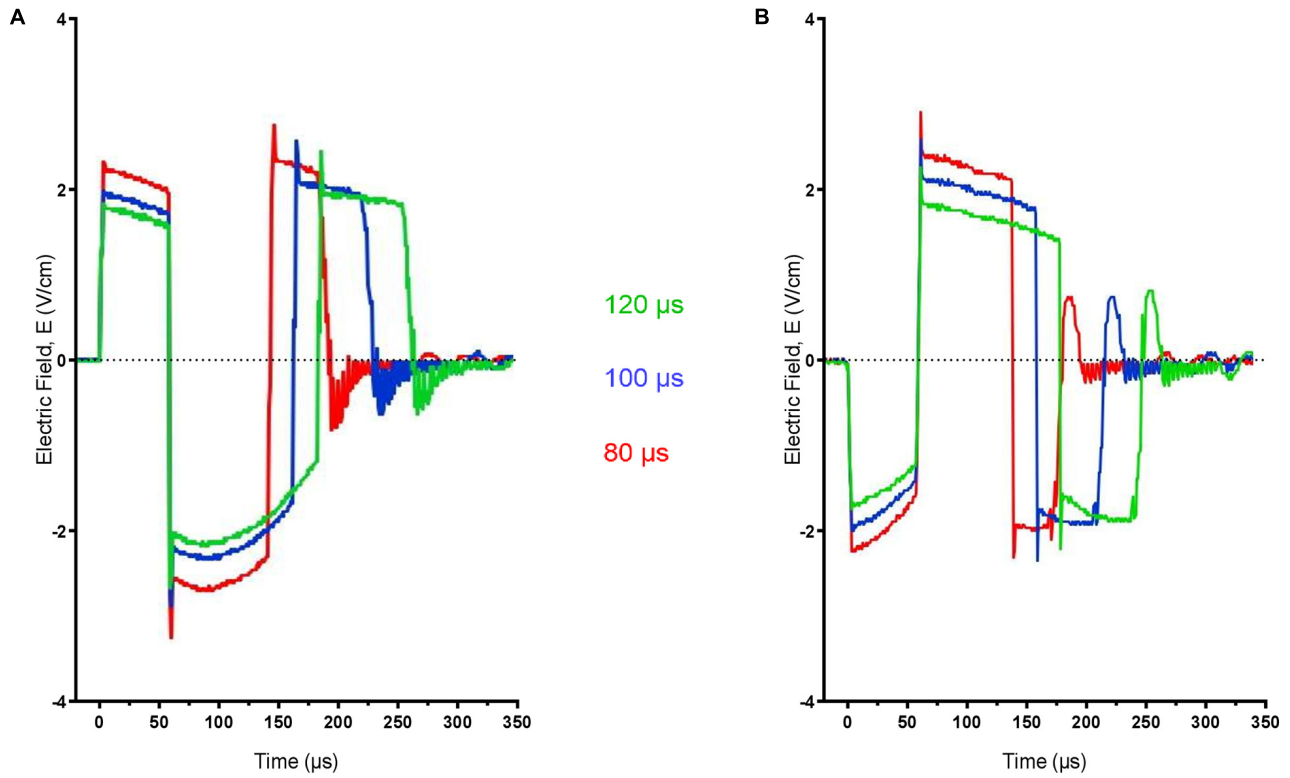

FIGURE 2 | Waveform and electric field strength of the repetitive transcranial magnetic stimulation (rTMS) pulse shapes recorded directly at the center 2 cm away from the TMS coil at the average threshold intensities for 5 Hz posterior–anterior (PA) stimulation **(A)** and 5 Hz anterior-posterior (AP) stimulation **(B)**.

813] with wider pulses resulting in significantly lower RMTs (**Figure 3A**). There was no significant variability in RMT values across the two intensity conditions of AP stimulation [$F_{(1,13)} = 0.398$, $p = 0.539$]. Direction dependent depolarization exhibited different patterns across pulse durations, relevant to the direction of the main phase. The longer AP pulses induced more depolarization in the AP direction but less in the PA direction (**Figure 3B**), while the longer PA pulses induced more depolarization in the PA direction but less in the AP direction (**Figure 3C**). The strength–duration time constant estimated separately for each individual was 71.57 ± 24.31 µs (mean ± SD) for the PA direction and 107.3 ± 29.81 µs for the AP direction ($p < 0.01$). Similarly, estimating a single group time constant and individual rheobase values gave a time constant of 67.85 µs

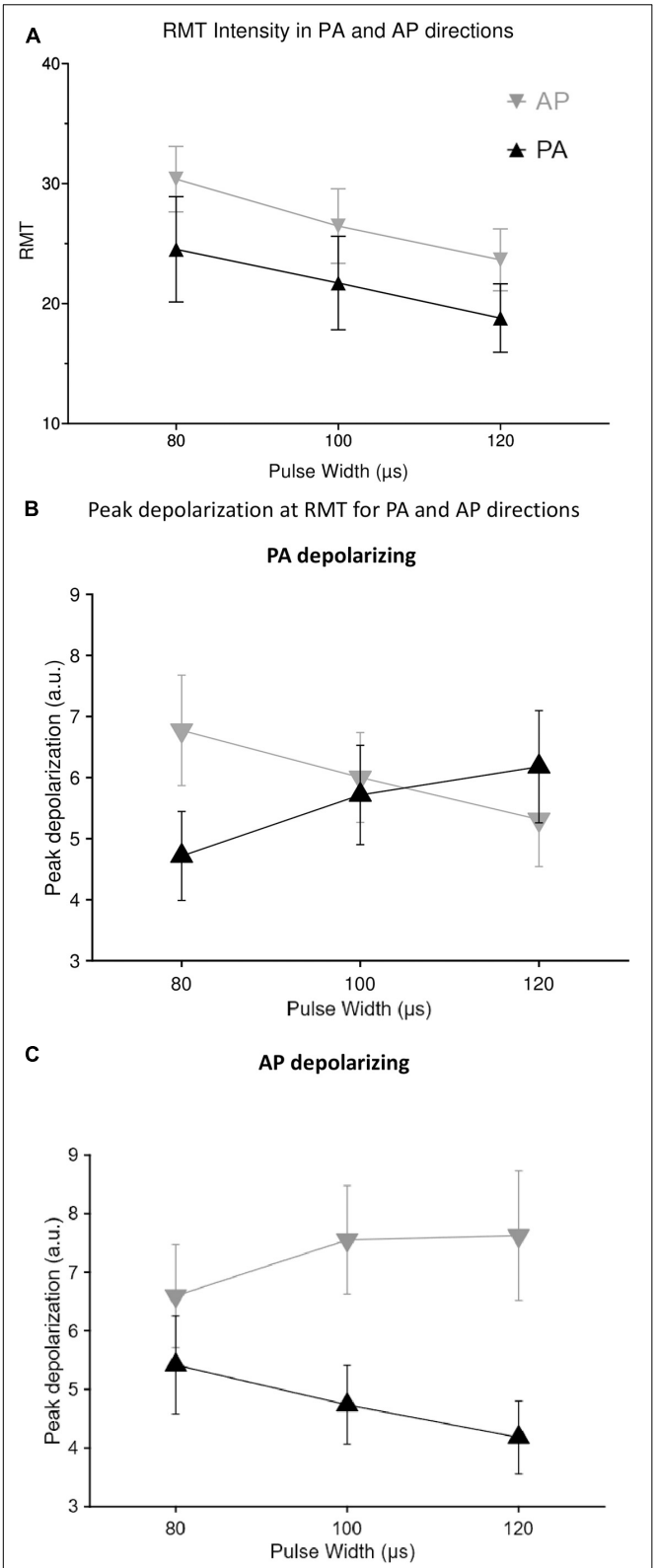

FIGURE 3 | Effect of pulse duration and stimulation direction on **(A)** intensity threshold and resulting depolarization for **(B)** posterior-anterior (PA) direction defined as depolarizing and **(C)** anterior-posterior (AP) direction defined as depolarizing.

[CI = (57.91 μs, 77.80 μs)] for PA and 102.13 μs [89.67 μs, 114.6 μ s] for AP.

Plastic Aftereffects

Baseline one-way ANOVA revealed no significant difference on MEP amplitude across sessions [$F_{(8,117)} = 0.4619$, $p = 0.8806$]. Intensity used in measuring the baseline and subsequent measurements was not significantly different across sessions [$F_{(8,117)} = 0.06611$, $p = 0.9988$].

Repeated measures ANOVA for the three conditions 80% PA, 80% AP, and 90% AP revealed significant main effects of condition [$F_{(2,26)} = 6.011$, $p = 0.007$], and time [$F_{(3,39)} = 4.645$, $p = 0.007$], and a significant interaction between these factors [$F_{(6,78)} = 3.126$, $p = 0.008$]. The main effect of pulse duration was not significant [$F_{(2,26)} = 0.052$, $p = 0.949$] as well as its interaction with condition [$F_{(4,52)} = 0.33$, $p = 0.857$], time [$F_{(6,78)} = 0.127$, $p = 0.993$], and condition with time [$F_{(12,156)} = 0.475$, $p = 0.927$]. Therefore, *post hoc* tests of the effect of pulse duration were performed on an exploratory basis.

For the 80% RMT, PA-directed 5 Hz rTMS, *post hoc t*-tests for the time bins during and after intervention with the baseline revealed no significant shift from the baseline (**Figure 4A**). Again, with the 80% RMT AP-directed stimulation, *post hoc t*-tests for the time bins with the baseline revealed no significant shift from the baseline (**Figure 4B**).

For the 90% AP stimulation conditions, *post hoc t*-tests of the in-between and the post bins showed that the 120 μs pulse shape produced significant excitation at the two post time bins: 0–15 min bin (Bonferroni adjusted $p = 0.0156$) and 20–30 min bin Bonferroni (adjusted $p = 0.0490$), as compared to baseline. The 100 μs condition produced excitation only at the 20–30 min bin (Bonferroni adjusted $p = 0.0461$). Eighty microseconds stimulation did not induce significant shift of excitability from the baseline at any time point and no significant difference was found between pulse durations (**Figure 4C**).

Finally, we simulated the polarization induced by each pulse scaled to the mean intensity applied experimentally across subjects and extracted the peak depolarization for each stimulation condition for both polarity assumptions (**Figure 5A**). Focusing first on a single time constant of 200 μs based on previous measurements with different cTMS pulses (Peterchev et al., 2013; D'Ostilio et al., 2016), the average normalized MEP amplitude was linearly correlated with the peak depolarization when AP E-field was defined as depolarizing in its main phase ($R^2 = 0.86$; $p < 0.001$), but not when PA was defined as depolarizing ($R^2 = 0.06$; $p = 0.520$) (**Figure 5B**). When the AP E-field direction was defined as depolarizing, the PA pulses were hyperpolarizing in their main phase. For the PA pulses, peak depolarization was therefore produced by the initial, reversed phase, which was 60 μs for all pulse waveforms. This produced an inverse correlation between main pulse duration and peak depolarization for PA pulses, as RMT, and consequently applied pulse intensity, decreased with pulse duration. As a result, the trend in peak depolarization relative to pulse duration matched the trend in mean MEP modulation. We found strongest correlations between the AP depolarizing linear membrane model and experimental data with the 200 μs time constant,

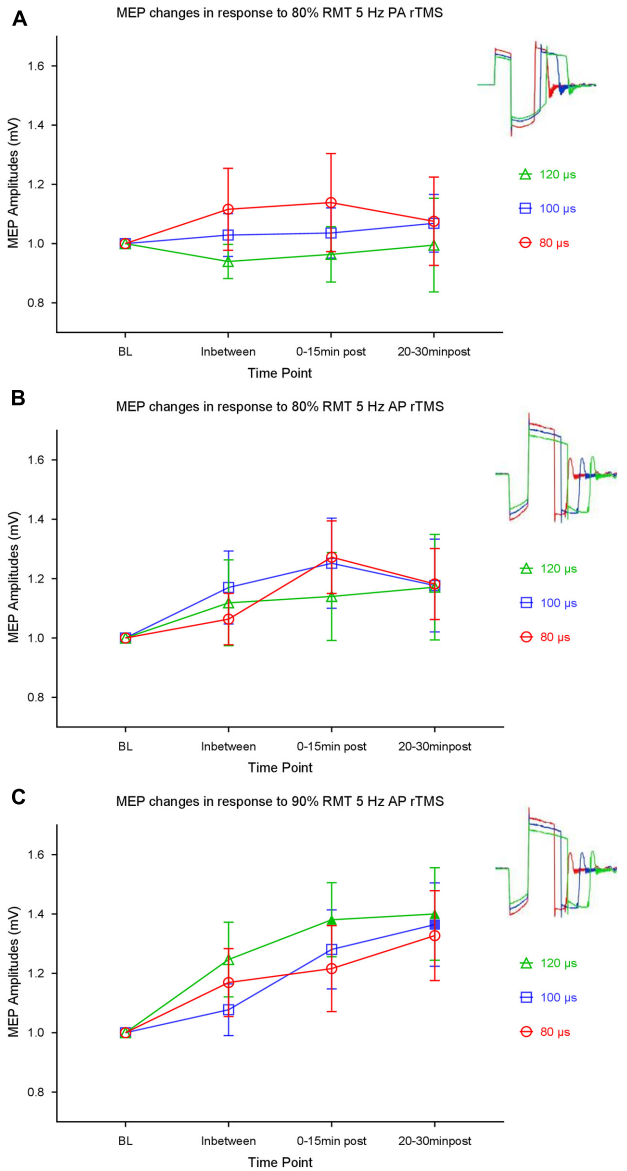

FIGURE 4 | Mean and SEM of motor evoked potential (MEP) amplitude changes in response to: **(A)** 80% resting motor threshold (RMT) 5 Hz stimulation using 80, 100, and 120 µs main component in the posterior-anterior (PA) direction. **(B)** 80% RMT 5 Hz stimulation using 80, 100, and 120 µs main component in the anterior-posterior (AP) direction. **(C)** 90% RMT 5 Hz stimulation using 80, 100, and 120 µs main components in the AP direction. Pulse shapes used for stimulation are illustrated in corresponding colors in the top right corner.

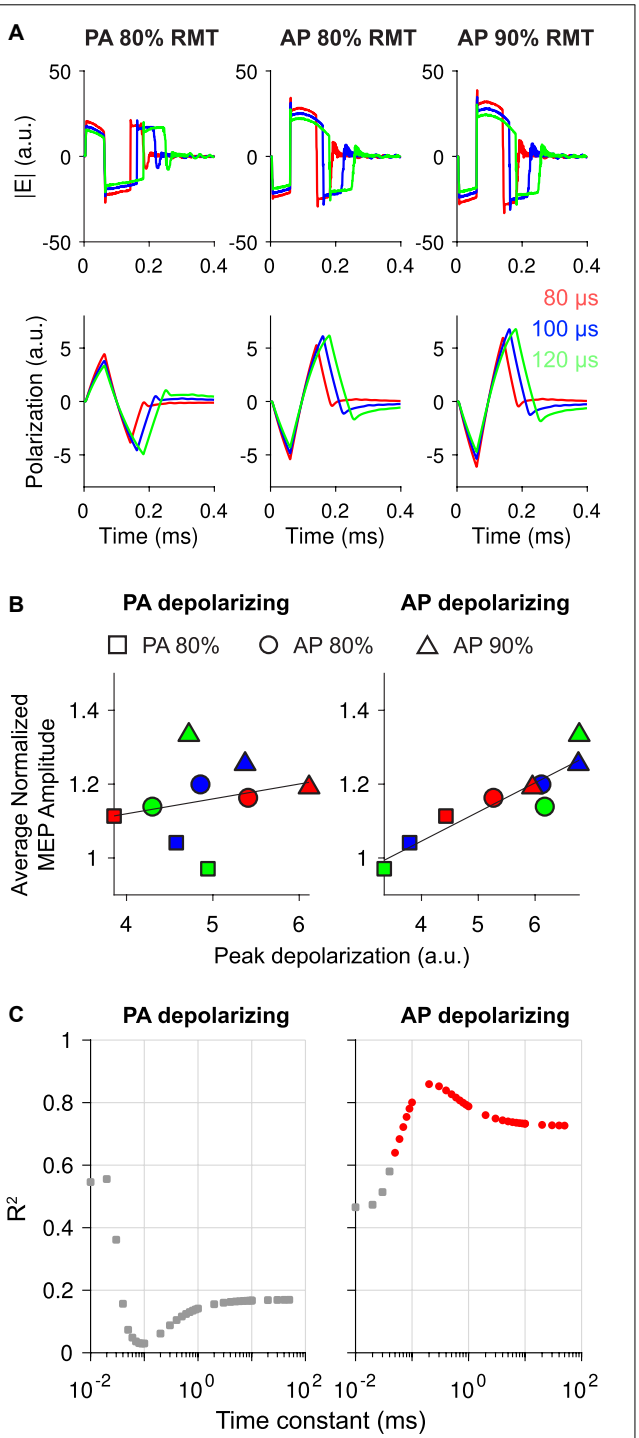

FIGURE 5 | (A) E-field waveforms scaled to mean intensity applied in experiments (top row) and simulated polarization for linear membrane model with 200 µs time constant (bottom row). **(B)** Correlation between average normalized motor evoked potential (MEP) amplitudes and peak depolarization values in panel **(A)**, with linear regression overlaid, for the main phase of posterior-anterior (PA) defined as depolarizing (left) or anterior-posterior (AP) defined as depolarizing (right). **(C)** R^2 values for linear regression of average normalized MEP amplitudes and peak depolarization as a function of membrane time constant. Red circles indicate $p < 0.01$, while gray squares indicate $p > 0.01$. PA depolarizing on left and AP depolarizing on right.

which corresponds to neural elements with higher time constants than the strength–duration time constant estimated from the motor threshold data (57.91–114.58 µs) (**Table 1**). Furthermore, the correlation coefficient was significantly reduced for shorter time constants ($R^2 = 0.47; p = 0.043$ for $\tau_m = 10\ \mu s$) and, to a lesser extent, for longer time constants, eventually reaching an asymptotic level ($R^2 = 0.73; p = 0.004$ for $\tau_m = 50\ ms$) (**Figure 5C**, right). In contrast, we did not find statistically

TABLE 1 | Strength–duration curve parameters estimated using measurements of resting motor threshold (RMT) with bidirectional cTMS3 pulses with main (2nd) E-field phase of 80, 100, and 120 μs duration applied in the posterior-anterior (PA) and anterior-posterior (AP) direction.

Model	Parameters	PA		AP	
		Mean	SD or 95% CI	Mean	SD or 95% CI
Individual rheobase and group time constant	Rheobase (% MSO)	13.82	1.97	13.10	1.66
	Time constant (μs)	67.85	[57.91, 77.80]	102.13	[89.67, 114.58]
Individual rheobase and individual time constant	Rheobase (% MSO)	13.72	3.08	13.10	3.46
	Time constant (μs)	71.58	24.31	107.27	29.81

significant correlations for the opposite polarity definition (PA depolarizing) for any membrane time constant (**Figure 5C**, left).

DISCUSSION

This study suggests that increasing both the pulse duration and intensity can increase 5 Hz rTMS excitatory aftereffects. An exploratory finding was that with the higher intensity of 90% RMT, 5 Hz rTMS in the AP direction increased cortical excitability relative to baseline for pulses with dominant E-field phase duration of 120 and 100 μs, whereas the 80 μs pulses did not. Hence, the effect of increasing the pulse duration is similar to what is already known for increasing stimulation intensity (Modugno et al., 2001; Fitzgerald et al., 2006). The difference between the 80 and 90% RMT AP conditions suggests that a certain degree of direct activation or depolarization, proportional to pulse intensity, is required to produce facilitation of the test pulse MEP. The increased rTMS excitatory effects are possibly a result of inducing cooperativity as demonstrated in the early LTP paper by McNaughton (McNaughton et al., 1978). AP stimulation was found to be more excitatory than PA stimulation as demonstrated earlier in rTMS studies with 5 Hz rTMS (Rothkegel et al., 2010; Sommer et al., 2013a).

RMT decreased consistently with increasing pulse duration (**Figure 3A**) in agreement with previous reports (D'Ostilio et al., 2016), and the canonical strength–duration model of membrane excitation. The strength–duration time constants estimated for both PA and AP pulses (∼60–110 μs) were significantly below previous estimates (∼200–250 μs) with magnetically monophasic pulses (Peterchev et al., 2013; D'Ostilio et al., 2016). This discrepancy may be due to the different pulse shapes: we used magnetically biphasic pulses (M = 1), inducing more symmetric, triphasic E-field waveforms, which potentially recruits a mixture of neuronal populations (Sommer et al., 2018). Activation of a mixture of populations with different membrane time constants would alter the overall shape of the strength–duration curve, making more ambiguous the physiological meaning of the strength–duration time constant estimates. Nevertheless, we estimated higher time constants for AP pulses relative to PA, which agrees with the trend observed for time constants measured during voluntary contraction, but not at rest (D'Ostilio et al., 2016).

We also sought to explain how changing the pulse duration might alter the effects of 5 Hz pulse trains on MEP modulation, despite each pulse duration producing equivalent motor output at either 80 or 90% RMT. Any differences in plastic aftereffects of pulse trains must be related to differences in the single pulse effects. Using a simple low-pass filter to model membrane polarization, we found that peak depolarization correlated well with MEP modulation across all conditions (**Figures 5B,C**), specifically for neural elements depolarized by AP-directed E-field and for membrane time constants near 200 μs. Previous studies have found that 5 Hz rTMS most effectively facilitates MEPs using biphasic pulses with the dominant phase in the posterior direction (AP) (Sommer et al., 2013a), suggesting neural elements activated by AP-directed E-field are involved in the neuromodulatory aftereffects. The polarity of membrane polarization (i.e., depolarization vs. hyperpolarization) is determined primarily by the relative orientation of the local E-field and secondarily by electrotonic interactions between differentially polarized branches within axonal and dendritic arbors (Tranchina and Nicholson, 1986; Arlotti et al., 2012; Aberra et al., 2018). Models and *in vitro* evidence suggest downward (pia to white matter) E-fields tend to depolarize the soma and basal dendrites of pyramidal cells while hyperpolarizing their apical dendrites (Bikson et al., 2004; Radman et al., 2009; Aberra et al., 2018). While cortical axons and dendrites typically have main branches aligned to the cortical columns, they also possess several oblique and transverse branches spanning virtually all possible directions, adding considerable complexity to polarization distributions induced within a given neuron. Therefore, the relevant neural elements may be axons belonging to the "AP-sensitive" neurons activated by single supra-threshold pulses with AP-directed E-fields, or dendritic elements oriented posteriorly, e.g., basal dendrites of neurons on the anterior side of the precentral gyrus or apical dendrites of neurons on the posterior side of the precentral gyrus (Sommer et al., 2013a).

The correlation between peak depolarization and MEP modulation was highest for model time constants between 0.1 and 1 ms (**Figure 5C**), while the estimated time constants from the motor threshold measurements (**Figure 3A**) were at the lower border of this range, suggesting the neural elements involved in producing the facilitatory effects at longer pulse durations were different from the directly activated elements. Additionally, since the pulse intensity is scaled to produce equivalent motor output, the directly activated elements producing corticospinal output likely experienced similar peak depolarization across pulse durations. Dendritic membrane time constants measured with intracellular electrodes are in the 1–10 ms range (Ranck, 1975),

although time constants are known to be lower for extracellular stimulation, depend on the field distribution (Ranck, 1975; Radman et al., 2009; Rattay et al., 2012), and respond preferentially to wider pulses (Rattay et al., 2012). Therefore, this simple model suggests the facilitatory effects were dependent on polarization of AP-sensitive neural elements with time constants longer than the neural elements responsible for the TMS-evoked motor output (pyramidal tract activation). While speculative, if these longer time constant neural elements are dendritic membranes, the increased MEP facilitation may correlate with increased recruitment of dendritic plasticity mechanisms.

This scenario is similar to what McNaughton and colleagues observed in rat cortices, where they demonstrated cooperativity of multiple afferents brought about by higher intensity and wider pulses as a mechanism of LTP (McNaughton et al., 1978). We propose that cooperativity is probably mediated by a stronger and wider dendritic activation, as a result of the unique membrane properties of dendrites and their important role in inducing synaptic plasticity. However, in a previous study with a 5 Hz biphasic (AP) rTMS protocol facilitation was not blocked by the glutamate receptor antagonist dextromethorphan; this led to the conclusion in the discussion that the mechanism was post-tetanic potentiation, which is NMDAr-independent (Sommer et al., 2013b). So another possibility is that the effect of pulse duration could be mediated by differential polarization of the presynaptic terminals activated by each pulse (Habets and Borst, 2006). Current injection into dendrites furthest from the soma produced longer and larger action potentials compared with somatic current injection (Larkum et al., 2007), especially in response to stimulation with higher frequency and longer pulse duration (Ledergerber and Larkum, 2010).

Dendritic stimulation can also generate back-propagating potentials that potentiate the anterograde potentials arising from somatic stimulation, thus producing LTP through associativity (Larkum, 2004), or cooperativity and spike-timing dependent plasticity (Lenz et al., 2015). The significance of dendritic activation in producing lasting plastic aftereffects through LTP in response to rTMS has been emphasized in *in vitro* studies (Sjöström et al., 2008; Müller-Dahlhaus and Vlachos, 2013). The large dendritic capacitance is mediated by the dendritic surface area, a significant portion of which is contributed by dendritic spines. Dendritic spines can also passively amplify local synaptic depolarization up to 50-fold due to their higher input resistance and increase cooperativity due to the high spine neck resistance (Harnett et al., 2012). Dendritic firing requires longer rTMS trains, but when finally achieved, the firing has significantly larger amplitudes and lasts for a longer period after stimulation ceases (Lee and Fried, 2017). If the dendritic activation hypothesis is verified, the therapeutic efficacy of high frequency rTMS in treating neurological or psychiatric diseases (Lefaucheur et al., 2020) might benefit from manipulating the duration of the individual pulses to modulate the extent of dendritic activation.

This study has several notable limitations. Absence of 90% PA conditions was a limitation that did not allow for a free comparison of the direction and intensity effects. Moreover, within the 90% AP condition, the effect of the pulse duration on the MEP amplitude change after rTMS was indicated by exploratory *post hoc* analyses in the absence of a significant ANOVA effect. A factor contributing to the small effect size may be the narrow range of pulse durations (80–120 μs), as compared to our previous study with 1 Hz rTMS, which explored a wider duration range (40–120 μs) as well as both bidirectional and unidirectional pulses (Halawa et al., 2019). Therefore, future studies could seek confirmation and enhancement of our exploratory findings, potentially by refining the experimental paradigm to include a wider range of pulse durations and directionality conditions. Finally, we used a very simple neural membrane response model. In the future, more realistic neuronal representations embedded in 3D models of the individual head and brain could be deployed to better understand the mechanisms underlying the effects of various TMS parameters (Aberra et al., 2020).

DATA AVAILABILITY STATEMENT

The raw data supporting the conclusions of this article will be made available by the authors, without undue reservation.

ETHICS STATEMENT

The studies involving human participants were reviewed and approved by the Local Ethics Committee of the University Medical Center Göttingen. The patients/participants provided their written informed consent to participate in this study.

AUTHOR CONTRIBUTIONS

IH, KR, MS, and WP conceived the research idea. IH and KR collected and analyzed the experimental data and prepared the initial figures and manuscript. AA and AP produced the modeling data. IH, KR, AA, MS, AP, and WP revised the manuscript and approved the final version. All authors contributed to the article and approved the submitted version.

FUNDING

The funding sources were not involved in the conduct of the research, the collection, analysis, or interpretation of data, the writing of the report, or in the decision to submit the article for publication. We thank the German Research Foundation (Deutsche Forschungsgemeinschaft, DFG) for funding the cTMS device (DFG grant application: NST1525/18-1 FUGG). We also thank the German Academic Exchange Service (Deutscher Akademischer Austauschdienst, DAAD) and the Egyptian Ministry of Higher Education and Scientific Research (MHESR) for jointly funding the Ph.D. scholarship for IH. The contribution of AP was supported by the U.S.A. National Institutes of Health (NIH) under award numbers R01NS088674, R01NS117405, R01MH111865, and RF1MH124943. AA was supported by the NIH (R25GM103765) as well as the U.S.A. National Science Foundation (DGF1106401).

ACKNOWLEDGMENTS

We thank Michael Nitsche for his contribution in particular with statistical support, Thomas Crozier for language editing, and Anthony Barker for his helpful communications.

SUPPLEMENTARY MATERIAL

The Supplementary Material for this article can be found online at: https://www.frontiersin.org/articles/10.3389/fnins.2021.773792/full#supplementary-material

REFERENCES

Aberra, A. S., Peterchev, A. V., and Grill, W. M. (2018). Biophysically realistic neuron models for simulation of cortical stimulation. *J Neural Eng.* 15:066023. doi: 10.1101/328534

Aberra, A. S., Wang, B., Grill, W. M., and Peterchev, A. V. (2020). Simulation of transcranial magnetic stimulation in head model with morphologically-realistic cortical neurons. *Brain Stimul.* 13, 175–189. doi: 10.1016/j.brs.2019.10.002

Arlotti, M., Rahman, A., Minhas, P., and Bikson, M. (2012). Axon terminal polarization induced by weak uniform DC electric fields: a modeling study. *Annu. Int. Conf. IEEE Eng. Med. Biol. Soc.* 2012, 4575–4578. doi: 10.1109/EMBC.2012.6346985

Barker, A. T., Garnham, C. W., and Freeston, I. L. (1991). Magnetic nerve stimulation: the effect of waveform on efficiency, determination of neural membrane time constants and the measurement of stimulator output. *Electroencephalogr. Clin. Neurophysiol. Suppl.* 43, 227–237.

Bikson, M., Inoue, M., Akiyama, H., Deans, J. K., Fox, J. E., Miyakawa, H., et al. (2004). Effects of uniform extracellular DC electric fields on excitability in rat hippocampal slices in vitro. *J. Physiol.* 557, 175–190. doi: 10.1113/jphysiol.2003.055772

Bliss, T. V. P., and Cooke, S. F. (2011). Long-term potentiation and long-term depression: a clinical perspective. *Clinics* 66, 3–17. doi: 10.1590/S1807-59322011001300002

Corthout, E., Barker, A. T., and Cowey, A. (2001). Transcranial magnetic stimulation. Which part of the current waveform causes the stimulation? *Exp. Brain Res.* 141, 128–132. doi: 10.1007/s002210100860

D'Ostilio, K., Goetz, S. M., Hannah, R., Ciocca, M., Chieffo, R., Chen, J.-C. A., et al. (2016). Effect of coil orientation on strength–duration time constant and I-wave activation with controllable pulse parameter transcranial magnetic stimulation. *Clin. Neurophysiol.* 127, 675–683. doi: 10.1016/j.clinph.2015.05.017

Fitzgerald, P., Fountain, S., and Daskalakis, Z. (2006). A comprehensive review of the effects of rTMS on motor cortical excitability and inhibition. *Clin. Neurophysiol.* 117, 2584–2596. doi: 10.1016/j.clinph.2006.06.712

Habets, R. L. P., and Borst, J. G. G. (2006). An increase in calcium influx contributes to post-tetanic potentiation at the rat calyx of Held synapse. *J. Neurophysiol.* 96, 2868–2876. doi: 10.1152/jn.00427.2006

Halawa, I., Shirota, Y., Neef, A., Sommer, M., and Paulus, W. (2019). Neuronal tuning: selective targeting of neuronal populations via manipulation of pulse width and directionality. *Brain Stimul.* 12, 1244–1252. doi: 10.1016/j.brs.2019.04.012

Hannah, R., Rocchi, L., Tremblay, S., Wilson, E., and Rothwell, J. C. (2020). Pulse width biases the balance of excitation and inhibition recruited by transcranial magnetic stimulation. *Brain Stimul.* 13, 536–538. doi: 10.1016/j.brs.2020.01.011

Harnett, M. T., Makara, J. K., Spruston, N., Kath, W. L., and Magee, J. C. (2012). Synaptic amplification by dendritic spines enhances input cooperativity. *Nature* 491, 599–602. doi: 10.1038/nature11554

Hebb, D. O. (1949). *The Organization of Behavior; A Neuropsychological Theory*. Oxford: Wiley.

Huerta, P. T., and Volpe, B. T. (2009). Transcranial magnetic stimulation, synaptic plasticity and network oscillations. *J. Neuroeng. Rehabil.* 6:7. doi: 10.1186/1743-0003-6-7

Koponen, L. M., Goetz, S. M., Tucci, D. L., and Peterchev, A. V. (2020). Sound comparison of seven TMS coils at matched stimulation strength. *Brain Stimul.* 13, 873–880. doi: 10.1016/j.brs.2020.03.004

Larkum, M. E. (2004). Top-down dendritic input increases the gain of layer 5 pyramidal neurons. *Cereb. Cortex* 14, 1059–1070. doi: 10.1093/cercor/bhh065

Larkum, M. E., Waters, J., Sakmann, B., and Helmchen, F. (2007). Dendritic spikes in apical dendrites of neocortical layer 2/3 pyramidal neurons. *J. Neurosci.* 27, 8999–9008. doi: 10.1523/JNEUROSCI.1717-07.2007

Ledergerber, D., and Larkum, M. E. (2010). Properties of layer 6 pyramidal neuron apical dendrites. *J. Neurosci.* 30, 13031–13044. doi: 10.1523/JNEUROSCI.2254-10.2010

Lee, S. W., and Fried, S. I. (2017). Enhanced control of cortical pyramidal neurons with micromagnetic stimulation. *IEEE Trans. Neural Syst. Rehabil. Eng.* 25, 1375–1386. doi: 10.1109/TNSRE.2016.2631446

Lefaucheur, J.-P., Aleman, A., Baeken, C., Benninger, D. H., Brunelin, J., Di Lazzaro, V., et al. (2020). Evidence-based guidelines on the therapeutic use of repetitive transcranial magnetic stimulation (rTMS): an update (2014–2018). *Clin. Neurophysiol.* 131, 474–528. doi: 10.1016/j.clinph.2019.11.002

Lenz, M., Platschek, S., Priesemann, V., Becker, D., Willems, L. M., Ziemann, U., et al. (2015). Repetitive magnetic stimulation induces plasticity of excitatory postsynapses on proximal dendrites of cultured mouse CA1 pyramidal neurons. *Brain Struct. Funct.* 220, 3323–3337. doi: 10.1007/s00429-014-0859-9

McNaughton, B. L., Douglas, R. M., and Goddard, G. V. (1978). Synaptic enhancement in fascia dentata: cooperativity among coactive afferents. *Brain Res.* 157, 277–293. doi: 10.1016/0006-8993(78)90030-6

Modugno, N., Nakamura, Y., MacKinnon, C., Filipovic, S., Bestmann, S., Berardelli, A., et al. (2001). Motor cortex excitability following short trains of repetitive magnetic stimuli. *Exp. Brain Res.* 140, 453–459. doi: 10.1007/s002210100843

Müller-Dahlhaus, F., and Vlachos, A. (2013). Unraveling the cellular and molecular mechanisms of repetitive magnetic stimulation. *Front. Mol. Neurosci.* 6:50. doi: 10.3389/fnmol.2013.00050

Oldfield, R. C. (1971). The assessment and analysis of handedness: the edinburgh inventory. *Neuropsychologia* 9, 97–113. doi: 10.1016/0028-3932(71)90067-4

Pell, G. S., Roth, Y., and Zangen, A. (2011). Modulation of cortical excitability induced by repetitive transcranial magnetic stimulation: influence of timing and geometrical parameters and underlying mechanisms. *Prog. Neurobiol.* 93, 59–98. doi: 10.1016/j.pneurobio.2010.10.003

Peterchev, A. V., D'Ostilio, K., Rothwell, J. C., and Murphy, D. L. (2014). Controllable pulse parameter transcranial magnetic stimulator with enhanced circuit topology and pulse shaping. *J. Neural Eng.* 11:056023. doi: 10.1088/1741-2560/11/5/056023

Peterchev, A. V., Goetz, S. M., Westin, G. G., Luber, B., and Lisanby, S. H. (2013). Pulse width dependence of motor threshold and input–output curve characterized with controllable pulse parameter transcranial magnetic stimulation. *Clin. Neurophysiol.* 124, 1364–1372. doi: 10.1016/j.clinph.2013.01.011

Peterchev, A. V., Murphy, D. L., and Lisanby, S. H. (2011). Repetitive transcranial magnetic stimulator with controllable pulse parameters. *J. Neural Eng.* 8:036016. doi: 10.1088/1741-2560/8/3/036016

Radman, T., Ramos, R. L., Brumberg, J. C., and Bikson, M. (2009). Role of cortical cell type and morphology in subthreshold and suprathreshold uniform electric field stimulation in vitro. *Brain Stimul.* 2, e1–e3. doi: 10.1016/j.brs.2009.03.007

Ranck, J. B. (1975). Which elements are excited in electrical stimulation of mammalian central nervous system: a review. *Brain Res.* 98, 417–440. doi: 10.1016/0006-8993(75)90364-9

Rattay, F., Paredes, L. P., and Leao, R. N. (2012). Strength–duration relationship for intra- versus extracellular stimulation with microelectrodes. *Neuroscience* 214, 1–13. doi: 10.1016/j.neuroscience.2012.04.004

Rossi, S., Hallett, M., Rossini, P. M., and Pascual-Leone, A. (2009). Safety, ethical considerations, and application guidelines for the use of transcranial magnetic stimulation in clinical practice and research. *Clin. Neurophysiol.* 120, 2008–2039. doi: 10.1016/j.clinph.2009.08.016

Rossini, P. M., Burke, D., Chen, R., Cohen, L. G., Daskalakis, Z., Di Iorio, R., et al. (2015). Non-invasive electrical and magnetic stimulation of the brain, spinal cord, roots and peripheral nerves: basic principles and procedures for routine clinical and research application. An updated report from an I.F.C.N.

Committee. *Clin. Neurophysiol.* 126, 1071–1107. doi: 10.1016/j.clinph.2015.02.001

Rothkegel, H., Sommer, M., and Paulus, W. (2010). Breaks during 5Hz rTMS are essential for facilitatory after effects. *Clin. Neurophysiol.* 121, 426–430. doi: 10.1016/j.clinph.2009.11.016

Sjöström, P. J., Rancz, E. A., Roth, A., and Häusser, M. (2008). Dendritic excitability and synaptic plasticity. *Physiol. Rev.* 88, 769–840. doi: 10.1152/physrev.00016.2007

Sommer, M., Ciocca, M., Chieffo, R., Hammond, P., Neef, A., Paulus, W., et al. (2018). TMS of primary motor cortex with a biphasic pulse activates two independent sets of excitable neurones. *Brain Stimul.* 11, 558–565. doi: 10.1016/j.brs.2018.01.001

Sommer, M., Norden, C., Schmack, L., Rothkegel, H., Lang, N., and Paulus, W. (2013a). Opposite optimal current flow directions for induction of neuroplasticity and excitation threshold in the human motor cortex. *Brain Stimul.* 6, 363–370. doi: 10.1016/j.brs.2012.07.003

Sommer, M., Rummel, M., Norden, C., Rothkegel, H., Lang, N., and Paulus, W. (2013b). Mechanisms of human motor cortex facilitation induced by subthreshold 5-Hz repetitive transcranial magnetic stimulation. *J. Neurophysiol.* 109, 3060–3066. doi: 10.1152/jn.01089.2012

Tranchina, D., and Nicholson, C. (1986). A model for the polarization of neurons by extrinsically applied electric fields. *Biophys. J.* 50, 1139–1156. doi: 10.1016/S0006-3495(86)83558-5

Vlachos, A., Funke, K., and Ziemann, U. (2017). Assessment and modulation of cortical inhibition using transcranial magnetic stimulation. *eNeuroforum* 23, A9–A17. doi: 10.1515/nf-2016-A103

Ziemann, U., Paulus, W., Nitsche, M. A., Pascual-Leone, A., Byblow, W. D., Berardelli, A., et al. (2008). Consensus: motor cortex plasticity protocols. *Brain Stimul.* 1, 164–182. doi: 10.1016/j.brs.2008.06.006

Author Disclaimer: The content is solely the responsibility of the authors and does not necessarily represent the official views of the funding agencies.

Conflict of Interest: AP is an inventor on patents and patent applications on TMS technology, related to TMS, he has received travel support as well as patent royalties from Rogue Research for cTMS, research and travel support, consulting fees, as well as equipment donations from Tal Medical/Neurex, patent application and research support as well as hardware donations from Magstim, equipment loans and hardware donations from MagVenture, and consulting fees from Neuronetics, BTL Industries, and Advise Connect Inspire.

The remaining authors declare that the research was conducted in the absence of any commercial or financial relationships that could be construed as a potential conflict of interest.

Publisher's Note: All claims expressed in this article are solely those of the authors and do not necessarily represent those of their affiliated organizations, or those of the publisher, the editors and the reviewers. Any product that may be evaluated in this article, or claim that may be made by its manufacturer, is not guaranteed or endorsed by the publisher.

Advantages of publishing in Frontiers

OPEN ACCESS
Articles are free to read for greatest visibility and readership

FAST PUBLICATION
Around 90 days from submission to decision

HIGH QUALITY PEER-REVIEW
Rigorous, collaborative, and constructive peer-review

TRANSPARENT PEER-REVIEW
Editors and reviewers acknowledged by name on published articles

Frontiers
Avenue du Tribunal-Fédéral 34
1005 Lausanne | Switzerland

Visit us: www.frontiersin.org
Contact us: frontiersin.org/about/contact

REPRODUCIBILITY OF RESEARCH
Support open data and methods to enhance research reproducibility

DIGITAL PUBLISHING
Articles designed for optimal readership across devices

FOLLOW US
@frontiersin

IMPACT METRICS
Advanced article metrics track visibility across digital media

EXTENSIVE PROMOTION
Marketing and promotion of impactful research

LOOP RESEARCH NETWORK
Our network increases your article's readership